THE CHEMICAL ANALYSIS OF MODERN TATTOO INKS

by

MICHELLE D. MIRANDA

VOLUME I

A dissertation submitted to the Graduate Faculty in Criminal Justice in partial fulfillment of the requirements for the degree of Doctor of Philosophy, The City University of New York

2012

This manuscript has been read and accepted for the Graduate Faculty in Criminal Justice in satisfaction of the dissertation requirement for the degree of Doctor of Philosophy.

Date	**Dr. Thomas A. Kubic, Chair of Examining Committee**
Date	**Dr. Joshua Freilich, Executive Officer**
	John Lombardi, Ph.D.
	Dr. John Lombardi, Committee Member
	Marco Leona, Ph.D.
	Dr. Marco Leona, Committee Member
	John Reffner, Ph.D.
	Dr. John A. Reffner, Committee Member

THE CITY UNIVERSITY OF NEW YORK

ABSTRACT

THE CHEMICAL ANALYSIS OF MODERN TATTOO INKS

by

Michelle D. Miranda

Adviser: Dr. Thomas A. Kubic

The application of vibrational spectroscopic methods to the analysis of modern organic pigments found in tattoo inks is explored in this project. In the field of forensic science, the recognition and identification of both inorganic and organic pigments in human tissue can aid in the identification of charred, decomposed, mummified or otherwise unidentifiable remains in criminal investigations and mass disasters (natural, accidental and as a result of terrorism). In the field of art conservation and cultural heritage, the characterization and archiving of organic pigments in traditional tattoo inks can aid in future anthropological and archaeological studies of human culture and history. The criminal justice field has long studied the culture and impact of tattooing, especially in criminal behavior and incarcerated individuals. A more detailed knowledge of the composition of tattoo inks can assist in understanding criminal behavior and cultural practices of individuals in prison settings and among social groups. Furthermore, by detailing the visual, microscopic and spectroscopic analysis of tattoo inks along with describing the theories of vibrational spectroscopy and color chemistry, a thorough analytical method can be developed and validated to conform to current forensic laboratory accreditation standards and the satisfaction of legal standards such as Frye, Daubert and the Federal Rules of Evidence.

The aim of this research is to scientifically evaluate tattoo inks by documenting the physical properties of the inks both macroscopically and microscopically and by identifying the optical

and chemical properties of the pigments spectroscopically. This is done in an effort to qualitatively identify tattoo inks resulting in the ability to discriminate between different colors, within similar colors and between different brands of tattoo inks. The lack of an established method of analysis of tattoo inks for identification and comparison is an additional catalyst for this research. The primary means of characterization is based upon molecular structural determination using normal micro-Raman spectroscopy. This method will be supplemented by several other methods commonly employed in forensic science and art conservation laboratories, such as Surface Enhanced Raman Scattering (SERS), Fourier-transform Raman spectroscopy (FT-Raman), Fourier-transform infrared spectroscopy (FT-IR), x-ray fluorescence (XRF) and ultraviolet-visible spectroscopy (UV/Vis).

ACKNOWLEDGEMENTS

I must first thank my mentors Thomas A. Kubic, John A. Reffner, John Lombardi, Marco Leona and Larry Sullivan, who not only provided support and education towards my pursuit of scientific knowledge but who enriched my life and helped me to appreciate other facets of life, especially the fine arts.

- Drs. Kubic and Reffner—I must thank you for you for extended time as my mentors, as you both were there when I first began graduate studies at the Master's level. Your encouragement and support has not waivered as time has passed; I owe a large part of my pursuit for graduate education to you. Dr. Kubic, I cannot say thank you enough for investing your time into educating me and imparting life lessons that have made me the forensic scientist I am today.
- Drs. Lombardi and Leona—I truly appreciate you taking a chance on me and welcoming me into your research endeavors. Dr. Lombardi, you have taught me to appreciate physical chemistry, and although my research only scratched to surface (pun intended) of physical science, I will continue to appreciate and pursue the studies of physical chemistry and quantum mechanics.
- Dr. Sullivan—I am so grateful for our friendship. You have taught me to appreciate the criminal justice system, the philosophy of science, fine art and tattooing. I enjoy our well-rounded, often cosmic conversations that always end too soon.

Dr. Deanna O'Donnell—Thank you, Dee. You were a very big part of my getting through my second examination/proposal defense. You took a lot of time to help me grasp physical chemistry so that I would not just be able to understand group theory and molecular symmetry and computational chemistry, but you took the time to make sure I could articulate and convey it to others. You were never selfish with your time even though you had your own work to do, and you never grew impatient with me (if you did you sure didn't show it).

Dr. Ed Suzuki (Supervising Forensic Chemist, Washington State Crime Laboratory, Washington State Patrol) and Dr. Patrick Buzzini (Professor, Forensic & Investigative Science Program, West Virginia University)—thank you for lending instant support to my project when it was still in its early stages. Thank you for your willingness to share your knowledge and personal research with me.

Dr. Chris Palenik (Research Microscopist and Vice President, Microtrace, LLC)—thank you for generously providing pigment standards and for lending support to my research.

Dr. Mark Taff—thank you for welcoming me into your professional world. Your help and support have been monumental and will never be forgotten.

Robyn Richie—thank you for unselfishly and without hesitation sharing your supplies and knowledge of tattoos with me.

Thank you to the members of the Metropolitan Museum of Art, some temporary fellows and some permanent staff, that helped me with administrative matters, instrumentation and sample

preparation, specifically Kathy Miller, Tony Frantz, Yae Takahashi, Adrianna Rizzo, and Federica Pozzi.

To my friends and colleagues, thank you for your shared support through my graduate studies. I would especially like to thank Nikolay Azar and Argeliz Pomales.

To my family—

- Michael, your understanding and support far outweighed your frustration at times over the course of my studies. Thank you for sitting through my presentations as I prepared for my examinations and defenses. You have been encouraging since I first filled out the application for the Ph.D. program and your support has never wavered.
- Emily and Joshua, thank you for being a source of comfort and entertainment in times of frustration when I was overwhelmed. I hope you understand one day how meaningful it was to have you express interest in my research by asking me about it, helping me at times and even getting fake tattoos as a show of support.
- To my parents, Dennis and Karen, and my brothers Brian and Dennis Jr. (D.J.). Thank you for being the best family- I would not be where I am today if it wasn't for your continuous support and comic relief. *Mom and Dad, this dissertation is dedicated to you.*

TABLE OF CONTENTS

VOLUME I

VOLUME II

LIST OF TABLES

LIST OF FIGURES

Chapter 1: Introduction

In the field of forensic science, the recognition and identification of both inorganic and organic pigments in human tissue will aid in the identification of charred, decomposed, mummified or otherwise unidentifiable remains in a criminal investigations, mass disasters (natural, accidental and acts of terrorism) and unmarked and mass burial sites. In the field of art conservation and cultural heritage, the characterization and archiving of organic pigments in traditional tattoo inks will serve as a reference point for the study of mummified remains, and can thus aid in anthropological and archaeological studies of human culture and history. The criminal justice field has long studied the culture and impact of tattooing, especially in criminal culture and among incarcerated individuals. A more detailed scientific understanding of the composition of tattoo inks can assist in understanding criminal behavior and cultural practices of individuals in prison settings. Furthermore, by detailing the visual, microscopic and spectroscopic analysis of tattoo inks along with describing the theories of vibrational spectroscopy and color chemistry, a thorough analytical method will be developed and validated to conform to current forensic laboratory accreditation standards and the satisfaction of legal standards such as Frye, Daubert and the Federal Rules of Evidence.

The aim of this research is to scientifically evaluate tattoo inks by documenting the physical properties of the inks both macroscopically and microscopically and by identifying the optical and chemical properties of the pigments spectroscopically. This is done in an effort to qualitatively identify tattoo inks resulting in the ability to discriminate between different colors, within similar colors and between different brands of tattoo inks. The lack of an established method of analysis of tattoo inks for identification and comparison is an additional catalyst for this research, as well as the need for comprehensive instrumental databases for tattoo inks.

Raman spectroscopy has been employed in the areas of forensic science and art conservation for the analysis of several different types of materials, including natural and synthetic paints and fibers, pigments and inks, explosives and suspected drugs, as well as a variety of mineralogical samples such as gemstones, glass, calcified tissue, and ceramics (Bouchard and Smith, 2003; Burgio and Clark, 2001; Edwards and Chalmers, eds., 2005; Centeno, *et. al.*, 2006; Thomas, *et. al.*, 2005, *etc.*). The application of Raman spectroscopic methods to the analysis of modern organic pigments found in tattoo inks is explored in this project. The primary means of characterization is based upon molecular structural determination using normal micro-Raman spectroscopy. This method will be supplemented by several other methods commonly employed in forensic science and art conservation laboratories, such as Surface Enhanced Raman Scattering (SERS), Fourier-transform Raman spectroscopy (FT-Raman), Fourier-transform infrared spectroscopy (FT-IR), x-ray fluorescence (XRF) and ultraviolet-visible spectroscopy (UV/Vis).

Much has been written about tattoos and tattooing, particularly in anthropological, medical/dermatological and forensic literature. With regards to the latter, many historical documents focus on the criminals and the description of tattoos for identification, affiliation and prior criminal activity for the purposes of criminal investigation. In addition, much has been addressed with regard to the prevalence of tattoos within different cultures and societies, with emphasis on the anthropological and psychological motivations and stigma behind the tattoos. Of special note is the attention to tattoos by several individuals that play an important role in the history of forensic science, including Edmond Locard (forensic science), Alphonse Bertillion (forensic science), Hans Gross (forensic science), J. Mathurin Felix Hutin (forensic science), Johann Ludwig Casper (pathology and forensic medicine), A. Ambroise Tardieu (forensic

medicine and toxicology). Additional literature concerning tattoos and their role in criminal justice was presented by Francois Vidocq, Alexandre Lacassagne, Cesare Lombroso, and a variety of other scientists, psychologists and criminologists of the time. Even the well-known fictional detective Sherlock Holmes has commented on the topic of tattoos, "The fish which you have tattooed immediately above your right wrist could only have been done in China. I have made a small study of tattoo marks, and have even contributed to literature of the subject. That trick of staining the fishes' scales of a delicate pink is quite peculiar to China" (1891, pp. 27). While some current scientific and medical literature has addressed tattoos and tattoo inks, forensic science literature has largely focused on forensic photography techniques with regard to the visualization of obscured tattoos on cadavers.

In the United States, laws concerning tattooing vary within different states and different jurisdictions. While the specifics of tattooing laws vary, it is generally accepted the tattooing of minors is illegal and socially immoral. This has not necessarily stopped adults from tattooing children, both in professional and private settings. A literature review of periodicals and news broadcasts demonstrates several instances in which adults and guardians were arrested for tattooing minors. Recent headlines have included "*Man tattoos gang symbol on 7 y(ear) o(ld) son*" (NBC News Broadcast), "*Dad charged with tattooing 3-year-old-son*" (Channel 2 News), "*Man arrested for tattooing toddler*" (Amy Hatch) and "*Parents arrested for home-tattooing 6 children*" (KTLA News). Additionally, tattooing or being in possession of tattooing equipment while incarcerated is also considered illegal. Several articles published in anthropological and medical and criminal justice journals have been focused on tattooing practices among the incarcerated. The potential of being able to identify the age of a tattoo by the location within the

layers of the skin along with identifying the type of ink used may assist in determining if a tattoo has been generated in a prison setting or while a minor was under the care of a particular adult.

Tattoos can also be used to identify charred, decomposed, mummified or otherwise unidentifiable remains. This is especially useful in death investigations, which can be non-criminally motivated (accident, suicide, natural) or the result of criminal activity (homicide). Tattoo recognition and identification is also used in instances of mass fatality and casualty incidents such as accidents and crashes (*i.e.* building collapse, plane or train crash), natural disasters (*i.e*. tsunami or hurricane), war, and terrorist attacks. An example demonstrating the effective use of a tattoo to aid in identification is apparent in the case of a female that was found burned and dumped in a remote region in New York in 2010. The woman's body was marked by a colorful rose tattoo and a name, which was used to aid in her identification and subsequently aid in the identification and arrest of the perpetrator (Figure 1). In many instances, when human remains are found, police agencies will release to the media physical characteristics and the types and locations of any tattoos in an attempt to identify the decedent and aid in the death investigation (Figure 2).

Man indicted in slaying, *body dumping*

Woman was found in Monsey; child abandoned in Del.

Joshua Burd
mycentraljersey.com

Keith Muccilli/Home News
Dwayne Jackson appeared in New Jersey state Superior Court on March 1.

NEW BRUNSWICK, N.J. — A grand jury has indicted a New Jersey man accused of abandoning his 21-month-old daughter at a Delaware gas station and killing the girl's mother, whose body was found burned and dumped in a Monsey park.

Dwayne Jackson, 27, of Edison was indicted on charges of murder, kidnapping, endangering the welfare of a child and hindering his own apprehension.

The indictment, handed up Tuesday, also charges 27-year-old Ritu Loi of New Brunswick with kidnapping, endangering the welfare of a child and hindering Jackson's apprehension. Prosecutors have described her as an acquaintance who accompanied Jackson as he traveled to Delaware and New York.

Jackson is accused of asphyxiating 25-year-old Patricia Belizaire on Feb. 21 in her one-bedroom unit in the Oakleaf Village apartments in North Brunswick. Authorities say her charred body was found a day later in Manny Weldler Park on West Maple Avenue in Monsey.

The woman's body was found by two newspaper carriers. Police discovered the body's most distinguishing feature was a colorful tattoo with the name "Patricia" and a red rose atop a green stem.

Their daughter, Hannah Jackson, [illegible] locked and crying in the bathroom of a Shell service station in Newark, Del., after the father abandoned her there the day of the slaying, police and prosecutors say.

Loi was charged March 9, but the charges were not previously announced by authorities.

Jim O'Neill, a spokesman for the Middlesex County Prosecutor's Office, said LOi is accused of going with Jackson as he left his young daughter in Delaware and disposed of Belizaire's body. He declined to comment further on her alleged involvement or her relationship to Jackson.

Hannah Jackson had been living with her mother in North Brunswick, authorities said. A Family Court judge in Delaware ruled March 3 that she would stay with a foster family in that state. It was not immediately clear if her situation had changed.

Jackson pleaded not guilty to the New Jersey charges in a March 1 hearing before Superior Court Justice Bradley Ferencz, sitting in New Brunswick. He remained in the Middlesex County Adult Correction Center in North Brunswick with bail set at $2.75 million.

Jackson is a former Marine who worked as a security guard at Robert Wood Johnson University Hospital in New Brunswick. Belizaire worked as a patient monitor there but was not employed there at the time of her death, a friend said after the slaying.

Figure 1. (left) Photograph taken at autopsy of a tattoo found on the lower back of a homicide victim (Courtesy of Shivonne Hutson, Medicolegal Death Investigator, Rockland County Medical Examiner's Office) and (right) corresponding news article (J. Burd, The Journal News, 09/22/10). The suspect eventually pled guilty to the crime.

Locating a tattoo on a body and identifying its physical characteristics such as design and color serves as a rapid means of making a tentative identification and often provides enough investigatory information to guide the initial stages of a police investigation. In the case noted above, tentative identification was made by showing a photograph of the tattoo to the public in an effort to have someone recognize the tattoo, and thus the individual (which often follows with

the identification of possible suspects). This method is faster than fingerprint recovery followed by comparison and subsequent identification, dental recovery with comparison and subsequent identification, and DNA analysis. Furthermore, dentition and fingerprints may not be available, as in cases of decomposition, mummification, charring or dismemberment. When fingerprints, dentition and DNA are available, investigators are limited to the availability of standards for comparison, such as a fingerprint card on file with an employer or in an arrest record, dental records or a DNA profile on file (In addition, the investigators must have some idea of the identity of the decedent in order to begin the acquisition of medical records and related documents). In other words, even after finding a fingerprint or DNA sample of good enough quality for further comparison and identification, there may not be a 'hit' if fingerprint or DNA profile was never entered into a database. Generally, databases exist for fingerprints and DNA profiles, but the lack of a universal dental database further limits the ability of dental records to be useful in a tentative identification. In some regions of the world, lack of comprehensive medical records and databases prevents the use of such identification methods altogether. An example of this is demonstrated by Ambade *et. al.*, "Identification is one of the main concerns of investigating agencies (with regard to) decomposed or skeletonised bodies…Dental comparison is not practicable in India and hence not done…In India, police usually established the identity of a dead body, with the help of relatives and acquaintances. The clothes of the deceased and belongings help in the identity of the decomposed bodies along with *tattoos, scar and other peculiar features*" [emphasis in original] (2011, pp. 105).

Cops identify body of woman…

(J. Kemp, NY Daily News, published June 22, 2011)

"The remains of a Bronx woman found dead and set on fire in a Hudson Valley state park were identified…by a tattoo…"

Body of missing Bronx mom…found in woods; husband expected to turn himself in

(B. Kappstatter, *et. al.*, NY Daily News, published March 16, 2011)

"The body of a missing Bronx mother of four…was found in a patch of woods in Westchester County on Wednesday night by teens riding four wheelers…Investigators identified the body of Tina Adovasio through photographs and a tattoo after she was discovered off the Taconic Parkway in Yorktown Heights, the sources said…"

The girl with the peach tattoo

(J. Gallucci, Long Island's Unidentified Murder Victims, L.I. Press, July 1, 2010)

"Her handless, headless, legless torso was found in Hempstead Lake State Park during the summer of 1997. She was wrapped in a black plastic garbage bag and stuffed into a dark-green Rubbermaid container with a floral pillow sham and frayed red towel. The only identifying mark on her body: a bitten heart-shaped peach tattoo on her left breast with two drops underneath…"

The girl with the angel tattoo

(J. Gallucci, Long Island's Unidentified Murder Victims, L.I. Press, July 1, 2010)

"In 2003, Jessica Taylor's dismembered body was found in Manorville in the Pine Barrens. Her Hands and head have never been found. She is one of four bodies found in the area in a three-year period. She is the only one who has been identified. Her angel tattoo was partially gouged out by her killer in an attempt to conceal her identity…"

Figure 2. Several media reports demonstrating the reliance of tattoos to help aid in identification of human remains.

Due to the deep penetration of the tattoo needles, along with the embedding, encapsulation and storage of the tattoo ink within the cellular material of the deeper layers of skin tissue, tattoos are likely to be preserved in instances of charring, mummification and decomposition. Retention and preservation of the inks and their pattern of distribution (design) within the tissue allows for visualization even when superficial layers of tissue have been burnt, desiccated or subject to various environmental and chemical factors. This identification of tattoos for investigatory purposes is also useful in searching for missing and kidnapped individuals or for the rapid identification individuals that may be involved in a structural or vehicular fire, or some other non-criminally motivated death.

Finally, tattoo equipment may be used to facilitate a criminal act. In particular, a tattoo machine and its needles may be used to generate puncture marks in the stabbing of skin or fabric. The use of a tattoo machine to assault or murder an individual is possible, as is the use of a tattoo machine to cut out a section of fabric from a garment. In a New York City case, a man claimed to have been sexually assaulted by a police officer, who used his retractable baton to perforate his underwear and penetrate his rectum. At trial, the shape of the damage to the boxer shorts of the individual became key forensic evidence in determining how the hole in the boxers could have been made and what could have made such damage (Figure 3). Additionally, microscopic examination of the damaged fibers at the periphery of the hole was shown to be useful in establishing the presence of ink. Once isolated, components consistent with ink were identified by spectroscopic analysis and subsequent comparison to a chemical database.

Experts for Defense in Police Brutality Case Say Evidence Is Not Consistent With Claims

By KAREEM FAHIM

Defense witnesses testifying in a police brutality trial said Tuesday that neither the hole in Michael Mineo's boxer shorts nor his injuries were consistent with his claim of being sodomized by a police officer's baton.

Such a baton would have cut an L-shaped hole, not a square one in the shorts, and Mr. Mineo would have suffered bruises or broken bones, forensic and medical experts testified.

"I don't believe it happened," Dr. Frank T. Sconzo said in State Supreme Court in Brooklyn.

In their continuing efforts to portray Mr. Mineo as a liar, defense lawyers called witnesses on Tuesday who scrutinized some of the evidence in the case — in particular, the victim's medical records as well as the torn boxer shorts.

Officer Richard Kern is accused of repeatedly ramming his retractable baton between the buttocks of Mr. Mineo, a 25-year-old body piercer who was smoking marijuana outside the Prospect Park subway station on Oct. 15, 2008; Officers Alex Cruz and Andrew Morales are charged with helping to cover up the attack.

The lead prosecutor, Charles Guria, parried a series of strong attacks by defense lawyers throughout the day, making it hard for either side to gain much momentum.

In the end, the day's proceedings may have set the stage for a bigger event: testimony by one or more of the officers the next time court convenes, on Thursday, although lawyers for the officers said they had not yet decided whether their clients would take the stand.

Dr. Sconzo, a colorectal expert who was the first witness of the day, dismissed the idea that Mr. Mineo's initial injuries, or an ensuing infection, stemmed from trauma. He noted that Mr. Mineo's blood, taken at Brookdale University Hospital and Medical Center shortly after the episode in the subway station, suggested he had an "ongoing infection," that had most likely developed at least 48 hours before he went to the hospital.

An abscess that Mr. Mineo developed later "was not caused by anything from the anus or the rectum," Dr. Sconzo said, noting that a culture of fluids drained from the abscess was "not consistent with the colon or rectal area."

A graphic photo of Mr. Mineo's buttocks, first shown to the jury on Tuesday, did little to clear up several mysteries. While Dr. Sconzo noted that the photograph seemed to show evidence of an anal fissure — a crack or tear — he conceded that other areas where Mr. Mineo might have been injured were obscured by shadows or hair.

The defense lawyers also renewed their focus on Mr. Mineo's boxer shorts, which he has said were pierced by the baton.

Thomas A. Kubic, who teaches forensic science at John Jay College of Criminal Justice, declared that the baton "could not have made that square hole in the boxer shorts." And he testified that a black spot on the edge of the hole showed traces of organic compounds that can be found in tattoo ink.

(On several occasions, defense lawyers have suggested that Mr. Mineo, who worked in a tattoo parlor, cut the hole in his boxers himself.)

Trial testimony focuses on blood tests, medical records and a pair of boxer shorts.

When asked by Mr. Guria, the prosecutor, whether any of the compounds could also be found in everyday items, like skin lotions, hair products and perfume, Professor Kubic said that it could.

Mr. Guria also asked whether Professor Kubic had tested the baton, to see whether "carbon black" that he had found on the boxer shorts could have come from its rubbery handle.

"No, counselor," he answered. He also acknowledged: "I know very little about tattooing."

Defense lawyers have tried t
show that Mr. Mineo has, ove
time, given conflicting account
of what happened in the subwa
station. On Tuesday, they tried t
zero in on his claim that medica
tion may have made him forg
when police investigators inter
viewed him in the hospital.

An internal affairs investigator
Sgt. David Gomes, testified tha
Mr. Mineo was "very coherent"
and "very lucid" during their
conversation at Brookdale. Mr
Mineo pulled off his underwear
showing investigators the hole
Sergeant Gomes said.

But under questioning by Mr.
Guria, Sergeant Gomes added
that Mr. Mineo was also "agitat-
ed," and "animated in his
speech."

"He stated that there may be
video in the subway station," Ser-
geant Gomes recalled. But, in
fact, there was none.

Figure 3. (top) Photograph of victim (Mineo) testifying in court, holding clothing evidence with damage and (bottom) corresponding news article (K. Fahim, The New York Times, 12/10/10). Note: The circled portion reads, "On several occasions, defense lawyers have suggested that Mr. Mineo, who worked in a tattoo parlor, cut the hole in the boxers himself."

The current lack of comprehensive chemical classification methods of tattoo inks in addition to the lack of tattoo ink-specific spectroscopic databases serves as one impetus for the research in this project. The characterization of tattoo inks visually, microscopically and spectroscopically and the subsequent development of tattoo ink databases and analytical procedures will make it possible for forensic practitioners to recover, identify and analyze tattoo ink from a wound, a garment or any other substrate involved in a forensic investigation. This

research will also explore useful methods for detecting tattoo inks (and pigments) in tissue samples.

In art conservation and art history, the examination and analysis of tattoos found in ancient mummified remains has served to better understand the practices of different cultures over the course of time. From a cultural anthropology perspective, by examining the physical and chemical characteristics of tattoos on an individual or a group of related individuals, it is possible to understand religious beliefs, medical and therapeutic practices, travels and conquests, hierarchal ranking and social classes as well as daily life practices. The identification and collection of a tattoo ink database will serve to aid in art conservation in future endeavors to identify mummies and remains that correspond to periods where organic colored pigments were the main source of tattoo inks, which is the current trend in tattooing today.

The examination and analysis of tattoo inks can also serve other fields, such as medicine, where the interest lies in the human tissue allergic reaction to the chemical constituents of tattoo inks and, more recently, the ideal conditions for tattoo removal via laser methods.

Chapter 2: Historical Perspectives & Review of the Literature

Tattoos and Forensic Applications

The presence of a tattoo on a decedent has long served as an identifying characteristic in forensic medicine and pathology. If an individual is not able to be identified by facial recognition, death investigators may use confirmation of a tattoo to serve as a tentative means of identification, as it is faster than fingerprint, dental, x-ray and genetic methods of identification. The tentative identification serves as a tool that can be used to guide a death investigation. Tattoos can be characterized based on physical characteristics, such as design and color, as well as the location on the decedent's body. During a death investigation and subsequent autopsy, the tattoos are often described with regard to their physical characteristics and locations and documented photographically. These techniques of describing and photographically documenting tattoos are also done on living persons, typically criminals in a police precinct, jail or prison setting.

The human skin is described as having two major layers, the collagen-containing dermis, or inner layer, which is between 1mm and 4mm thick and the keratin-rich epidermis, or outer layer, which is typically ~40µm thick, but thicker in areas like the palms of the hands and soles of the feet (Caspers, 2003, pp. 572). The stratum corneum is the cornified layer of dead, flattened cells found at the skin's outermost surface of the epidermis with a thickness of 10-15 µm on most areas of the body (*ibid.*). Tattoo pigment particles are embedded within the dermal layer of the human skin (Figure 4).

The use of reflected infrared photography to resolve tattoos in cadavers that are barely discernable is common and has been reported in forensic and applied photographic literature. Due to the longer wavelength of infrared radiation, infrared light penetrates deeper into the skin

than visible and ultraviolet radiation. Photography coupled with the use of filters and forensic alternate light sources has been used for quite some time in forensic work to successfully document latent, superficial bruising of the epidermal and upper dermal layers of human skin with ultraviolet radiation (shorter wavelengths, less penetration) and deeper-set tattoos with infrared radiation (longer wavelengths, deeper penetration). Schematics of relative penetration depths of incident radiation into skin are provided in Figure 4. De Donno *et.al.* (2008) report the success of infrared photography in resolving tattoos in tissues exposed to various conditions. They report three cases in which they resolved tattoos from a body immersed in water for 20-25 days, charred remains and a mummified, partially skeletonized body. In all instances, infrared photography of the cadavers and subsequent resolution of their tattoos through this technique led to identification of each of the individuals. McKechnie *et.al.* (2008) were able to photograph and detect tattoos that had been removed by laser tattoo removal procedures using reflected infrared photography, demonstrating that it is possible to detect tattoos that have been 'erased' by laser surgery. According to Wright and Golden (2010), the shorter wavelengths of light interact with the surface of the skin while the longer wavelengths of light (700-900nm) can penetrate the skin up to 3mm (pp. 60).

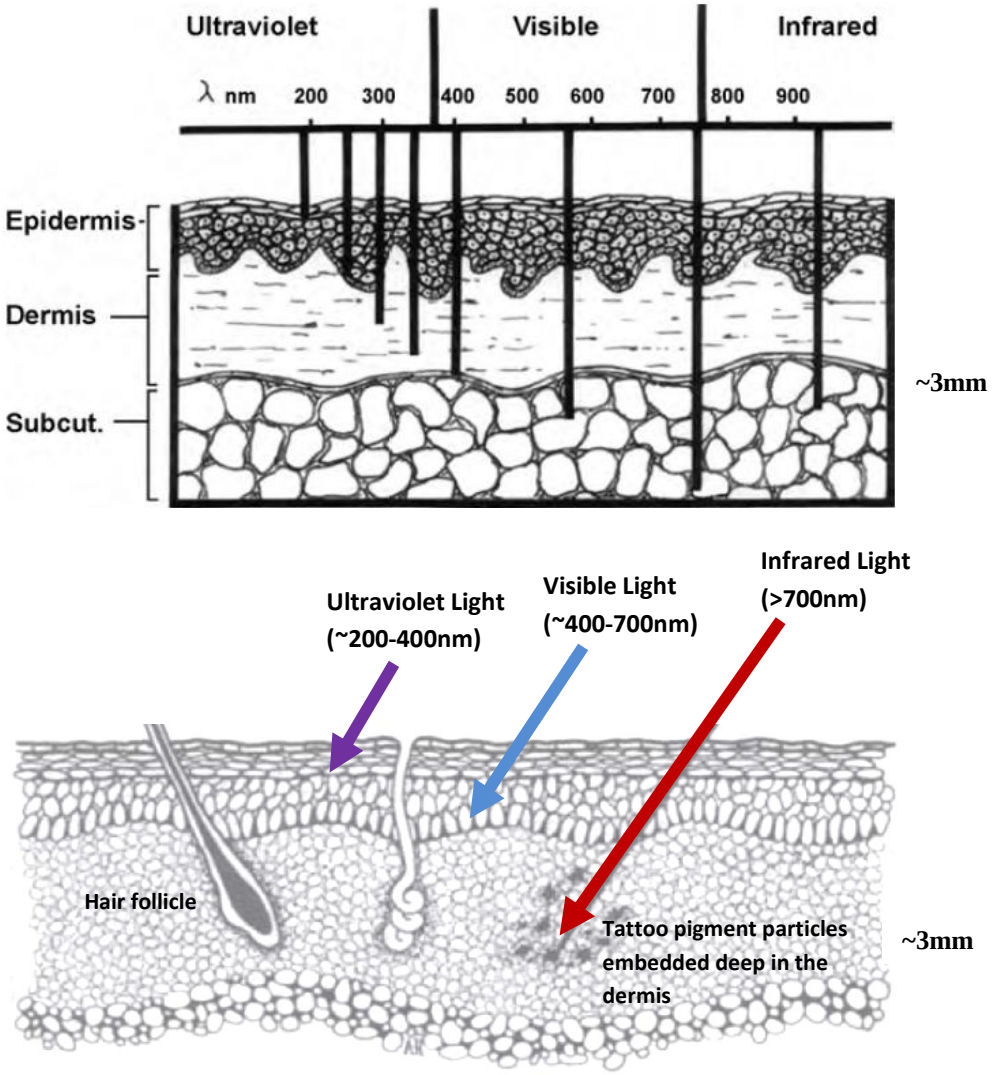

Figure 4. (top and bottom) Cross-section of skin, demonstrating the relative penetration depth of different wavelengths (Top image adapted from Wright and Golden, 2010; bottom image adapted from Morgan, 1974).

Tattoos may also be visualized with the assistance of an alternate light source (ALS). This technique has been reported by Bennett and Rockhold, specifically the use of a 450nm bandpass filter to produce fluorescence and an amber colored barrier filter to pass the emission as well as absorbance characteristics of inks to resolve the tattoo (1999). The authors studied tattoos in human cadavers as the tissue went through the various stages of decomposition and

they documented the visible characteristics of the tattooed area as these degenerative changes were taking place. The following table summarizes their observations:

Stage of Decomposition (proposed by Reed)	**Marked Changes to Tissue**	**Appearance of tattoo**
1 ("Fresh")	None Reported	No Change
2 ("Bloating")	Slight darkening of skin	
	Sloughage of epidermal layer followed by Formation of waxy layer	Enhanced tattoo visibility (brighter colors, defined lines) Decreased tattoo visibility
3 ("Decay")	Increase in skin discoloration	Decreased tattoo visibility
	Dehydration (Leathering)	Leathery appearance, muted colors
	Increasing discoloration	Decreased tattoo visibility
4 ("Dry")	Further decomposition	Continued obliteration of the tattoo design

Table 1. Resultant observations of tattoos through the stages of decomposition (Adapted from Bennett and Rockhold, 1999).

The authors add that in several instances, recognition during stage 4 of decomposition was only possible due to prior knowledge of tattoo location (*ibid.*)

Another method that has been reported as being useful for the visualization of tattoos is the use of hydrogen peroxide (H_2O_2). Haglund and Sperry reported that rubbing 3% H_2O_2 on tissue would resolve tattoos otherwise obscured by the stages of decomposition that result during the postmortem interval (PMI). According to the authors, "during decomposition… accumulated hydrogen sulfide (produced by bacteria) reacts with hemoglobin to produce sulfmethemoglobin and iron sulfide, which creates colors that vary from… dirty crimson or light green to dark green, brown or black" (1993, pp.147). The ferric iron is available to bind with many of the products of decomposition leading to the color production of greens, browns and blacks. The stages of

decomposition produce a variety of colors; for example, when the hemoglobin loses oxygen, deoxyhemoglobin forms resulting in a purple color. Bilirubin, a bile pigment produced by the breakdown of hemoglobin, and its byproducts produce shades of reds, and greens. All of these colors, along with other factors that occur during the PMI can obscure tattoos or contribute to the breakdown of the pigments in the skin. Haglund and Sperry hypothesize that the peroxide reduces the bonds within the chemical structures of the decomposition products causing the colors to fade and thus render the tattoo pigments visible against a light background. The sequence of decomposition products and corresponding color changes is described in the Figure 5.

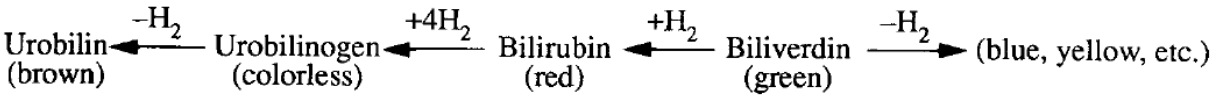

Figure 5. Bile pigments produced by oxidation and reduction reactions of biliverdin, the initial product of hemoglobin breakdown (Adapted from Gill-King in Haglund and Sorg, eds., 1996). These pigments are present in the later stages of decomposition and may mask tattoos.

Light scattering is the basis for skin color, which is based on the presence of melanins, the natural pigments in human skin which can be found in the epidermal layers of the skin. It is this concept of light interacting with skin that enables us to perceive a variety of skin colors and tattoos placed into the layers of skin. Considering that the purpose of the tattoo is to be 'viewable', the tattoo ink would have to be located at a depth such that visible radiation can penetrate and traverse the skin and reflect back in order for the viewer to perceive the colors of the design. By interacting with visible radiation, the pigments that make up the tattoo are able to be detected by the human eye.

Tattoo Inks and Pigments

Over the course of time, a variety of chemical substances have been used to impart color in and onto different substrates. As these chemical substances have changed, so has their use in art, architecture and automobiles. This change in chemical composition has also affected the changing chemistry of tattoo inks. The most basic definition of tattoo is to mark the skin with pigments. The pigments used in tattooing vary greatly and have changed throughout history. Generally, tattoo inks have transitioned from carbonaceous materials and natural organic and inorganic pigments originating from vegetable and mineral sources to synthetic organic pigments and colorants. The inorganic pigments are generally classified based on the various metallic elements of which they are composed while organic pigments can be classified in different manners, according to such characteristics as carbon content, functional groups, molecular structure and synthesis methods.

Modern tattoo types include amateur tattoos (also called street tattoos or prison tattoos), which are usually homemade inks that are tattooed by a non-professional. These tattoos are often described as lacking in artistic detail and usually monochromatic, uneven in color distribution and not deep within the layers of the skin. A wide variety of materials may be used to make the ink and the tattooing implements commonly used in amateur tattooing. In contrast, professional tattoos are generated using higher quality inks and pigments and are done with either a tattoo gun (modern) or using tattooing implements according to cultural traditions. Two additional tattoo types are medical tattoos and cosmetic tattoos, the latter used for permanent makeup, tattoo cover ups, and instances of plastic and reconstructive efforts. Medical and cosmetic tattoo inks are usually neutral and represent skin tones, typically ranging in shades of whites, beiges, pinks, browns and blacks. In instances of permanent makeup, cosmetic tattoo

colors include a wider range of options in order to be used for lip liner, lipstick, eyeliner and blush. A fifth type of tattoo is described as traumatic tattoos, pigmentation under the skin which generally results from the embedding of dirt and rocks, gunpowder, fireworks and explosives, or other debris beneath the skin. These types of tattooing are not typically characterized by the introduction and retention of colored pigments into the skin, and will not be discussed further in this document.

Commercial tattoo inks can vary in color and luminescence in addition to chemical composition. Non-permanent tattoo ink includes materials such as henna, while permanent tattoo ink includes pigments common to the visible spectrum, fluorescent and blacklight-active inks, and magnetite (Fe_3O_4). Due to the increasing tattoo removal market, there is also an ink that, while permanent, is designed to break down more efficiently when cosmetic laser removal is conducted (*i.e.* InfinitInk™).

The technique of tattooing has been traced back thousands of years, and conservators have made an effort to study and evaluate the methods and materials that were used in tattooing practices by studying recovered mummified remains. In addition, anthropologists and historians have documented the practices of various cultures in order to understand the meaning and mechanisms of tattooing over time. Ancient tattoos have been described as being carbonaceous in nature, describing carbon black as being developed from burnt bones, tar, pitch, and soot. Research and publications referencing tattooing have identified compositions and components such as India ink, China ink, lamp black, bone black and pine soot. In order to introduce color to ancient tattooing practices, pigments were extracted from mineral and plant sources (such as trees, flowering plants and roots). Interestingly, the resultant quality of the tattoos and their

ability to last and not fade over time is what likely drove the evolution of pigments used in tattooing practices.

It is reported in the literature that a French forensic scientist, Jean Mathurin Felix Hutin, described the process of tattooing based on a study conducted in the early 1850s. In his account of Hutin's resultant research, Dye writes, "Colored materials, apparently nearly always Indian or Chinese ink (lampblack mixed with animal glue, sold in solid rolls or cakes), laundry bluing, or vermilion (artificial cinnabar, *i.e.* alpha mercuric sulfide, ground with white wine and then mixed with white of egg), were prepared with a little water or saliva in small cups or shells" (1989, pp. 530). Laundry bluing is a process of adding a blue dye to laundry in order to counteract the yellowing of fabrics and make the fabric appear whiter. Laundry bluing is akin to adding fluorescent optical brighteners or bleach to laundry, both of which are commonly done today. Based on the time of Hutin's research, the materials that could have been used for laundry bluing (and thus tattooing) include ultramarine (in its natural form) and smalt ($K_2CoSi_4O_{10}$). Ultramarine is referred to as lapis lazuli and its principle blue mineral component, lazurite, while synthetic ultramarine is described as a three dimensional aluminosilicate lattice with sodalite structure containing entrapped sodium ions and ionic sulfur groups; $Na_7Al_6Si_6O_{24}S_3$ (The Pigment Compendium). The work of Hutin was also cited by Dr. Johann Ludwig Casper, who also studied tattoos in his capacity as a forensic pathologist. Dr. Casper lists "cinnabar or gunpowder…Indian ink, charcoal, ink or Prussian (washing) blue[1]" as being the coloring-matter rubbed into patterned wounds to create tattoos in his Handbook of Forensic Medicine (1861, pp.105). Dr. Casper adds that Hutin mentioned the same coloring-matters, with "cinnabar being the general favourite" (*ibid.*).

[1] Iron (III) hexacyanoferrate (II)

Gross describes the importance of tattooing in criminal investigations and discusses instances in which tattoos may fade and even disappear based upon the inks used. He refers to the common tattooing materials of the time, including cinnabar, gunpowder, washing-blue, ink and chalk mixed with lampblack. With regard to microscopic examination of tissue sections of the lymph glands from a decedent, Gross adds, "…(the small colouring particles) can naturally be better seen through the microscope, but the cinnabar so often employed as colouring matter looks reddish when rays of light fall upon the gland and has a black aspect when they traverse it" (1924, pp. 113).

Discovered in 1991, Ötzi, the Tyrolean Iceman, was determined to be the oldest complete mummified body being approximately 5,200-5,300 years old. Upon examination of Ötzi, tattoos were found at different areas of his body. Pabst, *et. al.* prepared unstained histological sections of the tattooed skin and examined the prepared sections using optical microscopy, bright field transmission electron microscopy, energy dispersive x-ray spectroscopy, electron energy loss spectrometry, energy filtering transmission electron microscopy and electron diffraction in an effort to study the tattoos and their chemical and structural compositions. The authors identified black colored particles that consisted mainly of carbon; more specifically, they identified double bonded carbon atoms that are typically found in soot (2009, pp. 2336). They also identified ash particles that consisted of carbon, oxygen, nitrogen and calcium (*ibid.*). In their conclusions, Pabst, *et. al.* note that quartz and 'probable almandine[2]' crystals they identified between the soot particles in the tattooed regions of the skin may have come from stones in a fireplace from which the soot was taken (2009, pp. 2336).

[2] $Fe^{+2}{}_3Al_2Si_3O_{12}$

Most of the historical literature pertaining to tattoos has focused on the tattooing methods and rituals, designs and semiotics, and the significance within a region or amongst a group of individuals. The specific details of tattoo ink composition and the ink-making process is often markedly absent or limited within the literature. A review of historical literature has resulted in the following timeline, which provides a suitable means to trace the composition and methodology of early tattoo inks within various cultures:

1888- Buckland indicates that while various colors were employed, indigo blue was the chief pigment utilized (pp. 322). She adds that the blue dye used by Maories was made from the soot obtained by burning the heart of certain trees. Buckland also mentions lamp black as a source of indelible markings and reports that different cultures would have tattoo marks of various colors, some using reds and blacks, others using blues, and some cultures containing marks that were "highly colored".

1901- Roth provides different accounts of materials used to produce the pigments in tattoos, including charcoal from various sources, gunpowder and the soot of wood. In one account, "The pigment was a mixture of lampblack and either milk or fat. A dog starved for the purpose was fed upon this. His excreta were remixed and buried in (pumice stone) boxes until wanted" (pp. 43).

1909- Geare provides information regarding tattooing practices of different cultures, reporting burned candle-nut (*Aleurites triloba*) and coconut ashes (pp. 790), burned leaves from a plant called 'ti' moistened with the juice of the 'poporo' berry (pp. 794), burnt resin (pp. 795), vermilion (pp. 797), cinnabar and India ink (pp. 798), and burnt bark from the birch (pp. 798).

1928- It was reported that the pigment was made from “the soot of seal oil lamps which is taken from the bottom of tea kettles or similar containers used to boil meat and other food over an open flame. The soot is mixed with urine, often that of an older woman…” (Smith and Zimmerman, 1975, pp. 435).

1932- Clark describes an ink from the lamp black of sesame oil or kerosene with water added and continues that red ochre may be used in some instances (1932, pp. 67).

1937- After spending time studying tattooing in Iraq, Smeaton describes kohl, in which the chief ingredient is carbon in the form of lamp black, and indicates that other additives include indigo, bile from the gall bladder of an ox, fat, milk, water or kerosene (1937, pp. 59).

1947- Matthews describes the use of tree-gum soot as the tattooing medium and details the use of dyes, “These must be relatively insoluble, stable to light and unaffected by tissue reaction…I have used ochres (oxides of iron)…in shades of brown and red…I have also used cadmium selenides…in nine shades ranging from tangerine, through yellow and pink to brick red. I have not used mercuric sulphide (cinnabar)…although it has been recommended by tattooists for cosmetic purposes…” The dyes are then mixed with absolute ethanol to form a paste suitable for tattooing. He further adds, “… (early literature recommends) to obtain the requisite shade by mixing the dyes with a white base,” such as zinc oxide and barium sulphate (1947, pp. 19).

1958- Lake reports his experiences using different colors to administer tattoos for surgical and cosmetic purposes. He reports achieving a true black by mixing carbon with the dye golden umber, using red oxide R. 93A (iron oxide) and irgalite orange P to achieve long-lasting red hues, and he reports using iron oxide and golden umber for brown hues (1958, pp. 1085).

Additional literature cites ink made of gunpowder (black powder) and ox-gall. The liquid suspension varied from saliva to urine to various types of alcohols.

According to Lynnerup, most tattoos were made with a puncture/dot method, whereby a pricking pin containing the pigment is introduced into the skin depositing the pigment into the dermis of the skin. He also notes that facial tattoos in mummies were made by the technique of sewing, which produced long lines that went across the facial region. This method was done by drawing a soot blackened strong string through the skin, which deposited the pigment into the dermis (2007, pp. 178). These techniques of using a sharpened object to either puncture or sew the ink in are still employed in amateur tattooing practices. In some instances, a homemade rotary machine representing a rudimentary tattoo gun is used in lieu of a manually operated needle or sharp pointed object. Another method describes rubbing the ink on the skin first, followed by pricking the skin with a sharp object or needle to push the ink into the skin. One historical reference described a method of cutting a design deep into the skin and subsequently rubbing ink or pigment into the cuts such that the pigment would remain in the deep cuts upon healing of the tissue.

Traditional tattoo inks are described as containing pigments that were typically inorganic mineral pigments such as metallic oxides, hydroxides, sulphides and aluminates. The following color trends were observed:

Red: mercury sulphide (HgS, cinnabar) and cadmium selenide (CdSe)

Yellow: cadmium sulphide (CdS)

Green: chromic oxide (Cr_2O_3)

Blue: cobalt (CoO, Co_3O_4)

Indigo/Purple: manganese oxide (MgO)

White: lead carbonate ($PbCO_3$), zinc oxide (ZnO), titanium dioxide (TiO_2, anatase/rutile)
Brown (inc. reds, yellows and blacks): iron oxides (FeO, Fe_2O_3, Fe_3O_4 [magnetite])

With regard to tattoo inks, titanium dioxide white is a general term for various titanium dioxide pigments, specifically the anatase and rutile forms of titanium (IV) oxide. Black colors are generally carbon black and lamp black (80-95% carbon with traces of sulfur and organic material; produced from burning a variety of materials and collecting the resultant sooty residues), graphite (40-90% carbon with mineral ash) or an iron oxide. Lamp black is generally described as being an older pigment than carbon black, being used for thousands of years by ancient cultures such as the Chinese and the Egyptians. 'Carbon-based blacks' is the general class for those black and brown pigments that are composed primarily of carbon. General distinction is made by the manufacturing process, source material or method of preparation. Examples of sources for carbon-based pigments may include minerals, soots and smokes, vegetable materials and animal materials (for example, bone).Variations in color and particle size and degree of crystallinaty, when viewed microscopically, can be used to distinguish the different types of black pigments.

In a 2008 research project by Poon, the tattoo pigments of interest were ancient and traditional pigments typically found in ancient mummified remains. The purpose of his research was to examine the chemical composition of pigments believed to be found in ancient tattoo inks and to design an experimental method for analyzing the pigments in mummified remains *in situ*. This was evaluated using an animal model to simulate mummification of tissues tattooed with ancient pigments as reported in early literature. The pigment standards that were the focus of this study included flame carbon/soot, bone black, vine charcoal, magnetite (Fe_3O_4), lapis lazuli

($(Na,Ca)_8[(Al,Si)_{12}O_{24}](S,SO_4)$; lazurite, the dominant constituent) and indigo (the molecular structure of which is depicted in figure 6).

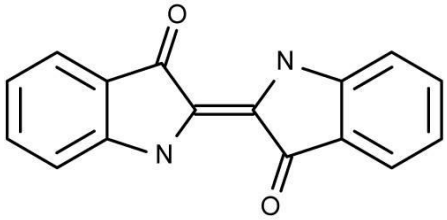

Figure 6. Molecular structure of indigo.

These pigments were evaluated using micro-Raman spectroscopy, scanning electron microscopy/energy dispersive spectroscopy (SEM-EDS), Fourier transform infrared spectroscopy (FT-IR), powder x-ray diffraction (XRD) and laser ablation inductively coupled plasma mass spectrometry (ICP-MS). With respect to the Raman portion, the author used a 632.8nm He/Ne laser at 1.8mW as his only means of excitation. According to Poon, despite the ability of Raman spectroscopy to provide positive identification of carbonaceous materials, the technique failed to discriminate between the particular forms, which made it necessary to use SEM-EDS for determination of morphology and elemental composition.

Modern tattoo inks are composed of pigment particles mixed with a solution to disperse them. The pigment portion is compromised of organic pigments such as azo dyes (reds, oranges, yellows), polycyclic amines, oxazines (magentas, purples, violets), phthalocyanines (greens, blues), quinacridones (reds) and arylides. The solution portion of tattoo inks can be composed of a variety of components, including a vehicle (to facilitate transfer of the pigment particles to the needle and the skin), additives (such as wetting agents, preservatives, stabilizers, thickeners and pH regulators) and solvents. Since there is no regulation of tattoo ink compositions, the variation is extensive and subject to change based upon material availability, manufacturer capabilities,

and fiscal considerations. Modern tattoo inks can also contain mineral pigments such as titanium dioxide (whites, lighteners) or iron oxide (reds, yellows, browns).

Water may function as a vehicle in the liquid portion of the tattoo ink; its function is to keep the pigment evenly distributed in the fluid matrix, carry the pigments from the bottle to the needle of the tattoo gun and into the dermis of the skin. Wetting agents can include glycerine, which affects the viscosity of the ink and acts as a thickener and alcohols such as ethanol or isopropanol, which thin out the ink. Barium sulfate may be added as a stabilizer and preservatives include witch hazel and benzoic acid. According to the packaging labels, the tattoo inks in this study include distilled water (dH_2O), isopropanol [isopropyl alcohol; $CH_3CHOHCH_3$], glycerine [$CH_2OHCHOH\ CH_2OH$], polyethylene glycol [$HOCH_2(CH_2OCH_2)_nCH_2OH$] and witch hazel (dried leaves of *Hamamelis virginiana*; using HPLC, Wang *et. al.* identified hamamelitannin, catechins and gallic acid in the leafy and woody portions of the *H.virginiana* plant, 2003). The molecular structure of hamamelitannin is depicted in figure 7. A review of updated Material Safety Data Sheets (MSDS) for the inks examined in this study demonstrates the presence of propylene glycol [$OHCH_2CHOHCH_3$] as an ingredient also.

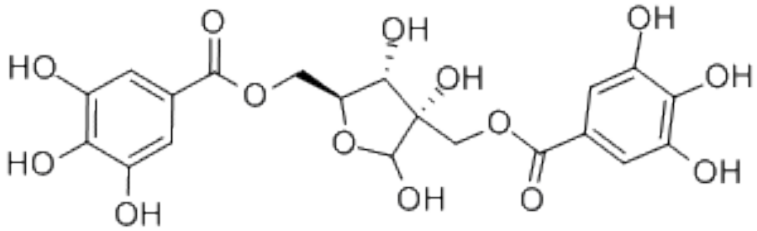

Figure 7. Molecular structure of hamamelitannin

With regard to most modern, professional tattoos, the tattooing process is conducted using a tattoo machine. Into the early 1900s, electromagnetic coil tattoo machines were manufactured based on a device initially developed by Thomas A. Edison in the late 1800s. This type of tattoo machine, with some minor modifications since its inception, is commonly used today by tattoo artists. The tattoo process involves dipping the tip of the needle, which is attached to the tattoo machine, into a small cup of ink and then moving the needle over a portion of the skin, depositing the ink into the region of skin being punctured by the needle. The process of dipping the needle into the ink is repeated as the ink is depleted from the needle surface. The types and brands of inks and pigments used by tattoo artists will vary, with some preferring pre mixed, liquid inks of a specific brand and others preferring dry, powder pigments to which they can add liquid carriers to create their own ink. Tattoo artists may also work with a small selection of ink colors, mixing these colors with whites or blacks to create different shades.

Home-made tattoo inks are those inks that are made in both residential and prison settings. Ingredients may include residue from burning an object such as paper, a Styrofoam™ cup, plastic cutlery, a toothbrush, a plastic chess piece or any plastic object that could be melted to generate black sooty material. Also reported was the use of ash from a cigarette. Ink from a writing implement such as a pen or Sharpie marker, shoe polish or shoe soles, or powdered pigment are also used. The solution, or liquid portion of the homemade ink, may be made up of a combination of water, saliva, shampoo, witch hazel, vodka, Listerine® mouthwash which, according to the MSDS sheet contains ethanol, eucalyptol, thymol, menthol, methyl salicylate, benzoic acid, sodium hydroxide, hydrochloric acid and water. Glycerin, propylene glycol(s), rubbing alcohol and nail polish remover (acetone) are also commonly employed in home-made

tattoo inks. The inks are typically introduced into the skin by crude methods such as glass, pins, razor blades, paper clips, staples, metal coils or light bulb filaments. The basic process is to burn the plastic/paper-based material and collect the smoke in or on a material held above it (such as a bottle cap or foil). The resultant sooty residue is collected and mixed with the suspending liquid (soap, water, alcohol, *etc*.) and then applied into the skin using the injection tool.

Sperry provides a detailed account of the tattooing process with regard to ink deposition and retention into the tissue (1992, pp. 7). The needle penetrates through the epidermis and just into the papillary and reticular dermis, but no deeper. He reports this depth to be between 1-2mm. Sperry notes that during the tattoo process, the pigment will be deposited along the length of the needle track throughout the epidermis and any superficial dermal layers, but only the pigment left within the dermis will permanently remain, making up the final tattoo (Figure 8).

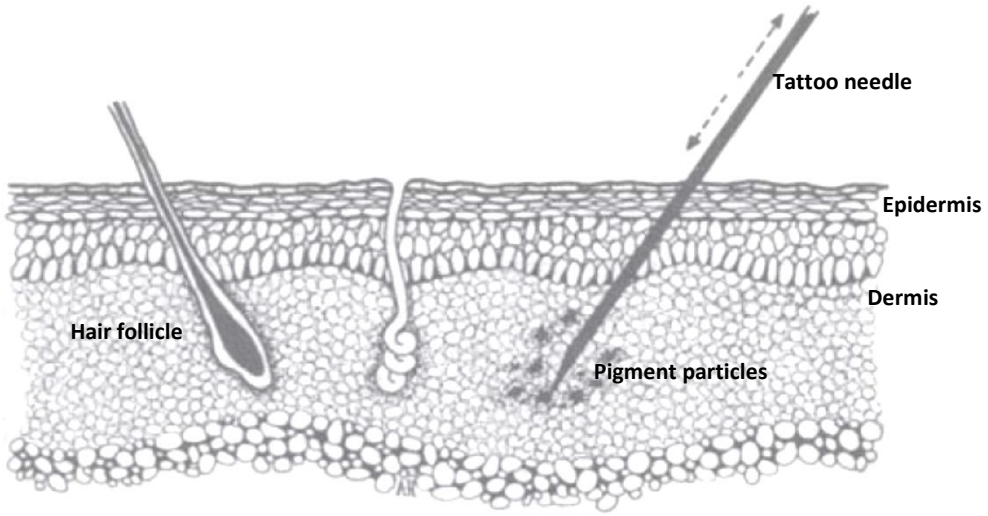

Figure 8. Cross-section of skin demonstrating the penetration of the tattoo needle and subsequent deposition of pigments into the dermis of the skin (Adapted from Morgan, 1974).

As the tissue heals, the superficial epidermal layers are peeled away leaving behind the deeper, regenerative basal epidermal layers. Eventually, sloughing off of cellular layers during

healing removes all of the pigmented layers of the epidermis with the exception of the dermis. Eventually, the epidermis regenerates and the epidermal layers grow back to their usual thickness over the pigmented dermal layer (1992, pp. 9). Over time, the body will react to the foreign pigment particles that have been introduced; "…the pigment particles are assimilated by dermal macrophages, which slowly carry them into the regional lymphatics and thus to the corresponding draining lymph nodes. The macrophages also engulf pigment granules and then migrate short distances within the dermis…" in which the majority of pigments will be assimilated by the macrophages, with unassimilated pigment granules remaining within dermal loose fibrous connective tissue between collagen bundles (*ibid.*). The effects of healing exhibited by the diffusion of light by the reformed epidermal layers and subsequent pigment migration result in a tattoo that appears smooth, diffuse, and hazy. An individual examining a tattoo that has healed and aged will often describe the tattoo as appearing faded.

Repeated exposure to ultraviolet light may affect the pigmentation of the tattoo, further degrading the overall tattoo pattern and the pigments themselves. Research concerning the photodecomposition of tattoo pigments in human tissue has become prevalent in medical forums, with dermatological complications being reported as a result of production of pigment breakdown by-products and their redistribution in tissue subsequent to ultraviolet or visible laser light exposure (Figure 9). References to such studies of the formation of pigment breakdown by-products include literature by Cui, *et.al.* (2004), Vasold, *et.al.* (2004), Engel, *et.al.* (2007) and Pfirrmann, *et.al.* (2007). Pfirrmann, *et.al.* provide a summary of the suitability of different lasers for breaking down the different tattoo colors (2007, pp. 892). In their paper, the authors demonstrate the usefulness of understanding pigment composition, morphology and histopathology in tattooing, particularly when removal is considered.

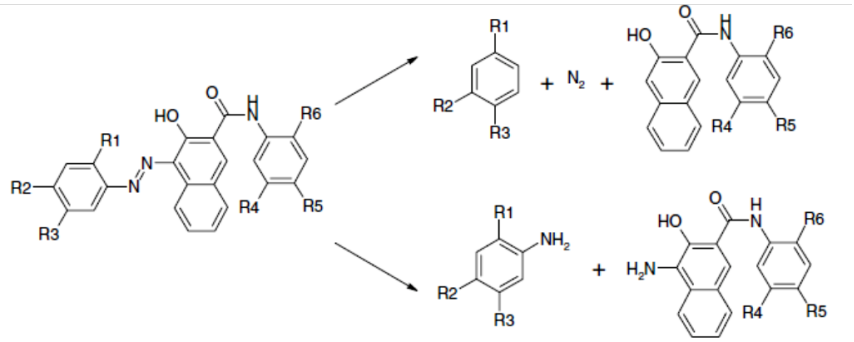

R1	R2	R3	R4	R5	R6	Pigment
Cl	H	Cl	H	H	OCH_3	P.R. 9 (I8)
CH_3	H	NO_2	H	H	H	P.R. 22 (Cardinal Red)

Figure 9. Decomposition products of red pigments as a result of solar or laser light exposure (as reported by Vasold, *et. al.*, 2004, pp. 186).

Raman Spectroscopy: Theory and Practice

When radiation interacts with matter, several processes can occur, including the absorption, emission, scattering, reflection and refraction of the incident radiation. The scattering of electromagnetic radiation forms the basis for Raman spectroscopy. The Raman effect is the scattering phenomenon that involves a net energy change between the scattered and incident beams of radiation. In contrast, a scattering process that involves no change in the energy of the scattered beam relative to the incident beam is defined as Rayleigh scattering. Elastic scattering occurs when the scattered radiation is the same frequency as the incident radiation (Rayleigh) and inelastic scattering occurs when the scattered radiation is of a different frequency (Raman). Raman scattering is caused by rotational and vibrational transitions in molecules, thereby allowing for structural determination of molecular species.

The Raman effect was observed by C.V. Raman in 1928 with the assistance of K.S. Krishnan. According to the literature, the phenomenon of inelastic light scattering was predicted five years earlier by A. Smekal (Haynes, *et.al*, 2005, pp. 339A) and "figured into the theory of dispersion due to Kramers and Heisenberg and in the papers of Schrödinger." (Raman and Krishnan, 1928, pp. 24). Raman found that a small fraction of scattered radiation will differ in wavelength from that of the incident beam and that shifts in frequency depend upon the chemical structure of the molecules causing the scattering. Raman and Krishnan note that the incident quantum radiation is either scattered as a whole or absorbed in part by the molecules in the medium, where the part absorbed shifts the molecule to an energy level different from its initial state. According to the Raman theory, if an oscillating electric field is incident upon a sample, this field will interact with polarizable electron clouds of the sample molecules. A molecule can undergo a change in polarizability during one of its normal modes of vibration, and polarizability

is a measure of how efficiently a given incident frequency induces a dipole in a polyatomic molecule. The Raman effect results from the effect of the polarizability with the normal modes of vibration of the molecules. A molecule's polarizability will vary based upon bond distances and inter-nuclear separations of a molecule. A normal mode that involves a change in polarizability is described as a Raman active mode, whereas a normal mode that results in no change in polarizability is referred to as a Raman inactive mode.

In Raman spectroscopy, a dipole moment is induced by an external electric field of light. When a molecule is placed in such an electric field (ε), the induced dipole moment (μ_i) is given by

$$\mu_i = \varepsilon\alpha$$

where α is the molecule's polarizability. Molecular dipoles are generally on the order of one Debye while α values are generally in units of cubic Ångströms. The magnitude of polarizability will vary with the frequency of the incident electric field and can be described as how easily a molecule's electronic configuration can be distorted by this field. If monochromatic light of frequency (ν_0) is incident upon a molecule, then light frequency of ν_0 and $\nu_0 \pm \nu$ is subsequently emitted from the molecule. In general, Raman scattering occurs when $\alpha \neq 0$.

From a quantum mechanical viewpoint, the Raman effect involves transitions between energy levels, where molecules in the ground vibrational state can interact with a photon of some energy and reemit a photon of energy at a lower frequency, or molecules in the lowest excited vibrational state can interact with a photon of energy and reemit a photon of energy and the higher frequency. An atomic or molecular system will scatter a photon if the energy of the photon equals the energy difference between two states of the molecular species. If scattering

occurs, the molecular species will occupy a higher energy level known as an excited virtual state. Smith and Dent (2005, pp. 72) describe the virtual state as a 'complex' between the incident radiation and the molecule; when the oscillating dipole interacts with the molecule, the electrons are polarized to a higher energy state. At the instant when the energy is transferred to the molecule, there is a complex that forms between the light energy and the molecule's electrons in which the nuclei do not have time to move appreciably. The authors add that this virtual state 'complex' is unstable and the light is released immediately as scattered radiation. Over time, the excited state will give off energy and the scattering species will return to a lower energy state. With Raman scattering, the amount of energy lost between incident radiation and the resultant emitted photon equals the energy difference between two quantized vibrational energy levels of the molecules causing the scattering. These energy differences are generally characteristic of the molecular species. Note the equation,

$$E = h\nu = h(c/\lambda) = h\acute{\upsilon}$$

in which the energy (E) between the ground state and excited state is directly proportional to the frequency, ν, and inversely proportional to the wavelength, λ, of the absorbed light (where $\acute{\upsilon} = 1/\lambda$ in wavenumbers, cm^{-1}).

The intensity of Raman scattering is defined by the equation

$$I = Kl\alpha^2\omega^4$$

in which the intensity is the product of a series of constants (represented by *K*), the power of the incident laser radiation (*l*), the polarizability of the molecule and the frequency of the incident radiation (ω). This equation is important in demonstrating the contribution of the incident frequency on the overall Raman scattering intensity (ω^4); in that there is signal enhancement to the fourth power.

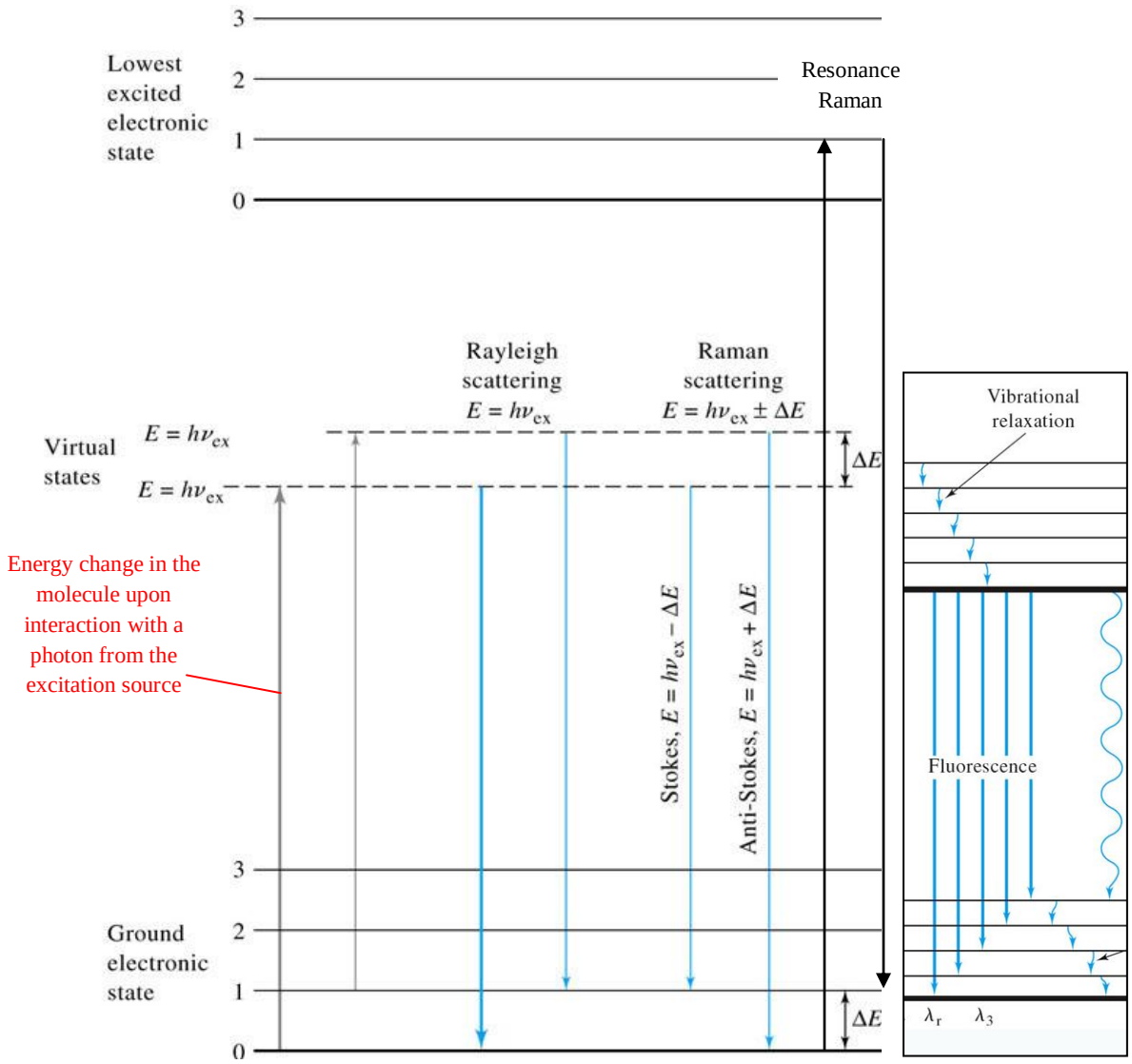

Figure 10. Energy level diagram outlining the scattering processes. The relative widths of the arrows indicate the probabilities of these processes occurring. Not that the numbered horizontal lines represent vibrational levels within the given electronic state (the spacing between them is exaggerated to show detail).In addition, Stokes emission is favored over Anti-Stokes (Adapted from Skoog, Holler and Nieman, 1998). Fluorescence is demonstrated in the inset.

Resonance Raman scattering is a phenomenon in which the Raman band intensities are enhanced when the excitation wavelength is near that of the electronic absorption band of the molecular species of a sample. This enhancement can be a factor of 10^2-10^6, which increases the detection sensitivity by molecules present in a sample at low concentrations. The resonance enhancement effect is observed in those Raman bands associated with functional groups that

contain valence electrons with low excitation energies (chromophores). This is due to the presence of absorbing species containing π (bonding) and n (non bonding) electrons and their transitions to π anti-bonding electron energy levels. According to White, *et. al.*, "provided a molecule has a suitable chromophore and the laser excitation wavelength matches, or is very close to the absorbance maximum of the analyte, then under resonance conditions sensitivity can be increased by up to three to four orders of magnitude over traditional Raman spectroscopy" (1998, pp. 78). Determination of a sample's wavelength absorbance maxima using a UV/Visible spectrophotometer can provide the approximate range of excitation wavelengths that are capable of producing the resonance Raman effect. In resonance Raman, an electron is promoted to an excited electronic state followed by instantaneous (10^{-12} -10^{-14}s) relaxation to a vibrational level within the electronic ground state. In contrast, the relaxation by fluorescence is not instantaneous, but instead involves a relaxation to the lowest vibrational level of the excited electronic state (Figure 10, inset) prior to returning to the ground state. In fluorescence, the molecular species emits a new photon after absorption and subsequently returns to the ground state. The lifetime of the excited state is of the order of 10^{-6}-10^{-8}s in fluorescence. Pre-resonance Raman spectra are those that are obtained when the excitation sources are set to a frequency slightly lower than that which would cause resonance Raman, thereby resulting in a lower degree of enhancement. The mechanisms of light scattering processes are compared in the energy level diagram below (Figure 11).

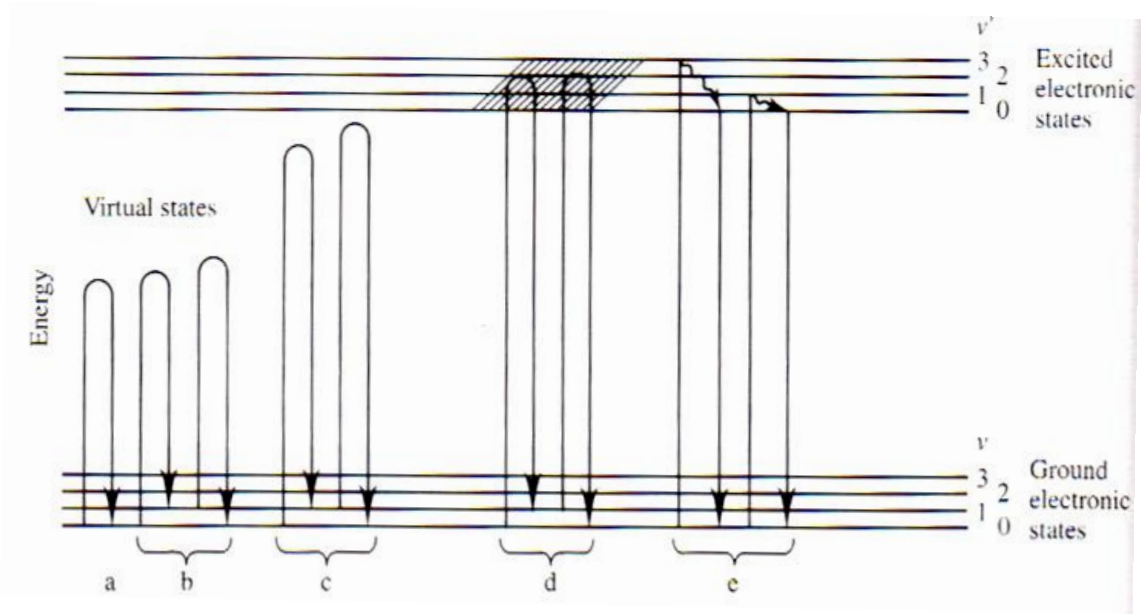

Figure 11. Mechanisms of light scattering processes. (a) Rayleigh, (b) non-resonance Raman (Stokes and Anti Stokes), (c) pre-resonance Raman, (d) resonance Raman and (e) resonance fluorescence (Reproduced with permission from Academic Press).

As with most spectroanalytical instrumentation, current Raman instrumentation contains a source, a sample holder, a wavelength selector or interferometer, a detector and a data processing/readout system. With dispersive Raman systems, the wavelength selector is a grating or series of gratings and with Fourier-Transform Raman systems, a Michelson interferometer is employed. Sources are almost always lasers coupled with filters, which provide bright, monochromatic radiation. A variety of laser sources are available and selection will vary based upon the instrument, the types of samples being analyzed and the needs of the analyst. Figure 12 (top) depicts some of the laser excitation wavelengths available for use with Raman spectrometers. In order to evaluate which monochromatic laser excitation wavelength and corresponding laser power (intensity) to apply to the sample being analyzed, it is necessary to consider fluorescence effects, absorption effects and possible photodecomposition of the sample. Selection of excitation wavelength will also be important when considering desired sample

penetration depth, as this may affect resultant spectra, especially in the cases of thin films or layered samples (Figure 12, bottom).

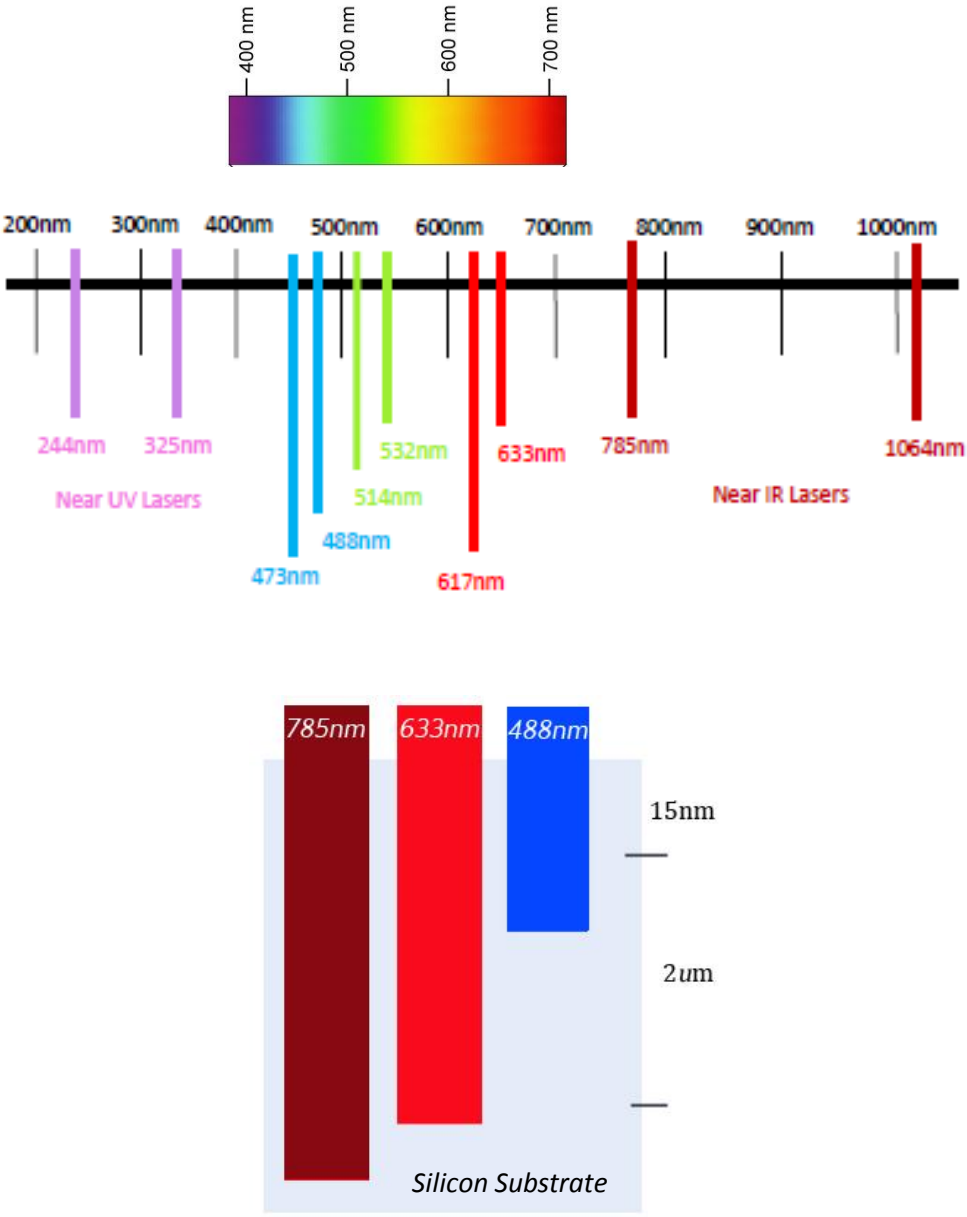

Figure 12. (top)Typical laser sources used in Raman spectroscopy and (bottom) some corresponding depth profiles. When considering the penetration depth of lasers of varying wavelength into Silicon, the depth of penetration will increase when moving from a shorter wavelength to a longer wavelength (Adapted from Horiba Scientific). This trend of penetration depth related to excitation wavelength is important when considering a pigment –containing tissue substrate (such as tattooed skin).

Raman systems may be stand-alone spectrometers or the Raman spectrometer can be coupled with an optical microscope for the analysis of smaller samples or samples composed of micro (10μg) amounts of molecular species. For stand-alone spectrometers, liquid and solid (for example, powder) samples may be placed in a capillary tube, sample cell or alternate sample holder and inserted into the path of the incident beam. For microscopic work, the solid or liquid sample is placed within a sample holder, mounted on a glass or aluminum-coated slide or placed directly on the microscope stage. It is important to note that obtaining Raman spectra is not limited by materials that affect infrared data collection, such as glass sample holders and optical components, aqueous solutions and some solvents. Many sample types require little to no sample preparation for Raman analysis, which is not always the case with classic infrared analysis techniques, with the exception of attenuated total reflection (ATR).

Current Raman instruments are typically of two types, Fourier transform instruments with low band gap semiconductor detectors such as Germanium (Ge) and indium gallium arsenide (InGaAs) or dispersive, multichannel instruments with charge coupled device (CCD) detectors. CCD detectors are not sensitive to the spectral area near the 1064nm Nd/YAG lasers, and as such, 1064nm lasers are typically used with a Germanium detector in Fourier Transform instruments. With dispersive systems, in order to observe the Raman spectrum, it is necessary to separate the collected Raman scattered light into individual wavelengths, which is accomplished with a grating or series of gratings. Since Raman scattering intensity depends on the fourth power of the frequency (referred to as the ω^4 or ν^4 rule), the high frequency lasers found in dispersive systems are ideal with respect to increased sensitivity. Conversely, the longer wavelength/shorter frequency of the 1064nm laser used in FT-Raman instrumentation decreases electron excitation and reduces the chance for fluorescence. Advantages of Fourier transform

instruments include the elimination of many fluorescence interferences and acquisition of the full spectrum which minimizes loss of spectral regions (no need to 'stitch' spectral regions together when switching between gratings in a dispersive system, and no need to switch gratings to change resolution since the moving mirror controls resolution in an FT system). Additionally, there is an increase of signal to noise ratio with concomitant enhanced sensitivity due to the multiple scan capability with signal averaging and the increased energy throughput of the interferometer.

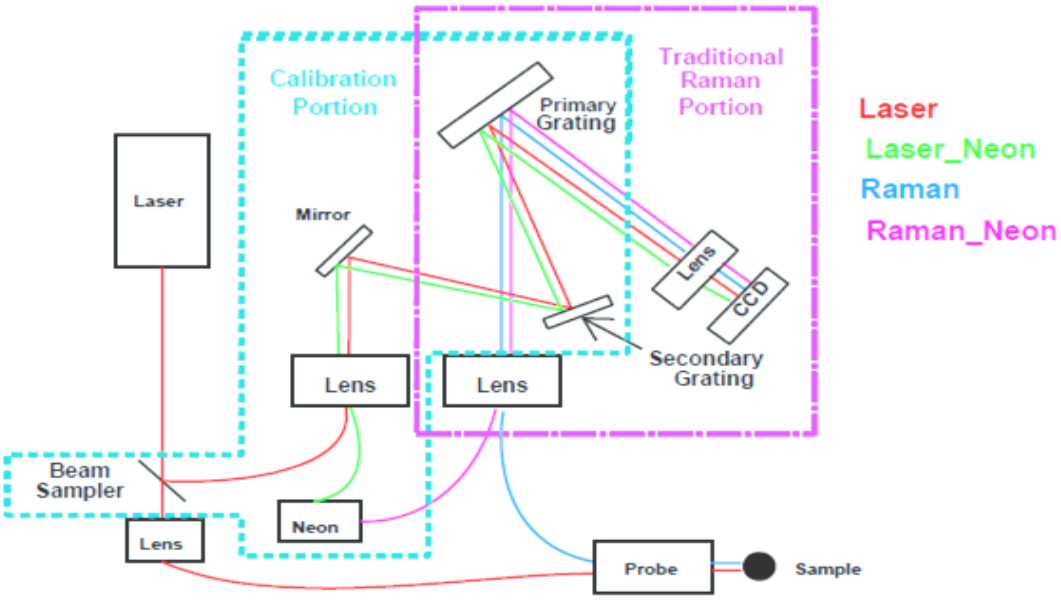

Figure 13. Schematic of the spectrograph of the Bruker Optics dispersive Raman microscope (Senterra). The ray diagrams correspond to Bruker Optics SureCal internal calibration system. SureCal (US Patent number 6,141,095) is an automatic calibration of the spectrometer without external standards and calibrates both frequency and intensity values by using an internal Neon line source (Source: Bruker Optics).

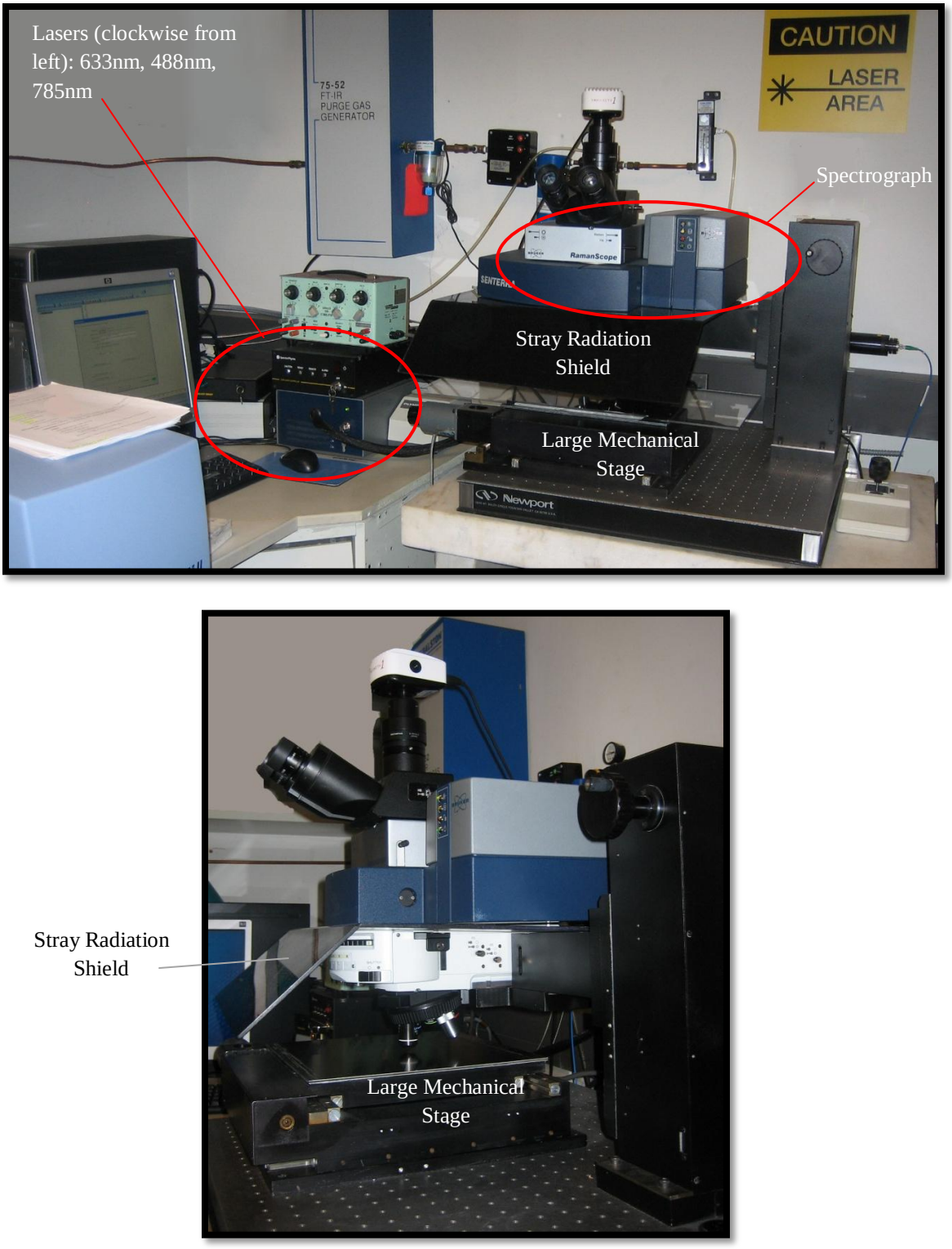

Figure 14. A Bruker Optics Senterra RamanScope (a spectrograph coupled with an Olympus BX51 microscope), (top) front view and (bottom) side view. The set-up has been modified to include a large mechanical stage for analyzing large works of art that would not fit on a normal microscope stage [The Metropolitan Museum of Art].

In a dispersive Raman microscope, the laser light travels through the objective, impacts the sample and scatters back through the objective. The Raman scattered light passes through the objective and travels to the spectrometer module (spectrograph). Narrow bandpass interference filters are in place to produce monochromatic incident laser lines and notch filters are in place to block any additional radiation (*i.e.* Rayleigh) such that only the Raman scattered radiation reaches the detector (Figure 15). The FT-Raman spectrometer uses an interferometer and series of filters to generate spectral data (Figure 16). The Fourier transform process is described in more detail in the *Infrared Spectroscopy: Theory and Practice* section of this paper.

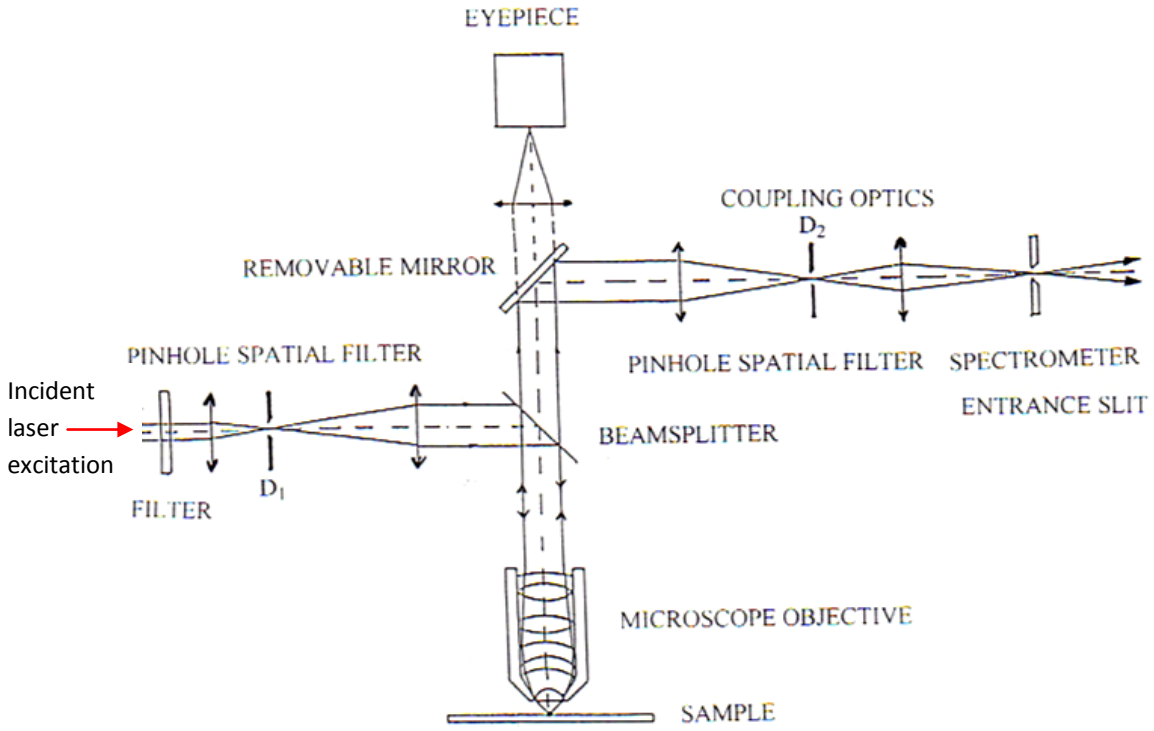

Figure 15. Collection geometry of some Raman spectrometers coupled with an optical microscope. The pinhole spatial filters (D_1 and D_2) are employed in confocal Raman systems. When confocal imaging is not being used, the pinhole filters are replaced with rectangular-shaped apertures (Reproduced with permission from Academic Press).

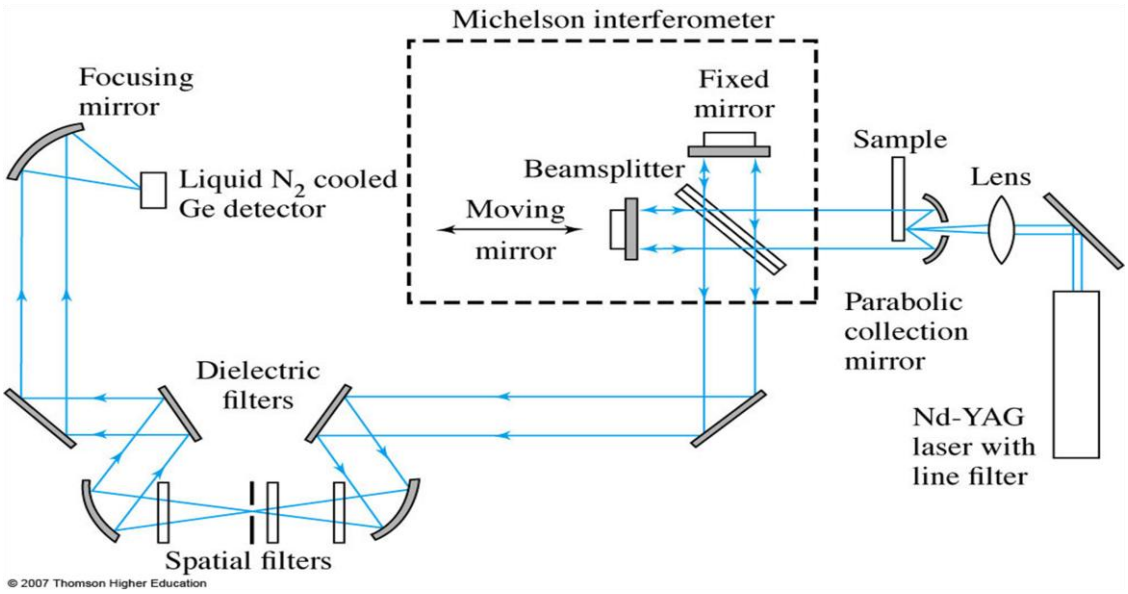

Figure 16. Schematic of a FT-Raman Spectrometer. Filters are inserted to remove radiation from the source and the stronger Rayleigh radiation so that only the Stokes scattering reaches the detector (Adapted from Skoog, Holler and Nieman, 1998).

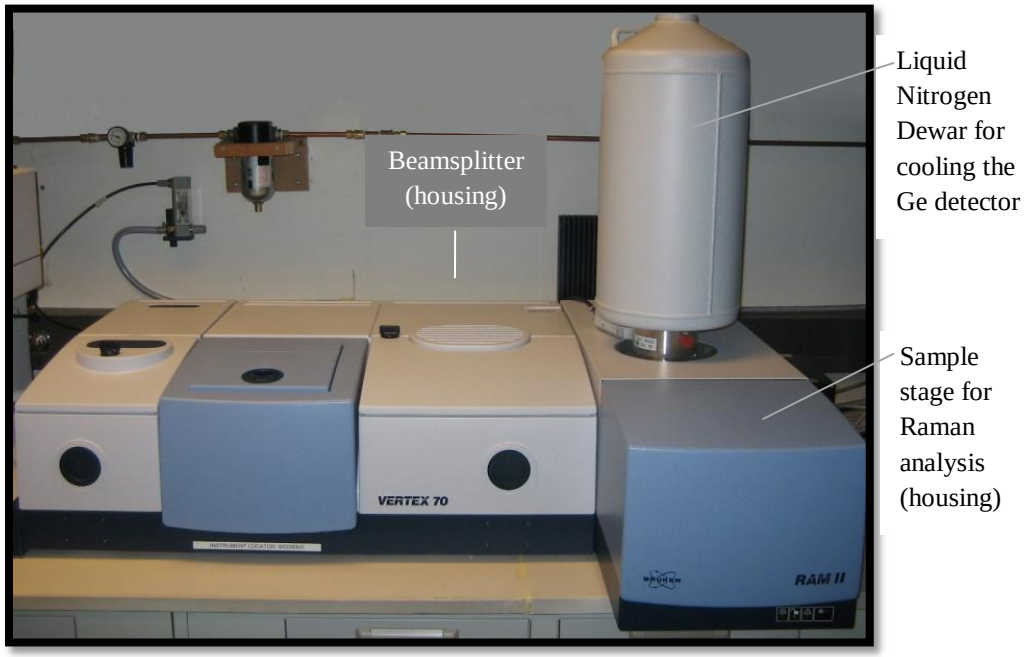

Figure 17. A Bruker Optics Vertex 70 Ram II Instrument (Ge detector), which can be used for both Fourier transform infrared spectroscopy and Raman spectroscopy. The instrument can also be coupled with a microscope for infrared microscopy using ATR and reflection optics on trace samples (not shown) [The Metropolitan Museum of Art].

Figure 18. A Thermo NXR FT-Raman Instrument (InGaAs detector), which can be used for both Fourier transform infrared spectroscopy (left) and Raman (right) spectroscopy [John Jay College of Criminal Justice, CUNY].

With Raman spectra, the abscissa (x axis) is the wavenumber shift (the difference in frequency between the observed radiation and the source). This value is usually labeled as units of reciprocal centimeters (cm^{-1}). The ordinate (y axis) is the Raman intensity and may be labeled as photons per second or arbitrary intensity units. The intensity of a Raman peak is affected by several factors, including but not limited to the molecule's polarizability, the concentration of the active molecular species within a sample, the intensity of the excitation source and the efficiency of the detector.

Raman spectroscopy can be impeded by sample degradation (thermal and photo degradation), inherently weak intensities, fluorescence interferences, and inefficient collection and subsequent detection of radiation. Current instrumentation has been able to overcome these factors, due to the availability of various laser excitation wavelengths, the introduction of interferometer-based instruments, improved detectors and electronics as well as enhancement

techniques such as surface enhanced Raman scattering (SERS) and resonance Raman spectroscopy.

Surface Enhanced Raman Scattering (SERS) is the technique employed to enhance the normal Raman signal by a factor of 10^6 or more by placing a molecular species on or near a metal substrate (for example, a metal nanoparticle or quantum dots), followed by analysis with standard Raman instrumentation. It has been found that there are three factors which contribute to this enhancement effect, molecular resonance (from the molecular species), surface plasmon resonance (from the conduction band of the metal nanoparticle) and charge transfer resonance (transfer of electrons between the molecule and the metal). In addition to the signal enhancement, there is also a resulting quenching of fluorescence. SERS benefits include the ability to generate high resolution spectra of molecular species in ultra trace concentrations and the ability to generate spectra in cases where fluorescence interference is otherwise overwhelming with normal Raman.

Much work has been done to establish the mechanism of the enhancement and to determine the relative effects of the contributing sources. According to Lombardi and Birke, the enhancements can be described by a single expression in which all three resonance effects contribute. Furthermore, these resonances (surface plasmon, charge transfer and molecular) contribute as multipliers rather than sums. The authors note that the three resonance effects contribute differently to the overall enhancement, depending on several factors. These factors include the nature of both the metal nanoparticle and the molecular species as well as the characteristics of the excitation wavelength. According to the equation that resulted from their research, the enhancement factor (R) can be determined based upon the contribution of the different resonance effects (2008, pp. 5609):

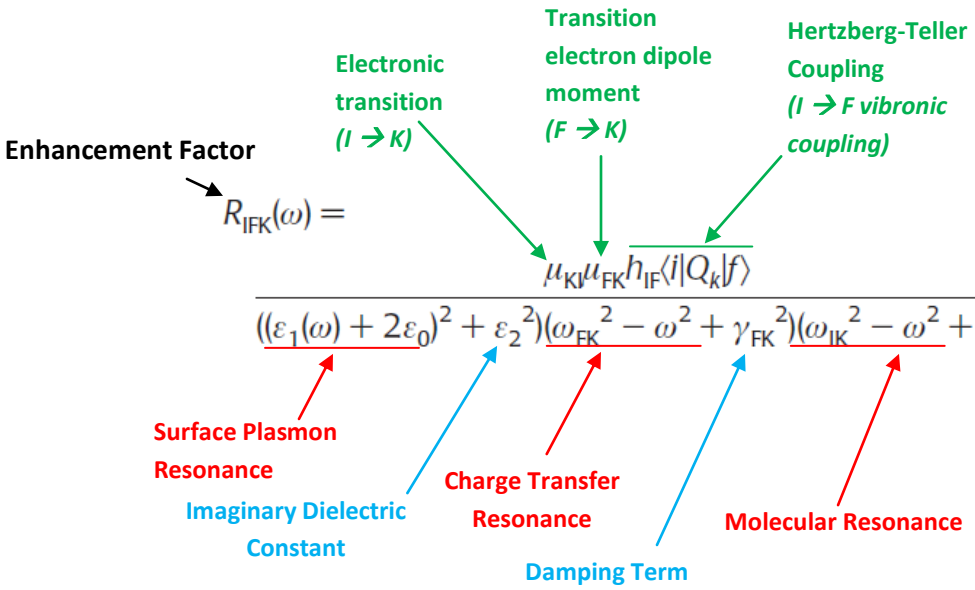

Figure 19. Equation used to determine the resonance enhancement effects for SERS.

Lombardi and Birke determined that the resonances are represented in a single expression linked by coupling terms where the three resonances contribute as multipliers with regard to the overall enhancement. In the above equation the numerator represents the Raman signal, where I, F, and K represent the ground state (HOMO), a charge-transfer state (Fermi) and an excited molecular state (LUMO) of the molecule-metal system, respectively, and the denominator represents the product of the three resonances (surface plasmon, charge transfer and molecular, respectively). In the numerator, $h_{IF}\langle i|Q_k|f\rangle$ represents the B-term (non-totally symmetric modes) in the Hertzberg-Teller equation, which gives rise to normal Raman spectra. In the denominator, the values are all energies that are affected by the excitation wavelength. These resonance factors correspond to the surface plasmon resonance, the charge transfer resonance and electromagnetic resonance. According to the authors, the magnitude of the SERS enhancement, the contribution of each of the three resonance effects and the appearance of the resultant Raman spectra depend on several factors, including the excitation wavelength, the size and shape of the metal

nanoparticle, the strength of the oscillator, the energy of the nanoparticle and the bandwidth of the resonance. Several publications have been generated evaluating the contribution of resonance effects to different dye molecules, an example of which is seen in figure 20 below):

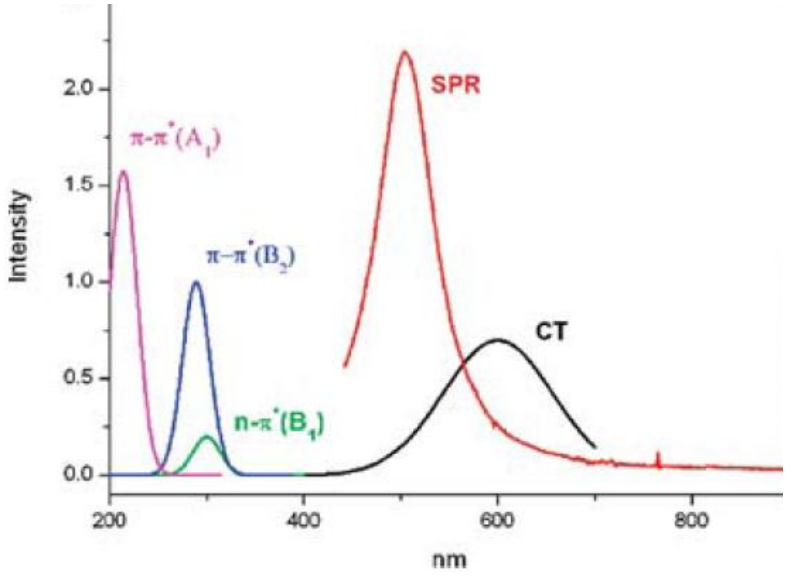

Figure 20. Resonances of Pyridine-Silver nanoparticle system (Adapted from Lombardi and Birke, 2009, pp. 734).

Of the metal substrates, copper, gold and silver are commonly employed for SERS work. Preparation of metal substrates has varied and has included surface roughening by a series of oxidation-reduction cycles, thin film depositions on different substrates by different methods of deposition (*i.e.* sputtering or evaporation), and the preparation of colloids. A study by Lee and Meisel (1982) attempted to detect SERS by examining dyes adsorbed on colloidal gold and silver by preparing a series of silver and gold sols using sodium citrate solution as a reducing agent. In addition to observing the surface enhancement phenomenon due to the molecular species (dyes) adsorbed on the surface of the colloids, the authors demonstrated the efficiency of adsorption of the dye molecules onto the colloids. Many researchers have employed the Lee and Meisel

method (or a slightly modified version) since its development to produce silver sols for their SERS work. While effective for SERS, the Lee and Meisel colloids had limited stability and reproducibility with regard to particle size, aggregation and absorption light maxima. As such, other support systems have been developed, such as roughened electrodes, Tollens mirrors (colloidal silver films on a glass substrate), silver nanoisland films and alternative metal colloids.

In order to improve the analytical performance of SERS in the analysis of microscopic samples, Leona (2009) developed a sensitive, stable silver colloid support that could be reproducibly prepared microwave activated reduction of silver sulfate with glucose and sodium citrate. By controlling the reaction and providing rapid, uniform heating, Leona developed a stable silver colloid of narrow particle size range absent of aggregates. Compared to the Lee and Meisel method, the microwave reduction method established by Leona produced a narrow absorption range, narrow particle size distribution and increased colloid stability over a longer period of time. Leona, *et.al.* (2006) also reported that the poly(L-lysine) used by Lee and Meisel to facilitate the adsorption of dyes onto the silver nanoparticles was not necessary. The authors report that superior results were obtained when using potassium nitrate (KNO_3) as the aggregant, or as an alternate, gently heating the microscope slide containing the dye solution-colloid. Sodium chloride (NaCl) has been proposed as a suitable aggregant by Bell, *et. al.*, where they reported "dramatic growth in the intensity" of the Raman bands resulting from its addition (2007, pp. 1064). The use of other aggregants has been reported (nitrates, chlorates, nitric acid, *etc.*) and aggregant selection may depend on the nature of the dye or sample being analyzed with regard to its functional groups and charges on the atoms. The presence of a background produced by the citrate-reduced silver colloid from the citrate ion and reduction reaction by-products has been noted by Teslova, *et. al.* (2007, pp. 807) and should be considered when interpreting SERS

spectra that incorporate this type of colloid (Figure 21). The procedure for the microwave synthesis of the silver colloid is outlined in the methods and materials section.

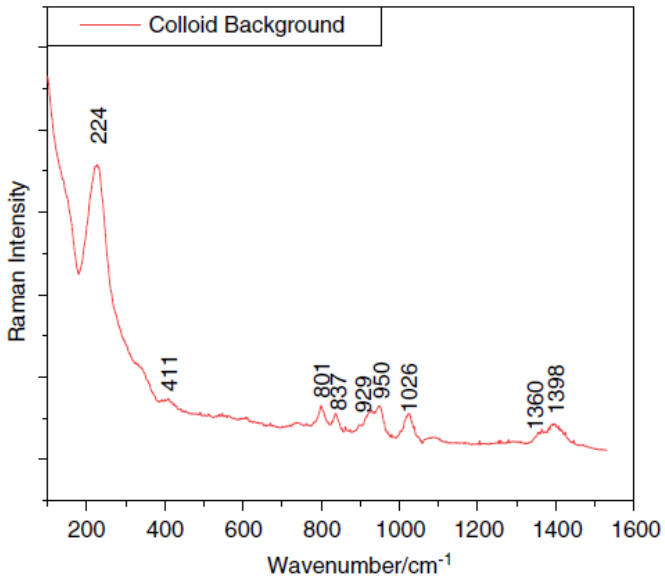

Figure 21. The colloid-citrate background. The silver-aggregant bond is typically observed in the region of 220-250cm^{-1}. The additional, weaker bands are due to the citrate ions (Adapted from Teslova, *et.al*., 2007, pp. 807).

Much has been published demonstrating the use of SERS to enhance signals and quench fluorescence. Istvan, *et.al.* reported the effect of adding silver sols to TLC spots, stating that the strongest Raman band was enhanced and many additional weak spectral features were then detectable above the noise level (2003, pp. 1717). SERS has been used in many fields of study, including art conservation and forensic science. SERS has been applied to the analysis of various natural, organic pigments and dyes, including rhodamine 6G, flavones and derivatives, flavonoids, berberine, alizarin, carminic acid, laccaic acid, photoberberine alkaloids, indanthrone and flavanthrone and many others. In the forensic science field, SERS has been used to analyze paints, pigments and inks, fibers and controlled substances such as morphine, codeine and hydrocodone, amphetamines and methamphetamines (Rana, *et.al.*, 2011 and Taplin, 2011)

Surface enhanced resonance Raman scattering (SERRS) is a technique that couples resonance Raman techniques with those of normal surface enhanced Raman scattering. According to Haynes, *et.al.,* SERRS occurs when the laser excitation wavelength overlaps with an electronic absorption band, thereby amplifying the Raman scattering intensities of the totally symmetric vibrational modes of the chromophore (2005, pp. 342A),. White *et.al.* analyzed acidic, basic and neutral dyes using a silver colloid based upon a modified Lee and Meisel method with poly(L-lysine) as the aggregating agent. Using excitation wavelengths of 457.9nm, 514.5nm and 632.7nm, the authors analyzed an assortment of dyes. They found no difficulties with the analysis of basic dyes and concluded that SERRS analysis is useful for the analysis of dyes in a mixture and the technique demonstrates that it is not necessary to perform any chromatography or extraction on the dyes prior to conducting SERRS (1998, pp. 86). For acidic and neutral dyes, White *et.al.* found that when ascorbic acid was added to the colloid-aggregant complex, there was an improvement in detection of the dye (pp. 80). The authors report that they were able to distinguish the dyes tested, including geometric isomers and tautomers (pp. 78). SERRS has been applied to the analysis of several materials encountered in forensic science and art conservation, including colorants, lipsticks, inkjet dyes and organic pigments and glazes.

Infrared Spectroscopy: Theory and Practice

Infrared spectrometry is a branch of vibrational spectroscopy that also provides important information about a compound's chemical nature and molecular structure. For a molecule to absorb infrared radiation, it must undergo a change in dipole moment brought about by its vibrational or rotational motion. A molecule can be continuously rotating and vibrating in space, and infrared active moments are those movements in which the molecule has a change in dipole moment. A dipole moment occurs when atoms within a molecule are chemically different so as to result in an asymmetric distribution of electron density because of unequal electron sharing (separation of charge within a molecule). The magnitude of the moment is determined by the distance between the centers of charge of the atoms and the charge distribution between the atoms. If the frequency of incident infrared radiation is equivalent to the molecule's natural vibrational or rotational frequency, then a net transfer of energy occurs. This energy transfer causes a change in the amplitude of the molecular vibration or rate of rotation, resulting from absorption of the incident infrared radiation. Energy transfer occurs because there is an electronic transition from one vibrational or rotational energy level up to another. The incident infrared radiation will be composed of a continuum of various wavelengths, and thus various frequencies. The frequencies that meet the above criteria will be absorbed by the molecule, while the frequencies that do not will be transmitted. Vibrational modes which do not involve a change in dipole moment are said to be infrared inactive.

Fourier transform infrared instruments allow for working with weak signals that may be lost amongst instrumental noise. Due to the decrease in optical elements and types of detectors employed in FT-IR instruments, the power of the radiation that reaches the detector is larger than that in dispersive infrared instruments, and greater signal-to-noise ratios are observed. Fourier

transform also results in high resolving power and wavelength reproducibility. An important advantage of Fourier transform is that since all of the wavelengths of the source reach the detector at the same time, an entire spectrum can be obtained within seconds. Non-Fourier transform instruments have to examine each wavelength individually to generate the spectrum, which can take much longer for comparable resolutions. Fourier transform can be described as a mathematical algorithm that is applied to the data generated by the spectrometer. Because the interferometer modulates the infrared light in a very specific way, the Fourier transform algorithm enables the instrument to process all of the wavelengths of infrared light at once. This produces a high quality spectrum almost immediately.

Fourier transform spectroscopy incorporates an interferometer for the purpose of achieving useable frequency-domain spectroscopy from time-domain (changes in radiant power with time) data through a series of mathematical computations and signal modulations. The interferometer splits a beam of radiation into two beams of nearly equal power and then recombines them such that intensity variations of the combined beam can be measured as a function of differences in the path lengths of the two beams. After a signal called an interferogram is generated, the mathematical Fourier transform of this signal occurs and is plotted. These interference patterns undergo data processing to produce a 'readable' spectrum; the interferogram shifts from the faster light frequency to a slower audio frequency, which can be ‘read’ by the detector and subsequently plotted.

The common Michelson interferometer possesses both a fixed and a movable mirror. The movable mirror travels away from and toward the beamsplitter with a constant velocity allowing for its location to be determined by fluctuations in the power of the reference laser radiation incident on a detector. The difference in pathlength that the infrared light travels can

be determined at any point in time by reference to the interference pattern generated by the laser. The difference between this pathlength and the pathlength that the infrared light travels to the fixed mirror part of the interferometer is called the optical path difference (OPD). As the optical path difference changes as the moving mirror is moved, the power at the infrared radiation also changes due to the constructive and destructive interferences of the various wavelengths. An interferogram is the result, which is the plot of the infrared energy power (or detector signal) versus the time (a function of the OPD).

Although routine infrared spectroscopic analysis is done in absorbance mode, the technique employed in this research used internal reflection, an infrared reflection method. Internal reflection spectroscopy is based on total internal reflection of radiation within an internal reflection crystal. Reflection will occur when radiation moves from a more refractive to a less refractive media, or vice versa. In this method, the more refractive media is the internal reflection element (IRE) and the less refractive is the sample. If the radiation is applied at an angle greater than the critical angle, reflection is described as being complete and total internal reflection occurs. The electric field of the radiation penetrates some distance into the less refractive material and thus can interact with the less refractive material. This distance the field extends into the less refractive media is called the depth of penetration. This depth of penetration depends upon the refractive indices of the sample and IRE, the angle of the incident radiation, and the wavelength of the incident radiation. As the wavelength increases, the wave number decreases and the depth of penetration increases. The electric field that penetrates into the sample is called the evanescent wave. If this radiation is absorbed by the sample, the reflected radiation will be attenuated at the wavelengths corresponding to the sample's absorption bands. Thus, this technique is called attenuated total reflection (ATR). Using attenuated total reflection

spectroscopy, the sample is placed into direct contact with an internal reflection crystal. For ATR to occur efficiently, the sample must come into contact with an IRE (also called an ATR crystal), which has a higher refractive index than the sample. Typical IRE's are zinc selenide (ZnSe), which has a refractive index (RI) of 2.2, Germanium (Ge), which has a refractive index of 4 and a composite IRE in which diamond (RI of 2.4) comes into contact with the sample. Most samples have refractive indices between 1.0 and 1.5, so typical IREs are suitable for most sample analysis. ATR is ideal for homogeneous, strongly absorbing and thick samples and a variety of samples that may normally produce intense, saturated peaks difficult to interpret when measured in transmission mode.

For routine work, the region of interest is the mid-infrared region from 4000-200 reciprocal centimeters (cm^{-1}). Within this range, the commonly displayed infrared spectrum can be split into two major regions, the group frequency region from approximately 4000-1300cm^{-1} and the fingerprint region from approximately 1300-400cm^{-1} (and down to 200cm^{-1}). Spectra are displayed as wavenumbers (cm^{-1}) on the x axis and absorbance, reflectance or percent transmittance on the y axis. When comparing ATR spectra to transmission spectra, the peak locations are very similar (with some small shifts occurring), but differ in intensities. One of the major differences between typical absorbance spectra and ATR spectra is the dependency on sample thickness; ATR spectra being generally independent of sample thickness as long as the sample is thicker than the depth of penetration. This is because the radiation penetrates a small distance into the sample, whereas absorption spectra require the incident radiation to traverse the entire sample prior to reaching the interferometer and ultimately the detector. When compared to transmission spectra for a given material, ATR spectra have less intense absorption bands at higher wavenumbers and more intense absorption bands at lower wavenumbers. An ATR

reflectance spectrum is a plot of the intensity of the internally reflected radiation as a function of wavelength (or wavenumber). When comparing sample preparation techniques of ATR and transmission, since ATR is based on the reflection of radiation from the surface of the sample, no special sample preparation is needed beyond making sure the sample is in intimate contact with the IRE (Figure 22).

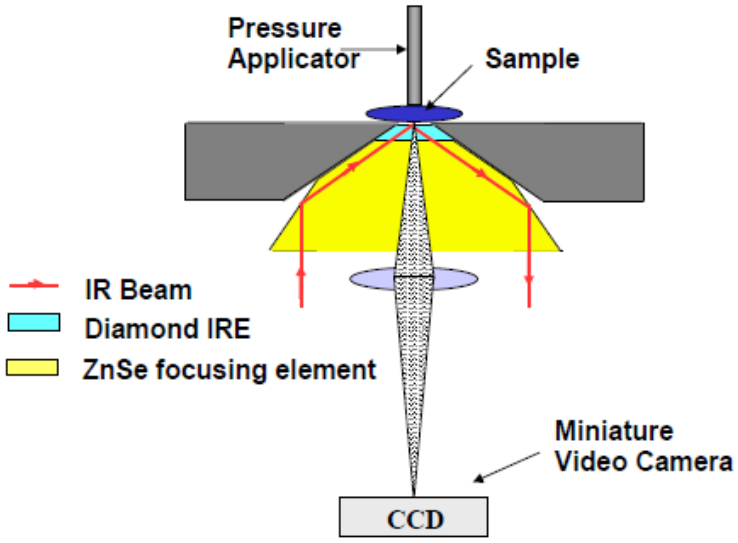

Figure 22. Schematic of FT-IR ATR Durascope™ instrumentation demonstrating sample orientation and contact with the IRE (Courtesy: John A. Reffner, Ph.D.).

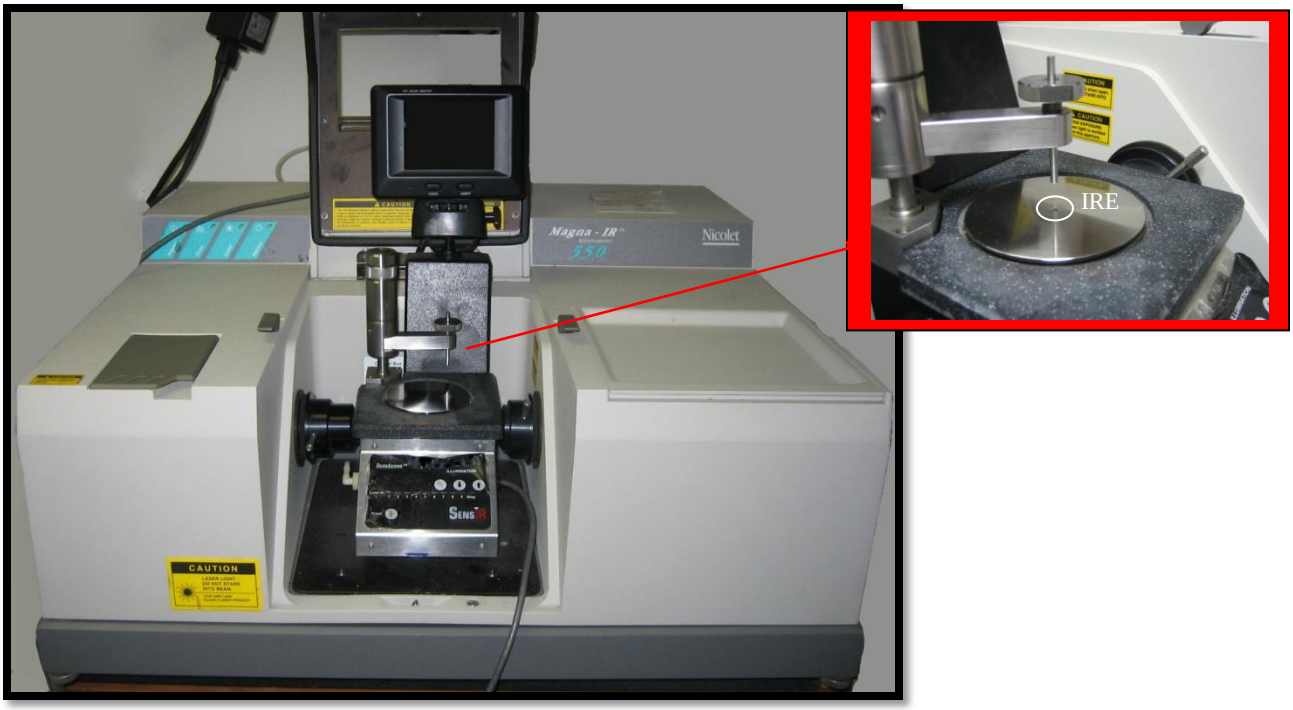

Figure 23. A Nicolet Magna IR 550 FT infrared spectrometer with a Durascope™ attachment for ATR. The insert shows the sample stage in order to provide a closer view of the internal reflection element (IRE) [Thomas A. Kubic and Associates, TAKA].

In order to routinely identify a compound and determine the molecular structure using infrared or Raman spectrometry, correlation charts are used to identify the functional groups in a molecule based upon the observed vibrational bands. After determination of the functional groups based upon the band locations, reference libraries and computer-based searches can be used to aid in the compound identification. For structural determination, calculations can be conducted to provide information about the expected infrared active modes wherein predictions are made about the structure and symmetry of a molecule. These calculations are based upon molecular symmetry and group theory considerations. By coupling infrared data with Raman spectrometry, interpretations for qualitative identification can be done with high confidence. A table of common Raman bands can be found in Appendix A. In addition, a comprehensive infrared Correlation Chart can be found in Appendix B.

Molecular Symmetry and Group Theory

Raman scattered radiation corresponds to vibrational energy levels, which are also characteristic of infrared spectroscopy. As previously stated, in order for Raman scattering to occur, there must be a change in polarizability (distortion of bond electrons) during the vibration resulting from the interaction of the incident field with the molecule. In contrast, infrared absorption requires a change in the dipole moment (overall charge distribution of the molecule) during the vibration resulting from the interaction of the incident field with the molecule. These concepts are described as the basic selection rules and are the basis for understanding resultant spectra based on molecular symmetry and group theory. Selection rules are rules for determining which transitions are allowed and which are forbidden. Raman and infrared are often described as complimentary techniques, on the basis that the vibrations that cause the largest changes in a molecule's polarizability are the symmetric vibrations, while the vibrations that cause the largest change in a molecule's dipole moment are the asymmetric stretches.

Molecules can undergo a variety of motions, including movement of the entire molecule in space (translational motion), rotational motion of the entire molecule, and movement of atoms in the molecule relative to other atoms in the molecule (individual vibrations). The transitions between the various energy levels (Figure 24) will be affected by the incident radiation that impinges on the sample resulting in molecular motions that affect the electronic cloud distribution about the molecule. It is these changes that generate a change in polarizability (Raman) and/or dipole moment (infrared) of the molecule.

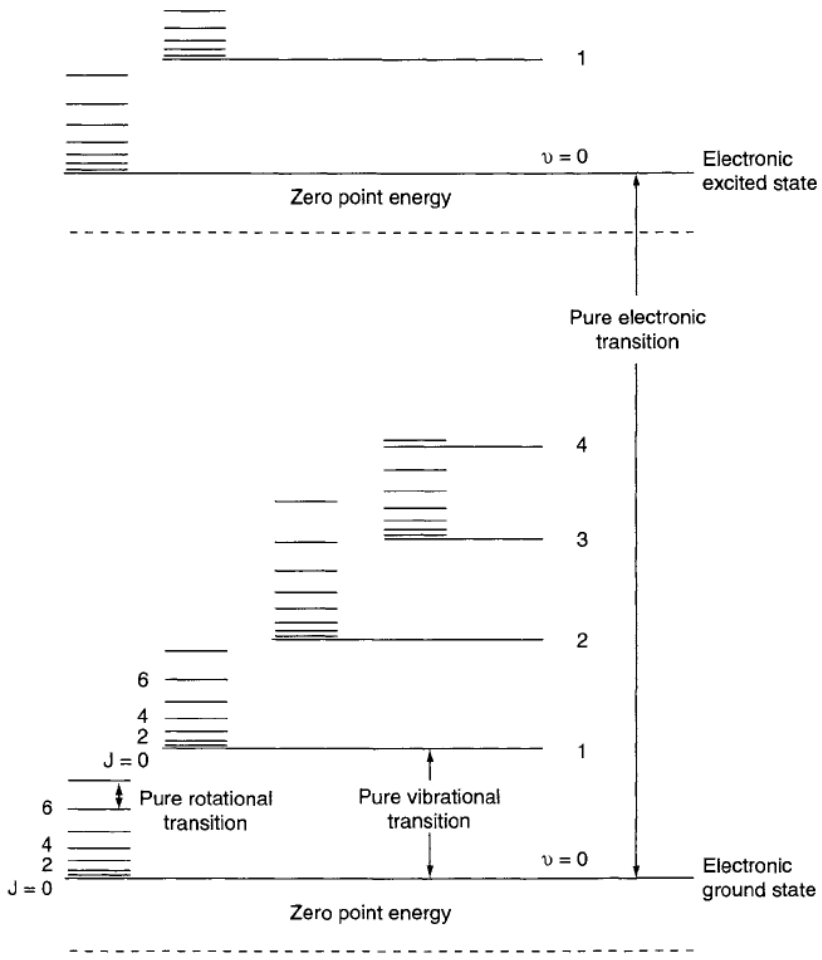

Figure 24. Energy levels of a diatomic molecule, including the relationships between the electronic, vibrational and rotational states. The space between electronic levels is actually much larger, which the space between rotational levels is substantially smaller (Ferraro, Nakamoto and Brown, 2003, pp. 7).

Motions that can potentially give way to either a change in polarizability or a dipole moment can include stretching, bending (scissoring), rocking, wagging, twisting or ring breathing. These normal modes are described as the overall vibrations of the atoms in a molecule and are broken into two classes, stretching vibrations which result in a change in bond length and bending vibrations, which result in a change in bond angle (Figure 25).

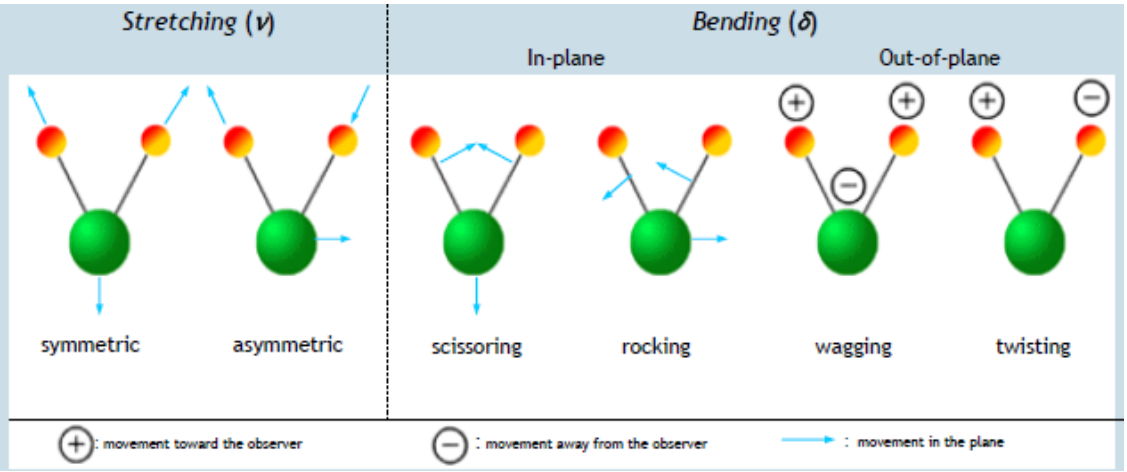

Figure 25. Molecular motions that can result in changes to either a molecule's dipole moment or polarizability. Some motions may not produce a change in dipole moment, but may produce a change in a molecule's polarizability and vice versa (Courtesy: Patrick Buzzini, Ph.D.).

For a harmonic oscillator, only the transitions involving $\Delta\upsilon = \pm 1$ are allowed. In anharmonic systems, transitions involving $\Delta\upsilon = \pm 2, \pm 3\ldots$ are allowed by the selection rules. These energy level transitions are often weak and classified as overtones. The fundamental transition from $\upsilon = 0 \leftrightarrow 1$ appears strongly in both Raman and infrared spectra. A potential energy curve for a diatomic molecule demonstrating the energy levels is provided in Figure 26. A harmonic system follows a quadratic equation whereas an anharmonic system moves away from the quadratic equation format, which causes a decline in linearity between the energy and intranuclear distance.

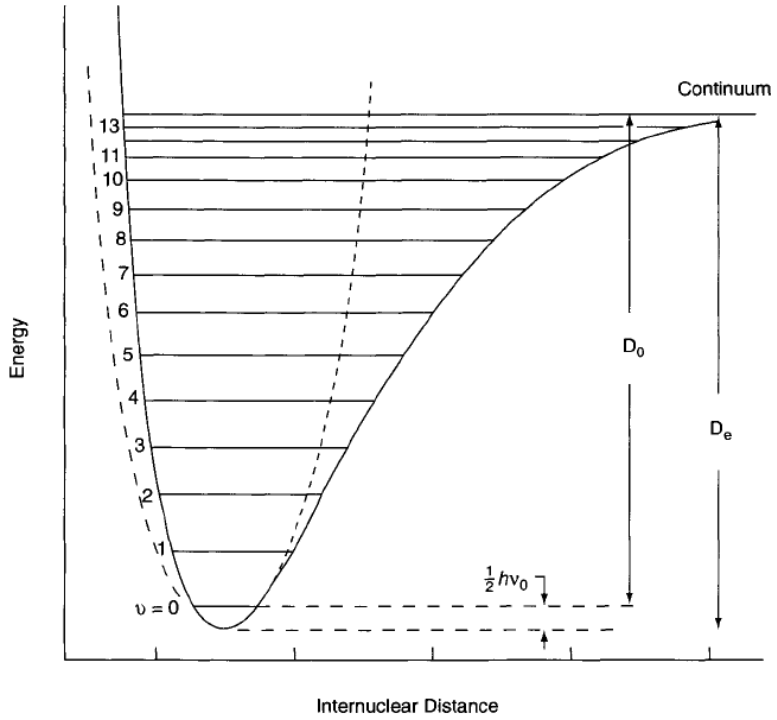

Figure 26. Potential energy curve for a diatomic molecule, where the solid line depicts an approximate potential (Morse potential) and the dashed line is the potential for a harmonic oscillator (Ferraro, Nakamoto and Brown, 2003, pp. 12).

The number of normal modes within a molecule is dictated by the number of atoms in the molecule and is represented as the net vibrational degrees of freedom, or 3N-6 for nonlinear molecules and 3N-5 for linear molecules, where the 3 comes from the three directions in which an atom can move (x, y and z), the 6 represents the six degrees of freedom originating from translational motions of the whole molecule about the three principle axes of rotation, which go through the center of gravity (Ferraro, Nakamoto and Brown, 2003, pp. 20), and the lack of rotation about the molecular axis results in the 3N-5 equation. All of these movements taken together will produce unique infrared absorption and Raman spectra, since each vibration has its own characteristic frequency. Because the various changes in dipole moment occur within the molecule upon this interaction, absorption of a number of quantized frequencies will occur, and

an absorption band should appear for each vibration or rotation in which there is a change in the dipole moment.

The infrared spectrum of a polyatomic molecule can be quite complex due to the possible vibrational transitions (sometimes described as fundamental transitions). In addition, several factors exist that could affect the amount or characteristics of absorption bands (sometimes referred to as non-fundamental transitions). Factors that can affect the resultant infrared spectrum can include degeneracy, weak absorptions, unresolved or undetected peaks, vibrational coupling, the presence of overtones, combination bands and difference bands. These factors, coupled with the combinations of vibrational transitions in a given molecule, are what make the infrared spectrum for a molecule unique and allow for qualitative identification of a material. Additional factors can lend themselves to affecting the infrared spectrum, including a change in a molecule's bond strength and length (which can be brought about by changing an atom in the molecule), its mass or polarity. Raman spectra are similar to infrared spectra in that they provide specific bands that can be used to identify a molecular species, but are less complex since Raman spectra do not display overtones or combination bands.

Group theory enables the determination of the symmetry elements of a molecule in order to assign the molecule to a finite number of groups (while there are an infinite number of combinations, only a small fraction of combinations are relevant to molecules). By determining the symmetry elements in a molecule, it is possible to identify the vibrational and rotational modes in order to predict the resultant infrared and Raman spectra. In order to assign a molecule to a group, it is necessary to identify the symmetry elements of the molecule and, using character tables, assign the molecule to a point group. A flowchart used to assign a point group to a

molecular species is provided in Figure 27. Character tables have been generated for each point group; after determining the point group with the aid of the flowchart, referring to the point group's character table will provide information about the symmetry operations and irreducible representations that characterize that particular point group. Symmetry elements describe identity operations (which leave the molecule unchanged), reflections through mirror planes, rotations about defined axes and inversions through defined points, and some combinations of these operations. A sample character table with the major components labeled is provided in Figure 28. The complete series of the Character Tables can be found in Appendix C.

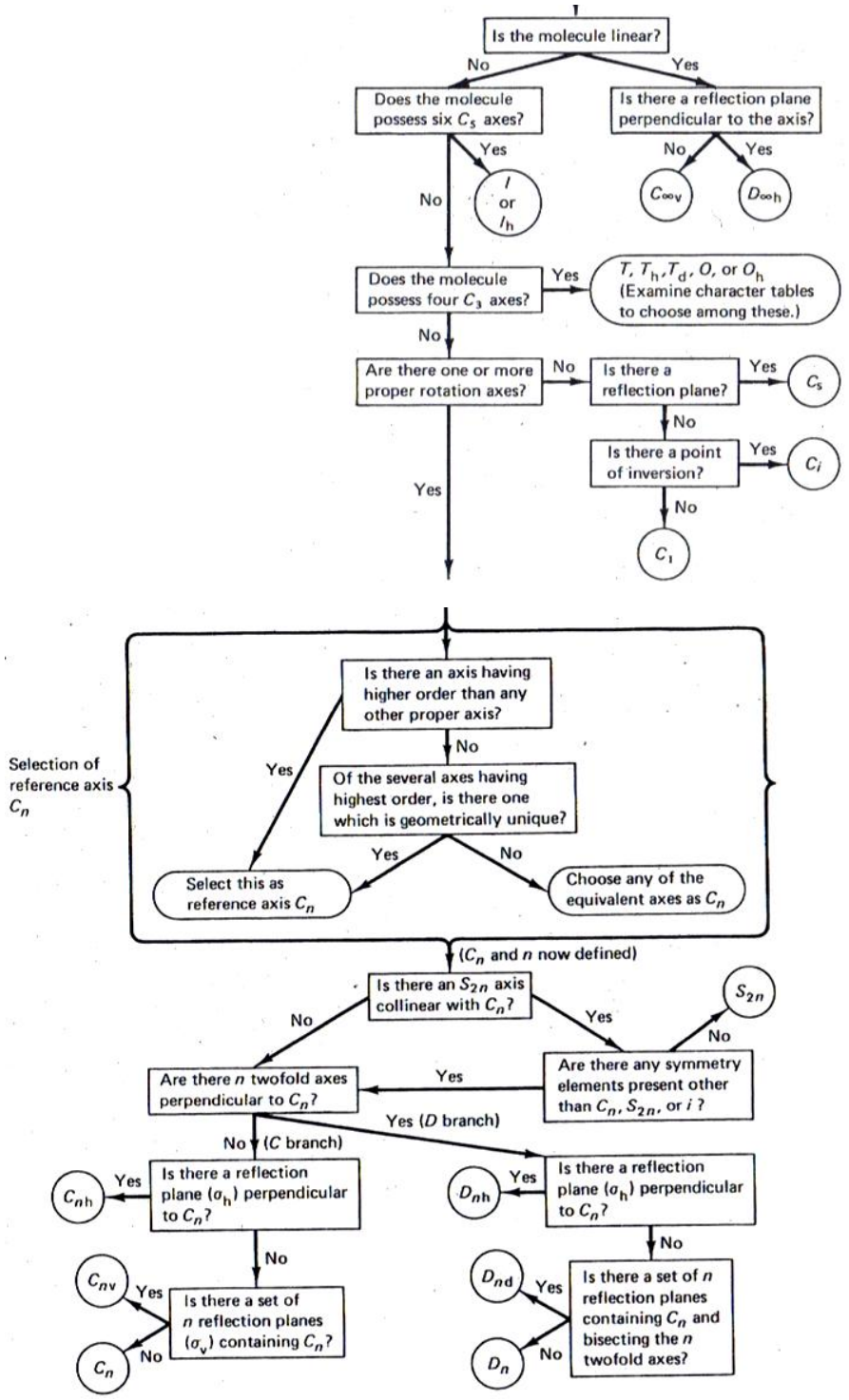

Figure 27. Flow chart outlining the procedure for determining the point group of a molecule based upon its observed symmetry elements (Adapted from Cotton, 1964). The point groups are located within the circles.

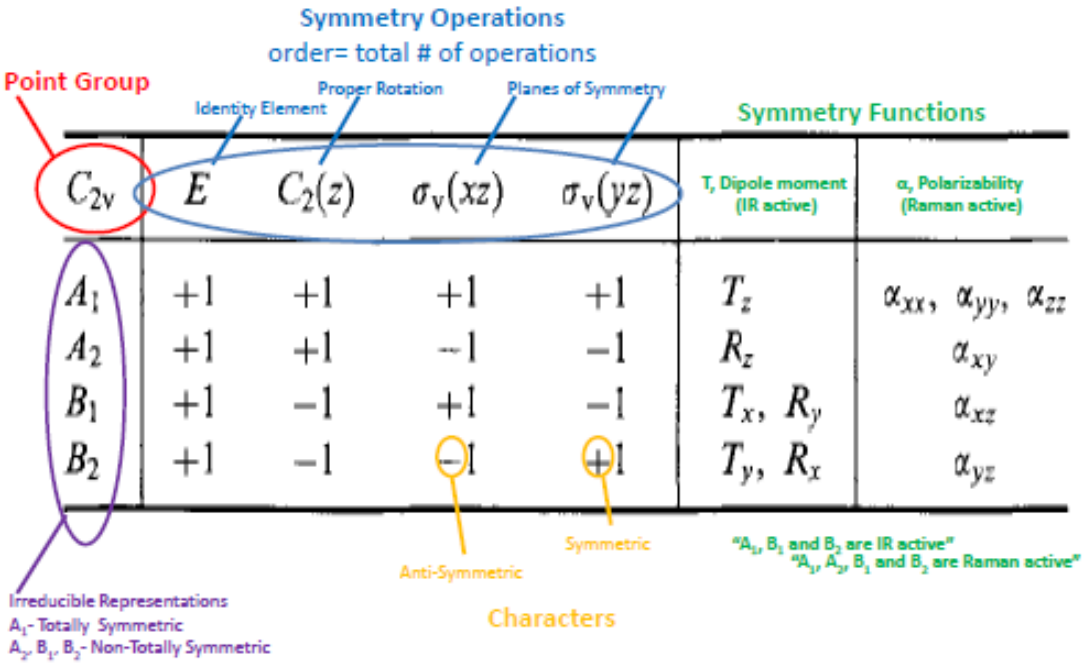

Figure 28. Character table for the C_{2v} point group with labels describing regions of the table.

Once structural information and knowledge of a molecule's vibrational excitations are elucidated, symmetry selection rules can be applied to determine which transitions will actually be observed in the molecule. Using group theory, symmetry properties of the molecular states and the infrared and Raman selection rules, it is possible to determine whether a transition is forbidden or not in either infrared or Raman spectroscopy (in other words, which vibrational modes will be active). The irreducible representations include the genuine normal vibrations and non genuine motions of pure molecular rotations and translations. By calculating the totally symmetric vibrational irreducible representation, the vector components of the dipole moment, and the irreducible representation of the vibrational mode, it is possible to determine whether or not the fundamental transition is active or inactive with respect to Raman and IR.

For determining infrared and Raman activity, it is necessary to consider vibrational transitions that result from a change in polarizability (a non vanishing transition moment). In

order to do this, the reducible representations are determined using the character table of the molecule of interest. This step describes how bonds are affected by the symmetry elements in a point group and can be done by assigning x, y and z Cartesian coordinates to each atom in the molecular species, which represent the directions of motions of each atom. By evaluating each plane relative to the symmetry operation, it is possible to determine the total reducible representations of the molecule. From the total reducible representation value, one can determine the vibrational reducible representation (Γ_{vib}) using the following equations:

$$\Gamma_{total} = \Gamma_{vib} + \Gamma_{trans} + \Gamma_{rot}$$

$$\Gamma_{trans} = A_1 + B_1 + B_2$$

$$\Gamma_{rot} = A_2 + B_1 + B_2$$

where Γ_{trans} and Γ_{rot} are calculated using the character table for the molecular species of interest and Γ_{total} is calculated using the equation described above.

To calculate the irreducible representations for all of the normal vibrations (Γ_{vib}), the following equations are used:

$$\Gamma_{vib} = a_1\Gamma A_1 + a_2\Gamma A_2 + b_1\Gamma B_1 + b_2\Gamma B_2$$

$$a_1 = \tfrac{1}{4}(\Gamma_{vib} \cdot \Gamma A_1)$$

$$a_2 = \tfrac{1}{4}(\Gamma_{vib} \cdot \Gamma A_2)$$

$$b_1 = \tfrac{1}{4}(\Gamma_{vib} \cdot \Gamma B_1)$$

$$b_2 = \tfrac{1}{4}(\Gamma_{vib} \cdot \Gamma B_2)$$

In some molecules, a symmetric mode may produce no change in the dipole moment as two atoms move away from a central atom (or central portion of the molecule), but may cause a change in the polarizability with the movement. This would render the molecule's symmetric mode infrared inactive and Raman active. In the anti-symmetric mode, the two atoms around the

central atom may move in a manner to produce an uneven distribution of charge, causing a change in the dipole moment but no net change in the polarizability, rendering the anti-symmetric mode infrared active and Raman inactive.

More often, an individual will evaluate the bands in a spectrum based upon their location (frequency, cm^{-1}) and band shape in order to determine the functional groups in a unknown sample in an effort determine a sample's composition. Conversely, it is also possible to evaluate a known sample's molecular make-up and chemical structure in order to determine how the spectrum should appear based upon the behavior of the functional groups comprising the sample and their interaction with the incident radiation (and how these interactions may affect the molecule's rotational and vibrational states). In predicting the transitions that will occur (according to the different electronic and vibrational states diagrammed in an energy level diagram), it is also necessary to consider which transitions are allowed and which are forbidden according to the laws of quantum mechanics. By correlating the predicted transitions to the resultant spectra, is it possible to determine which transitions are forbidden (based upon their marked absence from the resultant spectrum).

In vibrational spectroscopic techniques (both Raman and infrared), there are transitions between vibrational states of a molecule, in either the electronic ground or excited states (refer to the energy level diagram in figure 10). Each vibrational state can be characterized in terms of a vibrational wave function (ψ) and can be described by quantum numbers (which refer to the absorbed quanta in the molecule's normal modes). In addition to the ground state transformation (the totally symmetric irreducible representation), there are electronic state transformations for the excited states above ground (fundamental vibrational levels, combination levels and overtone levels). Those transitions which connect ground and fundamental levels are called fundamental

transitions. It is these transitions that give rise to infrared and Raman bands and are more intense than other transitions. In addition to the molecular vibrations, infrared radiation will also excite molecular rotations (if the molecule is free to rotate). It is the combination, overtone and rotational bands that make infrared spectra more complicated when compared with Raman spectra.

Using the equation derived from their research concerning surface enhanced Raman scattering, Lombardi and Burke describe the Hertzberg-Teller selection rules governing SERS intensities in order to determine allowable transitions and in what contribution they will have to the overall spectrum. The authors note that the relative intensities of the SERS bands of a given symmetry will be proportional to the relative oscillator strengths of the observed optical transitions (2008, pp. 5608). This, along with other contributing factors, can allow for the prediction of relative band intensities in SERS spectra. By being aware of the selection rules and contributing electrochemical factors of both normal Raman spectra, SERS spectra and SERRS spectra, one is able to account for spectral differences when interpreting and comparing spectra of the same material generated using different Raman techniques. In other words, resonance effects and orientation effects may result in variation of band intensities and overall relative band intensities, causing a difference in the SERS spectrum and the normal Raman spectrum of the same molecular species. In addition, bands may be subjected to frequency shifts and broadening due to the different techniques employed (normal Raman, FT Raman or surface enhanced Raman), laser excitation wavelength and intensity, and matrix effects. Careful consideration of selection rules and resonance effects are crucial to interpreting these spectra, as failure to do so may result in false positives or false negatives with respect to identifications.

As a result of atomic composition, bonding and selection rules, functional groups will vary in their strength or weakness as a Raman scatterer or infrared radiation absorber. For example, water (H_2O) is a weak Raman scatterer due to the polar, weak vibrations exhibited in the O-H stretching, but because the water molecule exhibits a dipole moment, water is easily detectable in infrared spectra. Furthermore, when observing an infrared spectrum of water, the asymmetric and symmetric stretches of water can be observed in the region of 3000-3500cm^{-1} and the scissoring can be observed in the region of approximately 1600cm^{-1}. Highly polarized N-H stretches are also weak in Raman, while backbone C-C stretches can be readily resolved in Raman spectra. The C-N stretch (commonly found in dyes and pigments) can be resolved in both infrared and Raman spectra.

Density Functional Theory

Density functional theory calculations are an excellent way to observe the behavior of a molecule with regard to its normal modes and to correlate these normal modes to peaks in vibrational spectra. Several factors should be considered when employing computational methods to derive vibrational spectra, as there can and will be differences between actual and calculated spectra with regard to peak shifts (frequency changes), peak heights (relative intensities) and peak areas. Of primary concern is that the output is dependent upon the input, meaning that, in addition to setting the functional and basis set, the user can control such factors as the matrix, the amount of molecules in the system, and the actual point group of the molecule (for example- one pigment molecule in vacuum set at the default point group of C1). Koch and Holthausen note that the selection of the functional and basis set to describe the chemical system requires the software to make "a best approximation of the exact wave function that can be obtained for a particular subset… By restricting the search to a subset, the exact wave function itself cannot be identified (ground state wave function)…" (2001, pp. 8). In "real world" cases, experimental examination will be based upon a system that is a mixture, impure or in a solution. It should also be remembered that the Gaussian software is making a harmonic calculation of an anharmonic system (refer to figure 26). It should also be noted that three dimensional structures may exhibit intramolecular hydrogen bonding within the molecule. By analyzing many similar molecules in a matrix, inter and intra molecular bonds are always a possibility, which could result in changes in vibrational intensities. In the absence of data generated from techniques like single crystal x-ray diffraction, the actual molecular structure and orientation (for example, planarity, bond angles, *etc.*) cannot be known and thus assumptions must be made by the analyst and software regarding the molecular structure. By coupling the pigment data with x-ray

diffraction data, such as that described by Hunger (1999), it may be possible to accurately reconstruct the molecular structure to eliminate a subjective variable from the DFT calculations.

Density function theory calculations have been used in the analysis of organic pigments in art conservation and cultural heritage studies, and have recently been applied in forensic applications, specifically with the analysis of controlled substances. It is important to note that DFT calculations are a useful tool for correlating experimental and calculated data and should not be used as a substitute for going into the lab and examining the sample to obtain a true spectrum.

Density functional theory (DFT) is used for the computation of molecular structure and vibrational frequencies. Density functional theory can help answer questions such as: *Does a peak correspond to a normal mode of vibration in a molecule*? *Does a particular band have a corresponding vibration and intensity*? Computational chemistry couples theoretical chemistry computer programs in order to accurately and more efficiently calculate the structures and properties of molecular species. DFT can be used to solve the Schrodinger's equation, $H\Psi = E\Psi$, which can be rewritten as:

$$\hat{H}|\phi\rangle = E|\phi\rangle$$

where H is the Hamiltonian (or functional used to define M nuclei and N electrons), E is the energy and ϕ is the basis set, or set of functions that describe the chemical system. The right side of the equation represents the properties of a system as defined by the left side of the equation. By providing the values on the left side of the equation and setting parameters to define the molecule and its structure, the computational software is able to calculate the properties of the

molecular system, which includes vibrational frequencies and dipoles which thereby give rise to Raman and infrared spectra.

Specifically, the basis set uses atomic functions to express molecular orbitals as linear combinations of atomic orbitals and is used to describe the electron density of a chemical system. Selection of a basis set is often done in an effort to constrain the spin orbitals to the lowest energy (done largely in an effort to maximize output and minimize computational time). In the DFT software, the basis set notation is specific for a set of functions used to classify the orbitals in a system. DFT calculation software assumes harmonic frequencies, in which the change in dipole moment is linearly proportional to the nuclear displacement of the atoms in the system. In addition to selecting the functional and the basis set, the software allows for controlling several parameters such as the environment in which the molecule is calculated (*i.e.* vacuum) and the symmetry of the molecule.

Each functional is designed to accurately calculate the specific property to which it is tailored. For example, B3LYP is the functional for calculating vibrational frequencies. The B3 notation indicates the Becke 3-parameter exchange and the LYP notation indicates the Lee-Yang-Parr correlation.

The basis set is a set of functions that describe the chemical system; the basis set functions are designed to describe the electron density of a chemical system. The basis set defines the parameters of the Hartree-Fock calculation and is a set of atomic functions used to express molecular orbitals as linear combinations of atomic orbitals. The Hartree-Fock calculation approximates the wave function using the Slater determinant (the relationship between energy and spin orbitals), which constrains the spin orbitals in order to yield the lowest

energy of the molecule. An example of a basis set notation is 6-311G, which is a split valence basis set characterized by the general format N-MPG. The split valence basis set describes the inner shell electrons by a single Slater orbital and the valence shell electrons by a sum of Slater orbitals. The Slater orbitals are then expressed as Gaussian functions. The split valence basis set is designed to limit functions to valence orbitals and minimize chemically inert inner orbitals. Generally speaking, the use of the split valence basis set can be employed in Gaussian calculations to provide a compromise between efficiency and accuracy, meaning the results are reasonable and can be obtained in a reasonable period of calculation time. The general notation, N-MPG outlines the number of Gaussian functions used to describe the inner shell electrons. A breakdown of the notation follows:

N: number of Gaussian functions used to describe the inner shell orbitals

-: indicates split valence basis set

M: number of Gaussian functions used to express the smaller Slater orbital

P: number of Gaussian functions used to express the larger Slater orbital

G: indicates Gaussian functions

The notation may get more complex depending on the parameters that define the system, such as 6-311++G (d,p), which incorporates diffuse functions (++) and polarization functions (d,p).

Density functional theory calculations have been used in the analysis of organic pigments in art conservation and cultural heritage studies, and have recently been applied in forensic applications, specifically with the analysis of controlled substances.

Instrument Calibration, Method Development & Standard Practices

Current trends in the forensic field have been evolving towards increasing the use of and developing unified laboratory standards of analysis. A comprehensive publication addressing the current status of forensic science was recently published by the National Academy of Science (2009). Entitled *Strengthening Forensic Science in the United States: A Path Forward*, the panel of authors address the accreditation process and standards and guidelines for quality control within the forensic science community. In recent years, accreditation of forensic laboratories has begun shifting from meeting the standards set forth by the American Society of Crime Lab Directors/Laboratory Accreditation Board (ASCLD/LAB) to those established under the International Organization of Standardization (ISO) ISO/IEC 17025 guideline, which outlines the requirements for the competence of a laboratory to carry out testing and calibrations using standard methods, non-standard methods and laboratory-developed methods. Major aspects of any accreditation program are validating and documenting both administrative and technical procedures, developing and maintaining calibration procedures and using appropriate controls and standards.

Any instrumentation to be employed in an accredited forensic laboratory must undergo qualification and calibration, which is a documented process usually done upon instrument installation. In addition, the instrumentation must undergo routine performance monitoring to ensure that the instrument is maintaining a standard level of operation. The establishment of an instrument's acceptable performance is usually referred to as the instrument qualification.

Most forensic laboratories will define how frequently the instrument should be calibrated and what the accepted limits are to declare the instrument suitable for casework. The calibration serves as a check of wavelength accuracy and is usually done with a standard that has known,

reported peak assignments. The standard selected for instrument calibrations and subsequent function checks is selected based on its ability to provide reproducible results regardless of external conditions such as environment, instrument manufacturer, *etc*. For example, a polystyrene standard is employed in order to evaluate the wavelength accuracy of a Fourier-transform infrared spectrometer. Polystyrene has well established, reproducible peaks across the range of the infrared region, making it a suitable calibration standard for routine wavelength calibrations. These polystyrene peak values obtained from a laboratory's FT-IR spectrometer can be compared to known values that have been established in the literature and be recorded and retained. The laboratory will often define an acceptable deviation range for each peak or a number of 'major' peaks. Several other measures may be used to ensure good performance the FT-IR spectrometer before use, such as aligning the instrument optics, conducting a battery of tests to evaluate the robustness of the instrument by examining and evaluating the background and interferogram, and using the polystyrene for absorbance and resolution tests. These methods may be called the 'function check' and are often done prior to use of the instrument. By running a standard, a laboratory is able to evaluate instrument performance on a daily basis and determine whether or not there are problems with the instrument hardware, settings, alignment or software settings.

Several documents have been published and several standards have been developed concerning the calibration of Raman instrumentation, including standard guides and practices released by the American Society for Testing and Materials (ASTM) and standards developed by the National Institute of Standards and Technology (NIST). According to McCreery, there are a variety of standards that can be used to calibrate and evaluate the performance of different features of the Raman instrumentation (2000, pp. 251).

The *Standard Practice for Testing the Performance of Scanning Raman Spectrometers* (ASTM Designation E 1683-02) outlines a methodology for evaluating and testing a Raman spectrometer by describing the instrument components and what affects these components may have on overall instrument performance. The standard also outlines guidelines for obtaining and reporting Raman spectra and provides a short list of materials that can be used to evaluate instrument performance, including carbon tetrachloride and cyclohexane.

The *Standard Guide for Raman Shift Standards for Spectrometer Calibration* (ASTM Designation E 1840-96) lists Raman shift values for eight materials (both liquids and solids) that can be used for wavenumber calibration checks of Raman spectrometers. The standard materials include cyclohexane, polystyrene, sulfur, 4-acetamidophenol (the active ingredient in analgesics like Tylenol®) and 50/50 (v/v) toluene/acetonitrile mixture. The spectra reported in the literature were generated with a SPEX 1403 scanning double monochromator with a 12000 lines/mm grating, a photomultiplier tube (PMT) detector and an excitation source of 514.5nm. The *Standard Guide for Testing the Resolution of a Raman Spectrometer* (ASTM Designation E 2529-06) is concerned with using low pressure arc lamp emission lines (such as xenon, argon, krypton or neon; where neon was referenced in the document but was not evaluated) or calcite to assess the spectral resolution of Raman spectrometers.

The use of a neon lamp for the calibration of Raman instruments is well-established and literature providing a table of the neon lamp lines that can be found quite readily (for example, the article by Kim, *et. al.*, 1986). McCreery notes that examination of the full width at half max (FWHM) of an emission line from a neon bulb provides a good indication of instrumental linewidth (2002). The Bruker Optics dispersive Raman microscope (Senterra) employs a patented SureCal internal calibration system using a neon source. SureCal is an automatic

calibration of the spectrometer without external standards that calibrates both frequency and intensity values by using an internal neon line source, measuring and applying instrumentation correction to produce a standard spectrum (Allen, *et. al.*, 2000). The authors describe the apparatus as a fully automated system providing standard reference data capable of achieving superior precision and accuracy. The calibration system is designed to be independent of instrument components and effects and to eliminate instrument variability as having an effect on a Raman spectrum. The apparatus incorporates a frequency calibration standard which is known and stable, and can be used to monitor Raman beams and account for any instrument fluctuations, thereby resulting in high resolution Raman spectra.

A validation process known as qualification is used to confirm that the instrumentation employed for routine testing is suitable for intended use. This validation is done by running a set of experiments with a set of standards in order to establish the reliability of the instrument and the specific method that is to be used in routine casework. The accredited laboratory will establish a procedure for qualification of their instrument followed by establishing any methods that are to be used with the instrument. Instrument qualification is a portion of the validation process that verifies that the instrument itself meets required specifications as described by the manufacturer or client. Typically, the qualification of the instrument is conducted upon installation of the instrument; the manufacturing company technician will install and set-up the instrument and then run a series of tests to ensure that the instrument has been installed properly and meets the required factory specifications. The series of tests will be conducted in order to ensure that the accuracy, precision and performance characteristics are optimized as per manufacturer's specifications. After testing and calibrating the instrument, the instrument is considered qualified and the laboratory can proceed to method development for setting standard

operating procedures and quality assurance measures. Routine preventative maintenance by the manufacturer and any instrument service are usually stored in a file in order to monitor and support the instrument qualification status. Retention of these records is critical to accreditation and may be critical in legal proceedings, both civil and criminal.

Upon instrument installation, the instrument service technician will conduct one or more service tests to ensure that the instrument has been installed properly and is performing according to its specifications. The technician will often provide the laboratory with documents outlining the tests performed and any relevant results. These documents should be retained by the lab, and may often be useful in assisting the analysts with setting up quality assurance procedures to monitor instrument performance. For example, a series of tests were conducted by the technician upon installation of the Bruker Senterra Raman instrument. The documentation outlines the procedures used by the technician and demonstrates that the instrument was set-up according to its factory specifications. The series of tests includes a background test, a beam focusing alignment test (using a silicon wafer), a frequency accuracy test (using acetaminophen, a main ingredient in Tylenol®), a spectral resolution test (using a Neon lamp), a spectral cut-off test (using NIST glass or other fluorescent material), a throughput test (using polystyrene) and a confocal Raman test (using a silicon wafer). Additional information regarding the OPUS validation program for Raman spectrometers is provided in the OPUS Software Users Manual and the OPUS Reference Manual, provided by Bruker. The latter provides a detailed procedure for performance and operational qualifications of their instrument.

This current research included the use of sulfur, cyclohexane, 4-acetamidophenol, polystyrene, silicon and a 50/50 mixture of acetonitrile/toluene as standards for evaluating and monitoring instrument performance. Elemental sulfur is a strong Raman scatterer that has

several low-frequency Raman bands that enable the ability to observe low Raman shifts. Cyclohexane and 4-acetamidophenol are also strong Raman scatterers which have a wide frequency range that makes them useful as a standard for spectral resolution. Silicon provides a large, sharp peak at around 520cm^{-1}, which can make it a useful, rapid check of wavelength accuracy.

The peak shift values obtained were checked against several sources, including ASTM Designation E 1840-96 and the McCreery text (standard spectra can also be found online at the McCreery Group website: http://www.chem.ualberta.ca/~mccreery/ramanmaterials.html). A series of reference spectra for calibration and function check standards can be found in Appendix H.

Previous Studies Concerning the Analysis of Tattoo Inks

In 1984, Slater and Durrant conducted x-ray microanalysis on the tattoos of seventeen (17) patients in conjunction with light and transmission electron microscopy (TEM) examinations. The results of their study (tattoo color and corresponding elemental composition) are reported below in Table 2. Sowden *et.al.* examined histological sections of red tattoos in eighteen (18) patients and determined the chemical composition of the pigments using x-ray microanalysis (1991, pp. 578). The elements reported included iron, sulfur, titanium, phosphorous, aluminum, silicon, calcium, mercury and cadmium.

Colour	**Metals**
Red	Al, Cl
Blue/Green	Cu/Ti
Yellow	Fe
Brown	Fe
Red	ND
Red	Hg, Cl
Blue/Red	Cr/Hg
Yellow	Cd, Pb, P
Purple	Mn
Blue	Co
Red	Hg
Blue/Red	Cr/Hg
Yellow	ND
Green/Blue	Ti/Cu
Red	Hg
Green	Cr
Red/Green	Hg/Ti

Table 2. Results of study conducted by Slater and Durrant using x-ray microanalysis on tattoos. (Note: ND= no elements detected) (1984, pp. 168). There are several reasons why a ND result may be reported, such as the detection limits of the instrument, the window material used or physical characteristics of the sample.

In 2000, Bäumler, *et. al.* analyzed forty-one (41) tattoo pigments (blues, greens, yellows, oranges, reds, violets) using visible absorption spectroscopy, FT-IR spectroscopy, x-ray diffraction (XRD), mass spectrometry (MS) and transmission electron microscopy (TEM). The

samples were taken from a variety of wholesalers from the US, the UK, the Netherlands and Germany. The authors identified the following pigments in the tattoo inks (pp. 16-17):

> Reds: Pigment Reds 112 and 170, Pigment Red 5 (Carmine), Pigment Reds 9 and 22 (yellowish red), Pigment Red 122 (bluish red)
>
> Orange: Pigment Orange 13 (yellowish orange)
>
> Yellows: Pigment Yellow 14, Pigment Yellows 55, 83 and 87 (reddish yellow), Pigment Yellow 74 (greenish yellow)
>
> Green: Pigment Green 7 (bluish green)
>
> Blue: Pigment Blue 15
>
> Violet: Pigment Violet 23 (bluish violet)

A table of the pigments with their corresponding chemical structures is provided in Table 3:

Pigments	**Chemical Structure**
Pigment Red 112	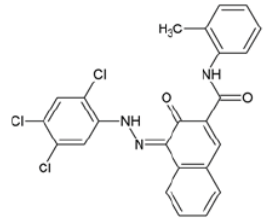
Pigment Red 170	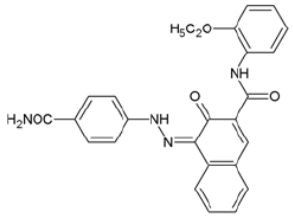
Pigment Red 5	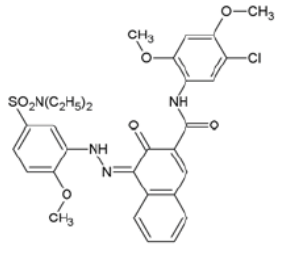

Table 3, continued

Pigment Red 9	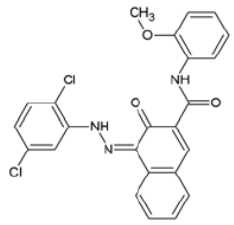
Pigment Red 22	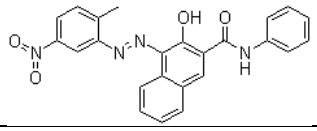
Pigment Red 122	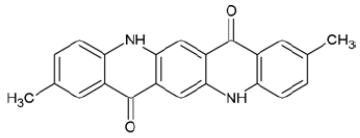
Pigment Orange 13	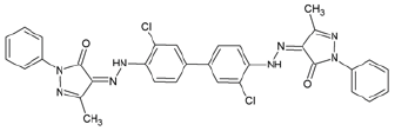
Pigment Yellow 14	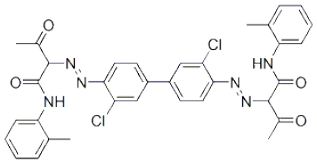
Pigment Yellow 55	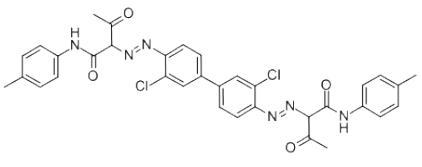

Table 3, continued

Pigment Yellow 83	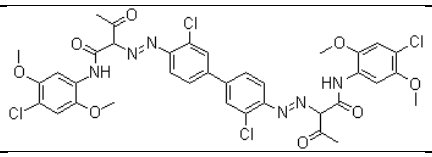
Pigment Yellow 87	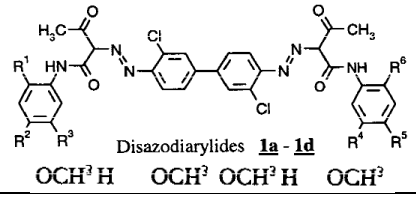
Pigment Yellow 74	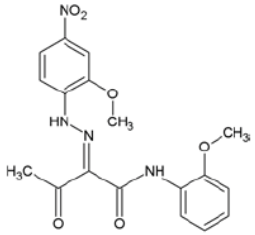
Pigment Green 7	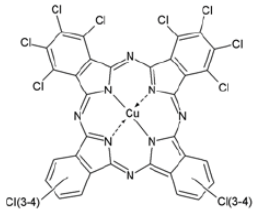
Pigment Blue 15	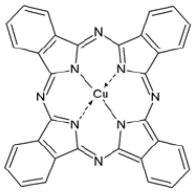
Pigment Violet 23	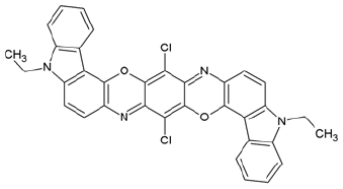

Table 3. Pigments identified in Baümler, *et. al.* 2000 study of tattoo inks.

Timko, *et.al.* (2001) analyzed twenty-nine (29) tattoo inks (Huck Spaulding Enterprises, Inc., USA) and India ink using SEM/EDS (for all atomic numbers greater than 11) and compared

the resultant data to that reported on manufacturer MSDS sheets. The authors report, "The technique (quantitative electron x-ray microanalysis by EDS) reliably identifies all elements with the exception of those with z<11…including H, He, Li, Be, B, C, N, O, F, Ne…H, He and Li are not recognized by EDS"…and … "quantifying these elements by EDS remains problematic." Timko, *et. al.* further note that they used a "standardless technique" (Timko, 2001). The authors then conclude that 73% of samples contain oxygen, 67% contain carbon, 87% contain aluminum and 67% contain titanium. Although they note the lower atomic numbers cannot be detected and that quantitative determinations are problematic, the authors report the results of x-ray diffraction on the samples in the following table:

	Element†										
Color	Titanium (22)	Aluminum (13)	Silica (14)	Copper (29)	Chromium (24)	Iron (26)	Chlorine (17)	Sulfur (16)	Carbon (6)	Oxygen (8)	Magnesium (12)
Black	...	0.25	...	...	...	85.95	...	0.29	...	13.51	...
White	98.55	1.45	...	...	...	...	...	...	...	...	...
Fire red	...	26.21	...	...	...	...	9.68	10.76	23.29	30.06	...
Flesh No.1 (tan)	74.27	1.75	...	...	...	23.98	...	...	...	...	...
Indian brown	41.98	0.76	...	...	...	57.26	...	...	...	...	...
Crimson red	...	...	17.2	...	...	...	...	...	49.36	22.25	11.19
Devil's red	27.65	2.6	0.53	...	...	...	...	...	51.67	17.55	...
Lotus (red)	40.17	3.2	...	...	...	...	...	...	17.71	38.92	...
Venetian brown	...	0.38	1.73	...	...	79.85	...	...	...	18.04	...
Florida orange	...	...	...	...	...	...	...	...	84.35	15.65	...
Lemon yellow	53.06	1.86	...	...	...	...	...	...	23.9	21.18	...
White	96.41	3.59	...	...	...	...	...	...	...	...	...
Black	...	...	...	...	...	87.98	...	...	...	12.02	...
Permanent green	...	0.89	...	13.32	...	...	51.55	...	34.24	...	...
Emerald green	5.45	0.49	...	...	72.66	...	4.15	...	...	17.25	...
Pine green	44.34	4.08	...	8.27	...	...	6.71	...	14.64	21.96	...
Parrot green	58.57	2.51	...	...	...	...	4.61	...	17.12	17.19	...
Sky blue	37.95	1.9	...	11.06	...	...	2.16	...	35.41	11.52	...
Blue green	...	1.14	...	14.46	...	...	52.24	...	32.16	...	...
Cerise (red)	51.51	2.18	...	...	...	15.34	...	...	9.81	21.16	...
Yukon white	94.98	5.02	...	...	...	...	...	...	...	...	...
Misty green	51.5	2.51	...	...	...	...	3.59	...	18.43	23.97	...
Misty blue	94.82	4.13	...	...	...	...	1.05	...	...	...	...
Tulip yellow	27.29	2.29	0.22	...	...	...	2.29	0.3	37.3	30.31	...
Peony (pink)	63.77	2.38	...	...	...	...	...	...	13.85	20	...
New blue	50.93	2.36	...	8.54	...	...	1.39	...	18.21	18.57	...
Blush (orange)	58.06	2.25	...	...	...	...	2.87	...	14.39	22.43	...
Wild violet	65.29	2.88	...	...	...	...	...	...	9.56	22.27	...
Tulip red	...	0.19	13.4	...	...	...	...	...	52.29	25.12	9
India ink	...	...	...	...	...	...	...	...	92.19	7.81	...

Table 4. Summary of results from Timko *et.al.*, 2001 demonstrating the percent elemental composition of tattoo pigments by x-ray diffraction.

In 2002, Lundsgaard presented the results of interviews with both 'traditional' tattooists and 'cosmetic' tattooists in addition to communication with pigment suppliers/manufacturers in

an effort to identify the pigments used in tattoo inks found on the Danish market. The author was able to identify a total of seventeen (17) pigments used in traditional ("general") tattooing and eleven (11) pigments used in cosmetic tattooing (pp. 7). No chemical or instrumental tests were conducted to confirm the reports of the tattoo artists and suppliers/manufacturers. The following table summarizes Lundsgaard's findings (pp. 15-16):

Pigments Used in General Tattoo Colors	**Pigments Used in Cosmetic Tattoo Colors**
Pigment Orange 36	Pigment White 6 (Titanium Dioxide)
Pigment Yellow 74	Pigment Brown 6 (Iron Oxide)
Pigment Red 170	Pigment Red 101 (Iron [III] Oxide)
Pigment Yellow 97	Jernoxid (Iron [II] Oxide)
Pigment Red 146	Pigment Yellow 42 (Ironhydroxidoxide)
Pigment Brown 25	Sudan Red
Pigment Red 266	Food Yellow 13
Pigment Violet 23	Mangan Violet
Pigment Red 122	Food Red 1
Pigment Yellow 1	Food Blue 2
Pigment Orange 43	Acid Red 87
Pigment Green 7	
Pigment White 6 (Titanium Dioxide)	
Pigment Red 101	
Pigment Blue 15	
Pigment Blue 15:3	
Pigment Black 7 (Carbon Black)	

Table 5. Resultant data from interview-based study conducted by Lundsgaard (2002)

Baeumler *et.al.* presented "Chemicals used in tattooing and permanent make up products" at a European Commission Workshop in 2003, which focused on the scientific analysis and regulation of tattoo and piercing practices. According to their report, the data obtained concerning pigments was obtained from the Council of Europe Committee of Experts on Cosmetics who have direct contact with "market players" in addition to some scientific articles and the presenter's own contact with "market players" (pp. 22-23). Baeumler *et. al.* (2003) cite the following chemicals based on these various sources

- From a 1994 study (pp. 23):

Colour	Pigments Used in Cosmetic Tattoo Colors
Blue	Cobalt blue (*cobaltous aluminate*) and indigo
Green	Trivalent chromic oxide, hydrated chromium sesquioxide
Red	Mercury sulphide (cinnabar)
Yellow	Cadmium sulphide, ochre (*ferric oxide*), curcuma yellow (curcumine)
Purple	Manganese (*non-identifiable manganese salt*)

Table 6. From Baeumler's 2003 presentation on accumulated data concerning pigments in tattoo inks.

- From a report on colorants in permanent makeup (Norway, Denmark and Finland) (pp. 24-25):

  Pigment Reds: 22, 23, 7, 170, 210, 57:1, 57:2, 181 (Vat Red 1), 122, 101 and 102
  Pigment Orange: 16
  Pigment Yellows: 74, 87, 42 and 43
  Pigment Greens: 7, 36, 17
  Pigment Blues: 15, 29 (Ultramarine Blue), 27 (Prussian Blue)
  Pigment Violet: 16 (Manganese Violet)
  Pigment Browns: 25, 6 and 7
  Pigment Blacks: 6 and 7 (Graphite), 11
  Pigment White: 6
  Acid Red 18, 87, 51
  Acid Yellow 9, 23, 3
  Acid Blue 9
  Basic Violet 10
  Solvent Red 1
  Food Red 17
  Natural Red: 22/23

- From a report on colorants in tattoo and permanent makeup studios (Germany, 2001) (pp. 25-26):

  Pigment Reds: 22, 23, 170, 146, 49, 181 (Vat Red 1), 122, 15, 101 and 102
  Pigment Oranges: 13, 34, 16, 43
  Pigment Yellows: 1, 74, 83, 42 and 43
  Pigment Greens: 7, 17
  Pigment Blue: 15
  Pigment Violets: 19, 23
  Pigment Browns: 25, 6 and 7
  Pigment Blacks: 6 and 7 (Graphite), 11
  Pigment Whites: 6, 4

- From a report on colorants in inks used for traditional tattooing (Danish) (pp. 26-27):

  Pigment Reds: 266, 170, 146, 101 and 102

Pigment Orange: 43
Pigment Yellows: 1, 74, 97, 36
Pigment Green: 7
Pigment Blue: 15
Pigment Violet: 19
Pigment Browns: 25, 6 and 7
Pigment Blacks: 6 and 7 (Graphite)
Pigment White: 6

Baeumler *et.al.* (2003, pp. 29) also list auxiliary ingredients used in tattoo inks and permanent make up, including distilled water (dH_2O), ethanol (CH_3CH_2OH), isopropanol ($CH_3CHOHCH_3$), glycerol ($OHCH_2CHOH\ CH_2OH$), hydrochloric acid (HCl), sodium hydroxide (NaOH), benzoic acid (), poloxamer 407 ($HO[CH_2CH_2O]_x[C(CH_3)HCH_2O]_y\ [CH_2CH_2O]_zH$, where x=98, y=67, z=98), rosa canina extract, aroma, barium sulfate ($BaSO_4$), aluminum hydroxide ($Al[OH]_3$), rosin, neodecanoic acid ($C_{10}H_{20}O_2$), butanamide, amorphous silica and kaolin ($Al_2Si_2O_5[OH]_4$), thickening powder, emulsifier (unspecified), resin (unspecified), sodium hyalonate, methylparaben (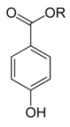 where $R=CH_3$), aqua rosae, dexpanthenol ($C_9H_{19}NO_4$), urea ($(NH_2)_2CO$), phenol(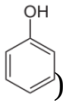). The authors add that Listerine and vodka have been reported as being used as a means of thinning the tattoo ink prior to its use.

Beute *et.al.* (2008) measured the absorption spectra of twenty-eight (28) pigments and India ink, which were mixed in an agar medium prior to instrumental analysis. The samples used in their study were the same inks and pigments used from the earlier research of Timko *et.al.* (2001). The authors reported that black inks exhibited absorption over the entire spectrum with no true peak, white pigments increased in absorbance from 404nm to peak at 790nm, and flesh inks had no maximum absorption (pp. 510). The results are reported below (pp. 511):

Color	No.	Max Absorption (nm)	Spectrum	Lowest Absorption (nm)	Spectrum	Secondary Peak	Spectrum
Black	2	600–800	Orange, red and near IR				
India ink	1	600–800	Orange, red and near IR				
Browns	2	410–550	Violet, blue, green	730–740	Red		
Blue (misty, new blue)	2	590–770	Orange to red	460–490	Blue		
Blue green	1	656–808	Red and near IR	488	Blue, green	450	Blue, violet
Permanent green	1	570–800	Yellow, orange, red	492	Blue, green		
Emerald green	1	602–680	Red, orange	532	Green	470	Blue
Pine green	1	620–785	Red to near IR	512	Green		
Parrot green	1	420–480	Violet, blue	532	Green	620–740	Red
Misty green	1	440–480	Blue	532	Green	630–710	Red
Yellow (tulip and lemon)	2	470–485	Blue	580	Yellow	780–795	Near IR
Orange (Florida orange and blush)	2	420–540	Violet, blue, green	580–610	Yellow to orange		
Red (cerise, fire red, devil's red, crimson red, tulip red, lotus, wild violet and peony)	8	500–570	Green	615–654	Red		
Flesh	1	None	None	600 to 800	Red		
White	3	790	Near IR				

Table 7. Summary of results from Beute, *et.al.* demonstrating absorption spectra peaks by pigment color grouping (2008, pp. 511).

In 2008, a paper was published by Poon *et. al.* concerning the analysis of tattoo inks using Raman spectroscopy. This study, a portion of a larger research project by the primary author (concerning analysis of ancient pigments, which was described in an earlier section of this research), appears to be the only investigation of tattoo inks using micro-Raman instrumentation. The authors analyzed five inks form Millennium Colorworks, Inc. (U.S.A.), specifically a blue, yellow, red, green and black ink (pp. 1229). The analysis was conducted on a Raman microscope with a laser excitation of 632.8nm (1.8mW laser power) and a 600 line/mm grating (pp. 1231). Each ink was subjected to a solvent extraction method[3] in order to separate the organic pigment from the solution portion and any inorganic extender/lightener (titanium dioxide). The authors identified the following pigments in the tattoo inks by comparison to known pigment standards:

[3] The solvent extraction method employed by Poon, *et. al.* (2008, pp. 1229) is described in the methods and materials section of this document

Red: naphthol AS (Pigment Red 170), diarylide yellow (Pigment Yellow 14)

Yellow: diarylide yellow (PY14), titanium dioxide

Green: chlorinated copper phthalocyanine (Pigment Green 7), diarylide yellow (PY 14)

Blue: copper phthalocyanine (Pigment Blue 15:1)

Black: carbon black

In addition to direct analysis of the pigment extracted from the ink in the bottle, the authors also tattooed pig tissue and subsequently analyzed the tissue cross sections for the presence of the pigments, which were detected and compared to the known reference pigments. Upon preparation of histological sections, the researchers located pigment particles and analyzed them directly using the Raman microscope. According to the authors, even in situations where the tattoo ink is made of a mixture of pigments (as in the case of the green pigment), discrimination and subsequent identification is possible with the appropriate reference compounds and databases. With regard to sample preparation and based upon his larger research study of ancient pigments in mummified remains, Poon recommends preparing thin, histological sectioning of the tissue in the absence of embedding media and a process of flash, cryogenic freezing of the tissue samples. Both techniques are invasive, as they involve excision of a portion of tissue and both require extensive sample preparation methods.

More recently, in February of 2011, an article appeared in the New York Times reporting that a German study found “dangerous materials” in tattoo inks. The Chemischen und Veterinäruntersuchungsämter (CVUA) ter Freiburg & Karlsruhe examined a total of 38 red, orange and yellow tattoo inks in a 2010 study and evaluated the ingredients listed on the labels. The inks were found to contain “prohibited” pigments/dyes including materials that are not

regulated for tattooing or cosmetic use, and some ingredients are considered harmful and/or carcinogenic. The pigments listed include:

Pigment Reds: PR 170, PR 179, PR 210, PR 254, PR 266

Pigment Oranges: PO 13, PO 34

Pigment Yellows: PY 65, PY 74, PY 97, PY 138, PY 151

Other: Titanium Dioxide

The CVUA lists additional studies concerning tattoo inks and references a study by Regensburger, *et.al.* (2010) in which polycyclic aromatic hydrocarbons (described as carcinogenic and mutagenic) were detected in black tattoo inks analyzed with HPLC-MS. In general, current research interests in tattoo inks, especially in European countries, are concerned with the medical risks of tattoo inks and an increased desire to move toward regulating tattoo inks such that only approved, 'safe' ingredients are utilized. An additional area of interest is in optimizing laser tattoo removal techniques and is prevalent in the fields of dermatological and cosmetic medicine.

Organic Pigment Chemistry

Colorants are generally classified as to whether they are organic or inorganic, natural or synthetic, and whether they are dyes or pigments. Further classification is done according to their method of application onto a substrate (such as textile dyes), according to the chemical class of the chromophore, or on the basis of their color. Dyes are coloring materials that are partially or completely soluble in a variety of liquids, and can be applied to a variety of substrates based on their affinity to a particular substrate. Pigments are small, dry particles that are virtually insoluble in liquids and the media in which they are applied. They often require a vehicle or substrate on which they can bind in order to color materials. Dyes and pigments are similar with respect to chemistry and structure and tend to differ in application and usage.

Organic pigments are carbon-based, polycyclic compounds that contain one or more characteristic functional groups called chromophores. The shades and physical properties of organic pigments depend on the nature and number of chromophores and salt forming groups within the molecular species and the relative disposition of these functional groups within the molecule. Chromophores are classified as either chromogens, which are color generating functional groups, or auxochromes, which are color augmenting functional groups. Color-displaying molecules vary in the amount and type of functional groups they contain, which will impact the color they exhibit. The production of color is related to the resonance by delocalization of the π electrons from the presence of conjugated unsaturated systems.

Common chromogens include: C=C and -C=C-C=C-, C=O (carbonyl), C=S (thiol), CH=N (azomethine), N=N (azo), $N=N^{+}O^{-}$, N=O (nitroso), NO_2 (nitro), and ringed structures. Common auxochromes include: $-OCH_3$, -OH, $-NH_2$, NH-R, NR_2, O-R, halogens, salts, phenyls and naphthyls and other conjugated heterocyclic groups. The carbonyl and vinyl groups have

chromophoric properties only when they are present in the molecule in multiple conjugated order (Juster 1962, pp. 598).

Organic pigments include azo compounds, phthalocyanines, oxazines and quinacridones. Azo pigments are characterized by the presence of the chromophore azo group –N=N–. Lomax and Learner (2006, pp.110) further specify that most of the α-keto azo pigments exhibit tautomerism with a ketohydrazone form (see figure 29).

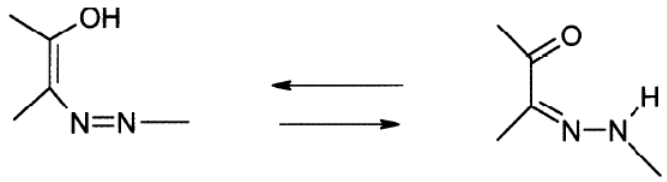

Figure 29. Hydroxyazo-ketohydrazone tautomerism in which the structure on the left represents the α-keto azo form and the structure on the right represents the ketohydrazone form (Lomax and Learner, 2006, pp.110).

The azo pigments are described as the largest class of synthetic pigments and are subdivided into the following classes based upon their general formulae: monoazo (one azo group), disazo (two azo groups), trisazo (three azo groups), and additional polyazo (four or more azo groups) classes. Pigment red 146 (PR 146, 2-hydroxy-3-naphtharylide azo pigment), pigment red 170 (PR 170, 2-hydroxy-3-naphtharylide azo pigment), pigment yellow 3 (PY 3, Hansa Yellow 10G, acetoacetarylide azo pigment), pigment yellow 151 (PY151) are examples of monoazo pigments. Pigment orange 16 (PO 16, Dianisidine Orange), pigment orange 34 (PO 34) and pigment yellow 83 (PY 83, Permanent Yellow HR) are examples of a disazo pigments. PR 146 and PR 170 are further characterized as aromatic azo compounds, with the general formula Ar–N=N–Ar' (Figure 30 a-g immediately below). Polymorphisms of PR 170 exist as α, β and γ polymorphs.

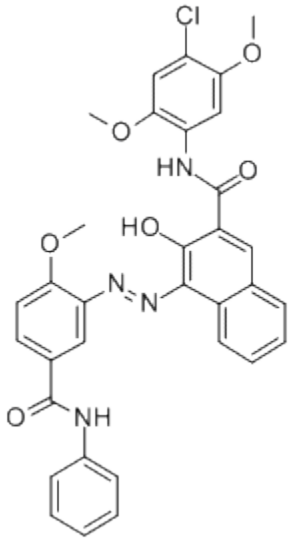

Pigment Red 146

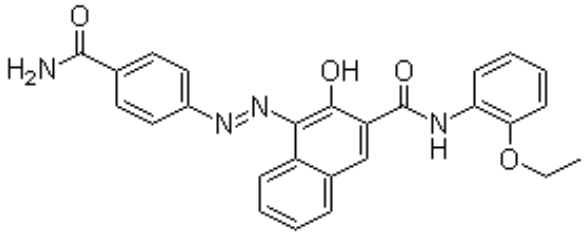

Pigment Red 170

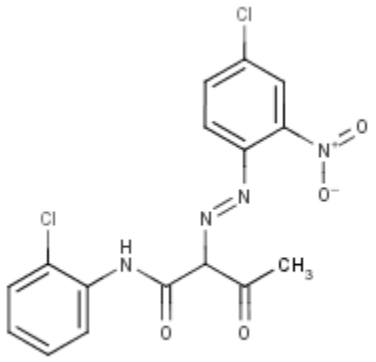

Pigment Yellow 3

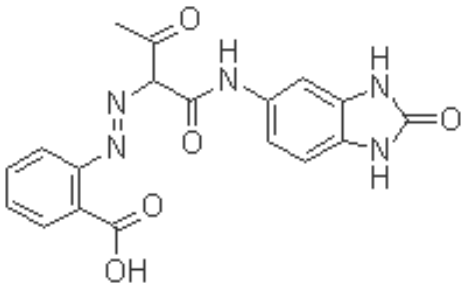

Pigment Yellow 151

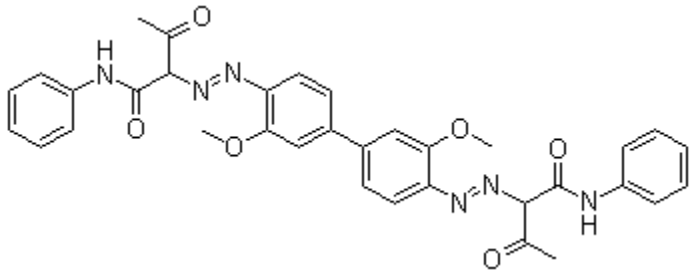

Pigment Orange 16

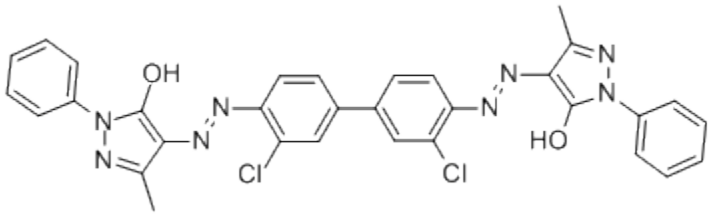

Pigment Orange 34

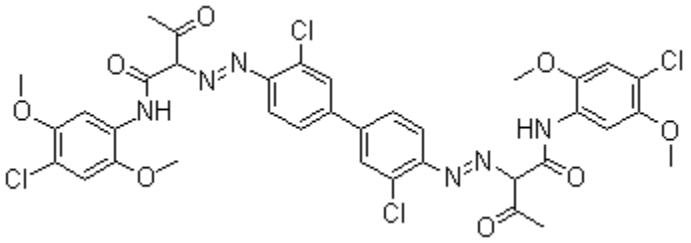

Pigment Yellow 83

Figure 30a-g. Various azo pigments.

Phthalocyanines consist of dyes and pigments that contain the tetrabenzoporphyrazine (TBP) nucleus (Figure 31 a). The principal metal ion is copper and peripheral substituents are chlorine and bromine. Pigment green 7 (PG 7, Phthalocyanine Green) and pigment blue 15 (PB 15, Phthalocyanine Blue) are examples of phthalocyanines (Figure 31b and c). Pigment blue is characterized by the copper centered within the TBP nucleus (Copper-tetrabenzo-tetraazo-porphin), and pigment green is characterized by the chlorination of the benzene rings with the copper centered TBP nucleus (chlorinated Copper-tetrabenzo-tetraazo-porphin). According to Thompson, the halogen bromine may also be incorporated along with the chlorine, where the more bromine used, the more yellow the shade (known as pigment green 36) (1977, pp. 447).

Phthalocyanines are subject to modifications through substitutions, and reports of α, β, γ, δ, ε, π, ρ, and R crystal forms of metal phthalocyanines have been described. Pigment blue 15 is the primary blue pigment in the phthalocyanines class, with nine forms of copper phthalocyanine

being reported, including four crystal forms of copper phthalocyanine. According to the Pigment Compendium (pp. 305),

> PB 15 is an unstablized (against crystal modification), non-halogenated copper phthalocyanine with the α-crystal modification, 15:1 is the same but with 0.5-1 chlorine substitutions, 15:2 is a non-flocculating version of 15:1, 15:3 is an unsubstituted β-copper phthalocyanine, 15:4 is a non-flocculating version of 15:3, and 15:6 is a stabilized, unsubstituted ε-modification form. Pigment blue 16 designates a metal-free phthalocyanine and Pigment Blue 7 is a cobalt phthalocyanine. Pigment Green 7 describes a copper phthalocyanine with 14-15 chlorine substitutions and Pigment Green 36 is a copper phthalocyanine with 4-9 bromine and 8-2 chlorine substitutions.

The color attributed to the phthalocyanines is due to both the inorganic metal ion of the central copper atom (described in the crystal field theory developed by Bethe and van Vleck) and the organic conjugated bond system of the annulated system.

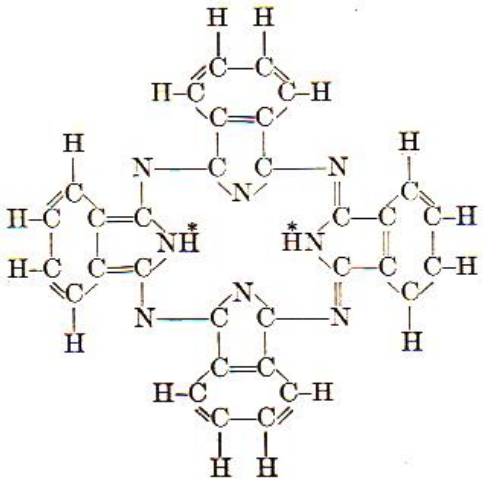

Tetrabenzoporphyrazine nucleus

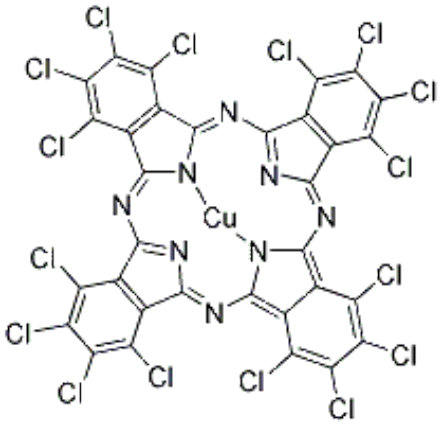

Pigment Green 7

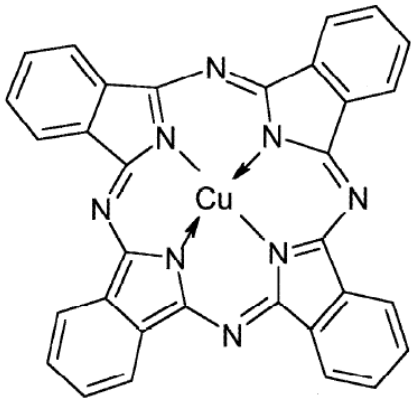

Pigment Blue 15

Figure 31 a-c. The phthalocyanines.

Oxazines are characterized by the presence of the chromophore oxazine ring, which forms the center of three condensed rings (Figure 32, top). Pigment violet 23 (PV 23) is an example of a dioxazine, a linear system of five anellated rings (Figure 32, bottom). According to The Pigment Compendium, PV 23 is used to shade phthalocyanine pigments, to counteract the yellowish cast of titanium dioxide whites and to shade carbon-based blacks that have a brownish cast (2008, pp. 309). Polymorphisms of PV 23 exist as α, and β polymorphs.

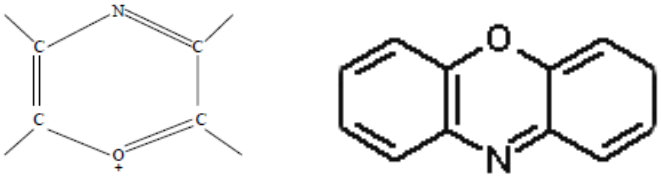

Oxazine ring, left, and bound into a three ringed structure, right

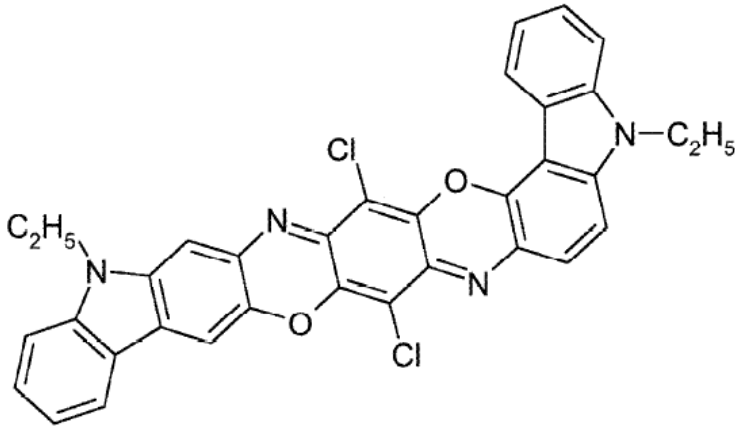

Pigment Violet 23

Quinacridones are a ring system with the following general structure (the linear, trans form is shown below in figure 33a).

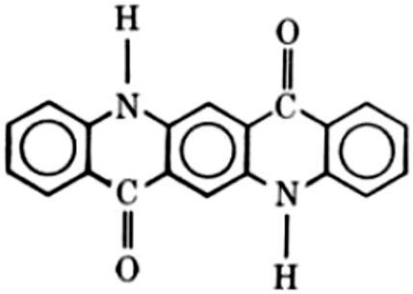

Pigment red 122 (PR 122), 2,9-dimethyl-quinacridone, is an example of a quinacridone (figure 33b below). It is describes as a linear cis-quinacridone and is reported to have α, β and γ forms.

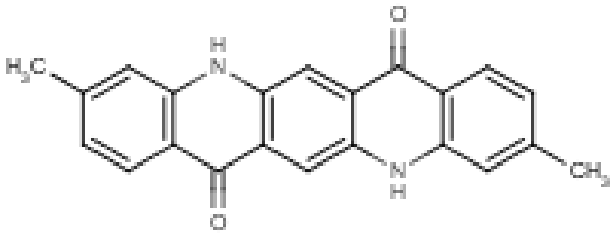

An extensive amount of literature concerning the chemical analysis of pigments can be found within a vast array of scientific journals, with the focus of these articles addressing color science, forensic science and art conservation science. Scherrer, *et. al* (2009) appear to have the

most comprehensive spectral reference collection of synthetic organic pigments to date, which includes approximately 120 pigments (excitation wavelength varied). The pigments analyzed include (pp. 508-510):

Pigment Red: 2, 3, 4, 5, 7, 8, 9, 10, 11, 12, 16, 18, 48:3, 49, 49:1, 49:2, 53, 53:1, 57, 57:1, 68, 83:1, 112, 122, 144, 146, 149, 166, 170, 179, 185, 187, 188, 214, 242, 254, 255, 264

Pigment Orange: 5, 13, 34, 36, 43, 48, 49, 62, 73

Pigment Yellow: 1, 1:1, 2, 3, 5, 10, 16, 65, 73, 74, 81, 83, 93, 95, 97, 109, 111, 120, 129, 139, 150, 151, 154, 155, 175, 181, 194

Pigment Green: 7, 9, 36

Pigment Blue: 15, 15:1, 15:2, 15:3, 15:4, 15:6, 16, 60

Pigment Violet: 5, 19, 23, 32, 36, 37

Pigment Brown: 23, 25

A 2008 article by Shulte *et. al.* contains reference spectra of 23 pigments (excitation wavelength varied), including (pp. 1457):

Pigment Red: 2, 49, 83:1, 88, 122, 123, 146, 176, 179, 181

Pigment Orange: 13, 34, 43

Pigment Yellow: 3, 83, 109, 110

Pigment Green: 7

Pigment Blue: 15:3

Pigment Violet: 1 , 2, 5:1, 19

A 2000 article by Vandenabeele *et.al.* contains reference spectra of 21 azo pigments. This database is limited to red and yellow pigments, and the excitation wavelength used was 780nm. The pigments compromising the database include (pp. 510-511):

Pigment Red: 3, 8, 9, 17, 22, 23, 49:1, 52:1, 53:1, 57:1, 112, 170

Pigment Yellow: 1, 3, 12, 13, 14, 17, 83, 65, 74

A 2010 article by Colombini *et.al.* contains reference spectra of 23 orange and yellow organic pigments (in addition to fluorescent orange and yellow pigment samples), which were analyzed using 514nm and 785nm excitation wavelengths. The pigments compromising the database include (pp. 17):

Pigment Orange: 34, 36, 43, 48, 49, 59, 61, 65, 73

Pigment Yellow: 1,3, 16, 24, 74, 83, 109, 129, 138, 139, 151, 154, 173

Ropret, *et.al.* (2008, pp. 488-489) present a reference library of 21 yellow pigments, which were analyzed with an excitation wavelength of 785nm. The yellow pigments analyzed include PY 6, 73, 75, 97, 111, 213, 100, 55, 81, 16, 155, 95, 128, 151, 154, 129, 153, 109, 110, 173 and 139.

Several of these pigment reference spectra can be found in Appendix I.

Chapter 3: Methods & Materials

Tattoo Inks and Analysis

Selection of tattoo inks for this study was based on origin of manufacture (U.S.A., Brazil and China) and color variation (red, orange, yellow, green, blue, purple, white, brown, gray and black). Each tattoo ink was obtained in its original bottle and the details of each ink were recorded form the label (including name, ingredients, lot number and production date). An effort to locate any chemical information was attempted, for example, a search for MSDS sheets. MSDS sheets were located for the U.S. manufactured Skin Candy inks[4] (these MSDS sheets were dated 2010 and thus may not correspond to those in this study in which production dates dated 2008 and 2009). MSDS sheets (or the equivalent) were not located for inks from Brazil and China.

The tattoo inks included in this study are detailed below:

Iron Works Brasil (Made In Brazil): Vermelho (Red), Pink, Citrus (Orange), Amarelo Canario (Canary Yellow), Amarelo Fluor (Fluorescent Yellow), Verde Claro (Green), Azul Royal (Royal Blue), Magenta, Lilas Claro (Lilac/Light Purple), Preto Escuro (Dark Black).

The contents listed on the packaging for all Iron Works Brasil inks include (translated from Spanish) "mineral/organic pigment, distilled water (dH_2O), surfactant, humectants, preservative." No information is given regarding specific pigment contents.

[4] http://skincandytattoosupply.com/ (Important Links → MSDS Reports)

Figure 34. Iron Works Brasil Tattoo Inks used in this study

Skin Candy (Made in the United States of America): Candy Apple Red, Red Hot, Marz (Orange), Dolemite (Orange-Yellow), Blisterene (Yellow), Sassygrass (Green), Tastywaves (Blue), BellBottom Blue, S.R.V. Teal 2, Razberry Creem (Pink), Muddy Water Blue, Ripple (Purple), San Brownadino (Brown), Whitegirl, Tokyo Pink, Dark Cherry Roan 1, 2 and 3 (Neutral Brown hues).

The contents listed on the packaging for Skin Candy inks include "distilled water (dH_2O), polyethylene glycol, witch hazel and 'proprietary'." Information is given regarding specific pigment contents with the exception of Tokyo Pink, which lists no contents on its bottle.

Figure 35 a-c. Skin Candy Tattoo Inks used in this study (Note: the bottle of Whitegirl is not included in the series of photographs)

Information concerning the pigment compositions of the Skin Candy Tattoo Inks is provided below. A detailed review of the molecular structure and chemistry of each pigment is provided in the *Organic Pigment Chemistry* section of this document. Although the inks were dated 2008 and 2009 while the MSDS sheets were labeled 2010, there was agreement between the MSDS sheets and contents listed on the labels. This indicates that, according to the manufacturer's records, the chemical composition of these particular tattoo inks has not changed within the last couple of years.

Skin Candy Tattoo Inks (contents, from packaging label: distilled water, polyethylene glycol, witch hazel, "proprietary")	
Candy Apple Red	CI 12485 (PR 146)
Red Hot	CI 12475 (PR 170)
Marz	CI 21160 (PO 16)
Dolemite	CI 13980 (PY 151), CI 21108 (PY 83)
Blisterene	CI 11710 (PY 3), CI 21115 (PO 34), CI 77891 (TiO_2)
Sassygrass	CI 74260 (PG 7), CI 11710 (PY 3), CI 21115 (PO 34)
Tastywaves	CI 77891 (TiO_2), CI 74260 (PG 7)
Bell Bottom Blue	CI 74160 (PB 15), CI 77891 (TiO_2)
S.R.V. Teal 2	CI 74160 (PB 15), CI 74260 (PG 7), CI 77891 (TiO_2)
Razberry Creem	CI 73915 (PR 122), CI 77891 (TiO_2)
Muddy Water Blue	CI 74160 (PB 15)
Ripple	CI 51319 (PV 23), CI 77891 (TiO_2)
San Brownadino	CI 77491 (Fe_2O_3)
Whitegirl	CI 77891 (TiO_2)
Skin Candy Tattoo Inks (contents, from packaging label: distilled water, witch hazel, polyethylene glycol)	
Black Cherry Roan 1	CI 12485 (PR 146), CI 77266 (PBl 7- Carbon Black)
Black Cherry Roan 2	CI 12485 (PR 146), CI 77266 (PBl 7- Carbon Black)
Black Cherry Roan 3	CI 12485 (PR 146), CI 77266 (PBl 7- Carbon Black)

Table 8. Skin Candy Tattoo Inks listed ingredients (from bottle labels)

Flying Tigers (Made in China): Salmon Pink, Pink Red, Magenta, Chinese Red, Bright Red, Rose Red, Mulberry (Red), Dark Red, Orange Red, Orange, Bright Yellow, Mid-Yellow,

Yellow, Golden Yellow, Khaki, Grass Hopper (Green), Light Green, Verdancy (Green), Lawngreen, Dark Green, Blue Sky, Turquoise Blue, Cyan, Dark Cyan, Blue, Navy Blue, Dark Blue, Grape (Purple), Purple, Violet, Gray, Bright Black, Black, Eggplant Black, Black, Sayonara Suede (Gray), Dark Brown, Light Chocolate, Skin Tone, White.

The contents listed on the packaging for all Flying Tigers inks include "isopropanol, water, glycerin and 'proprietary'." No information is given regarding specific pigment contents.

Figure 36. Flying Tigers Tattoo Inks used in this study

A search of manufacturers and distributors was conducted in an attempt to assess the variation in tattoo ink manufacturing. It is apparent that some tattoo ink manufacturers will generate different brand names under their main company name. For example, Skin Candy Tattoo Inks list separate ink brands under the "Skin Candy" umbrella, including Skin Candy, Bloodline, Kabuki, Tribal One, Eternal, Dynamic, Panther and Roan Bloodline. Additional tattoo inks from other manufacturers include Intenze, Starbrite, Iron Butterfly, Alla Prima, Silverback, Black Buddha, Dynamic Color Co., Scream, Immortal, National, Fusion, Eternal, Dispersion,

Talons/Talens, Joker, Katana, Twilight MOMs Millennium and MOMs Nuclear (where MOM's is labeled as a distributor) and Chameleon (the latter two are newer, "Blacklight UV Reactive" inks), Sta-Glo and Cosmetic Colors (Huck Spaulding Distributors), Prizm, Ichiban Sumi, Forever Natural, Lightning, Flesh-Tone, EO One, Infinitink. It is difficult in many instances to ascertain common origin from distributors and may be possible by looking at the information on the bottle label (to correlate manufacturer name, location/address, *etc.*). Tattoo ink lines named after famous tattoo artists are also available, and generally are an 'artist series' of a particular manufacturer (*i.e.* Feldman's Inks). The primary Japanese manufactured tattoo ink is Kuro Sumi (a Kokkai Sumi ink was found at one distributor's website, likely a cheaper alternative to the well-known Kuro Sumi brand).

One supply company offered powder pigment for tattoo inks and recommended mixing their colors with witch hazel, their own dispersing solution (listed as "Made in the U.S.A.", but no additional information was made available), Listerine or alcohol[5]. Interestingly, the website lists (and provides an image of) Higgins black ink (Sanford). The Sanford logo is more commonly associated with clerical ink and inscription, and a subsequent search of this ink lists it as for use with technical pens, airbrushes, dip pens or brushes (not tattoo inks). In another instance, it was alleged that Pelikan ink (advertised as a drawing/fountain pen ink) was being used as a tattoo ink but was later removed from the market because its usage as a tattoo ink caused allergic reactions and led to legal ramifications.

[5] http://www.nationaltattoo.com/index.asp?PageAction=VIEWCATS&Category=3

Figure 37. Sanford Black Magic Ink available on a tattoo ink website

One problem in attempting to understand the trends in manufacture and distribution of tattoo inks is the potential for counterfeit products; for example, a search of tattoo inks on popular online marketplaces offers brand-name tattoo inks at a fraction of the cost, and a careful examination of packaging (bottle type and shape, labels) demonstrates differences between the 'originals' and those offered at a discount through online marketplaces. It is possible that the determination of counterfeiting based on comparison of chemical composition of the real and counterfeited product (as well as chemical composition and physical characteristics of the packaging and associated labels) may further enhance the usefulness of tattoo ink databases and methods of analysis.

Figure 38. Some packaging and advertisements feature a licensed logo such as these, likely in a effort to demonstrate that they are selling the original products and not counterfeit inks

Sample Preparation

The tattoo ink samples were placed on a microscope slide and allowed to dry at room temperature for several days in order to allow for evaporation of any volatile solvents. Each prepared slide was examined with a stereomicroscope followed by examination on an Olympus BH metallurgical microscope with Neo objectives using both reflected brightfield and darkfield illumination to observe and document particle and color characteristics. Each tattoo ink was photographed under darkfield and brightfield conditions.

A sample of the ink was scraped off of the microscope slide and mounted in a Cargille oil with a Refractive Index (RI) of 1.5509 [$n^{25°C}$ (+/- 0.0002) $D_{5893Å}$] for examination with an Olympus BHSP Polarized Light Microscope with DPlan PO achromat objectives. The selection of refractive index oil was made in order to allow for the ability to conduct relative refractive index measurements on the particles, if necessary. The particles were examined under crossed polars and slightly uncrossed by approximately 5-10°. Photomicrographs were obtained for each tattoo ink under uncrossed and crossed polarizing filters.

Upon removal of some ink from the slide for microscopic examination, the consistency of the tattoo inks was markedly different from one another. Some samples scraped off with little

effort (pressure) and were very powdery and dry. Other tattoo inks were difficult to scrape off of the microscope slide several and had a ‘gummy’ consistency; as if the solvent had not completely evaporated. This was especially the case for the majority of Flying Tigers tattoo inks (China). In some instances, the samples were still ‘wet’, even a year after having been mounted on the slides, left to dry and stored in a microscope box.

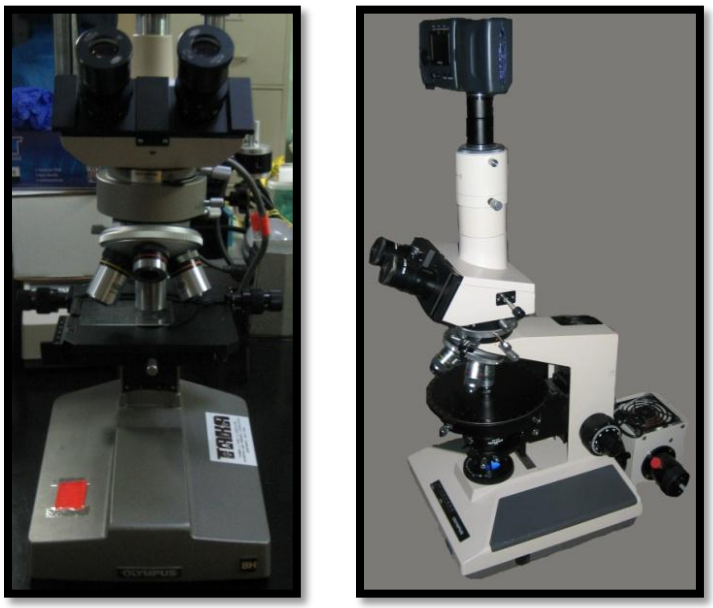

Figure 39. (left) Olympus BH metallurgical microscope and (right) Olympus BHSP Polarized Light Microscope (PLM) *[Thomas A. Kubic and Associates, TAKA]*.

A table of resultant visual and microscopic examinations was prepared to facilitate examination and comparison of the optical characteristics of the pigments, including particle sizes, color, *etc*. Visual and microscopic observations were presented in this format in order to conduct comparisons across origin of manufacture and color. The table includes images based upon visual/stereoscopic examinations, brightfield and darkfield images generated with the metallurgical microscope, crossed and uncrossed polarizers with the polarized light microscope and images generated with the Raman microspectrometer. This information is in conjunction

with any information concerning the chemical composition as provided through product labels, MSDS sheets and any additional relevant information pertaining to the ink compositions.

Instrument Calibration and Set-up

Prior to the analysis of the tattoo inks using the Raman instrumentation, several samples recommended for calibration were analyzed in order to assess the calibration guidelines outlined in the literature. Samples include Silicon, Sulfur, acetaminophen (4-acetamidophenol), cyclohexane and polystyrene. In addition, the Bruker Optics dispersive Raman employs a patented Sure-Cal procedure, which calibrates internally based on a Neon lamp within the instrument housing. A standard Sulfur sample was run prior to sample analyses in order to ensure the instrument was performing properly. In addition, samples of black (K-O Tattoo Ink), blue (Buddha Blue, Kuro Sumi Tattoo Ink, Japan) and brown (Hibachi Brown, Kuro Sumi Tattoo Ink, Japan) tattoo inks were obtained and analyzed on the dispersive Raman microscope, changing power settings of each excitation wavelength and integration times in order to assess sample damage and quality of spectra. This was used to develop a preliminary guideline for sample analysis. It was determined that it is best to start with the lowest power setting in order to limit sample damage and to increase the integration time. If there was no improvement to the spectrum (in terms of signal to noise ratio), then the power was increased. Standards were employed to serve as a function check prior to the use of any instrument.

Instrumental Analysis-Raman

The normal Raman spectra of the tattoo inks were obtained with a dispersive Raman spectrometer, specifically a Bruker Optics Senterra Raman spectrometer coupled to an Olympus microscope employing Bruker OPUS 6.5 software (Figure 14). The objectives are Olympus 100x, 50x, and 20x LM Plan Fl with numerical apertures (NAs) of 0.80, 0.50 and 0.40 and

excitation spot sizes of approximately 1 micron, 2 microns, and 5 microns, respectively. The spectrometer utilizes holographic gratings with 1200 rulings per mm (low resolution/9-15cm^{-1}) and 1800 rulings per mm (high resolution /3-5cm^{-1}) and a Si charge coupled device (CCD) detector. The excitation sources are a blue 488nm Argon ion (Ar^{+}) laser (with six fixed power settings from 0-25mW), a red 632.8nm (633nm) Helium/Neon (He-Ne) laser (with six fixed power settings from 0-20mW), and a near-infrared 785nm diode laser (with six fixed power settings from 0-100mW). In order to obtain the best spectrum for each sample, the laser power settings and integration time are varied to maximize signal without causing photodecomposition of the sample while attempting to limit or eliminate any potential background noise or fluorescence. Using the high resolution grating, the spectral ranges are set to 70-3350cm^{-1} for the 488nm laser, 70-2630 cm^{-1} for the 633nm laser and 70-2610 cm^{-1} for the 785nm laser. (Note: due to the use of longer spectral ranges, the movement of the gratings resulted in overlap in spectral regions, which would occasionally be apparent in the resultant spectrum. The regions of overlap are as follows: 488nm 1870-1880 cm^{-1}, 633nm: 1450-1520 cm^{-1}, 785nm 1500-1520cm^{-1}. It is recommended that the user be aware of the spectral stitching features of their instrument and software, as it may produce spectral distortion in regions of the spectra). The dried tattoo ink samples that had been placed on the microscope slide were analyzed by placing the microscope slide directly on the sample stage for analysis. The majority of the spectra were cropped to include the spectral region from approximately 100-1800 cm^{-1} which is considered the region where pigments exhibit their characteristic bands.

The tattoo inks were also analyzed using Fourier-Transform Raman Spectroscopy. The instruments used include a Bruker Optics Vertex 70 (Ram II) Fourier-transform spectrometer with a liquid-Nitrogen (lN_2) cooled germanium (Ge) photodiode detector with a near-infrared

1064nm Neodymium-Yttrium Aluminum Garnet (Nd/YAG) laser excitation source employing Bruker OPUS software (Figure 17) and a Thermo NXR Fourier transform spectrometer with an indium gallium arsenide (InGaAs) detector with a 1064nm laser excitation source employing Thermo OMNIC software (Figure 18). Both instruments use a calcium fluoride (CaF) beamsplitter, which is manually installed into the light path prior to sample analysis. The instrument resolution was set to 4 cm^{-1} and both the laser power setting and scan rate were varied to maximize signal without causing photodecomposition of the sample and to reduce or eliminate any potential background noise or fluorescence. For the Bruker instrument, the sample holder used is a 2mm disk with a central well for the sample material and for the Thermo instrument, the sample holder is either a glass microscope slide or a glass capillary tube. A portion of the ink on the microscope slide was scraped off and placed into the sample holder for analysis using FT Raman. A standard Sulfur sample was analyzed prior to sample analyses in order to ensure the instrument is performing properly. In instances of overwhelming fluorescence and the presence of highly absorbing species (blacks, browns, grays, and the darker purples, blues and greens), the pigment was ground with potassium bromide (KBr) and put in a glass capillary tube prior to analysis in the Thermo FT-Raman.

SERS was conducted on some of the tattoo ink pigment extracts as well as the powder pigment standards. The silver colloid was prepared using Leona's microwave digestion method (Leona, 2009). Spectra were obtained using the dispersive Raman instrument with an excitation wavelength of 488nm. The resultant spectra were compared to the normal Raman spectra at 488nm in an effort to evaluate whether or not there was any improvement in using SERS to generate spectral information, especially with samples that exhibited overwhelming fluorescence with normal Raman. The development of a SERS library of tattoo inks was also developed.

Calculations relative to Leona's preparation method were made to determine the amount of silver nitrate, sodium citrate and glucose needed to generate a substantial supply of silver colloid. The silver nitrate was converted to silver sulfate to remove any of the nitrate by formation of a silver sulfate precipitate. To generate the colloid, calculated amounts of the glucose, citrate and the silver were then combined in a microwave digestion vessel and subjected to the temperature and time controlled microwave digestion method using a CEM MDS-2100 microwave digestion system. The colloid was stored in a capped sample holder wrapped with aluminum foil and kept refrigerated. For analysis of the pigment standards, a small portion of pigment was placed on a microscope slide. An approximately 0.8 microliter drop of colloid was placed on the pigment and left for several minutes (approximately 5-10min). An approximately 0.1 microliter drop of potassium nitrate (KNO_3) was added and left for approximately 1-2 minutes. The sample was then viewed with the dispersive Raman, with the colloid-molecular species aggregate being located and analyzed with the 488nm laser (with the focus being varied as necessary). This technique was attempted with the tattoo inks, but was quite inefficient. An attempt was made to put the tattoo ink in solution using methanol, but this was limited due to solubility issues with many of the pigments. Instead of removing some of the tattoo ink from the slide, a drop of colloid (approximately 0.8 microliter) was placed directly on the tattoo ink smear and allowed to sit for several minutes (5-10min) followed by addition of the potassium nitrate and subsequent analysis with the instrument. This technique proved to be quite successful in generating interactions between the pigment and the colloid, which resulted in quality SERS spectra for several of the tattoo inks and pigments.

Examination and comparison of the Raman spectra (normal and Fourier transform) for a given pigment were conducted in order to determine whether there is band shifting and changes

in relative band intensities due to changing the excitation wavelength. While the band locations are relative for a given molecular species and most literature indicates that resultant Raman spectra of a sample are independent of the incident energy, it is anticipated that when changing from 488nm to 633nm to 785nm to 1064nm laser excitation wavelengths, there may be some shifting of bands and changes in band relative ratios. This evaluation was used to assert that the excitation wavelength is an important factor in the evaluation and comparison of questioned and known samples and should thus be noted in any Raman analysis, especially when reporting band locations in both tabular and spectral formats. Examination and comparison of the normal Raman spectra and SERS spectra were conducted to evaluate whether or not SERS was useful in enhancing weak signals and quenching fluorescence. In addition, any variation in band locations and relative band intensities is noted.

Instrumental Analysis-Infrared

The infrared spectra of the tattoo inks was obtained with a Nicolet FT-IR spectrometer employing Thermo OMNIC software with a Durascope™ (SensIR Technologies, Danbury, CT) attachment, used for micro-attenuated total reflection (ATR) infrared measurements (Figure 23). A portion of the ink on the microscope slide was scraped off and placed into the internal reflecting element for direct analysis without any additional sample preparation. A polystyrene spectrum was obtained in order to ensure the FT-IR instrument was calibrated prior to sample analysis.

Resultant Raman (normal, Fourier transform and SERS) spectra and infrared spectra from the tattoo inks were processed and displayed using Grams AI® software (Thermo-Fisher, Madison, WI). Spectral processing was minimal in an effort to minimize the amount of 'spectral manipulation' applied to the data. Peak identification was conducted in order to label and

classify the strongest bands (major) for comparison to pigment reference material and to determine the modes of vibration based on previously published correlation tables (Appendix A). All tattoo inks were evaluated to determine possible pigment compositions based upon band locations and comparison to pigment standards. Reference pigments were obtained and analyzed, where possible, in an effort to have a set of standard pigments that have been analyzed on the same instruments and under the same conditions as the tattoo inks and were used to compile known pigment databases for the various instrumental techniques employed. A list of known pigment standards obtained and analyzed in this study can be found in Table 9 below. The spectra from the reference pigments and tattoo inks were compared to data tables that are available in the literature, specifically articles by Vandenabeele *et. al.* (2000), Ropret *et. al*. (2007), Schulte *et. al*. (2008), and Scherrer *et. al.* (2009) and Colombini *et. al.* (2010). The data tables in the literature and available Raman pigment libraries within the software (Tate Pigments-Fogg Library and Metropolitan Museum of Art Pigments Library) were also used to aid in the identification of pigments in the tattoo samples.

Reference Pigments	Chemical Structure
Pigment Blue 15 Pigment Blue 15.1 Pigment Blue 15.2 Pigment Blue 15.3	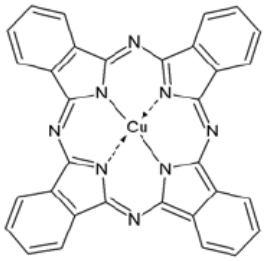
Pigment Green 7	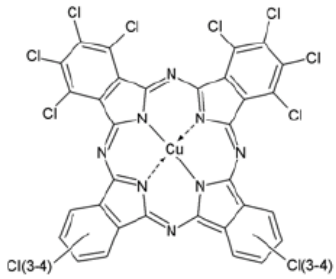
Pigment Orange 16	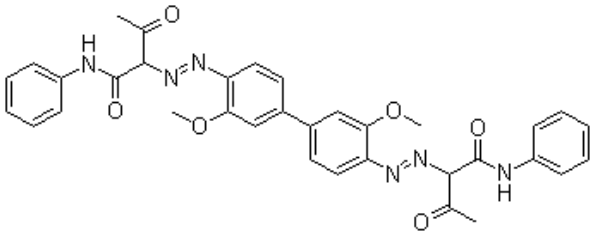
Pigment Orange 34	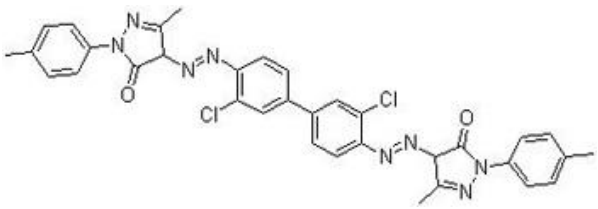

Table 9, continued

Pigment Orange 62	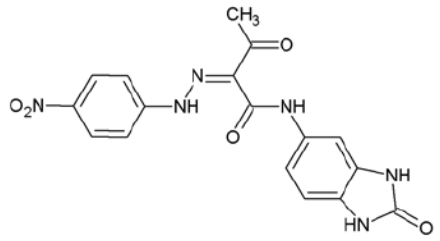
Pigment Red 122	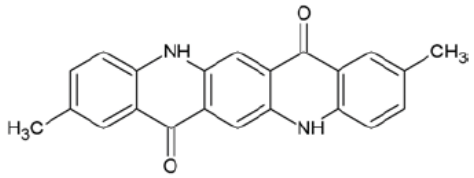
Pigment Red 146	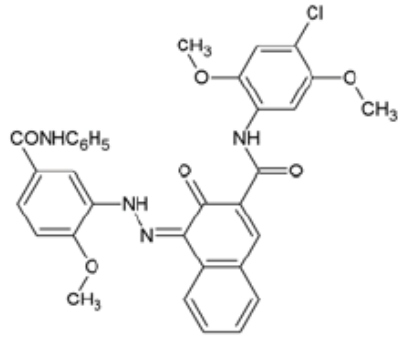

Table 9, continued

Pigment Red 170	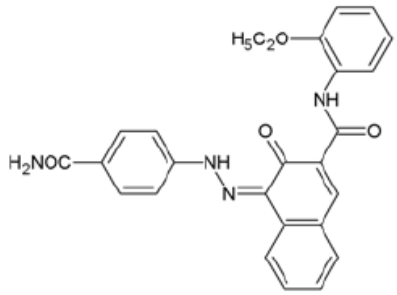
Pigment Red 255	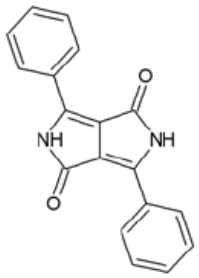
Pigment Yellow 3	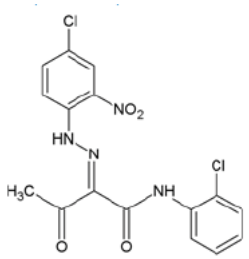
Pigment Yellow 73	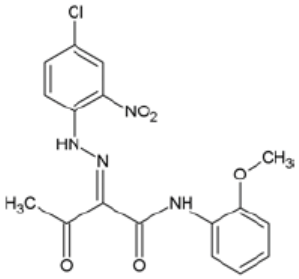
Pigment Yellow 83	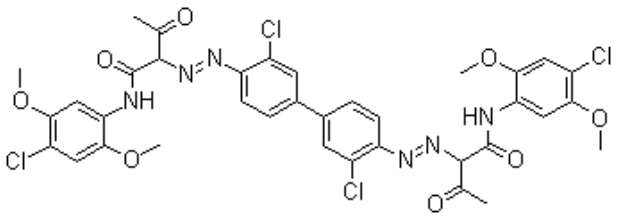

Table 9, continued

Pigment Yellow 151	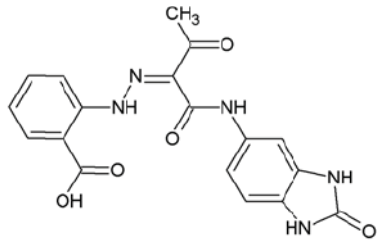
Pigment Violet 23	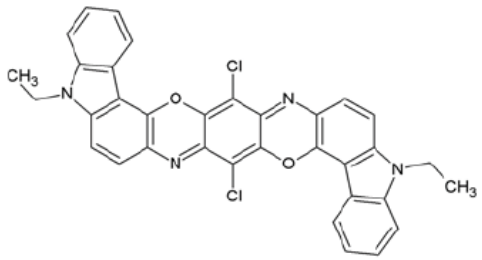

Table 9. Standard pigments analyzed in the current research.

Instrumental Analysis-X-Ray Fluorescence

X-ray fluorescence (XRF) measurements were conducted using a Bruker Artax x-ray fluorescence spectrometer. The Artax VRF employed a Rhodium target and a SiLi detector. A 1.5mm aperture was attached to the collimator in order to conduct 'bulk' analysis of the tattoo inks. The samples were prepared by placing the inks on a thin polymer sample support (Chemplex Mylar® Polyester thin film; typical impurities (ppm): Ca, P, Sb, Fe, Zn), which was pulled taut in a plastic circular sample cup. Calibration of the instrument was conducted prior to tattoo ink analysis using a Tin-Bronze sample.

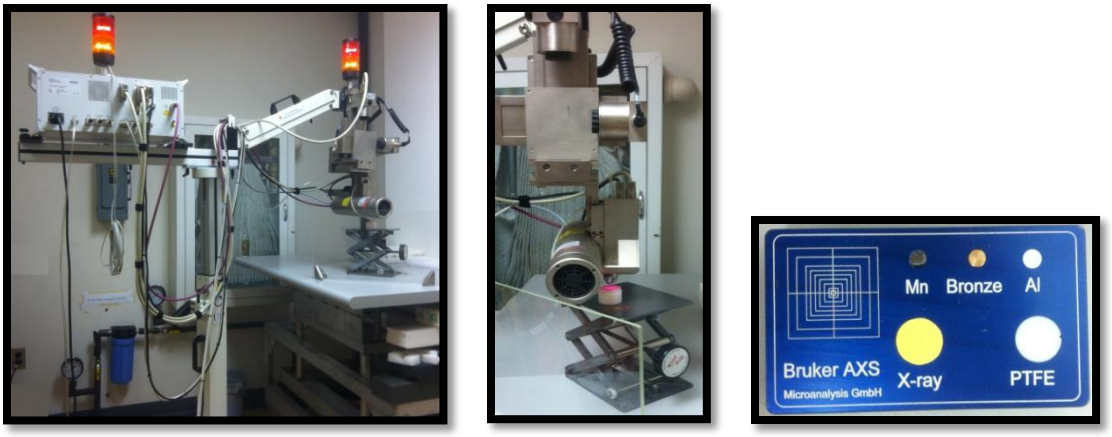

Figure 40. (left) Bruker Artex XRF, (middle), close up of sample mount and (right) mounted standards.

Instrumental Analysis-UV/Vis

The primary examination of the pigment samples was done without separating the pigment from the carrier solution, which means that there are potential matrix interferences inherent in all instrumental examinations. For example, a portion of the solution in which the pigment(s) is dispersed may produce fluorescence that inhibits the detection of the pigment. It is expected that the SERS technique will be the best way to reduce fluorescence and at the same time, enhance the signal of the pigment. Matrix effects may also render the pigment molecule unable to bind to the colloid. The solution may also present solubility issues that introduce problems in UV/Vis spectrometric measurements, which determine the absorption maxima (useful for resonance Raman). One method to minimize matrix effects is to conduct extractions of the tattoo inks in order to remove any residues from the solution and any inorganic materials (such as titanium dioxide).

As such, a solvent extraction similar to the procedure used by Poon, *et. al.* (2008) was conducted on a selection of tattoo inks to separate the pigment from the carrier solution and any inorganic substances. The extraction method was conducted and evaluated in order to provide an

accurate method for the extraction and recovery of the organic pigment portion of the tattoo ink. The extraction procedure was also able to elucidate whether or not an inorganic pigments such as titanium oxide was present in the tattoo ink. This extraction process would allow for recovery and subsequent instrumental analysis of the inorganic portion, for example, analysis of titanium dioxide in order to confirm its presence and identify its polymorph (of the three forms of titanium dioxide, only anatase and rutile have been reported as being found in tattoo inks).

A selection of extracted pigments were analyzed using both Raman (normal and FT-Raman) and infrared (ATR) techniques, and a comparison of spectral data between direct analysis of the tattoo ink and the extracted pigment(s) was conducted to elucidate any differences in data according to the state of the sample. In order to assess the resonance effects of the tattoo inks, some of the tattoo inks were analyzed using UV/Vis spectrometry. The region of absorption of the tattoo ink can provide additional insight into the best excitation wavelength necessary to get maximum signal and quality spectra due to resonance effects. The solubility of the pigments and additional wet chemistry methods may provide insight into chemical composition and general tattoo ink differentiation. It should be noted that there may be problems associated with extraction techniques, including contamination, incomplete or inefficient extraction of the pigment and possibility of changing the form of the chromophore or overall structure of the molecule. With regard to extractions, White *et.al.* (1998, pp. 82) report that it is important to control both the pH and solvent polarity during extraction to ensure there are no changes to the chemical structure of the dye, as this change my impact the resultant Raman spectrum and lead to problems in identification.

With regard to differentiation of organic and inorganic pigments, separation was conducted using solvent extraction methods. Generally, inorganic pigments are expected to be

heavier than the organic components, and it is expected that centrifugation coupled with solvent extraction will aid in the separation of organic and inorganic components. Due to its extensive use as a lightener, it is hypothesized that the majority of inorganic material recovered will consist of titanium dioxide. Caution must be taken during extraction, since some organic pigments, such as the phthalocyanines, may behave more like inorganics due to their composition and molecular structure, specifically the presence of the copper and chlorine atoms. According to the procedure in Poon *et. al.*, (2008, pp. 1229) separation and isolation of the pigments was done by transferring an aliquot of tattoo ink to an Eppendorf™ tube with water and centrifuged at 12,000 RPM for ten minutes. After discarding the supernatant, the water wash process was repeated for a total of three washes. After air drying for thirty minutes, carbon tetrachloride was added to the precipitate and again centrifuged at 12,000 RPM for ten minutes. The authors describe "a defined partition in the precipitate clearly observed between the organic pigment layer and the denser extender/lightener" (Poon, 2008, pp. 1234). It should be noted that the solvent extraction was conducted on a small number of samples with not all colors represented. Therefore, where this extraction method may have been suitable for the limited sample size, it may not be as efficient with a wider variety of samples. It is likely that solvent extraction with water or an organic solvent may not be suitable in all instances, and the extraction may require a solvent such as methylene chloride or chloroform in order to increase the extraction efficiency.

Spectrophotometric measurements made with the UV/Vis require consideration of pigment solubility; the pigments will need to be dissolved in an appropriate solvent (such as acetone [CH_3COCH_3], methanol [CH_3OH], cyclohexane [C_6H_6], methylene chloride [CH_3Cl] or a dilute (0.1M) or concentrated acid [for example sulfuric acid, H_2SO_4]). Due to the change in protonation with a change in pH, any wavelength shifts (bathochromic, shift toward longer

wavelengths [red shift], or hypsochromic, shift towards shorter wavelengths [blue shift]) in the UV/Vis spectra will be documented along with any potential pigment color changes, as these observations can aid in pigment identification and classification.

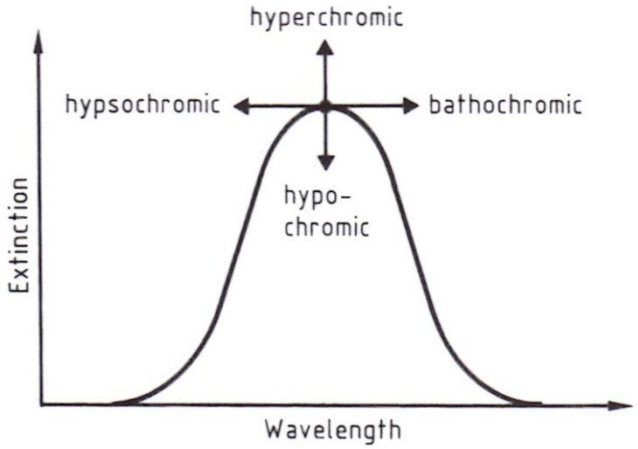

Figure 41. Shifts observed in UV/Vis Spectrophotometry (Adapted from Zollinger, 2003, pp. 18)

The UV/Vis spectrophotometer is an instrument in which a monochromatic light is passed through the sample (which is in a sample holder such as a cuvette made of quartz or silica and having a fixed pathlength), to the detector. Wavelength selection is done by either a filter or a monochromator. The technique is based upon the detection of electromagnetic radiation generally from the region of 160nm to 780nm (abscissa) in solution measurements wherein a solution's percent transmittance (%T) or absorbance (abs.) is plotted on the ordinate. The measurement is made against a reference, which typically consists of the solvent used to dissolve the pigment.

Billmeyer, *et.al.* (1981) describe a range of solvents useful for dissolving organic pigments for solution spectrophotometry. According to the authors, concentrated sulfuric acid (H_2SO_4) is the most powerful solvent for all organic pigments, having the ability to dissolve

virtually all pigments of this type. A series of solvents is listed according to their solubility parameter (defined as a measure of the cohesive energy which must be overcome in the solution process), in which the components of the solubility parameter include dispersion, dipole and hydrogen bonding. Useful solvents include pentane, cyclohexane, carbon tetrachloride, toluene, xylene, chloroform, methylene chloride, ethyl acetate, acetone, pyridine, ethanol, dimethyl formamide (DMF) and methanol. It is important to consider the effect the solvents will have on the absorption maxima; while these shifts may be useful for identification of the pigment using solution spectrometry, the shifts may provide misleading information pertaining to molecular resonances. This is especially the case with concentrated sulfuric acid, in which the authors note that there are often drastic shifts in absorption maxima and visible color changes when using this solvent (pp. 308). H_2SO_4 is not only a solvent, but also a sulfonation reagent and catalyst that can cause acid hydrolysis of amide bonds (Zollinger, 2003, pp. 414).

According to Billmeyer, *et.al.* , pigment yellow 3 will dissolve in all of the solvents tested but gave different spectra depending on solvent polarity, with a hypsochromic shift occurring with polar solvents and a bathochromic shift occurring with conc. H_2SO_4 (1981, pp. 308). Pigment reds 146 and 170 were found to be mostly soluble in all solvents tested with the exception of cyclohexane. Their behavior is reported as being similar to that of pigment yellow 3 (1981, pp. 309). Disazo pigments, such as pigment orange 16 and pigment yellow 83 are soluble in toluene, xylene, chloroform, DMF and conc. H_2SO_4 (1981, pp. 309). Pigment violet 23 was reported as being soluble in weakly polar solvents such as toluene, xylene and chloroform, insoluble in acetone and methanol, and soluble in DMF and H_2SO_4. The authors add that in DMF and H_2SO_4, the solutions are fluorescent (1981, pp. 309). Pigment red 122 is soluble in ethanol: NaOH (9:1), DMF and H_2SO_4. These solutions also exhibit fluorescence (1981, pp.

309). The phthalocyanines (pigment blue 15 and pigment green 7) are reported as being only soluble in conc. H_2SO_4. The authors add that the absorption maxima of these solutions are shifted from the visible region to the near infrared (between 800 and 900nm) (1981, pp. 309-310).

Of important note in their research, the authors assert that Beer's law holds for solutions of inorganic pigments in the solvents used, allowing for the possibility of quantitative analysis to be conducted in addition to the qualitative analysis presented. In addition, an analytical scheme is provided by the authors in order to facilitate the separation and identification of samples that may be composed of two or more pigments (Billmeyer, *et. al.*, 1981, pp. 311-312).

UV/Vis measurements were made with a Shimadzu UV-2550 UV/Vis spectrophotometer. Pigment standard samples and pigment extracts from the selected tattoo inks were dissolved in concentrated hydrochloric acid and placed in a 1mm path length fused silica cuvette. Concentrated sulfuric acid was used as the solvent in order to ensure complete dissolution of the pigment. Although this solvent can have a great effect on the molecular chemistry of the pigments, it is well-suited for the dissolution of the phthalocyanines and their metal complexes. Furthermore, for identification and comparison, it was important to maintain a single solvent system for all pigments. It is also important to note that the UV/Vis analysis and corresponding solution chemistry were intended for qualitative, not quantitative analysis (thus strict adherence Beer's Law was not factored into the spectroscopic analysis). The initial color change upon addition of the pigment particles into the concentrated sulfuric acid was recorded, and absorption measurements were extended beyond the visible region of the electromagnetic spectrum (approximately 400nm-700nm) into the near infrared region (to approximately 900nm) to account for any bathochromic and hypsochromic shifts due to the use of the conc. H_2SO_4 (as

reported by Billmeyer, *et. al.*, 1981). The samples were analyzed against a solvent blank of concentrated sulfuric acid. Holmium oxide and didymium glass reference spectra were obtained in order to ensure the UV/Vis instrument was calibrated prior to sample analysis. Instrument settings were set at the following:

Wavelength range (Absorbance, x axis): 200-1000nm
Scan speed: Medium
Sampling Interval: 0.5nm
Slit Width: 1nm

Figure 42. Shimadzu UV-2550 UV/Vis spectrophotometer [John Jay College of Criminal Justice, CUNY].

The color of the pigment before and after dissolution in concentrated H_2SO_4 was noted in an effort to make preliminary assessments about absorption and to determine whether or not a bathochromic or hypsochromic shift may have occurred upon dissolving in the concentrated acid. It has also been suggested that upon separation of pigment mixtures by thin layer chromatography (TLC), spraying the plate with concentrated H_2SO_4 can provide a useful color test to determine pigment class (Thomson, 1977, pp. 434).

λ Wavelength absorbed (Å)	Color observed (transmitted)
4000 (violet)	greenish-yellow
4250 (dark blue)	yellow
4500 (blue)	orange
4900 (blue-green)	red
5100 (green)	purple
5300 (yellow-green)	violet
5500 (yellow)	dark blue
5900 (orange)	blue
6400 (red)	bluish-green
7300 (purple)	green

Table 10. Relationship between absorption and transmission (Adapted from Juster, 1962, pp. 596).

Method Development

A general scheme of analysis for tattoo inks includes microscopic examination (such as polarized light microscopy to determine optical properties in addition to particle dispersion and particle size), wet chemistry (solvent extractions and solubility testing) and instrumental analysis (UV/Vis, Raman spectroscopy, infrared spectroscopy). Additional analytical techniques to determine the inorganic composition of the tattoo inks should be conducted to include bulk x-ray fluorescence (XRF) or electron microprobe analysis using low vacuum SEM/EDS instrumentation (although care should be taken in interpretation due to the potential difference in results from a bulk technique and a more area specific technique such as SEM/EDS). Chromatography can also be used to identify ink composition, including thin layer chromatography (TLC), gas chromatography (GC) and high performance liquid chromatography (HPLC) All techniques employed should consider both the pigment portion and vehicle portion of the tattoo inks.

Density Functional Theory (DFT) Calculations

Of the tattoo ink samples obtained for this study, only the Skin Candy brand lists the pigments in the ingredients section of the label (and provides MSDS sheets). Three pigments from the Skin Candy Tattoo Inks were selected for DFT calculations, selection was made based on the following criteria: the pigment composition of the tattoo ink (only pigments with one pigment listed according to the ingredients list were considered to avoid any affects from pigment mixtures), the type of pigment (chemical class and structure) making up the ink, and the resultant spectra of the tattoo inks and pigment standards obtained from instrumental analysis using infrared and Raman spectroscopies. Pigment red 170 (monoazo), found in Red Hot tattoo ink, was selected because all of the normal Raman spectra of the tattoo ink were considered good quality (a substantial amount of bands were detected and the bands were well resolved). Pigment red 122 (quinacridone), found in Razberry Creem tattoo ink was selected because none of the normal Raman spectra of the tattoo ink would be considered good quality; all spectra exhibited fluorescence and little to no peaks were resolved. Pigment orange 16 (disazo; found in Marz tattoo ink) produced moderate quality Raman spectra, where the overall quality of the spectra were dependent upon the laser excitation wavelength.

Some of the known, listed pigments were evaluated via group theory (to determine the symmetry elements of the pigment molecule) followed by entering these selected pigment molecules into DFT calculation software in order to obtain the predicted Raman and infrared spectra. A comparison of the experimentally observed Raman (normal, Fourier transform and SERS) and infrared spectra for selected pigment molecules with the theoretical DFT (mathematically generated spectra) was conducted to evaluate the correlation between experimental and calculated vibrational spectra.

The molecules were generated using ChemDraw and imported in to GaussView5™ (Gaussian, Inc., Wallingford, CT) to build the molecule, followed by entering the molecule into the Gaussian03™ software (Gaussian, Inc., Wallingford, CT) to conduct the computational chemistry portion. GaussView5™ is a graphical interface that enables the building and defining of features of molecular structures for submission to Gaussian03™ and subsequent retrieval of calculations from Gaussian03™. Gaussian03™ is a software program that predicts molecular structures, molecular properties, energies and vibrational frequencies using fundamental quantum mechanics. After defining the molecule and setting up the desired parameters for analysis in GaussView5™, Gaussian03™ was used to predict vibrational Raman and infrared spectra, which was then compared to experimental spectra. The Gaussian03™ software assumes harmonic frequencies, in which the change in dipole moment is linearly proportional to nuclear displacement. As described previously, most molecules are more accurately characterized as anharmonic systems.

The pigment molecules were made planar initially with the exception of Pigment Red 170 where it was not possible to achieve planarity. In GaussView5™, the molecules were "cleaned" in order to correct for bond angles and bond lengths and any additional geometric oddities. This process is done to prevent errors in the DFT analysis, where errors such as closeness of adjacent or localized atoms could stop the DFT calculation. This assessment of the molecule is a subjective process in which the analyst and the Gaussian program re-orient the molecule so that it looks structurally sound. Although "cleaned" and restructured, the planarity of the molecules was maintained.

All molecules were subjected to an optimization process in Gaussian prior to running the DFT calculations, in which the Gaussian program attempts to orient the molecule in its lowest

energy structure in order to minimize the total energy of the ground state as a function of the molecule's electron density. The optimization was done using the STO3G (Slater-type orbital in which three Gaussian orbitals are fit) minimal basis set, which is used to make a preliminary determination of the geometry of an organic molecule.

After completion of the initial optimization, the resultant molecules were subjected to a second optimization and frequency calculation in order to generate vibrational spectra. The basis set used was 6-311G d,p with no diffuse functions applied. The frequency calculation method used was RB3LYP (described as density functional Becke's three parameter hybrid method which uses the LYP correlation function). Point groups were not assigned and the symmetry elements were not considered for the molecules.

After minimizing the energy of the molecule and optimizing the molecule's geometry, the Raman and infrared spectra were obtained with the Gaussian software. The frequencies of the spectra are obtained by determining the change in energy that results from the molecular displacements from the normal modes of vibration. Several differences are noted between the experimental and calculated spectra, including the matrix effects of the molecule. Gaussian assumes one pigment molecule in a vacuum, while the actual experimental techniques were done on pigments within a tattoo ink matrix (ingredients are described on each ink's bottle) and pigments extracted from this tattoo ink. These differences can account for the presence or absence of bands, band shifting, band heights and relative band intensities, since each individual vibration in a molecule is not isolated, but is coupled with and affected by other vibrations.

Pigskin Study

The initial portion of this research project was directed towards the evaluation and characterization of tattoo inks since, while there is an abundance of literature concerning organic pigments, there is a deficiency in the amount of comprehensive analytical information concerning tattoo ink composition and chemistry. Reference material, instrumental libraries or standard operating procedures need to be developed for the analysis and identification of tattoo inks. Upon completion of the analysis portion of the neat tattoo inks, a study of tattoo inks in tissue was conducted. Known tattoo ink was injected into pigskin using a tattoo gun and standard tattooing procedures and an attempt to analyze the inks in a minimally invasive fashion was conducted. The tattooed pigskin was preserved by freezing of tissues and storing the tissues in formalin (1:10 dilution, buffered-- formaldehyde, sodium phosphate, deionized water) in order to assess the effect of preservation on the tissue and tattoo ink. Formalin fixation preserves the tissue by preventing autolysis and stabilizing tissue structure and formalin fixation promotes the cross-linkage of amine groups in collagen (Huang, *et.al.*, 2003, pp. 649, 650)

An attempt to analyze the tissue sample directly was conducted first. If the ink was not detected by direct analysis then histological sectioning and affixing the tattooed tissue to slides in order to microscopically observe the pigment particles within the tissue and isolate the particles for spectral analysis would be considered. If it is not possible to detect the pigment particles in the tissues directly by either direct or sectioning methods, an attempt to extract the pigment from the tissues using hydroxyl gel techniques (as described by Leona, *et. al.*, 2011) was considered as an alternative. In addition, attempts to introduce silver nanoparticles on to the surface of the tissue or inject them into the tissue followed by SERS could serve as an alternative to detect the tattoo ink in the tissue.

A section of pigskin was obtained from a local butcher and stored in a refrigerator prior to tattooing. A tattoo artist was directed to tattoo two series of seven successive dots into the pigskin using the same Skin Candy tattoo inks analyzed in this research as follows:

White Girl, Red Hot, Marz, Blisterine, Tastywaves, Muddy Water Blue, Ripple

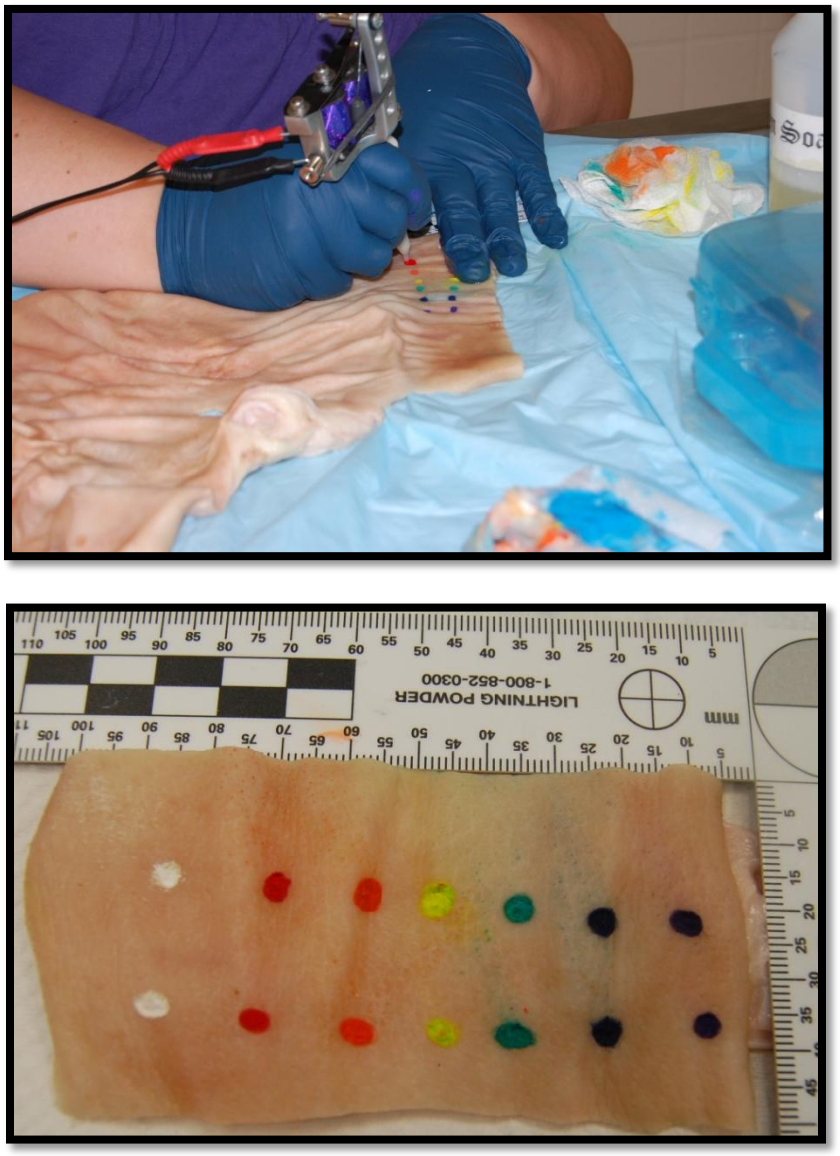

Figure 43. Tattooing of pigskin and resultant tattoos.

The skin was cut in between the two rows, with one set of colored dots being placed in formalin (1:10 dilution, buffered) and the other row being frozen. The tattooed skin samples

were then analyzed with the dispersive Raman using the three laser excitation wavelengths available (488nm, 633nm, 785nm).

A correlation to the resultant data with effects of the environmental conditions that produce post-mortem changes in tissue such as charring, decomposition and mummification are made. Consideration is also give to the possibility of detecting tattoo inks and pigments in instances where the tissue has healed and the pigment was able to migrate deeper into the skin. A proposed timed study analyzing a tattoo via Raman spectroscopy as the pigments migrate into the deeper layers of tissue and as the tissue heals is presented. The goal is to develop a method for detecting tattoo inks *in situ* with the most minimally invasive techniques, including conducting an analysis without the need to excise tissue from the body. Due to the current trends towards hand-held Raman spectrometers, this would be ideal and allow for more routine analysis of living and cadaveric tissue, and tissue in which removal of samples is undesired or nearly impossible, such as forensic specimens of limited size and historical samples in museums.

Summary

The Iron Works Brasil Tattoo Inks were examined and photographed microscopically and instrumentally analyzed with dispersive micro-Raman (488nm, 633nm, and 785nm excitation wavelengths), SERS (488nm), FT-Raman (1064nm), FT-IR (ATR) and XRF. The various Raman spectra of these inks were compared to evaluate that variation in techniques and laser excitation wavelength. A comparison of the dispersive Raman spectrum at 488nm was compared to the SERS spectrum obtained at 488nm for each ink in order to validate the use of SERS in routine analytical work. In addition, these inks were compared to pigment standards and libraries in an effort to determine the pigment composition of the tattoo inks.

The Flying Tigers Tattoo Inks were examined and photographed microscopically and instrumentally analyzed with dispersive micro-Raman (488nm, 633nm, and 785nm excitation wavelengths), FT-Raman (1064nm), FT-IR (ATR) and XRF. In addition, the Flying Tigers Tattoo Inks were subjected to the extraction method described earlier. The extracts were instrumentally analyzed with dispersive micro-Raman (488nm, 633nm, and 785nm excitation wavelengths). The various Raman spectra of these inks were compared to evaluate that variation in techniques and laser excitation wavelength. In addition, the dispersive micro-Raman spectra of the tattoo inks were compared to those of the pigment extractions to evaluate the usefulness of conducting extractions on tattoo inks. These inks were compared to pigment standards and libraries in an effort to determine the pigment composition of the tattoo inks.

The Skin Candy Tattoo Inks were examined and photographed microscopically and instrumentally analyzed with dispersive micro-Raman (488nm, 633nm, and 785nm excitation wavelengths), SERS (488nm), FT-Raman (1064nm), FT-IR (ATR) and XRF. In addition, the Skin Candy Tattoo Inks were subjected to the extraction method described earlier. The extracts

were instrumentally analyzed with dispersive micro-Raman (488nm, 633nm, and 785nm excitation wavelengths), FT- Raman (1064nm), FT-IR (ATR) and UV/Vis. The various Raman spectra of these inks were compared to evaluate that variation in techniques and laser excitation wavelength. A comparison of the dispersive Raman spectrum at 488nm was compared to the SERS spectrum obtained at 488nm for each ink in order to validate the use of SERS in routine analytical work. The Raman (normal and FT) and FT-IR spectra of the tattoo inks were compared to those of the pigment extractions to evaluate the usefulness of conducting extractions on tattoo inks. The resultant UV/Vis spectra were described and compared to that of known pigment standards. In addition, these inks were compared to pigment standards and libraries in an effort to determine the pigment composition of the tattoo inks.

The selection of known pigments were instrumentally analyzed with dispersive micro-Raman (488nm, 633nm, 785nm and 1064nm excitation wavelengths), SERS (488nm), FT-IR (ATR) and UV/Vis.

The pigments found in three of the Skin Candy Tattoo Inks (Red Hot-Pigment Red 170, Marz- Pigment Orange 16, and Razberry Creem- Pigment Red 122) were subjected to DFT calculations in order to compare the experimental spectral data (Raman and infrared) with the calculated spectral data. For the resultant spectra, the Raman bands were correlated to vibrational modes considering group theory and molecular symmetry. Assignment of vibrational modes to resultant bands was conducted.

A selection of Skin Candy Tattoo Inks (specifically White Girl, Red Hot, Marz, Blisterine, Tastywaves, Muddy Water Blue, Ripple) were used to tattoo pigskin. First, direct analysis using dispersive micro-Raman was conducted in an attempt to detect the inks. Other methods were considered as alternatives. Upon obtaining spectral data, the tattoo inks in pigskin

were compared to the original data obtained when the tattoo inks were analyzed directly on the microscope slides. Additional consideration was given to environmental factors that may affect the tissue in ‘real world’ cases and time-studies that result in the healing process and pigment migration.

All spectra played an integral part in establishing analytical methodology and searchable databases, both for tattoo inks in general and with regard to the specific instrumental techniques employed (namely dispersive Raman, FT-Raman, SERS and FT-IR/ATR). Furthermore, this research was able to validate SERS as a viable technique for use in conservation and forensic laboratories.

The following data tables summarize samples analyzed and techniques employed in analysis:

	Normal Raman (Dispersive)			SERS	FT Raman	FT-IR	XRF	Microscopy	
	488nm	633nm	785nm	488nm	1064nm	Durascope			(extraction)
IRON WORKS BRASIL- Tattoo Inks									
Vermelho	x	x	x	x	x	x	x	x	NA
Pink	x	x	x	x	x	x	x	x	NA
Citrus	x	x	x	ND	x	x	x	x	NA
Amarelo Canario	x	x	x	x	x	x	x	x	NA
Amarelo Fluor	x	x	x	ND	x	x	x	x	NA
Verde Claro	x	x	x	ND	x	x	x	x	NA
Azul Royal	x	x	x	x	x	x	x	x	NA
Magenta	x	x	x	x	x	x	x	x	NA
Lilas Claro	x	x	x	x	x	x	x	x	NA
Preto Escuro	x	x	x	NA	x	x	x	x	NA

LEGEND: x- analyzed; NA- not analyzed; ND- analyzed, no or poor data obtained; √-extracted; *-KBr (FT-Raman)

	Normal Raman (Dispersive)			SERS	FT Raman	FT-IR	XRF	Microscopy	
	488nm	633nm	785nm	488nm	1064nm	Durascope			(extraction)
SKIN CANDY- Tattoo Inks									
Candy Apple Red	x	x	x	x	x	x	x	x	√
Red Hot	x	x	x	x	x	x	x	x	√
Marz	x	x	x	ND	x	x	x	x	√
Dolemite	x	x	x	x	x	x	x	x	√
Blisterene	x	x	x	x	x	x	x	x	√
Sassygrass	x	x	x	x	x	x	x	x	√
Tastywaves	x	x	x	x	x	x	x	x	√
Bell Bottom Blue	x	x	x	ND	x	x	x	x	√
S.R.V. Teal 2	x	x	x	x	x	x	x	x	√
Razberry Creem	x	x	x	x	x	x	x	x	√
Muddy Water Blue	x	x	x	ND	x	x	x	x	√
Ripple	x	x	x	x	x	x	x	x	√
San Brownadino	x	x	x	x	ND	x	x	x	√
Black Cherry Roan 1	NA	NA	NA	NA	NA	NA	NA	x	NA
Black Cherry Roan 2	x	x	x	NA	ND	x	NA	x	√
Black Cherry Roan 3	NA	NA	NA	NA	NA	NA	NA	x	NA
Tokyo Pink	x	x	x	ND	x	x	x	x	√
White Girl	x	x	x	x	x	x	x	x	NA

LEGEND: x- analyzed; NA- not analyzed; ND- analyzed, no or poor data obtained; √-extracted; *-KBr (FT-Raman)

	Normal Raman (Dispersive)			SERS	FT Raman	FT-IR	XRF	Microscopy	
	488nm	633nm	785nm	488nm	1064nm	Durascope			(extraction)
FLYING TIGERS- Tattoo Inks									
Salmon Pink	x	x	x	NA	x	x	x	x	√
Pink Red	x	x	x	NA	ND*	x	x	x	√
Magenta	x	x	x	NA	x	x	x	x	√
Chinese Red	x	x	x	NA	x	x	x	x	√
Bright Red	x	x	x	NA	x	x	x	x	√
Rose Red	x	x	x	NA	x	x	x	x	√
Mulberry	x	x	x	NA	x	x	x	x	√
Dark Red	x	x	x	NA	x	x	x	x	√
Orange Red	x	x	x	NA	x	x	x	x	√
Orange	x	x	x	NA	x	x	x	x	√
Bright Yellow	x	x	x	NA	x	x	x	x	√
Mid-Yellow	x	x	x	NA	x	x	x	x	√
Yellow	x	x	x	NA	x	x	x	x	√
Golden Yellow	x	x	x	NA	x	x	x	x	√
Khaki	x	x	x	NA	x	x	x	x	√
Grass Hopper	x	x	x	NA	x	x	x	x	√
Light Green	x	x	x	NA	x	x	x	x	√
Verdancy	x	x	x	NA	x	x	x	x	√
Lawngreen	x	x	x	NA	x	x	x	x	√
Dark Green	x	x	x	NA	x	x	x	x	√
Blue Sky	x	x	x	NA	x	x	x	x	√
Turquoise Blue	x	x	x	NA	x	x	x	x	√

LEGEND: x- analyzed; NA- not analyzed; ND- analyzed, no or poor data obtained; √-extracted; *-KBr (FT-Raman)

Cyan	x	x	x	NA	x	x	x	x	√
Dark Cyan	x	x	x	NA	x	x	x	x	√
Blue	x	x	x	NA	x	x	x	x	√
Navy Blue	x	x	x	NA	x	x	x	x	√
Dark Blue	x	x	x	NA	x	x	x	x	√
Grape	x	x	x	NA	x	x	x	x	√
Purple	x	x	x	NA	x*	x	x	x	√
Violet	x	x	x	NA	x	x	x	x	√
Grey	x	x	x	NA	ND	x	x	x	√
Bright Black	x	x	x	NA	ND	x	x	x	√
Black	x	x	x	NA	ND	x	x	x	√
Eggplant Black	x	x	x	NA	ND	x	x	x	√
Dark Black	x	x	x	NA	ND	x	x	x	√
Sayonara Suede	x	x	x	NA	ND	x	x	x	√
Dark Brown	x	x	x	NA	ND	x	x	x	√
Light Chocolate	x	x	x	NA	ND	x	x	x	√
Skin Tone	x	x	x	NA	ND	x	x	x	√
White	x	x	x	NA	x	x	x	x	√

LEGEND: x- analyzed; NA- not analyzed; ND- analyzed, no or poor data obtained; √-extracted; *-KBr (FT-Raman)

	Normal Raman (Dispersive)			SERS	FT Raman	FT-IR	XRF	Microscopy	UV/Vis
	488nm	633nm	785nm	488nm	1064nm	Durascope			(extraction)
SKIN CANDY- Pigment Extracts									
Candy Apple Red	x	x	x	NA	x	x	NA	NA	x
Red Hot	x	x	x	NA	x	x	NA	NA	x
Marz	x	x	x	NA	x	x	NA	NA	x
Dolemite	x	x	x	NA	x	x	NA	NA	x
Blisterene	x	x	x	NA	x	x	NA	NA	x
Sassygrass	x	x	x	NA	x	x	NA	NA	x
Tastywaves	x	x	x	NA	x	x	NA	NA	x
Bell Bottom Blue	x	x	x	NA	x	x	NA	NA	x
S.R.V. Teal 2	x	x	x	NA	x	x	NA	NA	x
Razberry Creem	x	x	x	NA	x	x	NA	NA	x
Muddy Water Blue	x	x	x	NA	x	x	NA	NA	x
Ripple	x	x	x	NA	x*	x	NA	NA	x
San Brownadino	x	x	x	NA	x*	x	NA	NA	x
Black Cherry Roan 1	NA	NA	NA	NA	NA	NA	NA	NA	NA
Black Cherry Roan 2	x	x	x	NA	ND	x	NA	NA	x
Black Cherry Roan 3	NA	NA	NA	NA	NA	NA	NA	NA	NA
Tokyo Pink	x	x	x	NA	ND	x	NA	NA	x
White Girl	NA	NA	NA	NA	NA	x	NA	NA	NA

LEGEND: x- analyzed; NA- not analyzed; ND- analyzed, no or poor data obtained; √-extracted; *-KBr (FT-Raman)

	Normal Raman (Dispersive)		
	488nm	633nm	785nm
FLYING TIGERS- Pigment Extracts			
Salmon Pink	x	x	x
Pink Red	x	x	x
Magenta	x	x	x
Chinese Red	x	x	x
Bright Red	x	x	x
Rose Red	x	x	x
Mulberry	x	x	x
Dark Red	x	x	x
Orange Red	x	x	x
Orange	x	x	x
Bright Yellow	x	x	x
Mid-Yellow	x	x	x
Yellow	x	x	x
Golden Yellow	x	x	x
Khaki	x	x	x
Grass Hopper	x	x	x
Light Green	x	x	x
Verdancy	x	x	x
Lawngreen	x	x	x

LEGEND: x- analyzed; NA- not analyzed; ND- analyzed, no or poor data obtained; √-extracted; *-KBr (FT-Raman)

Dark Green	x	x	x
Blue Sky	x	x	x
Turquoise Blue	x	x	x
Cyan	x	x	x
Dark Cyan	x	x	x
Blue	x	x	x
Navy Blue	x	x	x
Dark Blue	x	x	x
Grape	x	x	x
Purple	x	x	x
Violet	x	x	x
Grey	x	x	x
Bright Black	x	x	x
Black	x	x	x
Eggplant Black	x	x	x
Dark Black	x	x	x
Sayonara Suede	x	x	x
Dark Brown	x	x	x
Light Chocolate	x	x	x
Skin Tone	x	x	x
White	x	x	x

LEGEND: x- analyzed; NA- not analyzed; ND- analyzed, no or poor data obtained; √-extracted; *-KBr (FT-Raman)

	Normal Raman (Dispersive)			SERS	FT Raman	FT-IR	Microscopy	UV/Vis	DFT
	488nm	633nm	785nm	488nm	1064nm	Durascope			
KNOWN PIGMENTS									
Pigment Blue 15	x	x	x	x	NA	x	NA	x	NA
Pigment Blue 15.1	x	x	x	NA	NA	x	NA	NA	NA
Pigment Blue 15.2	x	x	x	NA	NA	x	NA	NA	NA
Pigment Blue 15.3	x	x	x	NA	NA	x	NA	NA	NA
Pigment Green 7	x	x	x	x	x	x	NA	x	NA
Pigment Orange 16	x	x	x	x	x	x	NA	x	x
Pigment Orange 34	x	x	x	x	x	x	NA	x	NA
Pigment Orange 62	x	x	x	x	NA	x	NA	x	NA
Pigment Red 122	x	x	x	x	ND	x	NA	x	x
Pigment Red 146	x	x	x	x	x	x	NA	x	NA
Pigment Red 170	x	x	x	x	x	x	NA	x	x
Pigment Red 255	x	x	x	x	NA	x	NA	x	NA
Pigment Yellow 3	x	x	x	x	NA	x	NA	x	NA
Pigment Yellow 73	x	x	x	x	NA	x	NA	x	NA
Pigment Yellow 83	x	x	x	x	NA	x	NA	x	NA
Pigment Yellow 151	x	x	x	x	NA	x	NA	x	NA
Pigment Violet 23 a	x	x	x	x	ND	x	NA	x	NA
Pigment Violet 23 b	x	x	x	x	x	x	NA	x	NA

LEGEND: x- analyzed; NA- not analyzed; ND- analyzed, no or poor data obtained; √-extracted; *-KBr (FT-Raman)

	Normal Raman (Dispersive)		
	488nm	633nm	785nm
PIGSKIN			
7 SC Dots (Frozen)	x	x	x
7 SC Dots (Fixed)	x	x	x

LEGEND: x- analyzed; NA- not analyzed; ND- analyzed, no or poor data obtained; √-extracted; *-KBr (FT-Raman)

Chapter 4: Results & Discussion

The Iron Works Brasil Tattoo Inks were examined and photographed microscopically and instrumentally analyzed with dispersive micro-Raman (488nm, 633nm, and 785nm excitation wavelengths), SERS (488nm excitation wavelength), FT-Raman (1064nm excitation wavelength), FT-IR (ATR) and XRF. The Flying Tigers Tattoo Inks were examined and photographed microscopically and instrumentally analyzed with dispersive micro-Raman (488nm, 633nm, and 785nm excitation wavelengths), FT-Raman (1064nm excitation wavelength), FT-IR (ATR) and XRF. In addition, the Flying Tigers Tattoo Inks were subjected to the extraction method described earlier. The extracts were instrumentally analyzed with dispersive micro-Raman (488nm, 633nm, and 785nm excitation wavelengths).The Skin Candy Tattoo Inks were examined and photographed microscopically and instrumentally analyzed with dispersive micro-Raman (488nm, 633nm, and 785nm excitation wavelengths), SERS (488nm excitation wavelength), FT-Raman (1064nm excitation wavelength), FT-IR (ATR) and XRF. In addition, the Skin Candy Tattoo Inks were subjected to the extraction method described earlier. The extracts were instrumentally analyzed with dispersive micro-Raman (488nm, 633nm, and 785nm excitation wavelengths), FT- Raman (1064nm excitation wavelength), FT-IR (ATR) and UV/Vis. Photographs and spectra for the tattoo inks can be found in Appendix D and photographs and spectra for the tattoo ink pigment extractions can be found in Appendix E.

The selection of known pigments were instrumentally analyzed with dispersive micro-Raman (488nm, 633nm, and 785nm excitation wavelengths), SERS (488nm excitation wavelength), FT-Raman (1064nm excitation wavelength), FT-IR (ATR) and UV/Vis. Spectra for these pigment standards can be found in Appendix F. A selection of pigment reference spectra reported in the literature is provided in Appendix I.

The pigments found in three of the Skin Candy Tattoo Inks (Pigment Red 170 [Red Hot], Pigment Orange 16 [Marz], and Pigment Red 122 [Razberry Creem]) were subjected to DFT calculations in order to compare the experimental vibrational spectra with the calculated vibrational spectra. DFT data and spectra for these pigments can be found in Appendix J. Any band assignments and interpretations of normal vibrational modes and associated molecular species were assisted with the use of the Table of Raman Bands (Appendix A), Correlation Charts (Appendix B) and Character Tables (Appendix C).

A selection of Skin Candy Tattoo Inks (specifically White Girl, Red Hot, Marz, Blisterine, Tastywaves, Muddy Water Blue, Ripple) were used to tattoo pigskin and analyzed directly with dispersive micro-Raman. Spectra for these tattoo inks can be found in Appendix G.

Prior to every sample analysis, a selection of reference standards were analyzed to ensure that each particular instrument was calibrated and to ensure that the instrument settings were correct. Reference spectra (both experimental and reference from the literature) pertaining to instrument calibration and validation procedures can be found in Appendix H.

NOTE: All Raman, infrared and UV/Vis band assignments were reported to five significant figures.

Results-Pigment Standards

The pigment standards were examined first to evaluate their band locations relative to those reported in the literature[1] and in order to assign characteristic vibrational modes to the primary functional groups of the pigment molecule. Comparison of normal Raman and SERS spectra were also conducted with the pigment standards. General observations followed by correlation of the experimental data to the literature of the resultant spectra for the pigments are summarized:

Pigment Red 122- With an increase in the excitation wavelength (λ_0) from 488nm to 785nm, there is a substantial decrease in signal observed. The best normal Raman spectrum was obtained with λ_0=488nm. No spectrum was generated using the FT-Raman, even after mixing the pigment with KBr in order to minimize sample heating and reduce fluorescence. The spectrum obtained with SERS corresponds to the peaks observed with the normal Raman spectrum at λ_0=488nm. There was not any apparent signal enhancement observed going from normal Raman to SERS at this excitation wavelength. The FT-IR/ATR spectrum generated a number of well-resolved peaks; the peaks characteristic of quinacridones apparent with the series of peaks in the region of 1630-1550 cm^{-1}, and the peaks located at 1472 cm^{-1} and 1335cm^{-1}. With regard to UV/Vis, the absorbance maximum of Pigment Red 122 was 302.0nm, likely a bathochromic shift that resulted from the solvent system (conc. H_2SO_4). This is supported by the change in color observed (red to a bluish-red, or purple shade). Correlation can be made between the

[1] In the literature, the peaks are labeled very strong (vs), strong (s) and medium to strong (m-s), *etc.* by the authors (a subjective determination based on peak intensities of the resultant spectra). These 'strong' peaks were compared to the experimental data. Full spectra and peak assignments from the literature can be found in Appendix I.
The experimental spectra used for comparison were selected based on which λ_0 for that particular pigment exhibited the highest number of peaks and best peak resolution. If there was more than one spectrum that fit the criteria, the spectrum with the λ_0 closely matching the λ_0 of the literature was selected.

experimental data and reported data for PR 122 (using Scherrer *et.al.*, 2009 and Schulte *et.al.*, 2008).

Scherrer *et.al.*: (λ_0=514nm) 1649s, 1597s, 1568vs, 1311s

Schulte *et. al*.: (λ_0=476.5nm) 1645s, 1565s, 1309s

Experimental: (λ_0=488nm): 1644.5, 1595.8, 1566.8, 1310.7 (note: no bands were resolved from 700-1200cm^{-1} limiting peak correlation to reported data).

A detailed explanation of the vibrational modes and band assignments for pigment red 122 (a quinacridone) can be found in the DFT portion of the Results & Discussion section.

Pigment Red 146-Raman bands were resolved with Raman spectra at λ_0=488nm, 785nm and 1064nm. Overwhelming fluorescence was observed with λ_0=633nm and no useful data were obtained at this excitation wavelength. The spectrum obtained with SERS corresponds to the peaks observed with the normal Raman spectrum at λ_0=488nm. Signal enhancement was observed when going from normal Raman to SERS as well as resolution of peaks not observed in the normal Raman spectrum. The FT-IR/ATR spectrum generated a number of well-resolved peaks. With regard to UV/Vis, the absorbance maximum of Pigment Red 146 was 317.0nm, likely a bathochromic shift that resulted from thesolvent system (conc. H_2SO_4). This is supported by the change in color observed (red to a bluish-red, or purple shade). Correlation can be made between the experimental data and reported data for PR 146 (using Scherrer *et.al.*, 2009 and Schulte *et.al.*, 2008).

Scherrer *et.al.*: (λ_0=785nm): 1582vs, 1508s, 1427s, 1363vs, 1316s, 1293s, 956s

Schulte *et.al.*: (λ_0=1064nm): 1582vs, 1508s, 1428s, 1363s

Experimental: (λ_0=488nm): 1581.9, 1508.3, 1426.7, 1363.7, 955.79

Pigment Red 146 exhibits bands characteristic of a monoazo. Specifically, the C-N symmetric stretch at 1157 cm^{-1} and the N=N stretching at 1426 and 1449 cm^{-1}. In addition, the characteristic bands associated with naphthalene can be found at 955, 1363, 1552 and 1581cm^{-1}.

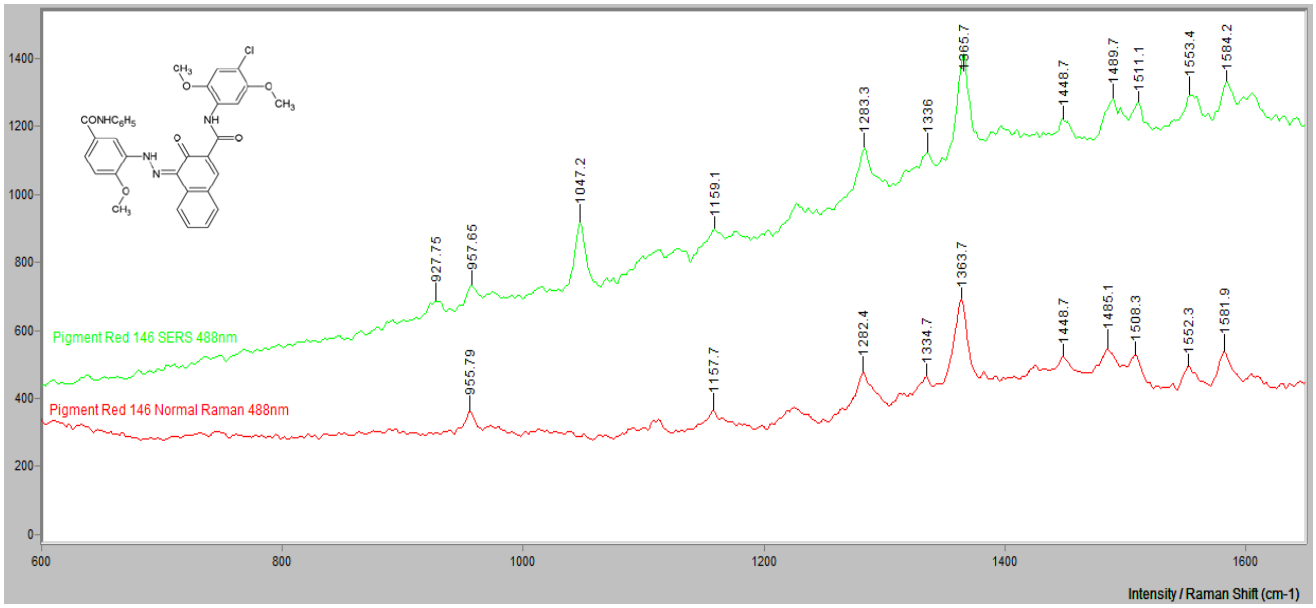

Figure 44. Comparison of Pigment Red 146 obtained with normal Raman (red) and SERS (green) , λ_0=488nm

Pigment Red 170- Bands were resolved with Raman spectra at all four excitation wavelengths. The best normal Raman spectrum was with λ_0=633nm. The spectrum obtained with SERS corresponds to the bands observed with the normal Raman spectrum at λ_0=488nm. Substantial signal enhancement was observed when going from normal Raman to SERS as well as resolution of bands not observed in the normal Raman spectrum. The FT-IR/ATR spectrum generated a number of well-resolved peaks. With regard to UV/Vis, the absorbance maximum of Pigment Red 170 was 312.50nm, similar to that of Pigment Red 146. Correlation can be made between the experimental data and reported data for PR 170 (using Scherrer *et.al.*, 2009 and Vandenabeele *et.al.*, 2000).

Scherrer *et.al.*: (λ_0=785nm): 1606vs, 1513s, 1363vs, 1289s, 1164s

Vandenabeele *et.al.*: (λ_0=780nm): 1363vs, 1605m-s

Experimental: (λ_0=633nm): 1604.9, 1511.7, 1362.1, 1286.8, 1164

A detailed explanation of the vibrational modes and band assignments for pigment red 170 (a monoazo) can be found in the DFT portion of the Results & Discussion section. Characteristic bands of a monoazo and naphthalene were found.

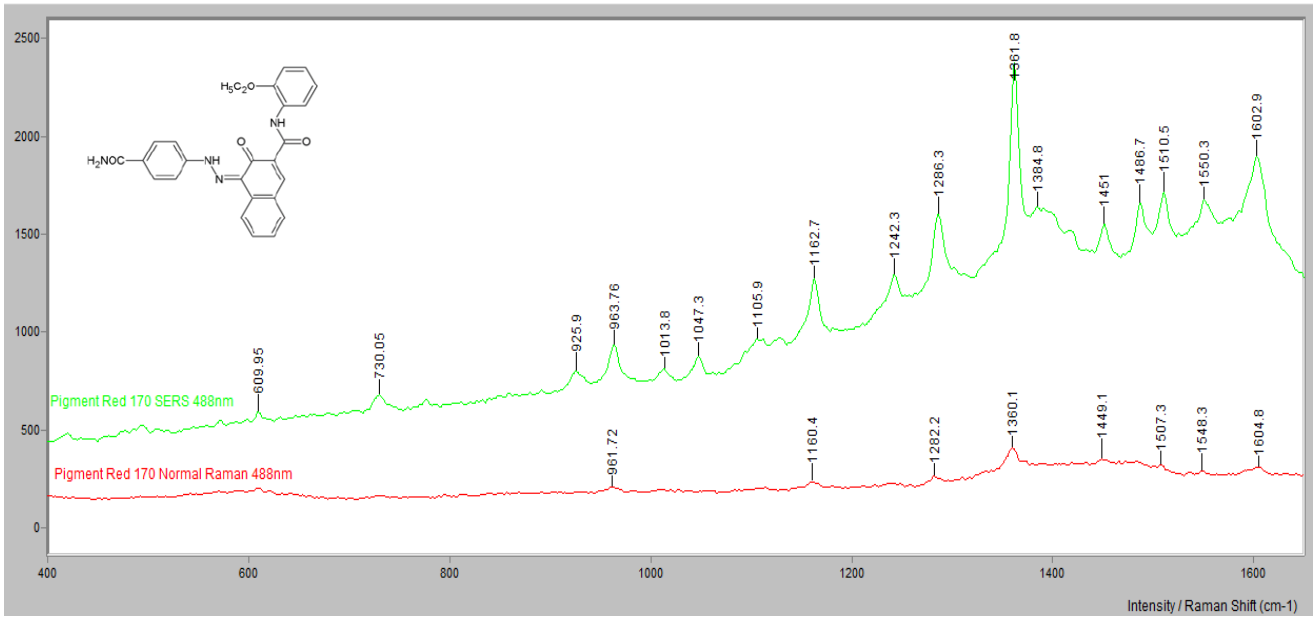

Figure 45. Comparison of Pigment Red 170 obtained with normal Raman (red) and SERS (green) , λ_0=488nm

Pigment Red 255- Pigment Red 255 is classified as a polycyclic diketopyrrolo-pyrrole, and has a structure different from the azo pigments that characterize many of the red pigments. Bands were resolved with normal Raman spectra with all three excitation wavelengths. The best normal Raman spectrum was with λ_0=785nm. The spectrum obtained with SERS corresponds to the peaks observed with the normal Raman spectrum at λ_0=488nm. Signal enhancement was observed when going from normal Raman to SERS. The FT-IR/ATR spectrum generated a number of well-resolved peaks. With regard to UV/Vis, the absorbance maximum of Pigment Red 255 was 521.50nm. This absorbance shift to a longer wavelength is in contrast to the

apparent color change observations in which the red/orange color of Pigment Red 255 changes to a yellow color upon introduction of conc. H_2SO_4. Correlation can be made between the experimental data and reported data for PR 255 (using Scherrer *et.al.*, 2009).

Scherrer *et.al.*: (λ_0=785nm): 1602vs, 1586s, 1562s, 1346vs, 1051s, 999s, 931s, 318s

Experimental: (λ_0=785nm): 1602.6, 1587.8, 1562.2, 1346.3, 1052.3, 999.57, 931.75, 319.34

Evaluation of the spectra of pigment red 255 exhibits bands characteristic of ring breathing (in the region of 930-1052cm^{-1}), C=C stretching (in the region of 1560-1602 cm^{-1}) and amide III and I bands at 1309 cm^{-1} and 1661 cm^{-1}, respectively.

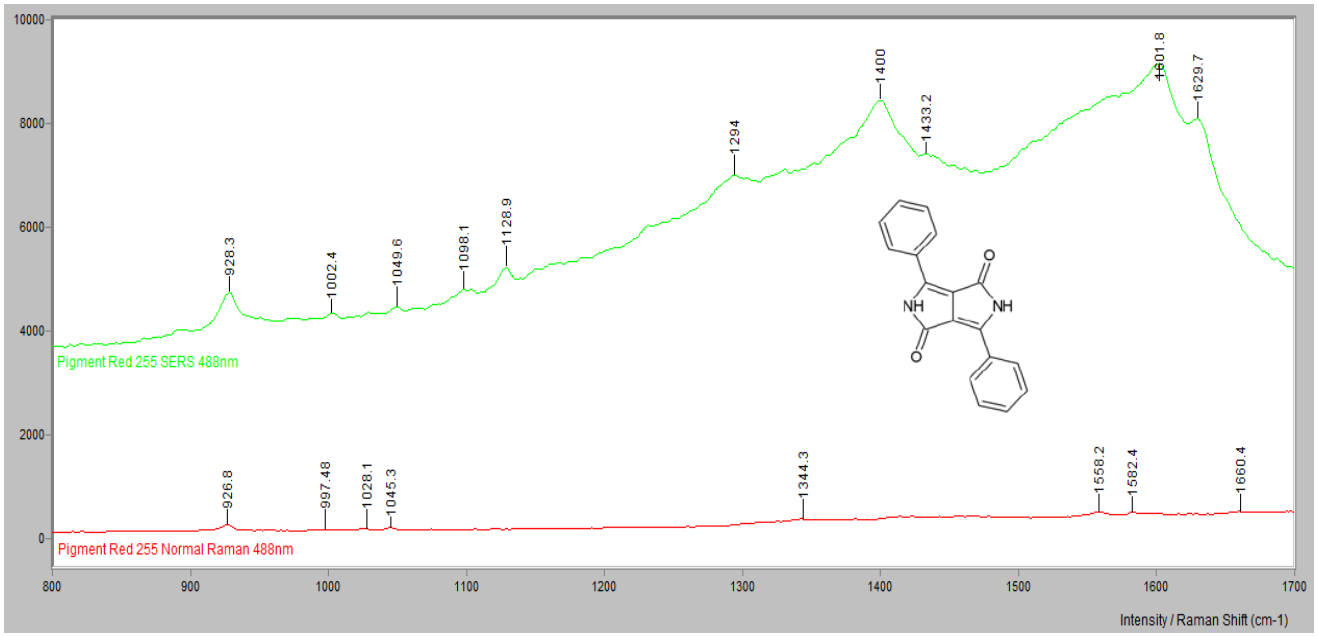

Figure 46. Comparison of Pigment Red 255 obtained with normal Raman (red) and SERS (green) , λ_0=488nm

Pigment Orange 16- Raman bands were resolved with Raman spectra at λ_0=633nm, 785nm and 1064nm. Overwhelming fluorescence was observed with λ_0=488nm and no useful data were obtained at this excitation wavelength. The spectrum obtained with SERS corresponds to the bands observed with the normal Raman spectrum at λ_0=633nm and 785nm. Substantial

signal enhancement was observed when going from normal Raman to SERS with λ_0=488nm since no bands were observed in the normal Raman spectrum. The FT-IR/ATR spectrum generated a number of well-resolved peaks. With regard to UV/Vis, the absorbance maximum of Pigment Orange 16 was 541.0nm, likely a bathochromic shift that resulted from the conc. H_2SO_4. This is supported by the change in color observed (orange to a reddish pink shade). No reference Raman spectra could be found for Pigment Orange 16 in the literature. The following major peaks are reported (assigned very strong [vs] and strong [s] according to peak intensity) for the spectrum with λ_0=785nm: 1601.8vs, 1397.3s, 1323.5vs, 1259.6s, 1123.4s, 669.65s, 371.07s, 120.07s.

A detailed explanation of the vibrational modes and band assignments for Pigment Orange 16 (a disazo) can be found in the DFT portion of the Results & Discussion section.

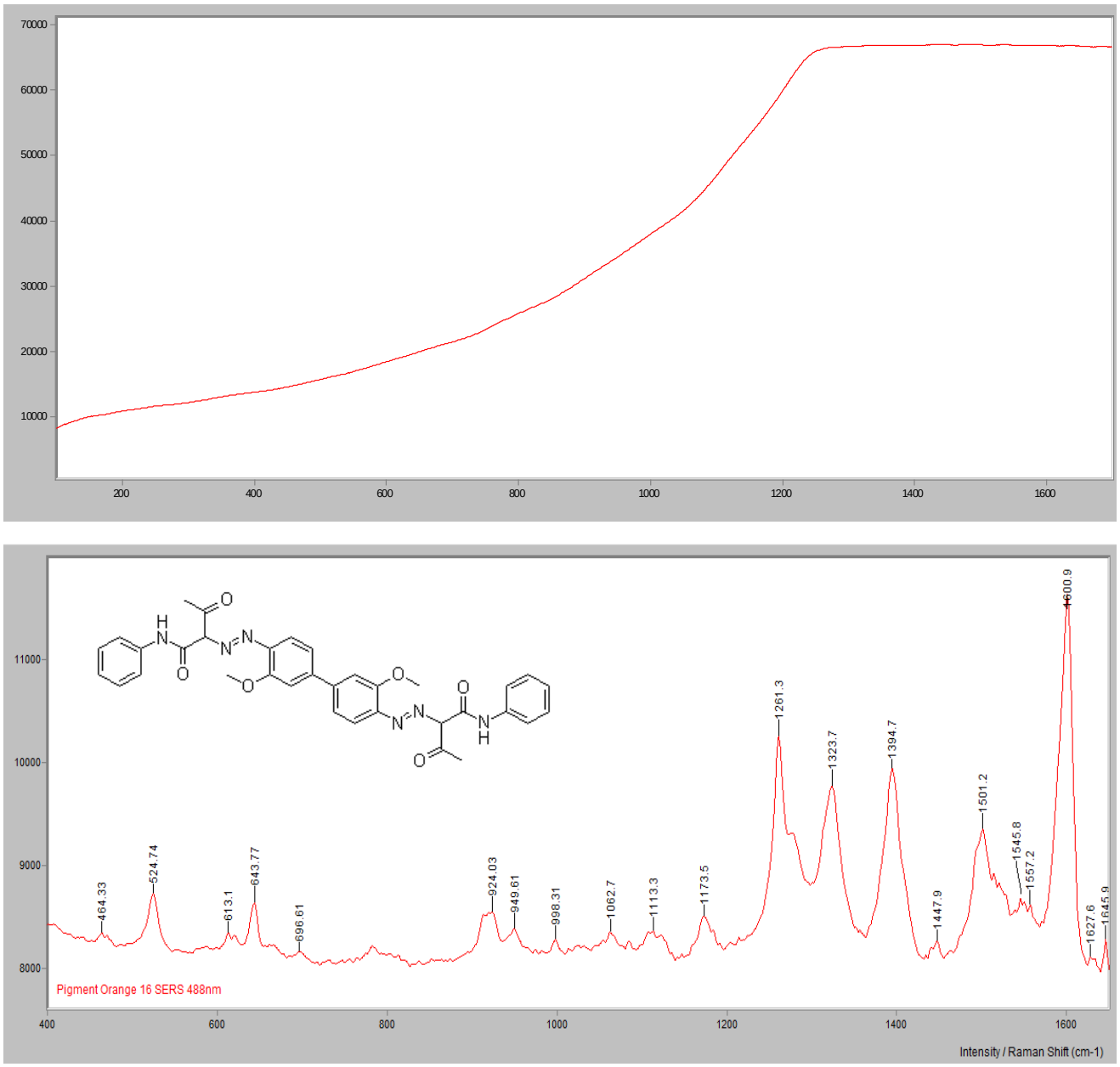

Figure 47. Comparison of Pigment Orange 16 obtained with normal Raman (top spectrum) and SERS (bottom spectrum), λ_0=488nm

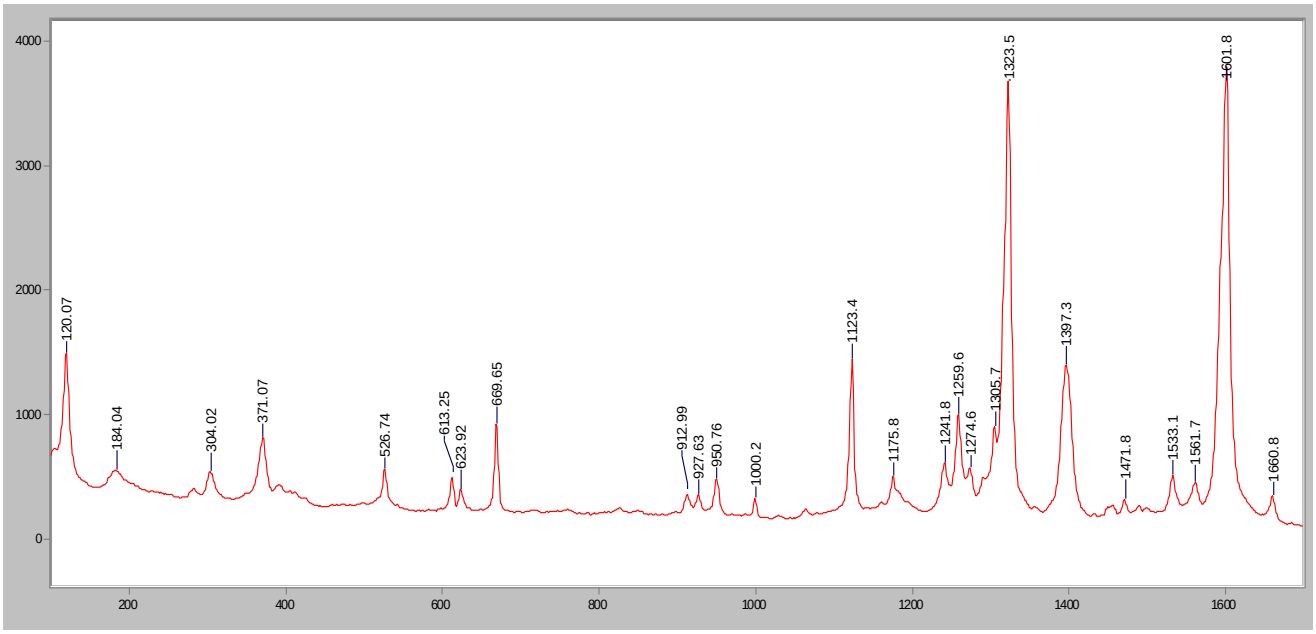

Figure 48. Pigment Orange 16, λ_0=785nm. (Intensity/Raman Shift [cm^{-1}])

Pigment Orange 34- Bands were resolved with Raman spectra with all four excitation wavelengths. The spectrum obtained with SERS corresponds to the bands observed with the normal Raman spectra. There was not any apparent signal enhancement observed when going from normal Raman to SERS. The FT-IR/ATR spectrum generated a number of well-resolved peaks. With regard to UV/Vis, the absorbance maximum of Pigment Orange 34 was 517.0nm, likely a bathochromic shift that resulted from the conc. H_2SO_4. This is supported by the change in color observed (orange to a reddish pink shade). Correlation can be made between the experimental data and reported data for PO 34 (using Colombini, *et.al.*, 2010, Scherrer *et.al.*, 2009 and Schulte *et.al.*, 2008).

Colombini *et. al*:. (λ_0=785nm): 1600vs, 1275s

Scherrer *et.al.*: (λ_0=785nm): 1597vs, 1273s

Schulte *et. al*.: (λ_0=1064nm): 1597vs, 1273m

Experimental: (λ_0=785nm): 1596.7, 1272.7

Pigment Orange 34 differs from pigment orange 16 with the presence of two methyl groups, with each group found on the outer-most rings located *para* to the rest of the molecule. Pigment Orange 34 exhibits bands characteristic of a disazo. Specifically, the C-N symmetric stretch at 1159 cm^{-1} and the N=N stretching at 1420cm^{-1}. A band at 1596 cm^{-1} is characteristic of the C=C (ring breathing) stretch.

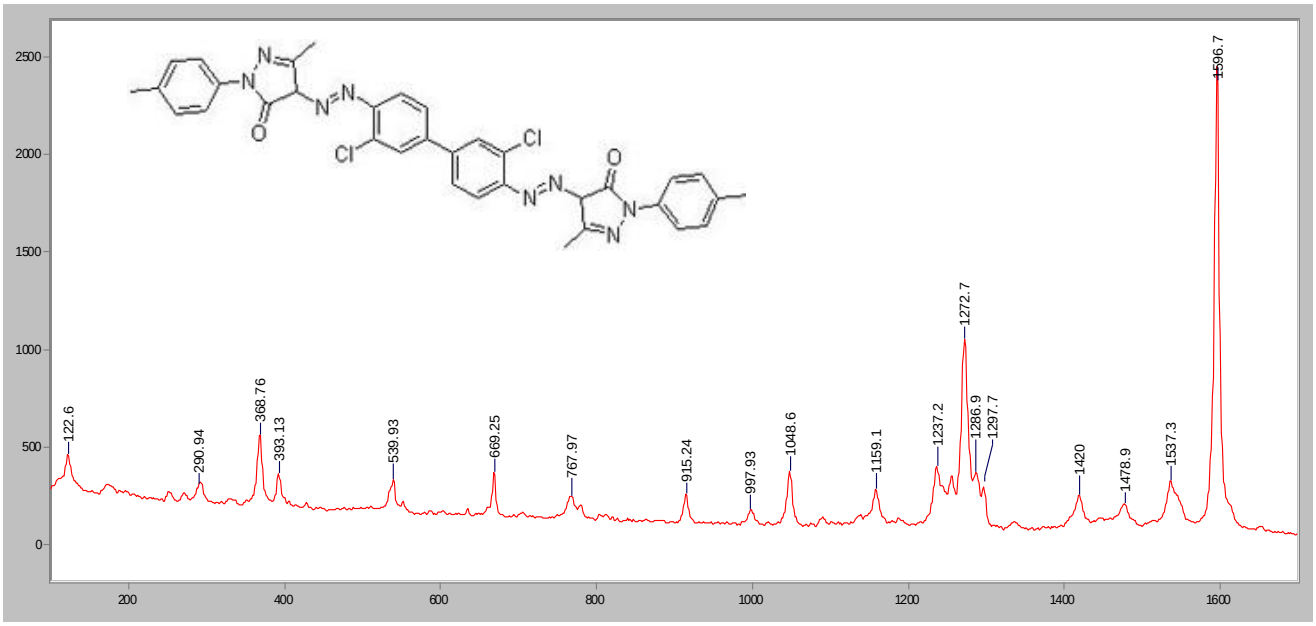

Figure 49. Pigment Orange 34, λ_0=785nm. (Intensity/Raman Shift [cm^{-1}]). An interesting feature of the above Raman spectrum for PO 34 is the appearance of evenly spaced, relatively intense bands. This may be due to the high molecular symmetry or the fundamental and overtones of a vibration (Franck-Condon scattering).

Pigment Orange 34 exhibited well resolved peaks across all excitation wavelengths. When comparing the three normal Raman spectra, it is apparent that using the 633nm (red) laser resulted in the most peaks being resolved and the highest intensity peaks followed by the 785nm (red/near IR) laser.

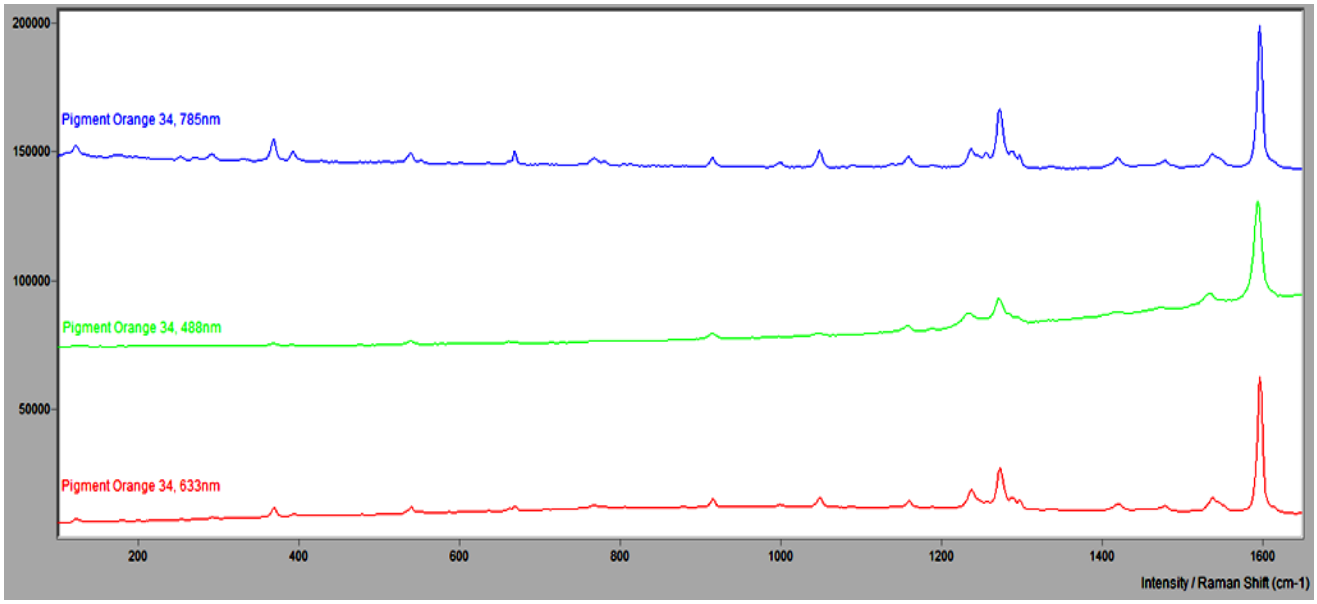

Figure 50. Comparison of Pigment orange 34 at different excitation wavelengths.

Pigment Orange 62- Bands were resolved with normal Raman spectra with all three excitation wavelengths. The spectrum obtained with SERS corresponds to the bands observed with the normal Raman spectra. There was not any apparent signal enhancement observed when going from normal Raman to SERS. The FT-IR/ATR spectrum generated a number of well-resolved peaks. With regard to UV/Vis, the absorbance maximum of Pigment Orange 62 was 401.5 nm, likely a hypsochromic shift that resulted from the conc. H_2SO_4. This is supported by the change in color observed (orange to a yellowish shade). Correlation can be made between the experimental data and reported data for PO 62 (using Scherrer *et.al.*, 2009).

Scherrer *et.al.*: (λ_0=785nm): 1601s, 1338vs, 1115s

Experimental: (λ_0=785nm): 1600.4, 1336.8, 1113.8

Pigment Orange 62 exhibits bands characteristic of a monoazo. Specifically, the C-N symmetric stretch at 1164 cm^{-1} and the N=N stretching at 1403cm^{-1}. In addition, bands likely associated with the double annulated structure can be found at 1336 and 1600cm^{-1}. Pigment

Orange 62 exhibited well resolved peaks across all three excitation wavelengths. When comparing the three spectra, it is apparent that using the 633nm (red) laser resulted in the most peaks being resolved and the highest intensity peaks followed by the 785nm (red/near IR) laser.

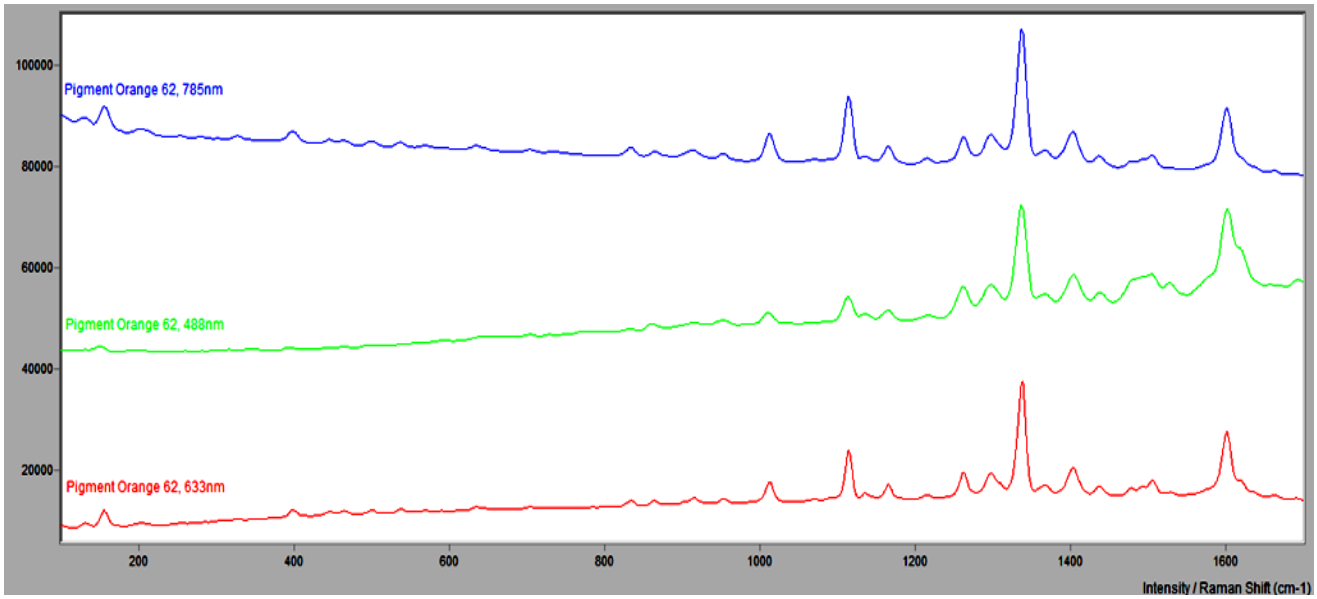

Figure 51. Comparison of Pigment Orange 62 at different excitation wavelengths.

Pigment Yellow 3- Bands were resolved with normal Raman spectra with all three excitation wavelengths. The spectrum obtained with SERS corresponds to the bands observed with the normal Raman spectra. There was not any apparent signal enhancement observed when going from normal Raman to SERS. The FT-IR/ATR spectrum generated a number of well-resolved peaks. With regard to UV/Vis, Pigment Yellow 3 dissolved in conc. H_2SO_4 produced a yellow color, with a corresponding absorbance maximum of 424.5nm. No major shifts were observed. Correlation can be made between the experimental data and reported data for PY 3 (using Colombini, *et.al.*, 2010, Scherrer *et.al.*, 2009 and Schulte *et.al.*, 2008 and Vandenabeele, *et.al.*, 2000).

Colombini, *et.al.*: (λ_0=785nm): 1614vs, 1596vs, 1496vs, 1388vs, 1311vs, 1246s, 1140vs, 988vs, 650m-s, 461m-s, 452m-s

Scherrer *et.al.*: (λ_0=785nm): 1613/1614vs, 1494/1495vs, 1387/1386s, 1337/1336vs, 1309/1310vs, 1139/1140vs, 650s

Schulte *et. al.*: (λ_0=514.5nm): 1609s, 1490s, 1386s, 1333s, 1305s, 1135vs

Vandenabeele, *et. al.*: (λ_0=780nm): 1336m-s, 1138vs

Experimental: (λ_0=488nm): 1613.3, 1495.1, 1387.7, 1336.4, 1309.4, 1140.6, 746.06, 650.23

Pigment Yellow 3 exhibits bands characteristic of a monoazo. Specifically, the C-N symmetric stretch at 1140 cm^{-1}, the C-N symmetric bend at 1170 and 1191 cm^{-1} and the N=N stretching at 1387cm^{-1}. Nitro group stretching can be found at 825, 1336 and 1566 cm^{-1}. Amide III and I bands can be found at 1244 cm^{-1} and 1675 cm^{-1}, respectively. The bands located at 650 cm^{-1} and 709 cm^{-1} are due to the C-Cl stretching vibrations. Pigment Yellow 3 exhibited well resolved peaks across all three excitation wavelengths. When comparing the three spectra, it is apparent that using the 488nm (green) laser resulted in the most peaks being resolved and the highest intensity peaks followed by the 633nm (red) laser.

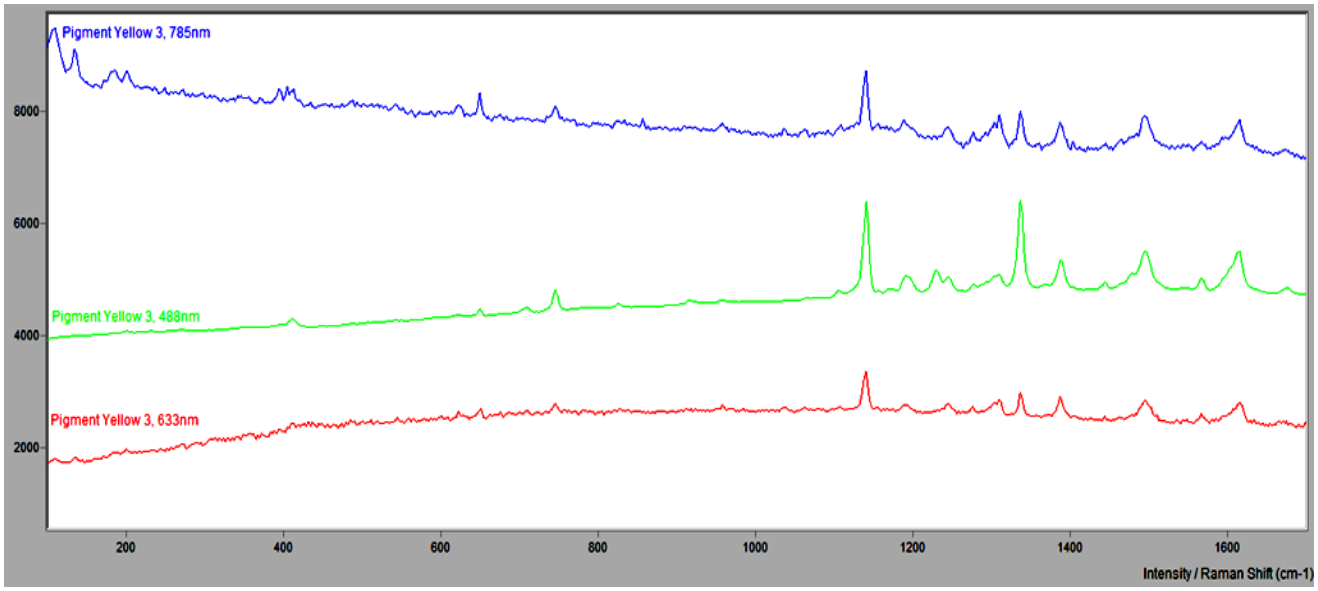

Figure 52. Comparison of Pigment Yellow 3 at different excitation wavelengths.

Pigment Yellow 73- Bands were resolved with normal Raman spectra with all three excitation wavelengths. The spectrum obtained with SERS corresponds to the bands observed with the normal Raman spectra. There was not any apparent signal enhancement observed when going from normal Raman to SERS. The FT-IR/ATR spectrum generated a number of well-resolved peaks. With regard to UV/Vis, Pigment Yellow 73 dissolved in conc. H_2SO_4 produced a yellow color, with a corresponding absorbance maximum of 428.0nm. No major shifts were observed. Correlation can be made between the experimental data and reported data for PY 73 (using Scherrer *et.al.*, 2009 and Ropret *et.al.*, 2007).

Scherrer *et.al.*: (λ_0=785nm): 1615s, 1598s, 1530s, 1480s, 1336vs, 1308s, 1137s

Ropret *et.al.*: (λ_0=785nm): 1616s-m, 1601s-m, 1532s-m, 1507s-m, 1481s-m, 1338vs, 1308s-m, 1138s

Experimental: (λ_0=633nm): 1613.2, 1599.8, 1529.1, 1504.8, 1479.4, 1332.8, 1306.5, 1250.8, 1138.8

Pigment Yellow 73 exhibits bands characteristic of a monoazo. Specifically, the C-N symmetric stretch at 1137cm^{-1} , the C-N symmetric bending at 1197 cm^{-1}, and the N=N stretching at 1390cm^{-1}. Nitro group stretching can be found at 824, 1335 and 1565 cm^{-1}. Amide III and I bands can be found at 1249 cm^{-1} and 1676 cm^{-1}, respectively.

Pigment Yellow 83- Bands were resolved with normal Raman spectra with all three excitation wavelengths. The spectrum obtained with SERS corresponds to the bands observed with the normal Raman spectra. Signal enhancement was observed when going from normal Raman to SERS as well as resolution of peaks not observed in the normal Raman spectrum. The FT-IR/ATR spectrum generated a number of well-resolved peaks; PY 83 contains a large band from about 1450-1500 cm^{-1}, which is due to the strong N=N azo vibrations. In addition, the series of peaks at around 1180-1310 cm^{-1} indicates a disazo, as well as the three peaks located

around 850-980 cm^{-1} (refer to IR spectrum in Appendix F). With regard to UV/Vis, Pigment Yellow 83 dissolved in conc. H_2SO_4 produced an orange color, with an absorbance maximum of 487.0nm. This color shift observed is consistent with the bathochromic shift absorbed instrumentally. Correlation can be made between the experimental data and reported data for PY 83 (using Scherrer *et.al*, 2009, Schulte *et.al.*, 2008 and Vandenabeele, *et.al.*, 2000).

*Colombini, *et.al.*: (λ_0=785nm): 1622s, 1486s, 1140s, 1000s, 988s, 952m-s, 787s

Scherrer *et.al.*: (λ_0=633nm): 1596vs, 1400s, 1254s

Schulte *et. al*.: (λ_0=632.8nm): 1593s, 1397s, 1255s

Vandenabeele, *et. al*.: (λ_0=780nm): 1595vs

Experimental: (λ_0=785nm): 1596.2, 1400.9, 1254.1

*Note: Initially, correlation was attempted using Colombini, *et al.*, but the peak list provided did not correspond to any of the reported data from the literature or the experimental data obtained in this study. In the text of the article, Colmbini *et.al.* indicate that there is a band present at 1280cm^{-1} which corresponds to the two carbon bridge of the aromatic function. This band is *not* noted in their table of "Pigments and their relevant Raman shifts" (see Appendix I for a complete copy of this table). Upon examination of the experimental Raman (normal and SERS) and infrared spectra obtained in this study, there is a band at 1290cm^{-1} present, which likely corresponds to the band mentioned in the Colombini *et.al.* article.

Pigment Yellow 83 exhibits bands characteristic of a disazo. Specifically, the N=N stretching at 1400cm^{-1}. A band at 1596 cm^{-1} is characteristic of the C=C (ring breathing) stretch. A band representing the C-Cl stretching is present at 662 cm^{-1} and symmetric C-O-C stretching band is present at 920 cm^{-1}.

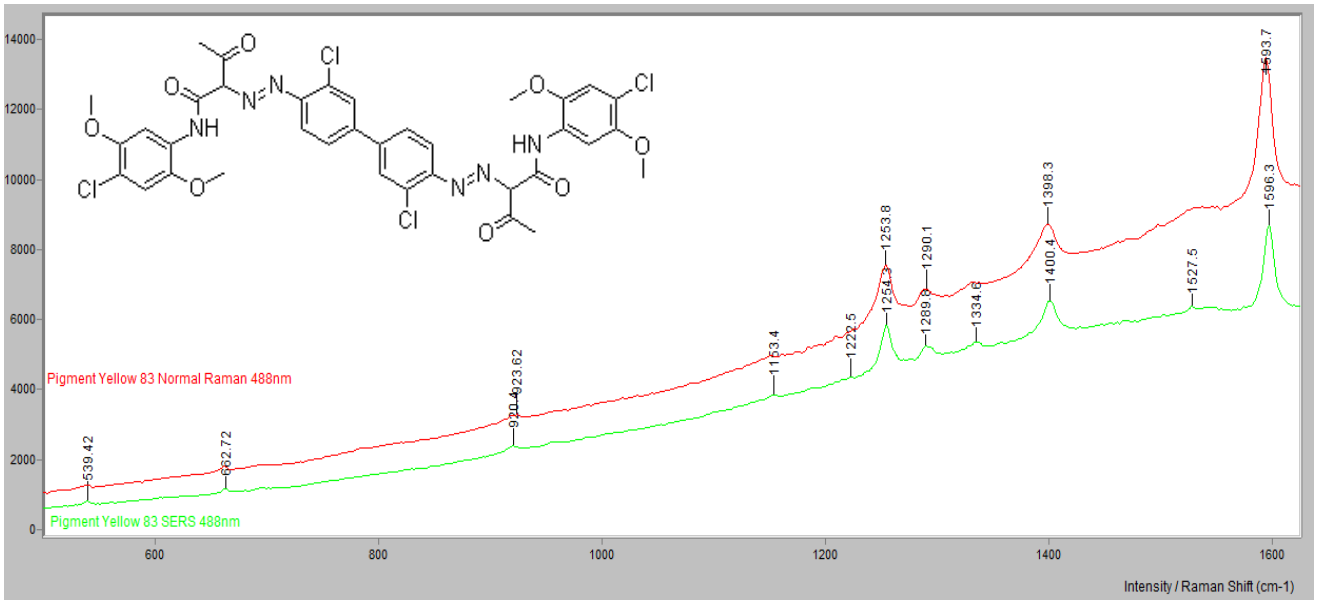

Figure 53. Comparison of Pigment Yellow 83 obtained with normal Raman (red) and SERS (green), λ_0=488nm

Pigment Yellow 151- Bands were resolved with normal Raman spectra with all three excitation wavelengths. The spectrum obtained with SERS corresponds to the bands observed with the normal Raman spectra. Signal enhancement was observed when going from normal Raman to SERS. The FT-IR/ATR spectrum generated a number of well-resolved peaks. With regard to UV/Vis, the absorbance maximum of Pigment Yellow 151 was 272.50nm, likely a hypsochromic shift that resulted from the conc. H_2SO_4. Correlation can be made between the experimental data and reported data for PY 151 (using Colombini, *et.al.*, 2010, Scherrer *et.al.*, 2009 and Ropret *et.al.*, 2007).

Colombini, *et.al.*: (λ_0=785nm): 1582s, 1388s, 1145s

Scherrer *et.al.*: (λ_0=785nm): 1581vs, 1387s, 1248s, 1144s

Ropret *et.al.*: (λ_0=785nm): 1602s-m, 1581vs, 1388s, 1248s-m, 1144s-m

Experimental: (λ_0=488nm): 1651.8, 1579.4, 1492.7, 1453.3, 1386.2, 1247.3

Pigment Yellow 151 exhibits bands characteristic of a monoazo. Specifically, the C-N symmetric stretch at 1143 cm^{-1} (and 1600 cm^{-1}) and the N=N stretching at 1386cm^{-1}. In addition,

bands likely associated with the double annulated structure can be found at 1579 cm^{-1} and 1600cm^{-1}. Amide III and I bands can be found at 1247 cm^{-1} and 1651 cm^{-1}, respectively.

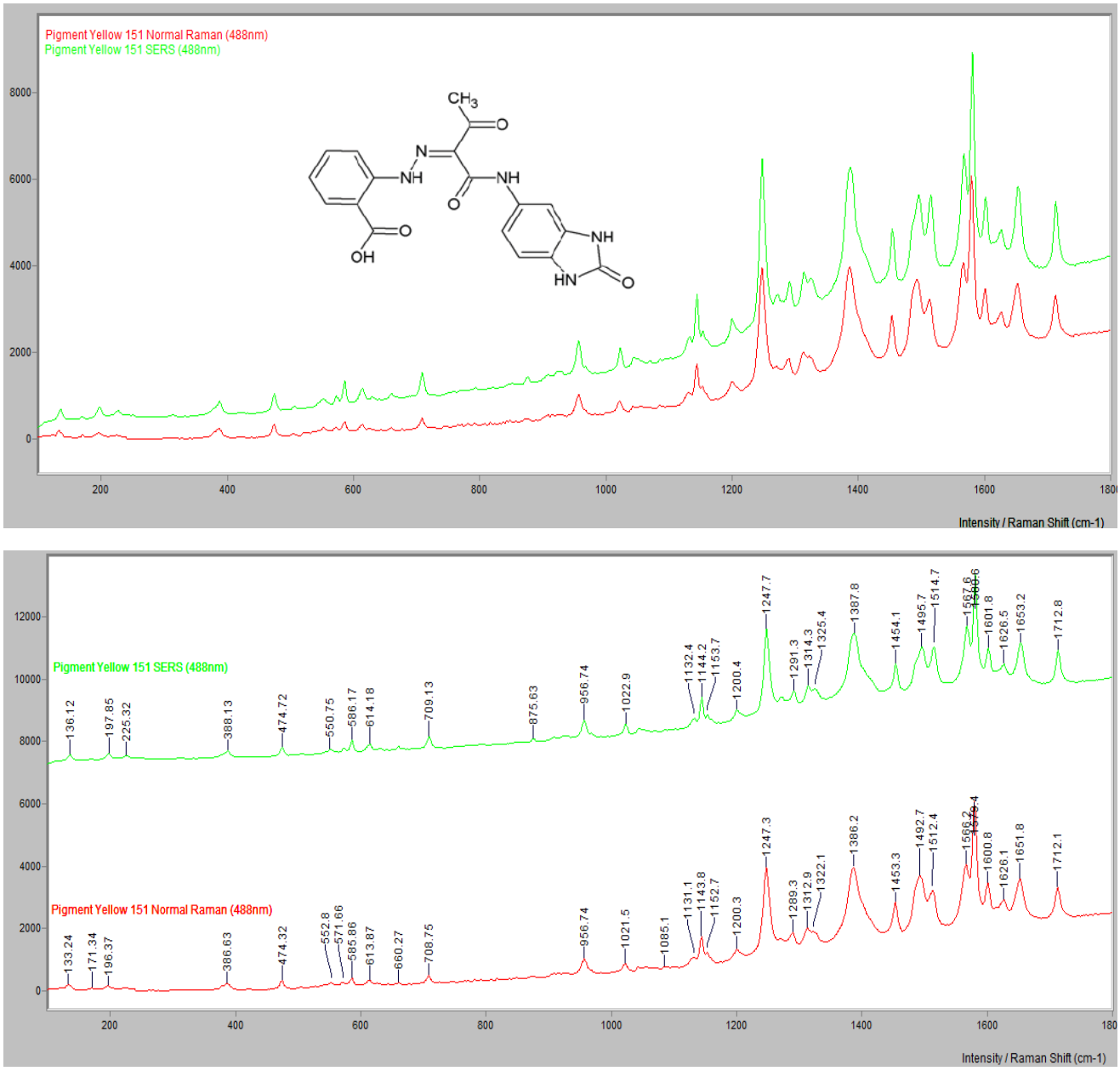

Figure 54 a and b. Comparison of Pigment Yellow 151 obtained with normal Raman (red) and SERS (green) , λ_0=488nm. The top window is displaying the spectra in 'overlaid' form to demonstrate increased signal from normal (red) to SERS (green) and the bottom window is displaying the spectra in 'stacked' form to demonstrate band location correlations.

Pigment Green 7- Bands were resolved with Raman spectra at all four excitation wavelengths. There was not any apparent signal enhancement observed when going from normal Raman to SERS. The FT-IR/ATR spectrum generated a number of well-resolved peaks. With regard to UV/Vis, absorbance maxima for Pigment Green 7 dissolved in conc. H_2SO_4 were observed at 859.50nm and 815.0nm. This was an obvious absorbance shift (bathochromic) from the purple region to the near infrared region, which is consistent with that reported in the article by Billmeyer, *et.al.* (1981). Correlation can be made between the experimental data and reported data for PG 7 (using Scherrer *et.al.*, 2009 and Schulte *et.al.*, 2008).

Scherrer *et.al.*: (λ_0=514nm): 1563s, 1538s, 1506vs, 1389s, 1283s, 1082s, 685vs

Schulte *et.al.*: (λ_0=487.9nm): 1495vs, 1380s, 1200vs, 1074s, 681vs

Experimental: (λ_0=488nm): *see spectra below*. Pigment Green 7 exhibited well resolved bands across all three excitation wavelengths. Interestingly, the spectra were quite different with a change in excitation wavelength, which is due to the resonance effects resulting from the $\Delta\ \lambda_0$ on the molecular structure of the phthalocyanine. This is important in that it not only lends support to the assertion that all reported Raman spectra should have the corresponding λ_0 listed, but it indicates that comparisons between two or more spectra should be done where the same λ_0 was used to generate the spectra.

Bands characteristic of the breathing and deformations of the phthalocyanine TBP nucleus can be found at around 680 cm^{-1} and in the region from about 750 to 800 cm^{-1}. The band located at around 230-235 cm^{-1} corresponds to the N-Cu metal bond. As the excitation wavelength changes, the relative ratios of these bands associated with the TBP nucleus change also. In some instances, the bands may not even be resolved above the background. The band located around 1520-1535cm^{-1} remains dominant in the spectra and can be attributed to the ring breathing of the molecule.

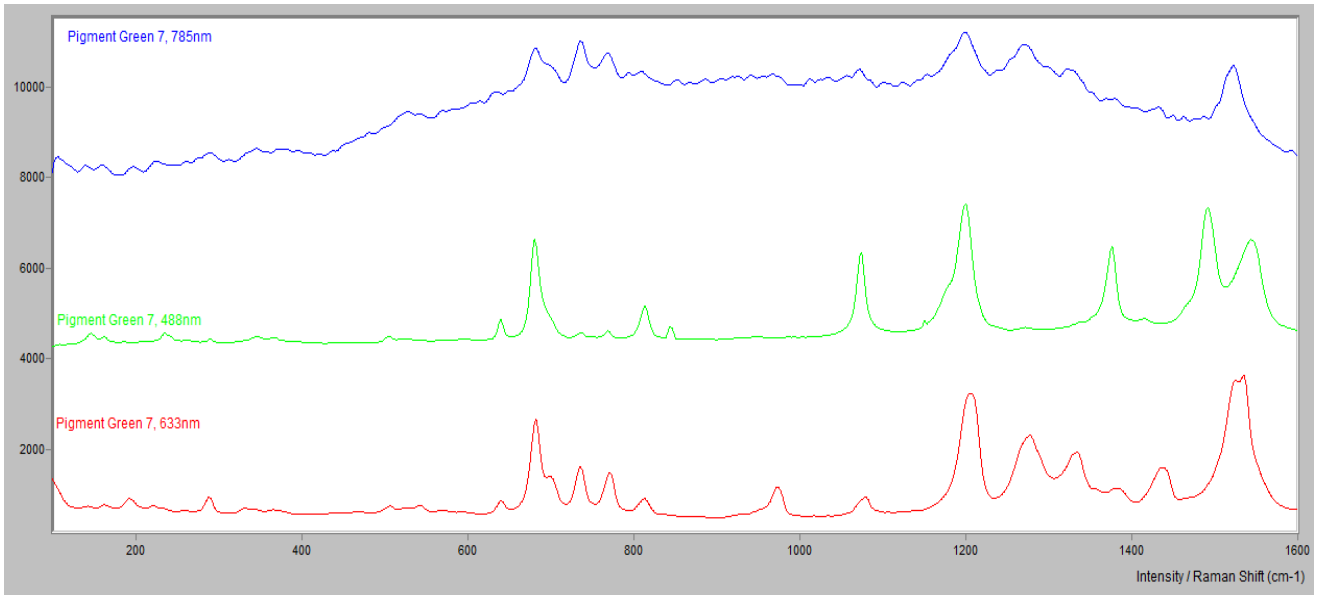
Pigment Green 7, 785nm
Pigment Green 7, 488nm
Pigment Green 7, 633nm
10000
8000
6000
4000
2000
200
400
600
800
1000
1200
1400
1600
Intensity / Raman Shift (cm-1)

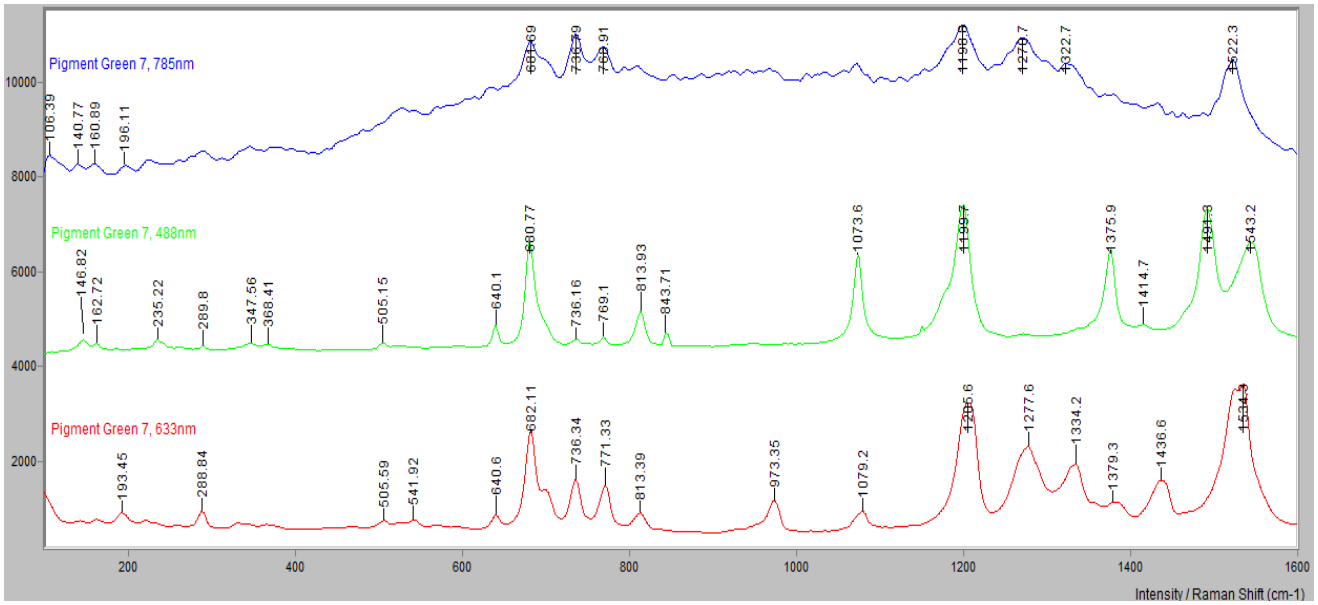
Pigment Green 7, 785nm
Pigment Green 7, 488nm
Pigment Green 7, 633nm
106.39
140.77
160.89
196.11
680.77
736.16
769.1
813.93
843.71
1073.6
1375.9
1414.7
1543.2
146.82
162.72
235.22
289.8
347.56
368.41
505.15
640.1
193.45
288.84
505.59
541.92
640.6
682.11
736.34
771.33
813.39
973.35
1079.2
1277.6
1334.2
1379.3
1436.6
10000
8000
6000
4000
2000
200
400
600
800
1000
1200
1400
1600
Intensity / Raman Shift (cm-1)

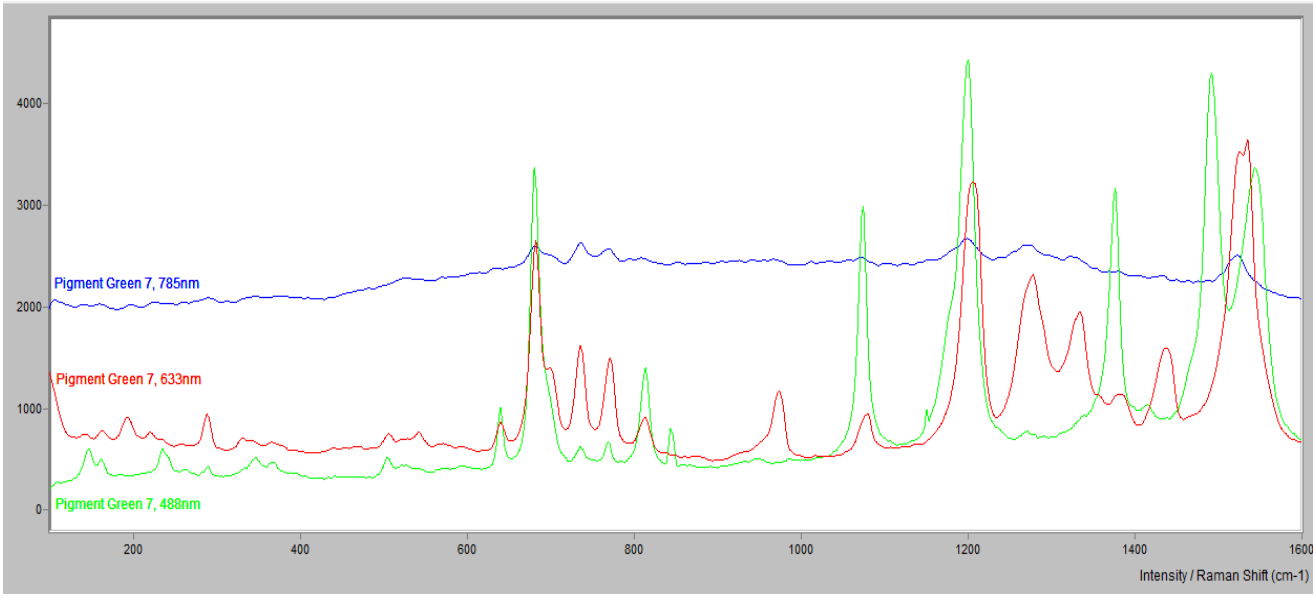

Figure 55 a, b and c. Comparison of Pigment Green 7 at different excitation wavelengths, stacked without band labels (top), stacked with labels (middle) and overlaid (bottom).

Pigment Blue 15, 15:1, 15:2, 15:3- Bands were resolved with normal Raman spectra with all three excitation wavelengths. Only Pigment Blue 15 was available for SERS. There was not any apparent signal enhancement observed when going from normal Raman to SERS. The FT-IR/ATR spectrum generated a number of well-resolved bands (Note: there was a very small amount of Pigment Blue 15 available for FT-IR/ATR. Spectral quality was not very high for Pigment Blue 15, but peaks were still resolved). With regard to UV/Vis, absorbance maxima for Pigment Blue 15 dissolved in conc. H_2SO_4 were observed at 791.0nm and 700.50nm. This was an obvious absorbance shift (bathochromic) from the orange region to the red/near infrared region, which is consistent with that reported in the article by Billmeyer, *et.al.* (1981). Correlation can be made between the experimental data and reported data for PB 15 (using Scherrer *et.al.*, 2009). Correlation between reported spectra and experimental spectra for the polymorphs of pigment blue were also made.

Scherrer *et.al.*: (λ_0=785nm): 1522vs, 1336s, 746/747vs, 679s

Experimental: (λ_0=488nm): *see spectra below*. In comparing experimental spectra with that in the literature, it became apparent that, while in most cases, band locations were relatively consistent with changing excitation wavelength (although variation in band presence/absence can be seen), the excitation wavelength used would affect the relative band intensities. This could be problematic in interpretation when comparing spectra of the same substance that were generated with different excitation wavelengths). When individuals report intensities in the literature (*e.g.* vs, s, s-m, *etc.*), an analyst should bear in mind that these values are subjective and will vary depending on the excitation wavelength. This can be seen with Pigment Blue 15, as correlation to the literature would vary based upon which excitation wavelength spectra was selected for comparison:

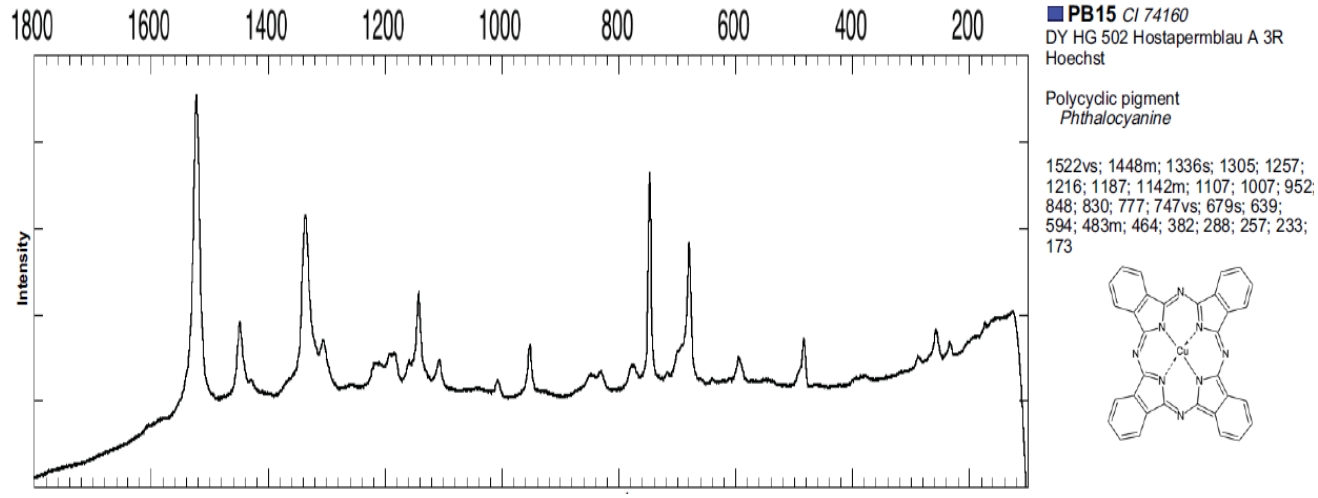

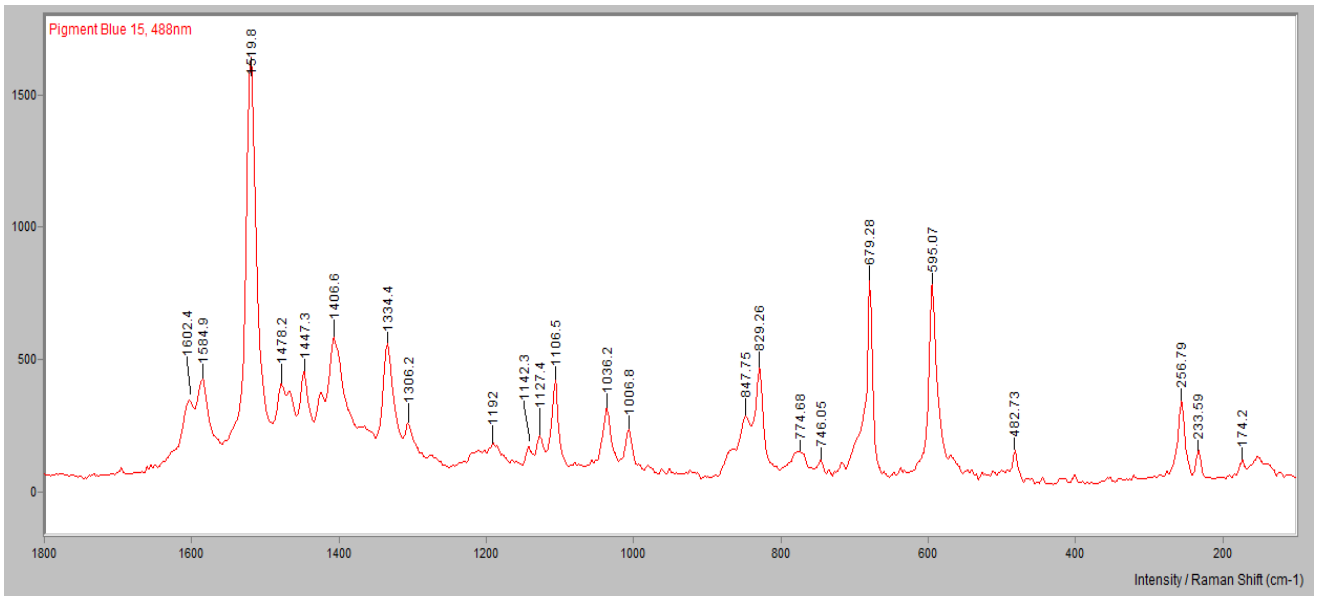

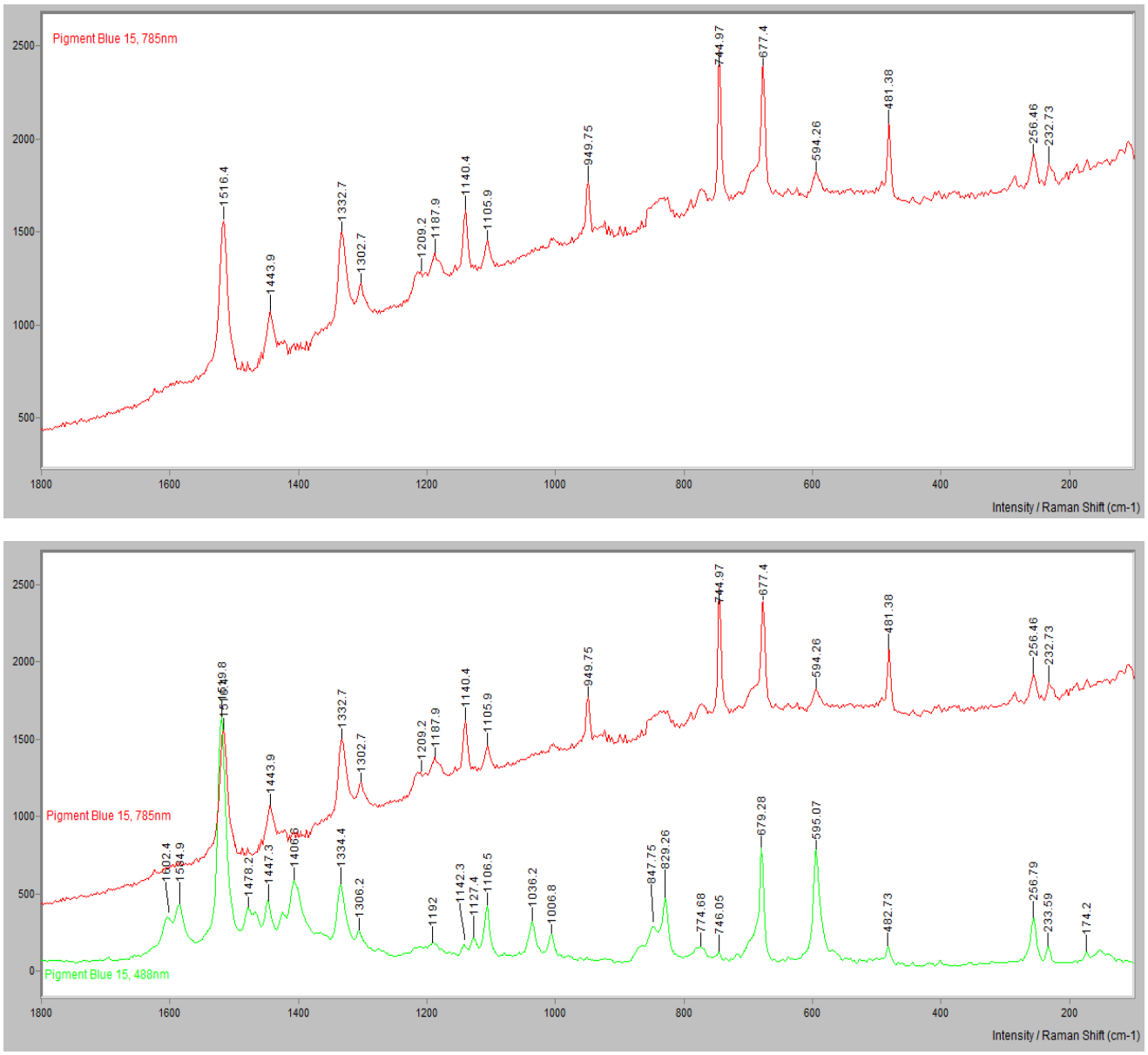

Figure 56 a-d. Pigment Blue 15 spectra from Scherrer, *et.al.*, λ_0=785nm (top), experimental, λ_0=488nm (upper middle) and experimental λ_0=785nm (lower middle) and an overlay of the two experimental spectra (bottom). Note the variation in band intensities in addition to the absence/presence of bands. (The series of spectra are provided with the x-axis in descending order to correspond to the Scherrer *et.al.* spectrum).

This variation in Raman spectra with a change in excitation wavelength can be attributed to resonance effects, specifically selective enhancement from resonance with different electronic states. It is reported that phthalocyanine molecules have a B (or Soret) band in the blue region of the absorption spectrum and a Q (allowed $\pi \rightarrow \pi^*$ transition) band in the red region of the

absorption spectrum.. The B and Q bands are associated with vibronic bands and the use of visible excitation wavelengths in these regions (blue and red, respectively) (will give rise to resonance or pre-resonance enhancements (Bovill, 1986, pp. 569). The metal ion incorporated into the porphyrin ring system can also affect the resultant spectra and band locations. The band located around 1520-1530cm^{-1} remains dominant in the spectra and can be attributed to the ring breathing of the molecule (C-N). Bands characteristic of the breathing and deformations of the phthalocyanine TBP nucleus can be found at around 680 cm^{-1} (C-N-C, N-C, N-C-C) and in the region from about 750 to 800 cm^{-1} (C-N-C, Cu-N). The band located at around 230-235 cm^{-1} corresponds to the N-Cu metal bond. As the excitation wavelength changes, the relative ratios of these bands associated with the TBP nucleus change also. In some instances, the bands may not even be resolved above the background.

Copper phthalocyanine is a planar molecule consisting of 57 atoms. It has 165normal vibrations and is in the symmetry group D_{4h}. The following irreducible representations are reported (Basova and Kolesov, 2000, pp. 771):

$$\Gamma_{vib} = 14A_{1g} + 13A_{2g} + 14B_{1g} + 14B_{2g} + 13E_g + 6A_{1u} + 8A_{2u} + 7B_{1u} + 7B_{2u} + 28E_u$$

in which the A_{1g}, B_{1g} and B_{2g} modes are Raman active and the A_{2u} and E_u modes are infrared active (Li, *et.al*., 2005, pp. 192). Experimental and calculated vibrational and absorption spectra of the phthalocyanines and their metal complexes has been reported in the literature along with detailed assignment of vibrational modes (Bovill, *et.al.*, 1985, Basova and Kolesov, 2000, Li, *et.al*., 2005, Liu, *et.al.*, 2007) . Basova, *et.al*. report, "…some contradictory assumptions concerning the assignments of the bands in (various phthalocyanines) still exist. The agreement between the data of symmetry assignments of the bands in IR spectra of CuPc obtained by

different authors is good, while the assignments in the Raman spectra are often very different." (2009, pp. 2081). The authors further add that the discrepancies in Raman band assignments are largely due to the lack of experimental support of the theoretical, calculated data. Evaluation of the data obtained by Baslova *et.al.*, 2009 correlates to the data reported by Bovill, *et.al.* in 1985 (concerning α copper phthalocyanine) and Li *et.al.* in 2005. It is important to note that with regard to experimental data, the authors of the various studies report the use of different excitation lasers (ranging in the blue, green and red regions), with some authors not specifically reporting the λ_0 used to generate their experimental data (they instead refer the reader to the literature in which the experimental data was acquired; see Li *et.al*, 2005 and Liu, *et.al.*, 2007).

Copper phthalocyanine is described as 'unusual' in regard to the fact that there is an increase in observed fluorescence with an increase in excitation wavelength (contrary to the tendency of fluorescence to decrease as the source approaches near infrared wavelength status). This fluorescence displays itself in a characteristic manner, and can be a means for preliminary identification of the copper phthalocyanines (blues and greens). It is believed that this phenomenon is due to the presence of the copper transition metal.

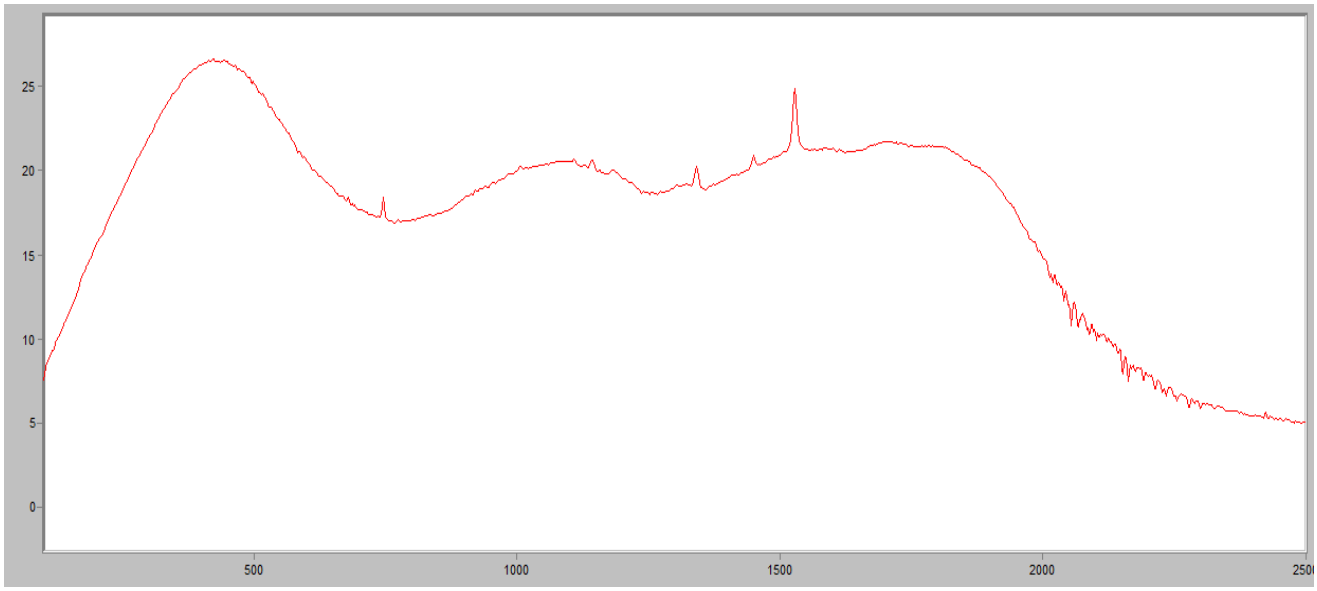

Figure 57. Characteristic fluorescence superimposed on a tattoo ink containing copper phthalocyanine (blue).

Pigment Violet 23α- Bands were resolved with normal Raman spectra with λ_0=488nm. Overwhelming fluorescence was observed with λ_0=633nm and 785nm, and no useful data were obtained at these excitation wavelengths. No spectrum was generated using the FT-Raman, even after mixing the pigment with KBr in an effort to minimize sample heating and reduce fluorescence. The spectrum obtained with SERS corresponds to the bands observed with the normal Raman spectrum at λ_0=488nm. Signal enhancement was observed when going from normal Raman to SERS as well as resolution of bands not observed in the normal Raman spectrum. The FT-IR/ATR spectrum generated a few broad peaks. With regard to UV/Vis, Pigment Violet 23α underwent a hypsochromic shift when dissolved in conc. H_2SO_4, the absorbance maximum being located at 317nm. The color exhibited upon mixing the powder with the conc. H_2SO_4 was a faint pinkish/red. No reference Raman spectra could be found for Pigment Violet 23α in the literature. The following major bands are reported for the spectrum with λ_0=488nm: 1481.1, 1406.8, 1329.2, 1283.5, 1166.7.

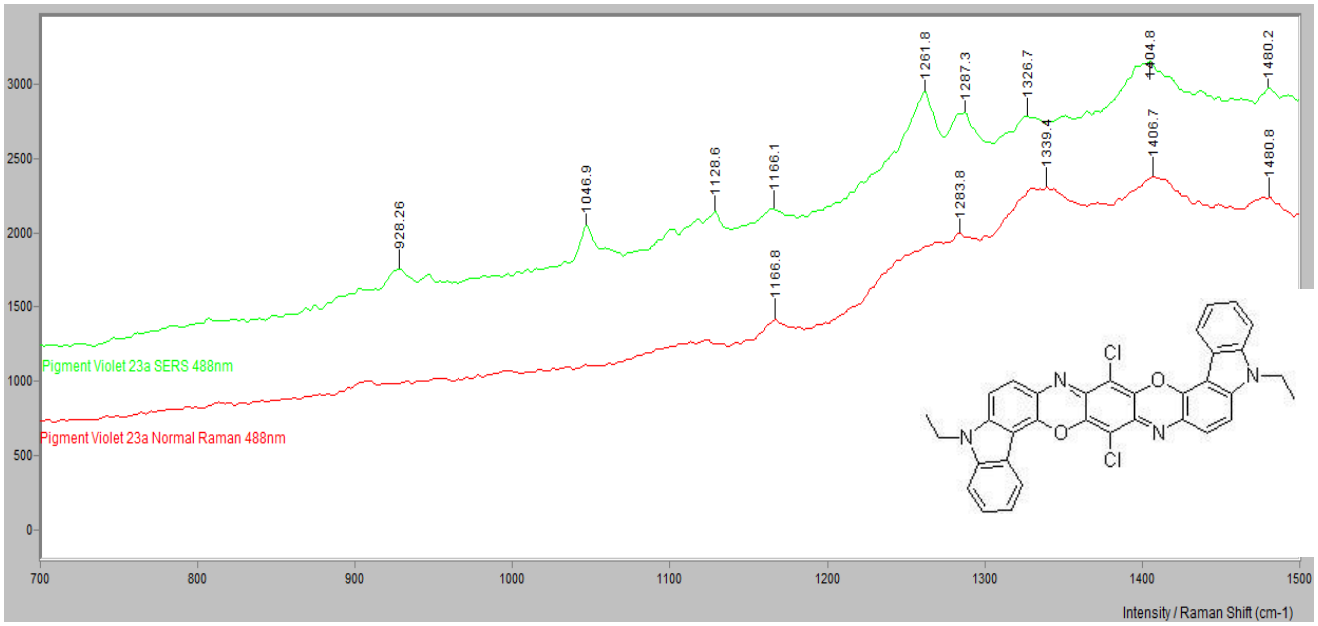

Figure 58. Comparison of Pigment Violet 23α obtained with normal Raman (red) and SERS (green) , λ_0=488nm

Pigment Violet 23β- Bands were resolved with Raman spectra at all four excitation wavelengths. The spectrum obtained with SERS corresponds to the bands observed with the normal Raman spectra. Signal enhancement was observed when going from normal Raman to SERS. The FT-IR/ATR spectrum generated a number of well-resolved peaks. With regard to UV/Vis, Pigment Violet 23β underwent a hypsochromic shift when dissolved in conc. H_2SO_4, the absorbance maximum being located at 313nm. Correlation can be made between the experimental data and reported data for PV 23β (using Scherrer *et.al.*, 2009).

Scherrer *et.al.*: (λ_0=514nm): 1391vs

Experimental: (λ_0=488nm): 1427.4, 1388.6, 1343.4, 1204.6

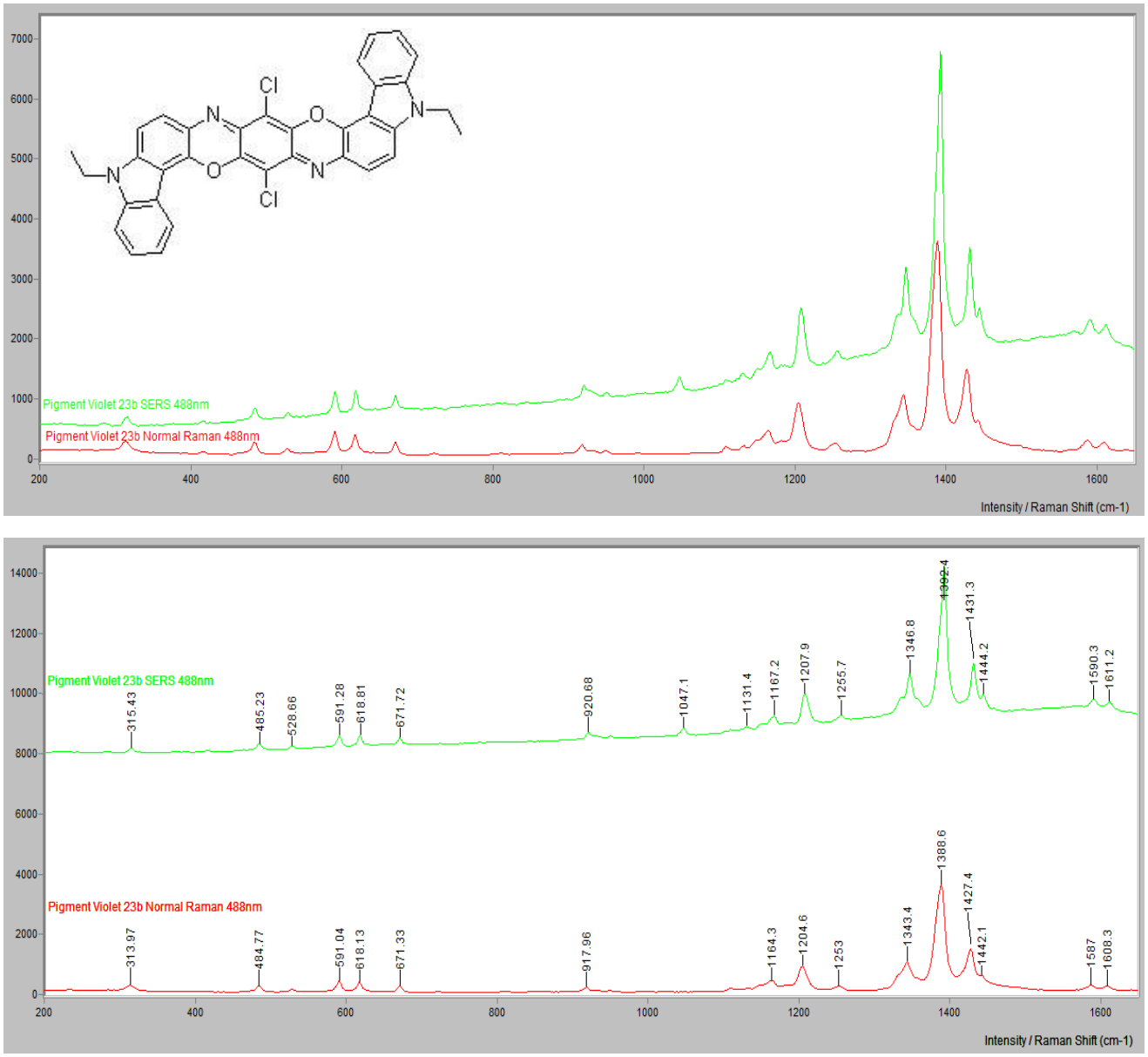

Figure 59 a and b. Comparison of Pigment Violet 23β obtained with normal Raman (red) and SERS (green) , λ_0=488nm. The top window is displaying the spectra in 'overlaid' form to demonstrate increased signal from normal (red) to SERS (green) and the bottom window is displaying the spectra in 'stacked' form to demonstrate band location correlations.

When comparing the Raman spectra of Pigment Violet 23α and Pigment Violet 23β, there are obvious differences. This indicates that it is possible to distinguish between the two polymorphs with Raman spectroscopy. It is interesting to note the difference between the α and β forms with regard to the normal Raman spectra, the SERS spectra, the infrared spectra and the

absorption spectra. These differences indicate that PV23α and PV23β likely differ in molecular structure or chemical constitution (for example, isomorphism) and not just in crystal form of the same molecule, making the 'polymorph' designation a misnomer. To test this hypotheses, crystal structure determination of the α and β forms can be carried out by x-ray diffraction. Additional evaluations of different molecular conformations (S-shape *vs.* linear, *cis vs. trans*) using DFT calculations may also enable the correlation of experimental spectral data with theoretical spectral data, allowing for the determination of correct molecular structure designation for PV23α and PV23β.

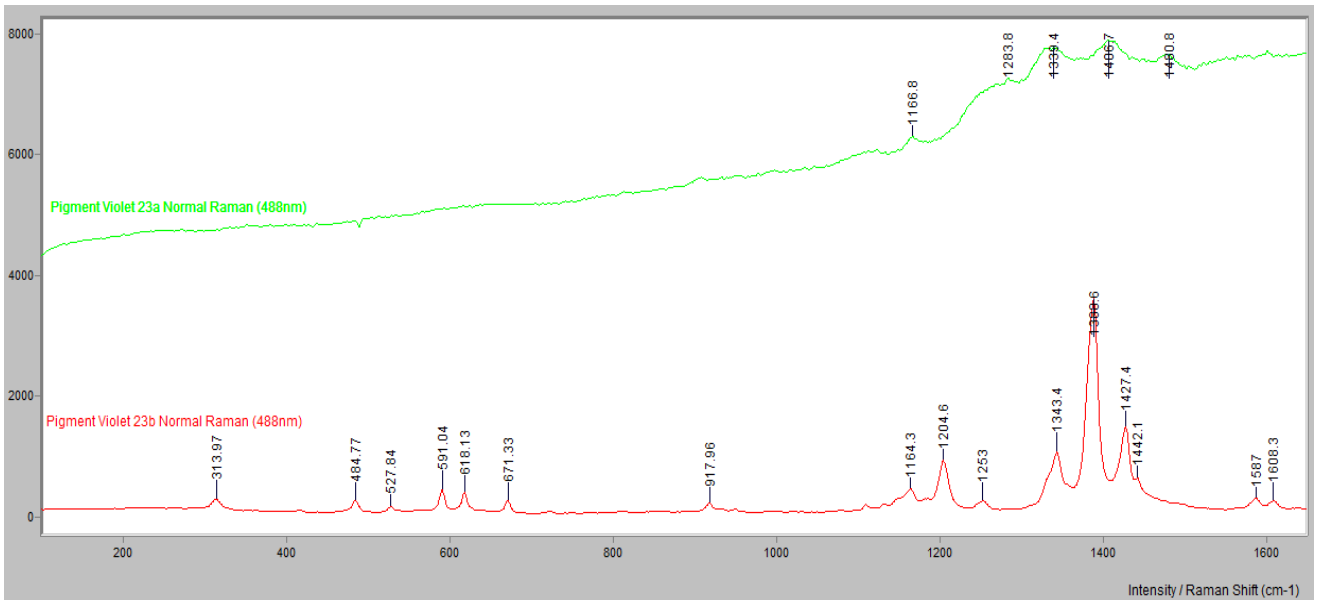

Figure 60. Comparison of the normal Raman spectra of Pigment Violet 23α (green spectrum) and Pigment Violet 23β (red spectrum) [λ_0=488nm].

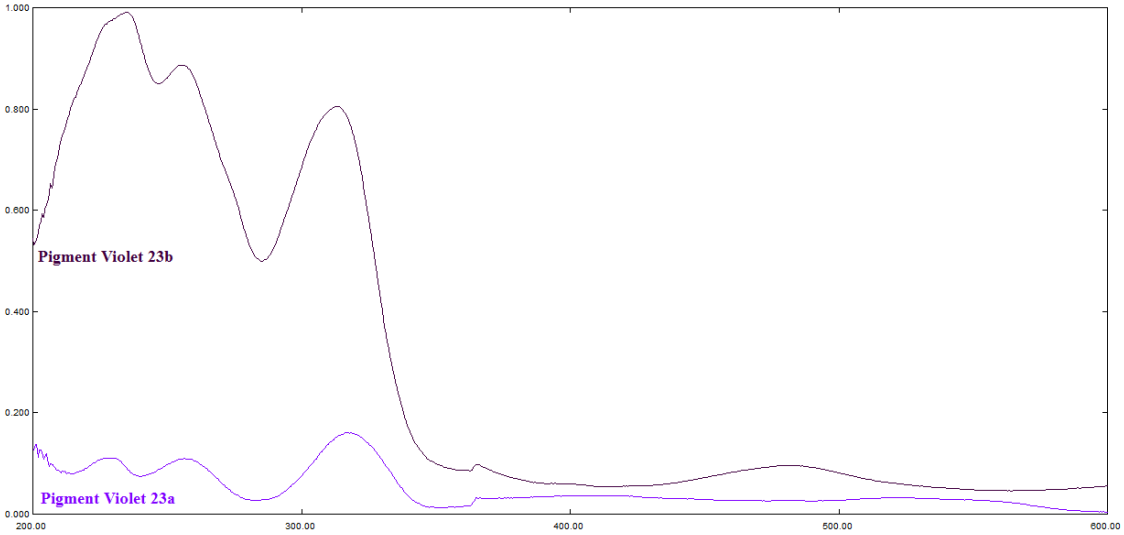

Figure 61.Comparison of Pigment Violet 23α and β absorbance spectra. Note the additional peak at 482nm present in the β polymorph.

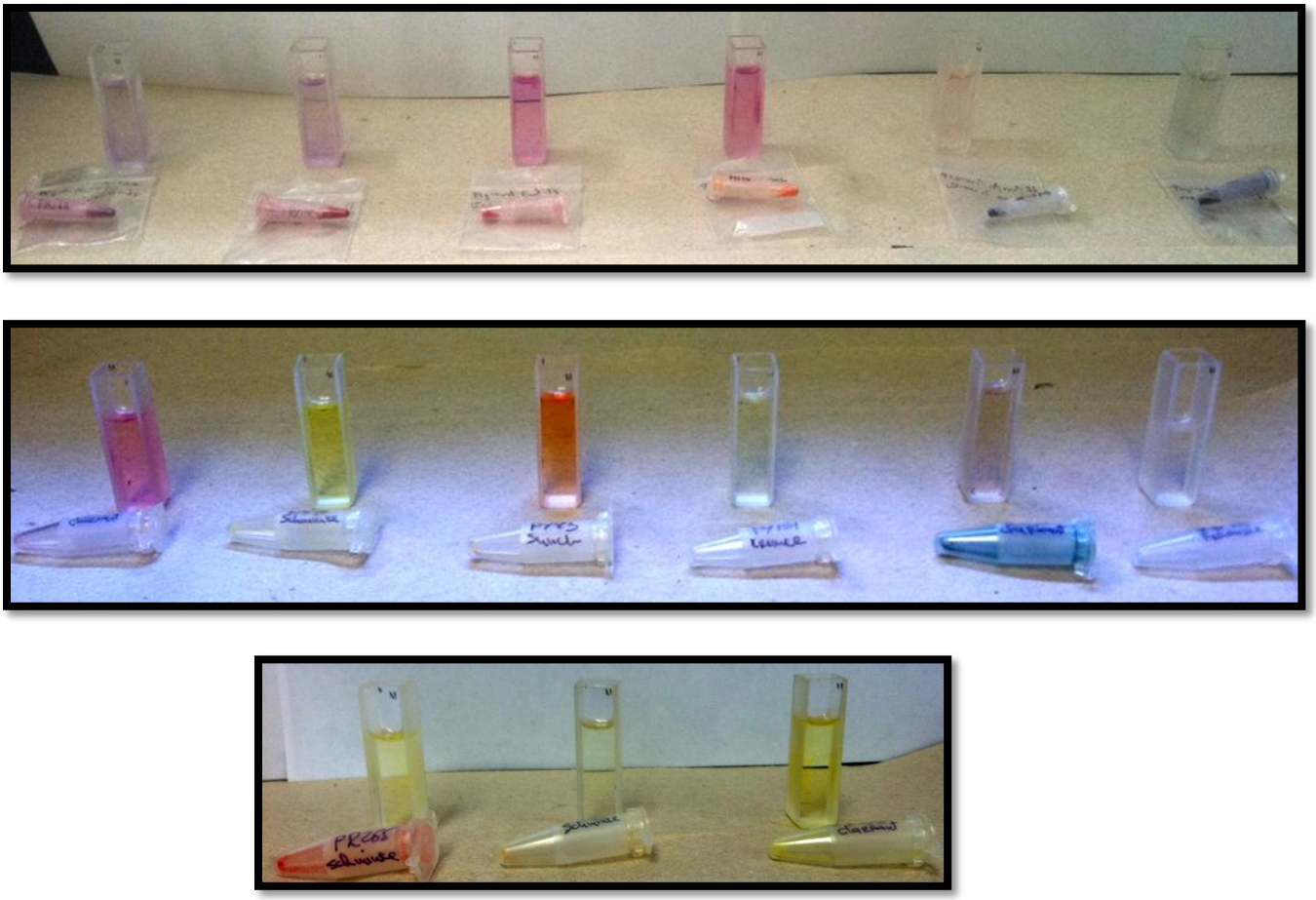

Figure 62 a, b and c. Pigment standards dissolved in conc. H_2SO_4 in fused silica cuvettes in preparation for UV/Vis analysis- (top) PR 122, PR 146, PR 170, PO 16, PV 23a, PV 23b; (middle) PO 34, PY 3, PY 83, PY 151, PG 7, PB 15; (bottom) PR 255, PO 62, PY 73.

Results- Tattoo Inks

Skin Candy

The Skin Candy Tattoo Ink set was analyzed extensively due largely to the fact that it was the only tattoo ink set that had available pigment composition data. This allowed for attainment of pigment standards that could be analyzed with similar instrumental parameters, facilitating spectral comparisons. Of the analyses conducted on the Skin Candy Tattoo Inks the following are considered:

- comparisons of the inks at different excitation wavelengths (Normal Raman-488nm, 633nm and 785nm and FT-Raman-1064nm) to evaluate the consistency of spectra with changing λ_0,
- comparison of the pigment extractions at the different excitation wavelengths (Normal Raman-488nm, 633nm and 785nm and FT-Raman-1064nm) to evaluate the consistency of spectra with changing λ_0,
- comparison of the tattoo ink to the pigment extraction to evaluate any spectra differences between direct analysis of the ink and the pigment extracted from the ink (using the procedure described in the Methods section),
- comparison of the tattoo ink to the pigment(s) listed on the bottle label to determine whether there is consistency with contents and ingredients listed on the label. In addition, this comparison may aid in determining whether or not there are other materials within the tattoo ink,
- comparison of the tattoo ink analyzed with normal Raman and SERS to further evaluate and validate the use of SERS,
- comparison of the SERS spectrum of the pigment extraction of the tattoo ink and the SERS spectrum of the pigment(s) listed on the bottle label also to further evaluate and validate the use of SERS,
- comparison of absorbance spectra of the tattoo ink pigment extraction and the corresponding pigment standard

In addition to the above, information pertaining to the visual and microscopic examinations, UV/Vis, FT-IR (ATR) and XRF spectra were collected and reported in order to characterize and develop a comprehensive tattoo ink database.

Overall, there were no substantial differences between the spectra of the tattoo inks and the pigment extractions. The extraction procedure was effective in separating the pigments and the titanium dioxide. In the case of the phthalocyanines (blue and green pigments), although

considered organic pigments, this class exhibited extraction characteristics consistent with inorganic pigments due to the metal complex, which made the extraction procedure less efficient when carbon tetrachloride was used as a solvent.

Candy Apple Red- Good correlation was found between Candy Apple Red and Pigment Red 146. Signal enhancement was observed when SERS was employed. XRF indicated the presence of titanium, chlorine and iron. It is probable that the titanium is due to the presence of titanium dioxide.

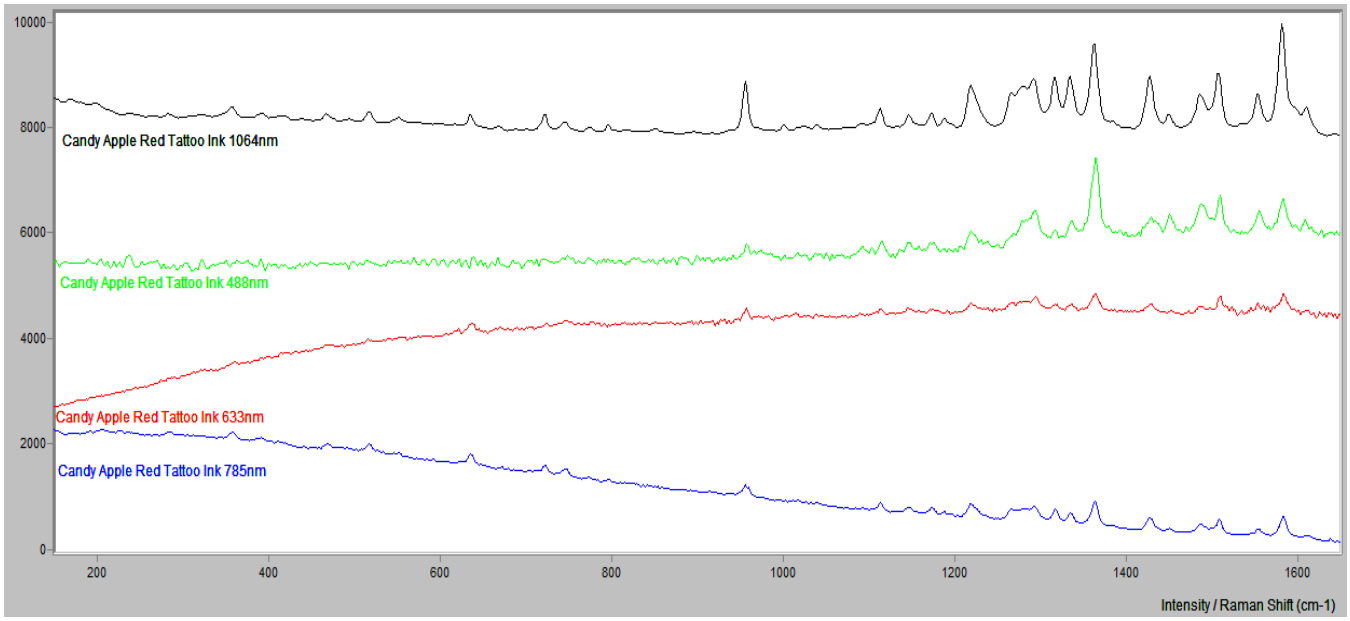

Figure 63. Raman spectra of Candy Apple Red ink at different excitation wavelengths.

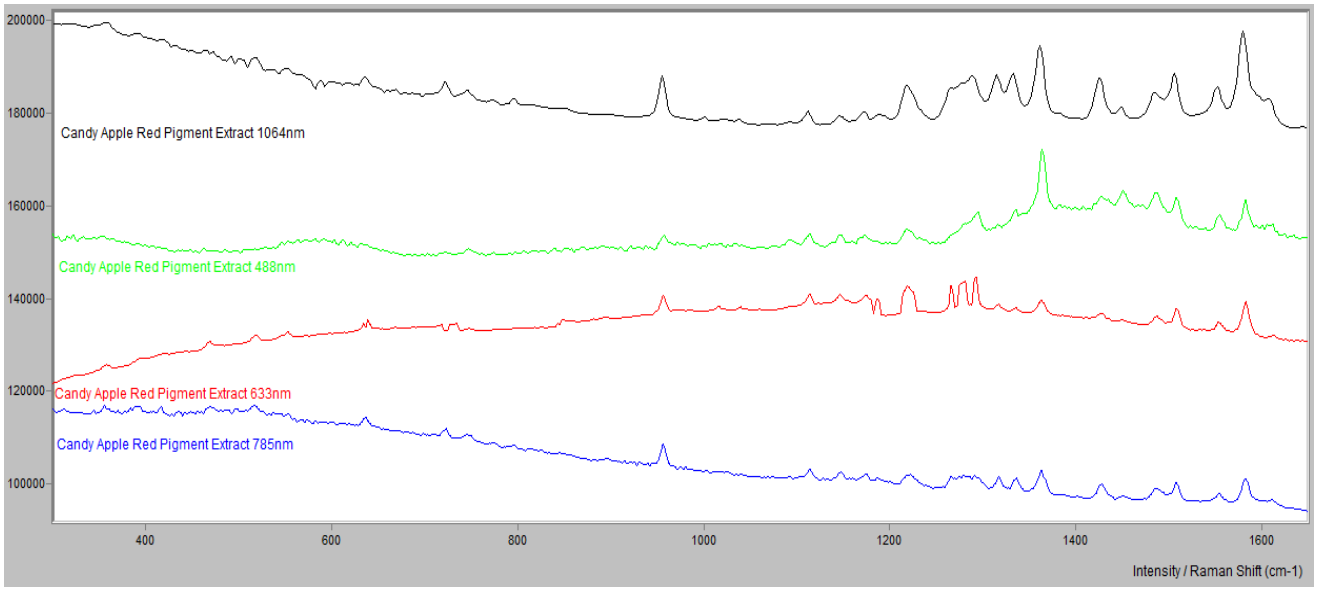

Figure 64. Raman spectra of Candy Apple Red pigment extraction at different excitation wavelengths.

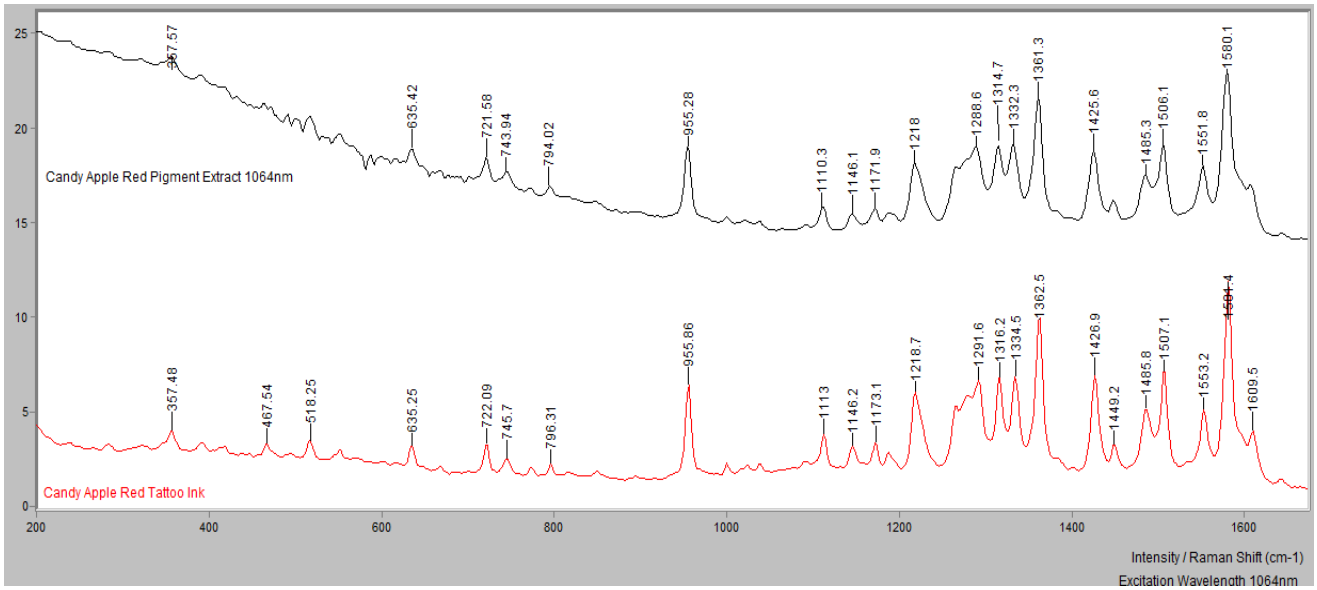

Figure 65. Comparison of Raman spectra of Candy Apple Red Tattoo ink and pigment extraction.

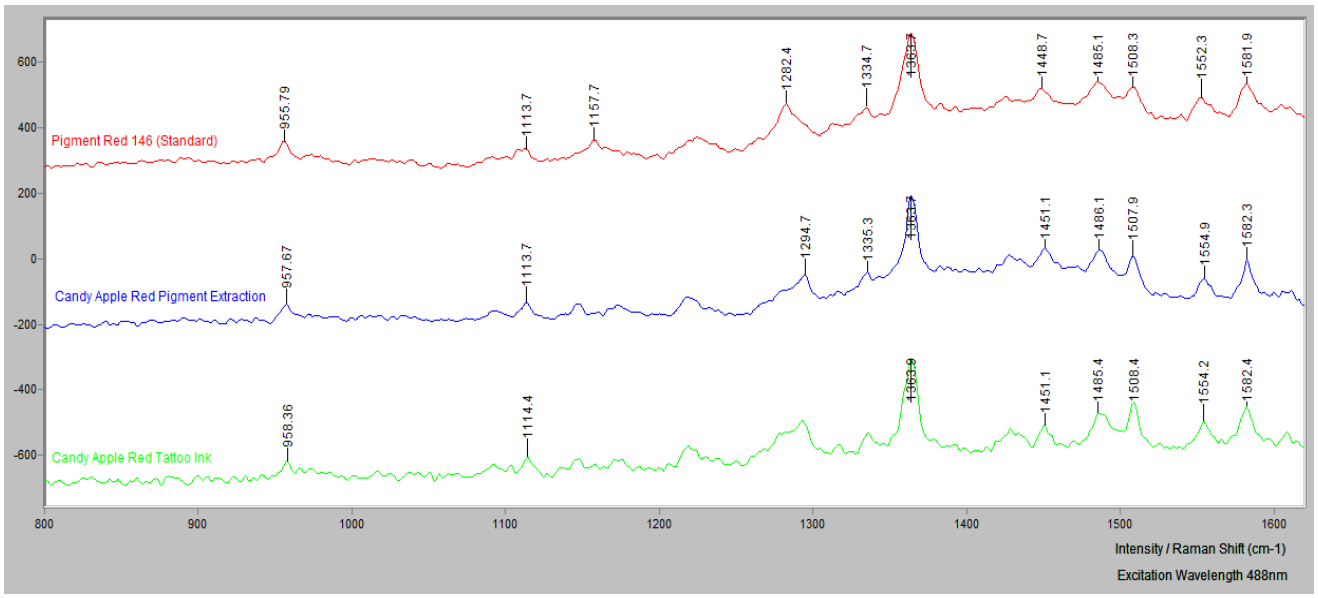

Figure 66. Normal Raman spectra of Candy Apple Red ink and pigment extraction compared to Pigment Red 146.

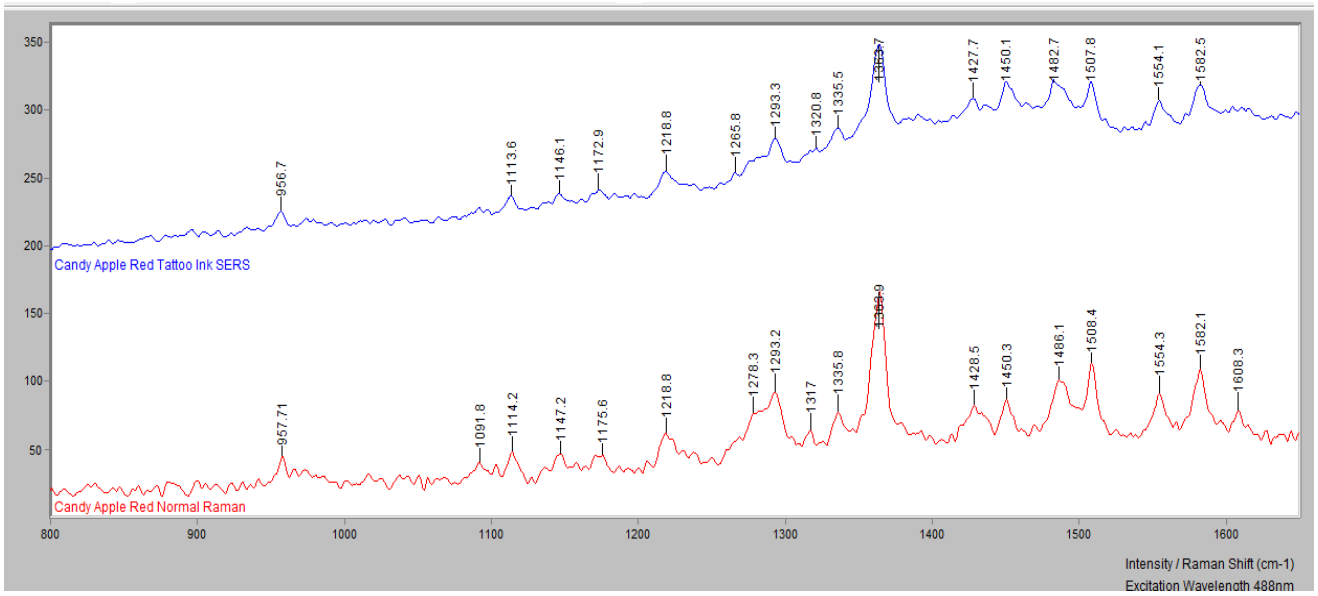

Figure 67. Normal Raman spectra of Candy Apple Red ink compared to SERS spectra of Candy Apple Red ink.

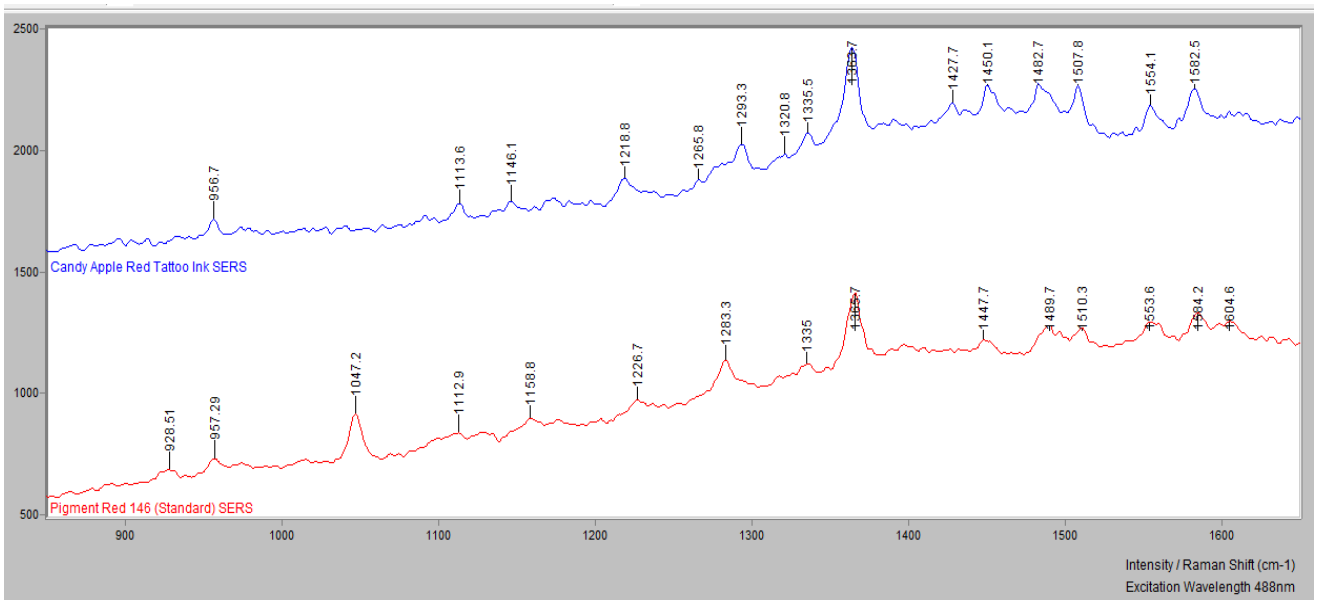

Figure 68. SERS spectra of Candy Apple Red ink compared to Pigment Red 146.

Red Hot- Good correlation was found between Red Hot and Pigment Red 170. Signal enhancement was observed when SERS was employed. XRF indicated the presence of chlorine and iron.

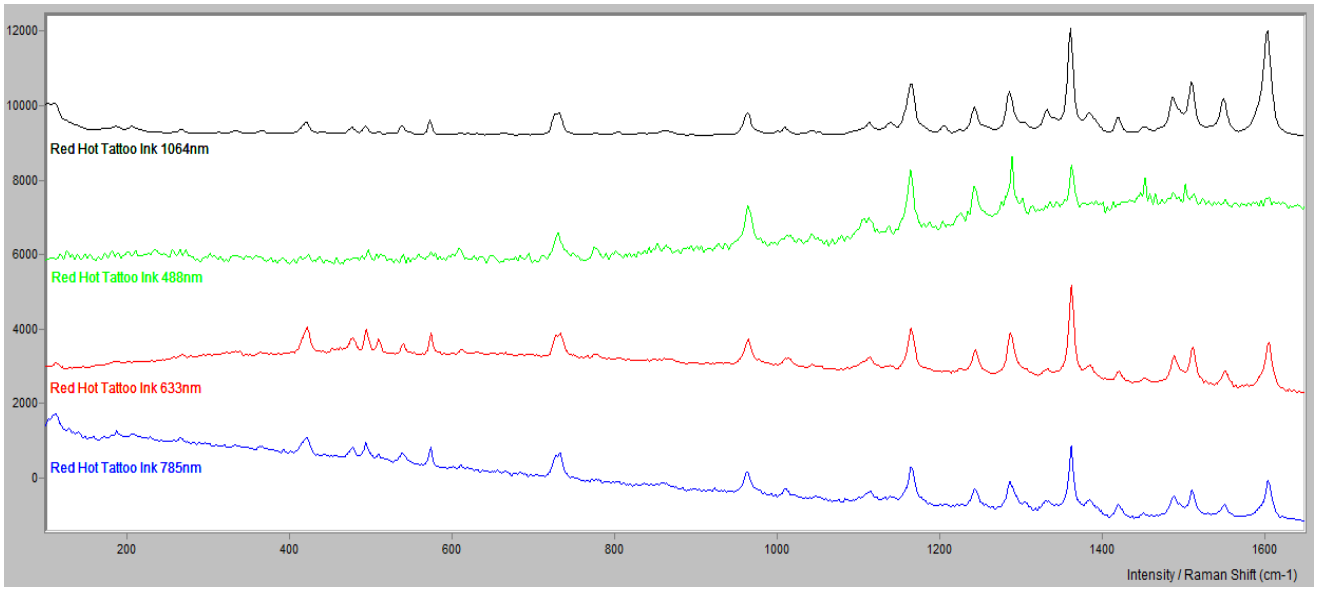

Figure 69. Raman spectra of Red Hot ink at different excitation wavelengths.

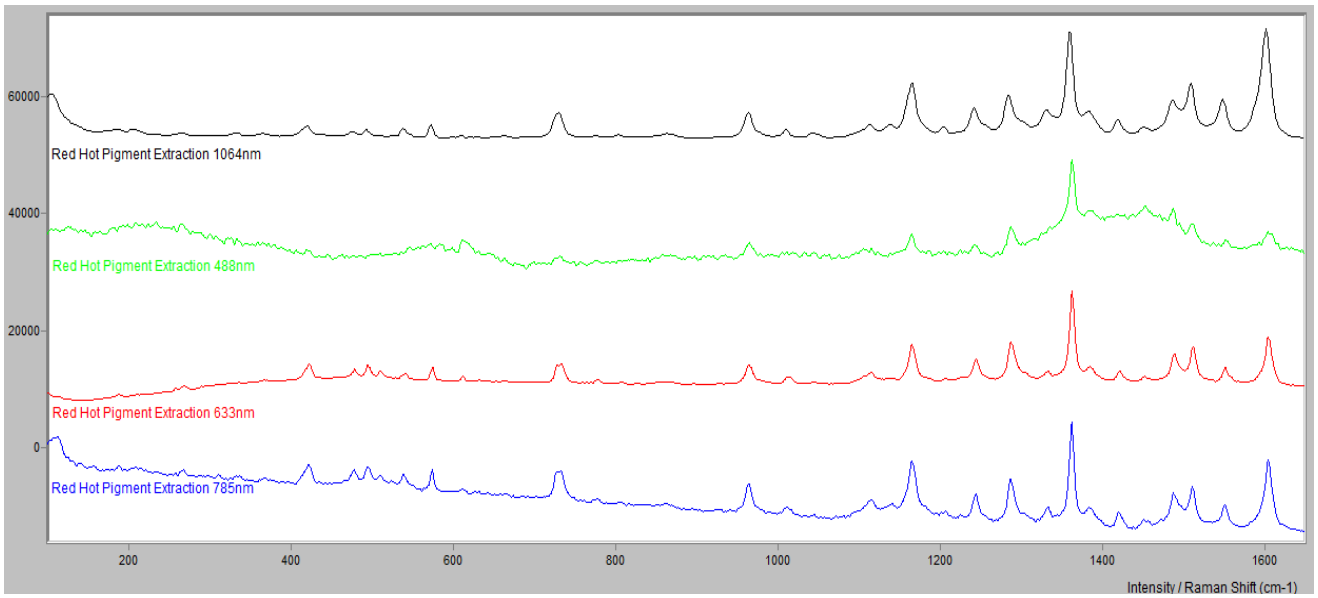

Figure 70. Raman spectra of Red Hot pigment extraction at different excitation wavelengths.

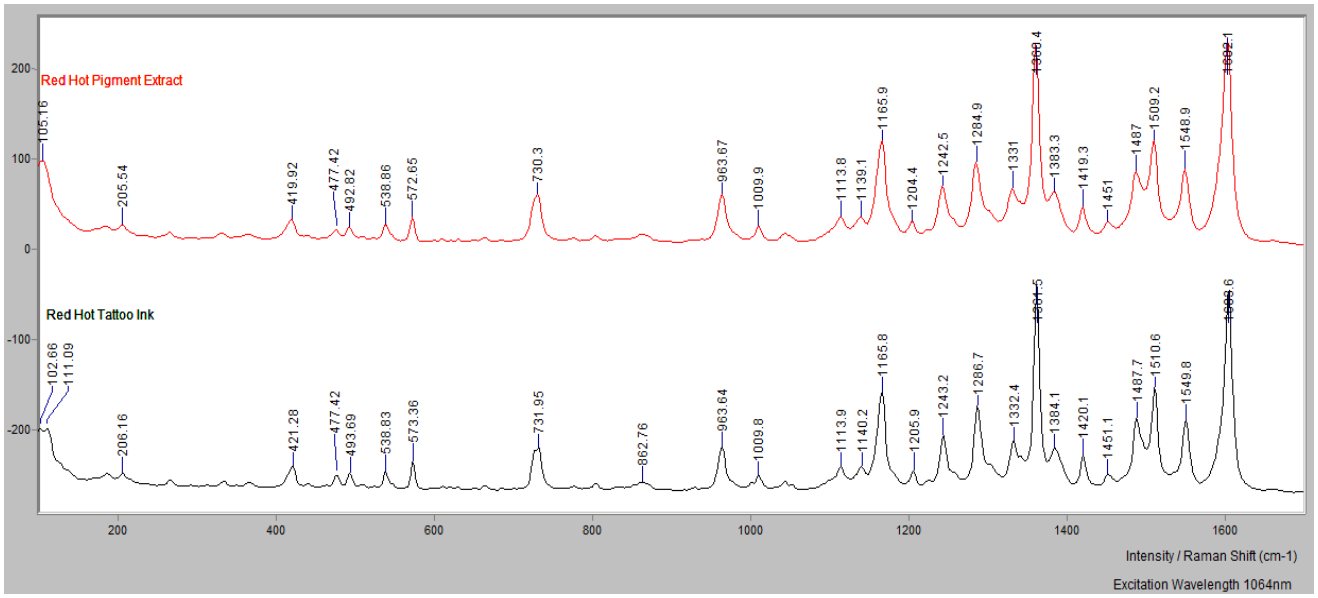

Figure 71. Comparison of Raman spectra of Red Hot ink and pigment extraction.

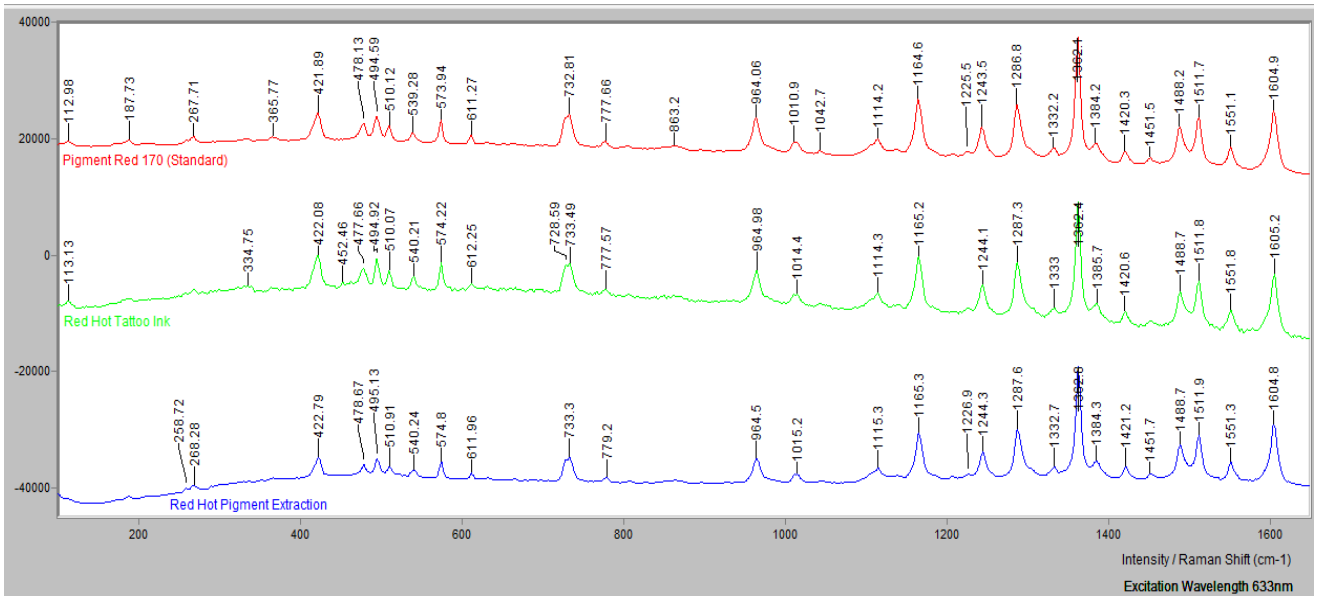

Figure 72. Normal Raman spectra of Red Hot ink and pigment extraction compared to Pigment Red 170.

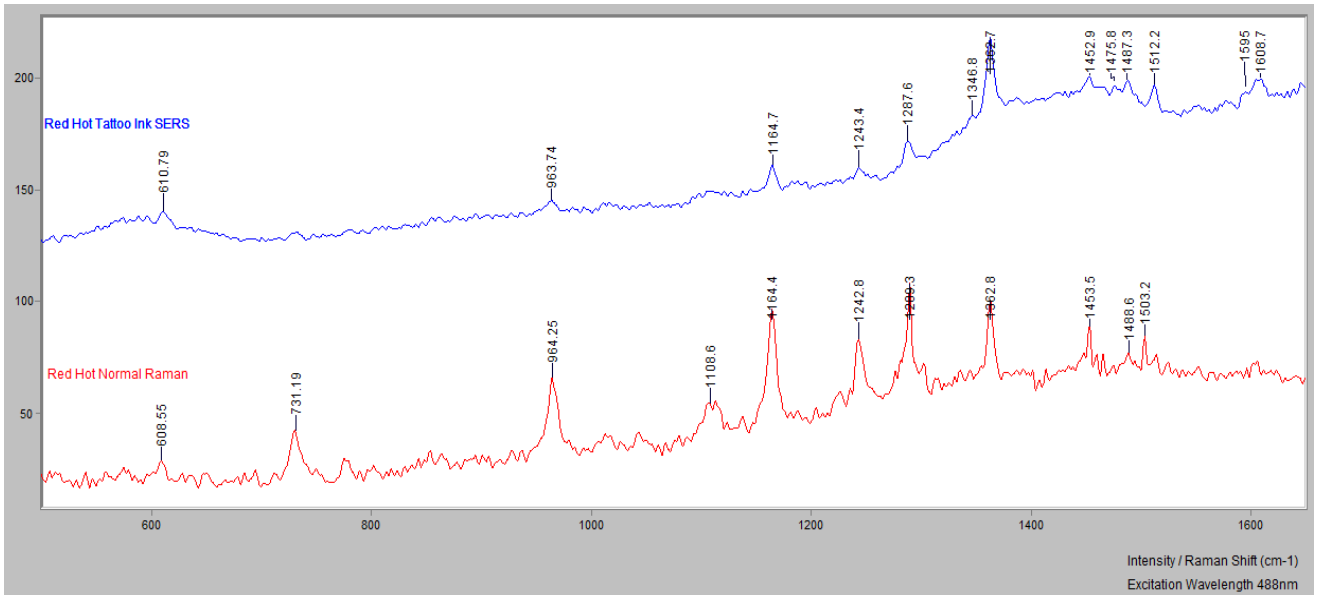

Figure 73. Normal Raman spectra of Red Hot ink compared to SERS spectra of Red Hot ink.

Marz- Good correlation was found between Marz and Pigment Orange 16. XRF indicated the presence of titanium, chlorine and iron. It is probable that the titanium is due to the presence of titanium dioxide.

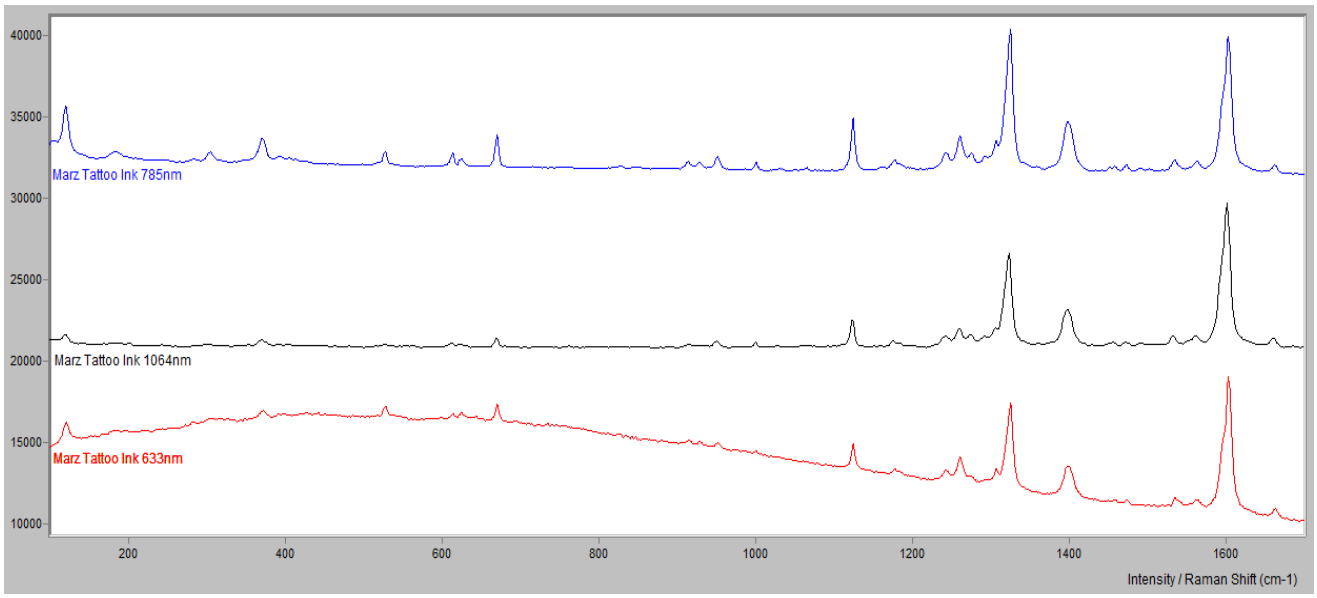

Figure 74. Raman spectra of Marz ink at different excitation wavelengths.

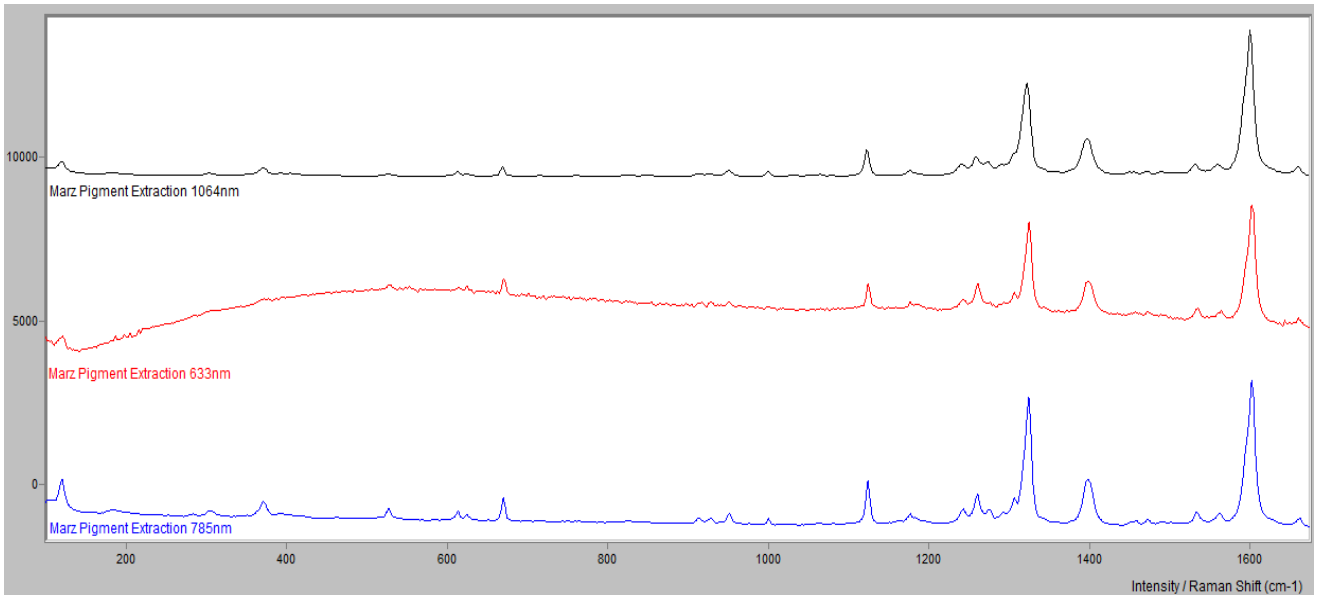

Figure 75. Raman spectra of Marz pigment extraction at different excitation wavelengths.

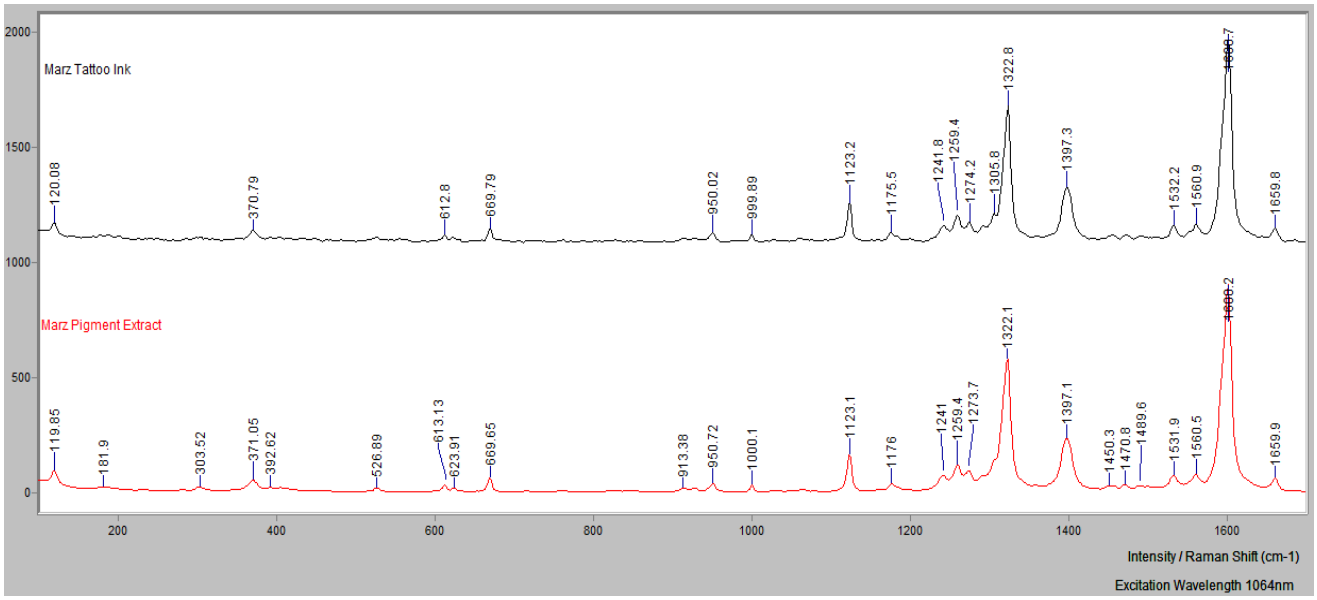

Figure 76. Comparison of Raman spectra of Marz ink and pigment extraction.

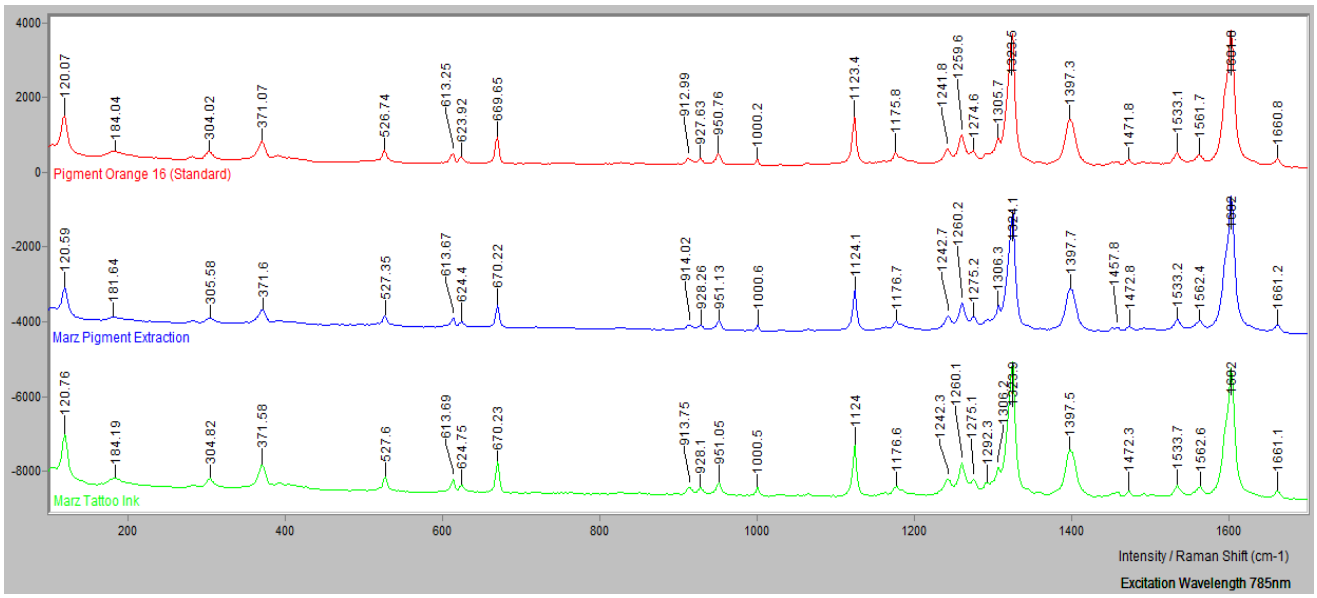

Figure 77. Normal Raman spectra of Marz ink and pigment extraction compared to Pigment Orange 16.

Dolemite- A comparison of Dolemite and the reported pigment composition is described below. XRF indicated the presence of titanium and iron. It is probable that the titanium is due to the presence of titanium dioxide.

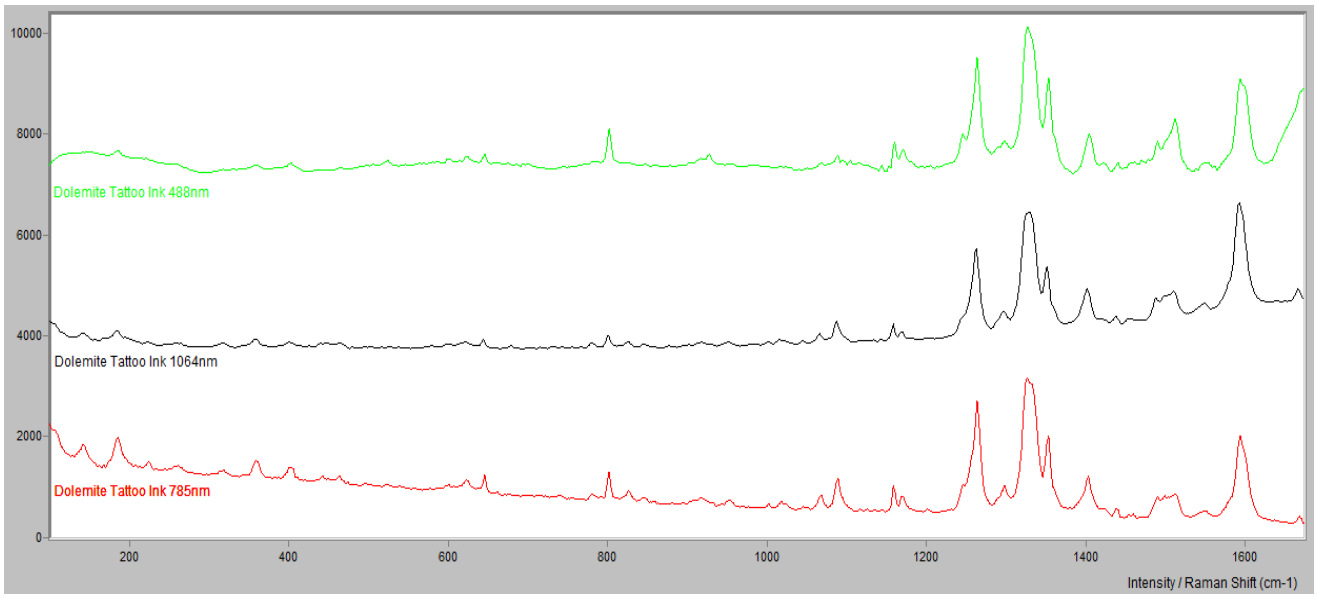

Figure 78. Raman spectra of Dolemite ink at different excitation wavelengths.

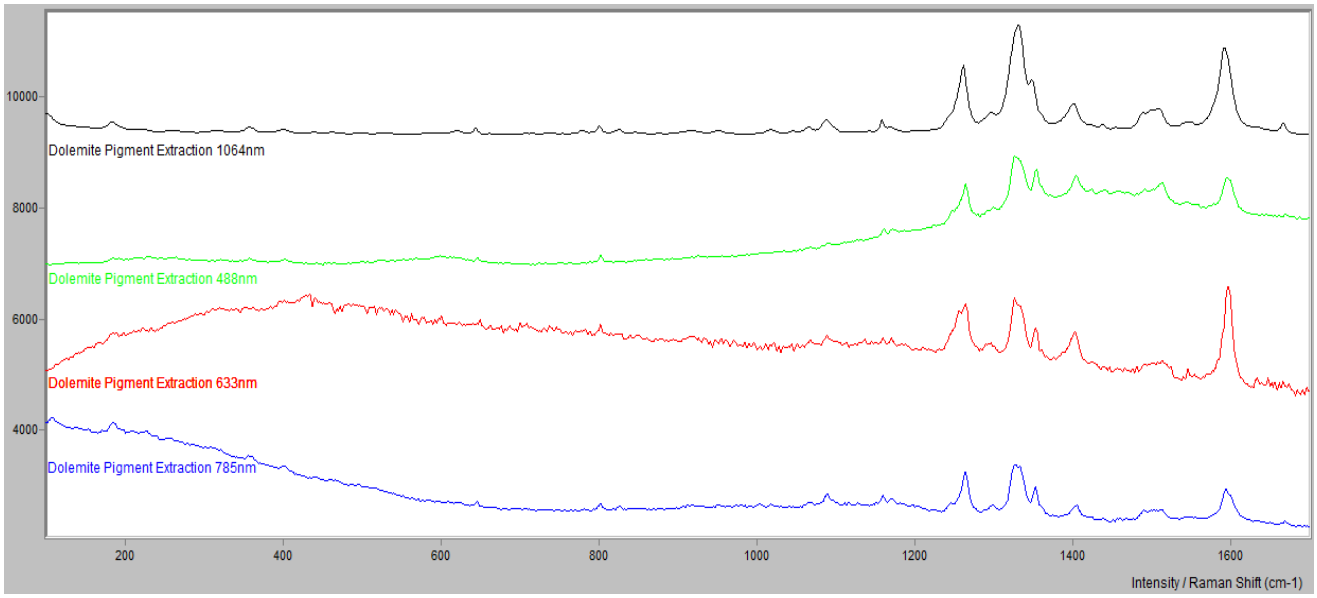

Figure 79. Raman spectra of Dolemite pigment extraction at different excitation wavelengths.

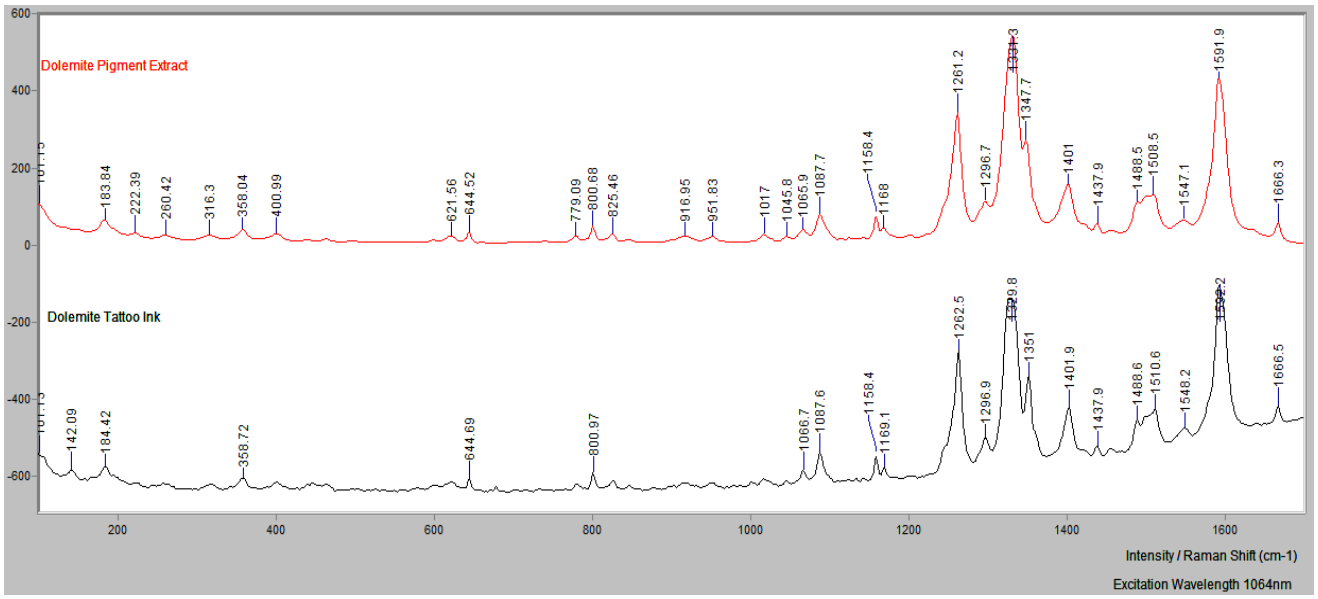

Figure 80. Comparison of Raman spectra of Dolemite ink and pigment extraction.

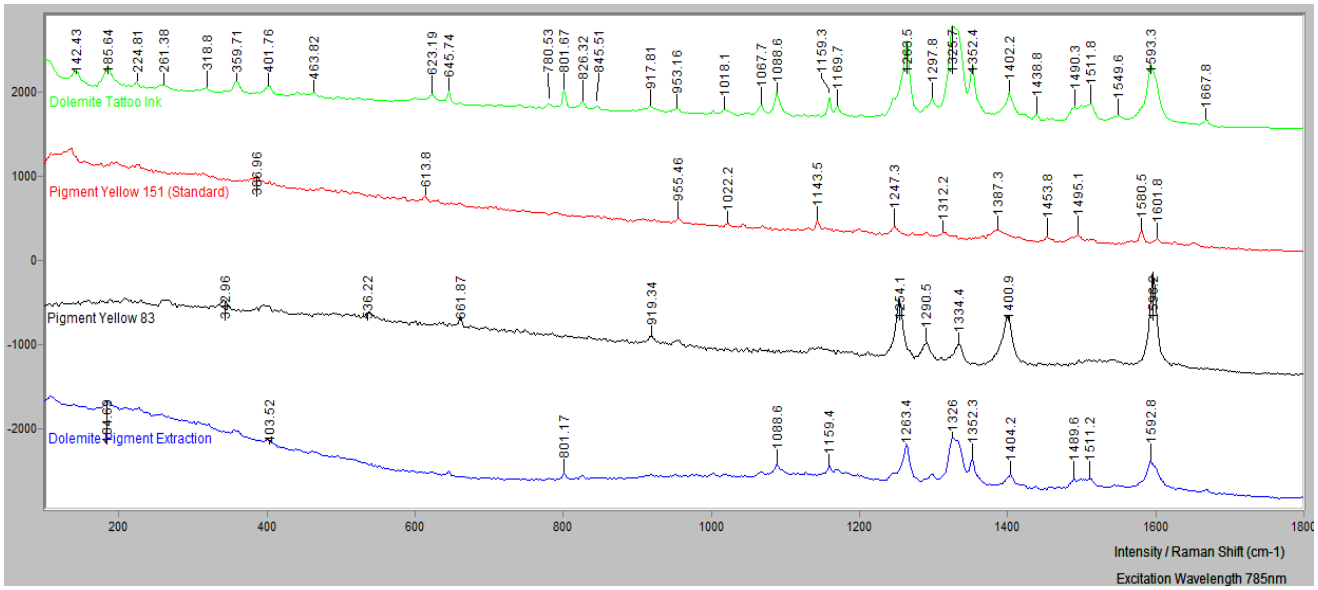

Figure 81. Normal Raman spectra of Dolemite ink and pigment extraction compared to Pigment Yellow 151 and Pigment Yellow 83.

According to the bottle label, Dolemite is supposed to contain Pigment Yellows 83 and 151. There is very little evidence to support the presence of PY 83, PY 151 or a mixture of the two. X-ray fluorescence did not disclose the presence of chlorine, which is found in PY83. Based on the literature, it appears that the bands present are more consistent with Pigment Yellow 74

(Note: No standard PY 74 was analyzed to directly correlate to the spectrum of Dolemite). The following bands are reported for PY 74 (using Colombini, *et.al.*, 2010, Scherrer *et.al.*, 2009 and Vandenabeele, *et. al*., 2000).

Colombini, *et.al.*: (λ_0=785nm): 1596s, 1403ms, 1355s, 1330vs, 1266s

Scherrer *et.al.*: (λ_0=785nm): 1593s, 1352s, 1328vs, 1263s

Vandenabeele, *et. al*.: (λ_0=780nm): 1327vs, 1263s

Comparison between the spectrum reported in Scherrer *et.al.* with the experimental data demonstrates a correlation between thirty-eight (38) of the bands labeled in the spectrum of Dolemite (Figure below; the list of bands reported by Scherrer *et.al.* can be found in Appendix I).

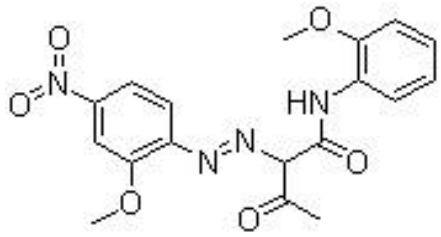

Figure 82. Pigment Yellow 74

The effect of mixtures cannot be ruled out as an important factor in evaluating spectral data. Extraction of the Dolemite tattoo ink resulted in the visualization of three components, a white portion which is likely to be titanium dioxide, a large yellow portion and a small orange portion. Based upon the disproportionate amount of yellow and orange pigment, two scenarios are possible: (1) the pigment detected for Dolemite was the yellow portion, with the small concentration of orange portion either being undetected or overwhelmed by the yellow or (2) the resultant spectra for Dolemite are a combination of the yellow and orange portions, with some spectral bands arising from the yellow portion and some spectral bands arising from the orange

portion. As such, it is recommended that an extraction or separation method be employed in order to determine the amount of pigments present and to isolate each pigment for subsequent qualitative spectroscopic analysis. In addition, the ratios of pigments (either relative ratios or more detailed quantitative analysis) may be a means to distinguish similar colors from different manufacturers or brands. Furthermore, Colombini *et.al.* state "PY83 is supposed to be containing some unknown percentage of PY1," adding that this class of pigment is often used in mixures, making them complex to study (2010, pp. 18).

Figure 83. Resultant extraction of Dolemite tattoo ink. Note the presence of three distinct color profiles- white (bottom), orange and yellow (top).

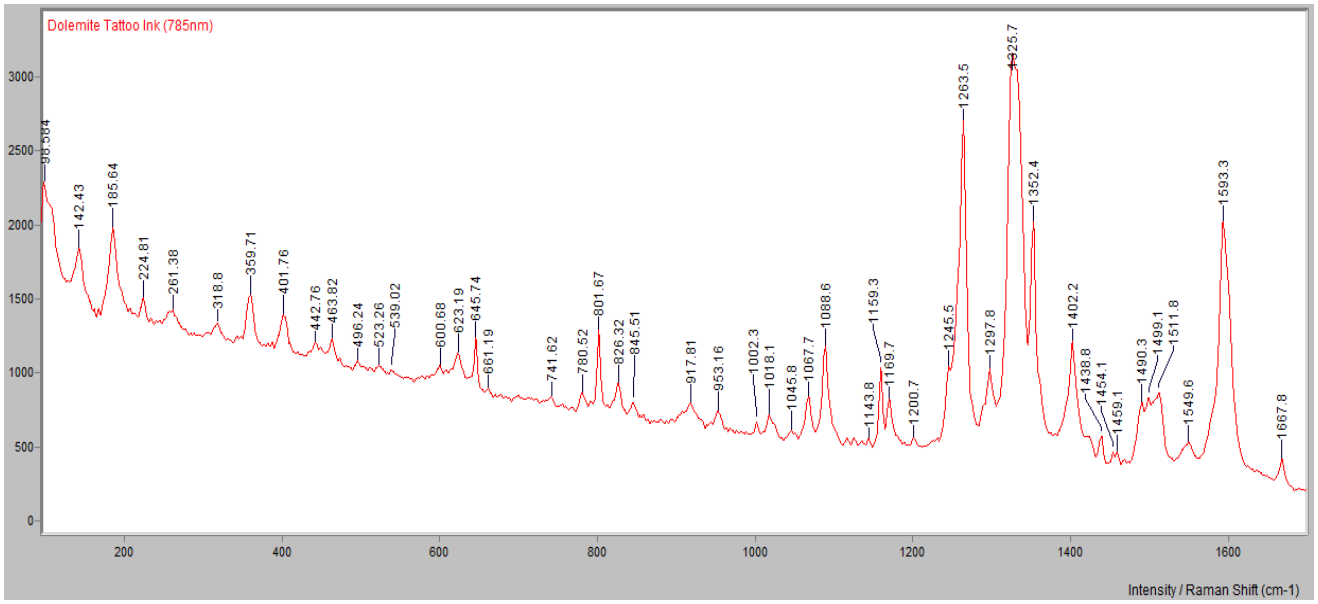

Figure 84. Dolemite Tattoo Ink showing band locations

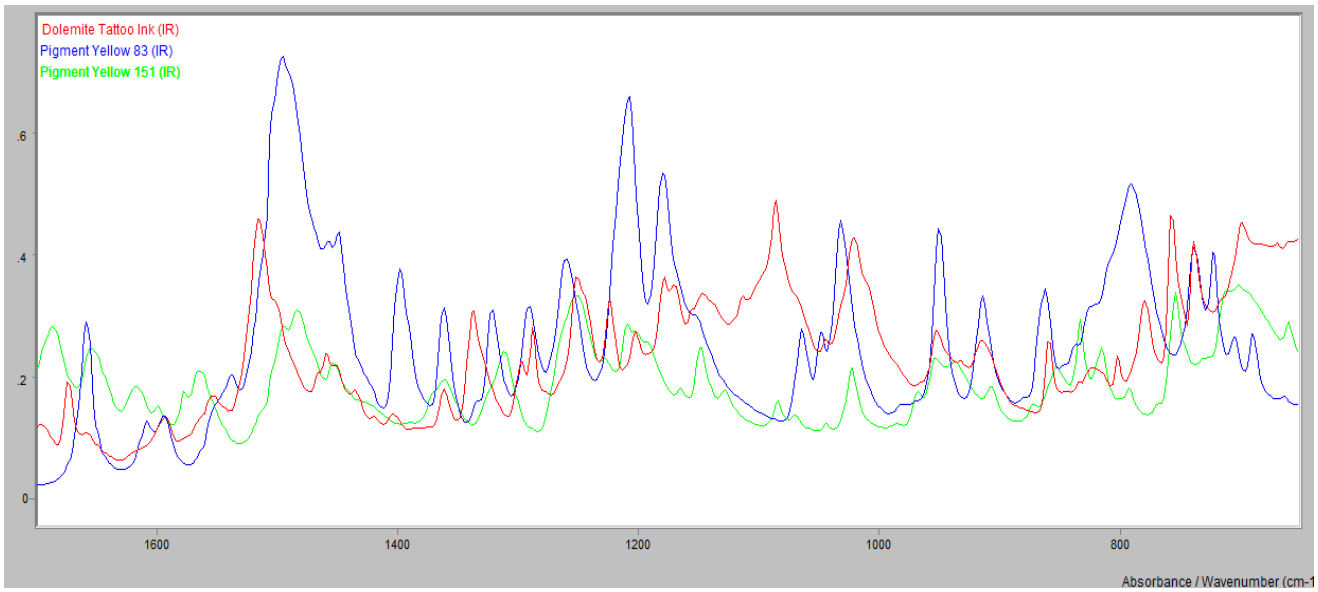

Figure 85. Infrared (ATR) spectra from the 'fingerprint' region of 1700-650cm^{-1} of Dolemite Tattoo Ink and Pigment Yellows 83 and 151. Note the lack of correlation of the pigment standards with the tattoo ink. Band assignments with infrared spectra similar to that done with Raman spectral data can be useful for providing information concerning the characteristic functional groups of the pigment molecules. For example, the disazo PY 83 (in blue) contains a large band from about 1450-1500 cm^{-1}, which is due to the strong N=N azo vibrations. This band is also present, but much weaker, in monoazo PY 151 and Dolemite (which is thought to be consistent with the monoazo PY 74). In PY 83, the series of peaks at around 1180-1310 cm^{-1} indicates a disazo, as well as the three peaks located around 850-980 cm^{-1}.

Blisterine- A comparison of Blisterine and the reported pigment composition is described below. XRF indicated the presence of titanium and iron. It is probable that the titanium is due to the presence of titanium dioxide.

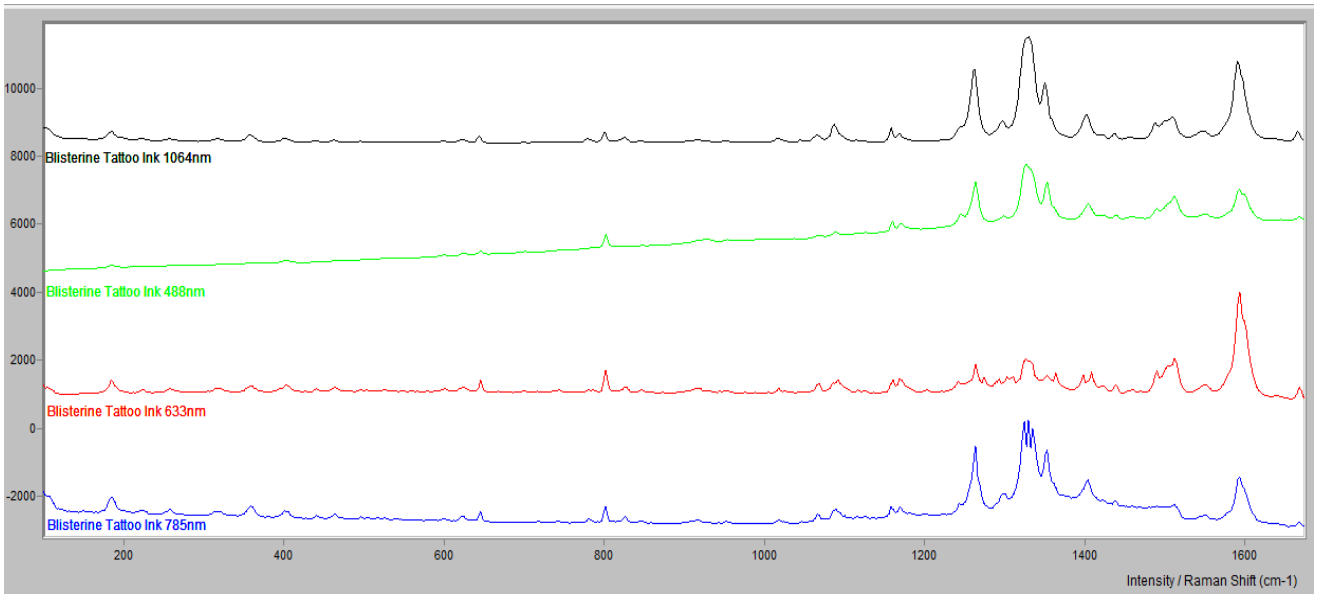

Figure 86. Raman spectra of Blisterine ink at different excitation wavelengths.

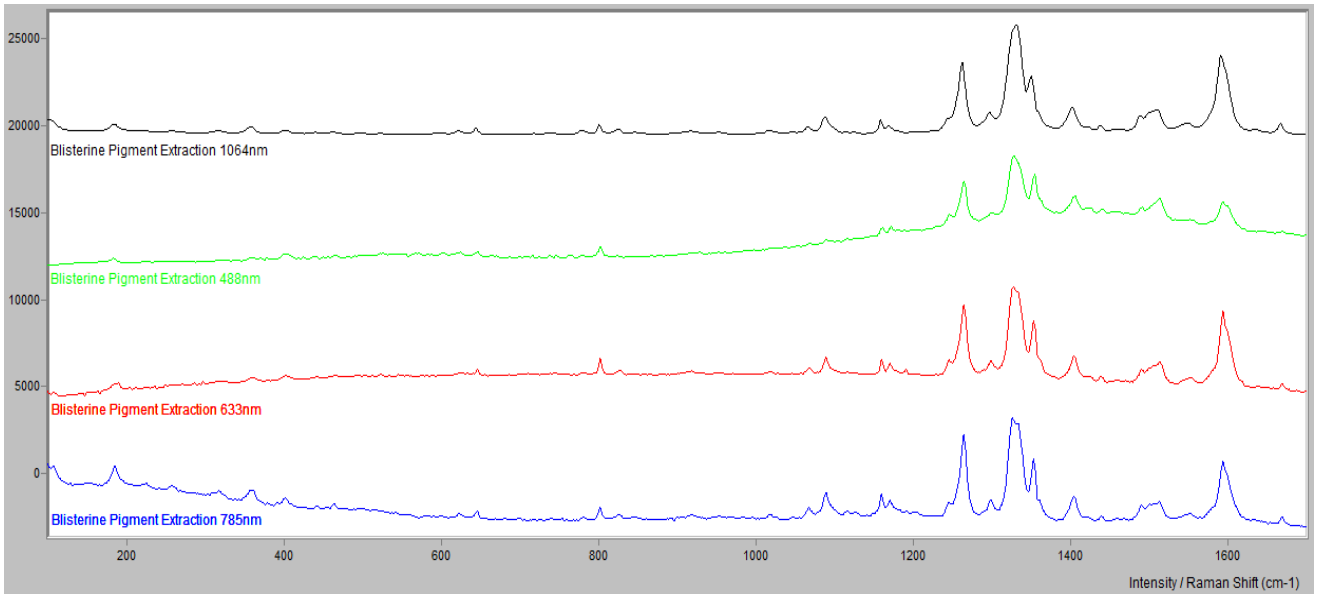

Figure 87. Raman spectra of Blisterine pigment extraction at different excitation wavelengths.

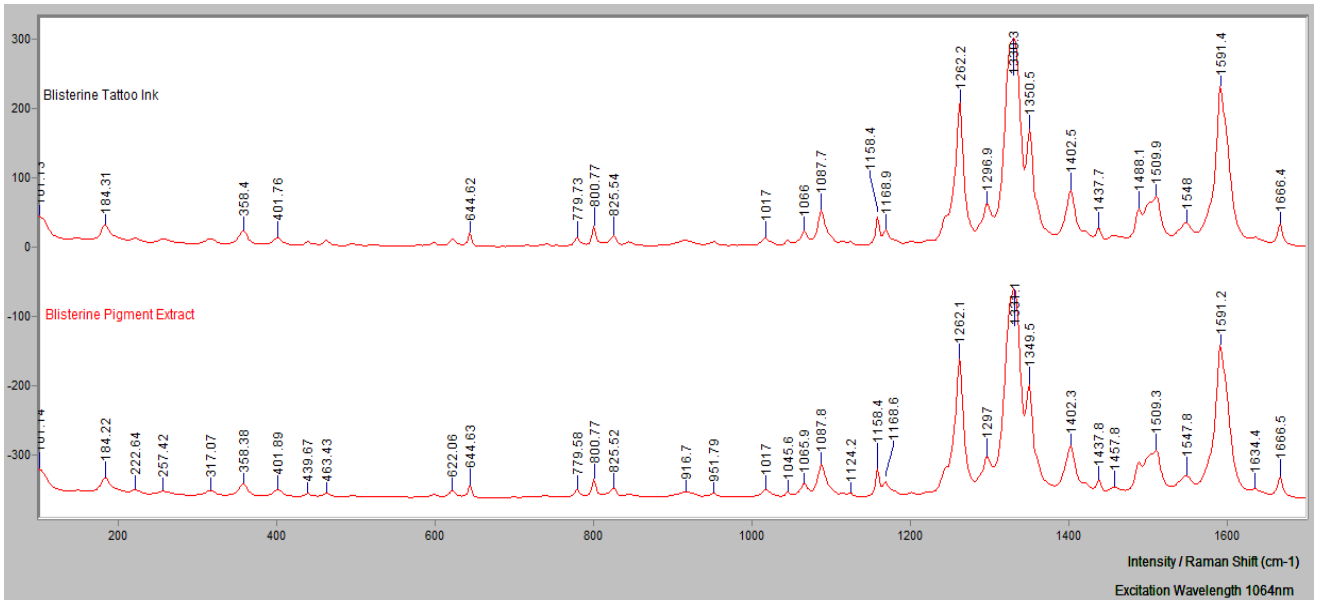

Figure 88. Comparison of Raman spectra of Blisterine ink and pigment extraction.

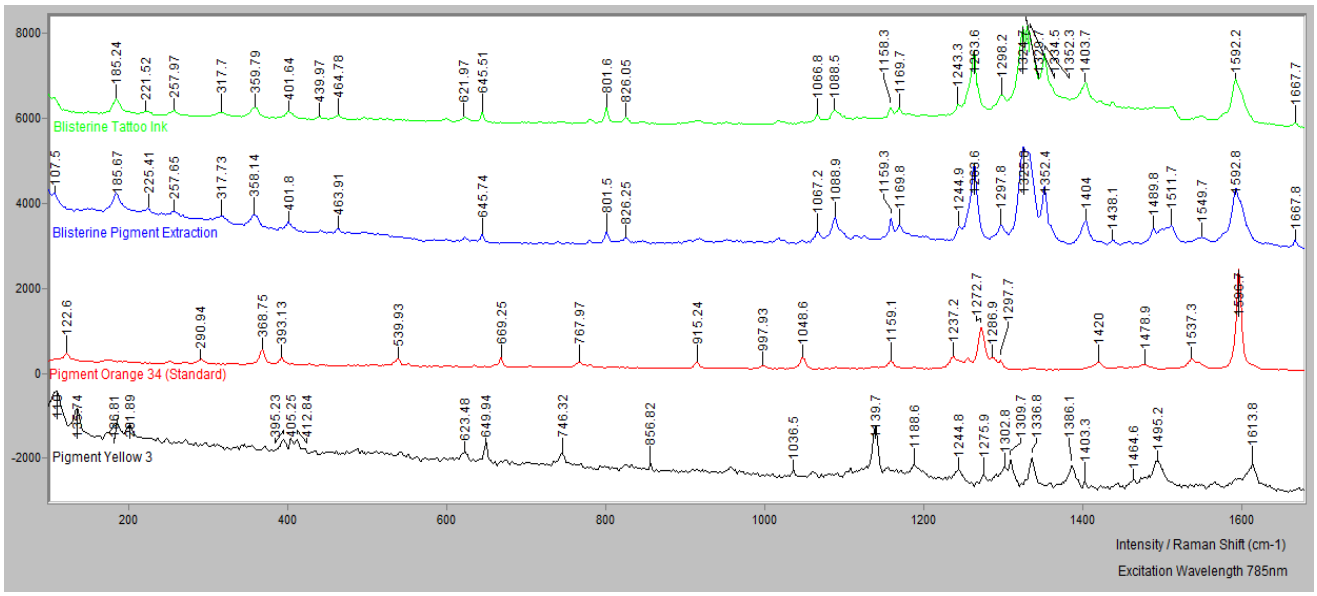

Figure 89. Normal Raman spectra of Blisterine ink and pigment extraction compared to Pigment Orange 34 and Pigment Yellow 3.

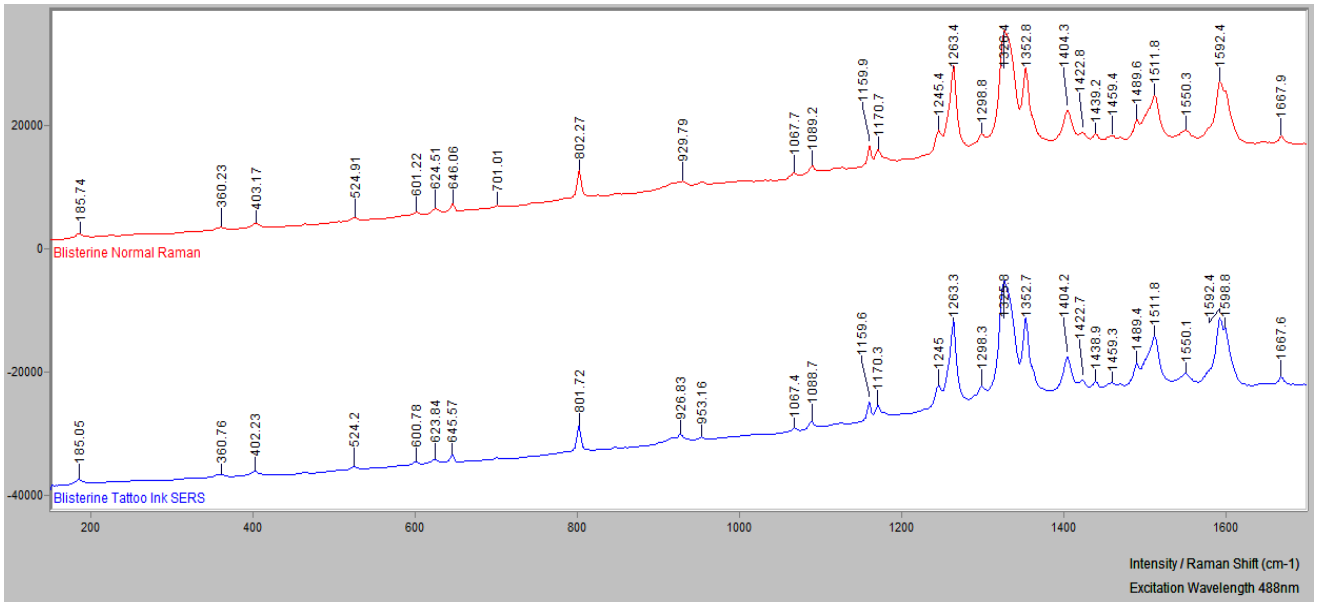

Figure 90. Normal Raman spectra of Blisterine ink compared to SERS spectra of Blisterine ink.

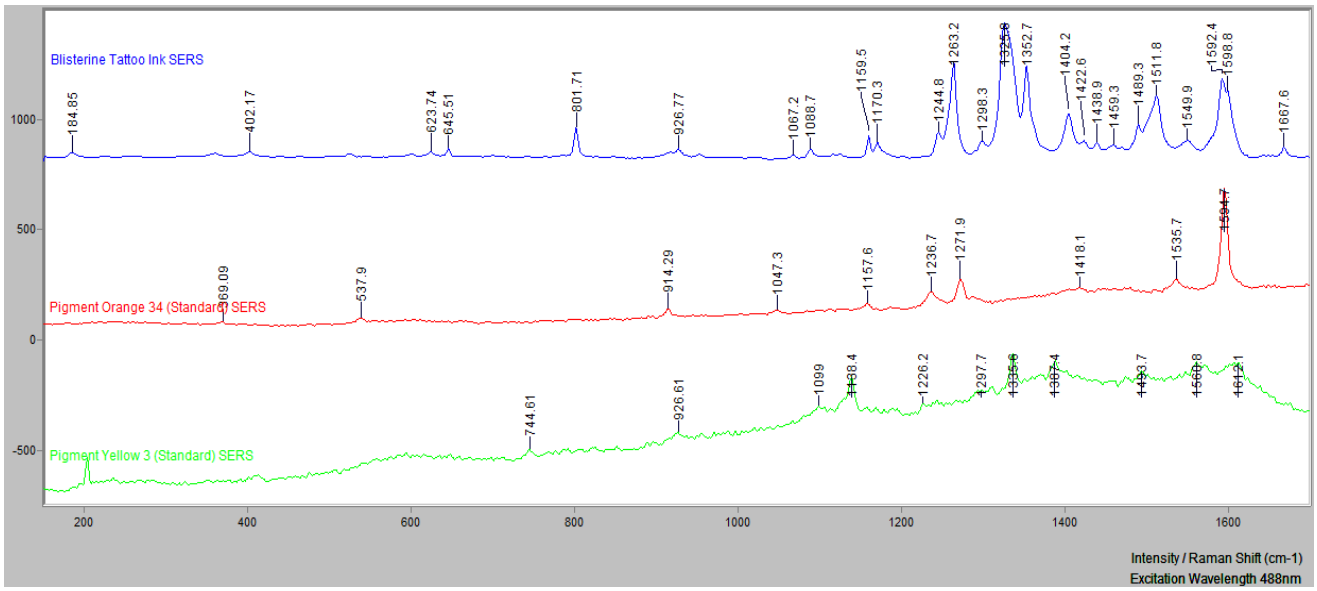

Figure 91. SERS spectra of Blisterine tattoo ink compared to Pigment Orange 34 and Pigment Yellow 3.

According to the bottle label, Blisterine is supposed to contain Pigment Yellow 3 and Pigment Orange 34. There is very little evidence to support the presence of PY 3 and PO 34. Based on the literature, it appears that the bands present are more consistent with Pigment

Yellow 74 as seen with the Dolemite Tattoo Ink. In addition, no chlorine was detected by x-ray fluorescence, which is found in both PY3 and PO34.

Comparison between the spectrum reported in Scherrer *et.al.* with the experimental data demonstrates a correlation between thirty-four (34) of the bands labeled in the spectrum of Blisterine (Figure below; the list of bands reported by Scherrer *et.al.* can be found in Appendix I). Due to the resultant Raman data and subsequent comparison to pigment standards, it is apparent that the labeling on the Blisterine packaging does not correspond to the actual ingredients.

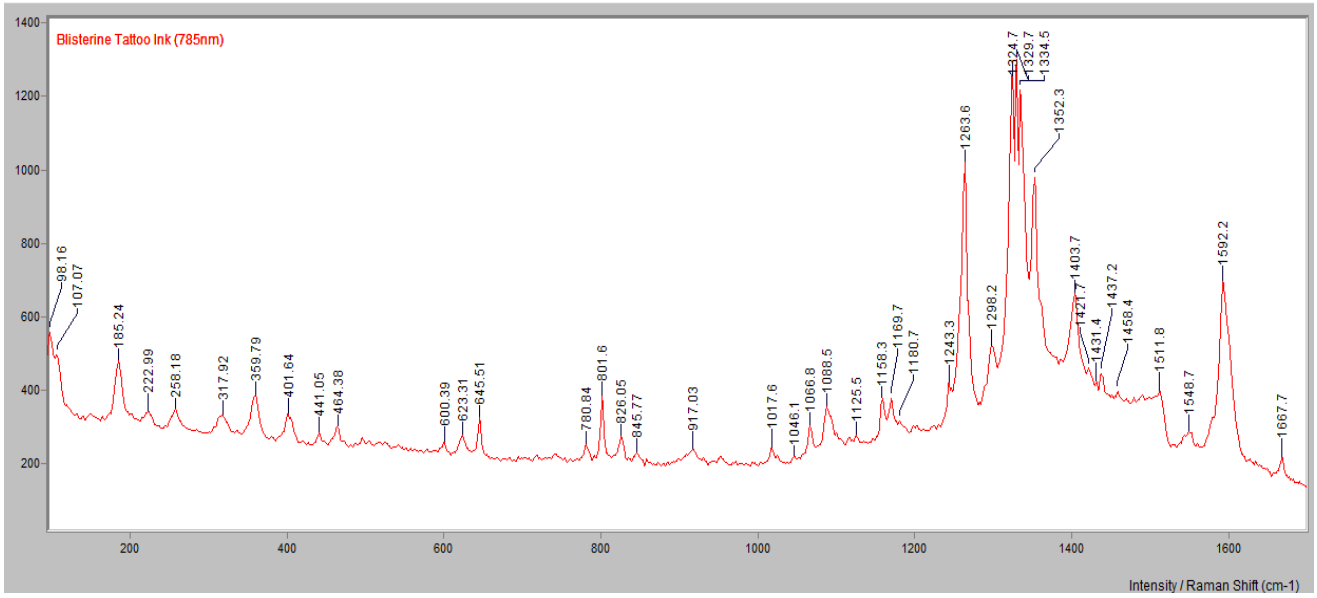

Figure 92. Blisterine Tattoo Ink showing band locations

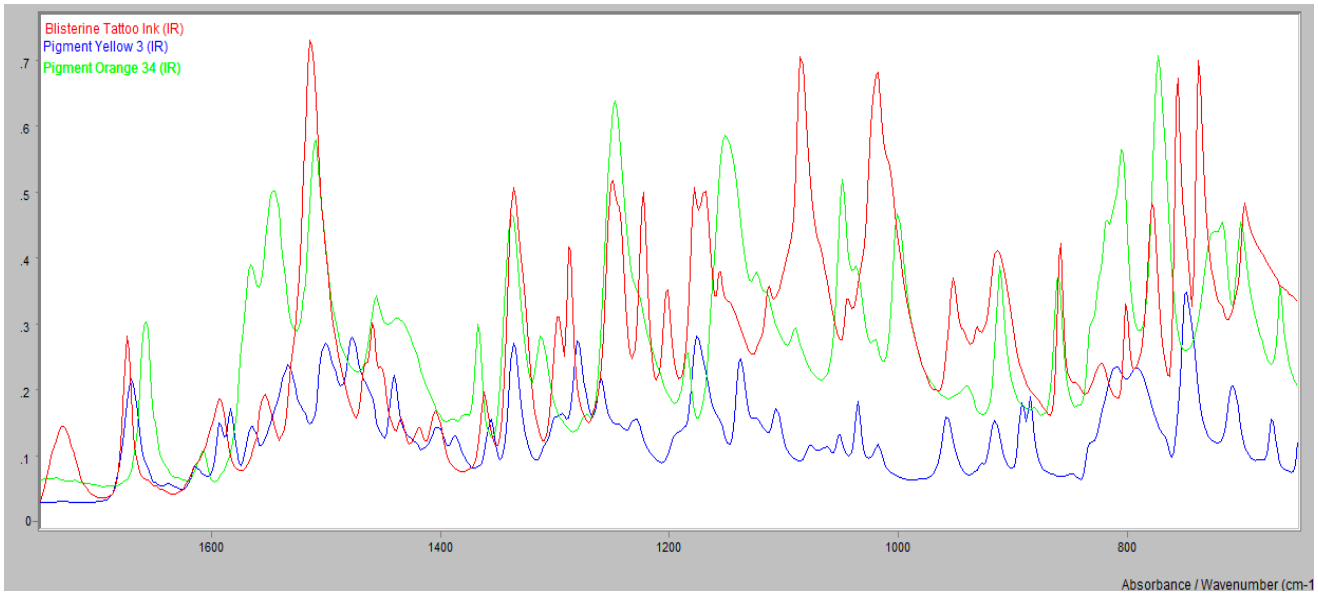

Figure 93. Infrared spectra from the region of 1750-650cm^{-1} of Blisterine Tattoo Ink and Pigment Yellow 3 and Pigment Orange 34. Note the lack of correlation of the pigment standards with the tattoo ink.

An overlay of the Raman spectra for Dolemite and Blisterine demonstrates that they are similar in chemical composition (Figure 94 below),

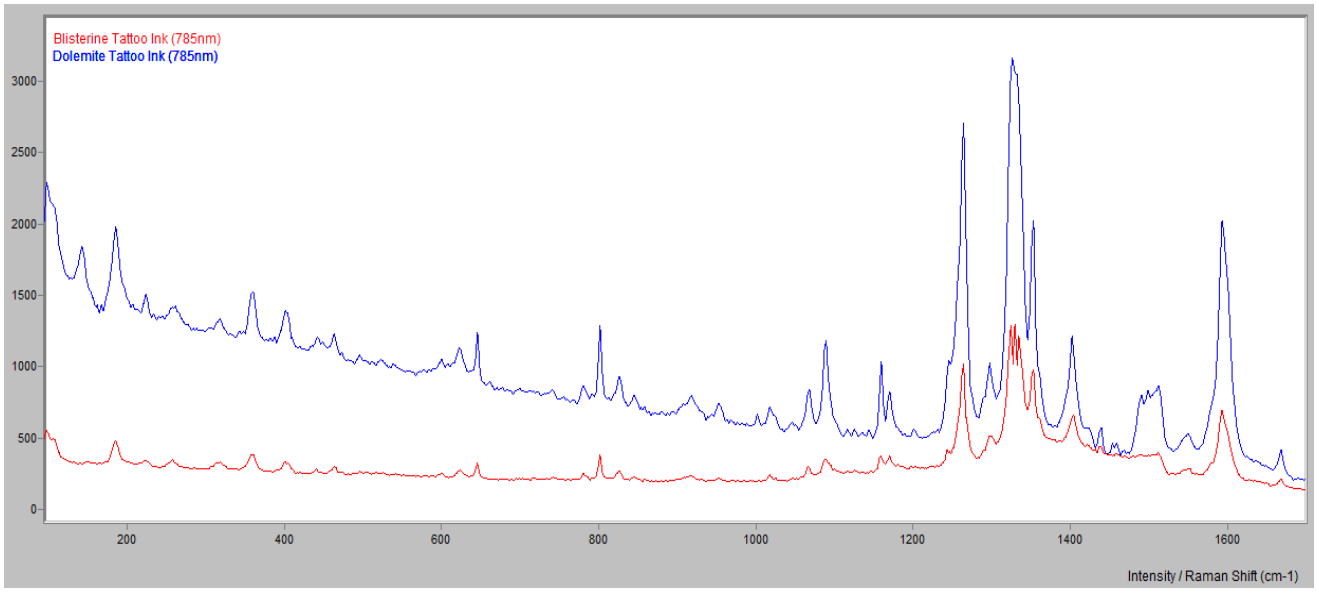

in addition to an overlay of the infrared spectra (Figure 95, below).

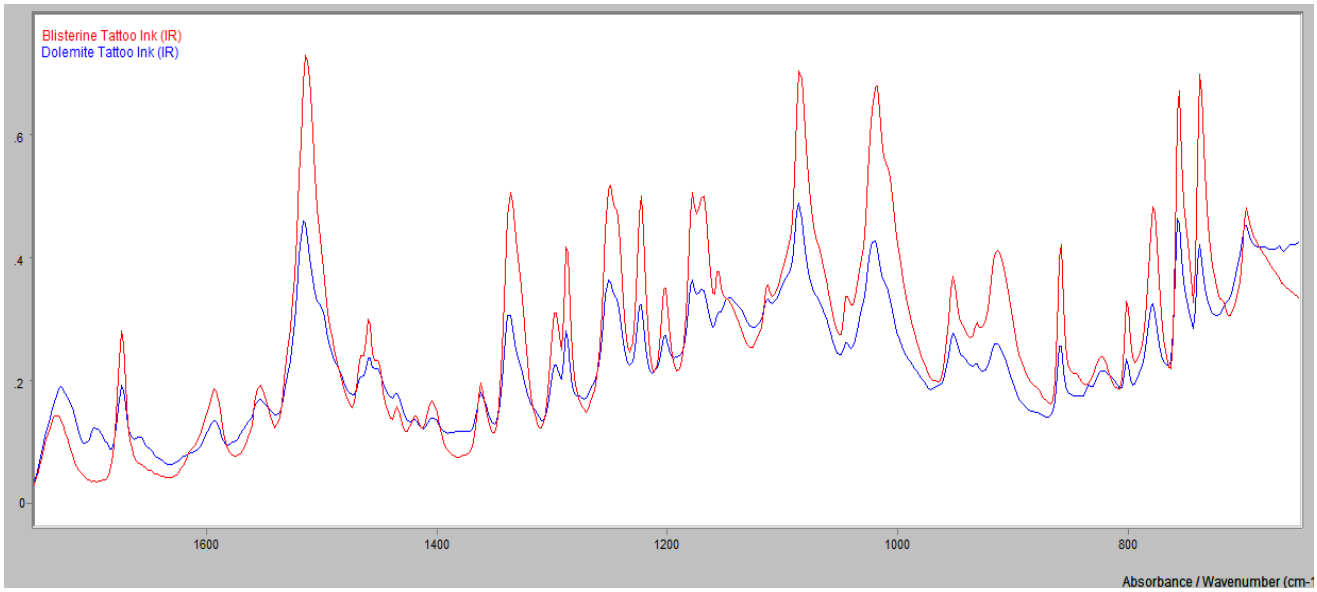

Sassygrass- Additional bands were detected when using SERS. XRF indicated the presence of titanium, chlorine, iron and copper. It is probable that the titanium is due to the presence of titanium dioxide and the chlorine and copper are indicative of Pigment Green 7.

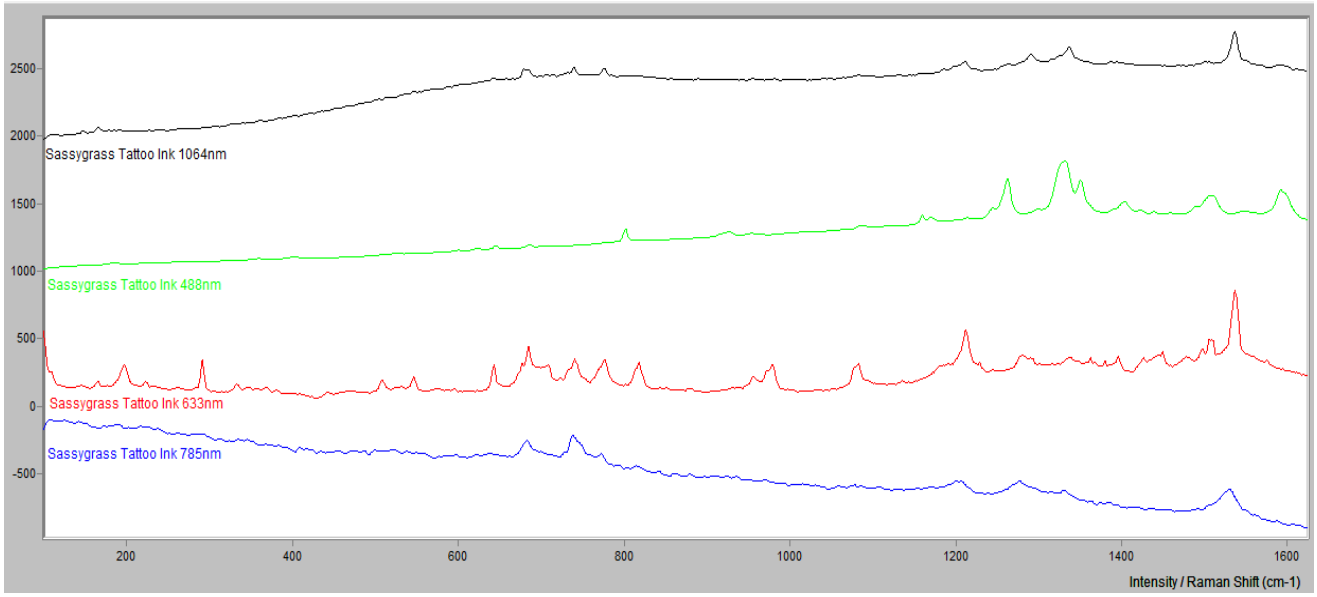

Figure 96. Raman spectra of Sassygrass ink at different excitation wavelengths.

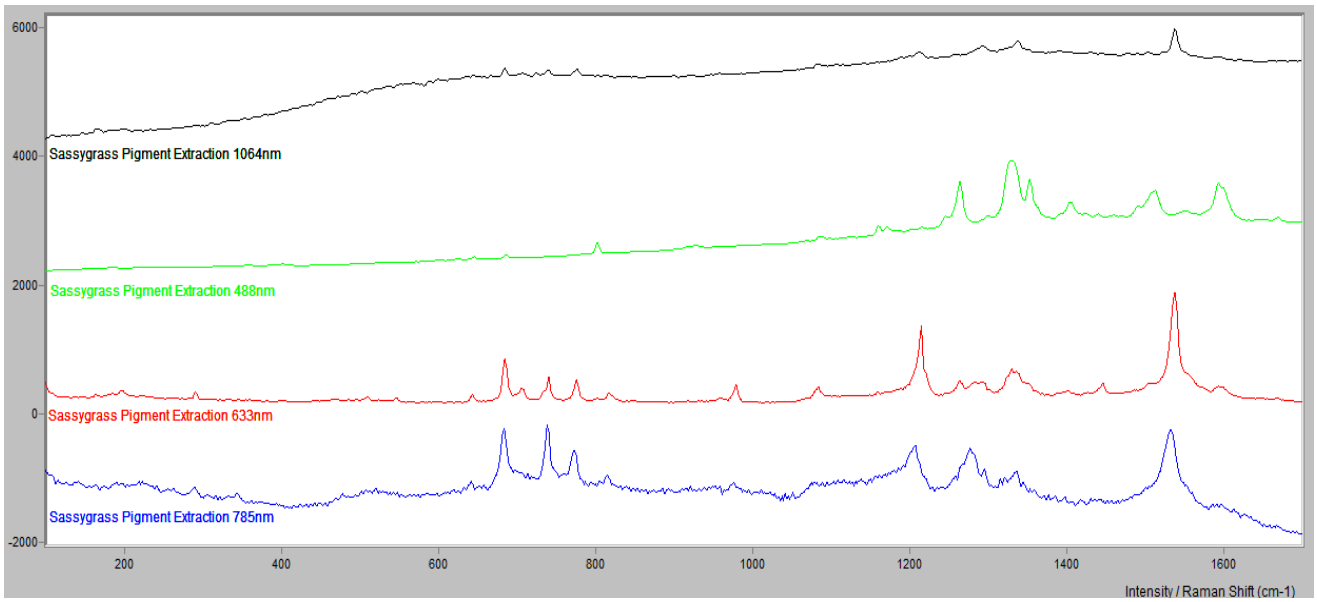

Figure 97. Raman spectra of Sassygrass pigment extraction at different excitation wavelengths.

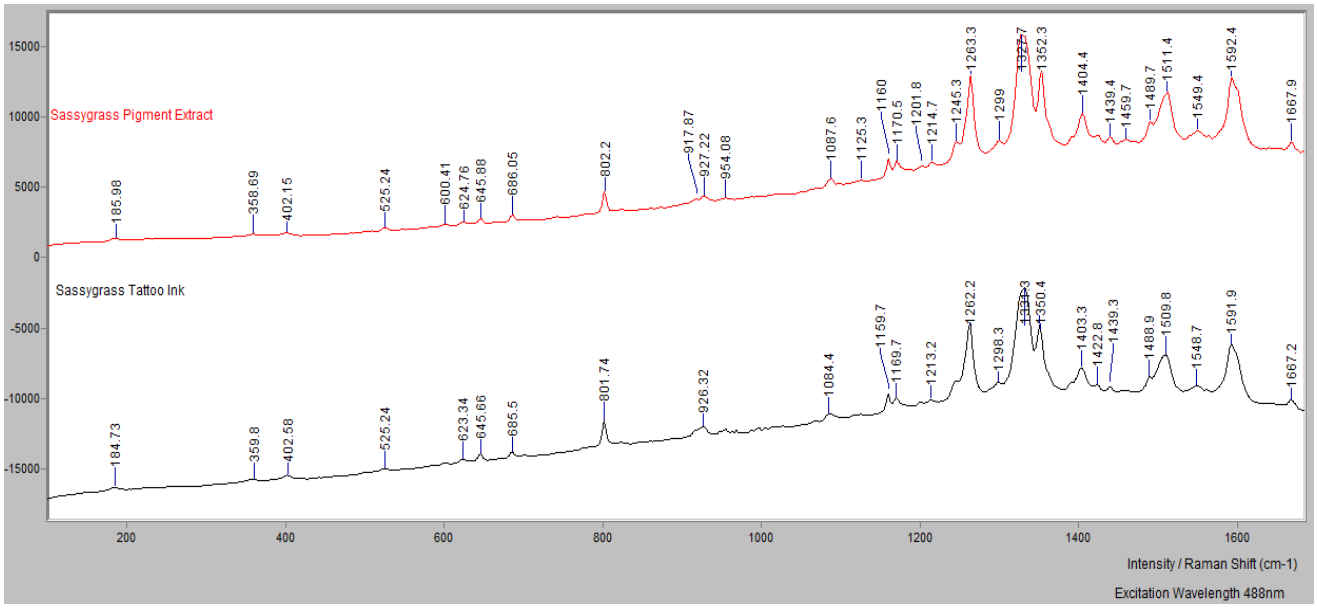

Figure 98. Comparison of Raman spectra of Sassygrass ink and pigment extraction.

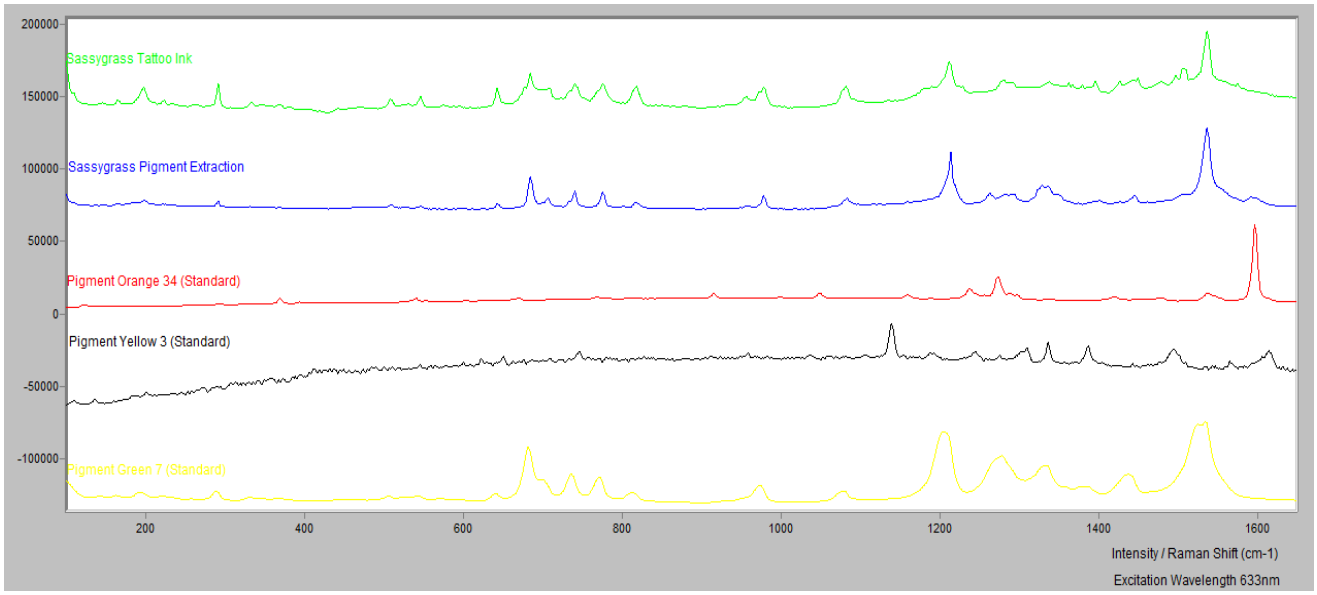

Figure 99. Normal Raman spectra of Sassygrass ink and pigment extraction compared to Pigment Orange and Pigment Yellow 3 and Pigment Green 7.

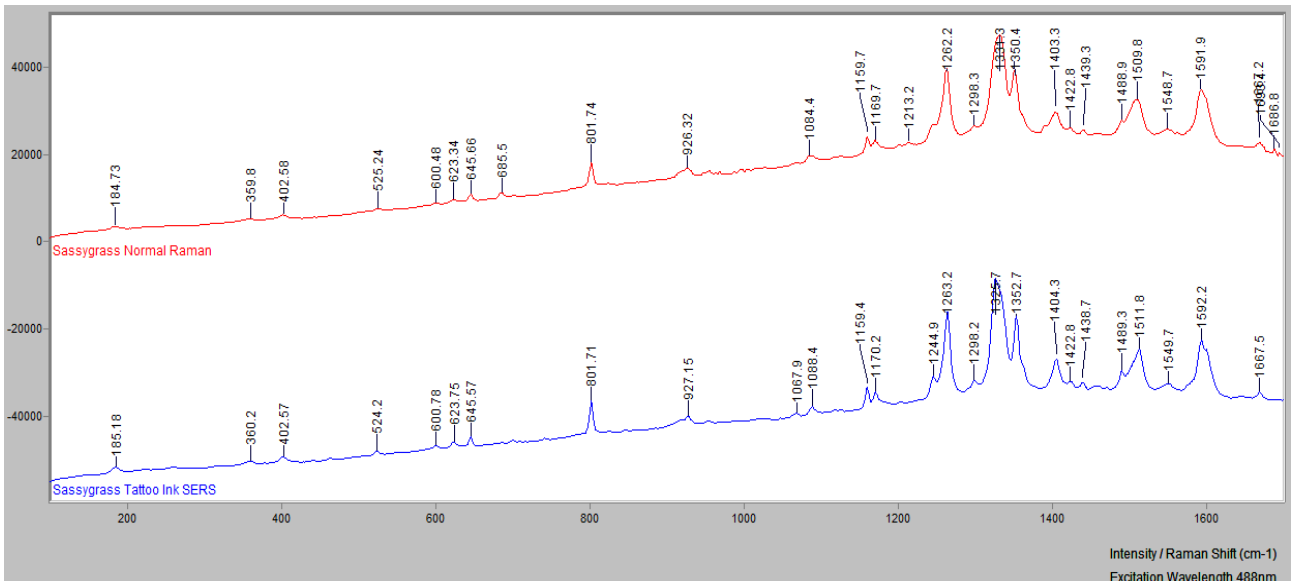

Figure 100. Normal Raman spectra of Sassygrass ink compared to SERS spectra of Sassygrass.

Many of the bands present in the Sassygrass tattoo ink correspond to the bands present in Pigment Green 7. Because Sassygrass is a green tattoo ink, it is probable that the majority of the pigment is green, thus rendering it difficult to detect any other pigments present in trace quantities, such as the Pigment Orange 34 and Pigment Yellow 3 that are supposed to be present according to the ingredients listed on the label.

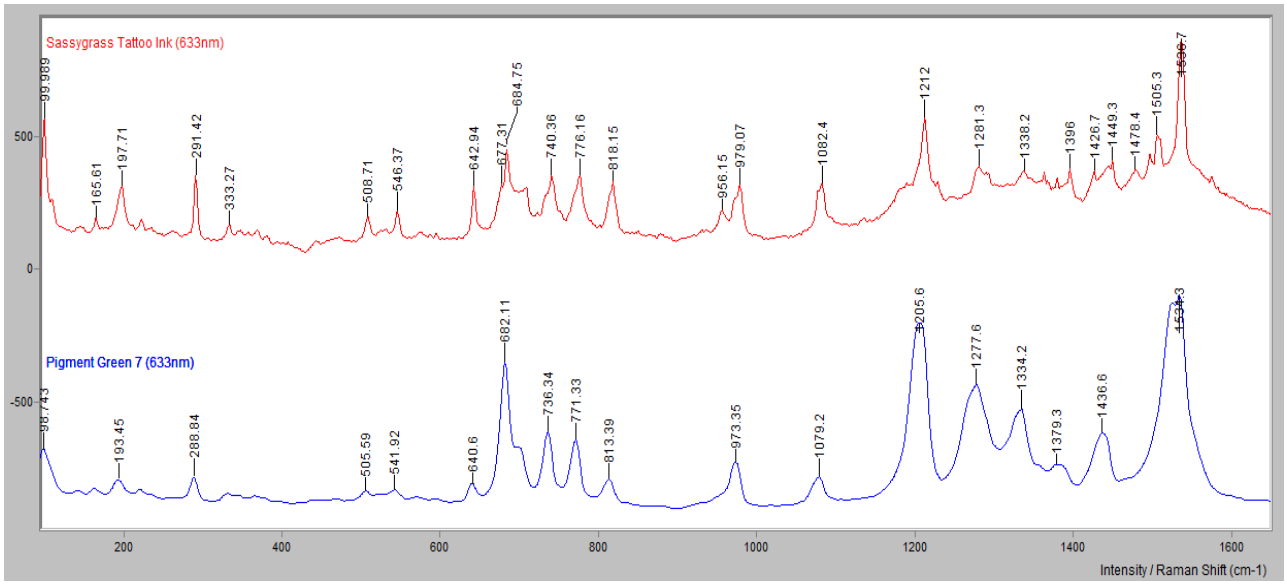

Figure 101. Sassygrass Tattoo Ink compared to PG 7 standard.

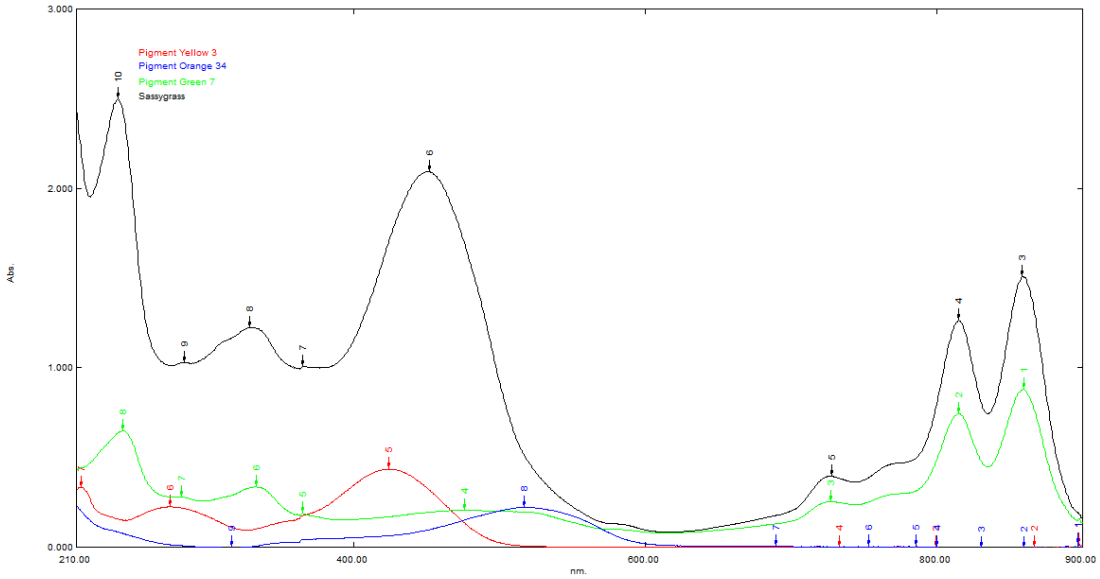

Figure 102. UV/Vis spectra of Sassygrass and corresponding pigments (according to manufacturer).

Tastywaves- XRF indicated the presence of titanium, chlorine, copper and bromine. It is probable that the titanium is due to the presence of titanium dioxide and the chlorine, copper and bromine are indicative of Pigment Green (Cu, Cl, Br). The presence of the bromine suggests the presence of Pigment Green 36, in which there is some of the chlorines are replaced with bromine.

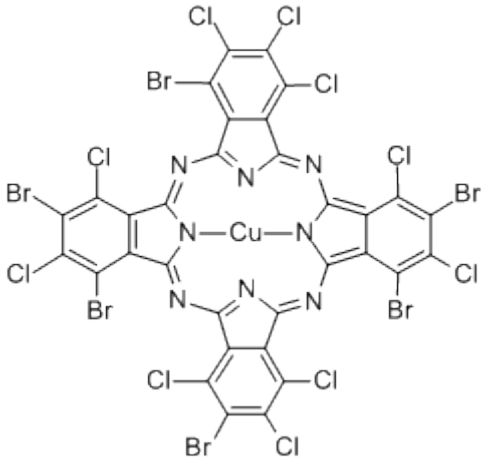

Figure 103. Pigment Green 36

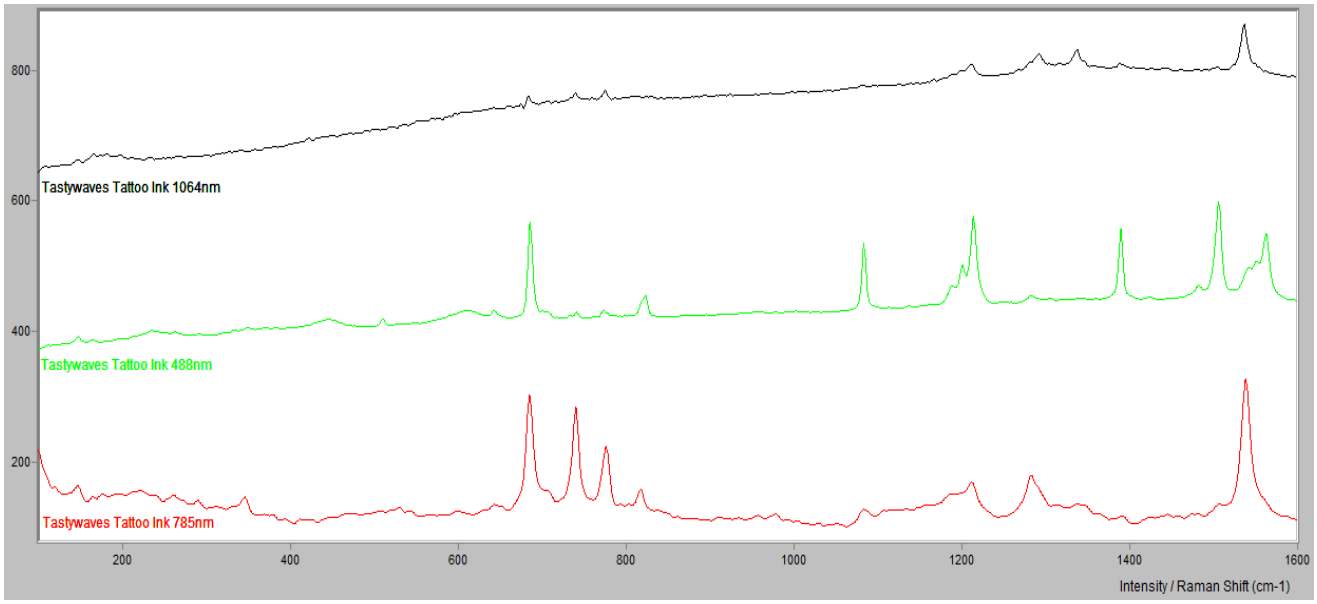

Figure 104. Raman spectra of Tastywaves ink at different excitation wavelengths.

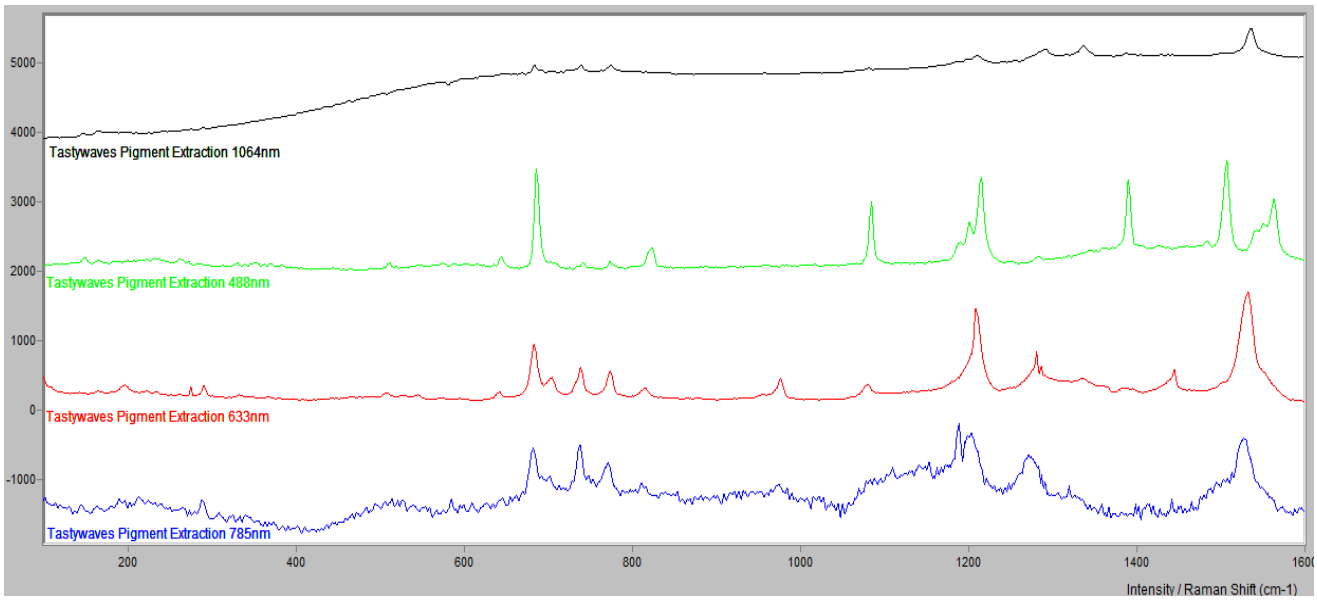

Figure 105. Raman spectra of Tastywaves pigment extraction at different excitation wavelengths.

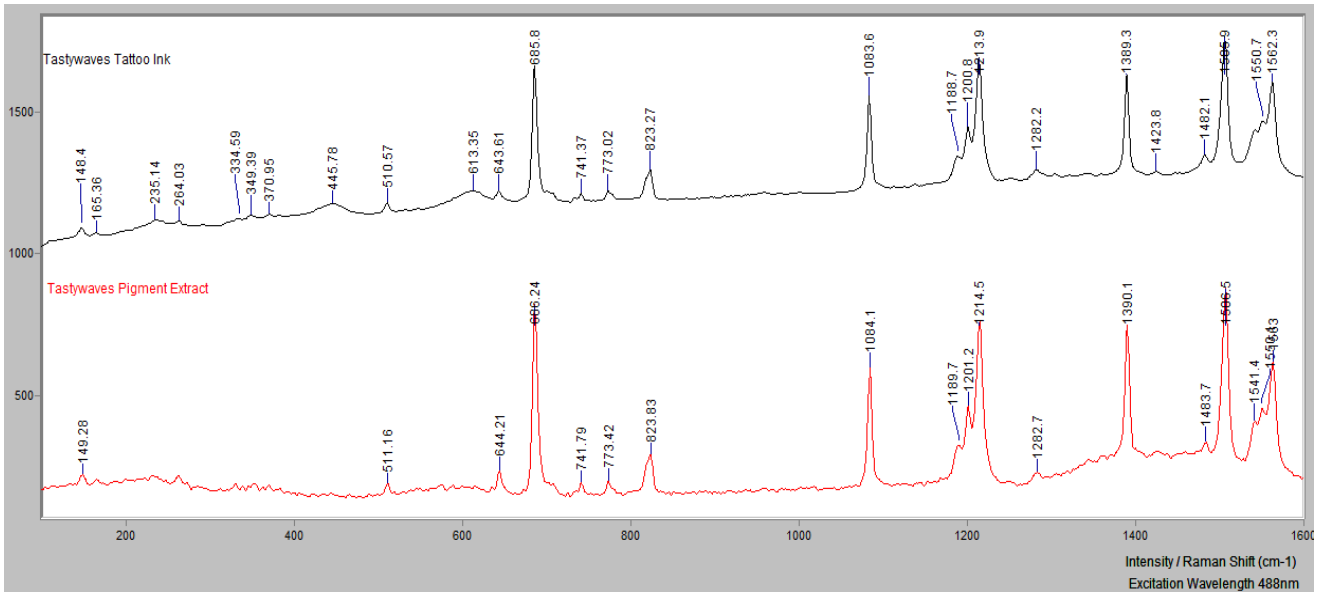

Figure 106. Comparison of Raman spectra of Tastywaves ink and pigment extraction.

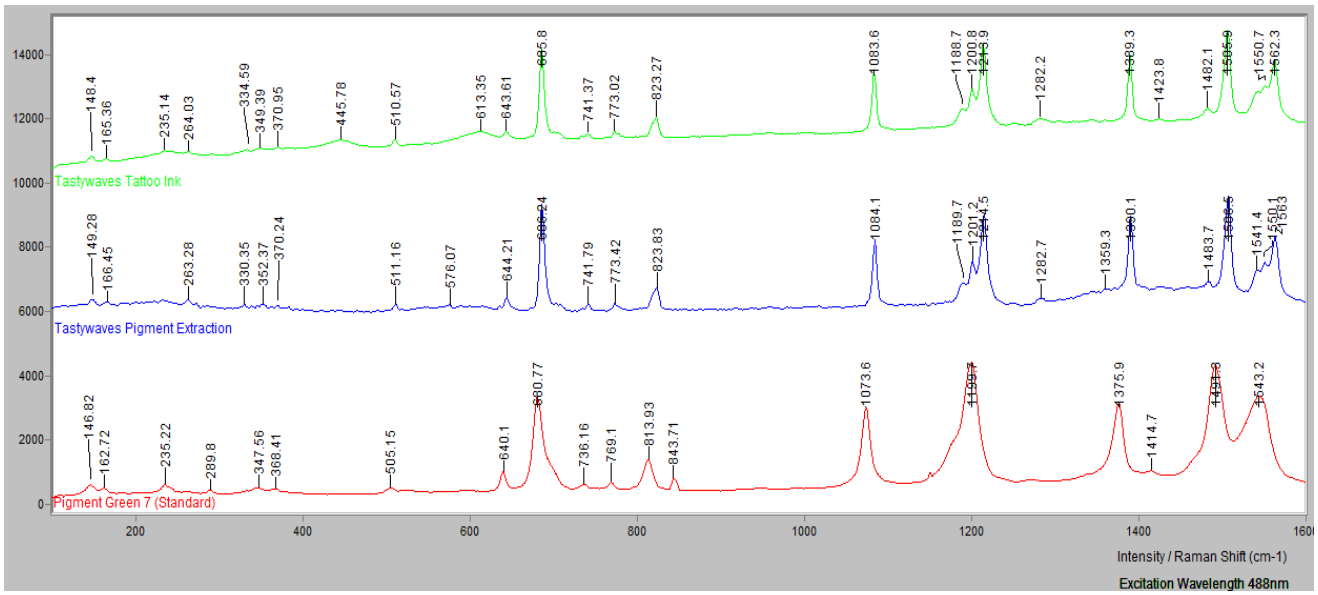

Figure 107. Normal Raman spectra of Tastywaves ink and pigment extraction compared to Pigment Green 7.

Bellbottom Blue- XRF indicated the presence of titanium and copper. It is probable that the titanium is due to the presence of titanium dioxide and the copper is indicative of Pigment Blue. UV/Vis data correlated to that of Pigment Blue 15.

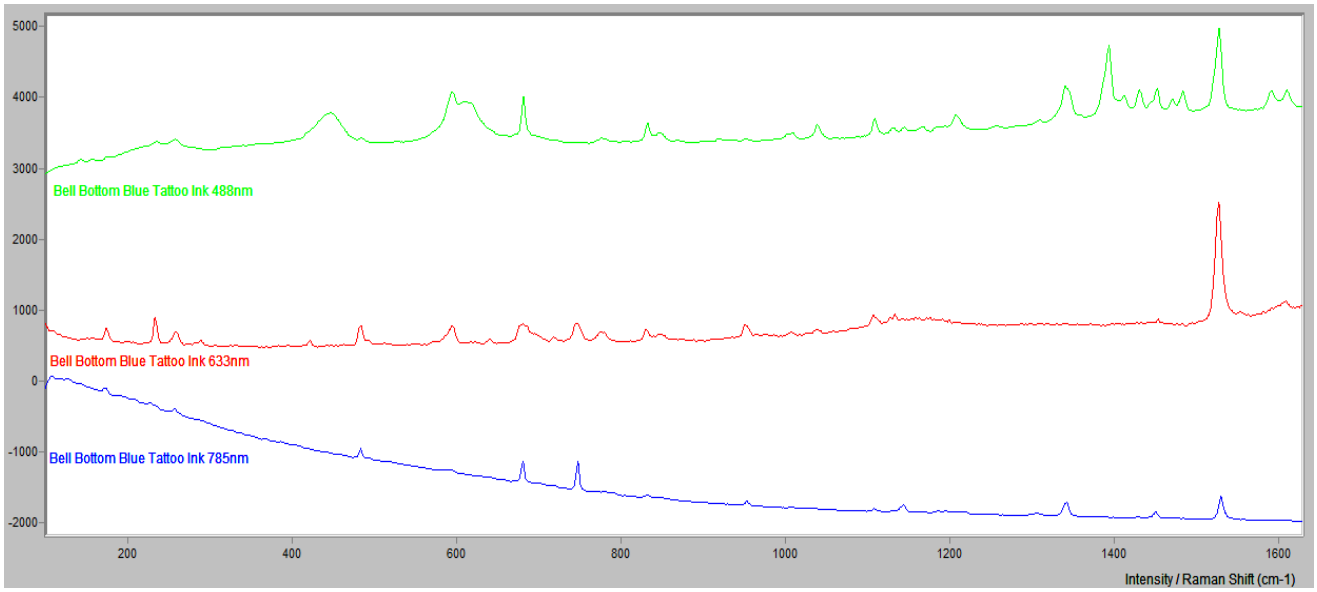

Figure 108. Raman spectra of Bell Bottom Blue ink at different excitation wavelengths.

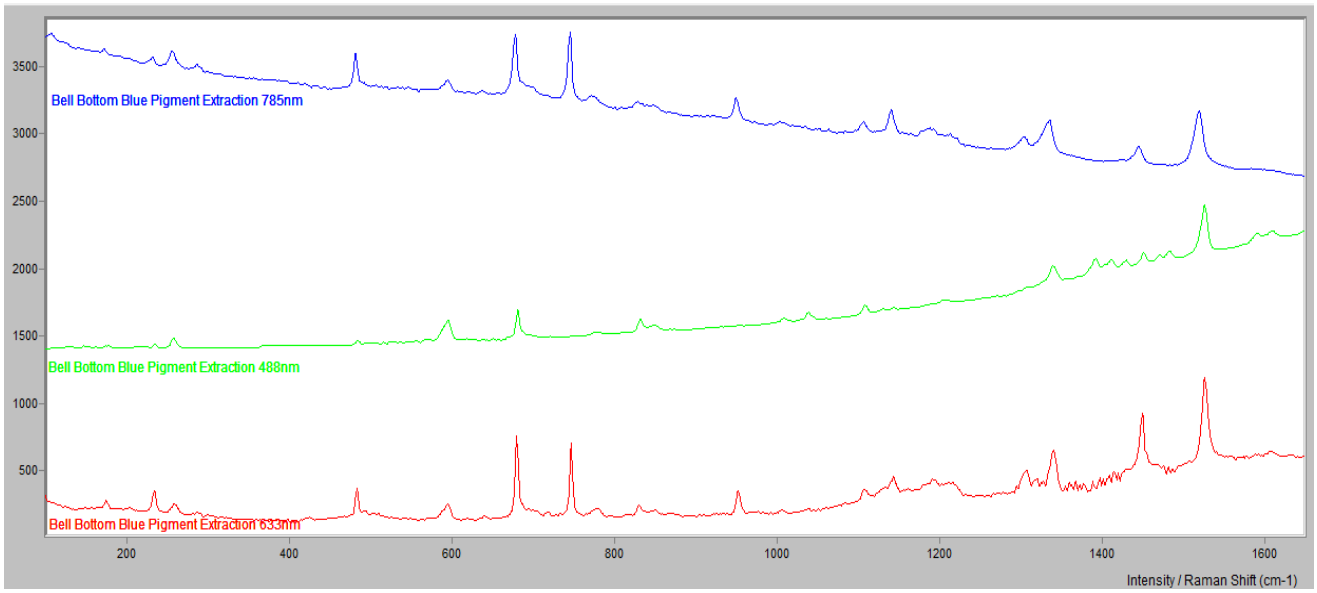

Figure 109. Raman spectra of Bell Bottom Blue pigment extraction at different excitation wavelengths.

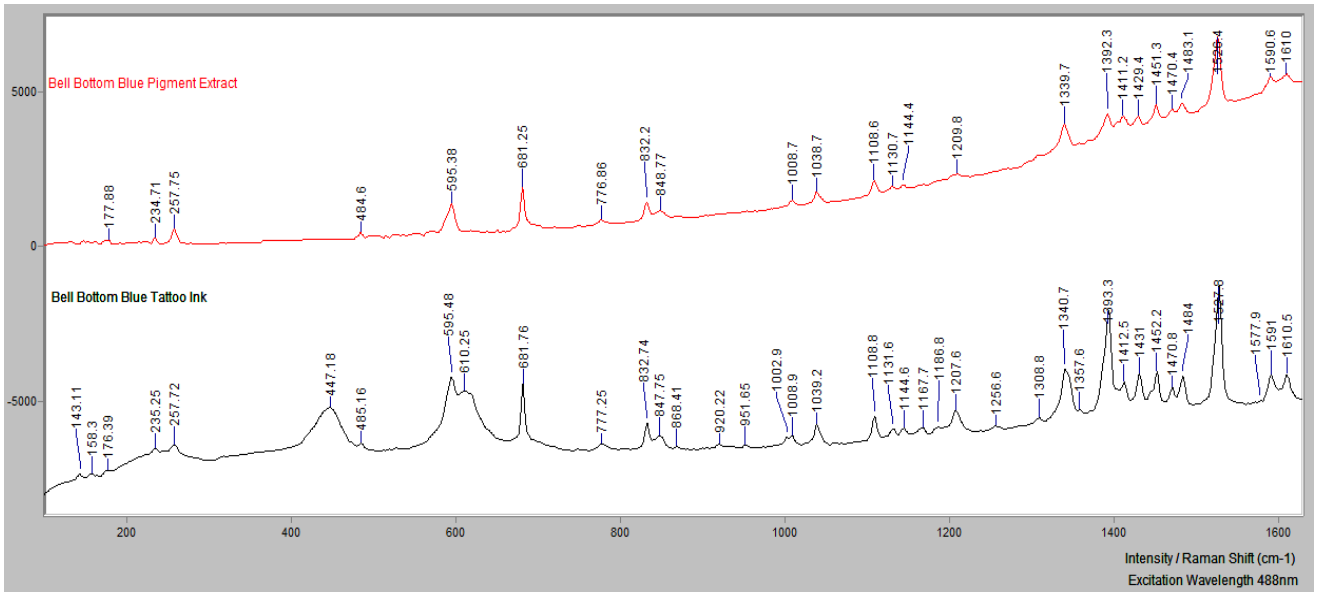

Figure 110. Comparison of Raman spectra of Bell Bottom Blue ink and pigment extraction.

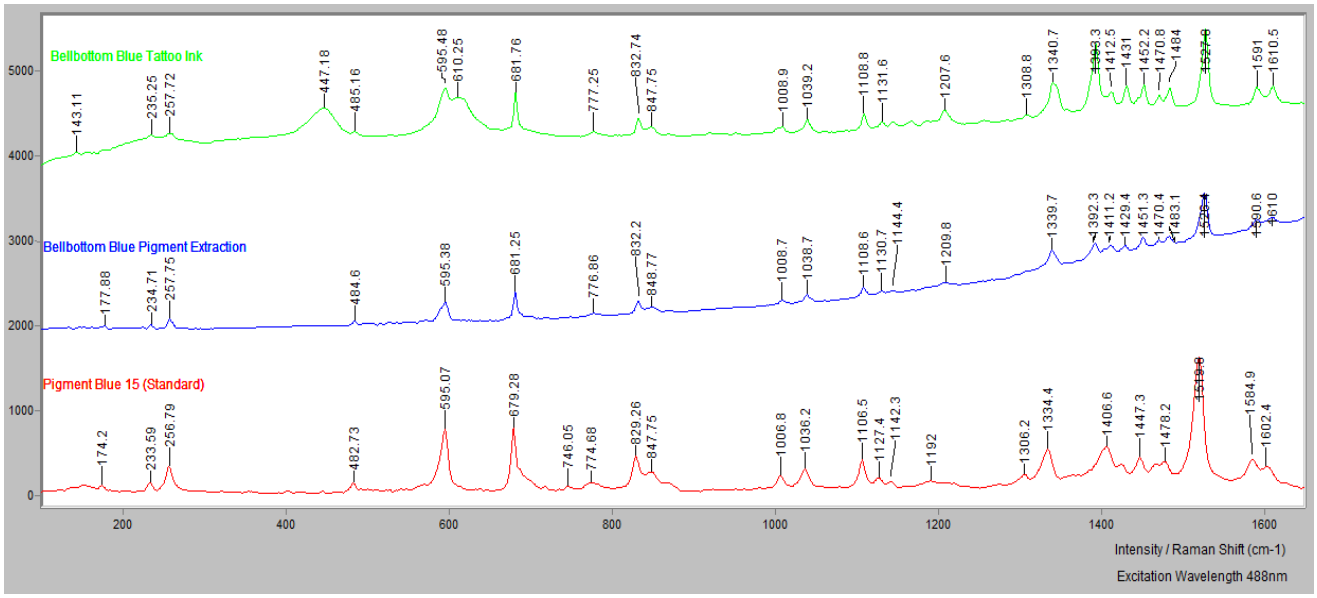

Figure 111. Normal Raman spectra of Bell Bottom Blue ink and pigment extraction compared to Pigment Blue 15.

SRV Teal 2- XRF indicated the presence of titanium, chlorine and copper. It is probable that the titanium is due to the presence of titanium dioxide and the chlorine and copper are indicative of Pigment Green (Cu, Cl) and Pigment Blue (Cu).

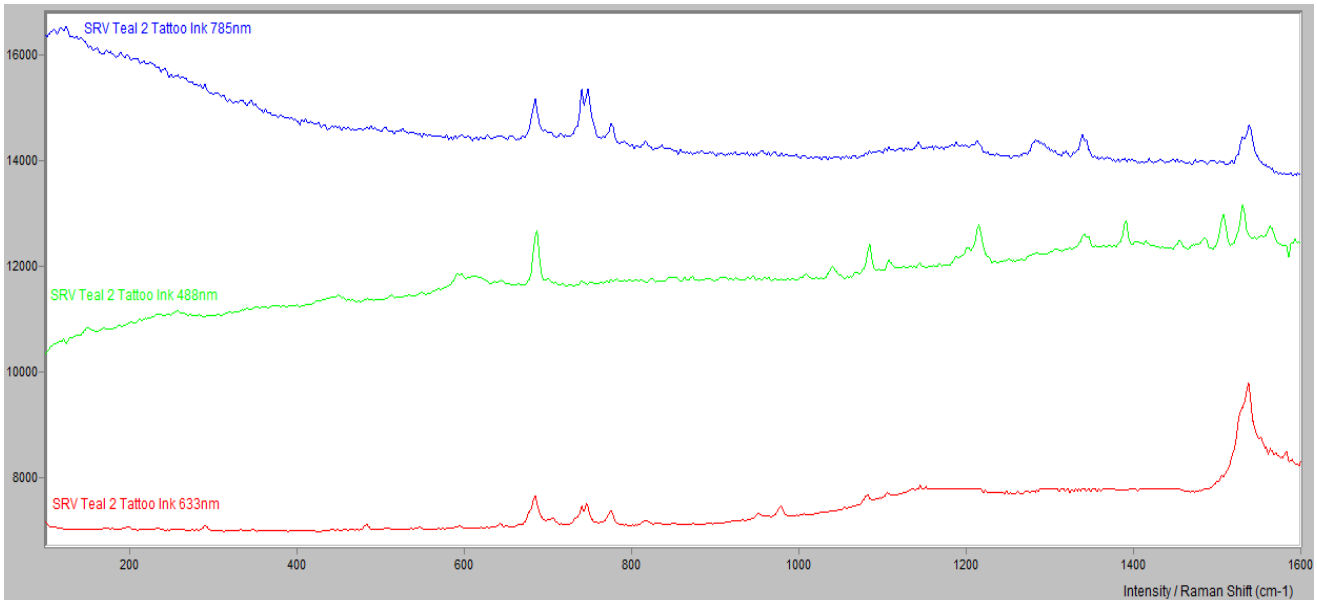

Figure 112. Raman spectra of SRV Teal 2 ink at different excitation wavelengths.

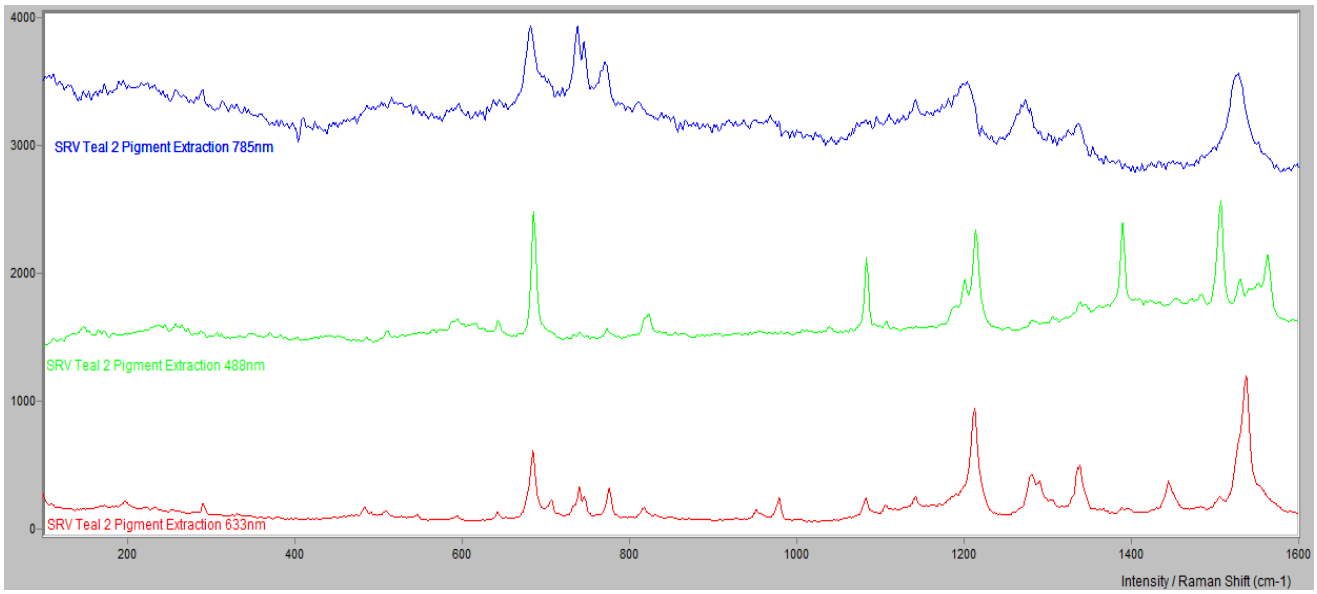

Figure 113. Raman spectra of SRV Teal 2 pigment extraction at different excitation wavelengths.

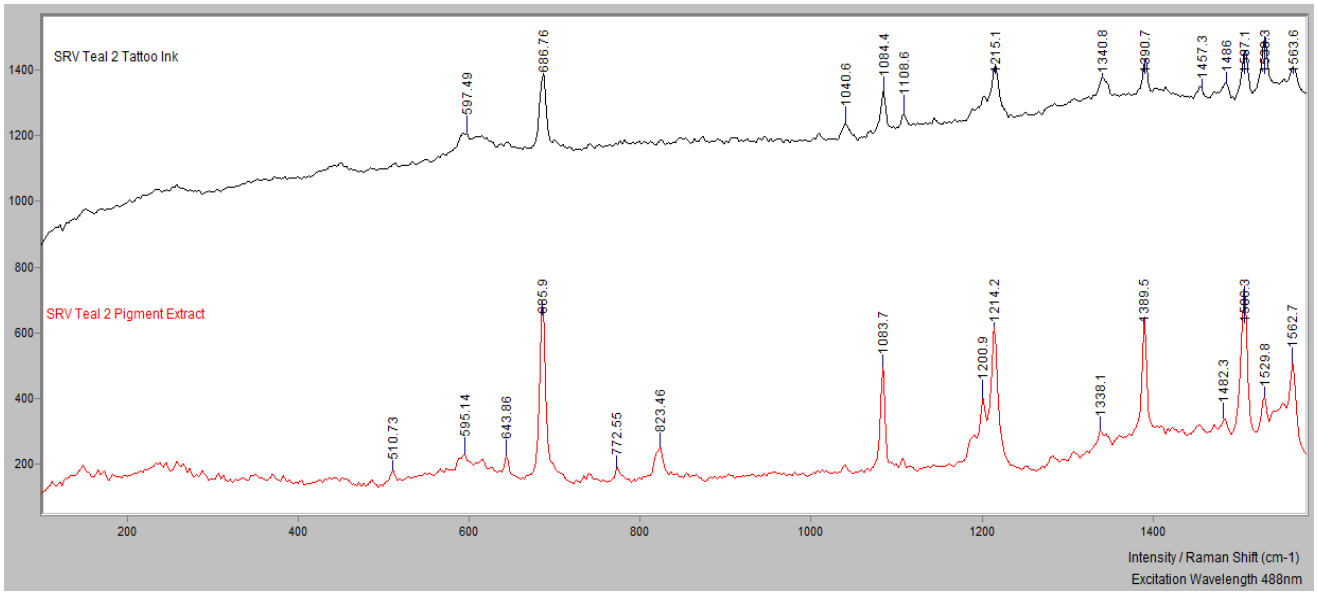

Figure 114. Comparison of Raman spectra of SRV Teal 2 ink and pigment extraction.

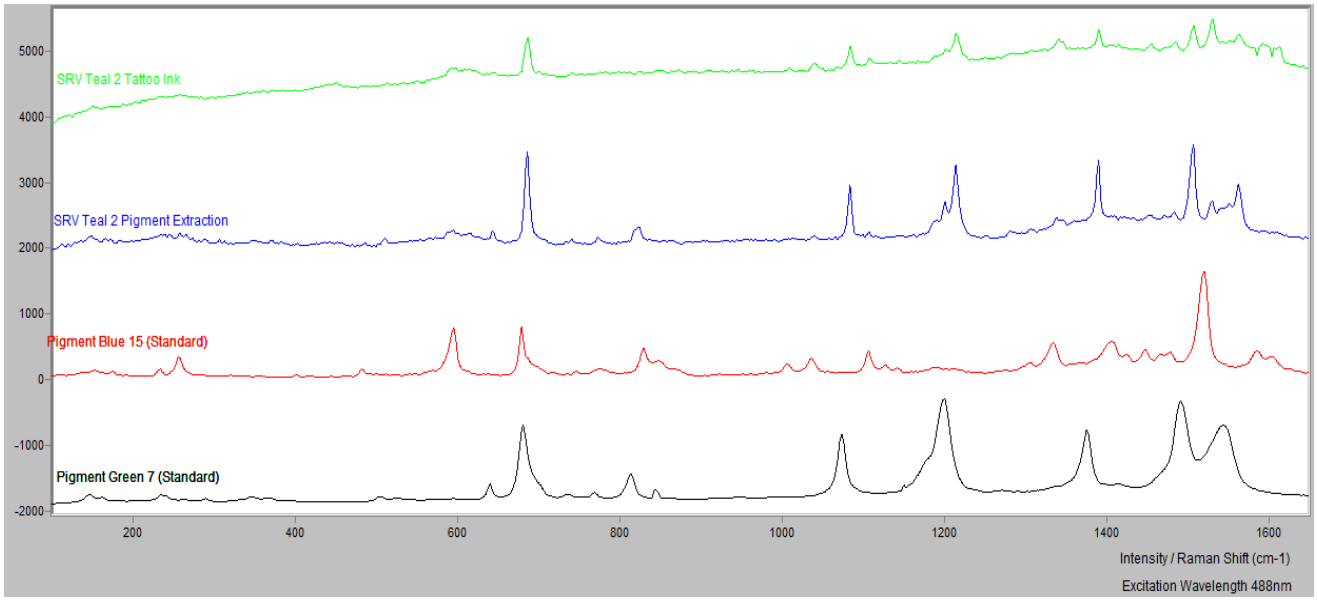

Figure 115. Normal Raman spectra of SRV Teal 2 ink and pigment extraction compared to Pigment Blue 15 and Pigment Green 7.

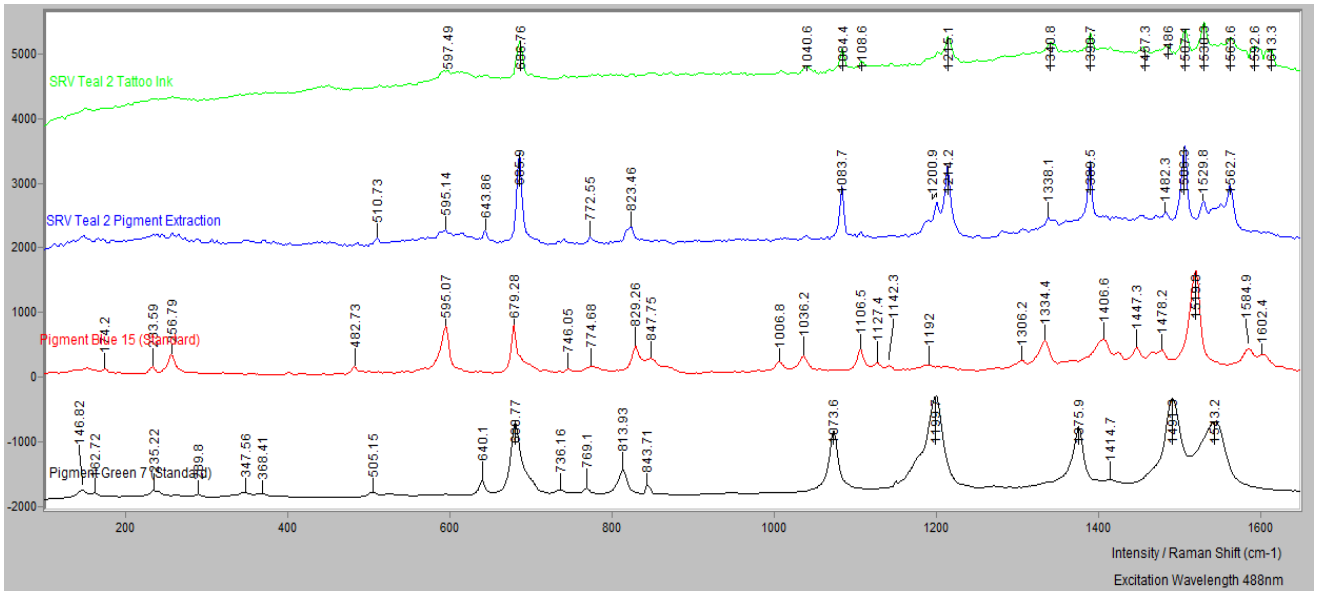

Figure 116. Normal Raman spectra of SRV Teal 2 ink and pigment extraction compared to Pigment Blue 15 and Pigment Green 7 (with peak labels).

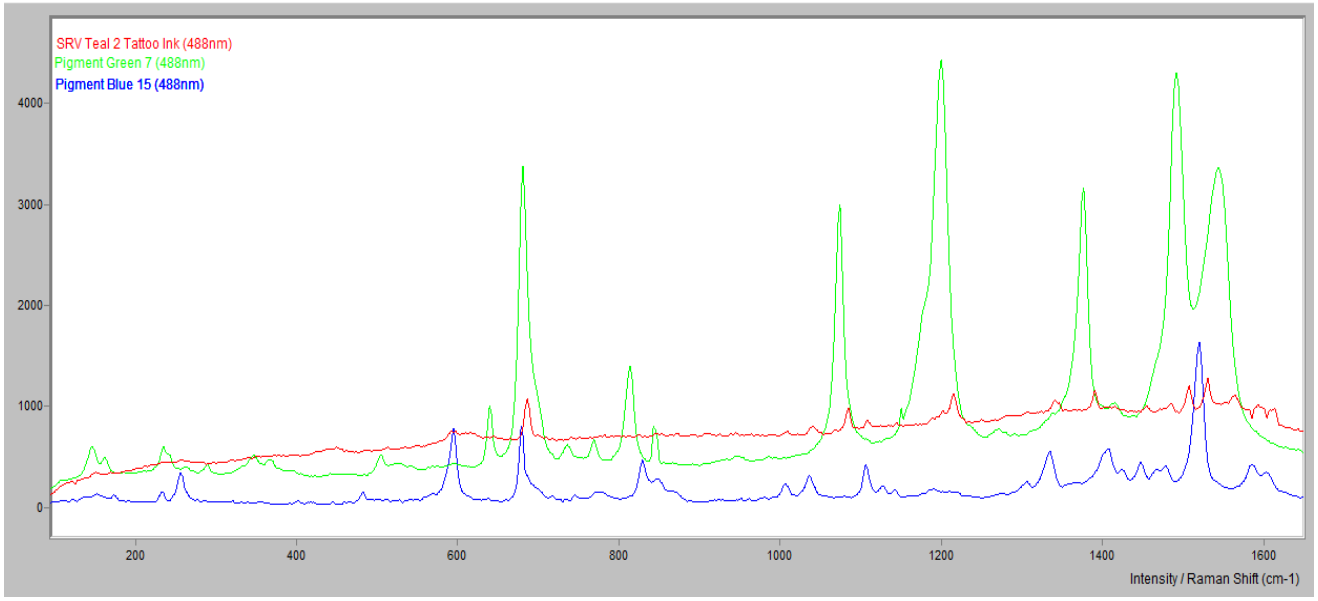

Figure 117. Overlaid Raman spectra of SRV Teal 2 with Pigment Green 7 and Pigment Blue 15. SRV Teal 2 does appear to exhibit bands present in both pigments.

Muddy Water Blue- XRF indicated the presence of copper. The copper is indicative of Pigment Blue. UV/Vis data correlated to that of Pigment Blue 15.

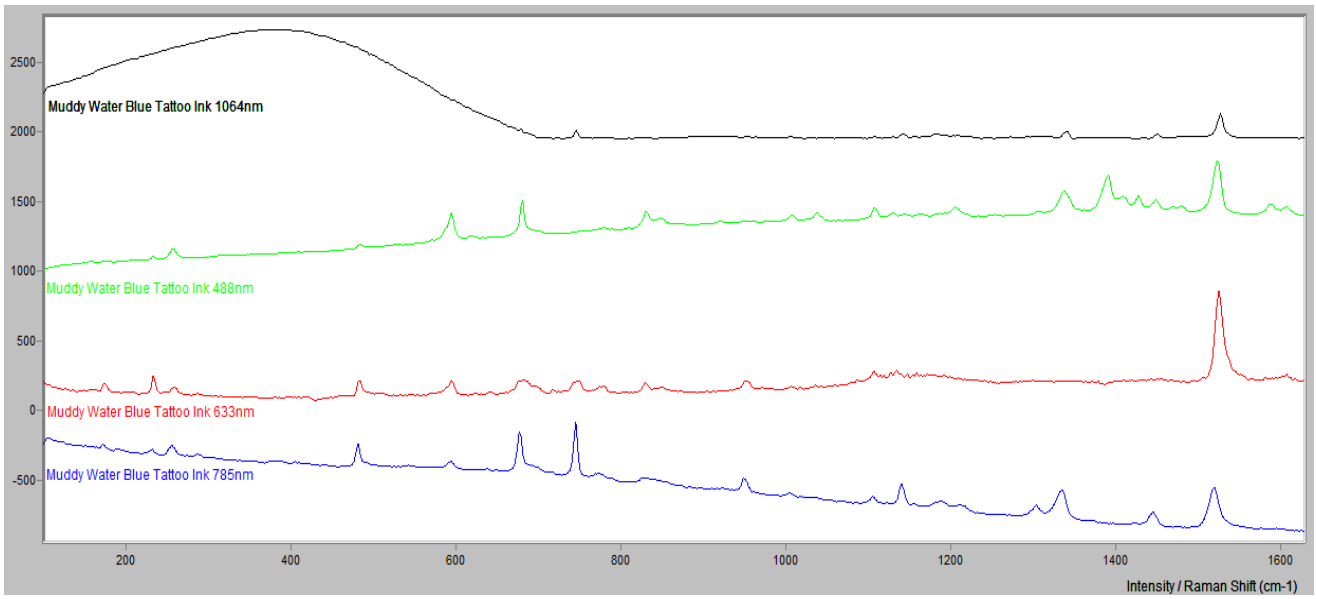

Figure 118. Raman spectra of Muddy Water Blue ink at different excitation wavelengths.

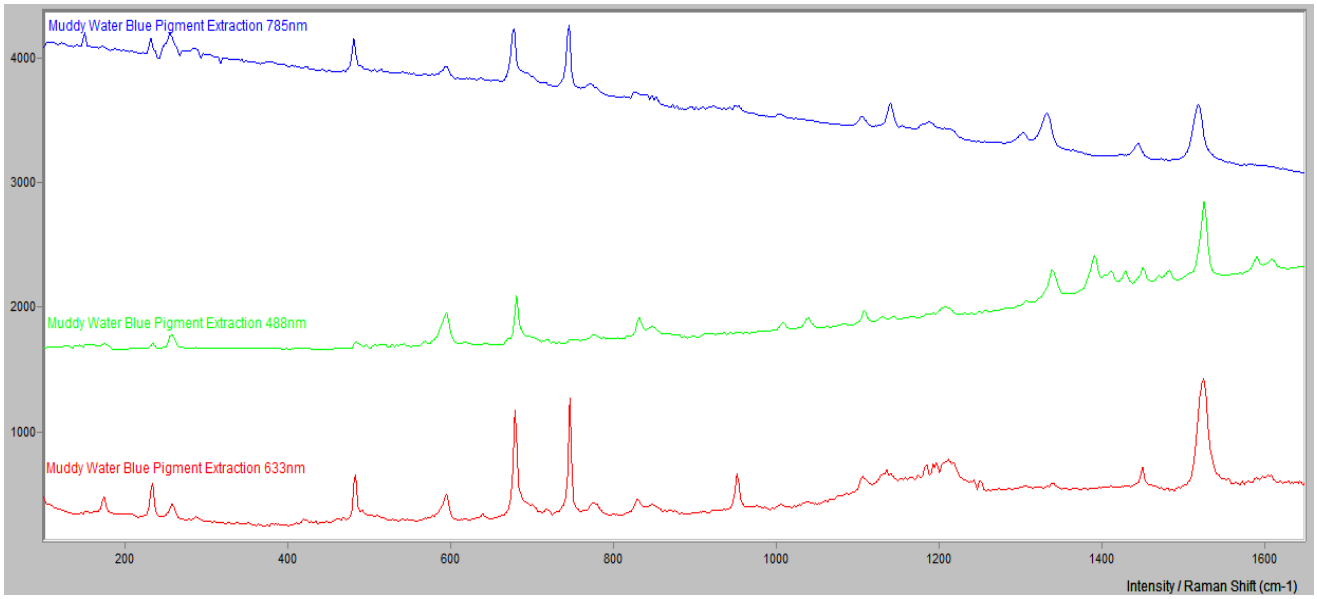

Figure 119. Raman spectra of Muddy Water Blue pigment extraction at different excitation wavelengths.

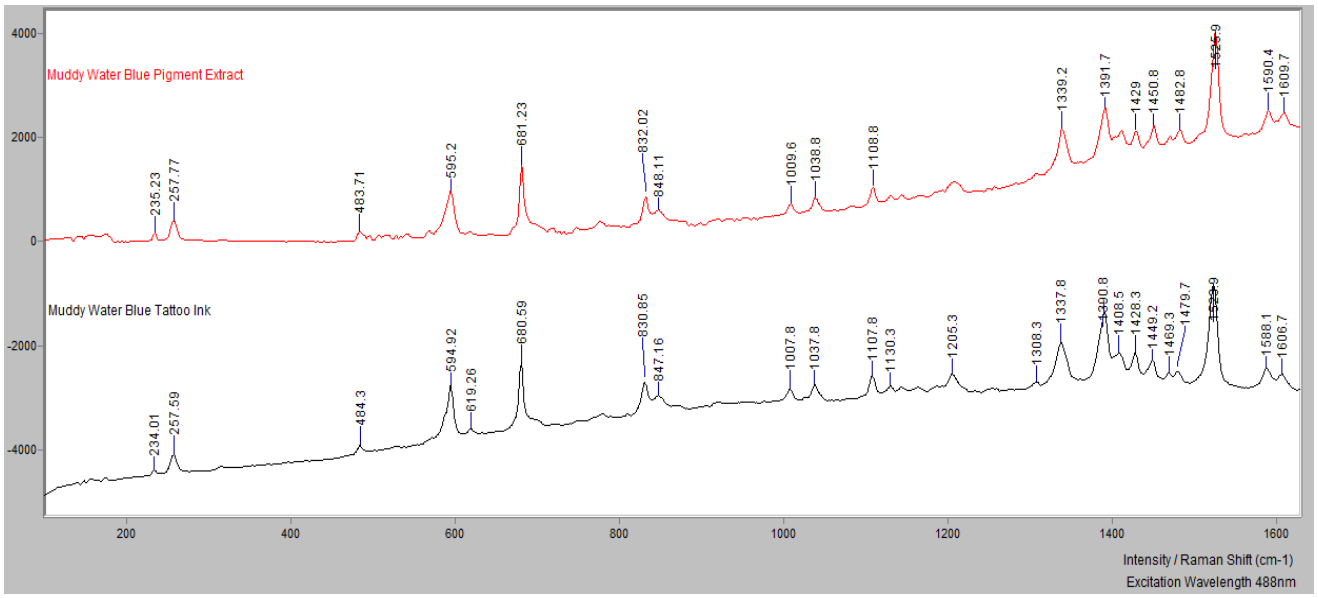

Figure 120. Comparison of Raman spectra of Muddy Water Blue ink and pigment extraction.

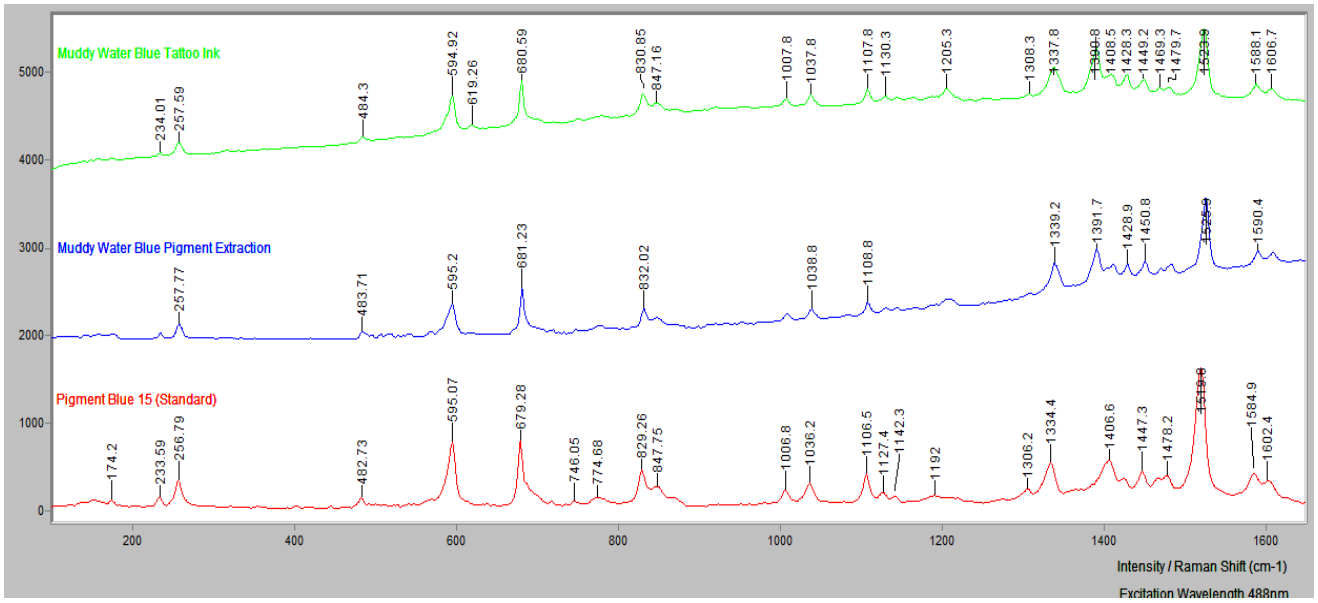

Figure 121. Normal Raman spectra of Muddy Water Blue ink and pigment extraction compared to Pigment Blue 15.

Ripple- XRF indicated the presence of titanium and chlorine. It is probable that the titanium is due to the presence of titanium dioxide.

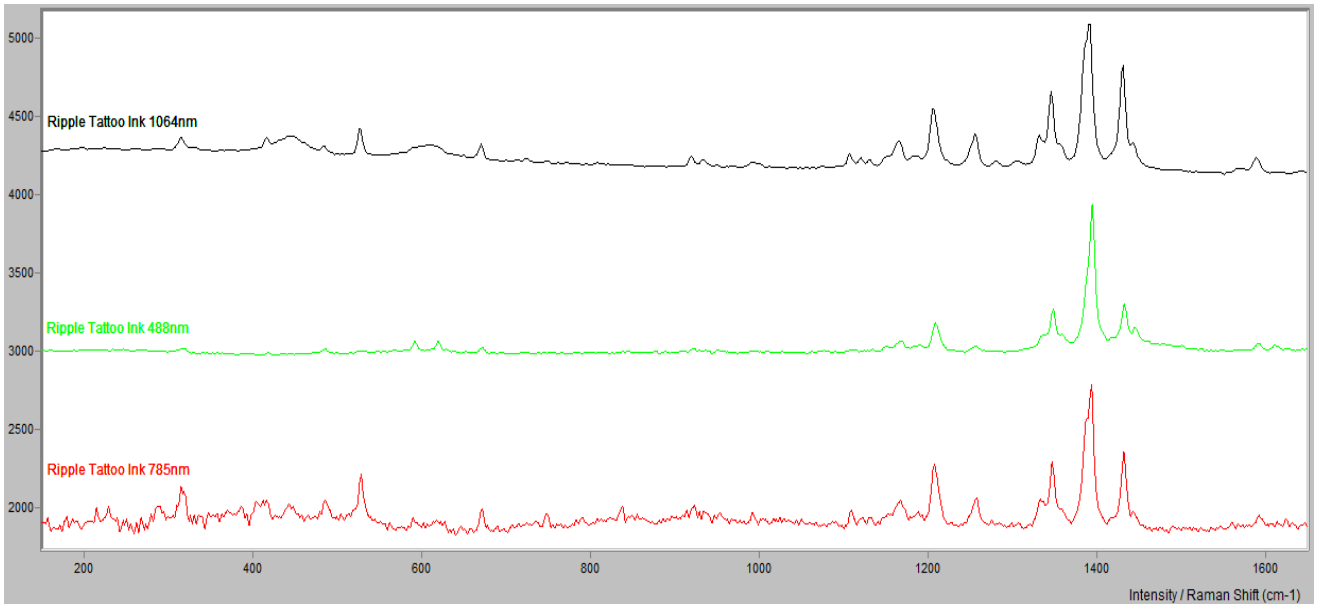

Figure 122. Raman spectra of Ripple ink at different excitation wavelengths.

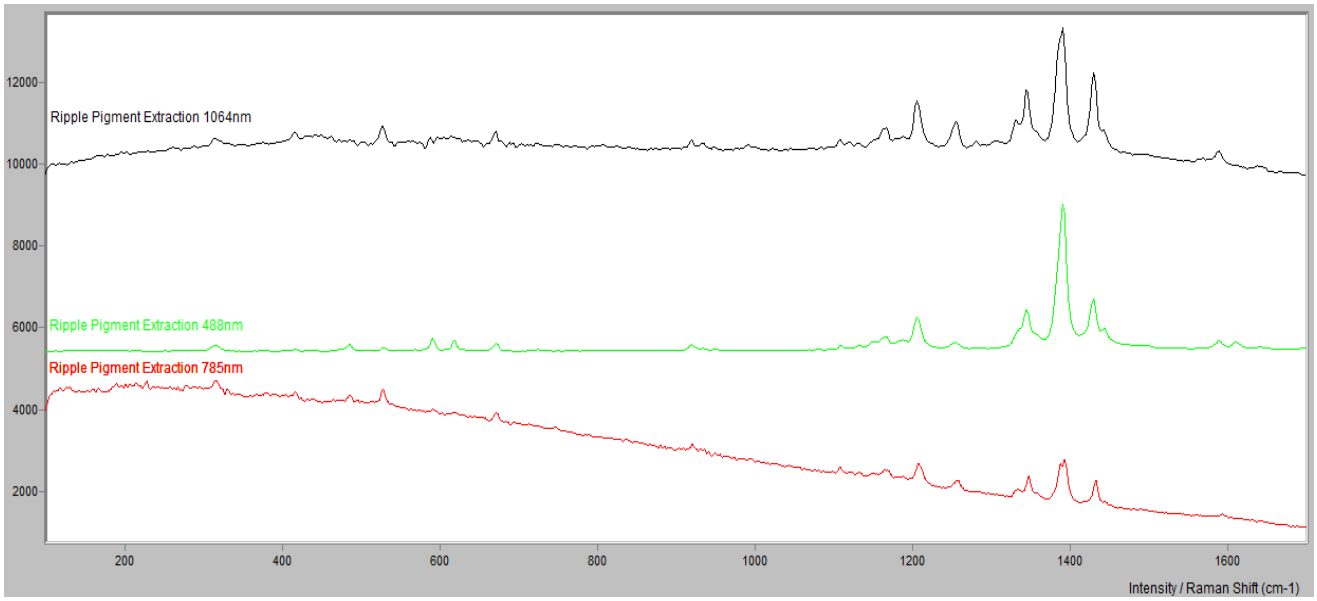

Figure 123. Raman spectra of Ripple pigment extraction at different excitation wavelengths.

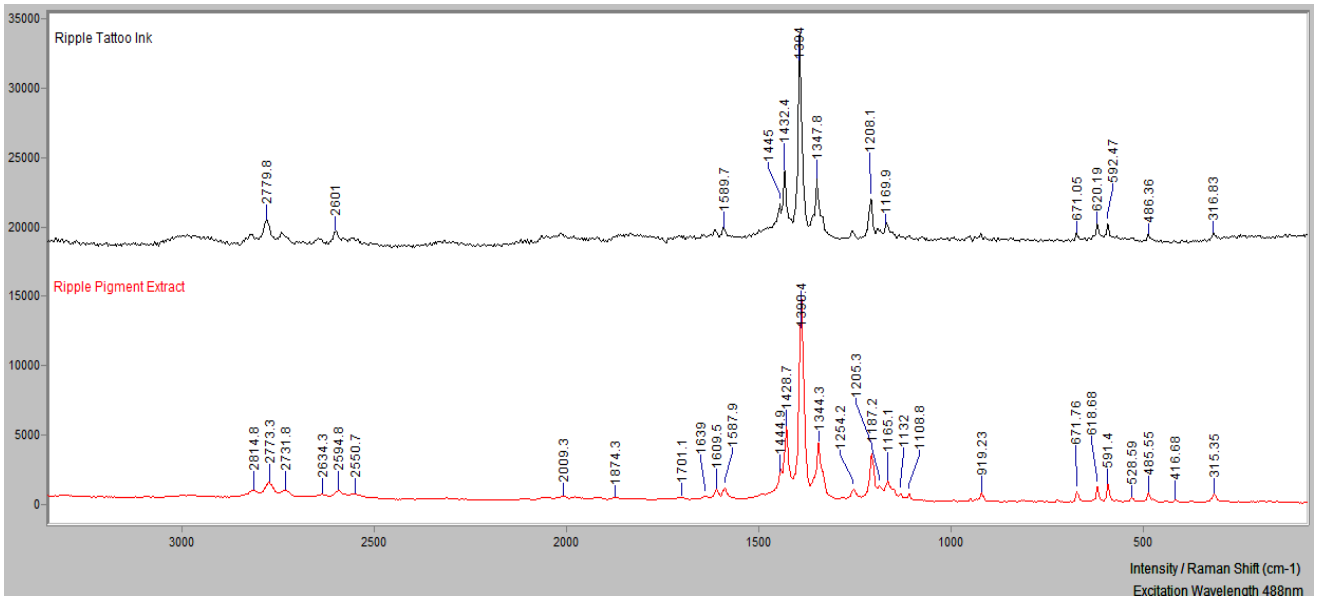

Figure 124. Comparison of Raman spectra of Ripple ink and pigment extraction.

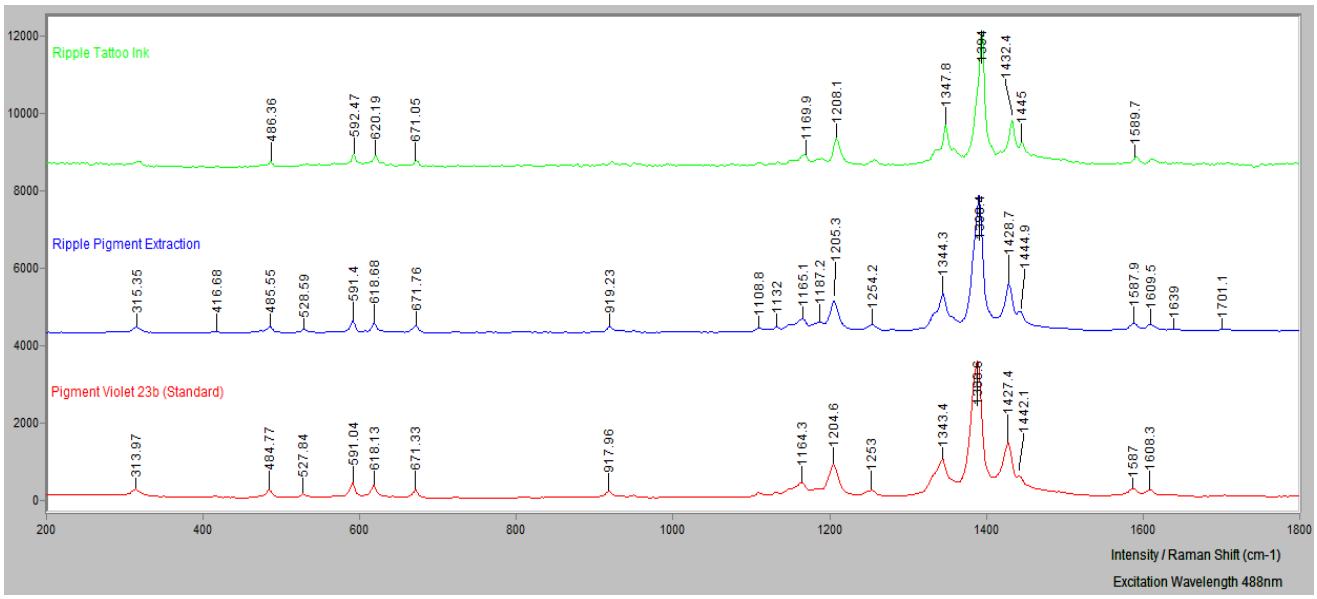

Figure 125. Normal Raman spectra of Ripple ink and pigment extraction compared to Pigment Violet 23β.

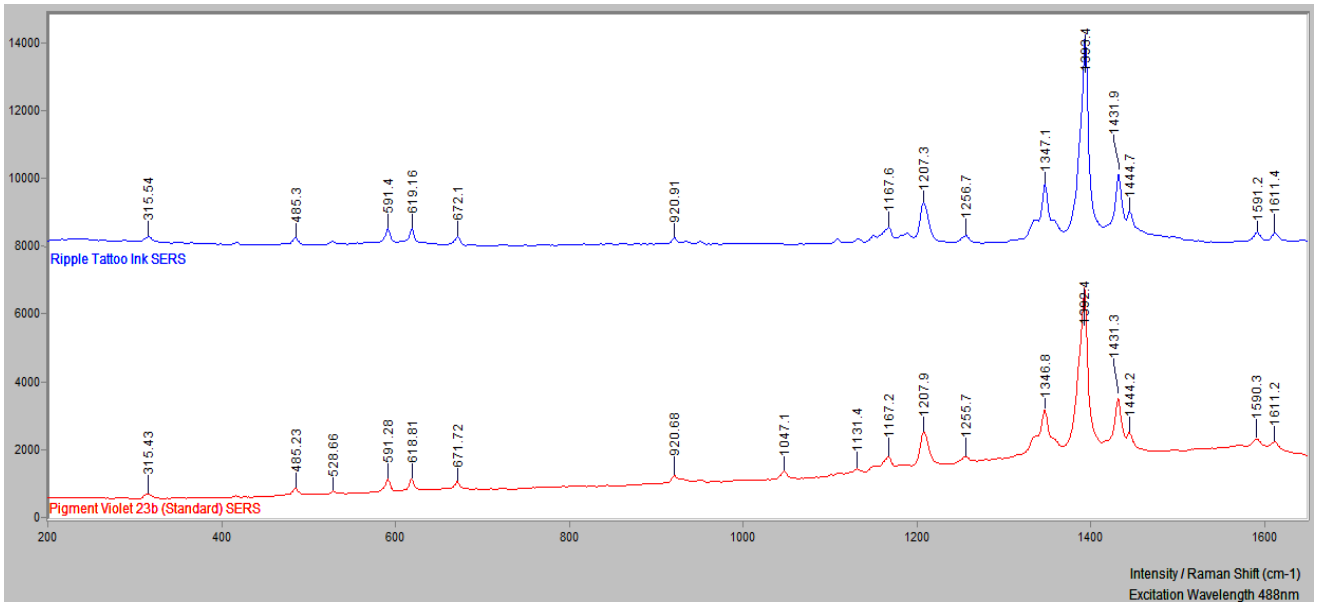

Figure 126. SERS spectra of Ripple ink compared to Pigment Violet 23β.

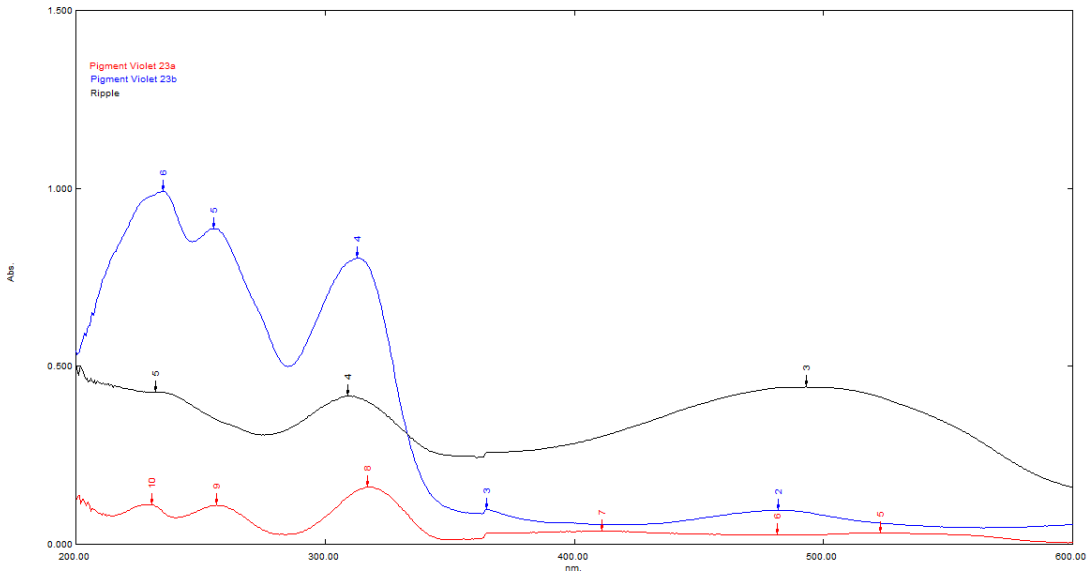

Figure 127. Comparison of Ripple Tattoo Ink and two polymorphs of PV23 (α and β).

Razberry Creem- All normal Raman spectra exhibited overwhelming fluorescence. A few very subtle bands are observed with λ_0=488nm. XRF indicated the presence of titanium. It is probable that the titanium is due to the presence of titanium dioxide. UV/Vis data correlated to that of Pigment Red 122.

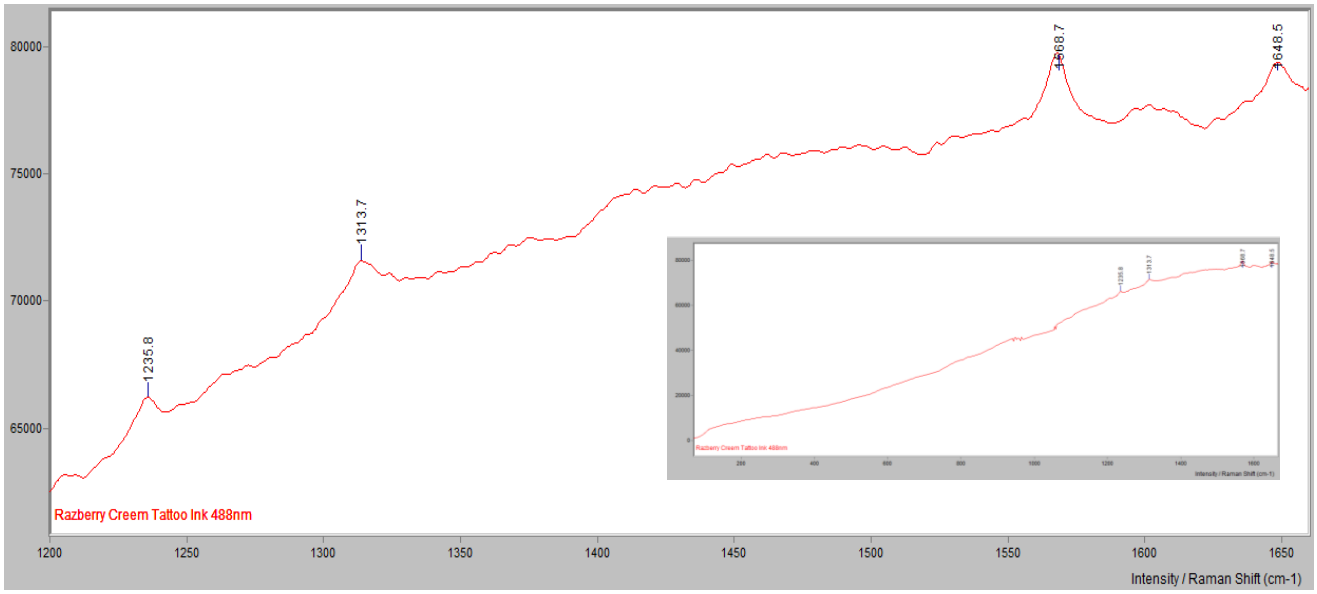

Figure 128. Normal Raman spectrum of Razberry Creem tattoo ink from the region of 1200nm to 1660nm (λ_0=488nm). The overwhelming fluorescence can be seen in the region from 70nm to 1660nm (inset).

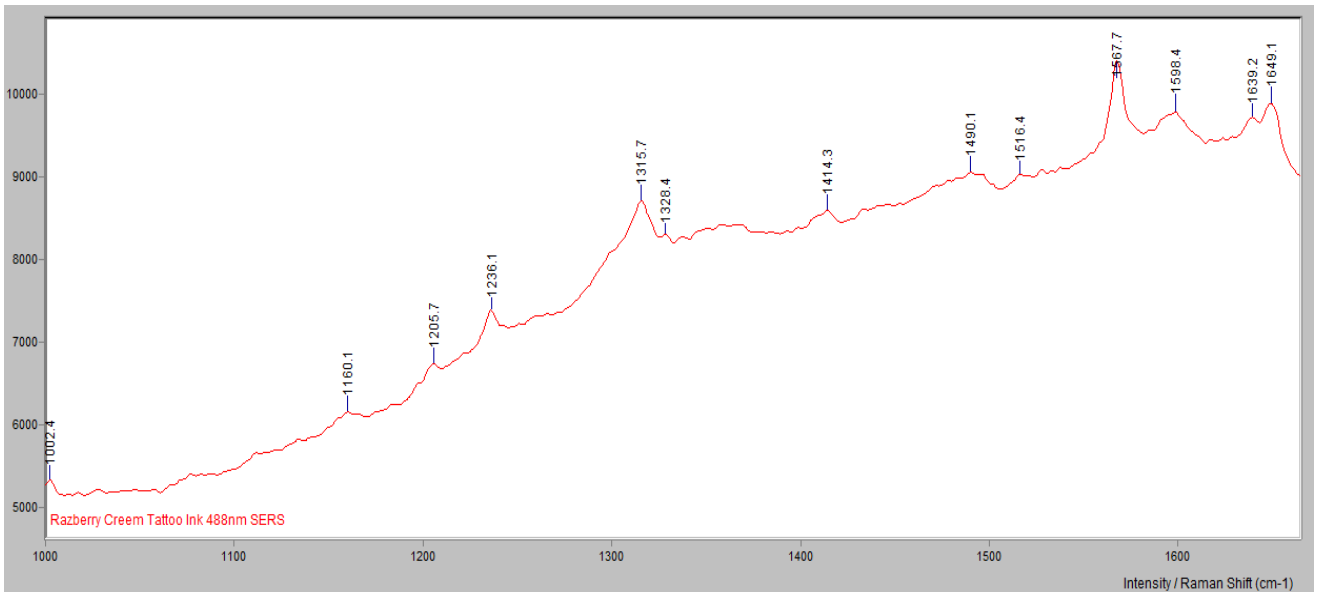

Figure 129. SERS spectrum of Razberry Creem tattoo ink from the region of 1000nm to 1660nm (λ_0=488nm). Although fluorescence is still apparent, the use of SERS enabled the resolution of additional bands.

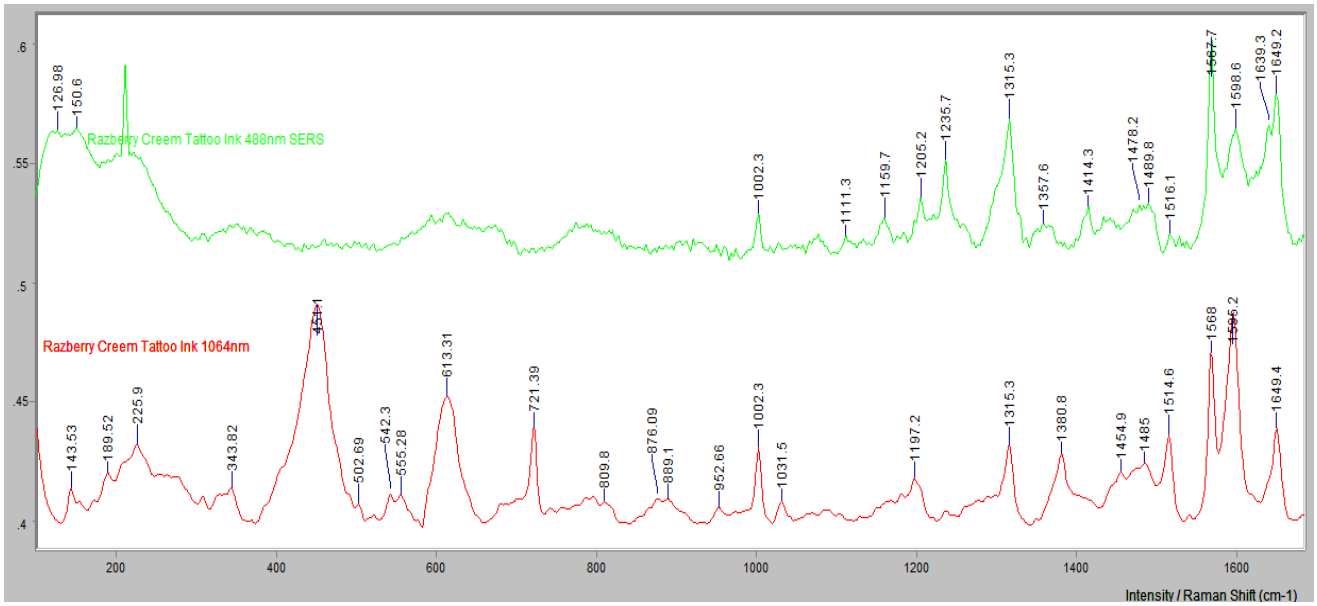

Figure 130. SERS spectrum and FT-Raman spectrum of Razberry Creem tattoo ink (baseline correction has been applied to both spectra).

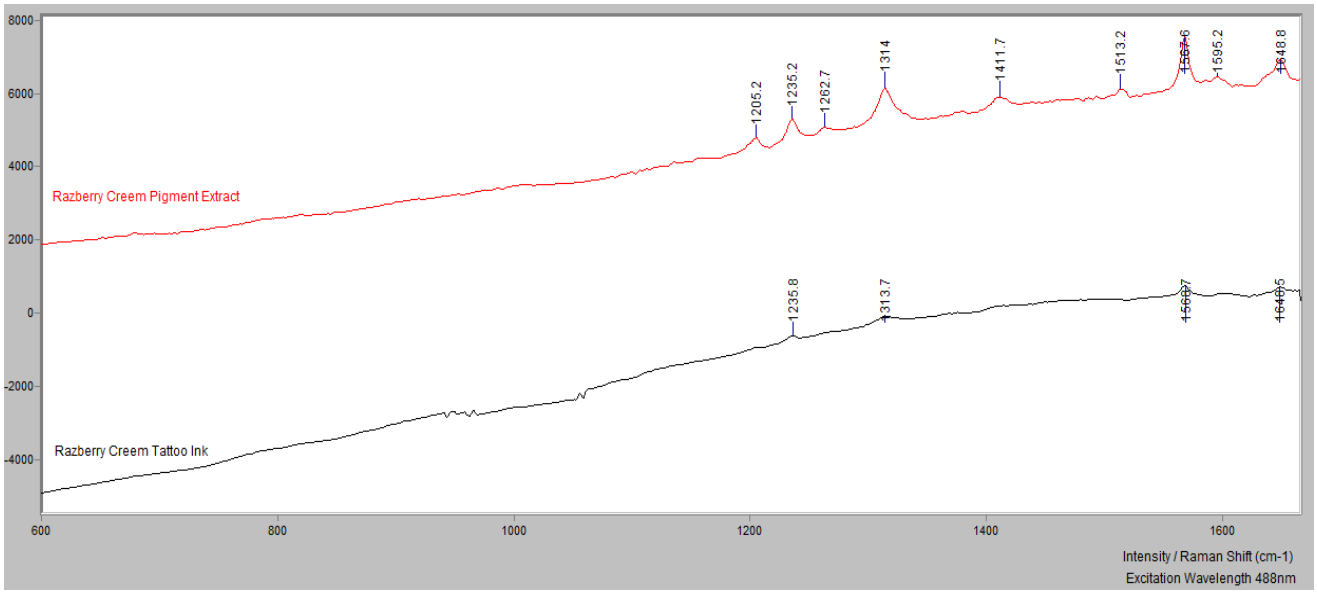

Figure 131. Comparison of Raman spectra of Razberry Creem ink and pigment extraction.

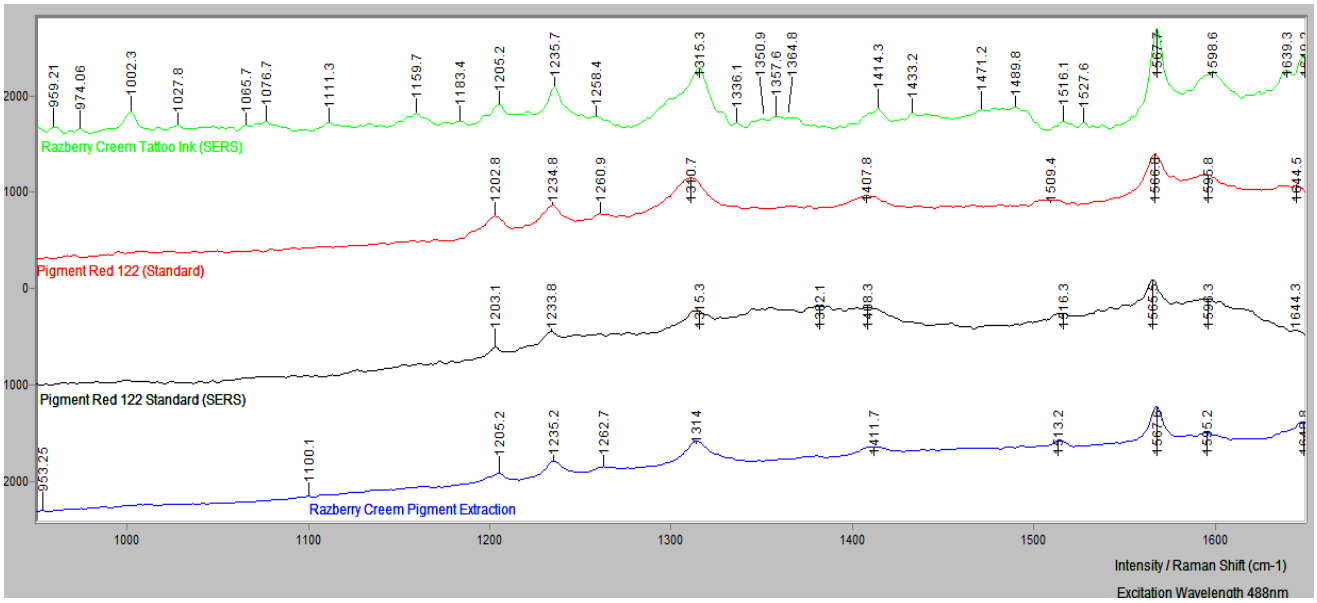

Figure 132. SERS spectrum of Razberry Creem tattoo ink and normal Raman spectrum of Razberry Creem pigment extraction compared to the normal Raman and SERS spectra of Pigment Red 122.

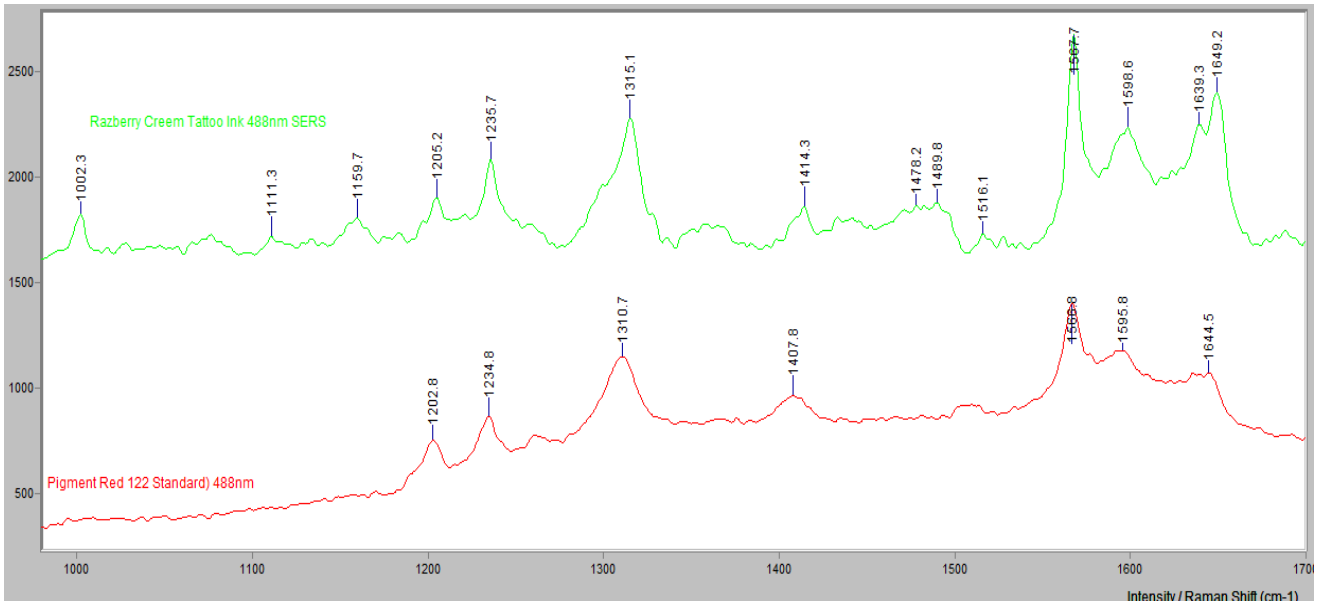

Figure 133. Comparison of SERS spectrum of Razberry Creem Tattoo ink and Pigment Red 122.

Black Cherry Roan 2- The Roan color series is described as neutral brown hues that are meant to be used to produce sepia-toned tattoos, often used with portrait or memorial tattoos. Although these colors appear different shades of brown (with Roan 1 being the darkest brown, almost black and Roan 3 being the lightest brown of the set), microscopic examination disclosed

the presence of green and reddish-pink/purple pigments, which ratios varied depending on the numerical assignments of the Roan color. UV/Vis data correlated to that of Pigment Red 146.

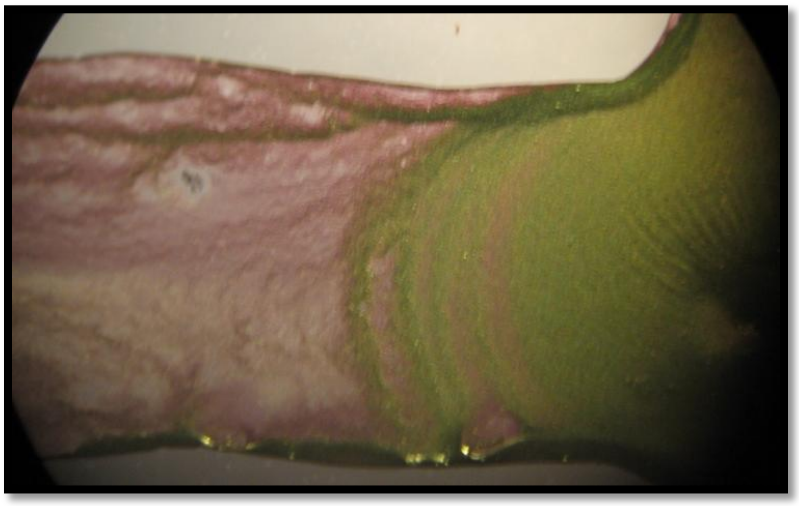

Figure 134. Photomicrograph of Roan tattoo ink (stereomicroscope, appx. 20x)

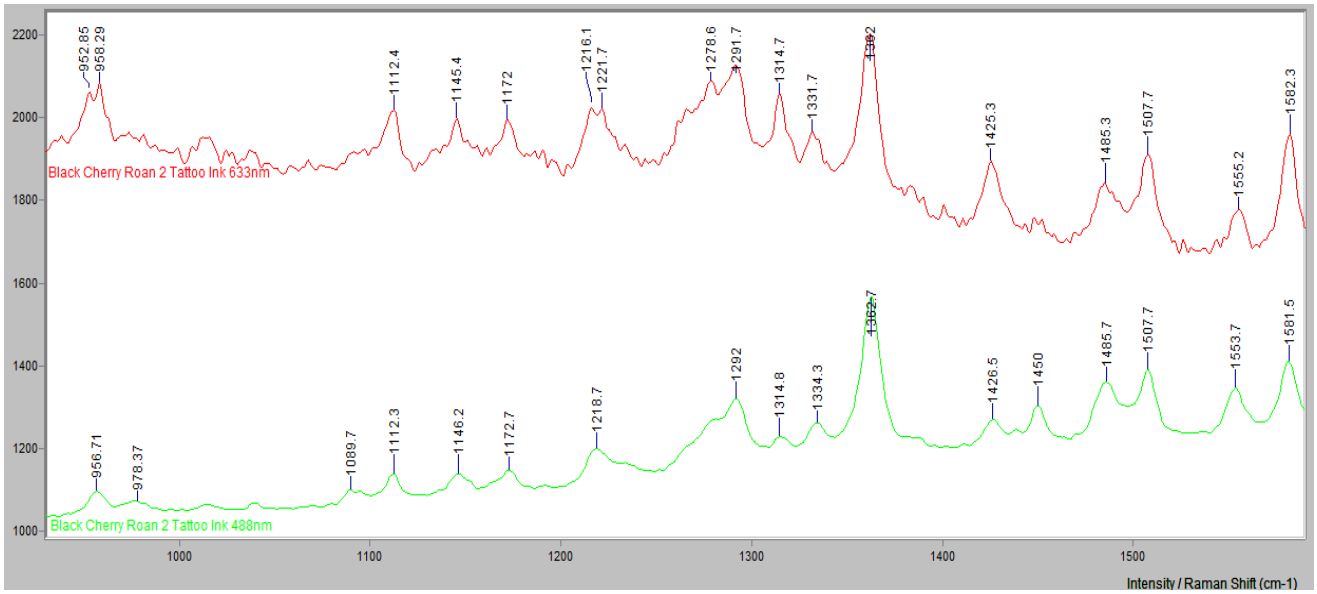

Figure 135. Comparison of Black Cherry Roan Tattoo ink at λ_0=488nm (green) and 633nm (red).

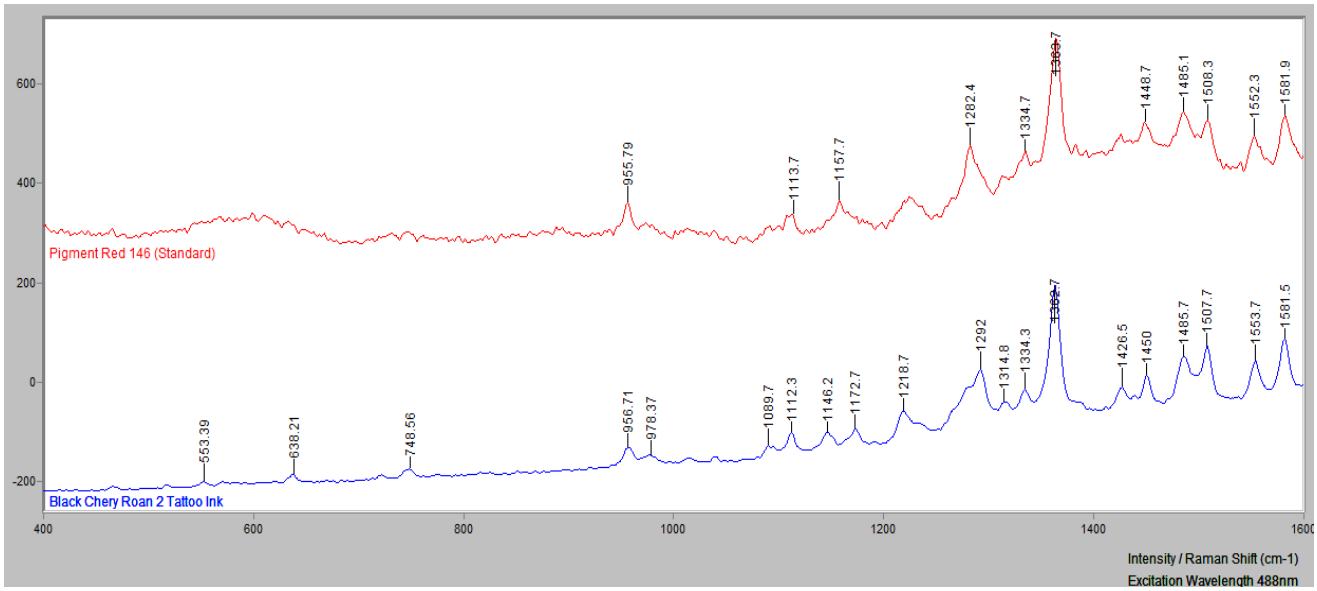

Figure 136. Comparison of Black Cherry Roan Tattoo ink (blue) and Pigment Red 146 pigment standard (red)

San Brownadino- The bands observed are consistent with iron oxide. According to Bell, *et. al*., 1997, synthetic iron (III) oxide, Fe_2O_3, exhibits bands at 224vs, 291vs, 407m, 494w, 608m (λ_0=632.8nm). XRF indicated the presence of iron. The iron is indicative of iron oxide.

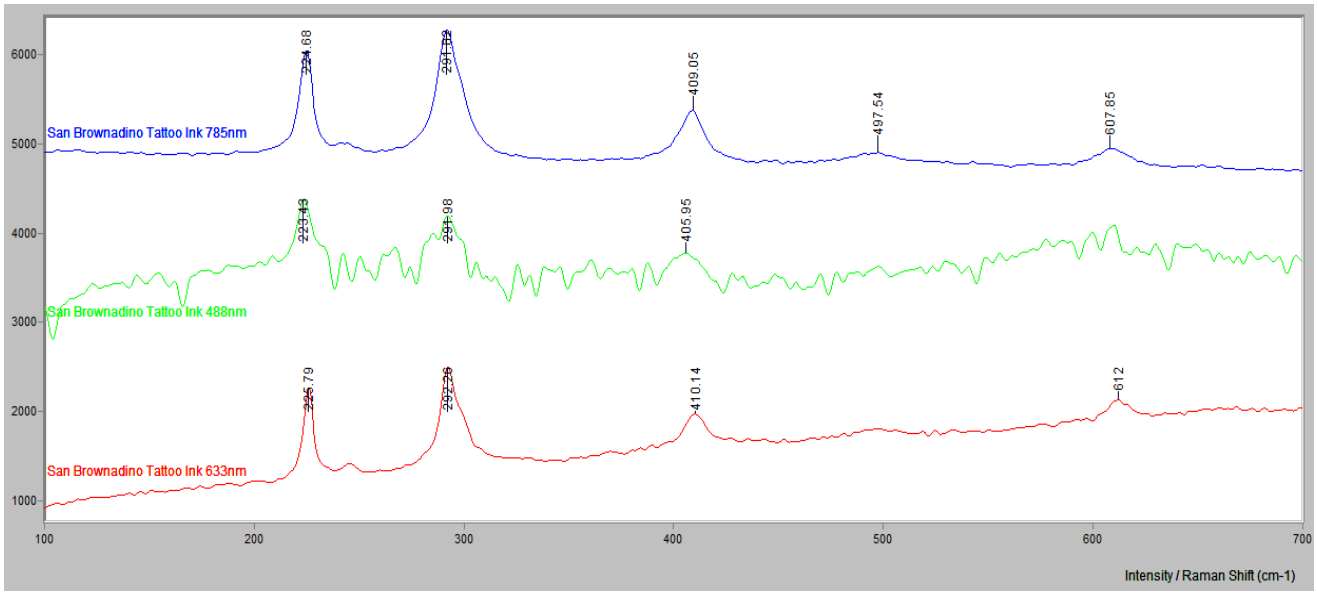

Figure 137. Raman spectra of San Brownadino ink at different excitation wavelengths.

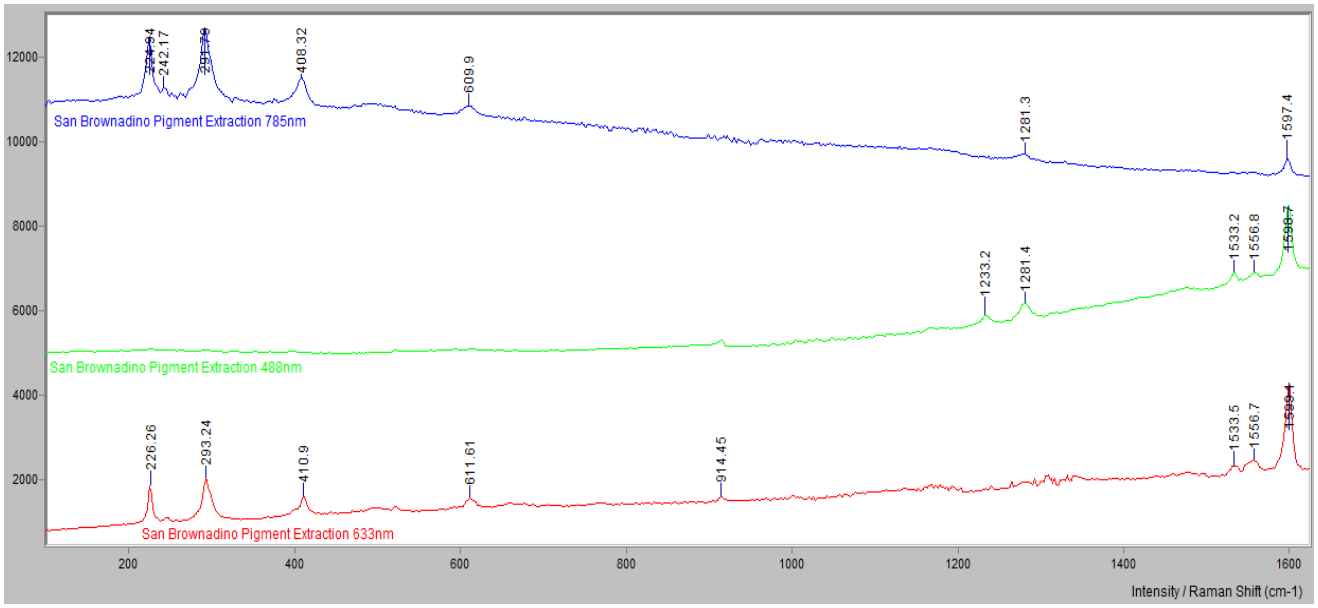

Figure 138. Raman spectra of San Brownadino pigment extraction at different excitation wavelengths.

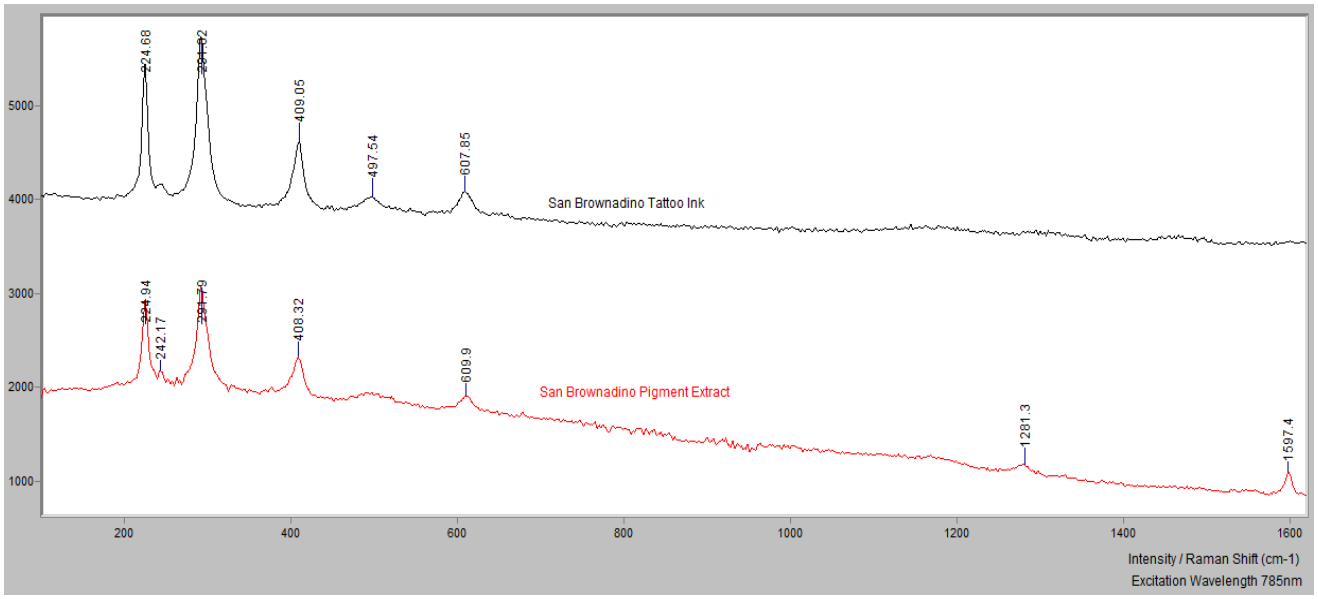

Figure 139. Comparison of Raman spectra of San Brownadino ink and pigment extraction.

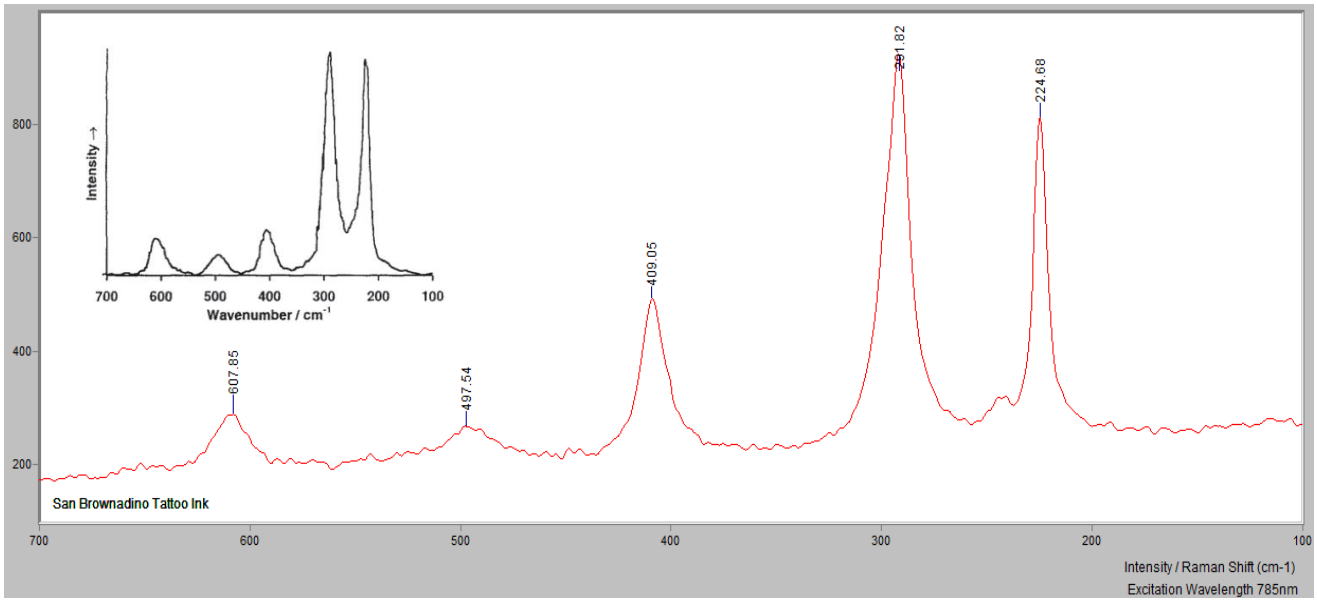

Figure 140. Normal Raman spectra of San Brownadino Tattoo Ink and synthetic iron (III) oxide (inset, from Bell, *et.al.*, 1997).

Whitegirl- The bands observed at the lower shifts are consistent with titanium dioxide, specifically rutile. According to Burgio, *et.al.*, 2001, the rutile form of titanium dioxide exhibits bands at 144(w), 232(m), 447(s) and 609(s)cm^{-1} (λ_0=1064nm). XRF indicated the presence of titanium, which is indicative of titanium dioxide. According to Ropret, *et.al.*, the anatase form of titanium dioxide is characterized by bands at 398, 515 and 639cm^{-1}. Most literature reports anatase as having three major bands (395, 515 and 640 cm^{-1}) and rutile as having two major bands (450 and 610 cm^{-1}).

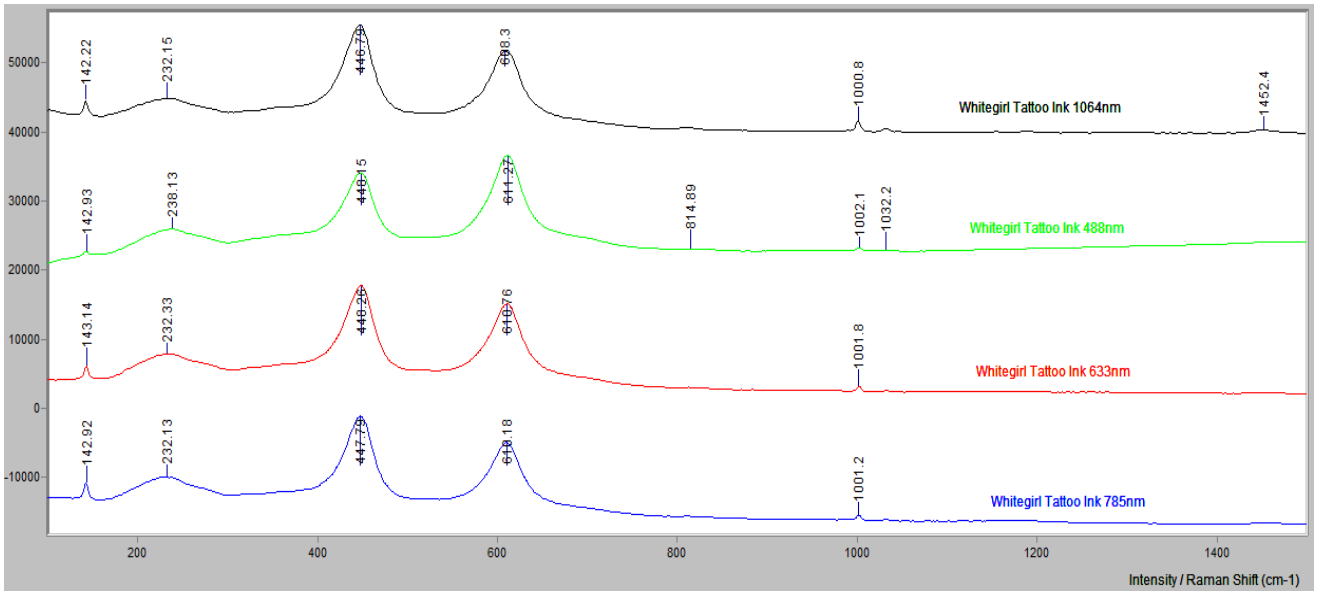

Figure 141. Raman spectra of Whitegirl ink at different excitation wavelengths.

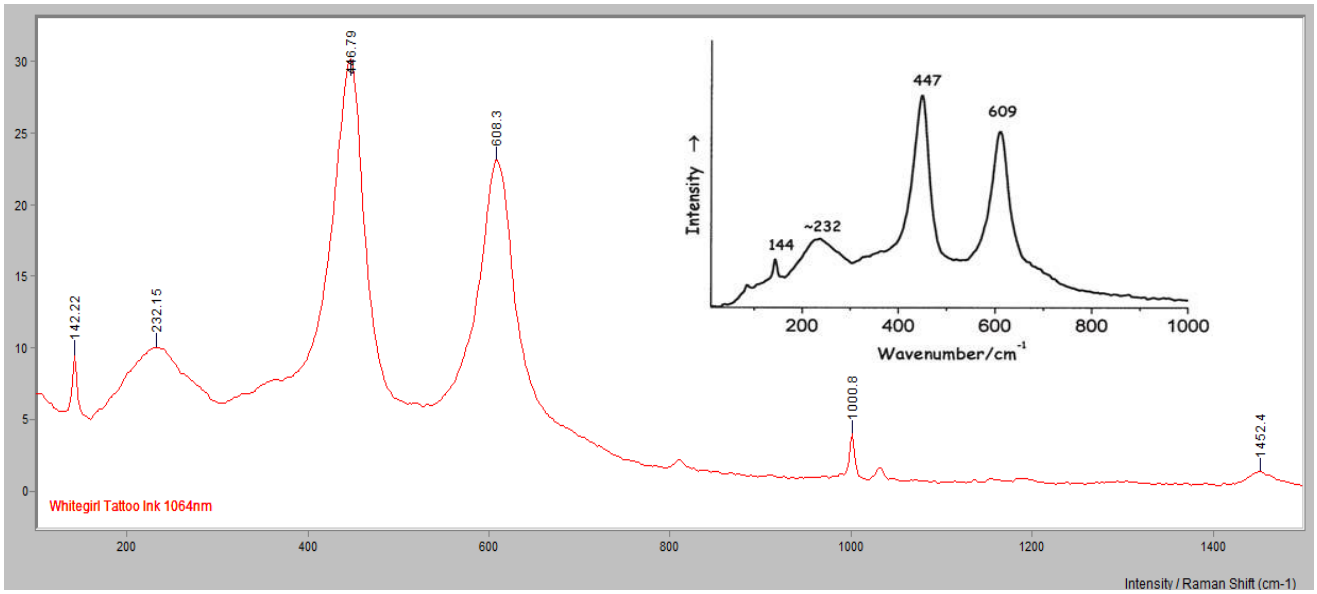

Figure 142. Normal Raman spectrum of Whitegirl Tattoo Ink and titanium dioxide (inset, from Burgio, *et.al.*, 2001).

Tokyo Pink- Tokyo Pink Tattoo Ink exhibited overwhelming fluorescence for normal Raman at all three excitation wavelengths. At λ_0=785nm, two faint bands were detected among the background. No information was obtained when attempting SERS on Tokyo Pink. FT-Raman was successful in producing a detailed spectrum. The two bands identified with normal Raman at

λ_0=785nm were detected in the FT-Raman spectrum (λ_0=1064nm). The spectrum does not appear consistent with that of any pigment standards analyzed in this research. The strong band at 1601.7cm^{-1} is consistent with that observed with Pigment Orange 16 and 62, a disazo and monoazo pigment, respectively. The band at 1601.7cm^{-1} is due to the C=N stretching vibration, and the band at 1003cm^{-1} is due to ring breathing. XRF indicated the presence of titanium, chlorine and iron. It is probable that the titanium is due to the presence of titanium dioxide.

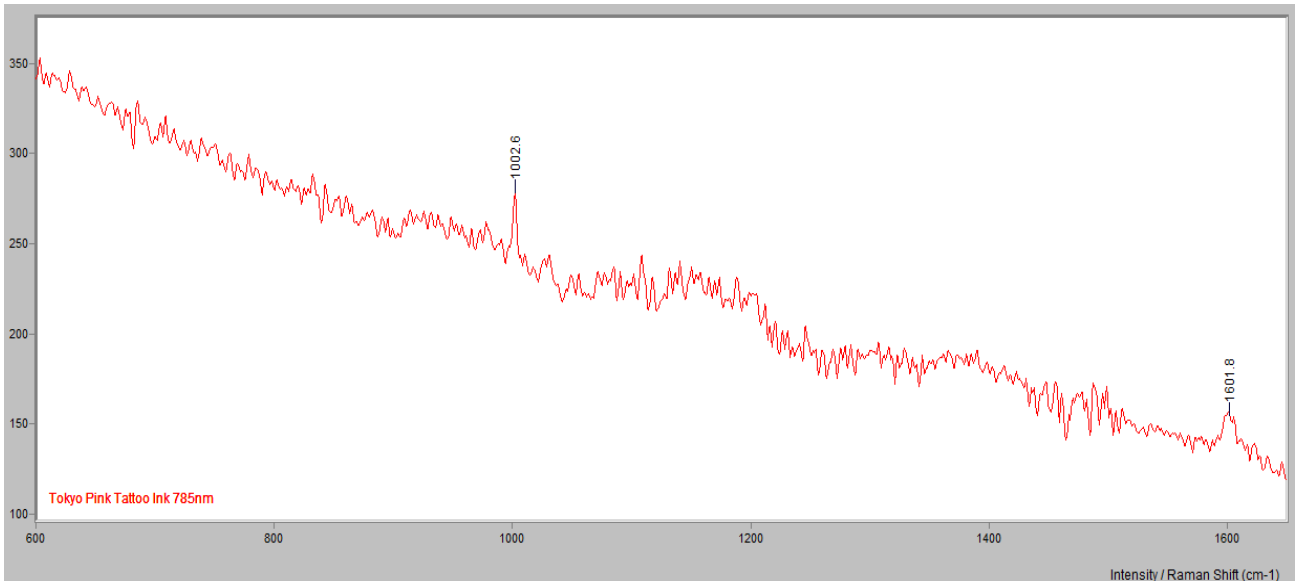

Figure 143. Normal Raman spectrum of Tokyo Pink (λ_0=785nm).

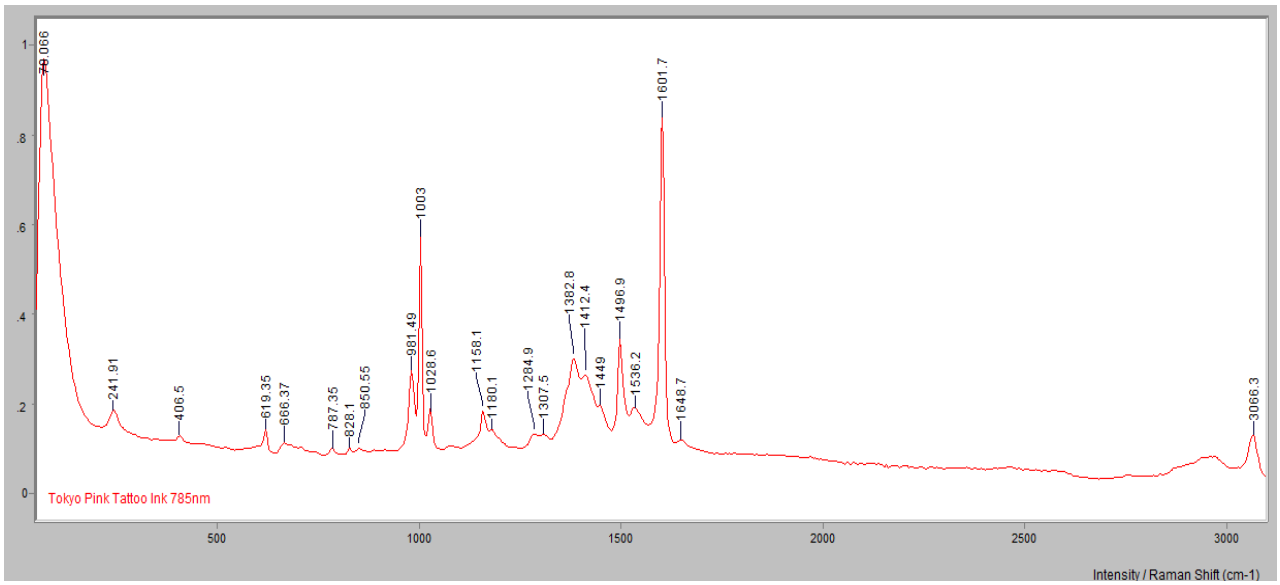

Figure 144. FT-Raman spectrum of Tokyo Pink (λ_0=1064nm).

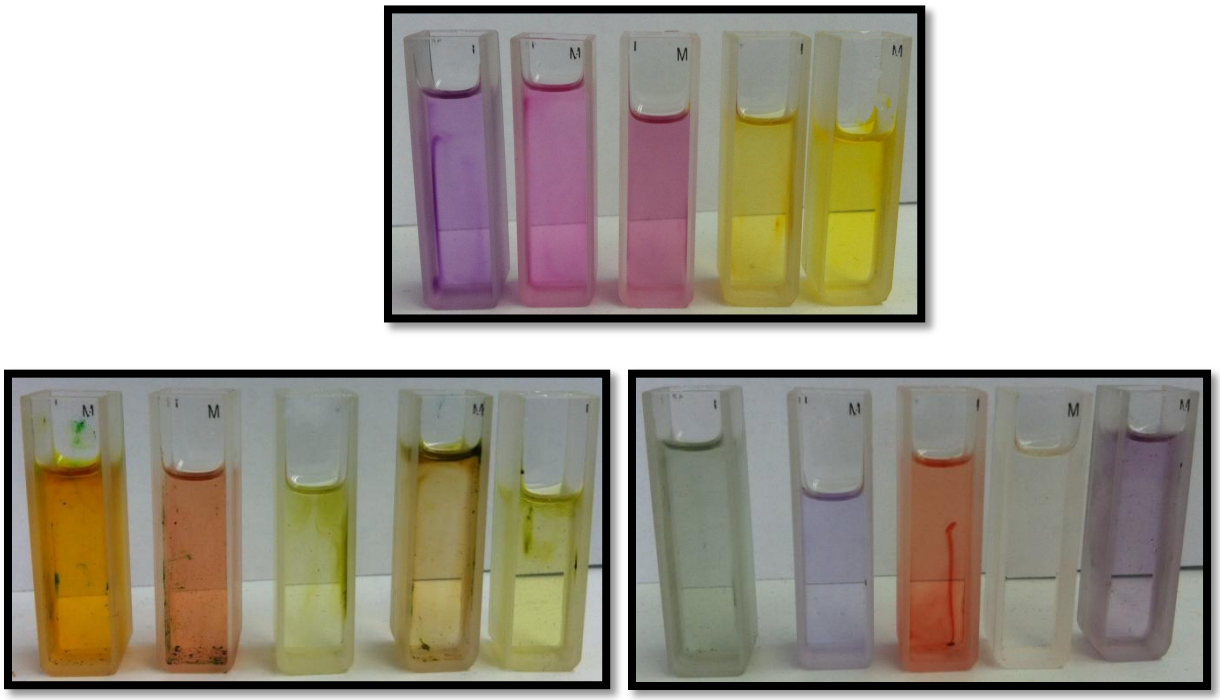

Figure 145 a, b and c. Tattoo ink pigment extractions dissolved in conc. H_2SO_4 in fused silica cuvettes in preparation for UV/Vis analysis (top) Candy Apple Red, Red Hot, Marz, Dolemite, Blisterine (bottom) Sassygrass, Tastywaves, Bellbottom Blue, SRV Teal 2, Muddy Water Blue, Ripple, Razberry Creem, San Brownadino, Tokyo Pink, Black Cherry Roan 2

Visual color characteristics, UV/Vis spectrometry, and color changes of the pigment upon introduction of the conc. sulfuric acid solvent system were recorded in an effort to characterize the pigments (in addition to the Skin Candy Tattoo Ink pigment extractions, which are reported below). Although it is not possible to establish structural information of the pigment molecule from 'coloristics' and solution chemistry, it is possible to gain information regarding the color class, functional groups (specifically chromophores) and resonance wavelength (for Raman spectroscopy) based upon visual characteristics and absorption maxima. Since the tattoo inks contain an abundance of various additives, including the presence of more than one pigment, it is recommended that pigment extracting be conducted prior to UV/Vis and wet chemistry methods. A proposed alternative to the extraction method conducted in this research is the use of the separation method Thin Layer Chromatography (TLC). Separation by a TLC plate in an appropriate solvent system followed by removal of the zone from the plate, extraction with an appropriate solvent system, and any necessary filtration and evaporation methods would be another option for separating the inks and extracting out any pigments for spectroscopic analysis.

Iron Works Brasil

The Iron Works Brasil Tattoo Ink set were analyzed via normal Raman and SERS. This was done in an effort to identify the pigment compositions within the inks and evaluate the use of SERS.

Vermelho- High quality spectra were resolved with normal Raman at all three excitation wavelengths and with FT-Raman. The FT-IR (ATR) spectrum also displayed a number of well-resolved peaks. XRF indicated the presence of iron, zinc and titanium. It is probable that the titanium is due to the presence of titanium dioxide. Microscopic examination of the Vermelho slide preparation proved to be very interesting, and lent support to the importance of microscopically examining the samples prior to instrumental analysis. Microscopic examination displayed a large concentration of red pigment particles, but a small aggregate of blue pigment particles was discovered. The region was subsequently analyzed using normal Raman along with the red region.

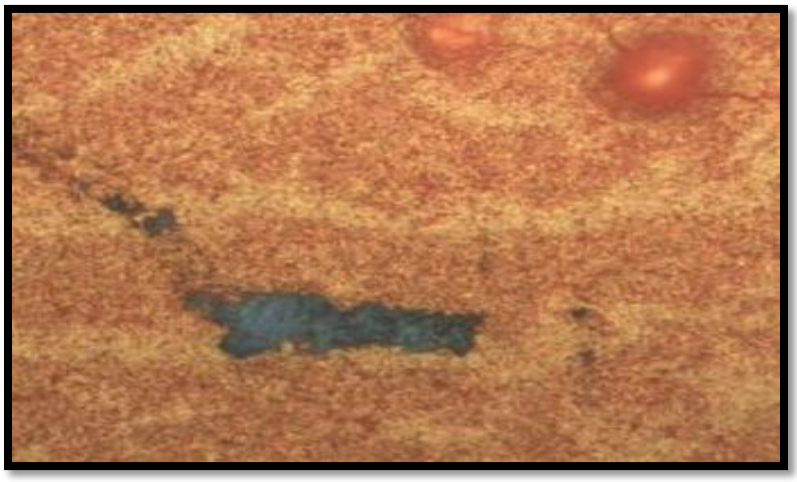

Figure 146. Image of region of Vermelho Tattoo Ink slide preparation through dispersive micro-Raman. Magnification is approximately 500x.

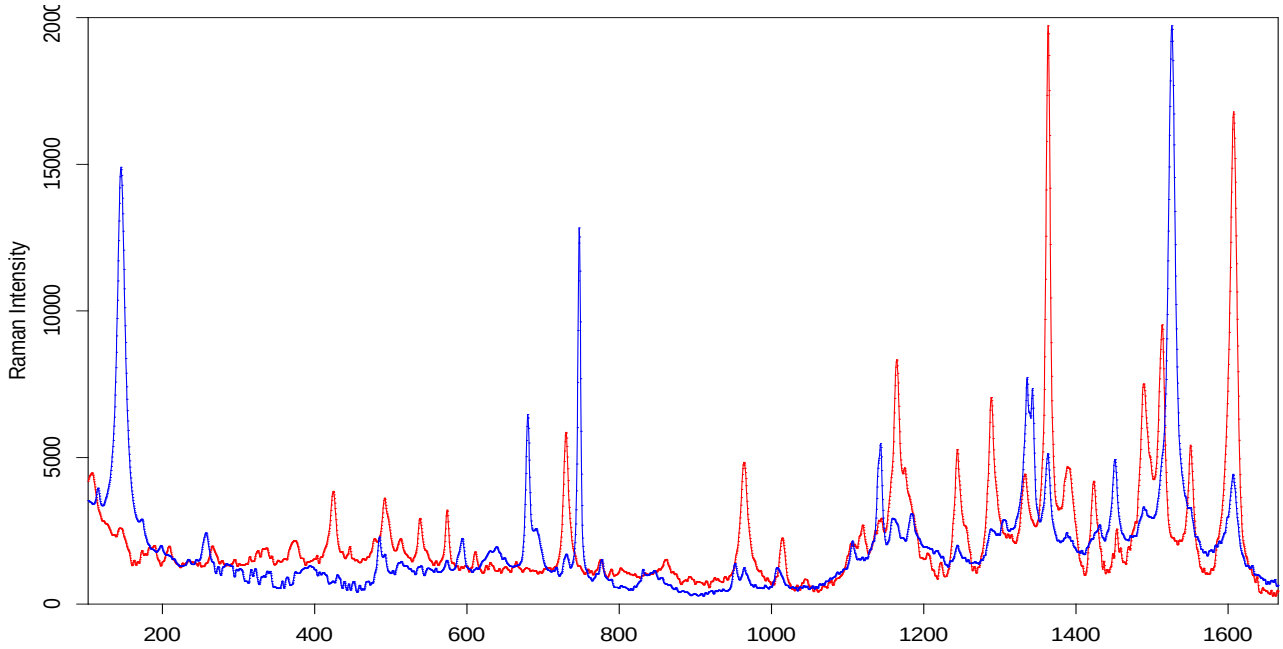

Figure 147. Overlay of red region (red) and blue aggregate (blue) from Vermelho sample (λ_0=785nm)

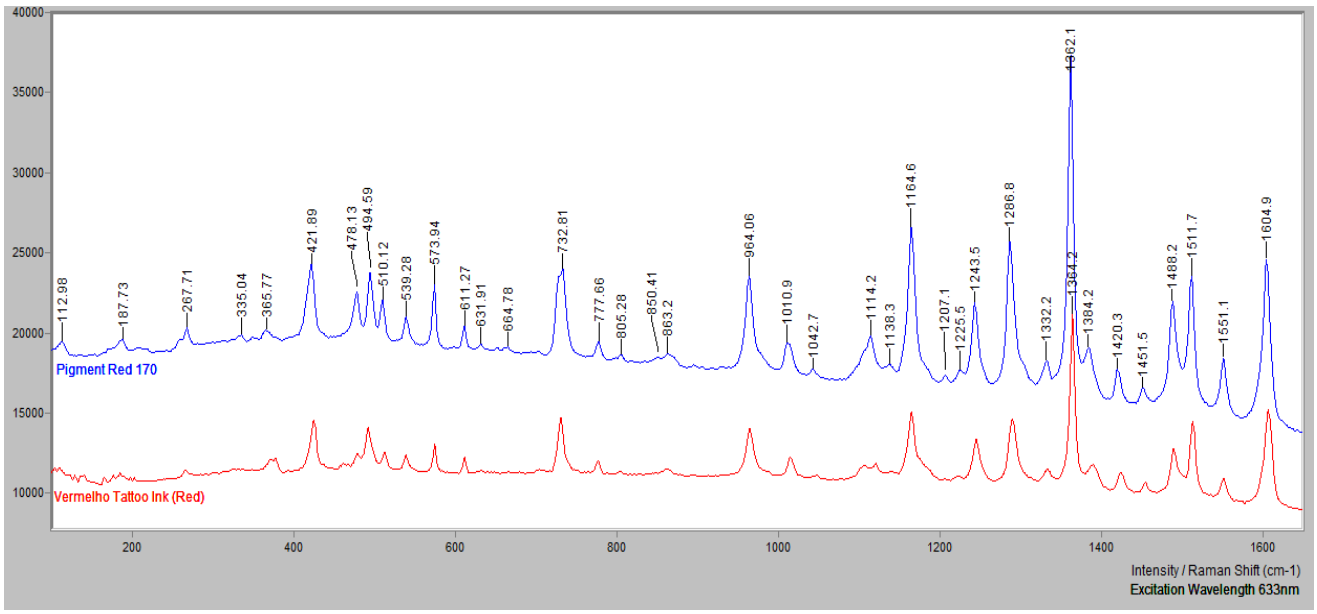

Figure 148. Red region of Vermelho and Pigment Red 170.

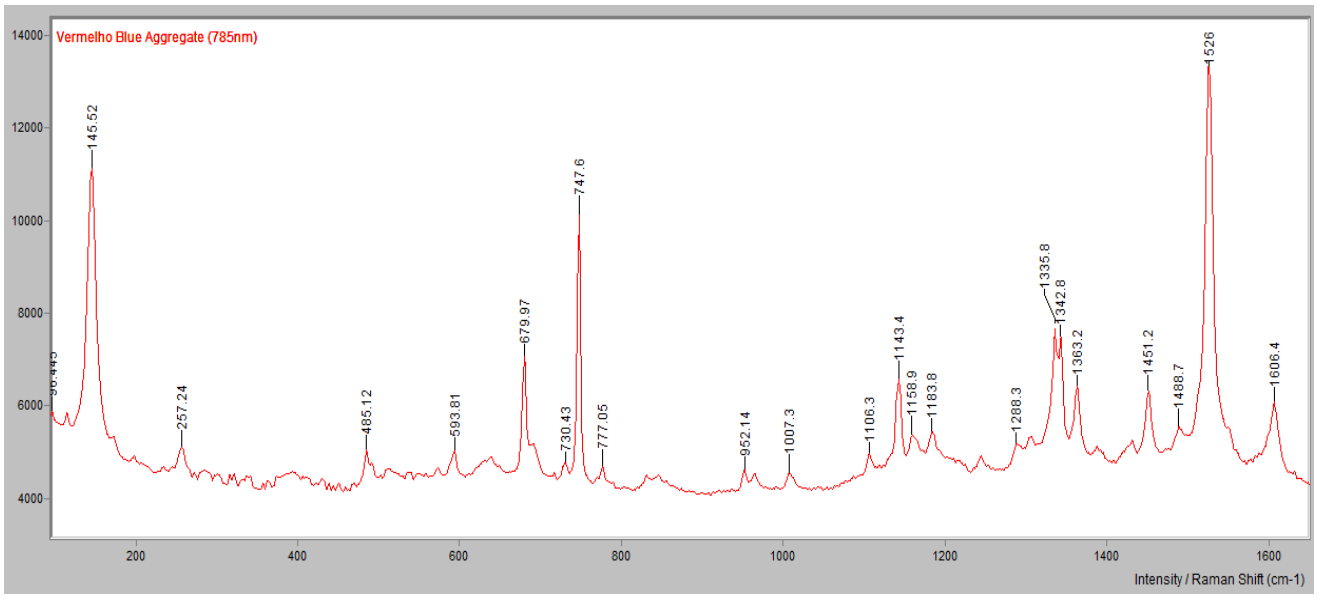

Figure 149. Blue aggregate of Vermelho. The region appears consistent with Pigment Blue 15 (no polymorph specified due to the lack of information and comprehensive comparison data).

Pink- Overwhelming fluorescence was observed with normal Raman at all three excitation wavelengths. A high quality spectrum was obtained with FT-Raman. SERS was useful in resolving Raman bands. The FT-IR (ATR) spectrum also displayed a number of well-resolved peaks. XRF indicated the presence of titanium. It is probable that the titanium is due to the presence of titanium dioxide. No pigment standard could be correlated to the resultant spectral data.

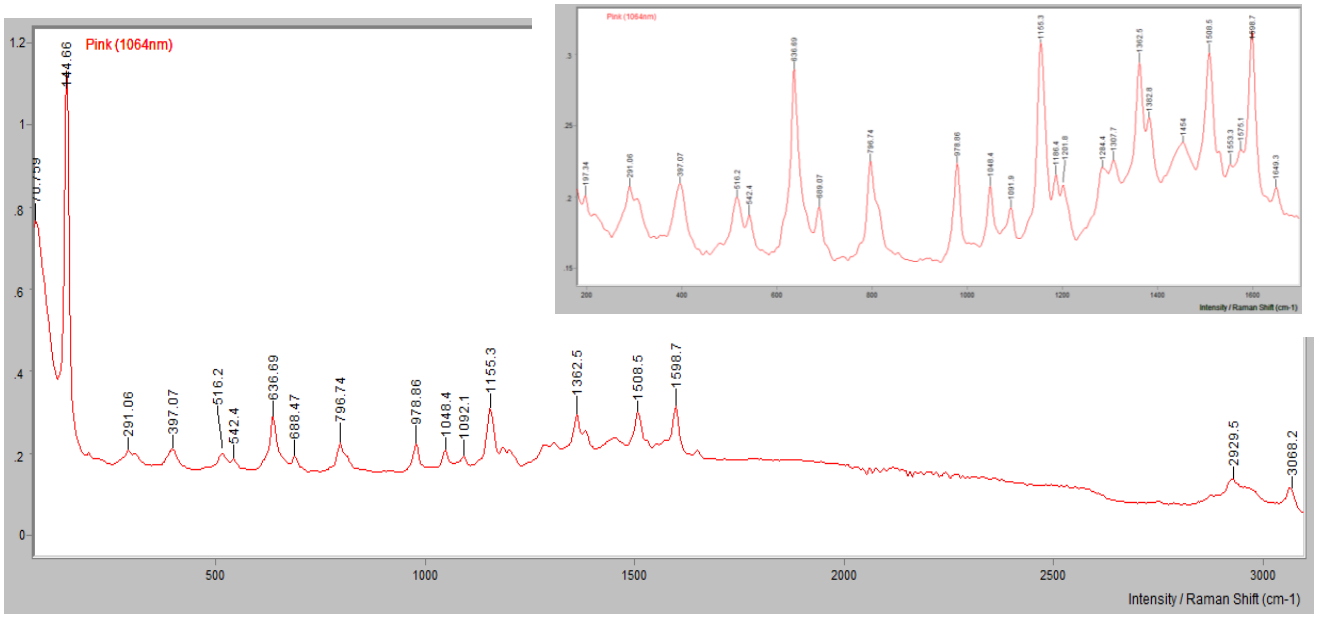

Figure 150. FT-Raman spectrum of Pink, with a close-up of the region from 170 to 1700cm^{-1} (inset).

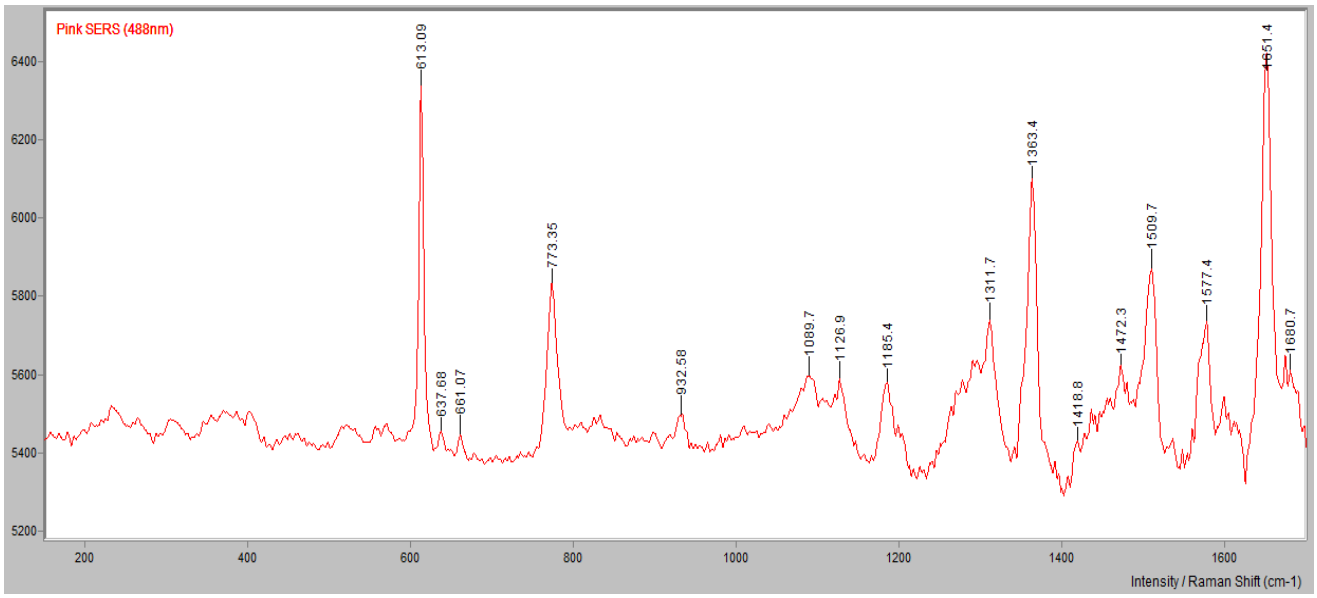

Figure 151. SERS spectrum of Pink (baseline corrected).

Citrus- Overwhelming fluorescence was observed with normal Raman at all three excitation wavelengths. A high quality spectrum was obtained with FT-Raman. The FT-IR (ATR) spectrum also displayed a number of well-resolved peaks. XRF indicated the presence of

titanium. It is probable that the titanium is due to the presence of titanium dioxide. No pigment standard could be correlated to the resultant spectral data.

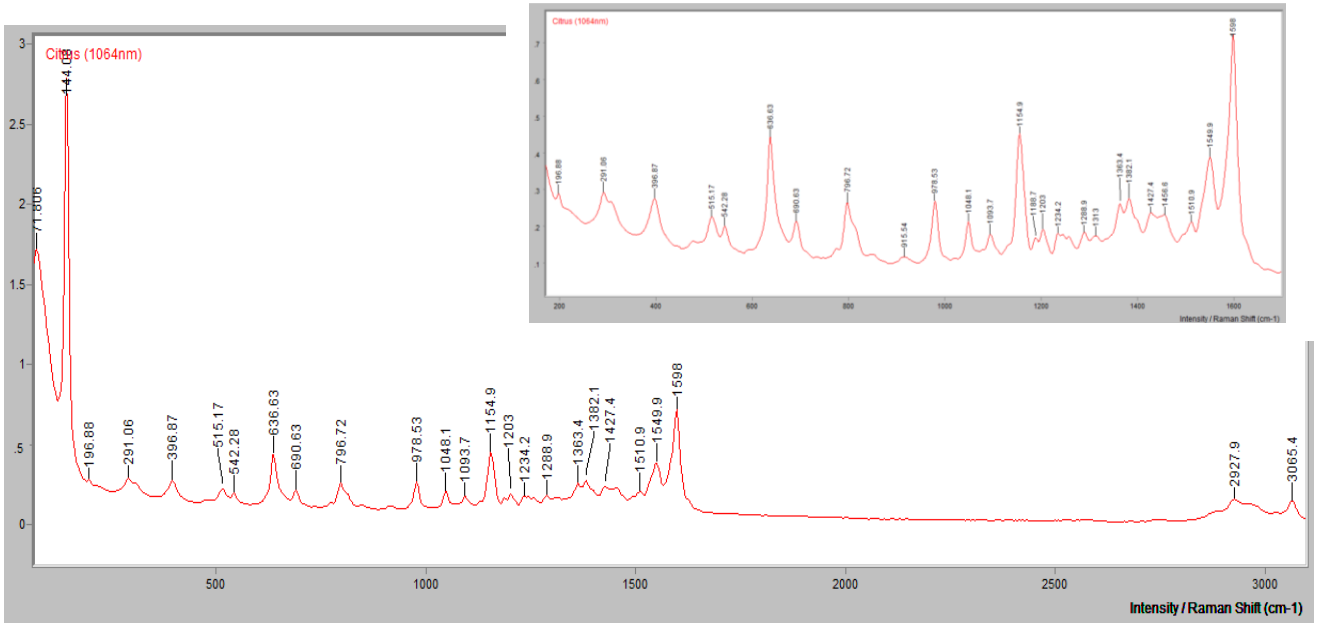

Figure 152. FT-Raman spectrum of Citrus, with a close-up of the region from 170 to 1700cm^{-1} (inset).

Correlation exists between the FT-Raman spectra of Pink and Citrus, which is interesting and indicates that both pigments have similar, but obviously not identical, molecular structures.

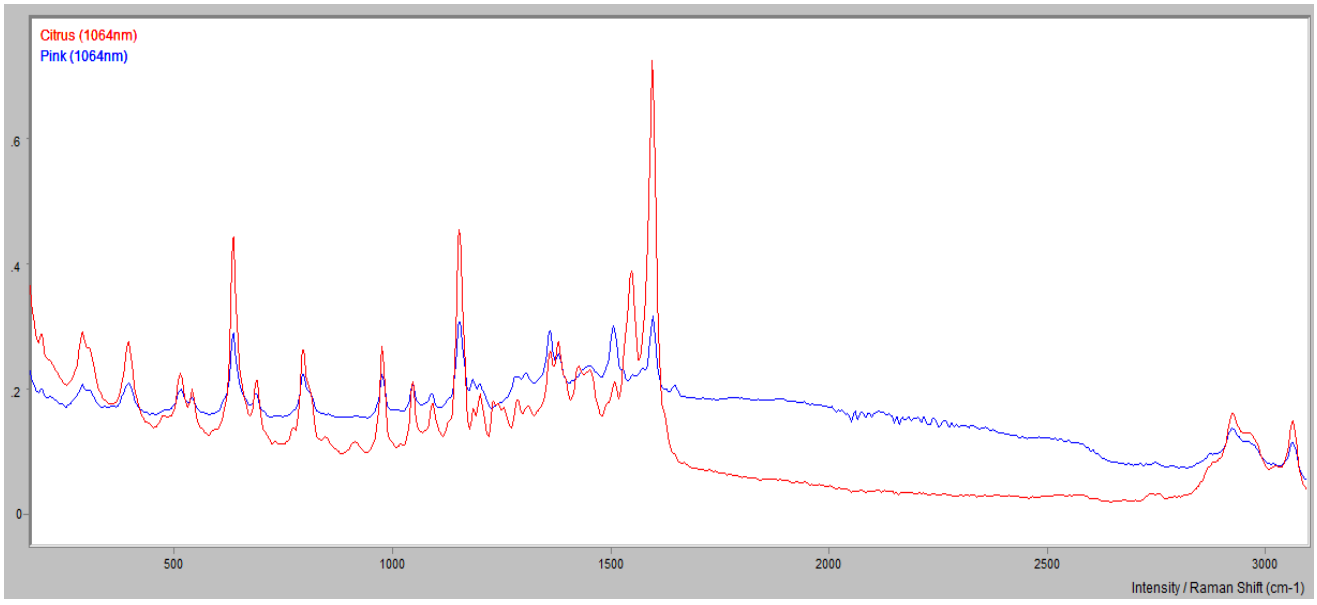

Figure 153. Spectral comparisons of IWB tattoo inks Citrus and Pink demonstrating the high degree of correlation between the two inks.

Amarelo Canario- Fluorescence was observed at λ_0=488nm, but some bands were present (1598, 1400.2, 1289.8 and 1247.8cm^{-1}). High quality spectra were obtained with λ_0=633nm, 785nm and 1064nm. SERS was useful in resolving Raman bands. The FT-IR (ATR) spectrum also displayed a number of well-resolved peaks. XRF indicated the presence of titanium. It is probable that the titanium is due to the presence of titanium dioxide.

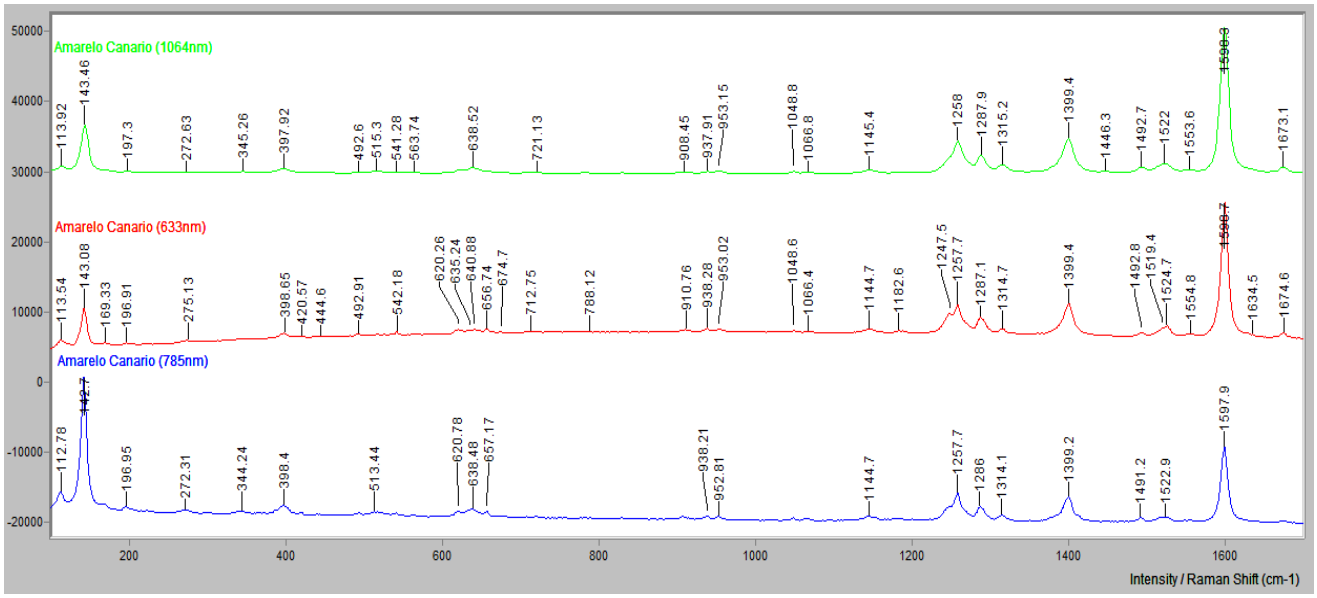

Figure 154. Comparison of Amarelo Canario and different excitation wavelengths.

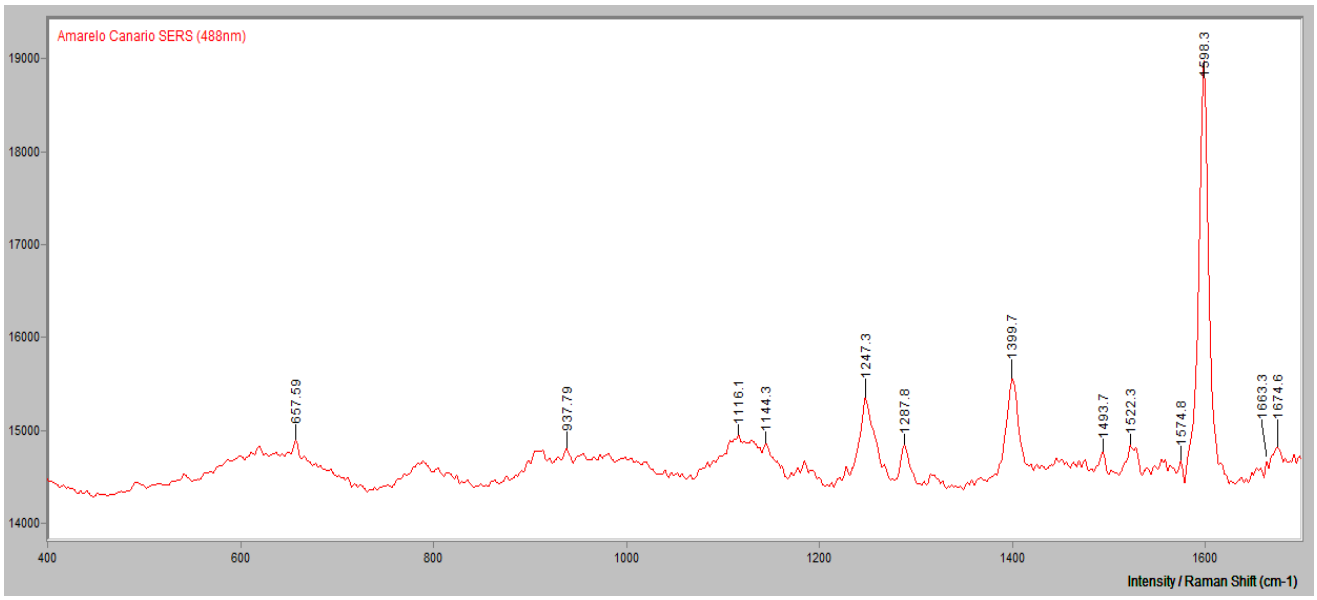

Figure 155. SERS spectrum of Amarelo Canario.

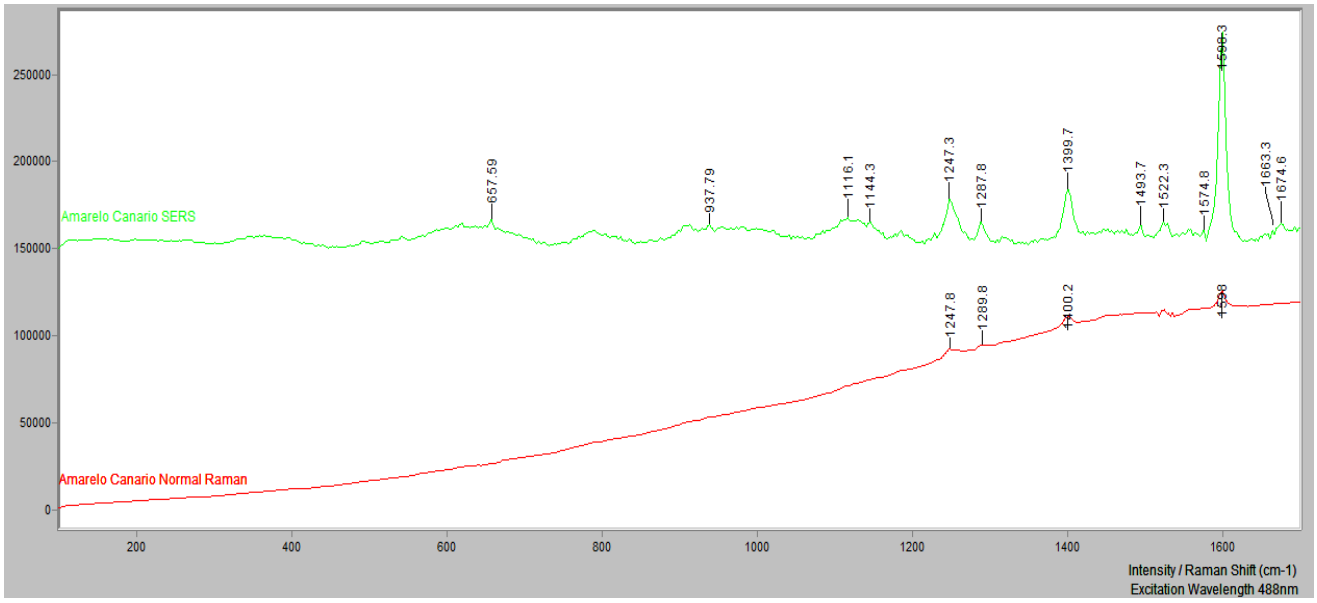

Figure 156. Comparison of normal Raman and SERS spectra of Amarelo Canario.

Amarelo Fluor- Overwhelming fluorescence was observed with normal Raman at λ_0= 488 and 633nm. A spectrum was obtained at λ_0=785 and a high quality spectrum was obtained at 1064nm. The FT-IR (ATR) spectrum also displayed a number of well-resolved bands. XRF indicated the presence of titanium. It is probable that the titanium is due to the presence of titanium dioxide. No pigment standard could be correlated to the resultant spectral data.

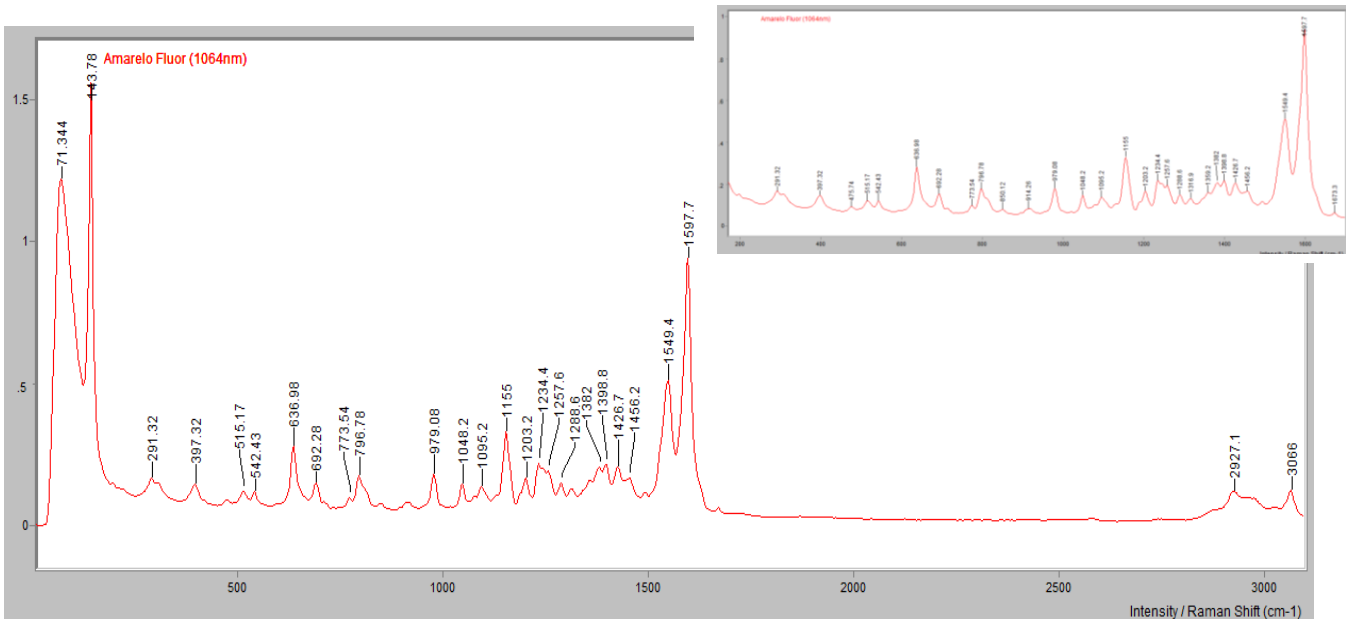

Figure 157. FT-Raman spectrum of Amarelo Fluor, with a close-up of the region from 170 to 1700cm^{-1} (inset).

The FT-Raman spectra of Amarelo Fluor, and Citrus are very similar, with little differences between the spectra.

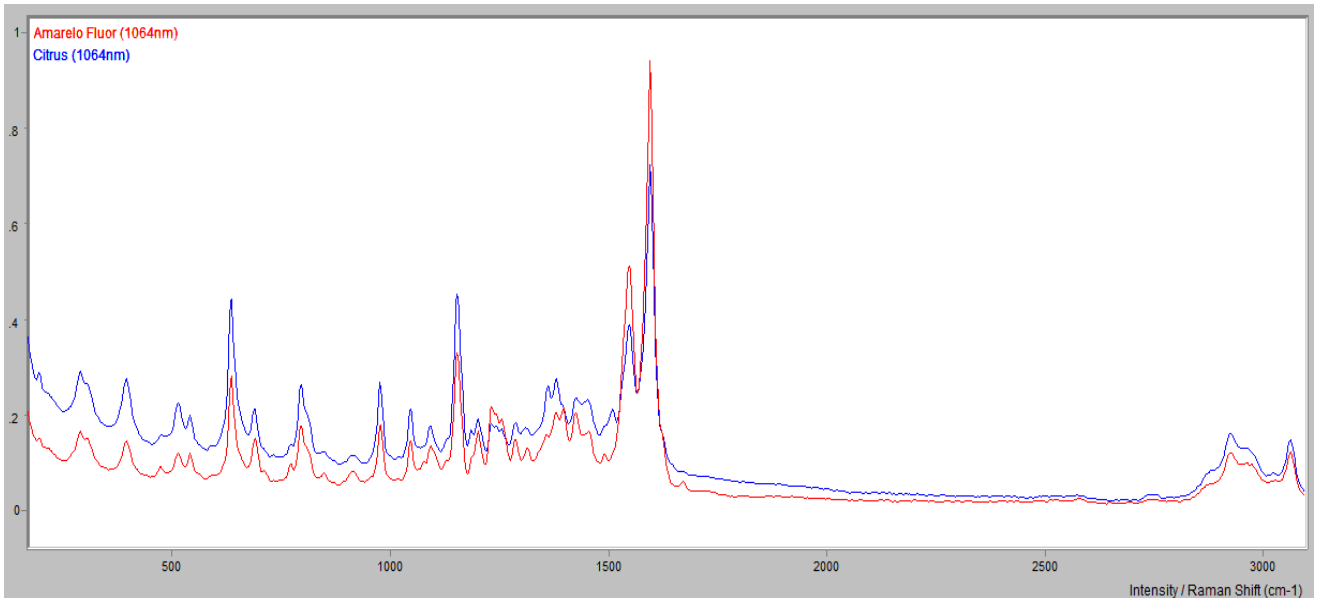

Figure 158. Spectral comparison of Amarelo Fluor and Citrus tattoo inks.

Verde Claro- Overwhelming fluorescence was observed at λ_0=488nm. A high quality spectrum was observed with λ_0=633nm and spectra were observed with λ_0=785nm and 1064nm (bands resolved at 146.84 and 1539.7cm^{-1}). The FT-IR (ATR) spectrum also displayed a number of well-resolved peaks. XRF indicated the presence of titanium, copper and bromine. It is probable that the titanium is due to the presence of titanium dioxide and the copper and bromine are indicative of Pigment Green. Verde Claro contains Pigment Green 7. The presence of bromine indicates that Verde Claro may also contain a trace amount of a bromine-containing pigment such as Pigment Green 36.

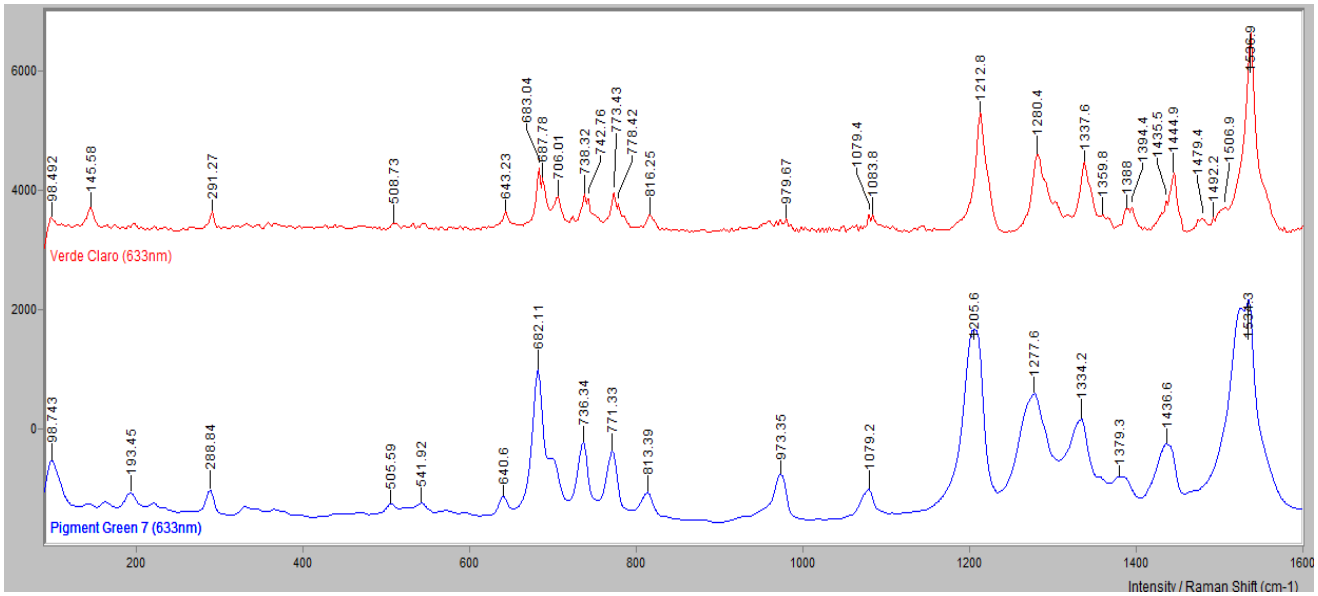

Figure 159. Comparison of Verde Claro with Pigment Green 7 standard.

Polarized light microscopy of verde claro disclosed the presence of colorless, green, yellow and blue pigment particles (Figure 160).

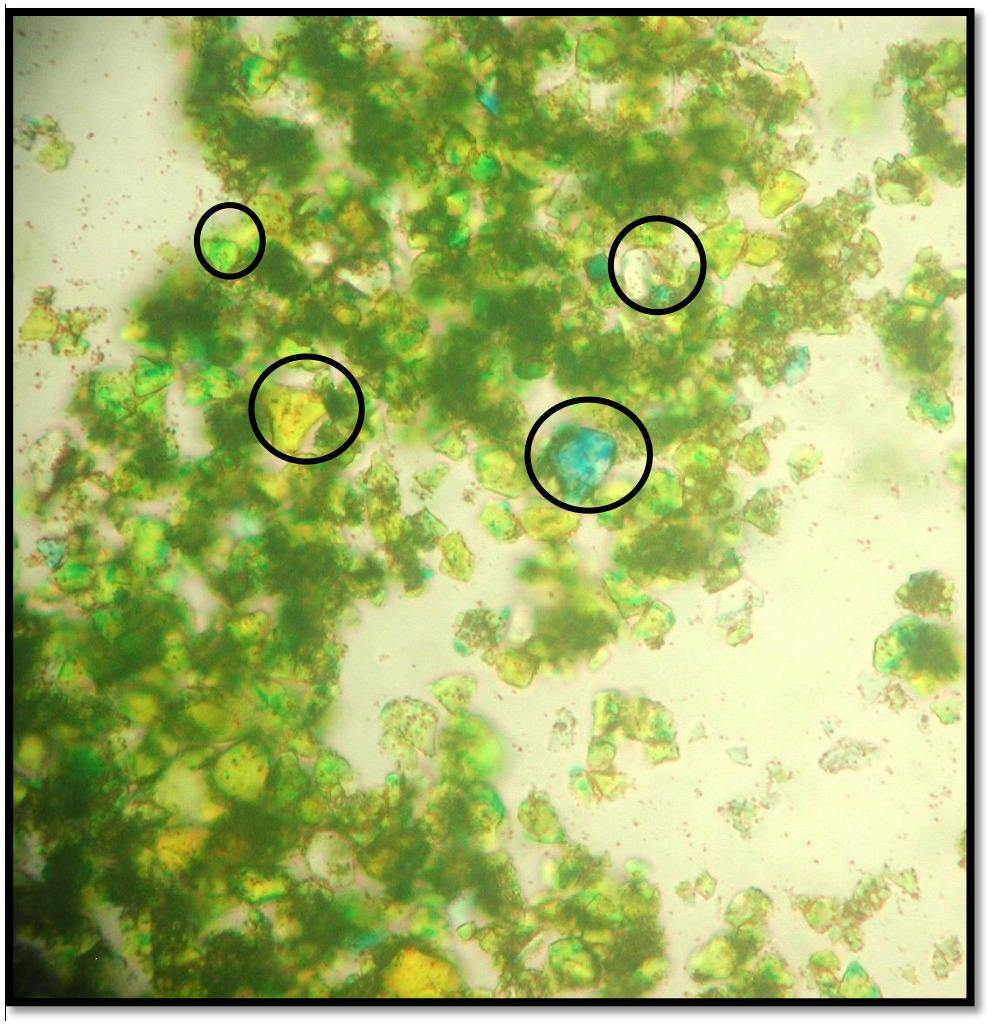

Figure 160. Photomicrograph of Verde Claro tattoo ink (Polarized light microscopy, 1.550 RI mounting media, 400x). Note the presence of colorless, green, yellow and blue pigment particles of varying particle size (circled).

Azul Royal- High quality spectra were resolved with normal Raman at all three excitation wavelengths and a spectrum was obtained with FT-Raman. The FT-IR (ATR) spectrum also displayed a number of well-resolved peaks. XRF indicated the presence of titanium and copper. It is probable that the titanium is due to the presence of titanium dioxide and the copper is indicative of Pigment Blue 15 or a related polymorph.

Magenta- Overwhelming fluorescence was observed at λ_0=633nm and 785nm. Spectra were observed with λ_0=488nm and 1064nm. SERS was useful in resolving Raman peaks. The

FT-IR (ATR) spectrum also displayed a number of well-resolved peaks. XRF indicated the presence of titanium. It is probable that the titanium is due to the presence of titanium dioxide. No pigment standard could be correlated to the resultant spectral data.

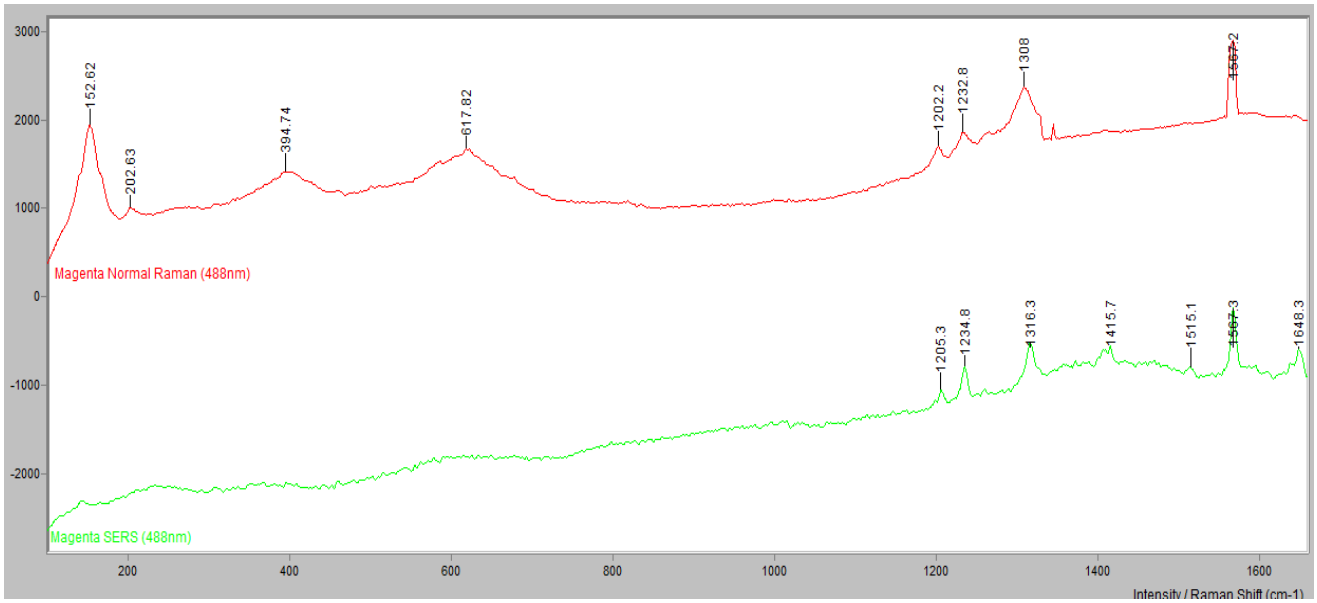

Figure 161. Comparison of normal Raman and SERS spectra of Magenta.

Lilas Claro- High quality spectra were obtained with all excitation wavelengths (both normal Raman and FT-Raman). Examination of the Raman spectra indicates the presence of titanium dioxide, anatase form ('light region') and Pigment Violet 23, specifically the β polymorph ('dark region'). The FT-IR spectrum resolved a few peaks and XRF indicated the presence of titanium. This titanium is due to the presence of titanium dioxide.

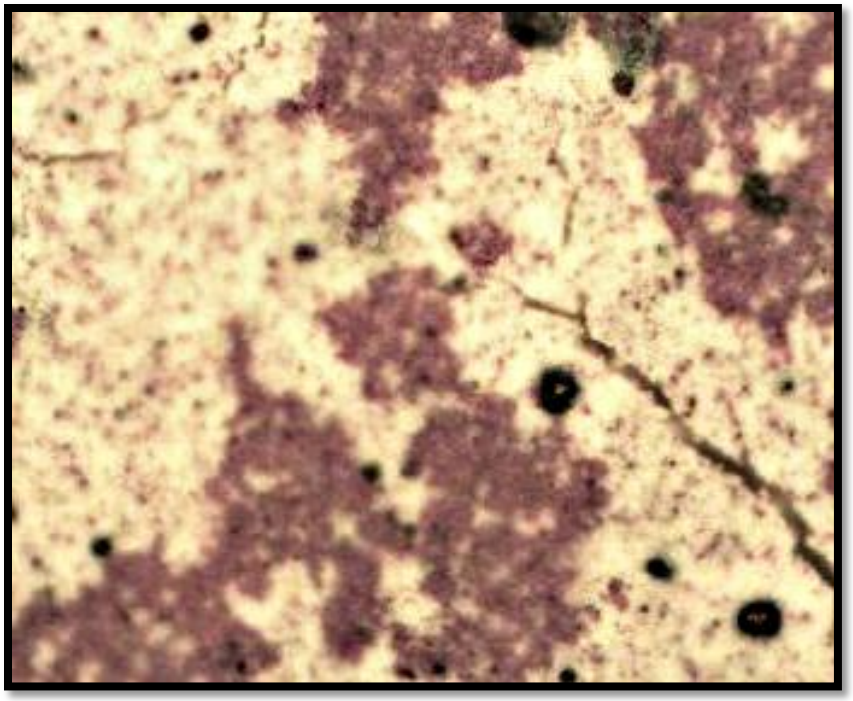

Figure 162. Image of region of Lilas Claro Tattoo Ink slide preparation through dispersive micro-Raman, demonstrating the dark and light regions. Magnification is approximately 2,000x.

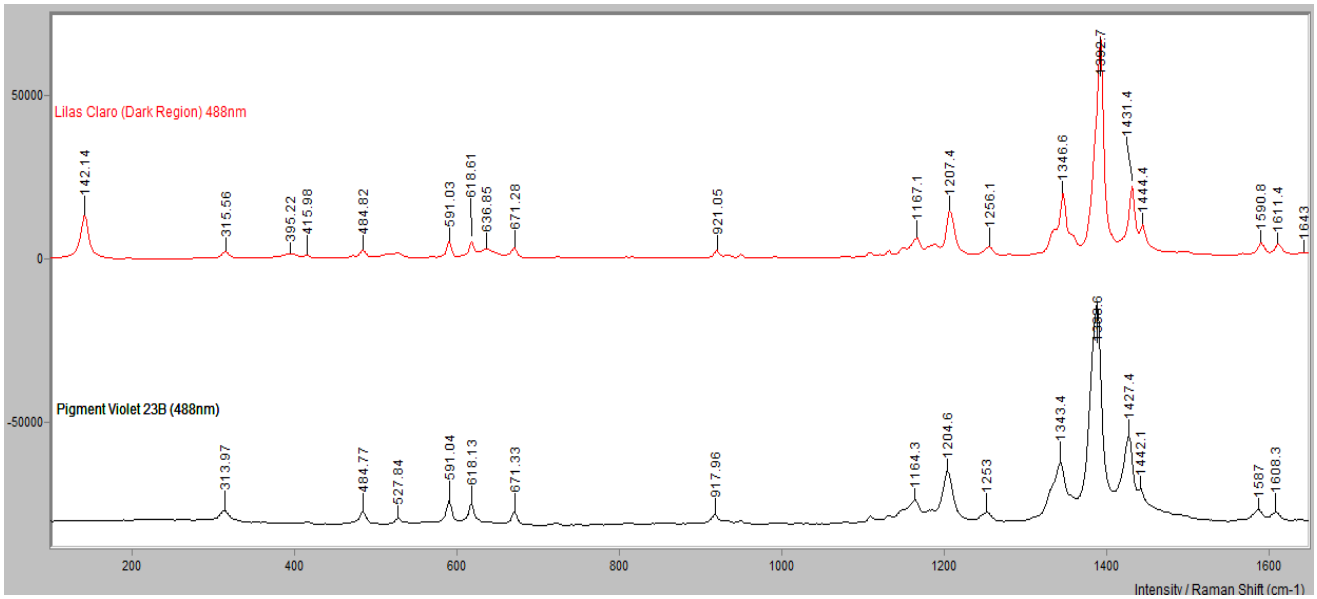

Figure 163. Normal Raman of Lilas Claro compared to Pigment Violet 23β pigment standard.

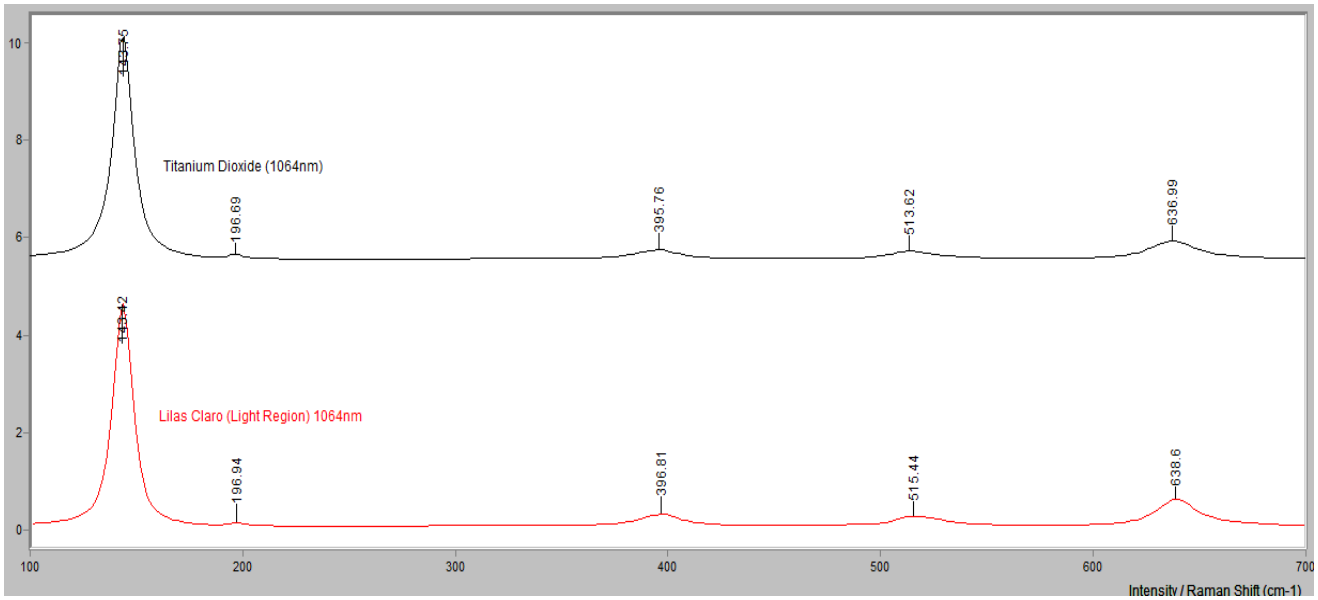

Figure 164. Normal Raman of Lilas Claro compared to titanium dioxide.

Flying Tigers

The Flying Tigers Tattoo Ink set was analyzed via normal Raman and subjected to pigment extraction. This was done in an effort to identify the pigment compositions. As expected, preliminary examinations indicate that the tattoo inks from China (and purchased inexpensively from an online auction site) exhibit a high degree of variation. A selection of inks is presented. More detailed information about each tattoo ink can be found in the corresponding Appendix.

Salmon Pink- Correlation was found between Salmon Pink and Pigment Orange 34.

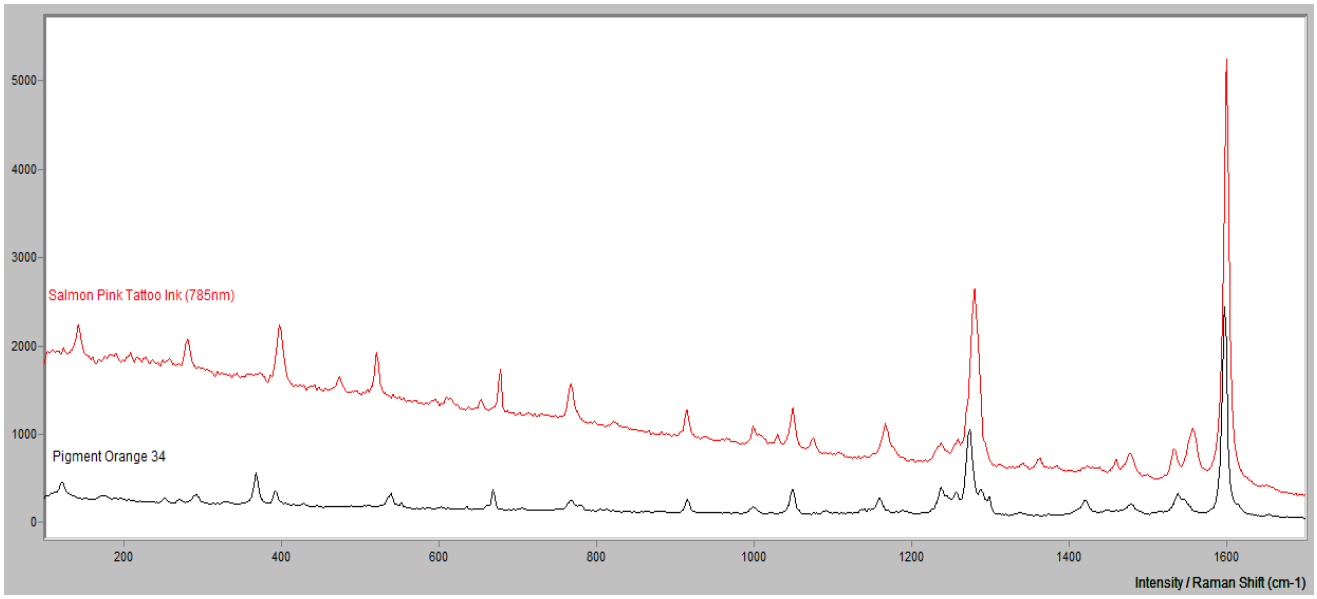

Figure 165. Comparison of Salmon Pink tattoo ink and PO 34 standard.

Pink Red- Comparison of the spectrum obtained at 488nm exhibited correlation with the SERS (488nm) spectrum of Pigment Red 170. The SERS spectrum was employed because there were more, better resolved peaks observed when compared to the normal Raman spectrum (488nm) of Pigment Red 170. Due to the detection of Zinc by XRF and the microscopic appearance of pink red, it is likely that zinc oxide (white) is present in the tattoo ink.

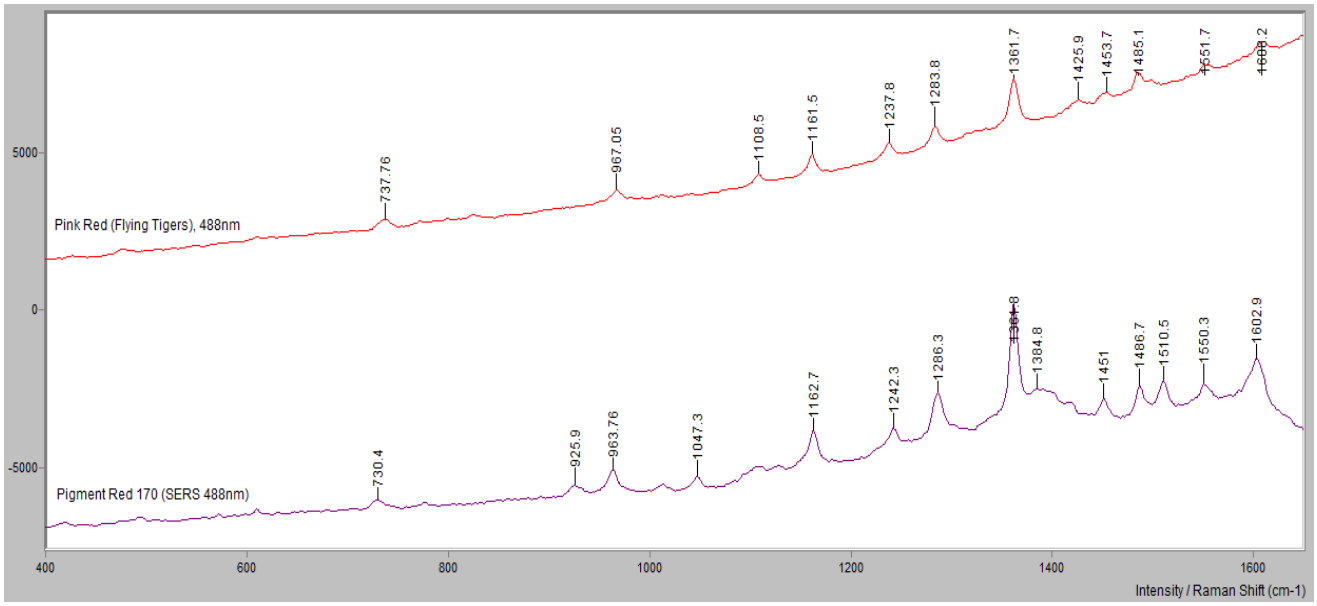

Figure 166. Comparison of Pink Red tattoo ink and PR 170 standard.

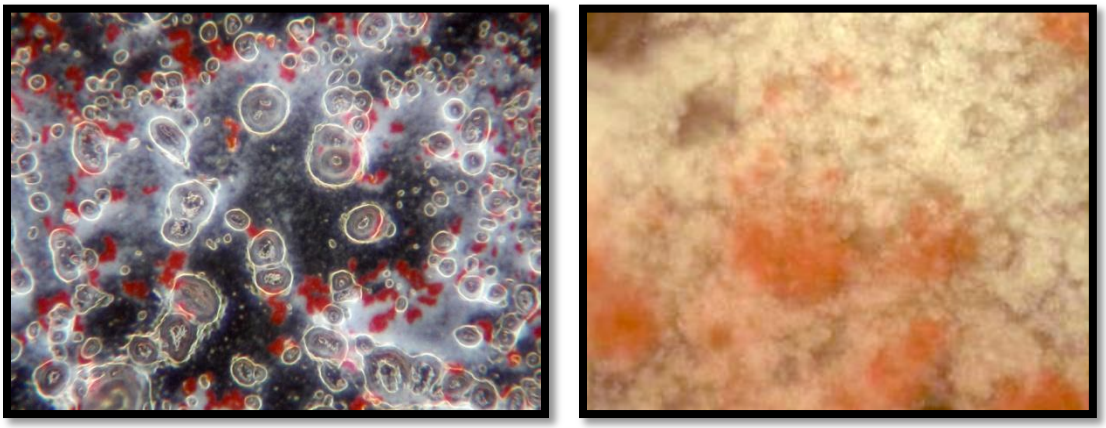

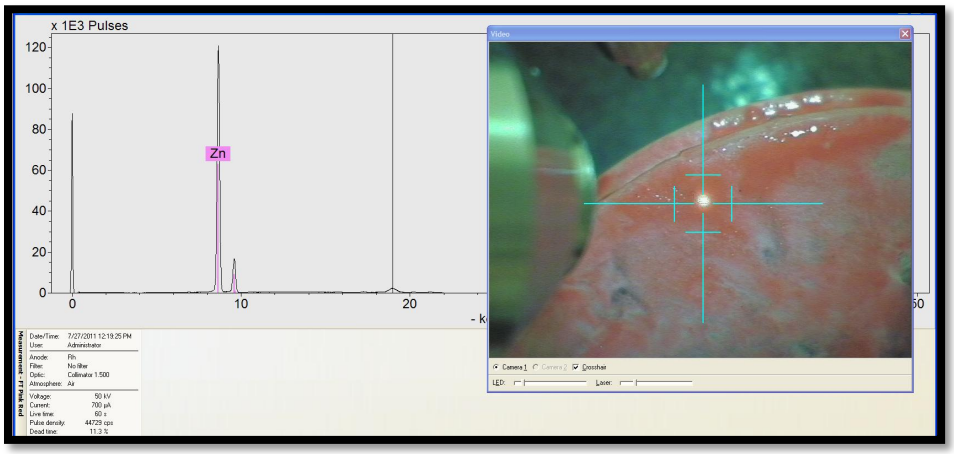

Figure 167 a, b and c. Flying Tigers Pink Red tattoo ink (darkfield microscopy 100x, left and Raman microscope, 1000x, right). Note the aggregates of pink/red particles and the aggregates of white particles. This can also be seen in the image from the XRF (bottom right), which detected Zinc.

Reds- ***Chinese Red***: Correlation was found with Pigment Red 170, specifically with regard to the more intense bands at 1163 (C-N symmetrical bend), 1283, 1360 (naphthalene), 1424 (N=N stretch), 1484, 1548, 1609 cm^{-1} (benzene stretch). There are a large number of unassigned bands, indicating that this tattoo ink is an azo dye in the red class and possibly a mixture. Similar conclusions can be drawn about the ***Rose Red*** tattoo ink, which exhibited peaks at 1289, 1360, 1424, 1486, 1547 and 1607 cm^{-1} and the ***Mulberry*** tattoo ink, which exhibited peaks at 1160, 1285, 1360, 1424, 1485, 1549 and 1609 cm^{-1}. An additional band at 1580 cm^{-1} was found at 1580 cm^{-1} for Rose Red and Mulberry, which was not present in Pigment Red 170. The intensity of the band at 1580 cm^{-1} is similar to that of the band at 1609 cm^{-1}. Similar results were found with ***Dark Red***. In summary, the selection of red tattoo inks exhibit characteristic Raman spectra consistent with azo dyes.

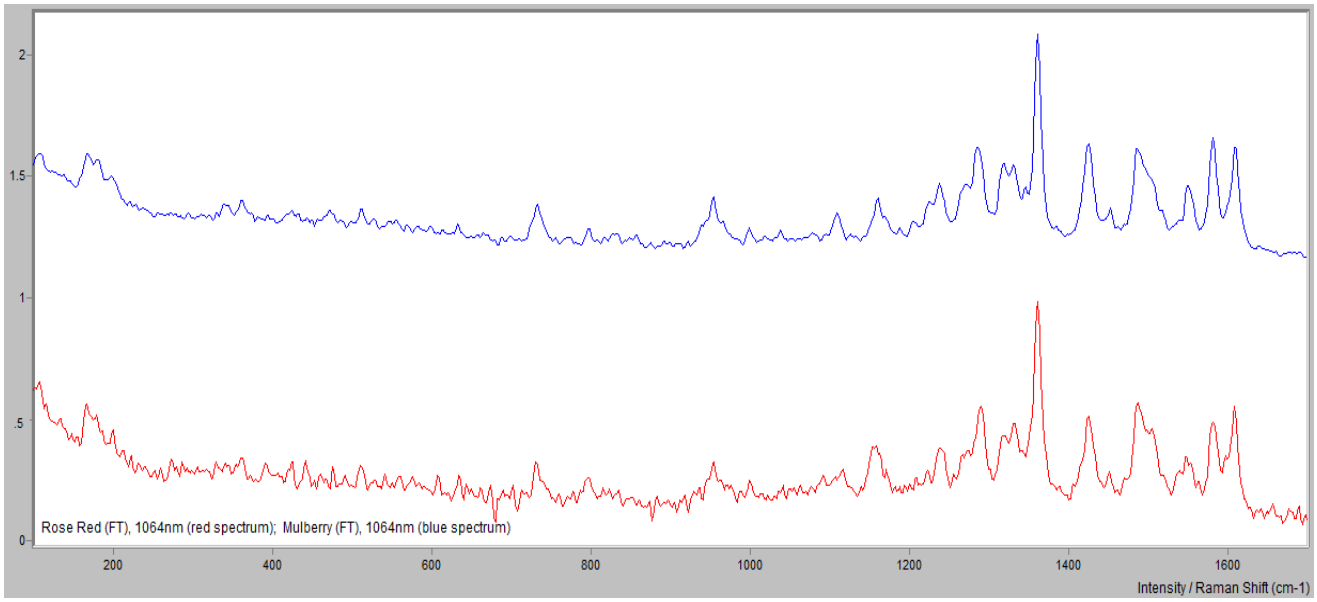

Figure 168. Comparison of Rose Red (red) and Mulberry (blue) spectra demonstrating correlation between the two inks.

Direct correlation was made between Pigment Red 170 and the ***Bright Red*** tattoo ink, with intense bands found at 1282, 1360, 1422, 1484, 1549 and 1609 cm^{-1}.

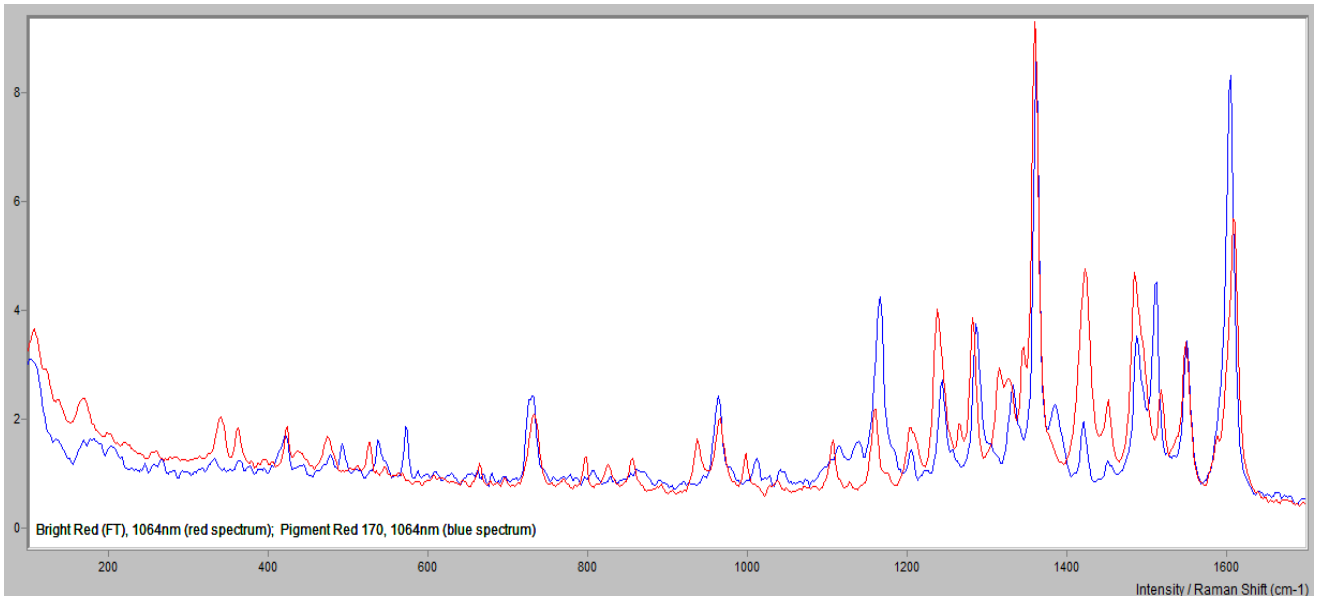

Figure 169. Comparison of Bright Red tattoo ink (red) and PR 170 pigment standard (blue).

Orange Red and **Orange**- Correlation was found between Orange Red, Orange and Pigment Orange 34. After closer inspection with the literature, better correlation was found between Orange Red, Orange and Pigment Orange 13 (Scherrer, *et.al.*, 2009), with the most intense peaks at 1280, 1555 and 1599 cm^{-1}. Pigment Orange 13 is structurally similar to Pigment Orange 34, the difference being the two methyl groups present of the outermost benzene rings (*para* orientation). The high degree of symmetry observed in the Raman spectrum of Pigment Orange 34 is apparent in that of Pigment Orange 13 (as reported in Scherrer, *et.al.*, 2009).

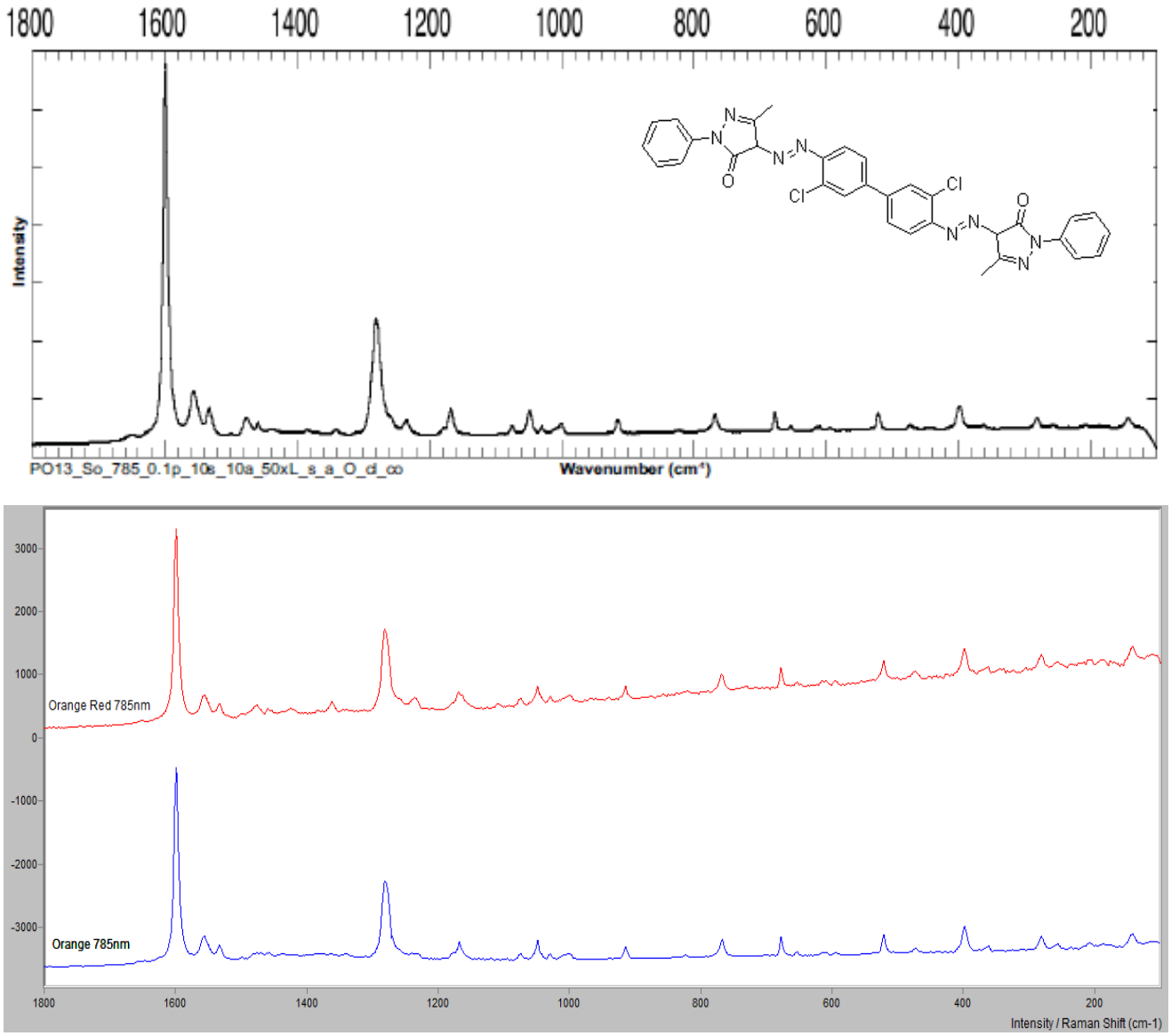

Figure 170 a and b. Pigment Orange 13 form the literature (top) and Orange Red (red spectrum) and Orange (blue spectrum) Flying Tigers Tattoo Inks (all spectra acquired with 785nm laser excitation).

Yellows- ***Mid-Yellow***, ***Yellow*** and ***Golden Yellow*** Tattoo Inks have the same composition. The spectra exhibit major bands at 1596 cm^{-1} (aromatic ring vibrations), 1399 cm^{-1} (azo N=N symmetric stretch), 1293 cm^{-1} (C-C stretching and CH bending vibrations, specifically the characteristic vibration between the C-C bridge between phenyl groups at the center of the molecule) and 1251 cm^{-1} (amide III band, with the amide I band around 1660 cm^{-1} and

benzylamide band at 950 cm^{-1}). The spectra clearly indicate a disazo pigment, specifically a diarylide (for example, Pigment Yellow 83). ***Bright Yellow*** has major bands at 1252, 1330, 1347, 1503, 1596 and 1404 cm^{-1} and ***Khaki*** has major bands at 1251, 1292, 1398 and 159.4 cm^{-1}, indicative of azo pigments.

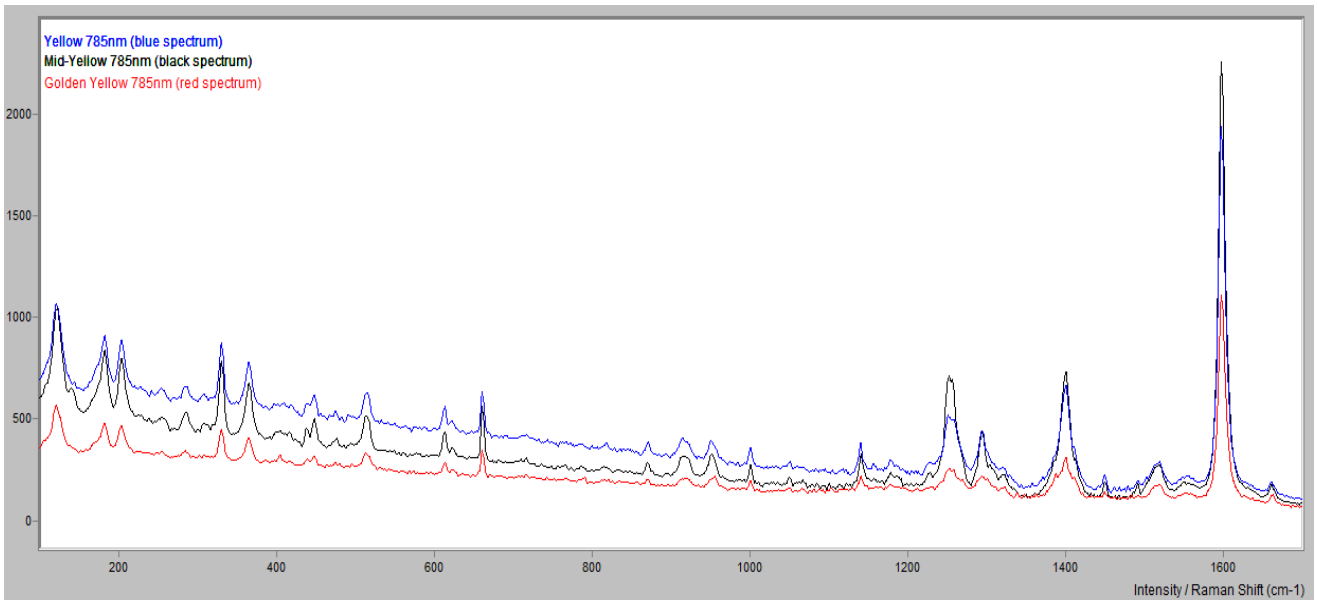

Figure 171. Comparison of yellow tattoo inks; Yellow (blue spectrum), Mid-Yellow (black spectrum) and Golden Yellow (red spectrum).

Greens- XRF disclosed the presence of Copper, Chlorine and Bromine in the ***Grass Hopper***, ***Light Green*** and ***Dark Green*** Tattoo Inks, and Copper and Chlorine in the ***Verdancy*** and ***Lawn Green*** Tattoo Inks. All of the green pigments exhibited bands at around 685 and 740 cm^{-1}, which is indicative of the vibrations inherent in the TBP nucleus characteristic of phthalocyanines (see Organic Pigment Chemistry section for a description of the phthalocyanines and the tetrabenzoporphyrazine nucleus). These two bands, along with the XRF data, assert that all of the green tattoo inks contain phthalocyanines. The presence of bromine indicates PG36 and the lack of bromine indicates PG7.

Blues- XRF disclosed the presence of Copper in ***Blue Sky***, ***Turquoise Blue***, ***Cyan***, ***Dark Cyan***, ***Blue***, ***Navy Blue*** and ***Dark Blue***. ***Cyan*** and ***Dark Cyan*** also contained Chlorine, and ***Navy Blue*** contained Chlorine and Bromine in addition to the Copper. All of the blue pigments exhibited bands at around 680 and 740 cm^{-1}, which is indicative of the vibrations inherent in the TBP nucleus. These two bands, along with the XRF data, assert that all of the blue tattoo inks contain phthalocyanines. Although it has been addressed earlier in this document about the spectral differences with a change in the excitation wavelength, one important observation is worth adding. In the blue tattoo inks, examination of the normal Raman spectra at 488nm shows a strong band around 680 cm^{-1} with little to no band around 745 cm^{-1}. The absence of this band may lead an inexperienced analyst to conclude that the TBP nucleus (ring vibrations) characteristic of the phthalocyanines is absent. These bands are present and of equal intensity in the normal Raman spectra at 785nm.

Purple and **Violet** - Correlation was found between Purple, Violet and Pigment Violet 23β.

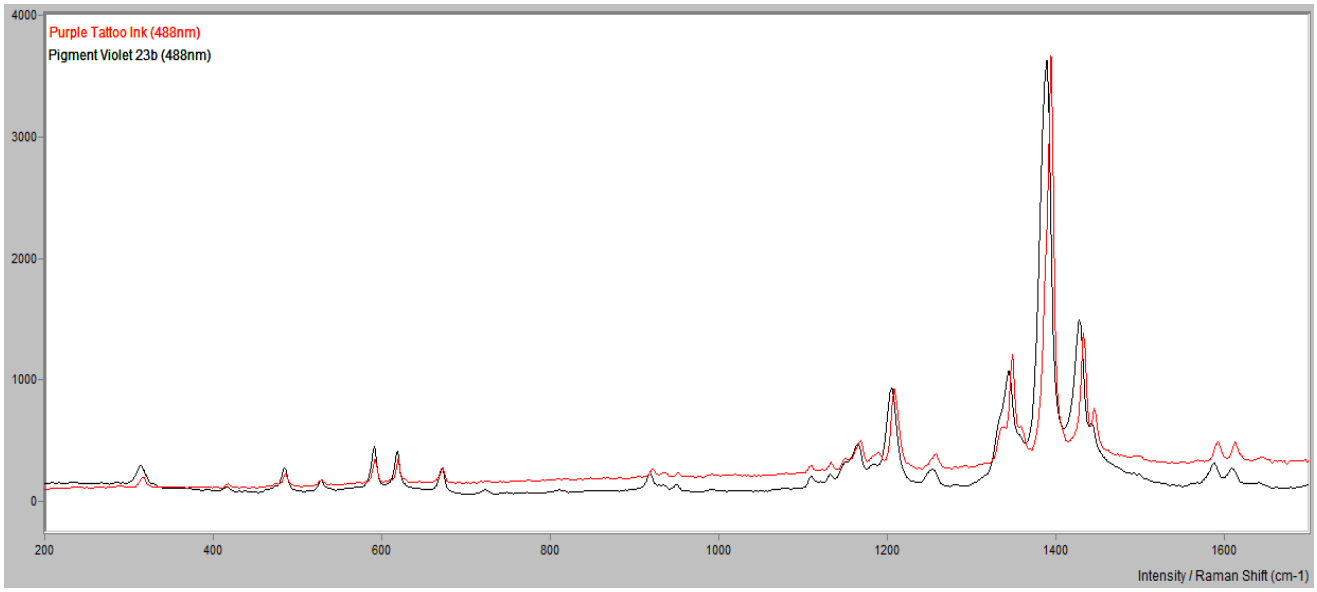

Figure 172. Comparison of Purple tattoo ink and PV 23β pigment standard.

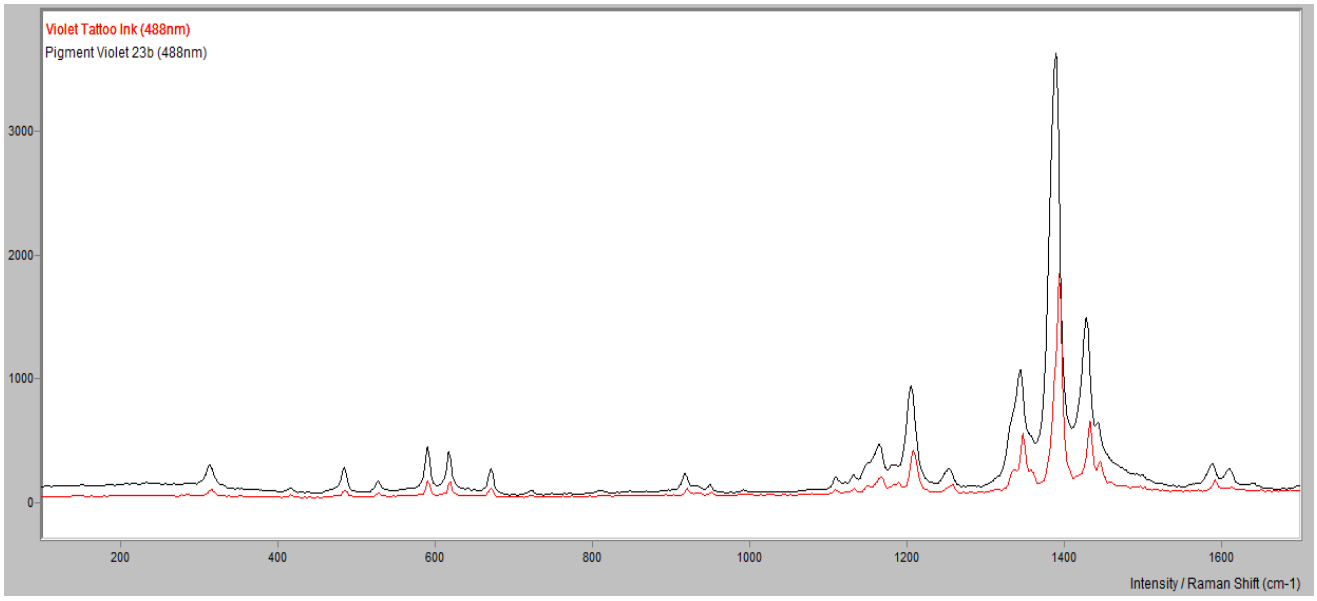

Figure 173. Comparison of Violet tattoo ink and PV 23β pigment standard.

Dark Brown and Light Chocolate- XRF indicated the presence of chlorine, chromium, iron, copper and zinc in dark brown and the presence of chlorine, chromium, iron, nickel and zinc in light chocolate. Correlation was found between Dark Brown and Light Chocolate, another Flying Tigers tattoo ink.

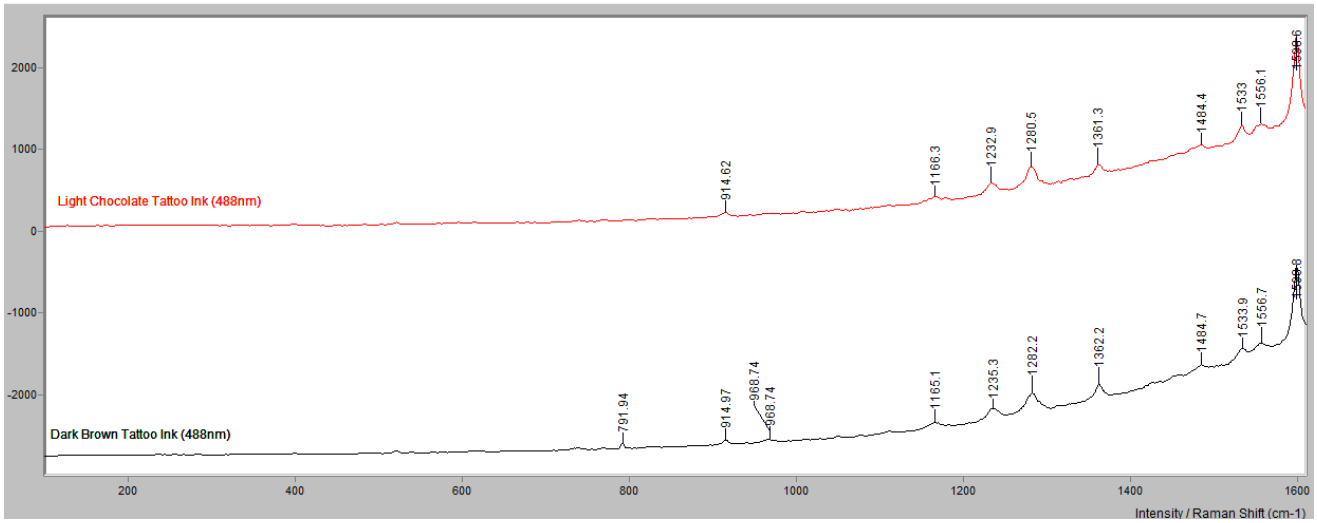

Figure 174. Comparison of Light Chocolate and Dark Brown tattoo inks demonstrating pigment composition correlation.

Skin Tone- No data with Raman, some peaks resolved with IR. XRF indicated the presence of zinc. This tattoo ink was still ‘wet’, even a year after being mounted on a glass slide and stored at room temperature in a microscope slide box.

White- XRF indicated the presence of titanium, which was consistent with the Raman spectrum corresponding to the titanium dioxide standard, specifically the anatase polymorph.

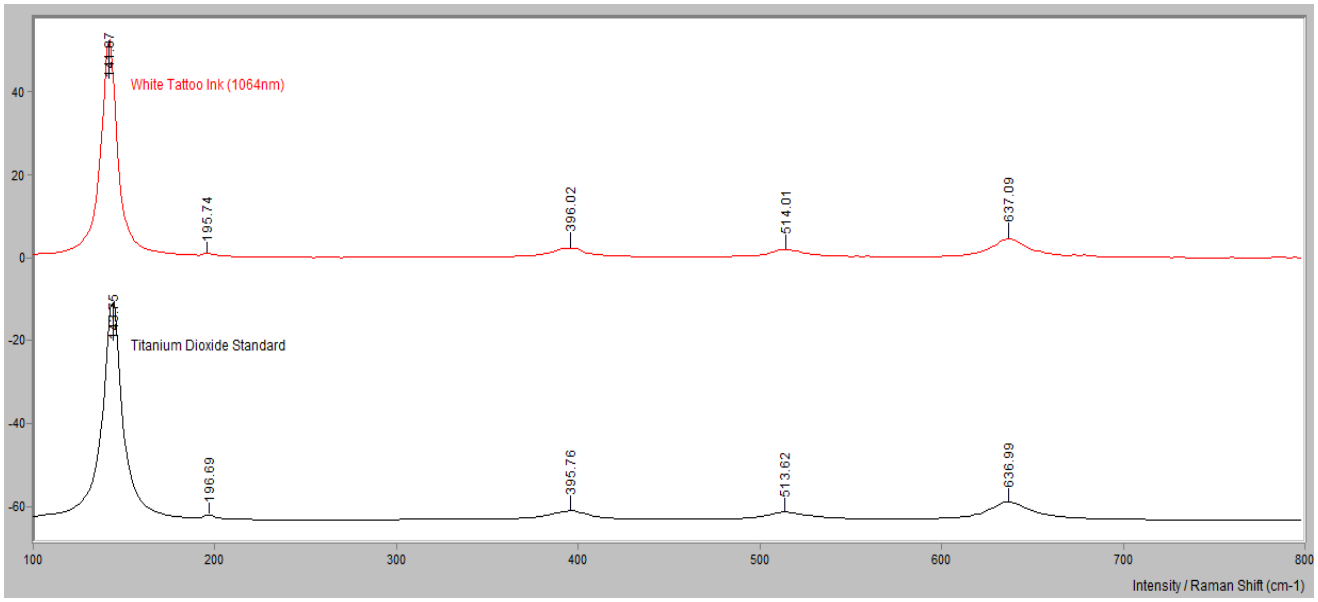

Figure 175. Comparison of White tattoo ink with titanium dioxide (anatase).

Results- Pigskin

A section of pigskin was obtained and two series of seven successive dots into the section of pigskin using the same Skin Candy tattoo inks analyzed in this research (refer to the Pigskin Study detailed in the Methods and Materials Section), one set of which was stored in formalin and one series was frozen. The tattoo inks used to tattoo were Whitegirl, Red Hot, Marz, Blisterine, Tastywaves, Muddy Water Blue, Ripple.

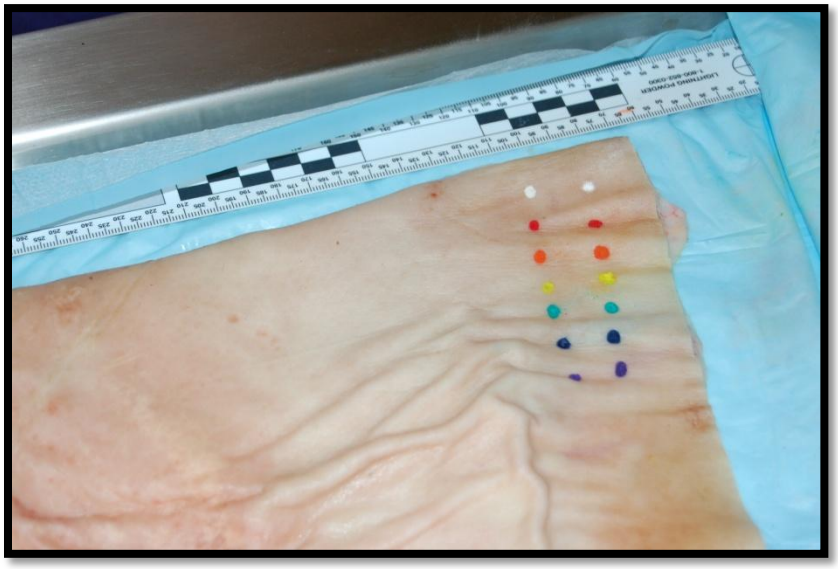

Figure 176. Section of pigskin with series of Skin Candy tattoo inks.

Preliminary examinations were used to compare the resultant spectra of the tattooed regions to the known pigments and to evaluate the effect of tissue preservation methods on the resultant spectra.

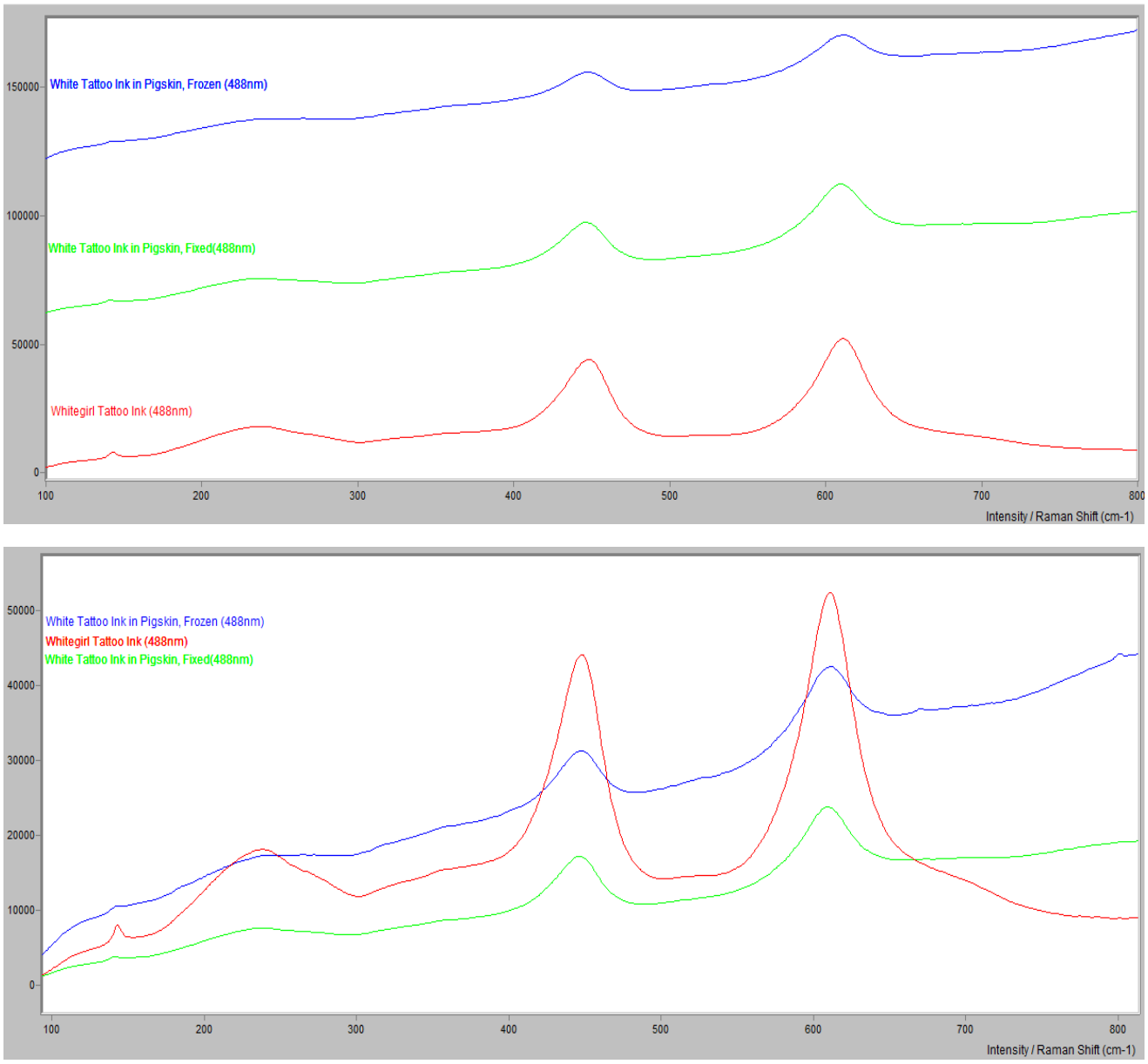

Figure 177 a and b. Comparison of white tattoo ink in pigskin (fixed and frozen) with Skin Candy Whitegirl tattoo ink [stacked (top) and overlay (bottom) formats].

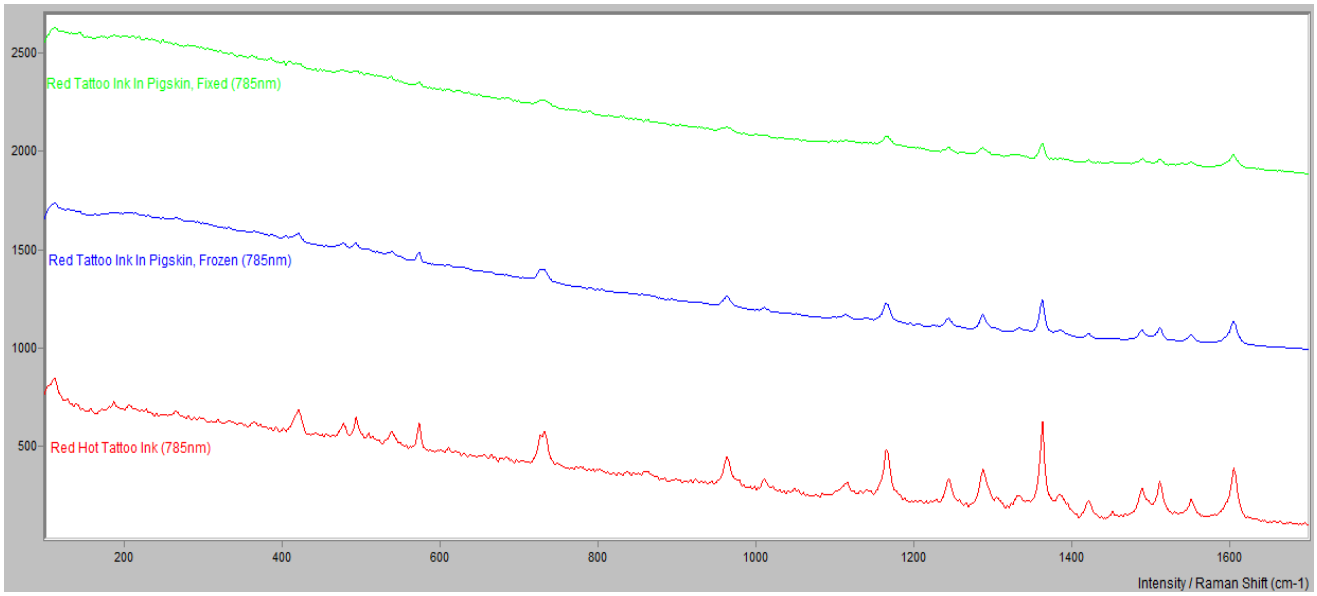

Figure 178. Comparison of red tattoo ink in pigskin (fixed and frozen) with Skin Candy Red Hot tattoo ink.

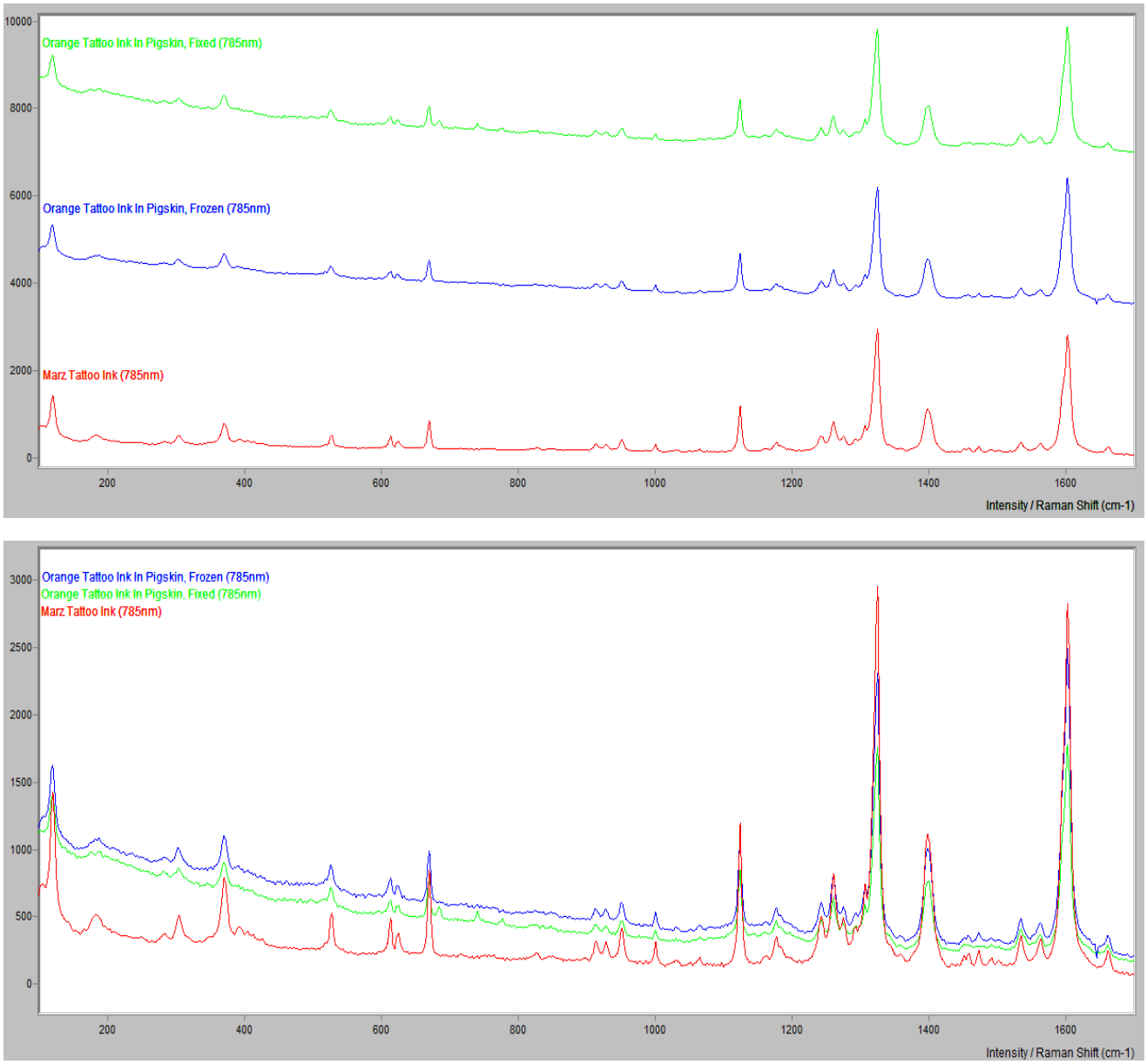

Figure 179 a and b. Comparison of orange tattoo ink in pigskin (fixed and frozen) with Skin Candy Marz tattoo ink [stacked (top) and overlay (bottom) formats].

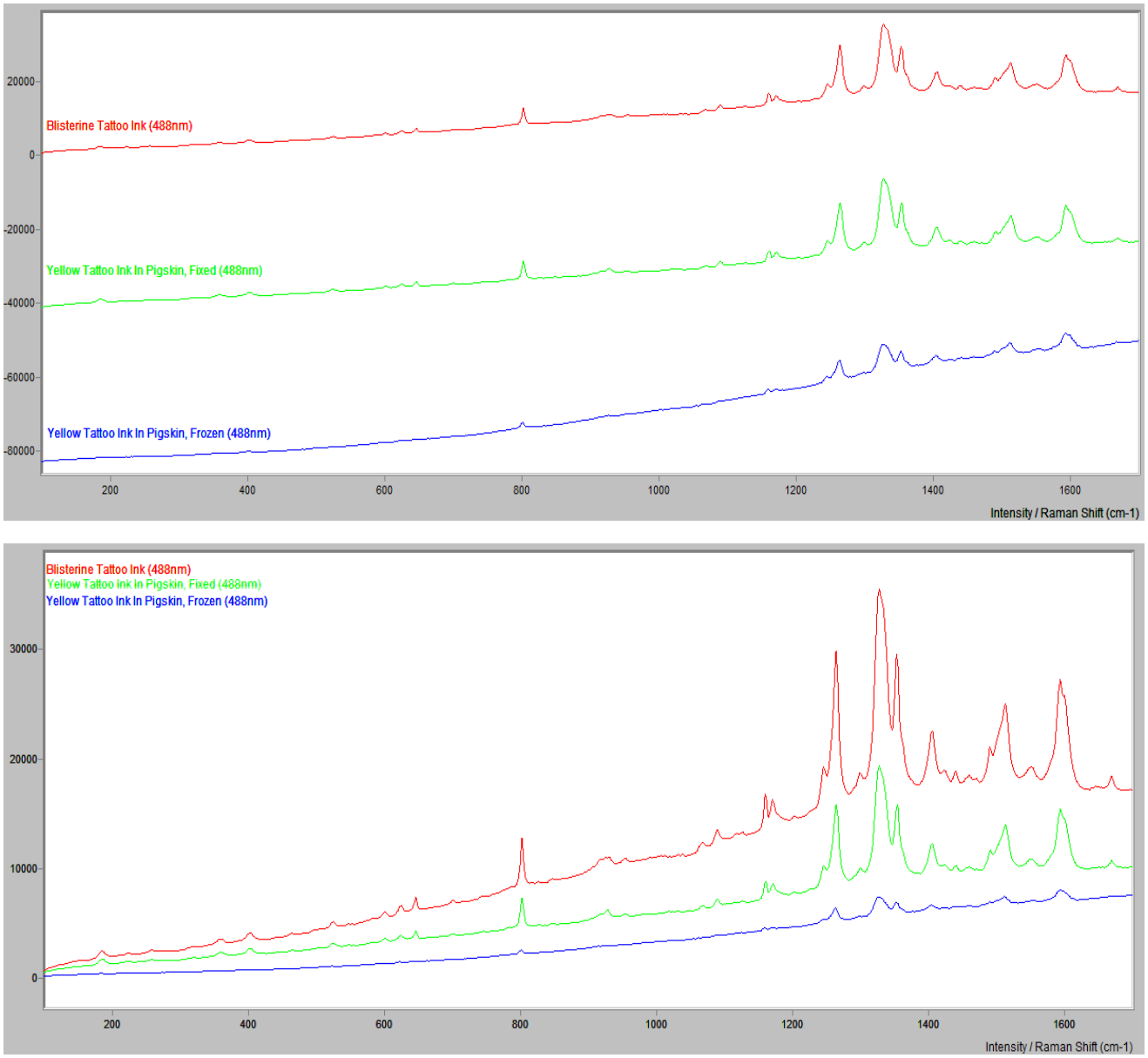

Figure 180 a and b. Comparison of yellow tattoo ink in pigskin (fixed and frozen) with Skin Candy Blisterine tattoo ink [stacked (top) and overlay (bottom) formats].

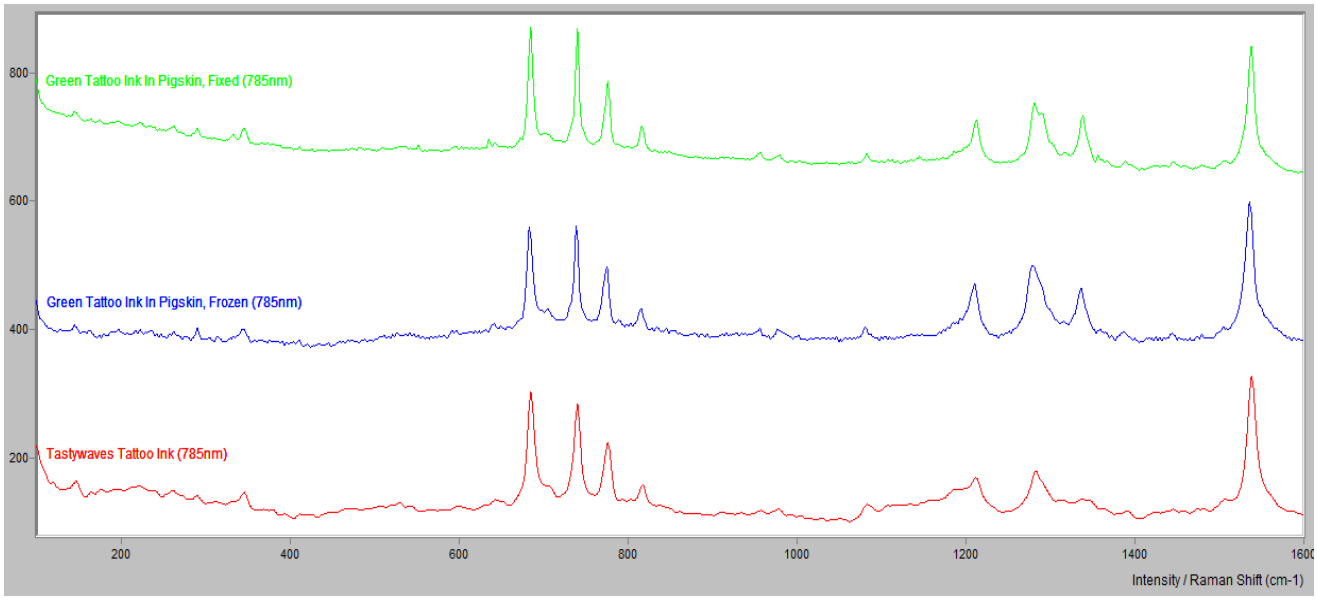

Figure 181. Comparison of green tattoo ink in pigskin (fixed and frozen) with Skin Candy Tastywaves tattoo ink.

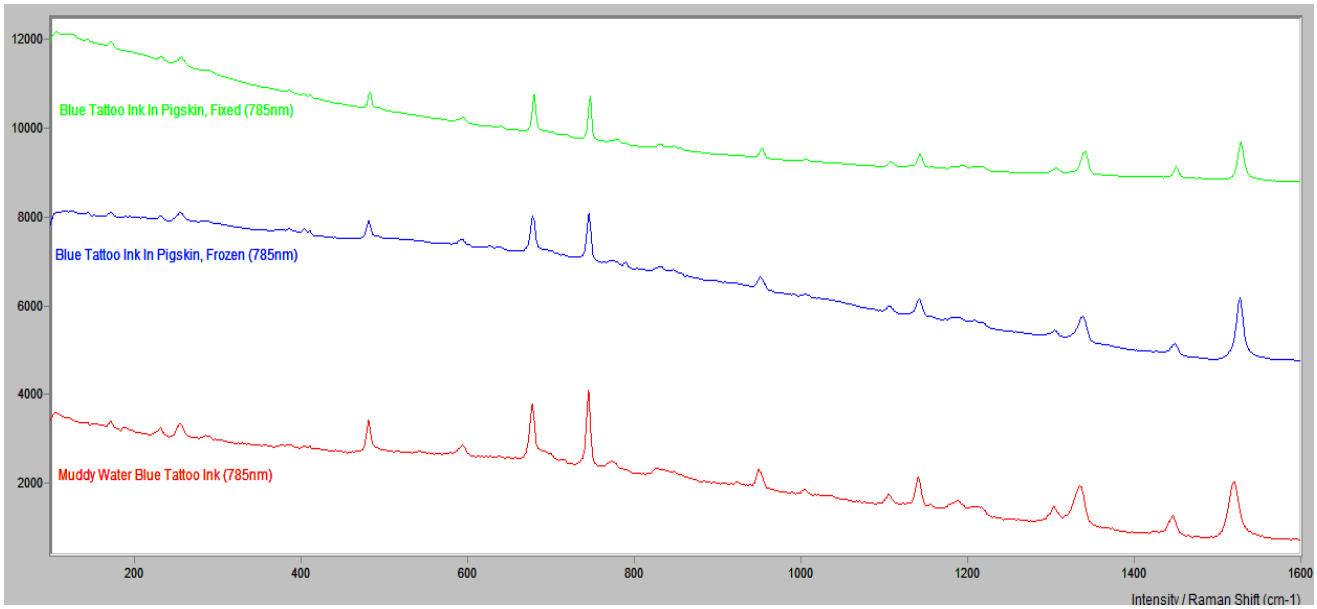

Figure 182. Comparison of blue tattoo ink in pigskin (fixed and frozen) with Skin Candy Muddy Water Blue tattoo ink.

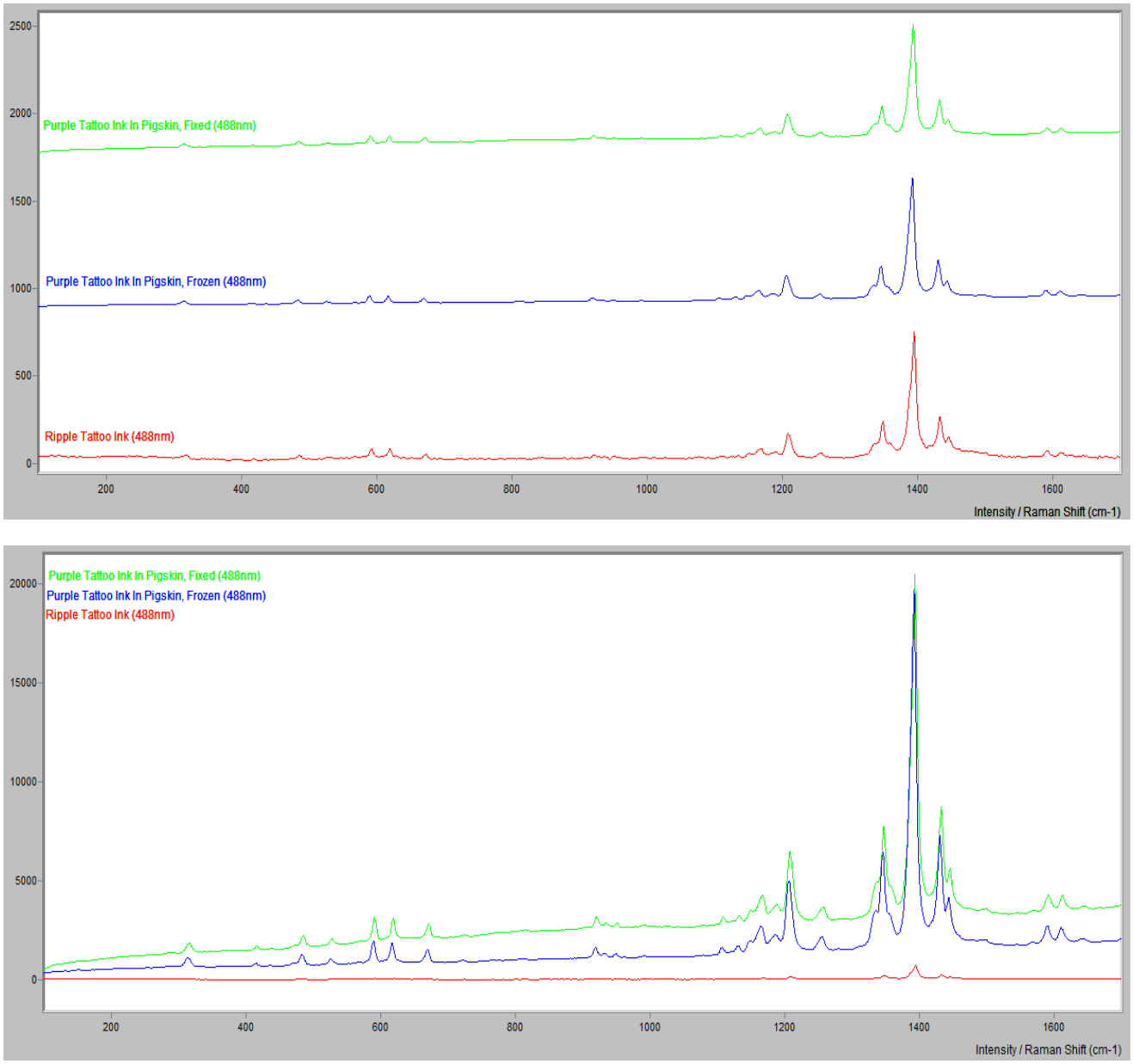

Figure 183 a and b. Comparison of purple tattoo ink in pigskin (fixed and frozen) with Skin Candy Ripple tattoo ink [stacked (top) and overlay (bottom) formats].

The first attempt, which was to directly analyze the tattooed regions, was successful, and no additional methodology needed to be used (*i.e.* thin sectioning, the addition of silver colloid or the use of the hydroxyl gel to extract the tattoo ink from the pigskin). For direct analysis, the sectioned tattooed pigskin was placed in a glass Petri dish and subsequently placed on the

sample stage of the Raman microscope. The sample was viewed under the microscope and focused on prior to Raman analysis. It is reasonable to conclude that direct analysis of unhealed, tattooed skin would easily disclose the presence of tattoo ink pigments due to both the absence of interfering layers of skin that would result from healing and due to the lack of migration of the pigments into deeper layers of skin also due to the healing process.

Although alternate methods were not employed, their use may become paramount in instances when the superficial, surface layers of tissue have healed and the pigment is embedded and stored in the deeper dermal layers. Direct analysis should be attempted first, with special attention paid to the excitation wavelength and its relative depth of penetration, as the source may be able to reach and therefore detect the pigments without intervention or destructive methodology. As described earlier, the longer wavelengths (such as 785nm for dispersive Raman and 1064nm for FT-Raman) penetrate deeper into the tissue and thus may be more useful in detecting the pigment particles that make up the tattoo (Refer to Figure 4).

Preliminary Investigation into the Analysis of Tattoo Inks in Healed, Human Tissue

Literature concerning the vibrational spectroscopic analysis of human tissue has been reported, with regard to biological implications with focus on dermatology and oncology (deFaria and Souza, 1999, Caspers, *et.al.*, 2003, Gniadecka, *et.al.*, 1998, and Huang, *et.al*., 2003) and anthropological and archaeological implications with focus on mummified remains (Edwards, *et.al.*, 2002, Petersen, *et.al.*, 2003). These studies demonstrate the ability of Raman spectroscopic methods to generate spectra of human skin, both normal (‘fresh’) and mummified, as well as human tissues from biopsies.

deFaria and Souza evaluated human skin and nail using an excitation wavelength of 632.8nm and compare their resultant data to that reported in the literature (in which an excitation

wavelength of 1064nm was employed). The results of deFaria and Souza, which demonstrate good agreement between reported and experimental data, are presented in the table below:

Human skin		Human nail		
This work ($\tilde{\nu}$/cm^{-1})	Literature ($\tilde{\nu}$/cm^{-1})	This work ($\tilde{\nu}$/cm^{-1})	Literature ($\tilde{\nu}$/cm^{-1})	Assignment
1650 s	1652 s	1649 s	1654	Amide I ν(C═O)
1460 sh	—	1457 sh	—	Amide II
1444 s	1438 s	1443 s	1449	Amide II
1409 m	—	1416 sh	—	
1340 s	1336 m	1338 sh	1341	
1293 w	1296 ms	1290	—	$\rho(CH_2)$
1170 w	1172 w	1168 w	—	ν(CC)
1152 w	1155 w	1150 w	—	ν(CC); δ(COH)
1125 w	1126 mw	1123 w	1127	ν(CC) lipid esq.
1085 w	1082 mw	1074 w	1087	ν(CC) lipid esq.
1058 w	1062 mw	1057 w	—	ν(CC) lipid esq.
1028 w	1032 mw	1026 w	—	ν(CC) queratin
1000 s	1002 m	1000 m	1003	ν(CC) aromatic ring breathing
848 m	850 w	849 w	858	δ(CCH) olefinic
640 w	644	638 w	643	ν(C–S) and amide IV
619 w	623 w	616 w	622	ν(C–S)
540 w,sh	—	542 w		
528 w	526 mw,br	528 w	520	ν(S–S)

[a] Intensities: s, strong; m, medium; w, weak; sh, shoulder; br, broad.

Table 18. Wavenumbers and band assignments for Raman spectra of human skin and nail excited at 632.8nm compared to the literature (λ_0=1064nm) (deFaria and Souza, 1999, pp. 170).

Gniadecka, *et.al.* employed FT-Raman spectroscopy to investigate the molecular conformation of proteins, lipids and water in human stratum corneum, whole skin, nail and hair (2001, pp. 394). The authors provide Raman spectral data of intact skin along with the band assignments and they add that skin spectra were highly reproducible, with only minor differences occurring in spectra with pigmented skin samples. These differences were increased background fluorescence as a result of increased pigmentation (*ibid.*).

With regard to mummified remains, research has been conducted on remains preserved by desiccation in various environments, including artificial mummification processes employed by ancient cultures. Overall, mummified skin exhibited bands characteristic of proteins and

lipids, and the remains tended to exhibit weaker hydroxyl (-OH) and amide (NH) bands due to the decrease in water content which results from the desiccation process (Petersen, *et.al.*, 2003, pp. 376). In the article by Edwards, *et.al.*, the authors provide a series of important observations that resulted from their comparisons of mummified and normal human skin, including the differences in Raman bands with regard to presence and absence, intensity variations, fluorescence and general features characteristic of the type of skin analyzed (2002, pp. 8-11). Generally, bands from tissue proteins (including collagen, phospholipids, *etc.*) are found in the regions of 1640-1680cm^{-1} (amide I), 1220-1300cm^{-1} (amide III) and in the regions associated with C-C vibrations, aromatic ring vibrations and assorted C-H vibrational modes. Differences may exist in band intensity, width and overall shape depending on the quality and moisture content of the tissue sample.

Huang *et.al.* addressed the effect of formalin fixation on Raman studies of human tissues. According to the authors, major Raman bands associated with formalin can be found in the ranges 980-1100 cm^{-1} and 1480-1650 cm^{-1}, with notable formalin peaks at 907cm^{-1} , 1041cm^{-1} and 1492cm^{-1} (2003, pp. 651). Their results showed that formalin fixation caused minimal influence on the tissue Raman spectra (*ibid.*), but the authors note that the effect of formalin on overall Raman spectra may be tissue-specific (*i.e.* animal *vs.* human, epithelial *vs.* tumor, *etc.*). Notably, an increase in formalin fixation time will decrease the overall Raman intensity of the skin and related proteins due to the formalin dehydrating the tissue (Huang, 2003, pp. 654) and changing the molecular structure of the tissue proteins. It should be noted that this is a positive aspect of formalin fixation with regard to this research, as the prolonged exposure of formalin to the tattooed tissue will reduce, if not eliminate, potential band interferences from the tissue substrate (as well as reducing potential fluorescence that could result from the analysis of tissue).

This is clearly demonstrated in the pigskin study, as little to no evidence of the tissue substrate is present. Furthermore, there appears to be little effect of the formalin on the resultant Raman spectra, with little to no evidence of the characteristic formalin Raman bands present in the fixed pigskin samples. Even with the tissue substrate and the formalin fixative, it was still possible to identify the pigments present in the pigskin by comparing the determined spectra to the previously obtained spectra of the tattoo ink and pigment standards.

When analyzing tattooed human tissue (whether normal, mummified, charred or decomposed) using vibrational spectroscopic methods, it is essential that the analyst be aware of the potential bands that could result from the tissue substrate in order to ensure proper interpretation of the resultant data and correct assignment of bands to the pigments present. In addition, the analyst should be aware of any bands that may arise from the fixation method, such as formalin.

Preliminary research into the analysis of tattoo inks in human tissue has demonstrated the ability to locate and isolate the pigment layer within a cross section of excised, fixed tissue, and subsequently detect the pigments via Raman spectroscopic methods (Miranda, unpublished study).

Results- Density Functional Theory (DFT) Calculations

The pigments analyzed using density functional theory calculations were Pigment Red 170 (listed as the main component of the Skin Candy Tattoo Ink Red Hot), Pigment Red 122 (listed as the main component of the Skin Candy Tattoo Ink Razberry Creem), and Pigment Orange 16 (listed as the main component of the Skin Candy Tattoo Ink Marz).

Due to the presence of ringed structures (benzene derivatives) within the pigment molecular structures and the conjugate π electron systems inherent in these structures, Raman bands can be expected in the aromatic C-H stretching region (3100-3000cm^{-1}). In some instances, these bands are readily apparent in both the pigment standards and the tattoo inks. In addition, bands (doublet) located in the range of 1630-1550cm^{-1} may also be present due to the ring stretching of the benzene derivatives. The presence and features of the doublet will vary based upon the atoms or functional groups located on the ring. Most of the pigments have their distinct bands located in the region of 1000 and 1700 cm^{-1}. In this region, a large number of vibrational modes can be found, including C=C, N=N, C-N, C=O and amide bands. At vibrations below 1000 cm^{-1}, additional vibrations associated with annulations can be found, along with C-C skeletal vibrations. For ring vibrations and deformations, the Wilson notation is listed[2].

Characteristic vibration information is reported for some of the pigment standards, followed by a more detailed interpretation of the pigments subjected to DFT calculations.

[2]The following website (http://boverhaus.dyndns.org/~wroth/gauss/varsanyi/molekuele/Bz/index.html) shows the normal modes of benzene according to the Wilson notation (originally reported in 1934) and as depicted by Varsanyi (1974). The site provides animations of each of the modes in order to demonstrate displacement of the atoms. A detailed analysis of the vibrational spectrum of the benzene molecule can be found in Wilson, *et.al.*,1955 (see References).

With regard to the phthalocyanines (PG 7, PB15, *et.al.*), the breathing and deformation of the TBP nucleus is exhibited in the band located at ~680 cm^{-1} with additional bands appearing in the region from ~750-800 cm^{-1}. A band at ~ 230-235 cm^{-1} can be attributed to the N-Cu bonding. A band at ~1070-1085 cm^{-1} is indicative of the aromatic chlorine, which can be used to distinguish the blues from the greens.

In general, the monoazo and disazo pigments exhibited an intense band ranging from ~1320-1401 cm^{-1}, which is characteristic of the N=N stretching vibration. Bands in the region of ~1100-1200 represents the C-N symmetric stretching and bending motions, between ~1650 and 1550 cm^{-1} represents the ring vibrations (C=C stretch), the amide I band (~1600-1700 cm^{-1}), which is characterized as the C=O stretching, and the amide III band (~1300-1250 cm^{-1}). The amide II band falls between the two regions, demonstrating the N-H bending and C-N stretching. It should again be noted that band position shifting and band intensity changes can occur and will depend on several factors, including neighboring groups, conjugation, intermolecular bonding and the tautomerism effect described earlier. The monoazo pigments exhibit a band at around 1490-1510 cm^{-1}, which can be attributed to the azobenzene ring vibration.

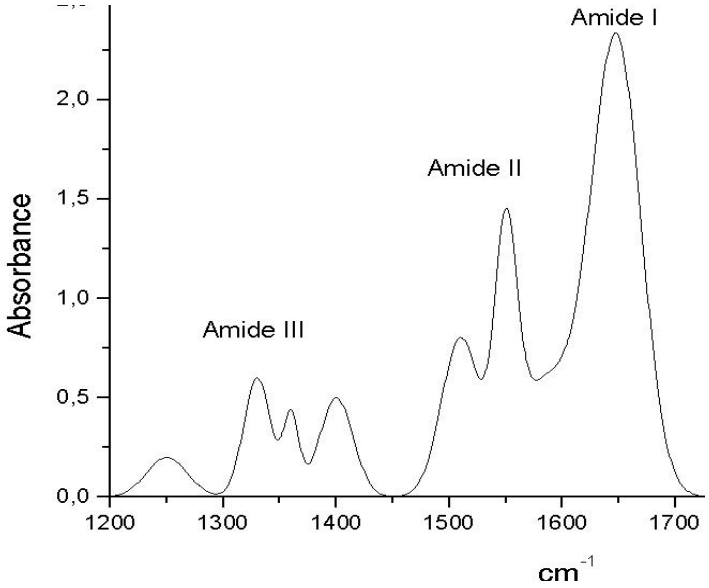

Figure 184. Characteristic amide bands and their locations in infrared spectra.

Pigment Red 122

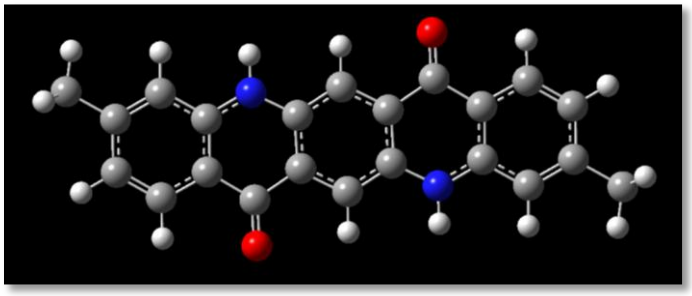

Figure 185. Molecular structure of PR 122.

Pigment Red 122 consists of 42 atoms and hence has 120 fundamental vibrations. Pigment Red 122 exhibits a center of symmetry, which indicates that the mutual exclusion rule will exist between the infrared and Raman spectra. According to the mutual exclusion rule, no spectral lines will appear in common to both due to the fact that any vibration in a molecule containing a center of symmetry can be either Raman or infrared active, but not both (Smith and Dent, 2005, pp. 86). This was exhibited in the vibrational output from the DFT calculations; a frequency with a vibrational mode in Raman did not exhibit a corresponding mode in the infrared and vice versa (see figure). Correlation was found between the calculated spectrum (after a .97 scaling factor was added; Chang, *et.al.*, 2009 note that a scaling factor is commonly needed in DFT calculations of Raman spectra in order to correct for correlation effects incompletely accounted for in DFT), especially with regard to the most intense lines. The normal Raman spectra of Pigment Red 122 exhibited fluorescence, which may have masked the less intense peaks. Quinacridones, of which PR 122 is a member, are characterized by a coupled ring breathing appearing ~1300 cm^{-1}, aromatic C=C vibrations at ~1580 cm^{-1}, and C=O stretching vibrations at ~1650 cm^{-1}.

Mode #	Freq	Infrared	Raman Activity
90	1488.90	0.0003	15.9644
91	1495.93	670.6039	0.0000
92	1498.72	53.4175	0.0001
93	1512.63	0.0001	124.3039
94	1527.94	51.4527	0.0000
95	1546.19	0.0001	114.6944
96	1581.15	589.6291	0.0001
97	1606.13	0.0000	40.6357
98	1613.17	0.0005	1340.9171
99	1617.03	66.2592	0.0066
100	1656.29	0.0194	233.0365
101	1660.43	760.3750	0.0050
102	1669.97	0.0010	49.6816
103	1701.36	549.1914	0.0007
104	1713.72	0.0006	722.5872
105	3026.54	63.8365	0.0106
106	3026.59	0.0007	987.2878
107	3076.23	7.1241	243.1736

Table 19. Excerpt of DFT calculation output. Note highlighted areas demonstrating the mutual exclusion rule.

Description	**DFT (raw data)**	**DFT (.97 scaling factor)**	**Normal Raman (λ_0=488nm)**	**SERS (λ_0=488nm)**
(Central) Ring stretch (Wilson 6a)	723.58 (w)	701.87	677.53	
			1202.8 (m)	1203.1 (m)
C-H rocking	1264.66 (w)	1226.72	1234.8 (m)	1233.8 (m)
C-H rocking	1313.65 (m)	1274.24		
(Central) Ring breathing (Wilson 1)	1331.97 (s)	1292.01	1310.7 (s)	1315.3 (s)
C=C stretch (Wilson 14)	1386.28 (m)	1344.69		
C-H wagging (methyl groups)	1414.44 (m)	1372.01		1382.1 (m)
			1407.8 (m)	1408.3 (m)
				1516.3 (m)
C-H rocking (methyl groups)	1512.63 (w)	1467.25		
C-H wagging	1546.19 (w)	1499.80		
C=C stretch (Wilson 8a)	1613.17 (vs)	1564.77	1566.8 (vs)	1565.5 (vs)
C=C stretch (Wilson 14), C=O stretch	1656.29 (m)	1606.60	1595.8 (m)	1596.3 (m)
C=O stretch, C=C stretch	1713.72 (s)	1662.31	1644.3 (m)	1644.3 (m)
C-H stretch (methyl groups)	3026.59 (s)	2935.79		
C-H rocking (methyl groups)	3076.23	2983.94		
C-H stretch (methyl group)	3107.67 (w)	3114.44		
C-H stretch	3168.65 (m)	3073.59		
C-H stretch (Central Ring)	3179.44 (w)	3084.06		
C-H stretch	3198.31(m)	3102.36		
N-H stretch	3625.63 (m)	3516.86		

Table 20. Wavenumbers (cm^{-1}) of DFT, normal Raman and SERS spectra of Pigment Red 122 (quinacridone); all of the reported vibrational modes were in the plane of the molecule.

Pigment Red 170

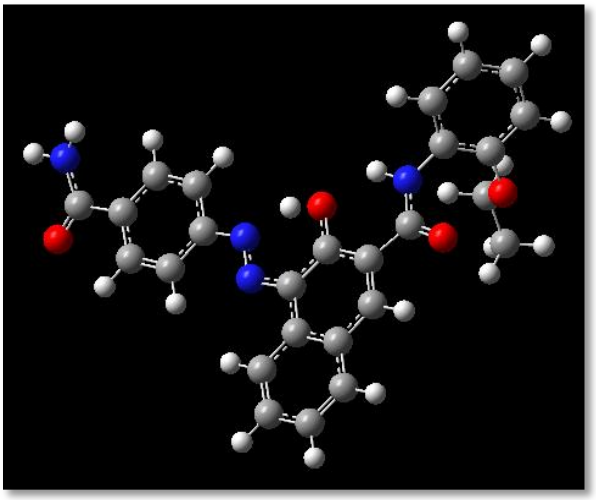

Figure 186. Molecular structure of PR 170.

Pigment Red 170 consists of 56 atoms and hence has 162 fundamental vibrations. Pigment Red 170 does not exhibit a large degree of symmetry. An extensive optimization phase was conducted prior to the DFT calculation, with the resultant molecule exhibiting planes almost perpendicular to one another (see figure).

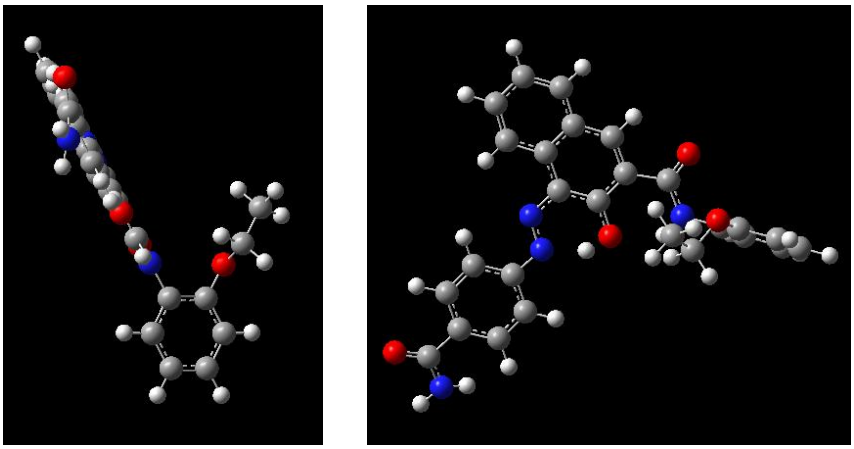

Figure 187 a and b. After rotating the Pigment Red 170 molecule around in space, it is apparent that the molecule is not completely linear.

Description	**DFT (raw data)**	**DFT (.97 scaling factor)**	**Normal Raman (λ_0=633nm)**	**SERS (λ_0=488nm)**
C=C Ring stretch (Wilson 6a)	728.37, 754.06	706.51, 731.44	732.81 (s)	730.05 (w)
Ring breathing (Wilson 1)	990.16	960.46	964.06 (s)	963.76 (m)
C-H wagging (Wilson 14, 15) Ring breathing (Wilson 1)	1172.60 (m)	1137.42	1138.3(w)	1128.4(w)
C-H wagging (Wilson 14, 15)	1187.92 (s)	1152.28		
Ring breathing (Wilson 1) C-H wagging (Wilson 14, 15)	1232.50 (s)	1195.53		
C_6H_5-C vibration, Ring breathing, C=N stretch, C=O stretch	1242.81 (s)	1205.53	1243.5(m) amide III	1242.3(m) amide III
C=C (ring) stretch (Wilson 8b), C-H wagging (Wilson 3)	1312.22 (s)	1272.85	1243.5 (s)	1242.3 (m)
C=C (ring) stretch (Wilson 8b), C-H wagging (Wilson 3)	1323.46 (m)	1283.76		
C=C stretch, C=N stretch, C-H wagging (Wilson 3)	1325.65 (m)	1285.88	1286.8 (s)	1286.3 (s)
C=C stretch (Wilson 12), C-H wagging (Wilson 14)	1353.68 (m)	1314.07		
C=C stretch (Wilson 8b), C-H wagging (Wilson 14)	1370.87 (s)	1329.74		
C=C (ring) stretch (Wilson 8b), C-H wagging (Wilson 14)	1427.78 (vs)	1384.95	1362.1 (vs)	1361.8 (vs)
N=N stretch, C=O stretch	1489.59 (vs)	1444.90	1420.3 (m)	1417.8 (m)
			1511.7(s)	1510.5 (m)
C=C stretch (Wilson 8b)	1642.97 (s)	1593.68	1551.1 (m)	1550.3 (m)
C=C stretch (Wilson 8b)	1652.07 (m)	1602.51	1604.9 (s)	1602.9 (s)
C=C stretch	1661.63 (w)	1611.78		
Aromatic C-H stretch	3192.05 (w)	3096.29		
Aromatic C-H stretch	3194.76 (w)	3098.92		

Table 21. Wavenumbers (cm^{-1}) of DFT, normal Raman and SERS spectra of Pigment Red 170 monoazo.

Using the spectrum of Pigment Red 170 acquired with an excitation wavelength of 633nm, the following assignments are made: 964cm^{-1}: benzylamide/naphthalene, 1114.2cm^{-1}: C-N symmetric stretch, 1164.6cm^{-1}: C-N symmetric bend, 1243.5cm^{-1}: amide III band, 1420.3cm^{-1}: N=N stretch and 1604.9cm^{-1}: benzene stretch. The band located in the 1360 range is due to the naphthalene.

Pigment Orange 16

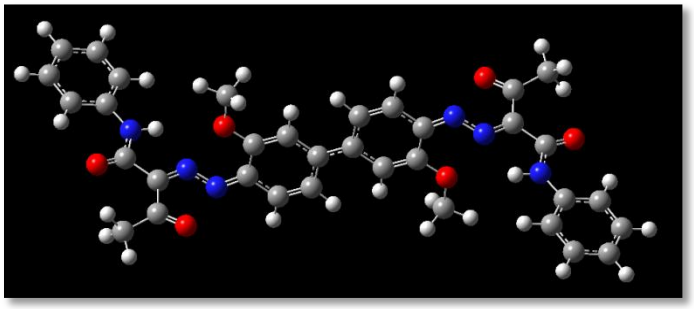

Figure 188. Molecular structure of PO 16.

Pigment Orange 16 consists of 76 atoms and hence has 222 fundamental vibrations. Pigment Orange 16 exhibits a center of inversion, which indicates that the mutual exclusion rule will exist between the infrared and Raman spectra. This was exhibited in the vibrational output from the DFT calculations; a frequency with a vibrational mode in Raman did not exhibit a corresponding mode in the infrared and vice versa. The resultant molecule exhibited planes almost perpendicular to one another (see figure).

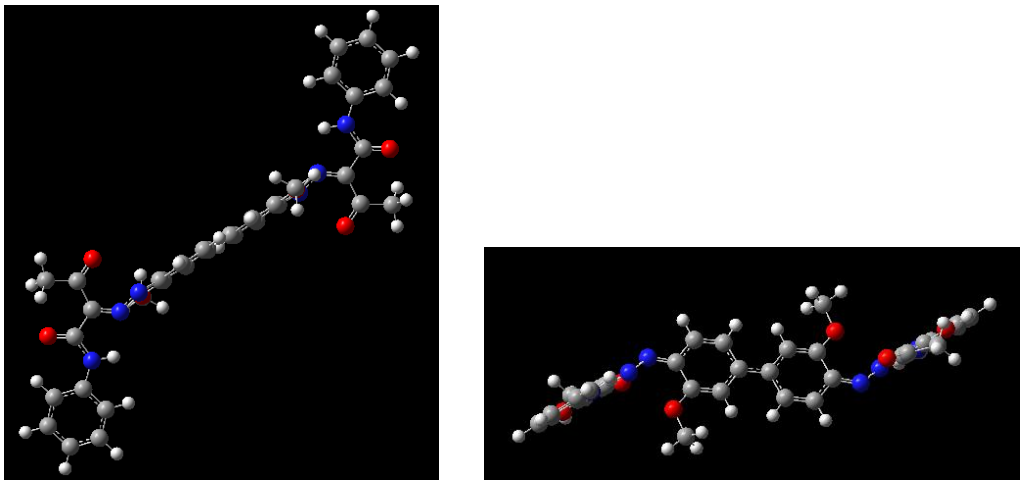

Figure 189 a and b. After rotating the Pigment Orange 16 molecule around in space, it is apparent that the molecule is not completely linear.

Description	DFT (raw data)	DFT (.97 scaling factor)	Normal Raman (λ_0=785nm)	SERS (λ_0=488nm)
Out-of-Plane C-C rocking	334.21 (m)	324.18		
Out-of-Plane C-C rocking	385.10 (m)	373.55	371.07 (m)	
Out-of-Plane C-C rocking	434.99 (m)	421.94		
Out-of-Plane C-C rocking	641.79 (m)	622.54	623.92 (w)	
C=C stretching (Wilson 6a)	670.86 (m)	650.73	669.65 (m)	643.86 (m)
Out-of-Plane rocking (C=C, C-H)	730.52 (m)	708.60		
Ring breathing (Wilson 1)	796.12 (m)	772.24		
C=C stretching, C=C rocking (Wilson 6a)	937.30 (m)	909.18	912.99 (w)	
C=N stretch, C=N and C-H rocking	1079.58 (m)	1047.19	1064.6 (w)	
C-H wagging	1181.81 (m)	1146.36		
C-H wagging	1183.30 (m-s)	1147.80	1123.4 (s)	1128.5 (w)
C=O and C-H rocking and wagging	1201.09 (m)	1165.06	1175.8 (m)	1175 (w)
C=C and C=O stretch, C-H rocking	1244.01 (s)	1206.69		
C=C (ring) stretching, C-H wagging	1256.20 (s)	1218.51		
C-H rocking	1273.37 (s)	1235.17	1259.6 (m)	1261.6 (m)
C=C stretching (outer-most rings)(Wilson 14)	1339.07 (m)	1298.90		
C=C stretching (2 central rings)	1360.03 (s)	1319.23	1305.7 (m)	
C=C (ring) stretching (between 2 central rings),	1382.46 (vs)	1340.99	1323.5 (vs)	1325.4 (s)
C-H_3 deformation, C-H wagging, C=C stretch	1468.43 (m)	1424.38	1397.3 (s)	1395.1 (s)
C-H_3 deformation, C-H wagging, C=C stretch	1473.14 (m-s)	1428.95		
C-H_3 deformation, C-H wagging, C=C stretch	1480.15 (s)	1435.75		
C-H_3 deformation, C-H wagging, C=C stretch	1498.88 (vs)	1453.91		
C-H_3 deformation, C-	1506.10 (m-s)	1460.92	1471.8 (m)	

H wagging				
C=N stretch, C=C stretch, N-H wagging	1553.85 (vs)	1507.23		1502.7 (m)
C=N stretch, N-H wagging C=C (ring) stretch	1566.62 (m)	1519.62		
C=N stretch, C=C stretch	1595.23 (vs)	1547.37	1533.1 (m)	
C=C stretch (Wilson 8b)	1633.38 (m)	1584.38		
C=C stretch (Wilson 8b)	1639.30 (m)	1590.12		
C=C stretch (Wilson 8b)	1646.11 (m)	1596.73	1601.8 (vs)	1601.4 (vs)
C=O stretch, (C=N-H wagging)	1734.68 (m)	1682.64	1660.8 (m)	
C=O stretch	1755.25 (m)	1702.59		
N-H stretch	3561.08 (m)	3454.25		

Table 22. Wavenumbers (cm^{-1}) of DFT, normal Raman and SERS spectra of Pigment Orange 16 (disazo).

It was possible to determine the pigments (both organic and inorganic) present in the tattoo inks examined in this study. In some instances, there was a lack of agreement between the pigments listed on the ink packaging and the experimental data. Several of the same pigments were found in the different brands of tattoo inks, making it difficult to determine tattoo origin based solely on pigment composition. For example, Pigment Blue 15, Pigment Green 7 and Pigment Violet 23β were found in the blue, green and purple inks (respectively) from the United States, Brazil and China inks sets. Therefore, detecting a pigment in tissue or on evidence is not likely to be able to point towards a specific manufacturing source.

In addition to being able to determine pigment compositions based upon comparison to pigment standards, reported spectra in the literature and computer databases, it was also possible to make determinations about functional groups (*i.e.* N=N, annulated systems, *etc.*) in an effort to classify pigments (*i.e.* azo, phthalocyanine, *etc.*). By making these determinations, one is able to interpret vibrational modes in the molecule, determine allowed and forbidden transitions, and elucidate the functional group chemistry of the molecular species. Furthermore, by analyzing the pigments with Raman spectroscopy and infrared spectroscopy, it is also possible to determine molecular symmetry of the molecule (such as the determination that the molecule has a center of inversion due to mutual exclusion).

The need to consider different excitation wavelengths in determination of unknowns using Raman spectroscopy cannot be understated. This is largely due to some variation in resultant spectra with a change in excitation wavelength, for example, as seen with the phthalocyanines. Caution must be taken in interpreting and reporting spectra when only one excitation wavelength is employed. Furthermore, the use of additional chemical and instrumental techniques such as pigment extractions, the use of concentrated sulfuric acid coupled with

UV/Vis spectrophotometry, infrared spectroscopy and x-ray fluorescence are especially helpful to the determination of a unknown as well as assignments of molecular and atomic features, both organic and inorganic.

DFT calculations and comparisons to the experimental Raman spectra enabled normal mode assignments for the pigments evaluated. Good correspondence was found with regard to band assignments of the major functional groups when a 0.97 scaling factor was applied to the calculated wavenumbers. According to Rana *et.al.*, a drift of the deviation with increasing wavenumber is to be expected in DFT calculations because of the high errors in correlation corrections (2011, pp. 202). The authors add that DFT calculations typically predict many more bands than are usually observed in the spectra. Differences in the intensities as well as the frequencies of the bands can be caused by the assumptions made in the calculations (*ibid.*).

Preliminary examination of tattoo inks in pigskin demonstrated the ability to detect the pigments easily, with little sample preparation. In addition, expected interferences from fixation methods, tissue substrate and fluorescence were minimal. The results show great promise for analyzing tattoo inks in tissue using minimally invasive techniques and little sample manipulation.

Chapter 5: Conclusions

A detailed evaluation was conducted on a variety of tattoo inks, and it was demonstrated that it is entirely possible to determine the chemical composition of tattoo inks. This study was able to determine the pigment compositions of a variety of tattoo inks, which varied in terms of color and origin of manufacture. Databases of tattoo inks were created with regard to microscopic characteristics, normal Raman data at different wavelengths of excitation, FT-Raman data, surface enhanced Raman scattering, FT-infrared data via attenuated total reflection and x-ray fluorescence. Similar pigments were found in tattoo inks from different manufacturers, which did not allow for individualization of tattoo inks based upon country of origin (with the limitation being the samples set examined). A revised hypothesis might include a more detailed evaluation of the microscopic and optical properties of the pigment particles and qualitative analysis of pigments within each tattoo ink in addition to an evaluation of the liquid portion of the inks.

Microscopy was an extremely useful tool for evaluating the physical properties of the tattoo inks. By examining the tattoo inks using bright field and dark field microscopic techniques, information concerning the uniformity and pigment distribution within the inks was able to be ascertained. It is highly recommended that any examination concerning tattoo inks and pigments (even paints and inks in general) begin with a thorough microscopic examination, beginning with stereomicroscopy, followed by bright field and dark field microscopy methods and polarized light microscopy of the pigment particles. Further analysis using scanning transmission electron microscopy (TEM) may also be useful in disclosing characteristics of the particles. Examination of the pigment particles can disclose additional information including

particle size, crystal morphology (forms) and class, and optical data such as (relative) refractive indices, birefringence, extinction characteristics, *etc*.

While it did not necessary improve the resultant spectral data, extractions of the tattoo inks were useful in resolving and isolating the individual pigments and separating the organic pigments from the inorganic, mineral pigments (such as titanium dioxide). Extractions allow for a more thorough qualitative assessment of the pigment composition of the inks and may be useful for determining qualitative aspects of pigment composition by evaluating relative ratios.

In analyzing samples in a laboratory, it is essential to employ instrumentation that will provide information concerning both the organic and inorganic fractions of the samples. Both Raman spectroscopy and infrared spectroscopy/attenuated total reflection provide a great deal of information concerning the chemical structure of the pigments that make up the inks, and either one of these techniques can be used to obtain detailed information about a sample. There is great benefit to using Raman spectroscopy due to the ability to use different excitation wavelengths to generate a useable spectrum. In addition, the use of SERS as an analytical tool in Raman spectroscopy is paramount; surface enhanced Raman scattering is a simple, yet powerful technique that enables the analyst to obtain data in instances where optical and physical characteristics of the sample would normally preclude the resolution of Raman bands. The microwave synthesis technique described by Leona demonstrates the ease with which a suitable colloid can be prepared and used for SERS work. In addition, x-ray fluorescence provided a simple, rapid method for obtaining data concerning the inorganic, elemental composition of the tattoo inks.

This research demonstrated the ease with which an instrument can be calibrated prior to analysis. Literature providing standards and corresponding spectral data in order to ensure that the instrument is performing properly is readily available. The use of internal checks in Raman spectrometers, such as Bruker's SureCal, demonstrates the robustness and accuracy of current instrumentation. It is imperative that any instrument be checked prior to analysis in order to ensure that the instrument is operating according to its specifications, and laboratories should maintain records demonstrating that their instruments are working properly in order to meet any quality assurance standards set forth by the laboratory or any accrediting agency.

Contributions to the fields of Forensic Science & Criminal Justice

This research contributed to the fields of forensic science and criminal justice in several ways. Namely, it has been able to (1) establish criteria for the examination, identification and comparison of tattoo inks and pigments in order to meet the admissibility standards set forth in court cases Frye and Daubert, and in the Federal Rules of Evidence; (2) establish standard operating procedures and quality control measures for the analysis of tattoo inks and pigments in forensic laboratories to ensure that the quality assurance needed to meet required accreditation standards is met, thereby working towards the general goal of strengthening forensic science and establishing good practices; (3) present novel databases and comprehensive reference data of tattoo inks to assist in criminal investigations where tattoo ink may be evidence in a crime or may aid in a death investigation or identification of a decedent, and (4) develop a method for detecting tattoo inks and pigments in tissue which can aid in criminal investigations of illegal activities.

Forensic science is routinely defined as the application of natural science to matters of law. Several court cases have proved pivotal to determining the admissibility of evidence in legal proceedings. A summary of some of the main cases are provided below. The standards set forth in state courts vary by jurisdiction, with some states using the Daubert standard and some states using the Frye standard (for example, New York is a Frye state). Additionally, in some states, Daubert and Frye may be used under a different case name in which a standard was applied to a specific case within the state (for example, *People v. Kelly* is California's equivalent to the Frye case dealing with general acceptance rule).

In *Frye v, United States*, 293 F. 1013 (D.C. Cir. 1923) [*Frye*], the Court determined that the standard for admissibility is whether the evidence has been generally accepted in the relevant

scientific community. *Frye* is described and being a stringent standard that makes it difficult to get novel scientific evidence into Courts due to the difficulty in meeting the general acceptance standard. Under *Frye*, the expert has the burden of demonstrating general acceptance. The problems with *Frye* are the difficulties in defining what constitutes general acceptance and who constitutes the relevant scientific community. Although case law has evolved and new standards for admissibility have been presented, the Frye standard is still applied in some jurisdictions.

In *Daubert v. Merrell Dow Pharmaceuticals, Inc.*, 509 U.S. 579 (1993) [*Daubert* I], the Court determined that the Judge should act as a gatekeeper to determine if the evidence is reliable and relevant. In order to be relevant, the testimony must fit the facts of the case. The Court in *Daubert* I set forth a non-exclusive, non-inclusive checklist for Courts to consider when determining reliability. The list includes whether the methods/techniques are testable (falsifiable), whether the techniques and methods have been subject to peer review and publication, whether the method/ technique has an established error rate and standards/controls, and if the method has gained general acceptance.

With regard to general acceptance, the Court referenced *Frye* but put forth that the relevant scientific community could be a small minority as opposed to the more global implication in *Frye*. In *Daubert v. Merrell Dow Pharmaceuticals, Inc.*, 43 F.3d 1311 (9th Cir. 1995) [*Daubert* II], the Court clarified and applied the conclusions in *Daubert* I. In addition, they considered another factor for the "checklist', that of whether the research/methods discussed in the testimony are litigation driven or a product of the witness's normal course of business.

In *General Electric Co. v. Joiner*, 522 U.S. 136 (1997) [*Joiner*], the question of admissibility was concerned with whether his exposure to toxic chemicals during his employment with General Electric had caused *Joiner*'s lung cancer. *Joiner*'s argument rested on

several scientific studies, including epidemiological studies which were presented by well-credentialed individuals. This case clearly demonstrates the intent of *Daubert*- that just because the expert is well-qualified does not mean that the evidence will automatically be admitted into the Court. The Judge determined that there existed too great an analytical gap between the evidence presented (including in vitro studies on mice that developed different types of cancer, European and Asian studies that involved different chemicals and different effects) and the facts of the case. He determined that the gap between the facts presented and the issues being questioned was too great when considering each study presented. Furthermore, the fact finders should not be clouded by the *ipse dixit* (say so) of the expert just because they are an expert. The facts and methods, while reliable, must fit the task at hand. If not, the evidence is inadmissible.

In *Kumho Tire Co. v. Carmichael*, 526 U.S. 137, 1999 [*Kumho*], the Court evaluated tire testimony to determine that *Daubert* is not limited to scientific evidence, but reaches not strictly scientific, but technical testimony as well.

Federal Rule of Evidence 702 states "If specific knowledge is necessary to assist the fact finder in determining the issue at hand then an expert deemed so by education, training, knowledge and experience is may to render an opinion or information, so long as the testimony is supported by reliable facts and data, the methods are applied reliably and the testimony addresses the issue at hand" (Federal Rules of Evidence Rule 702, 1975-revised 2000) [FRE 702]. In a note on the revised FRE 702 the advisory committee adds that the FRE 702 is subject to the opinions and conclusions from *Daubert* (I and II), *Joiner* and *Kumho*. In addition, other factors are outlined in the FRE Note. One of the factors states that there are no set guidelines (limitations) to the role of the gatekeeper and his admissibility evaluations, and another factor

states that testimony not based upon the scientific method (such as opinion evidence or testimony based on experience) is not necessarily inadmissible.

One purpose of this research is to demonstrate the scientific validity of tattoo ink analysis with vibrational spectroscopic methods in order to assert its evidential reliability. By demonstrating reliable, objective scientific principles and methodology, it can be established that the analysis of tattoo inks by the methods and techniques employed in this research is a valid technique that can withstand admissibility concerns. Furthermore, establishing sound scientific procedure and methodology with regard to analysis of tattoo inks can be used to assert confidence in the resultant data and its subsequent interpretation.

According to Moenssens' 1993 article, problems with forensic science include expert witnesses that are actually technicians who do not understand the theory behind the work that they perform in a laboratory and quality assurance is often lacking (pp. 3). In addition, technological advances, novel scientific evidence and methods of analyses are not accurately depicted in court and are not necessarily subject to admissibility hearings. In addition to criticisms concerning the lack of fundamental theoretical scientific knowledge of forensic practitioners and the unbalanced and sometimes lacking quality assurance in laboratory systems, critics of current practices in the forensic field tend to target the subjective nature of some interpretations and conclusions. This criticism rests in the thought that subjective analyses are affected by inherent biases.

Another purpose of this research project is to address some of the criticisms of the forensic science discipline presented by Moenssens (and still considered criticisms almost ten years later!). Namely, this research is conducted in an effort to provide a scientific, theoretical

background for the instrumental techniques applied in a forensic lab (namely Raman spectroscopy and SERS) and specific analysis of tattoo inks and pigments. This is done in an effort to foster a thorough understanding of the analysis of the tattoo inks that would enable an analyst to be able to successfully present evidence in legal proceedings, including admissibility hearings. One statement by Moenssens regarding admissibility of validating of underlying data and theory is especially poignant, "The gloss begins to fade as the technology transfer from research laboratories to crime laboratories began, and expert witnesses (true research scientists) became somewhat less credentialed, and also began to change (sometimes shortcutting) operational procedures…" (1993, pp. 9). This issue is especially important, as research conducted and protocols described in an academic forum should be completely embraced and considered in a forensic laboratory in order to ensure proper training and establishment of analytical procedures.

Moenssens also touches on the negative effects of computer assisted determinations with database programs, including the analyst's lack of understanding the database programs and how the program arrived at a result. He states, "In order to run an analysis, you do not need to be an expert anymore- you only need to be taught to run a sophisticated type of instrumentation that is hooked up to a computer, and then read off the result." (1993, pp. 9). Furthermore, the analyst will often read the result that the computer program generates and report that result without questioning the reliability of the output or validating the resultant determination. His research demonstrates the need to examine the resultant data and interpret the spectral data by conducting band assignments and by analyzing standards under similar instrumental conditions to aid in identifications and comparisons. Furthermore, while the use of DFT calculations provided information concerning vibrational modes and band assignments, it is meant to supplement

actual experimental data. The use of databases is paramount in forensic and analytical laboratories, but it should be noted that all spectral data should be evaluated by the analyst so ensure the identifications and comparisons are scientifically sound. An effort to understand the functions of instrumental databases should also be conducted by laboratory personnel in order to understand the limitations of the computer identification programs.

The National Academy of Sciences Report released a report based upon an extensive study conducted by the Committee on Identifying the Needs of the Forensic Science Community in 2009. In general, the NAS report recommends improving methods, practices and overall performance within the forensic sciences. The recommendations include the need for research and scientific advancement, improved education, well-established standards for accreditation, improved interface between the forensic science and medical examiner communities and well-established scientific bases for validation of forensic methods.

The report notes that by advancing the recommendations, law enforcement investigations can be performed more reliably, wrongful convictions can be minimized and advances can be made with regard to homeland security. This research is conducted in an effort to establish the scientific basis and validity of the analysis of modern tattoo inks in order to work towards meeting these goals. The analysis of tattoo inks, as presented in this research, demonstrates an analytical scheme that is strongly rooted in science and supported by objective data analysis that has been strengthened by accepted, fundamental calibration and validation methods (an additional recommendation presented in the NAS report). This research also addresses a concern in the NAS report, namely, "…some forensic science disciplines are supported by little rigorous systematic research to validate the discipline's basic premises and techniques" (2009,

pp. S-16). Since there is limited research concerning the analysis of tattoo inks, this research serves to work towards ameliorating this criticism.

Another NAS Report recommendation addressed in this research is that of collaboration between the forensic science and medical examiner communities. The forensic lab, which would commonly conduct instrumental analysis on inks, pigments, dyes, *etc.* would be directly working with medical examiners in instances where human tissue containing tattoo inks would require analysis in an effort to identify human remains. The analysis of tattoo inks in human tissue directly addresses the development and advancement of technical methods, the interfacing of forensic science and medical examiner communities and basic sciences and the creation of "fertile ground for the discourse among the communities" 2009, (pp. S-16). The analysis of tattoo inks and pigments recovered from human remains will certainly facilitate the investigatory process conducted by law enforcement officials and medicolegal death investigators. Finally, the research presented here could be an asset in issues of homeland security in providing intelligence and identification in instances of mass disasters that result from terrorist acts.

Future Studies

The advancement of analytical techniques and instrumentation coupled with the paradigm shift to a more objective, analytical approach to forensic science provides fertile ground for research that can contribute to forensic science and criminal justice, art conservation and cultural heritage, as well as anthropology and art history. During the course of this research, it became apparent that there are many additional studies that could be done with tattoo inks or related materials. A summary of future projects is presented; the list is not intended to be exhaustive, as the evolution of tattoo inks and the needs of the forensic science community will surely guide the course of future research.

General instrumental techniques would be extremely useful for further classifying each ink, namely x-ray diffraction (XRD) on the tattoo inks in an effort to elucidate specific structural information. XRD data would be an added tool, especially in instances where computational chemistry, or DFT calculations are to be made. Molecular electronic fluorescence spectroscopy would prove useful in the analysis of the tattoo inks and pigments in solution. A vast undertaking to understand the solubility of the inks and pigments with a variety of solvents using wet chemistry coupled with UV/Vis spectrophotometry and fluorescence spectrometry may provide increased discriminating power between tattoo inks and pigments. Additional microchemistry and solution chemistry (including color and microcrystalline tests) could be conducted to enhance any analytical schemes developed for identification and comparison of tattoo inks and pigments. Density functional theory calculations should be conducted for all of the pigments represented in this study, with detailed vibrational modes being assigned to the calculated and experimental Raman and infrared bands. Additional SERS spectra should be obtained, with the

use of alternate excitation wavelengths and aggregants used in an effort to evaluate optimum sample preparation methods of the tattoo inks.

Quantitative analysis of the tattoo inks in an effort to determine relative pigment abundances is another approach that could be undertaken in the characterization and discrimination of tattoo inks. By determining concentrations of specific pigments, including titanium dioxide, and demonstrating batch consistency, it may be possible to statistically assign an unknown tattoo ink to a particular manufacturer (or country of origin) based upon the relative ratios of pigments.

Aside from the need to continue building up databases and libraries by analyzing more tattoo inks and powder pigments, there are other substances similar to tattoo inks (in usage and application) that should be studied and characterized, both on and off of the skin. These include: henna, non-permanent, 'fake' tattoos, and ink based stamp pads. Furthermore, a more detailed analysis of both the inorganic portions of the tattoo inks along with a thorough investigation of the liquid portion of the inks may prove useful in discriminating ink brands and origins of manufacture.

During the course of this research, it has become apparent that it is possible to distinguish polymorphs of a given pigment, as reported in the literature (for example, authors in Venkataraman's text report on distinguishing the different polymorphs of Pigment Blue 15 using infrared spectroscopy and comparative x-ray powder data, 1977, pp. 446 and 289, respectively) and based on the experimental data presented in this research (both IR and Raman). One future research project that could be applied to increasing the discrimination power of pigment blue 15 is through the use of chemometrics. Specifically, by using software for data analysis that

incorporates statistical computing and graphical display methodologies (such as The R Project for Statistical Computing, http://www.r-project.org). By inputting the spectral data (peak locations) for the various pigment blues into the computer program, it is possible to use a discrimination algorithm such as partial least squares (PLS) analysis to determine the relationships between and discrimination of the data within the set).This use of statistics could also be applied across tattoo inks and manufacturers. This is an excellent way to support the paradigm shift from subjective analysis and interpretation within forensic science to the desired objective, statistical support for interpretations and conclusions regarding inclusions and exclusions. Additionally, like Raman spectroscopy, x-ray powder diffraction is a useful tool for differentiating between the different polymorphs of a given pigment. XRD coupled with wet chemistry methods to facilitate crystal growth or isolation a crystal form is a viable project that could provide insight into the polymorphs of existing synthetic/organic pigments. Caution must be taken during sample preparation methods to prevent the chance of changing the crystal form upon the application of pressure or solvents (for example, according to Thompson, "The (infrared) spectrum (of the Pigment Blue polymorph) must be run in Nujol since the high pressures involved in the potassium bromide [KBr] disk techniques effect changes in crystal form and hence in the peak ratio" (1977, pp. 447).

Since similar pigment types were found across the three origins of manufacture (U.S.A, Brazil and China), further microscopic and spectroscopic studies should be conducted to attempt to distinguish the pigment manufacturers based on a more comprehensive study of the pigment polymorphs present in the tattoo inks. The crystal form of the pigment is a key factor in the physical properties of the resultant tattoo ink. According to Brostoff *et. al.*, slight variations in the manufacturing process [of artists' pigments], including pH, drying processes and

corresponding temperatures and any milling methods can cause the transformation of polymorphs and affect the crystallinity and crystal quality of the pigment. An evaluation of the pigment manufacturing processes along with the manufacturing processes of the tattoo inks should be conducted and used to characterize tattoo inks originating from different sources. Since the physical and optical characteristics of the pigment particles are paramount in determining the color characteristics of a sample, more detailed evaluation of the particles in tattoo inks should be explored (although control over the drying, extraction and any additional isolation and preparation methods would be paramount to prevent modification of the crystals[(*i.e.* polymorph changes]). Again, microscopy would prove to be an extremely powerful tool in evaluating the pigment distribution, particle size and particle shapes.

Finally, expanding or improving upon any work presented in this research would be beneficial, specifically with regard surface enhanced Raman scattering (SERS). This should be done in an order to further validate the use of SERS as a routine analytical tool to be used in the lab, whether it be a forensic lab, conservation lab, industrial lab or any other laboratory setting (cosmetic, pharmaceutical, color chemistry, *etc.*). The increased application of SERS in the forensic field will help meet the criteria set forth in courtroom admissibility guidelines, such as those in Daubert.

Appendix A: Table of Raman and Infrared Bands[3]

A Summary of Characteristic Raman and Infrared Frequencies

A. Raman*
B. Infrared†

A.

A SUMMARY OF CHARACTERISTIC RAMAN FREQUENCIES

Frequency (cm^{-1})	Vibration	Compound
3400–3330	Bonded antisymmetric NH_2 stretch	Primary amines
3380–3340	Bonded OH stretch	Aliphatic alcohols
3374	CH stretch	Acetylene (gas)
3355–3325	Bonded antisymmetric NH_2 stretch	Primary amides
3350–3300	Bonded NH stretch	Secondary amines
3335–3300	≡CH stretch	Alkyl acetylenes
3300–3250	Bonded symmetric NH_2 stretch	Primary amines
3310–3290	Bonded NH stretch	Secondary amides
3190–3145	Bonded symmetric NH_2 stretch	Primary amides
3175–3154	Bonded NH stretch	Pyrazoles

*F. R. Dollish, W. G. Fateley, and F. F. Bentley, *Characteristic Raman Frequencies of Organic Compounds*, John Wiley & Sons Inc., New York, 1974, with permission.
†N. B. Colthup, L. H. Daly, and S. E. Wiberly, *Introduction to Infrared and Raman Spectroscopy*, Third Edition, Academic Press, Inc., 1990.

[3] Adapted from Lin-Vein, Colthup & Grasselli, The Handbook of Infrared and Raman Characteristic Frequencies of Organic Molecules, Academic Press, 1991.

Frequency (cm^{-1})	Vibration	Compound
3103	Antisymmetric $=CH_2$ stretch	Ethylene (gas)
3100–3020	CH_2 stretches	Cyclopropane
3100–3000	Aromatic CH stretch	Benzene derivatives
3095–3070	Antisymmetric $=CH_2$ stretch	$C=CH_2$ derivatives
3062	CH stretch	Benzene
3057	Aromatic CH stretch	Alkyl benzenes
3040–3000	CH stretch	C=CHR derivatives
3026	Symmetric $=CH_2$ stretch	Ethylene (gas)
2990–2980	Symmetric $=CH_2$ stretch	$C=CH_2$ derivatives
2986–2974	Symmetric NH_3^+ stretch	Alkyl ammonium chlorides (aqueous solution)
2969–2965	Antisymmetric CH_3 stretch	*n*-Alkanes
2929–2912	Antisymmetric CH_2 stretch	*n*-Alkanes
2884–2883	Symmetric CH_3 stretch	*n*-Alkanes
2861–2849	Symmetric CH_2 stretch	*n*-Alkanes
2850–2700	CHO group (2 bands)	Aliphatic aldehydes
2590–2560	SH stretch	Thiols
2316–2233	C≡C stretch (2 bands)	$R-C\equiv C-CH_3$
2301–2231	C≡C stretch (2 bands)	$R-C\equiv C-R'$
2300–2250	Pseudoantisymmetric N=C=O stretch	Isocyanates
2264–2251	Symmetric C≡C−C≡C stretch	Alkyl diacetylenes
2259	C≡N stretch	Cyanamide
2251–2232	C≡N stretch	Aliphatic nitriles
2220–2100	Pseudoantisymmetric N=C=S stretch (2 bands)	Alkyl isothiocyanates
2220–2000	C≡N stretch	Diaklyl cyanamides
2172	Symmetric C≡C−C≡C stretch	Diacetylene
2161–2134	N≡C stretch	Aliphatic isonitriles
2160–2100	C≡C stretch	Alkyl acetylenes
2156–2140	C≡N stretch	Alkyl thiocyanates
2104	Antisymmetric N=N=N stretch	CH_3N_3
2094	C≡N stretch	HCN
2049	Pseudoantisymmetric C=C=O stretch	Ketene
1974	C≡C stretch	Acetylene (gas)
1964–1958	Antisymmetric C=C=C stretch	Allenes
1870–1840	Symmetric C=O stretch	Saturated 5-membered ring cyclic anhydrides
1820	Symmetric C=O stretch	Acetic anhydride
1810–1788	C=O stretch	Acid halides

Frequency (cm^{-1})	Vibration	Compound
1807	C=O stretch	Phosgene
1805–1799	Symmetric C=O stretch	Noncyclic anhydrides
1800	C=C stretch	$F_2C=CF_2$ (gas)
1795	C=O stretch	Ethylene carbonate
1792	C=C stretch	$F_2C=CFCH_3$
1782	C=O stretch	Cyclobutanone
1770–1730	C=O stretch	Halogenated aldehydes
1744	C=O stretch	Cyclopentanone
1743–1729	C=O stretch	Cationic α-amino acids (aqueous solution)
1741–1734	C=O stretch	*O*-Alkyl acetates
1740–1720	C=O stretch	Aliphatic aldehydes
1739–1714	C=C stretch	$C=CF_2$ derivatives
1736	C=C stretch	Methylene cyclopropane
1734–1727	C=O stretch	*O*-Alkyl propionates
1725–1700	C=O stretch	Aliphatic ketones
1720–1715	C=O stretch	*O*-Alkyl formates
1712–1694	C=C stretch	RCF=CFR
1695	Nonconjugated C=O stretch	Uracil derivatives (aqueous solution)
1689–1644	C=C stretch	Monofluoroalkenes
1687–1651	C=C stretch	Alkylidene cyclopentanes
1686–1636	Amide I band	Primary amides (solids)
1680–1665	C=C stretch	Tetraalkyl ethylenes
1679	C=C stretch	Methylene cyclobutane
1678–1664	C=C stretch	Trialkyl ethylenes
1676–1665	C=C stretch	*trans*-Dialkyl ethylenes
1675	Symmetric C=O stretch (cyclic dimer)	Acetic acid
1673–1666	C=N stretch	Aldimines
1672	Symmetric C=O stretch (cyclic dimer)	Formic acid (aqueous solution)
1670–1655	Conjugated C=O stretch	Uracil, cytosine, and guanine derivatives (aqueous solution)
1670–1630	Amide I band	Tertiary amides
1666–1652	C=N stretch	Ketoximes
1665–1650	C=N stretch	Semicarbazones (solid)
1663–1636	Symmetric C=N stretch	Aldazines, ketazines
1660–1654	C=C stretch	*cis*-Dialkyl ethylenes
1660–1650	Amide I band	Secondary amides
1660–1649	C=N stretch	Aldoximes

Frequency (cm^{-1})	Vibration	Compound
1660–1610	C=N stretch	Hydrazones (solid)
1658–1644	C=C stretch	$R_2C=CH_2$
1656	C=C stretch	Cyclohexene, cycloheptene
1654–1649	Symmetric C=O stretch (cyclic dimer)	Carboxylic acids
1652–1642	C=N stretch	Thiosemicarbazones (solid)
1650–1590	NH_2 scissors	Primary amines
1649–1625	C=C stretch	Allyl derivatives
1648–1640	N=O stretch	Alkyl nitrites
1648–1638	C=C stretch	$H_2C=CHR$
1647	C=C stretch	Cyclopropene
1638	C=O stretch	Ethylene dithiocarbonate
1637	Symmetric C=C stretch	Isoprene
1634–1622	Antisymmetric NO_2 stretch	Alkyl nitrates
1630–1550	Ring stretches (doublet)	Benzene derivatives
1623	C=C stretch	Ethylene (gas)
1620–1540	Three or more coupled C=C stretches	Polyenes
1616–1571	C=C stretch	Chloroalkenes
1614	C=C stretch	Cyclopentene
1596–1547	C=C stretch	Bromoalkenes
1581–1465	C=C stretch	Iodoalkenes
1575	Symmetric C=C stretch	1,3-Cyclohexadiene
1573	N=N stretch	Azomethane (in solution)
1566	C=C stretch	Cyclobutene
1560–1550	Antisymmetric NO_2 stretch	Primary nitroalkanes
1555–1550	Antisymmetric NO_2 stretch	Secondary nitroalkanes
1548	N=N stretch	1-Pyrazoline
1545–1535	Antisymmetric NO_2 stretch	Tertiary nitroalkanes
1515–1490	Ring stretch	2-Furfuryl group
1500	Symmetric C=C stretch	Cyclopentadiene
1480–1470	OCH_3, OCH_2 deformations	Aliphatic ethers
1480–1460	Ring stretch	2 Furfurylidene or 2-furoyl group
1473–1446	CH_3, CH_2 deformations	*n*-Alkanes
1466–1465	CH_3 deformation	*n*-Alkanes
1450–1400	Pseudosymmetric N=C=O stretch	Isocyanates
1443–1398	Ring stretch	2-Substituted thiophenes
1442	N=N stretch	Azobenzene
1440–1340	Symmetric CO_2^- stretch	Carboxylate ions (aqueous solution)

Frequency (cm^{-1})	Vibration	Compound
1415–1400	Symmetric CO_2^- stretch	Dipolar and anionic α-amino acids (aqueous solution)
1415–1385	Ring stretch	Anthracenes
1395–1380	Symmetric NO_2 stretch	Primary nitroalkanes
1390–1370	Ring stretch	Naphthalenes
1385–1368	CH_3 symmetric deformation	*n*-Alkanes
1375–1360	Symmetric NO_2 stretch	Secondary nitroalkanes
1355–1345	Symmetric NO_2 stretch	Tertiary nitroalkanes
1350–1330	CH deformation	Isopropyl group
1320	Ring vibration	1,1-Dialkyl cyclopropanes
1314–1290	In-plane CH deformation	*trans*-Dialkyl ethylenes
1310–1250	Amide III band	Secondary amides
1310–1175	CH_2 twist and rock	*n*-Alkanes
1305–1295	CH_2 in-phase twist	*n*-Alkanes
1300–1280	CC bridge bond stretch	Biphenyls
1282–1275	Symmetric NO_2 stretch	Alkyl nitrates
1280–1240	Ring stretch	Epoxy derivatives
1276	Symmetric N=N=N stretch	CH_3N_3
1270–1251	In-plane CH deformation	*cis*-Dialkyl ethylenes
1266	Ring "breathing"	Ethylene oxide (oxirane)
1230–1200	Ring vibration	Para-disubstituted benzenes
1220–1200	Ring vibration	Mono- and 1,2-dialkyl cyclopropanes
1212	Ring "breathing"	Ethylene imine (aziridine)
1205	C_6H_5-C vibration	Alkyl benzenes
1196–1188	Symmetric SO_2 stretch	Alkyl sulfates
1188	Ring "breathing"	Cyclopropane
1172–1165	Symmetric SO_2 stretch	Alkyl sulfonates
1150–950	CC stretches	*n*-Alkanes
1145–1125	Symmetric SO_2 stretch	Dialkyl sulfones
1144	Ring "breathing"	Pyrrole
1140	Ring "breathing"	Furan
1130–1100	Symmetric C=C=C stretch (2 bands)	Allenes
1130	Pseudosymmetric C=C=O stretch	Ketene
1112	Ring "breathing"	Ethylene sulfide
1111	NN stretch	Hydrazine
1070–1040	S=O stretch (1 or 2 bands)	Aliphatic sulfoxides

Frequency (cm^{-1})	Vibration	Compound
1065	C=S stretch	Ethylene trithiocarbonate
1060–1020	Ring vibration	Ortho-disubstituted benzenes
1040–990	Ring vibration	Pyrazoles
1030–1015	In-plane CH deformation	Monosubstituted benzenes
1030–1010	Trigonal ring "breathing"	3-Substituted pyridines
1030	Trigonal ring "breathing"	Pyridine
1029	Ring "breathing"	Trimethylene oxide (oxetane)
1026	Ring "breathing"	Trimethylene imine (azetidine)
1010–990	Trigonal ring "breathing"	Mono-, meta-, and 1,3,5-substituted benzenes
1001	Ring "breathing"	Cyclobutane
1000–985	Trigonal ring "breathing"	2- and 4-Substituted pyridines
992	Ring "breathing"	Benzene
992	Ring "breathing"	Pyridine
939	Ring "breathing"	1,3-Dioxolane
933	Ring vibration	Alkyl cyclobutanes
930–830	Symmetric COC stretch	Aliphatic ethers
914	Ring "breathing"	Tetrahydrofuran
906	ON stretch	Hydroxylamine
905–837	CC skeletal stretch	*n*-Alkanes
900–890	Ring vibration	Alkyl cyclopentanes
900–850	Symmetric CNC stretch	Secondary amines
899	Ring "breathing"	Pyrrolidine
866	Ring "breathing"	Cyclopentane
877	OO stretch	Hydrogen peroxide
851–840	Pseudosymmetric CON stretch	*O*-Alkyl hydroxylamines
836	Ring "breathing"	Piperazine
835–749	Skeletal stretch	Isopropyl group
834	Ring "breathing"	1,4-Dioxane
832	Ring "breathing"	Thiophene
832	Ring "breathing"	Morpholine
830–720	Ring vibration	Para-disubstuted benzenes
825–820	C_3O skeletal stretch	Secondary alcohols
818	Ring "breathing"	Tetrahydropyran
815	Ring "breathing"	Piperidine
802	Ring "breathing"	Cyclohexane (chair form)
785–700	Ring vibration	Alkyl cyclohexanes
760–730	C_4O skeletal stretch	Tertiary alcohols

Frequency (cm^{-1})	Vibration	Compound
760–650	Symmetric skeletal stretch	*tert*-Butyl group
740–585	CS stretch (1 or more bands)	Alkyl sulfides
735–690	"C=S stretch"	Thioamides, thioureas (solid)
733	Ring "breathing"	Cycloheptane
730–720	CCl stretch, P_C conformation	Primary chloroalkanes
715–620	CS stretch (1 or more bands)	Dialkyl disulfides
709	CCl stretch	CH_3Cl
703	Ring "breathing"	Cyclooctane
703	Symmetric CCl_2 stretch	CH_2Cl_2
690–650	Pseudosymmetric N=C=S stretch	Alkyl isothiocyanates
688	Ring "breathing"	Tetrahydrothiophene
668	Symmetric CCl_3 stretch	$CHCl_3$
660–650	CCl stretch, P_H conformation	Primary chloroalkanes
659	Symmetric CSC stretch	Pentamethylene sulfide
655–640	CBr stretch, P_C conformation	Primary bromoalkanes
630–615	Ring deformation	Monosubstituted benzenes
615–605	CCl stretch, S_{HH} conformation	Secondary chloroalkanes
610–590	CI stretch, P_C conformation	Primary iodoalkanes
609	CBr stretch	CH_3Br
577	Symmetric CBr_2 stretch	CH_2Br_2
570–560	CCl stretch, T_{HHH} conformation	Tertiary chloroalkanes
565–560	CBr stretch, P_H conformation	Primary bromoalkanes
540–535	CBr stretch, S_{HH} conformation	Secondary bromoalkanes
539	Symmetric CBr_3 stretch	$CHBr_3$
525–510	SS stretch	Dialkyl disulfides
523	CI stretch	CH_3I
520–510	CBr stretch, T_{HHH} conformation	Tertiary bromoalkanes
510–500	CI stretch, P_H conformation	Primary iodoalkanes
510–480	SS stretch	Dialkyl trisulfides
495–485	CI stretch, S_{HH} conformation	Secondary iodoalkanes
495–485	CI stretch, T_{HHH} conformation	Tertiary iodoalkanes
484–475	Skeletal deformation	Dialkyl diacetylenes
483	Symmetric CI_2 stretch	CH_2I_2
459	Symmetric CCl_4 stretch	CCl_4
437	Symmetric CI_3 stretch	CHI_3 (in solution)
425–150	"Chain expansion"	*n*-Alkanes
355–335	Skeletal deformation	Monoalkyl acetylenes
267	Symmetric CBr_4 stretch	CBr_4 (in solution)
200–160	Skeletal deformation	Aliphatic nitriles
178	Symmetric CI_4 stretch	CI_4 (solid)

Appendix B: Correlation Chart for the Infrared Region[4]

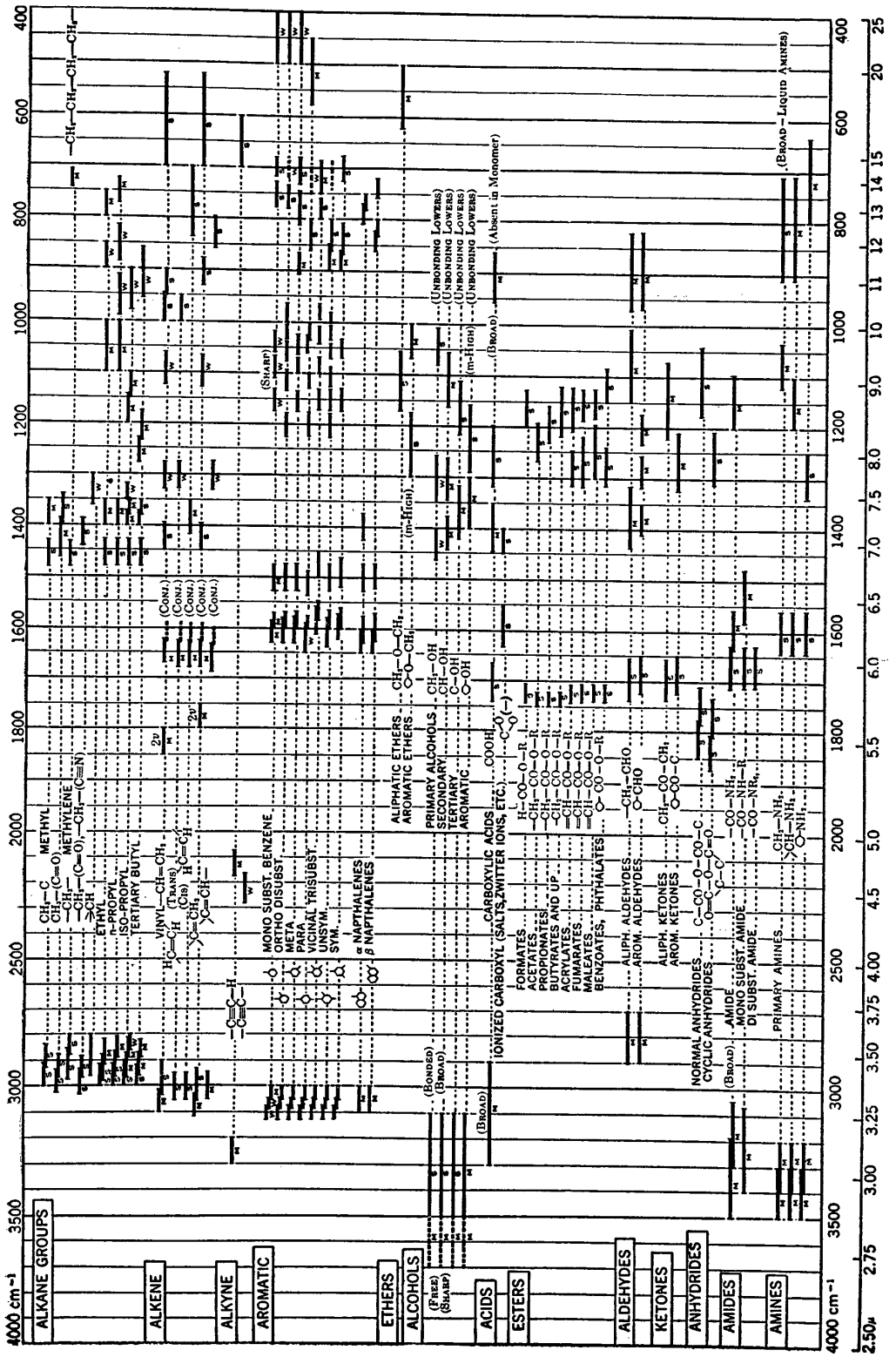

[4] Adapted from Colthup, 1950

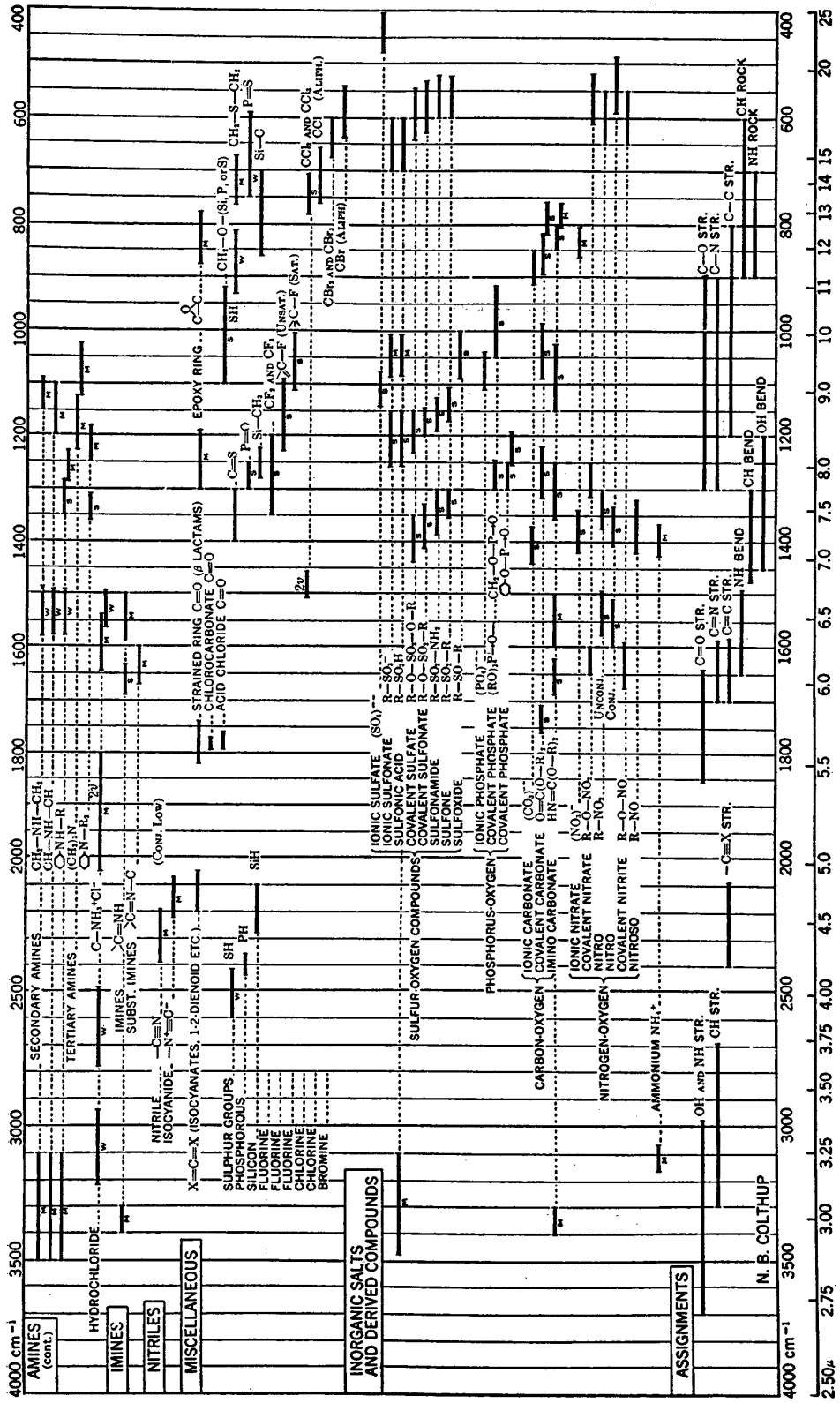
AMINES (cont.)
IMINES
NITRILES
MISCELLANEOUS
INORGANIC SALTS AND DERIVED COMPOUNDS
ASSIGNMENTS
HYDROCHLORIDE
SECONDARY AMINES
TERTIARY AMINES
IMINES
SUBST. IMINES
NITRILE
ISOCYANIDE
X=C=X (ISOCYANATES, 1-2-DIENOID ETC.)
SULPHUR GROUPS
PHOSPHOROUS
SILICON
FLUORINE
CHLORINE
BROMINE
STRAINED RING C=O (β LACTAMS)
CHLOROCARBONATE C=O
ACID CHLORIDE C=O
EPOXY RING
IONIC SULFATE
IONIC SULFONATE
SULFONIC ACID
COVALENT SULFATE
COVALENT SULFONATE
SULFONAMIDE
SULFONE
SULFOXIDE
SULFUR-OXYGEN COMPOUNDS
IONIC PHOSPHATE
COVALENT PHOSPHATE
PHOSPHORUS-OXYGEN
IONIC CARBONATE
COVALENT CARBONATE
IMINO CARBONATE
CARBON-OXYGEN
IONIC NITRATE
COVALENT NITRATE
NITRO
COVALENT NITRITE
NITROSO
NITROGEN-OXYGEN
AMMONIUM NH4+
OH AND NH STR.
CH STR.
-C≡X STR.
C=O STR.
C=N STR.
C=C STR.
NH BEND
CH BEND
OH BEND
C=O STR.
C=N STR.
C—C STR.
CH ROCK
NH ROCK
N. B. COLTHUP
4000 cm⁻¹
2.50μ
2.75
3.00
3.25
3.50
3.75
4.00
4.5
5.0
5.5
6.0
6.5
7.0
7.5
8.0
9.0
10
11
12
13
14
15
20
25

Appendix C: Character Tables

C_s	E	$\sigma(xy)$		
A'	+1	+1	$T_x,\ T_y,\ R_z$	$\alpha_{xx},\ \alpha_{yy},\ \alpha_{zz},\ \alpha_{xy}$
A''	+1	−1	$T_z,\ R_x,\ R_y$	$\alpha_{yz},\ \alpha_{xz}$

C_2	E	$C_2(z)$		
A	+1	+1	$T_z,\ R_z$	$\alpha_{xx},\ \alpha_{yy},\ \alpha_{zz},\ \alpha_{xy}$
B	+1	−1	$T_x,\ T_y,\ R_x,\ R_y$	$\alpha_{yz},\ \alpha_{xz}$

C_i	E	i		
A_g	+1	+1	$R_x,\ R_y,\ R_z$	all components of α
A_u	+1	−1	$T_x,\ T_y,\ T_z$	

C_{2v}	E	$C_2(z)$	$\sigma_v(xz)$	$\sigma_v(yz)$		
A_1	+1	+1	+1	+1	T_z	$\alpha_{xx},\ \alpha_{yy},\ \alpha_{zz}$
A_2	+1	+1	−1	−1	R_z	α_{xy}
B_1	+1	−1	+1	−1	$T_x,\ R_y$	α_{xz}
B_2	+1	−1	−1	+1	$T_y,\ R_x$	α_{yz}

C_{3v}	E	$2C_3(z)$	$3\sigma_v$		
A_1	+1	+1	+1	T_z	$\alpha_{xx}+\alpha_{yy},\ \alpha_{zz}$
A_2	+1	+1	−1	R_z	
E	+2	−1	0	$(T_x,\ T_y),\ (R_x,\ R_y)$	$(\alpha_{xx}-\alpha_{yy},\ \alpha_{xy}),\ (\alpha_{yz},\ \alpha_{xz})$

C_{4v}	E	$2C_4(z)$	$C_4^2\equiv C_2''$	$2\sigma_v$	$2\sigma_d$		
A_1	+1	+1	+1	+1	+1	T_z	$\alpha_{xx}+\alpha_{yy},\ \alpha_{zz}$
A_2	+1	+1	+1	−1	−1	R_z	
B_1	+1	−1	+1	+1	−1		$\alpha_{xx}-\alpha_{yy}$
B_2	+1	−1	+1	−1	+1		α_{xy}
E	+2	0	−2	0	0	$(T_x, T_y),\ (R_x,\ R_y)$	$(\alpha_{yz},\ \alpha_{xz})$

C_p^n (or S_p^n) denotes that the C_p (or S_p) operation is carried out successively n times.

$C_{\infty v}$	E	$2C_\infty^\phi$	$2C_\infty^{2\phi}$	$2C_\infty^{3\phi}$	...	$\infty\sigma_v$		
Σ^+	+1	+1	+1	+1	...	+1	T_z	$\alpha_{xx}+\alpha_{yy},\ \alpha_{zz}$
Σ^-	+1	+1	+1	+1	...	−1	R_z	
Π	+2	$2\cos\phi$	$2\cos 2\phi$	$2\cos 3\phi$	...	0	$(T_x,\ T_y),\ (R_x,\ R_y)$	$(\alpha_{yz},\ \alpha_{xz})$
Δ	+2	$2\cos 2\phi$	$2\cos 2.2\phi$	$2\cos 3.2\phi$	...	0		$(\alpha_{xx}-\alpha_{yy},\ \alpha_{xy})$
Φ	+2	$2\cos 3\phi$	$2\cos 2.3\phi$	$2\cos 3.3\phi$	...	0		
...	...	...	...	...	...	...		

C_{2h}	E	$C_2(z)$	$\sigma_h(xy)$	i		
A_g	+1	+1	+1	+1	R_z	$\alpha_{xx},\ \alpha_{yy},\ \alpha_{zz},\ \alpha_{xy}$
A_u	+1	+1	−1	−1	T_z	
B_g	+1	−1	−1	+1	$R_x,\ R_y$	$\alpha_{yz},\ \alpha_{xz}$
B_u	+1	−1	+1	−1	$T_x,\ T_y$	

D_3	E	$2C_3(z)$	$3C_2$		
A_1	+1	+1	+1		$\alpha_{xx}+\alpha_{yy},\ \alpha_{zz}$
A_2	+1	+1	−1	$T_z,\ R_z$	
E	+2	−1	0	$(T_x,\ T_y),\ (R_x,\ R_y)$	$(\alpha_{xx}-\alpha_{yy},\ \alpha_{xy}),\ (\alpha_{yz},\ \alpha_{xz})$

$D_{2d} \equiv V_d$	E	$2S_4(z)$	$S_4^2 \equiv C_2''$	$2C_2$	$2\sigma_d$		
A_1	+1	+1	+1	+1	+1		$\alpha_{xx} + \alpha_{yy}$, α_{zz}
A_2	+1	+1	+1	−1	−1	R_z	
B_1	+1	−1	+1	+1	−1		$\alpha_{xx} - \alpha_{yy}$
B_2	+1	−1	+1	−1	+1	T_z	α_{xy}
E	+2	0	−2	0	0	(T_x, T_y), (R_x, R_y)	$(\alpha_{yz}, \alpha_{xz})$

D_{3d}	E	$2S_6(z)$	$2S_6^2 \equiv 2C_3$	$S_6^3 \equiv S_2 \equiv i$	$3C_2$	$3\sigma_d$		
A_{1g}	+1	+1	+1	+1	+1	+1		$\alpha_{xx} + \alpha_{yy}$, α_{zz}
A_{1u}	+1	−1	+1	−1	+1	−1		
A_{2g}	+1	+1	+1	+1	−1	−1	R_z	
A_{2u}	+1	−1	+1	−1	−1	+1	T_z	
E_g	+2	−1	−1	+2	0	0	(R_x, R_y)	$(\alpha_{xx} - \alpha_{yy}, \alpha_{xy})$, $(\alpha_{yz}, \alpha_{xz})$
E_u	+2	+1	−1	−2	0	0	(T_x, T_y)	

D_{4d}	E	$2S_8(z)$	$2S_8^2 \equiv 2C_4$	$2S_8^3$	$S_8^4 \equiv C_2''$	$4C_2$	$4\sigma_d$		
A_1	+1	+1	+1	+1	+1	+1	+1		$\alpha_{xx} + \alpha_{yy}$, α_{zz}
A_2	+1	+1	+1	+1	+1	−1	−1	R_z	
B_1	+1	−1	+1	−1	+1	+1	−1		
B_2	+1	−1	+1	−1	+1	−1	+1	T_z	
E_1	+2	$+\sqrt{2}$	0	$-\sqrt{2}$	−2	0	0	(T_x, T_y)	
E_2	+2	0	−2	0	+2	0	0		$(\alpha_{xx} - \alpha_{yy}, \alpha_{xy})$
E_3	+2	$-\sqrt{2}$	0	$+\sqrt{2}$	−2	0	0	(R_x, R_y)	$(\alpha_{yz}, \alpha_{xz})$

$D_{2h} \equiv V_h$	E	$\sigma(xy)$	$\sigma(xz)$	$\sigma(yz)$	i	$C_2(z)$	$C_2(y)$	$C_2(x)$		
A_g	+1	+1	+1	+1	+1	+1	+1	+1		α_{xx}, α_{yy}, α_{zz}
A_u	+1	−1	−1	−1	−1	+1	+1	+1		
B_{1g}	+1	+1	−1	−1	+1	+1	−1	−1	R_z	α_{xy}
B_{1u}	+1	−1	+1	+1	−1	+1	−1	−1	T_z	
B_{2g}	+1	−1	+1	−1	+1	−1	+1	−1	R_y	α_{xz}
B_{2u}	+1	+1	−1	+1	−1	−1	+1	−1	T_y	
B_{3g}	+1	−1	−1	+1	+1	−1	−1	+1	R_x	α_{yz}
B_{3u}	+1	+1	+1	−1	−1	−1	−1	+1	T_x	

D_{3h}	E	$2C_3(z)$	$3C_2$	σ_h	$2S_3$	$3\sigma_v$		
A_1'	+1	+1	+1	+1	+1	+1		$\alpha_{xx} + \alpha_{yy}$, α_{zz}
A_1''	+1	+1	+1	−1	−1	−1		
A_2'	+1	+1	−1	+1	+1	−1	R_z	
A_2''	+1	+1	−1	−1	−1	+1	T_z	
E'	+2	−1	0	+2	−1	0	(T_x, T_y)	$(\alpha_{xx} - \alpha_{yy}, \alpha_{xy})$
E''	+2	−1	0	−2	+1	0	(R_x, R_y)	$(\alpha_{yz}, \alpha_{xz})$

$\mathbf{D}_{4h}$	E	$2C_4(z)$	$C_4^2 \equiv C_2''$	$2C_2$	$2C_2'$	σ_h	$2\sigma_v$	$2\sigma_d$	$2S_4$	$S_2 \equiv i$		
A_{1g}	+1	+1	+1	+1	+1	+1	+1	+1	+1	+1		$\alpha_{xx}+\alpha_{yy},\ \alpha_{zz}$
A_{1u}	+1	+1	+1	+1	+1	−1	−1	−1	−1	−1		
A_{2g}	+1	+1	+1	−1	−1	+1	−1	−1	+1	+1	R_z	
A_{2u}	+1	+1	+1	−1	−1	−1	+1	+1	−1	−1	T_z	
B_{1g}	+1	−1	+1	+1	−1	+1	+1	−1	−1	+1		$\alpha_{xx}-\alpha_{yy}$
B_{1u}	+1	−1	+1	+1	−1	−1	−1	+1	+1	−1		
B_{2g}	+1	−1	+1	−1	+1	+1	−1	+1	−1	+1		α_{xy}
B_{2u}	+1	−1	+1	−1	+1	−1	+1	−1	+1	−1		
E_g	+2	0	−2	0	0	−2	0	0	0	+2	(R_x, R_y)	$(\alpha_{yz}, \alpha_{xz})$
E_u	+2	0	−2	0	0	+2	0	0	0	−2	$(T_x,\ T_y)$	

$\mathbf{D}_{5h}$	E	$2C_5(z)$	$2C_5^2$	σ_h	$5C_2$	$5\sigma_v$	$2S_5$	$2S_5^3$		
A_1'	+1	+1	+1	+1	+1	+1	+1	+1		$\alpha_{xx}+\alpha_{yy},\ \alpha_{zz}$
A_1''	+1	+1	+1	−1	+1	−1	−1	−1		
A_2'	+1	+1	+1	+1	−1	−1	+1	+1	R_z	
A_2''	+1	+1	+1	−1	−1	+1	−1	−1	T_z	
E_1'	+2	$2\cos 72°$	$2\cos 144°$	+2	0	0	$+2\cos 72°$	$+2\cos 144°$	$(T_x,\ T_y)$	
E_1''	+2	$2\cos 72°$	$2\cos 144°$	−2	0	0	$-2\cos 72°$	$-2\cos 144°$	$(R_x,\ R_y)$	$(\alpha_{yz},\ \alpha_{xz})$
E_2'	+2	$2\cos 144°$	$2\cos 72°$	+2	0	0	$+2\cos 144°$	$+2\cos 72°$		$(\alpha_{xx}-\alpha_{yy},\ \alpha_{xy})$
E_2''	+2	$2\cos 144°$	$2\cos 72°$	−2	0	0	$-2\cos 144°$	$-2\cos 72°$		

$\mathbf{D}_{6h}$	E	$2C_6(z)$	$2C_6^2 \equiv 2C_3$	$C_6^3 \equiv C_2''$	$3C_2$	$3C_2'$	σ_h	$3\sigma_v$	$3\sigma_d$	$2S_6$	$2S_3$	$S_6^3 \equiv S_2 \equiv i$		
A_{1g}	+1	+1	+1	+1	+1	+1	+1	+1	+1	+1	+1	+1		$\alpha_{xx}+\alpha_{yy},\ \alpha_{zz}$
A_{1u}	+1	+1	+1	+1	+1	+1	−1	−1	−1	−1	−1	−1		
A_{2g}	+1	+1	+1	+1	−1	−1	+1	−1	−1	+1	+1	+1	R_z	
A_{2u}	+1	+1	+1	+1	−1	−1	−1	+1	+1	−1	−1	−1	T_z	
B_{1g}	+1	−1	+1	−1	+1	−1	−1	−1	+1	+1	−1	+1		
B_{1u}	+1	−1	+1	−1	+1	−1	+1	+1	−1	−1	+1	−1		
B_{2g}	+1	−1	+1	−1	−1	+1	−1	+1	−1	+1	−1	+1		
B_{2u}	+1	−1	+1	−1	−1	+1	+1	−1	+1	−1	+1	−1		
E_{1g}	+2	+1	−1	−2	0	0	−2	0	0	−1	+1	+2	$(R_x,\ R_y)$	$(\alpha_{yz},\ \alpha_{xz})$
E_{1u}	+2	+1	−1	−2	0	0	+2	0	0	+1	−1	−2	$(T_x,\ T_y)$	
E_{2g}	+2	−1	−1	+2	0	0	+2	0	0	−1	−1	+2		$(\alpha_{xx}-\alpha_{yy},\ \alpha_{xy})$
E_{2u}	+2	−1	−1	+2	0	0	−2	0	0	+1	+1	−2		

$\mathbf{D}_{\infty h}$	E	$2C_\infty^\phi$	$2C_\infty^{2\phi}$	$2C_\infty^{3\phi}$	$\cdots$	σ_h	$\propto C_2$	$\propto \sigma_v$	$2S_\infty^\phi$	$2S_\infty^{2\phi}$	$\cdots$	$S_2 \equiv i$		
Σ_g^+	+1	+1	+1	+1	$\cdots$	+1	+1	+1	+1	+1	$\cdots$	+1		$\alpha_{xx}+\alpha_{yy},\ \alpha_{zz}$
Σ_u^+	+1	+1	+1	+1	$\cdots$	−1	−1	+1	−1	−1	$\cdots$	−1	T_z	
Σ_g^-	+1	+1	+1	+1	$\cdots$	+1	−1	−1	+1	+1	$\cdots$	+1	R_z	
Σ_u^-	+1	+1	+1	+1	$\cdots$	−1	+1	−1	−1	−1	$\cdots$	−1		
Π_g	+2	$2\cos\phi$	$2\cos 2\phi$	$2\cos 3\phi$	$\cdots$	−2	0	0	$-2\cos\phi$	$-2\cos 2\phi$	$\cdots$	+2	$(R_x,\ R_y)$	$(\alpha_{yz},\ \alpha_{xz})$
Π_u	+2	$2\cos\phi$	$2\cos 2\phi$	$2\cos 3\phi$	$\cdots$	+2	0	0	$+2\cos\phi$	$+2\cos 2\phi$	$\cdots$	−2	$(T_x,\ T_y)$	
Δ_g	+2	$2\cos 2\phi$	$2\cos 4\phi$	$2\cos 6\phi$	$\cdots$	+2	0	0	$+2\cos 2\phi$	$+2\cos 4\phi$	$\cdots$	+2		$(\alpha_{xx}-\alpha_{yy},\ \alpha_{xy})$
Δ_u	+2	$2\cos 2\phi$	$2\cos 4\phi$	$2\cos 6\phi$	$\cdots$	−2	0	0	$-2\cos 2\phi$	$-2\cos 4\phi$	$\cdots$	−2		
Φ_g	+2	$2\cos 3\phi$	$2\cos 6\phi$	$2\cos 9\phi$	$\cdots$	−2	0	0	$-2\cos 3\phi$	$-2\cos 4\phi$	$\cdots$	+2		
Φ_u	+2	$2\cos 3\phi$	$2\cos 6\phi$	$2\cos 9\phi$	$\cdots$	+2	0	0	$+2\cos 3\phi$	$+2\ \cos\ 4\phi$	$\cdots$	−2		
$\cdots$	$\cdots$	$\cdots$	$\cdots$	$\cdots$	$\cdots$	$\cdots$	$\cdots$	$\cdots$	$\cdots$	$\cdots$	$\cdots$	$\cdots$		

$\mathbf{T}_d$	E	$8C_3$	$6\sigma_d$	$6S_4$	$3S_4^2 \equiv 3C_2$		
A_1	+1	+1	+1	+1	+1		$\alpha_{xx} + \alpha_{yy} + \alpha_{zz}$
A_2	+1	+1	−1	−1	+1		
E	+2	−1	0	0	+2		$(\alpha_{xx} + \alpha_{yy} - 2\alpha_{zz},\ \alpha_{xx} - \alpha_{yy})$
F_1	+3	0	−1	+1	−1	$(R_x,\ R_y,\ R_z)$	
F_2	+3	0	+1	−1	−1	$(T_x,\ T_y,\ T_z)$	$(\alpha_{xy},\ \alpha_{yz},\ \alpha_{xz})$

$\mathbf{O}_h$	E	$8C_3$	$6C_2$	$6C_4$	$3C_4^2 \equiv 3C_2''$	$S_2 \equiv i$	$6S_4$	$8S_6$	$3\sigma_h$	$6\sigma_d$		
A_{1g}	+1	+1	+1	+1	+1	+1	+1	+1	+1	+1		$\alpha_{xx} + \alpha_{yy} + \alpha_{zz}$
A_{1u}	+1	+1	+1	+1	+1	−1	−1	−1	−1	−1		
A_{2g}	+1	+1	−1	−1	+1	+1	−1	+1	+1	−1		
A_{2u}	+1	+1	−1	−1	+1	−1	+1	−1	−1	+1		
E_g	+2	−1	0	0	+2	+2	0	−1	+2	0		$(\alpha_{xx} + \alpha_{yy} - 2\alpha_{zz},\ \alpha_{xx} - \alpha_{yy})$
E_u	+2	−1	0	0	+2	−2	0	+1	−2	0		
F_{1g}	+3	0	−1	+1	−1	+3	+1	0	−1	−1	$(R_x,\ R_y,\ R_z)$	
F_{1u}	+3	0	−1	+1	−1	−3	−1	0	+1	+1	$(T_x,\ T_y,\ T_z)$	
F_{2g}	+3	0	+1	−1	−1	+3	−1	0	−1	+1		$(\alpha_{xy},\ \alpha_{yz},\ \alpha_{xz})$
F_{2u}	+3	0	+1	−1	−1	−3	+1	0	+1	−1		

$\mathbf{I}_h$	E	$12C_5$	$12C_5^2$	$20C_3$	$15C_2$	i	$12S_{10}$	$12S_{10}^3$	$20S_6$	15σ		
A_g	1	1	1	1	1	1	1	1	1	1		$\alpha_{xx}+\alpha_{yy}+\alpha_{zz}$
F_{1g}	3	$\frac{1}{2}(1+\sqrt{5})$	$\frac{1}{2}(1-\sqrt{5})$	0	−1	3	$\frac{1}{2}(1-\sqrt{5})$	$\frac{1}{2}(1+\sqrt{5})$	0	−1	$(R_x,\ R_y,\ R_z)$	
F_{2g}	3	$\frac{1}{2}(1-\sqrt{5})$	$\frac{1}{2}(1+\sqrt{5})$	0	−1	3	$\frac{1}{2}(1+\sqrt{5})$	$\frac{1}{2}(1-\sqrt{5})$	0	−1		
G_g	4	−1	−1	1	0	4	−1	−1	1	0		
H_g	5	0	0	−1	1	5	0	0	−1	1		$(2\alpha_{zz}-\alpha_{xx}-\alpha_{yy},$ $\alpha_{xx}-\alpha_{yy},$ $\alpha_{xy},\ \alpha_{yz},\ \alpha_{xz})$
A_u	1	1	1	1	1	−1	−1	−1	−1	−1		
F_{1u}	3	$\frac{1}{2}(1+\sqrt{5})$	$\frac{1}{2}(1-\sqrt{5})$	0	−1	−3	$-\frac{1}{2}(1-\sqrt{5})$	$-\frac{1}{2}(1+\sqrt{5})$	0	1	$(T_x,\ T_y,\ T_z)$	
F_{2u}	3	$\frac{1}{2}(1-\sqrt{5})$	$\frac{1}{2}(1+\sqrt{5})$	0	−1	−3	$-\frac{1}{2}(1+\sqrt{5})$	$-\frac{1}{2}(1-\sqrt{5})$	0	1		
G_u	4	−1	−1	1	0	−4	1	1	−1	0		
H_u	5	0	0	−1	1	−5	0	0	1	−1		

Appendix D: Tattoo Inks (Iron Works Brasil)

Vermelho

Bright Field, 100x

Dark Field, 100x

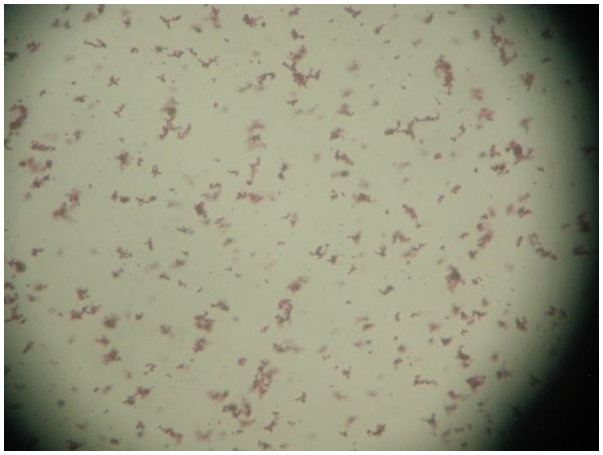

In RI 1.550, 400x

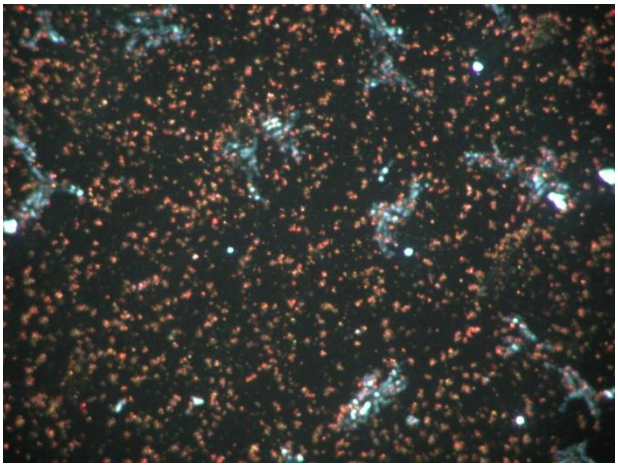

Crossed polars, In RI 1.550, 200x

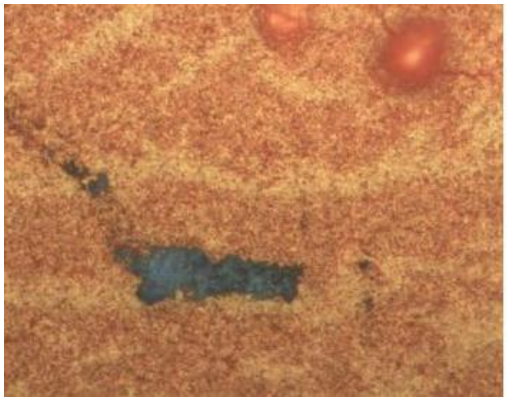

Raman microscope image, 200x

Normal Raman, 488nm

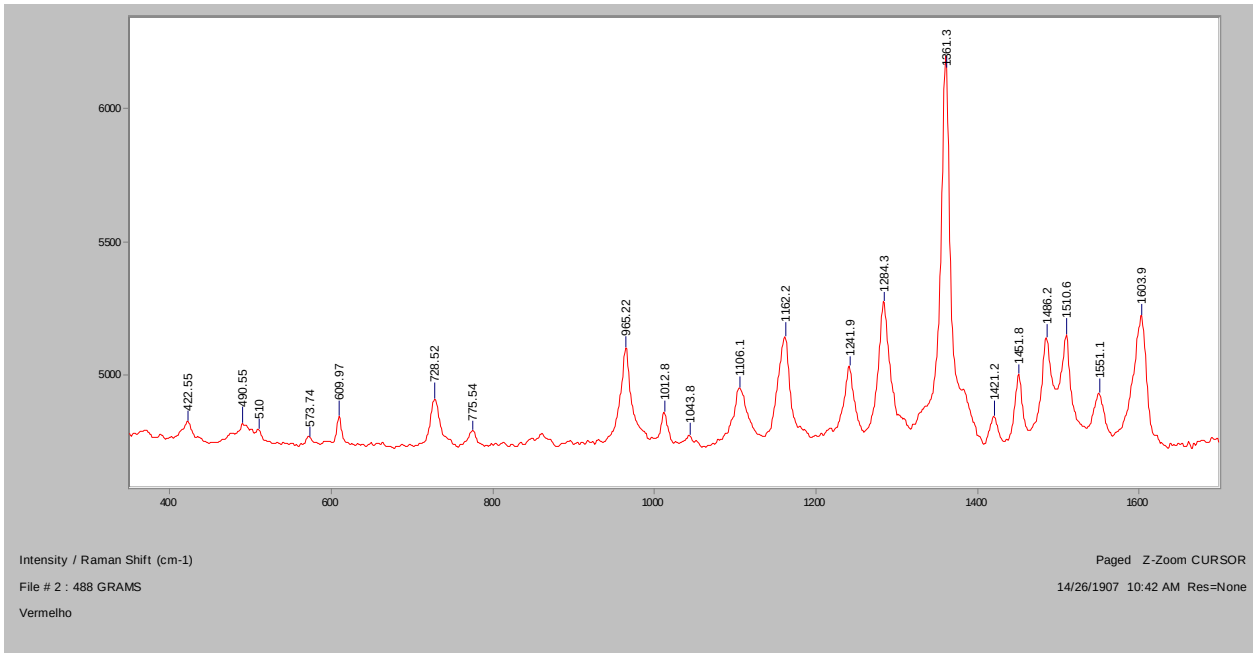

Normal Raman, 633nm

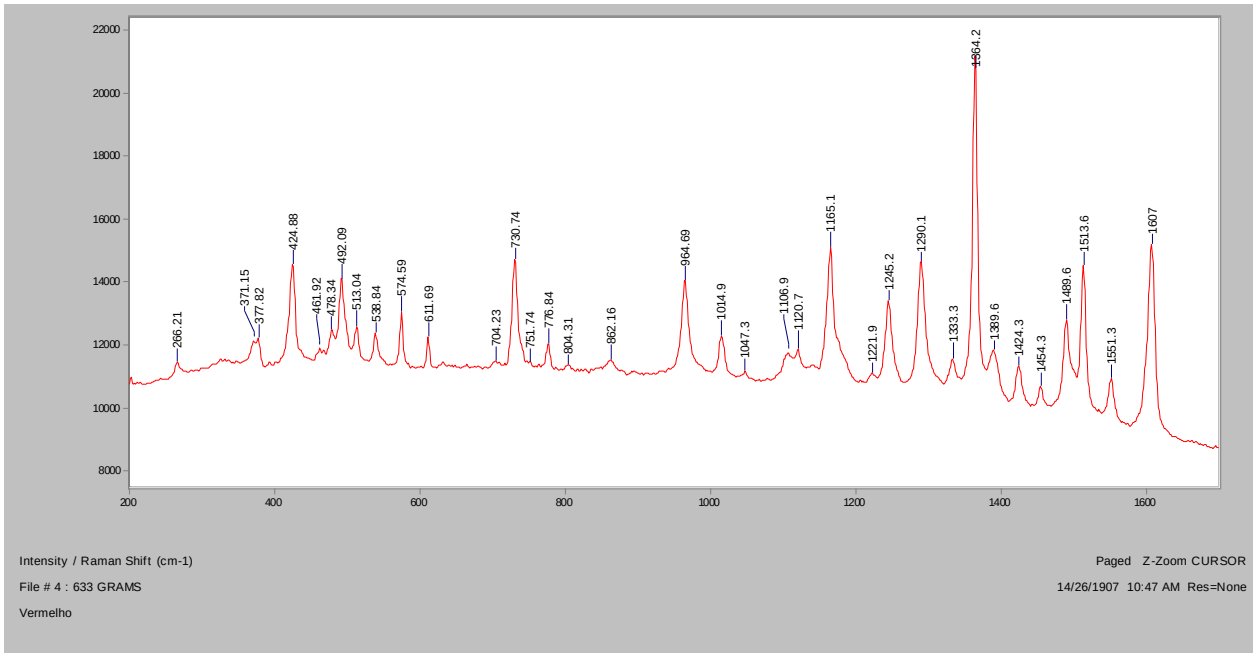

Normal Raman, 785nm

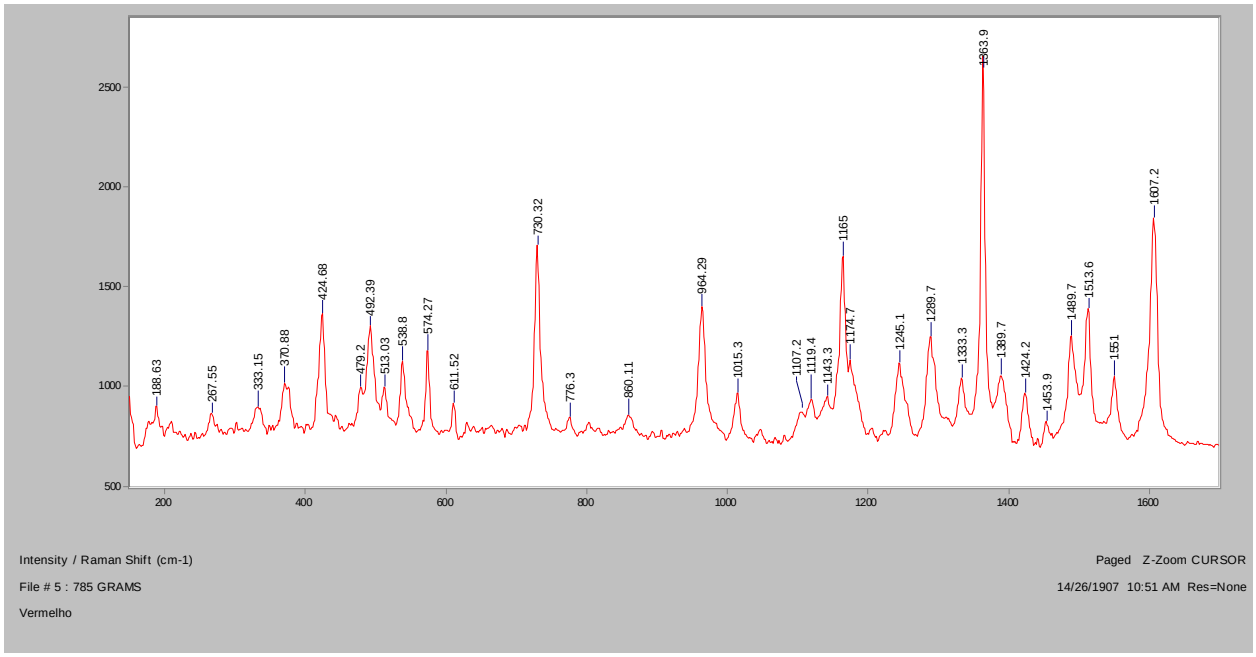

FT-Raman, 1064nm

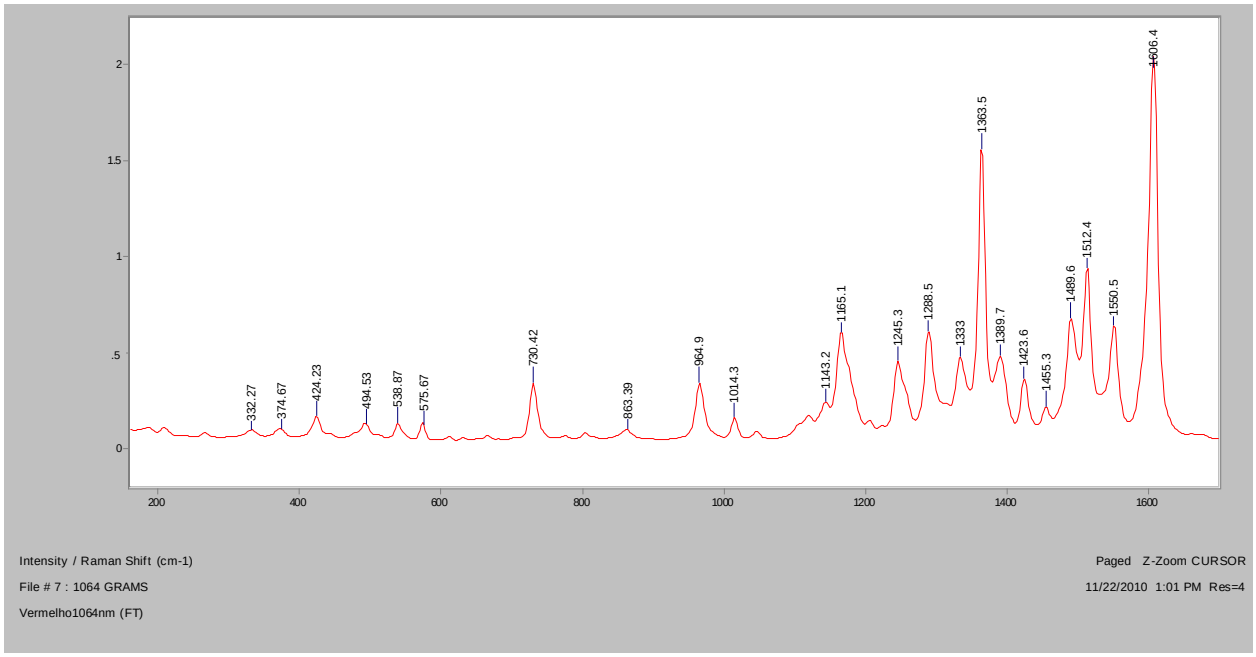

SERS, 488nm

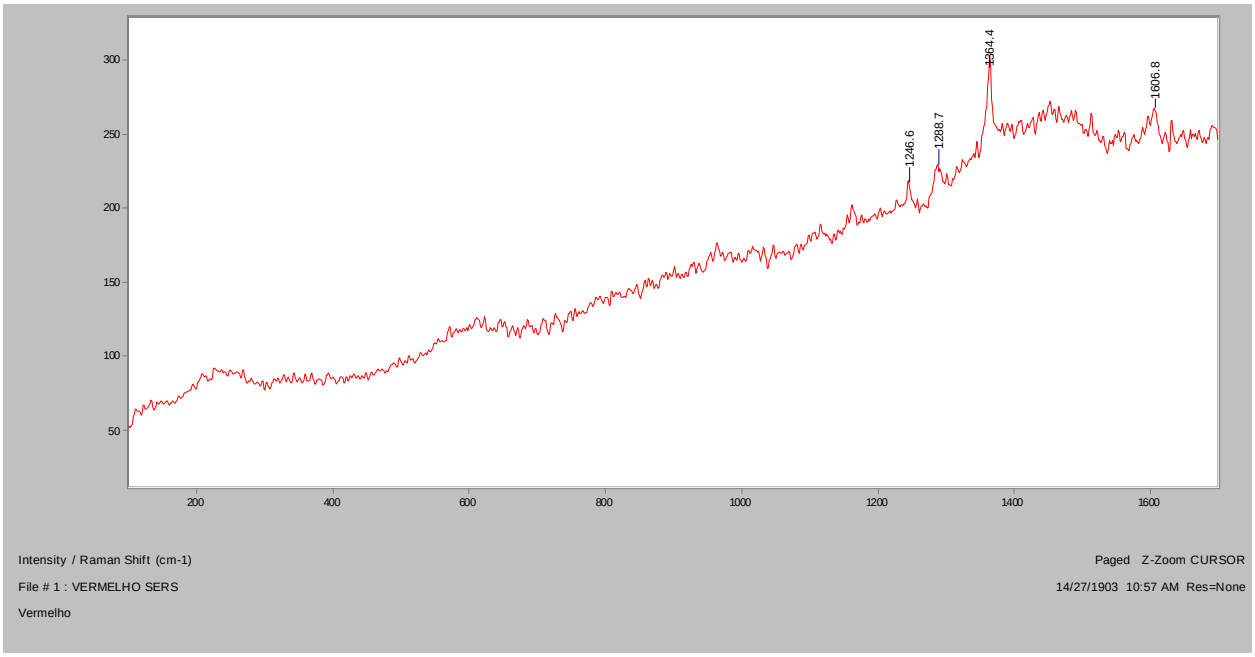

FT-IR (ATR)

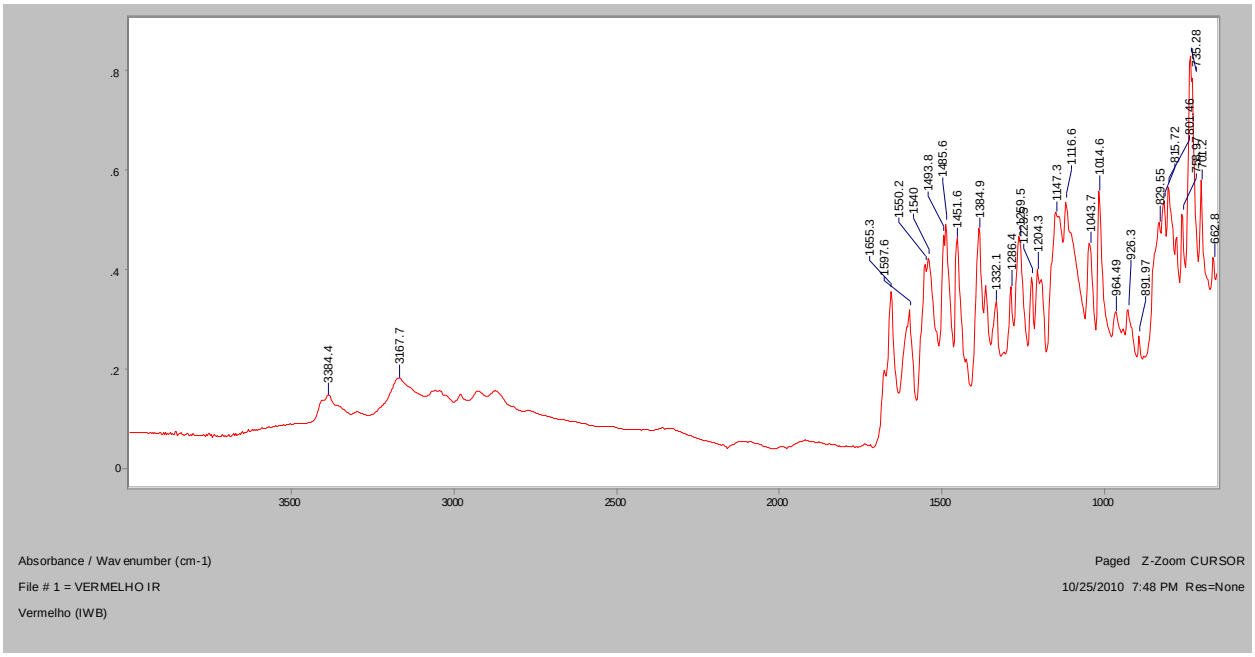

XRF

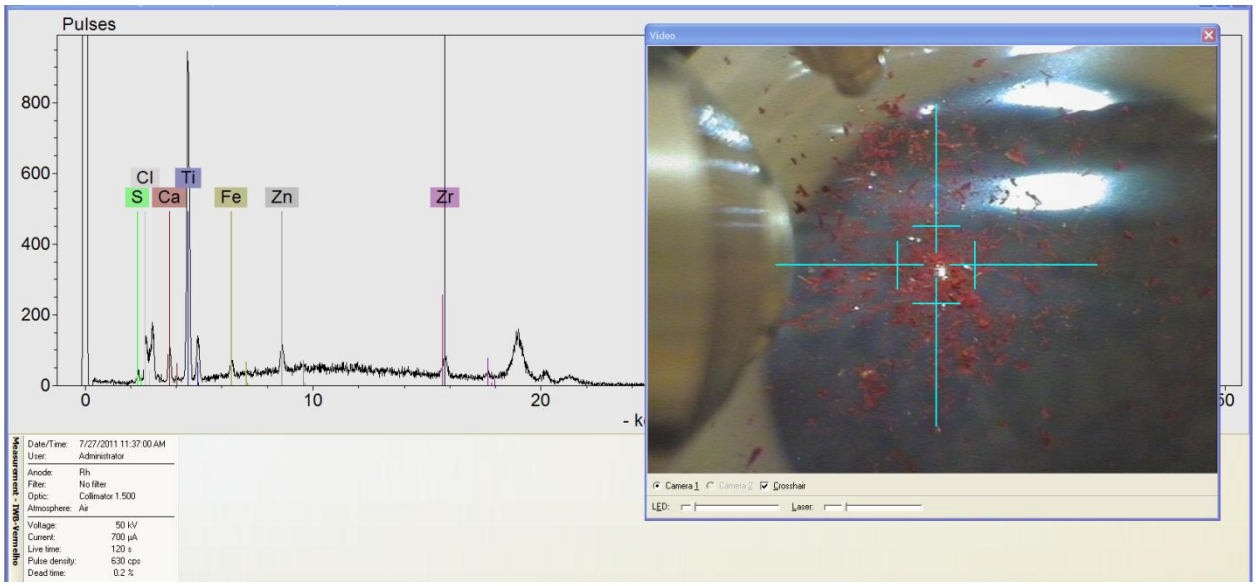
Pulses
800
600
400
200
0
0
10
20
Cl
Ti
S
Ca
Fe
Zn
Zr
Video
Camera 1
Camera 2
Crosshair
LED:
Laser:
Date/Time: 7/27/2011 11:37:00 AM
User: Administrator
Anode: Rh
Filter: No filter
Optic: Collimator 1.500
Atmosphere: Air
Voltage: 50 kV
Current: 700 µA
Live time: 120 s
Pulse density: 630 cps
Dead time: 0.2 %

Pink

Bright Field, 100x

Dark Field, 100x

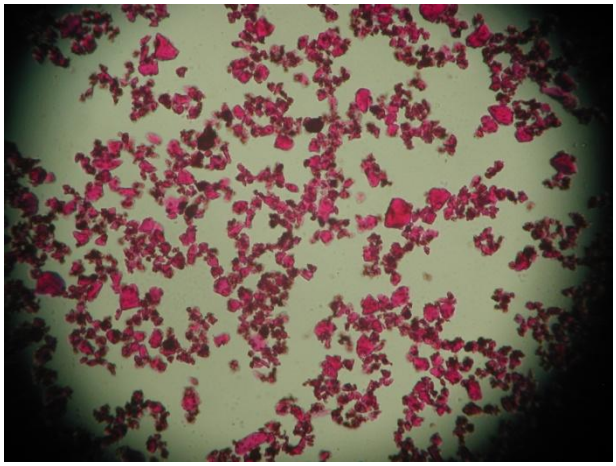

In RI 1.550, 200x

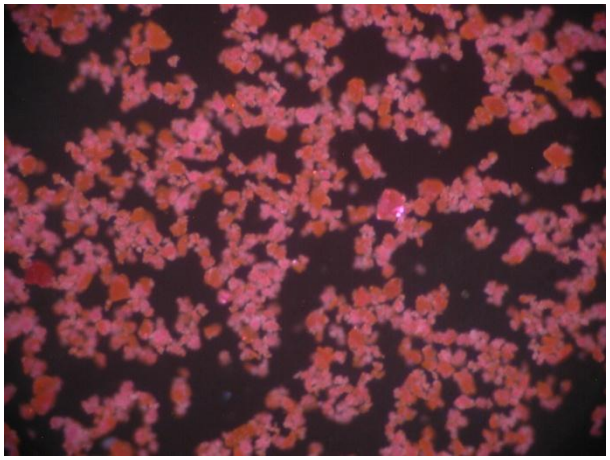

Crossed polars, In RI 1.550, 200x

Normal Raman, 488nm

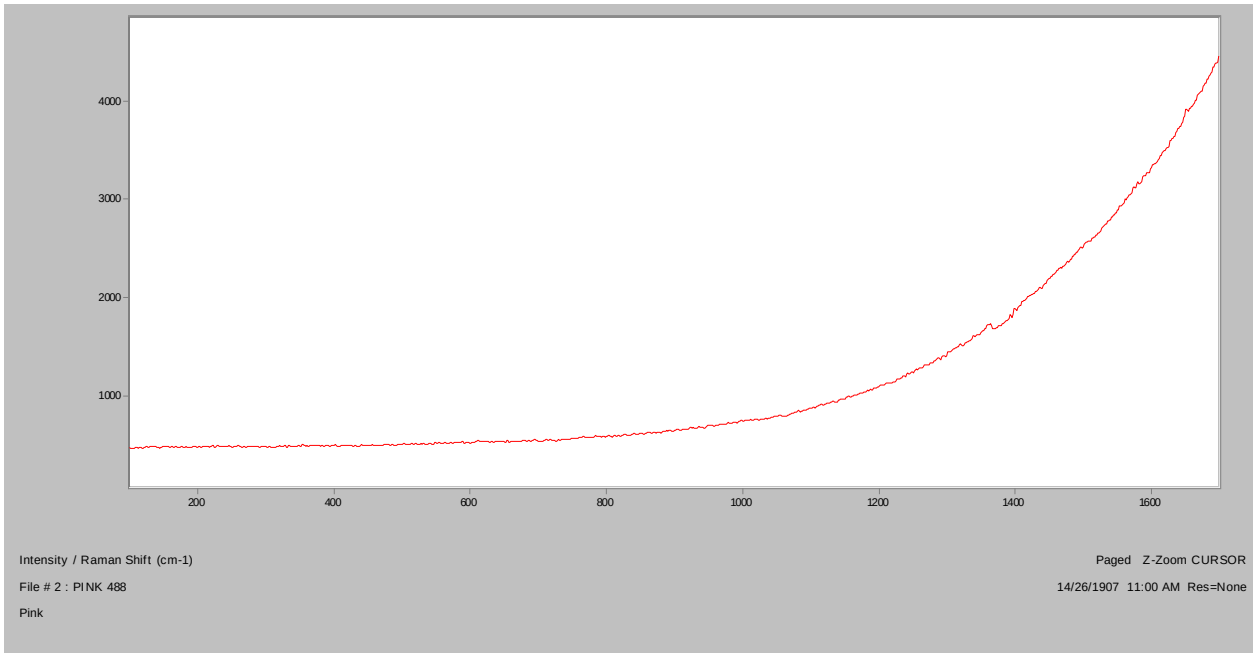

Normal Raman, 633nm

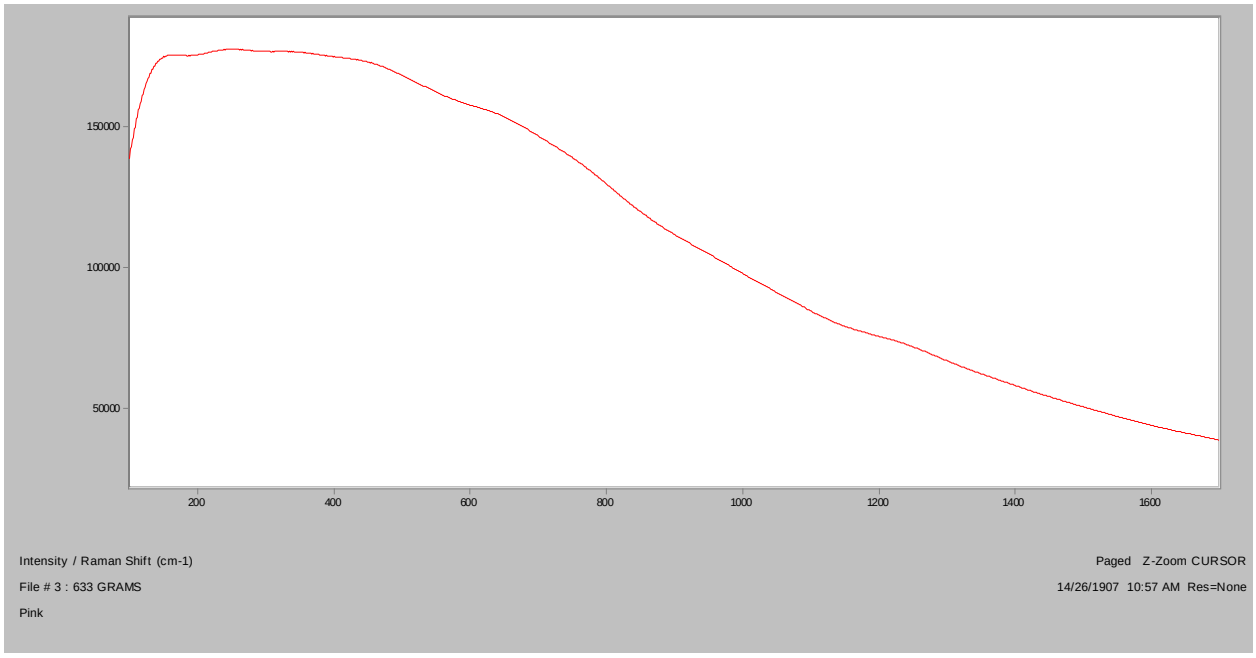

Normal Raman, 785nm

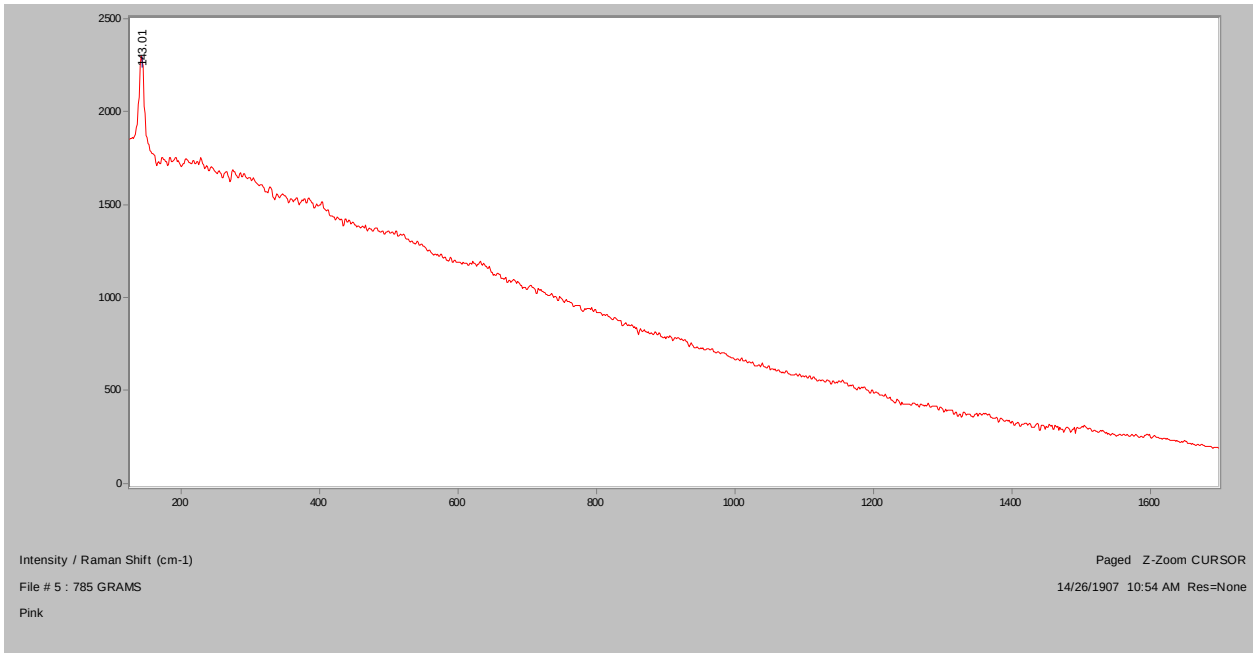

FT-Raman, 1064nm

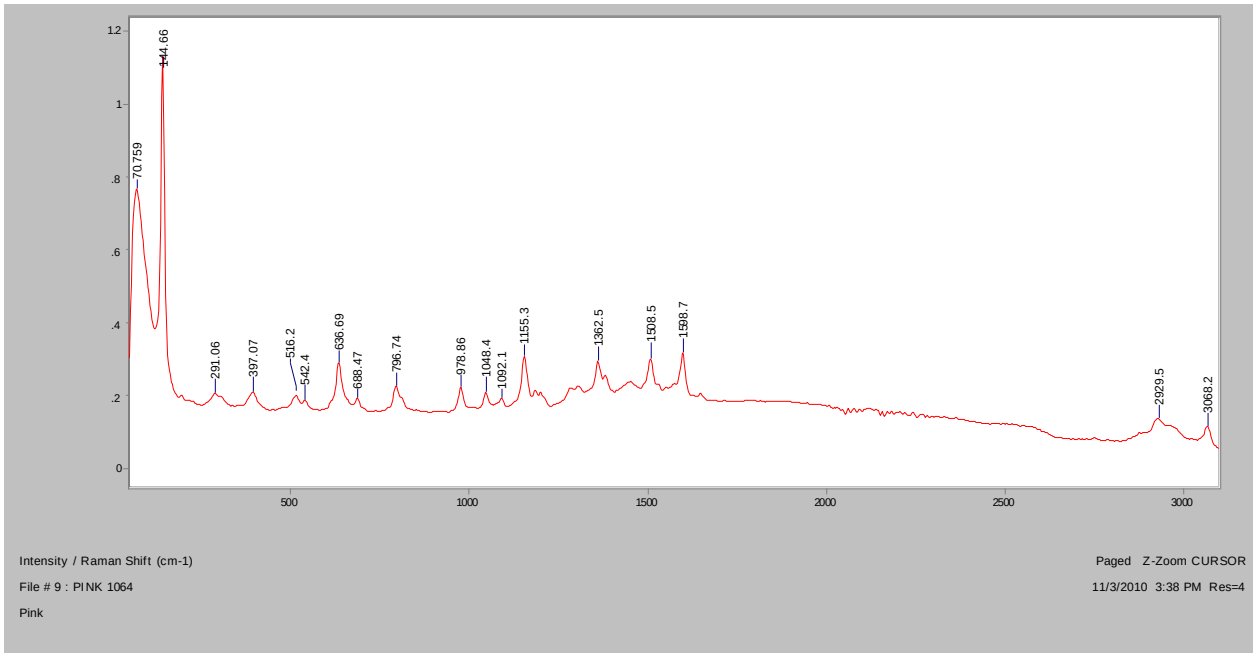

SERS, 488nm

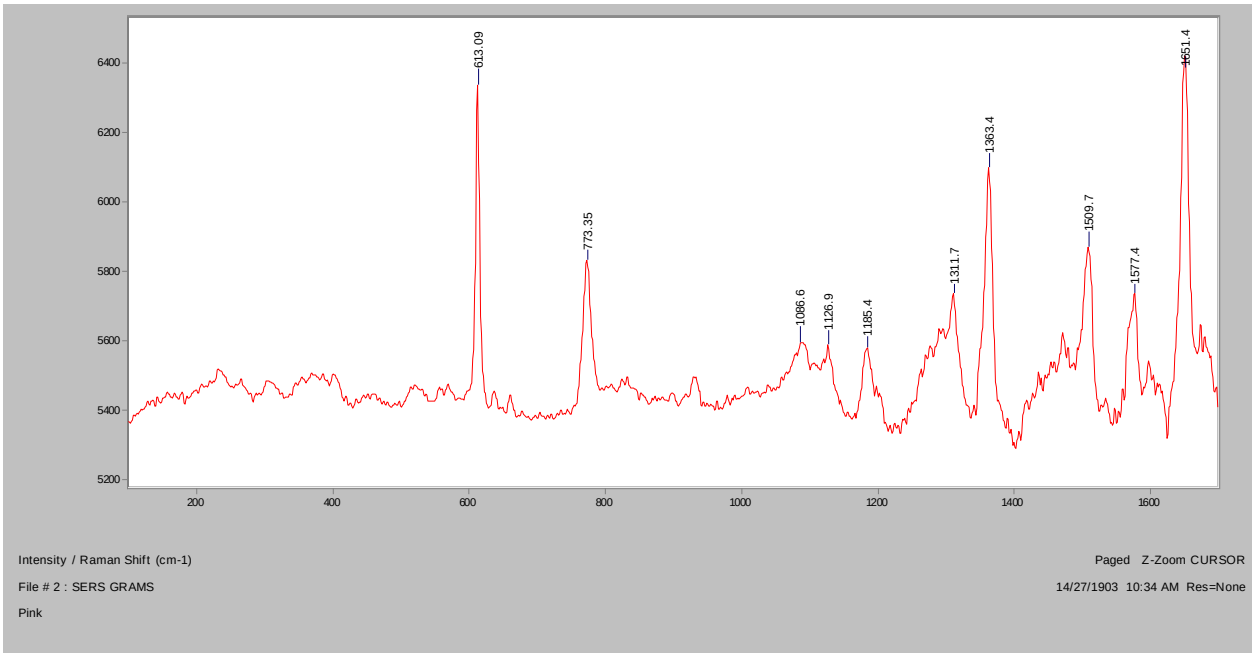

FT-IR (ATR)

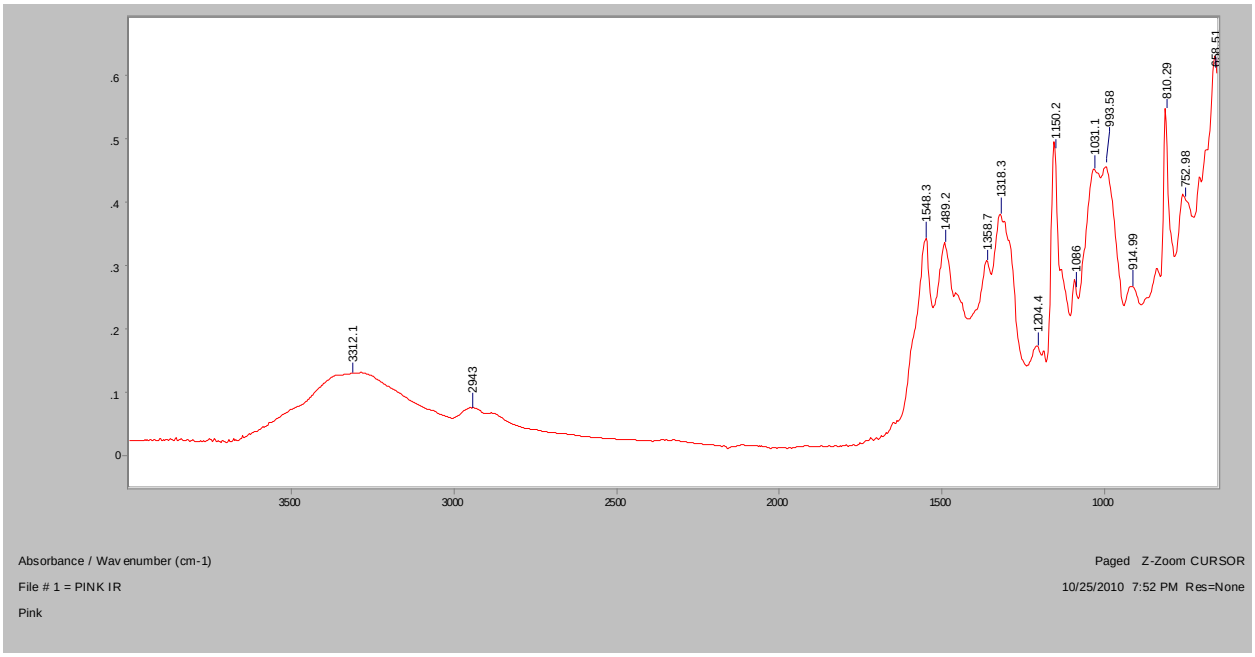

XRF

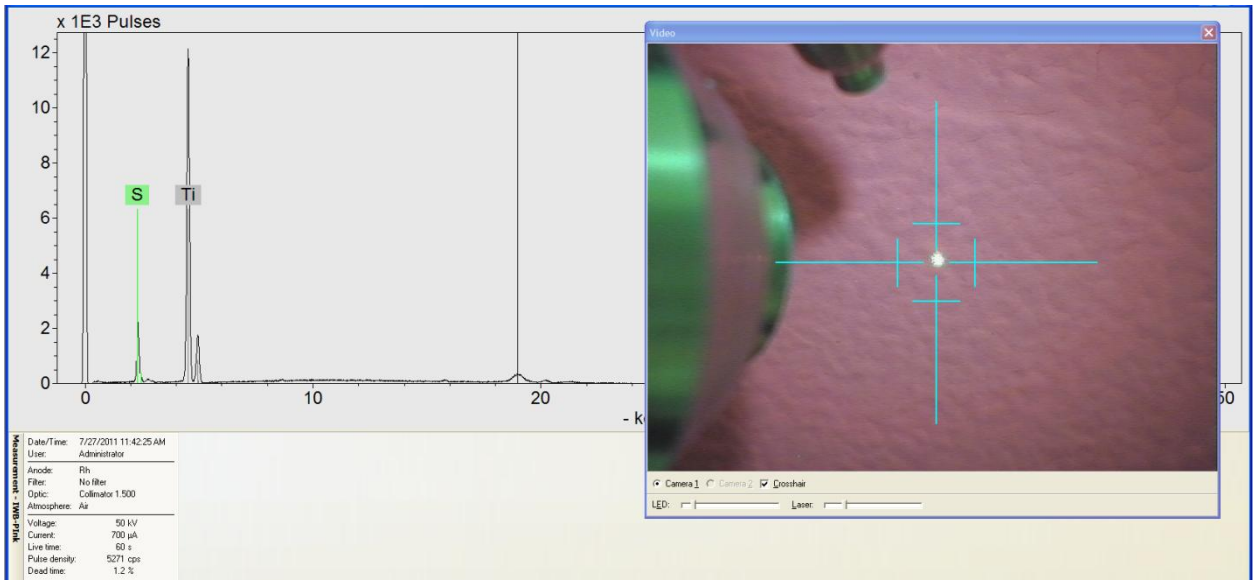
x 1E3 Pulses
12
10
8
6
4
2
0
S
Ti
0
10
20
Video
Camera 1
Camera 2
Crosshair
LED:
Laser:
Measurement - SMB-PHA
Date/Time: 7/27/2011 11:42:25 AM
User: Administrator
Anode: Rh
Filter: No filter
Optic: Collimator 1.500
Atmosphere: Air
Voltage: 50 kV
Current: 700 µA
Live time: 60 s
Pulse density: 5271 cps
Dead time: 1.2 %

Citrus

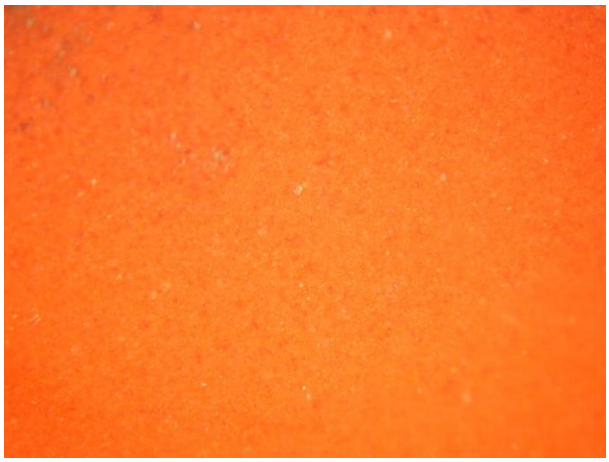

Bright Field, 100x

Dark Field, 400x

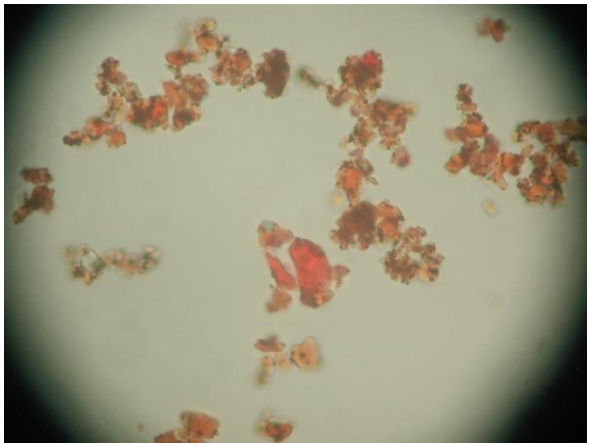

In RI 1.550, 400x

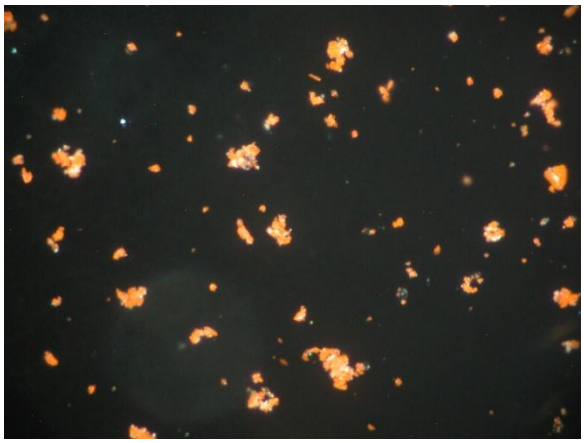

Crossed polars, In RI 1.550, 200x

Normal Raman, 488nm

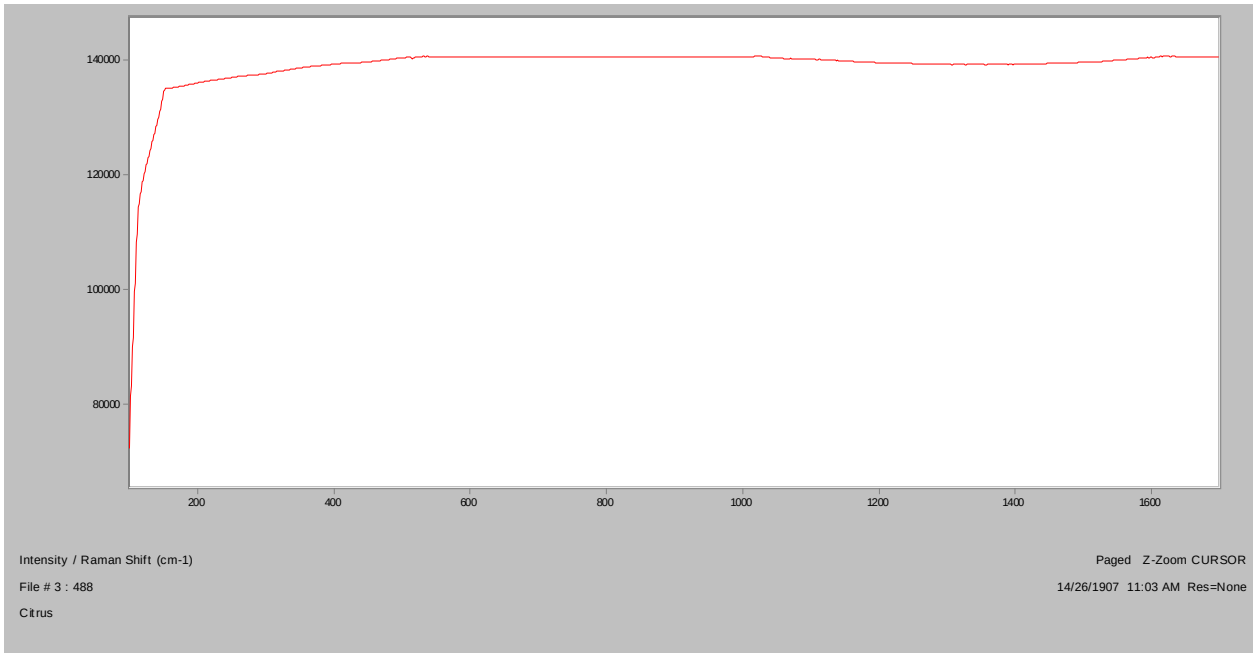

Normal Raman, 633nm

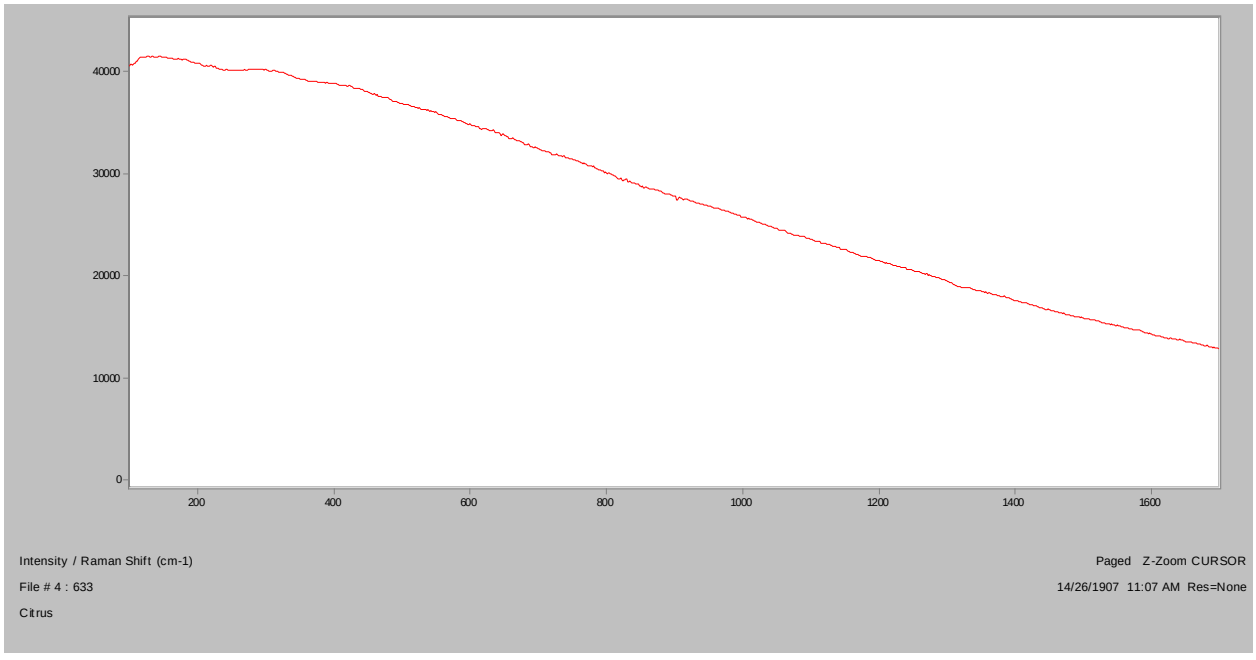

Normal Raman, 785nm

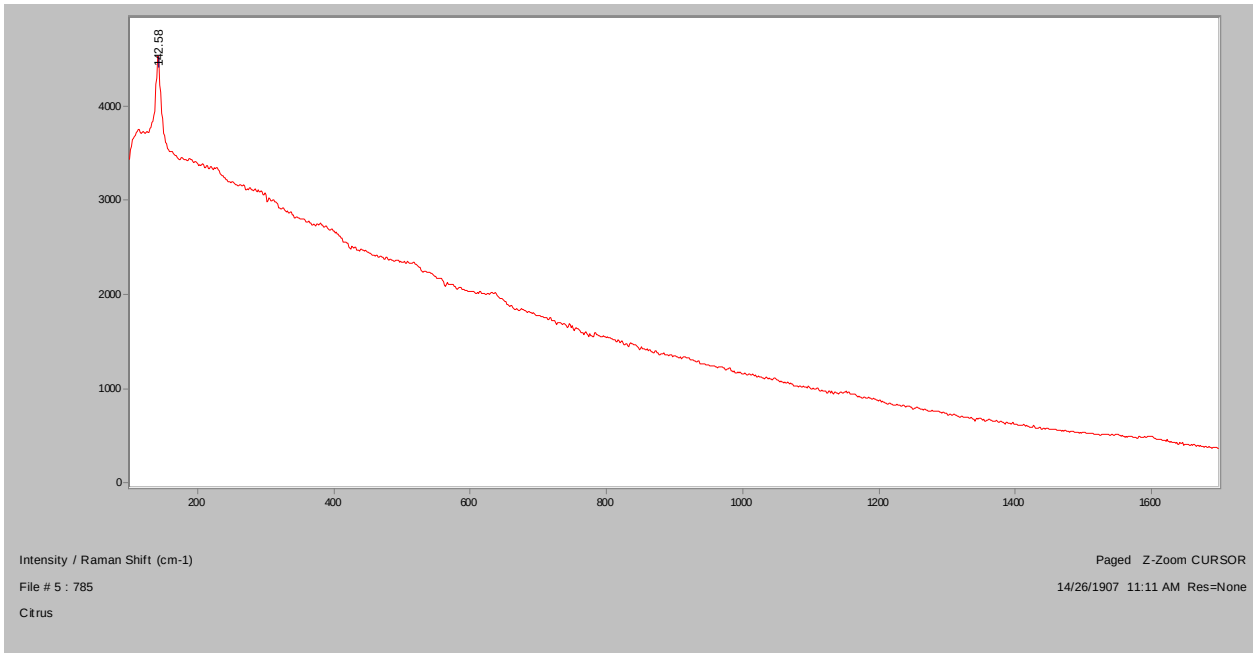

FT-Raman, 1064nm

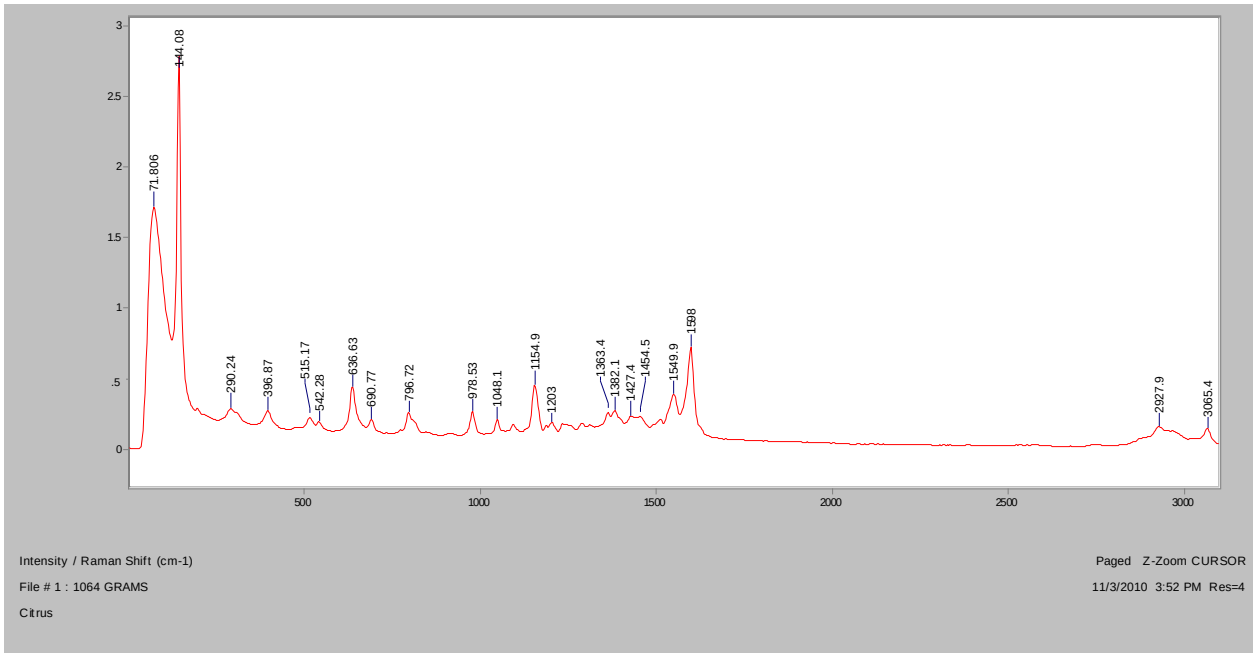

FT-IR (ATR)

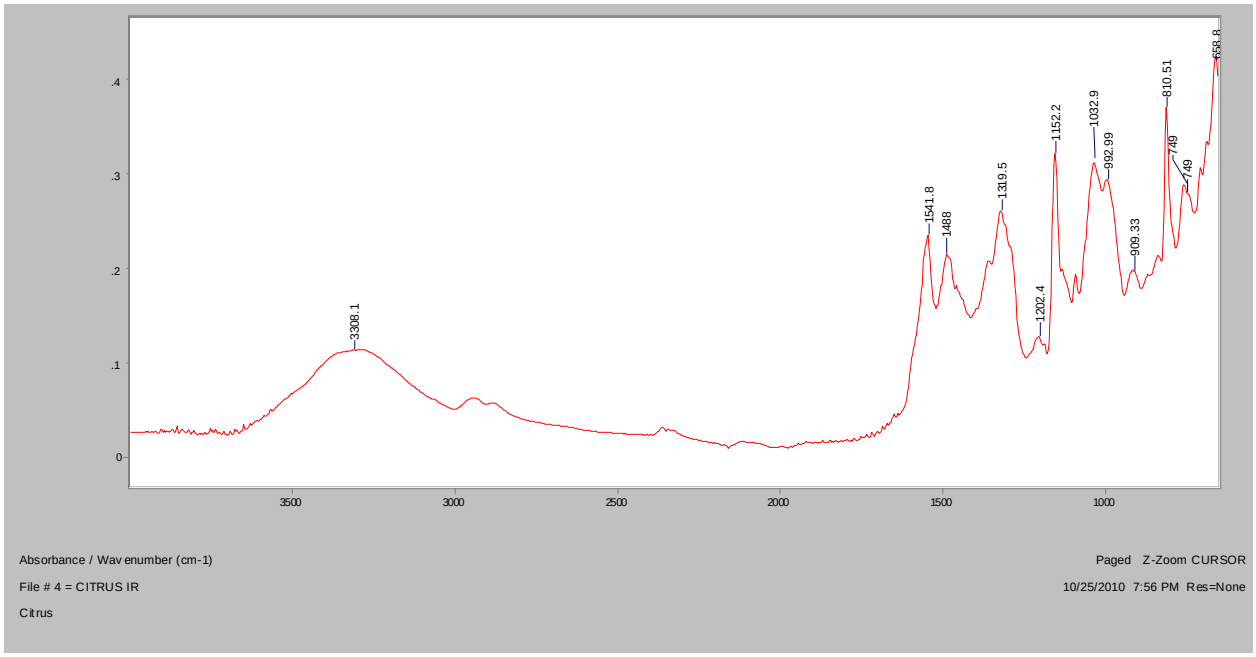
3306.1
1541.8
1488
1319.5
1202.4
1152.2
1032.9
992.99
909.33
810.51
749
749
668.8
.4
.3
.2
.1
0
3500
3000
2500
2000
1500
1000
Absorbance / Wavenumber (cm-1)
File # 4 = CITRUS IR
Citrus
Paged Z-Zoom CURSOR
10/25/2010 7:56 PM Res=None

XRF

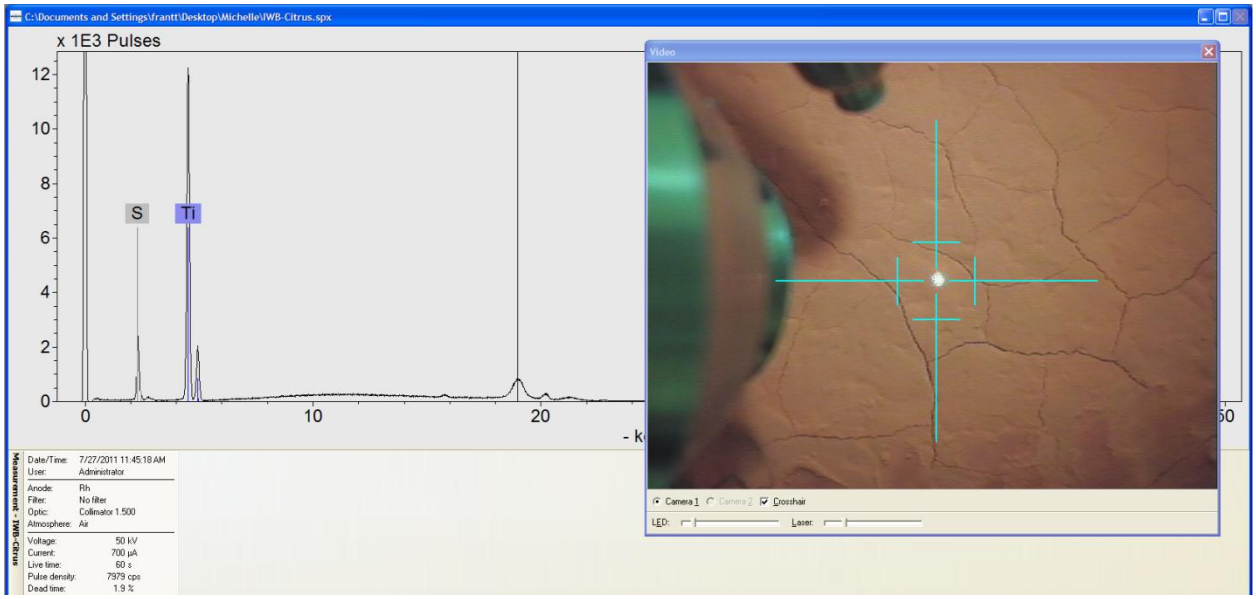
C:\Documents and Settings\frantt\Desktop\Michelle\IWB-Citrus.spx
x 1E3 Pulses
S
Ti
Video
Camera 1
Crosshair
LED:
Laser:
Date/Time: 7/27/2011 11:45:18 AM
User: Administrator
Anode: Rh
Filter: No filter
Optic: Collimator 1.500
Atmosphere: Air
Voltage: 50 kV
Current: 700 µA
Live time: 60 s
Pulse density: 7979 cps
Dead time: 1.9 %

Amarelo Canario

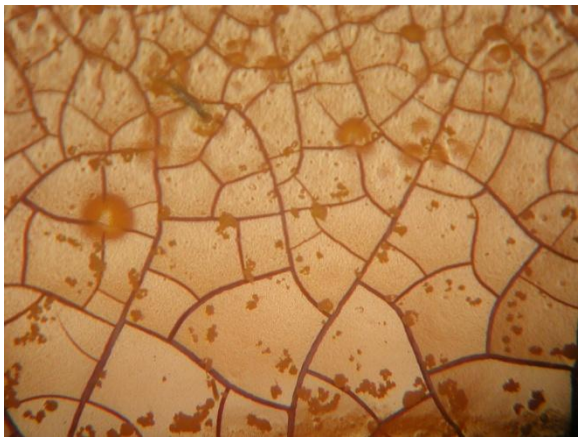

Bright Field, 100x

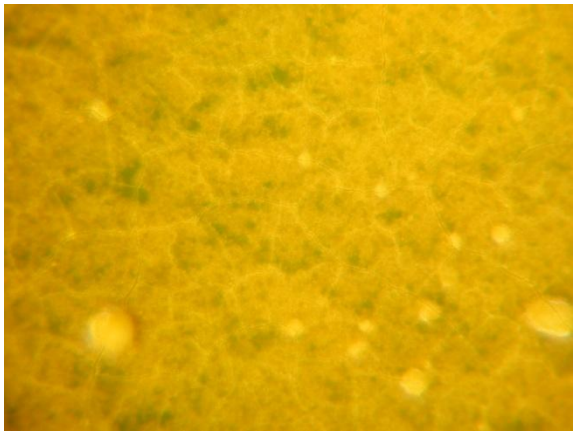

Dark Field, 400x

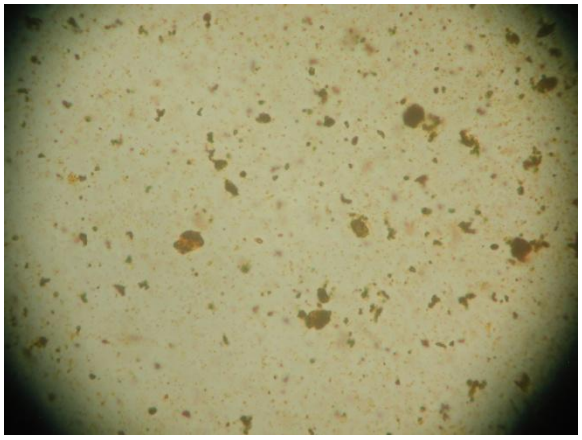

In RI 1.550, 400x

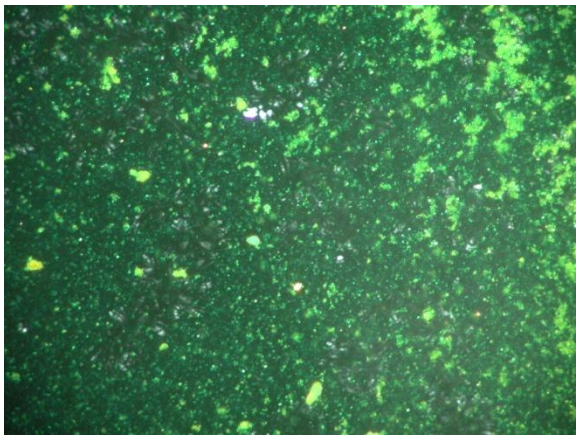

Crossed polars, In RI 1.550, 200x

Normal Raman, 488nm

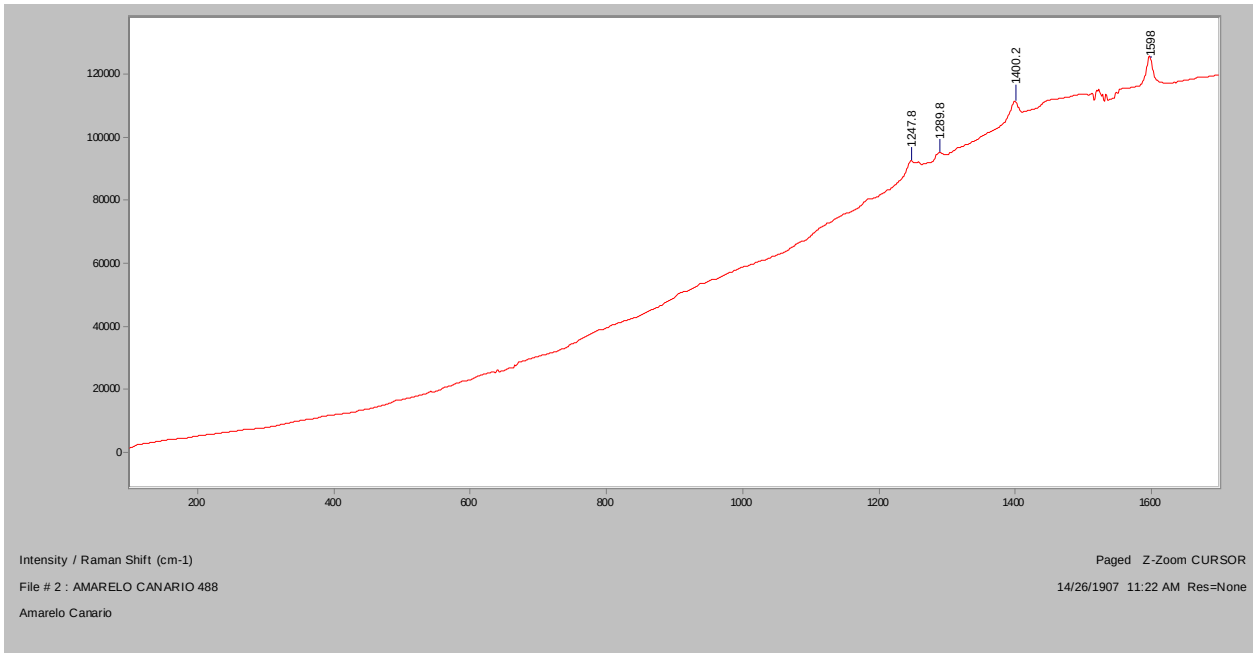

Normal Raman, 633nm

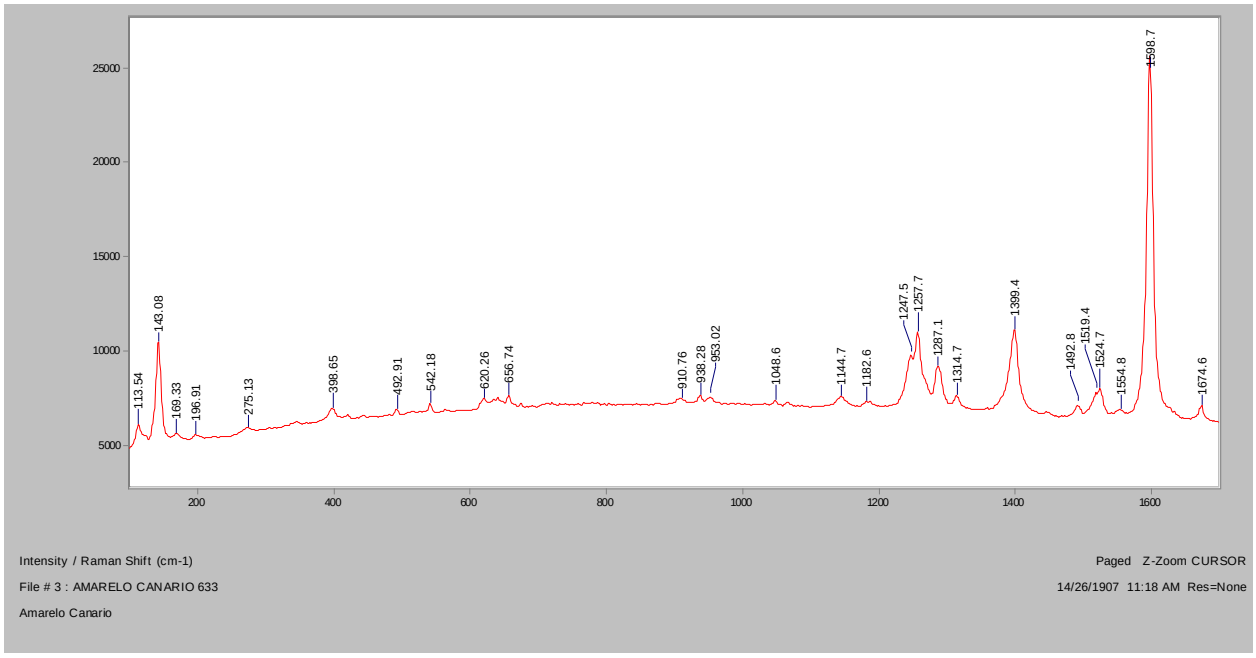

Normal Raman, 785nm

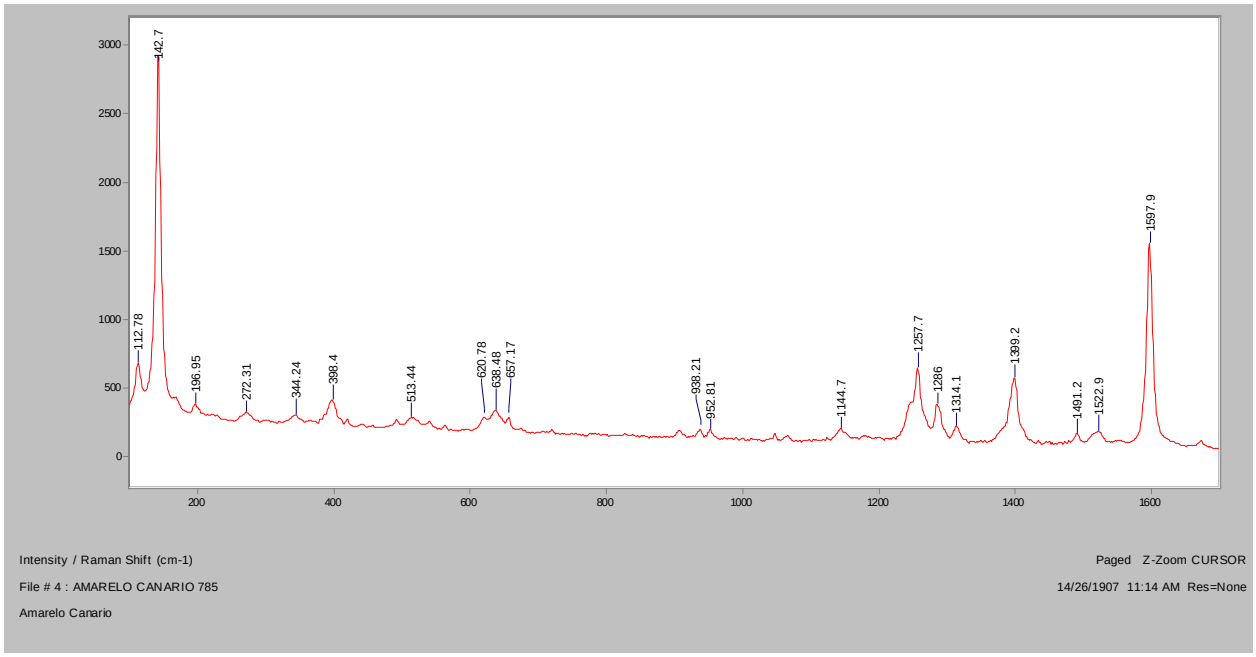

FT-Raman, 1064nm

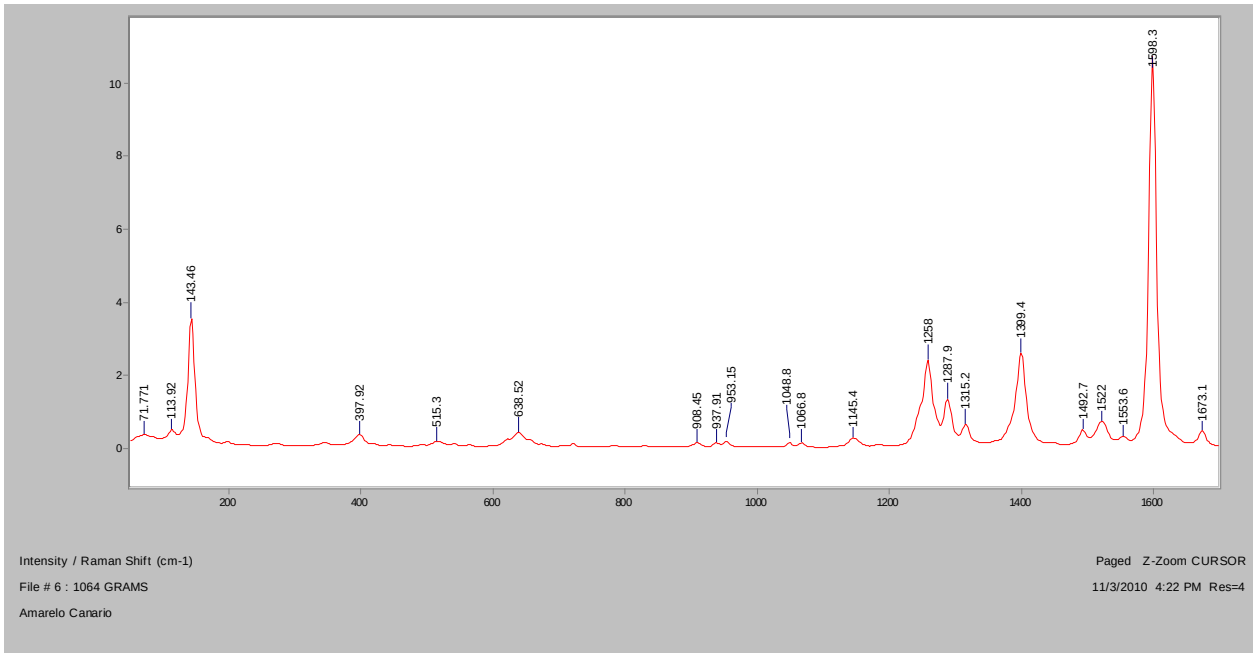

SERS, 488nm

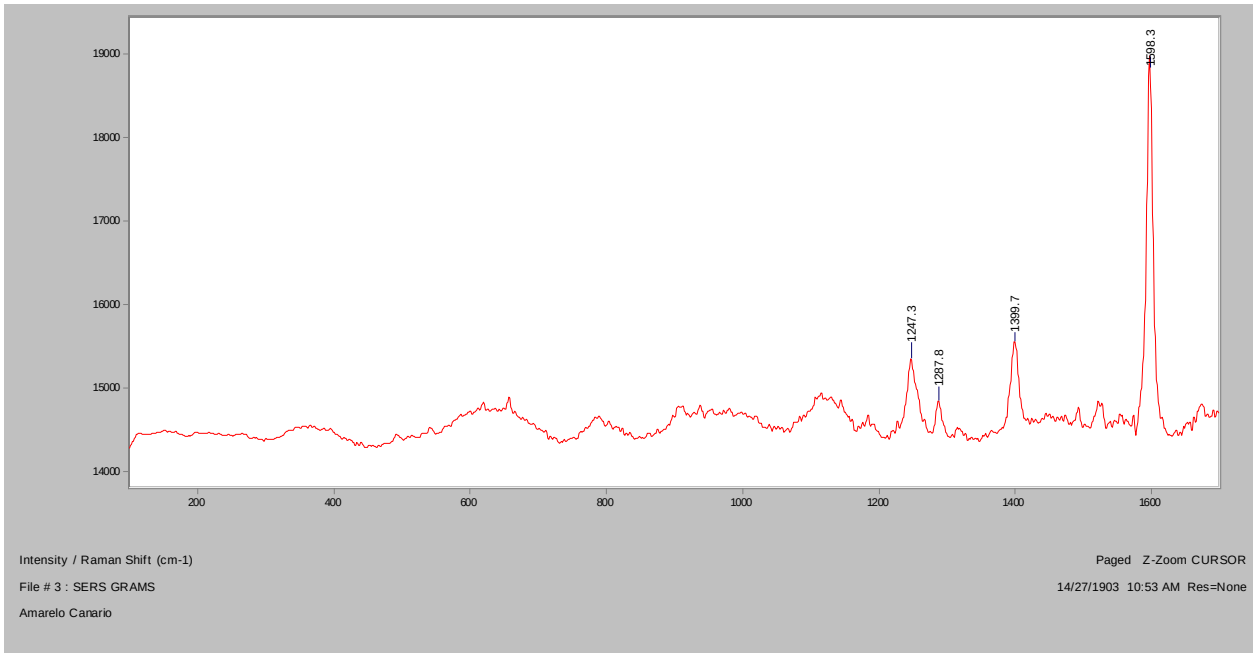

FT-IR (ATR)

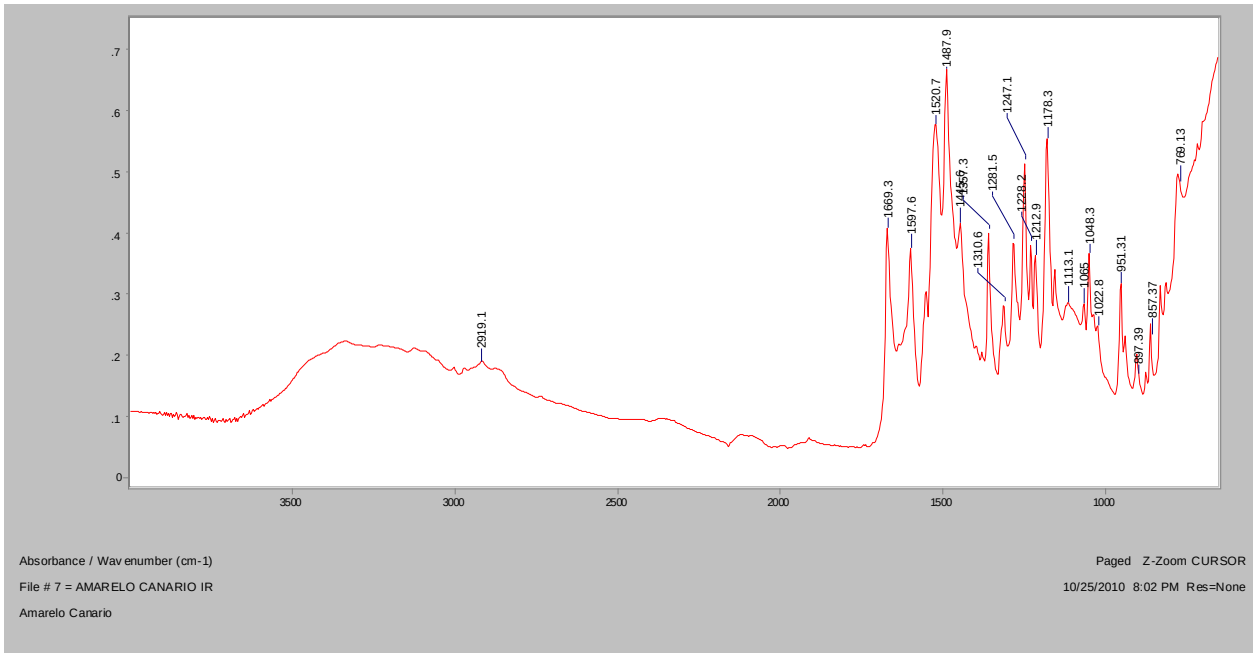

XRF

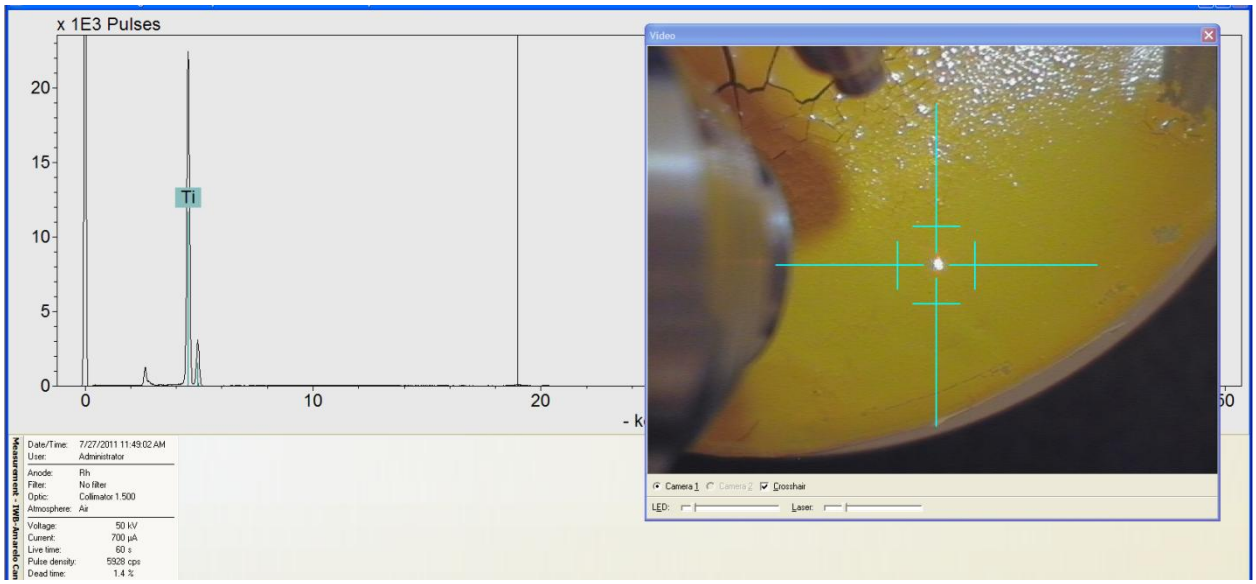
x 1E3 Pulses
20
15
10
5
0
Ti
0
10
20
Video
Camera 1
Crosshair
LED:
Laser:
Date/Time: 7/27/2011 11:49:02 AM
User: Administrator
Anode: Rh
Filter: No filter
Optic: Collimator 1.500
Atmosphere: Air
Voltage: 50 kV
Current: 700 µA
Live time: 60 s
Pulse density: 5928 cps
Dead time: 1.4 %

Amarelo Fluor

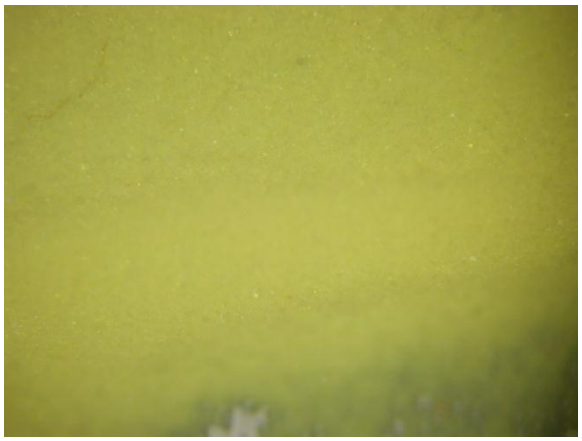

Bright Field, 100x

Dark Field, 100x

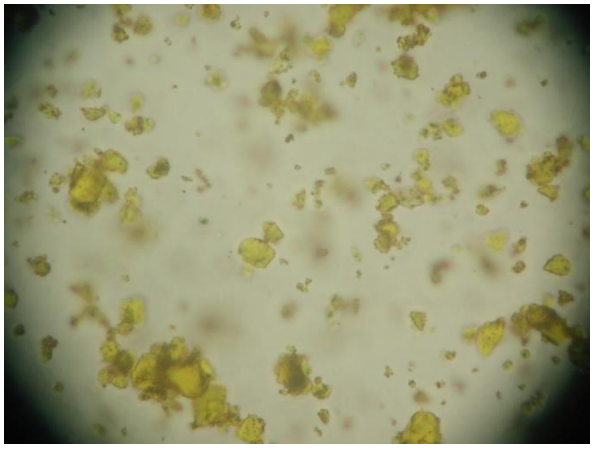

In RI 1.550, 400x

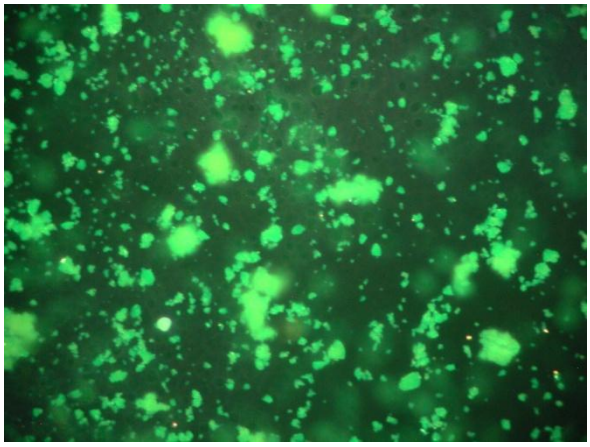

Crossed polars, In RI 1.550, 200x

Normal Raman, 488nm

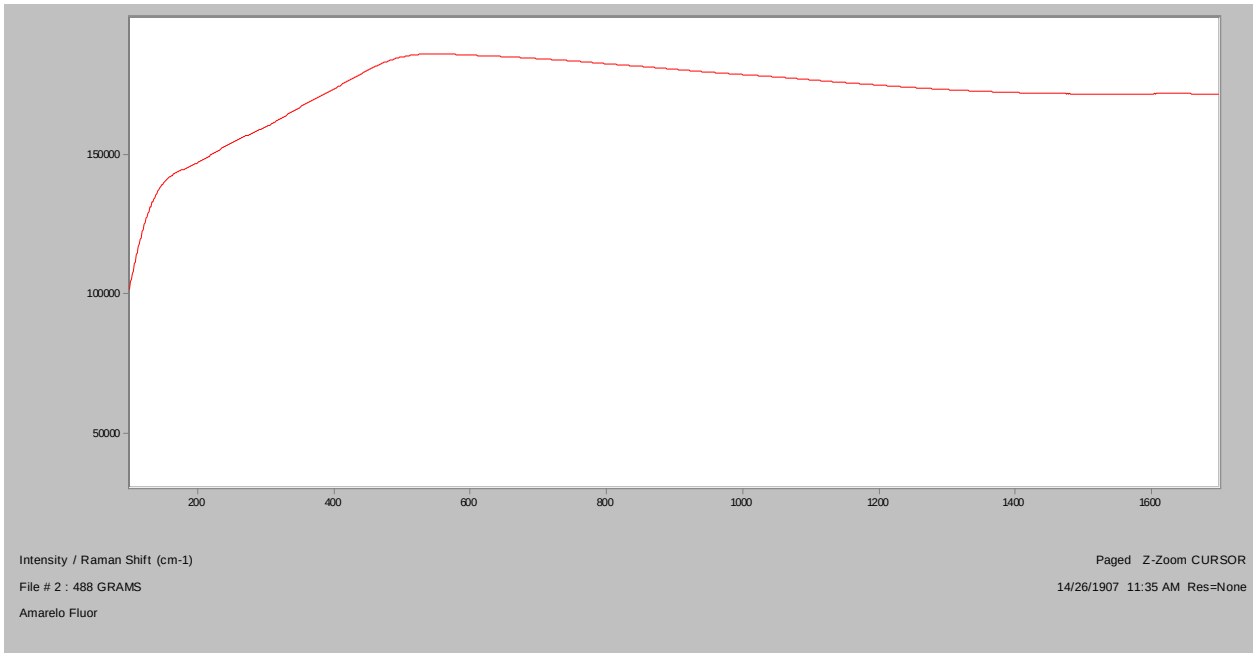

Normal Raman, 633nm

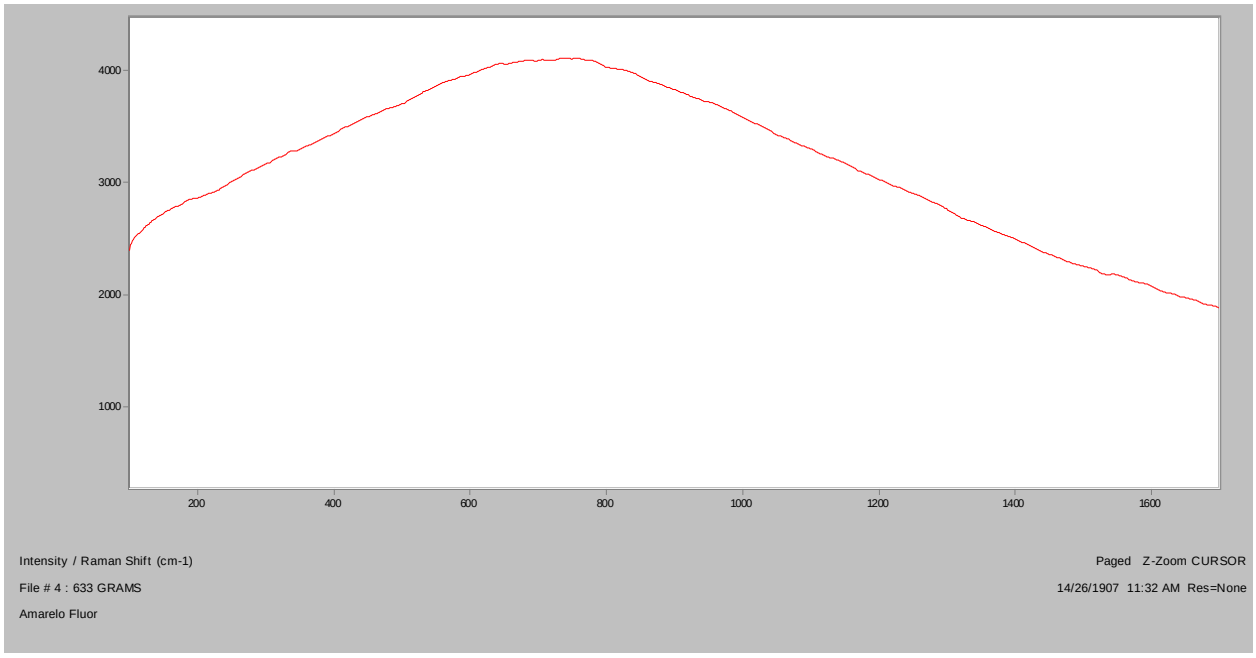

Normal Raman, 785nm

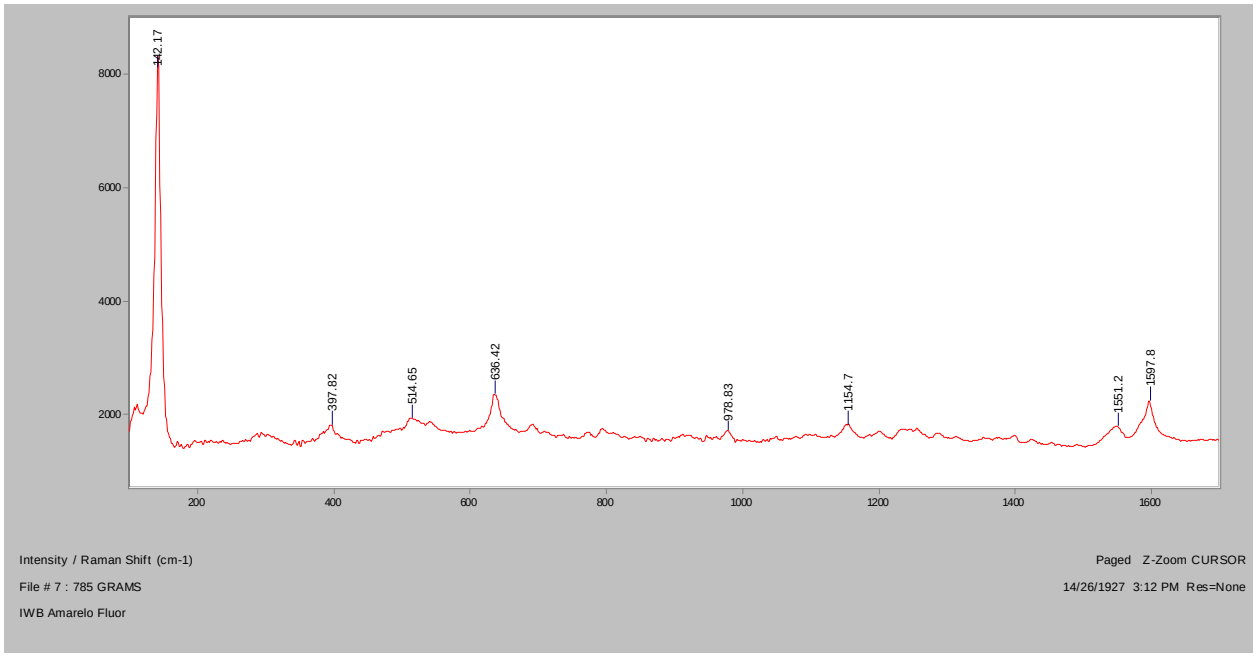

FT-Raman, 1064nm

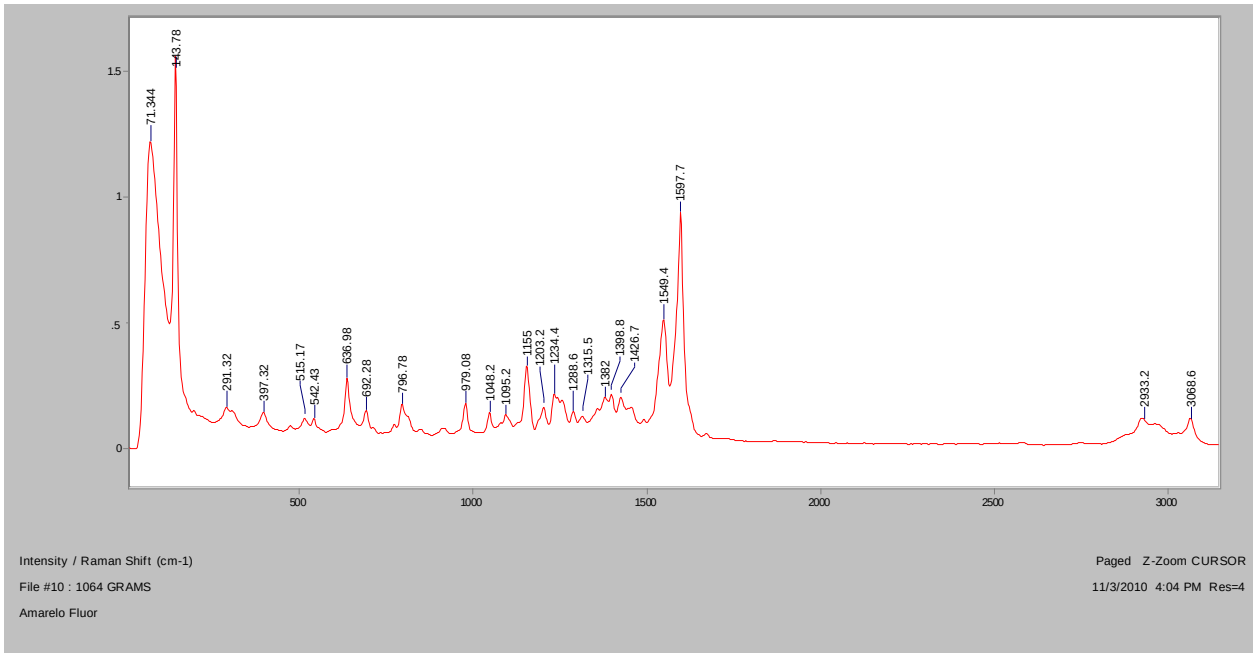

FT-IR (ATR)

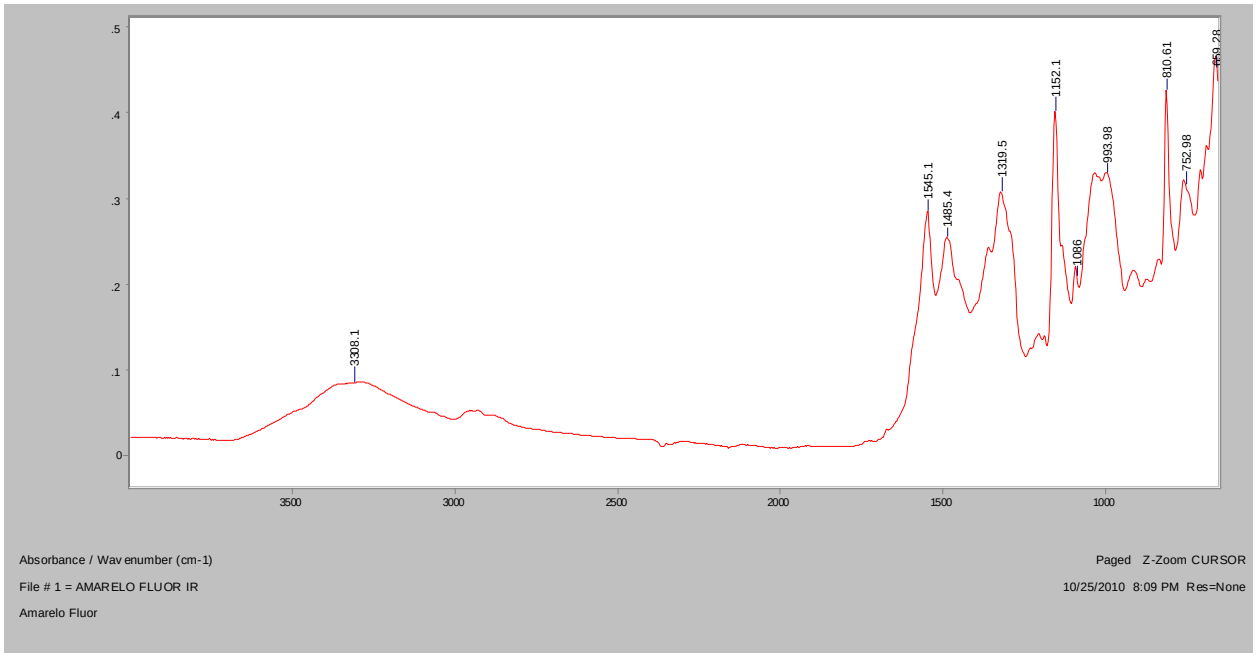
.5
.4
.3
.2
.1
0
3308.1
1545.1
1485.4
1319.5
1152.1
1086
993.98
752.98
610.61
469.28
3500
3000
2500
2000
1500
1000
Absorbance / Wavenumber (cm-1)
File # 1 = AMARELO FLUOR IR
Amarelo Fluor
Paged Z-Zoom CURSOR
10/25/2010 8:09 PM Res=None

XRF

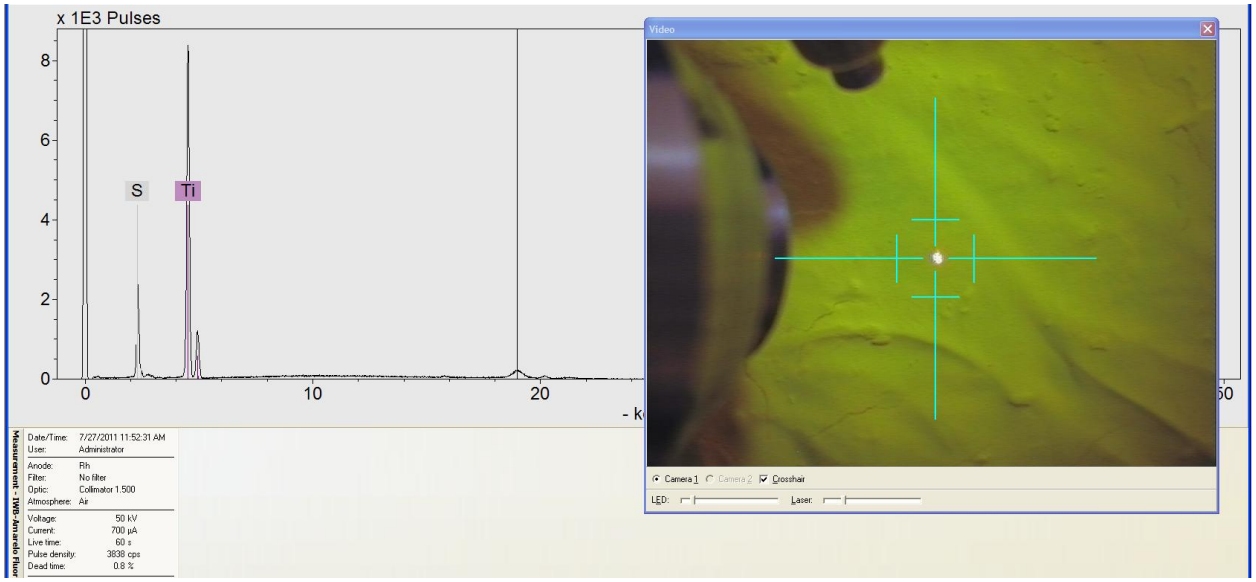
x 1E3 Pulses
8
6
4
2
0
S
Ti
0
10
20
Video
Camera 1
Camera 2
Crosshair
LED:
Laser:
Date/Time: 7/27/2011 11:52:31 AM
User: Administrator
Anode: Rh
Filter: No filter
Optic: Collimator 1.500
Atmosphere: Air
Voltage: 50 kV
Current: 700 µA
Live time: 60 s
Pulse density: 3838 cps
Dead time: 0.8 %

Verde Claro

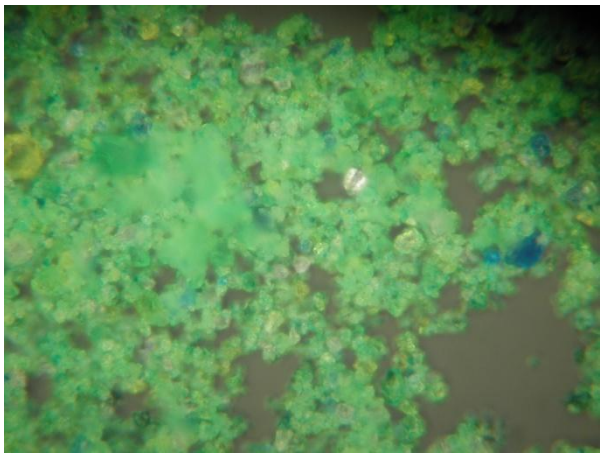

Bright Field, 400x

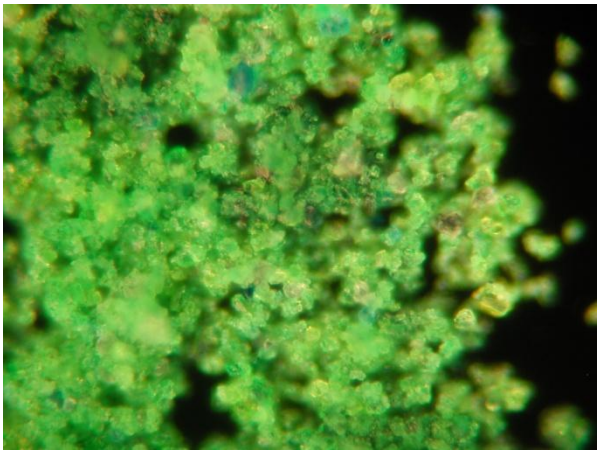

Dark Field, 400x

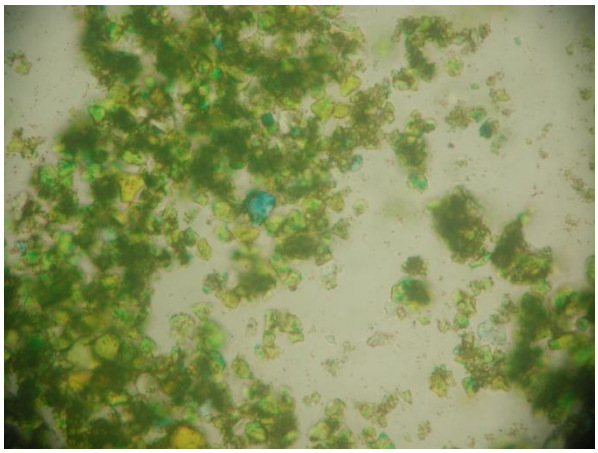

In RI 1.550, 400x

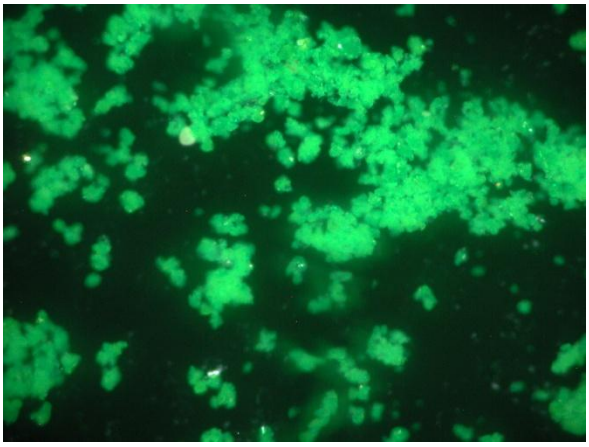

Crossed polars, In RI 1.550, 200x

Normal Raman, 488nm

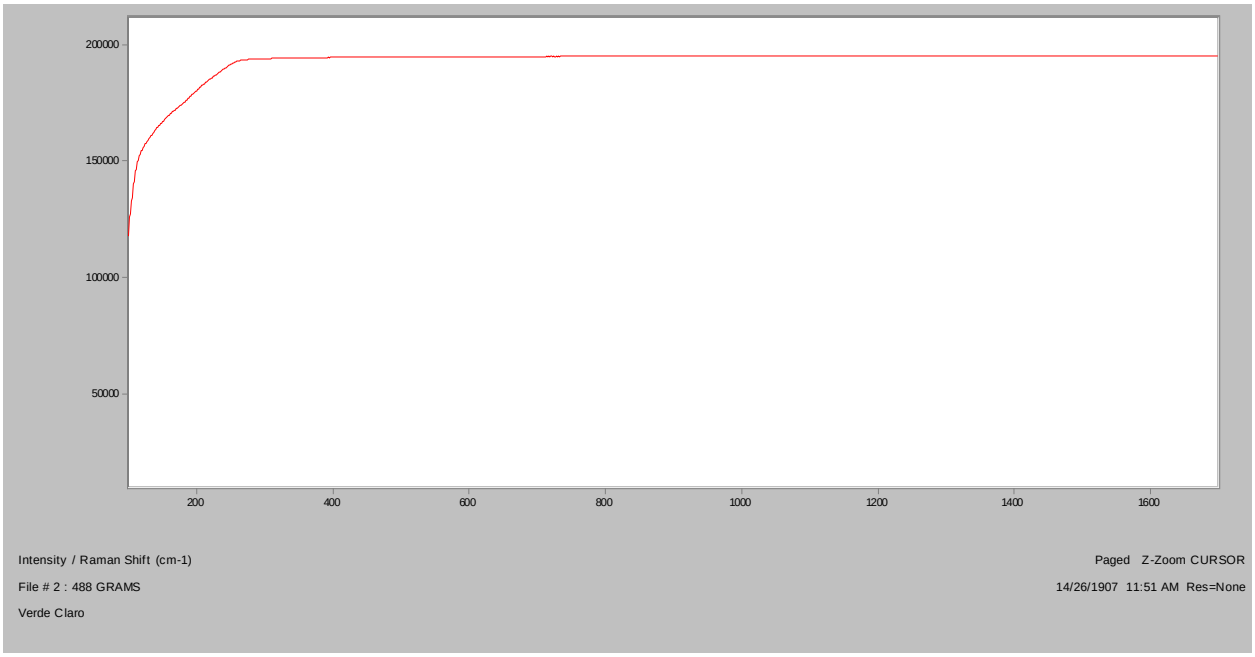

Normal Raman, 633nm

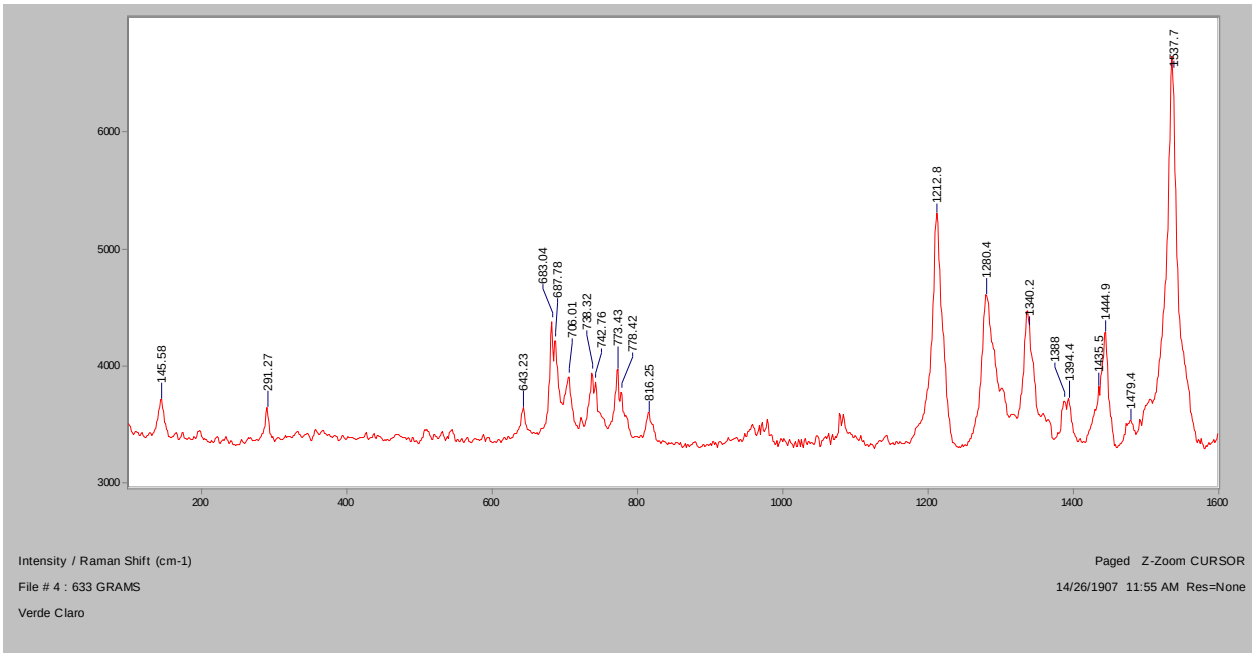

Normal Raman, 785nm

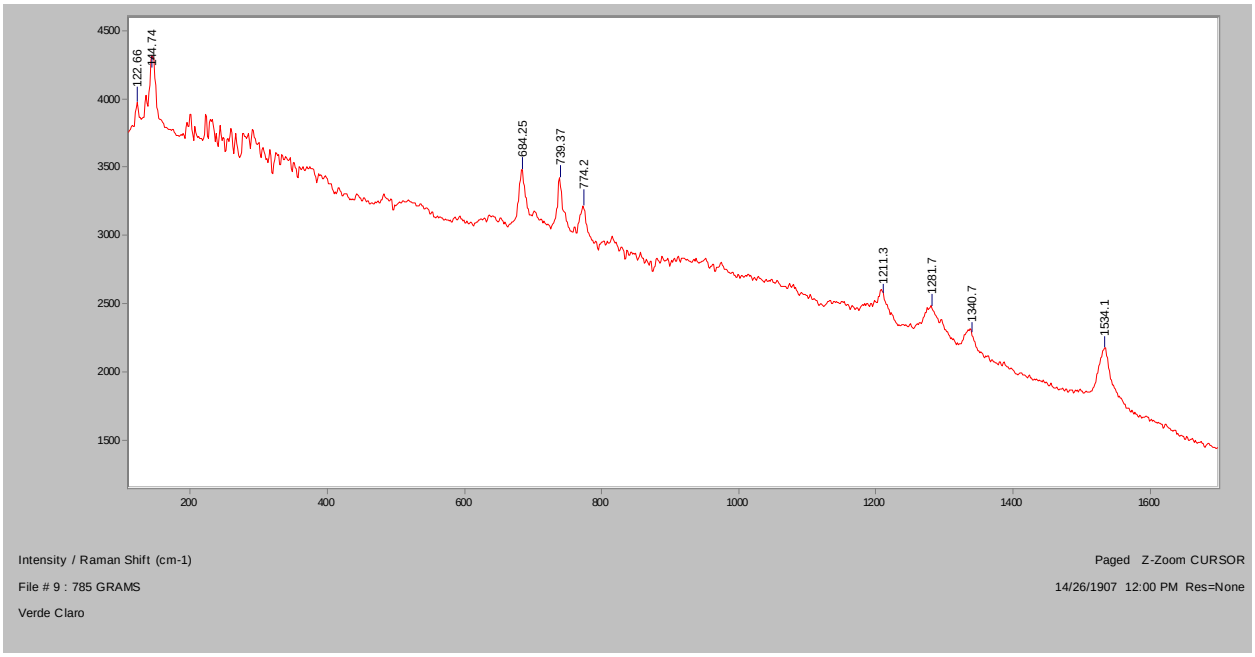

FT-Raman, 1064nm

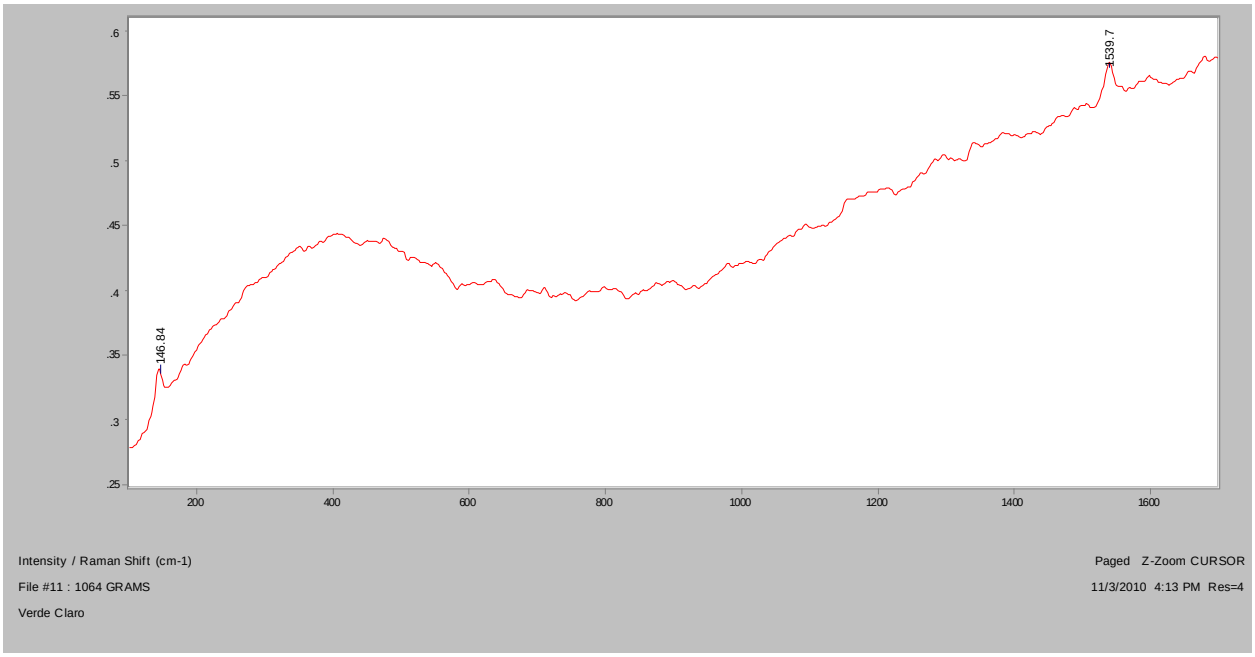

FT-IR (ATR)

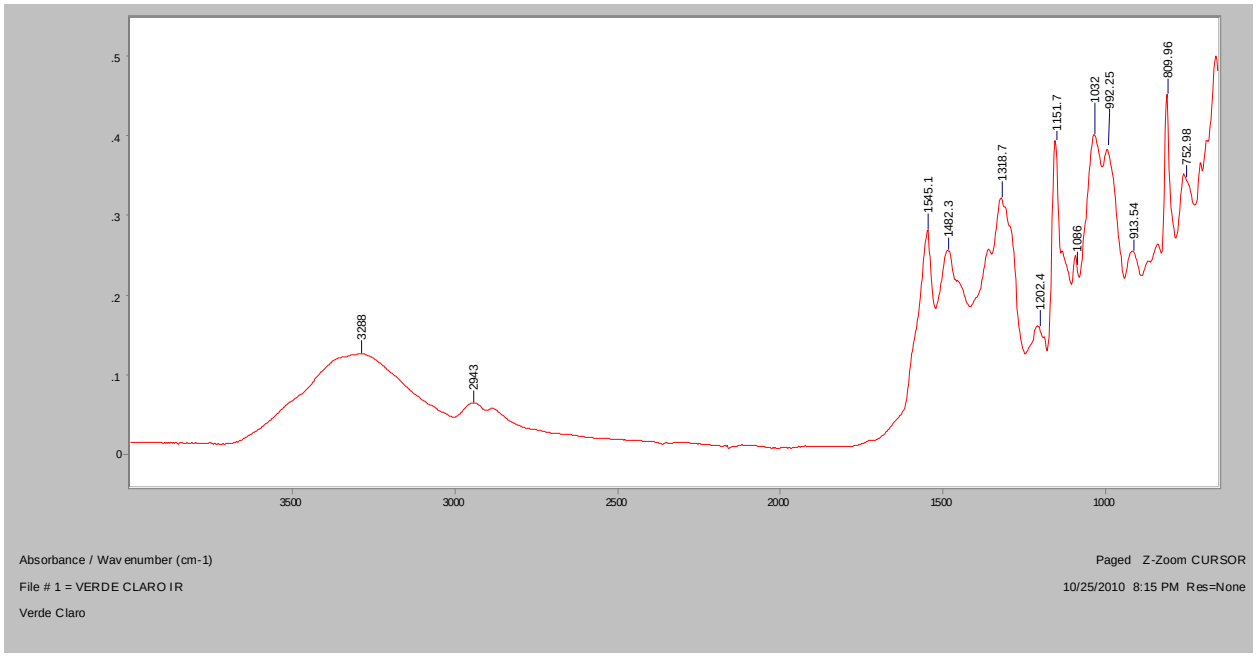
.5
.4
.3
.2
.1
0
3288
2943
1545.1
1482.3
1318.7
1202.4
1151.7
1086
1032
992.25
913.54
809.96
752.98
3500
3000
2500
2000
1500
1000
Absorbance / Wavenumber (cm-1)
File # 1 = VERDE CLARO IR
Verde Claro
Paged Z-Zoom CURSOR
10/25/2010 8:15 PM Res=None

XRF

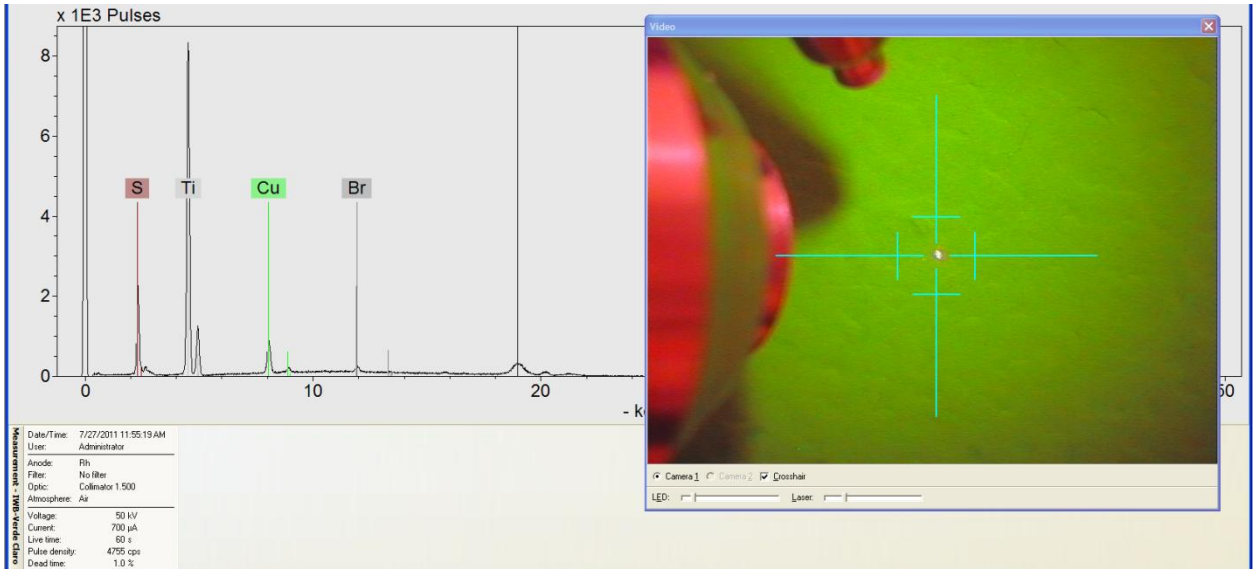
x 1E3 Pulses
8
6
4
2
0
S
Ti
Cu
Br
0
10
20
Video
Camera 1
Camera 2
Crosshair
LED:
Laser:
Date/Time: 7/27/2011 11:55:19 AM
User: Administrator
Anode: Rh
Filter: No filter
Optic: Collimator 1.500
Atmosphere: Air
Voltage: 50 kV
Current: 700 µA
Live time: 60 s
Pulse density: 4755 cps
Dead time: 1.0 %

Azul Royal

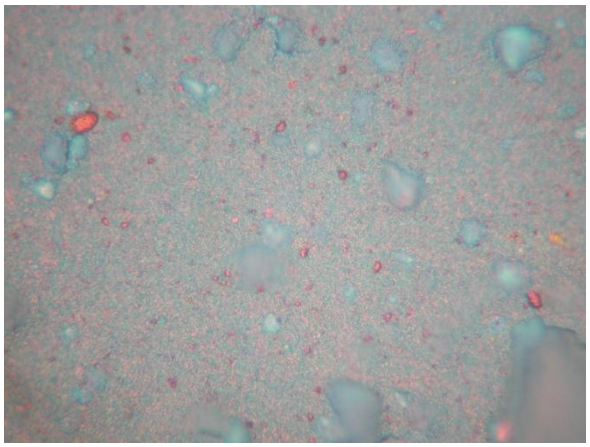

Bright Field, 400x

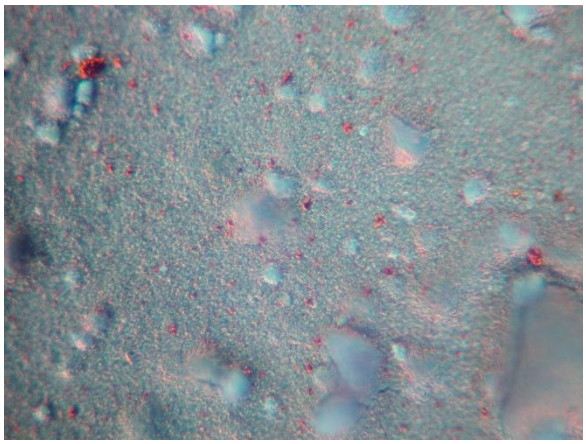

Dark Field, 400x

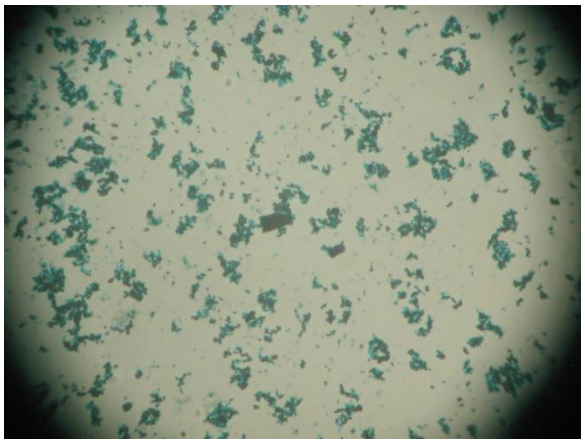

In RI 1.550, 400x

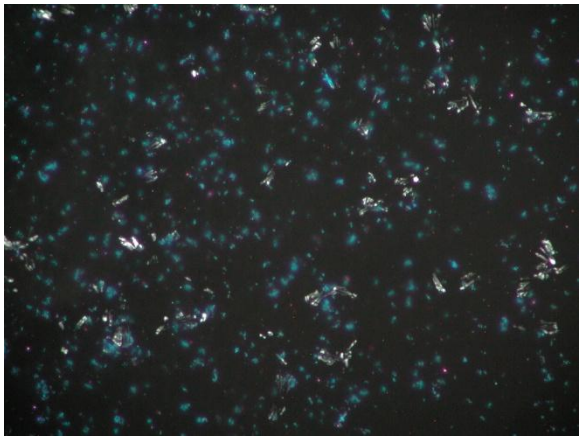

Crossed polars, In RI 1.550, 200x

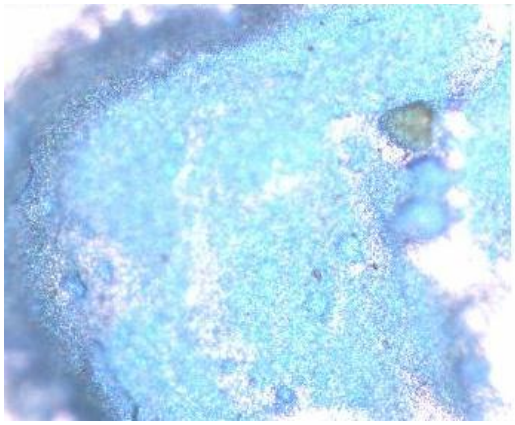

Raman microscope image, 200x

Normal Raman, 488nm

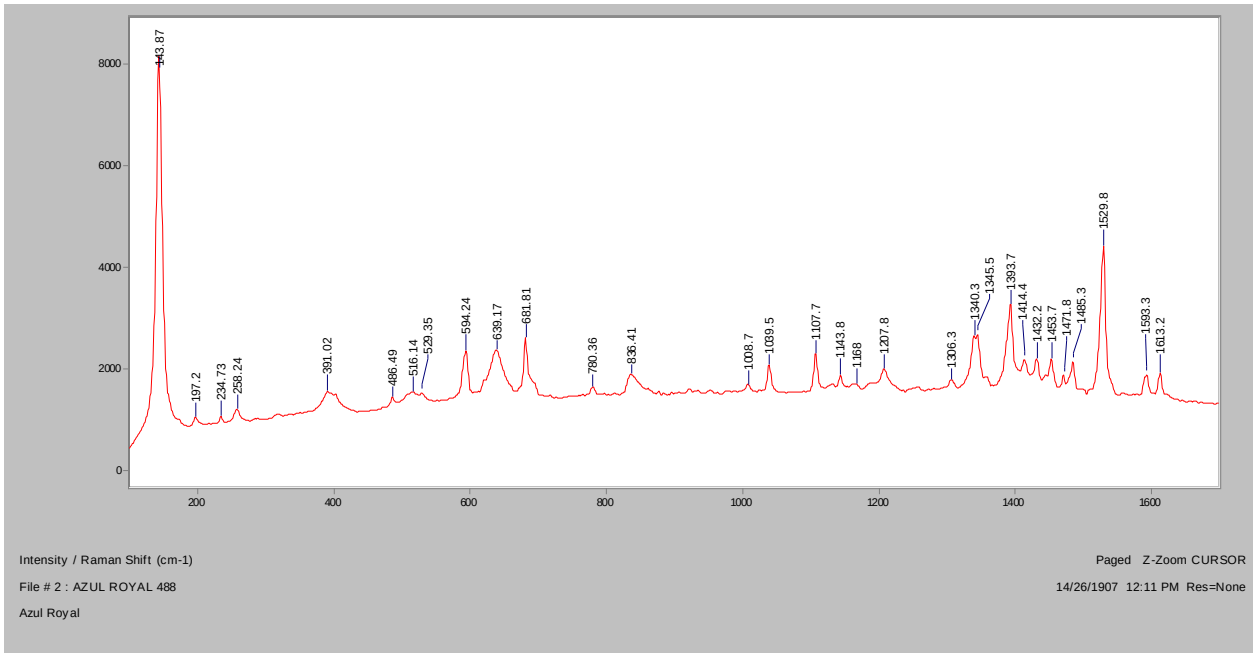

Normal Raman, 633nm

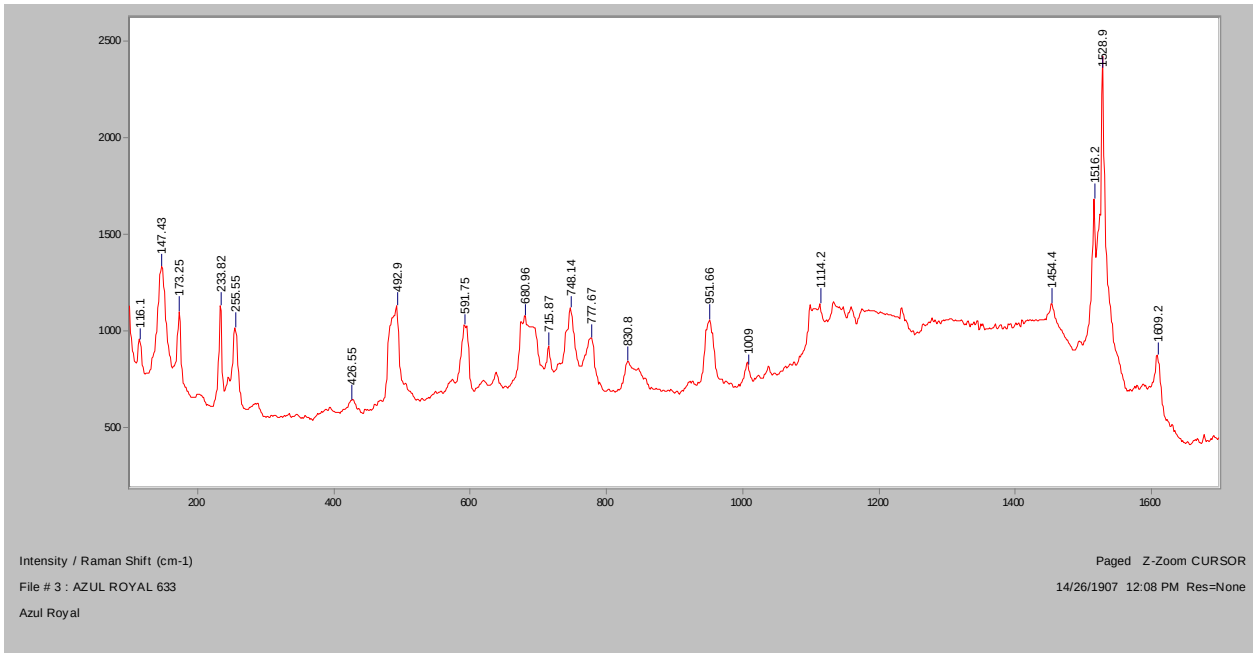

Normal Raman, 785nm

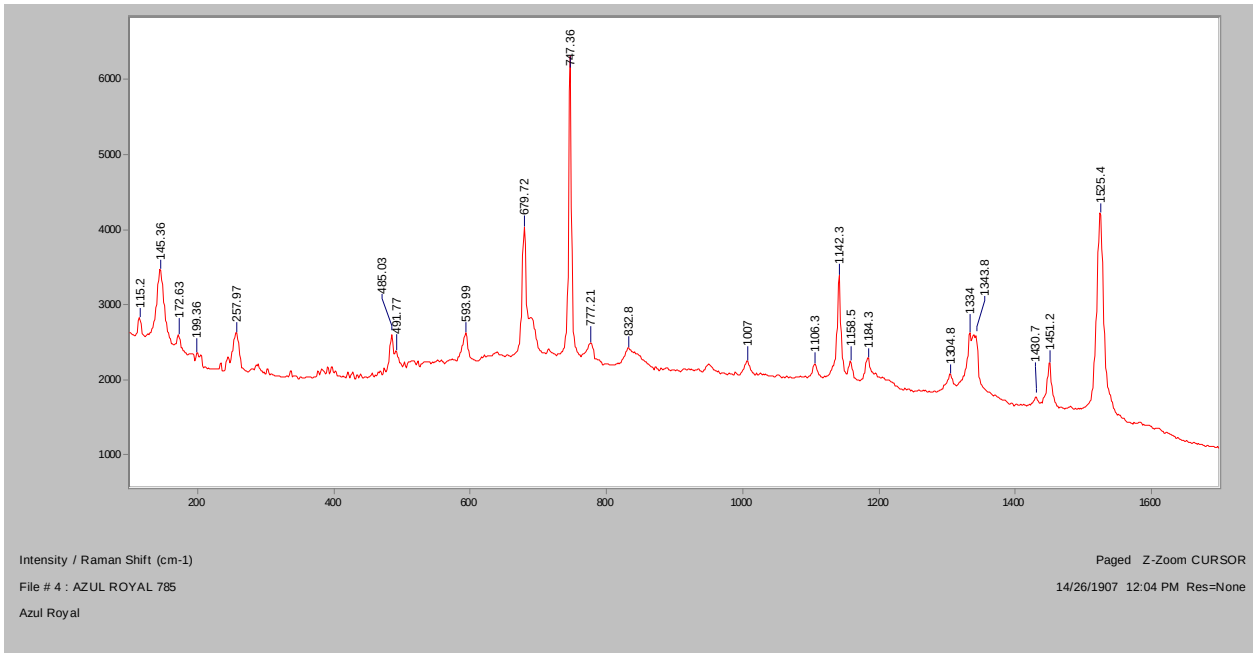

FT-Raman, 1064nm

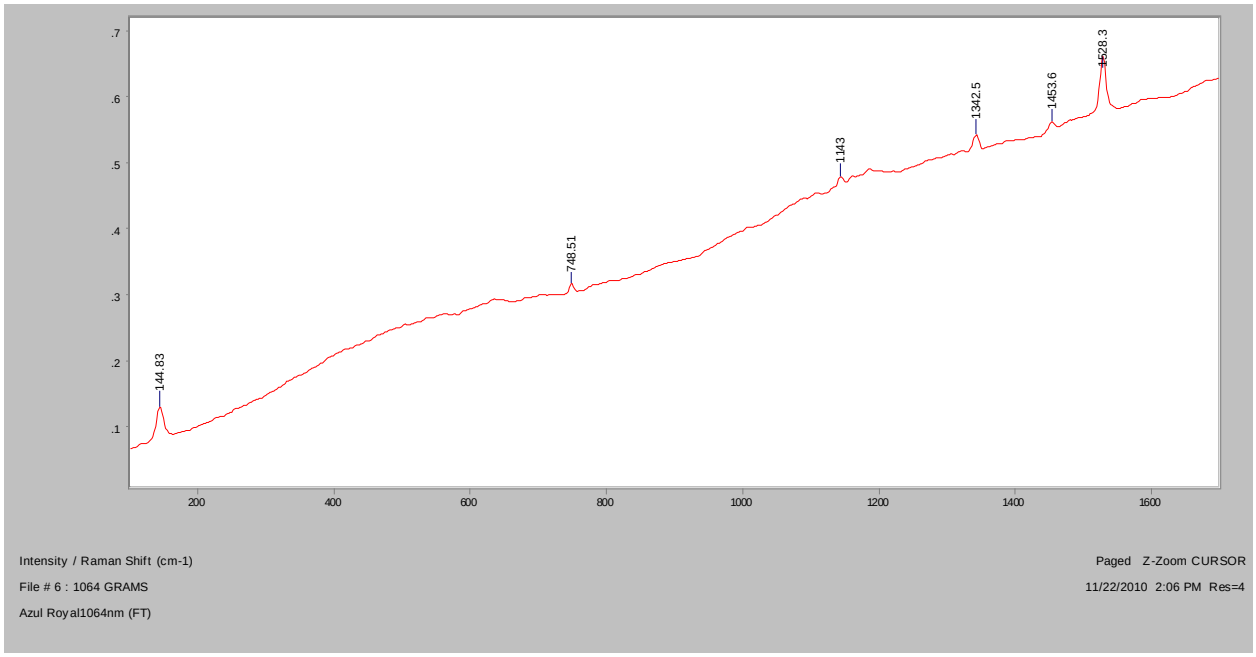

SERS, 488nm

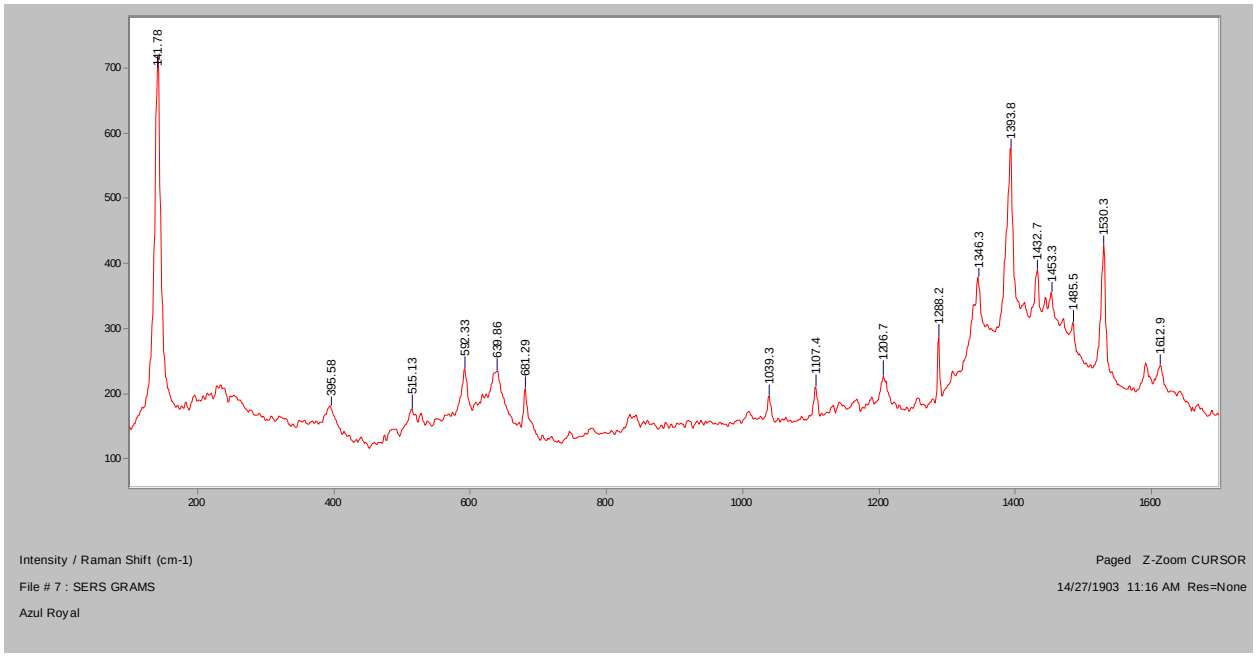

FT-IR (ATR)

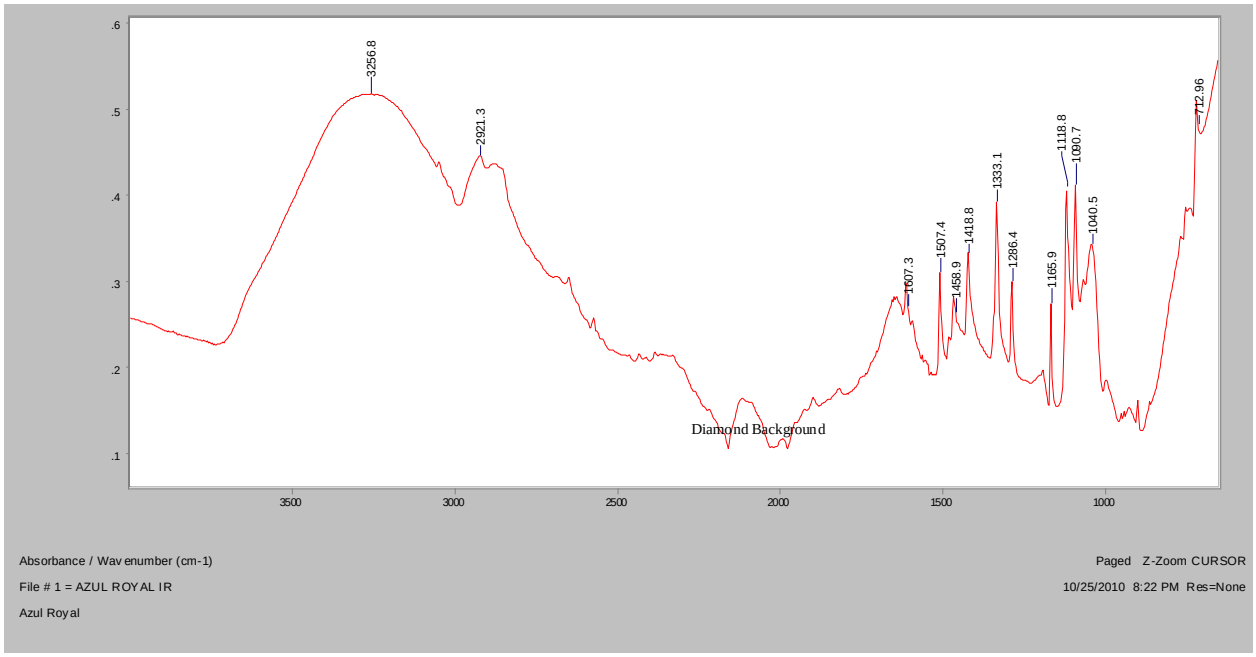

XRF

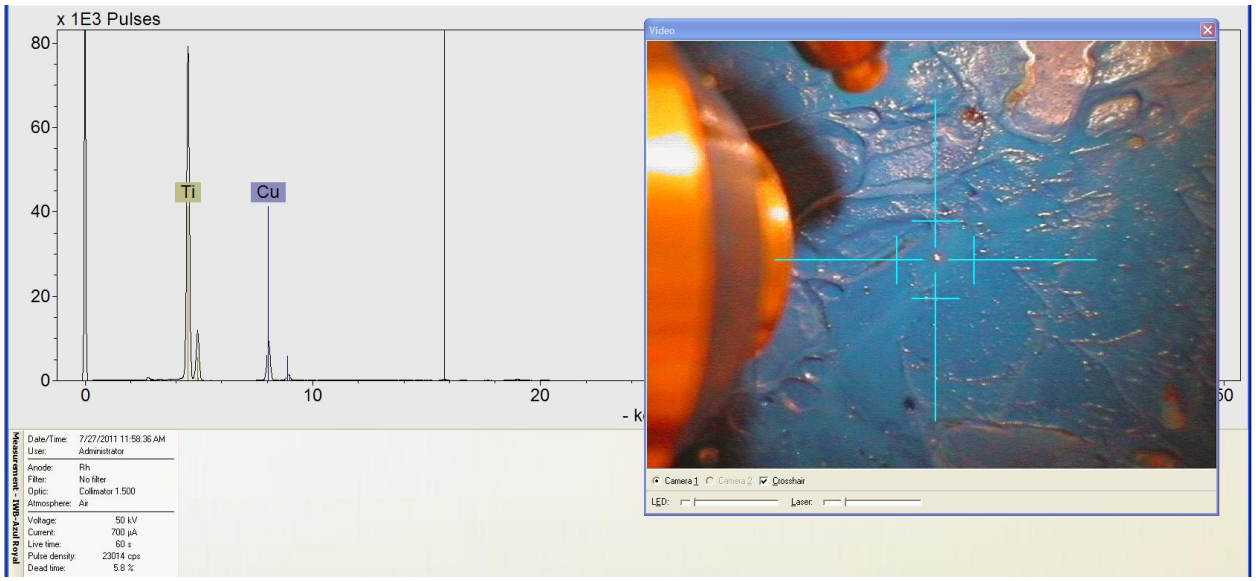
x 1E3 Pulses
80
60
40
20
0
Ti
Cu
0
10
20
Video
Camera 1
Camera 2
Crosshair
LED:
Laser:
Date/Time: 7/27/2011 11:58:36 AM
User: Administrator
Anode: Rh
Filter: No filter
Optic: Collimator 1.500
Atmosphere: Air
Voltage: 50 kV
Current: 700 µA
Live time: 60 s
Pulse density: 23014 cps
Dead time: 5.8 %

Magenta

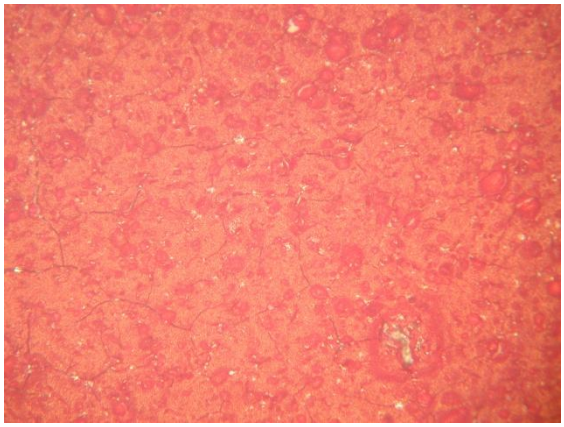

Bright Field, 100x

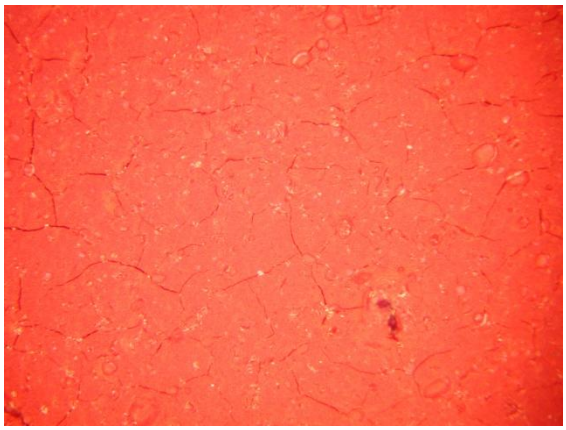

Dark Field, 100x

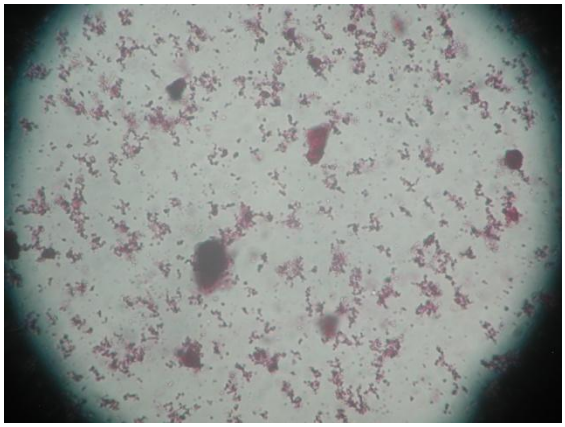

In RI 1.550, 400x

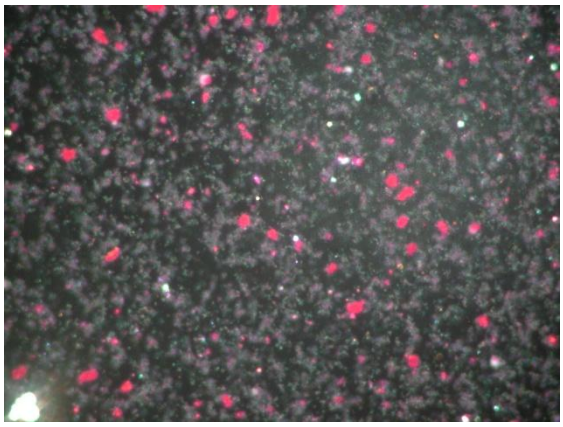

Crossed polars, In RI 1.550, 200x

Normal Raman, 488nm

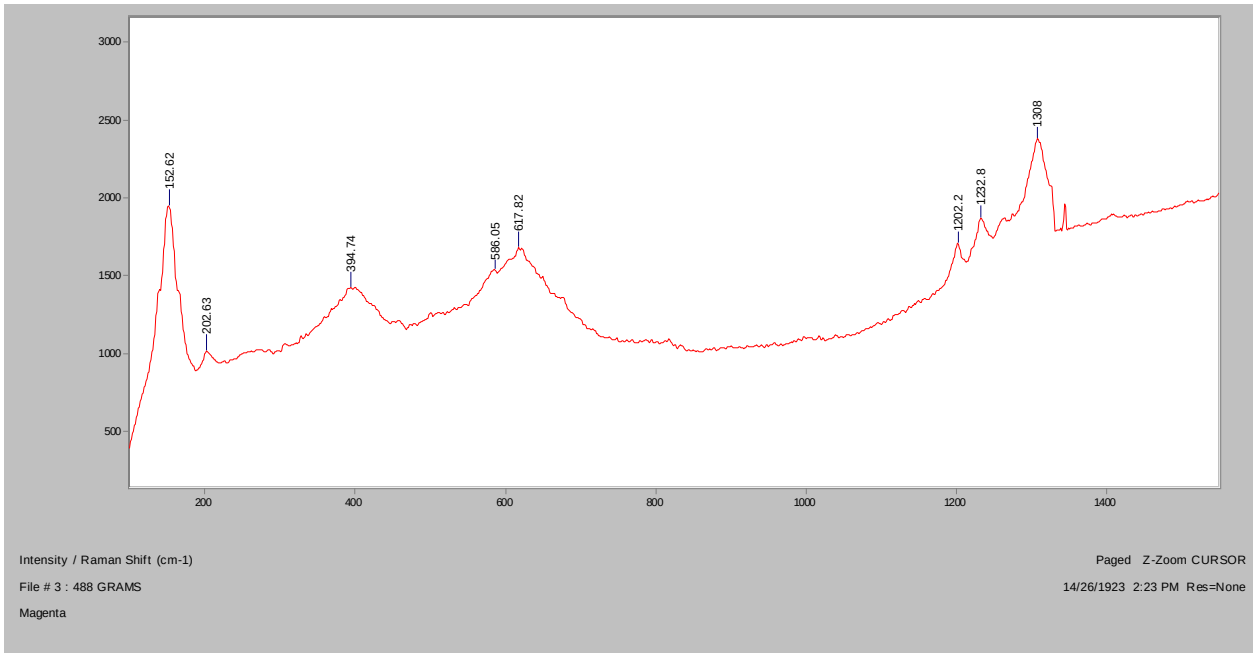

Normal Raman, 633nm

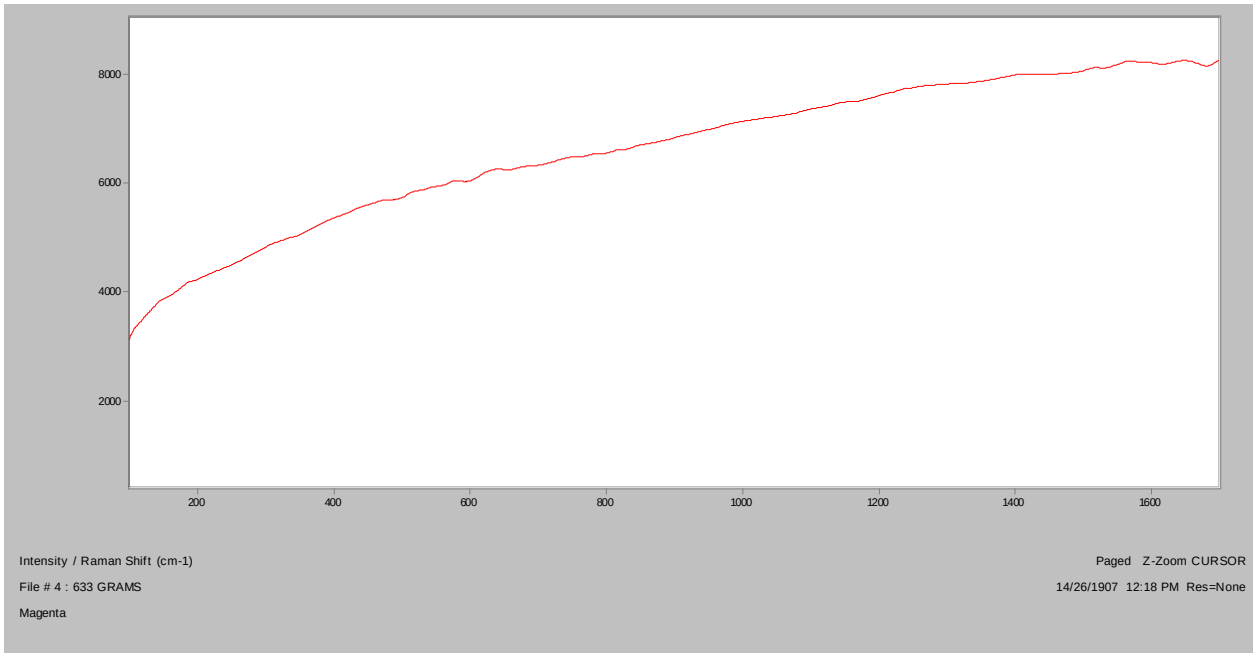

Normal Raman, 785nm

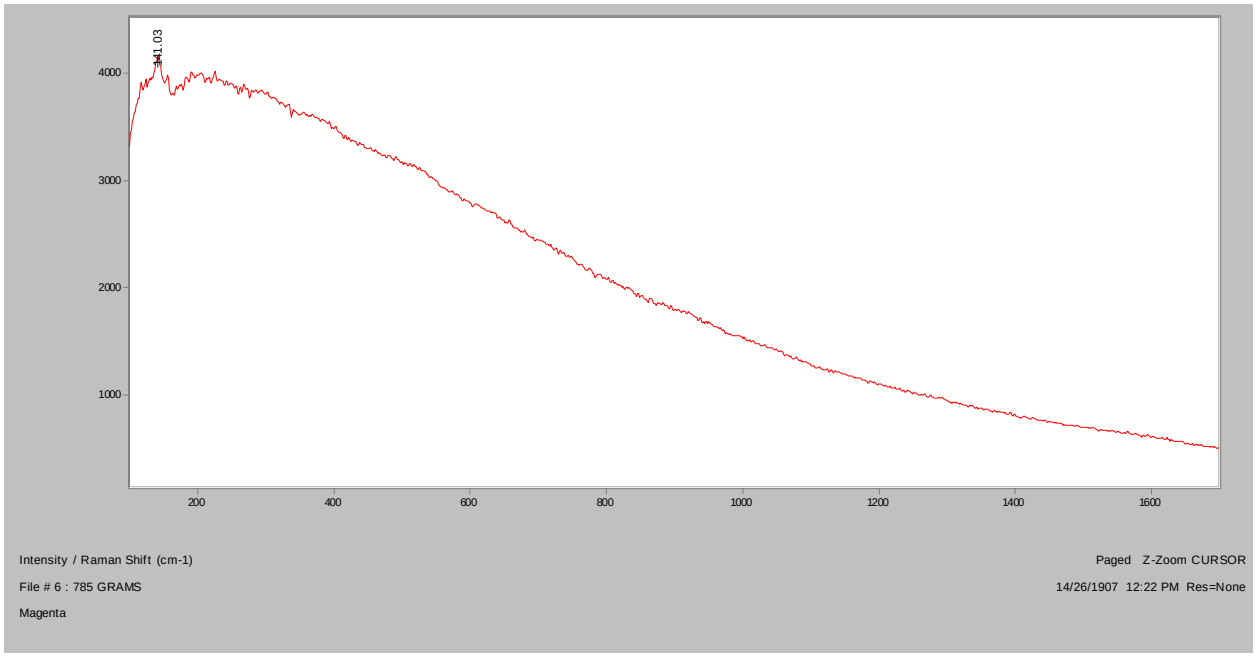

FT-Raman, 1064nm

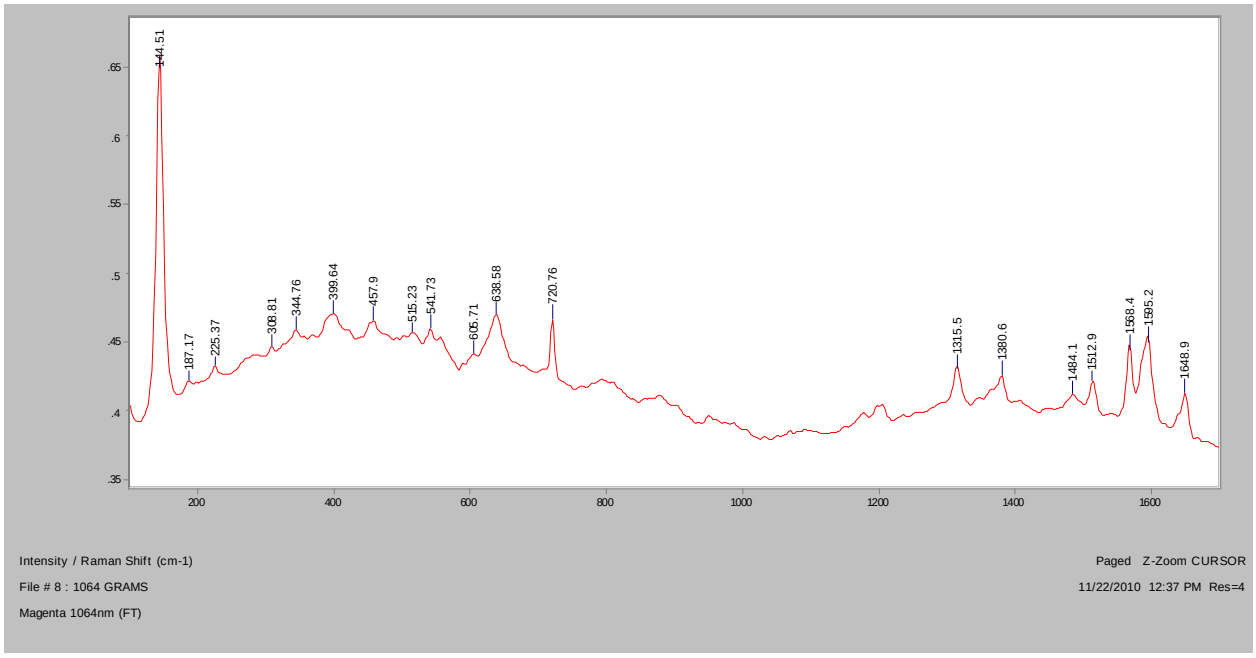

SERS, 488nm

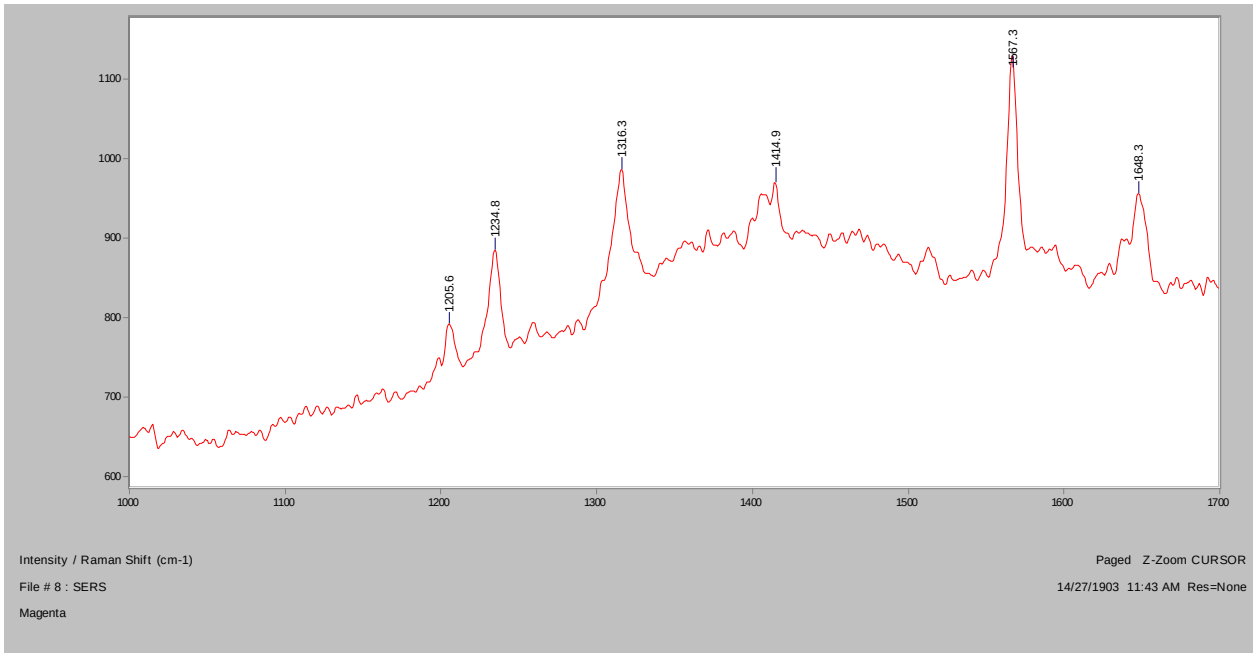

FT-IR (ATR)

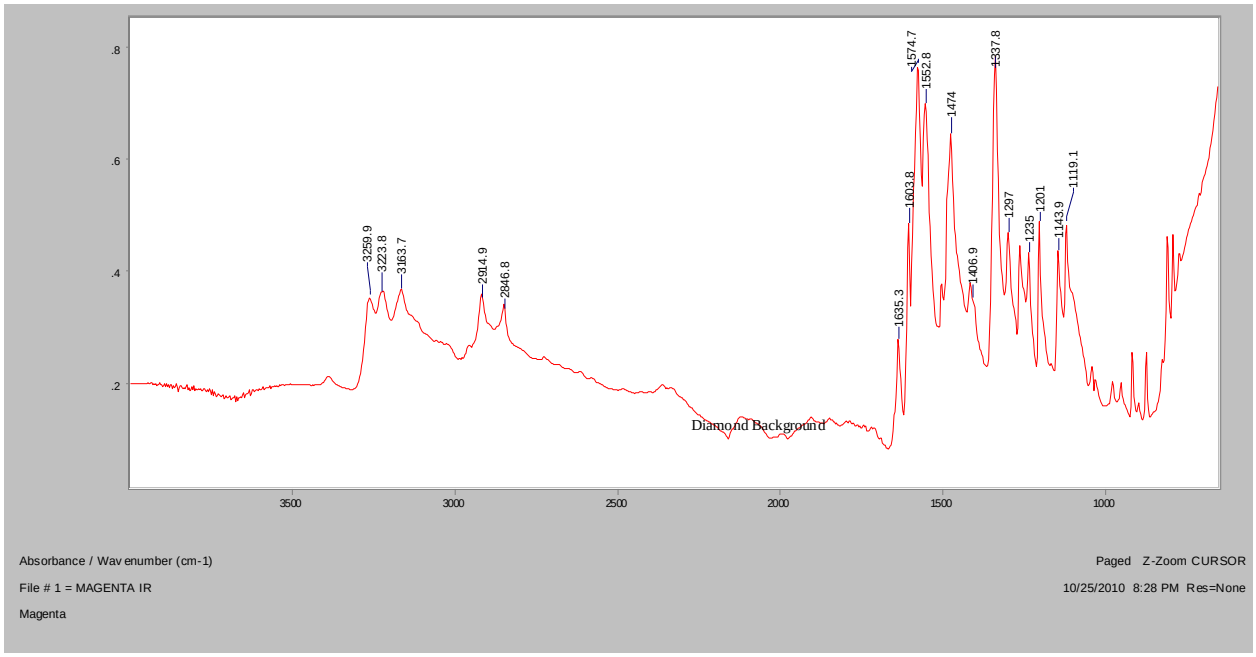

XRF

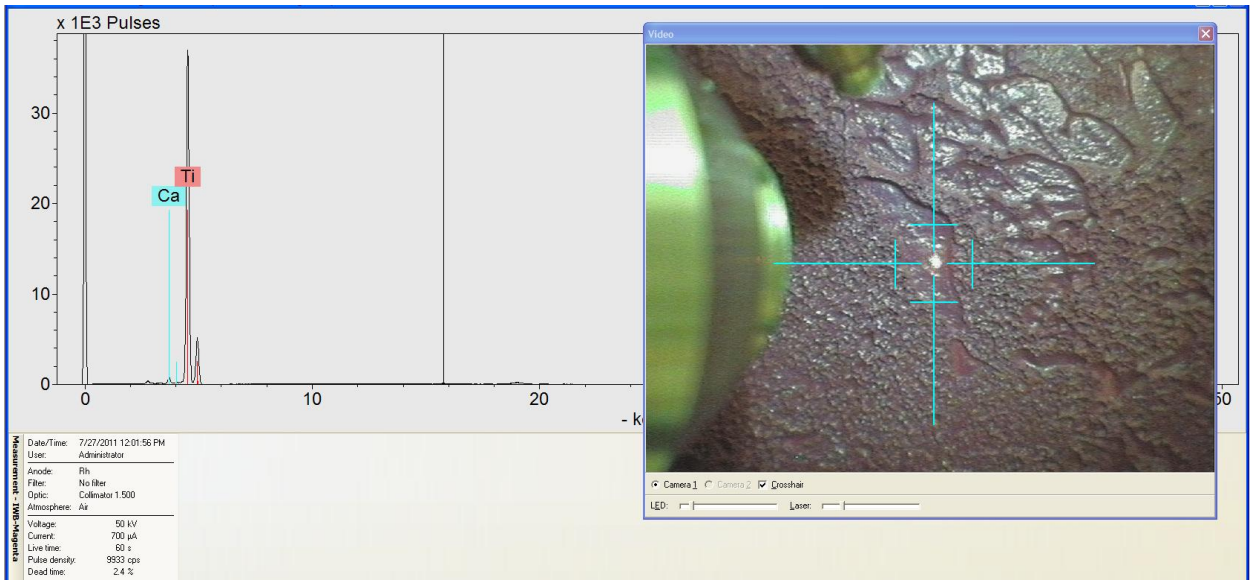
x 1E3 Pulses
30
20
10
0
Ti
Ca
0
10
20
Video
Camera 1
Camera 2
Crosshair
LED:
Laser:
Measurement - TMS-Negrita
Date/Time: 7/27/2011 12:01:56 PM
User: Administrator
Anode: Rh
Filter: No filter
Optic: Collimator 1.500
Atmosphere: Air
Voltage: 50 kV
Current: 700 µA
Live time: 60 s
Pulse density: 9933 cps
Dead time: 2.4 %

Lilas Claro

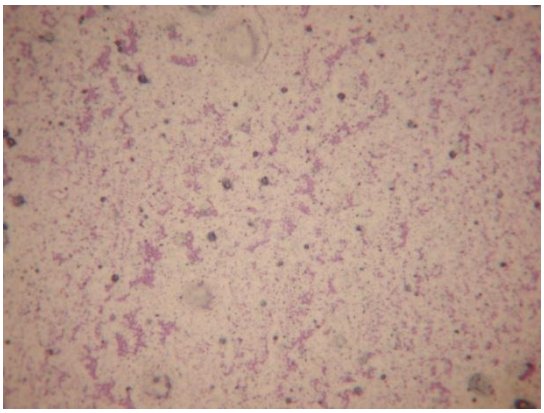

Bright Field, 100x

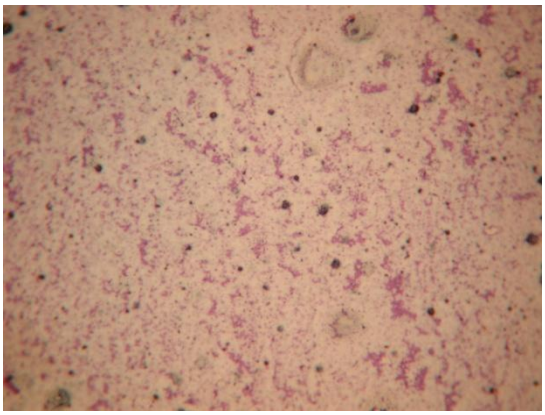

Dark Field, 100x

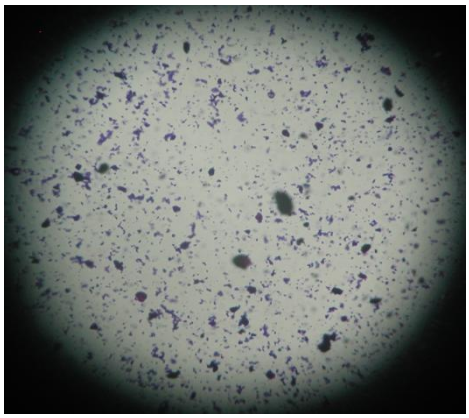

In RI 1.550, 400x

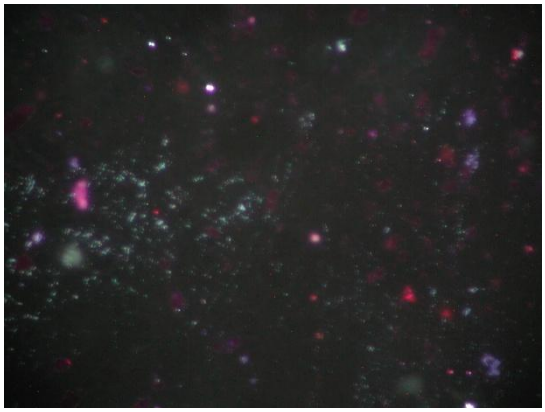

Crossed polars, In RI 1.550, 400x

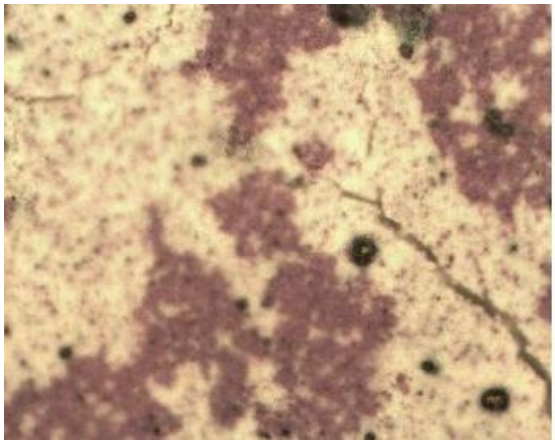

Raman microscope image, 200x

Normal Raman, 488nm

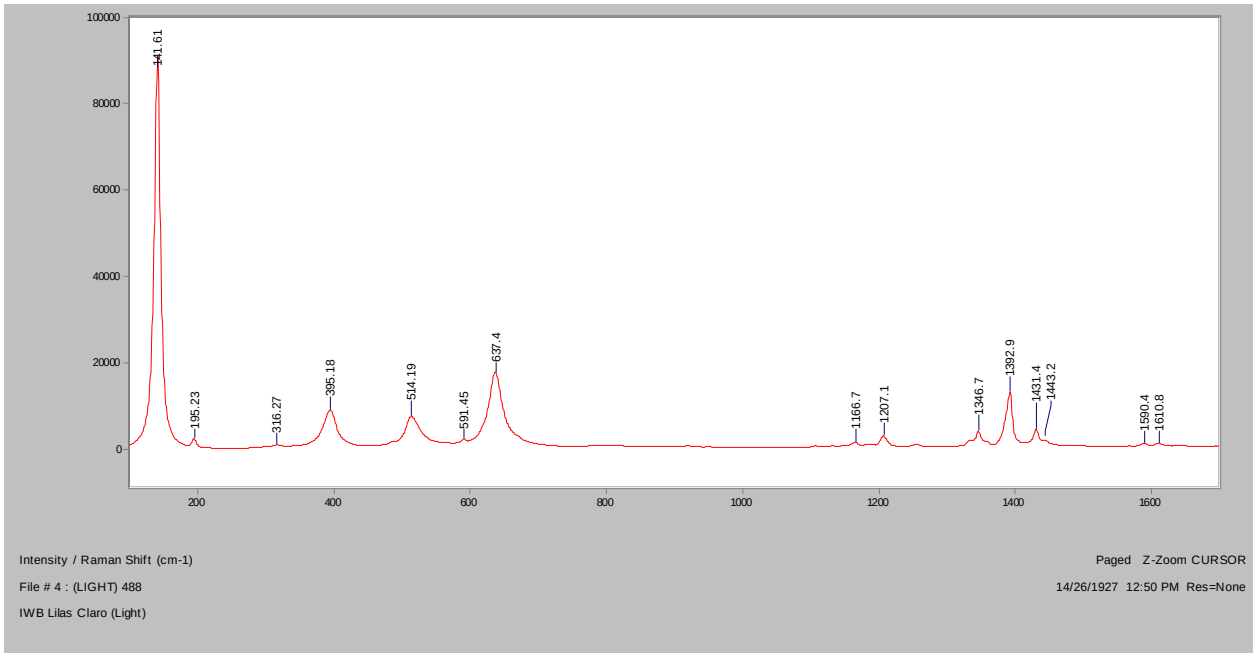

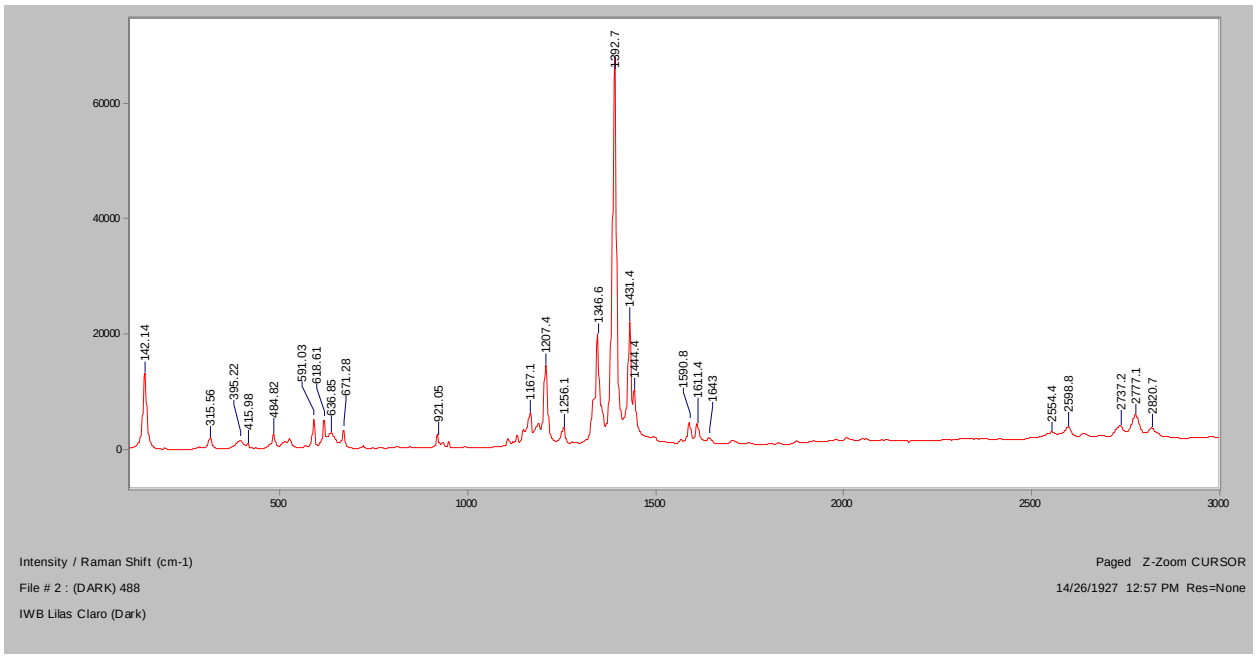

Normal Raman, 633nm

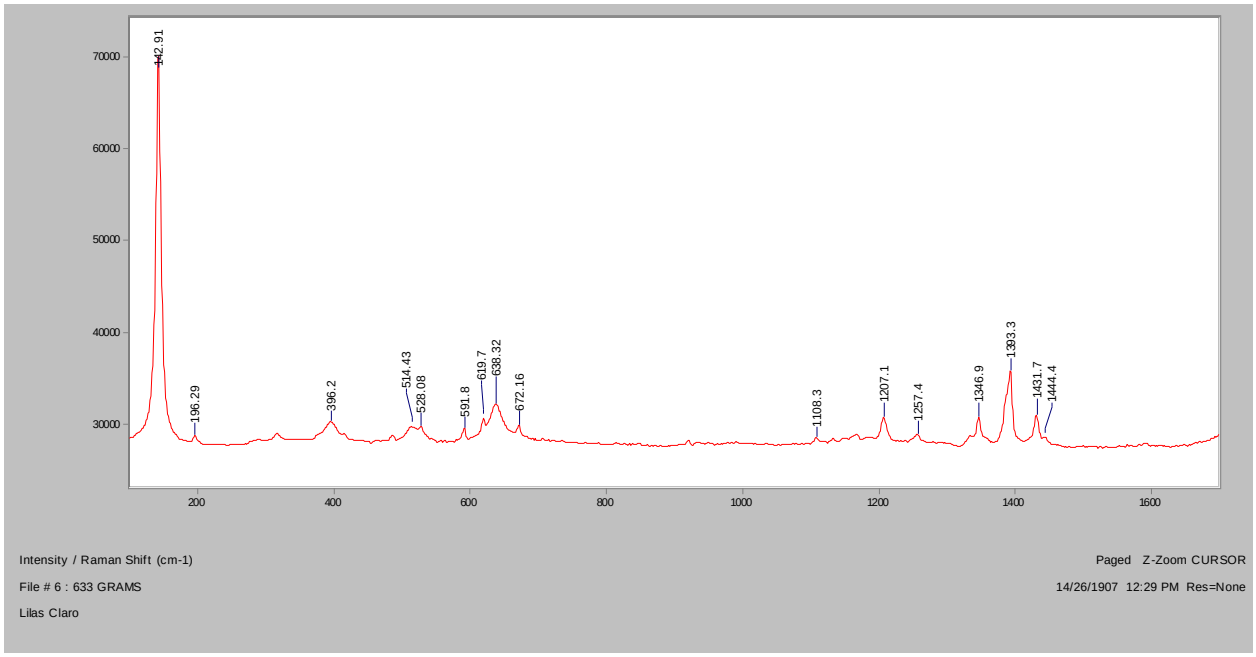

Normal Raman, 785nm

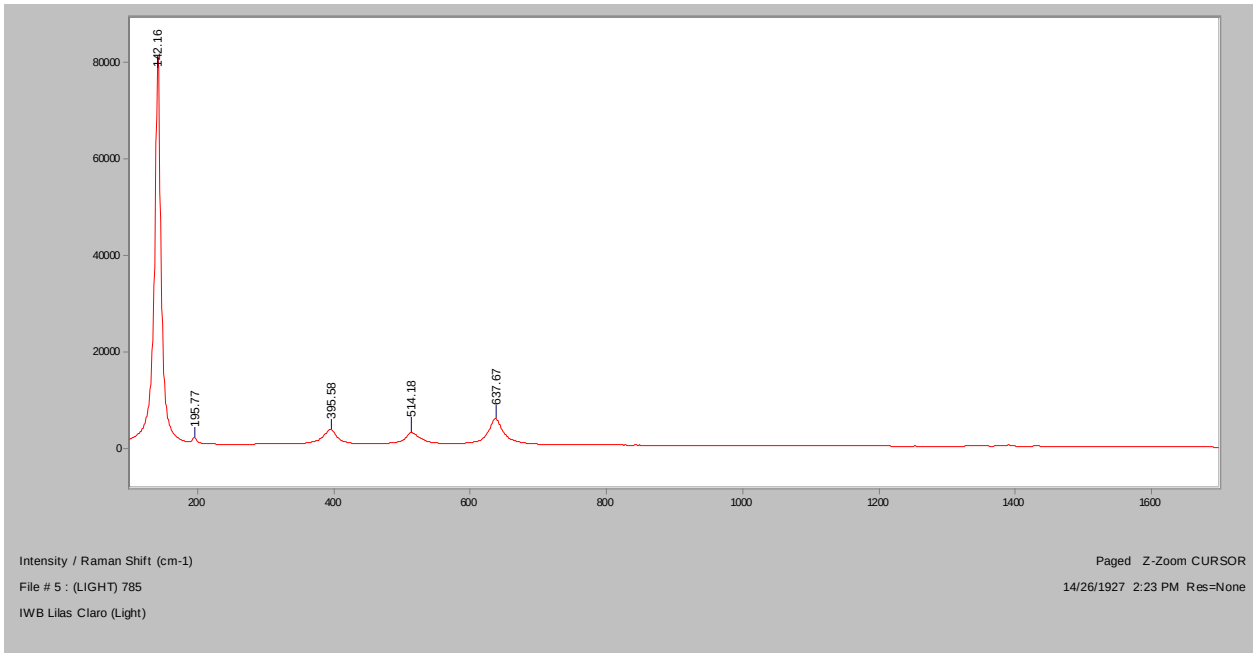

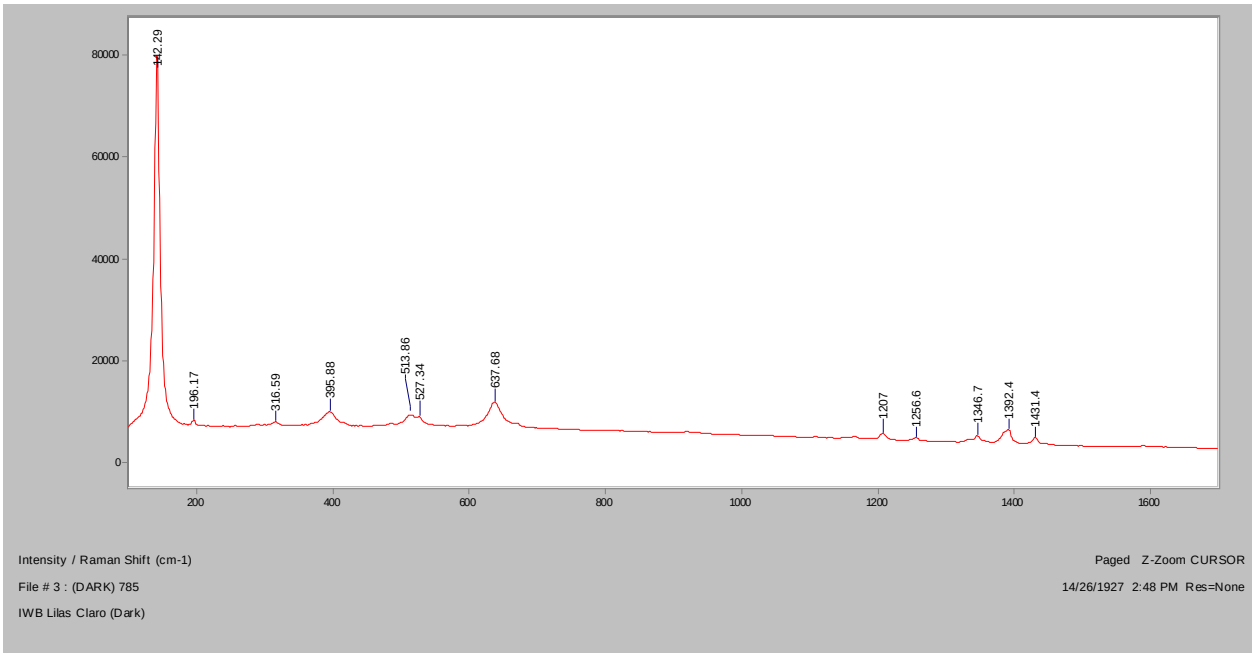

FT-Raman, 1064

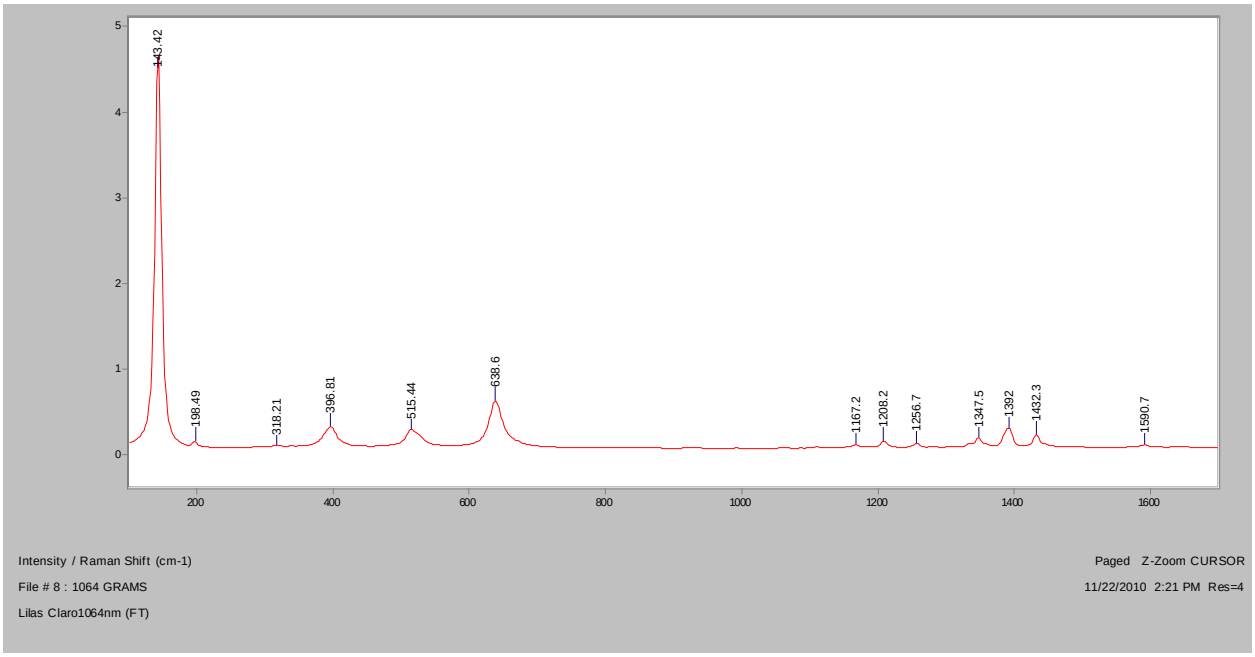

SERS

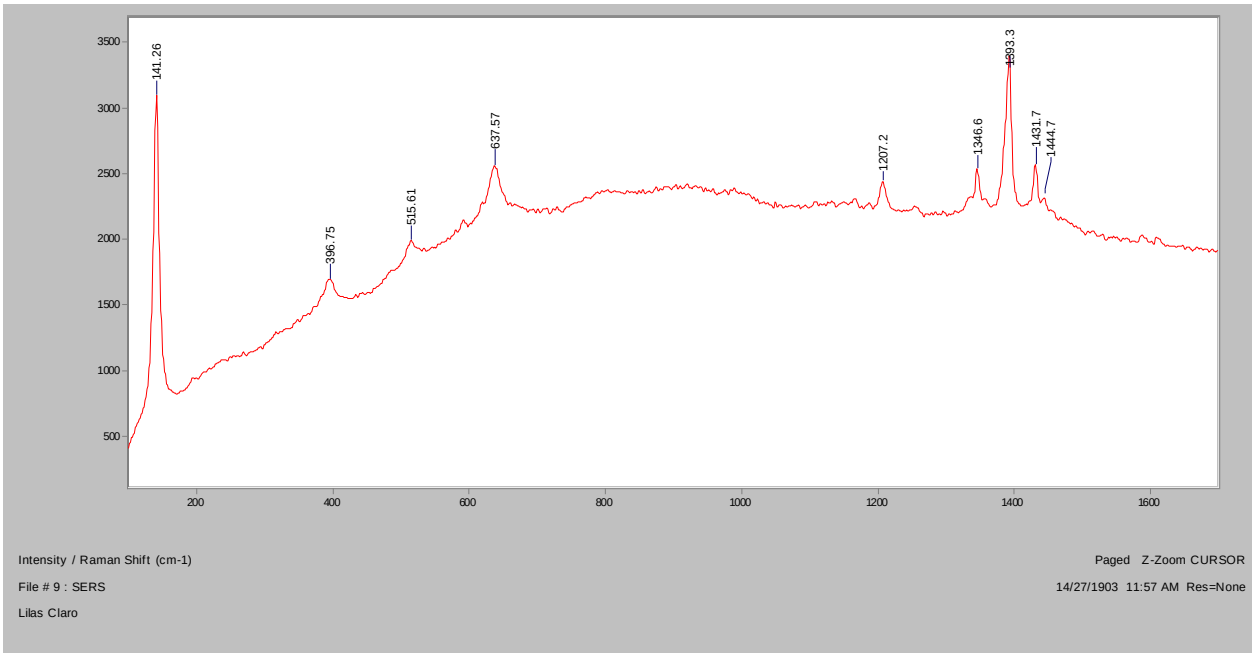

FT-IR (ATR)

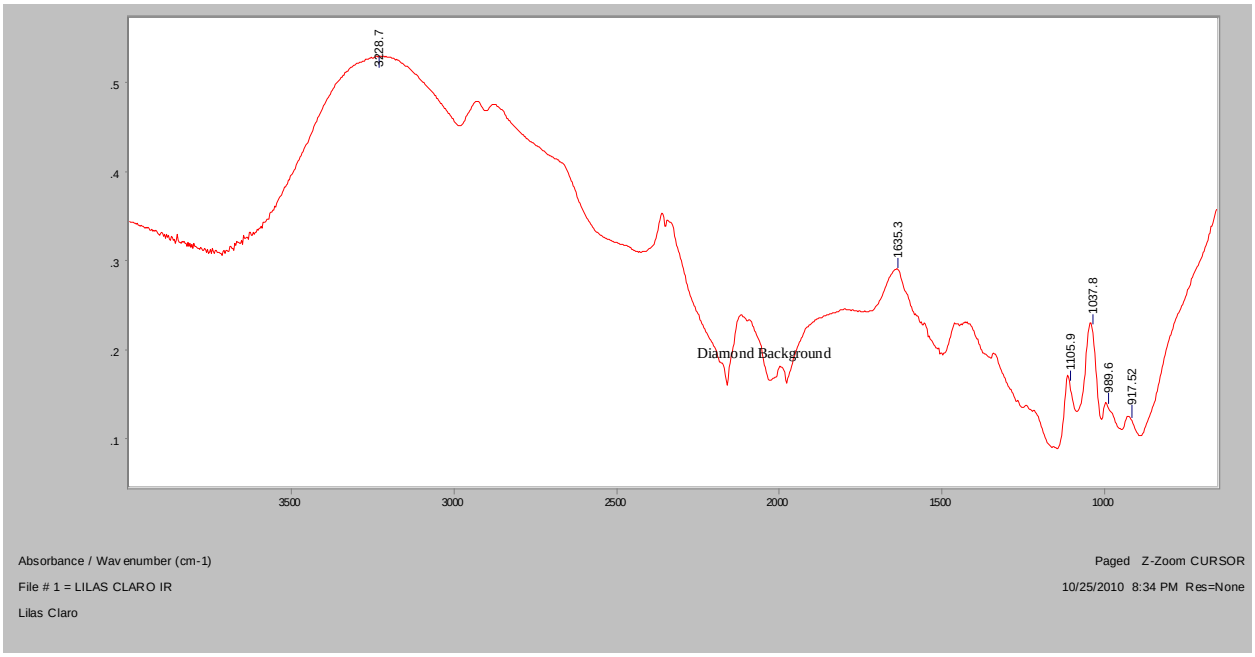

XRF

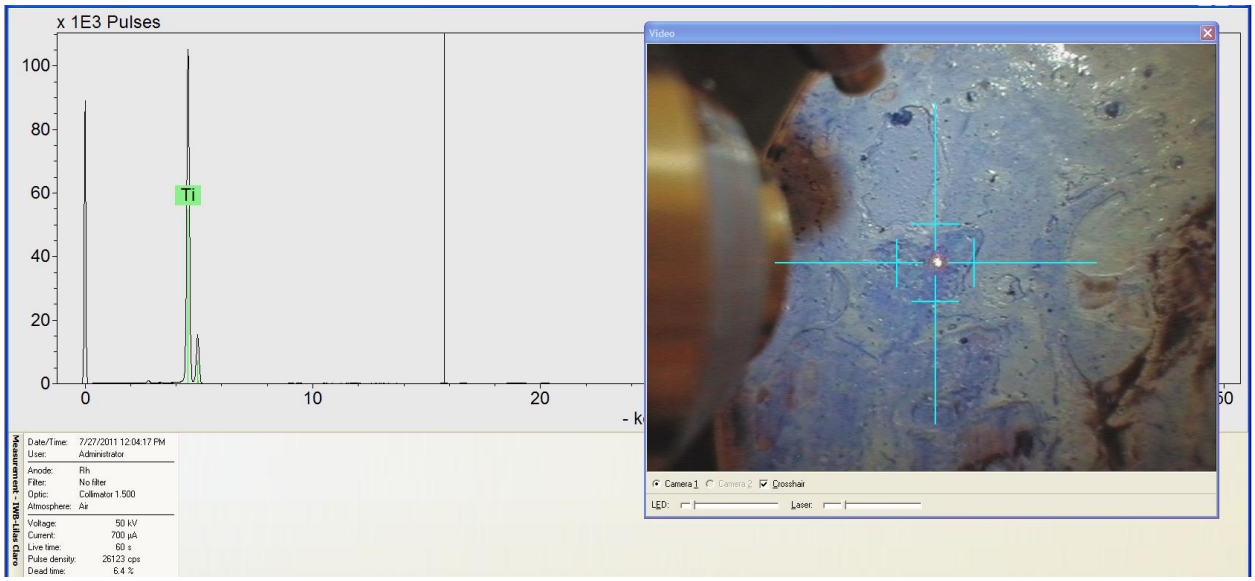
x 1E3 Pulses
100
80
60
40
20
0
Ti
0
10
20
Video
Camera 1
Camera 2
Crosshair
LED:
Laser:
Date/Time: 7/27/2011 12:04:17 PM
User: Administrator
Anode: Rh
Filter: No filter
Optic: Collimator 1.500
Atmosphere: Air
Voltage: 50 kV
Current: 700 µA
Live time: 60 s
Pulse density: 26123 cps
Dead time: 6.4 %

Preto Escuro

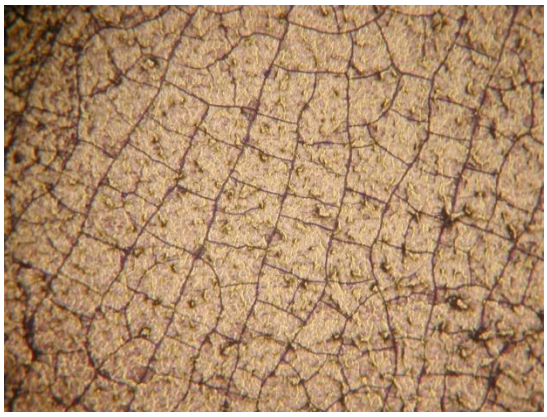

Bright Field, 100x

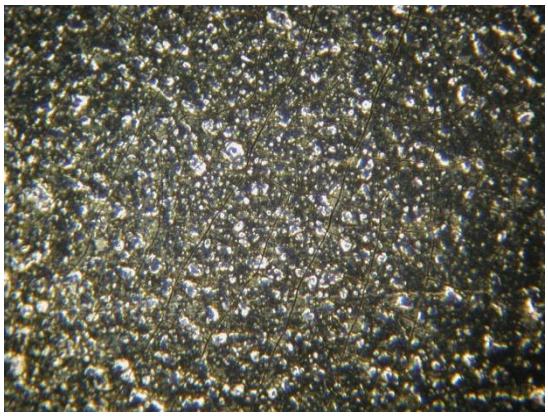

Dark Field, 100x

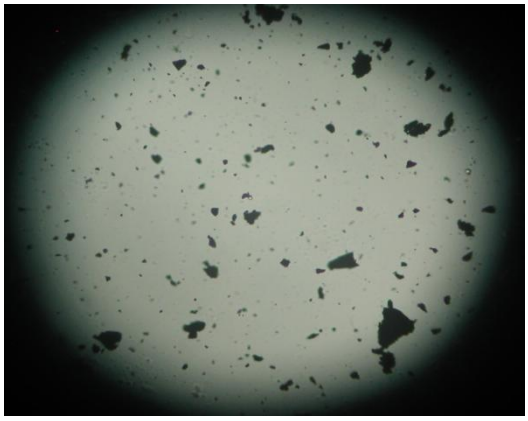

In RI 1.550, 400x

Normal Raman, 488nm

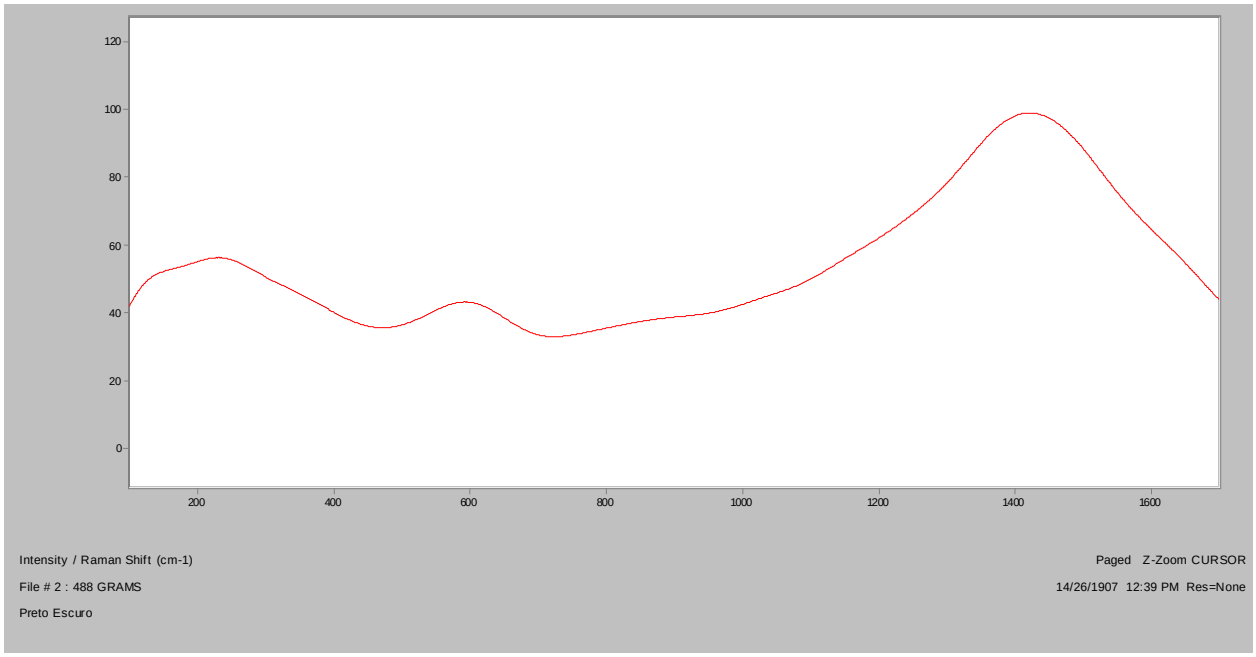

Normal Raman, 633nm

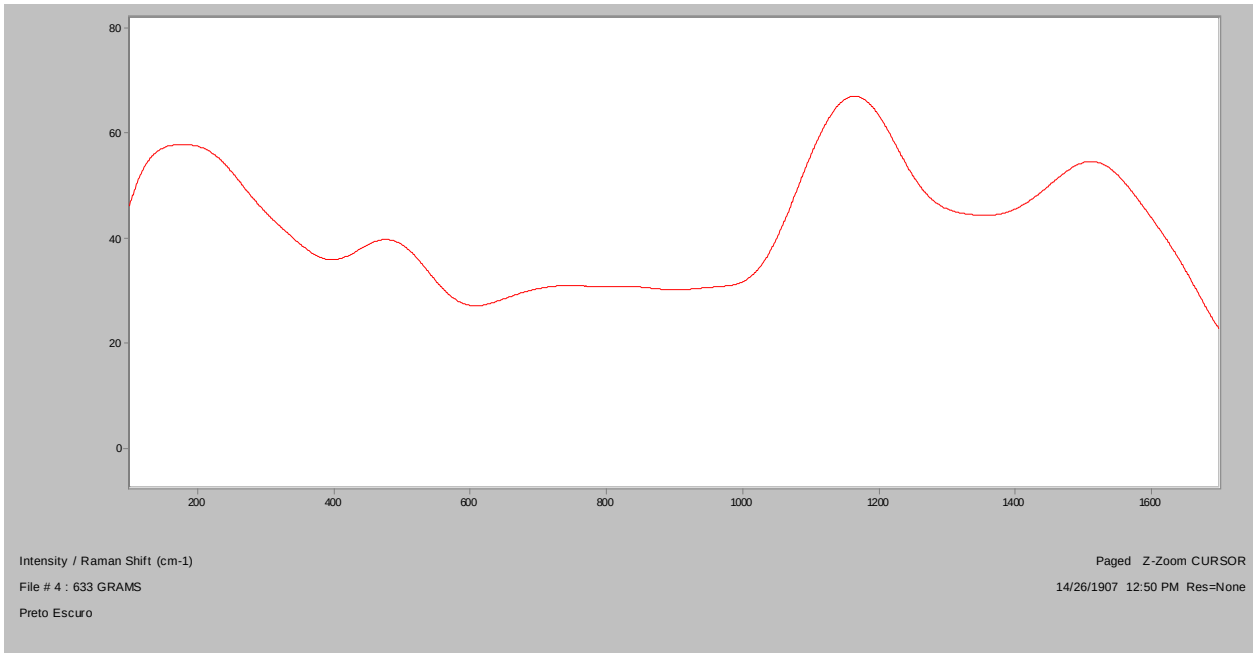

Normal Raman, 785nm

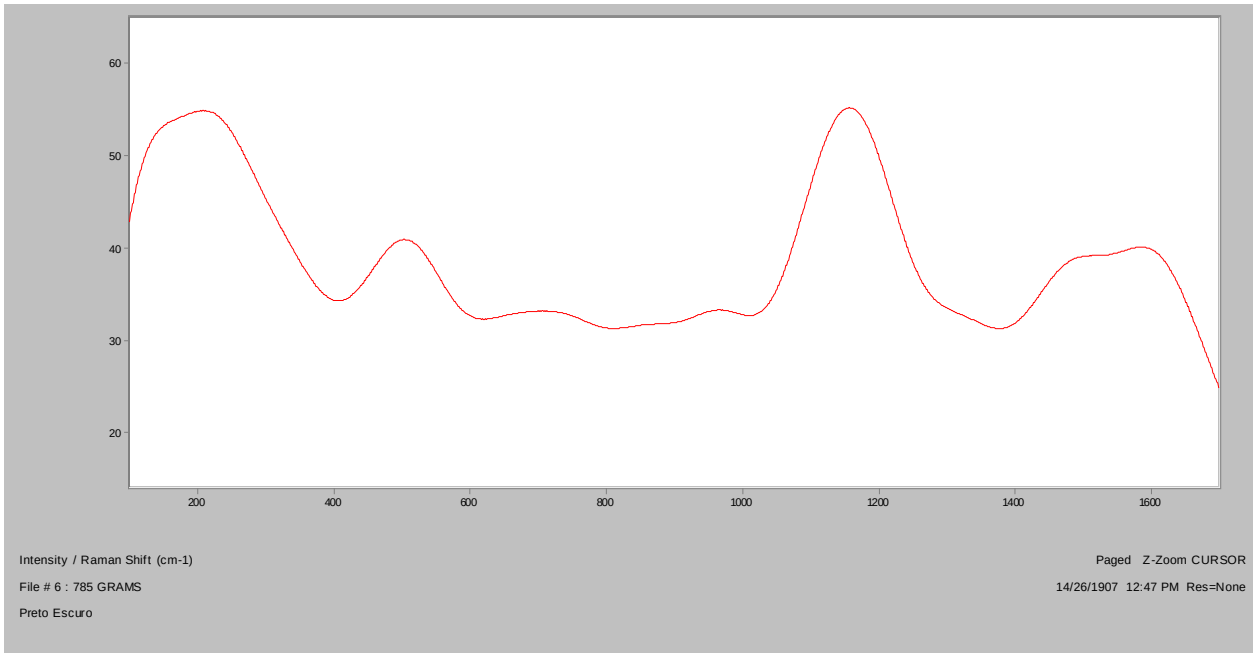

FT-Raman, 1064nm

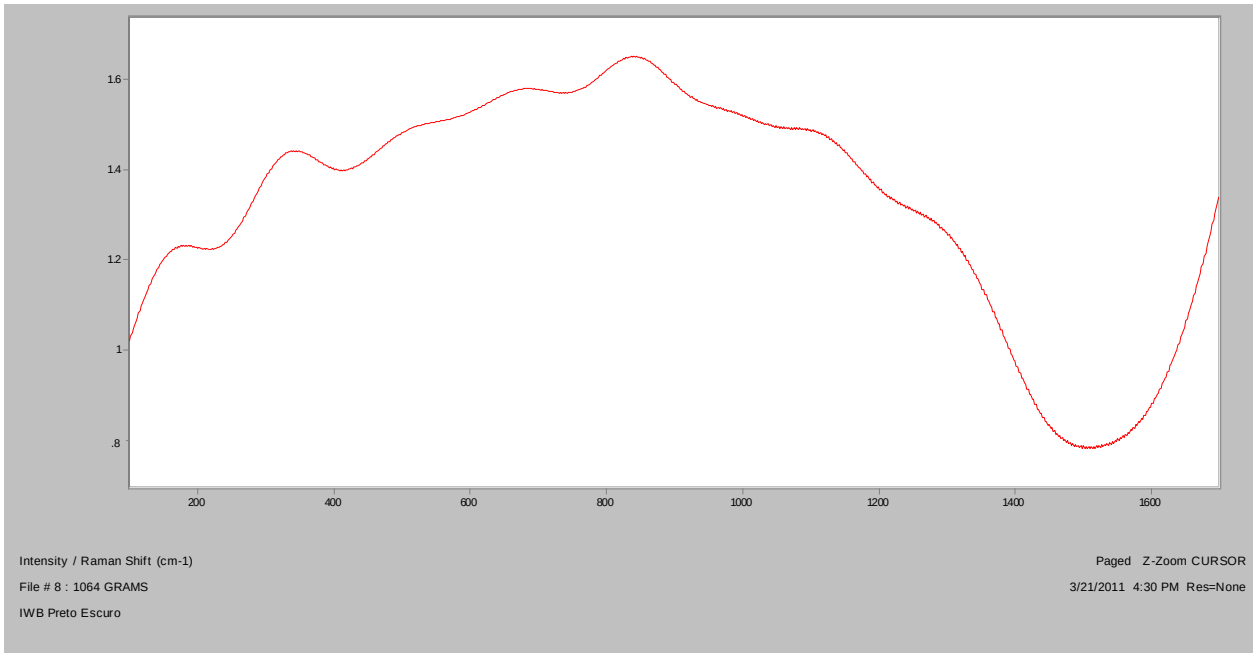

FT-IR (ATR)

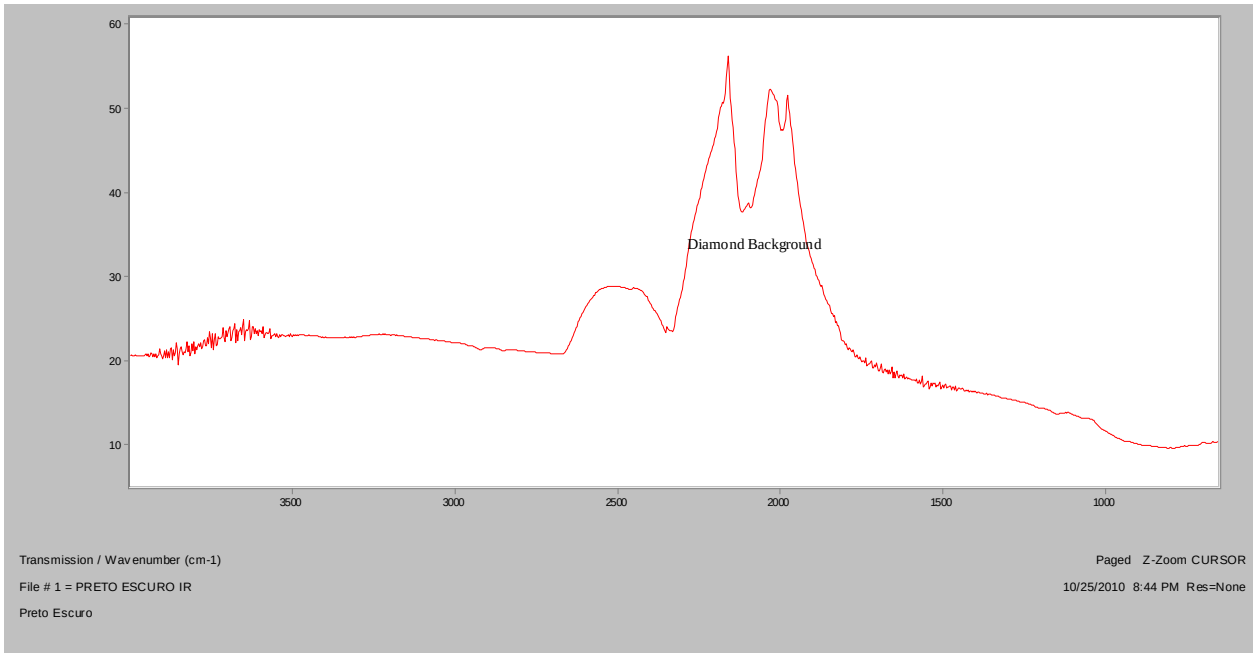
Diamond Background
Transmission / Wavenumber (cm-1)
File # 1 = PRETO ESCURO IR
Preto Escuro
Paged Z-Zoom CURSOR
10/25/2010 8:44 PM Res=None

XRF

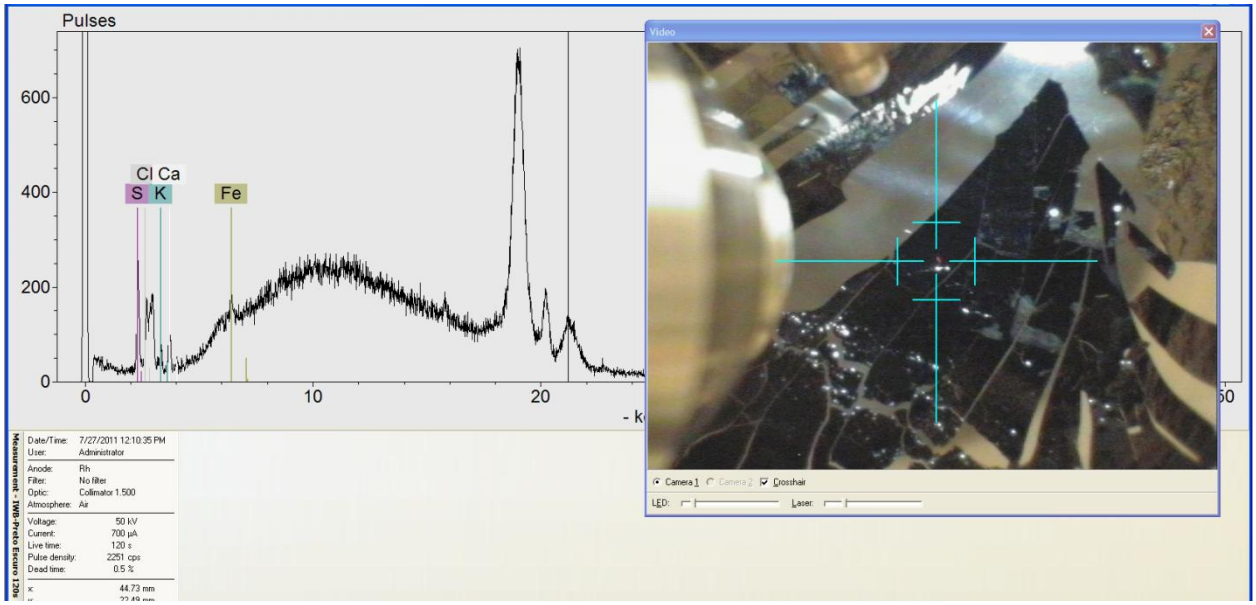
Pulses
Cl Ca
S K
Fe
Video
Camera 1
Crosshair
LED:
Laser:
Date/Time: 7/27/2011 12:10:35 PM
User: Administrator
Anode: Rh
Filter: No filter
Optic: Collimator 1.500
Atmosphere: Air
Voltage: 50 kV
Current: 700 µA
Live time: 120 s
Pulse density: 2251 cps
Dead time: 0.5 %
x: 44.73 mm

Appendix D: Tattoo Inks (Skin Candy)

Candy Apple Red

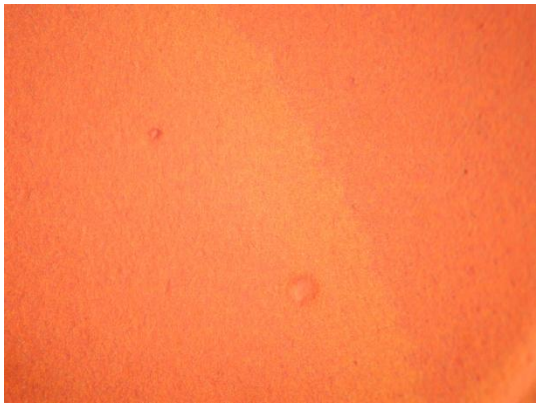

Bright Field, 400x

Dark Field, 100x

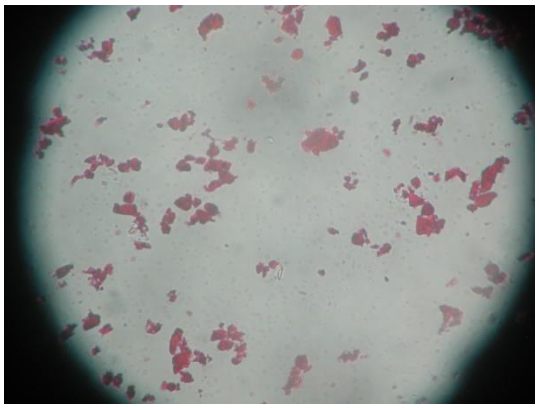

In RI 1.550, 400x

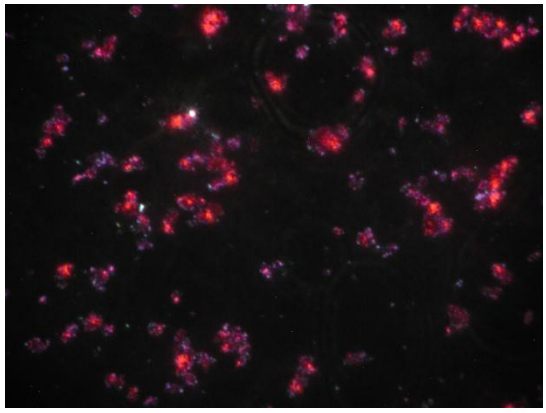

Crossed polars, In RI 1.550, 400x

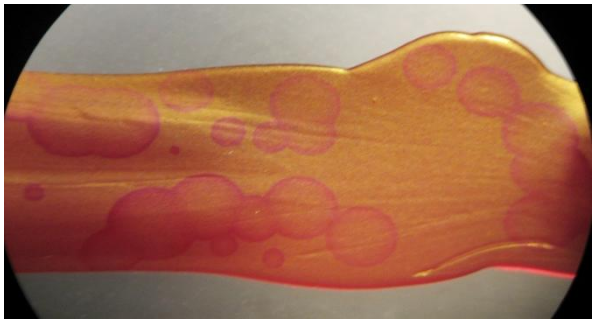

Smear on microscope slide after drying, ~20x

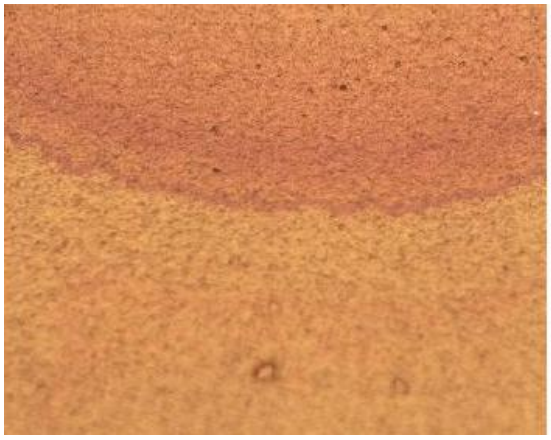

Raman microscope image, 200x

Normal Raman, 488nm

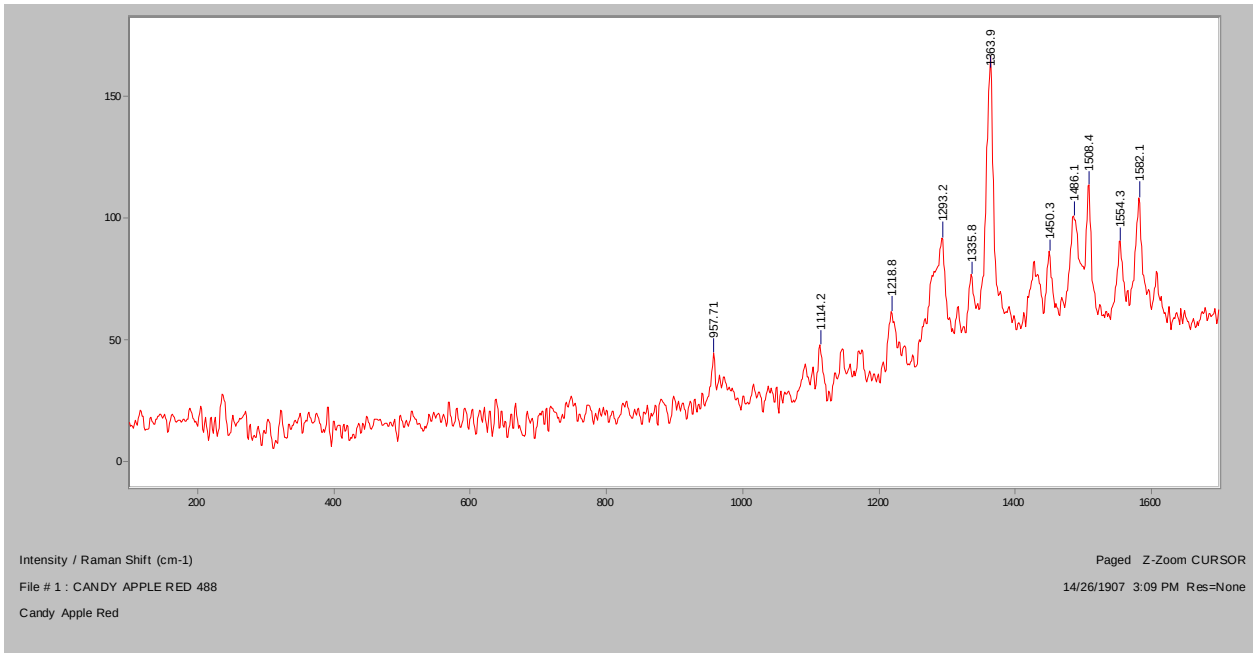

Normal Raman, 633nm

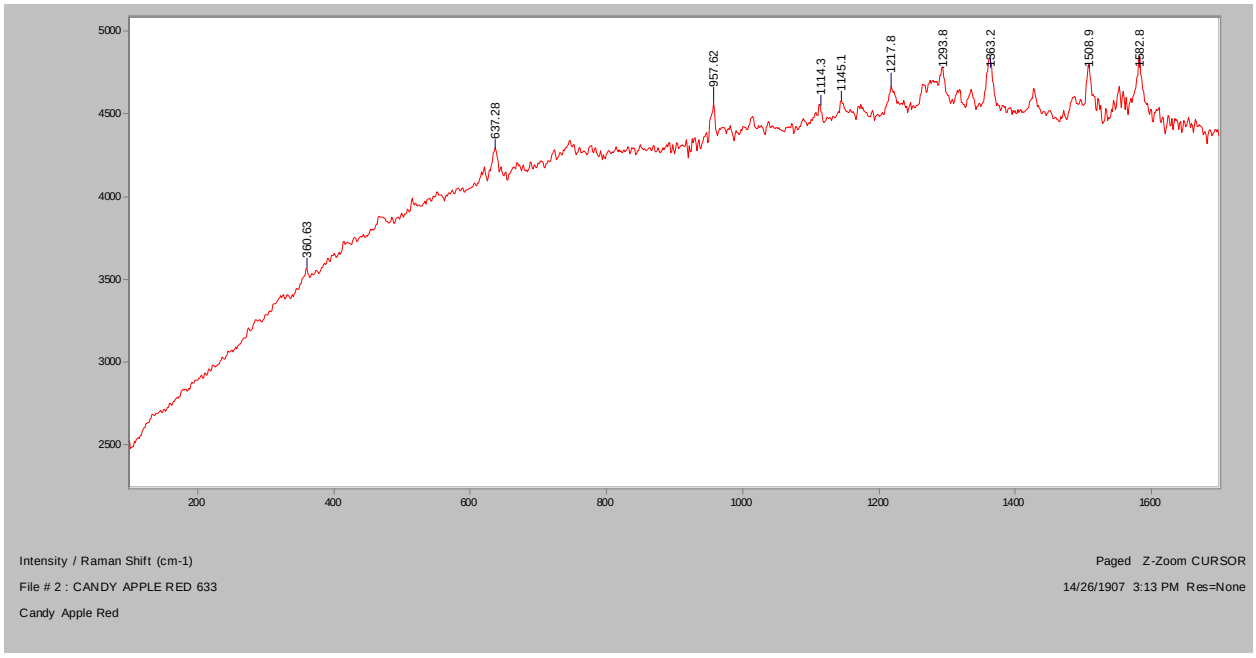

Normal Raman, 785nm

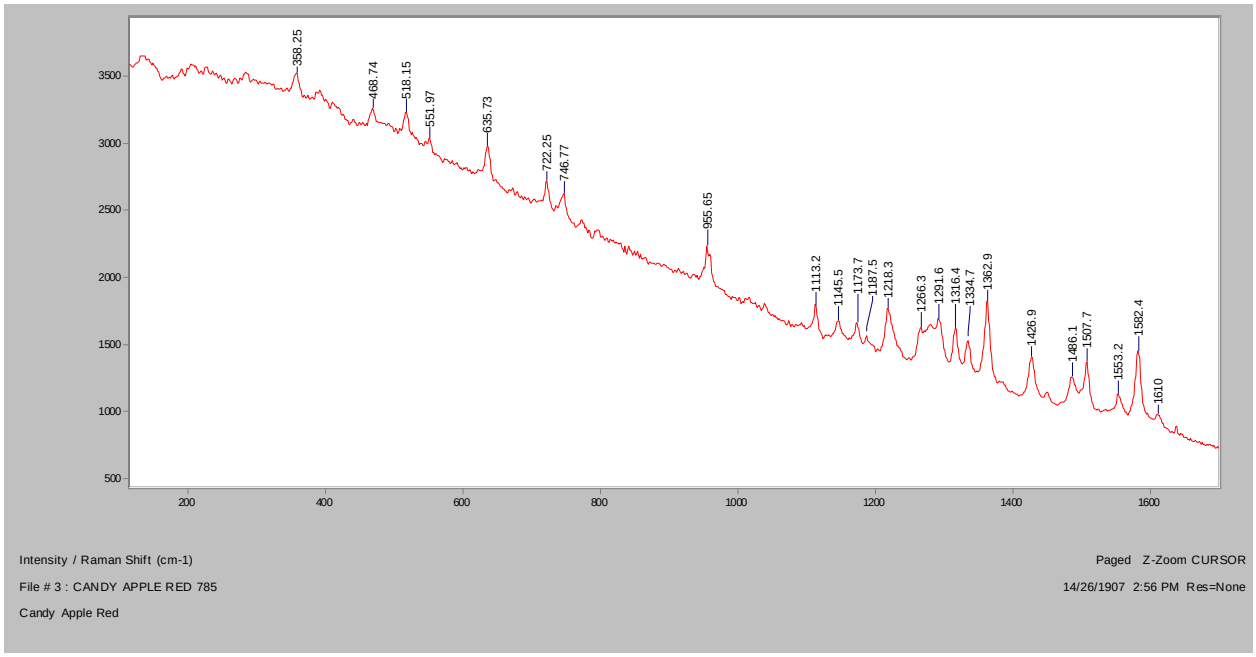

FT-Raman, 1064nm

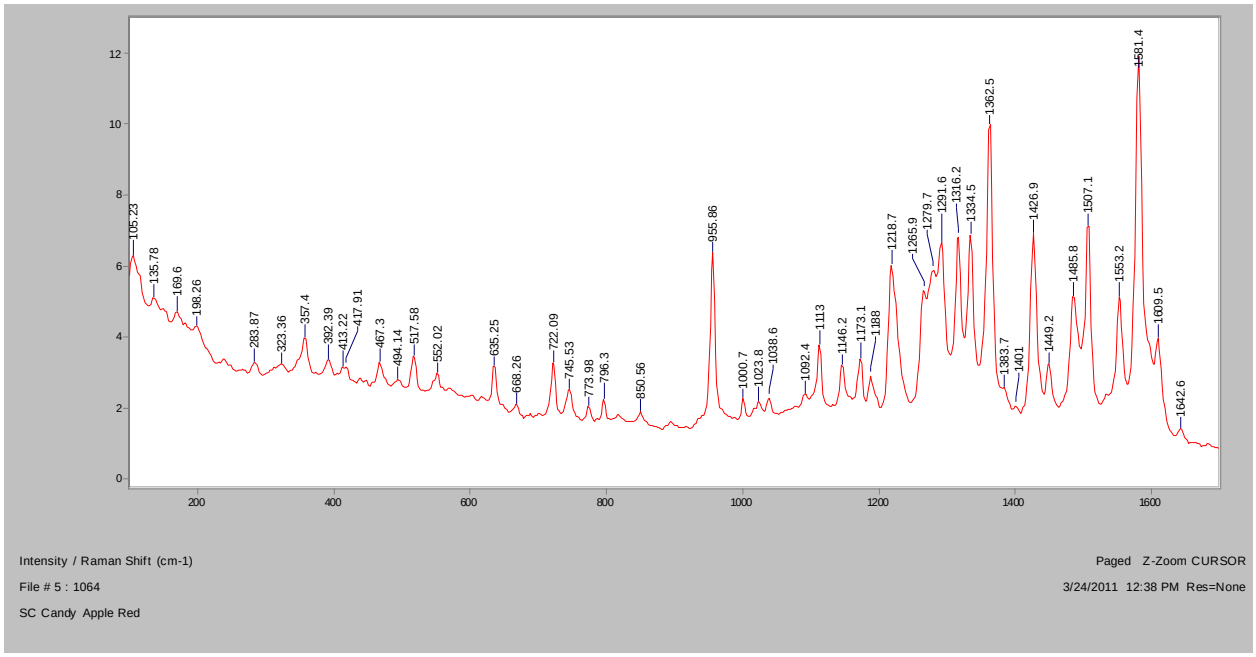

SERS, 488nm

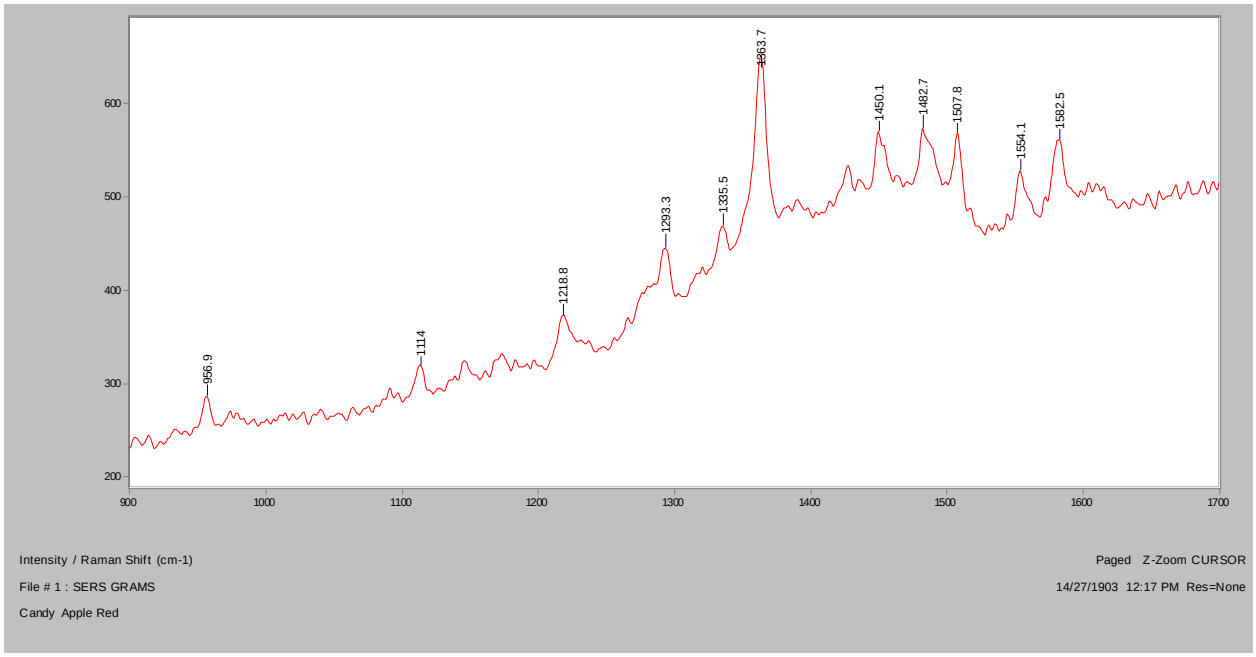

FT-IR (ATR)

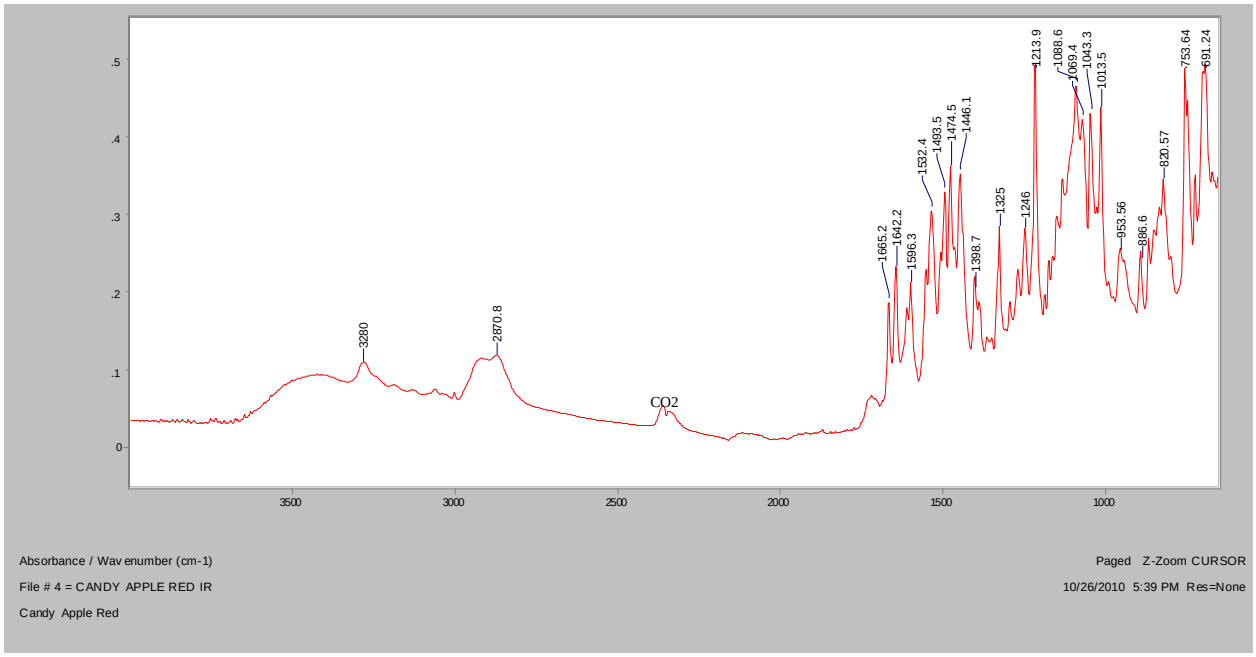

XRF

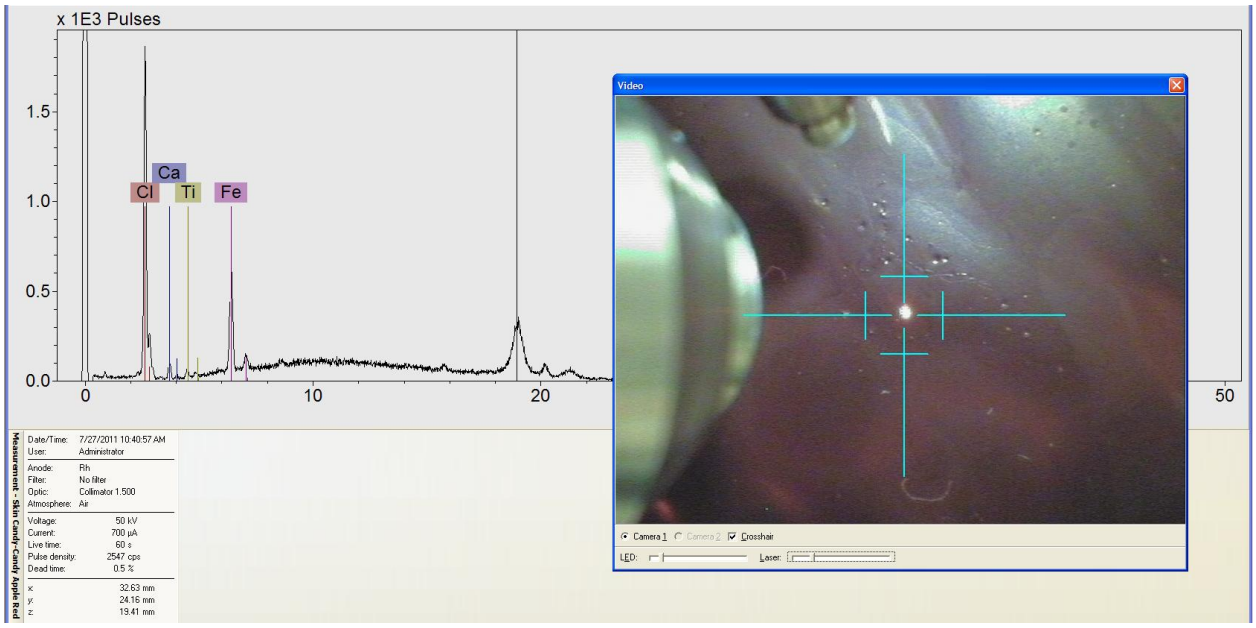
x 1E3 Pulses
1.5
1.0
0.5
0.0
0
10
20
50
Ca
Cl
Ti
Fe
Video
Camera 1
Camera 2
Crosshair
LED:
Laser:
Measurement - Skin Candy-Candy Apple Red
Date/Time: 7/27/2011 10:40:57 AM
User: Administrator
Anode: Rh
Filter: No filter
Optic: Collimator 1.500
Atmosphere: Air
Voltage: 50 kV
Current: 700 µA
Live time: 60 s
Pulse density: 2547 cps
Dead time: 0.5 %
x: 32.63 mm
y: 24.16 mm
z: 19.41 mm

Red Hot

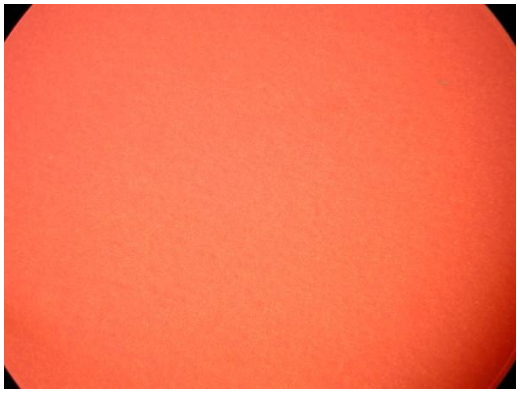

Bright Field, 100x

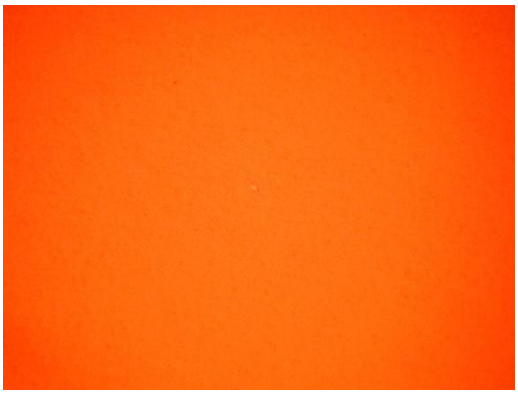

Dark Field, 100x

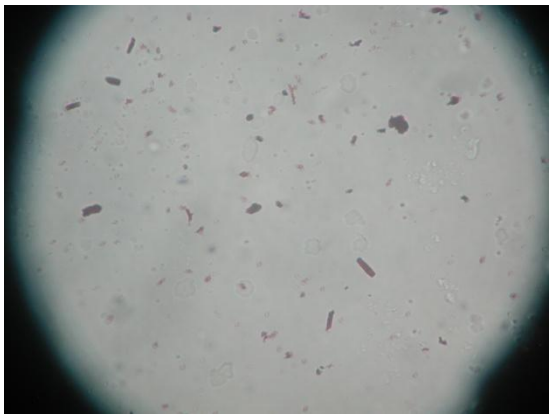

In RI 1.550, 400x

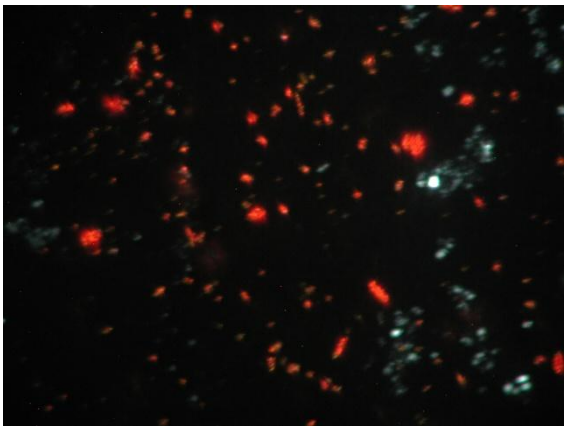

Crossed polars, In RI 1.550, 400x

Normal Raman, 488nm

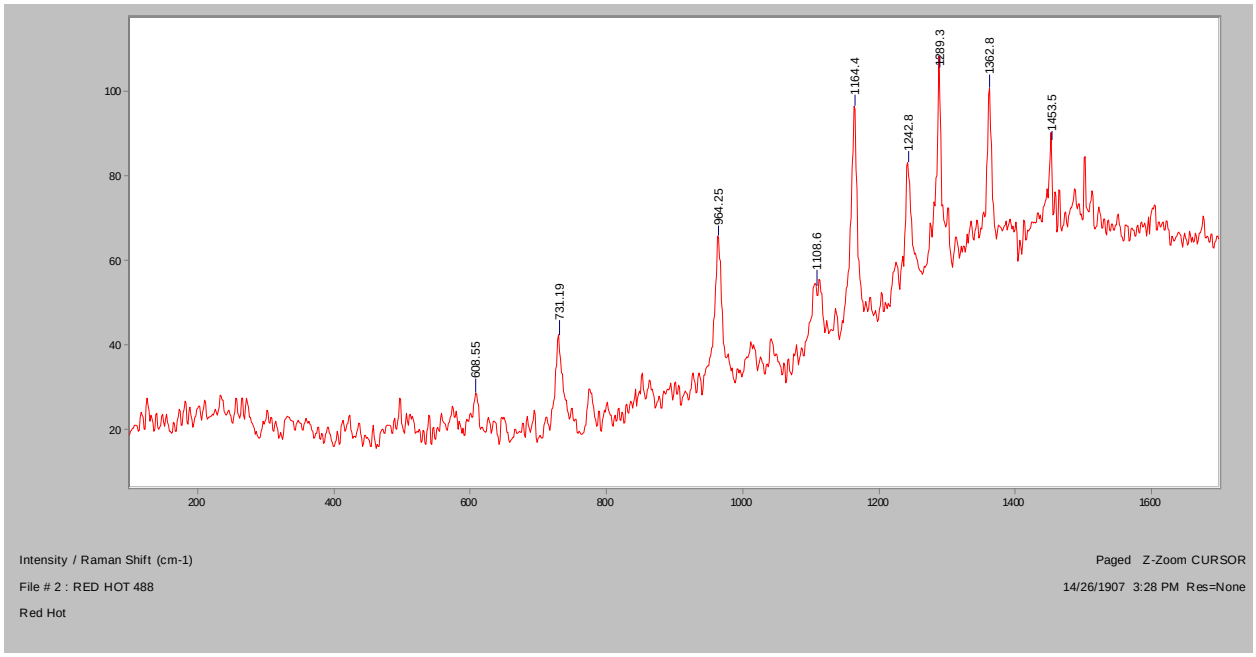

Normal Raman, 633nm

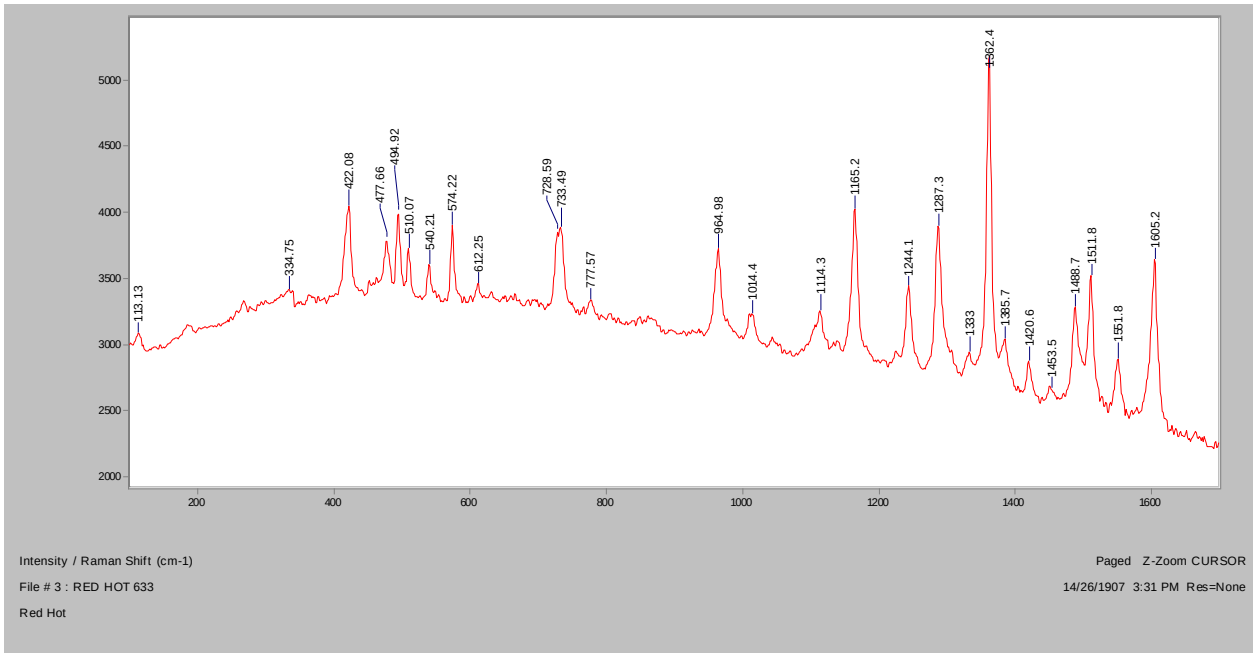

Normal Raman, 785nm

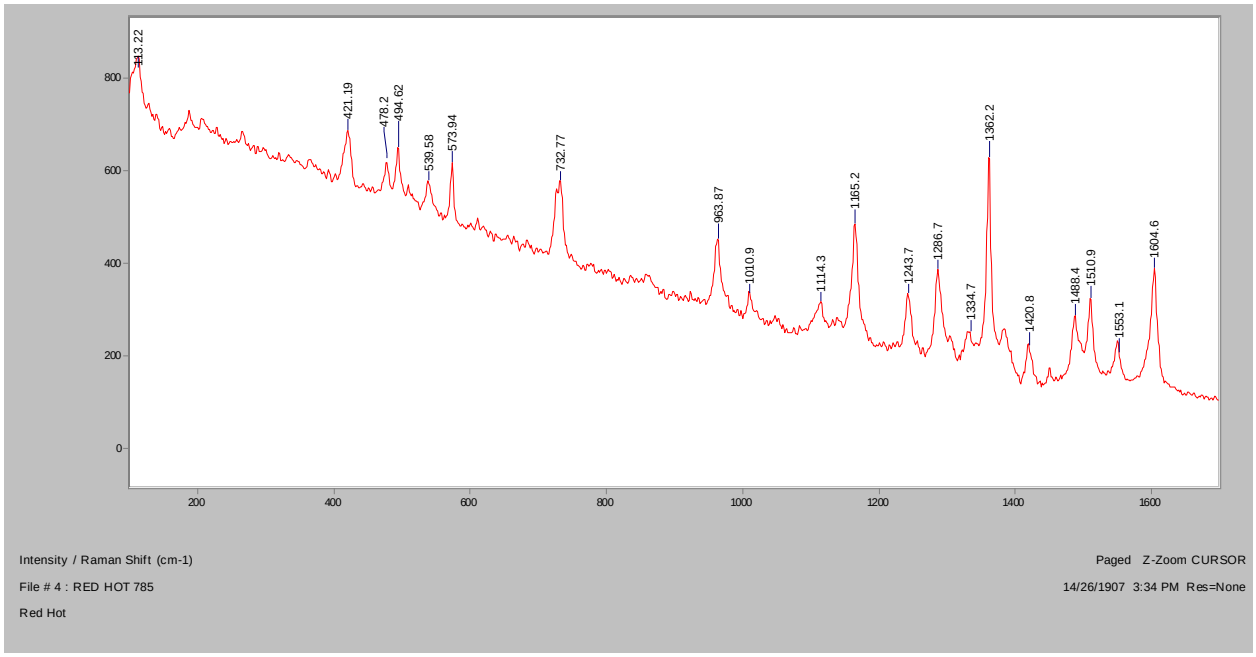

FT-Raman, 1064nm

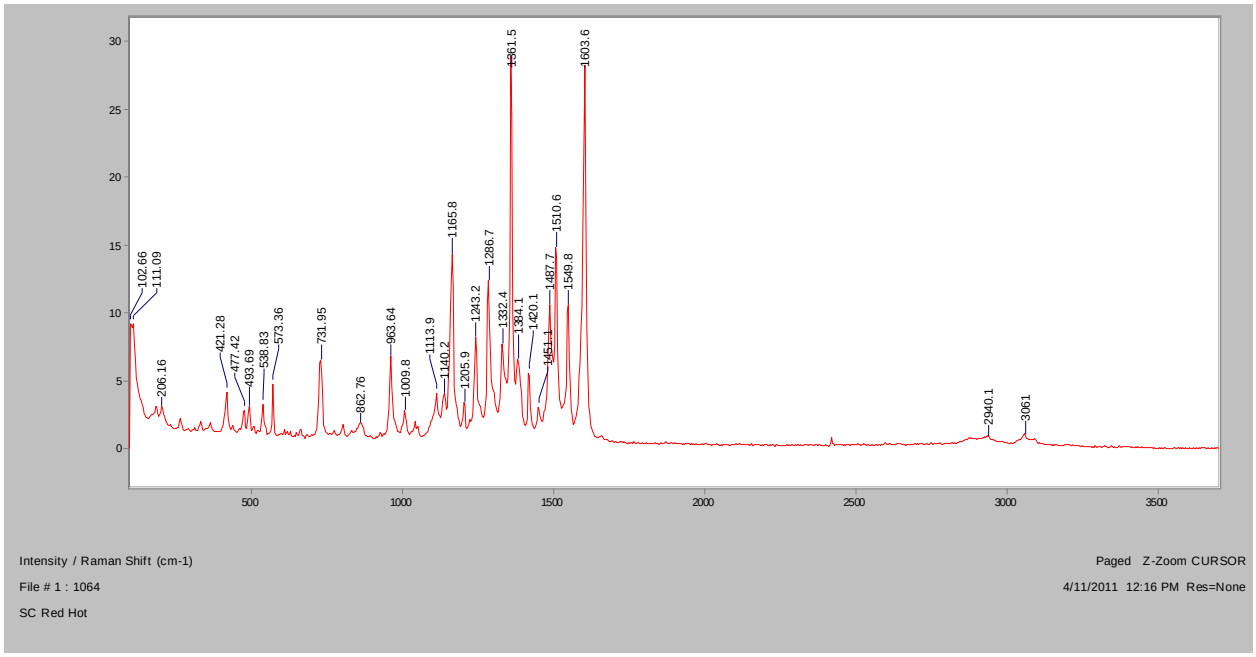

SERS, 488nm

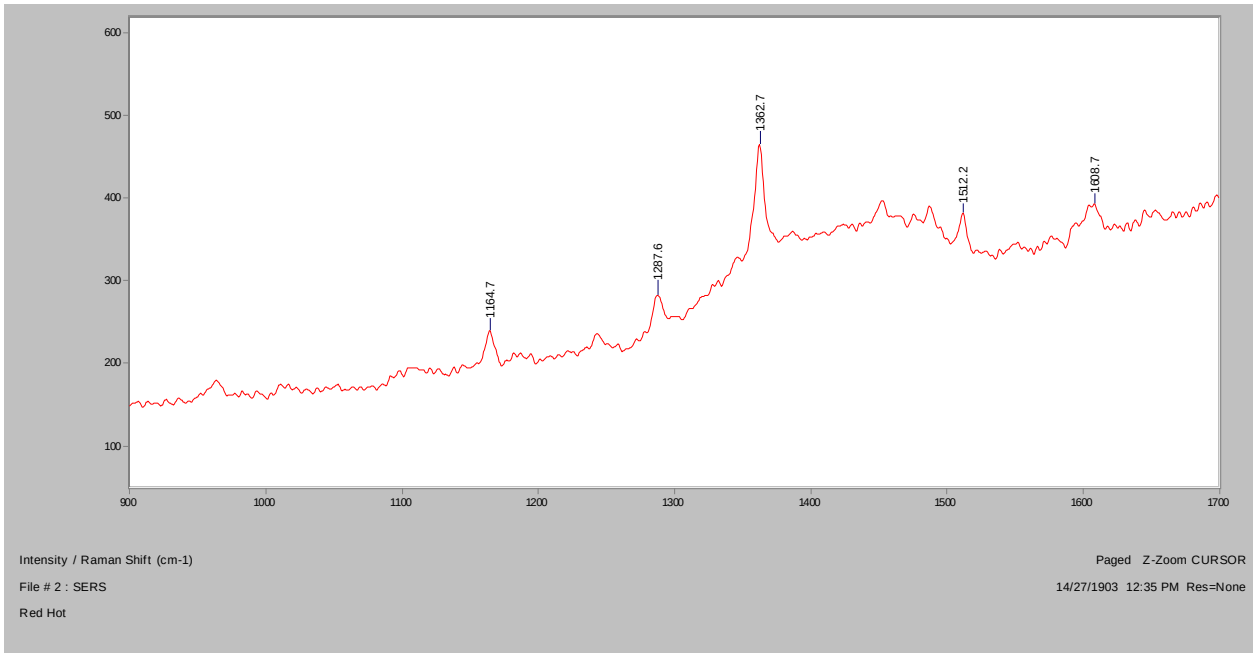

FT-IR (ATR)

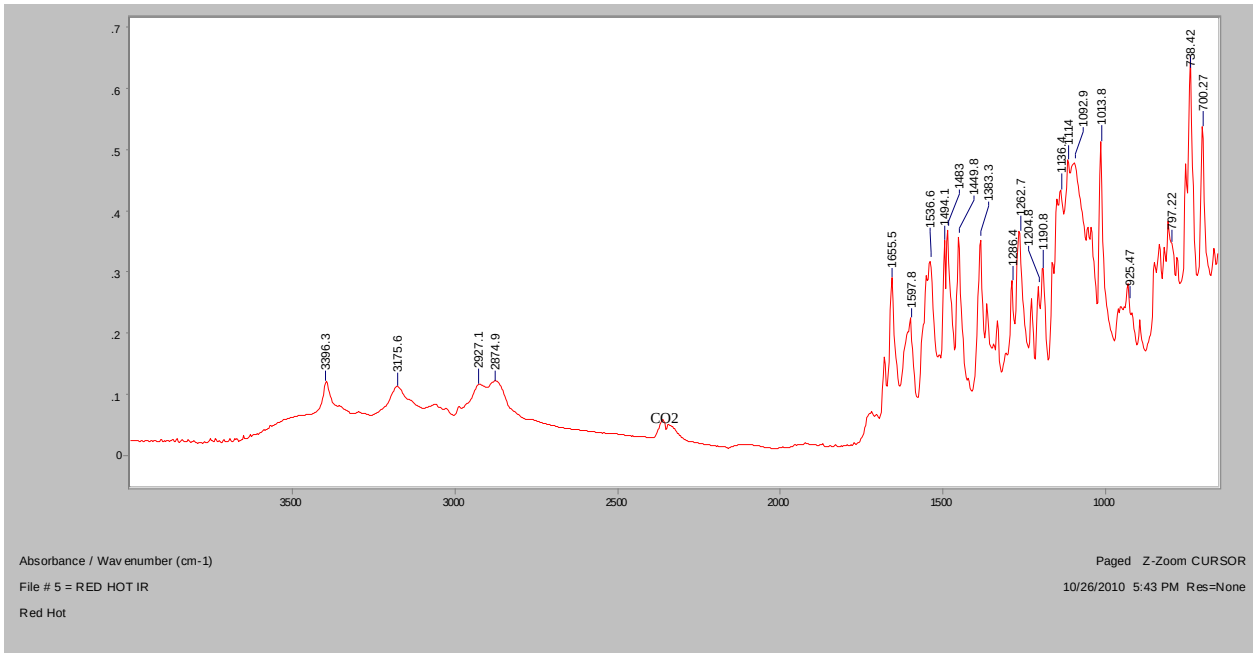

XRF

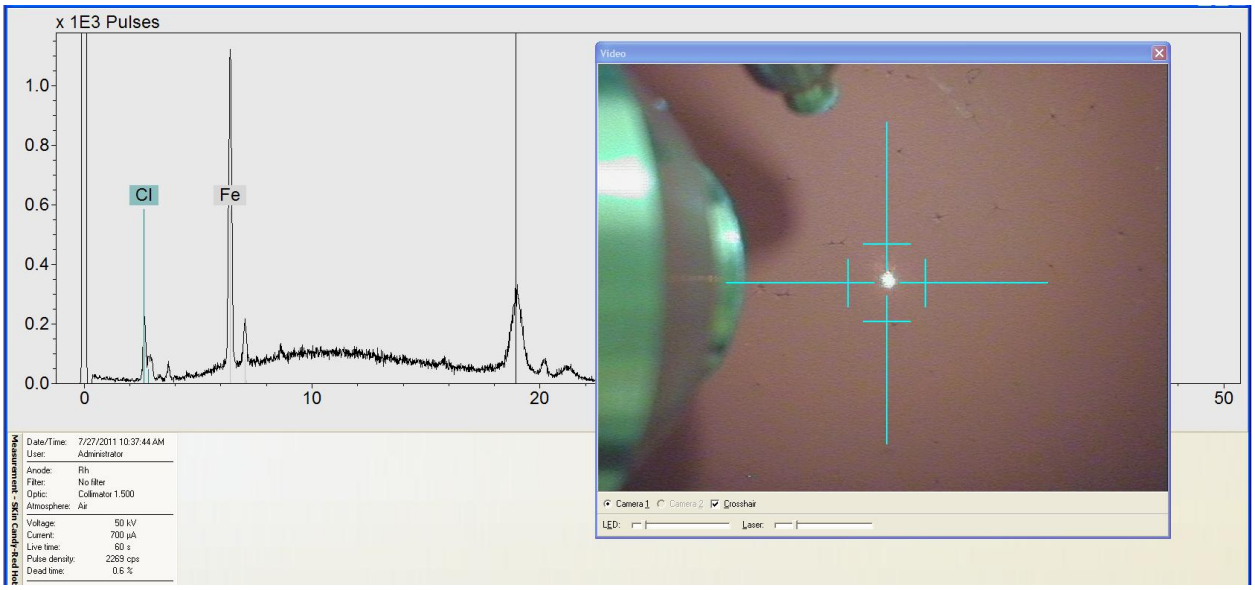
x 1E3 Pulses
1.0
0.8
0.6
0.4
0.2
0.0
Cl
Fe
0
10
20
50
Video
Camera 1
Camera 2
Crosshair
LED:
Laser:
Measurement - SKN Candy-Red Hot
Date/Time: 7/27/2011 10:37:44 AM
User: Administrator
Anode: Rh
Filter: No filter
Optic: Collimator 1.500
Atmosphere: Air
Voltage: 50 kV
Current: 700 µA
Live time: 60 s
Pulse density: 2269 cps
Dead time: 0.6 %

Marz

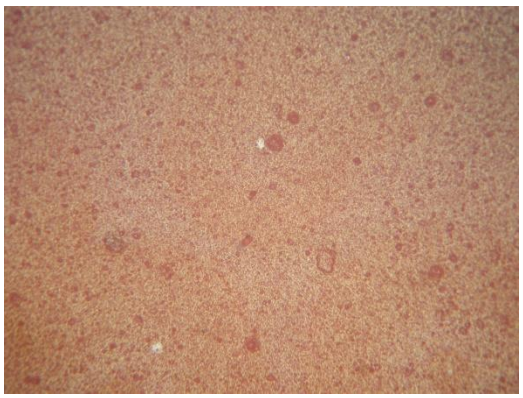

Bright Field, 100x

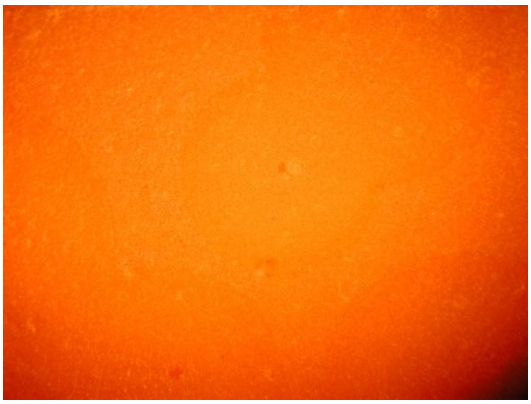

Dark Field, 100x

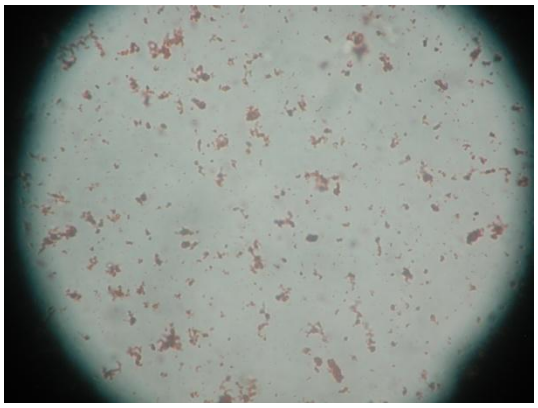

In RI 1.550, 400x

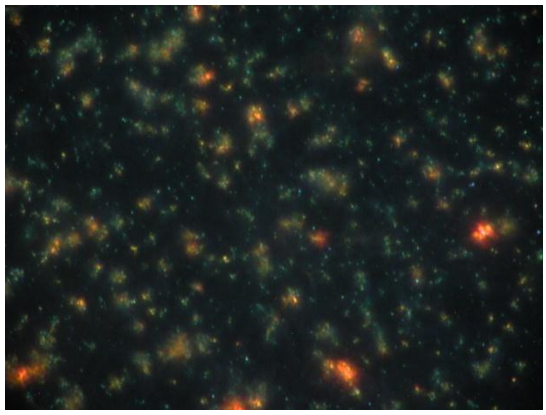

Crossed polars, In RI 1.550, 400x

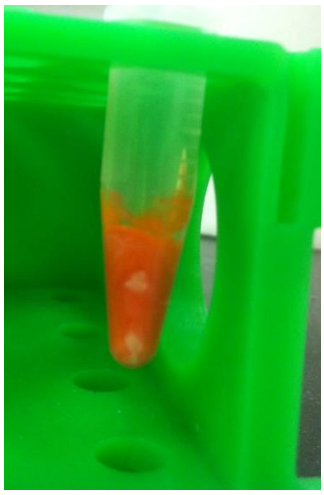

Post-extraction

Normal Raman, 488nm

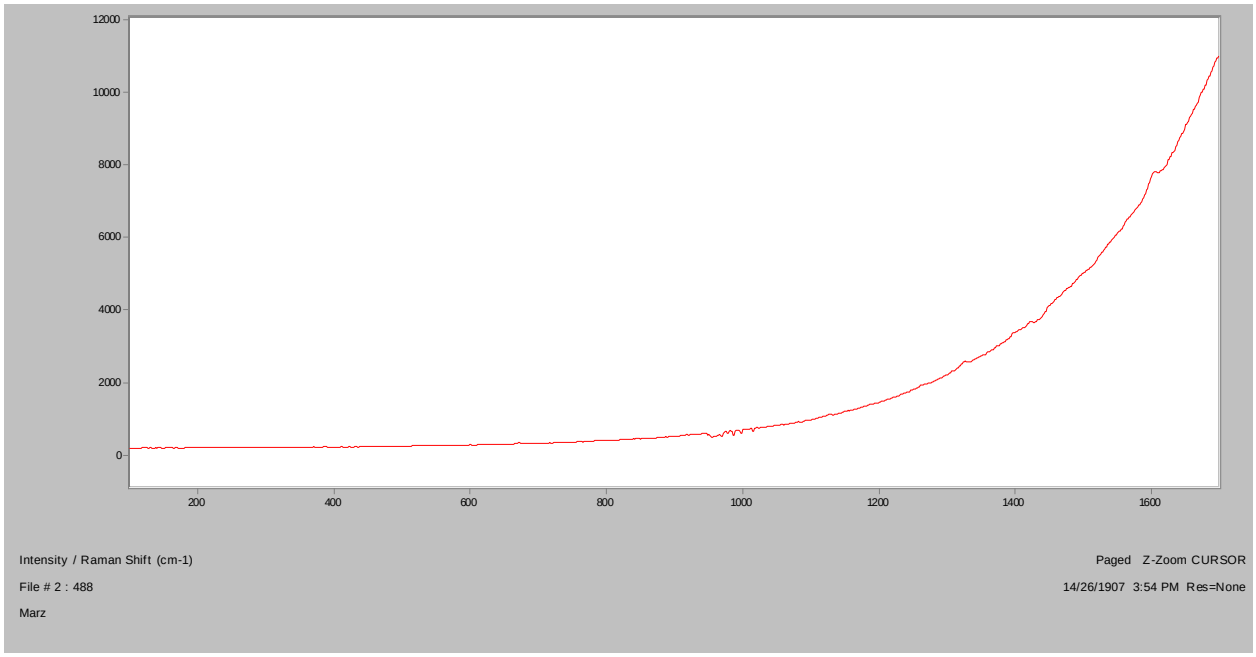

Normal Raman, 633nm

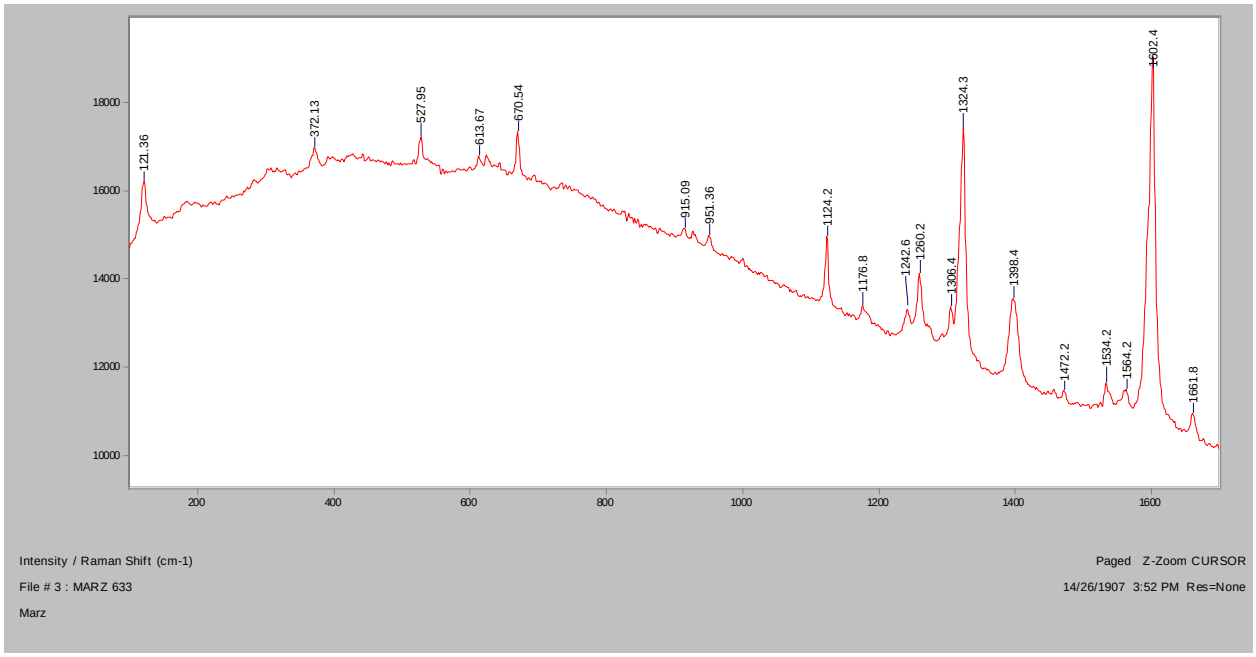

Normal Raman, 785nm

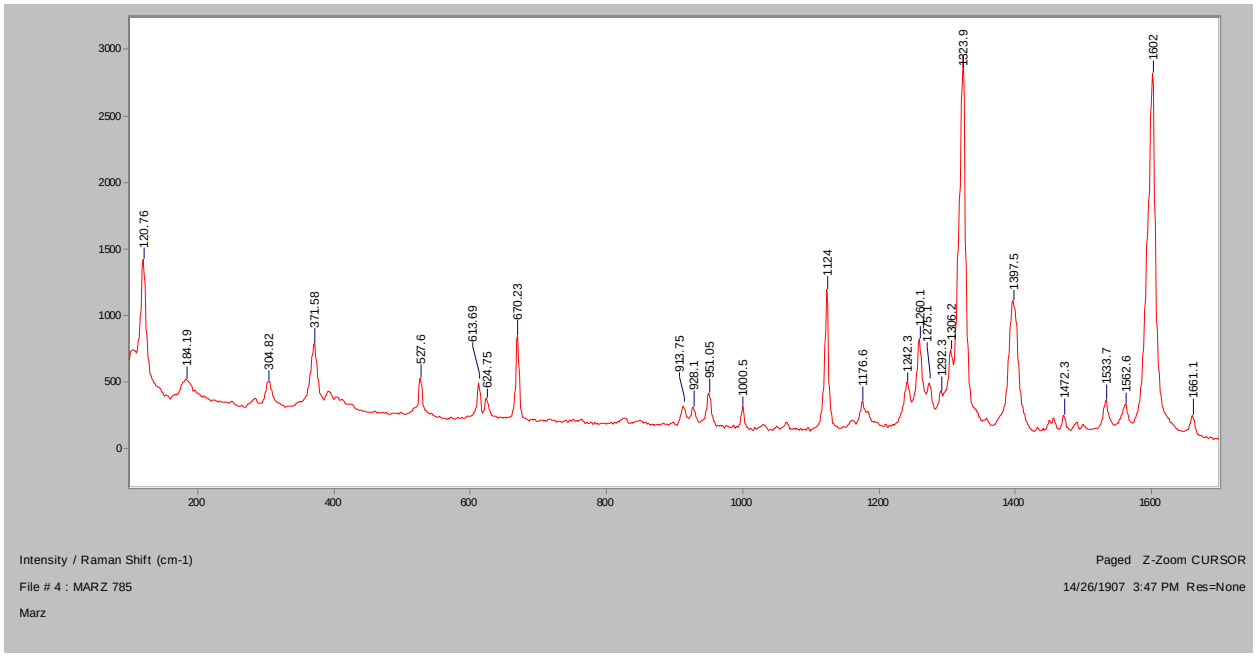

FT-Raman, 1064nm

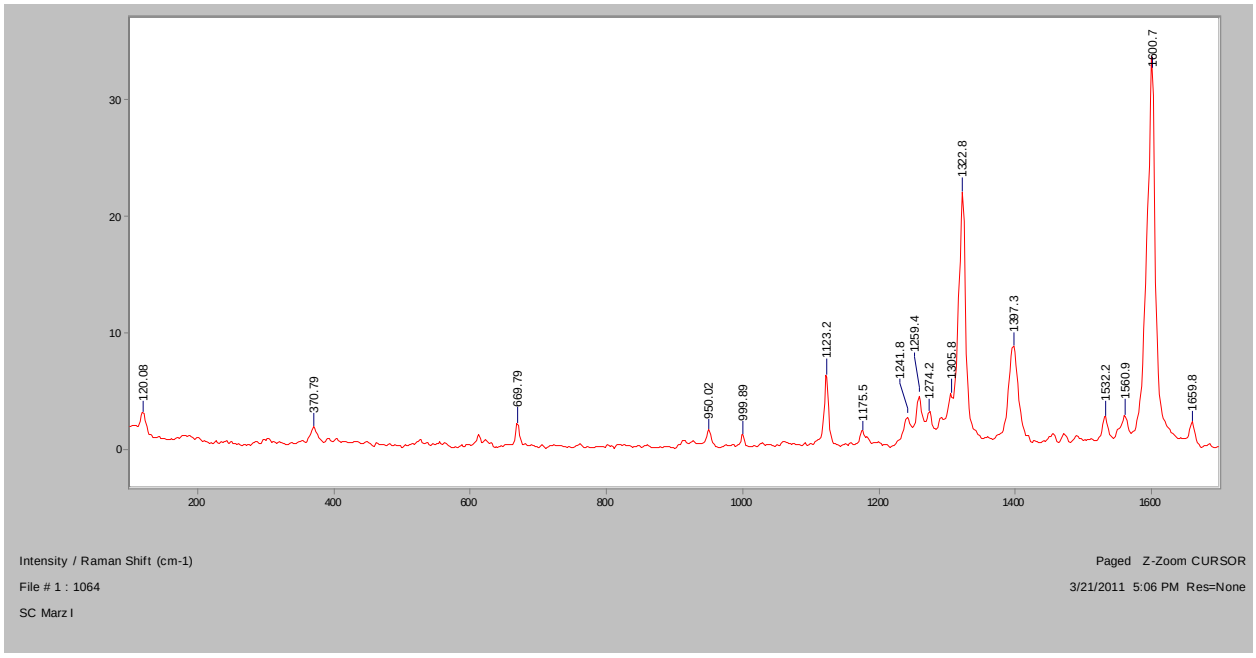

FT-IR (ATR)

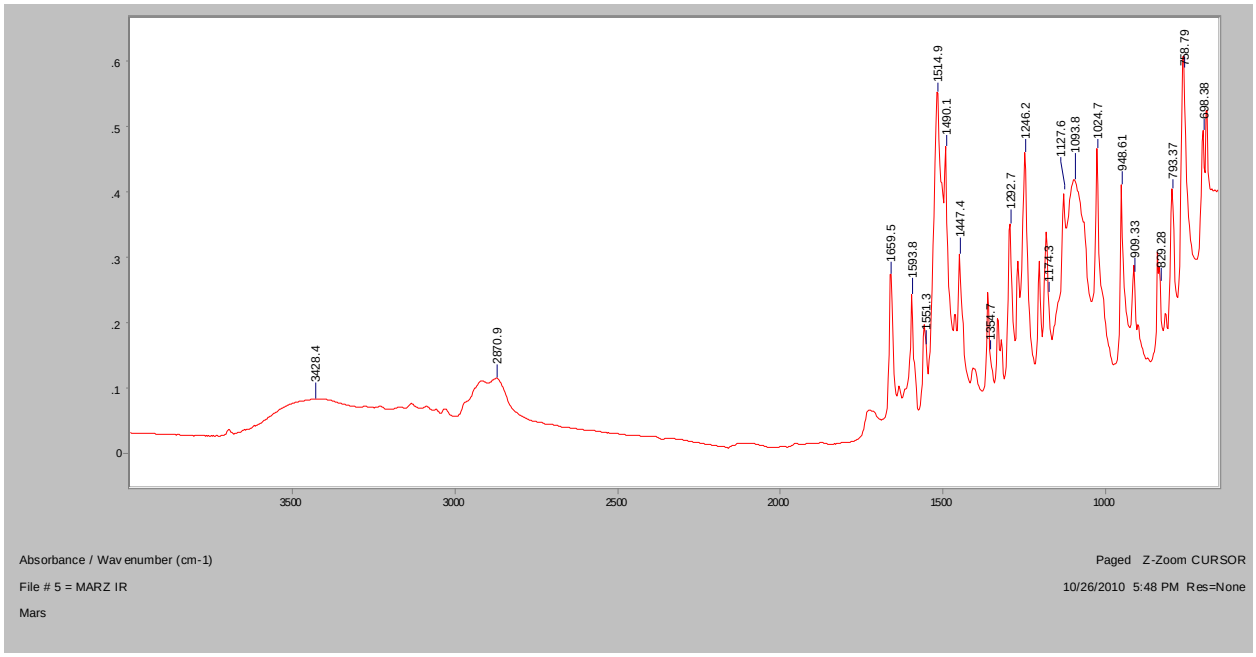
3428.4
2870.9
1659.5
1593.8
1551.3
1514.9
1490.1
1447.4
1354.7
1292.7
1246.2
1174.3
1127.6
1093.8
1024.7
948.61
909.33
829.28
793.37
758.79
698.38
.6
.5
.4
.3
.2
.1
0
3500
3000
2500
2000
1500
1000
Absorbance / Wavenumber (cm-1)
File # 5 = MARZ IR
Mars
Paged Z-Zoom CURSOR
10/26/2010 5:48 PM Res=None

XRF

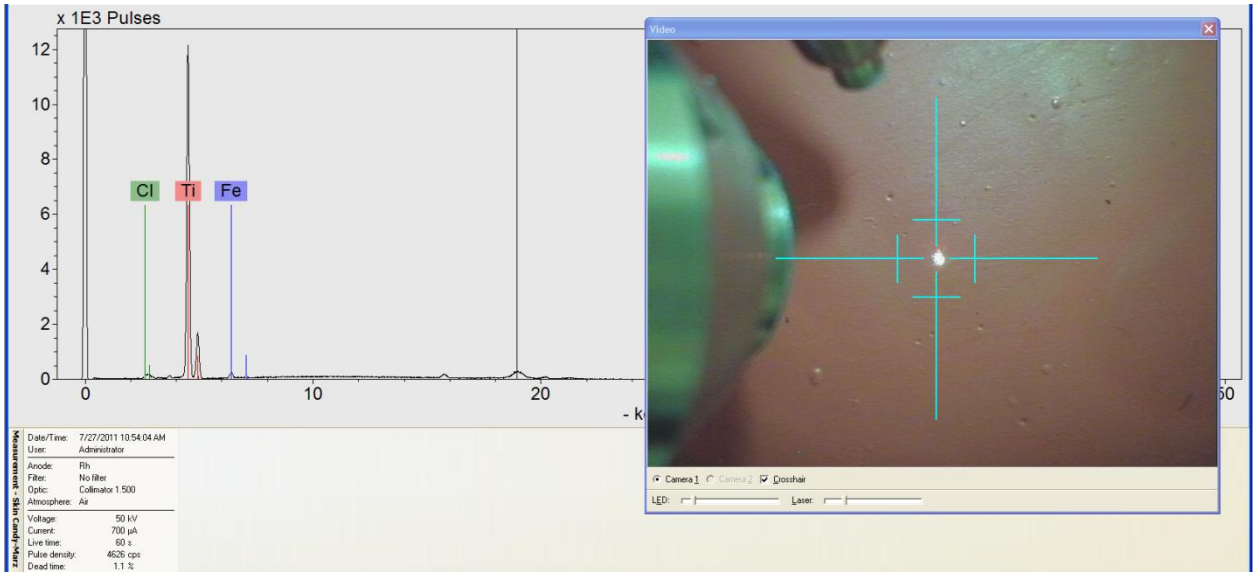
x 1E3 Pulses
12
10
8
6
4
2
0
Cl
Ti
Fe
0
10
20
Video
Camera 1
Camera 2
Crosshair
LED:
Laser:
Measurement - Skin Config.mkaz
Date/Time: 7/27/2011 10:54:04 AM
User: Administrator
Anode: Rh
Filter: No filter
Optic: Collimator 1.500
Atmosphere: Air
Voltage: 50 kV
Current: 700 µA
Live time: 60 s
Pulse density: 4626 cps
Dead time: 1.1 %

Dolemite

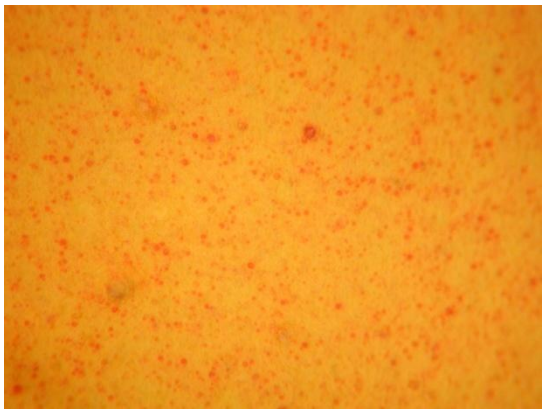

Bright Field, 400x

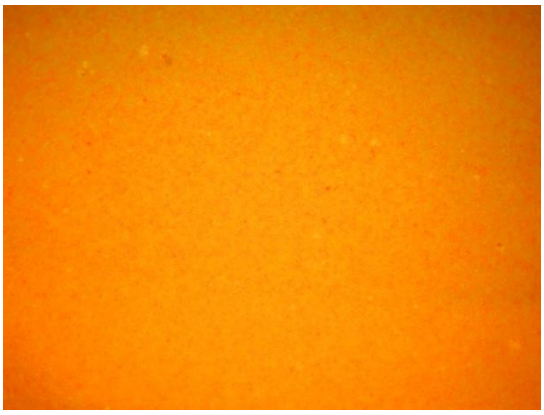

Dark Field, 100x

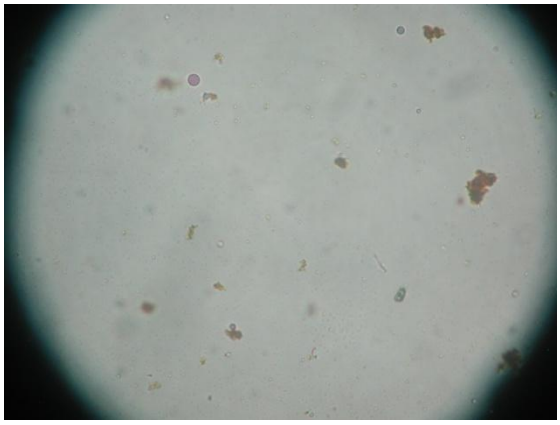

In RI 1.550, 400x

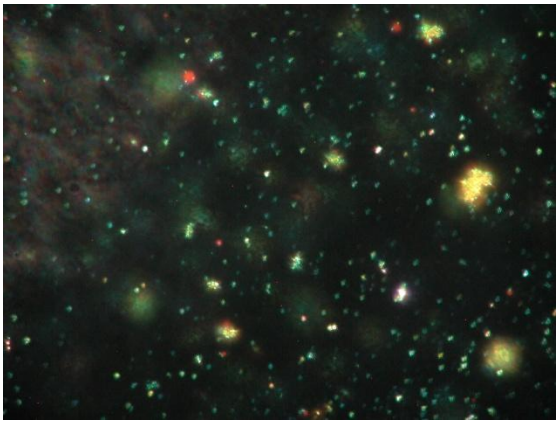

Crossed polars, In RI 1.550, 400x

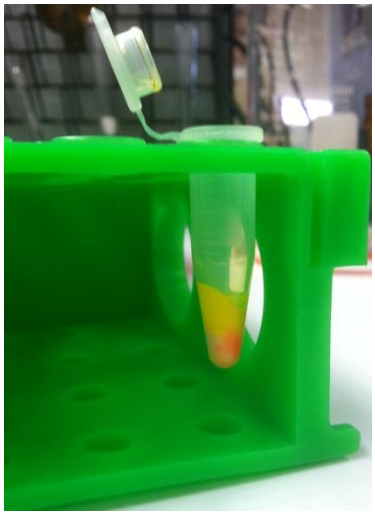

Post-extraction

Normal Raman, 488nm

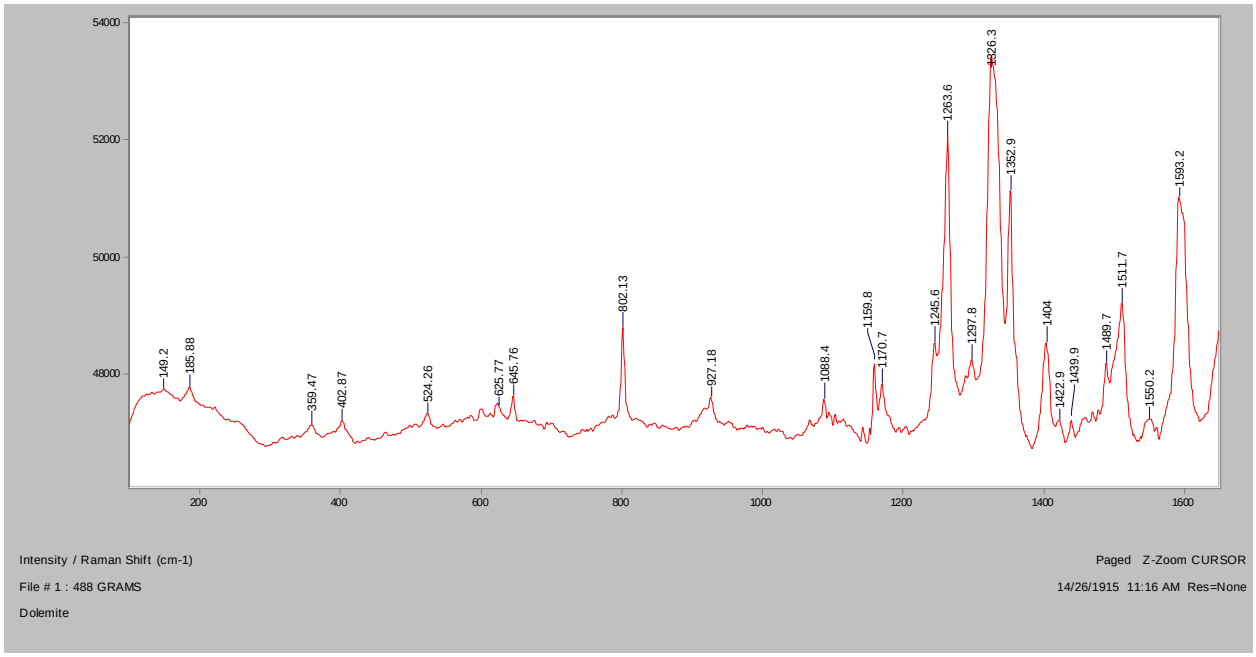

Normal Raman, 633nm

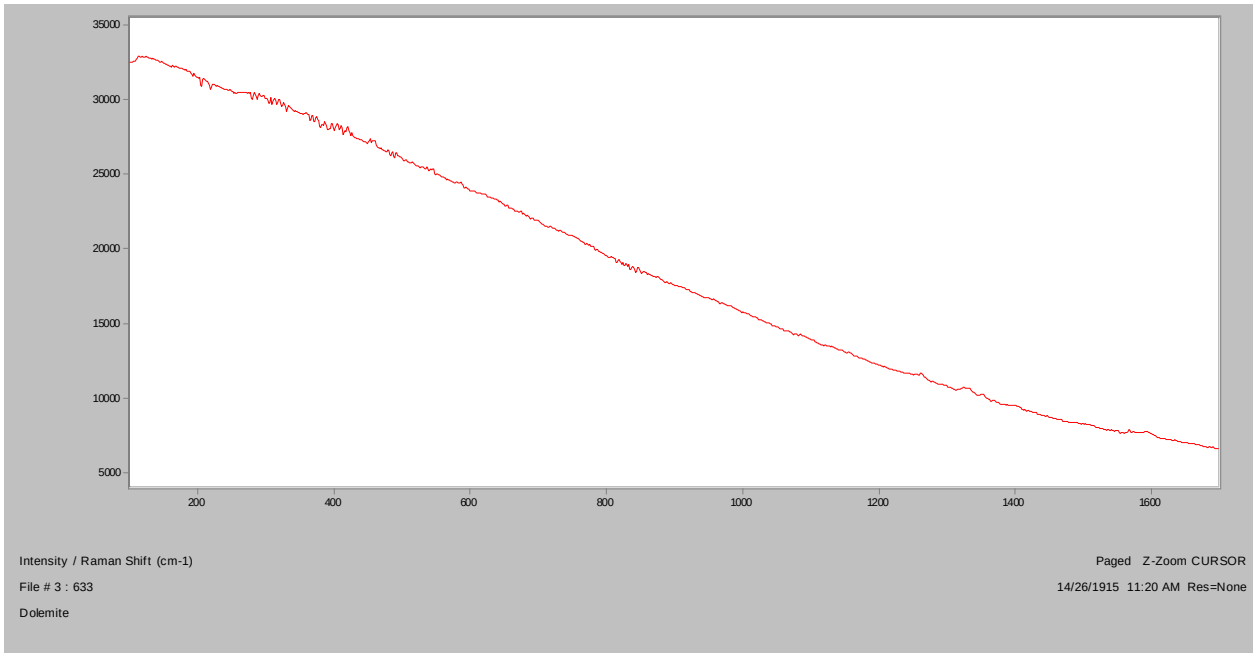

Normal Raman, 785nm

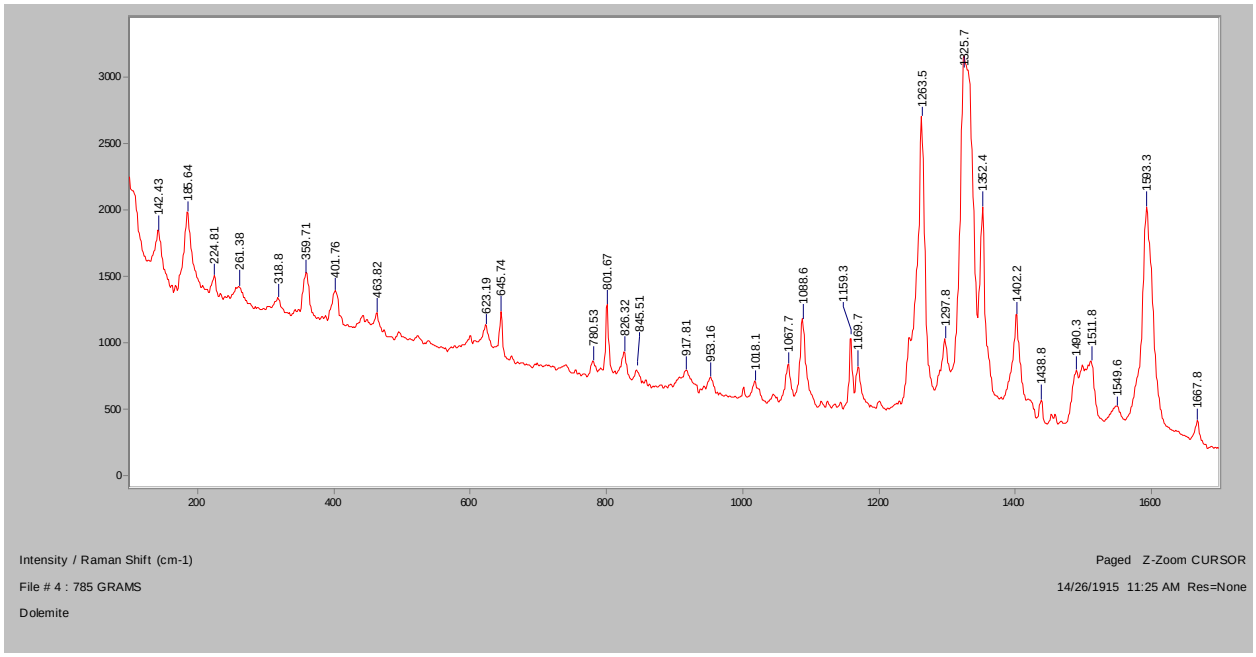

FT-Raman, 1064nm

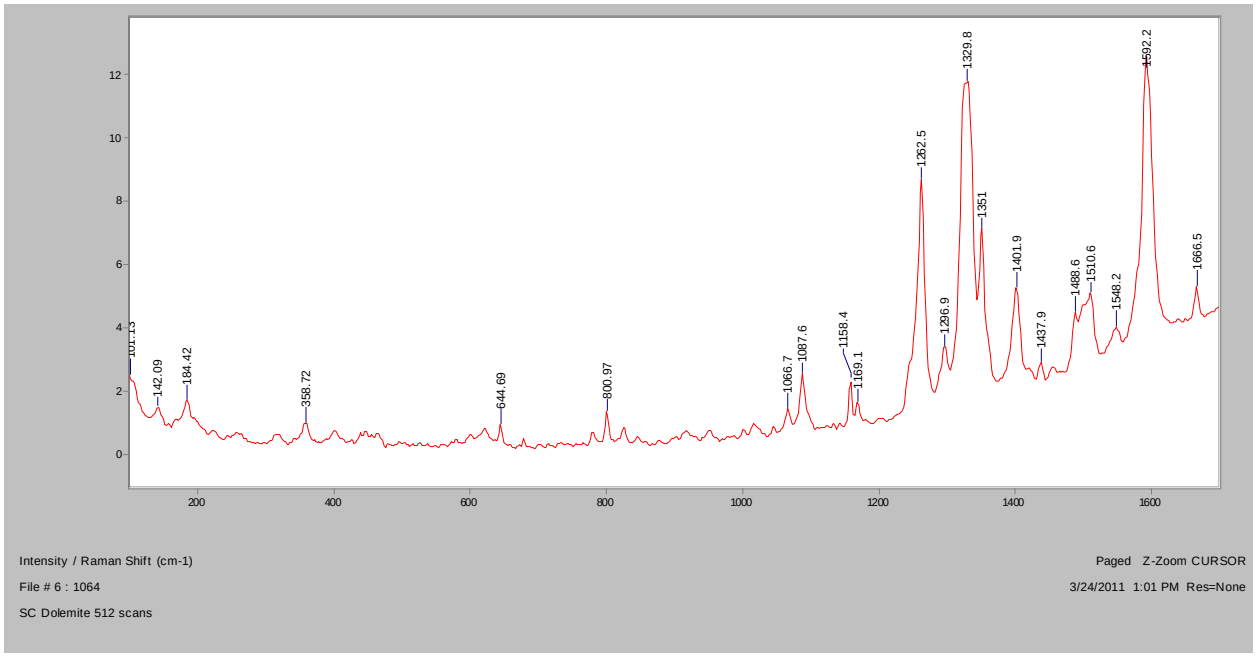

SERS, 488nm

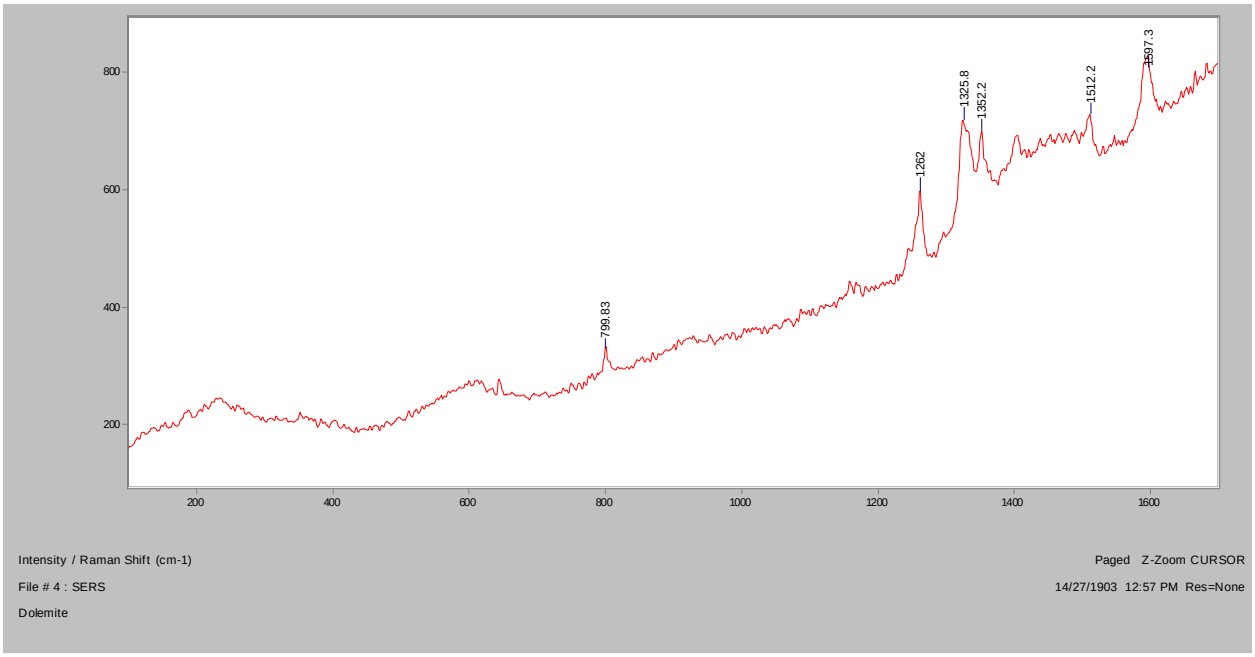

FT-IR (ATR)

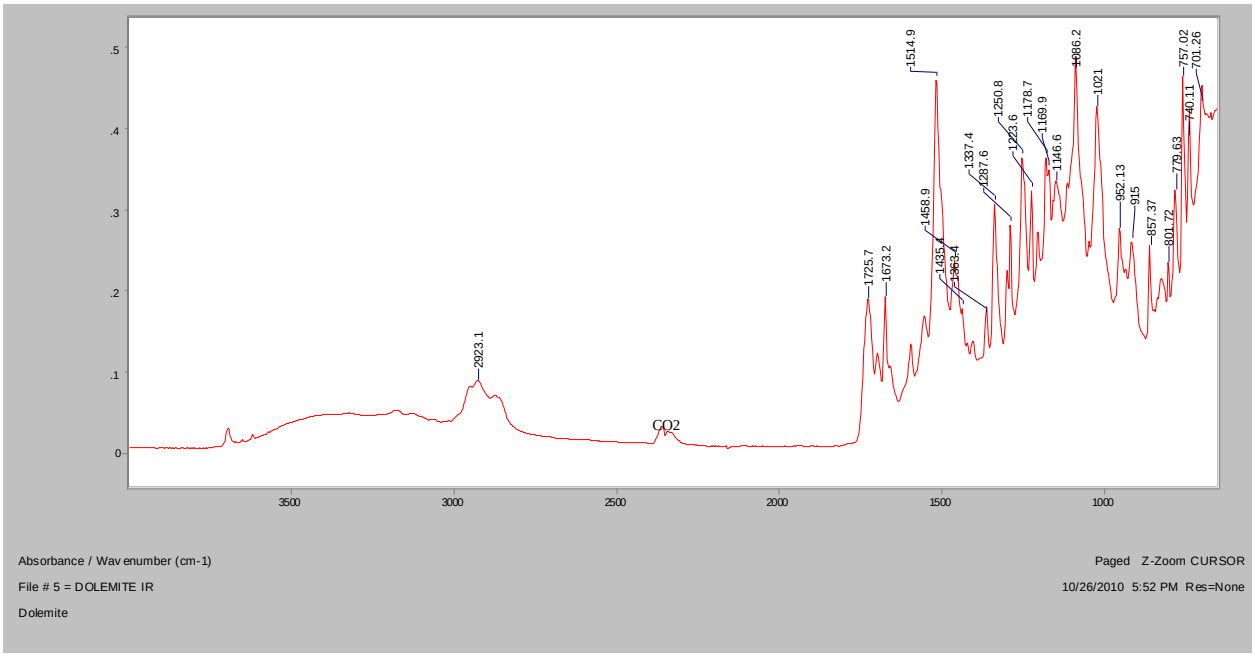

XRF

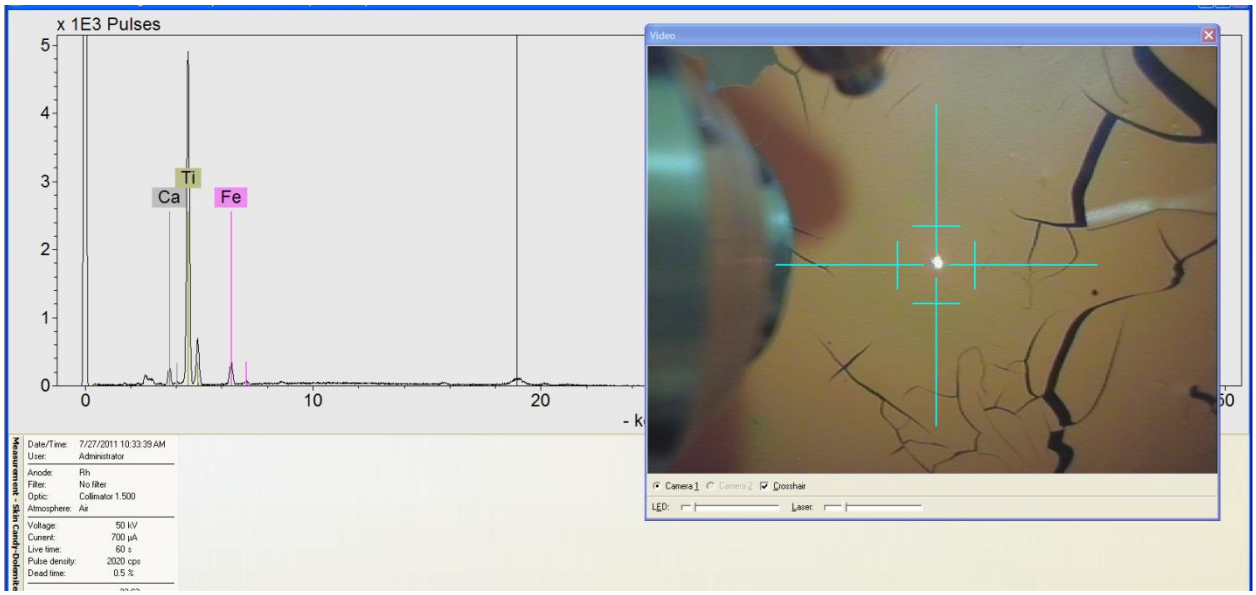
x 1E3 Pulses
5
4
3
2
1
0
Ti
Ca
Fe
0
10
20
Video
Camera 1
Camera 2
Crosshair
LED:
Laser:
Date/Time: 7/27/2011 10:33:39 AM
User: Administrator
Anode: Rh
Filter: No filter
Optic: Collimator 1.500
Atmosphere: Air
Voltage: 50 kV
Current: 700 µA
Live time: 60 s
Pulse density: 2020 cps
Dead time: 0.5 %

Blisterine

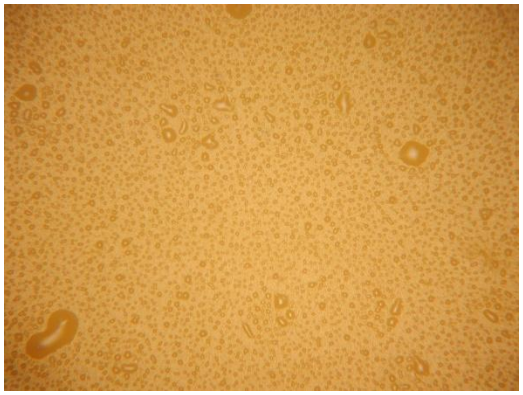

Bright Field, 100x

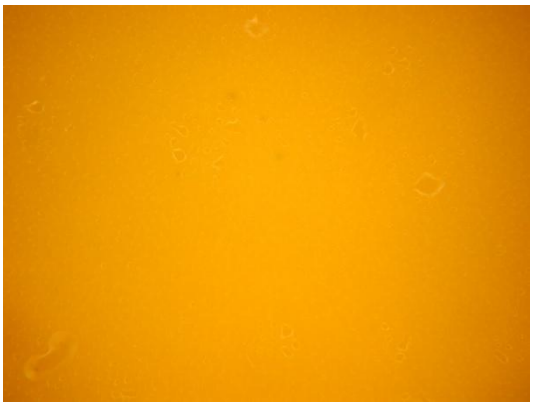

Dark Field, 100x

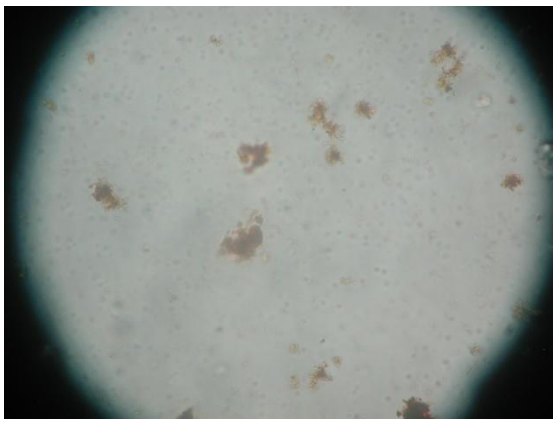

In RI 1.550, 400x

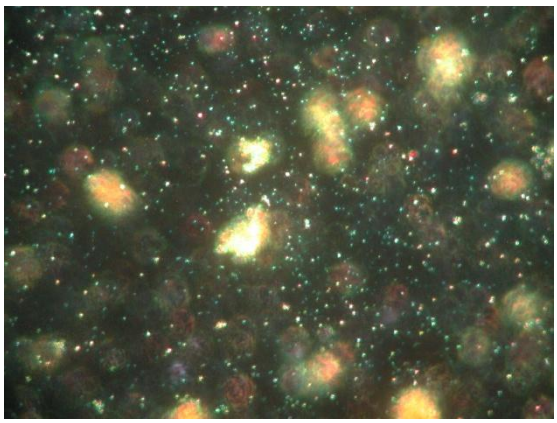

Crossed polars, In RI 1.550, 400x

Normal Raman, 488nm

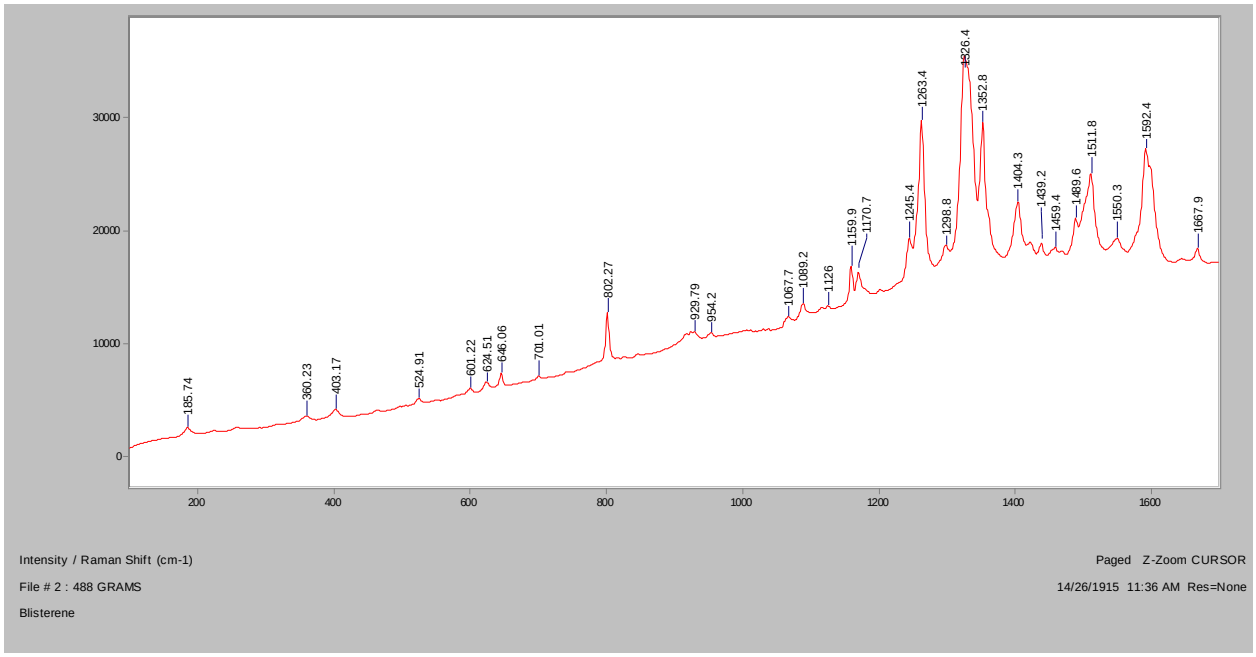

Normal Raman, 633nm

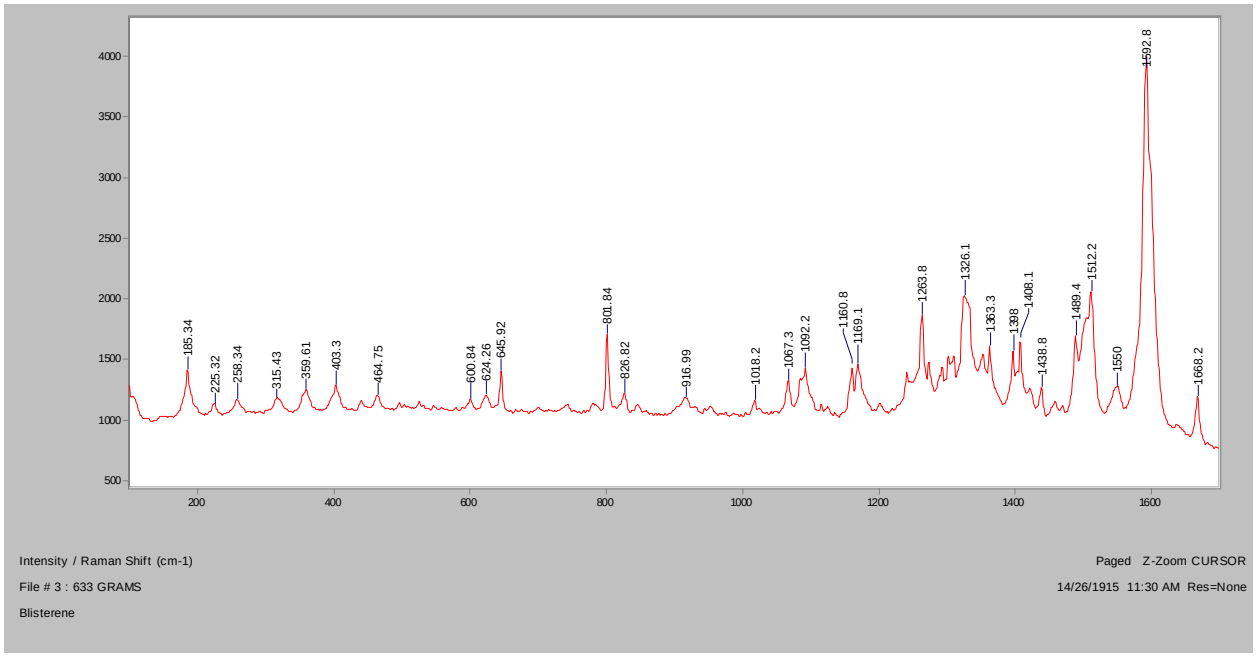

Normal Raman, 785nm

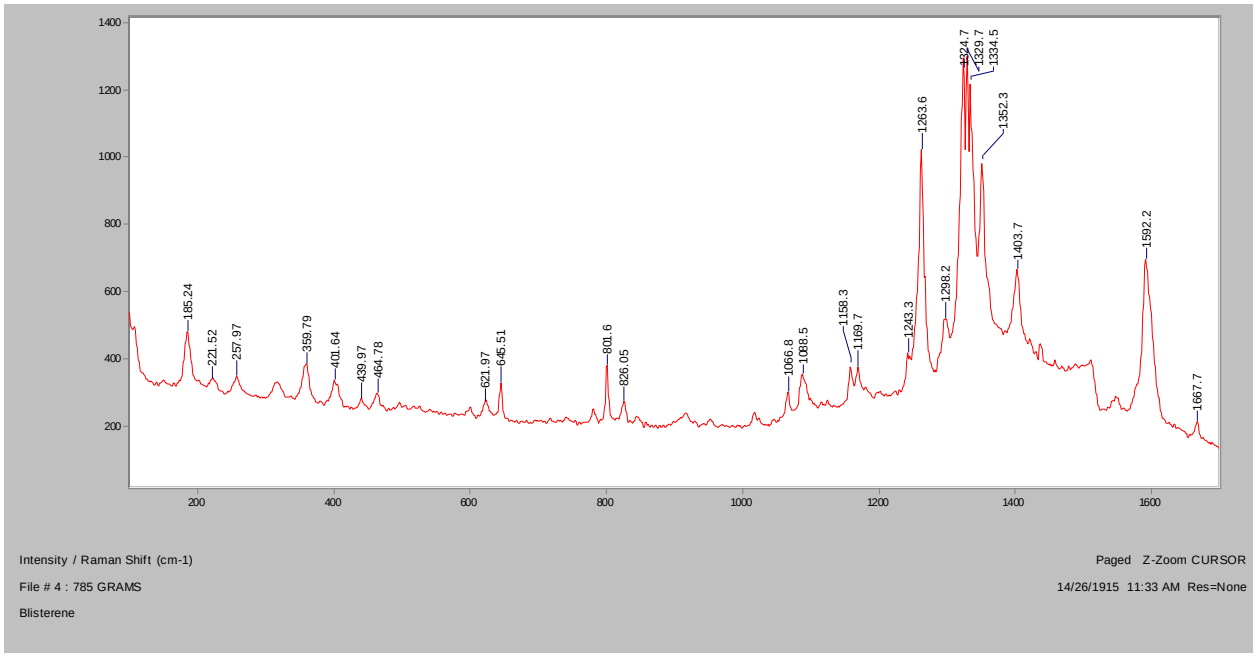

FT-Raman, 1064nm

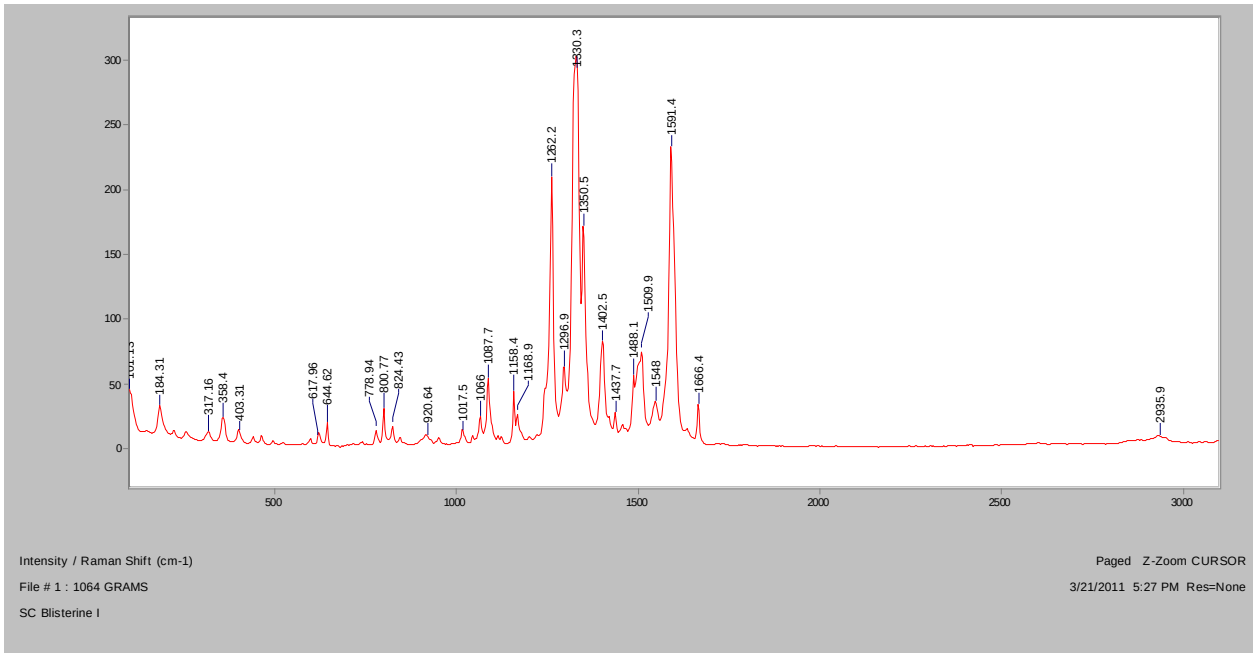

SERS, 488nm

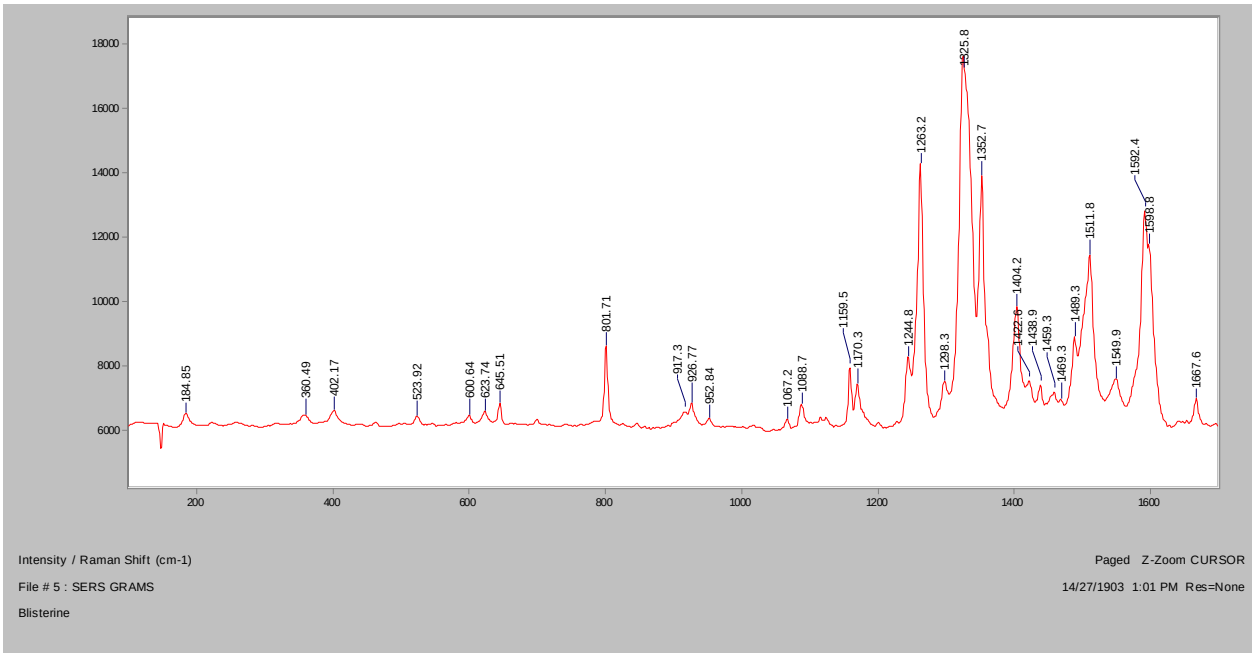

FT-IR (ATR)

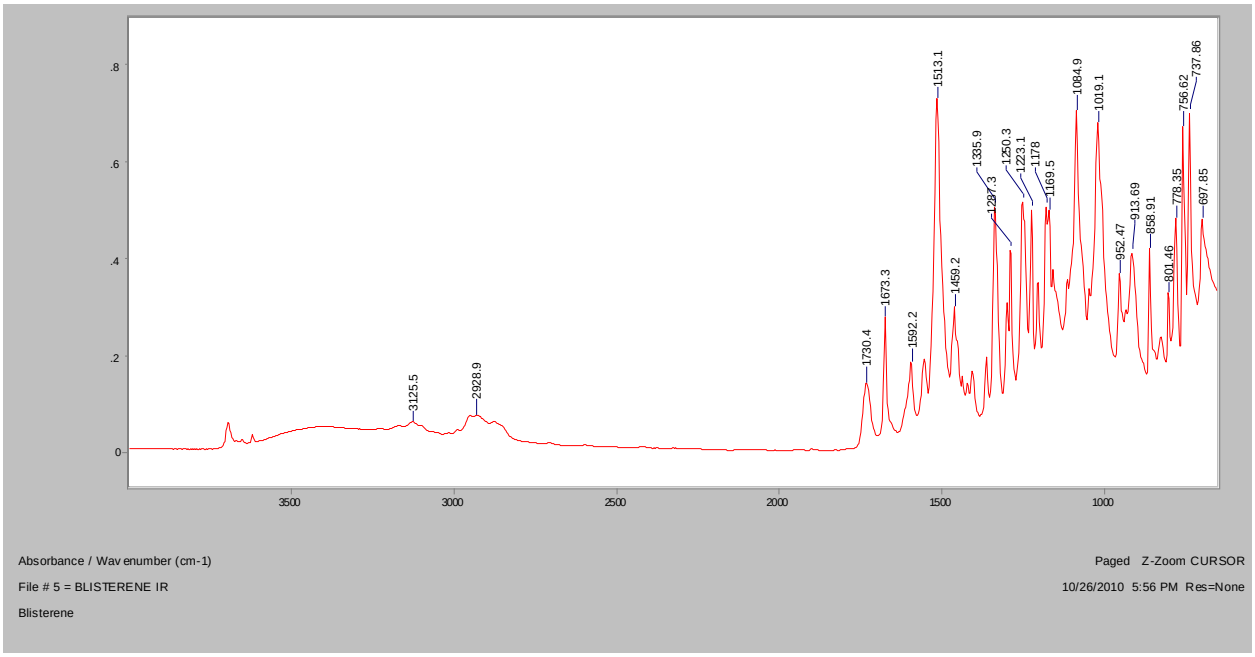

XRF

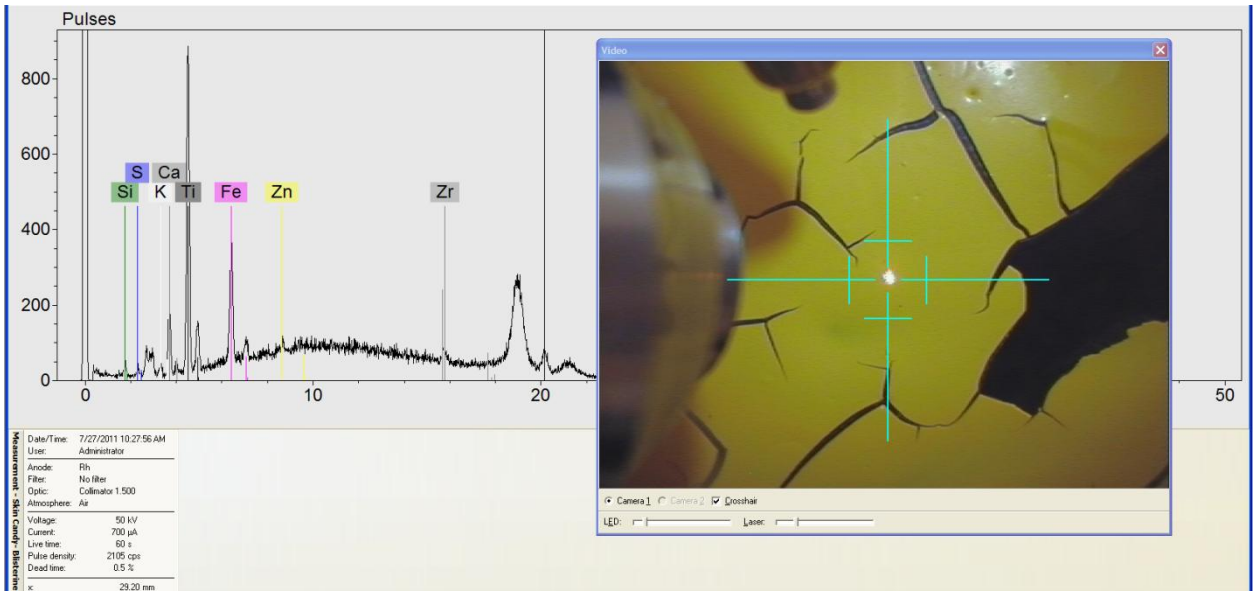
Pulses
800
600
400
200
0
0
10
20
50
S
Ca
Si
K
Ti
Fe
Zn
Zr
Video
Camera 1
Crosshair
LED:
Laser:
Measurement - Skin Candy - Diskrete
Date/Time: 7/27/2011 10:27:56 AM
User: Administrator
Anode: Rh
Filter: No filter
Optic: Collimator 1.500
Atmosphere: Air
Voltage: 50 kV
Current: 700 µA
Live time: 60 s
Pulse density: 2105 cps
Dead time: 0.5 %
x: 29.20 mm

Sassygrass

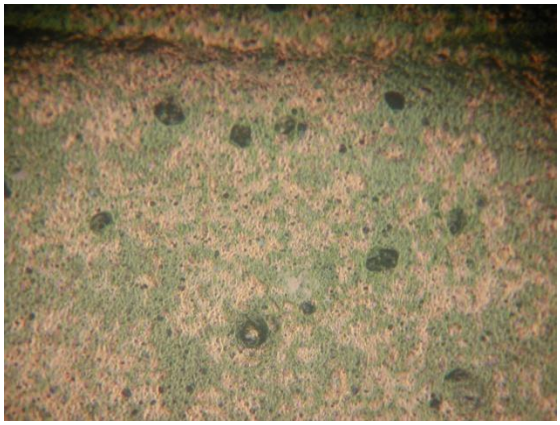

Bright Field, 100x

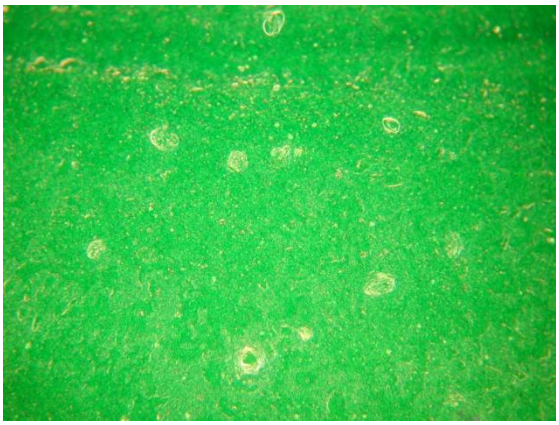

Dark Field, 100x

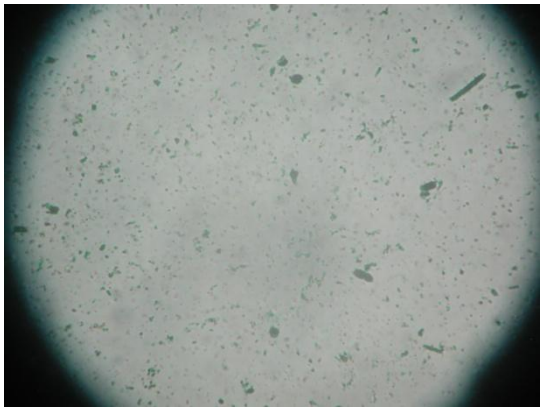

In RI 1.550, 400x

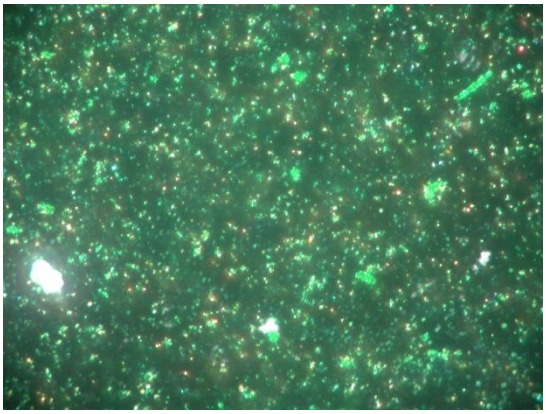

Crossed polars, In RI 1.550, 400x

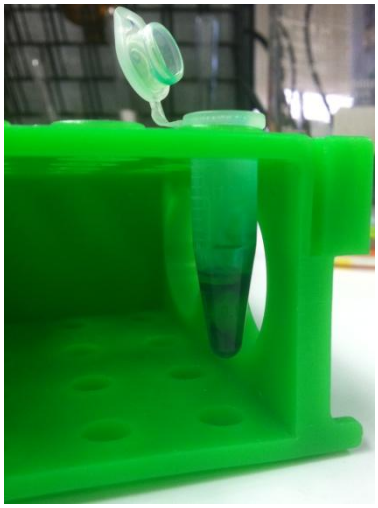

Post-extraction

Normal Raman, 488nm

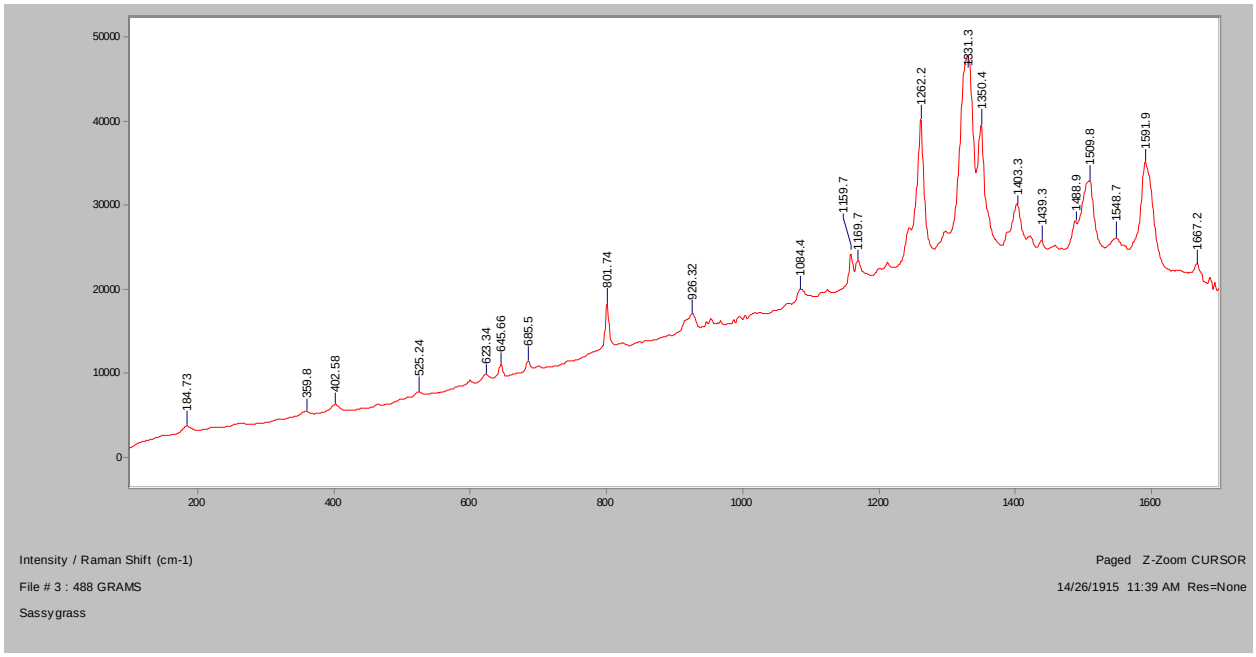

Normal Raman, 633nm

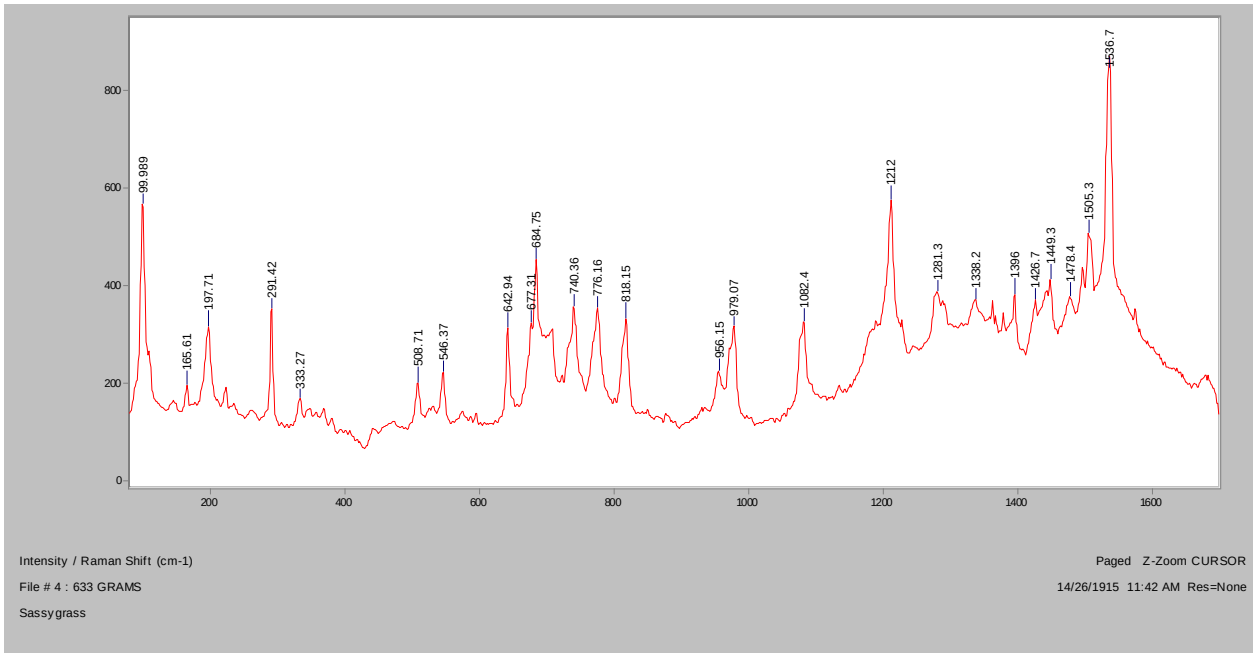

Normal Raman, 785nm

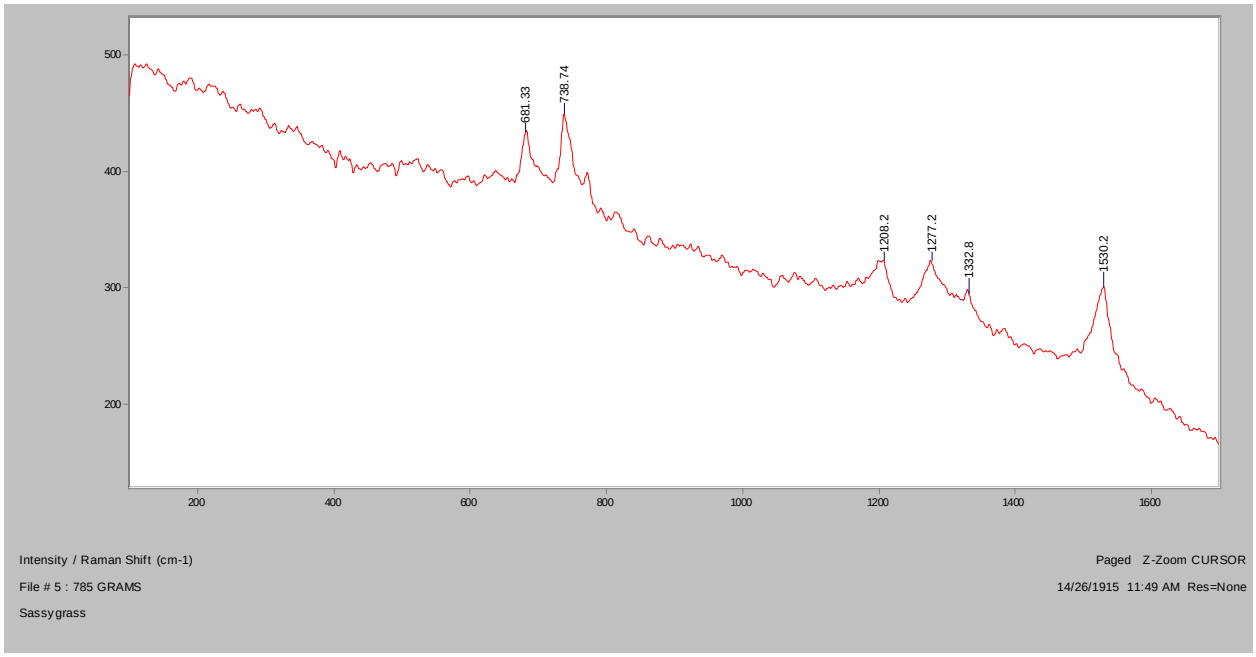

FT- Raman, 1064nm

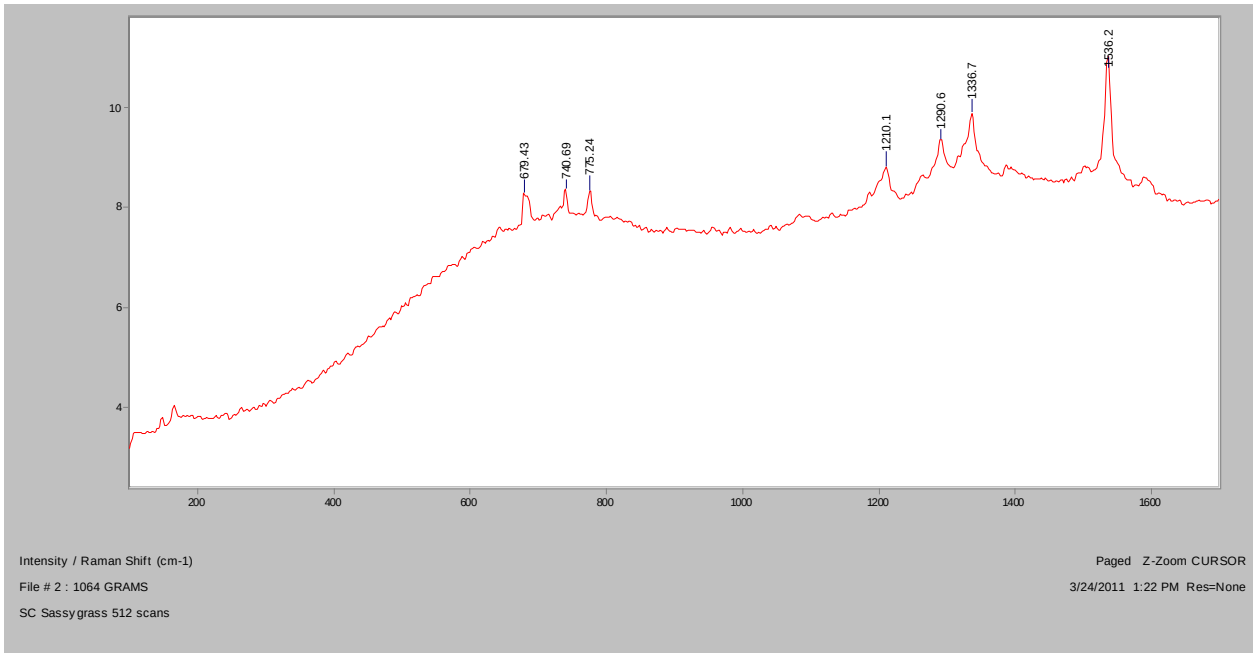

SERS, 488nm

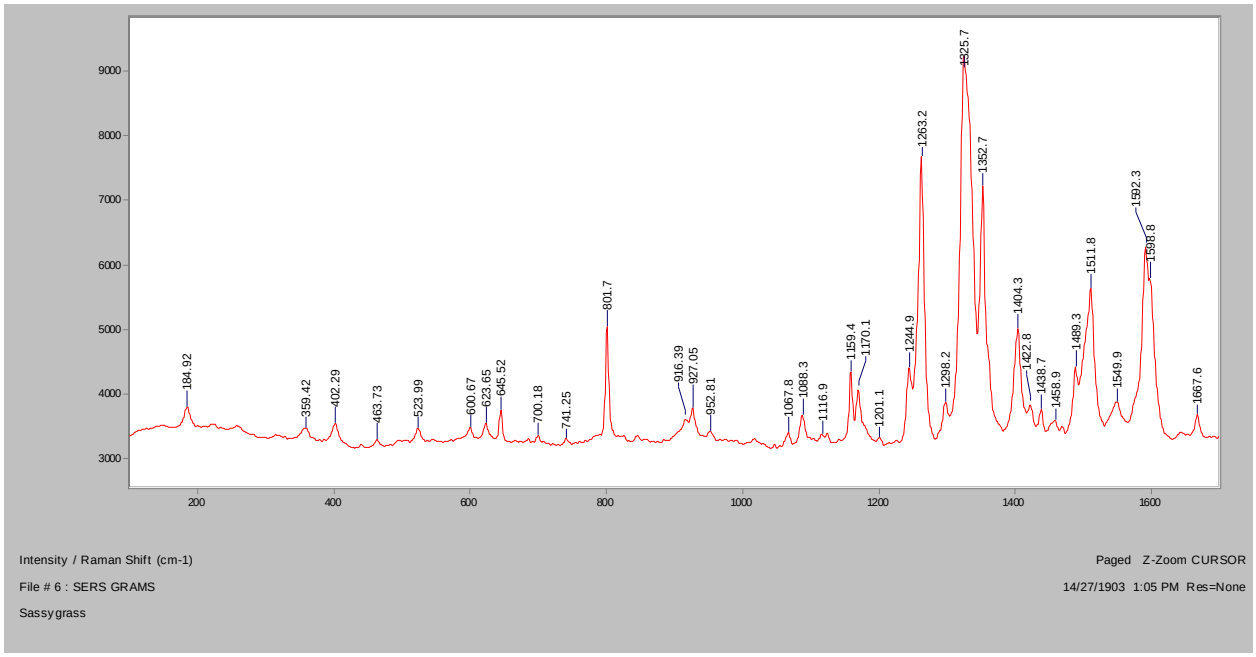

FT-IR (ATR)

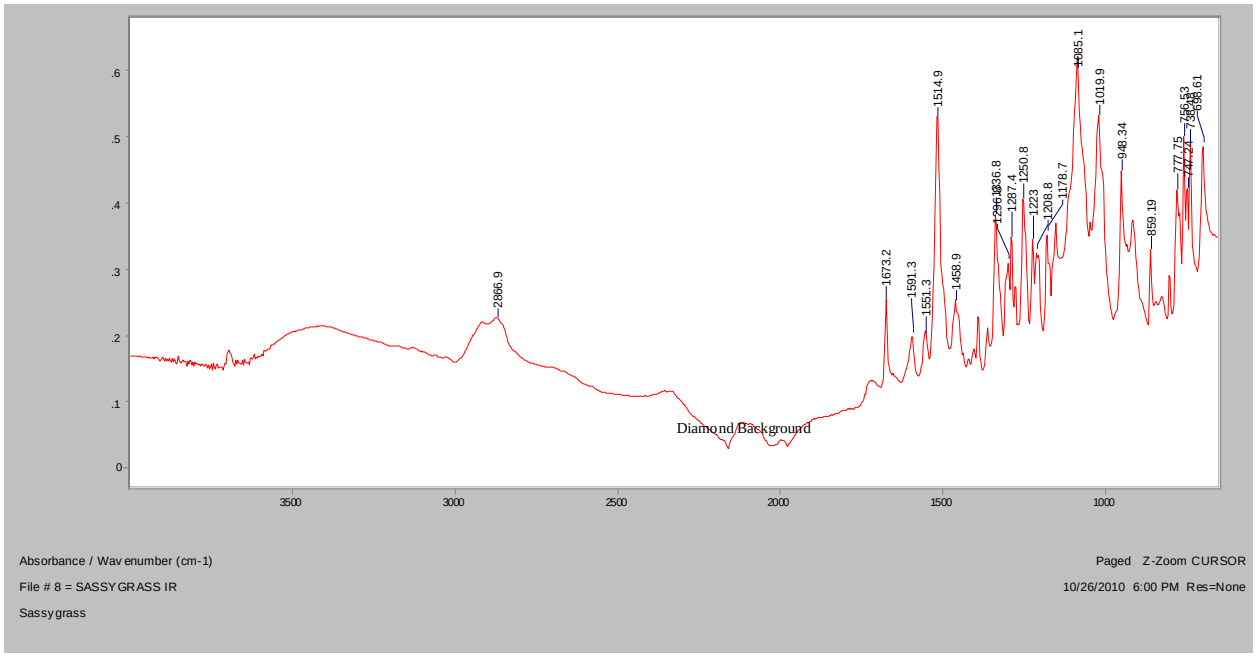

XRF

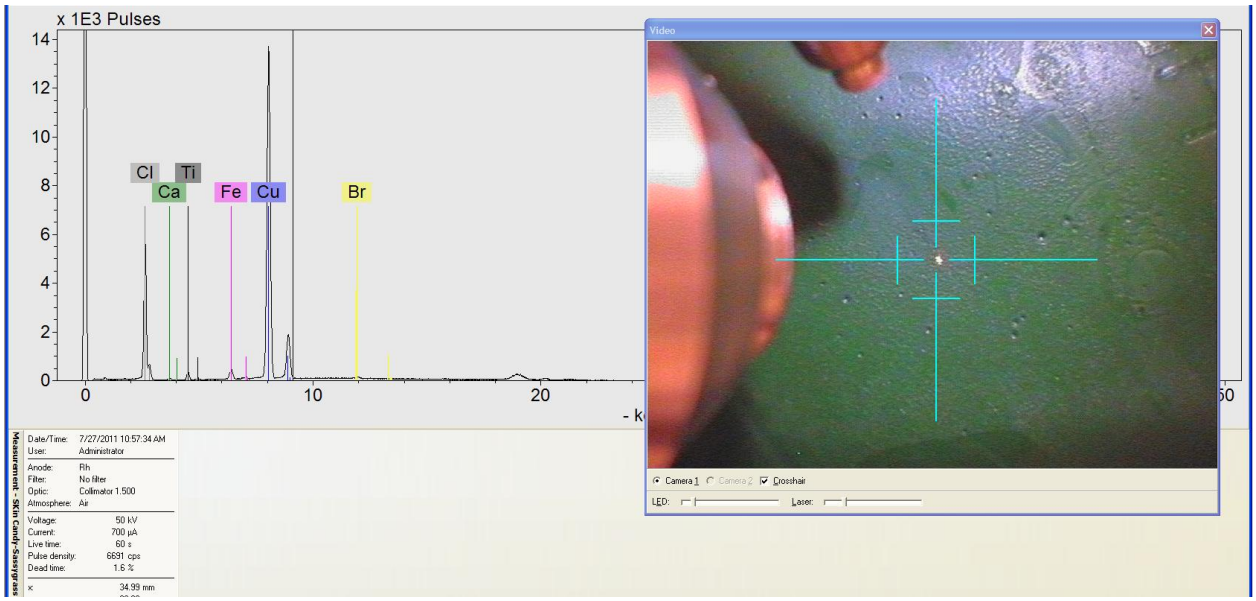
x 1E3 Pulses
14
12
10
8
6
4
2
0
Cl
Ti
Ca
Fe
Cu
Br
0
10
20
Video
Camera 1
Camera 2
Crosshair
LED:
Laser:
Date/Time: 7/27/2011 10:57:34 AM
User: Administrator
Anode: Rh
Filter: No filter
Optic: Collimator 1.500
Atmosphere: Air
Voltage: 50 kV
Current: 700 µA
Live time: 60 s
Pulse density: 6691 cps
Dead time: 1.6 %
x 34.99 mm

Tastywaves

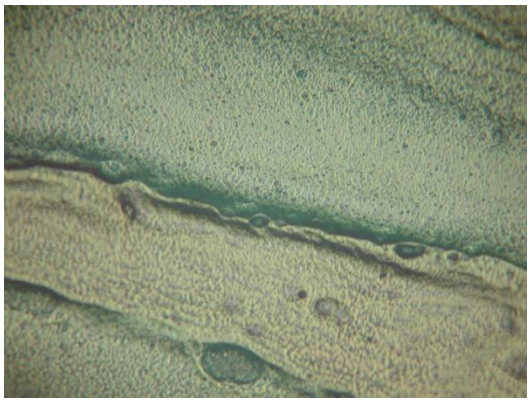

Bright Field, 100x

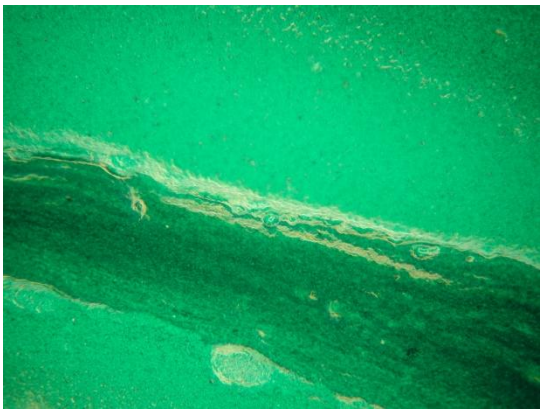

Dark Field, 100x

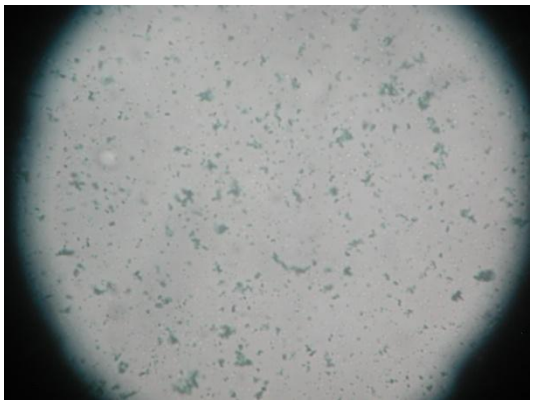

In RI 1.550, 400x

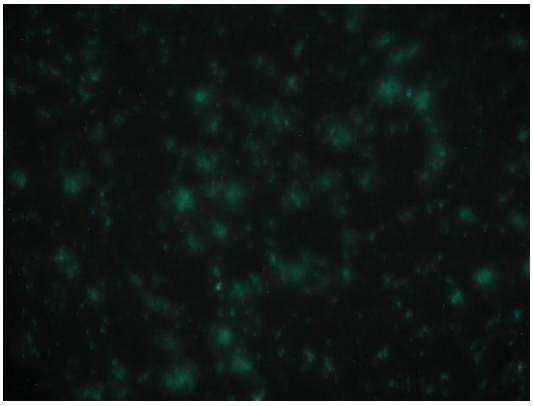

Crossed polars, In RI 1.550, 400x

Normal Raman, 488nm

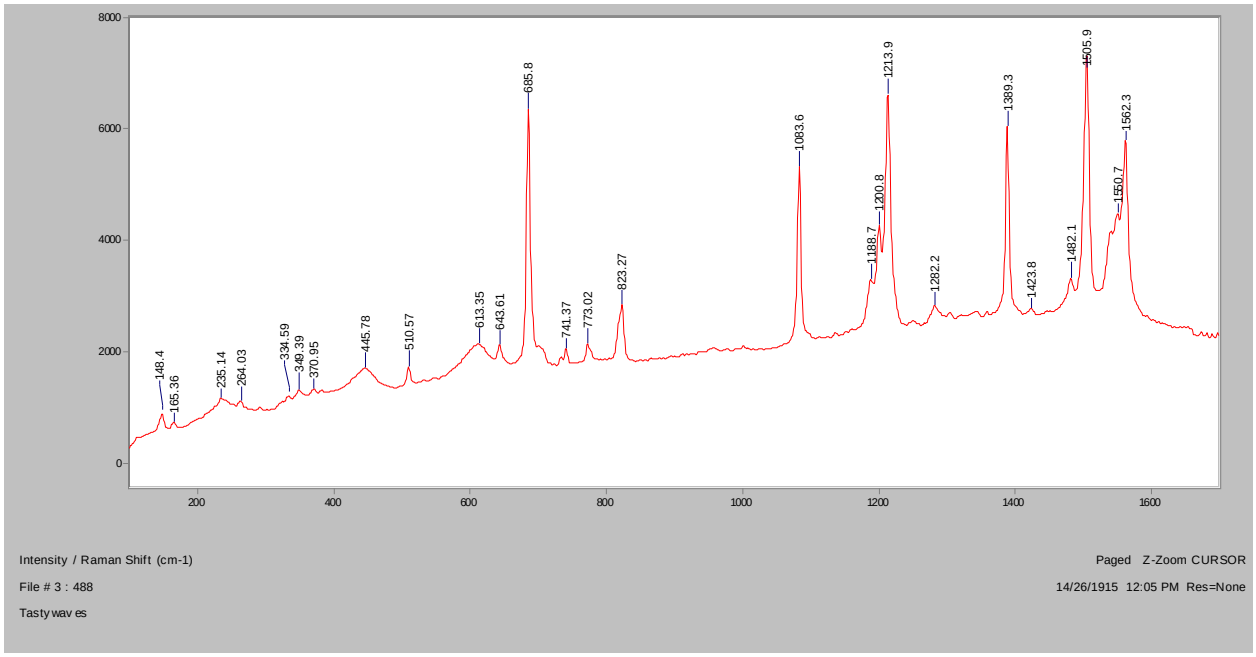

Normal Raman, 633nm

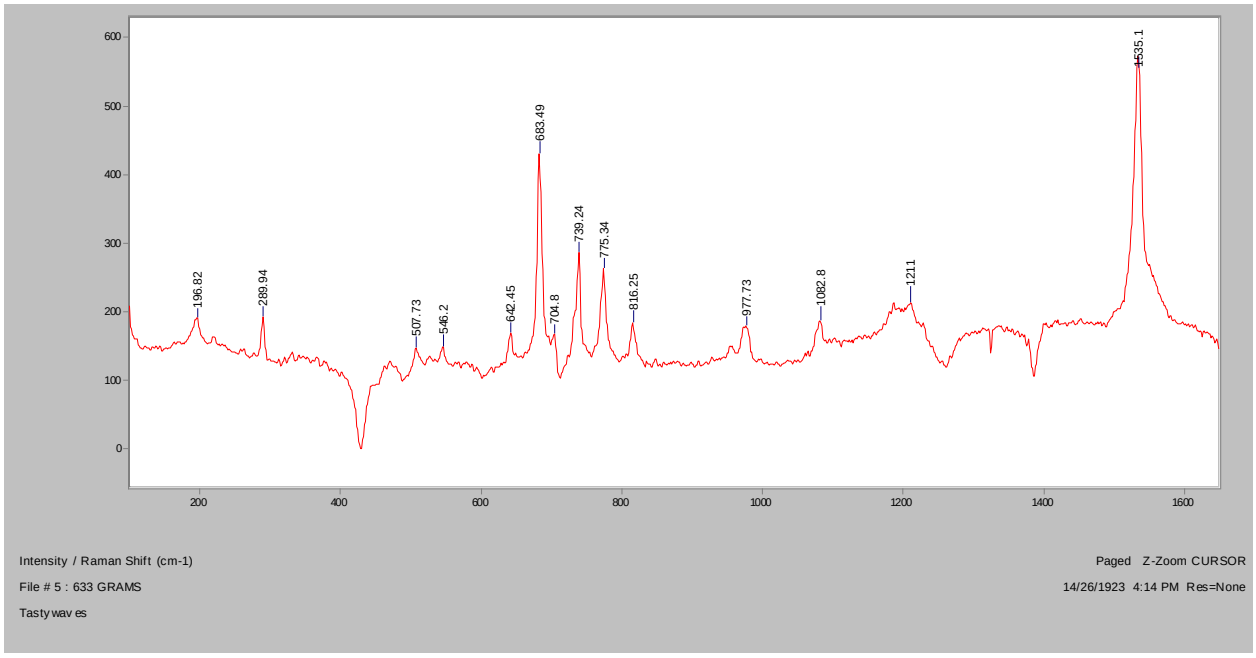

Normal Raman, 785nm

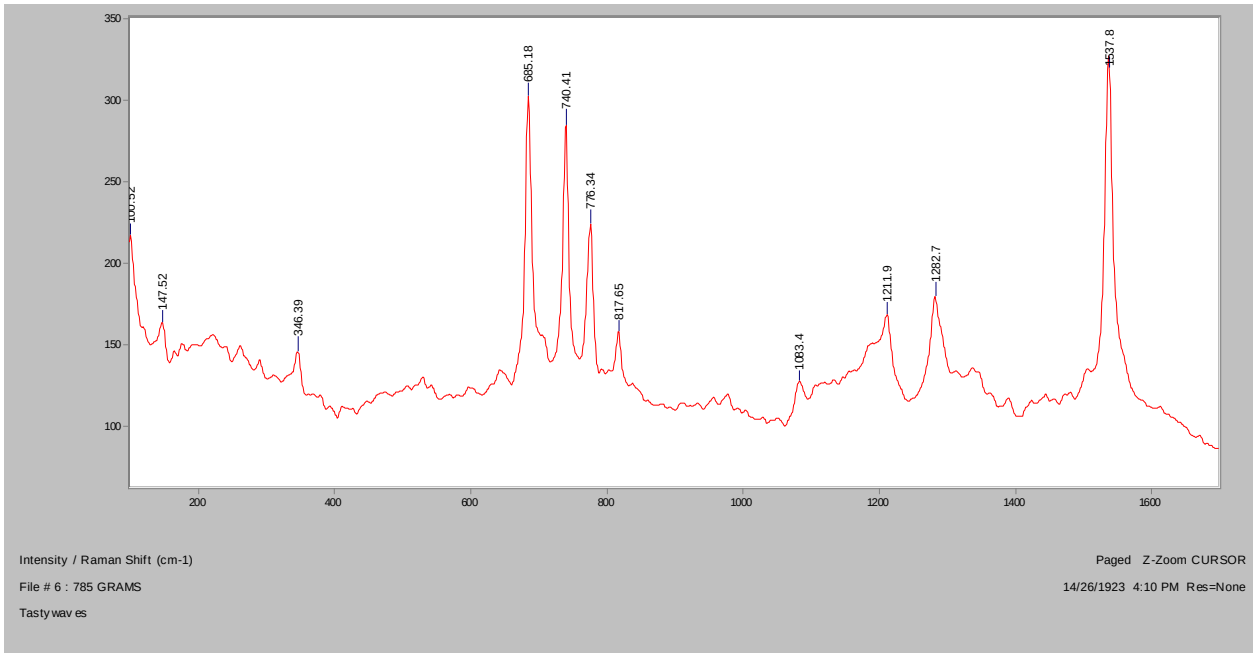

FT-Raman, 1064nm

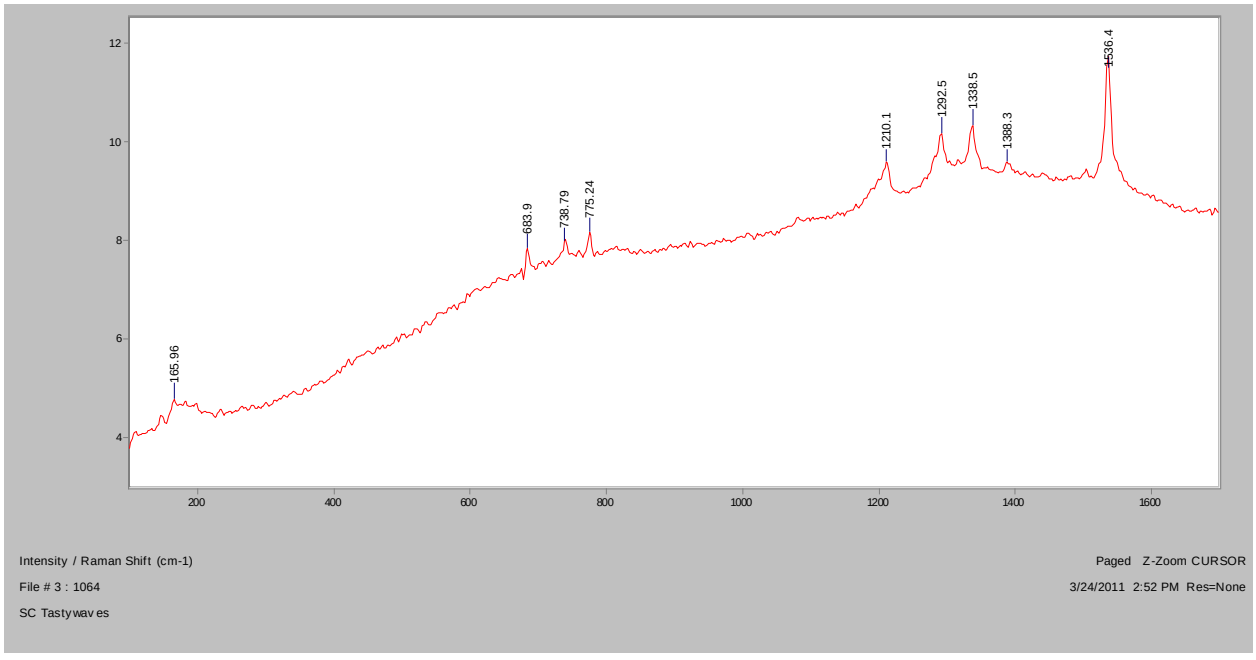

SERS, 488nm

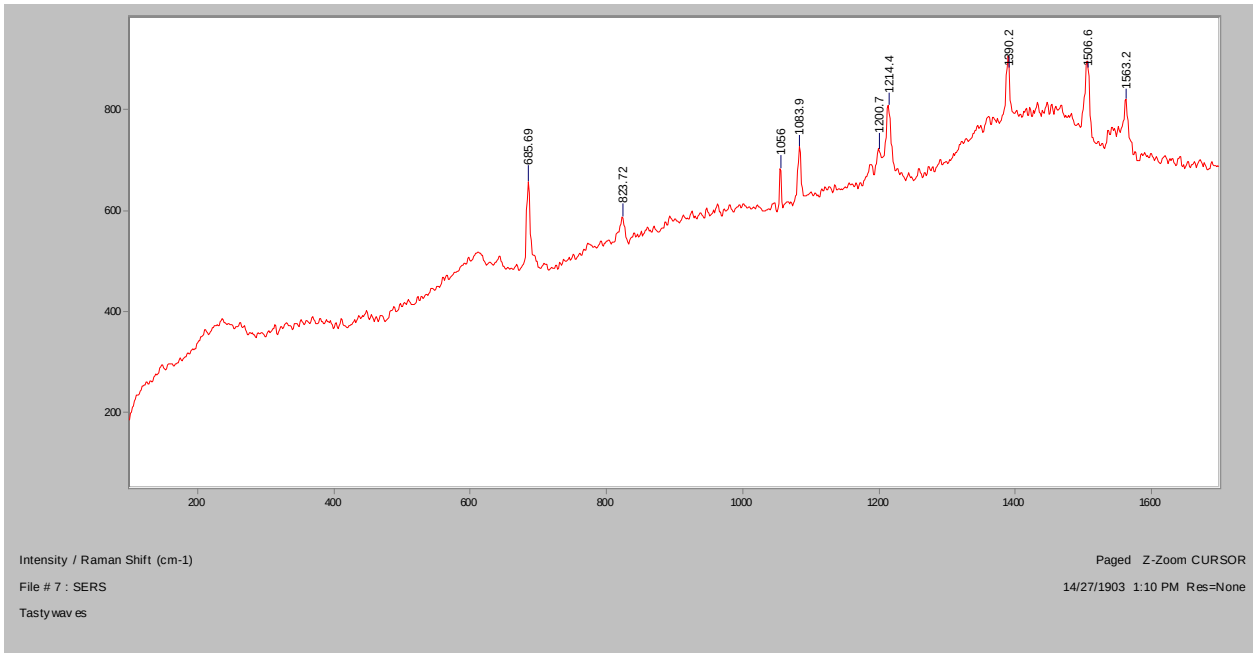

FT-IR (ATR)

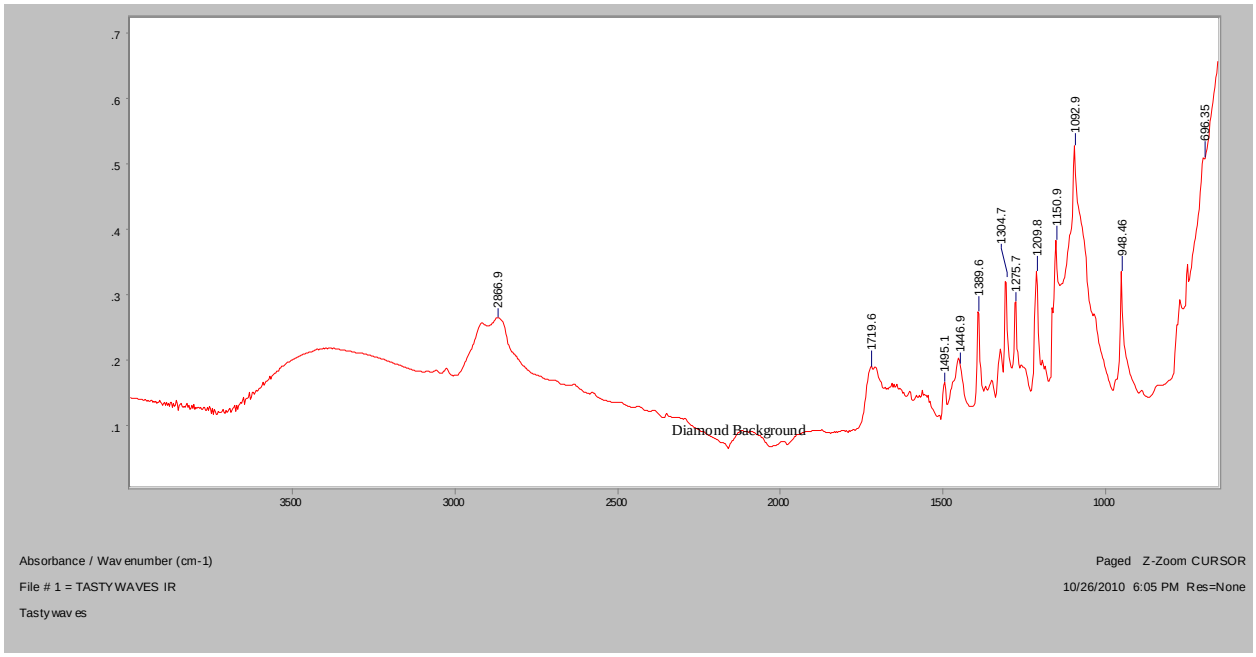

XRF

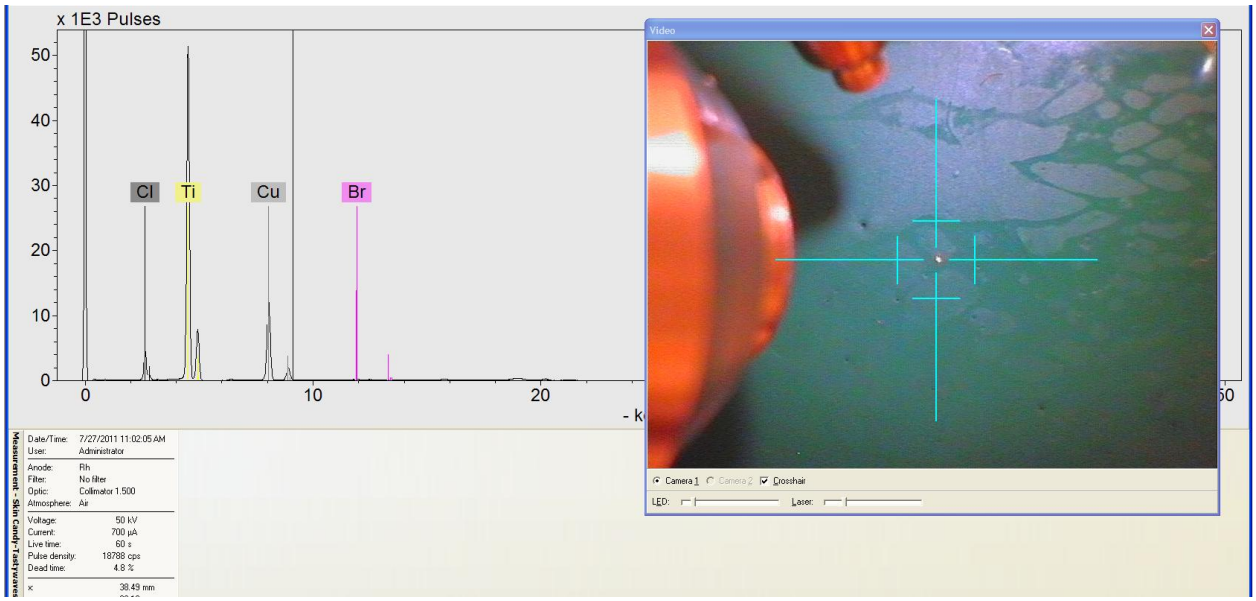
x 1E3 Pulses
50
40
30
20
10
0
Cl
Ti
Cu
Br
0
10
20
Video
Camera 1
Camera 2
Crosshair
LED:
Laser:
Date/Time: 7/27/2011 11:02:05 AM
User: Administrator
Anode: Rh
Filter: No filter
Optic: Collimator 1.500
Atmosphere: Air
Voltage: 50 kV
Current: 700 µA
Live time: 60 s
Pulse density: 18788 cps
Dead time: 4.8 %
x 38.49 mm

Bell Bottom Blue

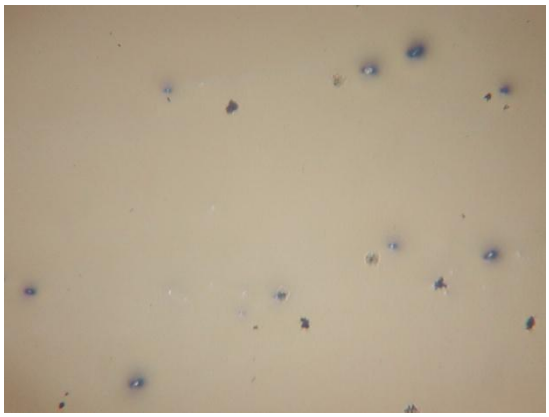

Bright Field, 100x

Dark Field, 100x

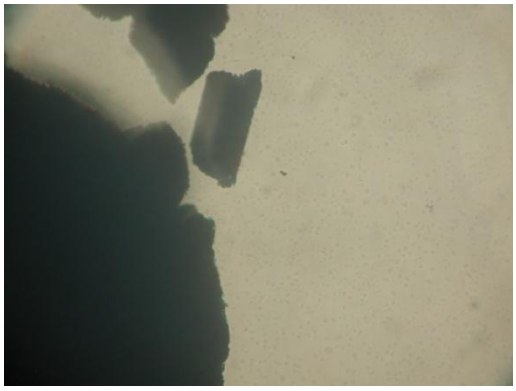

In RI 1.550, 400x

Crossed polars, In RI 1.550, 400x

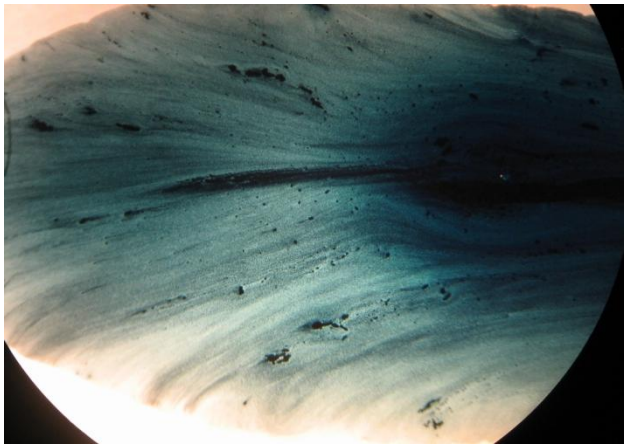

Smear on microscope slide after drying

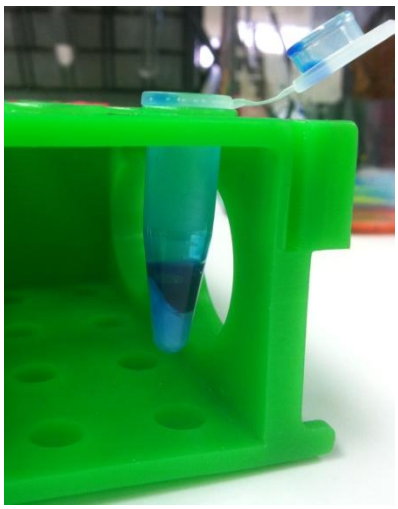

Post- extraction

Normal Raman, 488nm

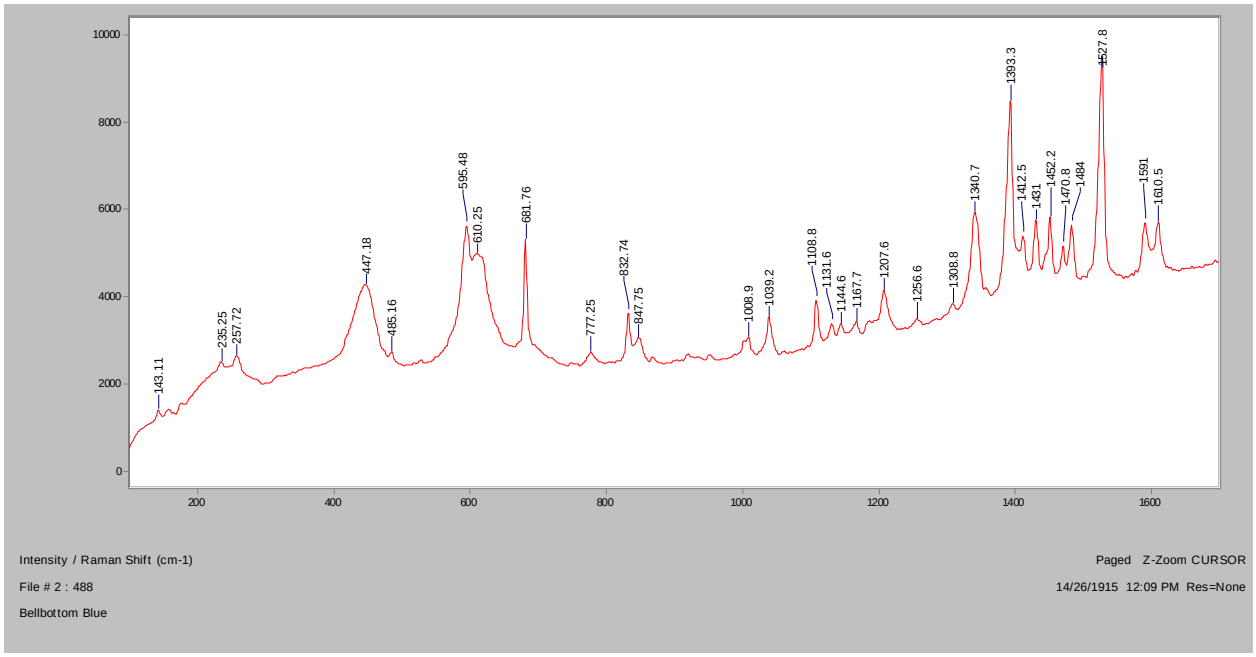

Normal Raman, 633nm

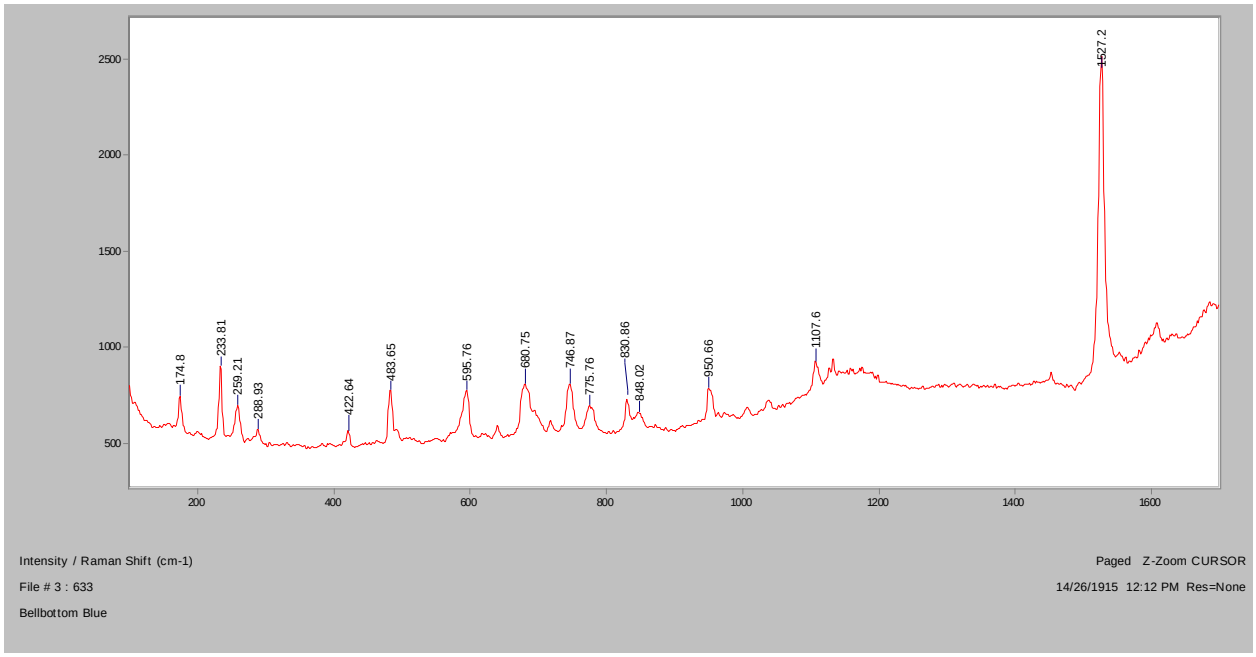

Normal Raman, 785nm

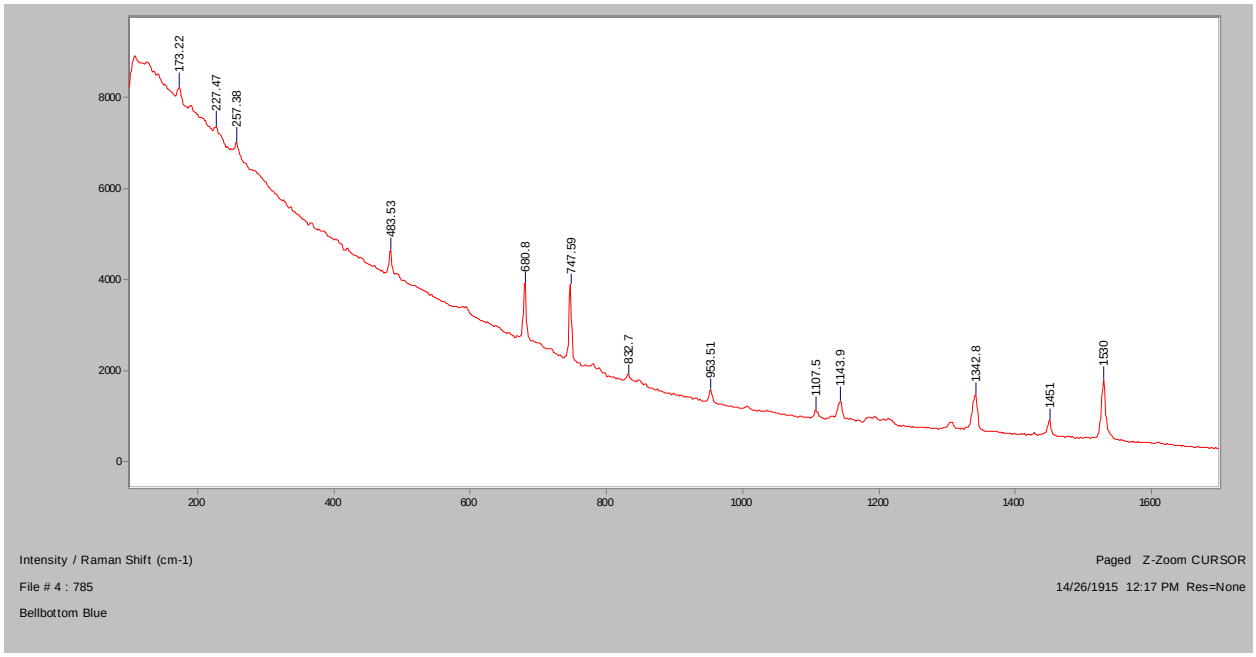

FT-Raman, 1064nm

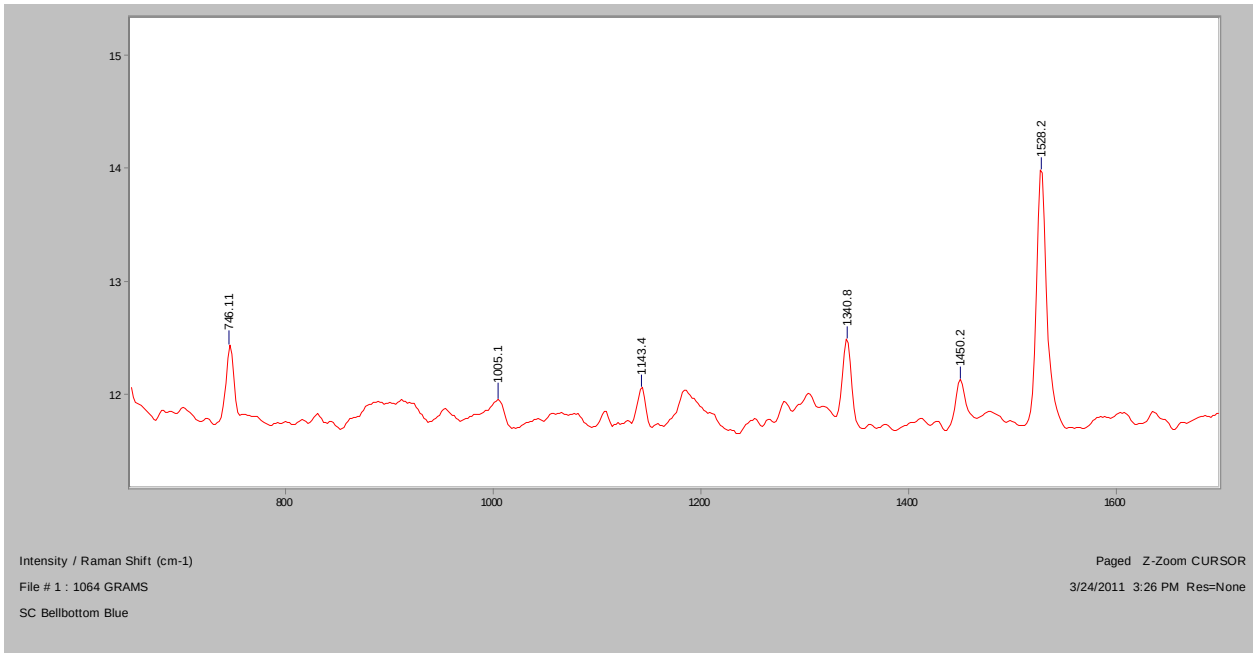

FT-IR (ATR)

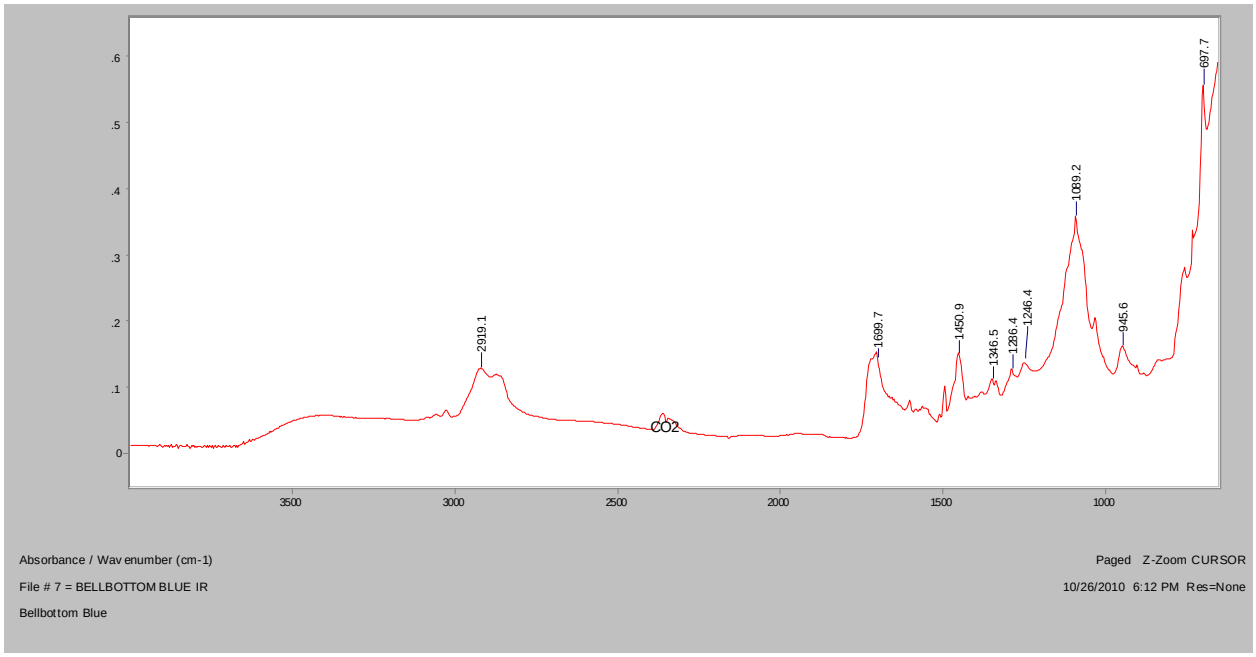
.6
.5
.4
.3
.2
.1
0
2919.1
CO2
1699.7
1450.9
1346.5
1286.4
1246.4
1089.2
945.6
697.7
3500
3000
2500
2000
1500
1000
Absorbance / Wavenumber (cm-1)
File # 7 = BELLBOTTOM BLUE IR
Bellbottom Blue
Paged Z-Zoom CURSOR
10/26/2010 6:12 PM Res=None

XRF

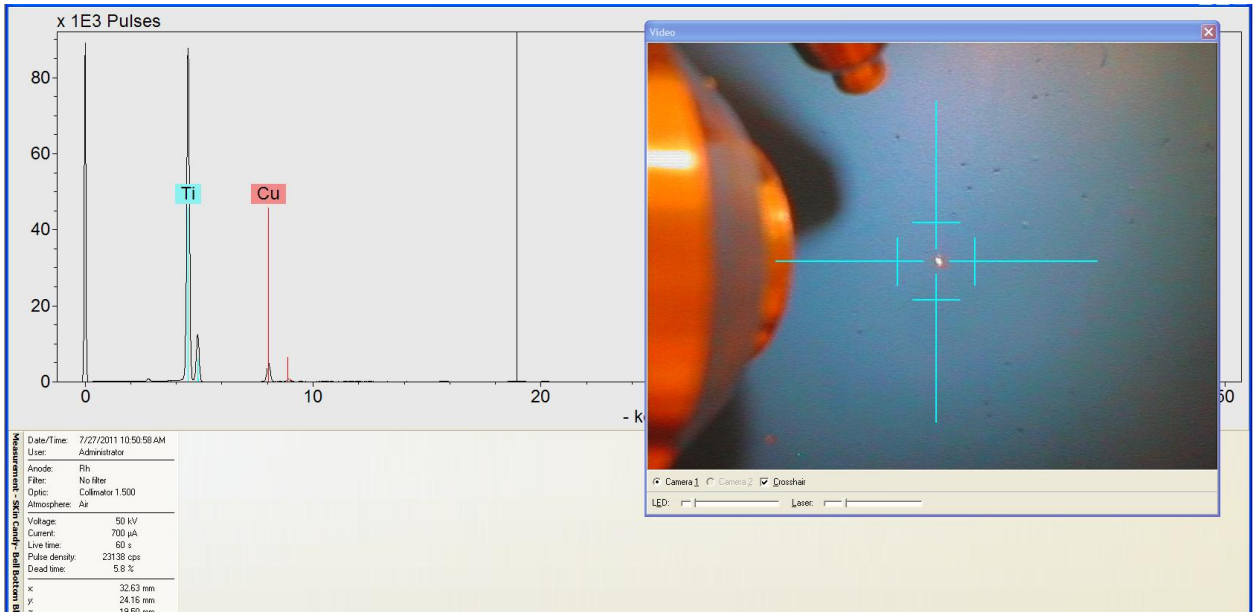
x 1E3 Pulses
80
60
40
20
0
Ti
Cu
0
10
20
Video
Camera 1
Camera 2
Crosshair
LED:
Laser:
Date/Time: 7/27/2011 10:50:58 AM
User: Administrator
Anode: Rh
Filter: No filter
Optic: Collimator 1.500
Atmosphere: Air
Voltage: 50 kV
Current: 700 µA
Live time: 60 s
Pulse density: 23138 cps
Dead time: 5.8 %
x 32.63 mm
y 24.16 mm

S.R.V. Teal 2

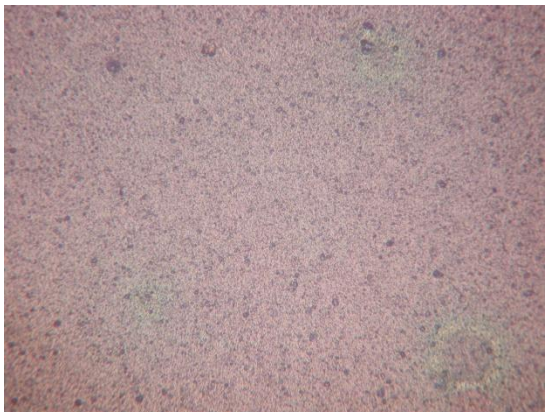

Bright Field, 100x

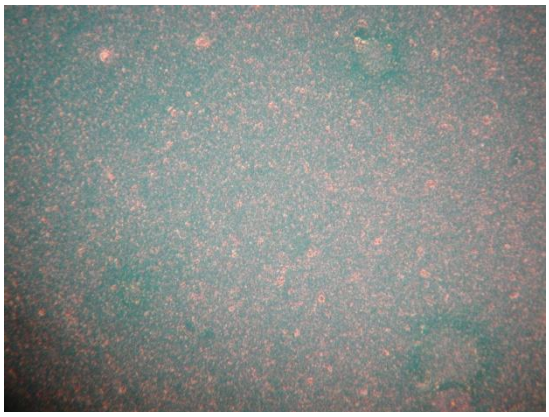

Dark Field, 100x

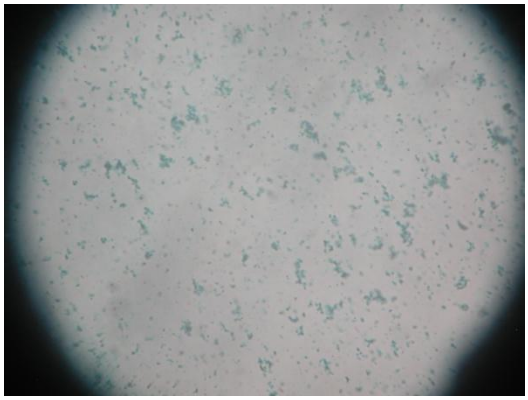

In RI 1.550, 400x

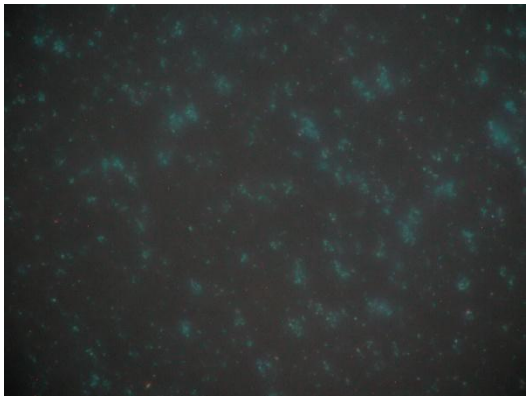

Crossed polars, In RI 1.550, 400x

Normal Raman, 488nm

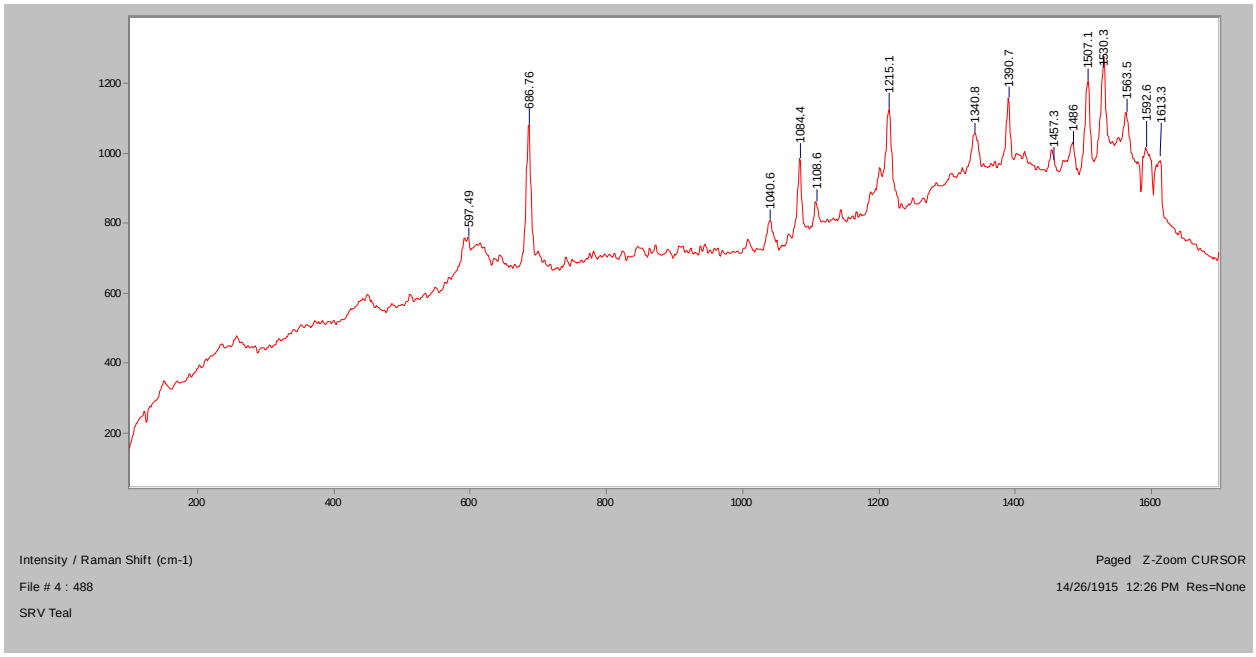

Normal Raman, 633nm

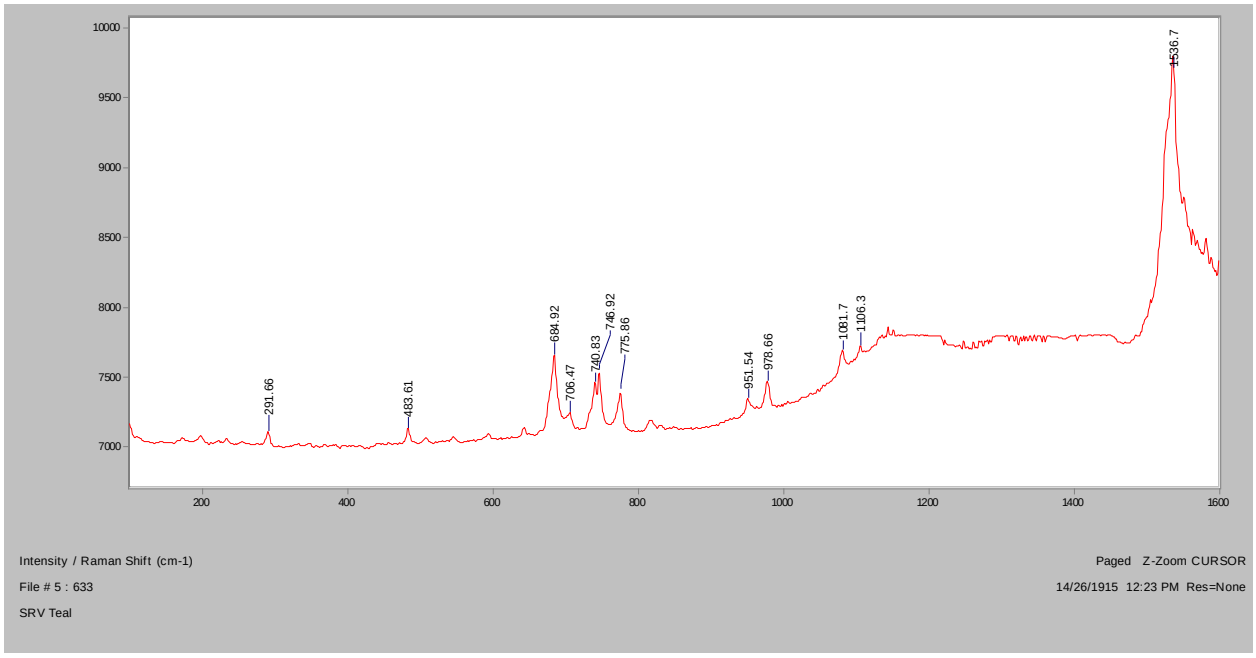

Normal Raman, 785nm

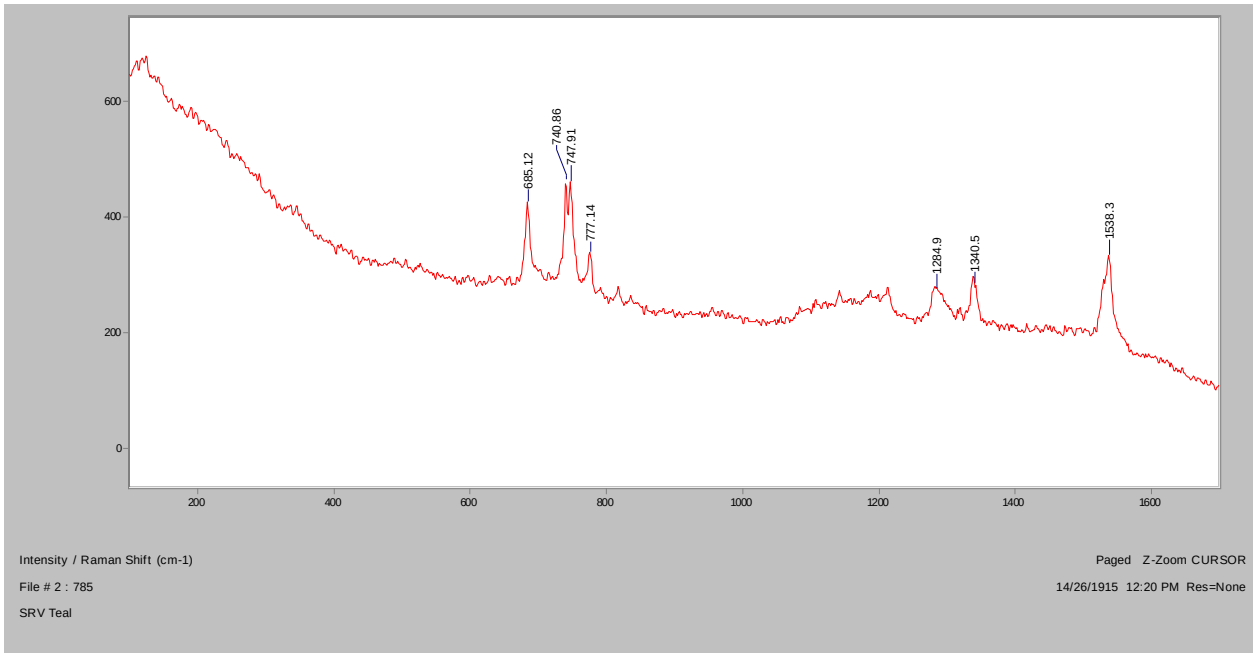

FT-Raman, 1064nm

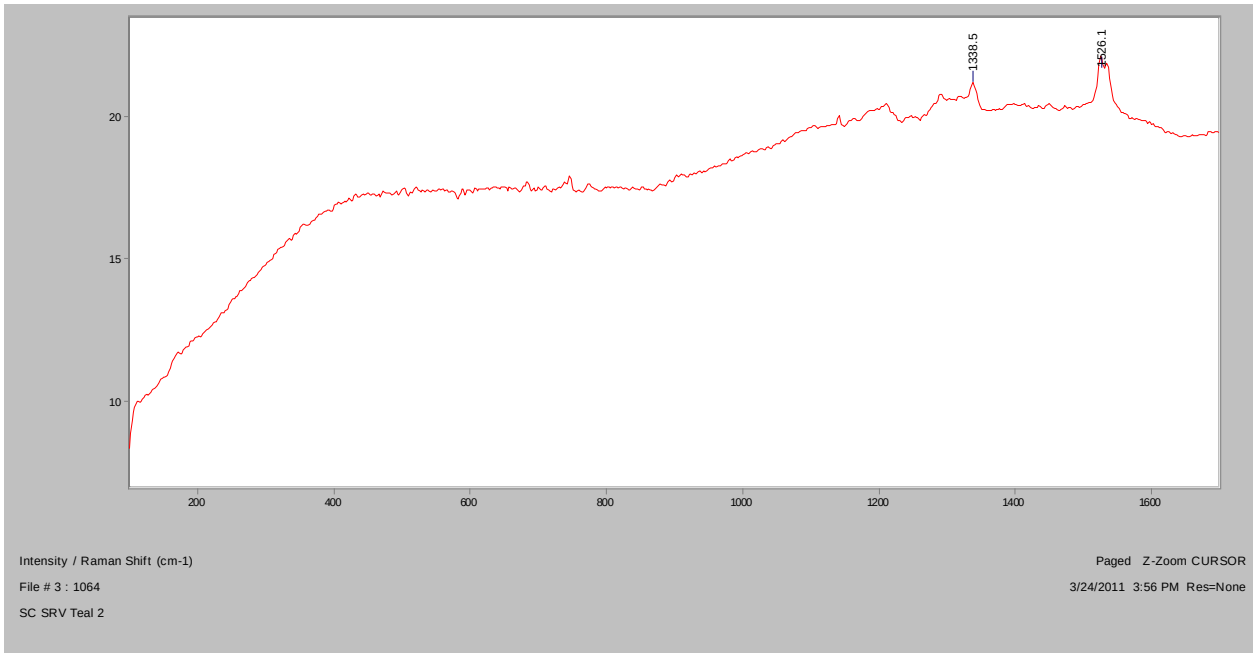

SERS, 488nm

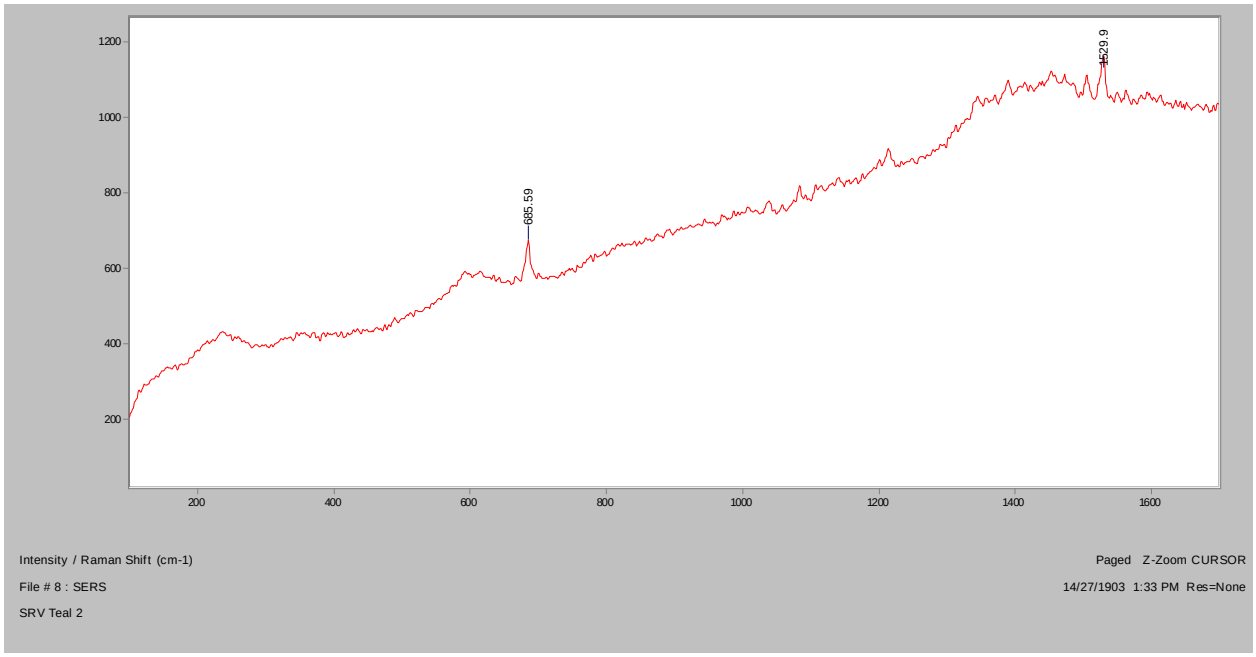

FT-IR (ATR)

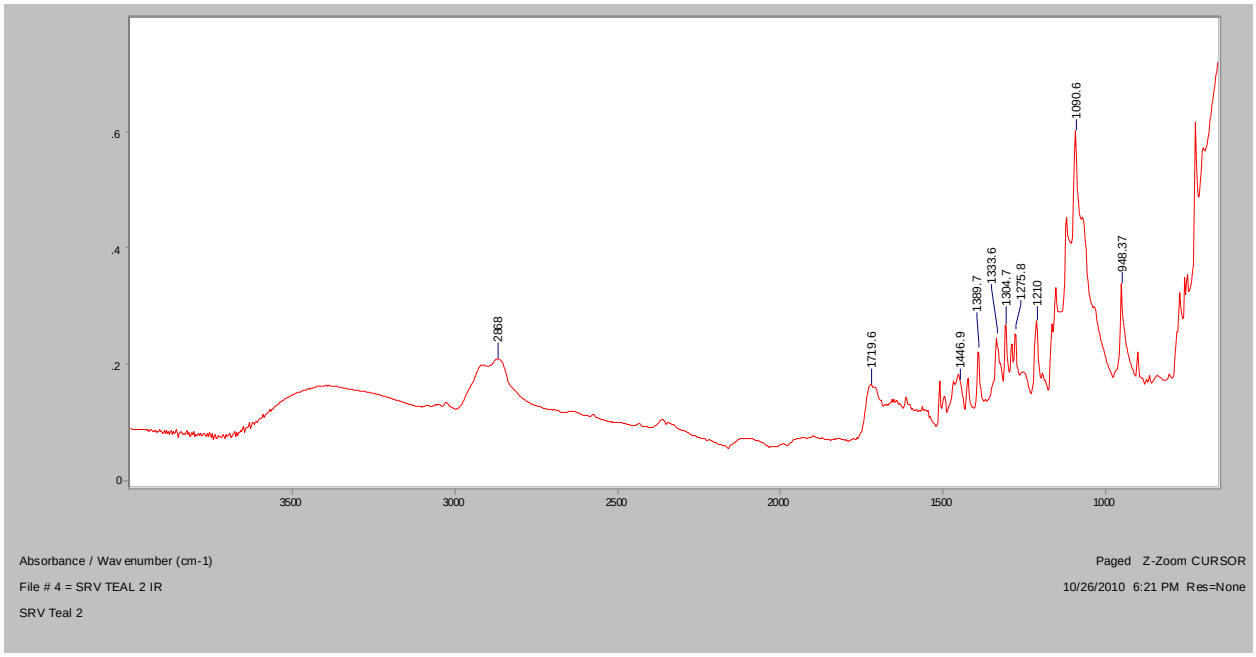

XRF

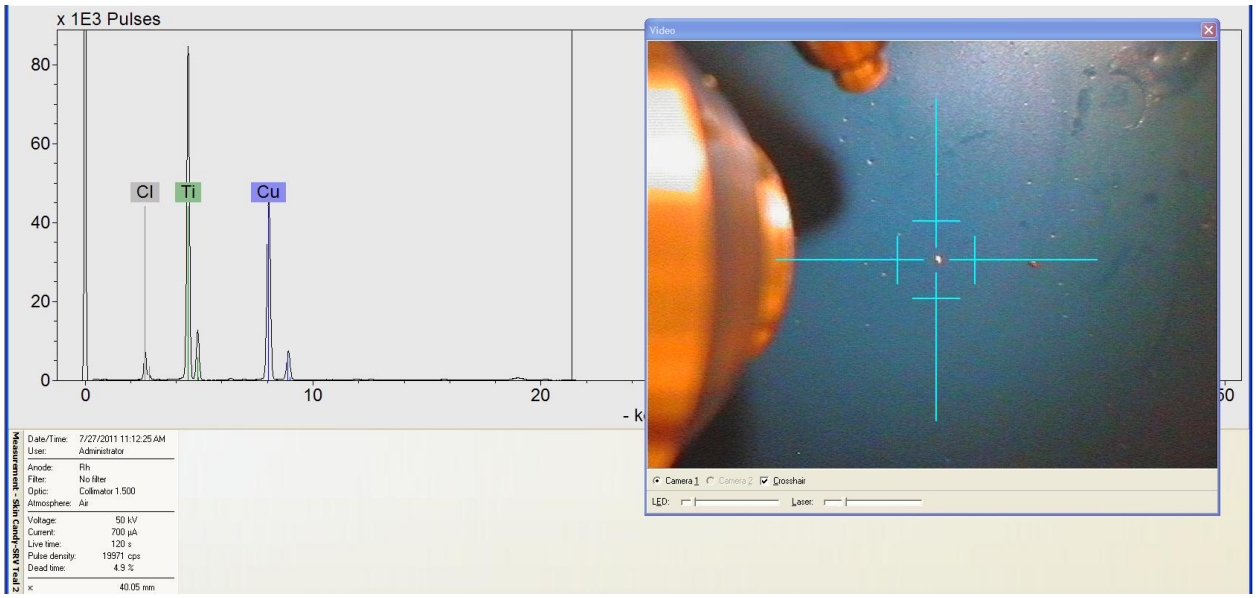
x 1E3 Pulses
80
60
40
20
0
Cl
Ti
Cu
0
10
20
Video
Camera 1
Camera 2
Crosshair
LED:
Laser:
Date/Time: 7/27/2011 11:12:25 AM
User: Administrator
Anode: Rh
Filter: No filter
Optic: Collimator 1.500
Atmosphere: Air
Voltage: 50 kV
Current: 700 µA
Live time: 120 s
Pulse density: 19971 cps
Dead time: 4.9 %
x 40.05 mm

Muddy Water Blue

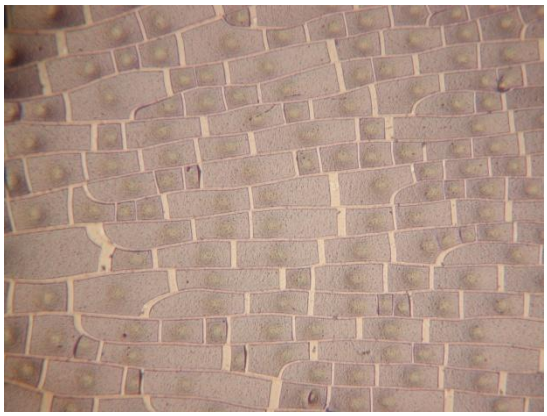

Bright Field, 100x

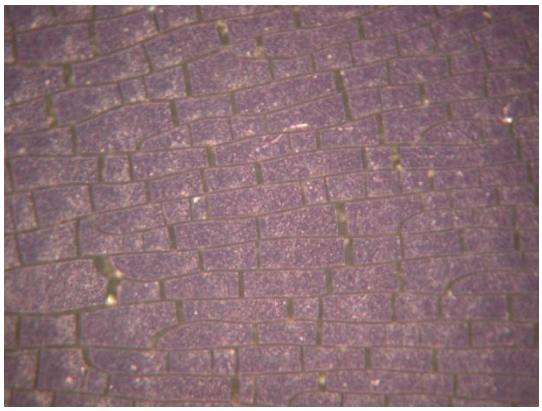

Dark Field, 100x

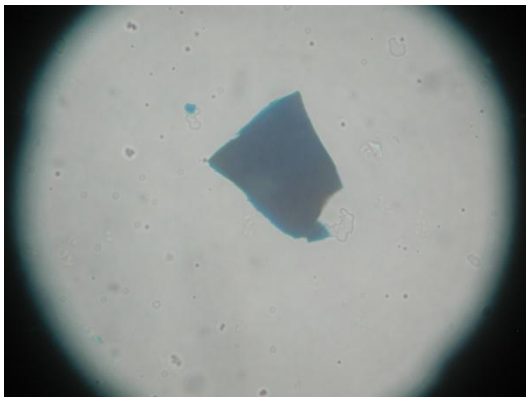

In RI 1.550, 400x

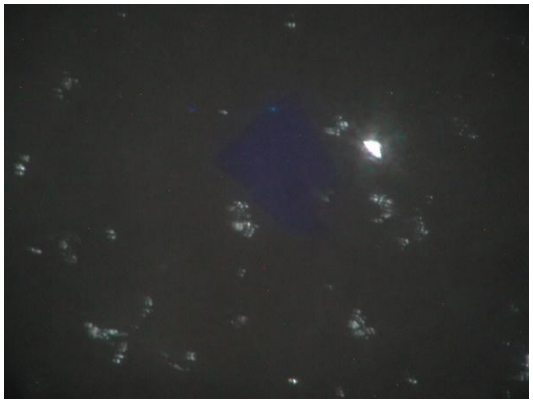

Crossed polars, In RI 1.550, 400x

Normal Raman, 488nm

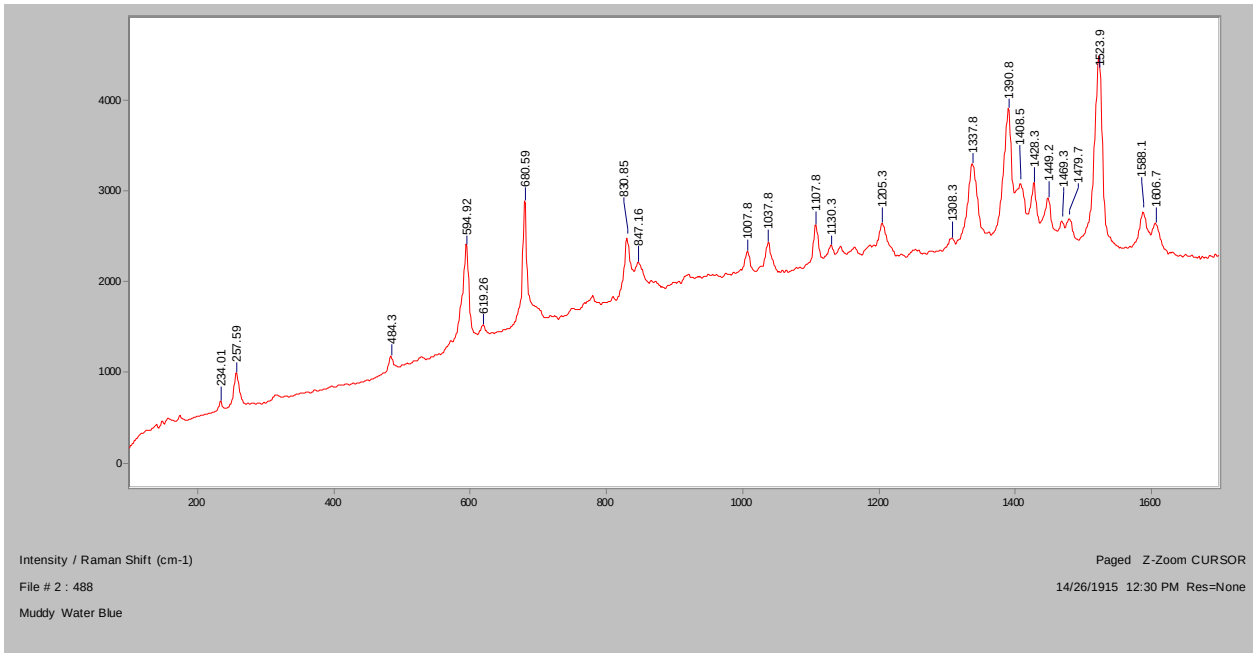

Normal Raman, 633nm

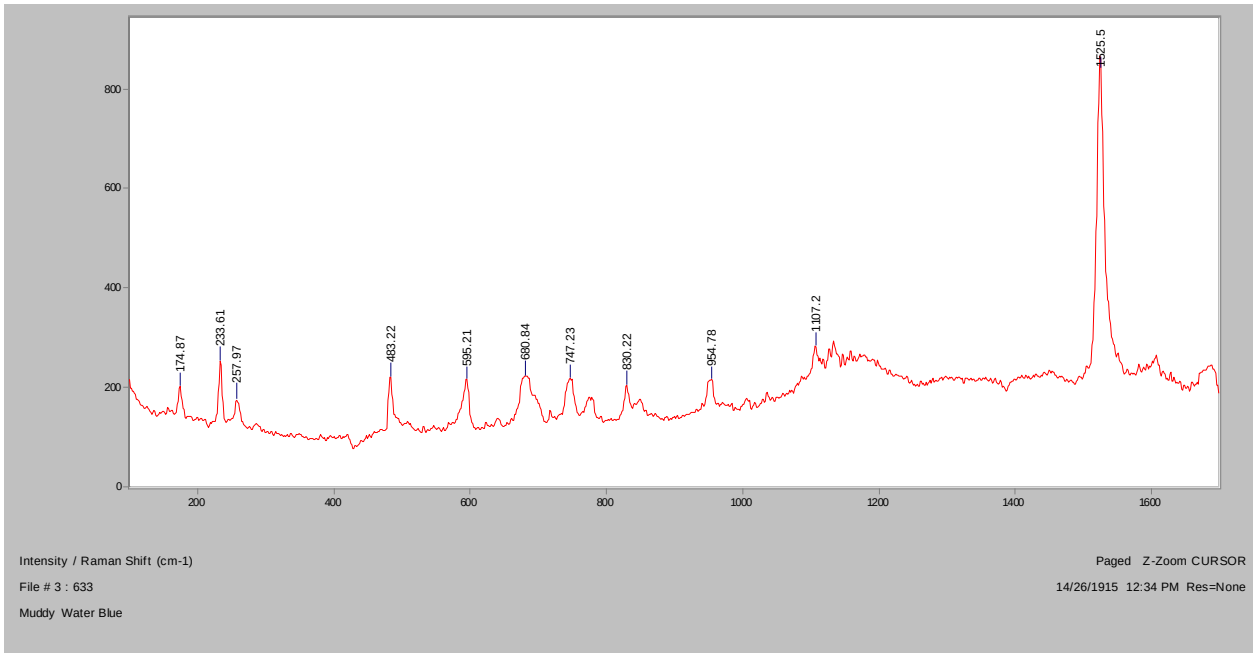

Normal Raman, 785nm

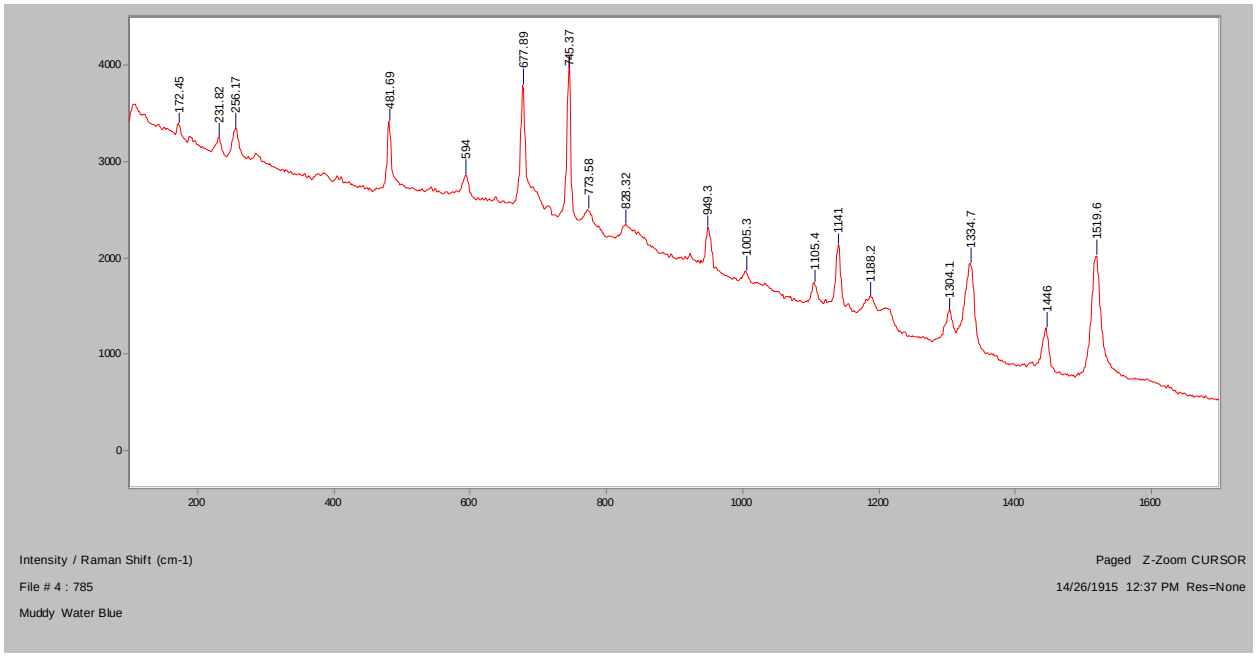

FT-Raman, 1064nm

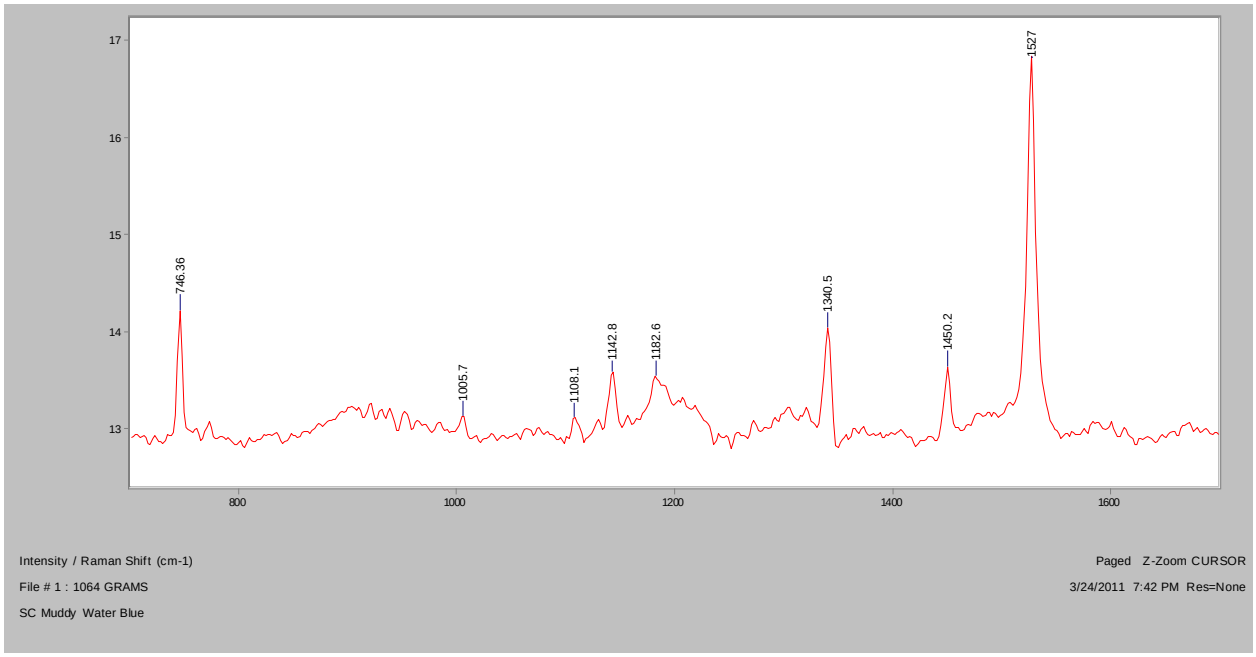

FT-IR (ATR)

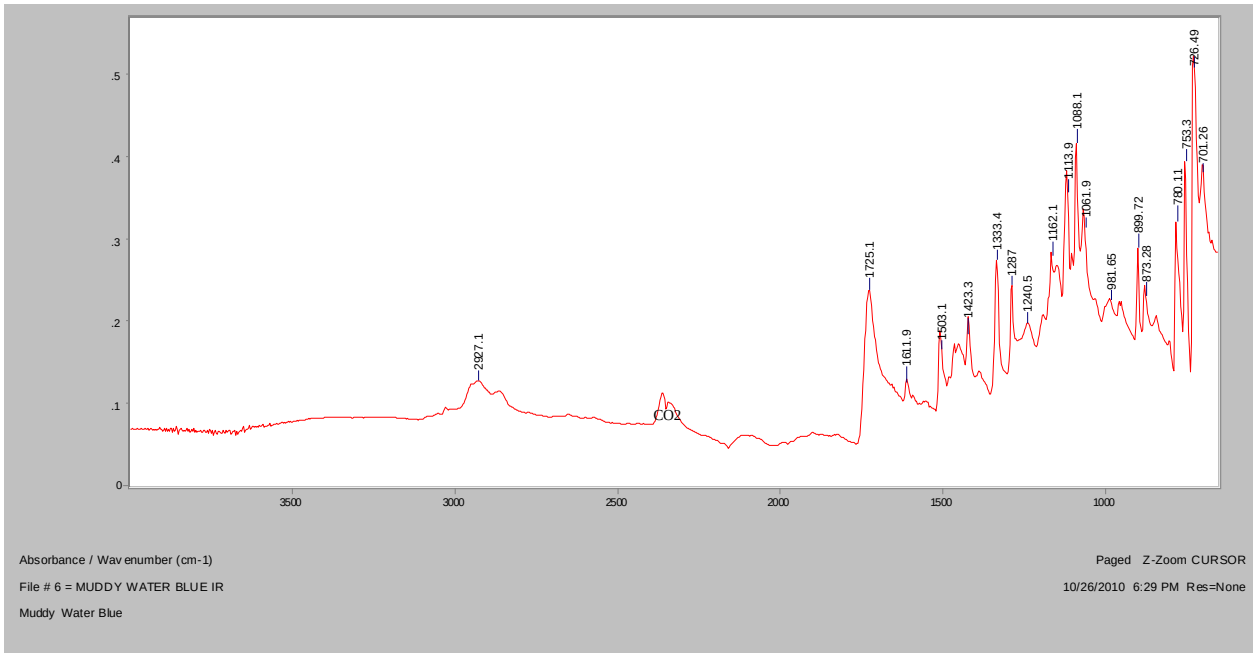
.5
.4
.3
.2
.1
0
3500
3000
2500
2000
1500
1000
2927.1
CO2
1611.9
1725.1
1503.1
1423.3
1333.4
1287
1240.5
1162.1
1113.9
1088.1
1061.9
981.65
899.72
873.28
780.11
753.3
726.49
701.26
Absorbance / Wavenumber (cm-1)
File # 6 = MUDDY WATER BLUE IR
Muddy Water Blue
Paged Z-Zoom CURSOR
10/26/2010 6:29 PM Res=None

XRF

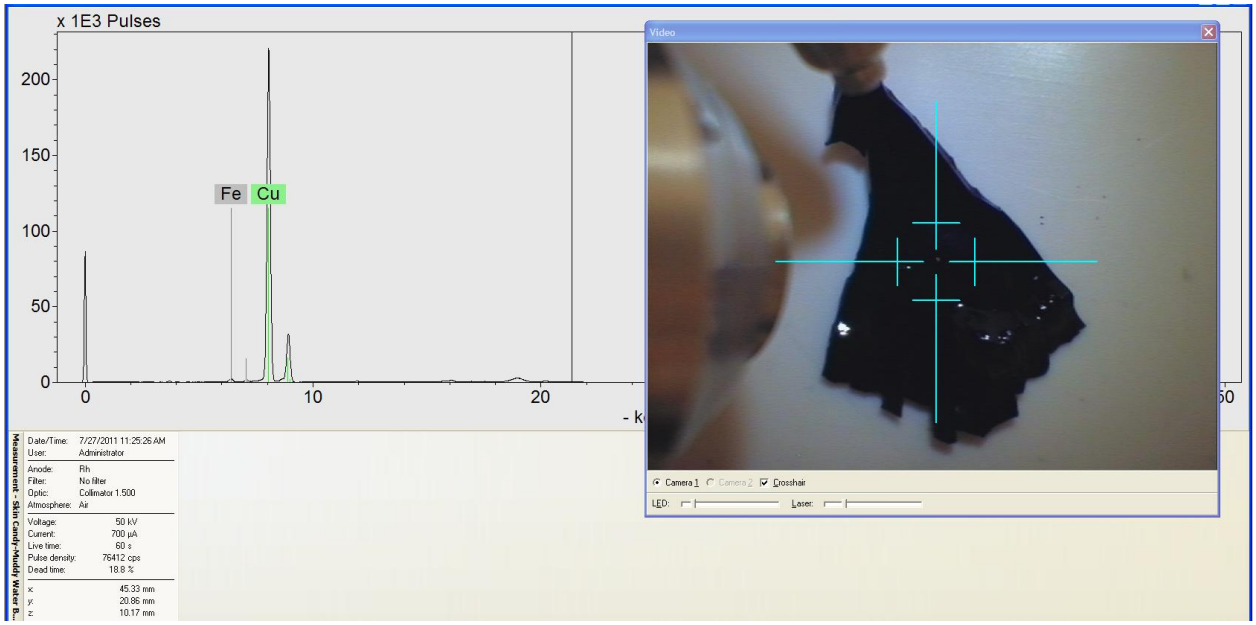
x 1E3 Pulses
200
150
100
50
0
0
10
20
Fe
Cu
Video
Camera 1
Camera 2
Crosshair
LED:
Laser:
Date/Time: 7/27/2011 11:25:26 AM
User: Administrator
Anode: Rh
Filter: No filter
Optic: Collimator 1.500
Atmosphere: Air
Voltage: 50 kV
Current: 700 µA
Live time: 60 s
Pulse density: 76412 cps
Dead time: 18.8 %
x 45.33 mm
y 20.86 mm
z 10.17 mm

Razberry Creem

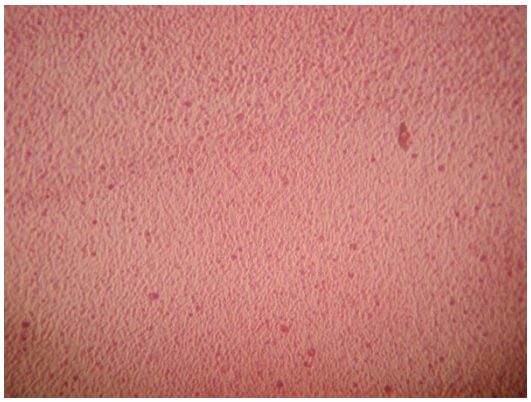

Bright Field, 100x

Dark Field, 100x

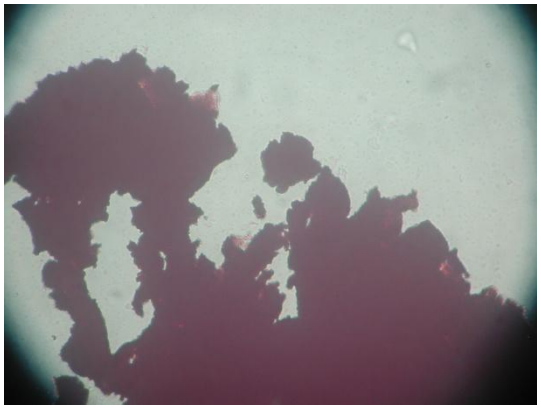

In RI 1.550, 400x

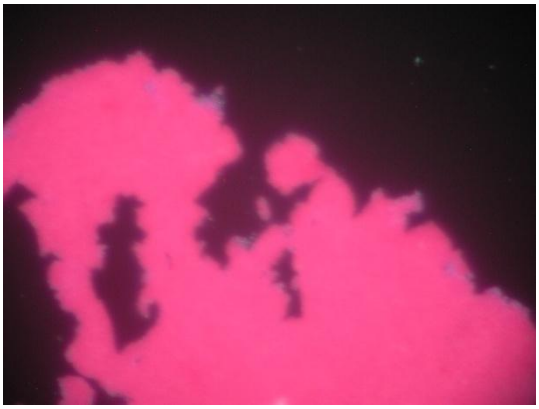

Crossed polars, In RI 1.550, 400x

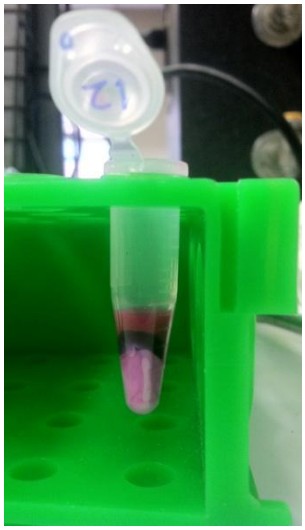

Post-extraction

Normal Raman, 488nm

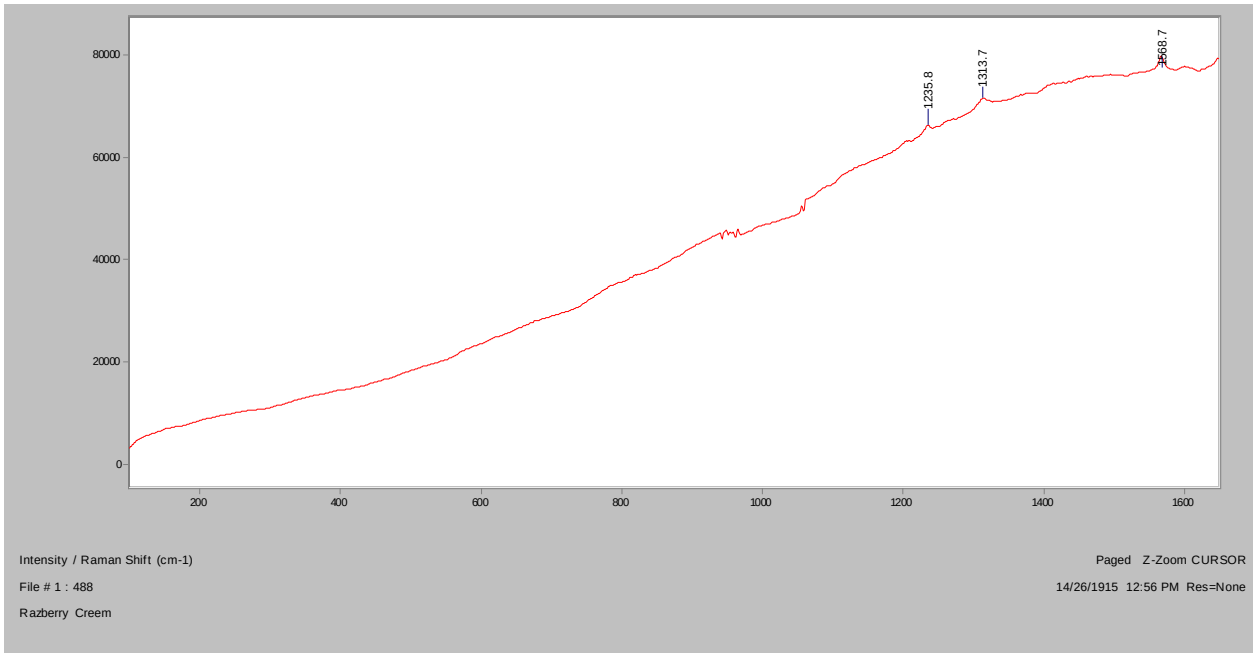

Normal Raman, 633nm

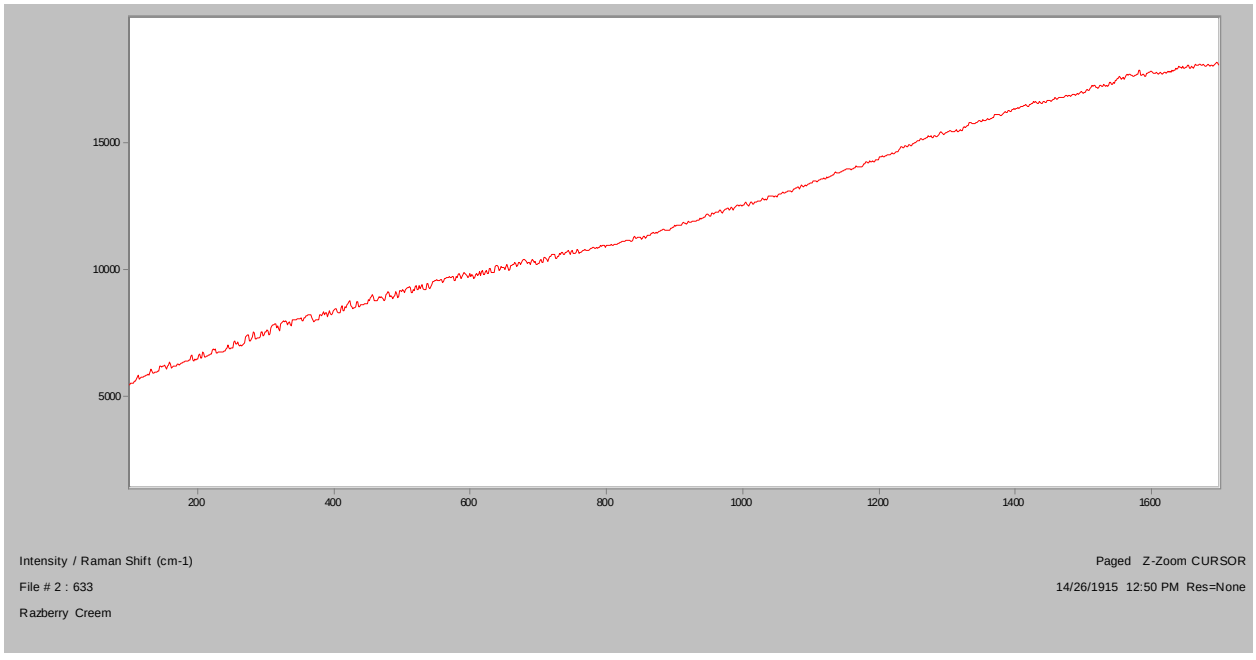

Normal Raman, 785nm

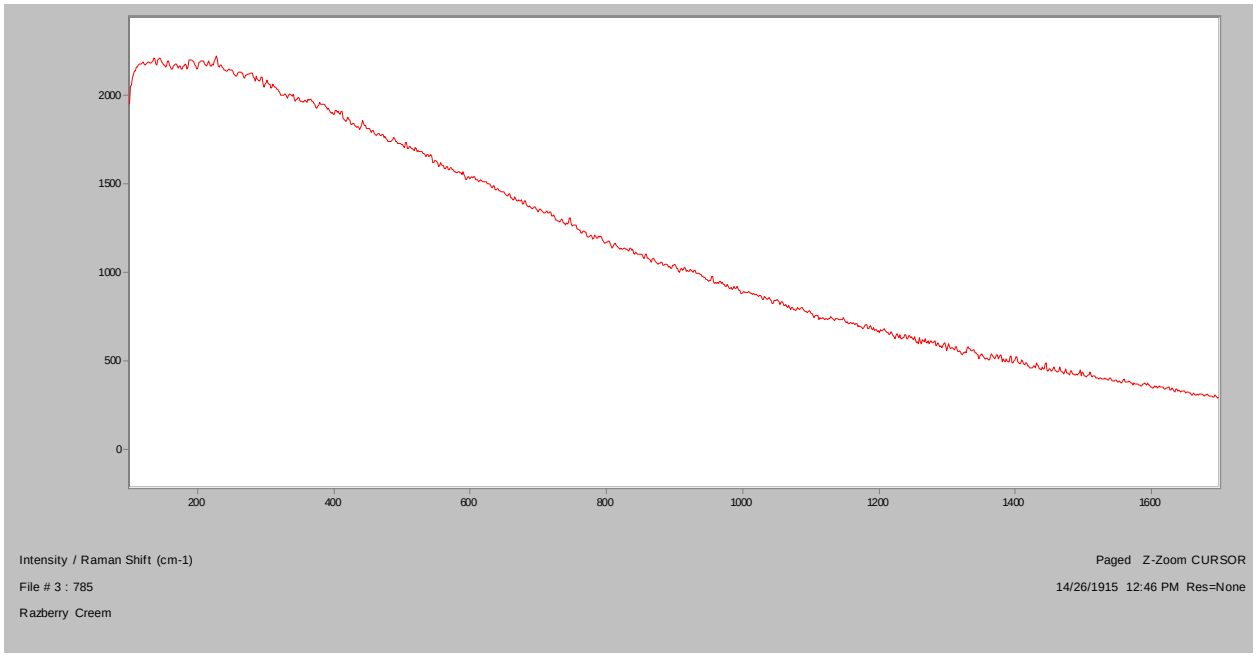

FT-Raman, 1064nm

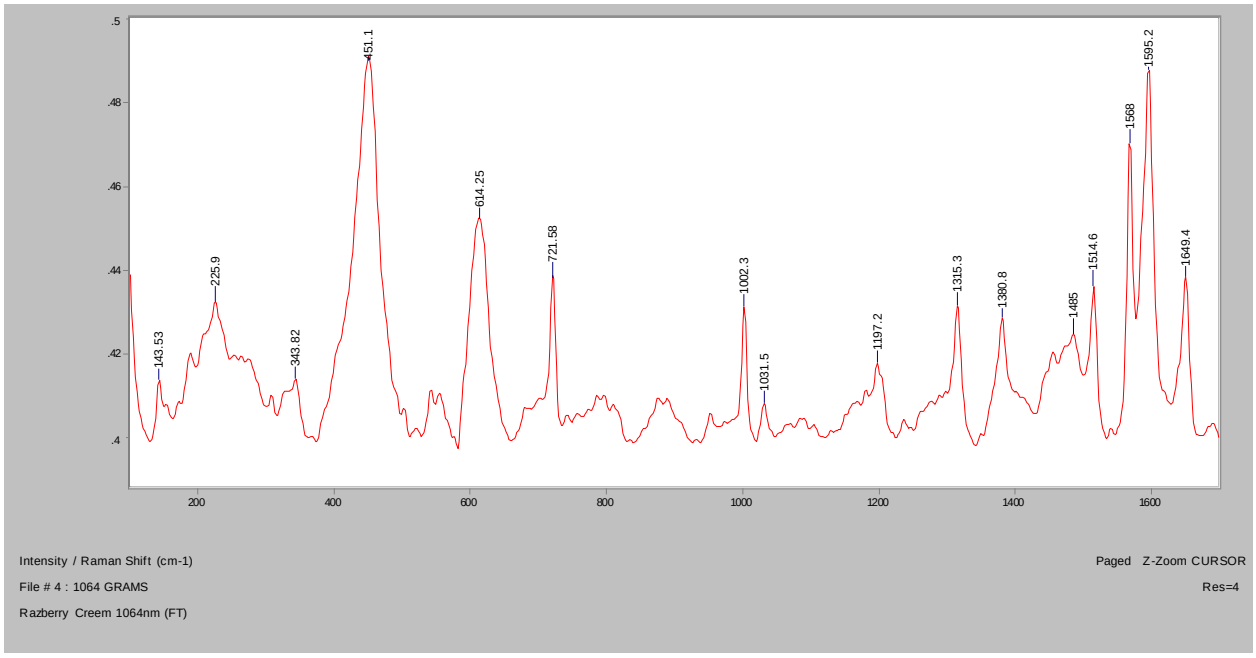

SERS, 488nm

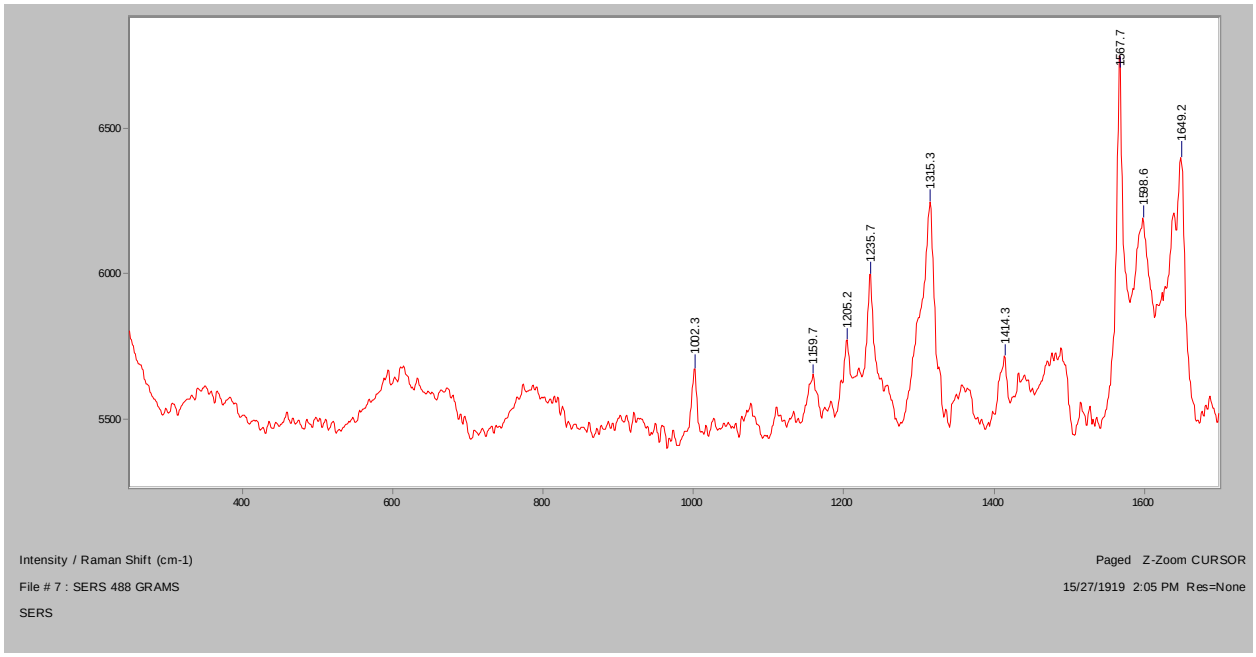

FT-IR (ATR)

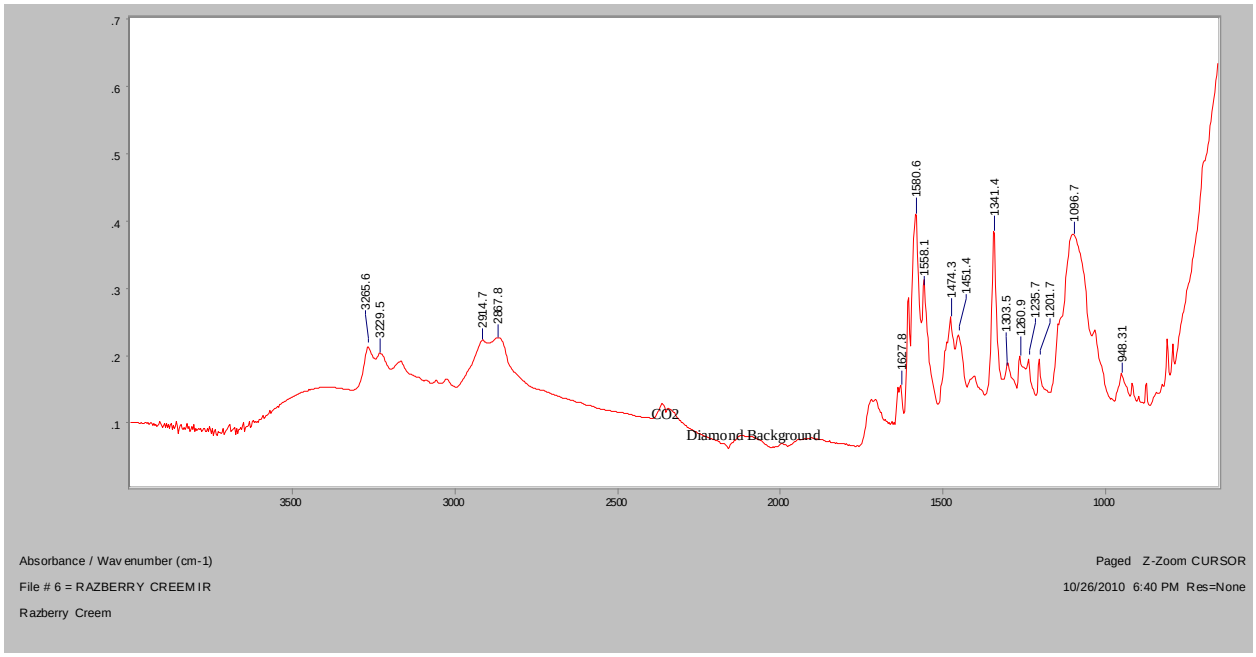

XRF

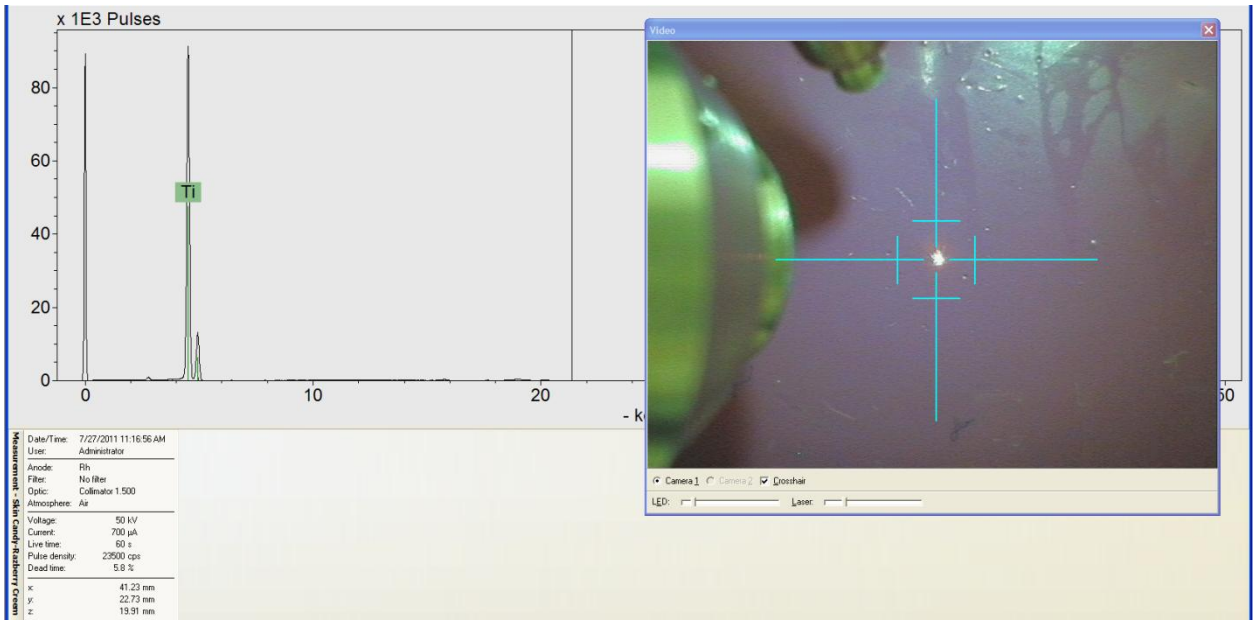
x 1E3 Pulses
80
60
40
20
0
Ti
0
10
20
Video
Camera 1
Camera 2
Crosshair
LED:
Laser:
Date/Time: 7/27/2011 11:16:56 AM
User: Administrator
Anode: Rh
Filter: No filter
Optic: Collimator 1.500
Atmosphere: Air
Voltage: 50 kV
Current: 700 µA
Live time: 60 s
Pulse density: 23500 cps
Dead time: 5.8 %
x: 41.23 mm
y: 22.73 mm
z: 19.91 mm

Ripple

Bright Field, 100x

Dark Field, 100x

In RI 1.550, 400x

Crossed polars, In RI 1.550, 400x

Smear on microscope slide after drying

Normal Raman, 488nm

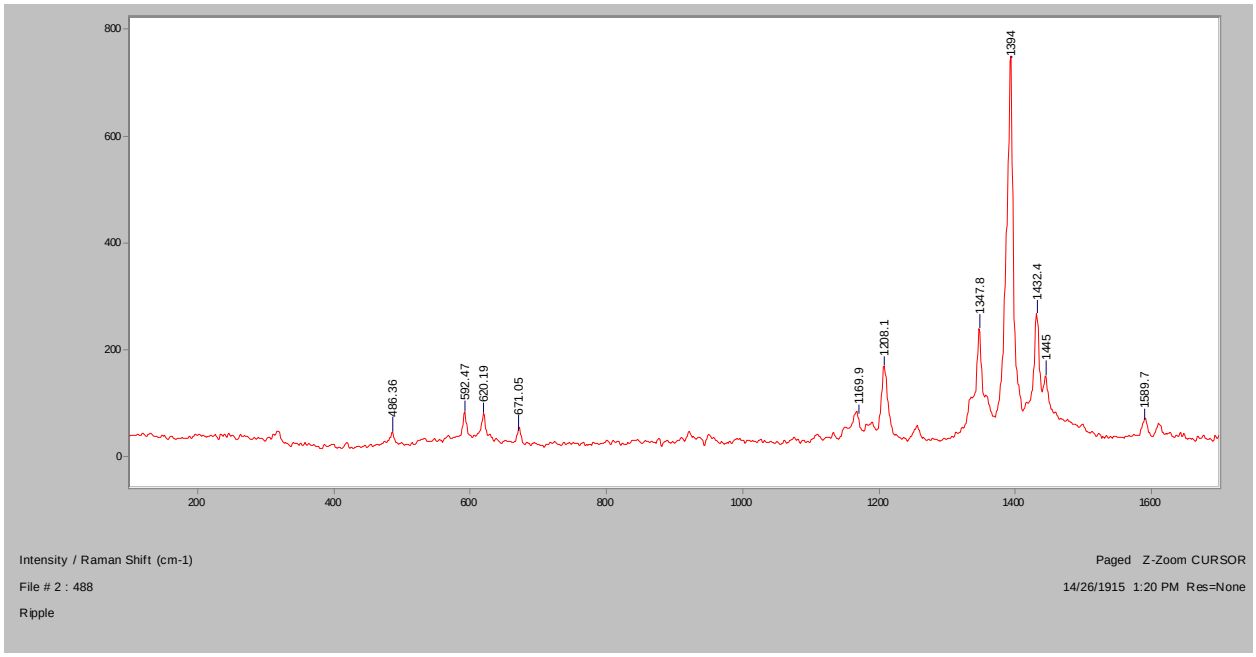

Normal Raman, 633nm

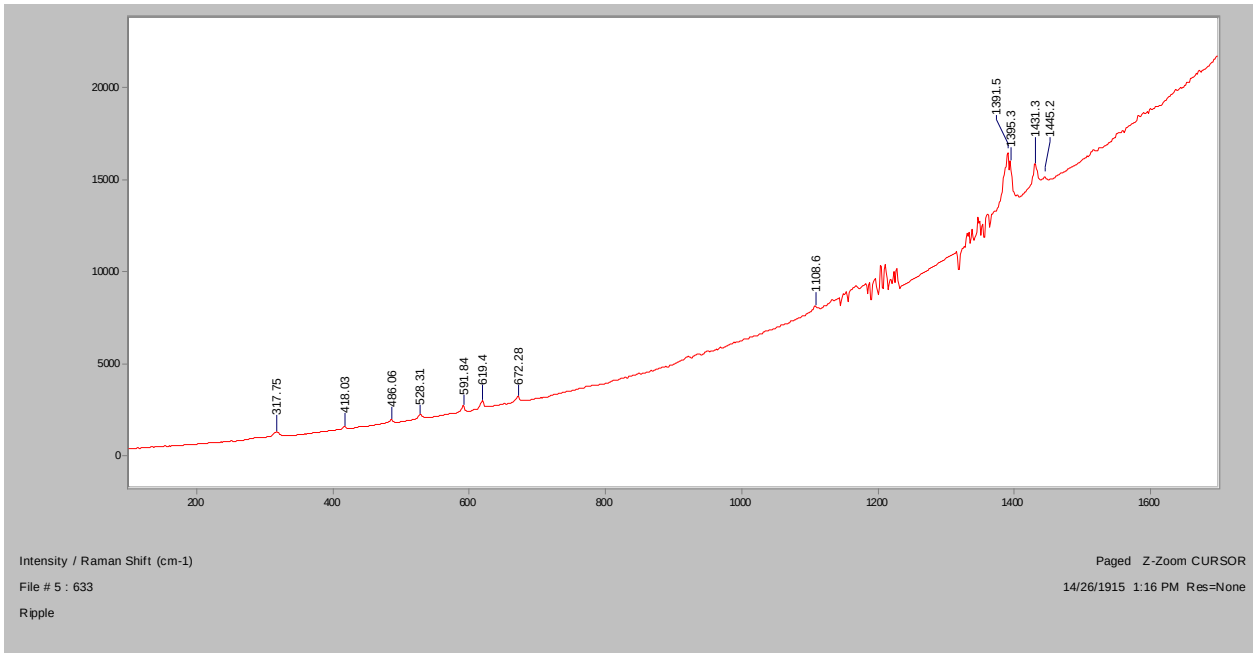

Normal Raman, 785nm

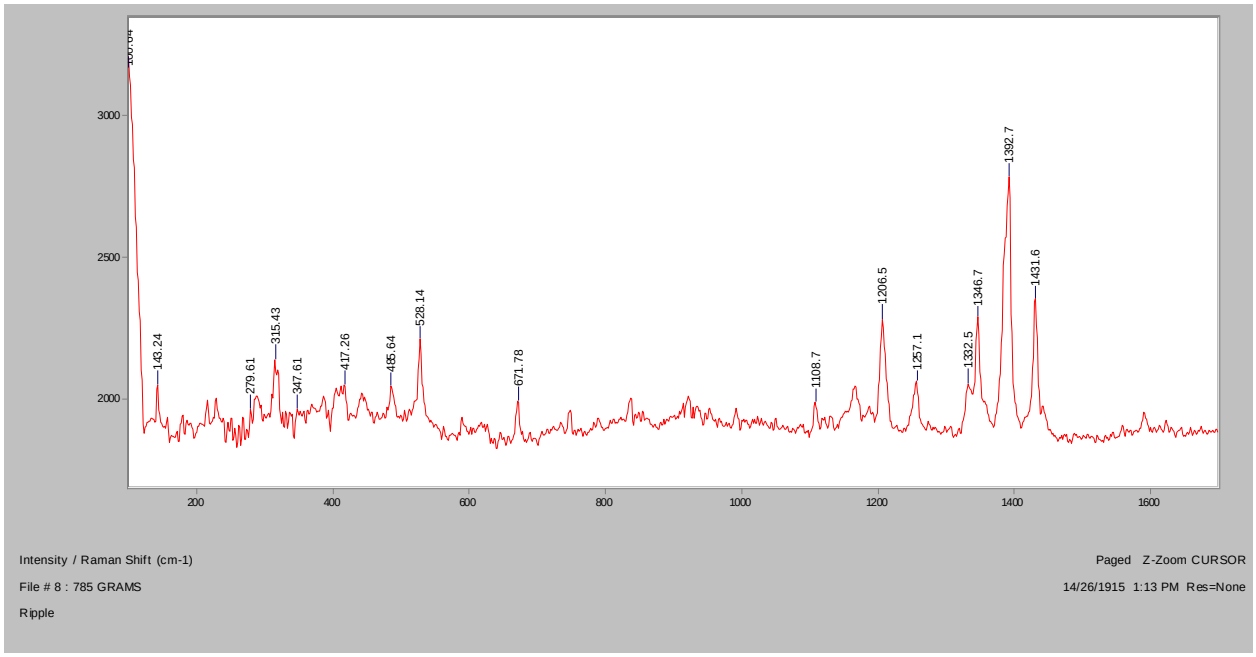

FT-Raman, 1064nm

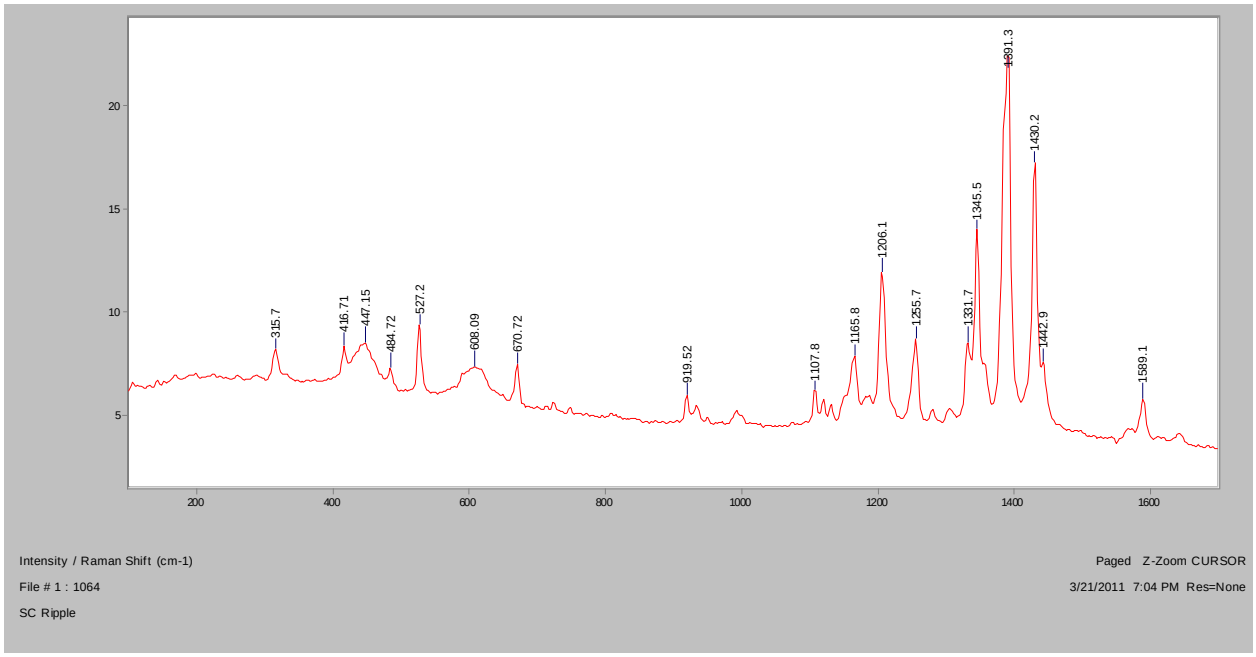

SERS, 488nm

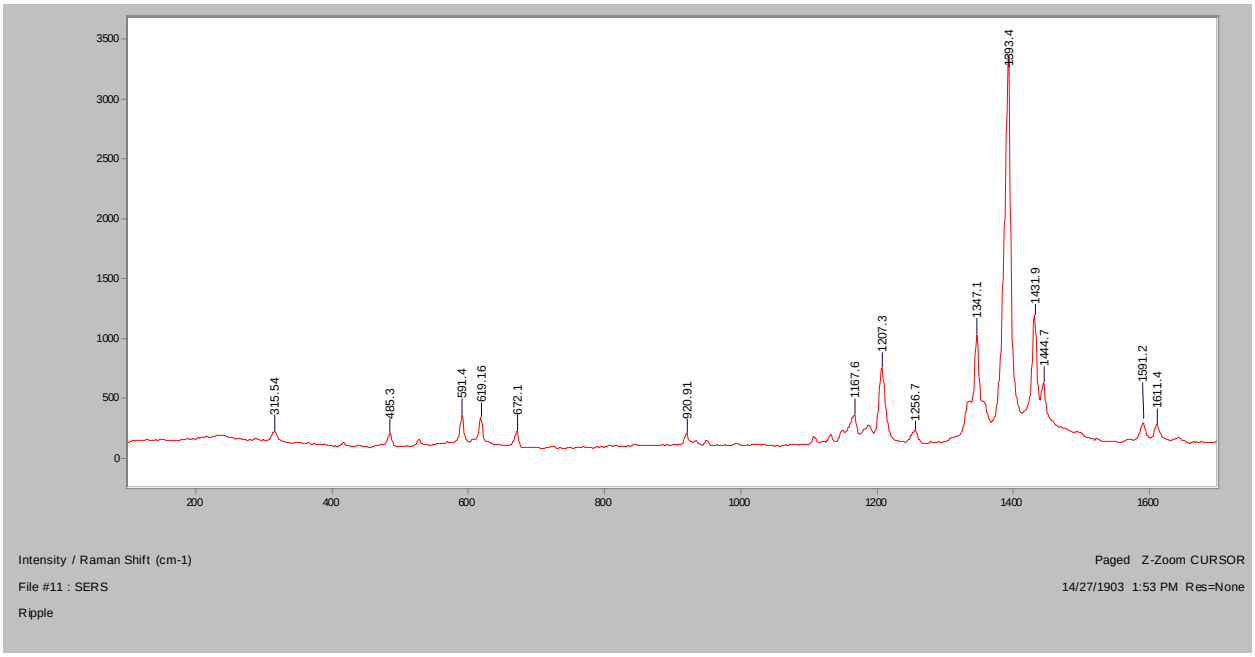

FT-IR (ATR)

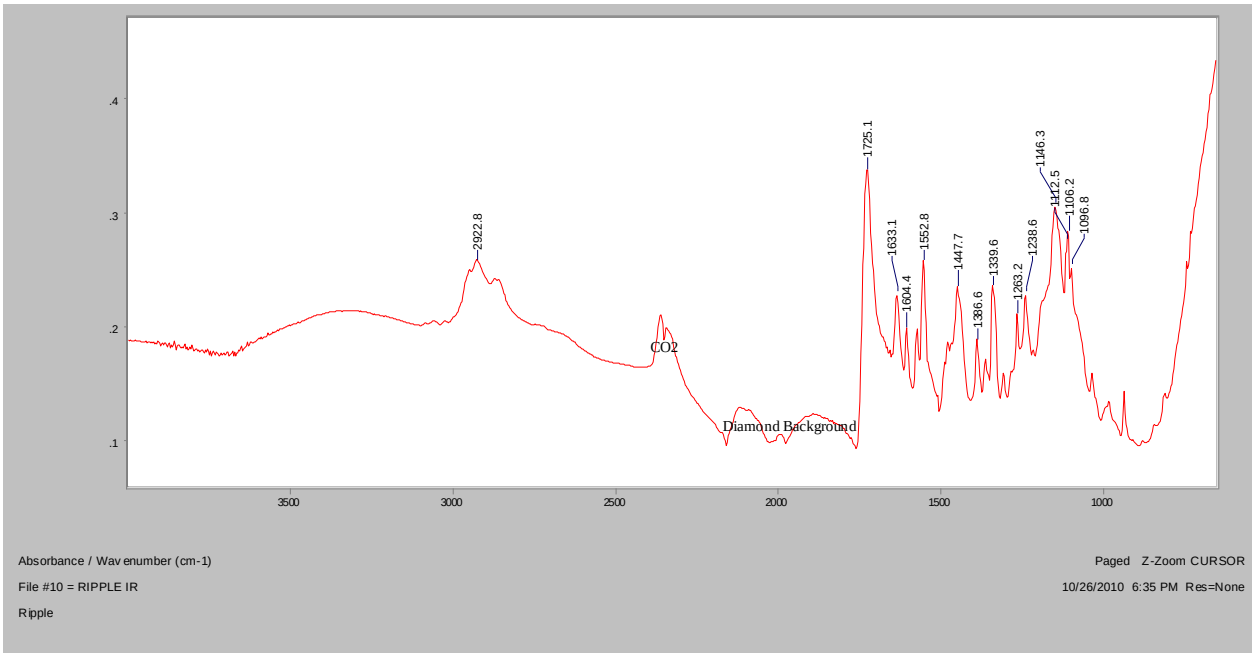

XRF

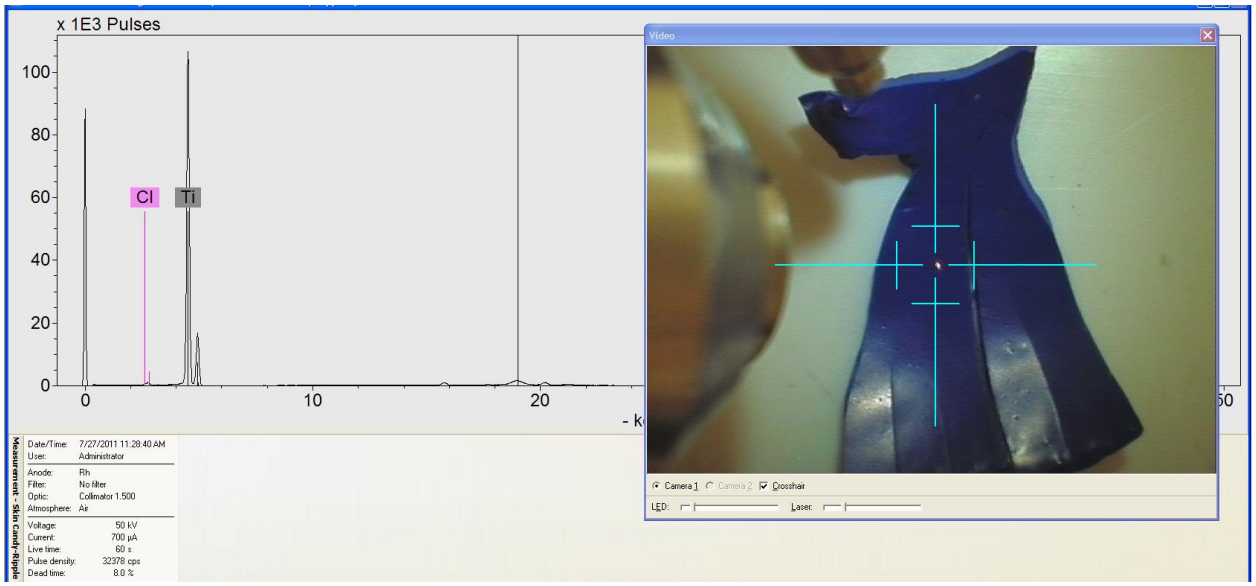
x 1E3 Pulses
100
80
60
40
20
0
Cl
Ti
0
10
20
Video
Camera 1
Camera 2
Crosshair
LED:
Laser:
Measurement - SDD Chart-Adobe
Date/Time: 7/27/2011 11:28:40 AM
User: Administrator
Anode: Rh
Filter: No filter
Optic: Collimator 1.500
Atmosphere: Air
Voltage: 50 kV
Current: 700 µA
Live time: 60 s
Pulse density: 32378 cps
Dead time: 8.0 %

San Brownadino

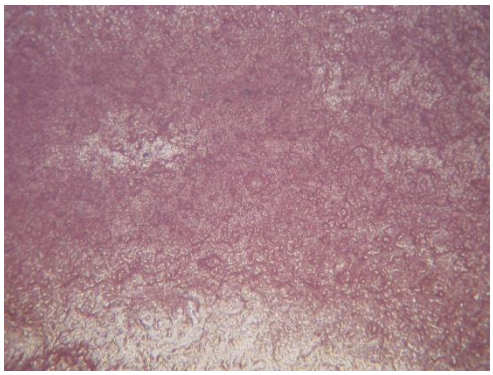

Bright Field, 100x

Dark Field, 100x

In RI 1.550, 400x

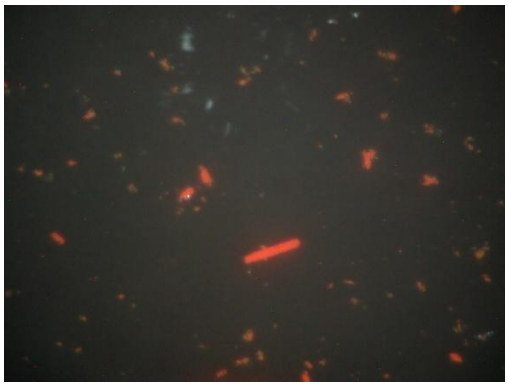

Crossed polars, In RI 1.550, 400x

Normal Raman, 488nm

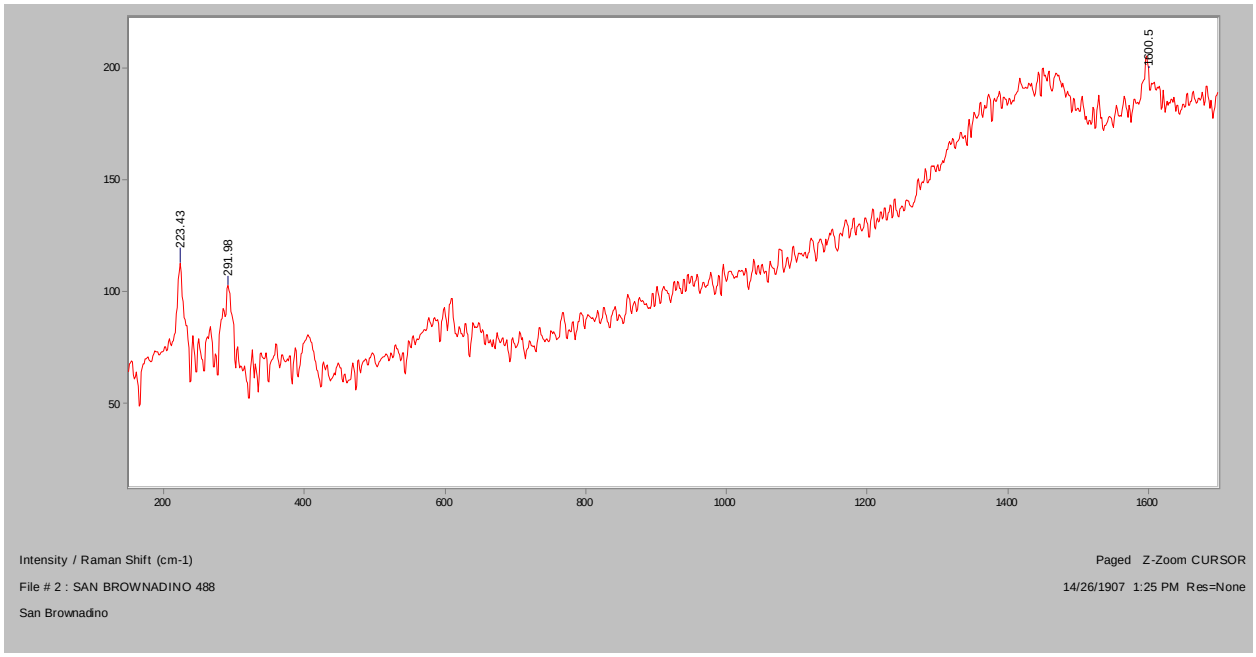

Normal Raman, 633nm

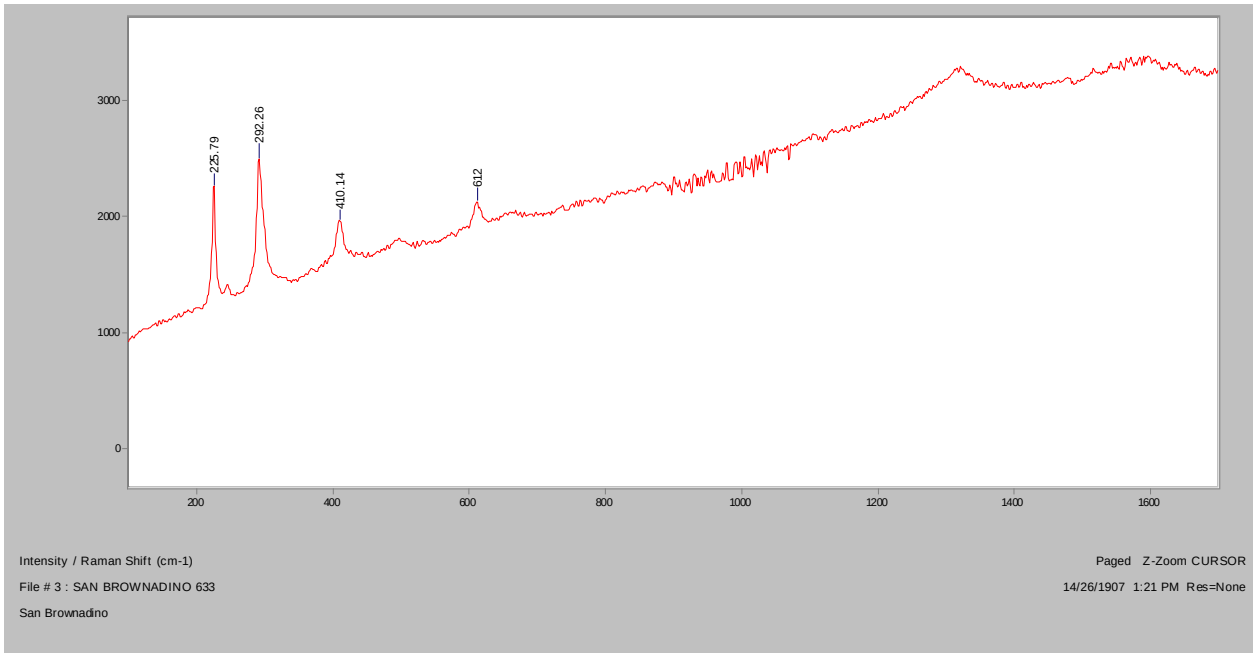

Normal Raman, 785nm

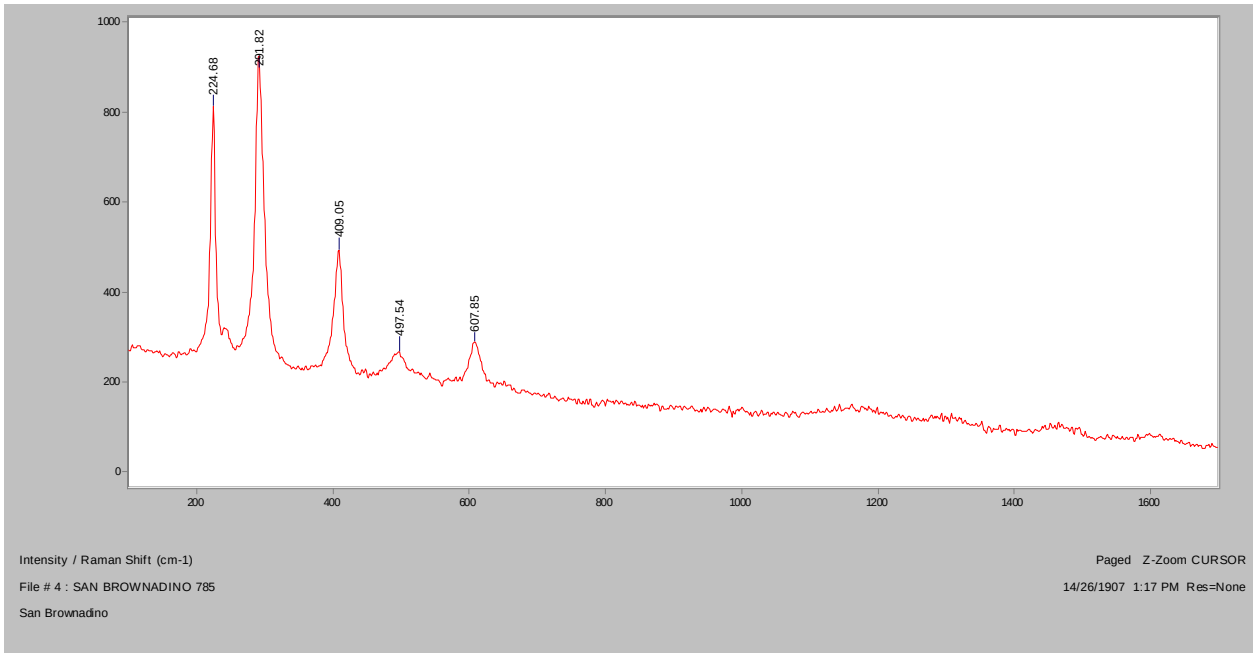

SERS, 488nm

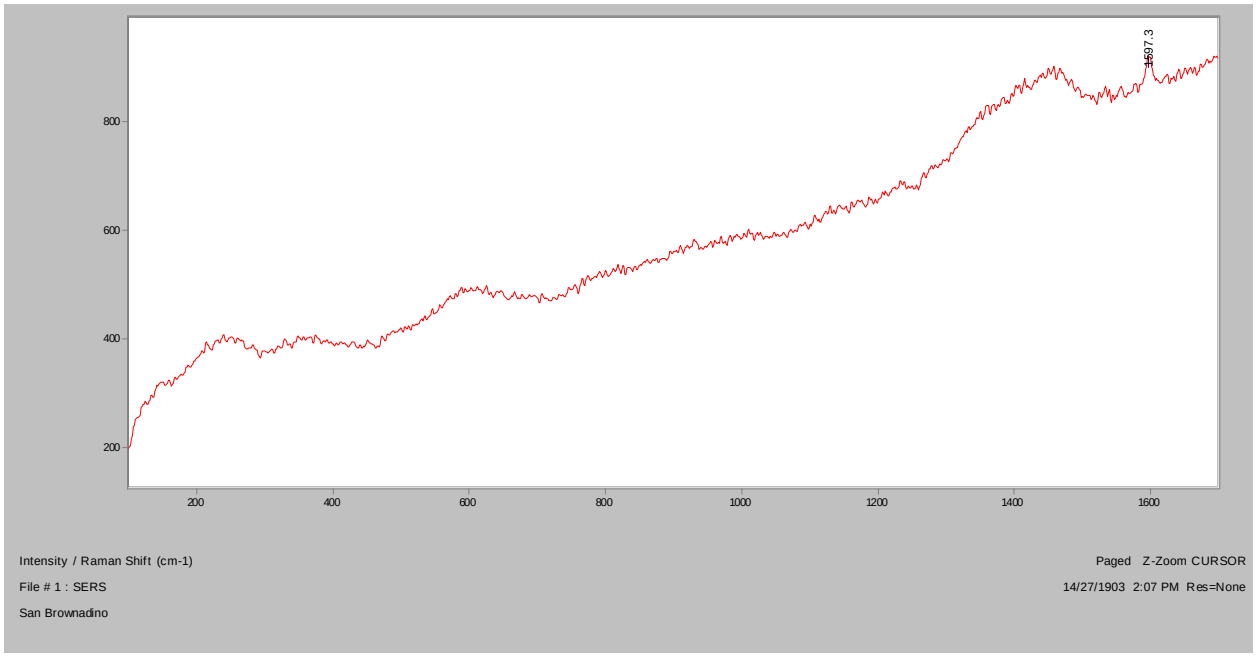

FT-IR (ATR)

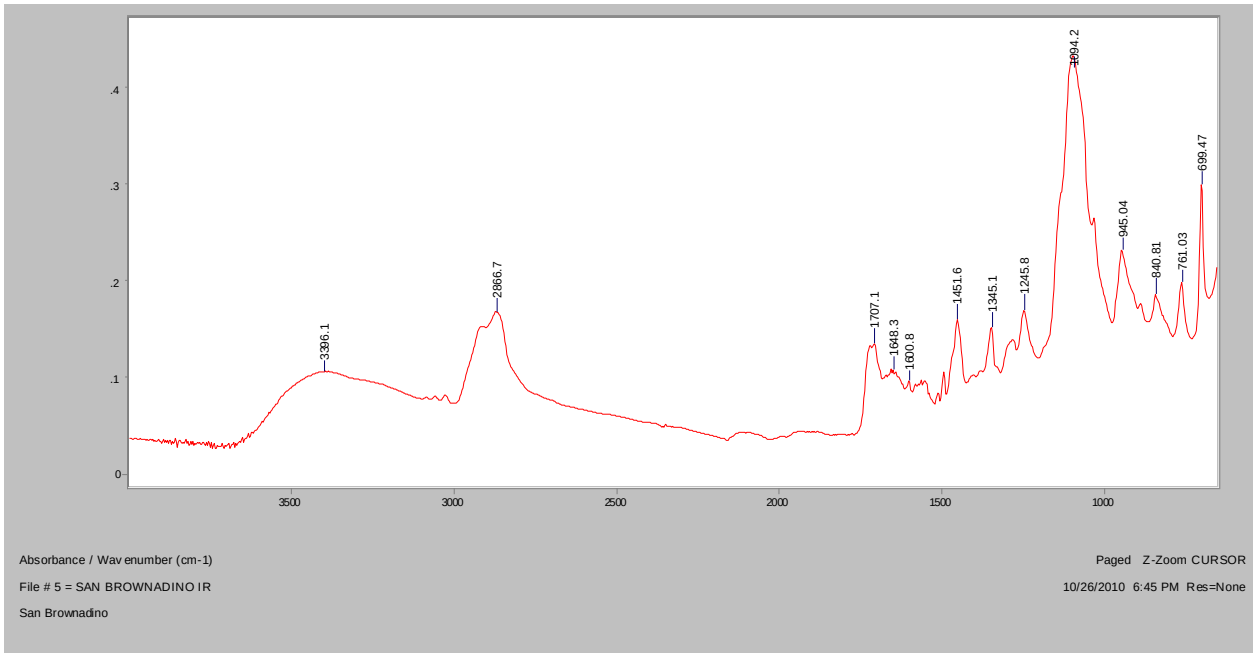
3396.1
2866.7
1707.1
1648.3
1600.8
1451.6
1345.1
1245.8
1094.2
945.04
840.81
761.03
699.47
3500
3000
2500
2000
1500
1000
Absorbance / Wavenumber (cm-1)
File # 5 = SAN BROWNADINO IR
San Brownadino
Paged Z-Zoom CURSOR
10/26/2010 6:45 PM Res=None

XRF

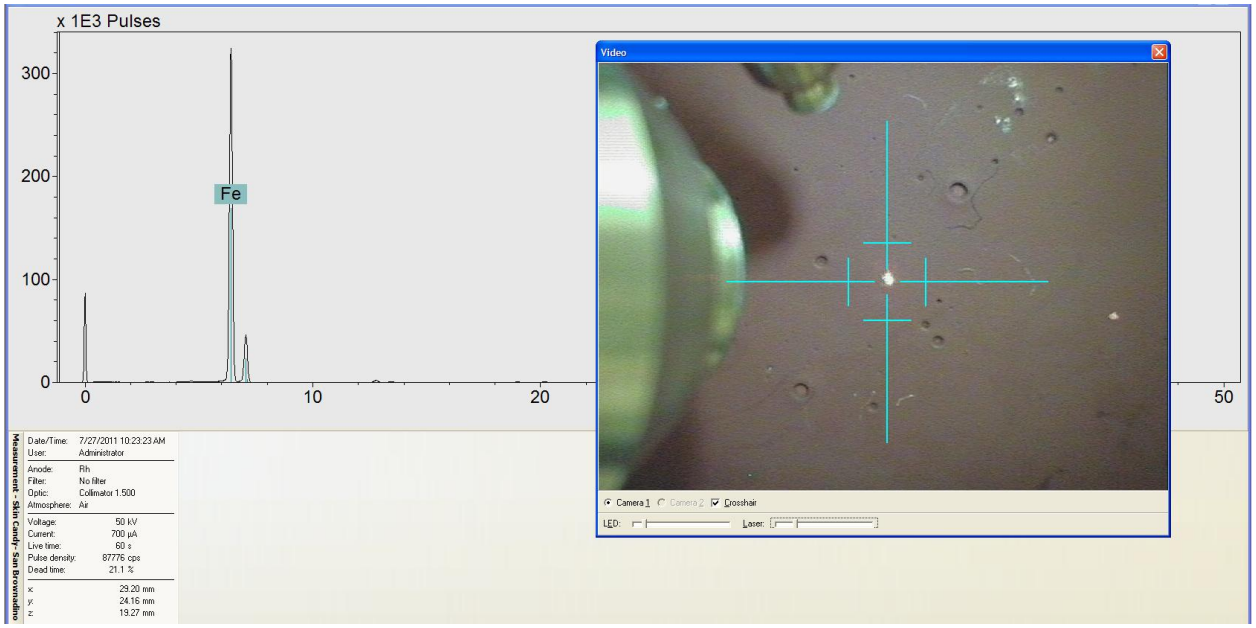
x 1E3 Pulses
Fe
Video
Camera 1
Crosshair
LED:
Laser:
Date/Time: 7/27/2011 10:23:23 AM
User: Administrator
Anode: Rh
Filter: No filter
Optic: Collimator 1.500
Atmosphere: Air
Voltage: 50 kV
Current: 700 µA
Live time: 60 s
Pulse density: 87776 cps
Dead time: 21.1 %
x 29.20 mm
y 24.16 mm
z 19.27 mm

Black Cherry Roan 2

Bright Field, 100x

Dark Field, 100x

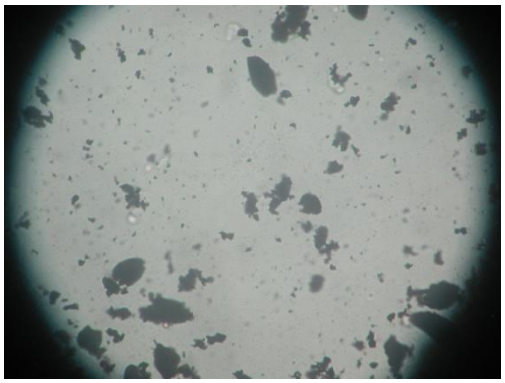

In RI 1.550, 400x

Crossed polars, In RI 1.550, 400x

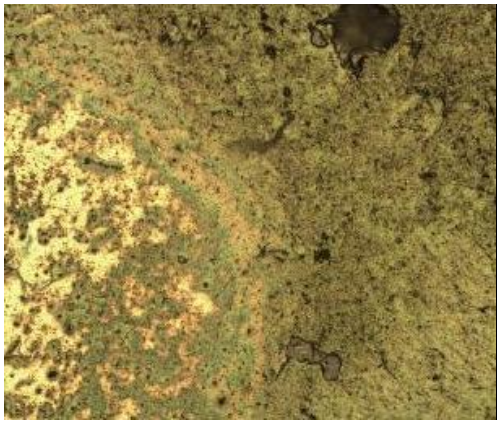

Raman microscope image, 200x

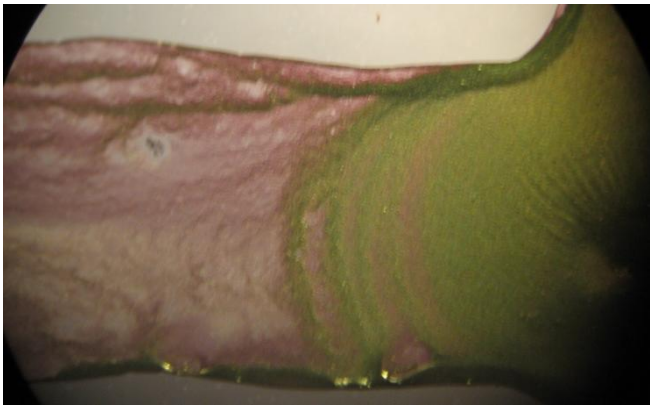

Smear on Microscope slide after drying, ~20x

Normal Raman, 488nm

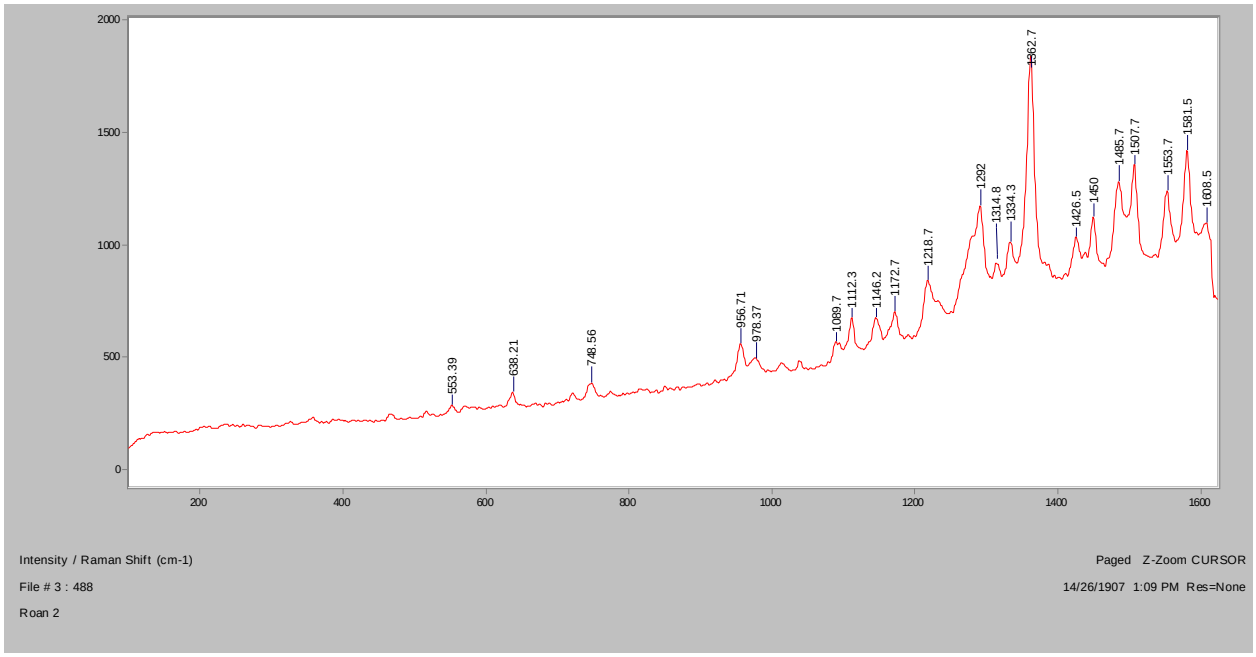

Normal Raman, 633nm

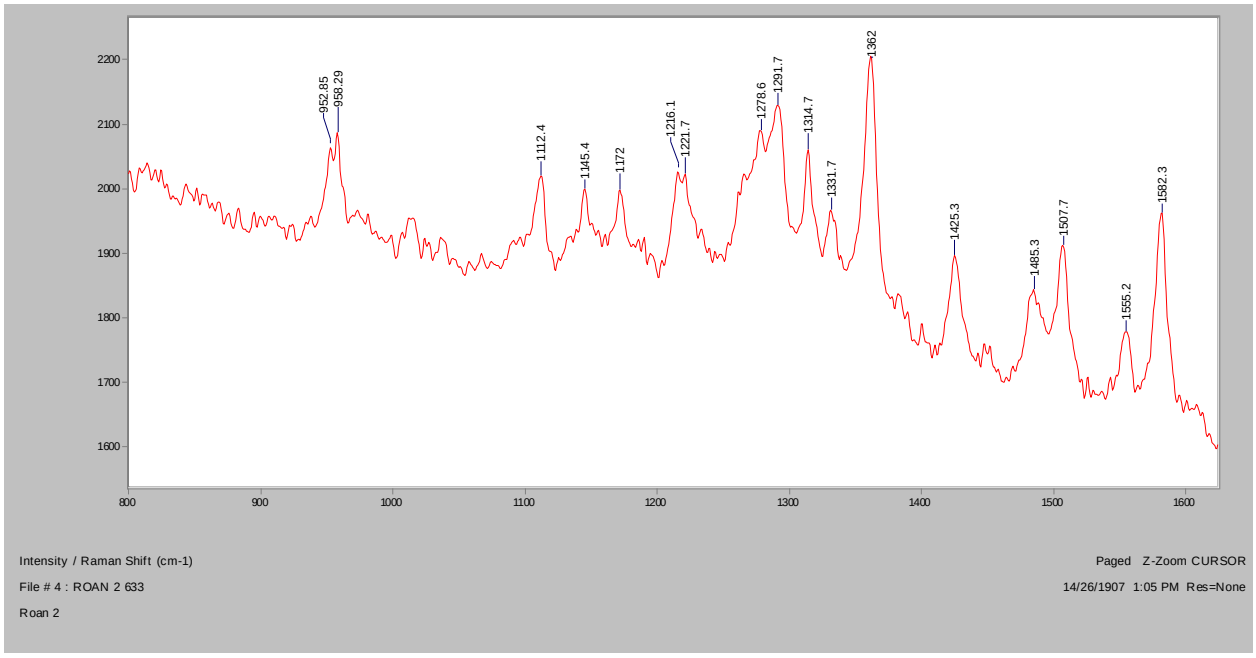

Normal Raman, 785nm

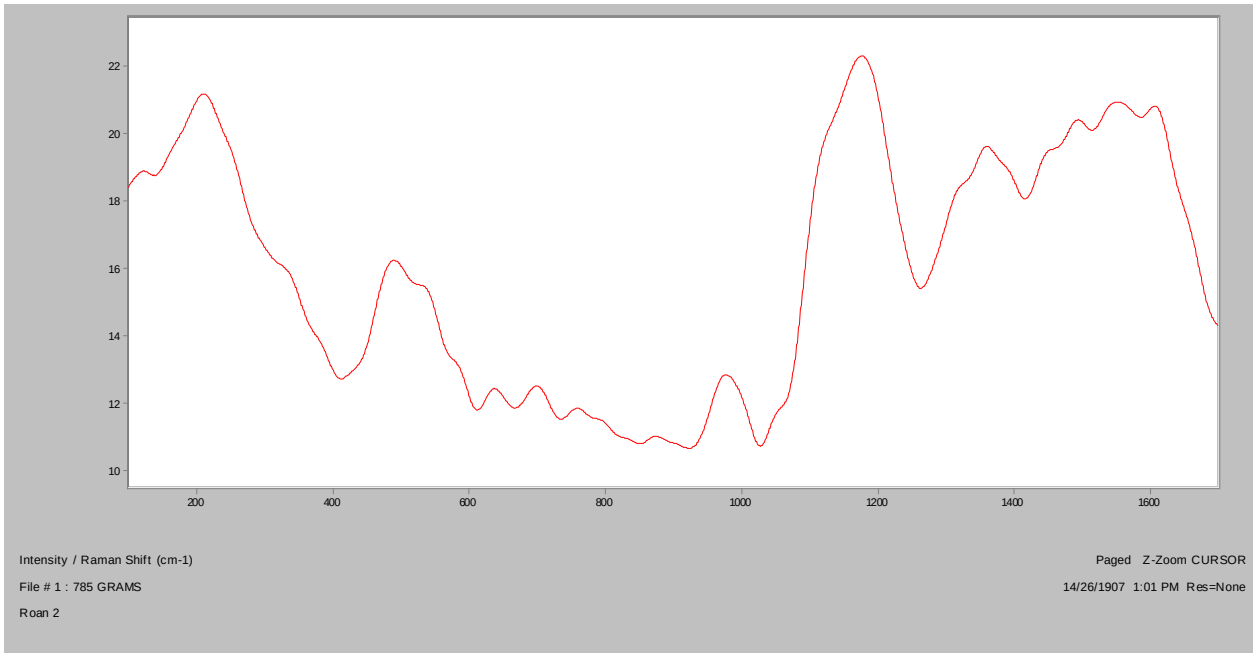

FT-IR (ATR)

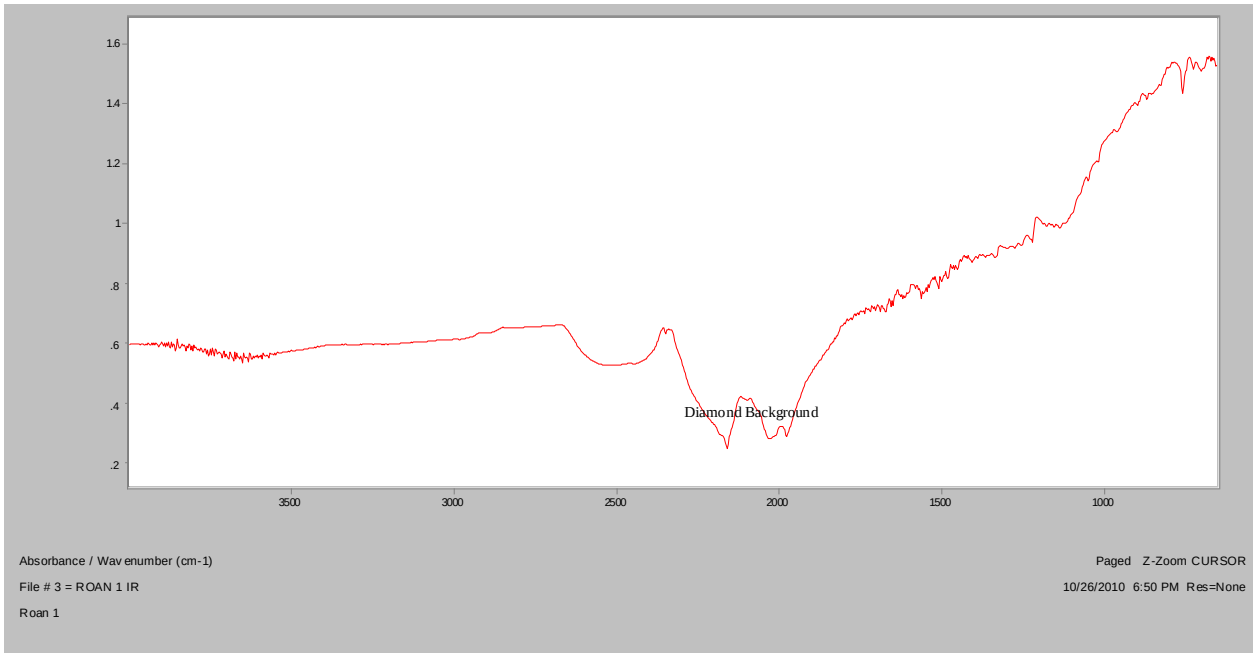

Roan 1

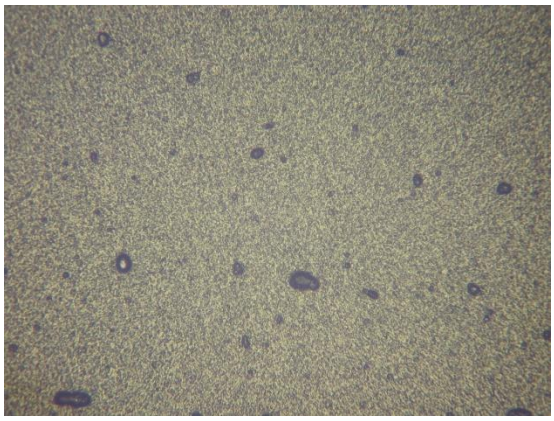

Bright Field, 100x

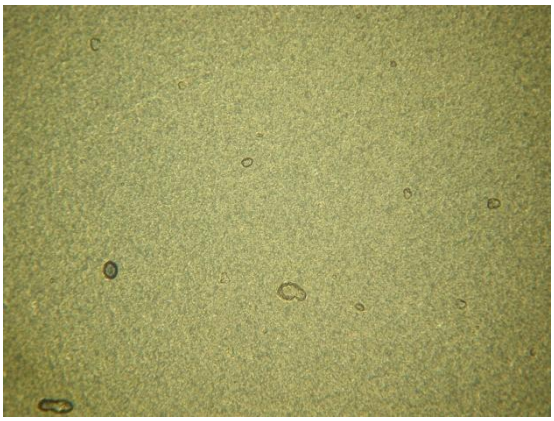

Dark Field, 100x

Roan 3

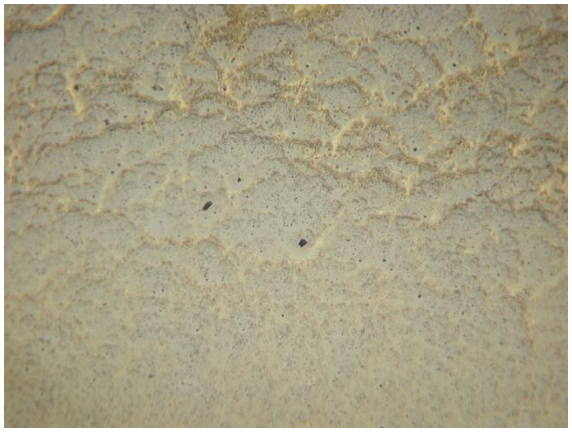

Bright Field, 100x

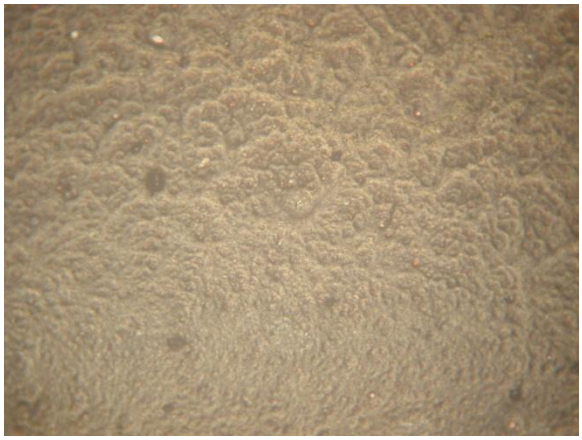

Dark Field, 100x

White Girl

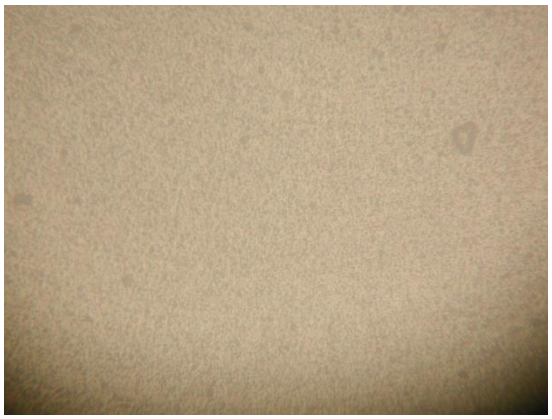

Bright Field, 100x

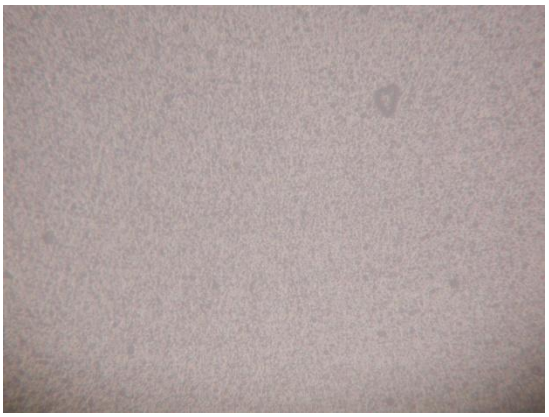

Dark Field, 100x

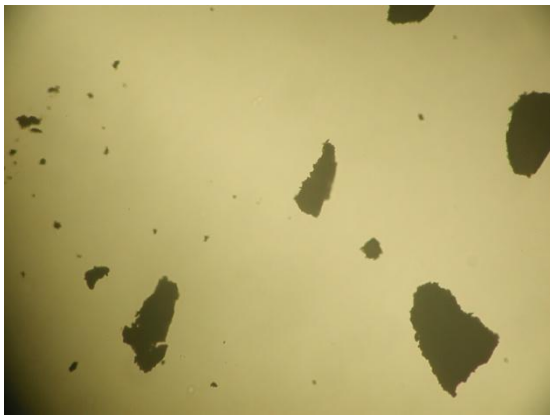

In RI 1.550, 200x

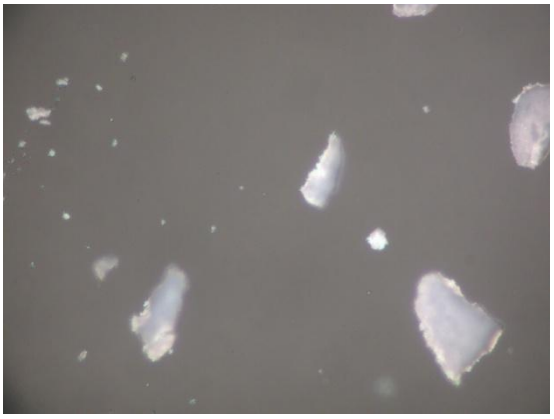

Crossed polars, In IR 1.550, 200x

Normal Raman, 488nm

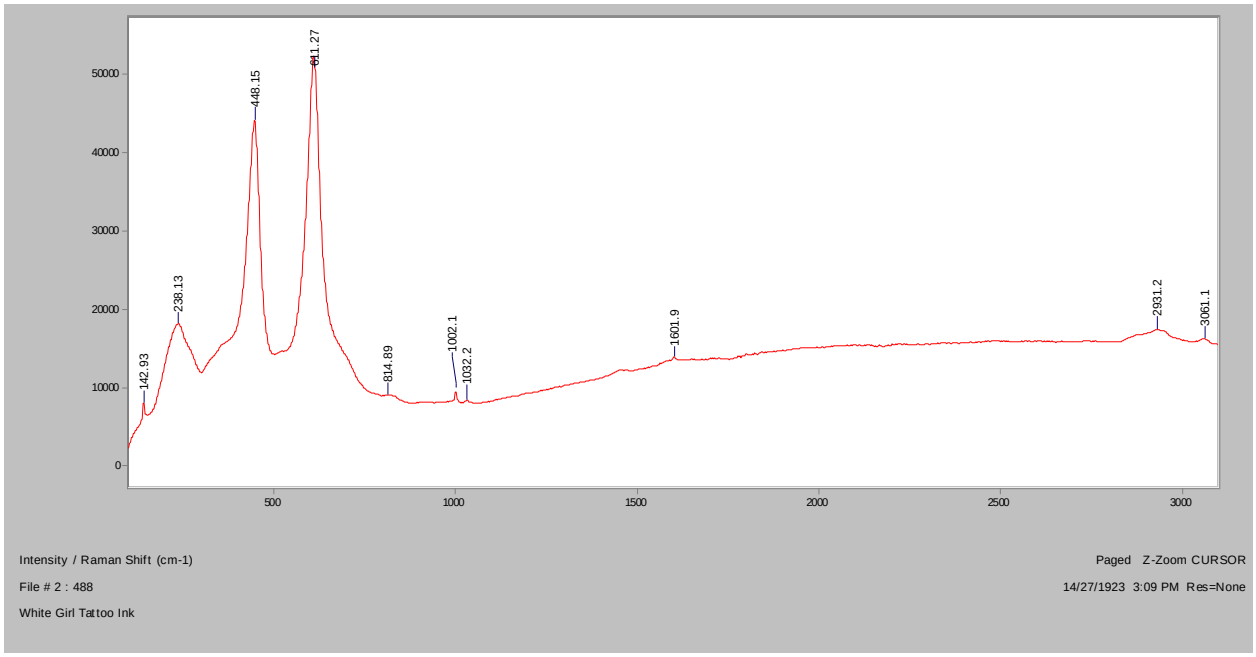

Normal Raman, 633nm

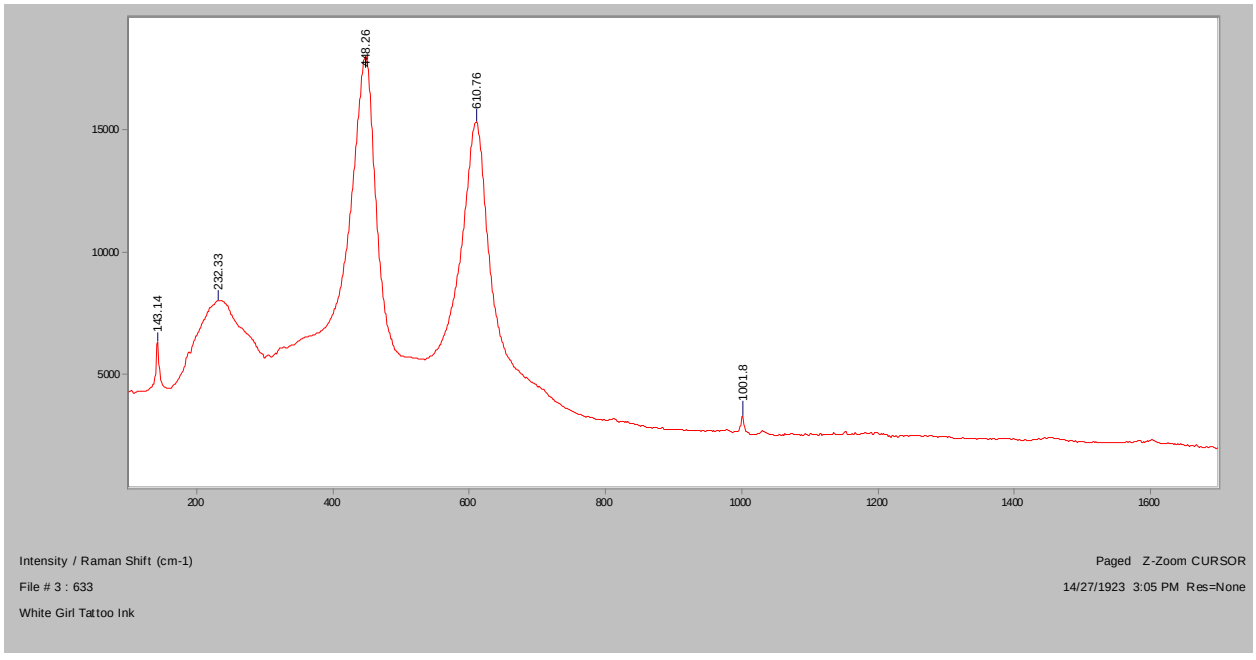

Normal Raman, 785nm

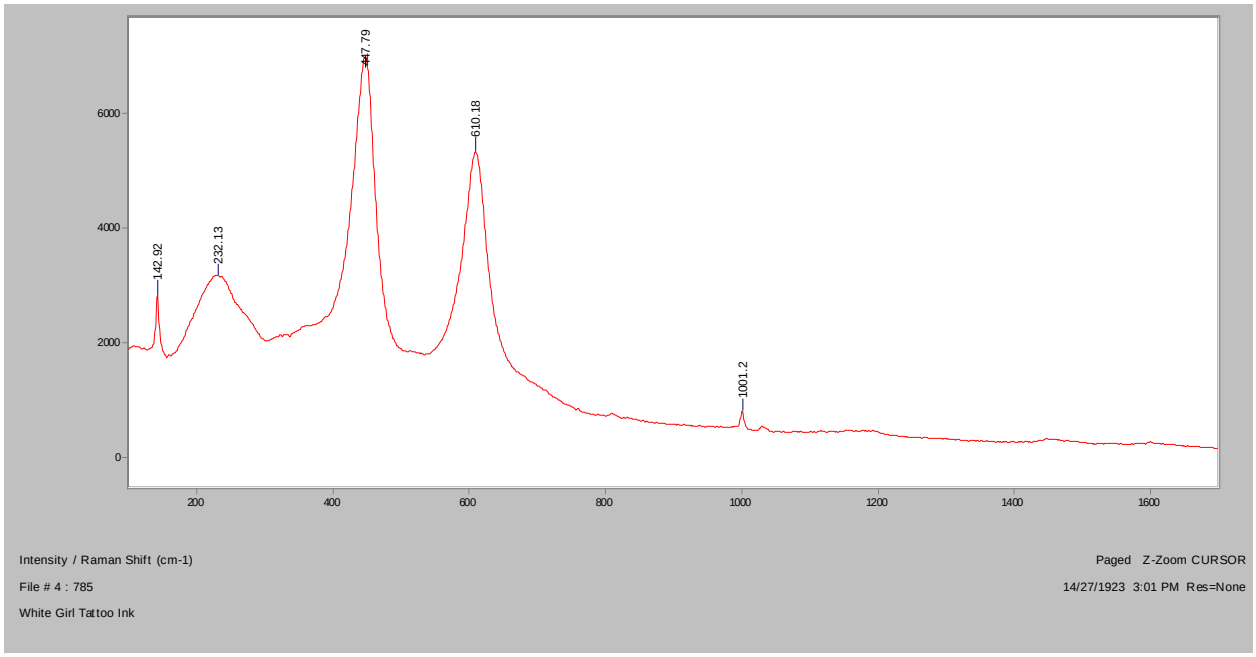

FT-Raman, 1064nm

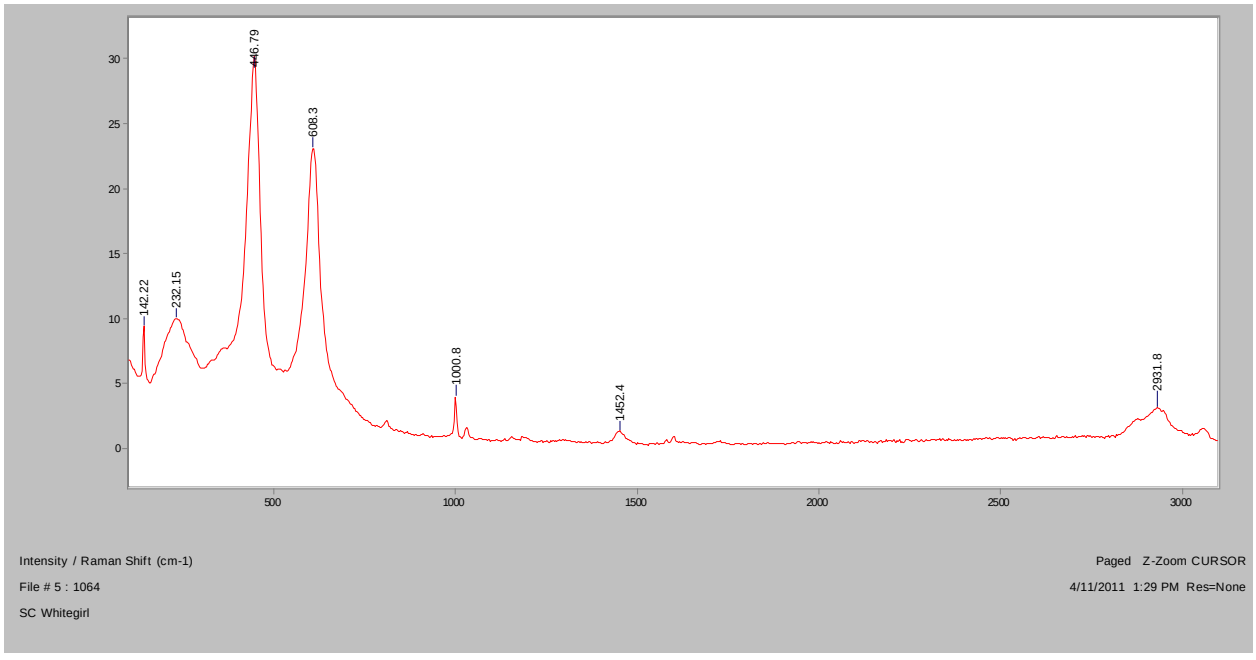

FT-IR (ATR)

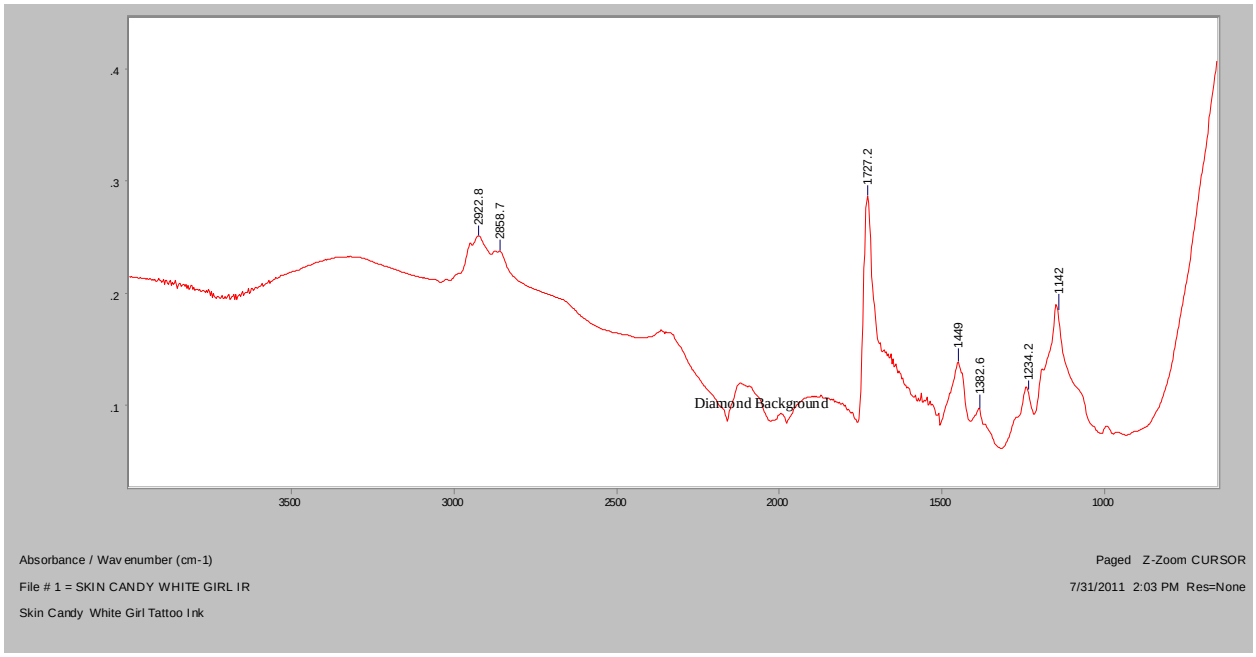
.4
.3
.2
.1
2922.8
2858.7
1727.2
1449
1382.6
1234.2
1142
Diamond Background
3500
3000
2500
2000
1500
1000
Absorbance / Wavenumber (cm-1)
File # 1 = SKIN CANDY WHITE GIRL IR
Skin Candy White Girl Tattoo Ink
Paged Z-Zoom CURSOR
7/31/2011 2:03 PM Res=None

XRF

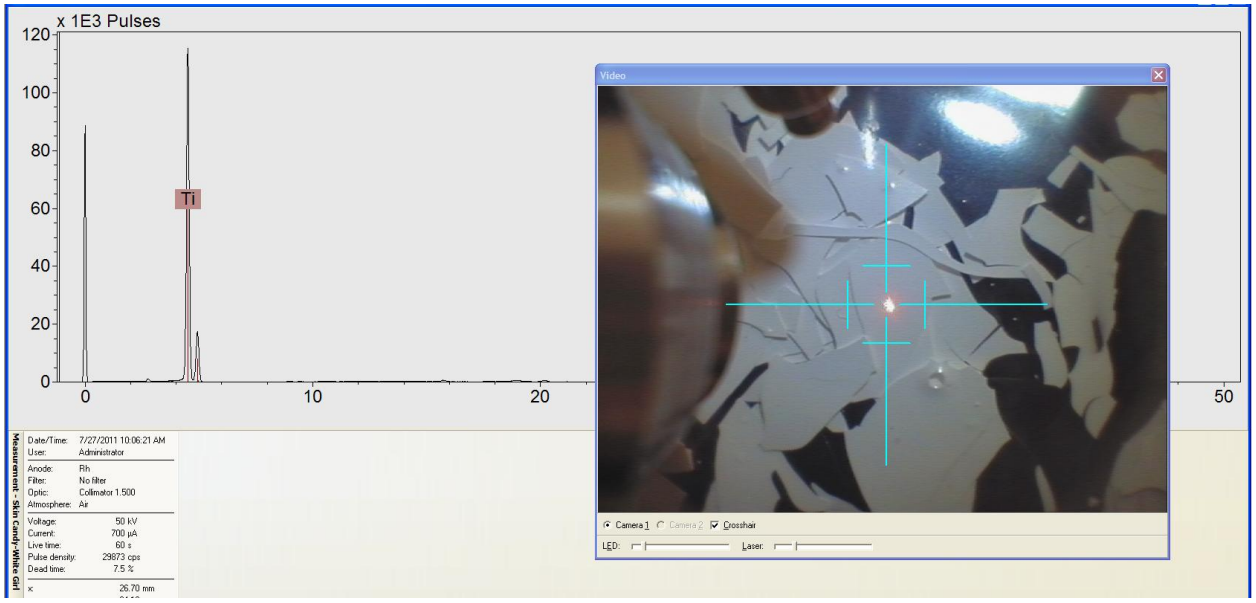
x 1E3 Pulses
120
100
80
60
40
20
0
Ti
0
10
20
50
Video
Camera 1
Camera 2
Crosshair
LED:
Laser:
Date/Time: 7/27/2011 10:06:21 AM
User: Administrator
Anode: Rh
Filter: No filter
Optic: Collimator 1.500
Atmosphere: Air
Voltage: 50 kV
Current: 700 µA
Live time: 60 s
Pulse density: 29873 cps
Dead time: 7.5 %
x: 26.70 mm
Measurement - Skin Candy White Girl

Tokyo Pink

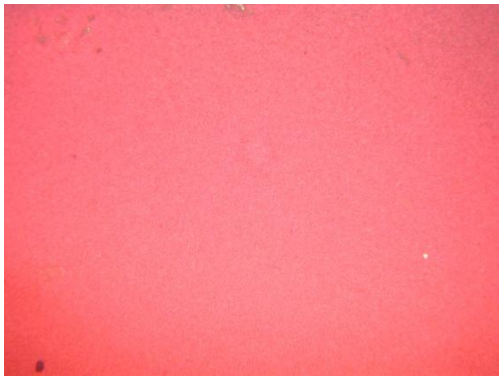

Bright Field, 100x

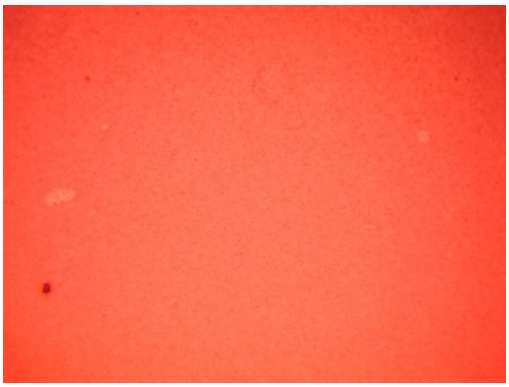

Dark Field, 100x

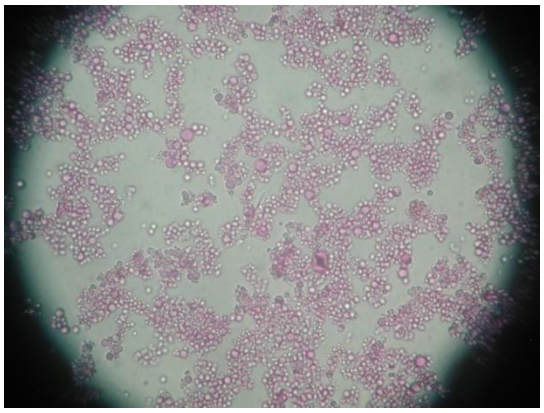

In RI 1.550, 400x

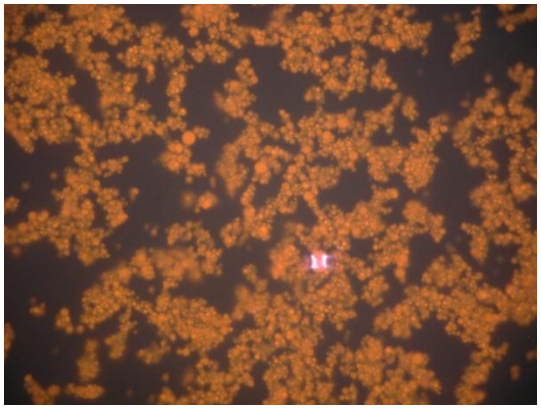

Crossed polars, In RI 1.550, 400x

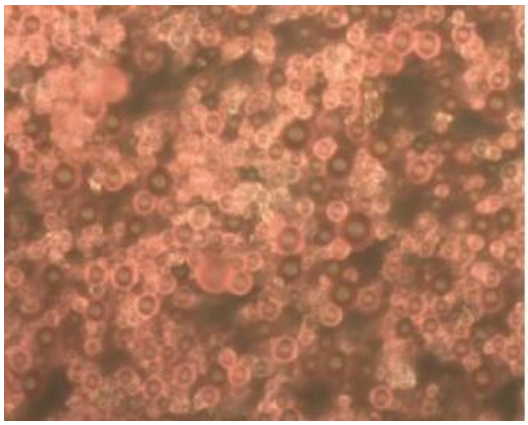

Raman microscope image, 1000x

Normal Raman, 488nm

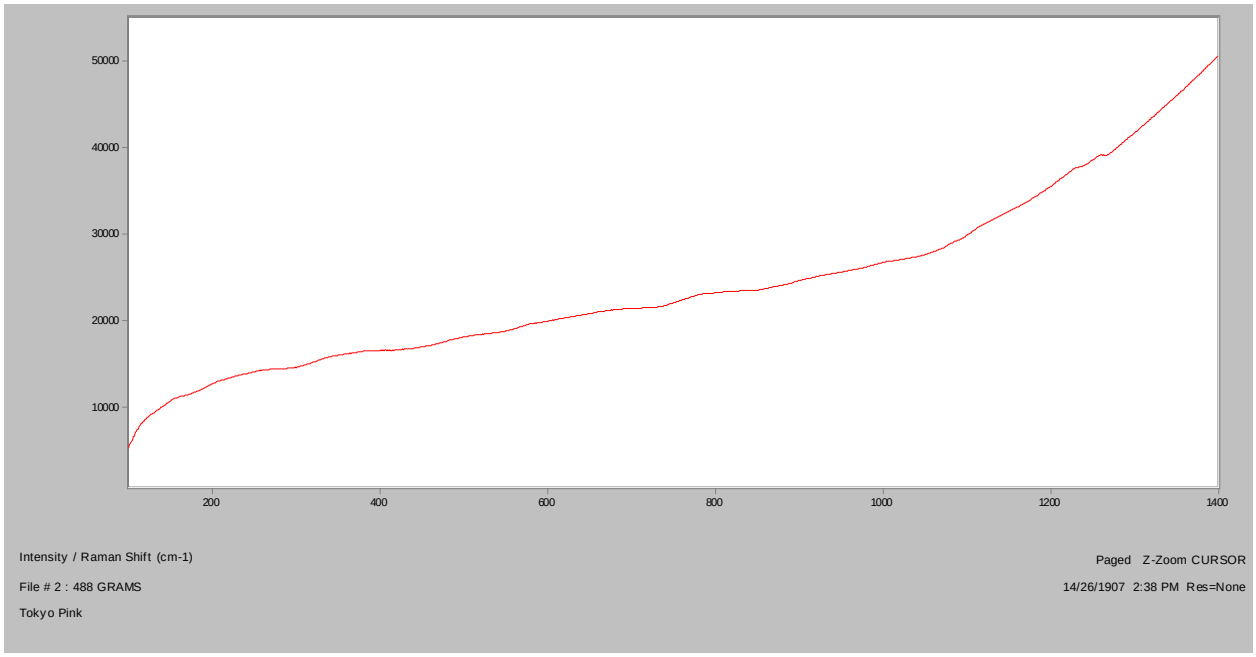

Normal Raman, 633nm

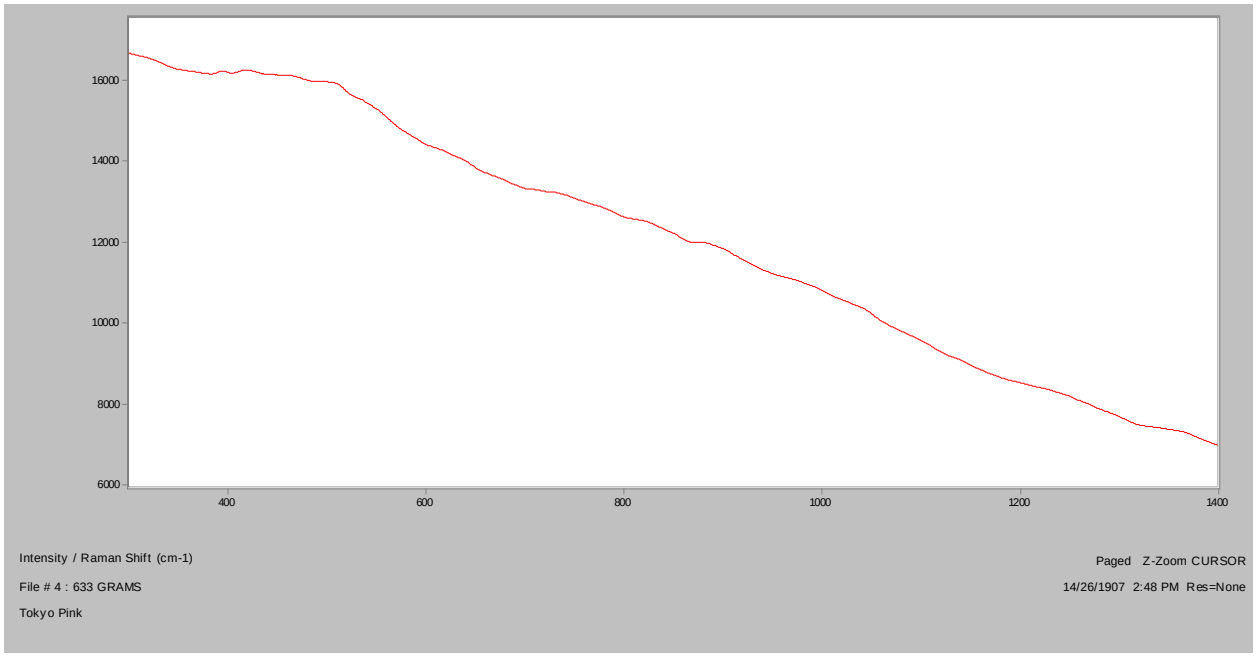

Normal Raman, 785nm

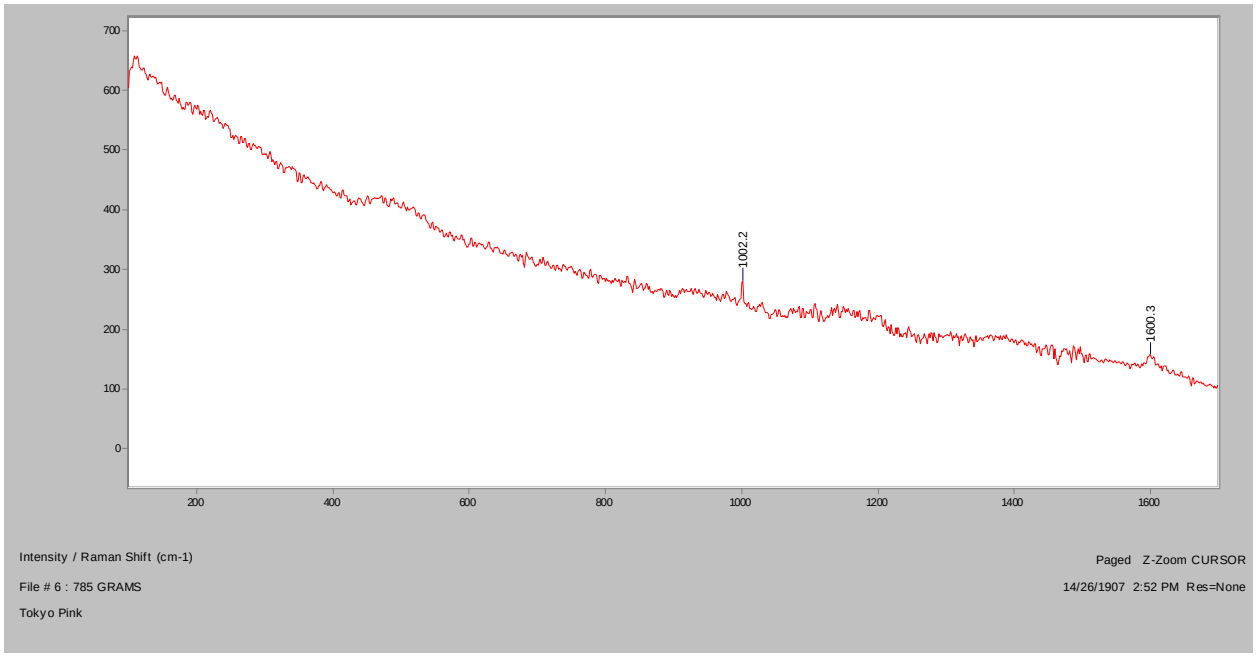

FT-Raman, 1064nm

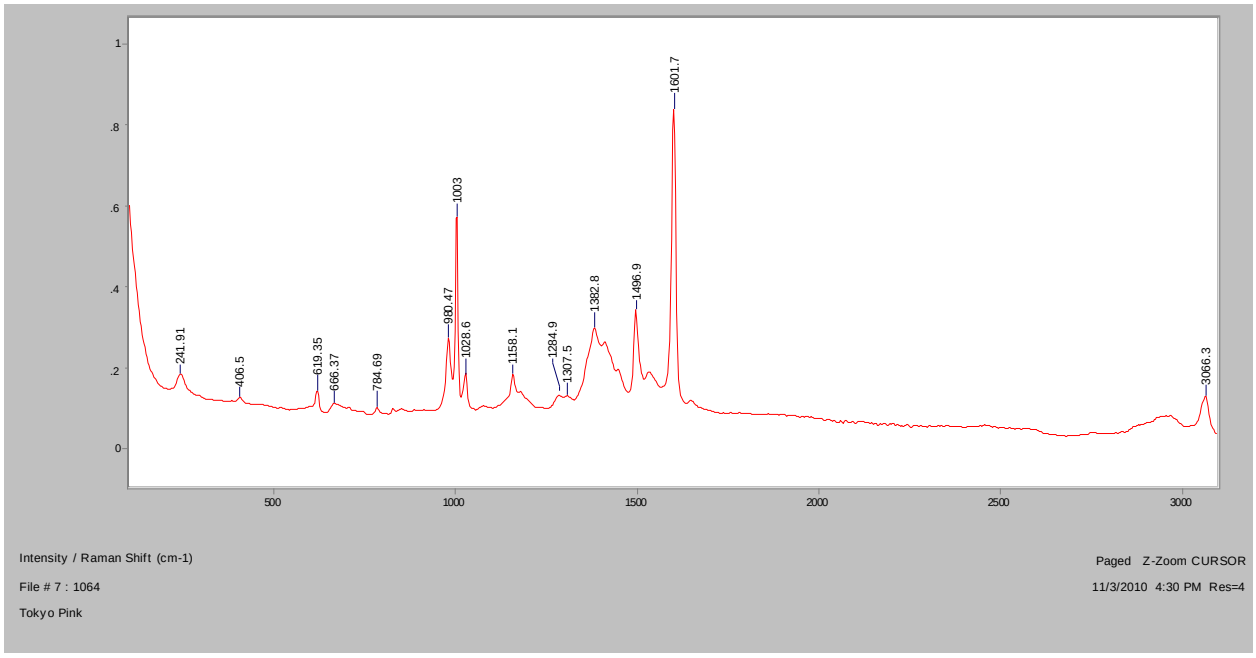

FT-IR (ATR)

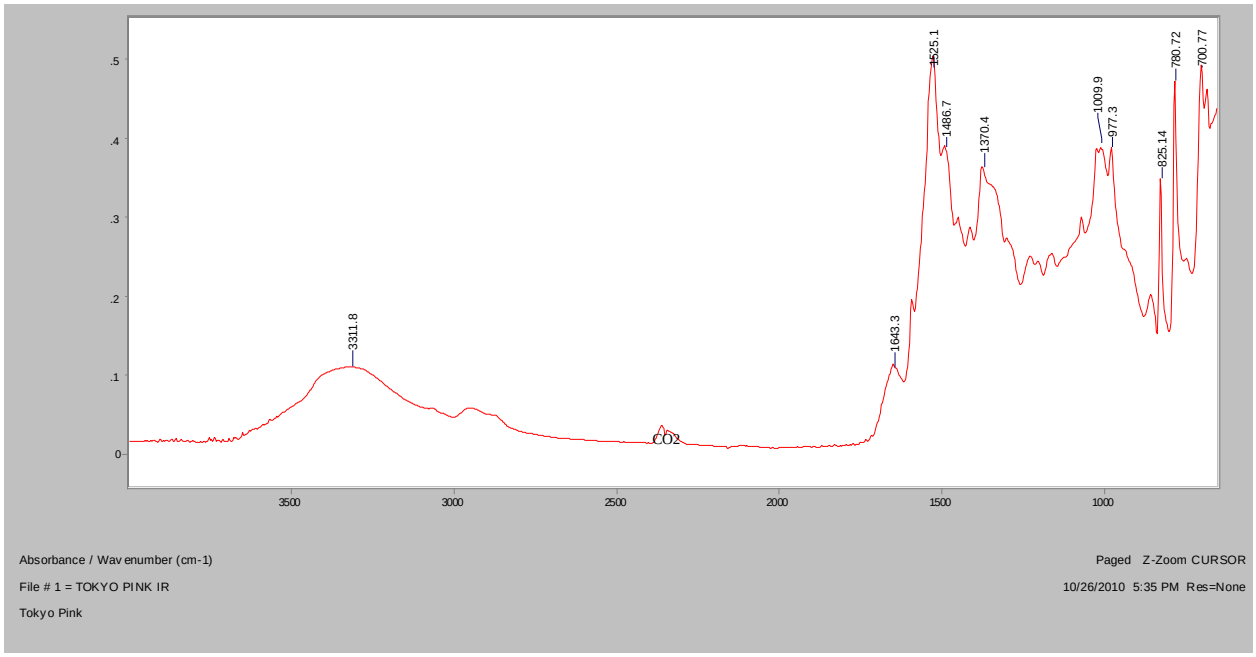
3311.8
1643.3
1525.1
1486.7
1370.4
1009.9
977.3
825.14
780.72
700.77
CO2
3500
3000
2500
2000
1500
1000
Absorbance / Wavenumber (cm-1)
File # 1 = TOKYO PINK IR
Tokyo Pink
Paged Z-Zoom CURSOR
10/26/2010 5:35 PM Res=None

XRF

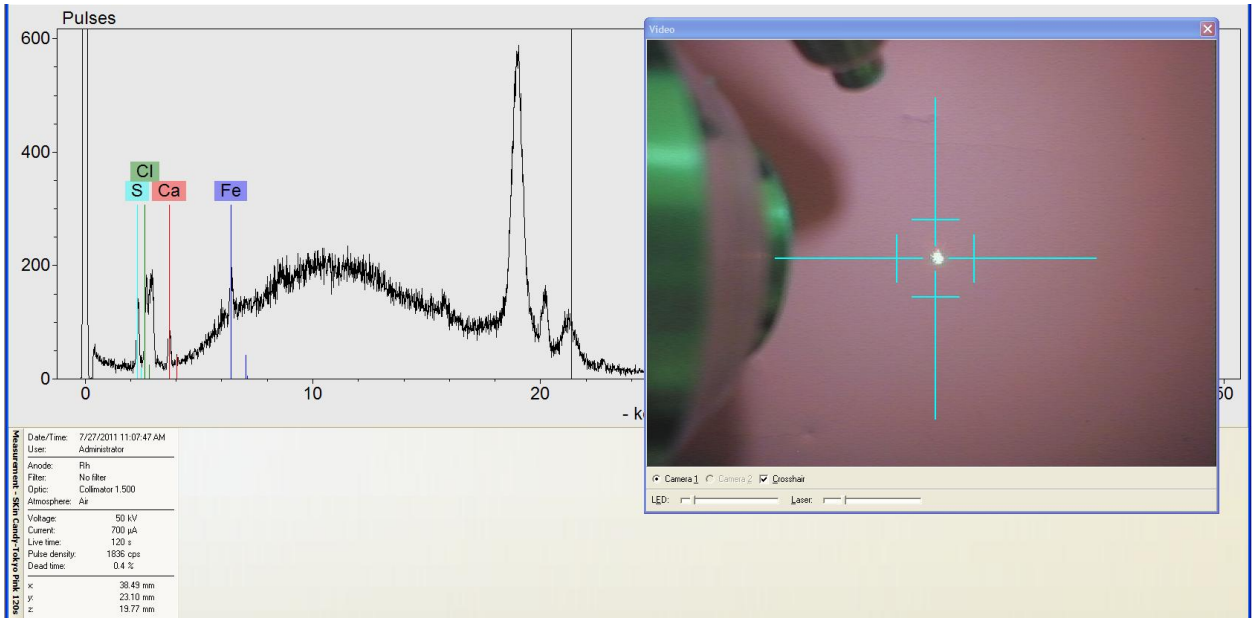
Pulses
Cl
S
Ca
Fe
Video
Camera 1
Camera 2
Crosshair
LED:
Laser:
Date/Time: 7/27/2011 11:07:47 AM
User: Administrator
Anode: Rh
Filter: No filter
Optic: Collimator 1.500
Atmosphere: Air
Voltage: 50 kV
Current: 700 µA
Live time: 120 s
Pulse density: 1836 cps
Dead time: 0.4 %
x: 38.49 mm
y: 23.10 mm
z: 19.77 mm

Appendix D: Tattoo Inks (Flying Tigers)

Salmon Pink

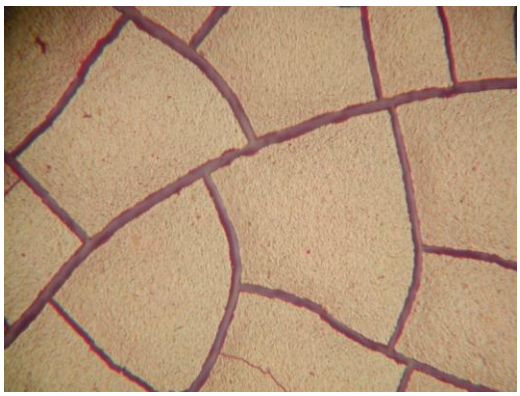

Bright Field, 100x

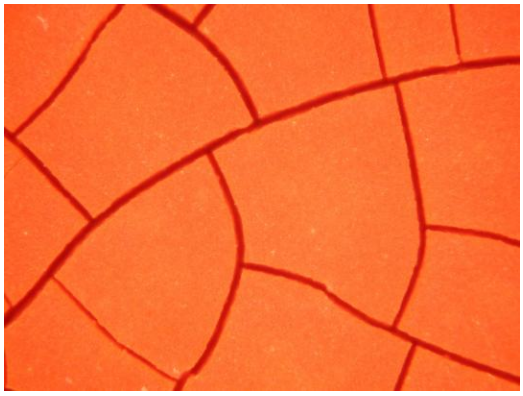

Dark Field, 100x

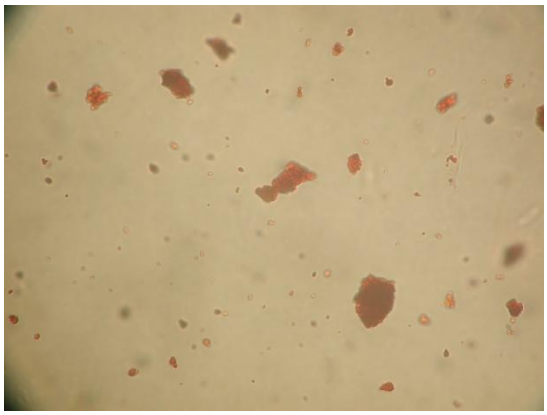

In RI 1.550, 400x

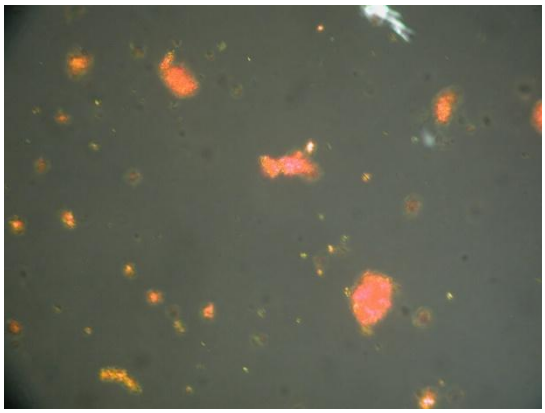

Crossed polars, In RI 1.550, 400x

Normal Raman, 488nm

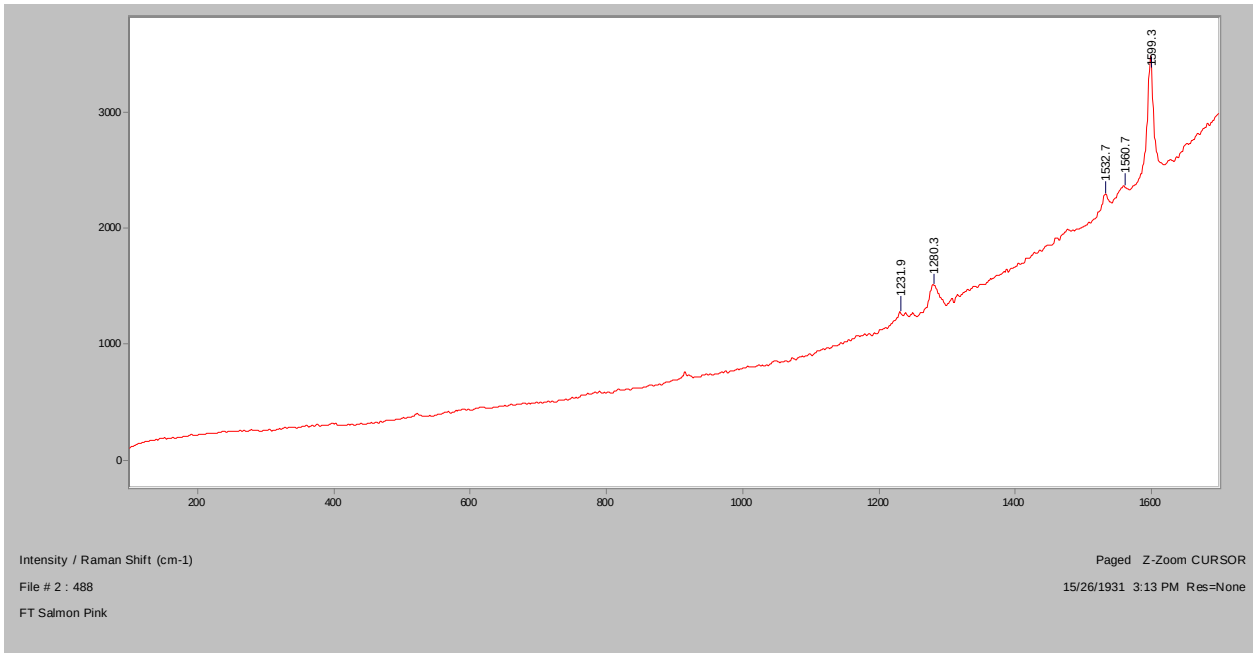

Normal Raman, 633nm

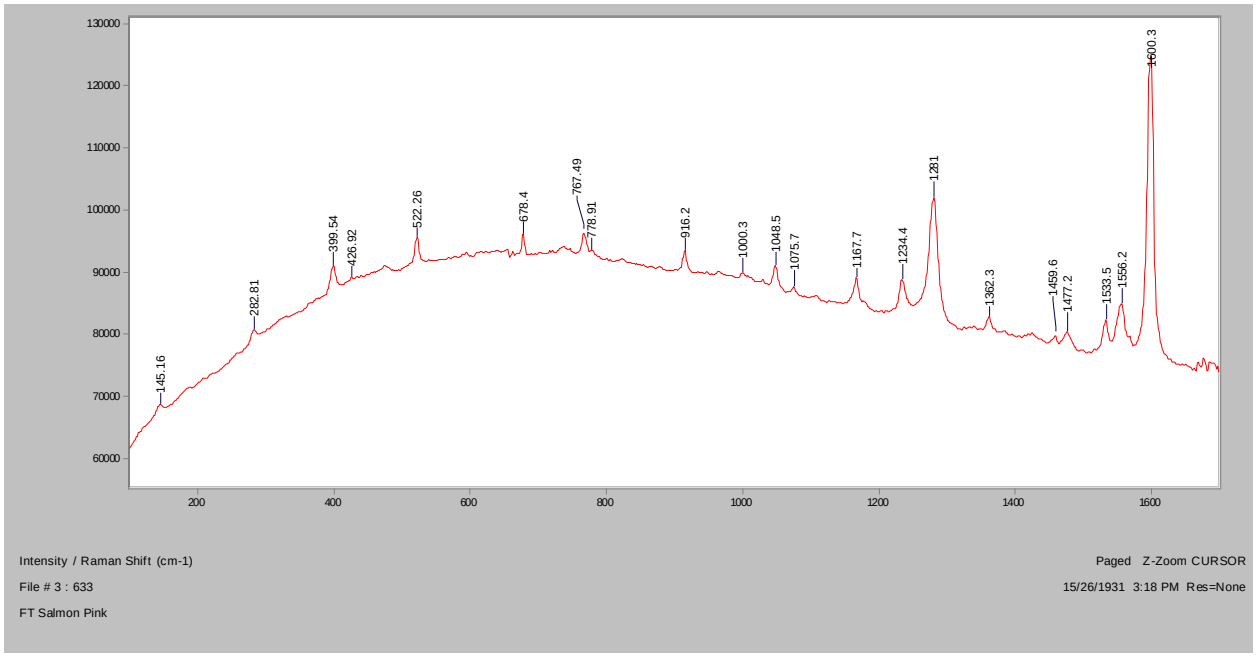

Normal Raman, 785nm

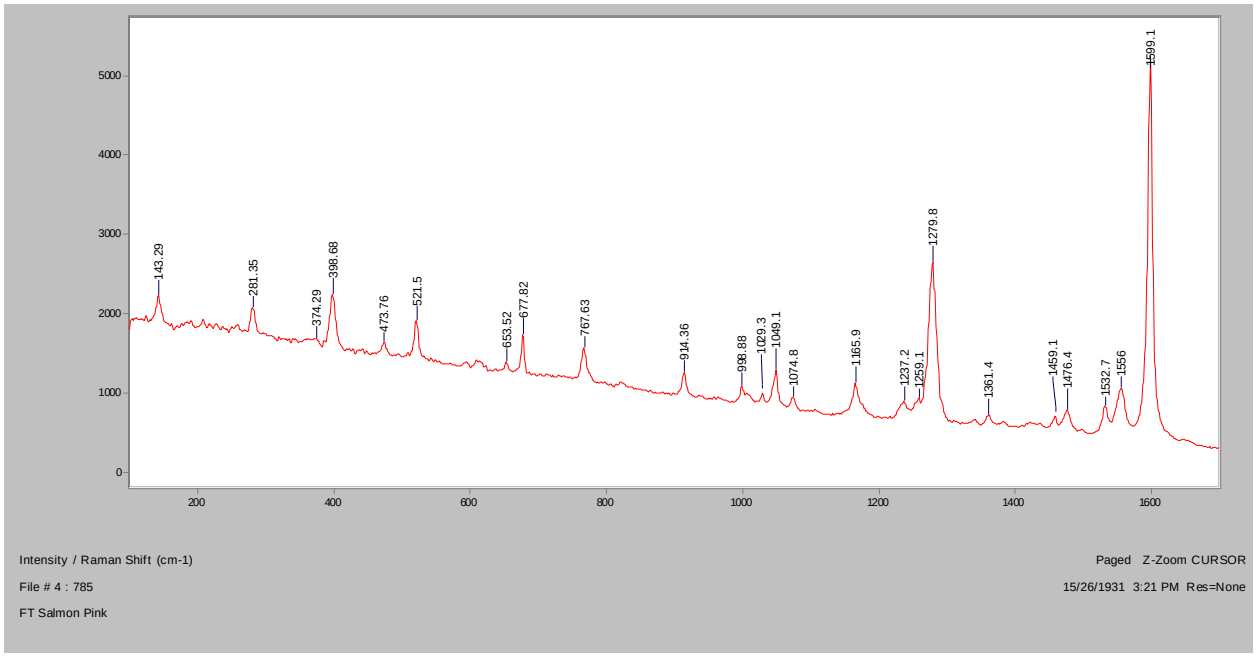

FT-Raman, 1064nm

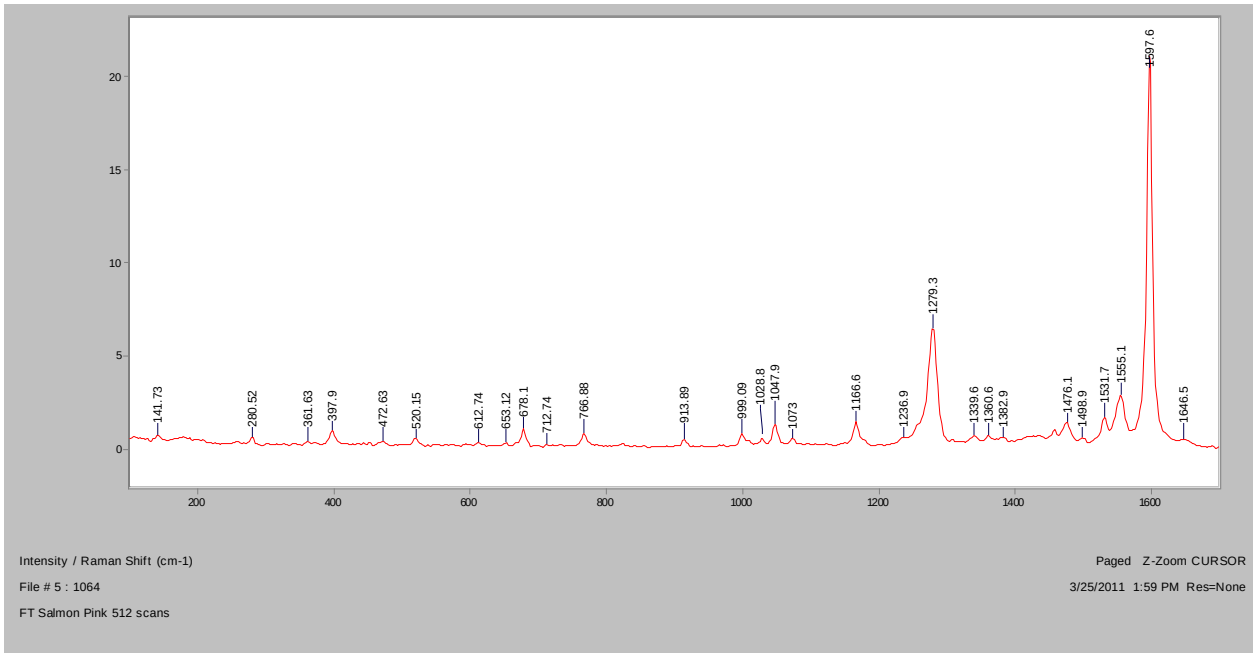

FT-IR (ATR)

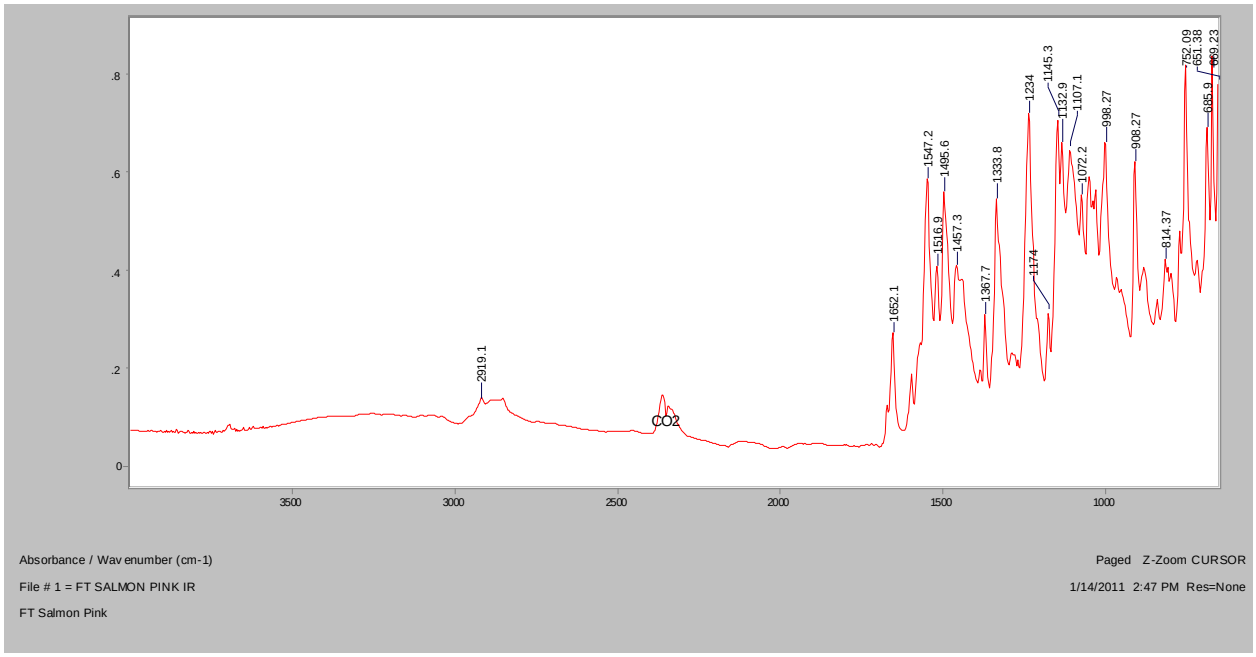
.8
.6
.4
.2
0
3500
3000
2500
2000
1500
1000
2919.1
CO2
1652.1
1547.2
1516.9
1495.6
1457.3
1367.7
1333.8
1234
1174
1145.3
1132.9
1107.1
1072.2
998.27
908.27
814.37
752.09
651.38
669.23
685.9
Absorbance / Wavenumber (cm-1)
File # 1 = FT SALMON PINK IR
FT Salmon Pink
Paged Z-Zoom CURSOR
1/14/2011 2:47 PM Res=None

XRF

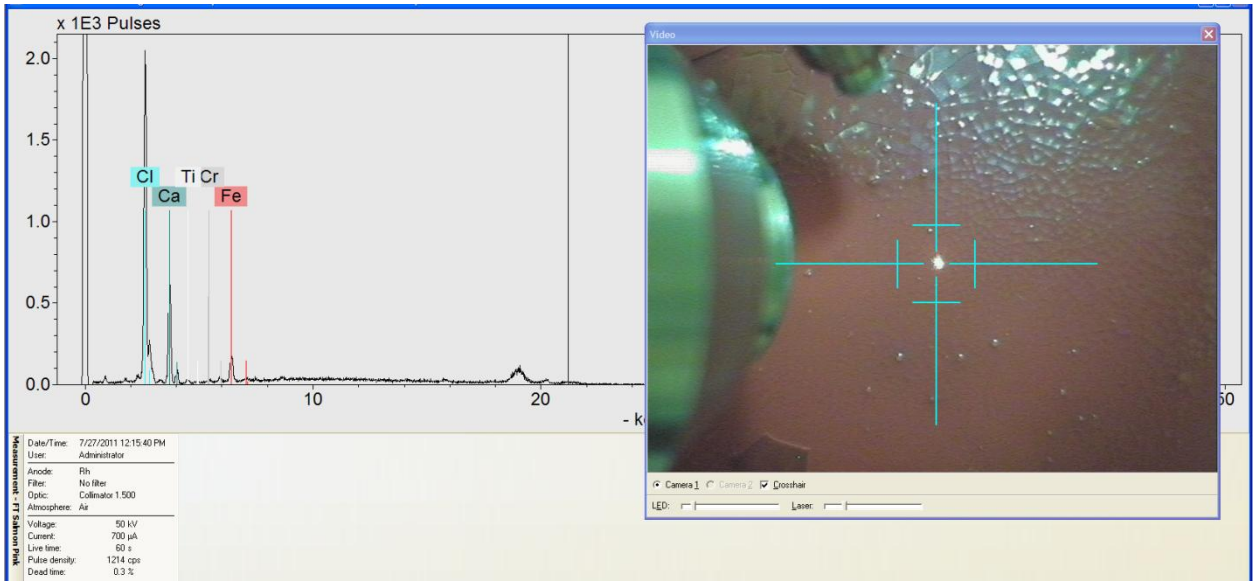
x 1E3 Pulses
2.0
1.5
1.0
0.5
0.0
0
10
20
Cl
Ti Cr
Ca
Fe
Video
Camera 1
Camera 2
Crosshair
LED:
Laser:
Date/Time: 7/27/2011 12:15:40 PM
User: Administrator
Anode: Rh
Filter: No filter
Optic: Collimator 1.500
Atmosphere: Air
Voltage: 50 kV
Current: 700 µA
Live time: 60 s
Pulse density: 1214 cps
Dead time: 0.3 %

Pink Red

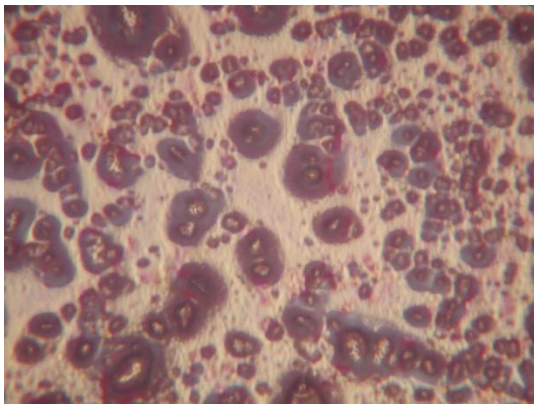

Bright Field, 100x

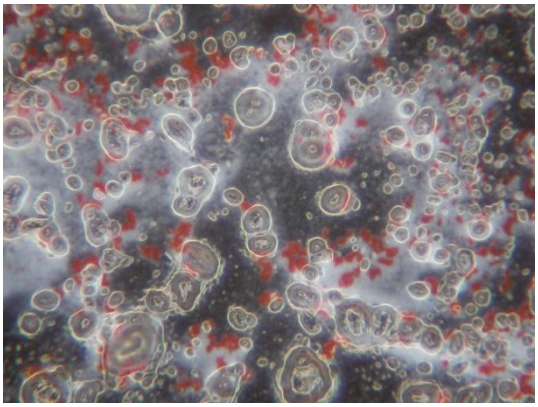

Dark Field, 100x

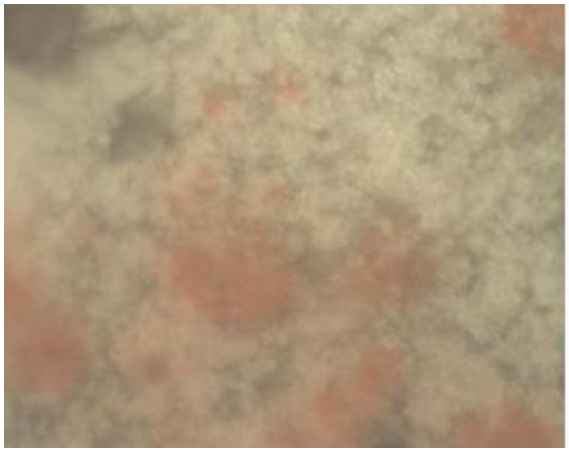

Raman microscope image, 1000x

Normal Raman, 488nm

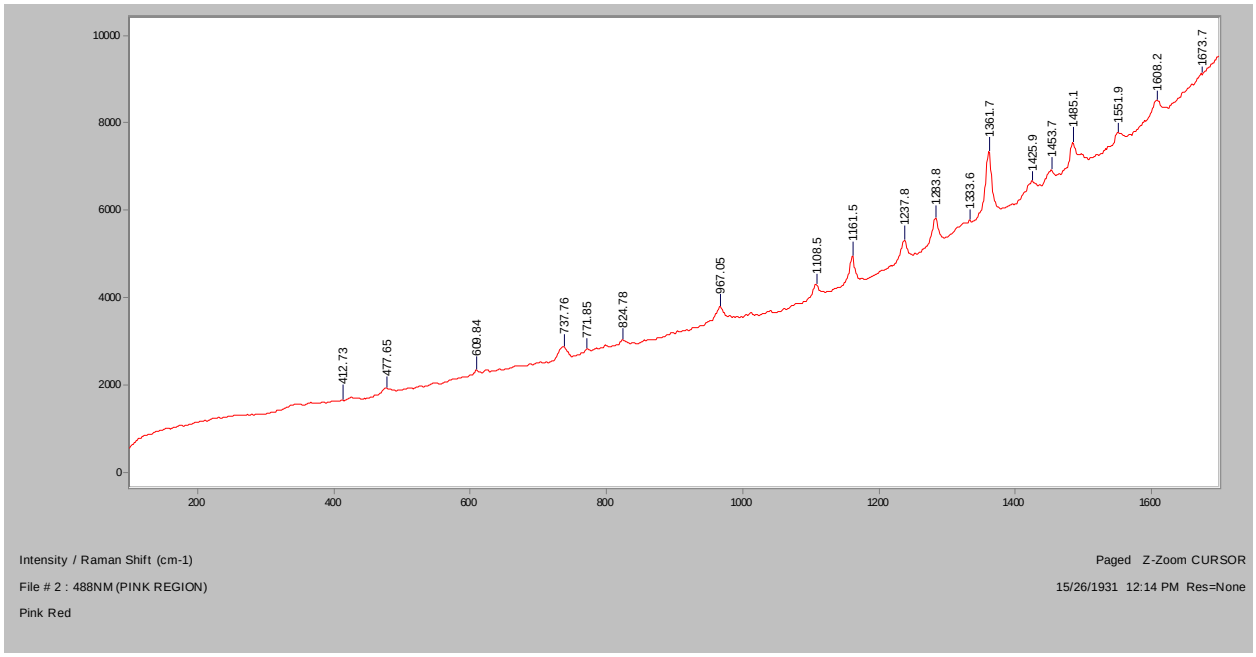

Normal Raman, 633nm

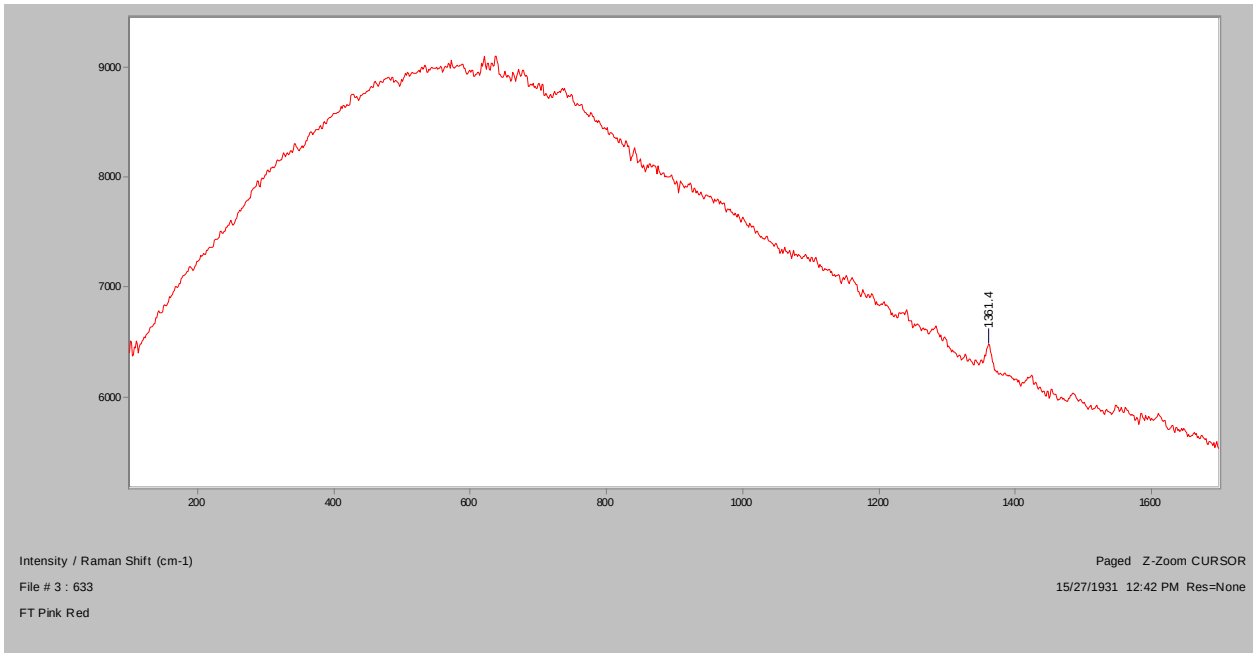

Normal Raman, 785nm

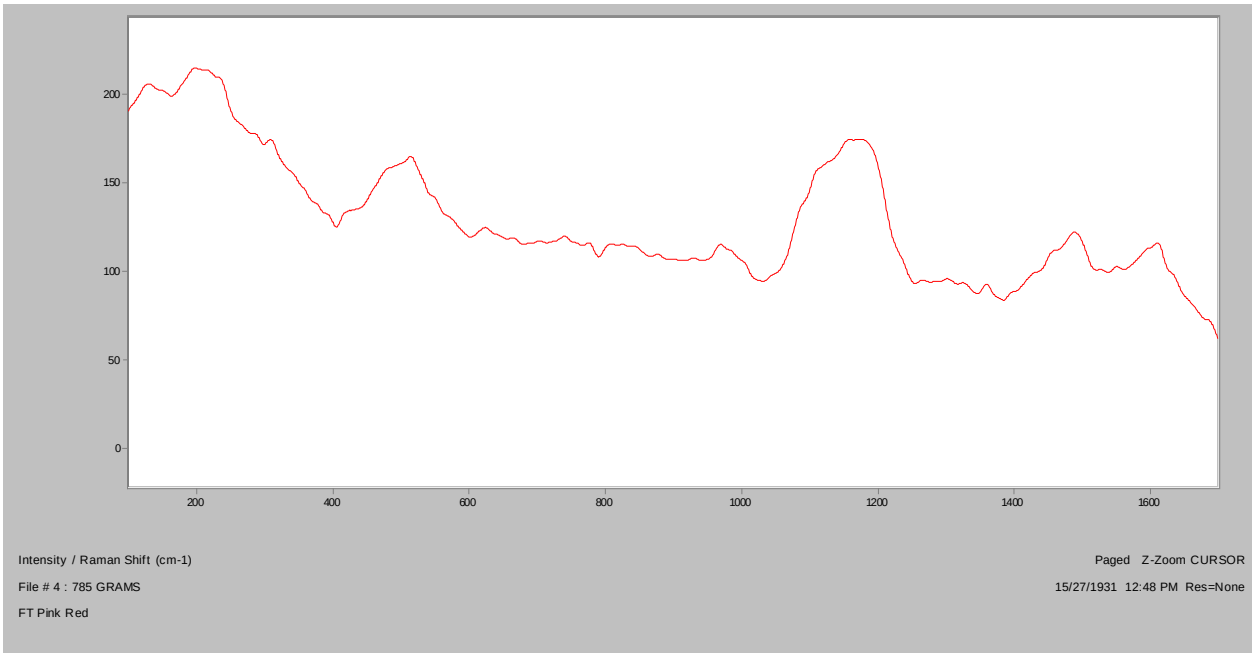

FT-IR (ATR)

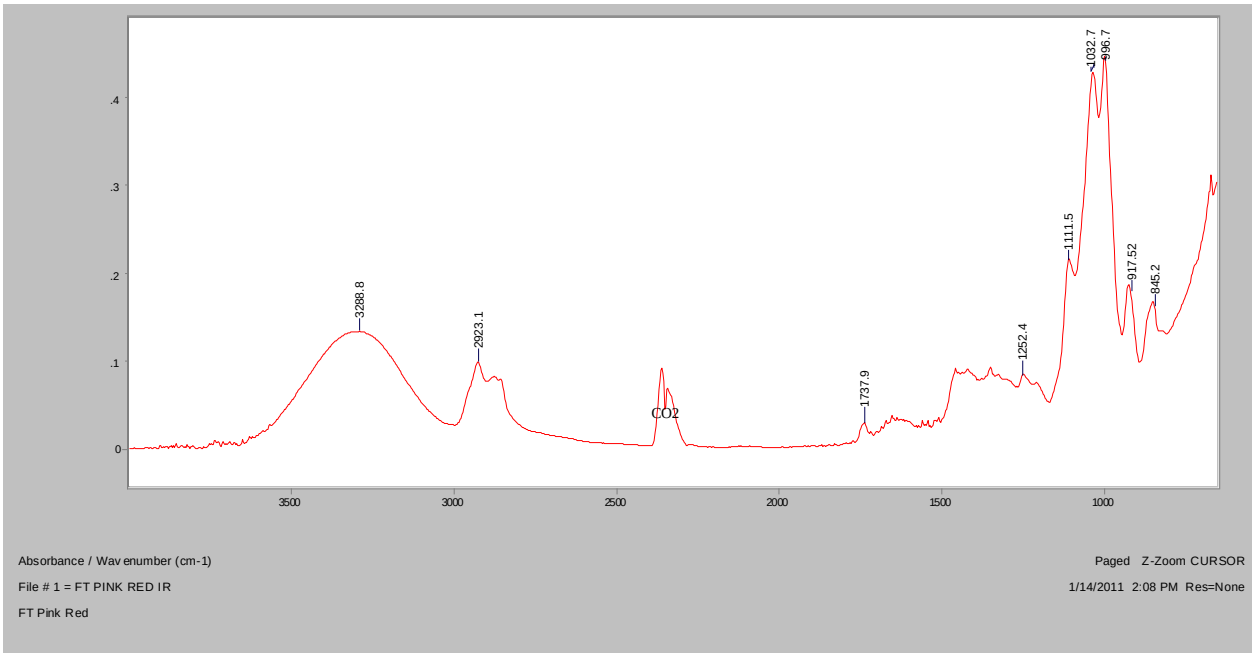

XRF

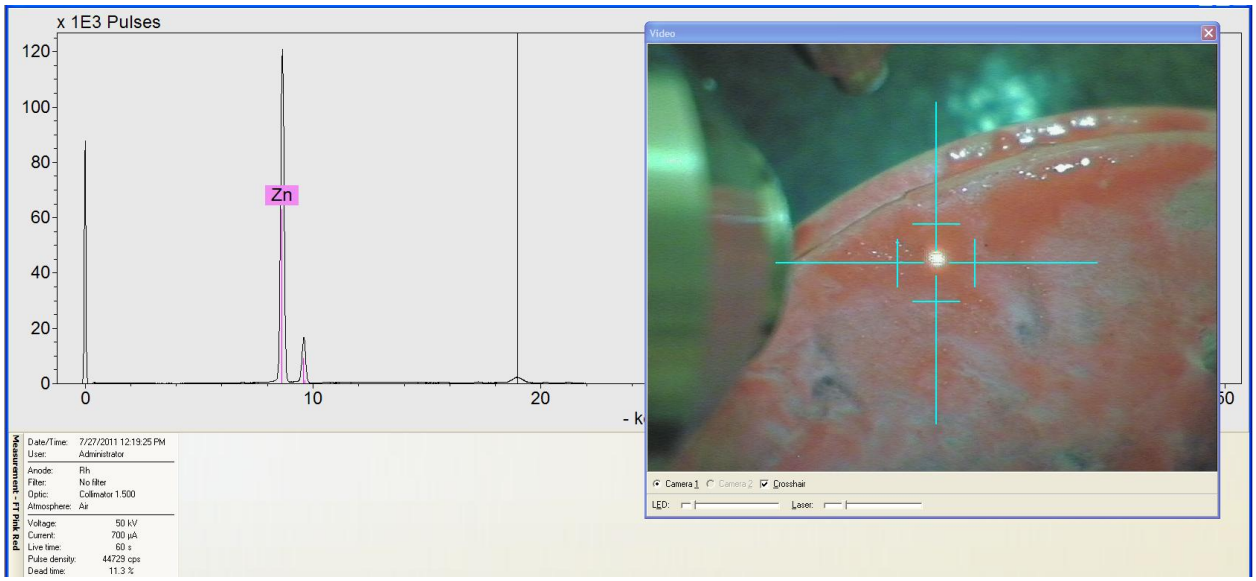
x 1E3 Pulses
120
100
80
60
40
20
0
Zn
0
10
20
Video
Camera 1
Camera 2
Crosshair
LED:
Laser:
Measurement - FT Pilot Rod
Date/Time: 7/27/2011 12:19:25 PM
User: Administrator
Anode: Rh
Filter: No filter
Optic: Collimator 1.500
Atmosphere: Air
Voltage: 50 kV
Current: 700 µA
Live time: 60 s
Pulse density: 44729 cps
Dead time: 11.3 %

Magenta

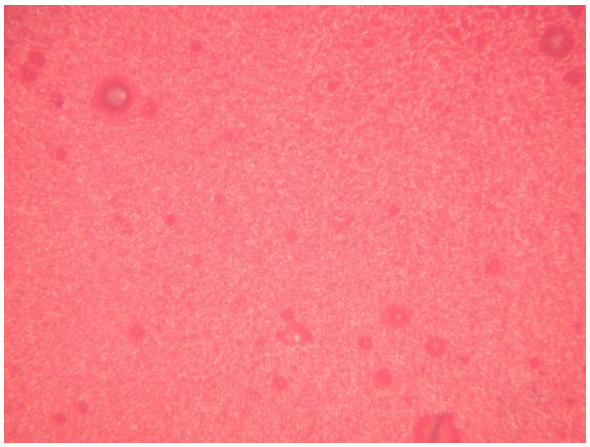

Bright Field, 100x

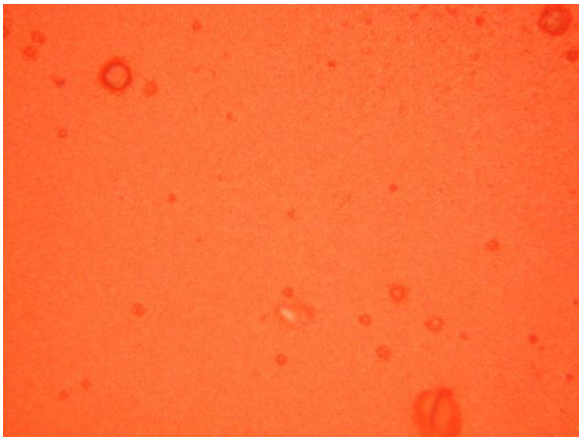

Dark Field, 100x

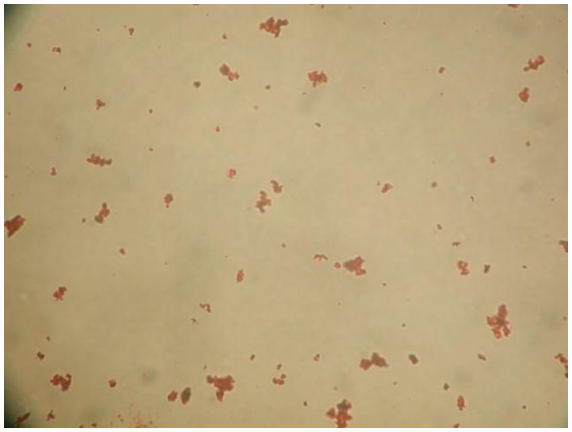

In RI, 1.550, 400x

Crossed Polars, In RI 1.550, 400x

Normal Raman, 488nm

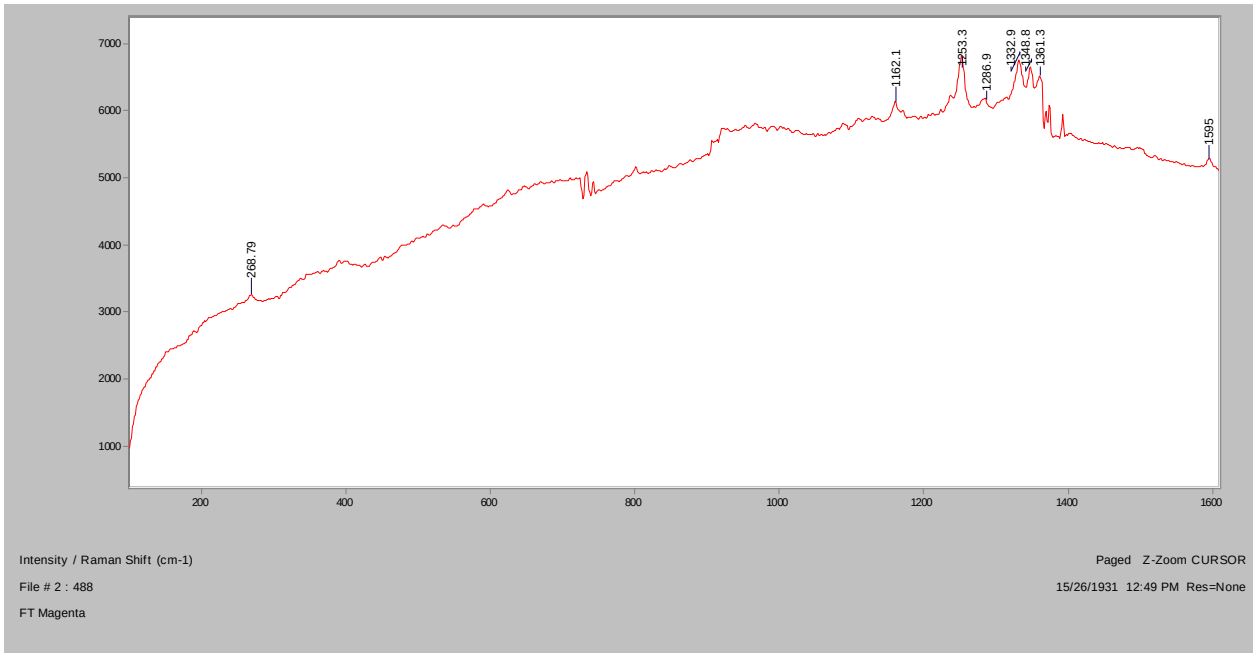

Normal Raman, 633nm

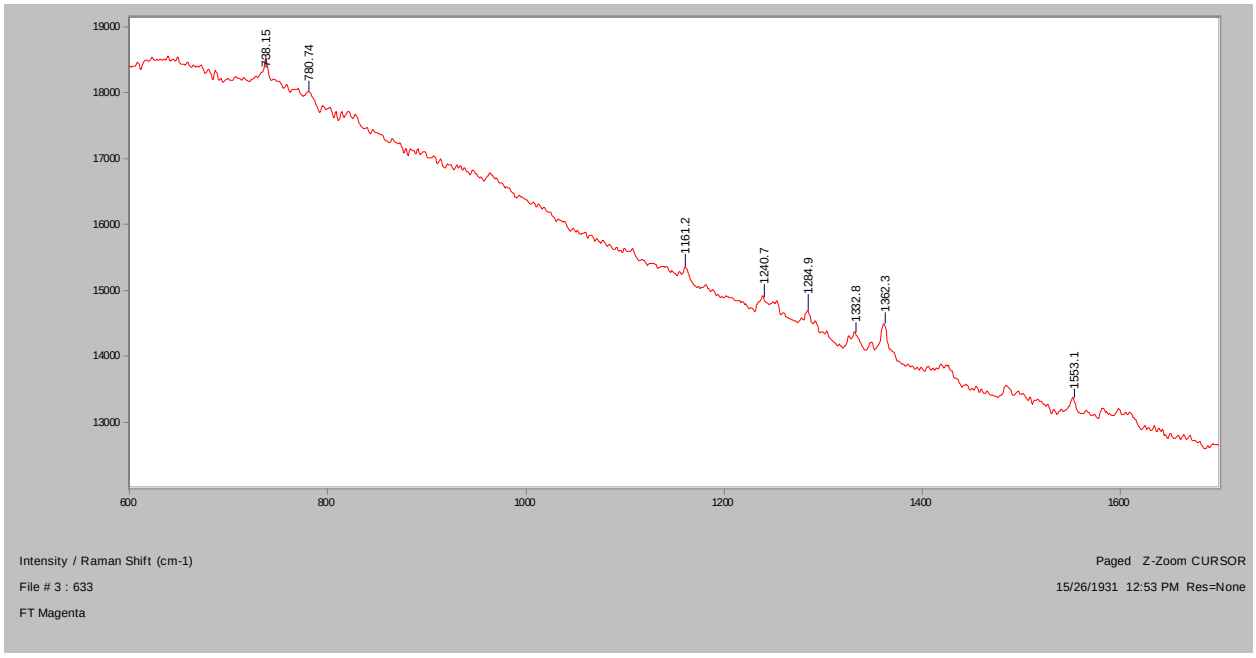

Normal Raman, 785nm

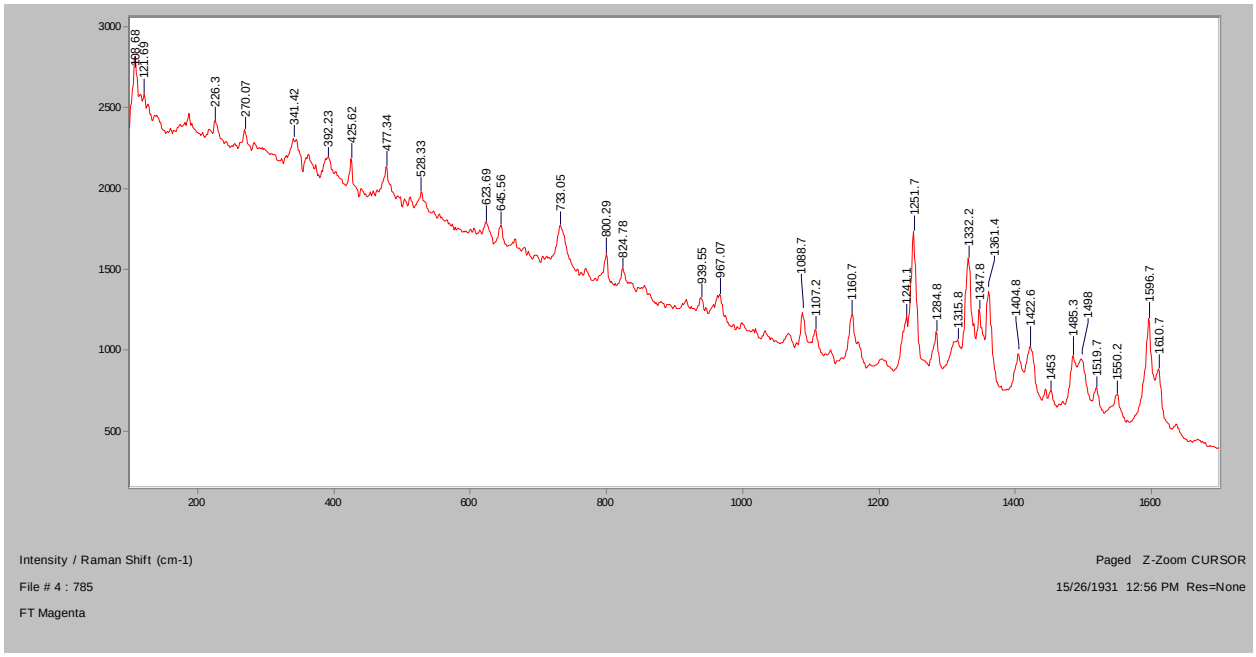

FT-Raman, 1064nm

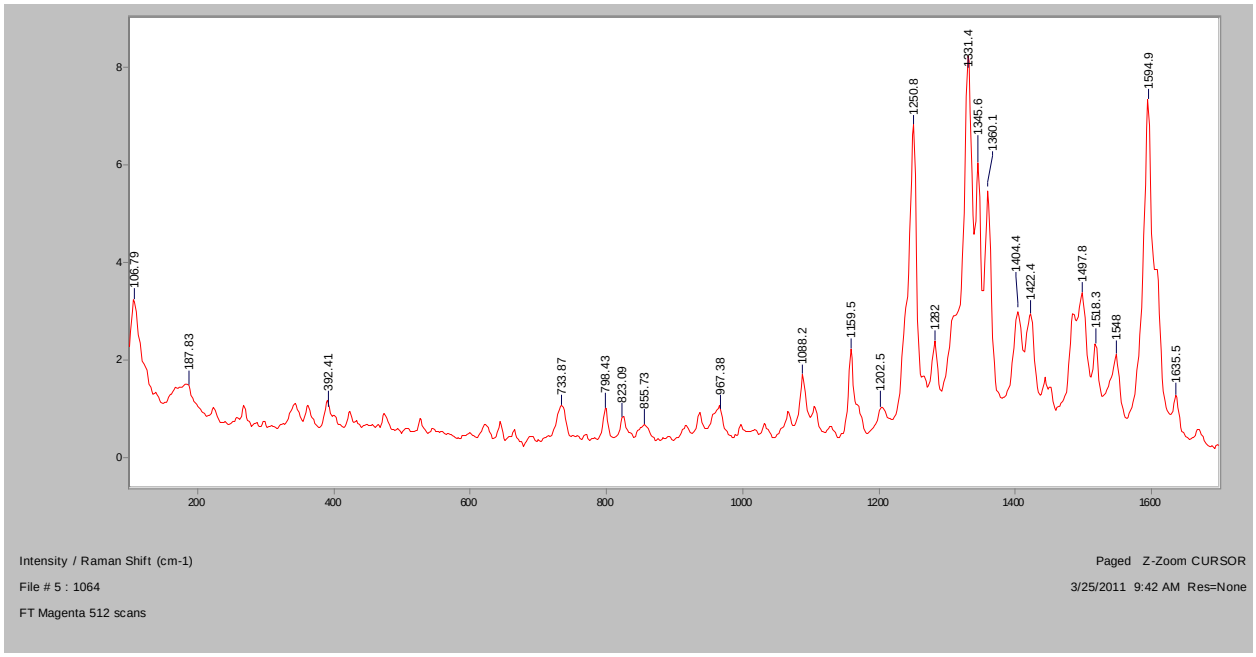

FT-IR (ATR)

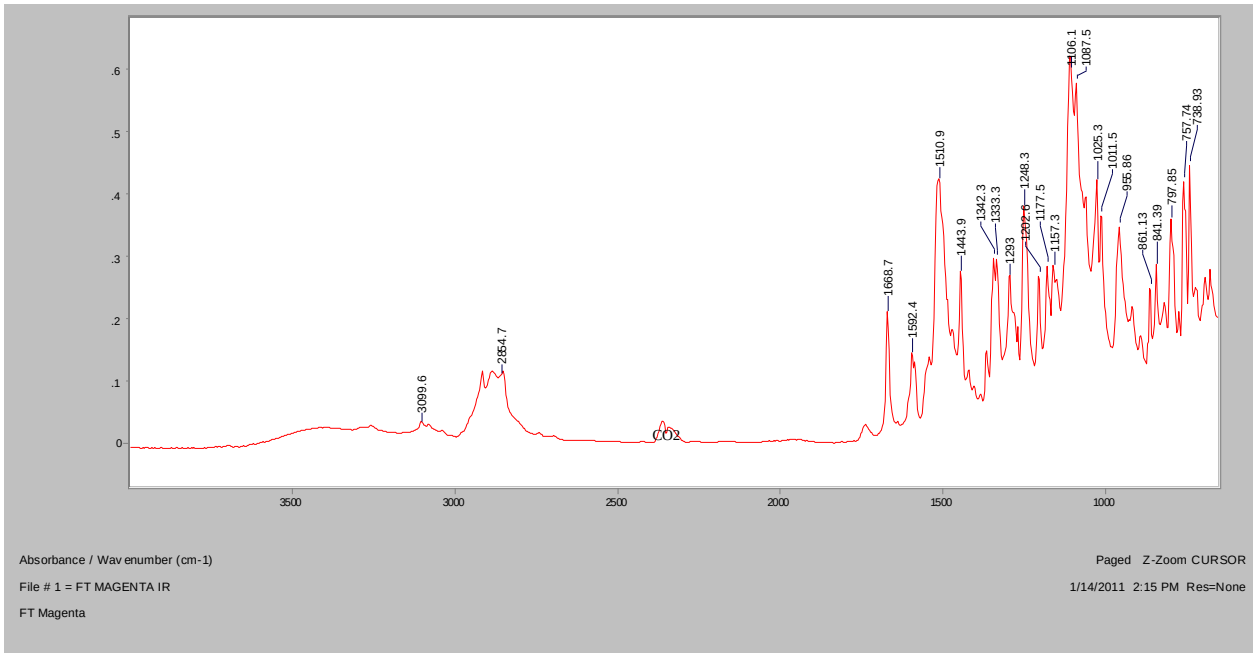
3099.6
2854.7
CO2
1668.7
1592.4
1510.9
1443.9
1342.3
1333.3
1293
1248.3
1177.5
1157.3
1106.1
1087.5
1025.3
1011.5
955.86
861.13
841.39
797.85
757.74
738.93
3500
3000
2500
2000
1500
1000
Absorbance / Wavenumber (cm-1)
File # 1 = FT MAGENTA IR
FT Magenta
Paged Z-Zoom CURSOR
1/14/2011 2:15 PM Res=None

XRF

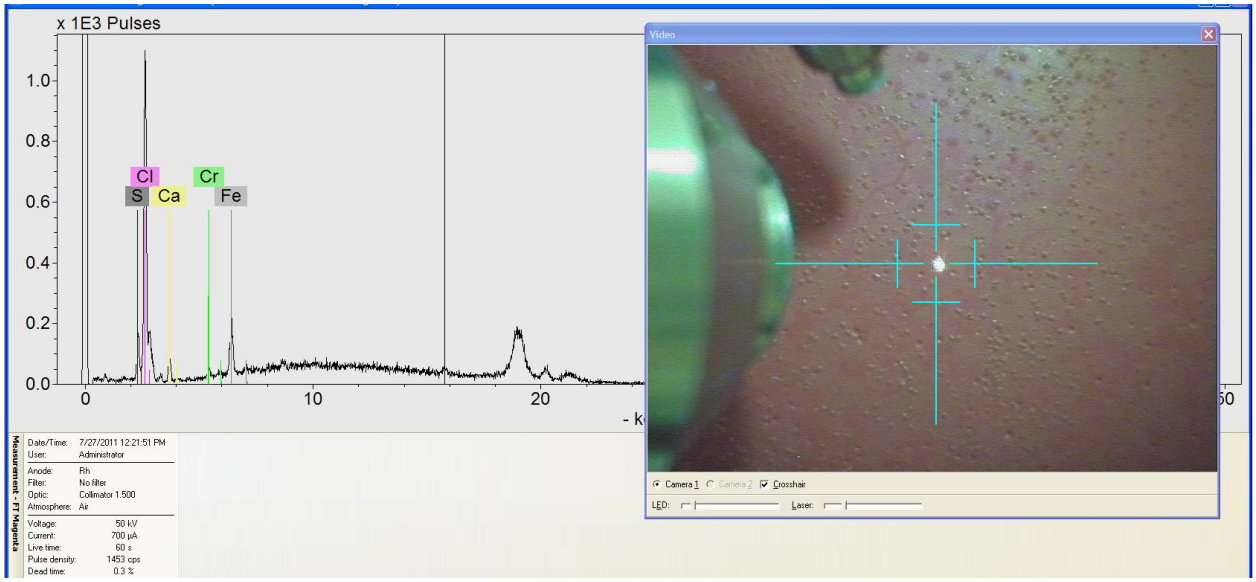
x 1E3 Pulses
Cl
S
Ca
Cr
Fe
Video
Camera 1
Crosshair
LED:
Laser:
Date/Time: 7/27/2011 12:21:51 PM
User: Administrator
Anode: Rh
Filter: No filter
Optic: Collimator 1.500
Atmosphere: Air
Voltage: 50 kV
Current: 700 µA
Live time: 60 s
Pulse density: 1453 cps
Dead time: 0.3 %

Chinese Red

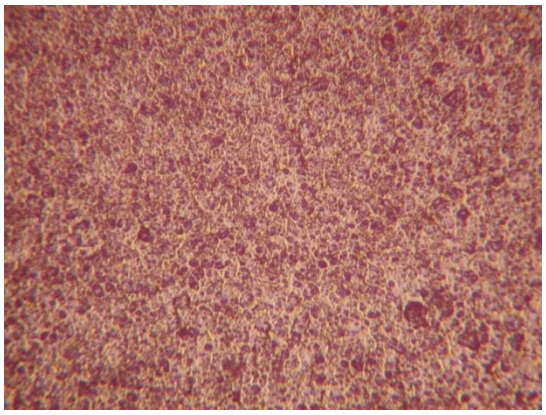

Bright Field, 100x

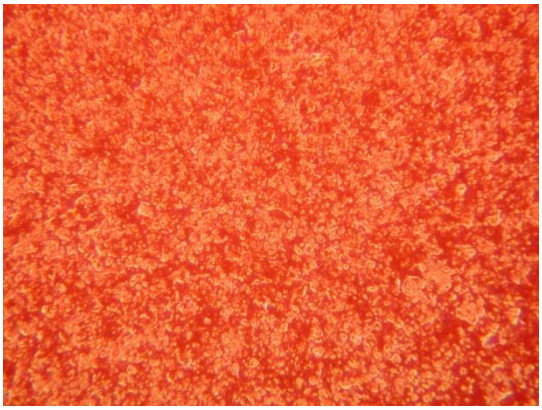

Dark Field, 100x

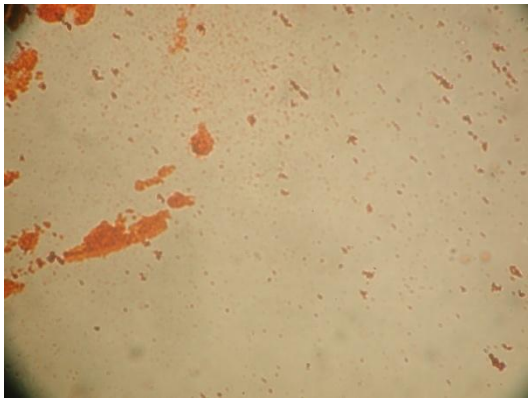

In RI 1.550, 400x

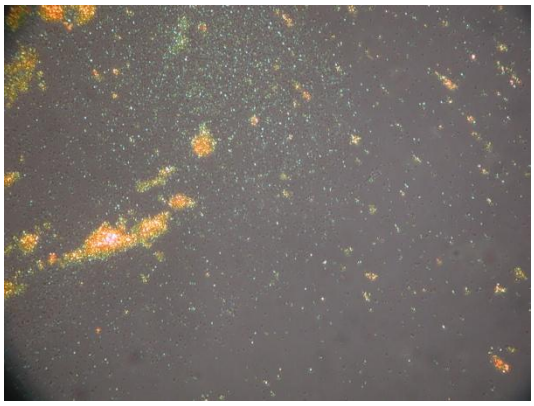

Crossed polars, In RI 1.550, 400x

Normal Raman, 488nm

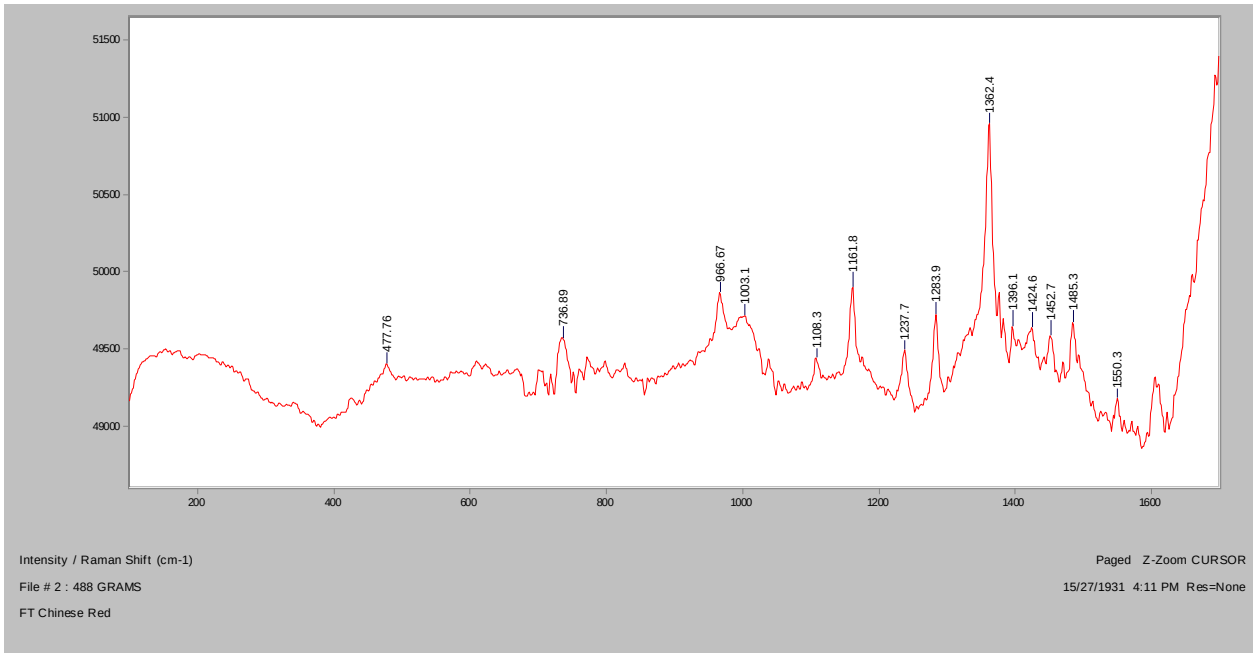

Normal Raman, 633nm

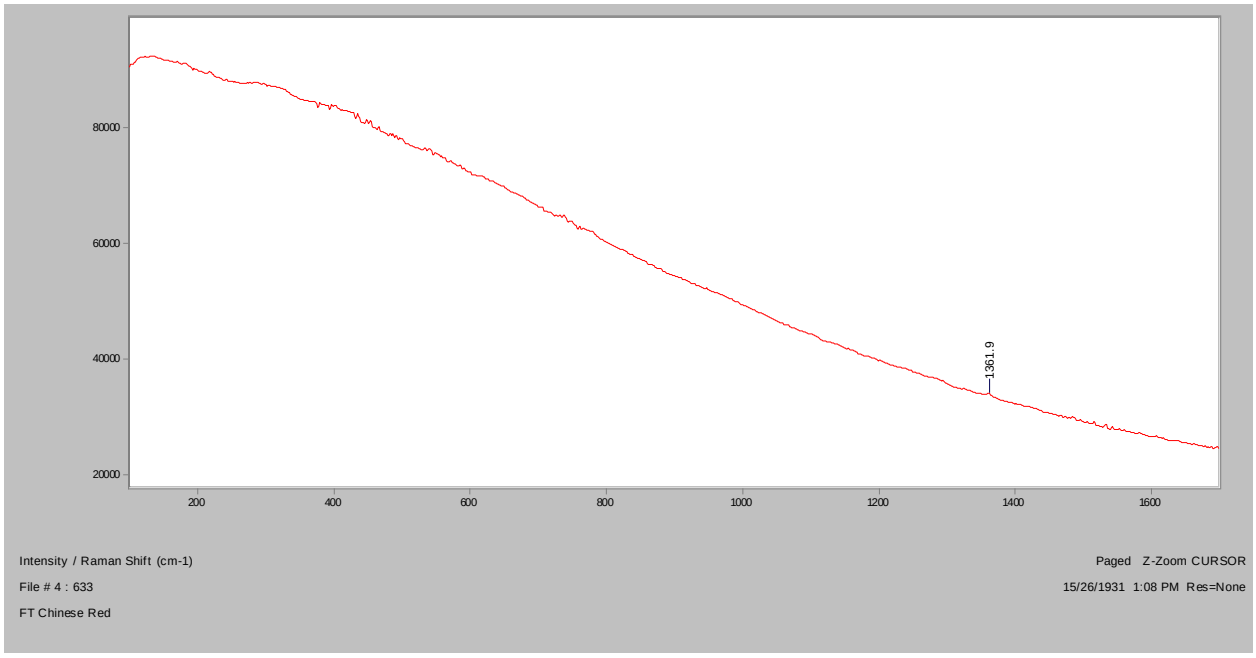

Normal Raman, 785nm

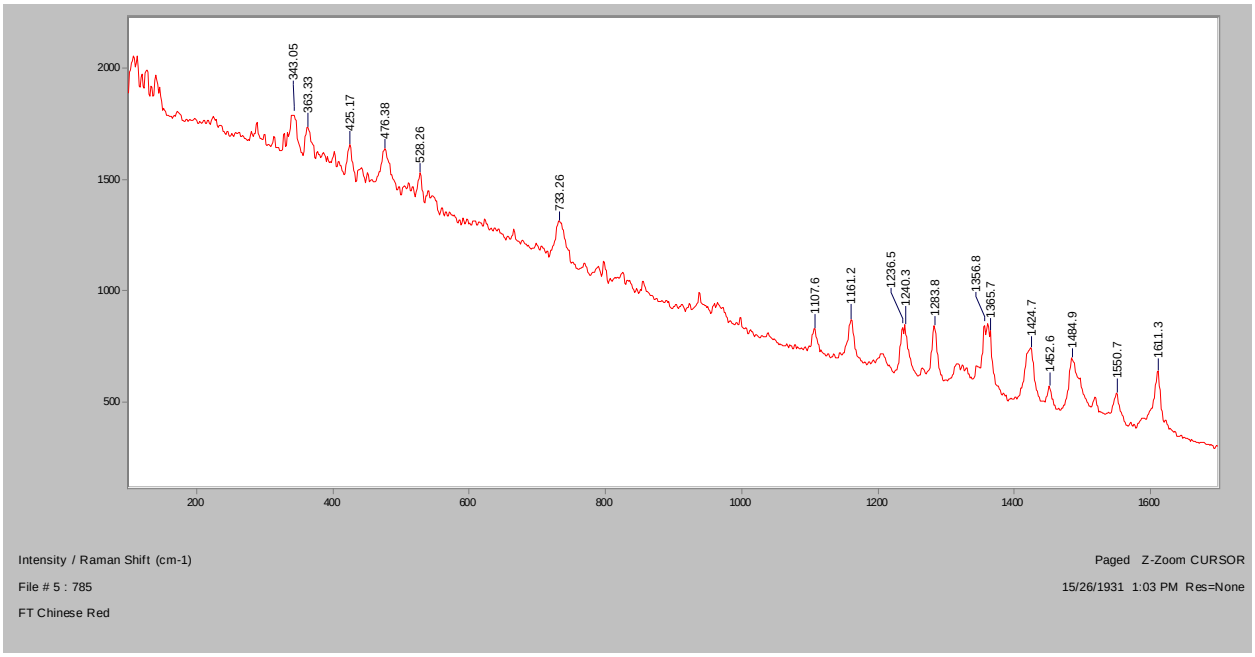

FT-Raman, 1064nm

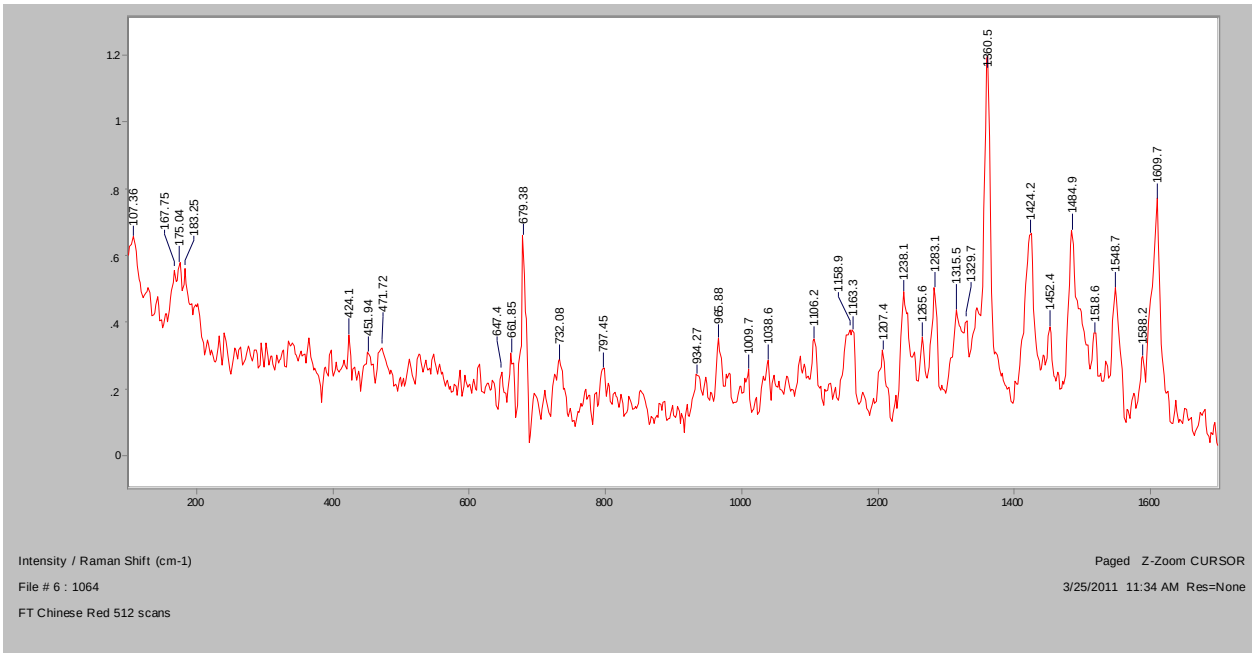

FT-IR (ATR)

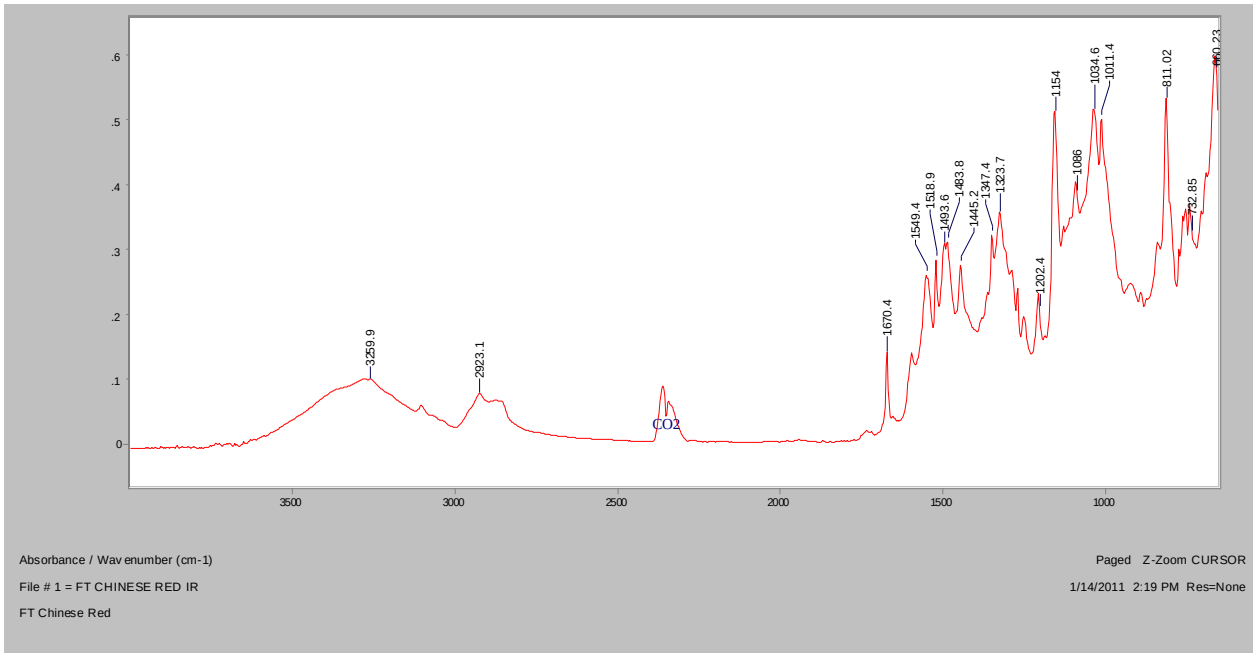
3259.9
2923.1
CO2
1670.4
1549.4
1518.9
1493.6
1483.8
1445.2
1417.4
1323.7
1202.4
1154
1086
1034.6
1011.4
811.02
752.85
660.23
3500
3000
2500
2000
1500
1000
Absorbance / Wavenumber (cm-1)
File # 1 = FT CHINESE RED IR
FT Chinese Red
Paged Z-Zoom CURSOR
1/14/2011 2:19 PM Res=None

XRF

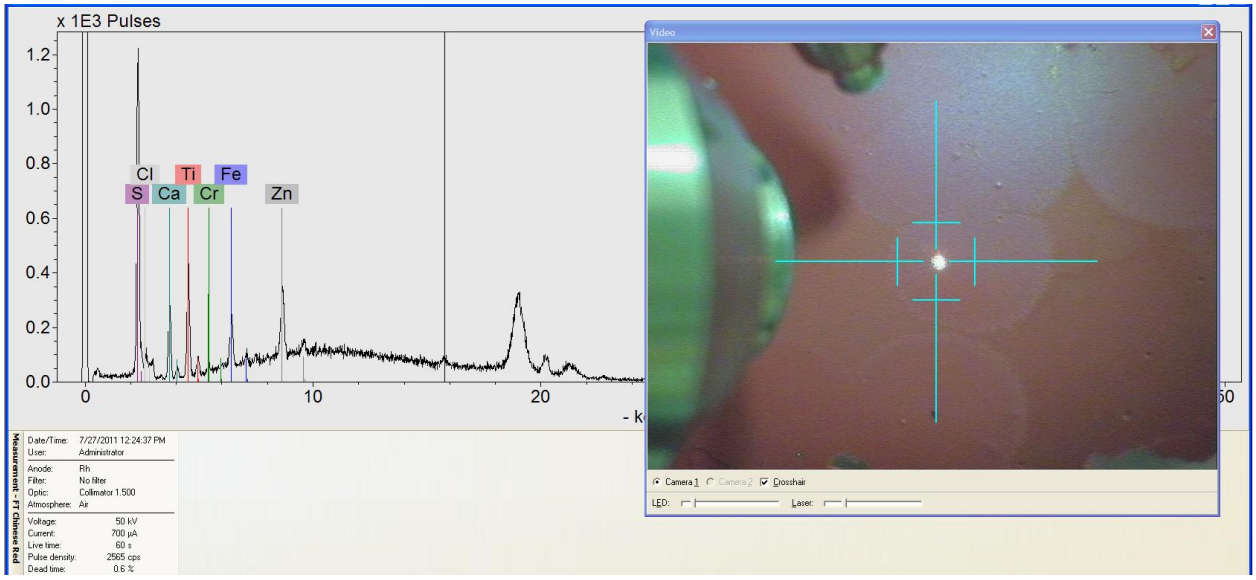
x 1E3 Pulses
Cl
Ti
Fe
S
Ca
Cr
Zn
Video
Camera 1
Camera 2
Crosshair
LED:
Laser:
Date/Time: 7/27/2011 12:24:37 PM
User: Administrator
Anode: Rh
Filter: No filter
Optic: Collimator 1.500
Atmosphere: Air
Voltage: 50 kV
Current: 700 µA
Live time: 60 s
Pulse density: 2565 cps
Dead time: 0.6 %

Bright Red

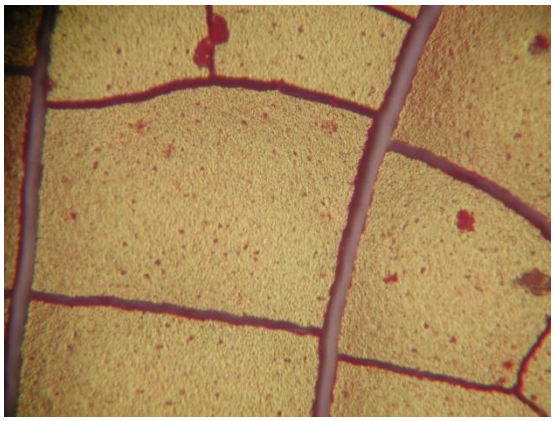

Bright Field, 100x

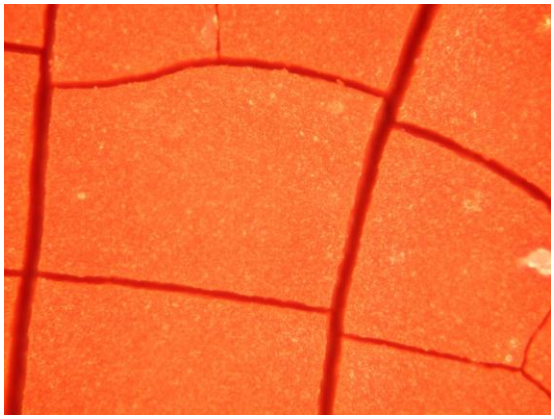

Dark Field, 100x

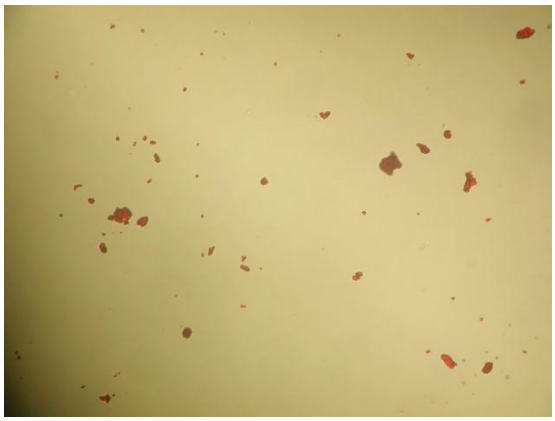

In RI 1.550, 400x

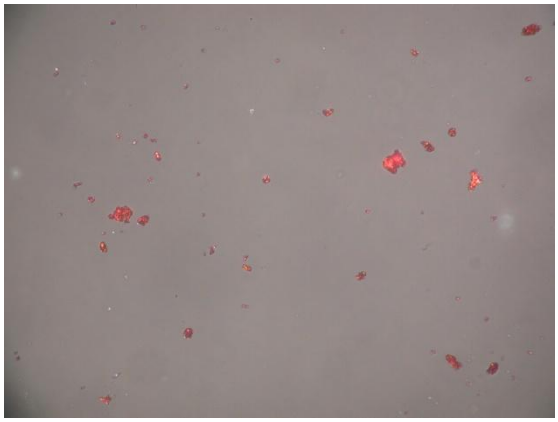

Crossed Polars, In RI 1.550, 400x

Normal Raman, 488nm

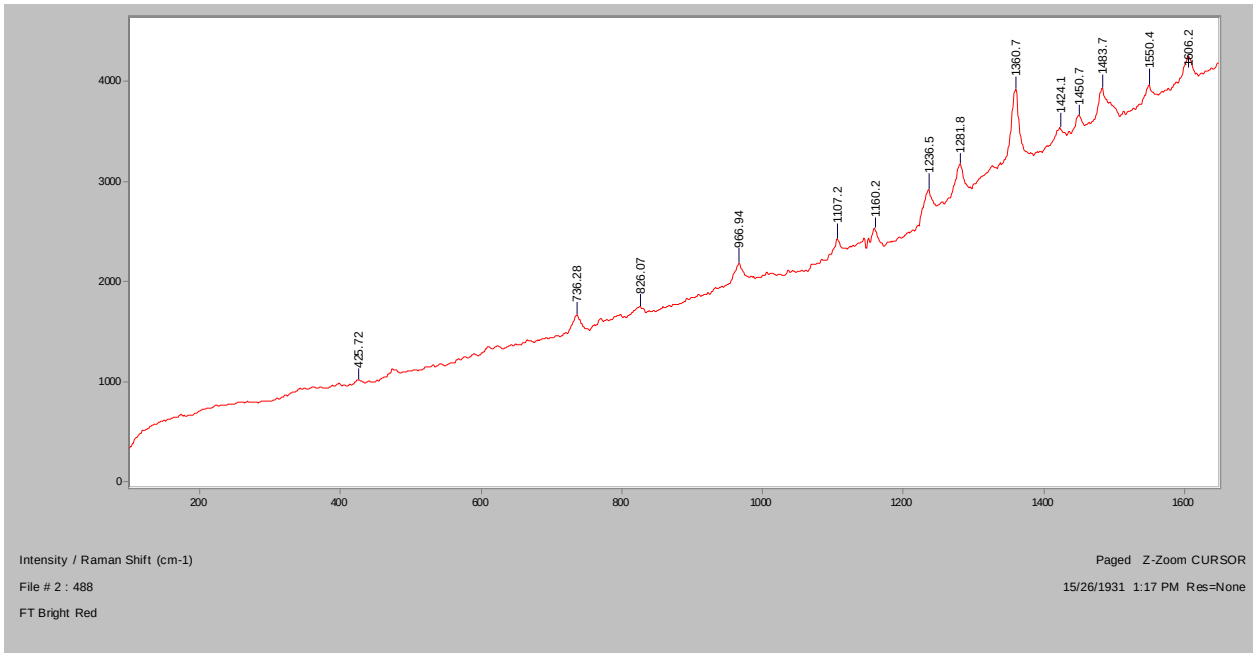

Normal Raman, 633nm

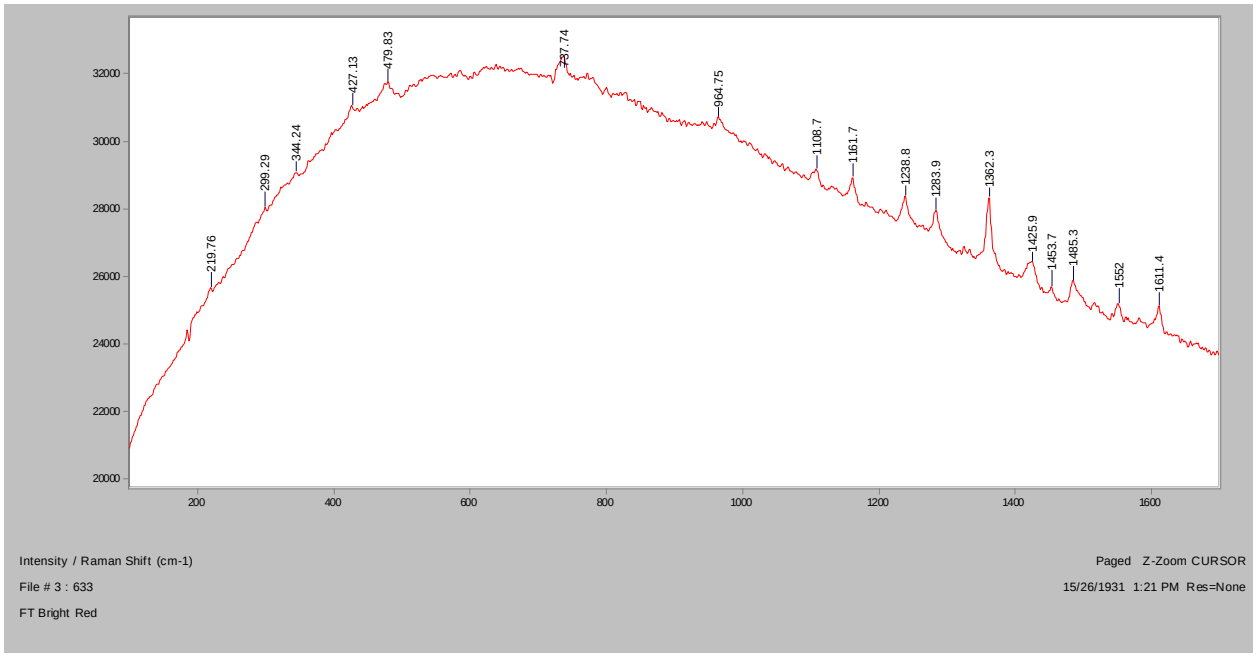

Normal Raman, 785nm

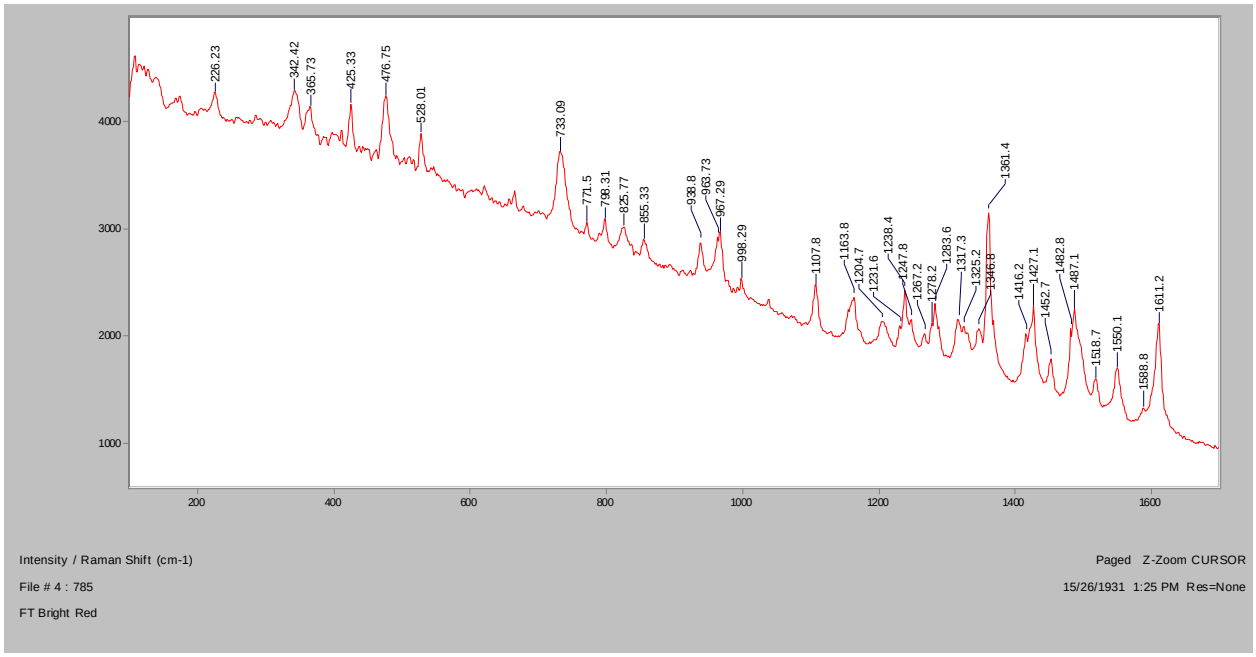

FT-Raman, 1064nm

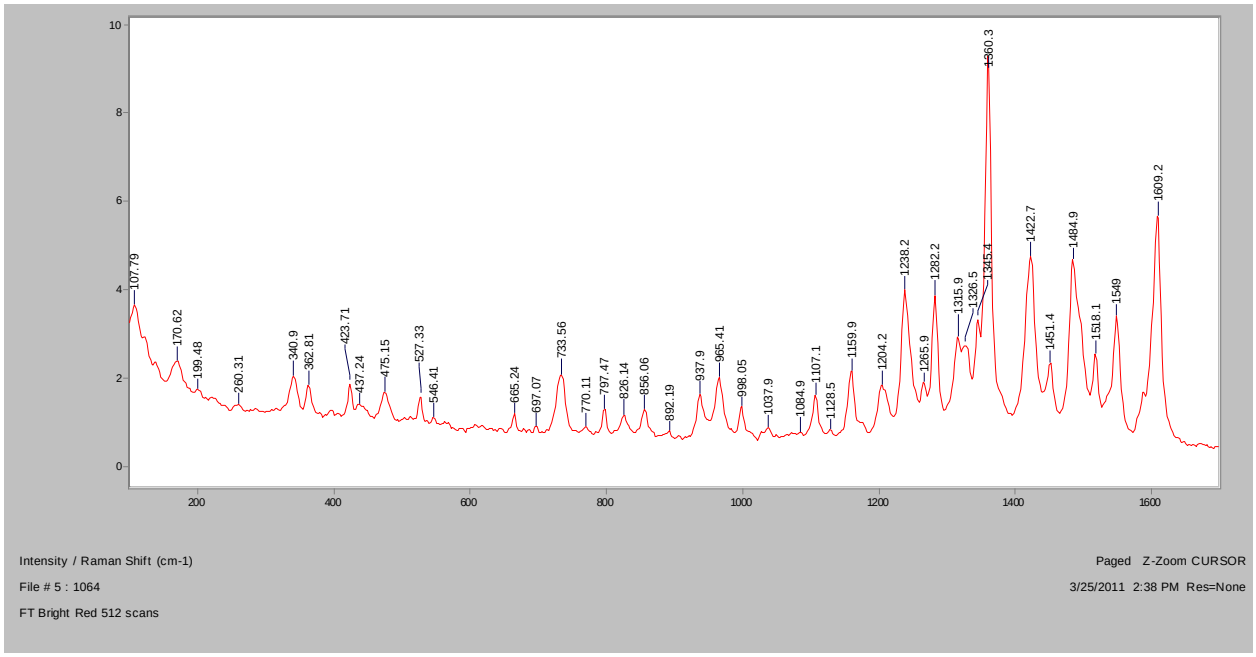

FT-IR (ATR)

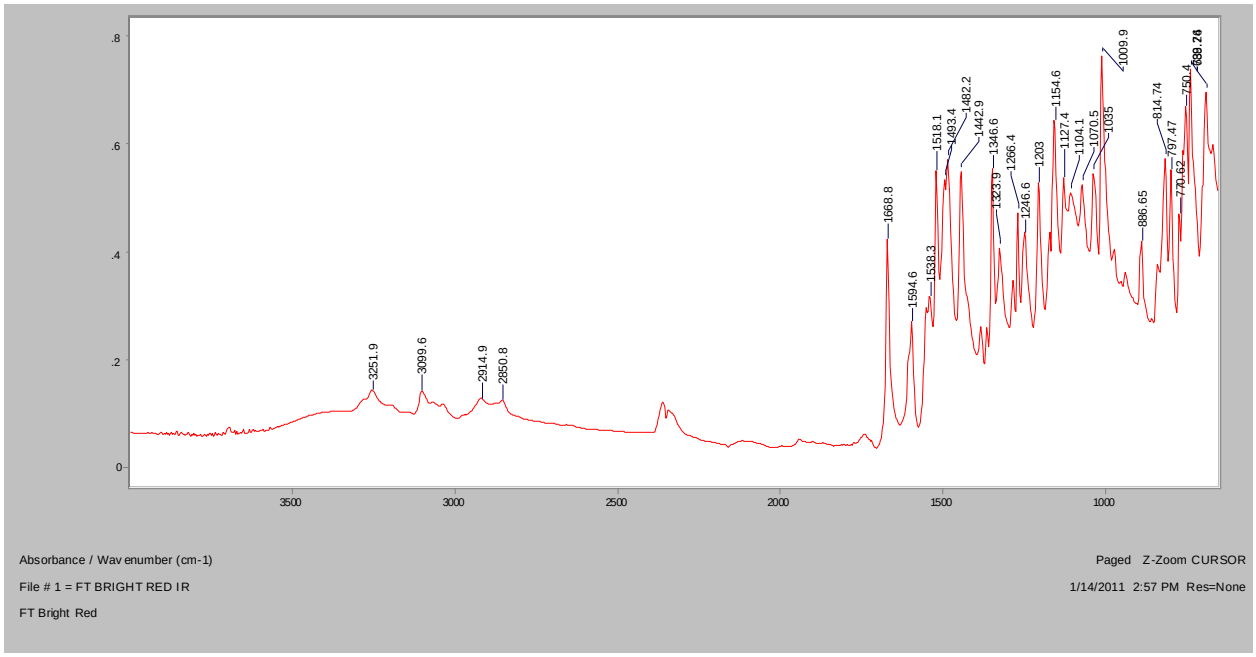
.8
.6
.4
.2
0
3500
3000
2500
2000
1500
1000
3251.9
3099.6
2914.9
2850.8
1668.8
1594.6
1538.3
1518.1
1493.4
1482.2
1442.9
1346.6
1323.9
1266.4
1246.6
1203
1154.6
1127.4
1104.1
1070.5
1035
1009.9
886.65
814.74
797.47
770.62
750.4
688.26
Absorbance / Wavenumber (cm-1)
File # 1 = FT BRIGHT RED IR
FT Bright Red
Paged Z-Zoom CURSOR
1/14/2011 2:57 PM Res=None

XRF

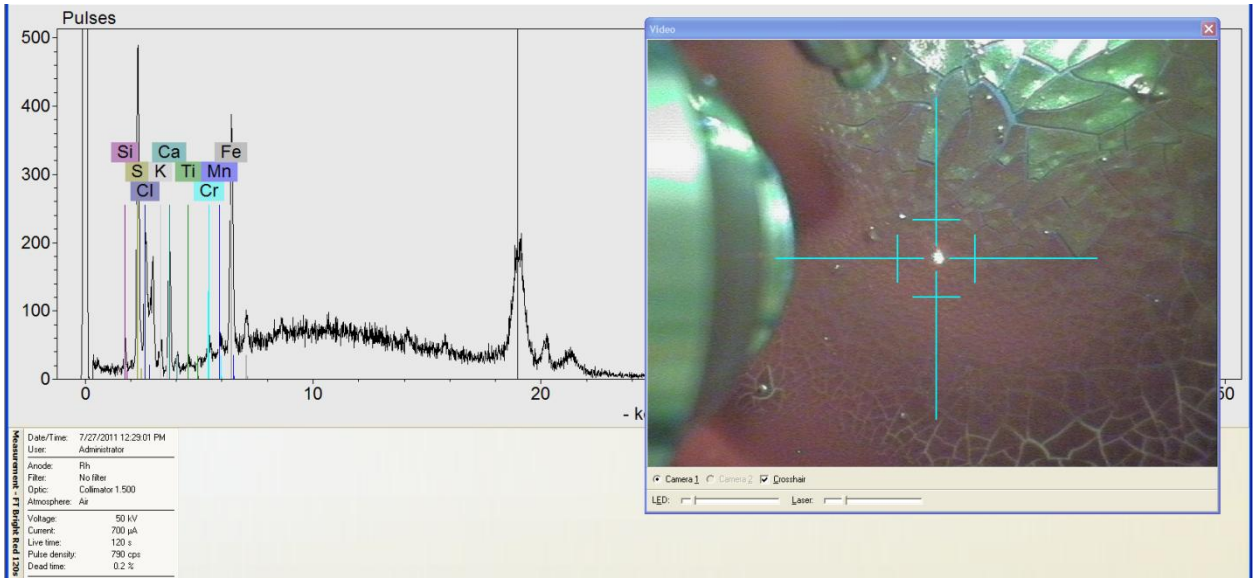
Pulses
500
400
300
200
100
0
0
10
20
Si
Ca
Fe
S
K
Ti
Mn
Cl
Cr
Video
Camera 1
Camera 2
Crosshair
LED:
Laser:
Date/Time: 7/27/2011 12:29:01 PM
User: Administrator
Anode: Rh
Filter: No filter
Optic: Collimator 1.500
Atmosphere: Air
Voltage: 50 kV
Current: 700 µA
Live time: 120 s
Pulse density: 790 cps
Dead time: 0.2 %

Rose Red

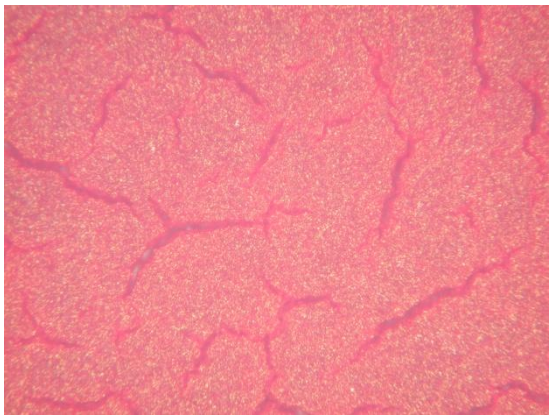

Bright Field, 100x

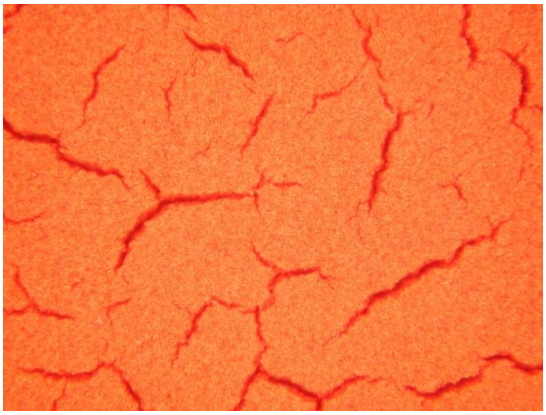

Dark Field, 100x

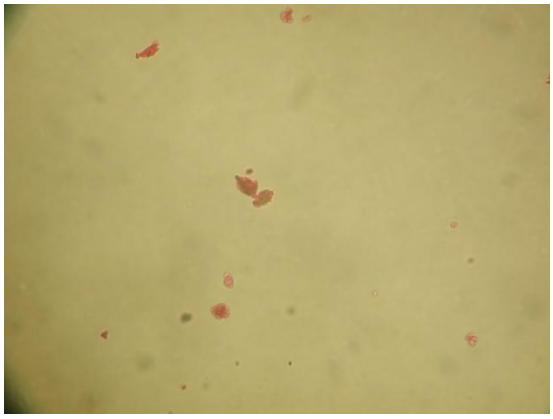

In RI 1.550, 400x

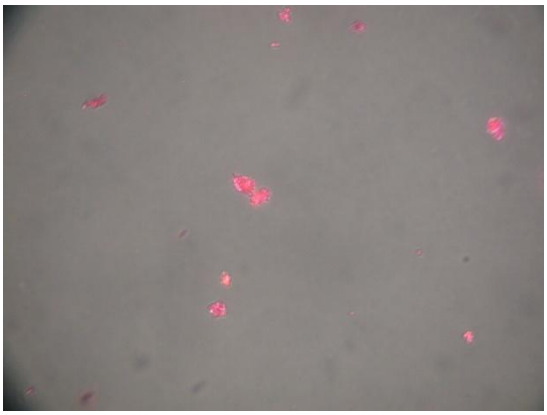

Crossed Polars, In RI 1.550, 400x

Normal Raman, 488nm

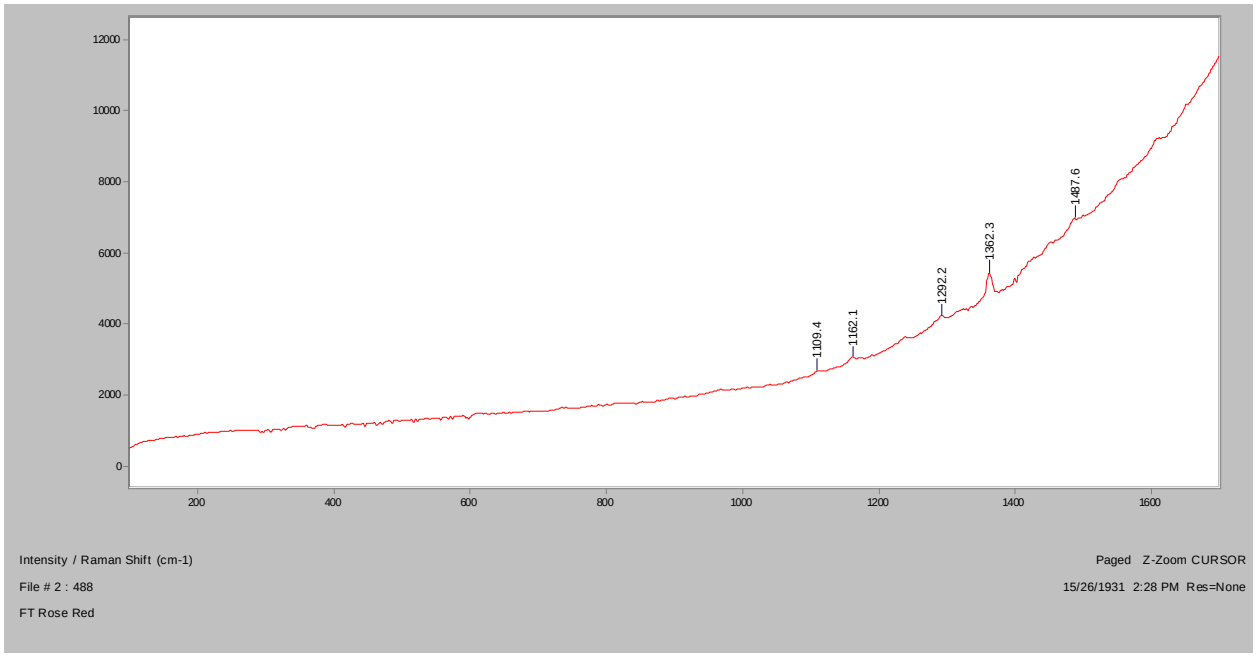

Normal Raman, 633nm

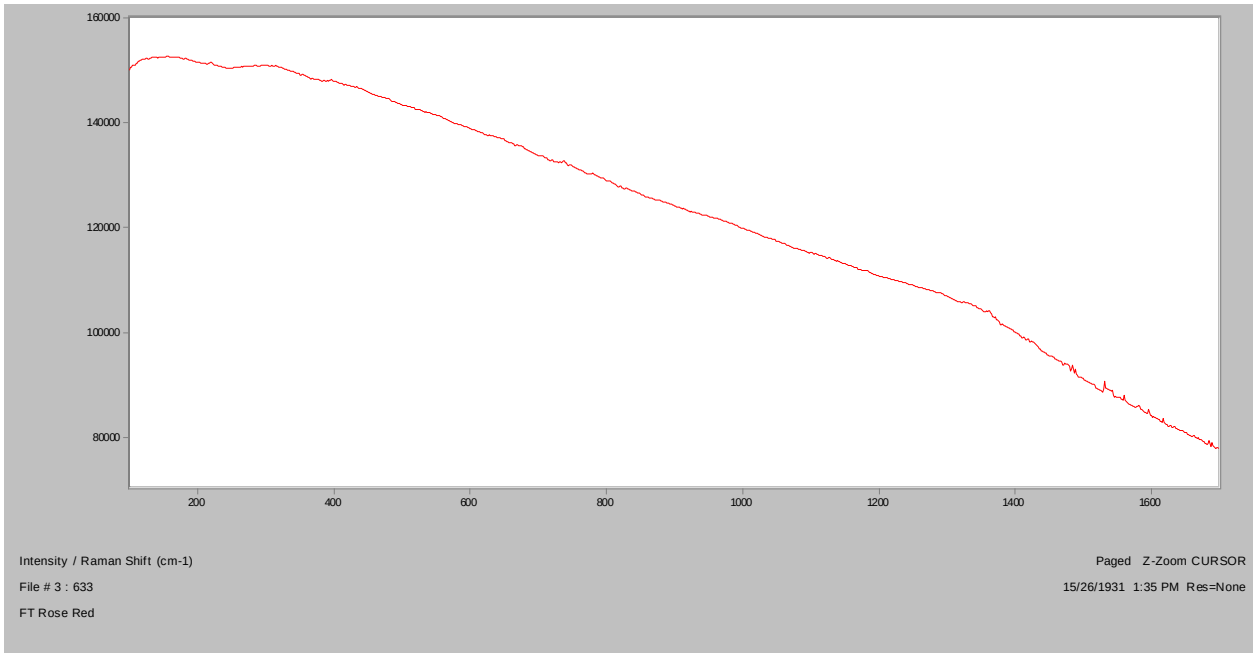

Normal Raman, 785nm

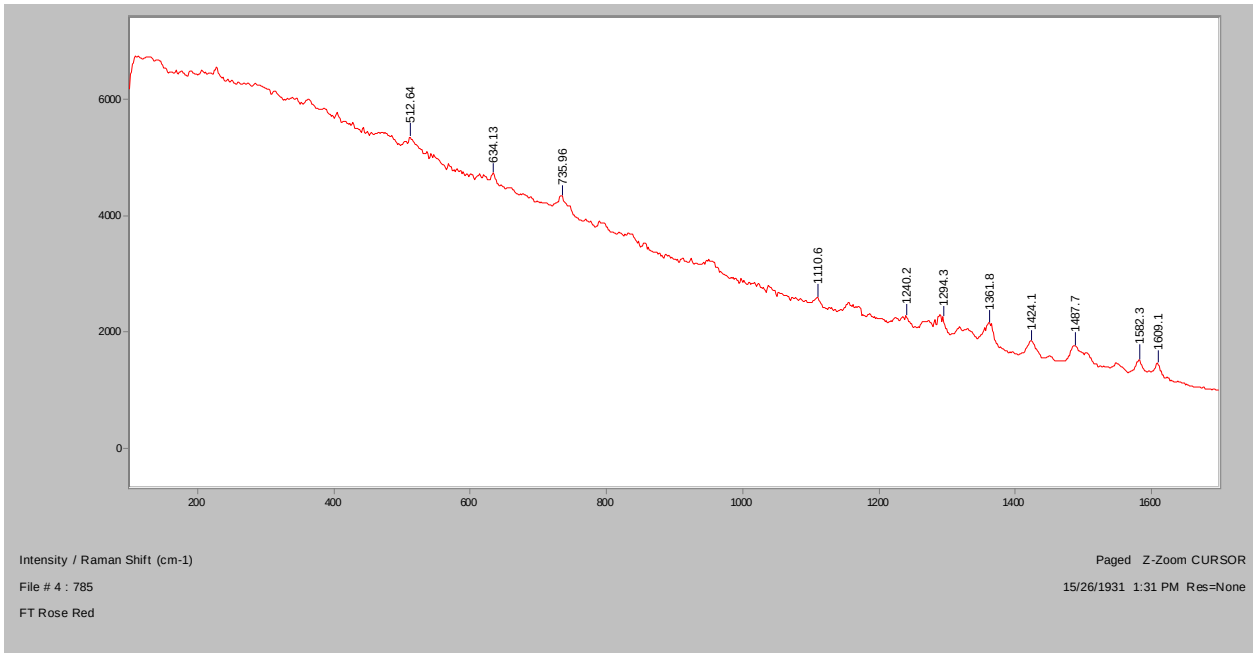

FT-Raman, 1064nm

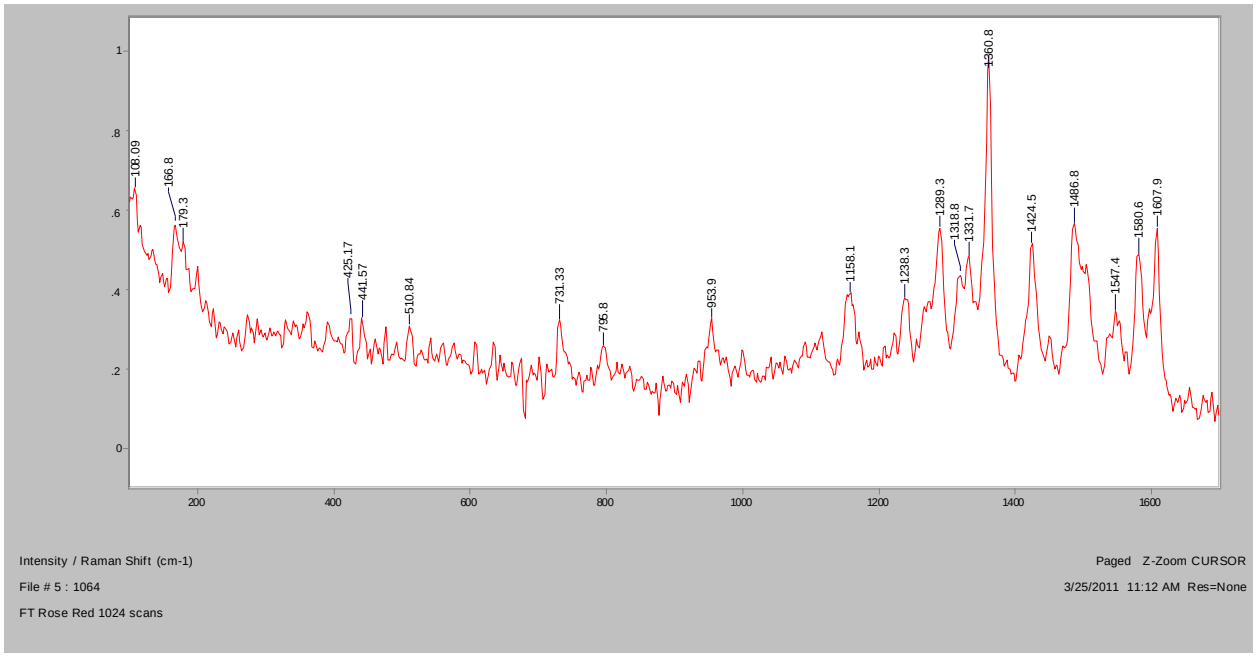

FT-IR (ATR)

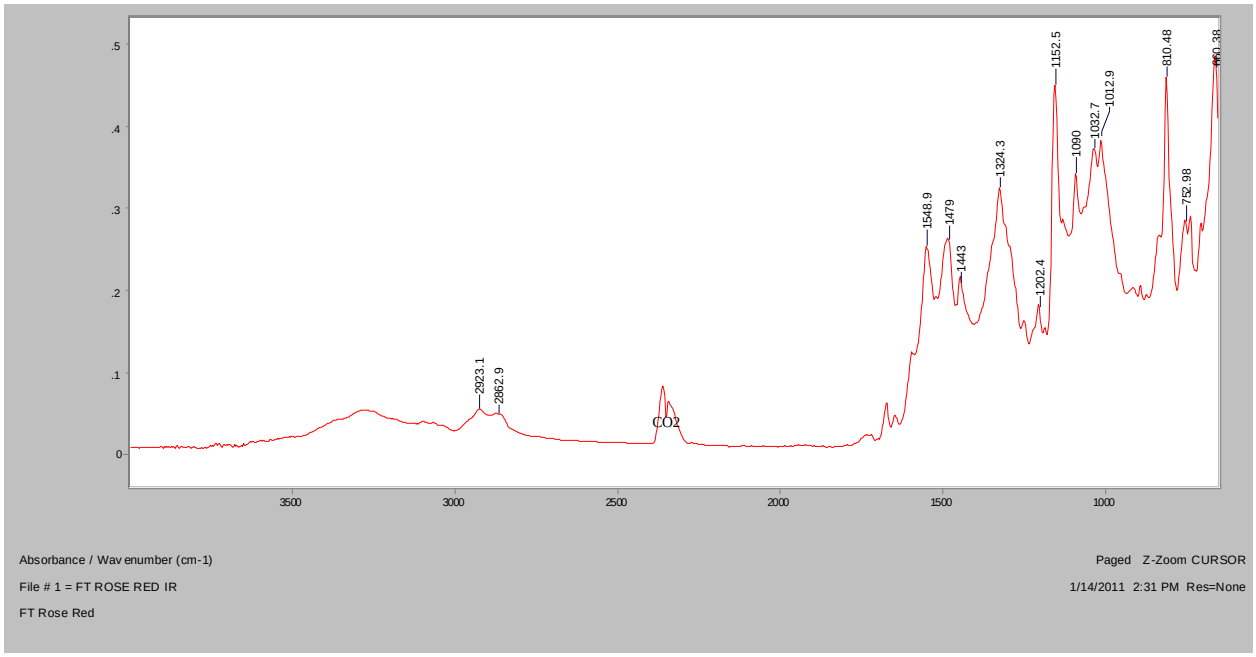
2923.1
2862.9
CO2
1548.9
1479
1443
1324.3
1202.4
1152.5
1090
1032.7
1012.9
810.48
752.98
3500
3000
2500
2000
1500
1000
Absorbance / Wavenumber (cm-1)
File # 1 = FT ROSE RED IR
FT Rose Red
Paged Z-Zoom CURSOR
1/14/2011 2:31 PM Res=None

XRF

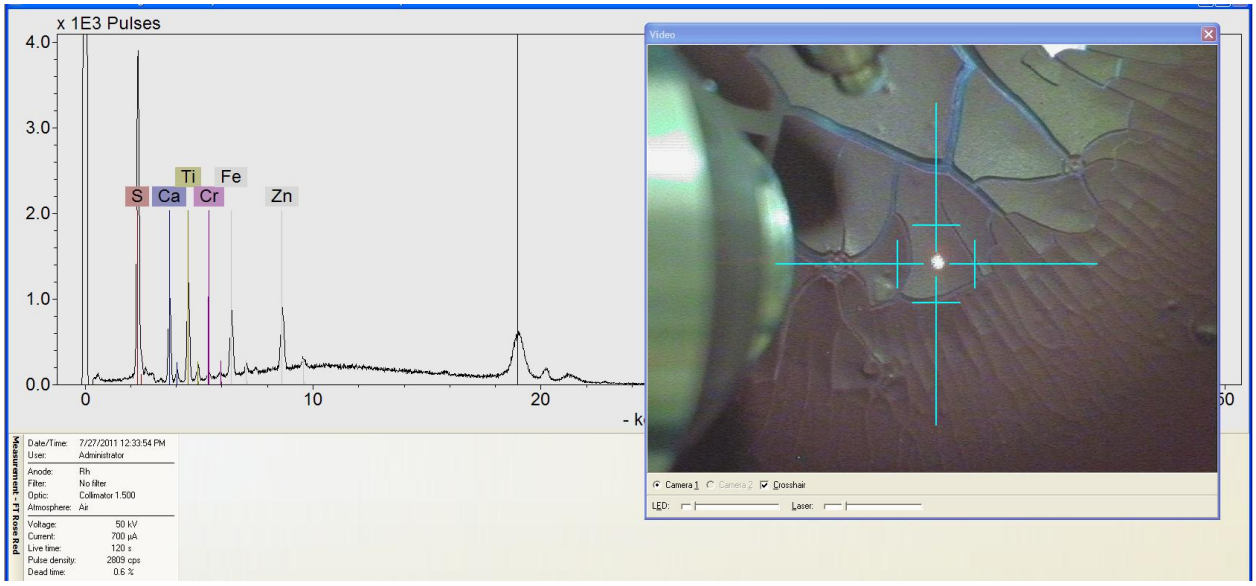
x 1E3 Pulses
Ti
Fe
S
Ca
Cr
Zn
Video
Camera 1
Camera 2
Crosshair
LED:
Laser:
Date/Time: 7/27/2011 12:33:54 PM
User: Administrator
Anode: Rh
Filter: No filter
Optic: Collimator 1.500
Atmosphere: Air
Voltage: 50 kV
Current: 700 µA
Live time: 120 s
Pulse density: 2809 cps
Dead time: 0.6 %
Measurement - FT Rose Red

Mulberry

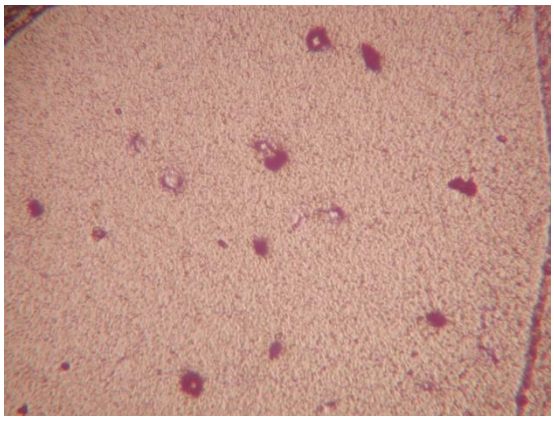

Bright Field, 100x

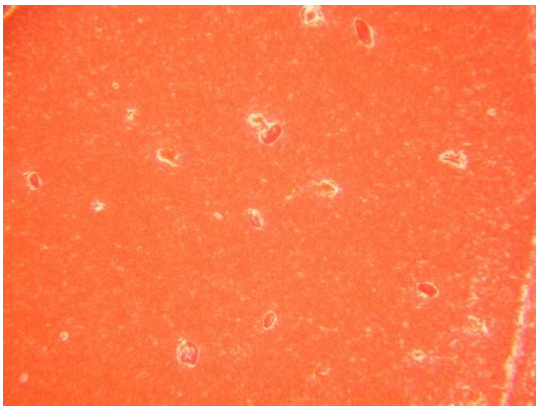

Dark Field, 100x

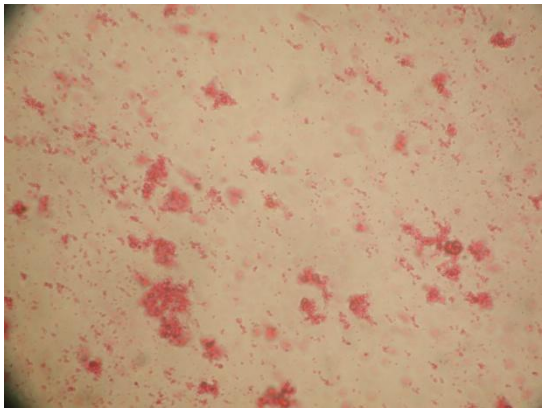

In RI 1.550, 400x

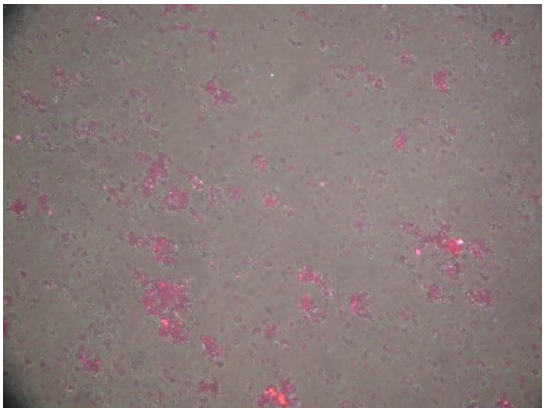

Crossed Polars, In RI 1.550, 400x

Raman microscope image, 500x

Normal Raman, 488nm

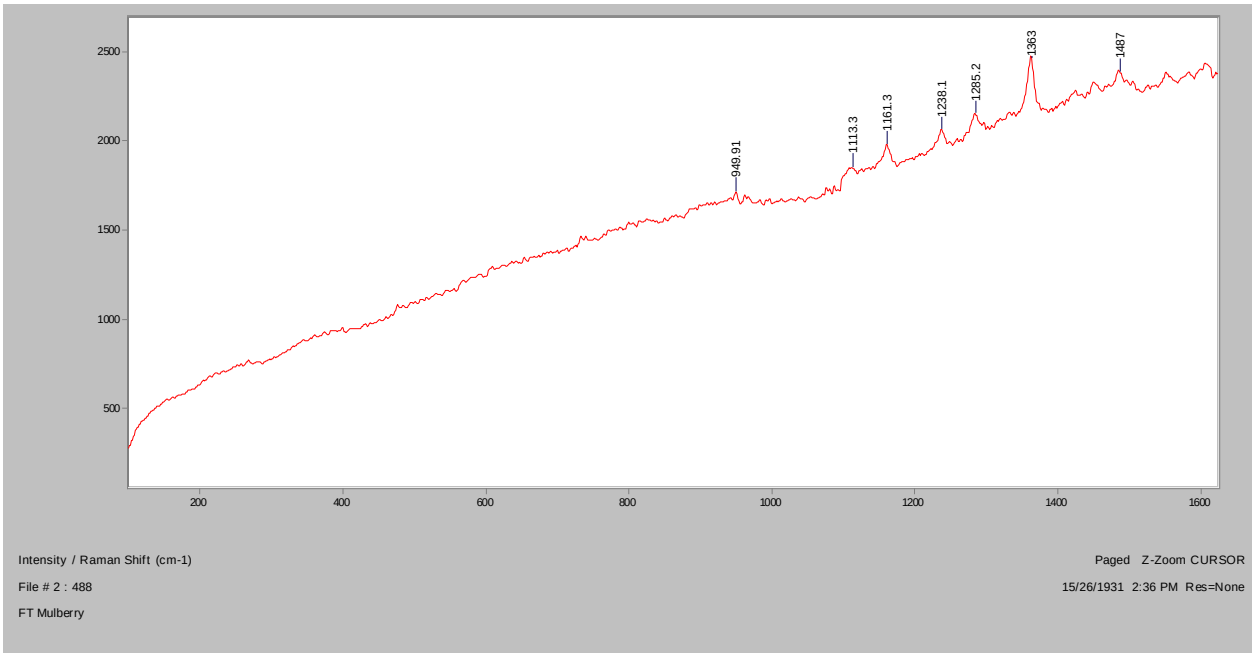

Normal Raman, 633nm

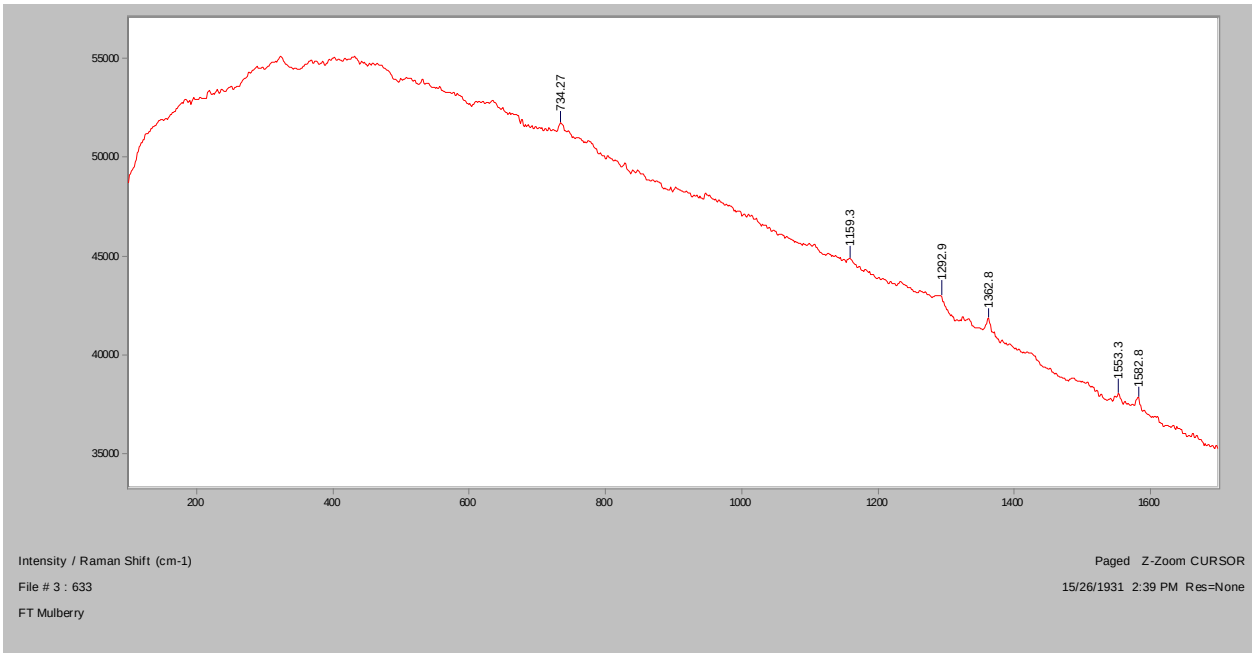

Normal Raman, 785nm

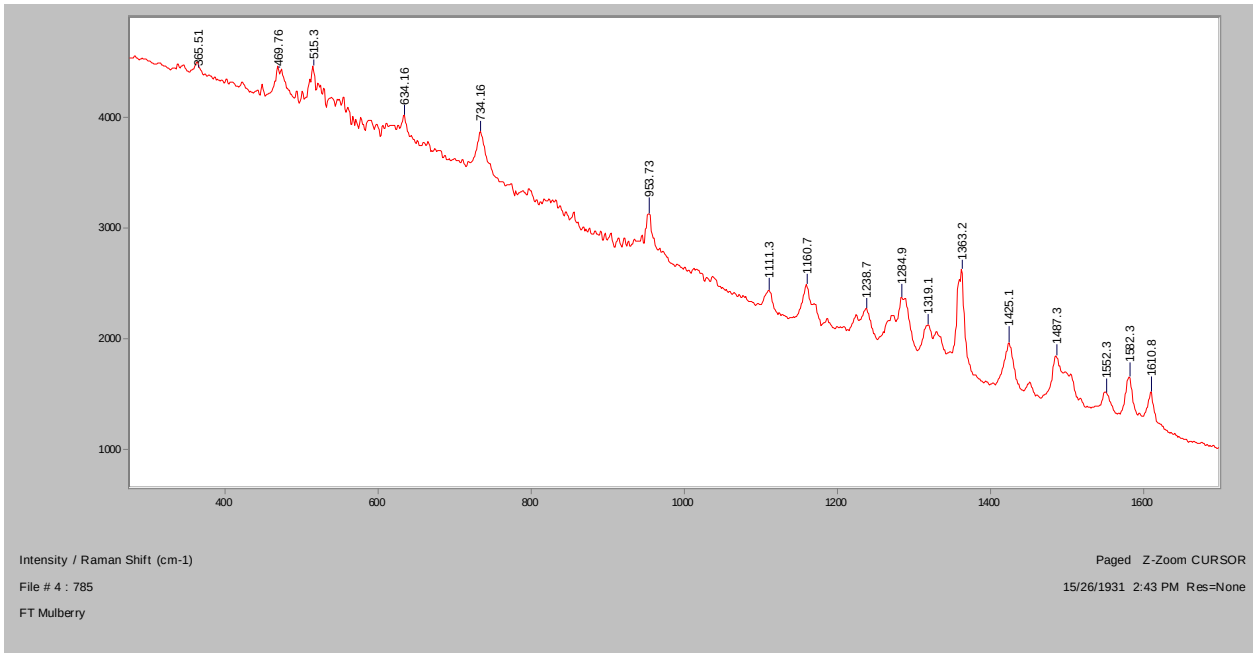

FT-Raman, 1064nm

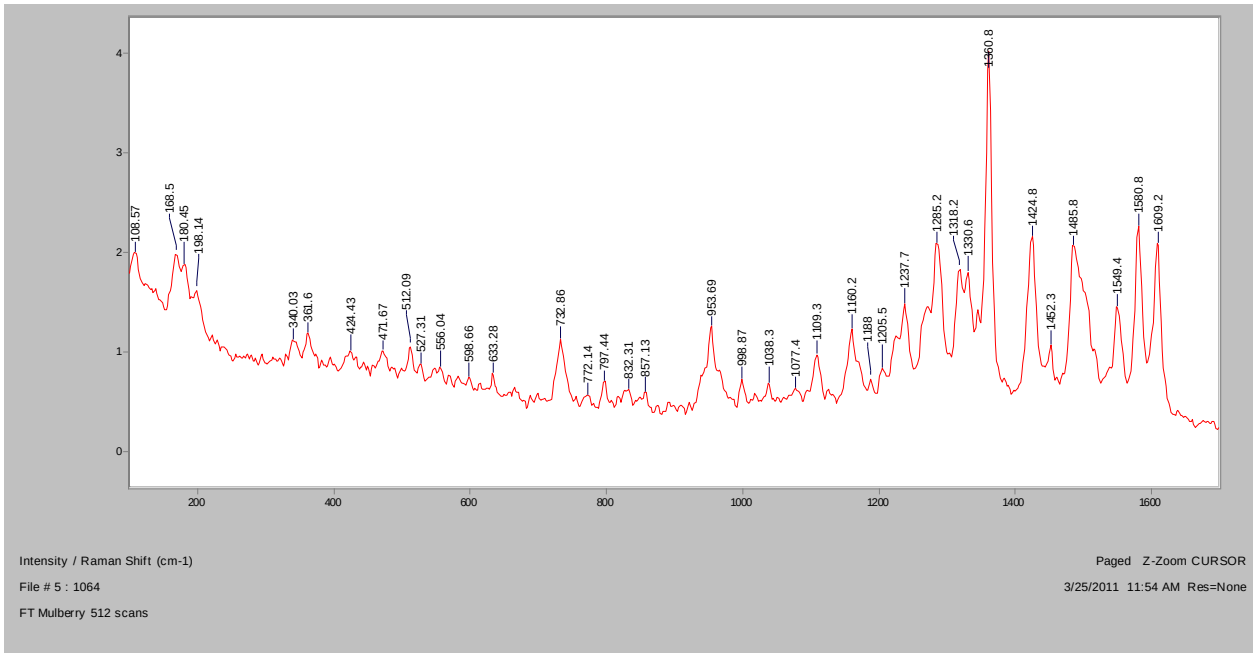

FT-IR (ATR)

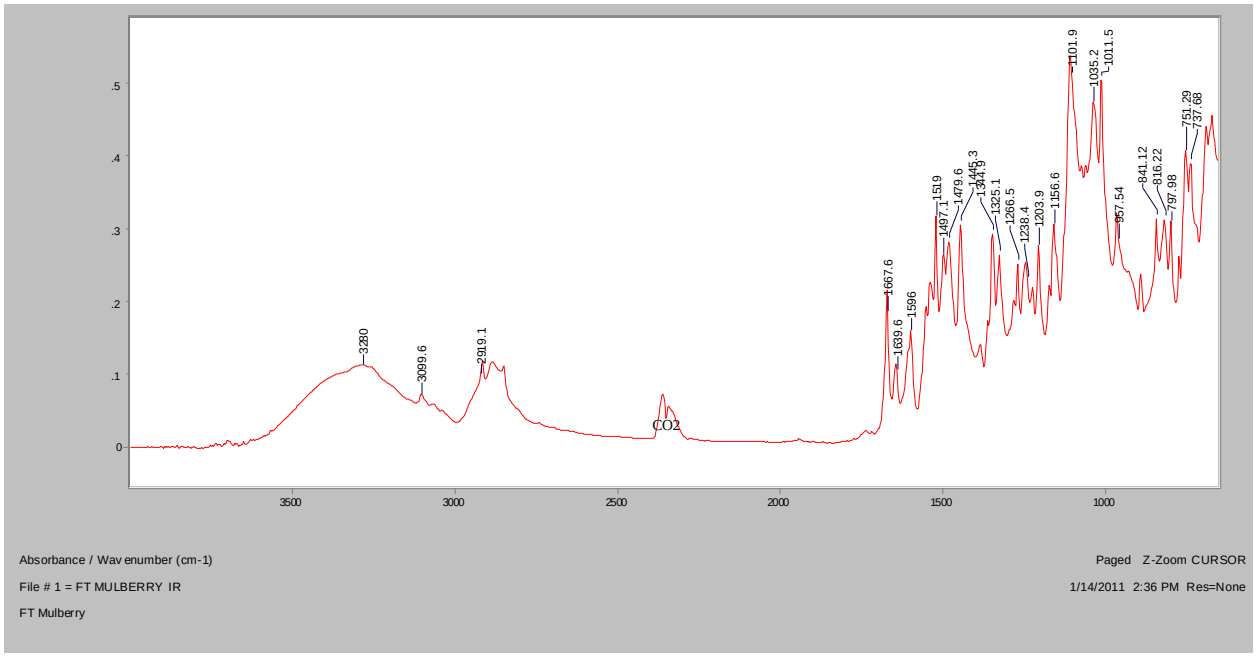
3280
3099.6
2919.1
CO2
1667.6
1639.6
1596
1519
1497.1
1479.6
1445.3
1434.9
1325.1
1266.5
1238.4
1203.9
1156.6
1101.9
1035.2
1011.5
957.54
841.12
816.22
797.98
751.29
737.68
.5
.4
.3
.2
.1
0
3500
3000
2500
2000
1500
1000
Absorbance / Wavenumber (cm-1)
File # 1 = FT MULBERRY IR
FT Mulberry
Paged Z-Zoom CURSOR
1/14/2011 2:36 PM Res=None

XRF

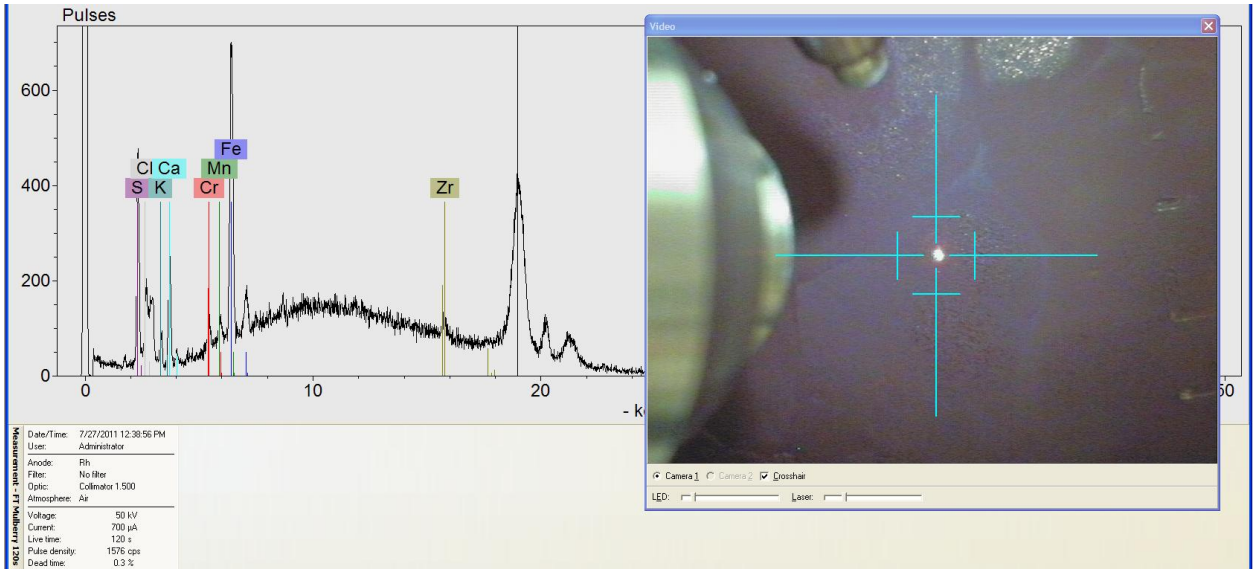
Pulses
600
400
200
0
Cl Ca
S K
Fe
Mn
Cr
Zr
0
10
20
Video
Camera 1
Camera 2
Crosshair
LED:
Laser:
Date/Time: 7/27/2011 12:38:56 PM
User: Administrator
Anode: Rh
Filter: No filter
Optic: Collimator 1.500
Atmosphere: Air
Voltage: 50 kV
Current: 700 µA
Live time: 120 s
Pulse density: 1576 cps
Dead time: 0.3 %

Dark Red

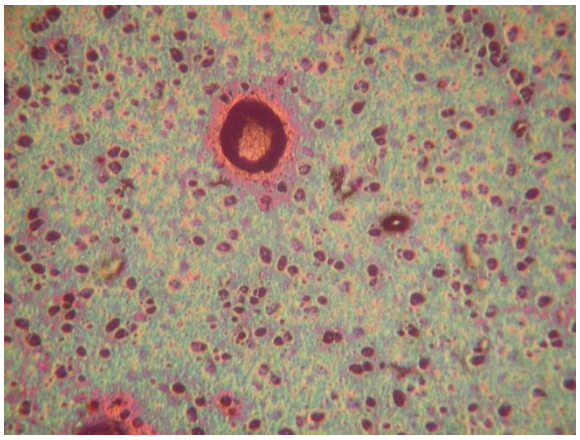

Bright Field, 100x

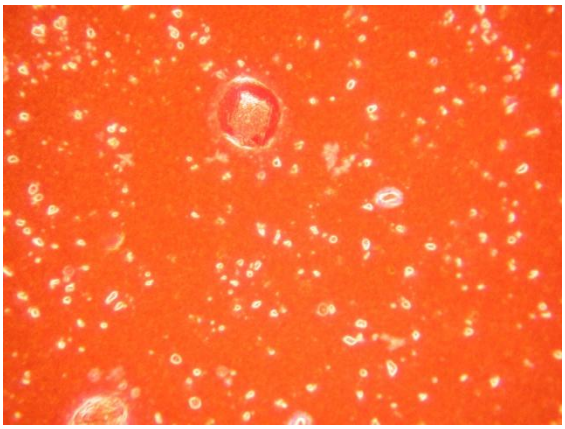

Dark Field, 100x

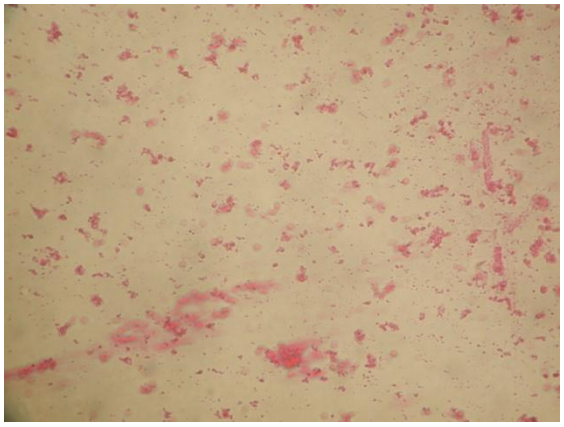

In RI 1.550, 400x

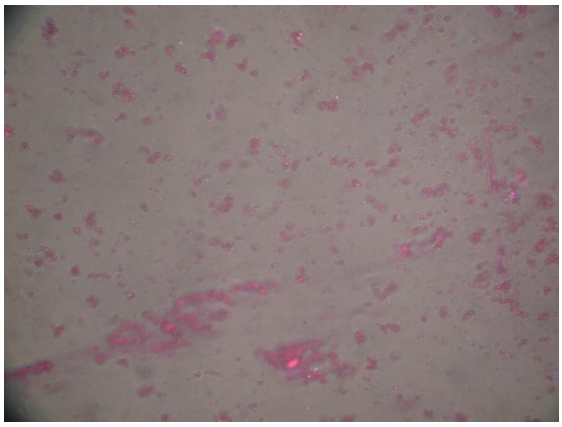

Crossed Polars, In RI 1.550, 400x

Normal Raman, 488nm

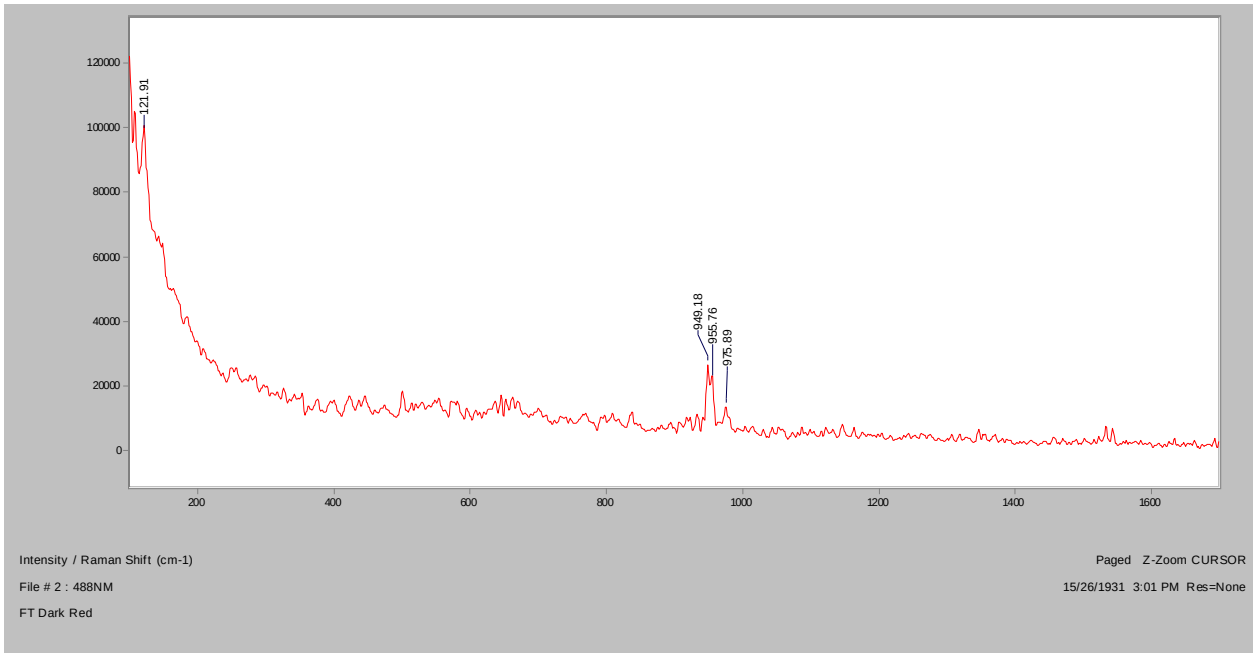

Normal Raman, 633nm

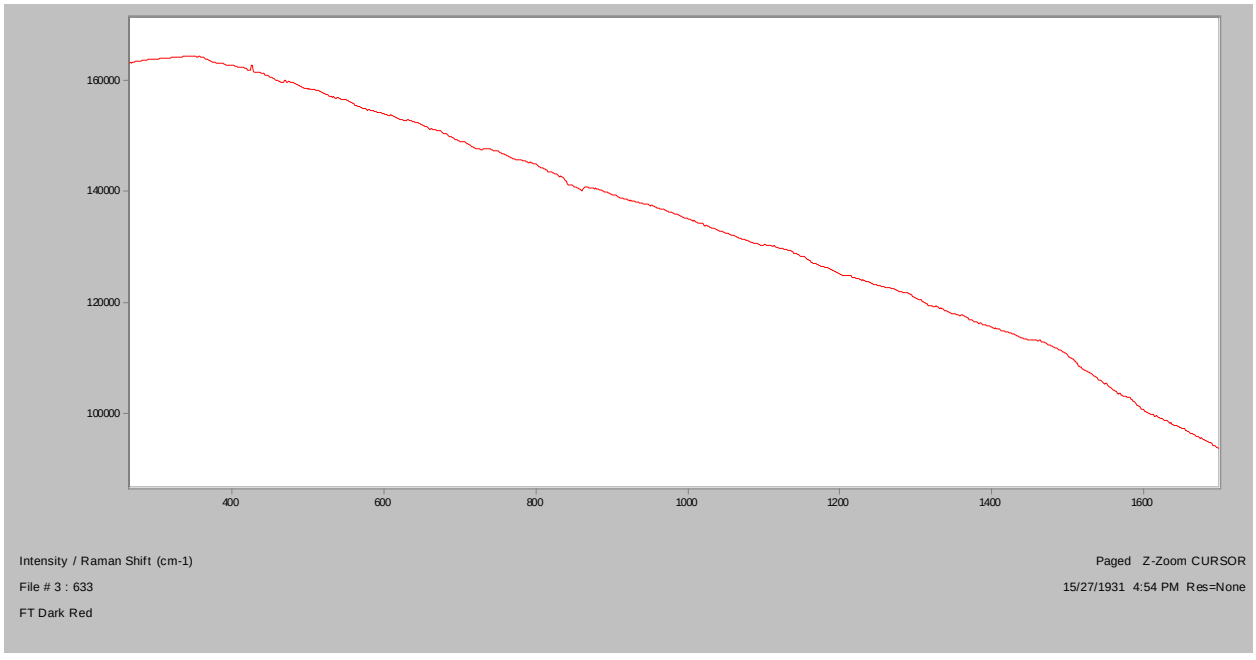

Normal Raman, 785nm

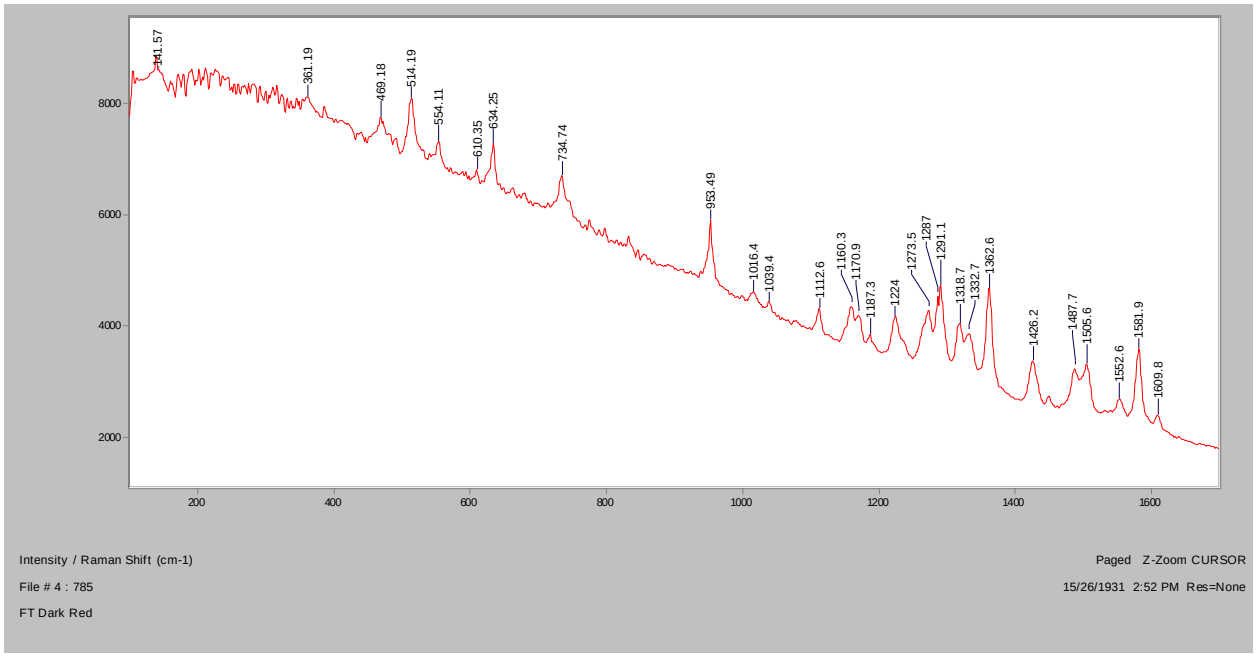

FT-Raman, 1064nm

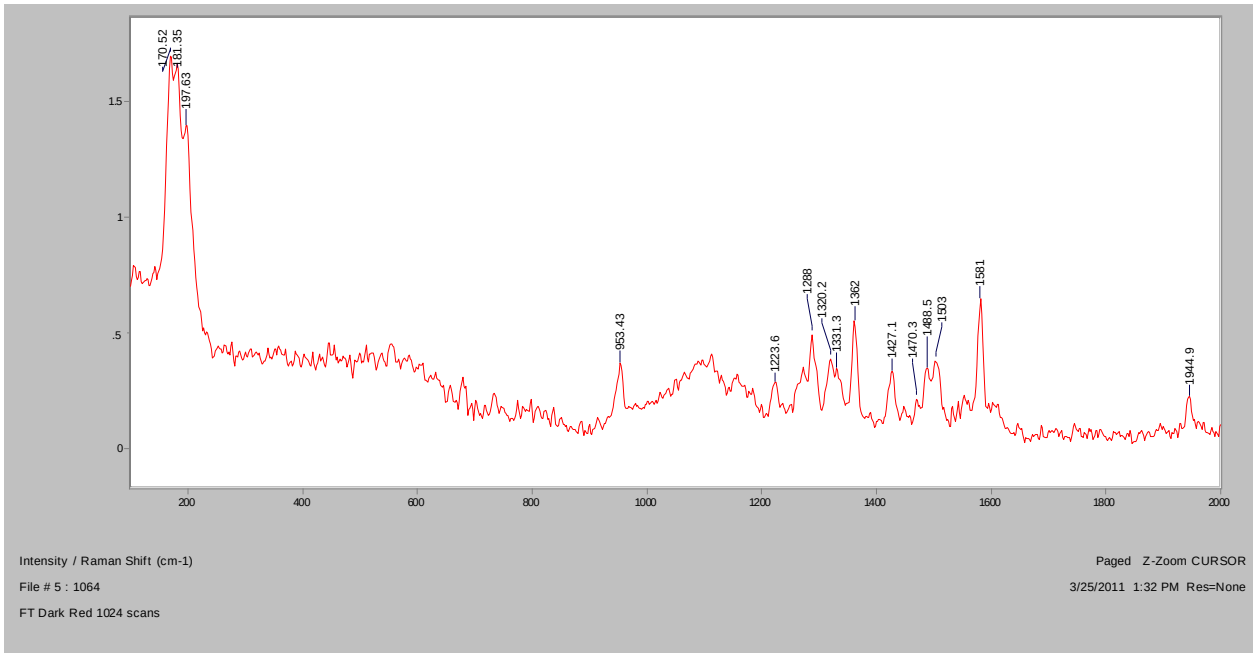

FT-IR (ATR)

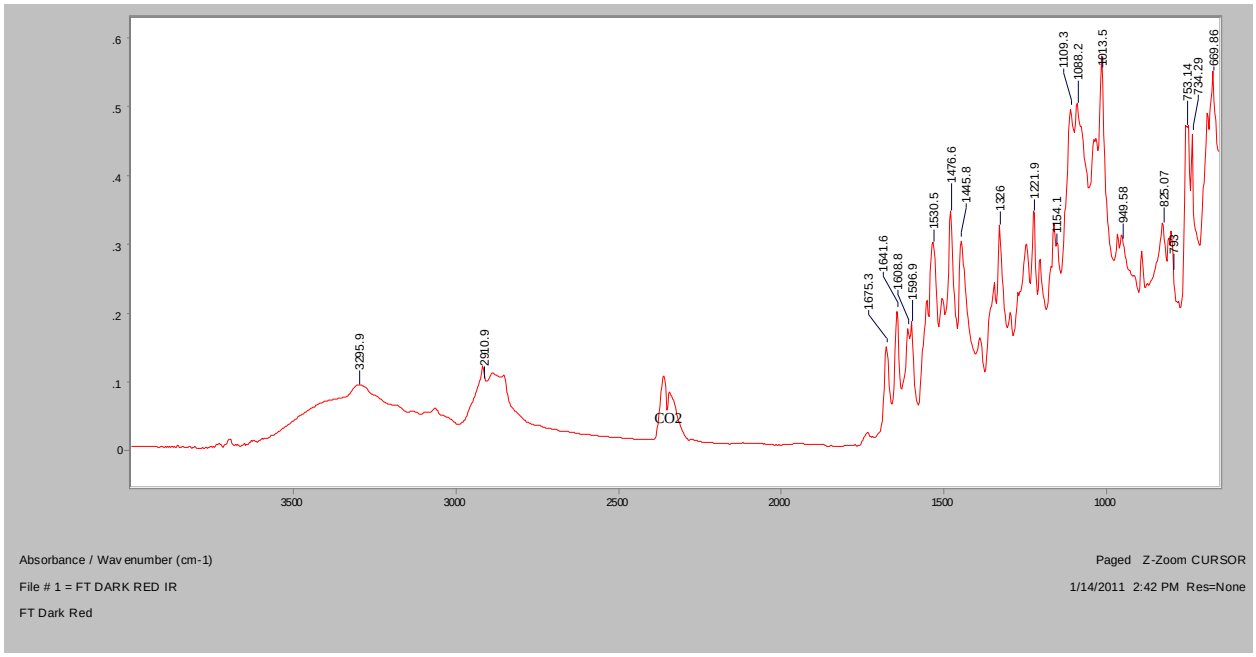
3295.9
2910.9
CO2
1675.3
1641.6
1608.8
1596.9
1530.5
1476.6
1445.8
1326
1221.9
1154.1
1109.3
1088.2
1013.5
949.58
825.07
753.14
734.29
669.86
Absorbance / Wavenumber (cm-1)
File # 1 = FT DARK RED IR
FT Dark Red
Paged Z-Zoom CURSOR
1/14/2011 2:42 PM Res=None

XRF

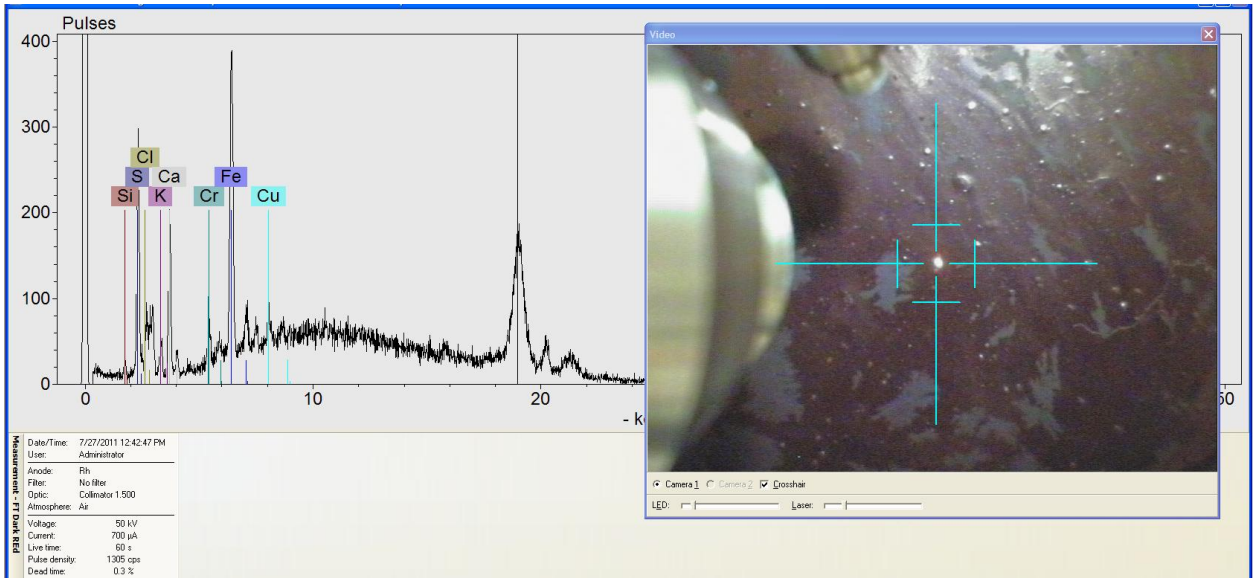
Pulses
Cl
S
Ca
Fe
Si
K
Cr
Cu
Video
Camera 1
Crosshair
LED:
Laser:
Date/Time: 7/27/2011 12:42:47 PM
User: Administrator
Anode: Rh
Filter: No filter
Optic: Collimator 1.500
Atmosphere: Air
Voltage: 50 kV
Current: 700 µA
Live time: 60 s
Pulse density: 1305 cps
Dead time: 0.3 %

Orange Red

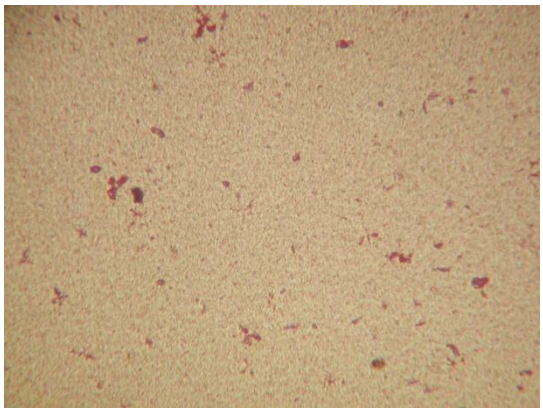

Bright Field, 100x

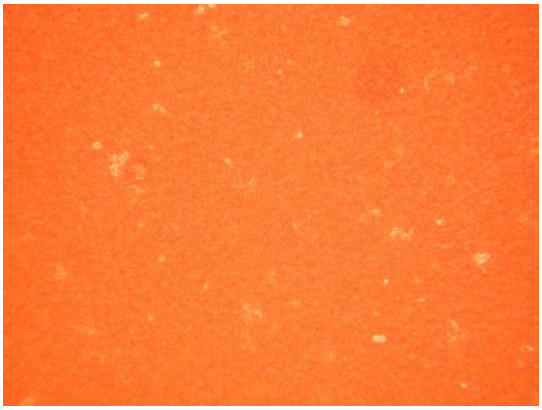

Dark Field, 100x

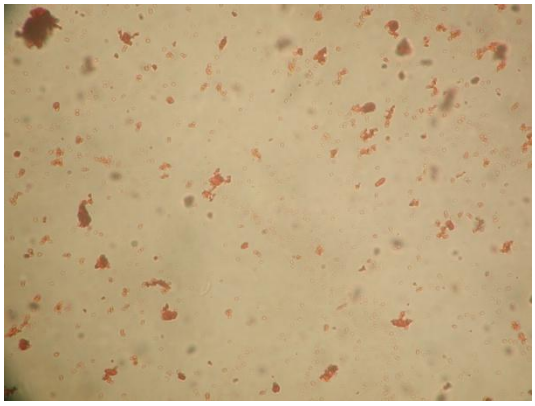

In RI 1.550, 400x

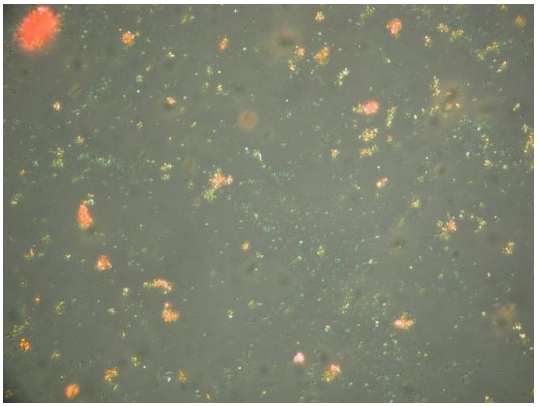

Crossed Polars, In RI 1.550, 400x

Normal Raman, 488nm

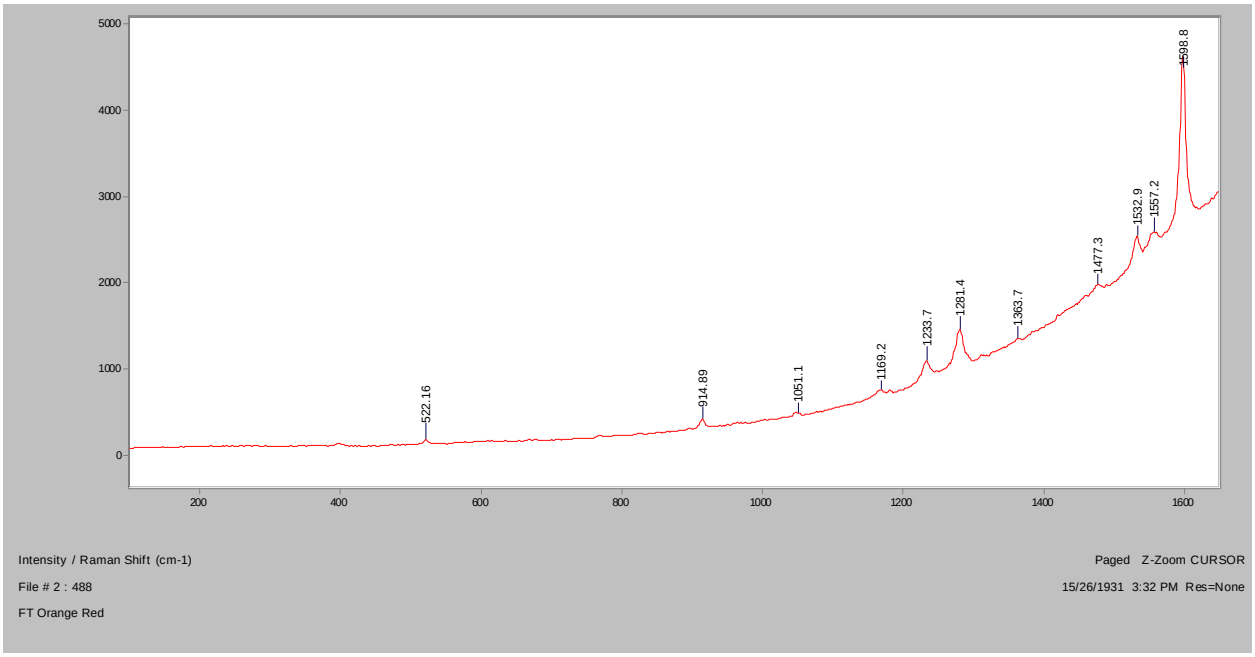

Normal Raman, 633nm

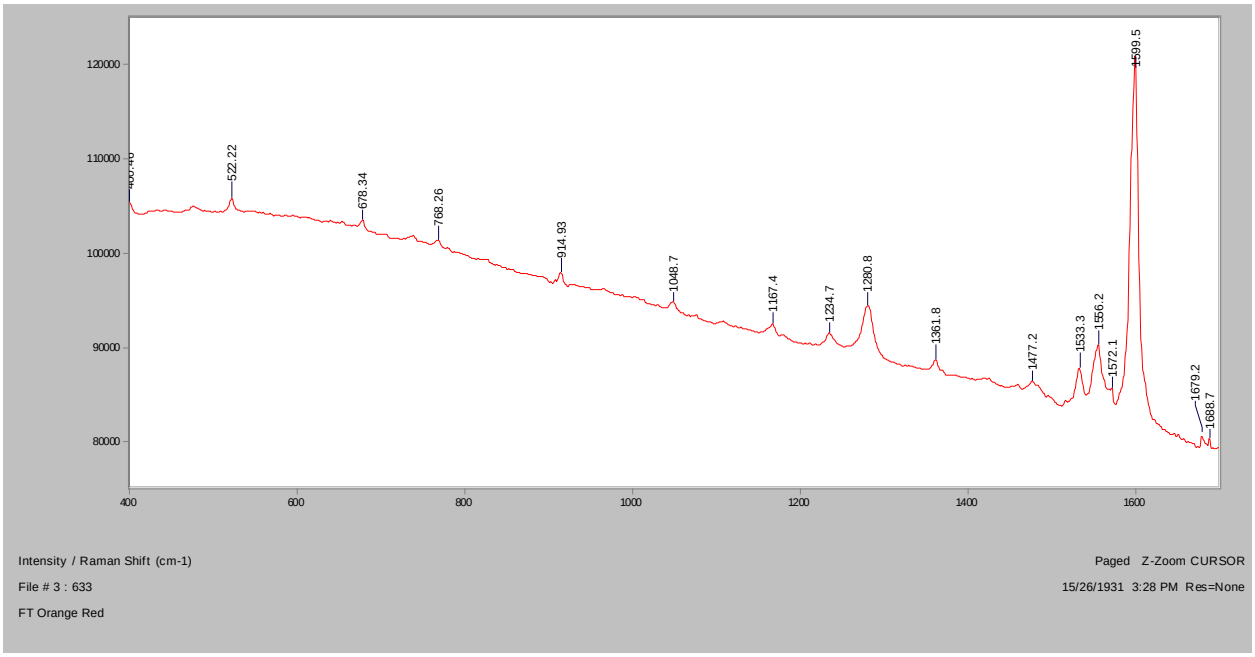

Normal Raman, 785nm

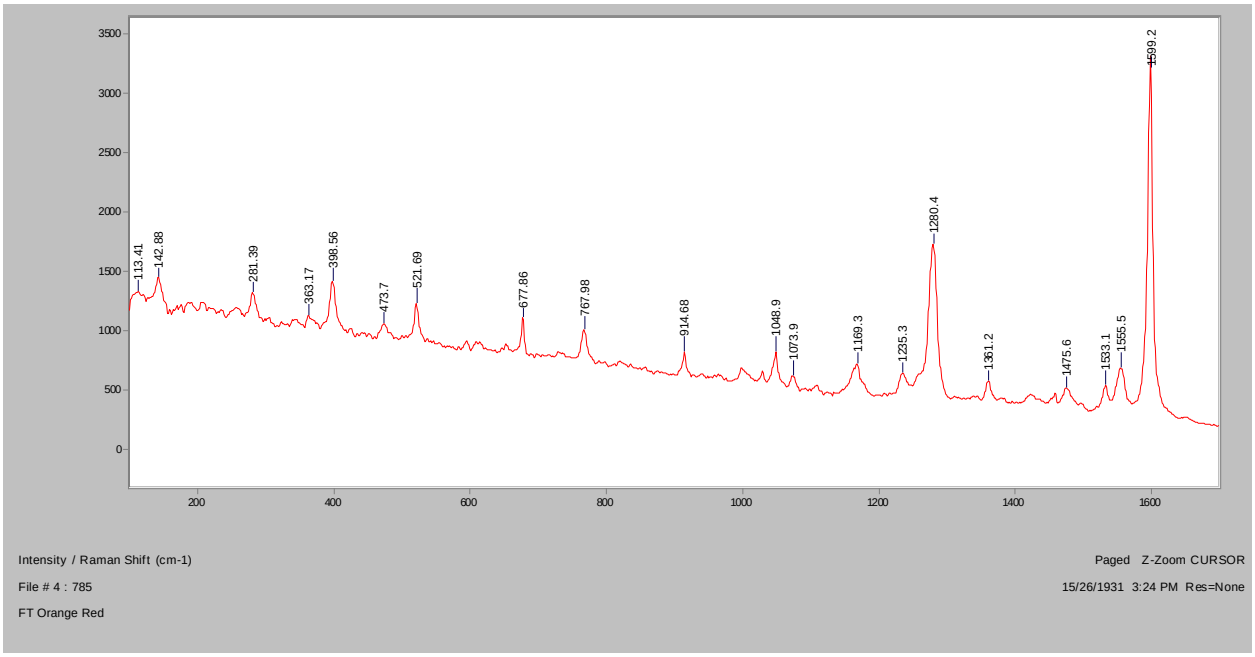

FT-Raman, 1064nm

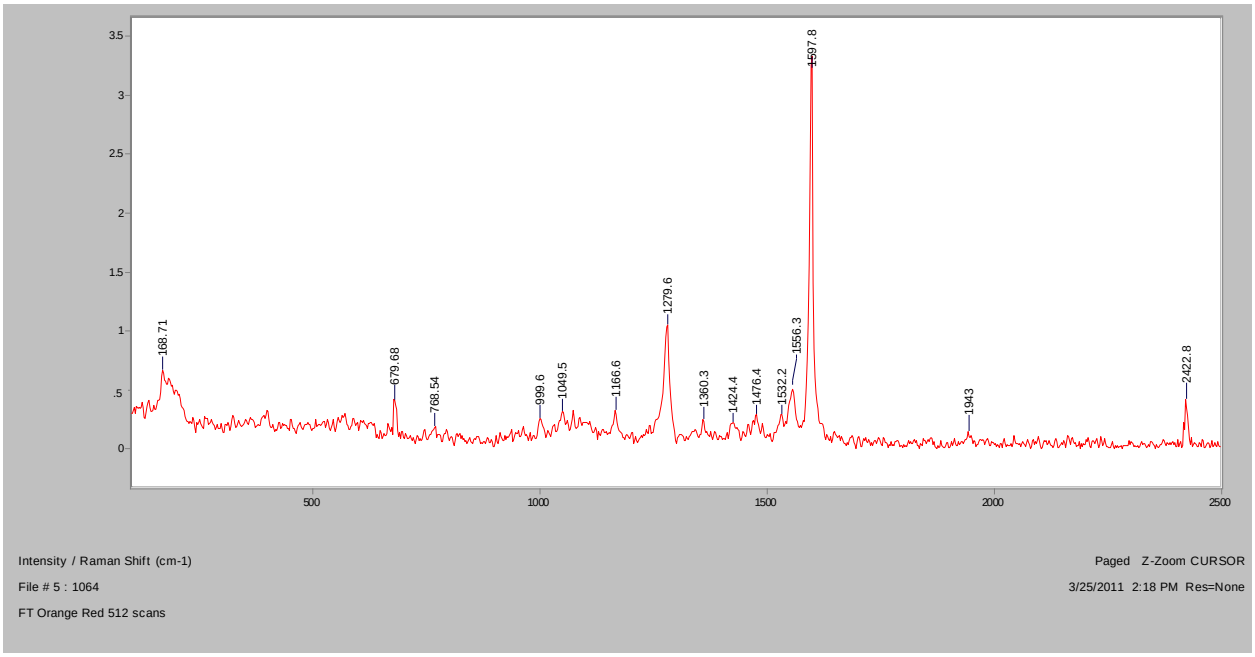

FT-IR (ATR)

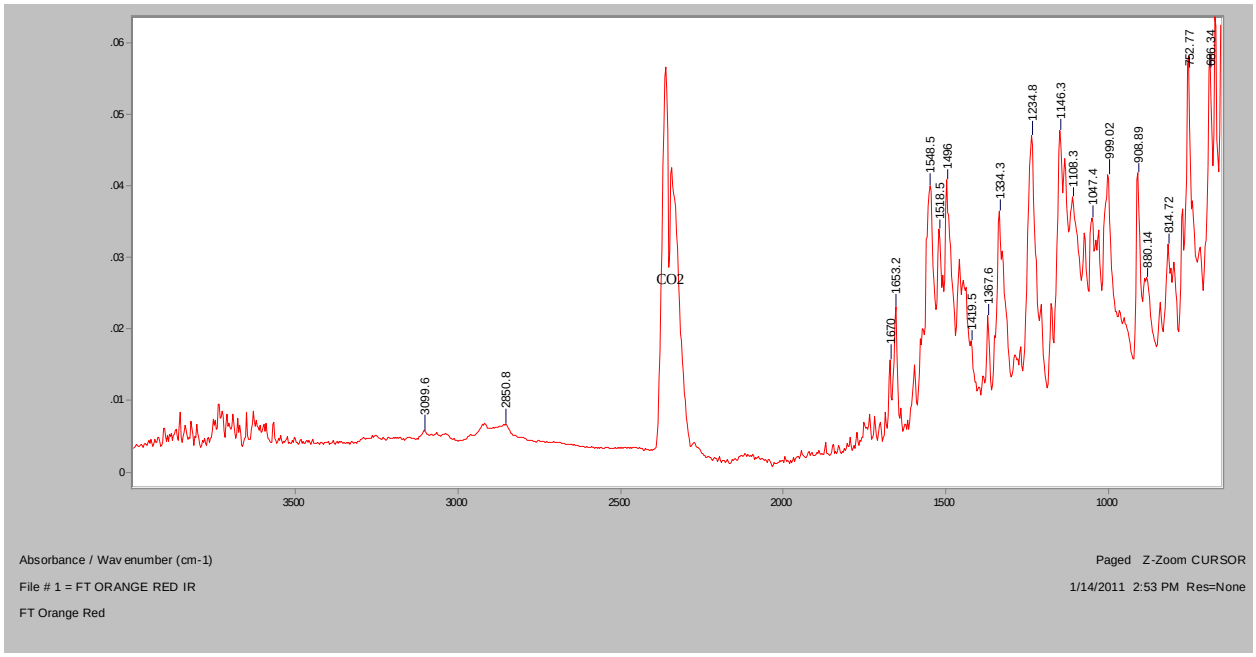
.06
.05
.04
.03
.02
.01
0
3500
3000
2500
2000
1500
1000
3099.6
2850.8
CO2
1653.2
1670
1548.5
1518.5
1496
1419.5
1367.6
1334.3
1234.8
1146.3
1108.3
1047.4
999.02
908.89
880.14
814.72
752.77
666.34
Absorbance / Wavenumber (cm-1)
File # 1 = FT ORANGE RED IR
FT Orange Red
Paged Z-Zoom CURSOR
1/14/2011 2:53 PM Res=None

XRF

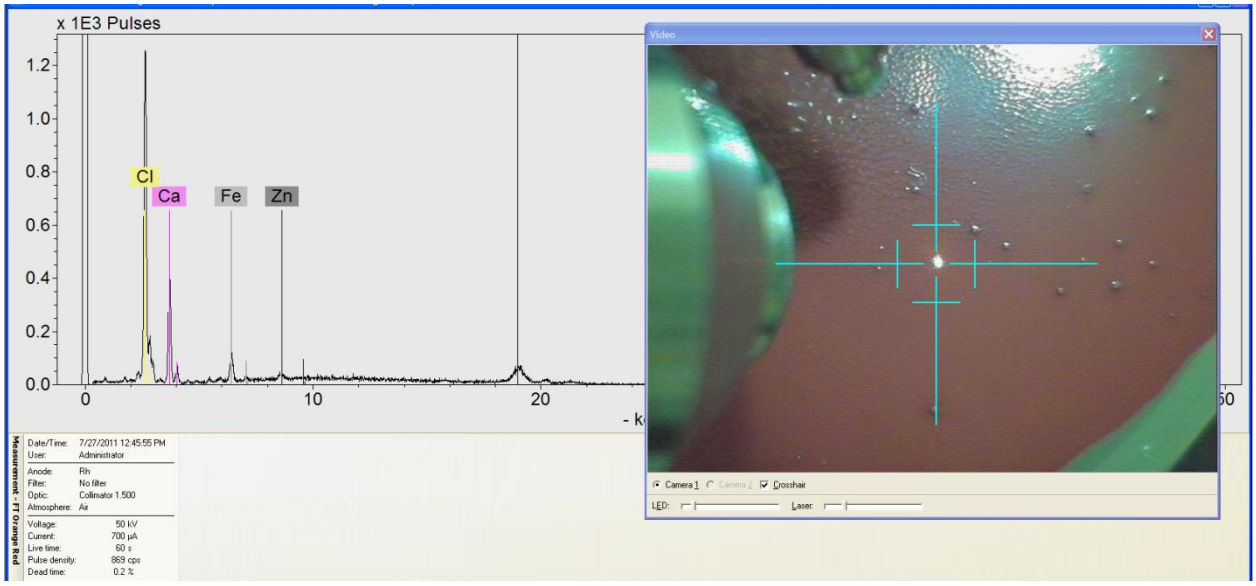
x 1E3 Pulses
1.2
1.0
0.8
0.6
0.4
0.2
0.0
Cl
Ca
Fe
Zn
0
10
20
Video
Camera 1
Camera 2
Crosshair
LED:
Laser:
Date/Time: 7/27/2011 12:45:55 PM
User: Administrator
Anode: Rh
Filter: No filter
Optic: Collimator 1.500
Atmosphere: Air
Voltage: 50 kV
Current: 700 µA
Live time: 60 s
Pulse density: 863 cps
Dead time: 0.2 %
Measurement - FT Orange Red

Orange

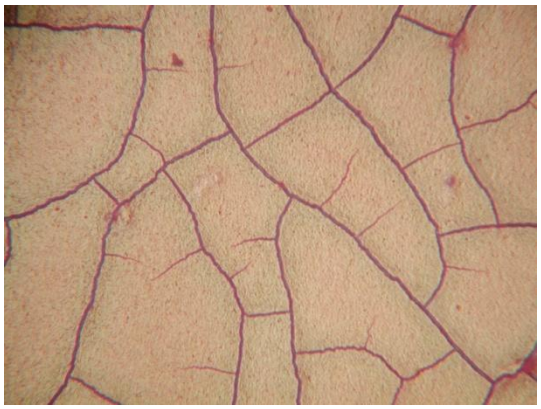

Bright Field, 100x

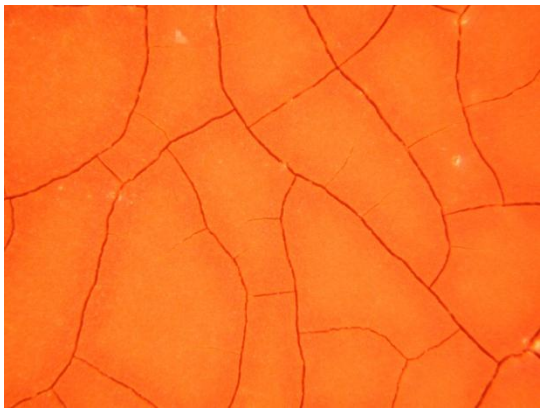

Dark Field, 100x

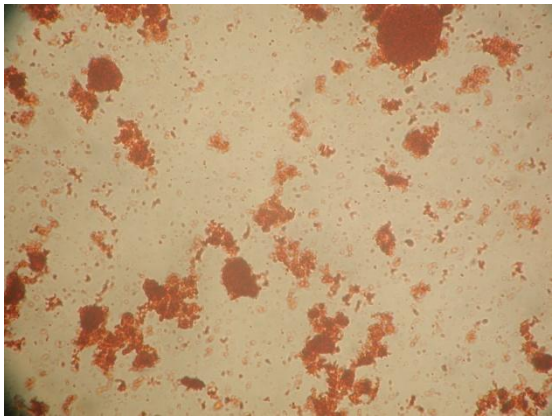

In RI 1.550, 400x

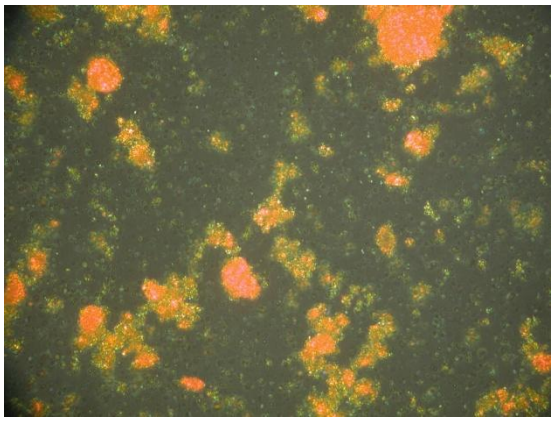

Crossed Polars, In RI 1.550, 400x

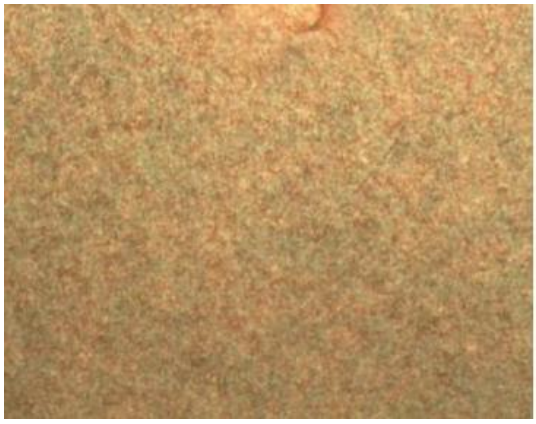

Raman microscope image, 1000x

Normal Raman, 488nm

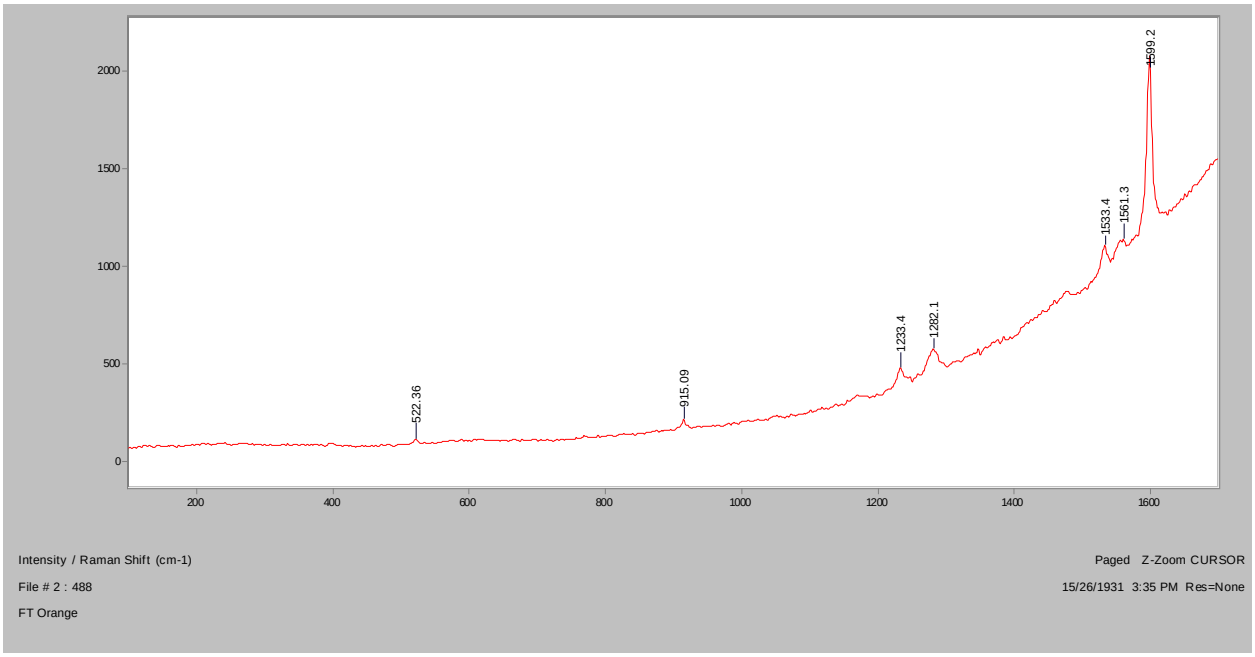

Normal Raman, 633nm

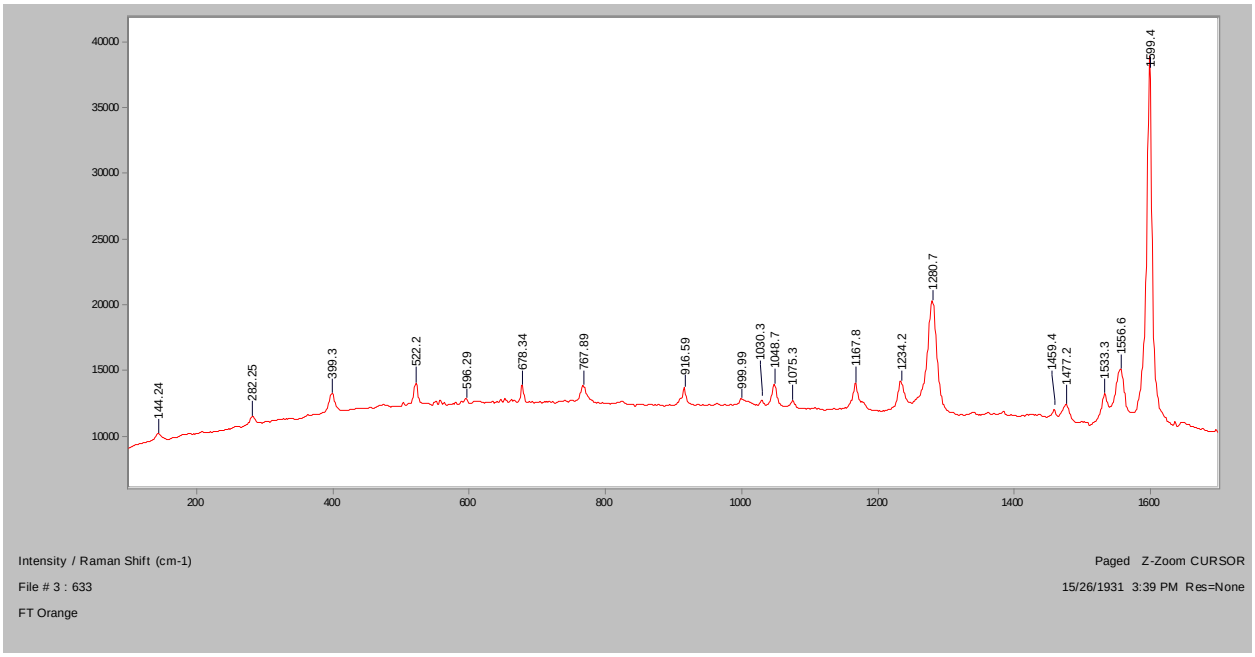

Normal Raman, 785nm

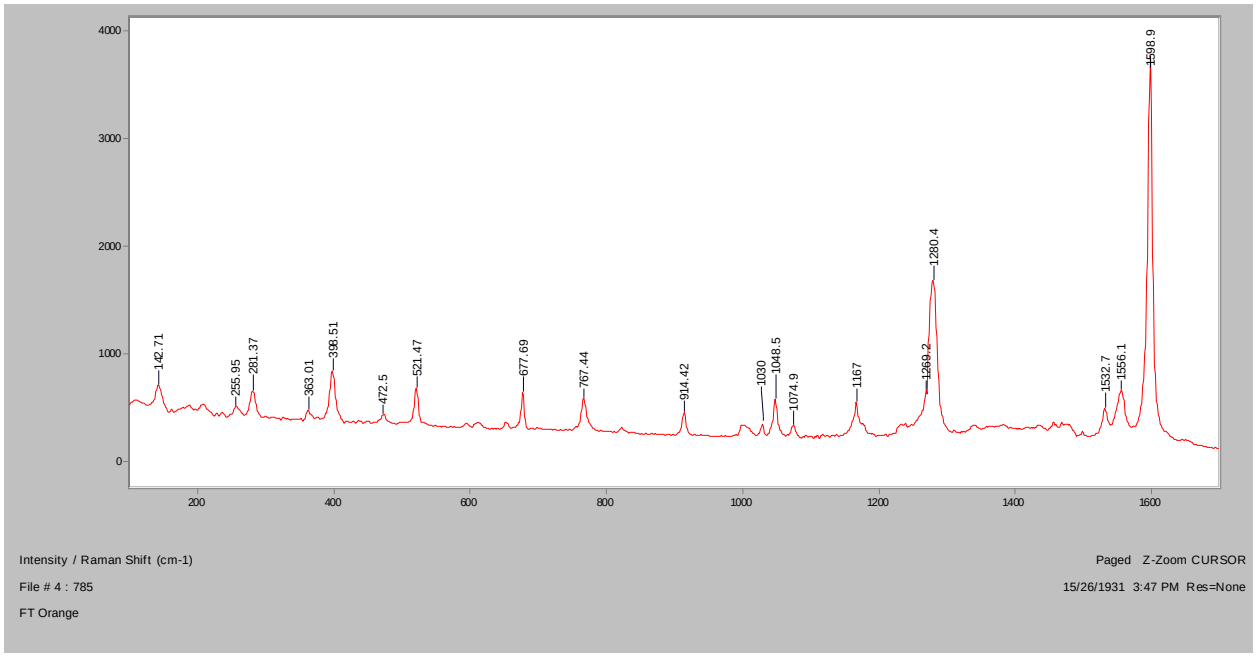

FT-Raman, 1064nm

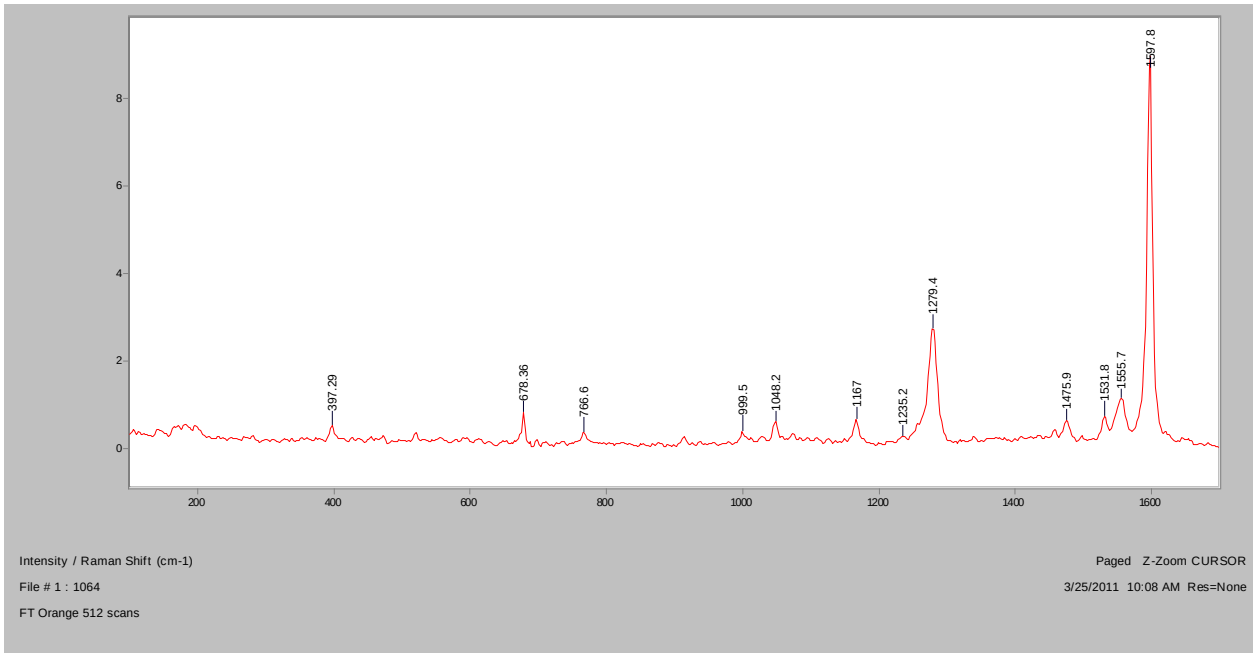

FT-IR (ATR)

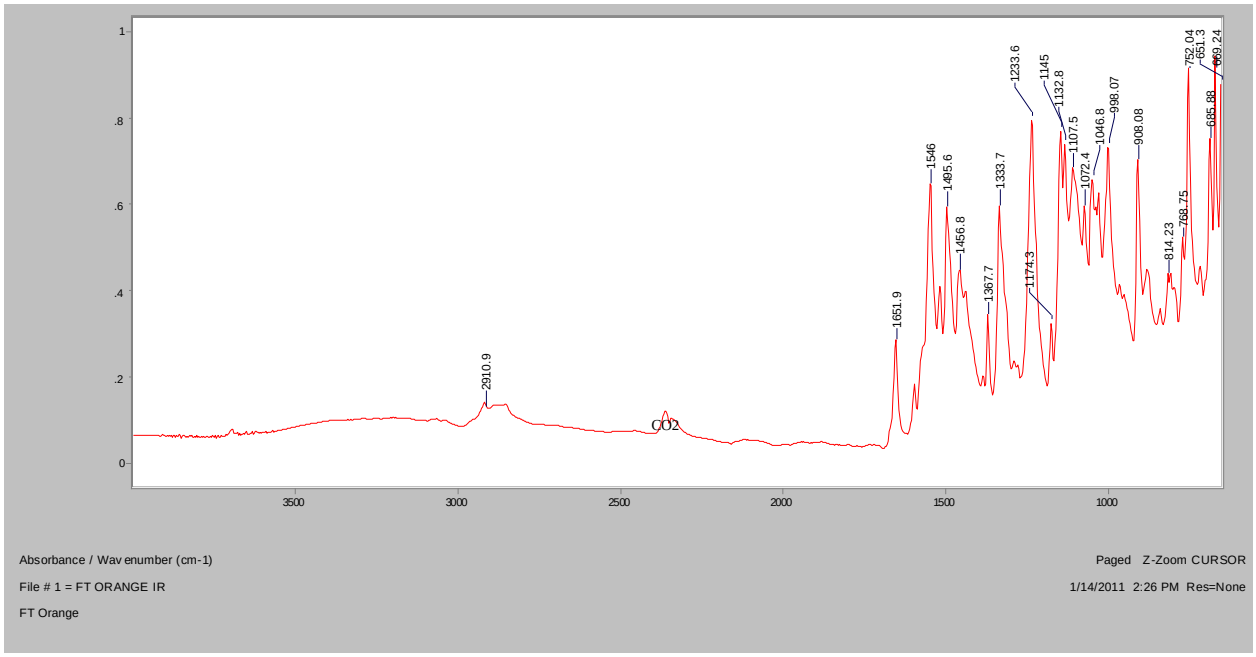
1
.8
.6
.4
.2
0
3500
3000
2500
2000
1500
1000
2910.9
CO2
1651.9
1546
1495.6
1456.8
1367.7
1333.7
1233.6
1174.3
1145
1132.8
1107.5
1072.4
1046.8
998.07
908.08
814.23
768.75
752.04
651.3
669.24
685.88
Absorbance / Wavenumber (cm-1)
File # 1 = FT ORANGE IR
FT Orange
Paged Z-Zoom CURSOR
1/14/2011 2:26 PM Res=None

XRF

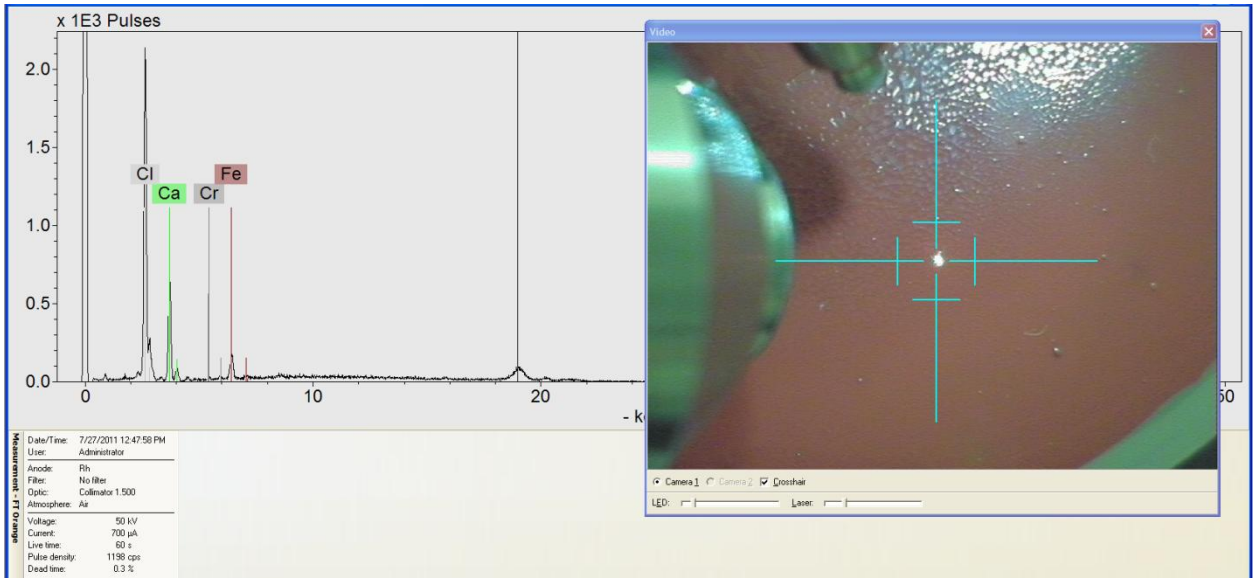
x 1E3 Pulses
2.0
1.5
1.0
0.5
0.0
0
10
20
Cl
Fe
Ca
Cr
Video
Camera 1
Camera 2
Crosshair
LED:
Laser:
Date/Time: 7/27/2011 12:47:58 PM
User: Administrator
Anode: Rh
Filter: No filter
Optic: Collimator 1.500
Atmosphere: Air
Voltage: 50 kV
Current: 700 µA
Live time: 60 s
Pulse density: 1198 cps
Dead time: 0.3 %

Bright Yellow

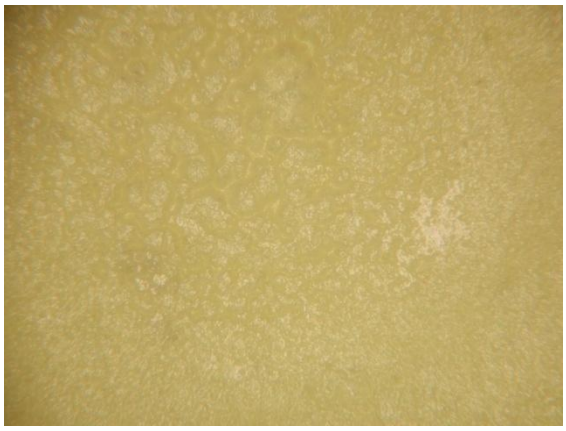

Bright Field, 100x

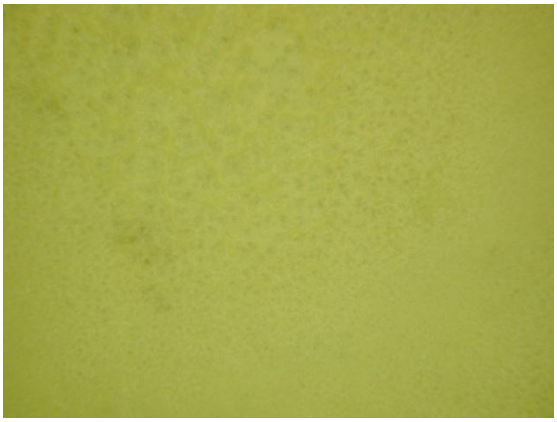

Dark Field, 100x

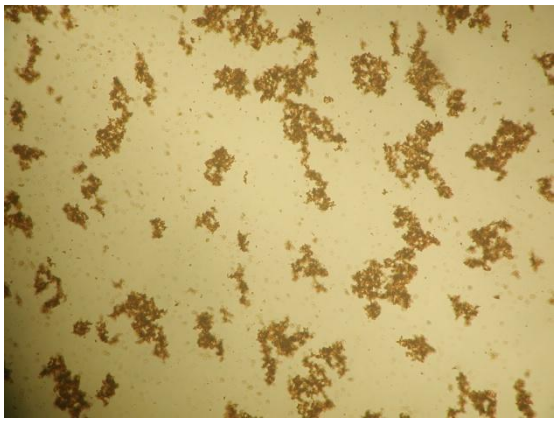

In RI 1.550, 200x

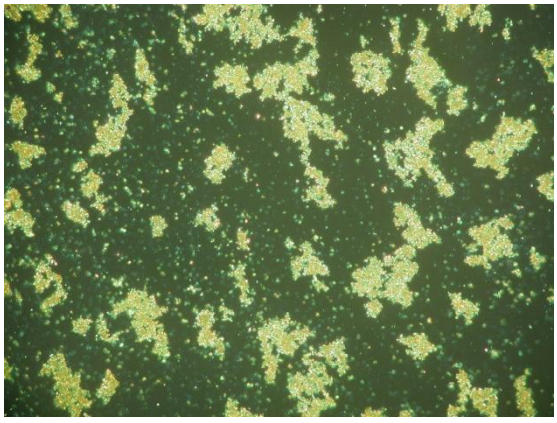

Crossed Polars, In RI 1.550, 200x

Normal Raman, 488nm

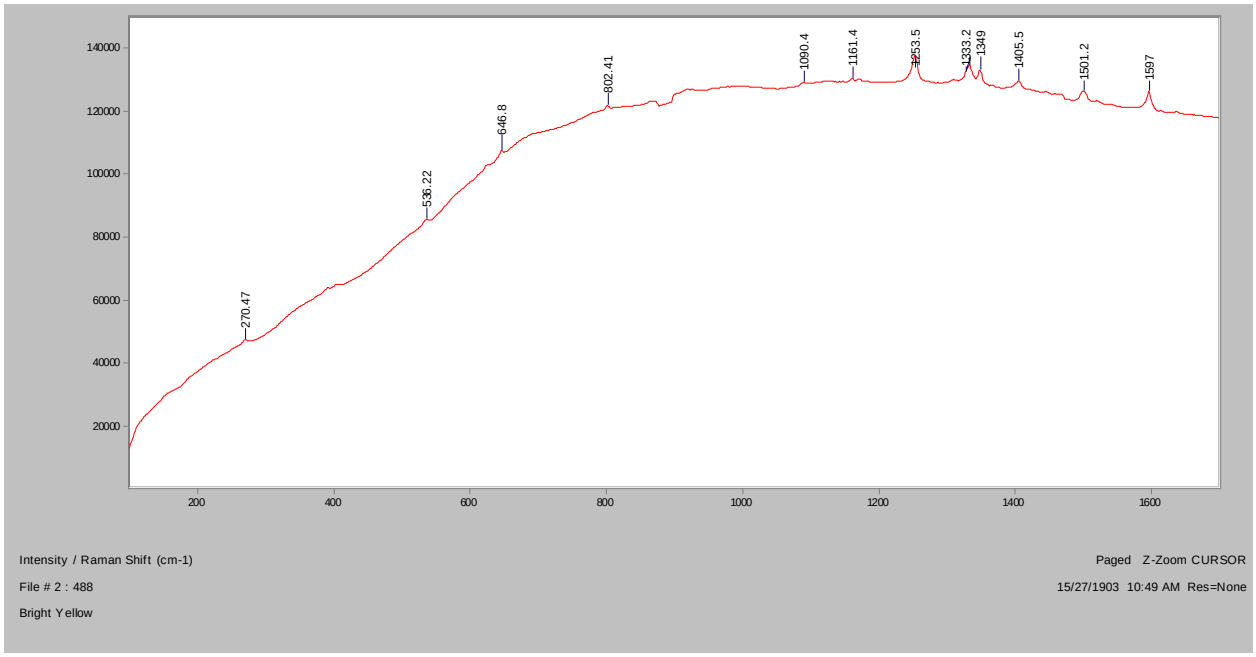

Normal Raman, 633nm

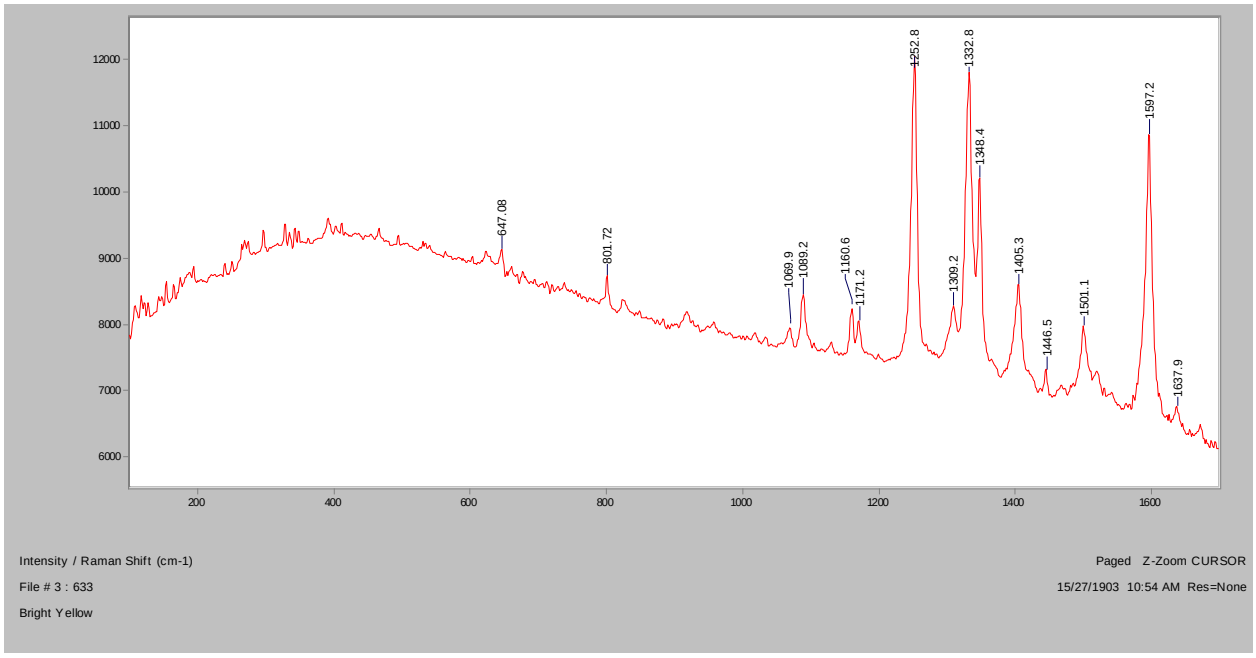

Normal Raman, 785nm

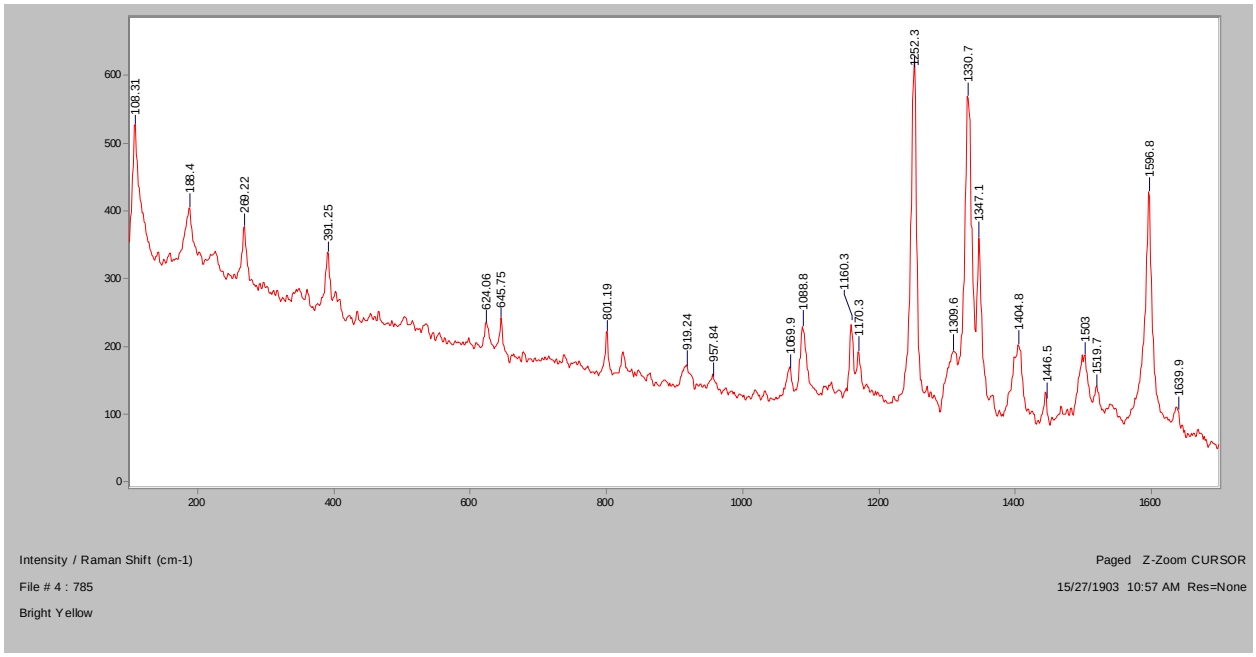

FT-Raman, 1064nm

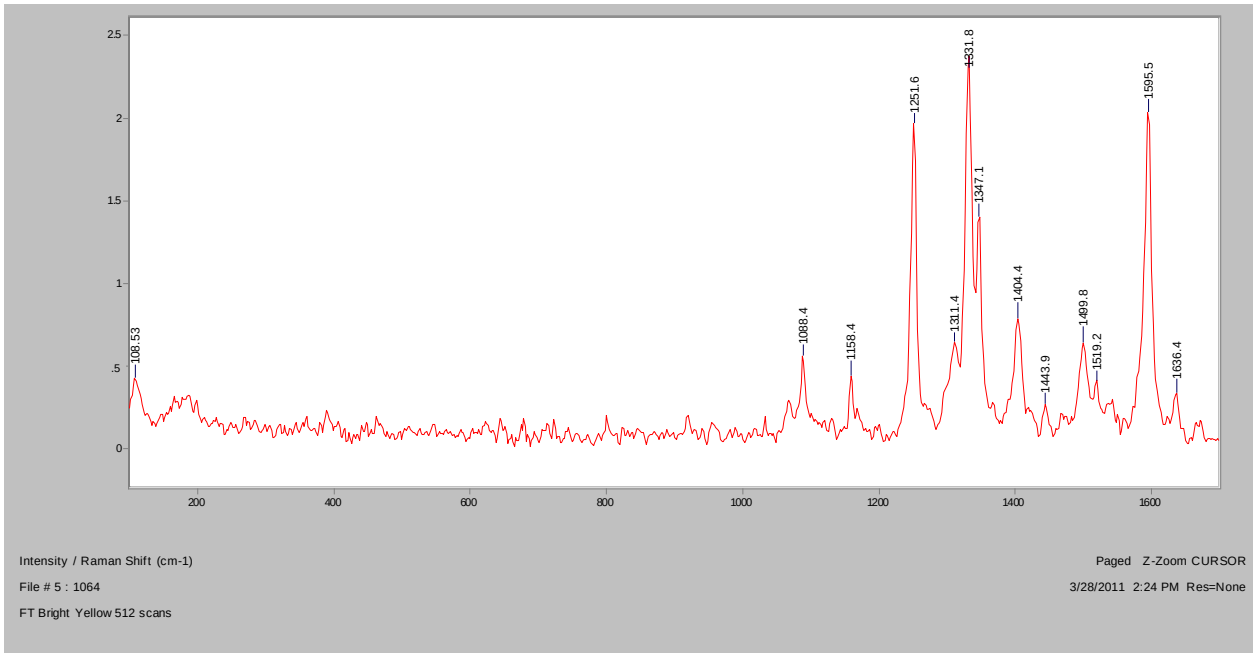

FT-IR (ATR)

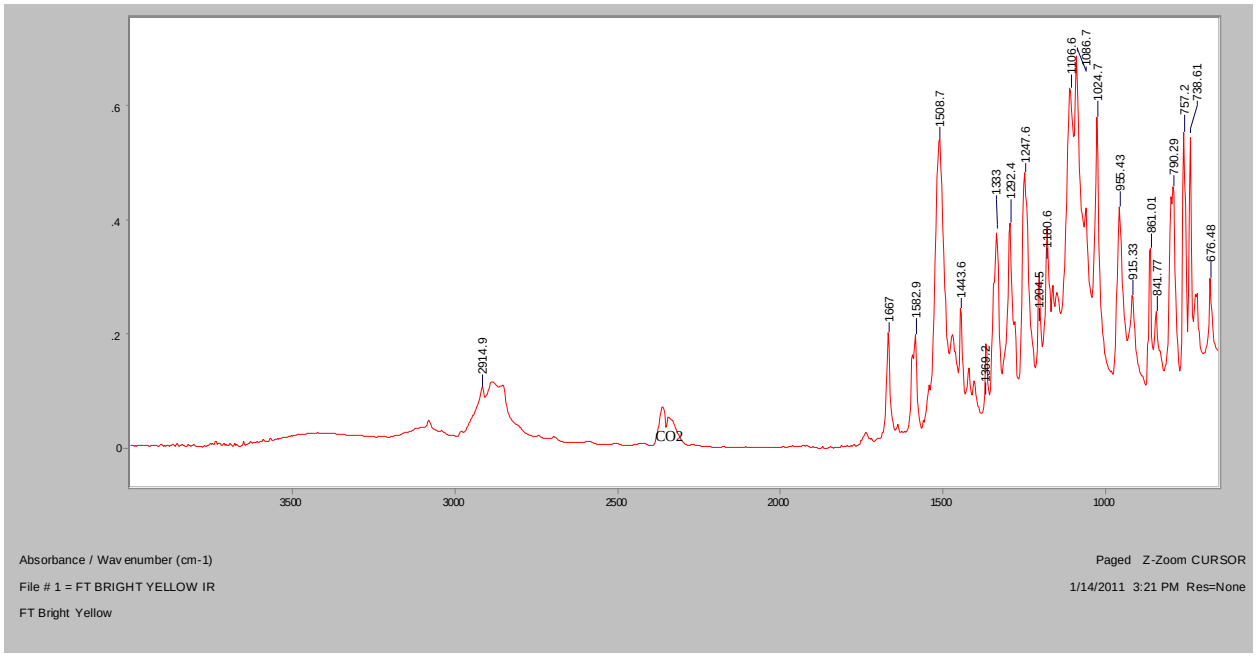
.6
.4
.2
0
3500
3000
2500
2000
1500
1000
2914.9
CO2
1667
1582.9
1508.7
1443.6
1333
1292.4
1247.6
1180.6
1106.6
1086.7
1024.7
955.43
915.33
861.01
841.77
790.29
757.2
738.61
676.48
Absorbance / Wavenumber (cm-1)
File # 1 = FT BRIGHT YELLOW IR
FT Bright Yellow
Paged Z-Zoom CURSOR
1/14/2011 3:21 PM Res=None

XRF

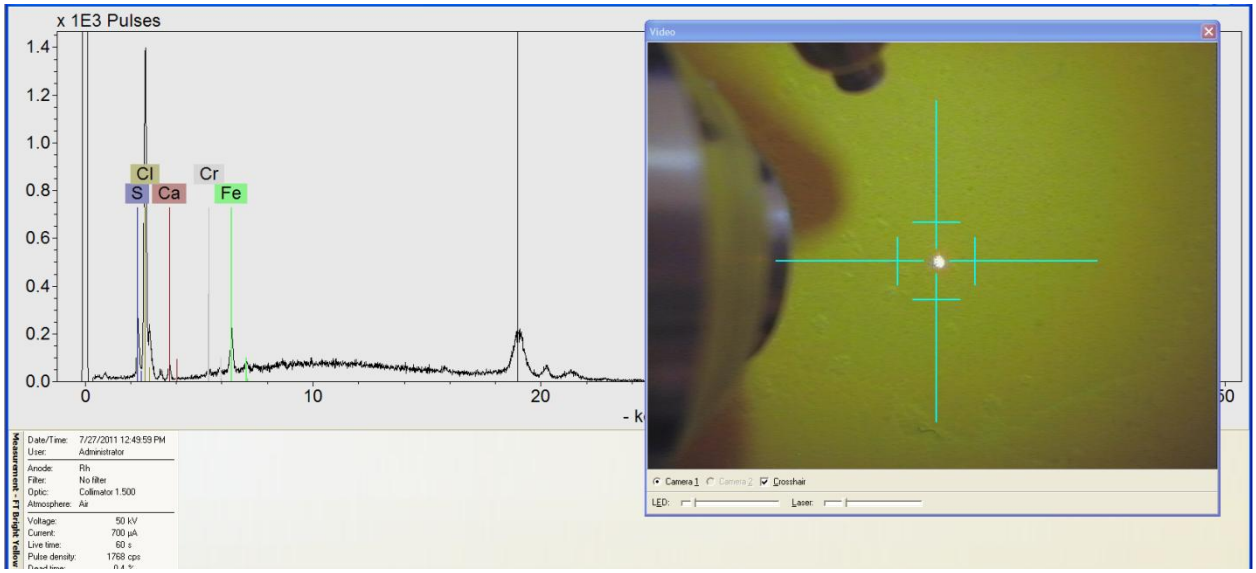
x 1E3 Pulses
1.4
1.2
1.0
0.8
0.6
0.4
0.2
0.0
0
10
20
Cl
S
Ca
Cr
Fe
Video
Camera 1
Camera 2
Crosshair
LED:
Laser:
Date/Time: 7/27/2011 12:49:59 PM
User: Administrator
Anode: Rh
Filter: No filter
Optic: Collimator 1.500
Atmosphere: Air
Voltage: 50 kV
Current: 700 µA
Live time: 60 s
Pulse density: 1768 cps

Mid-Yellow

Bright Field, 100x

Dark Field, 100x

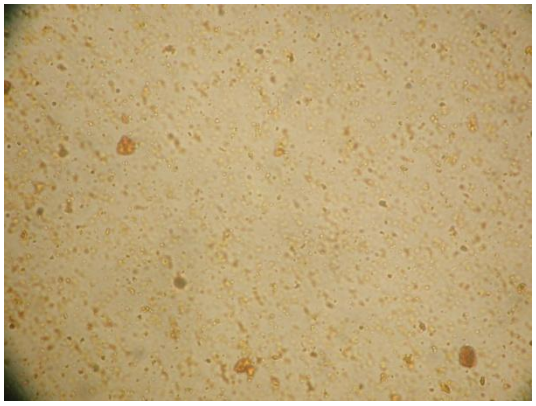

In RI 1.550, 400x

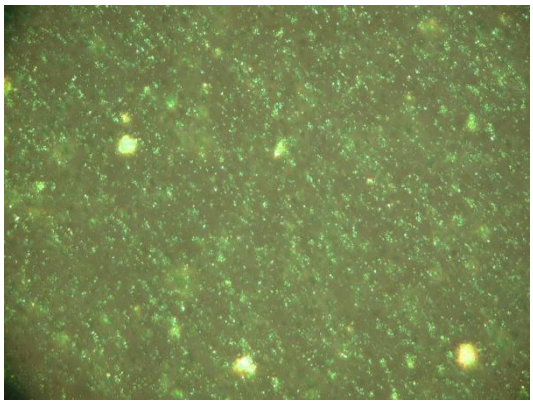

Crossed Polars, In RI 1.550, 400x

Normal Raman, 488nm

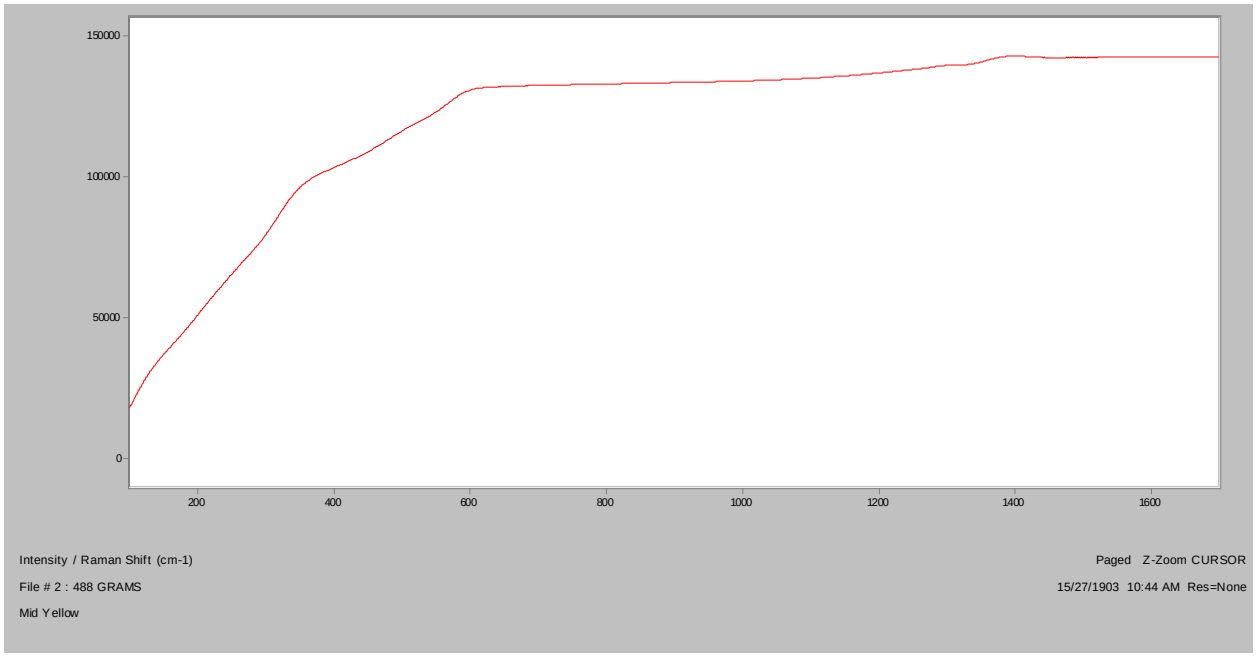

Normal Raman, 633nm

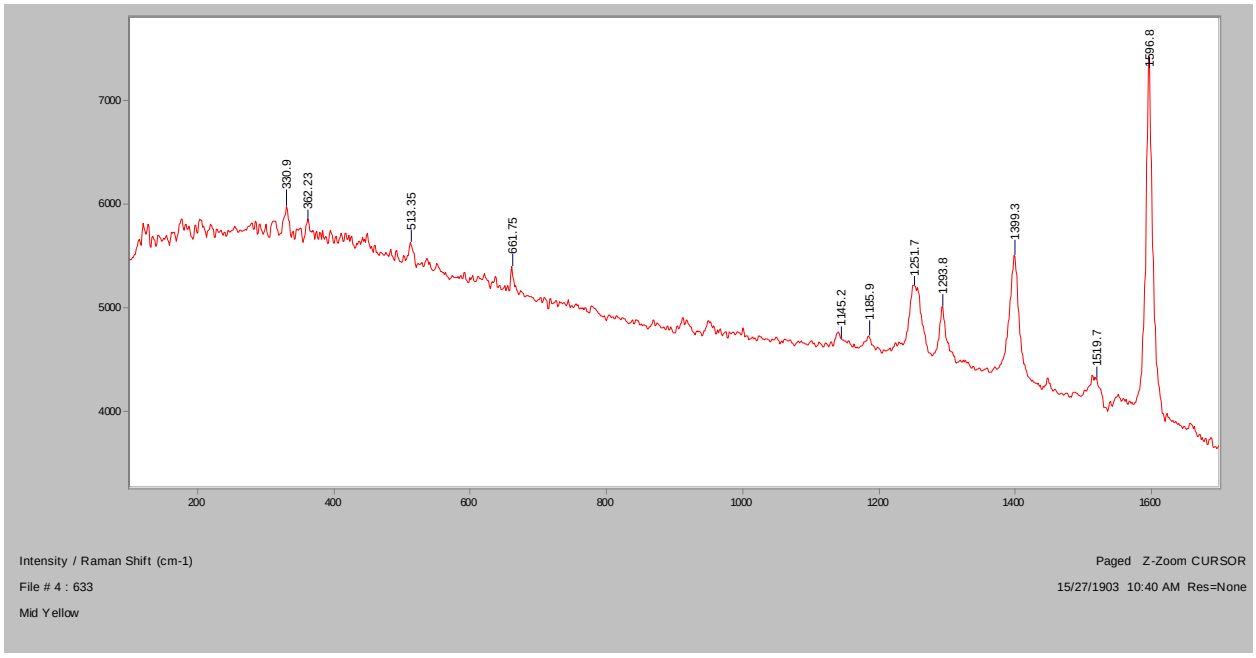

Normal Raman, 785nm

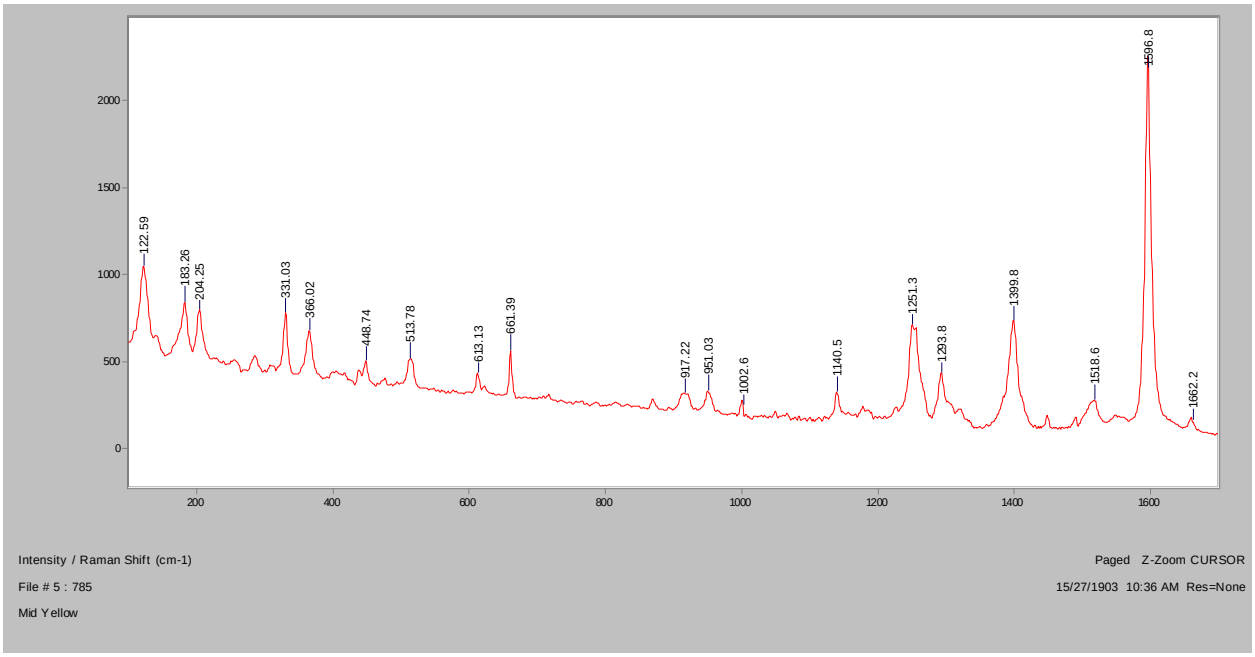

FT-Raman, 1064nm

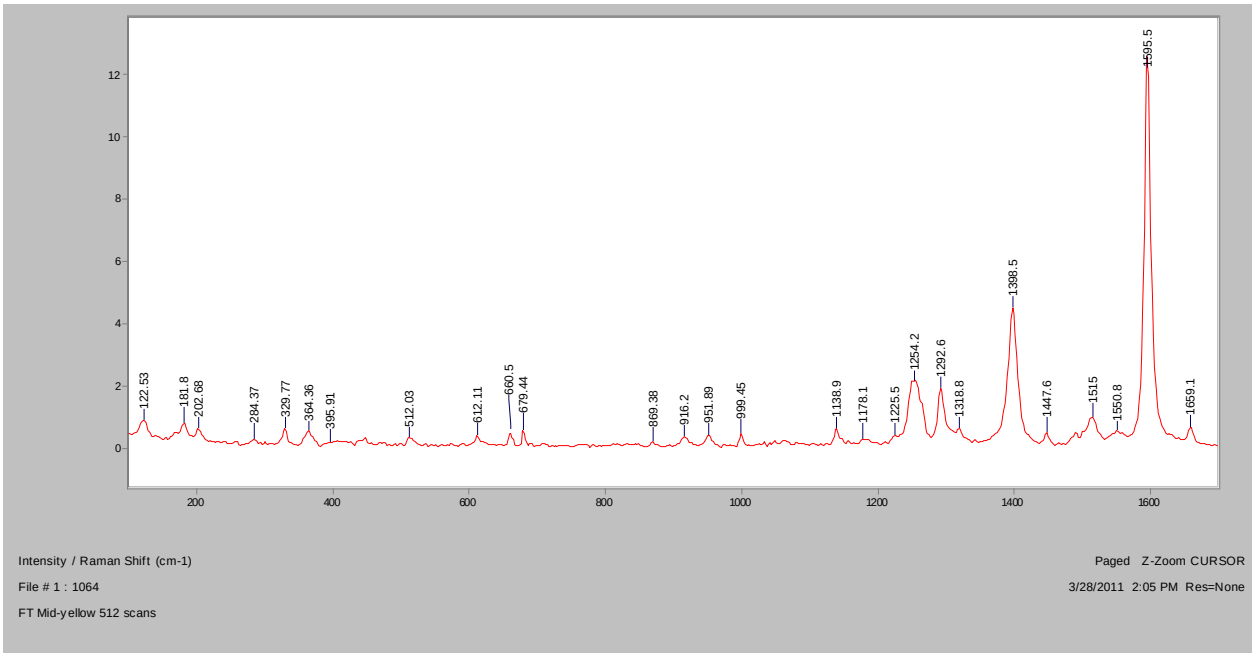

FT-IR (ATR)

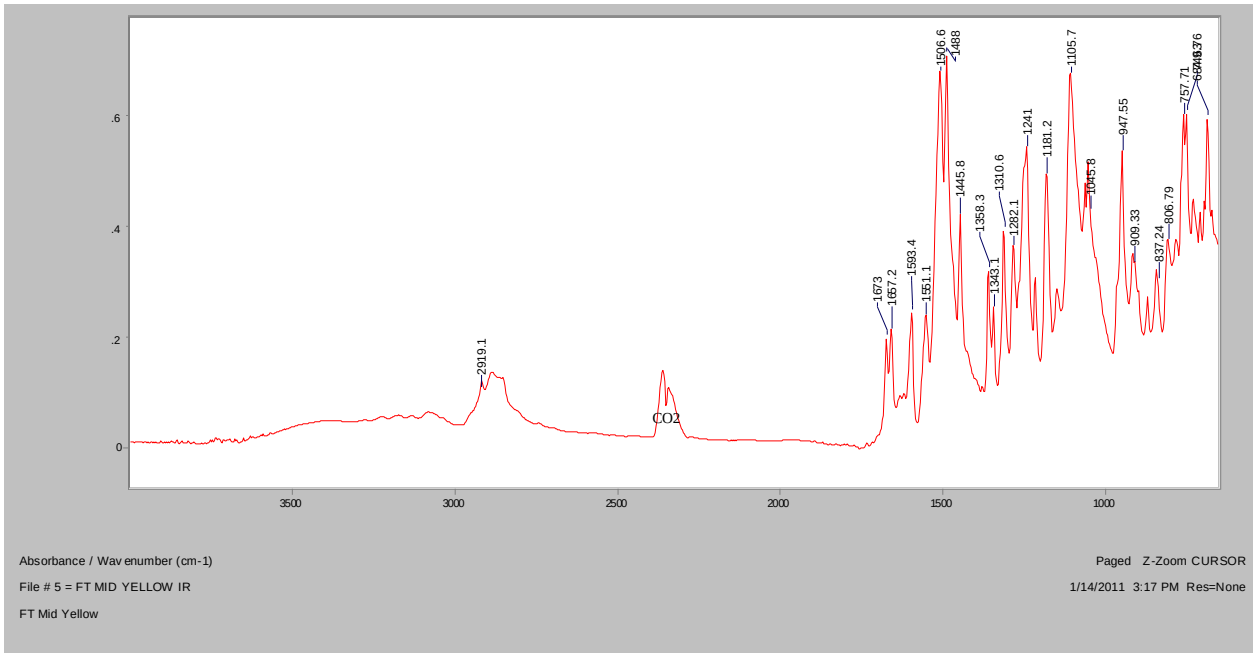
2919.1
CO2
1673
1657.2
1593.4
1551.1
1506.6
1488
1445.8
1358.3
1343.1
1310.6
1282.1
1241
1181.2
1105.7
1045.8
947.55
909.33
837.24
806.79
757.71
3500
3000
2500
2000
1500
1000
Absorbance / Wavenumber (cm-1)
File # 5 = FT MID YELLOW IR
FT Mid Yellow
Paged Z-Zoom CURSOR
1/14/2011 3:17 PM Res=None

XRF

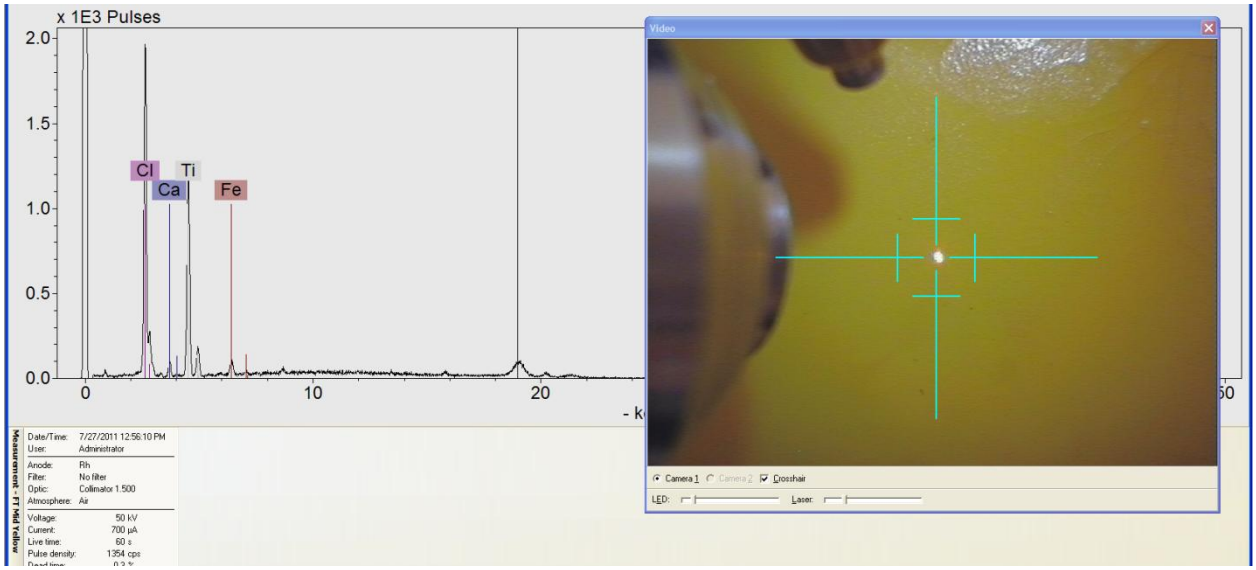
x 1E3 Pulses
Cl
Ti
Ca
Fe
Video
Camera 1
Crosshair
LED:
Laser:
Date/Time: 7/27/2011 12:56:10 PM
User: Administrator
Anode: Rh
Filter: No filter
Optic: Collimator 1.500
Atmosphere: Air
Voltage: 50 kV
Current: 700 µA
Live time: 60 s
Pulse density: 1354 cps

Yellow

Bright Field, 100x

Dark Field, 100x

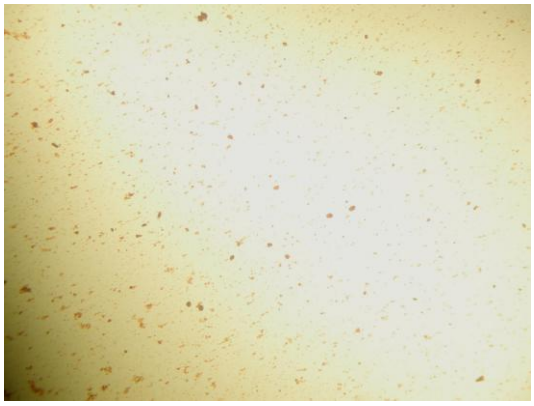

In RI 1.550, 400x

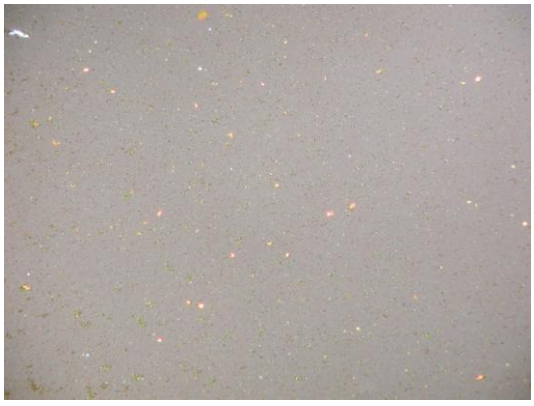

Crossed Polars, In RI 1.550, 400x

Normal Raman, 488nm

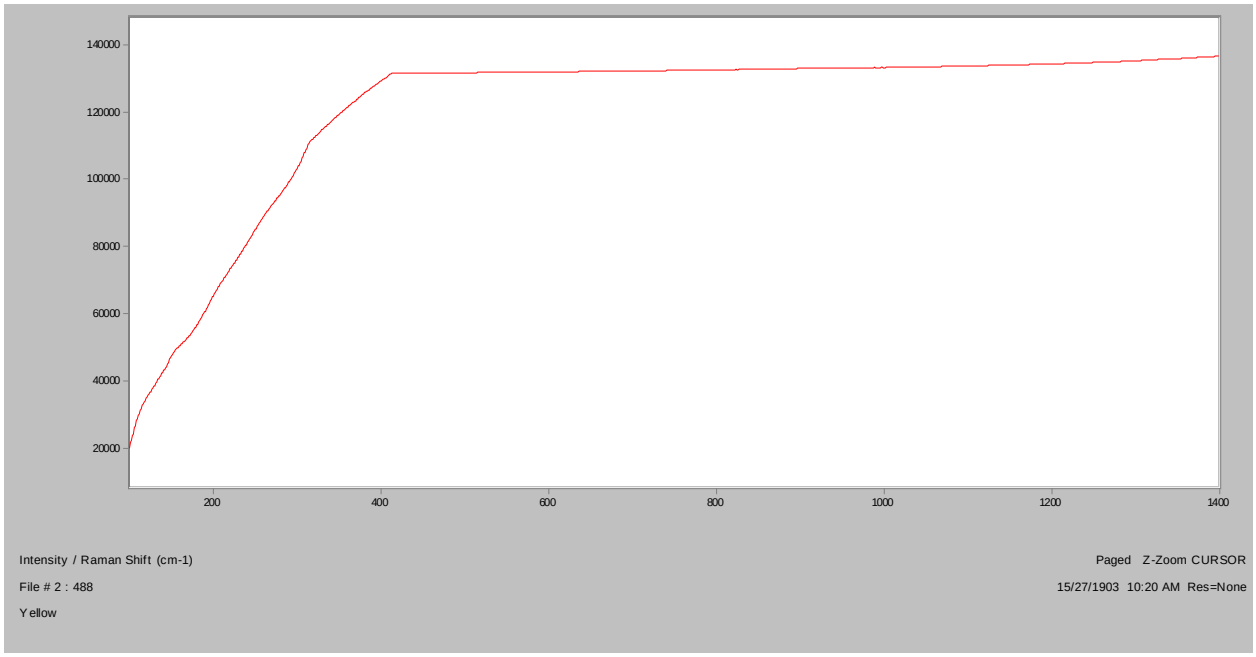

Normal Raman, 633nm

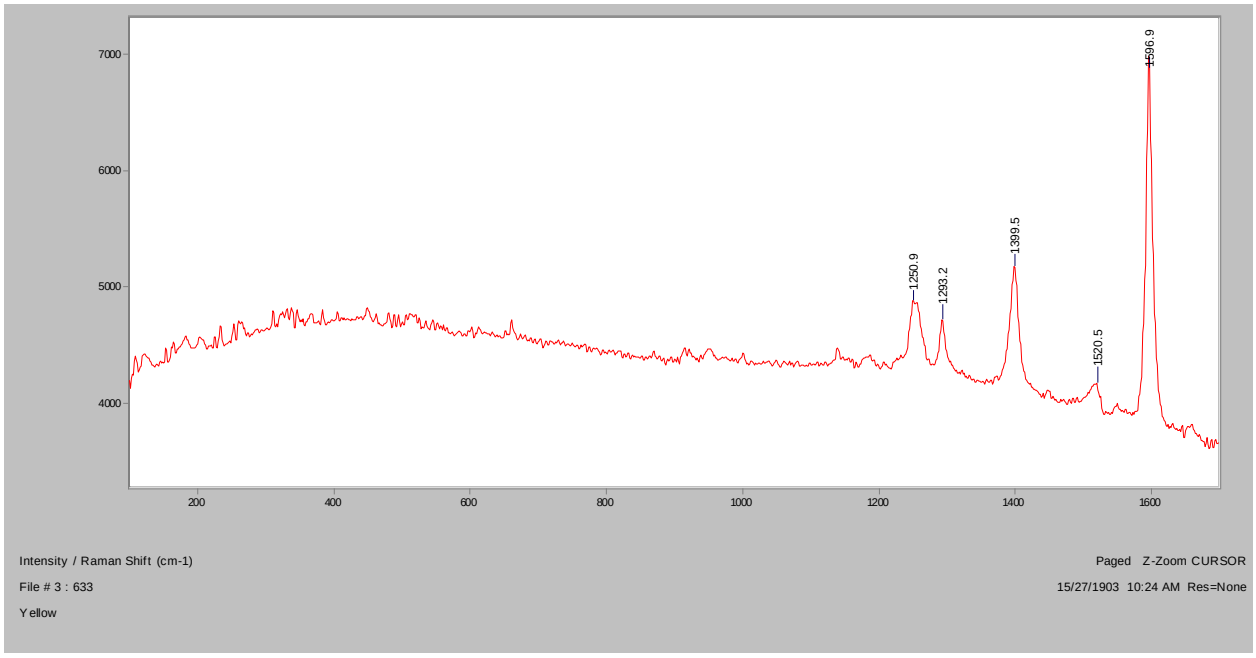

Normal Raman, 785nm

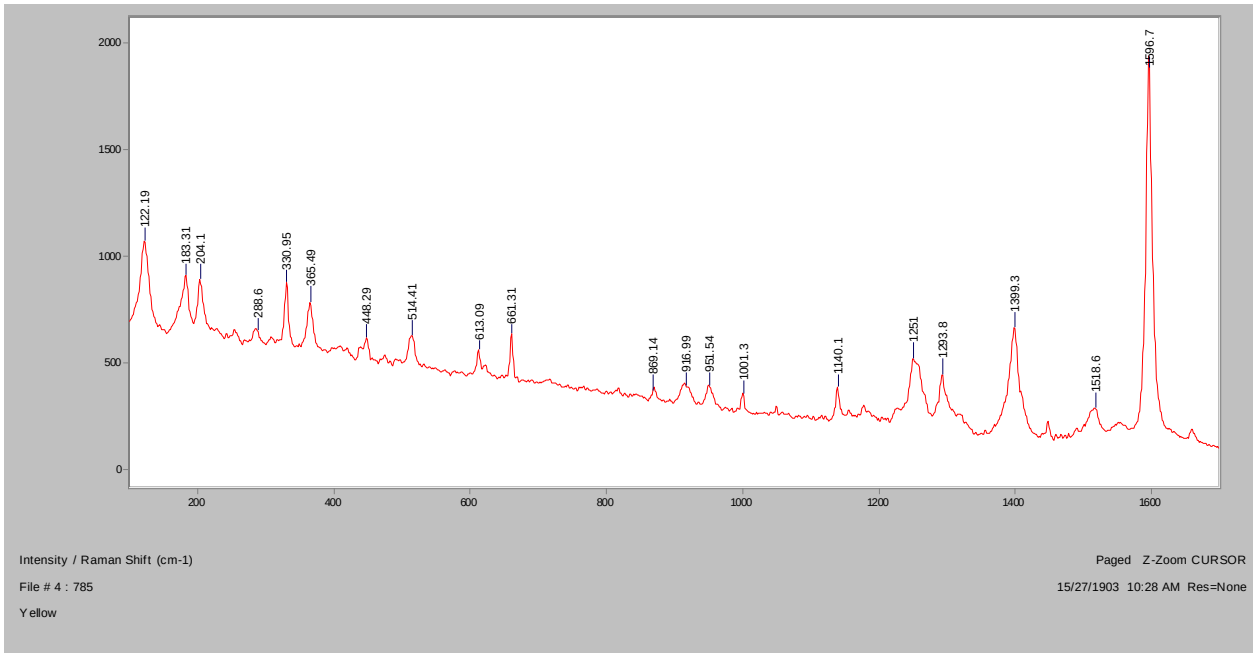

FT-Raman, 1064nm

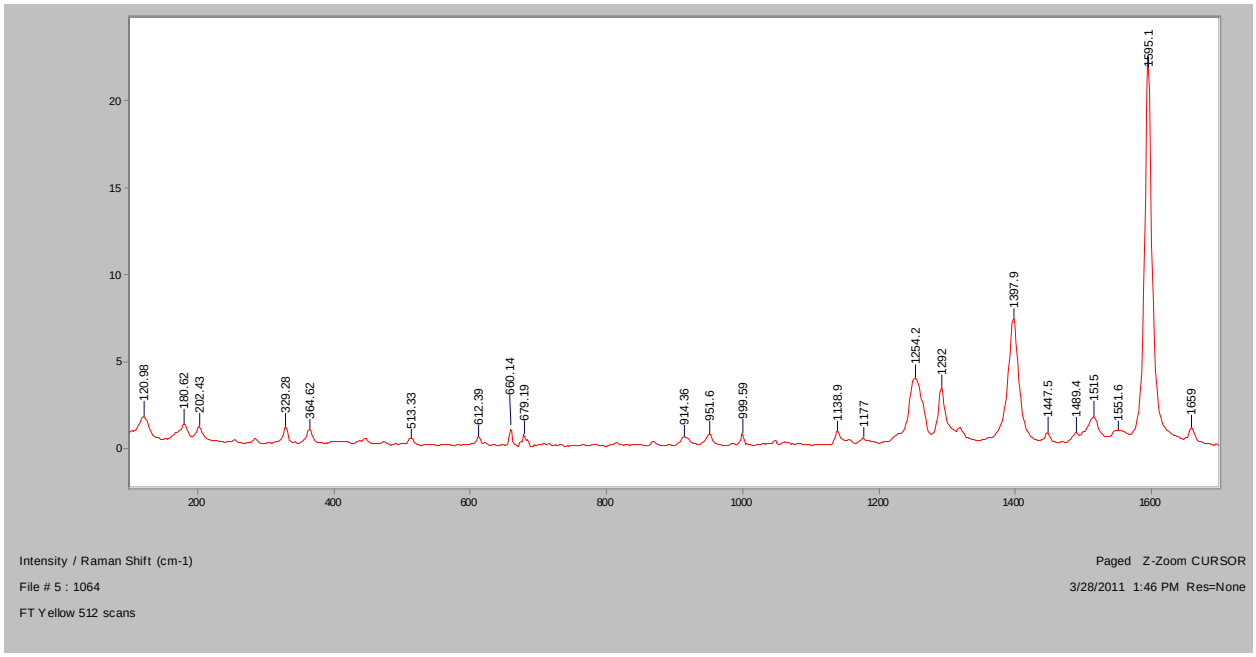

FT-IR (ATR)

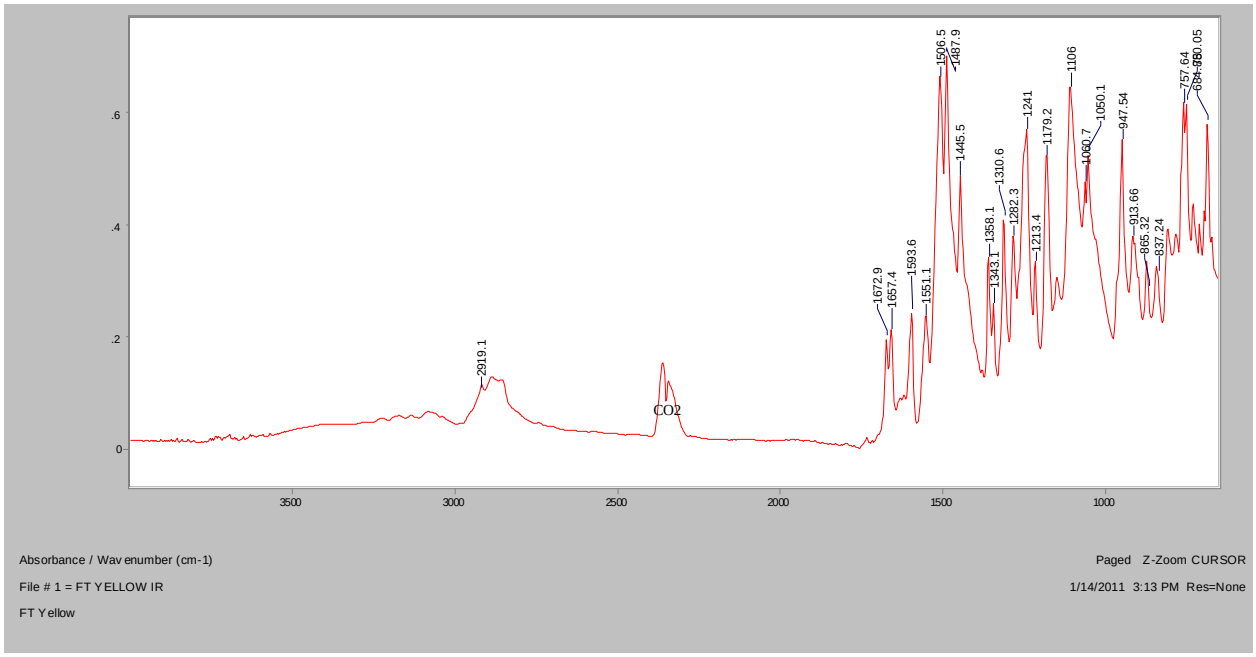
2919.1
CO2
1672.9
1657.4
1593.6
1551.1
1506.5
1497.9
1445.5
1358.1
1343.1
1310.6
1282.3
1241
1213.4
1179.2
1106
1060.7
1050.1
947.54
913.66
865.32
837.24
757.64
684.05
.6
.4
.2
0
3500
3000
2500
2000
1500
1000
Absorbance / Wavenumber (cm-1)
File # 1 = FT YELLOW IR
FT Yellow
Paged Z-Zoom CURSOR
1/14/2011 3:13 PM Res=None

XRF

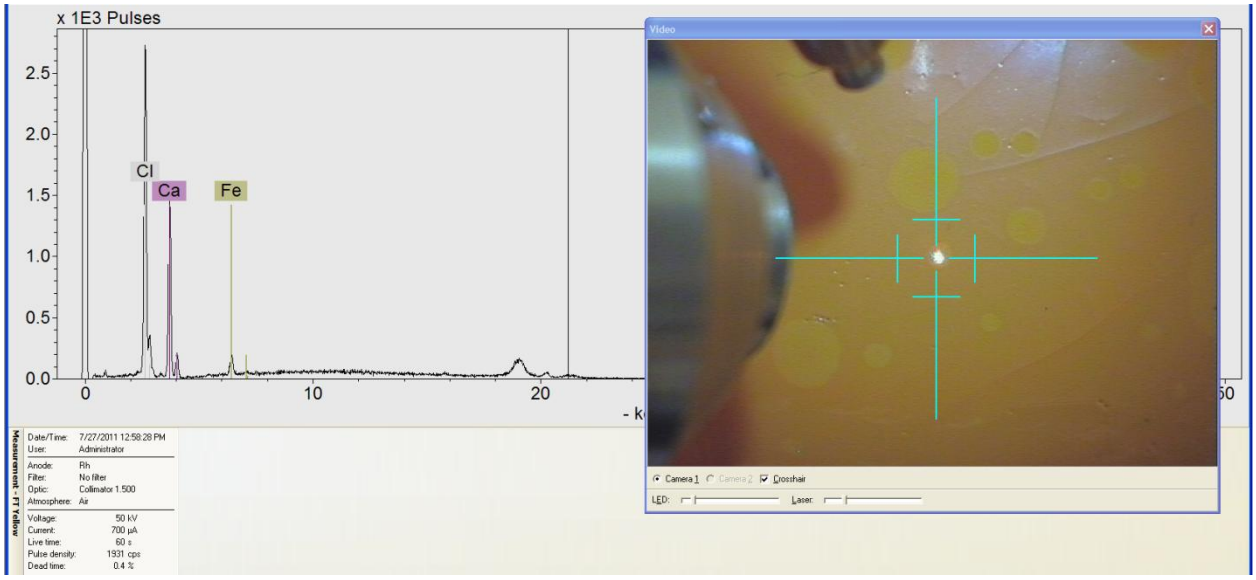
x 1E3 Pulses
2.5
2.0
1.5
1.0
0.5
0.0
0
10
20
Cl
Ca
Fe
Video
Camera 1
Camera 2
Crosshair
LED:
Laser:
Date/Time: 7/27/2011 12:58:28 PM
User: Administrator
Anode: Rh
Filter: No filter
Optic: Collimator 1.500
Atmosphere: Air
Voltage: 50 kV
Current: 700 µA
Live time: 60 s
Pulse density: 1931 cps
Dead time: 0.4 %

Golden Yellow

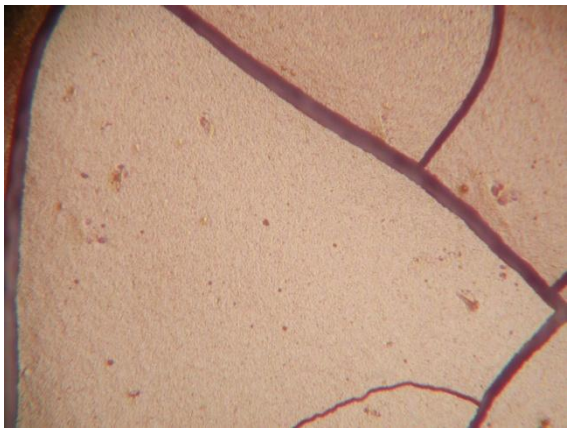

Bright Field, 100x

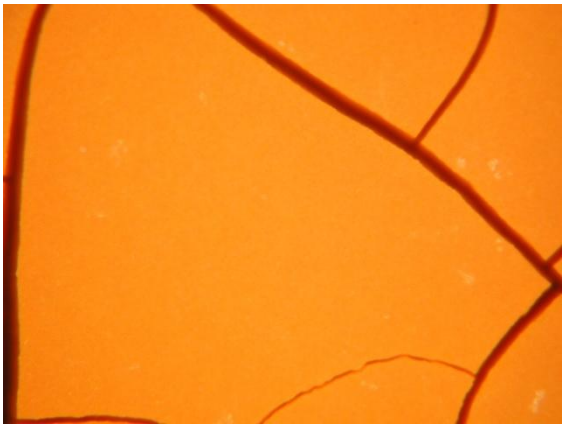

Dark Field, 100x

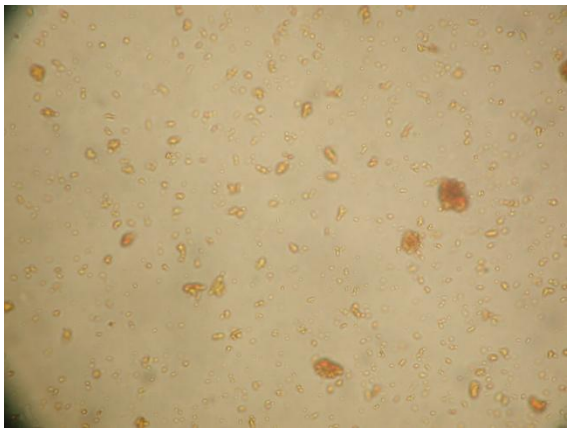

In RI 1.550, 400x

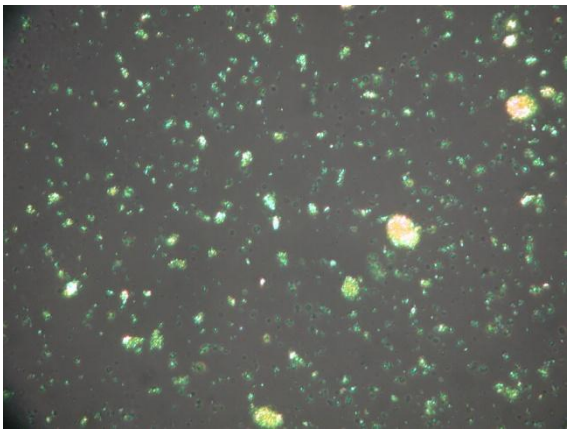

Crossed Polars, In RI 1.550, 400x

Normal Raman, 488nm

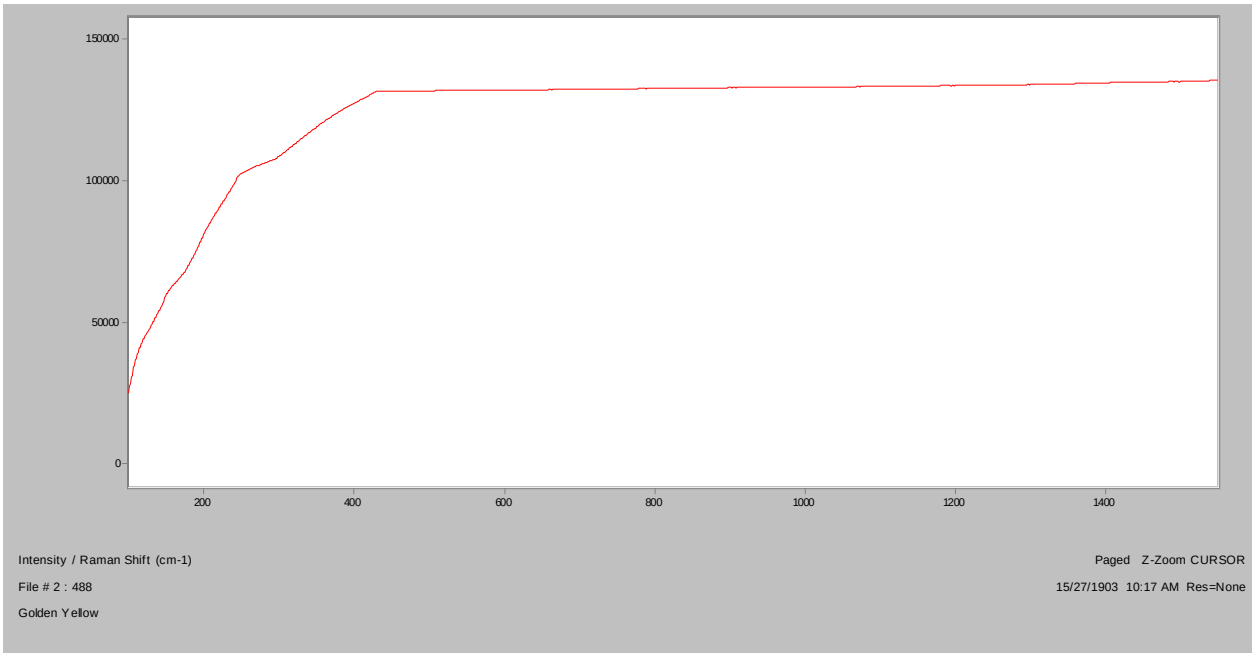

Normal Raman, 633nm

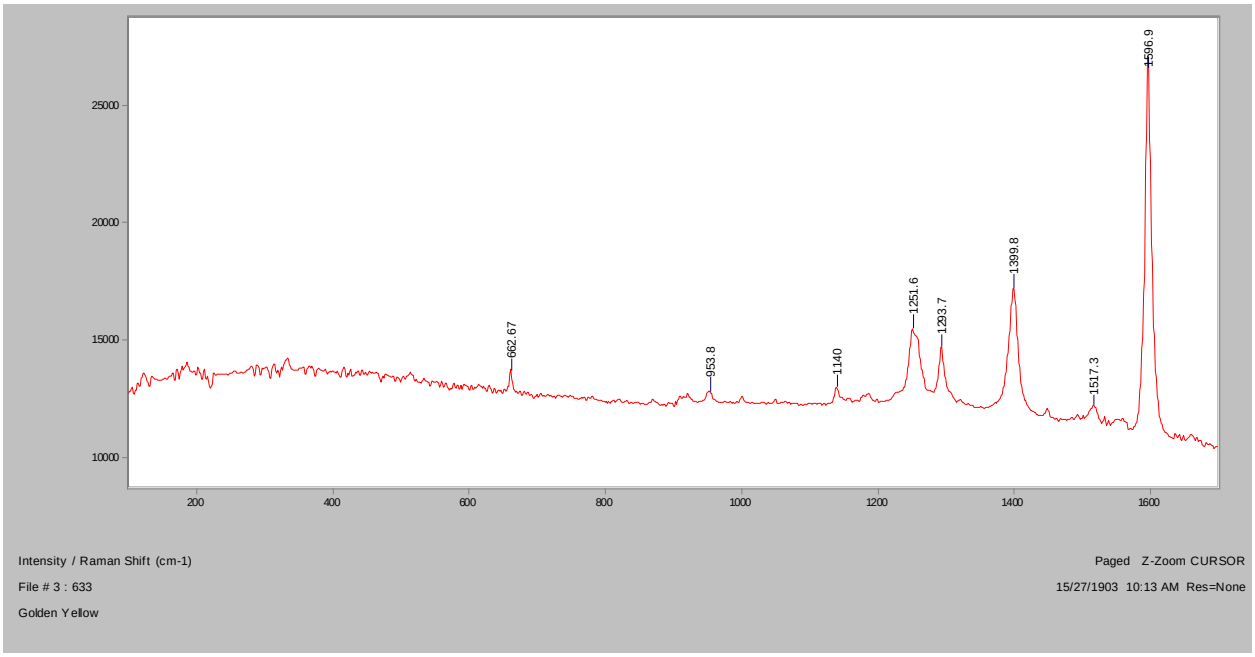

Normal Raman, 785nm

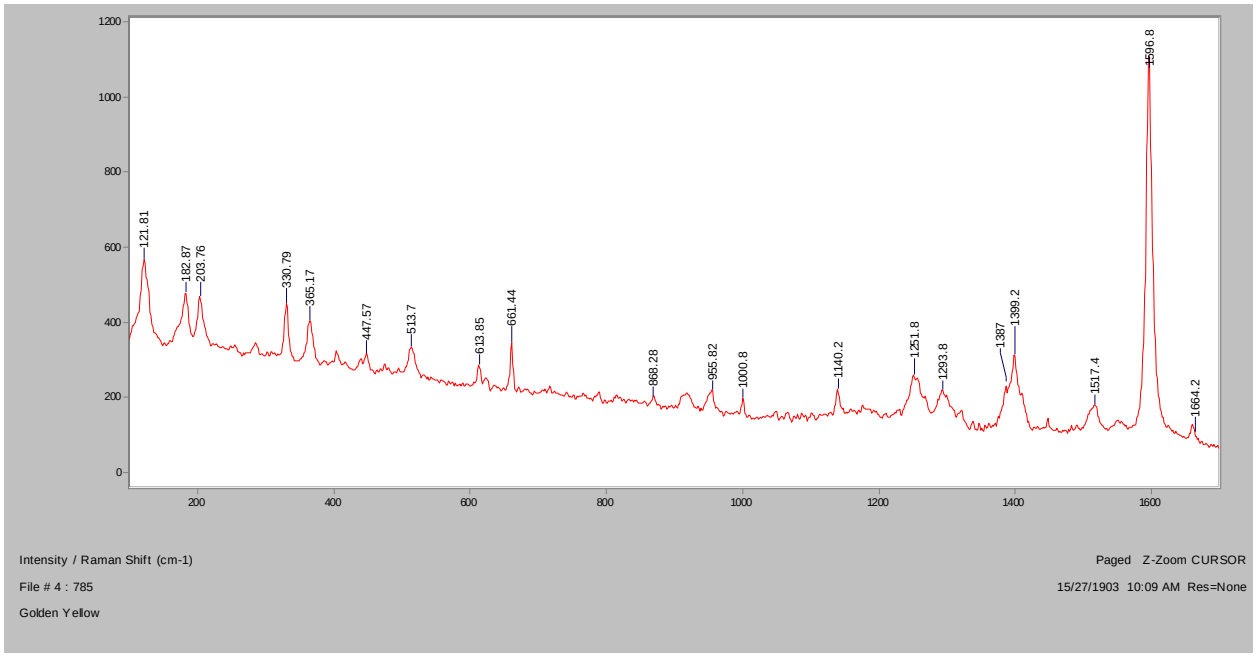

FT-Raman, 1064nm

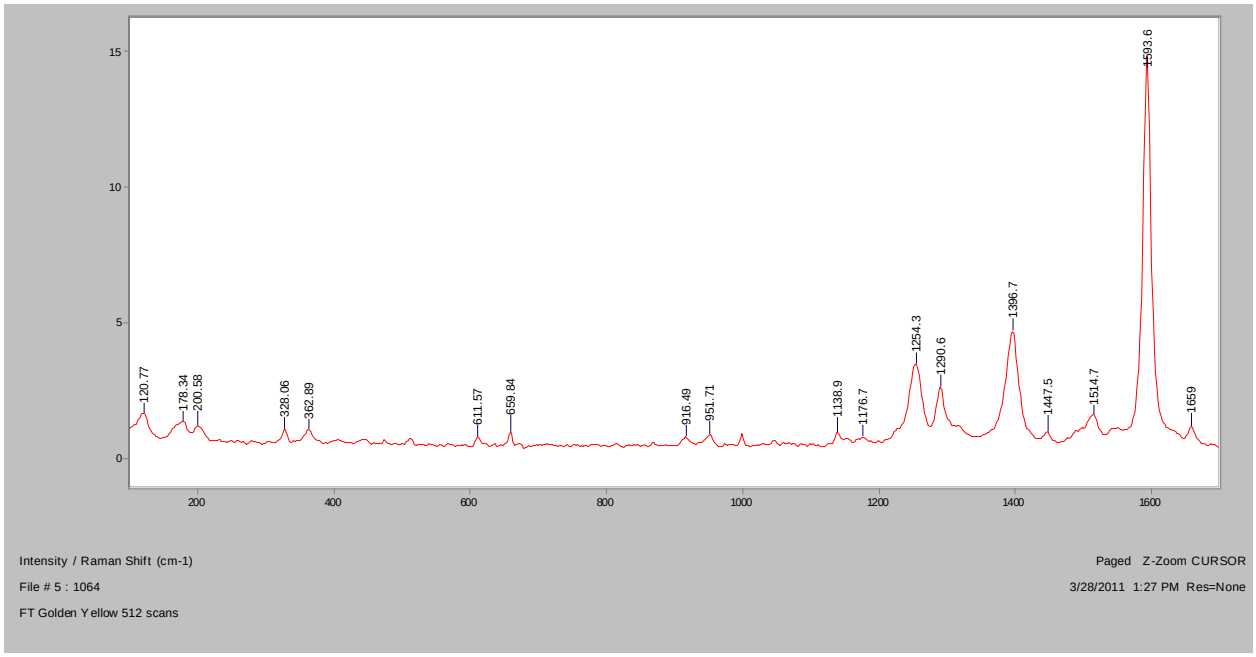

FT-IR (ATR)

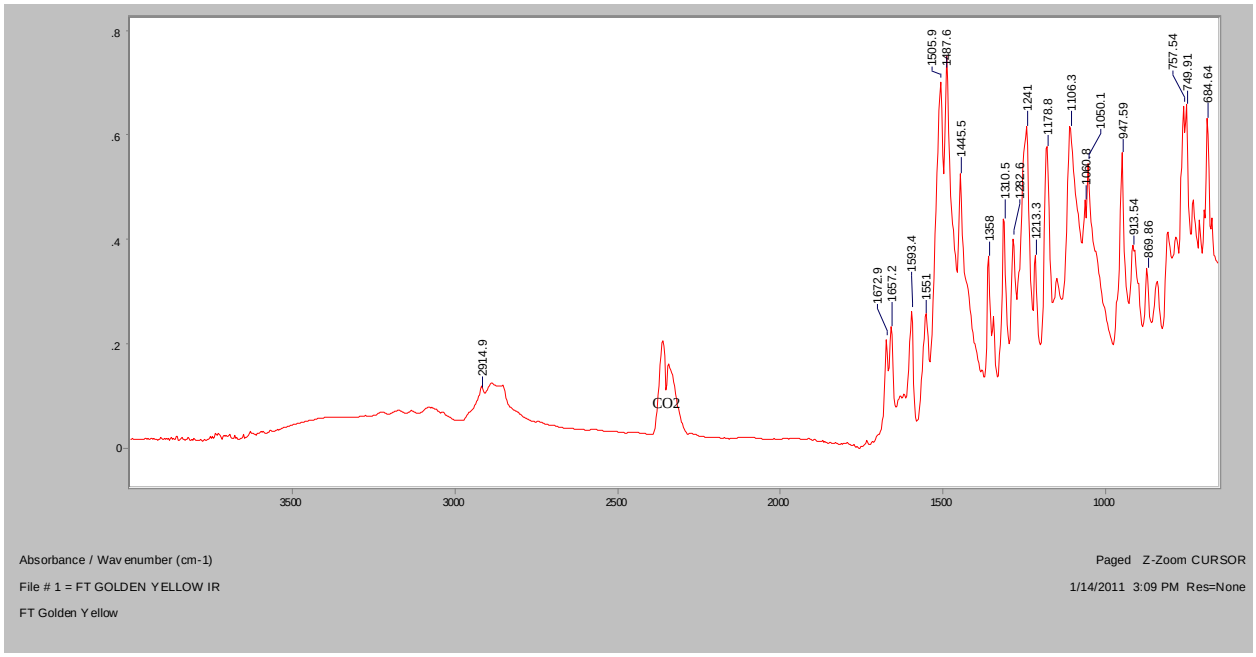
.8
.6
.4
.2
0
3500
3000
2500
2000
1500
1000
2914.9
CO2
1672.9
1657.2
1593.4
1551
1505.9
1487.6
1445.5
1358
1310.5
1282.6
1241
1213.3
1178.8
1106.3
1060.8
1050.1
947.59
913.54
869.86
757.54
749.91
684.64
Absorbance / Wavenumber (cm-1)
File # 1 = FT GOLDEN YELLOW IR
FT Golden Yellow
Paged Z-Zoom CURSOR
1/14/2011 3:09 PM Res=None

XRF

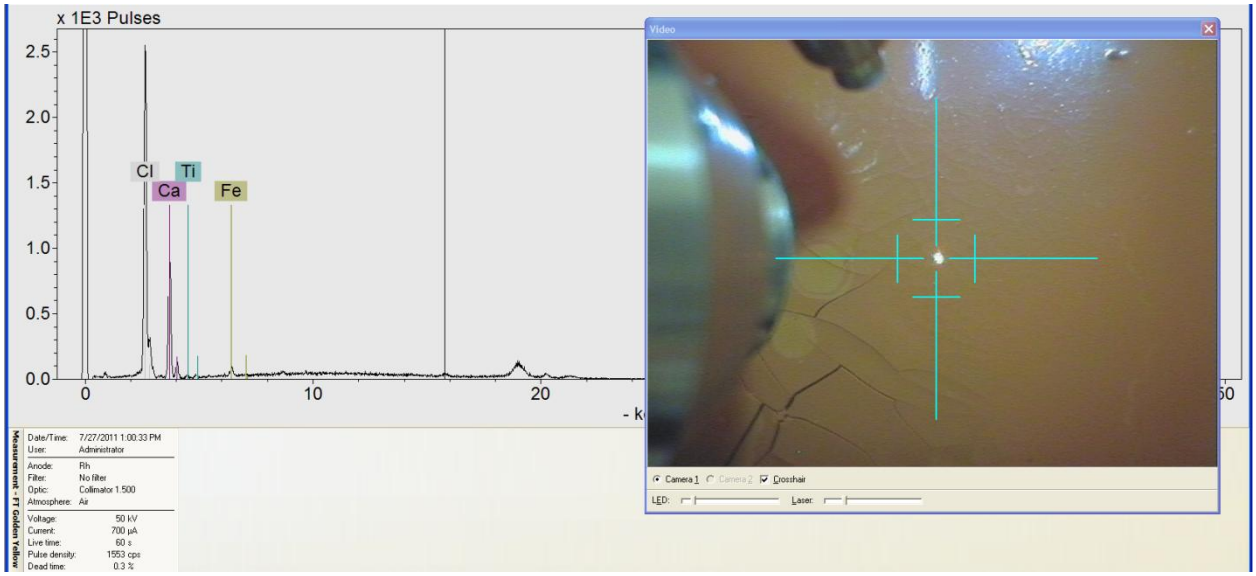
x 1E3 Pulses
2.5
2.0
1.5
1.0
0.5
0.0
0
10
20
Cl
Ti
Ca
Fe
Video
Camera 1
Camera 2
Crosshair
LED:
Laser:
Date/Time: 7/27/2011 1:00:33 PM
User: Administrator
Anode: Rh
Filter: No filter
Optic: Collimator 1.500
Atmosphere: Air
Voltage: 50 kV
Current: 700 µA
Live time: 60 s
Pulse density: 1553 cps
Dead time: 0.3 %

Khaki

Bright Field, 100x

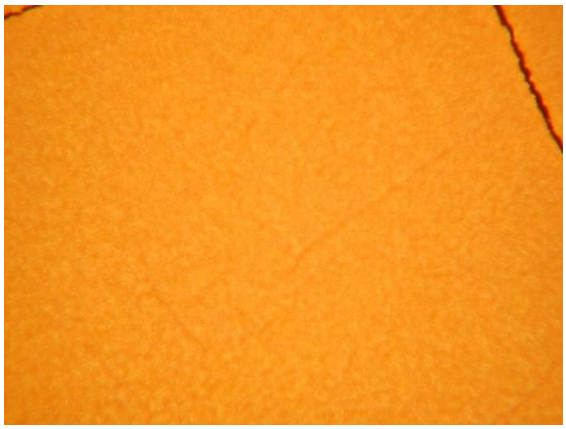

Dark Field, 100x

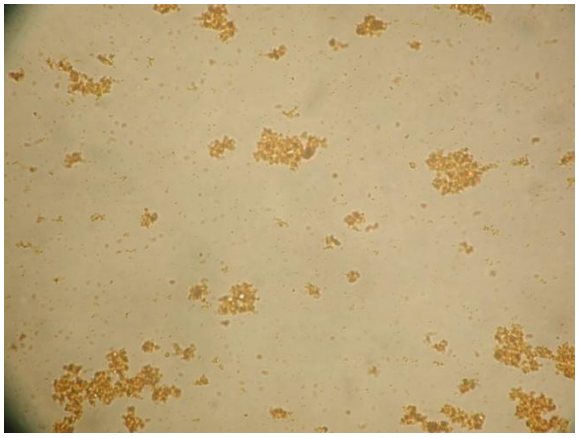

In RI 1.550, 400x

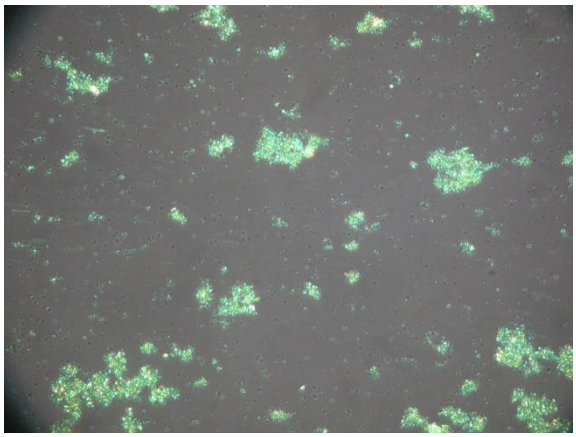

Crossed Polars, In RI 1.550, 400x

Normal Raman, 488nm

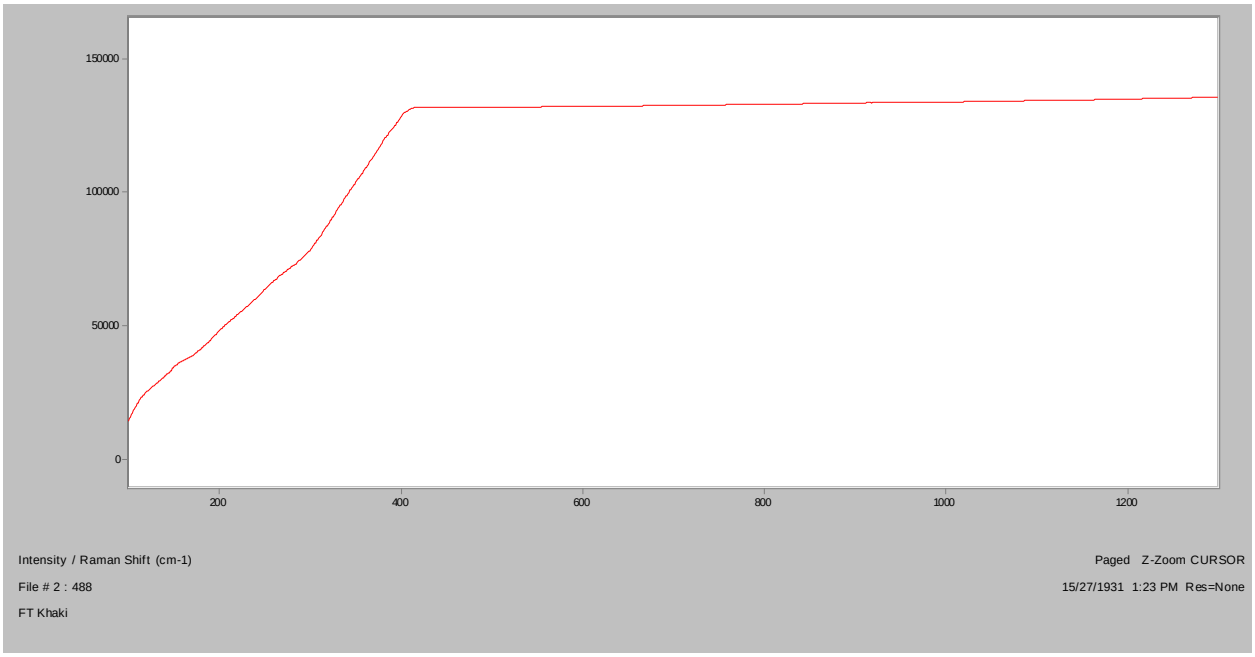

Normal Raman, 633nm

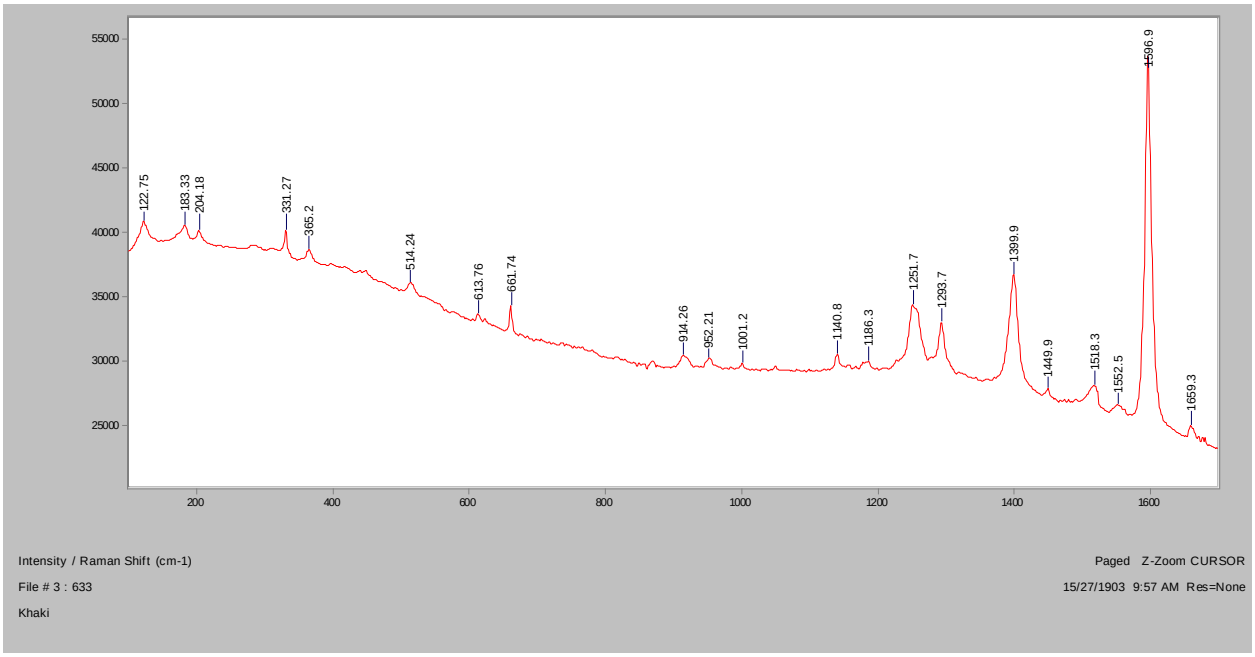

Normal Raman, 785nm

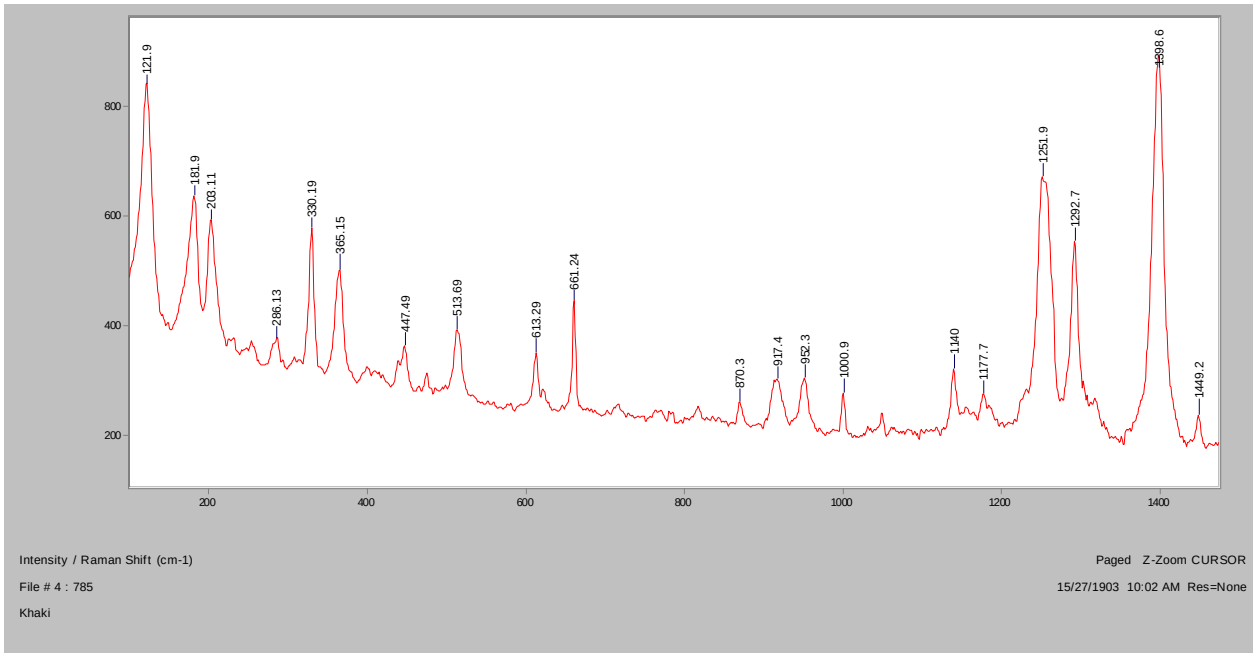

FT-Raman, 1064nm

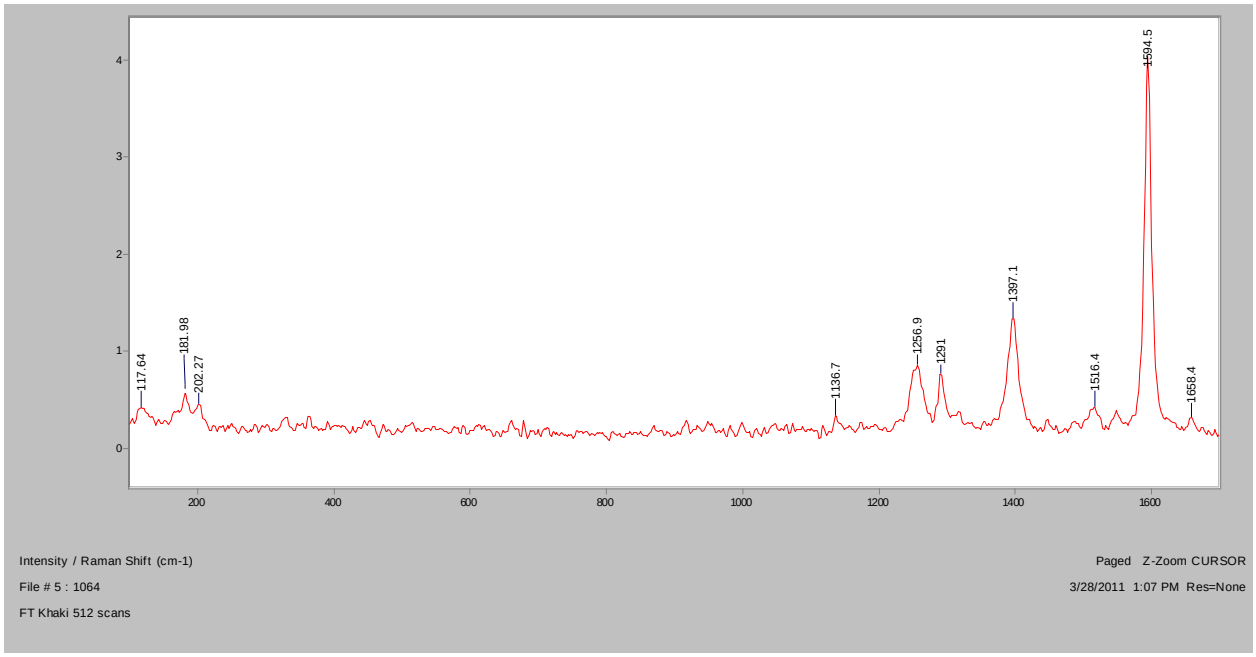

FT-IR (ATR)

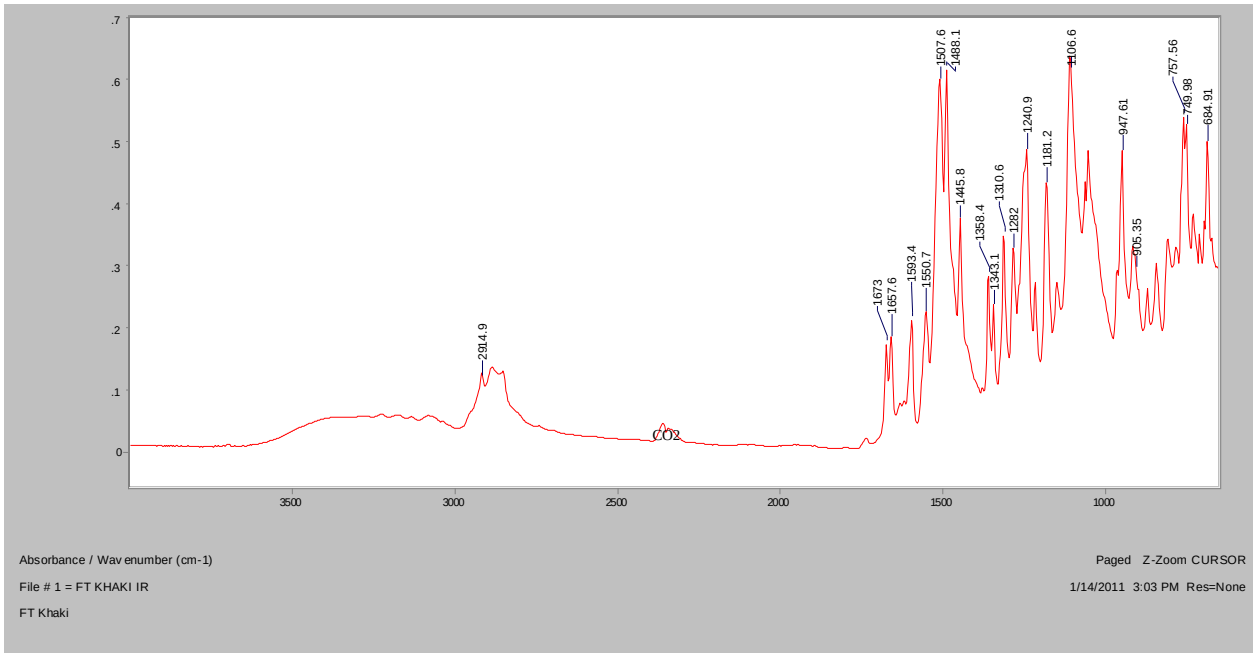
2914.9
CO2
1673
1657.6
1593.4
1550.7
1507.6
1488.1
1445.8
1358.4
1343.1
1310.6
1282
1240.9
1181.2
1106.6
947.61
905.35
757.56
749.98
684.91
3500
3000
2500
2000
1500
1000
Absorbance / Wavenumber (cm-1)
File # 1 = FT KHAKI IR
FT Khaki
Paged Z-Zoom CURSOR
1/14/2011 3:03 PM Res=None

XRF

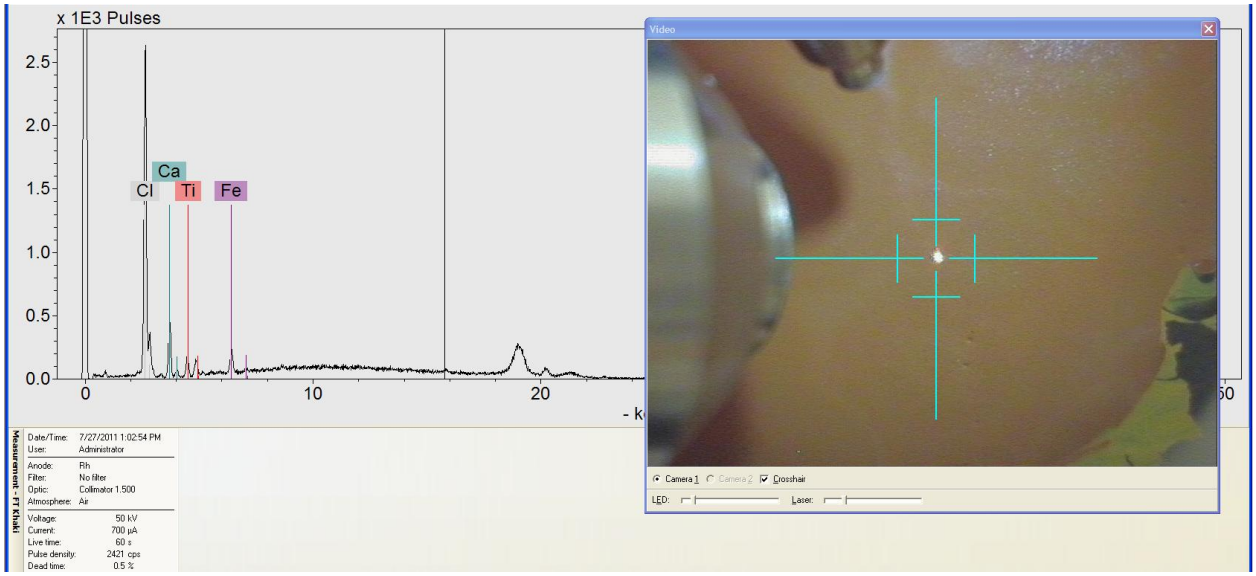
x 1E3 Pulses
Ca
Cl
Ti
Fe
Video
Camera 1
Camera 2
Crosshair
LED:
Laser:
Date/Time: 7/27/2011 1:02:54 PM
User: Administrator
Anode: Rh
Filter: No filter
Optic: Collimator 1.500
Atmosphere: Air
Voltage: 50 kV
Current: 700 µA
Live time: 60 s
Pulse density: 2421 cps
Dead time: 0.5 %

Grass Hopper

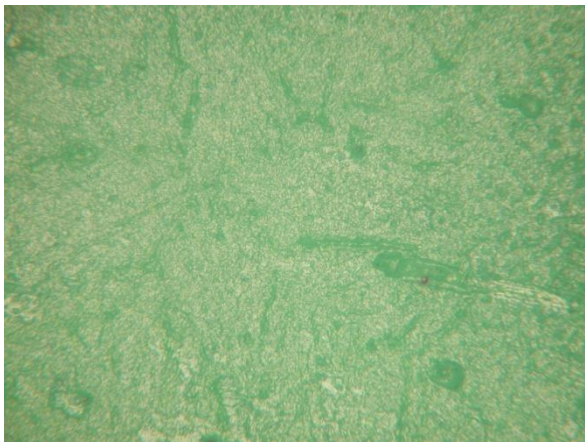

Bright Field, 100x

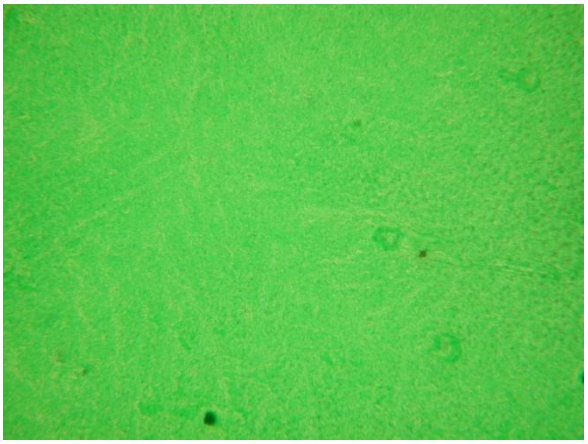

Dark Field, 100x

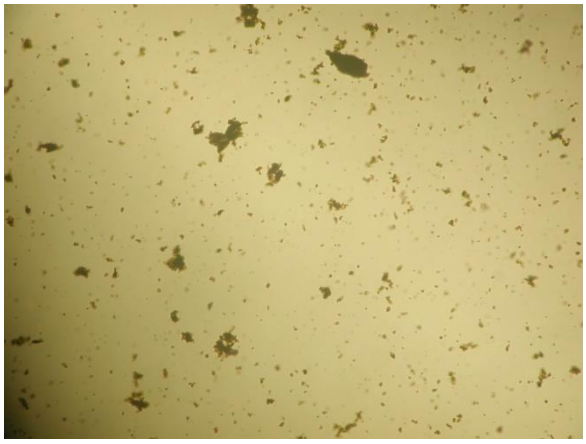

In RI 1.550, 200x

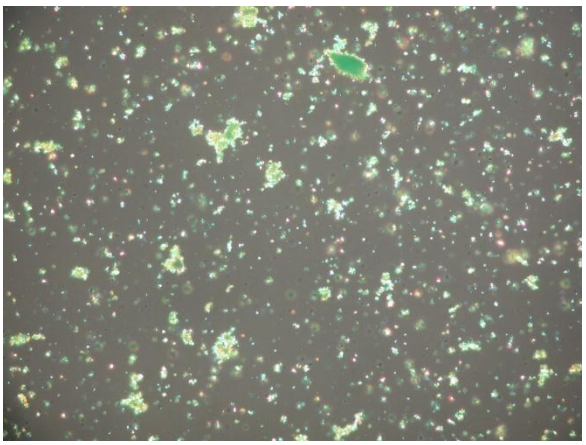

Crossed Polars, In RI 1.550, 200x

Normal Raman, 488nm

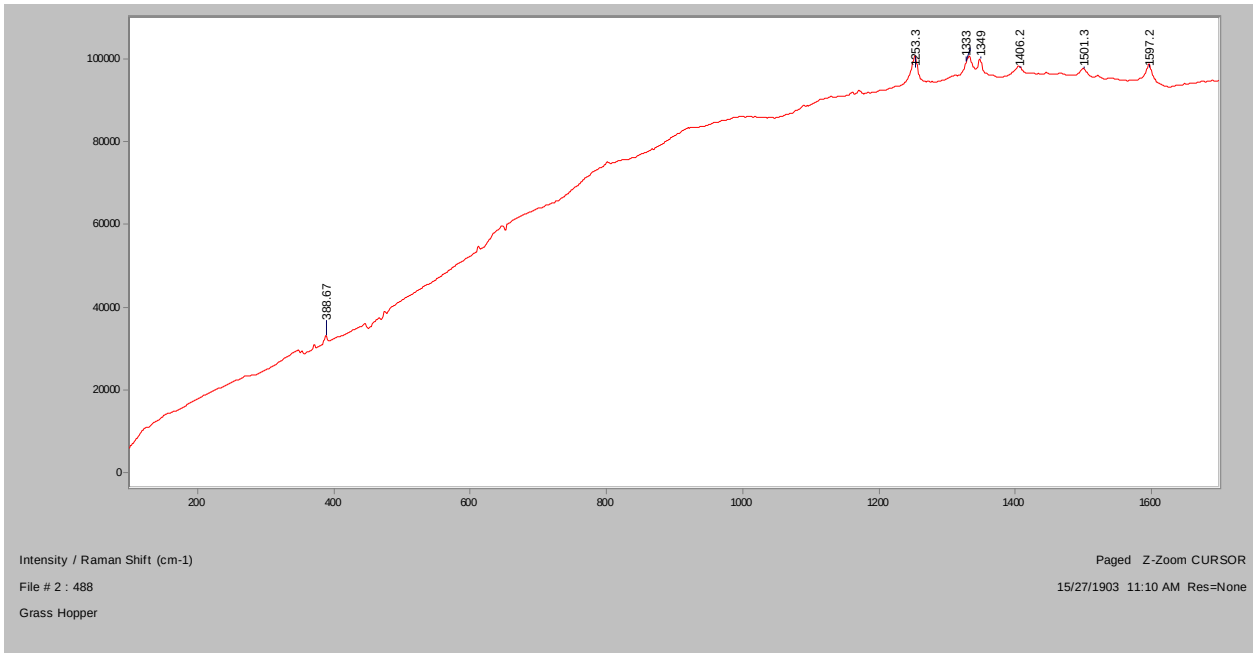

Normal Raman, 633nm

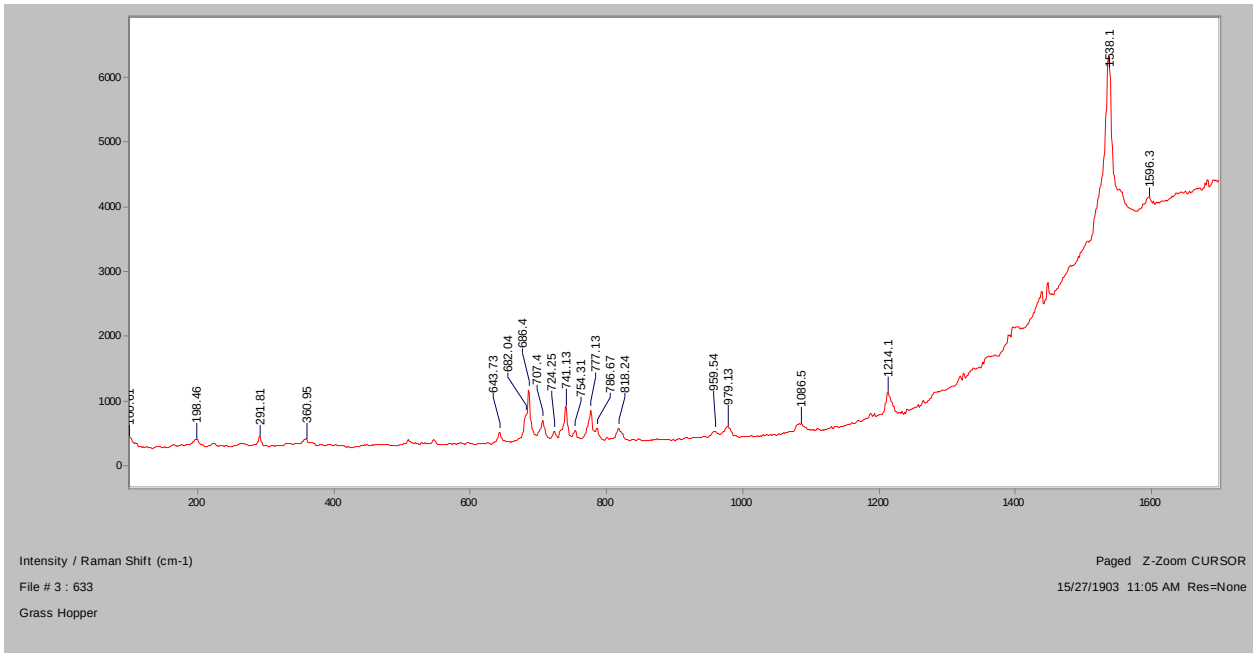

Normal Raman, 785nm

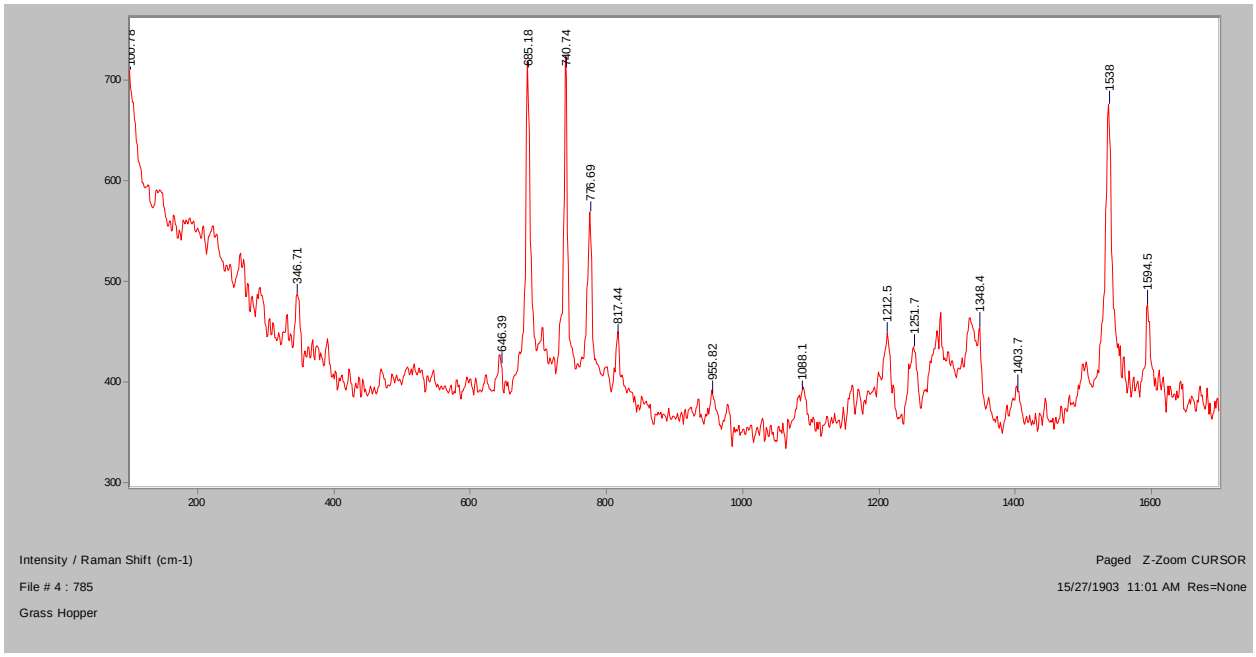

FT-Raman, 1064nm

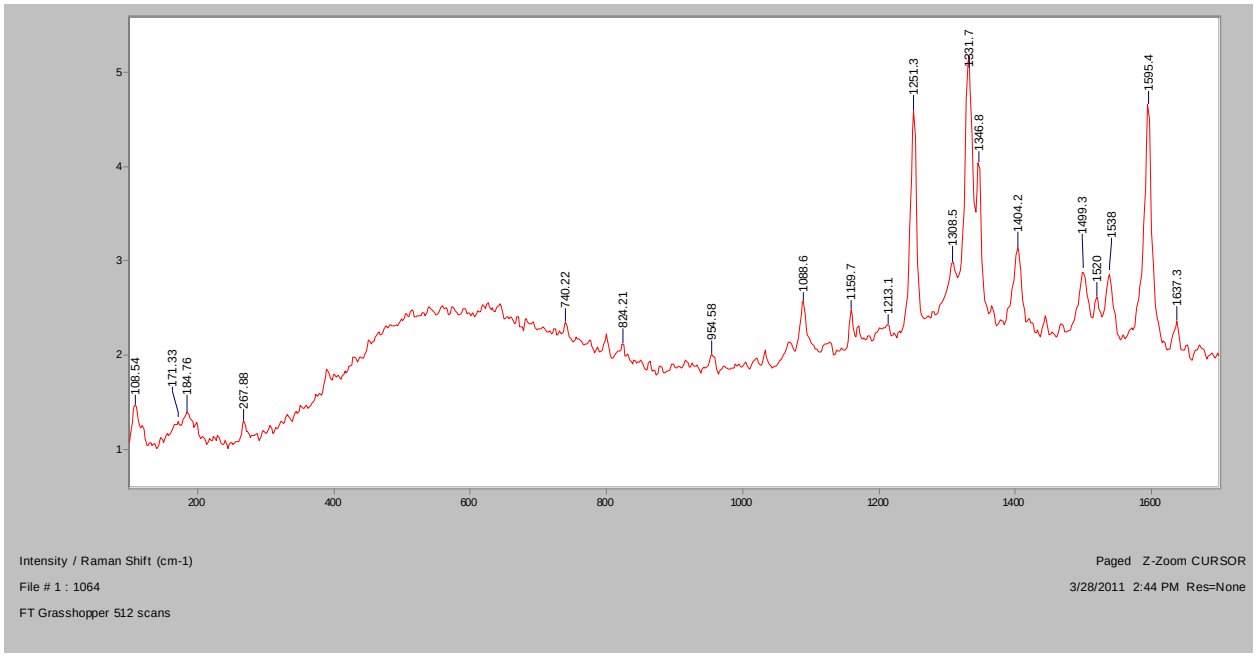

FT-IR (ATR)

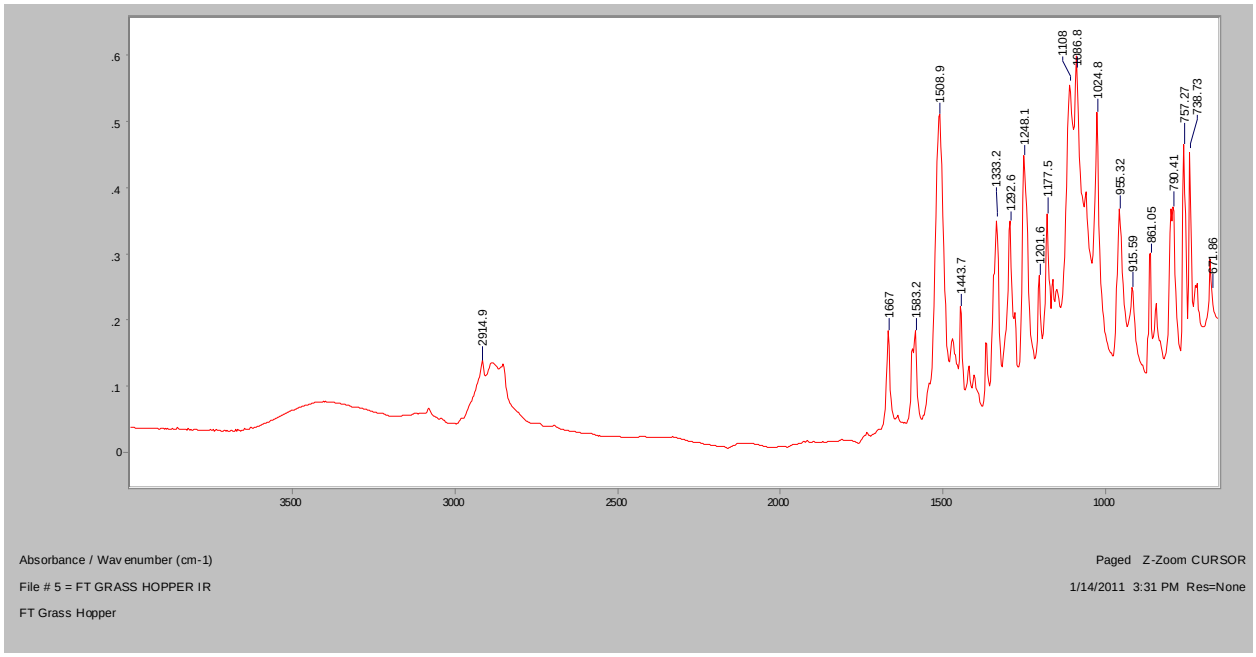
.6
.5
.4
.3
.2
.1
0
3500
3000
2500
2000
1500
1000
2914.9
1667
1583.2
1508.9
1443.7
1333.2
1292.6
1248.1
1201.6
1177.5
1108
1086.8
1024.8
955.32
915.59
861.05
790.41
757.27
738.73
671.86
Absorbance / Wavenumber (cm-1)
File # 5 = FT GRASS HOPPER IR
FT Grass Hopper
Paged Z-Zoom CURSOR
1/14/2011 3:31 PM Res=None

XRF

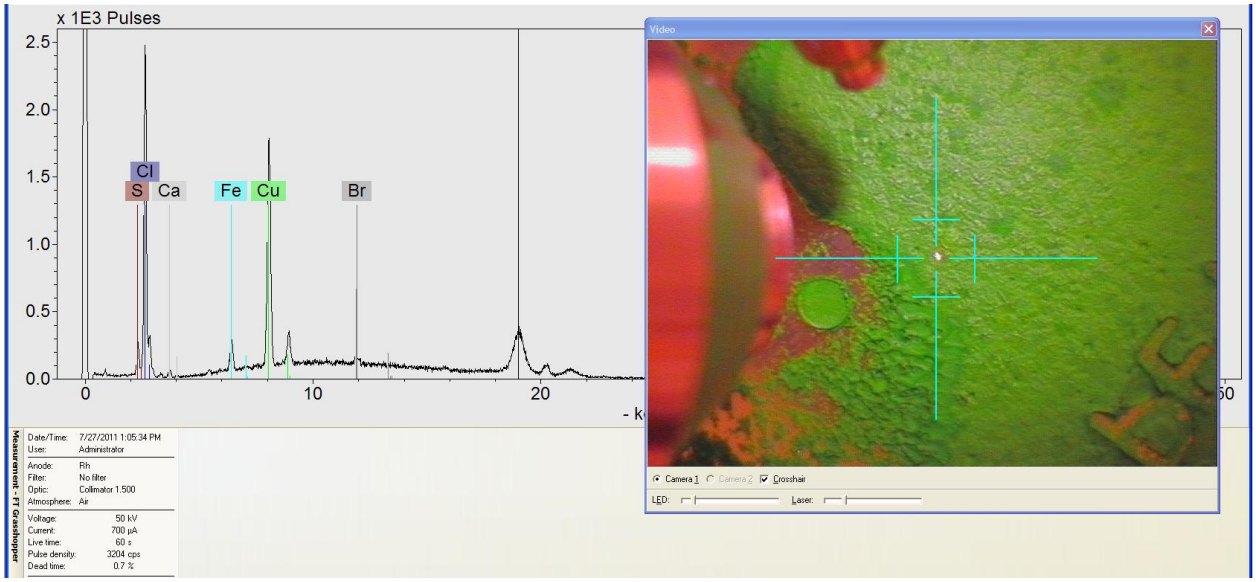
x 1E3 Pulses
2.5
2.0
1.5
1.0
0.5
0.0
0
10
20
Cl
S
Ca
Fe
Cu
Br
Video
Camera 1
Camera 2
Crosshair
LED:
Laser:
Date/Time: 7/27/2011 1:05:34 PM
User: Administrator
Anode: Rh
Filter: No filter
Optic: Collimator 1.500
Atmosphere: Air
Voltage: 50 kV
Current: 700 µA
Live time: 60 s
Pulse density: 3204 cps
Dead time: 0.7 %

Light Green

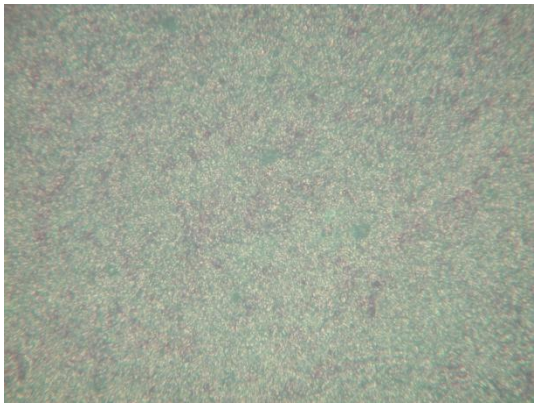

Bright Field, 100x

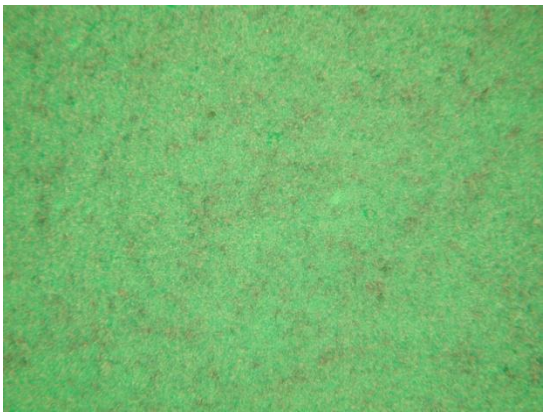

Dark Field, 100x

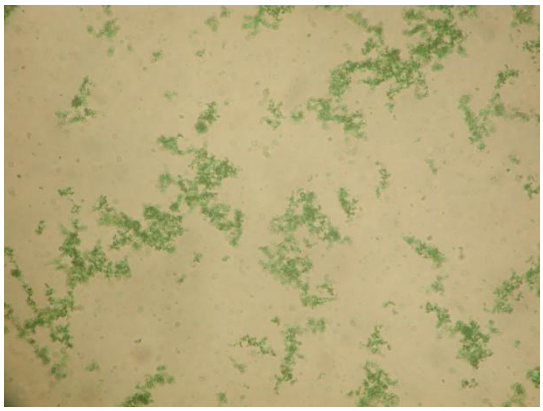

In RI 1.550, 400x

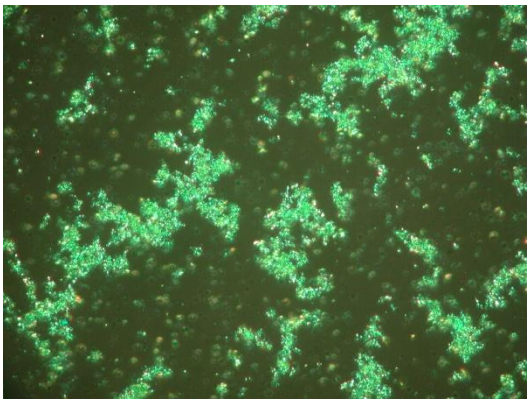

Crossed Polars, In RI 1.550, 400x

Normal Raman, 488nm

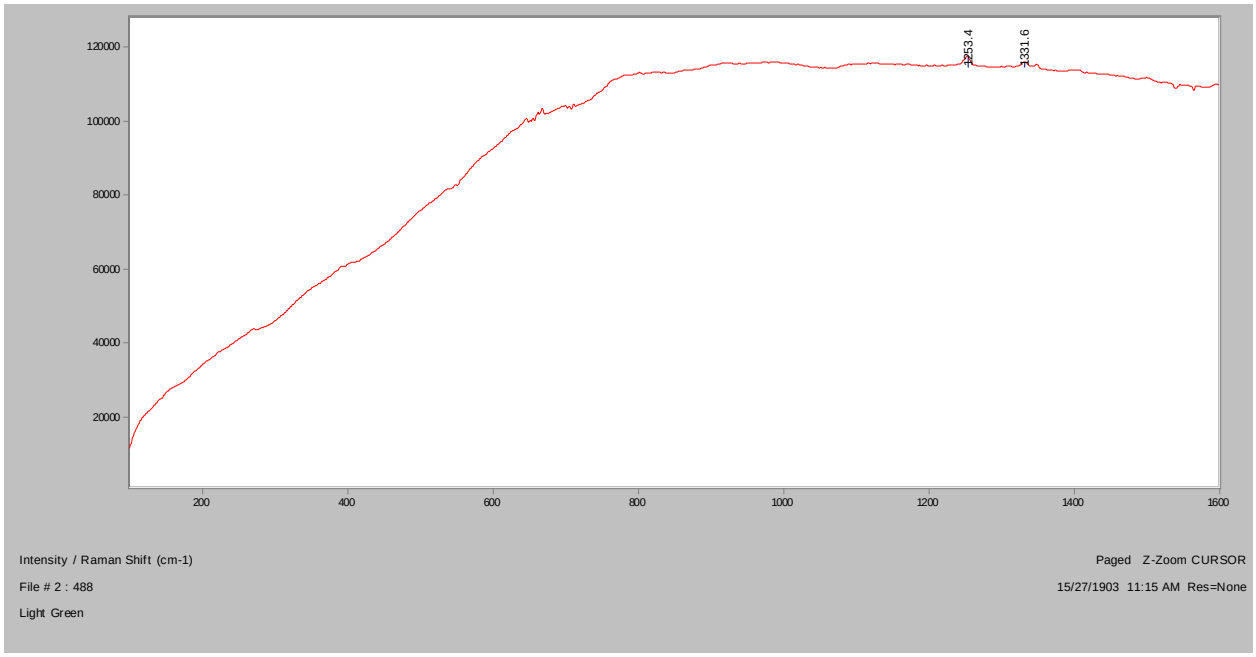

Normal Raman, 633nm

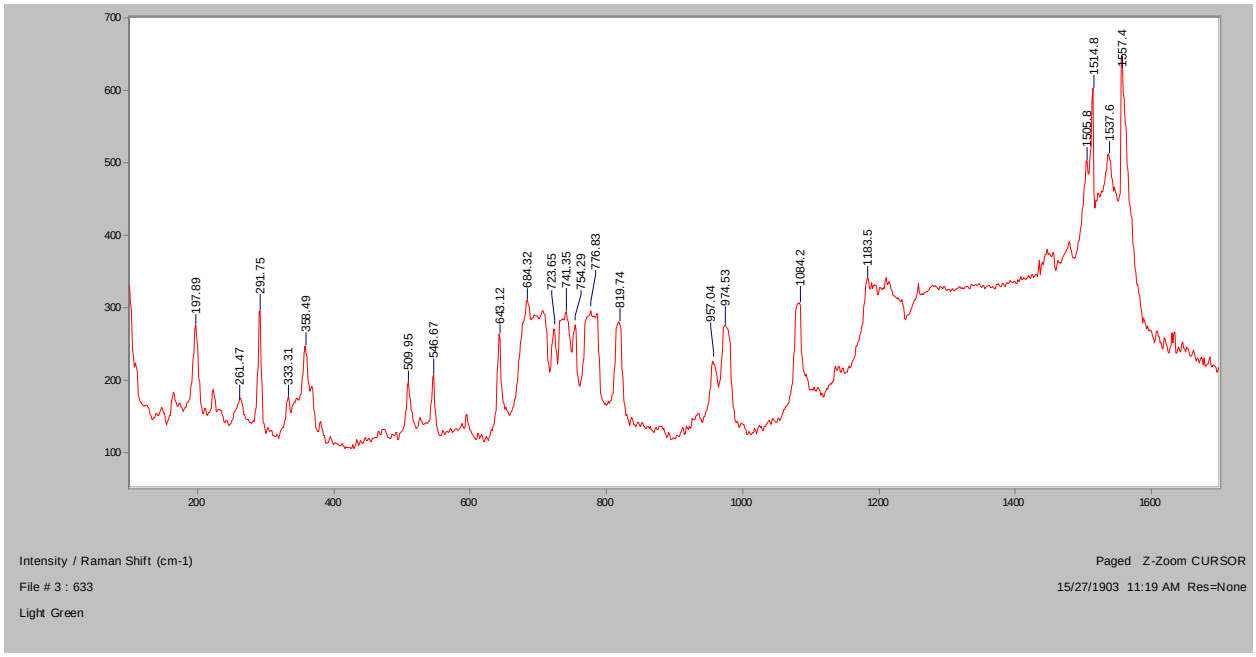

Normal Raman, 785nm

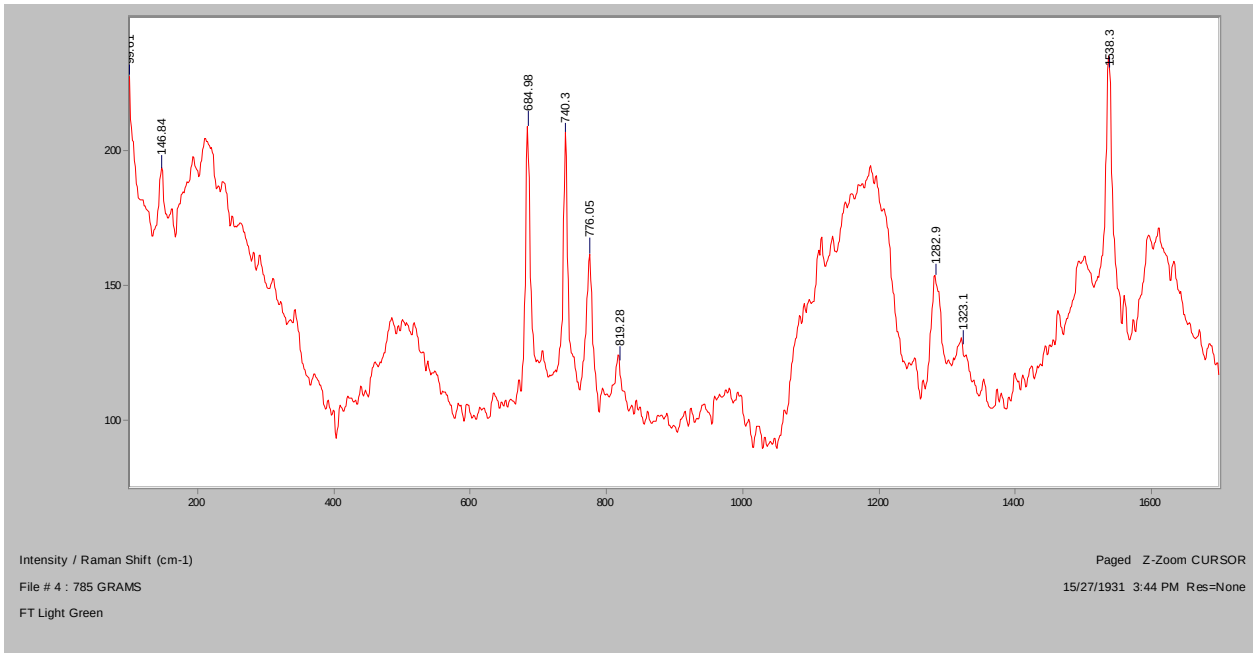

FT-Raman, 1064nm

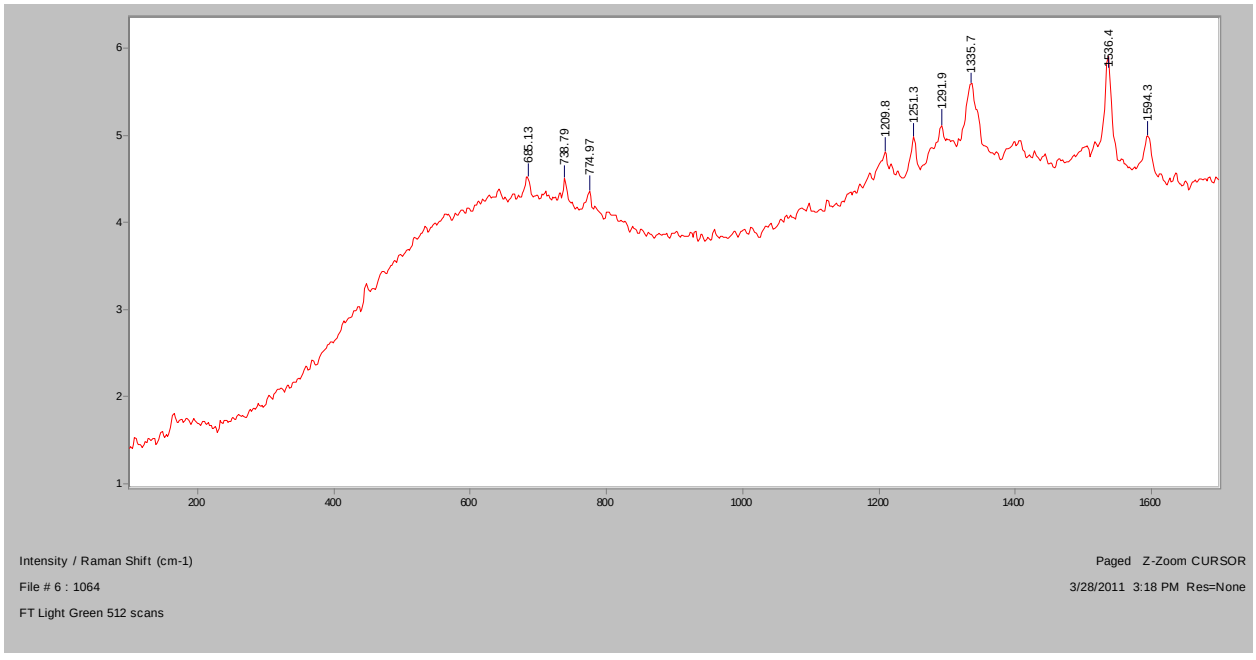

FT-IR (ATR)

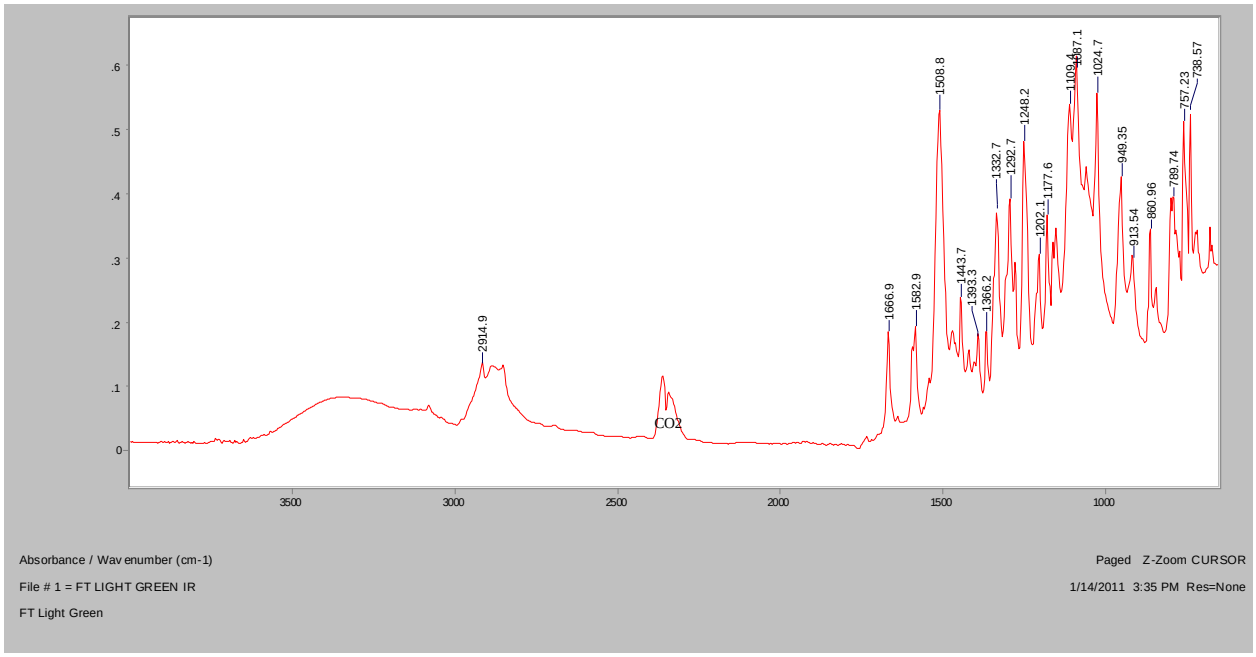
2914.9
CO2
1666.9
1582.9
1508.8
1443.7
1393.3
1366.2
1332.7
1292.7
1248.2
1202.1
1177.6
1109.4
1087.1
1024.7
949.35
913.54
860.96
789.74
757.23
738.57
3500
3000
2500
2000
1500
1000
Absorbance / Wavenumber (cm-1)
File # 1 = FT LIGHT GREEN IR
FT Light Green
Paged Z-Zoom CURSOR
1/14/2011 3:35 PM Res=None

XRF

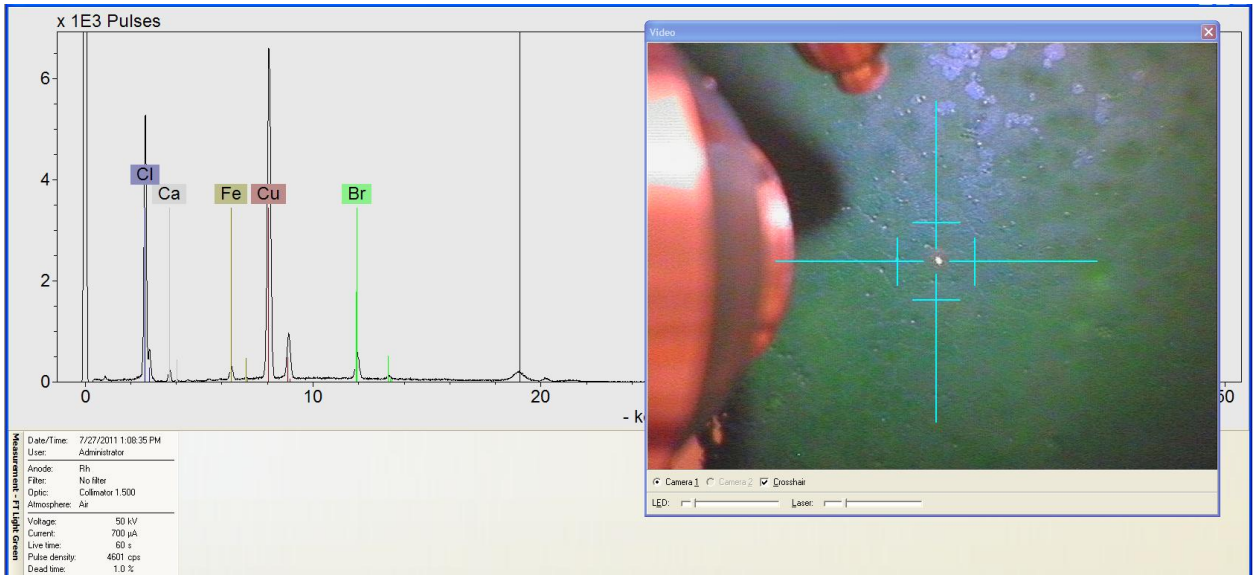
x 1E3 Pulses
Cl
Ca
Fe
Cu
Br
Video
Camera 1
Camera 2
Crosshair
LED:
Laser:
Date/Time: 7/27/2011 1:08:35 PM
User: Administrator
Anode: Rh
Filter: No filter
Optic: Collimator 1.500
Atmosphere: Air
Voltage: 50 kV
Current: 700 µA
Live time: 60 s
Pulse density: 4601 cps
Dead time: 1.0 %

Verdancy

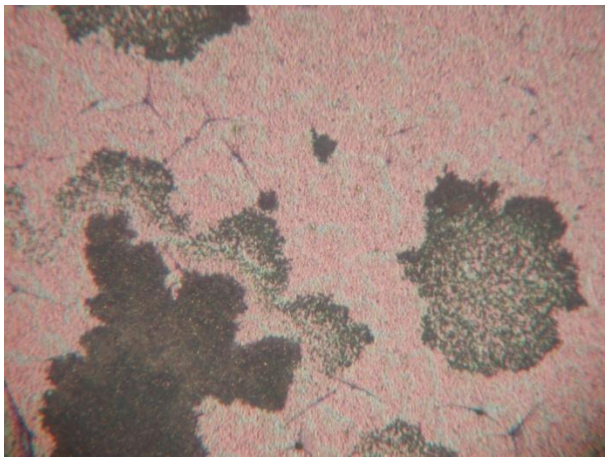

Bright Field, 100x

Dark Field, 100x

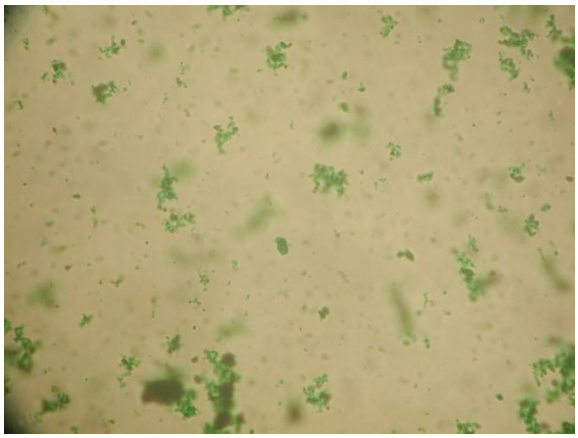

In RI 1.550, 400x

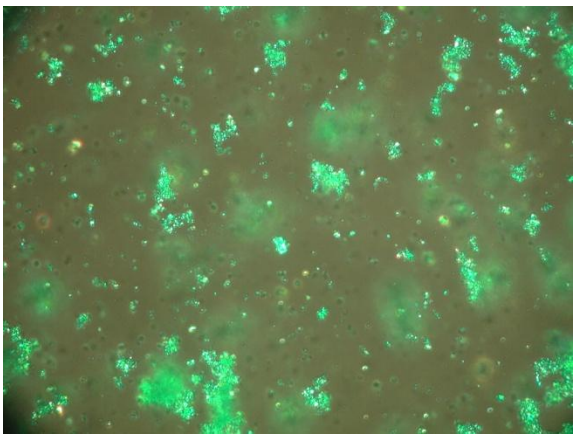

Crossed Polars, In RI 1.550, 400x

Normal Raman, 488nm

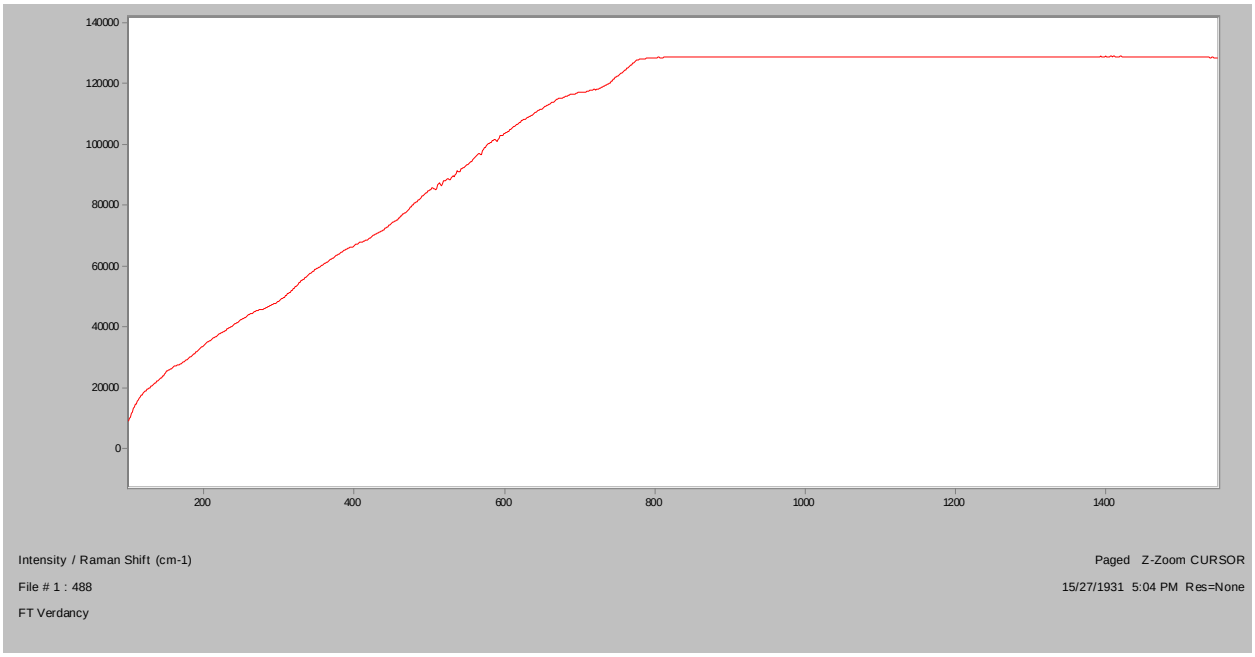

Normal Raman, 633nm

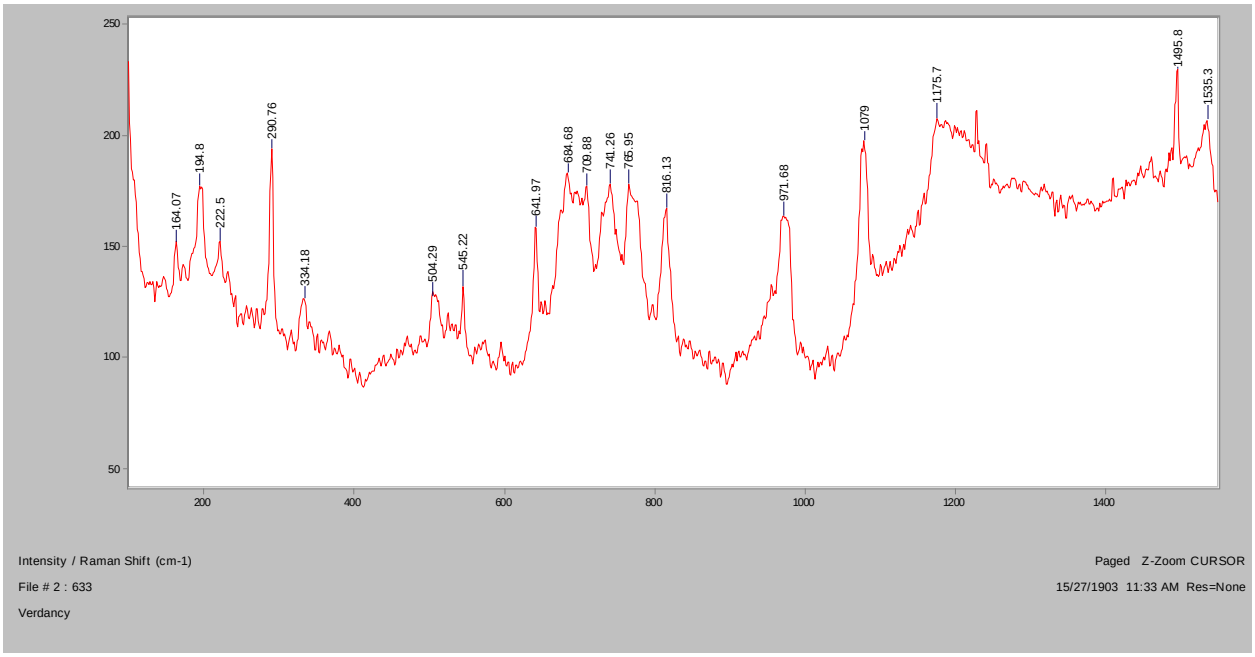

Normal Raman, 785nm

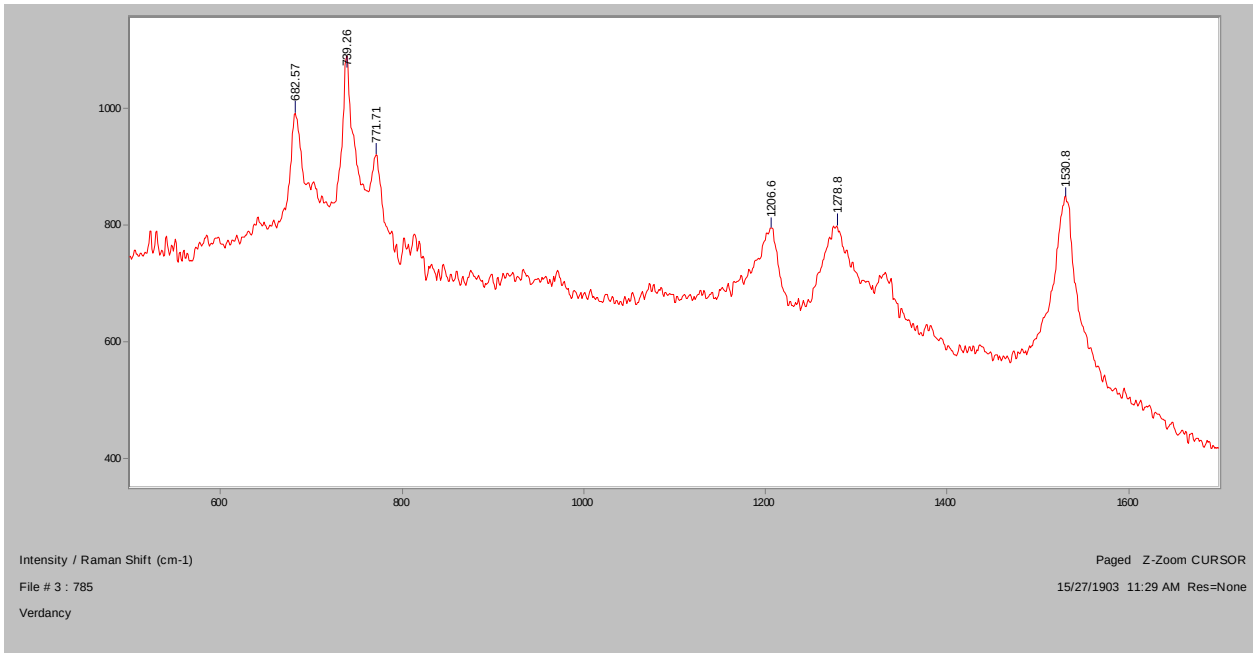

FT-Raman, 1064nm

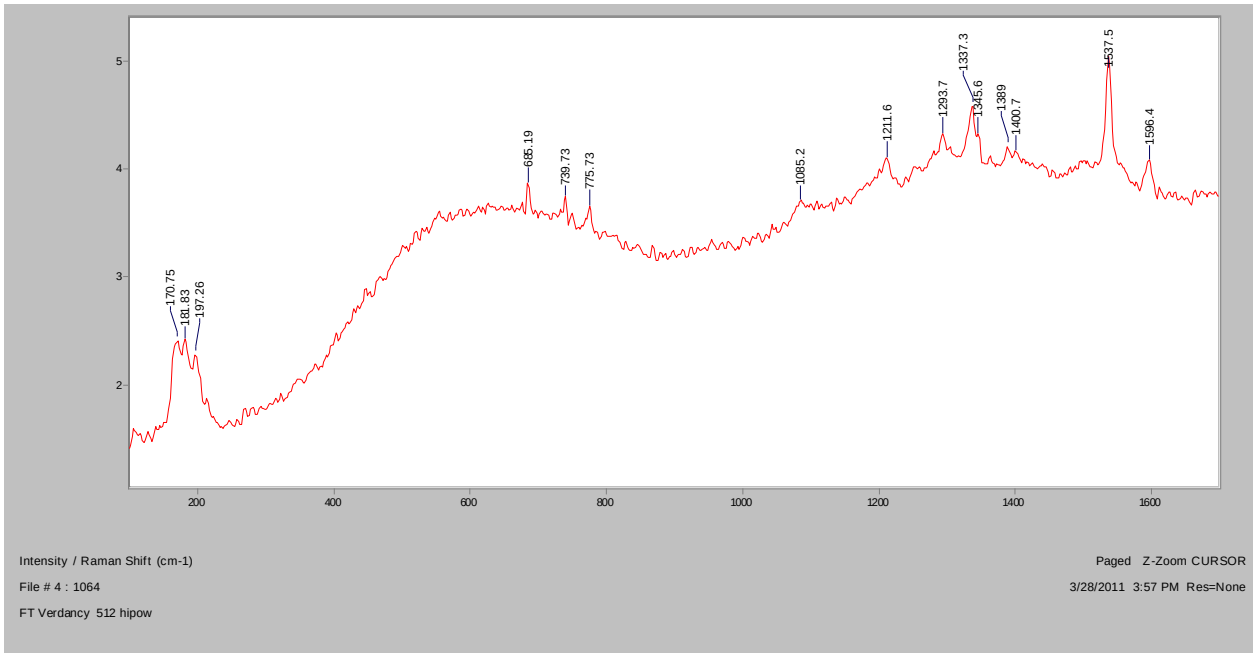

FT-IR (ATR)

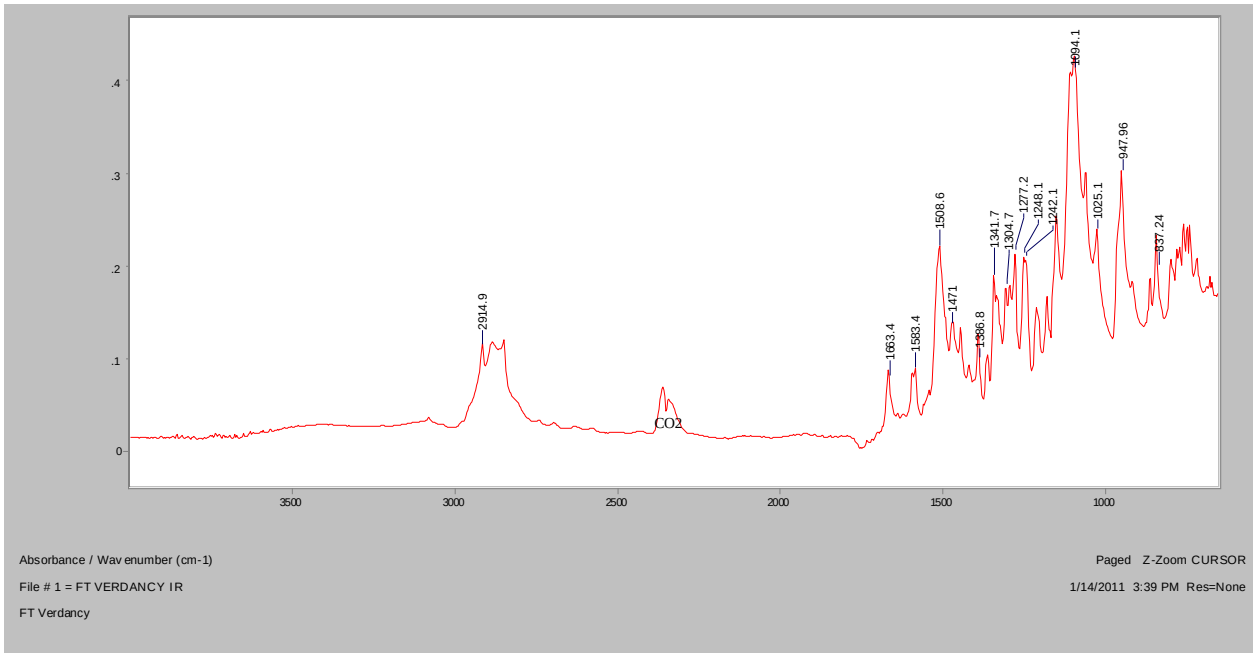
2914.9
CO2
1663.4
1583.4
1471
1396.8
1508.6
1341.7
1304.7
1277.2
1248.1
1242.1
1694.1
1025.1
947.96
837.24
.4
.3
.2
.1
0
3500
3000
2500
2000
1500
1000
Absorbance / Wavenumber (cm-1)
File # 1 = FT VERDANCY IR
FT Verdancy
Paged Z-Zoom CURSOR
1/14/2011 3:39 PM Res=None

XRF

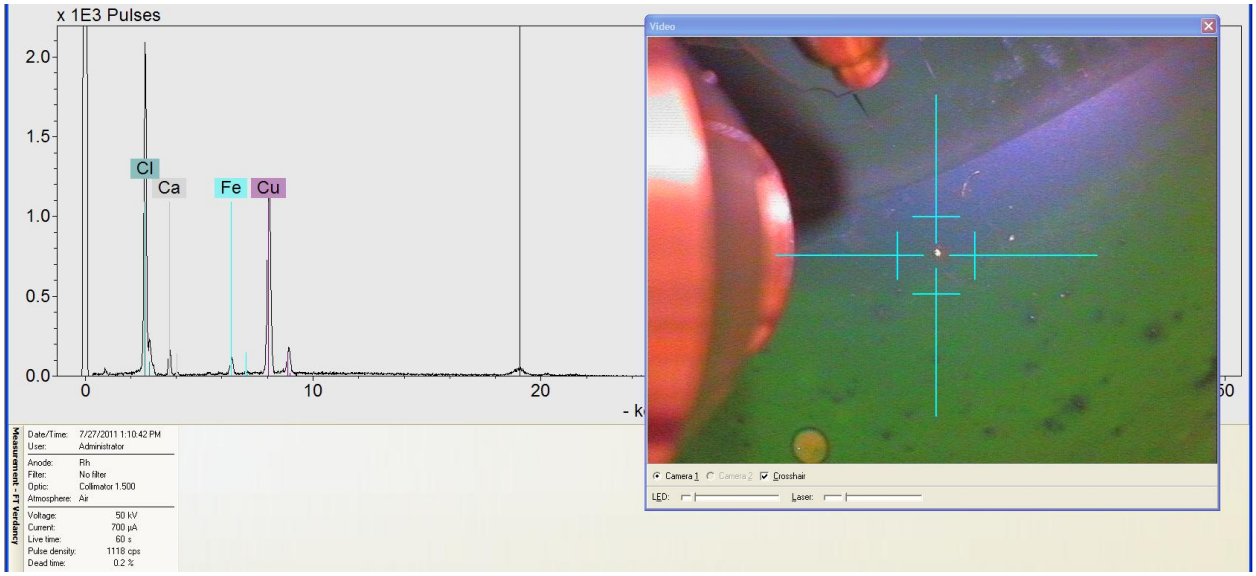
x 1E3 Pulses
2.0
1.5
1.0
0.5
0.0
Cl
Ca
Fe
Cu
0
10
20
Video
Camera 1
Camera 2
Crosshair
LED:
Laser:
Measurement - FT Verdancy
Date/Time: 7/27/2011 1:10:42 PM
User: Administrator
Anode: Rh
Filter: No filter
Optic: Collimator 1.500
Atmosphere: Air
Voltage: 50 kV
Current: 700 µA
Live time: 60 s
Pulse density: 1118 cps
Dead time: 0.2 %

Lawn Green

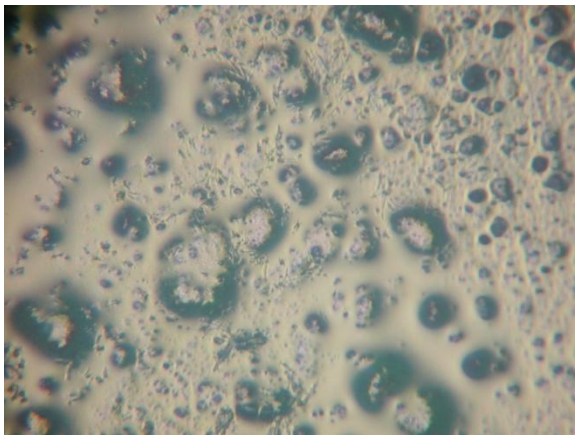

Bright Field, 100x

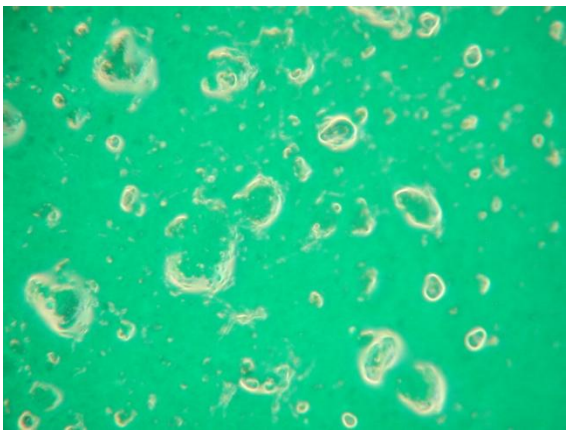

Dark Field, 100x

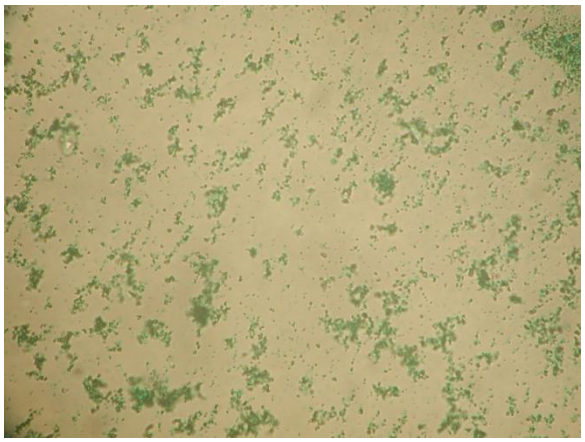

In RI 1.550, 400x

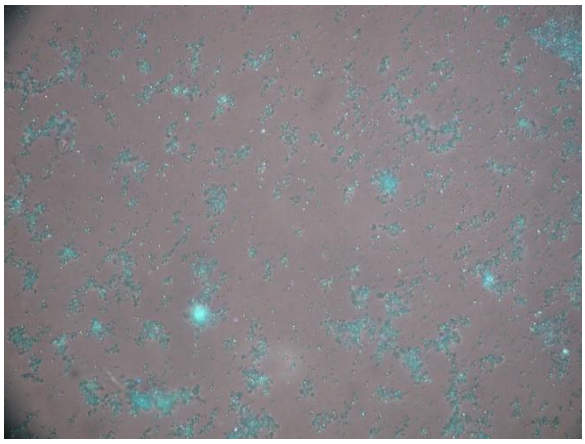

Crossed Polars, In RI 1.550, 400x

Normal Raman, 488nm

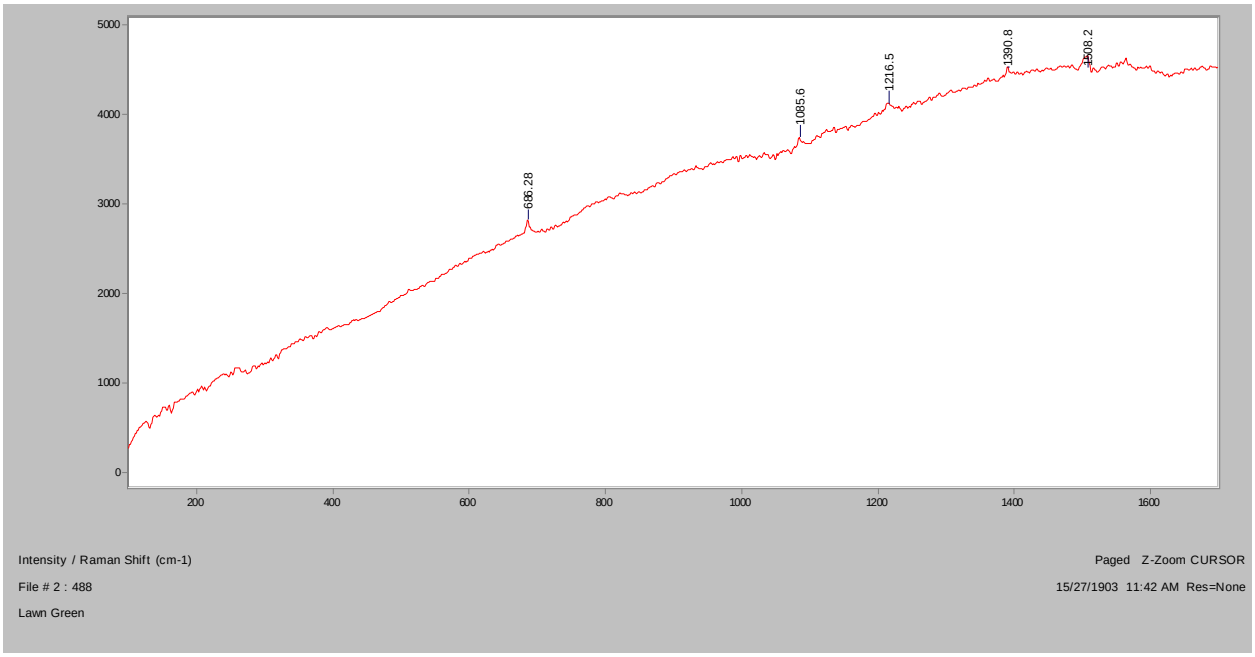

Normal Raman, 633nm

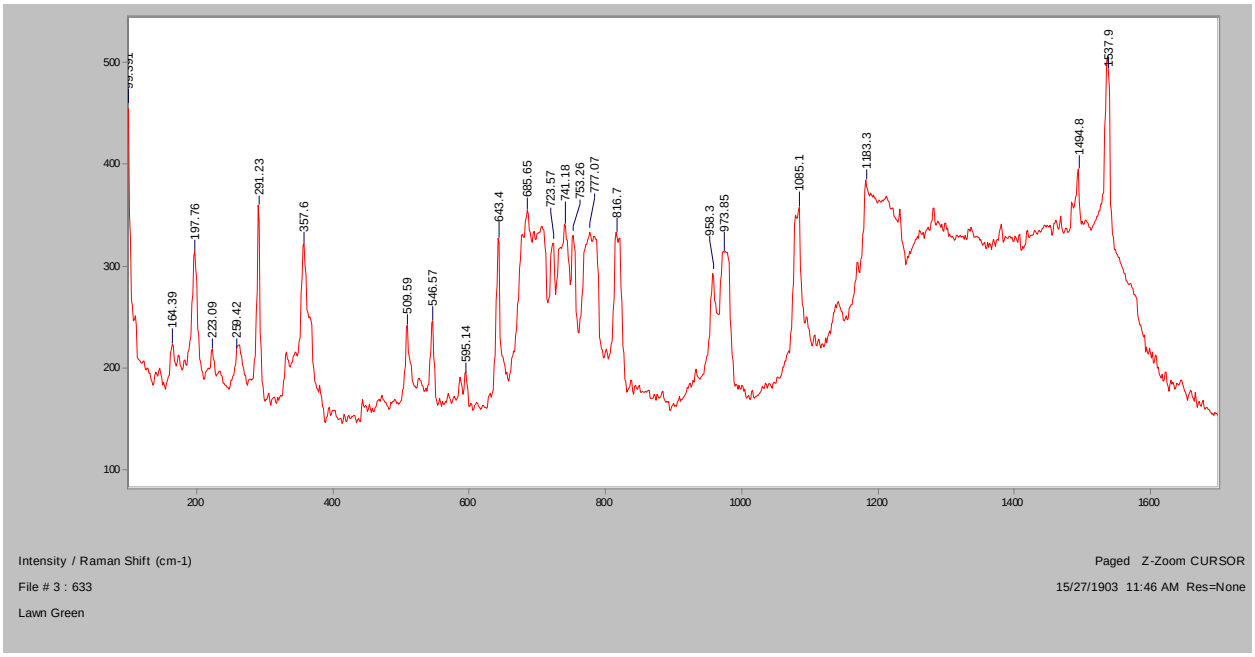

Normal Raman, 785nm

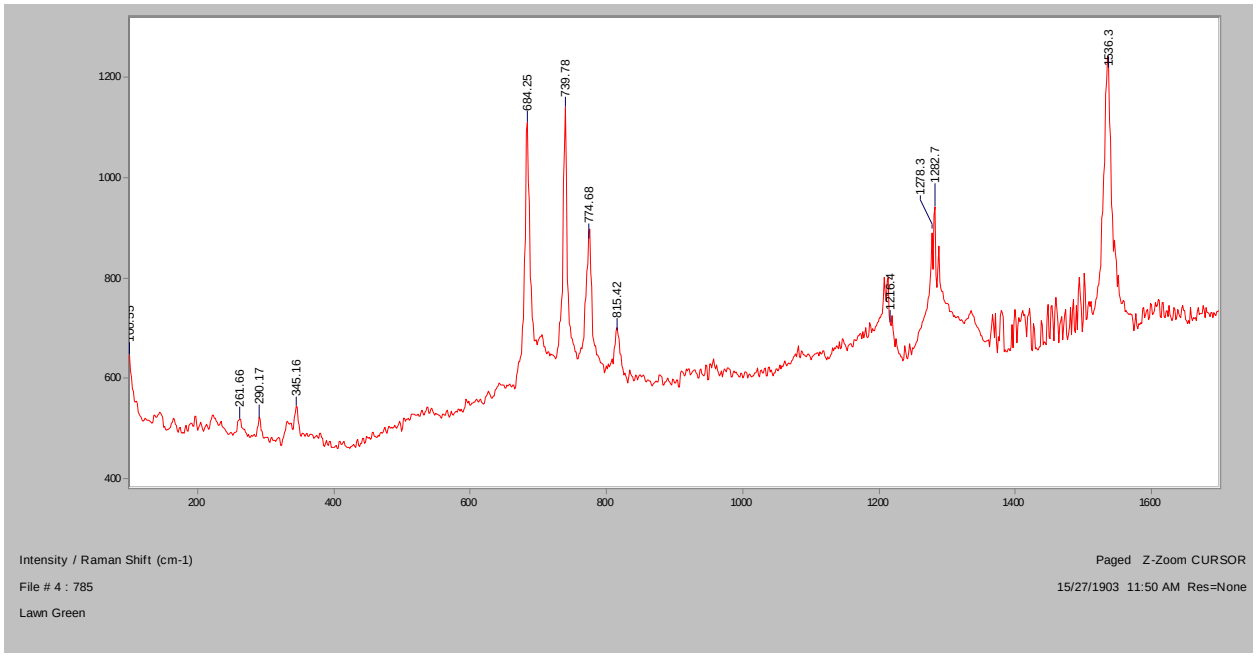

FT-Raman, 1064nm

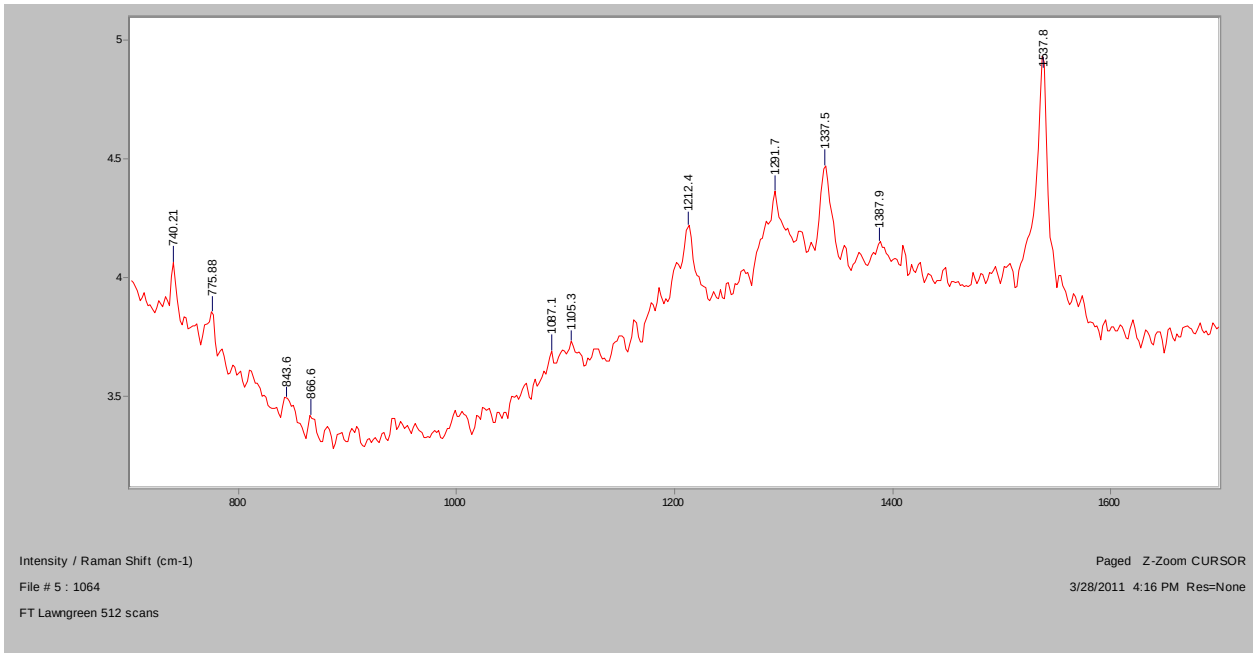

FT-IR (ATR)

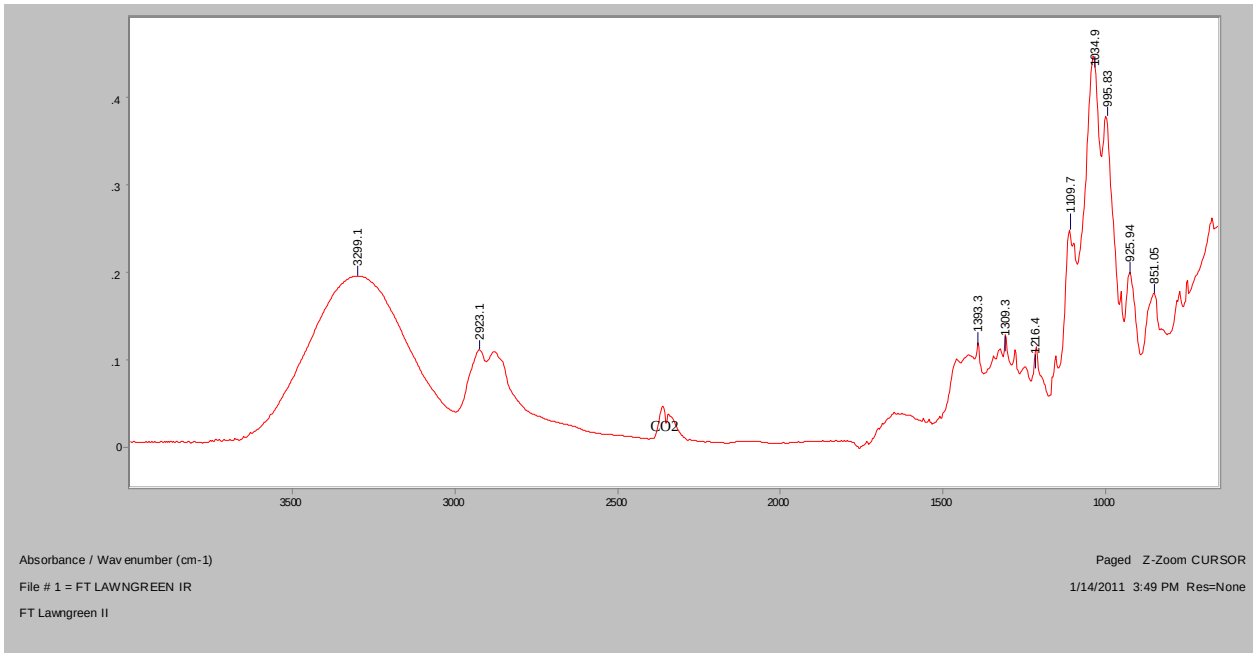
3299.1
2923.1
CO2
1393.3
1309.3
1216.4
1109.7
1034.9
995.83
925.94
851.05
.4
.3
.2
.1
0
3500
3000
2500
2000
1500
1000
Absorbance / Wavenumber (cm-1)
File # 1 = FT LAWNGREEN IR
FT Lawngreen II
Paged Z-Zoom CURSOR
1/14/2011 3:49 PM Res=None

XRF

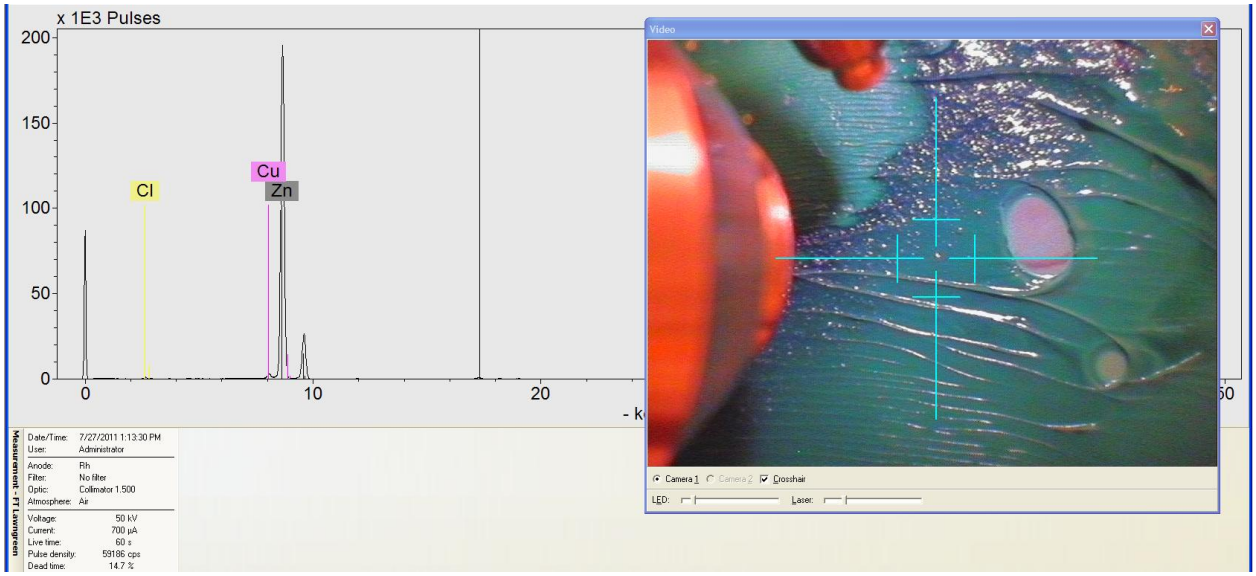
x 1E3 Pulses
200
150
100
50
0
Cl
Cu
Zn
0
10
20
Video
Camera 1
Camera 2
Crosshair
LED:
Laser:
Date/Time: 7/27/2011 1:13:30 PM
User: Administrator
Anode: Rh
Filter: No filter
Optic: Collimator 1.500
Atmosphere: Air
Voltage: 50 kV
Current: 700 µA
Live time: 60 s
Pulse density: 59186 cps
Dead time: 14.7 %

Dark Green

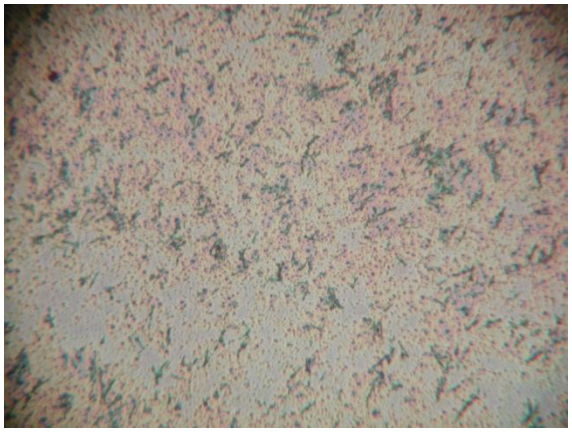

Bright Field, 100x

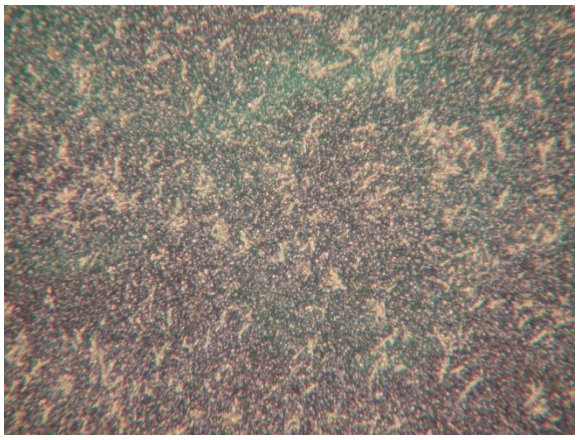

Dark Field, 100x

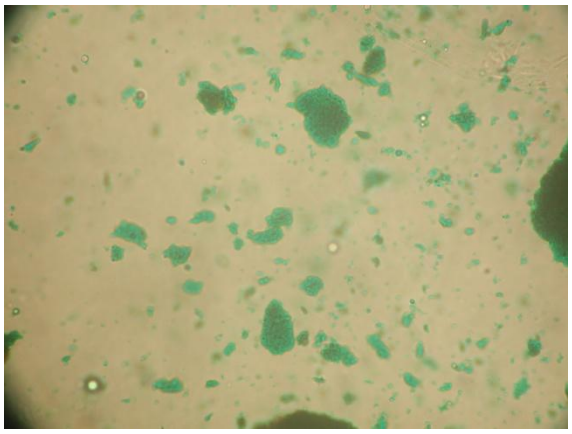

In RI 1.550, 400x

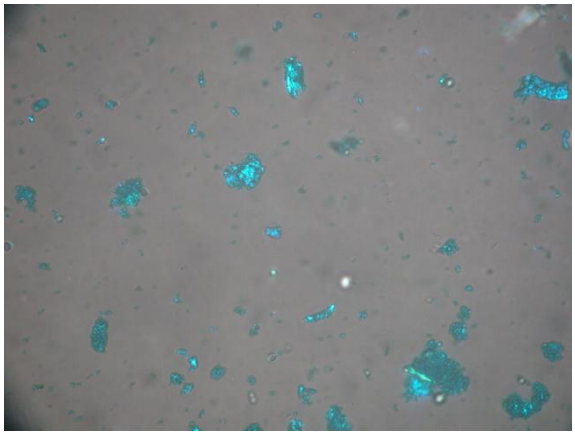

Crossed Polars, In RI 1.550, 400x

Normal Raman, 488nm

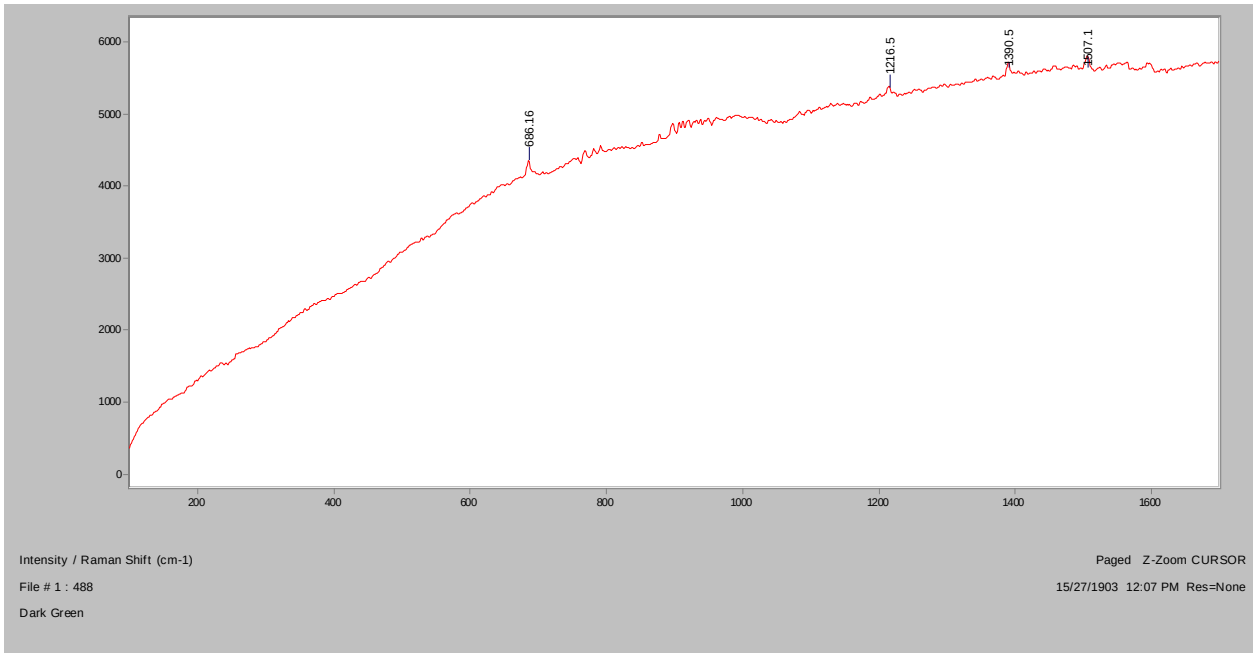

Normal Raman, 633nm

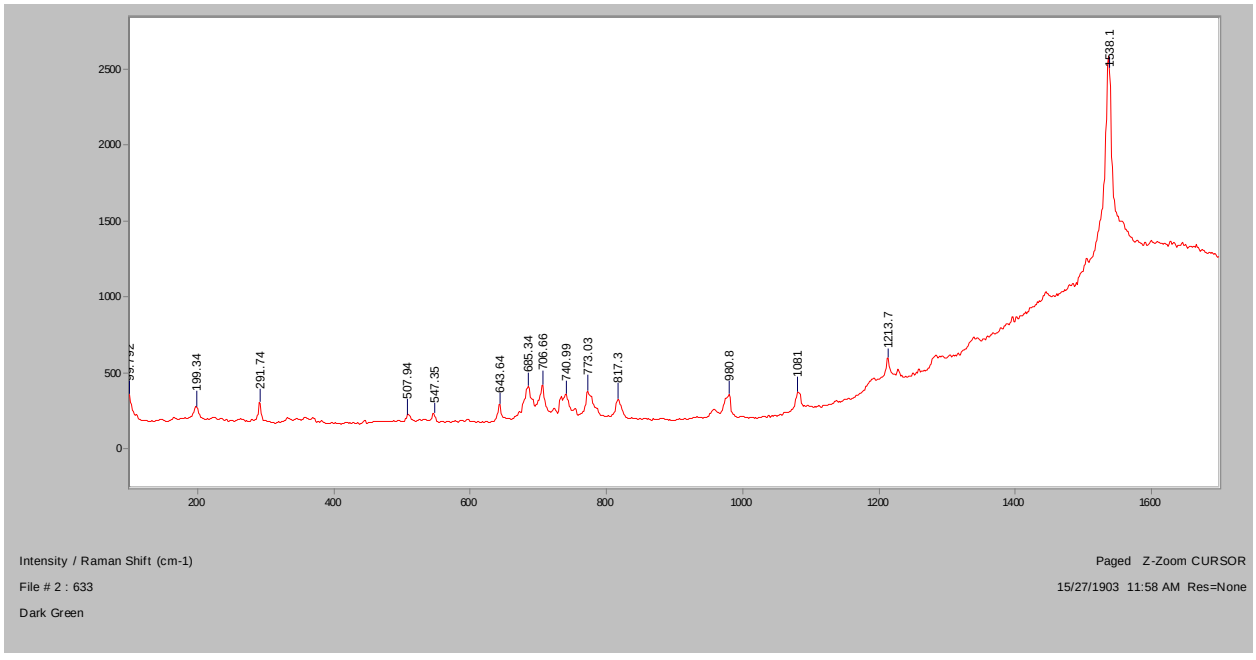

Normal Raman, 785nm

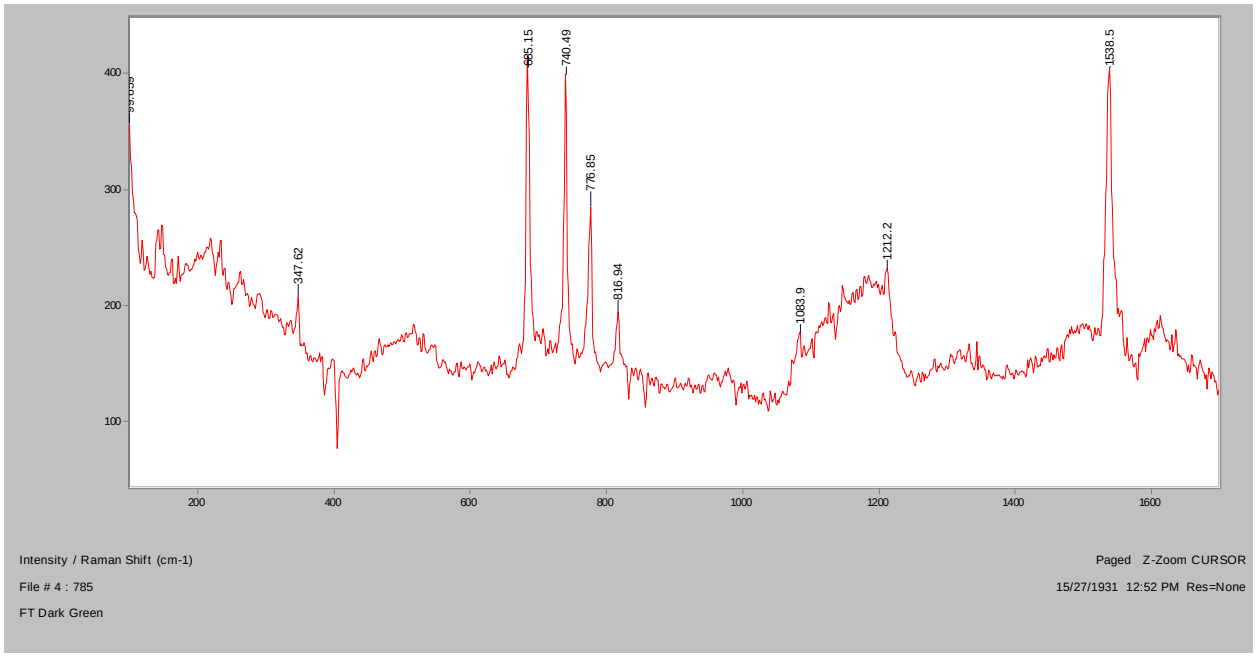

FT-Raman, 1064nm

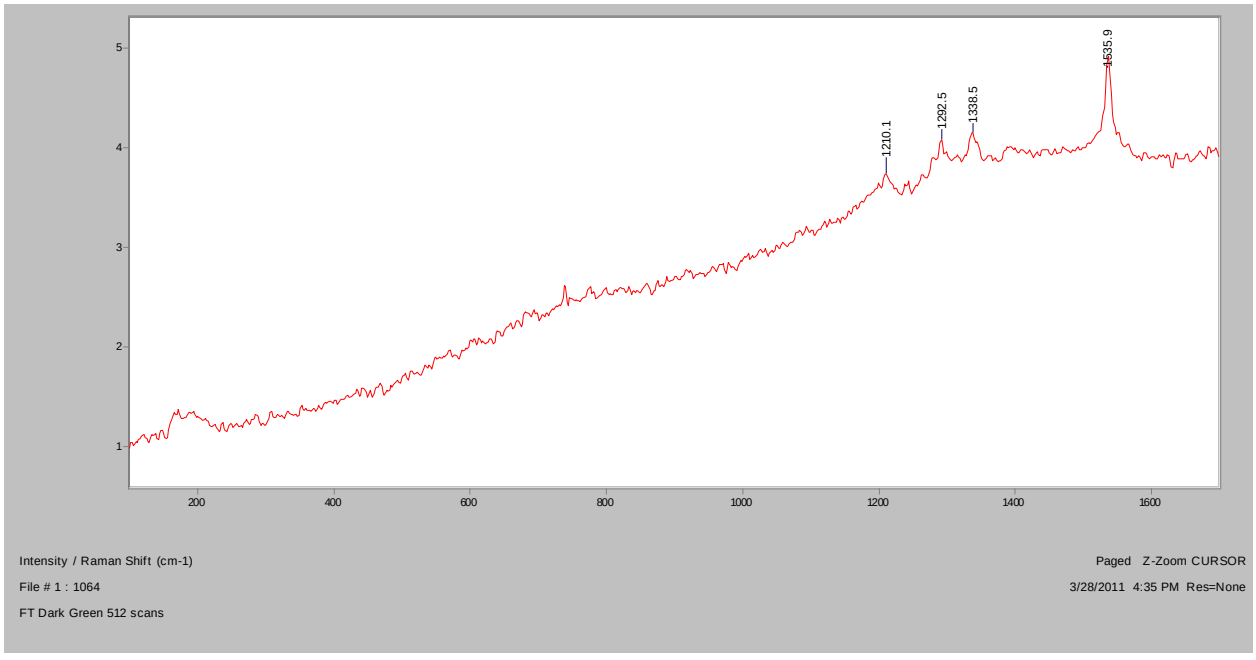

FT-IR (ATR)

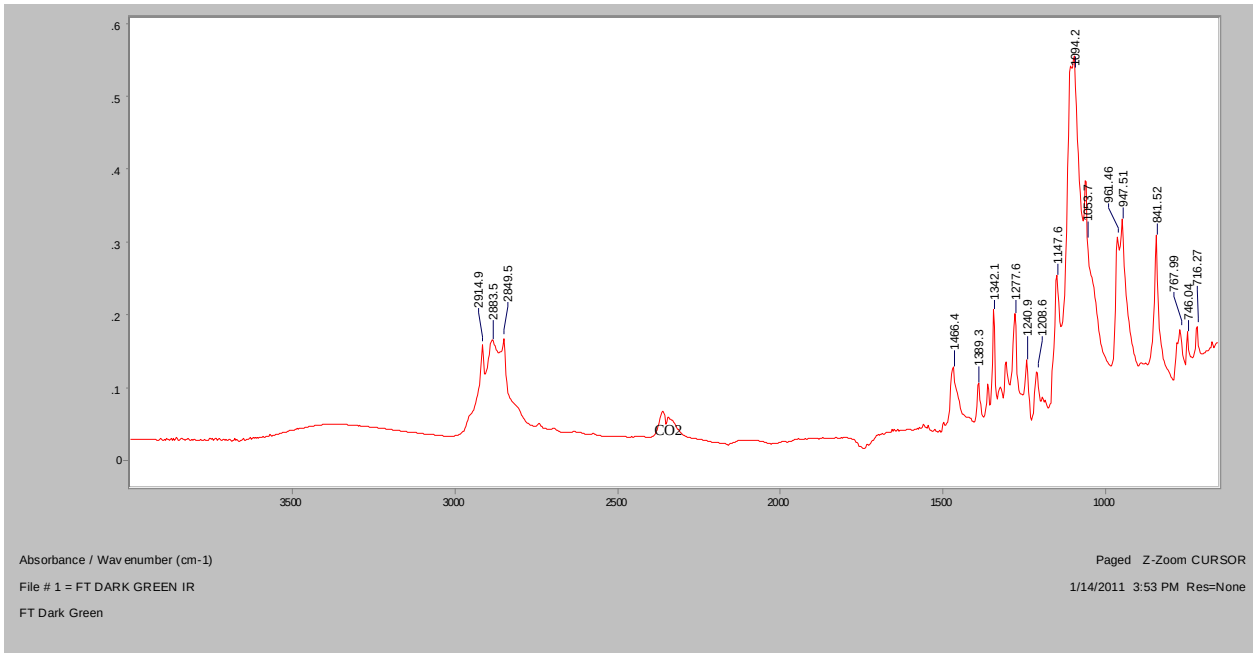
2914.9
2863.5
2849.5
1466.4
1389.3
1342.1
1277.6
1240.9
1208.6
1147.6
1053.7
994.2
961.46
947.51
841.52
767.99
746.04
716.27
CO2
3500
3000
2500
2000
1500
1000
Absorbance / Wavenumber (cm-1)
File # 1 = FT DARK GREEN IR
FT Dark Green
Paged Z-Zoom CURSOR
1/14/2011 3:53 PM Res=None

XRF

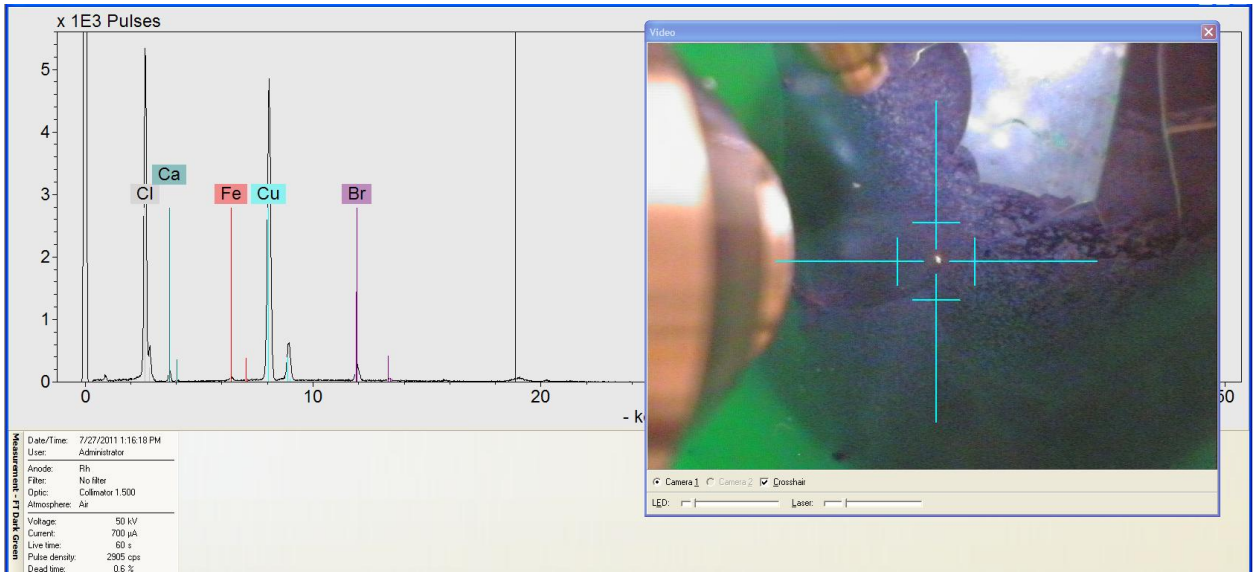
x 1E3 Pulses
Cl
Ca
Fe
Cu
Br
Video
Camera 1
Camera 2
Crosshair
LED:
Laser:
Date/Time: 7/27/2011 1:16:18 PM
User: Administrator
Anode: Rh
Filter: No filter
Optic: Collimator 1.500
Atmosphere: Air
Voltage: 50 kV
Current: 700 µA
Live time: 60 s
Pulse density: 2905 cps
Dead time: 0.6 %

Blue Sky

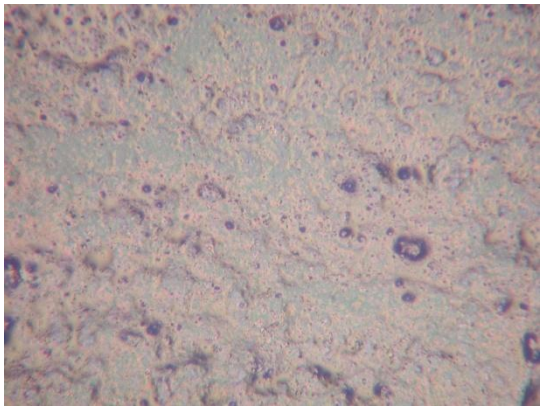

Bright Field, 100x

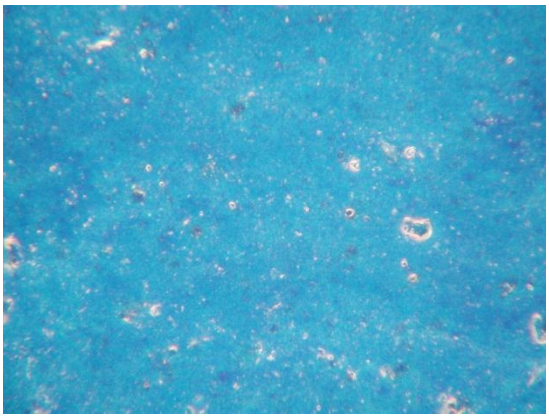

Dark Field, 100x

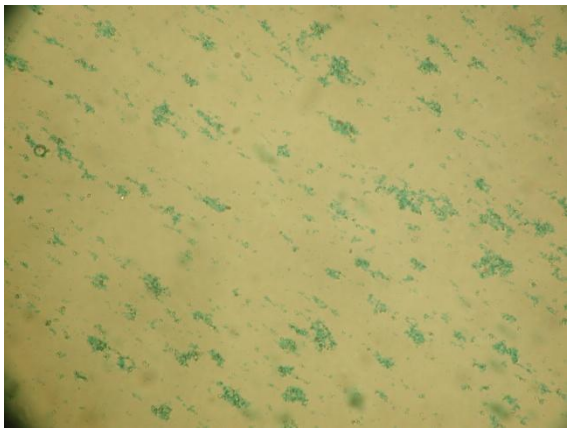

In RI 1.550, 400x

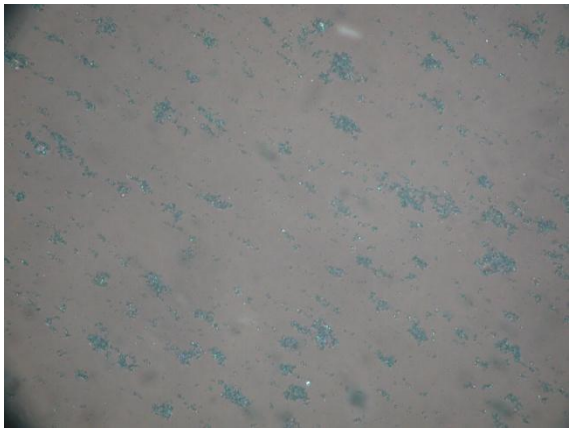

Crossed Polars, In RI 1.550, 400x

Normal Raman, 488nm

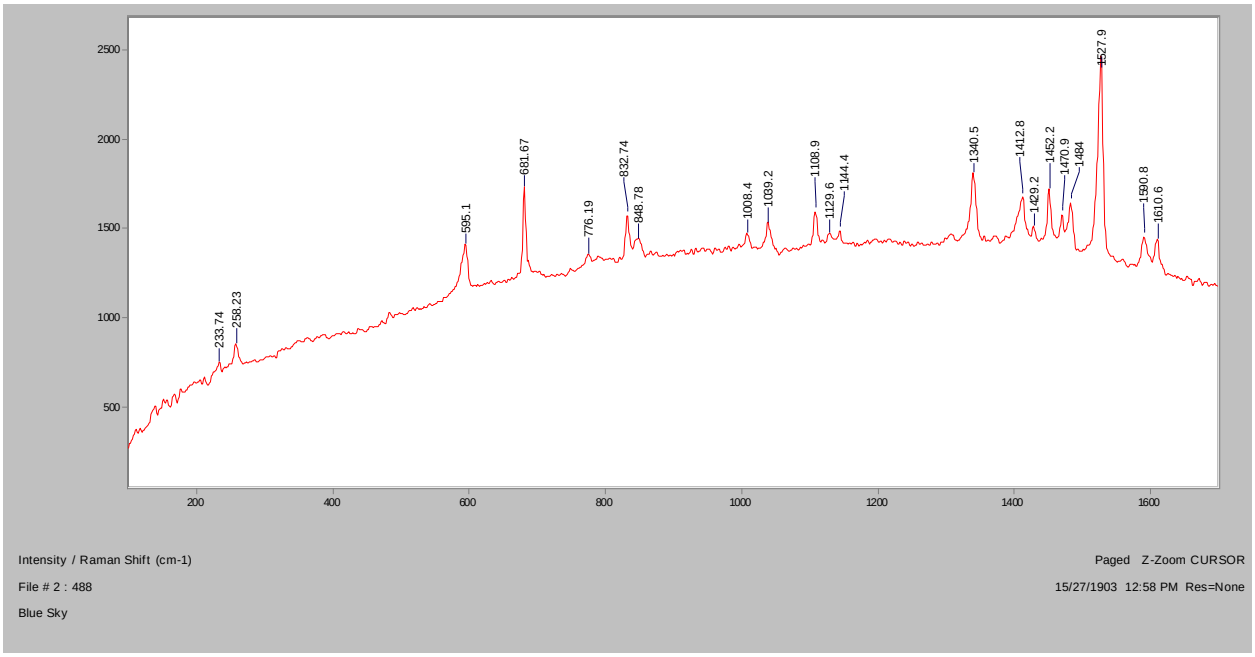

Normal Raman, 633nm

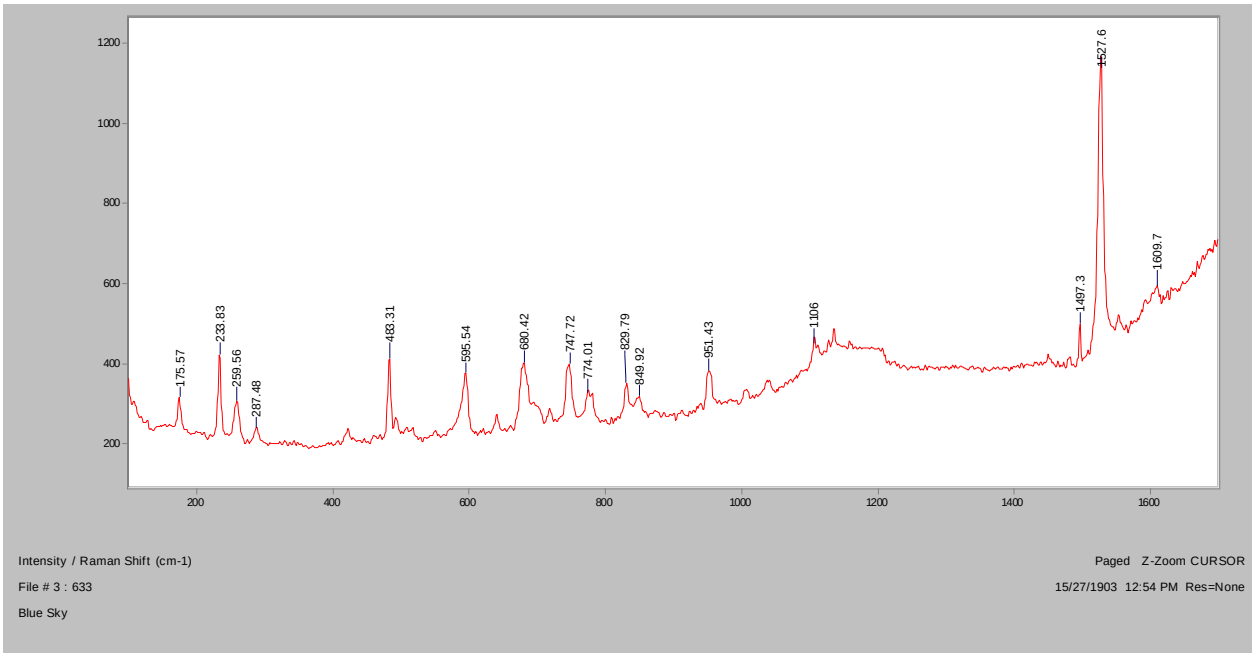

Normal Raman, 785nm

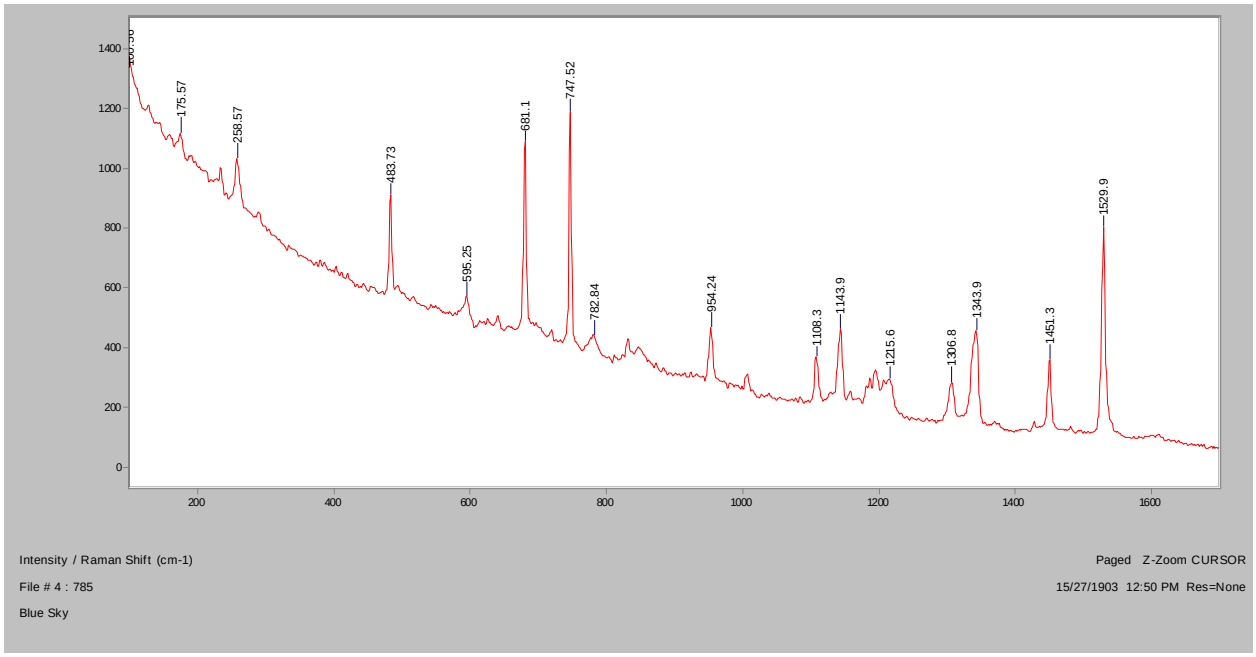

FT-Raman, 1064nm

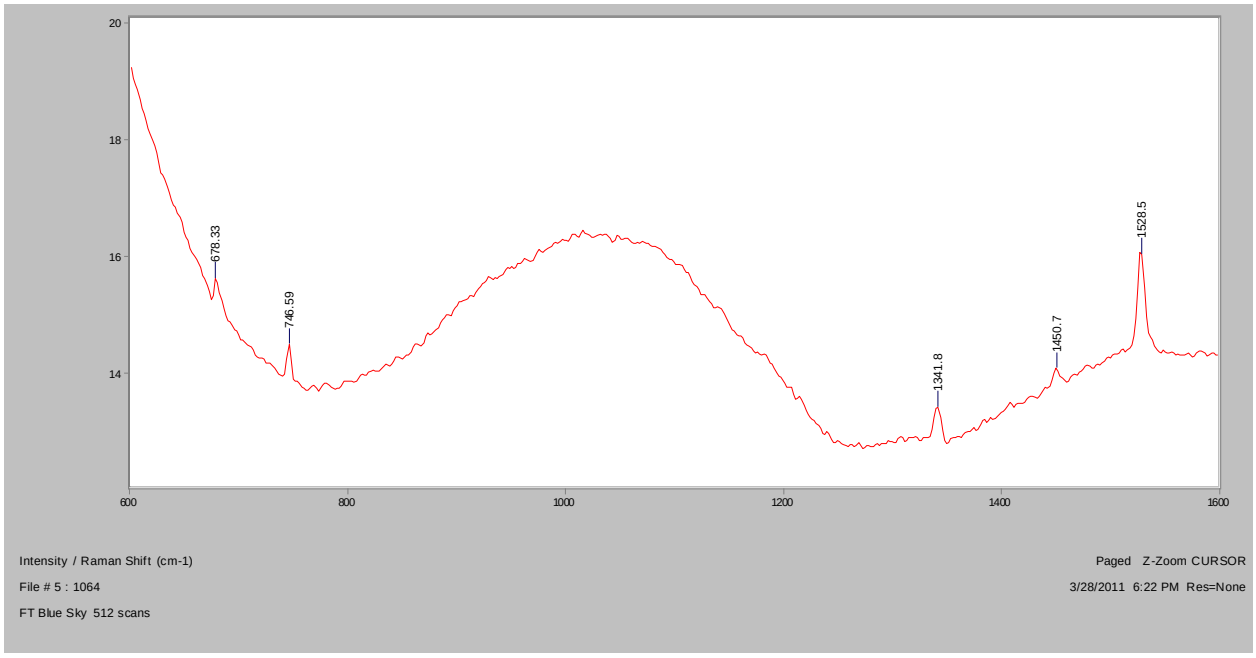

FT-IR (ATR)

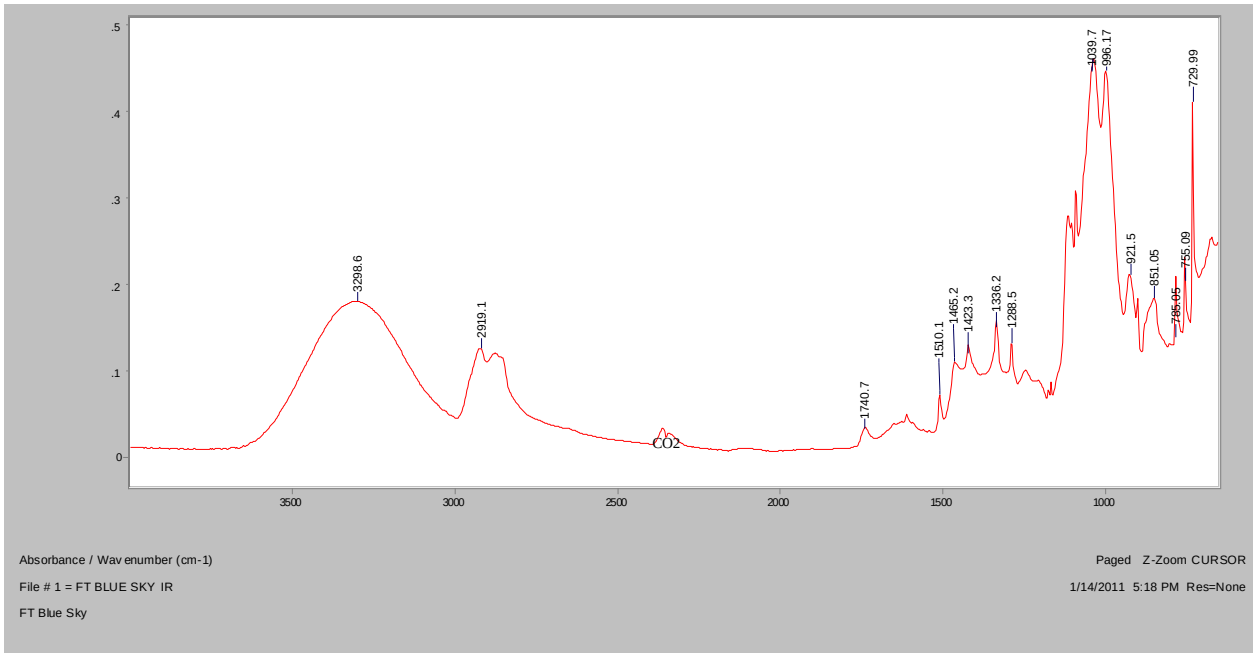
.5
.4
.3
.2
.1
0
3298.6
2919.1
CO2
1740.7
1510.1
1465.2
1423.3
1336.2
1288.5
1039.7
996.17
921.5
851.05
786.05
755.09
729.99
3500
3000
2500
2000
1500
1000
Absorbance / Wavenumber (cm-1)
File # 1 = FT BLUE SKY IR
FT Blue Sky
Paged Z-Zoom CURSOR
1/14/2011 5:18 PM Res=None

XRF

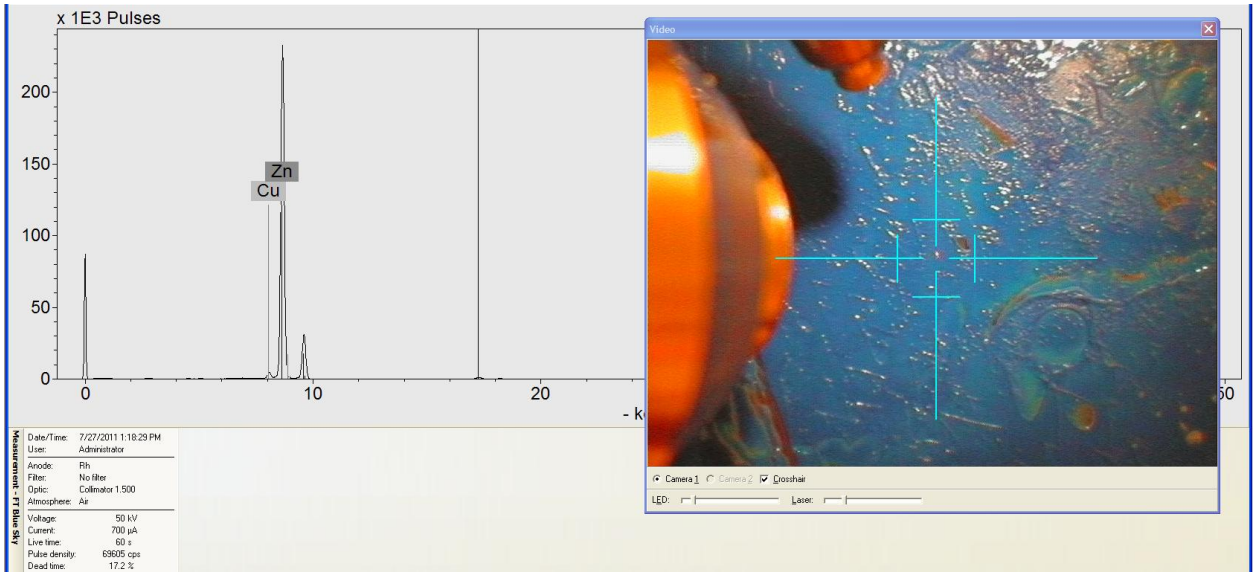
x 1E3 Pulses
200
150
100
50
0
Zn
Cu
0
10
20
Video
Camera 1
Camera 2
Crosshair
LED:
Laser:
Measurement: FT Blue Sky
Date/Time: 7/27/2011 1:18:29 PM
User: Administrator
Anode: Rh
Filter: No filter
Optic: Collimator 1.500
Atmosphere: Air
Voltage: 50 kV
Current: 700 µA
Live time: 60 s
Pulse density: 69605 cps
Dead time: 17.2 %

Turquoise Blue

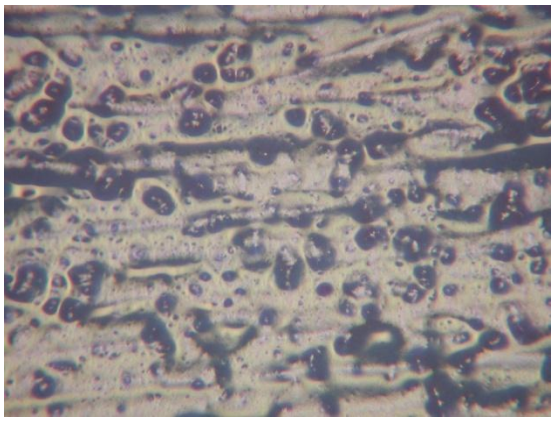

Bright Field, 100x

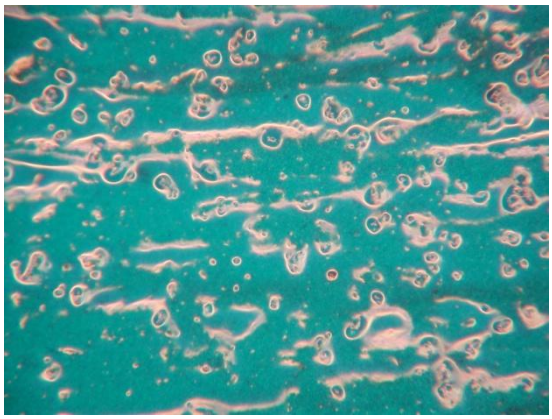

Dark Field, 100x

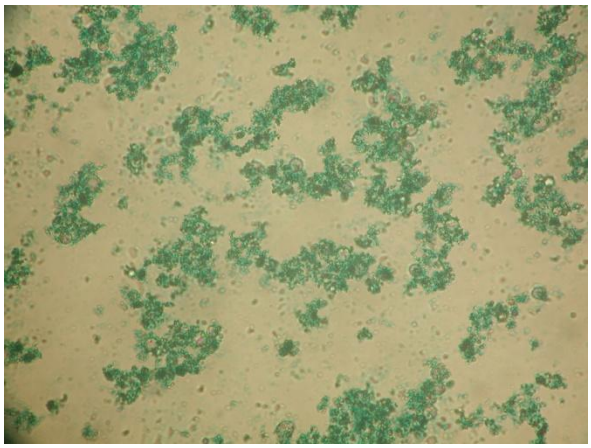

In RI 1.550, 400x

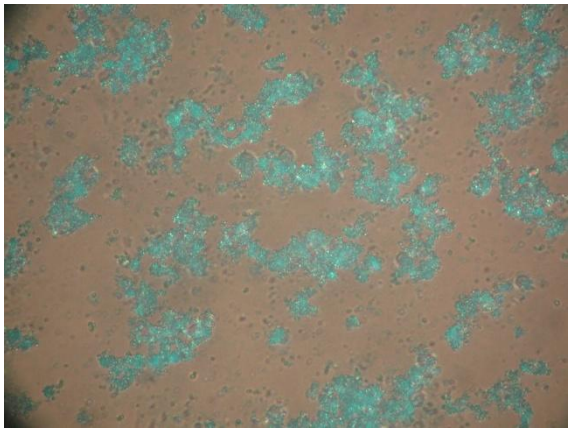

Crossed Polars, In RI 1.550, 400x

Normal Raman, 488nm

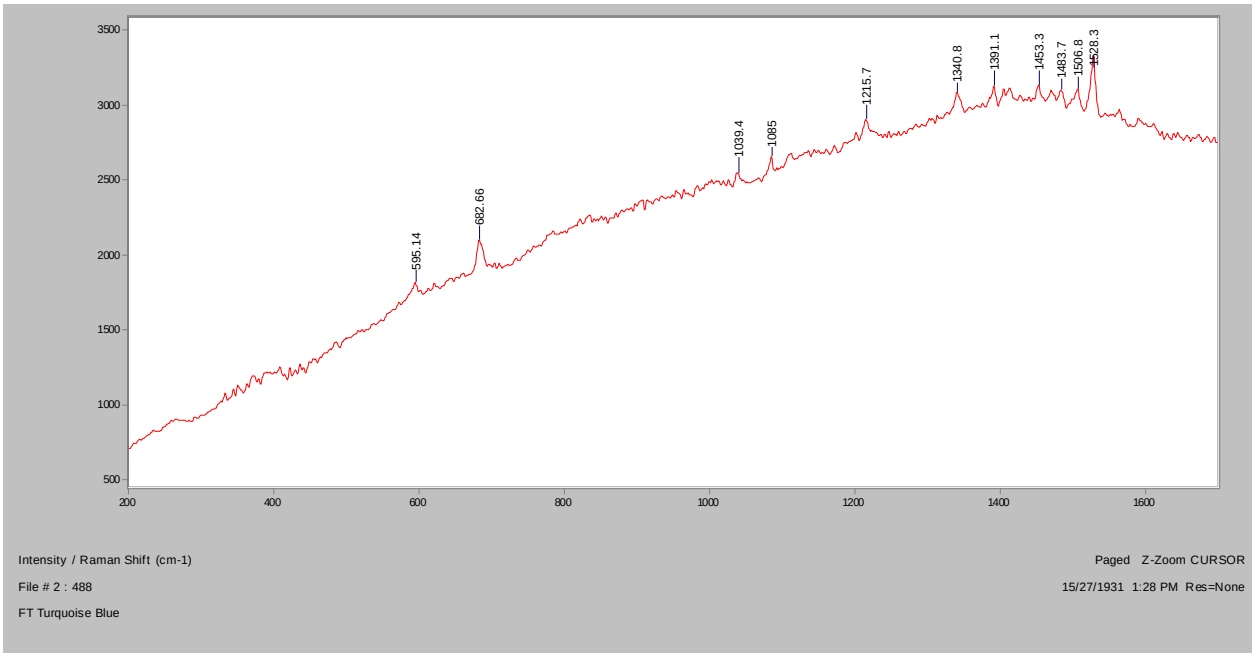

Normal Raman, 633nm

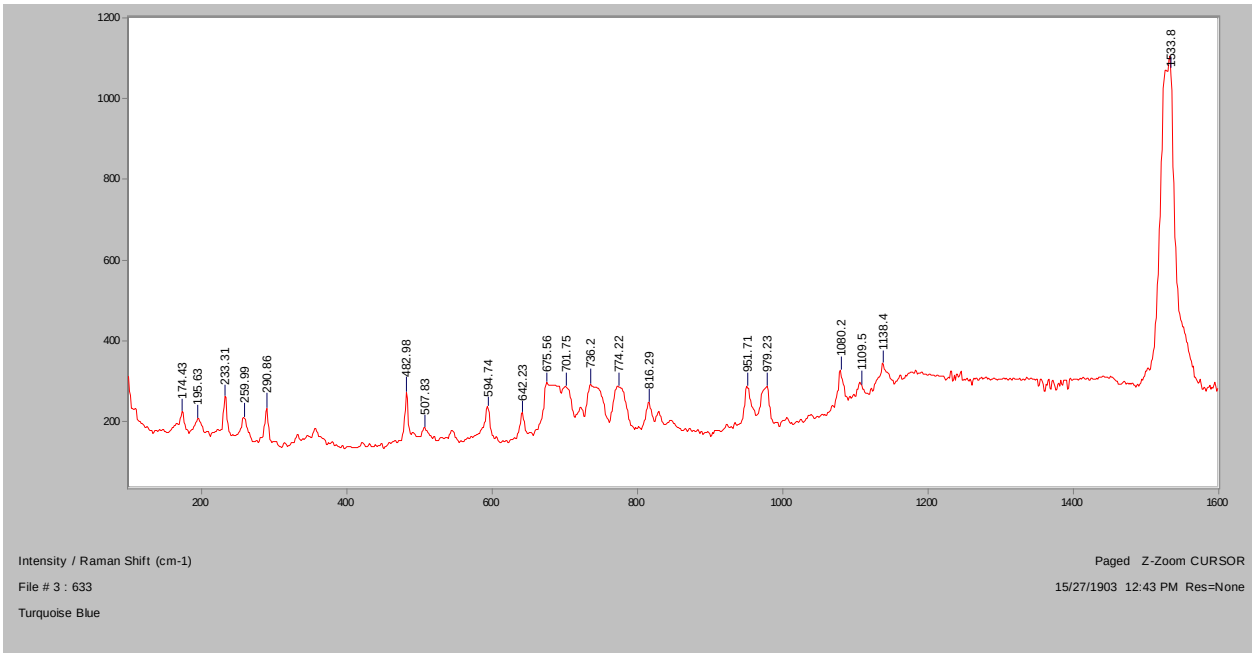

Normal Raman, 785nm

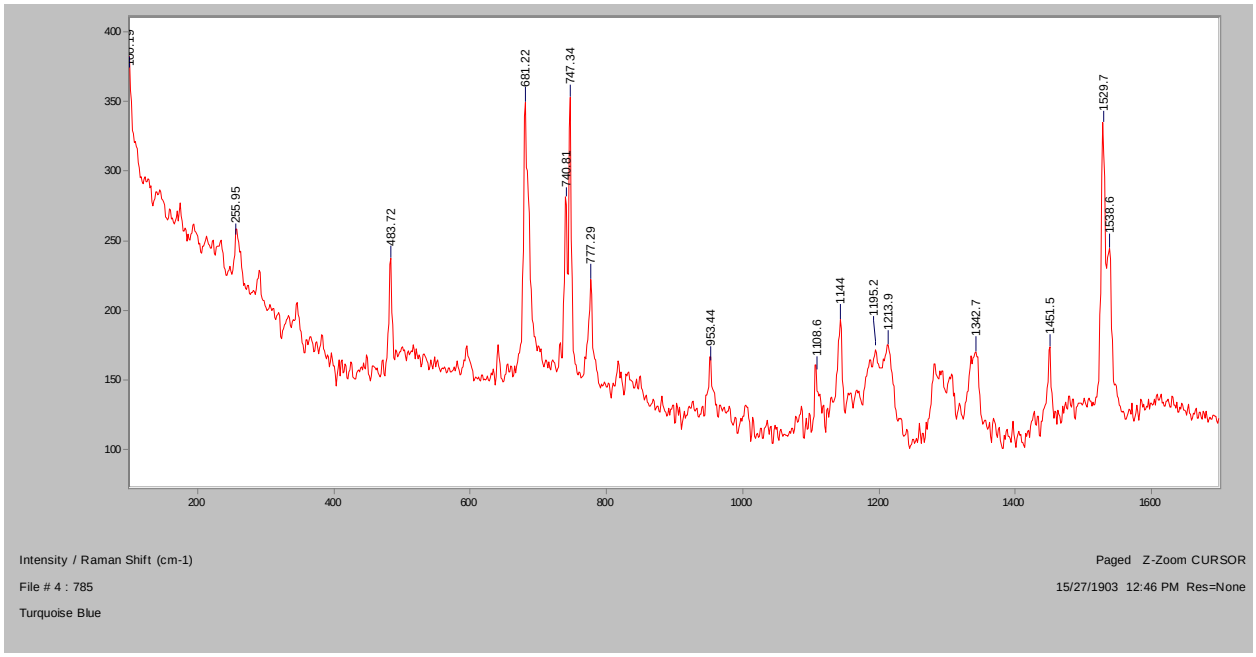

FT-Raman, 1064nm

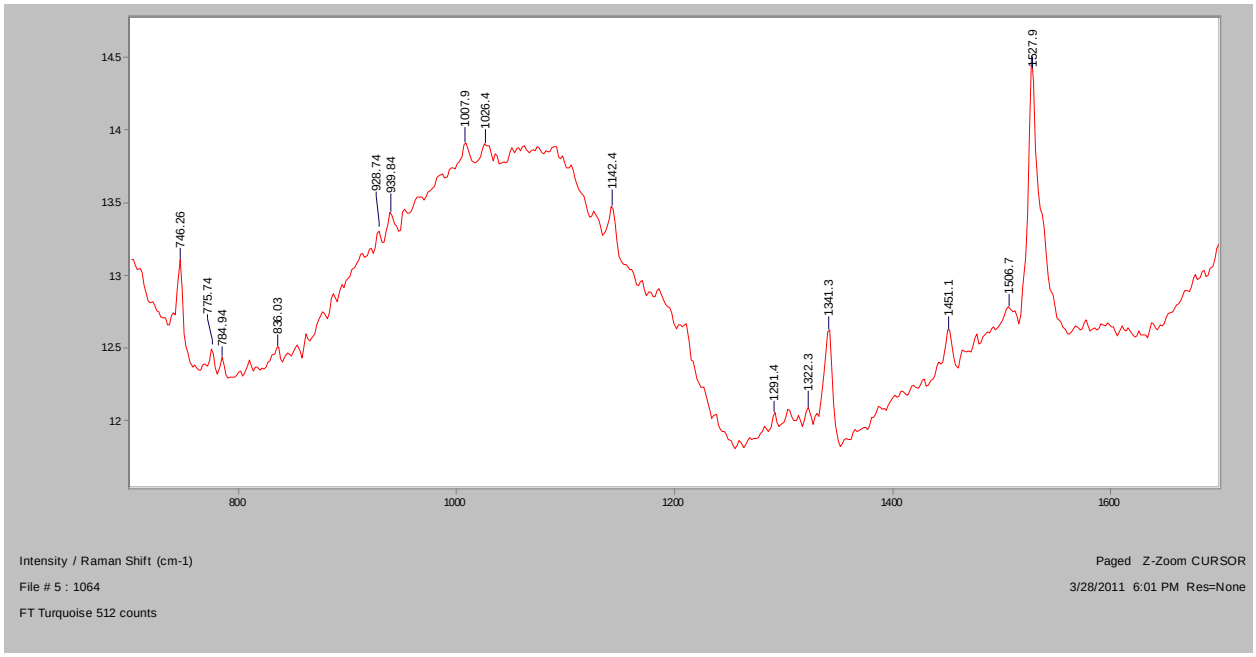

FT-IR (ATR)

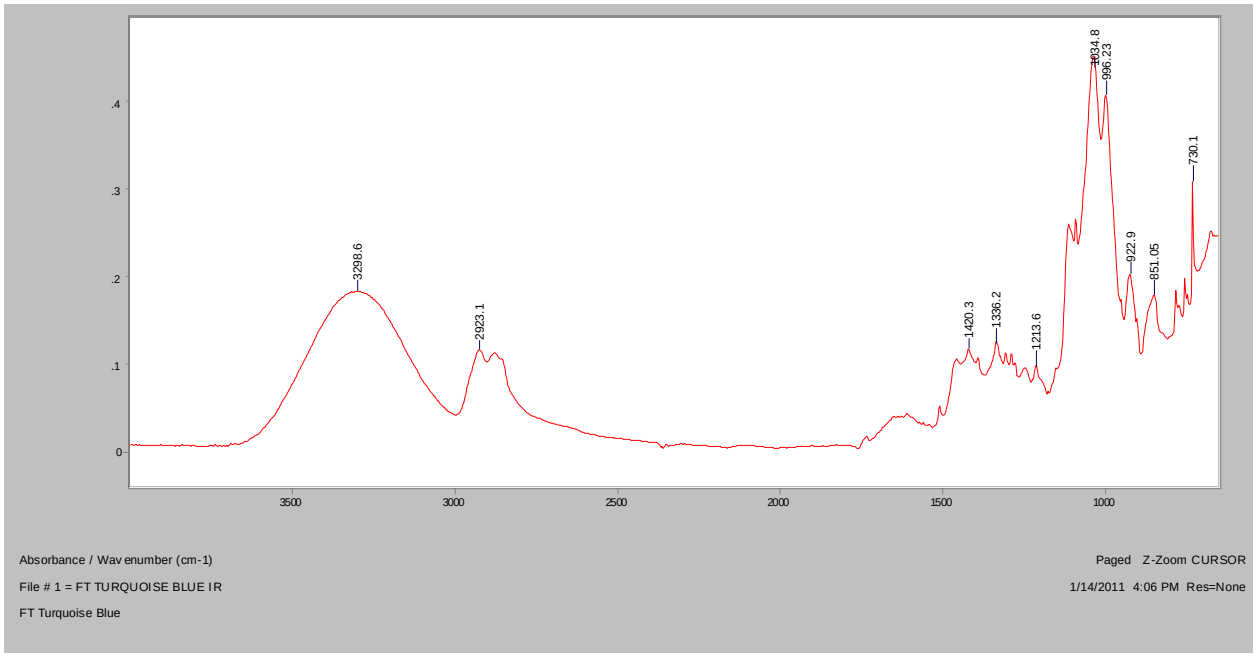
3298.6
2923.1
1420.3
1336.2
1213.6
1034.8
996.23
922.9
851.05
730.1
.4
.3
.2
.1
0
3500
3000
2500
2000
1500
1000
Absorbance / Wavenumber (cm-1)
File # 1 = FT TURQUOISE BLUE IR
FT Turquoise Blue
Paged Z-Zoom CURSOR
1/14/2011 4:06 PM Res=None

XRF

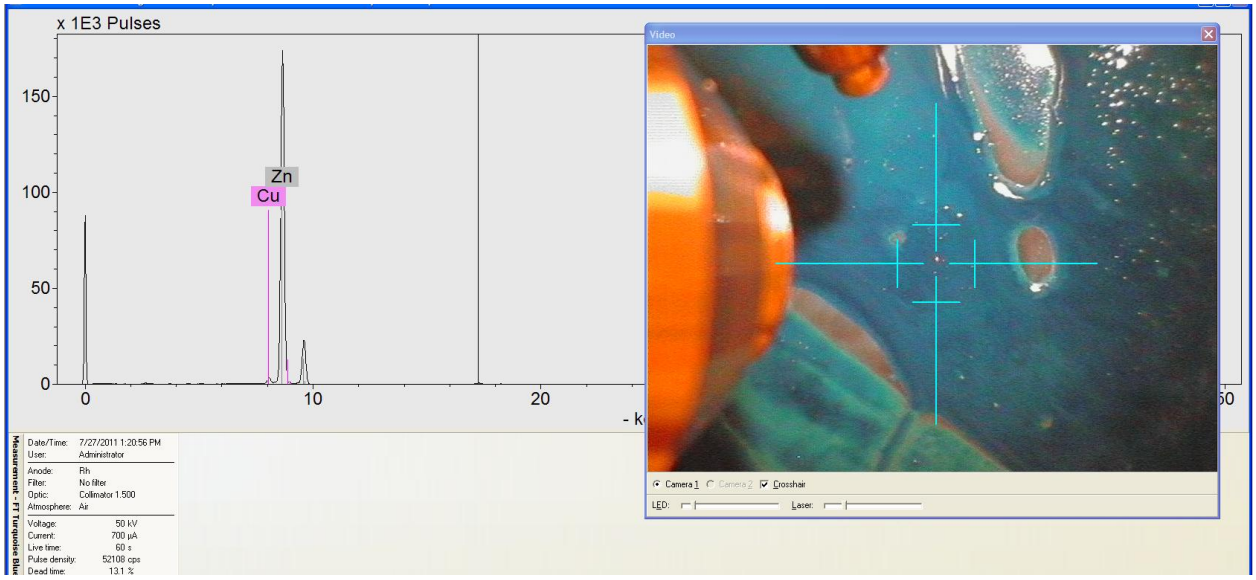
x 1E3 Pulses
150
100
50
0
Zn
Cu
0
10
20
Video
Camera 1
Camera 2
Crosshair
LED:
Laser:
Date/Time: 7/27/2011 1:20:56 PM
User: Administrator
Anode: Rh
Filter: No filter
Optic: Collimator 1.500
Atmosphere: Air
Voltage: 50 kV
Current: 700 µA
Live time: 60 s
Pulse density: 52108 cps
Dead time: 13.1 %

Cyan

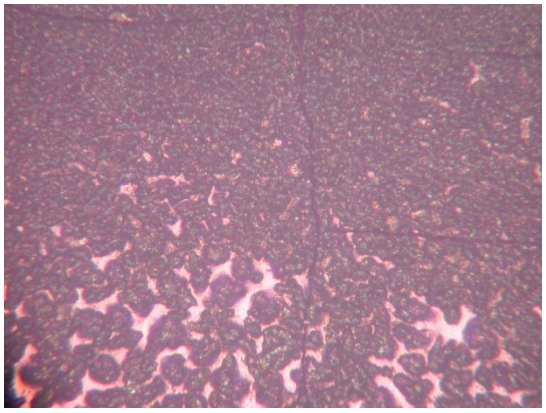

Bright Field, 100x

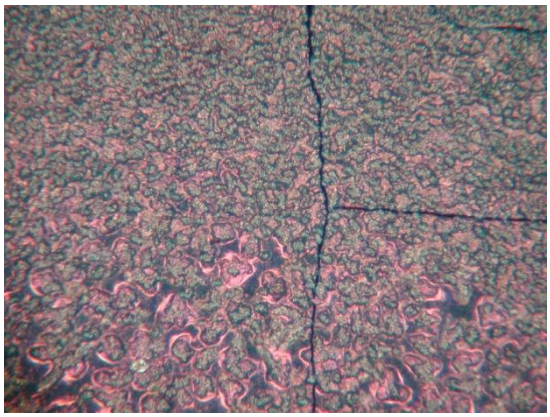

Dark Field, 100x

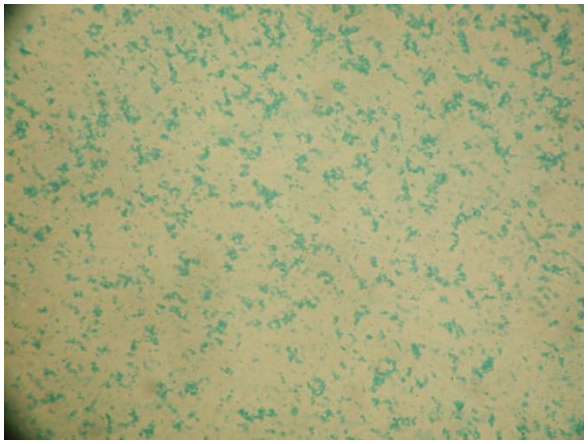

In RI 1.550, 400x

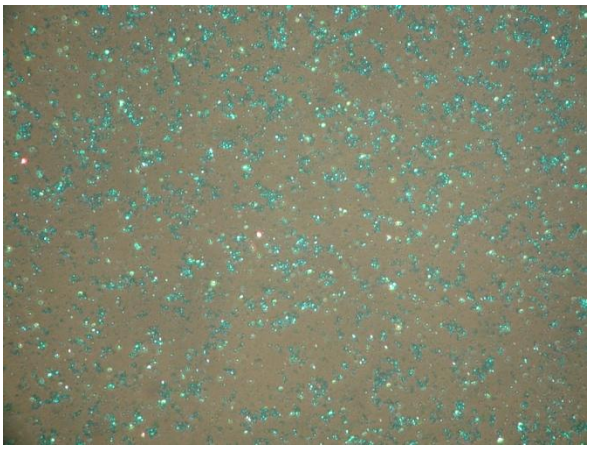

Crossed Polars, In RI 1.550, 400x

Normal Raman, 488nm

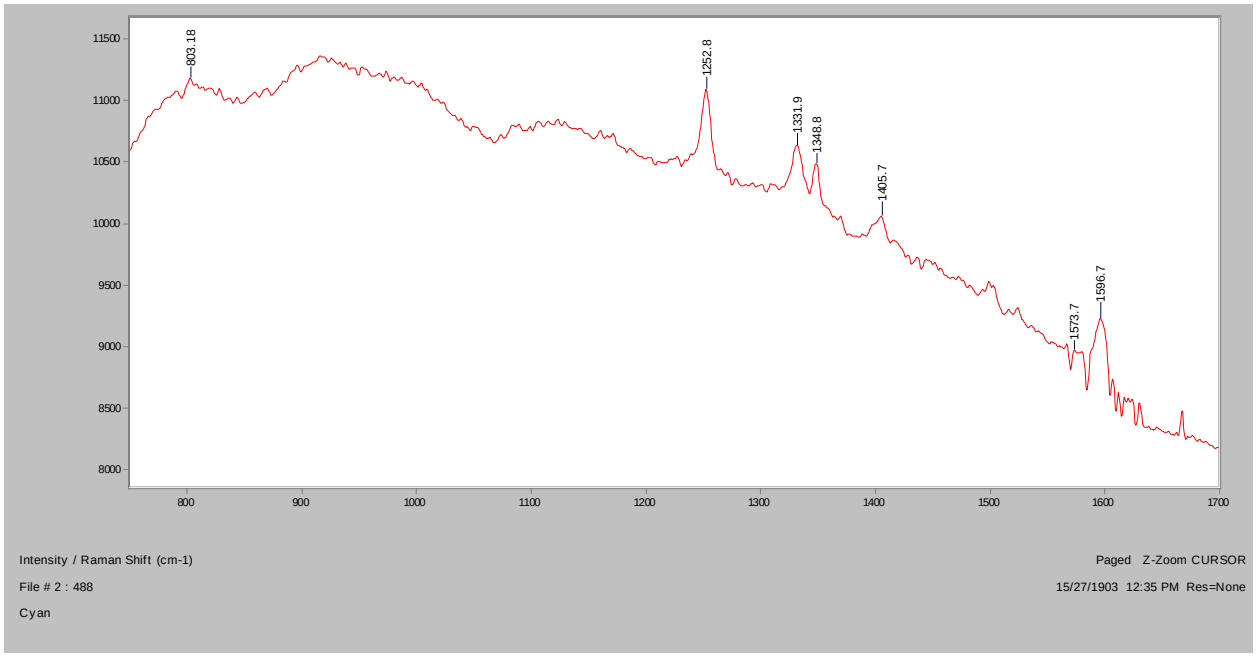

Normal Raman, 633nm

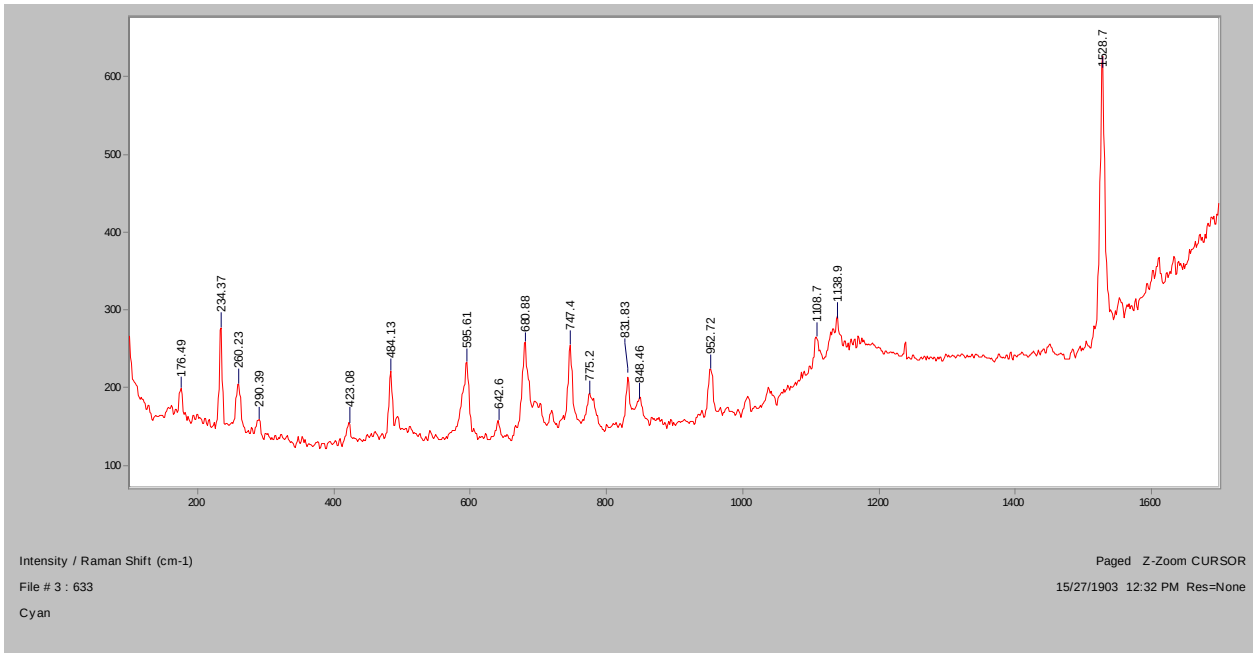

Normal Raman, 785nm

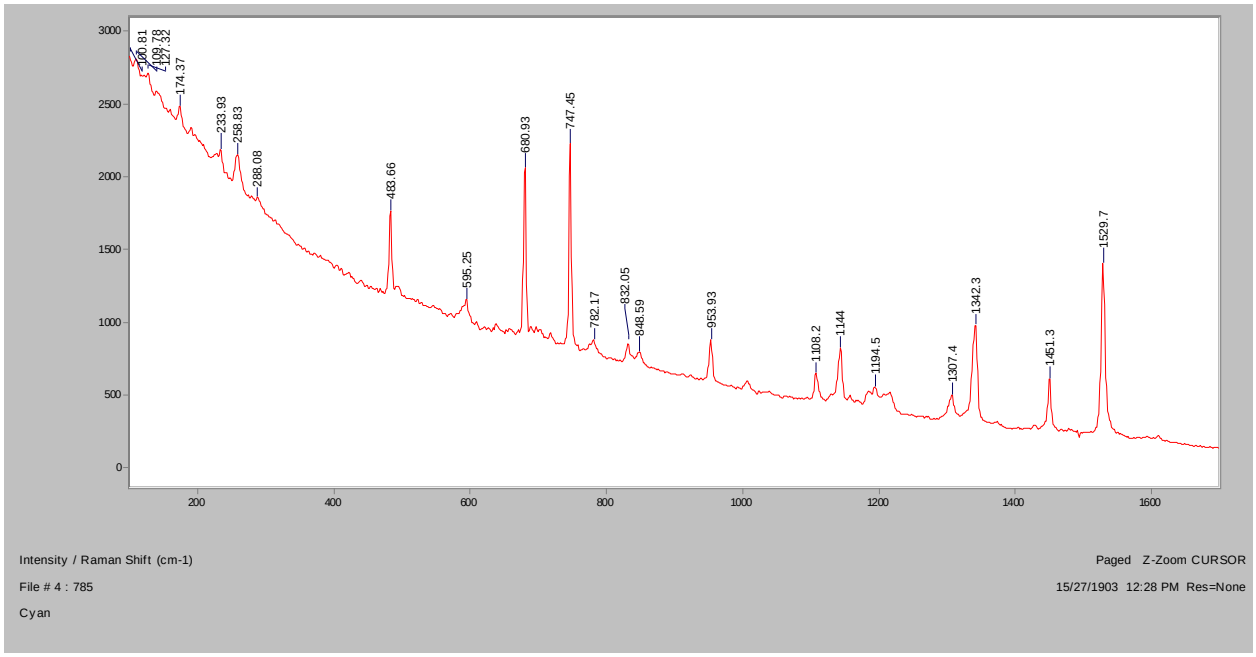

FT-Raman, 1064nm

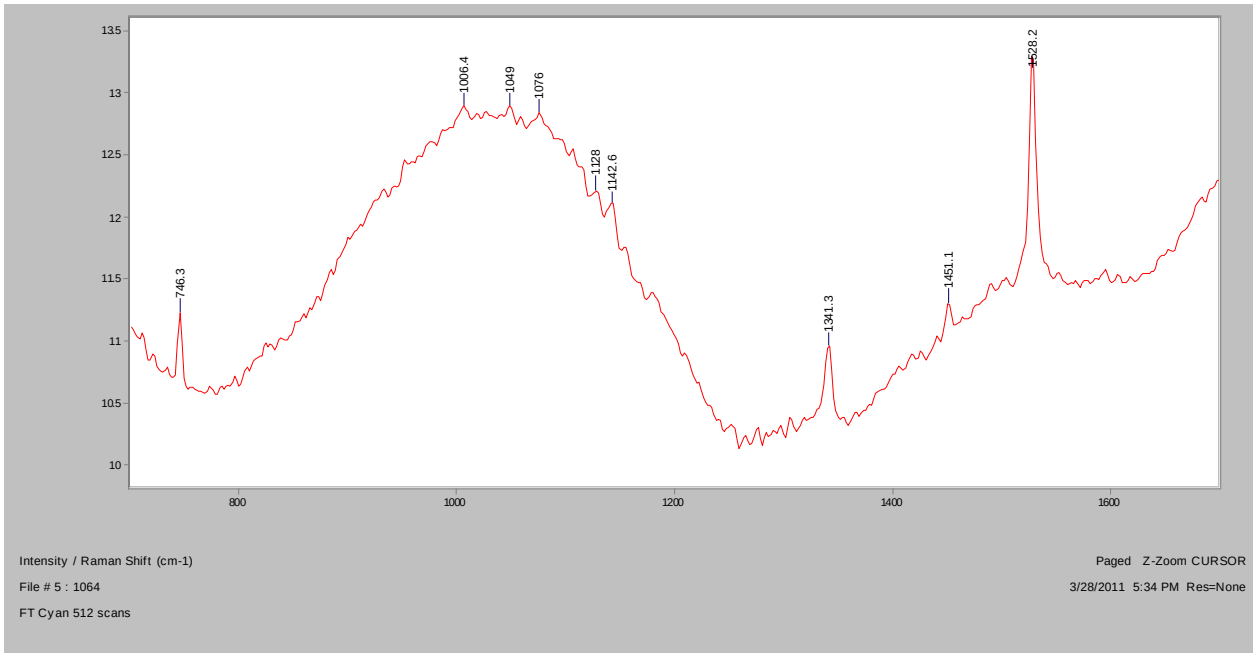

FT-IR (ATR)

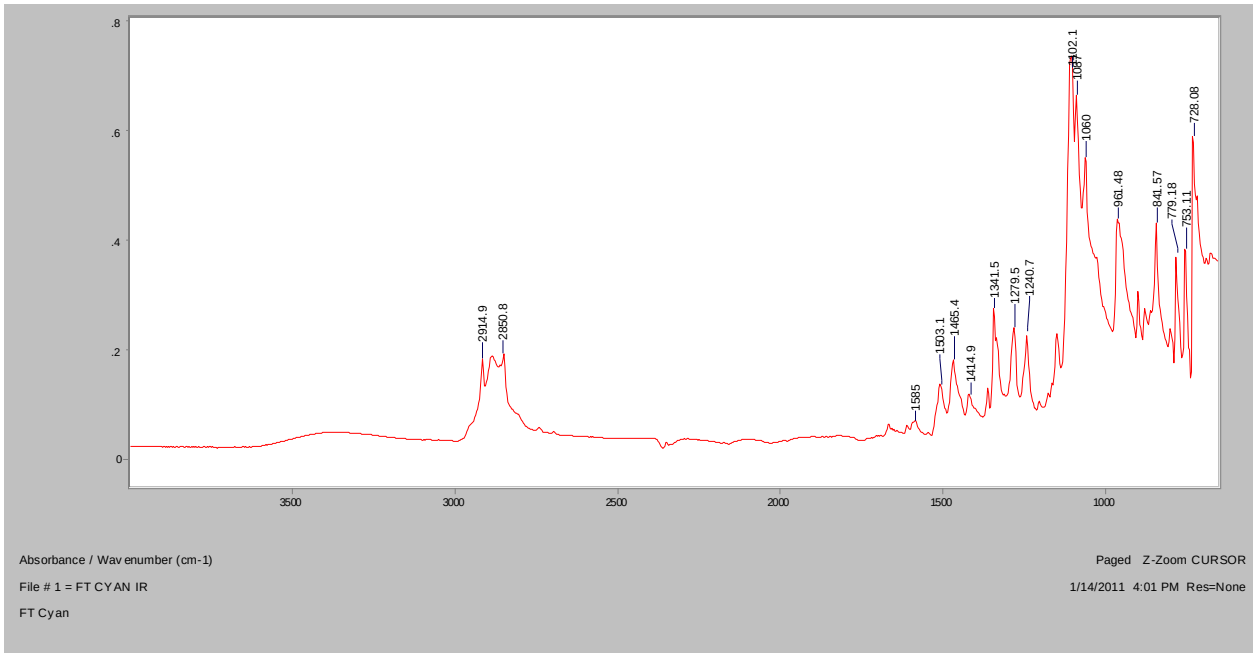
.8
.6
.4
.2
0
3500
3000
2500
2000
1500
1000
2914.9
2850.8
1585
1503.1
1465.4
1414.9
1341.5
1279.5
1240.7
1102.1
1060
961.48
841.57
779.18
753.11
728.08
Absorbance / Wavenumber (cm-1)
File # 1 = FT CYAN IR
FT Cyan
Paged Z-Zoom CURSOR
1/14/2011 4:01 PM Res=None

XRF

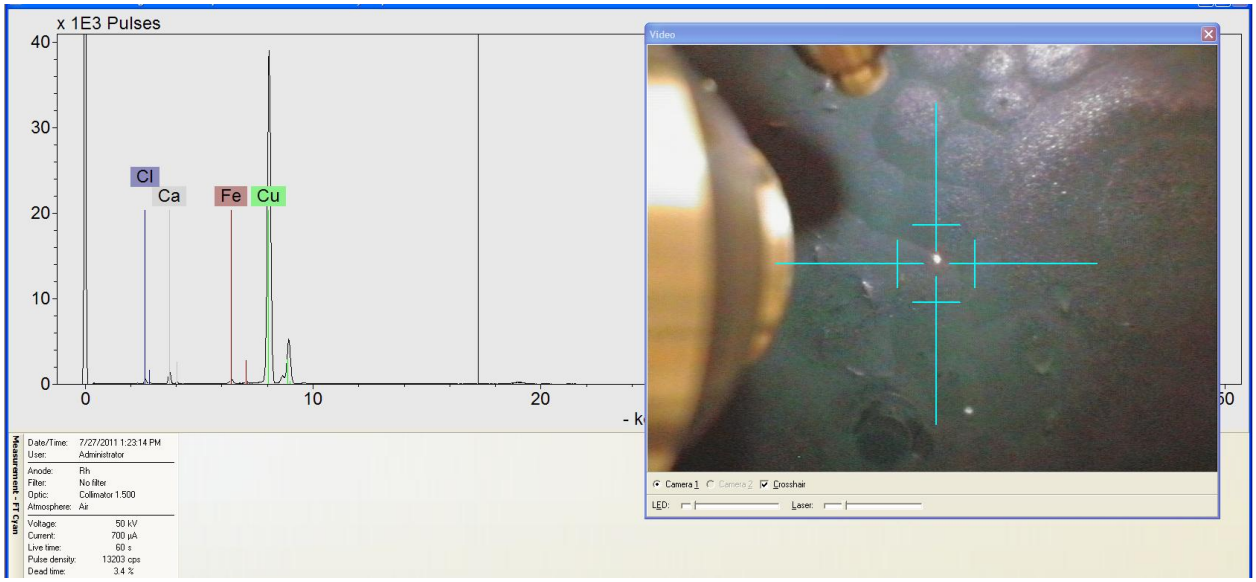
x 1E3 Pulses
40
30
20
10
0
0
10
20
Cl
Ca
Fe
Cu
Video
Camera 1
Camera 2
Crosshair
LED:
Laser:
Date/Time: 7/27/2011 1:23:14 PM
User: Administrator
Anode: Rh
Filter: No filter
Optic: Collimator 1.500
Atmosphere: Air
Voltage: 50 kV
Current: 700 µA
Live time: 60 s
Pulse density: 13203 cps
Dead time: 3.4 %

Dark Cyan

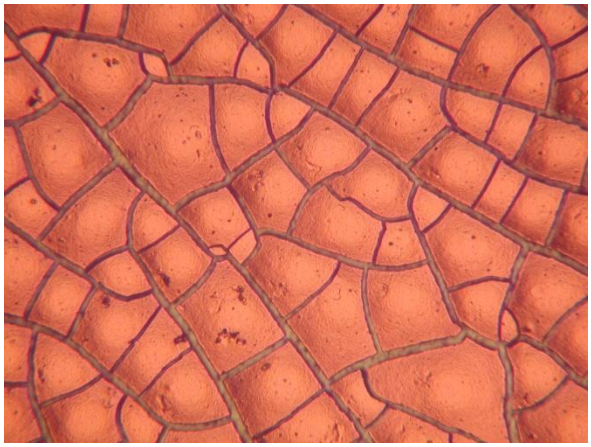

Bright Field, 100x

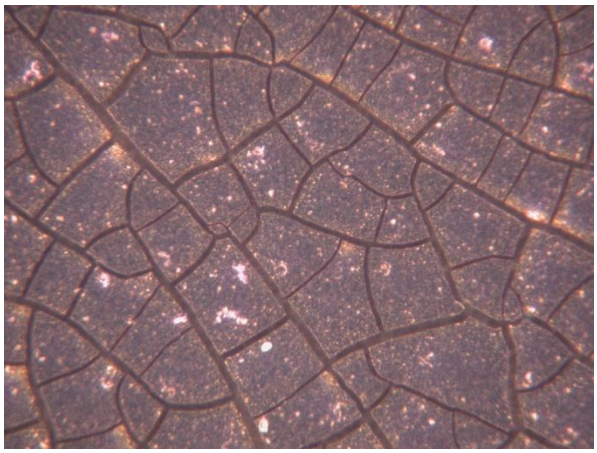

Dark Field, 100x

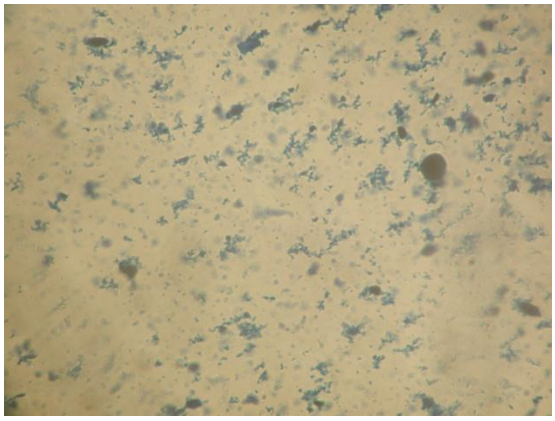

In RI 1.550, 400x

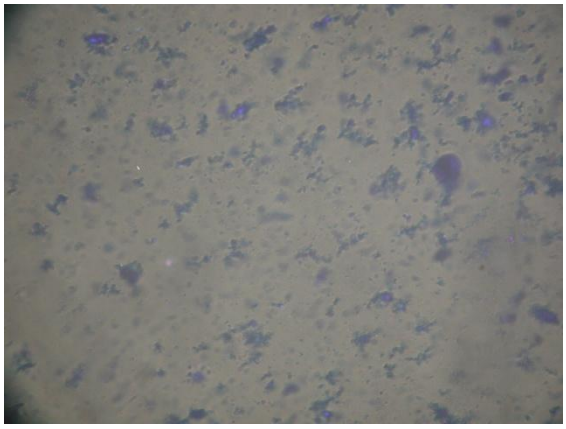

Crossed Polars, In RI 1.550, 400x

Normal Raman, 488nm

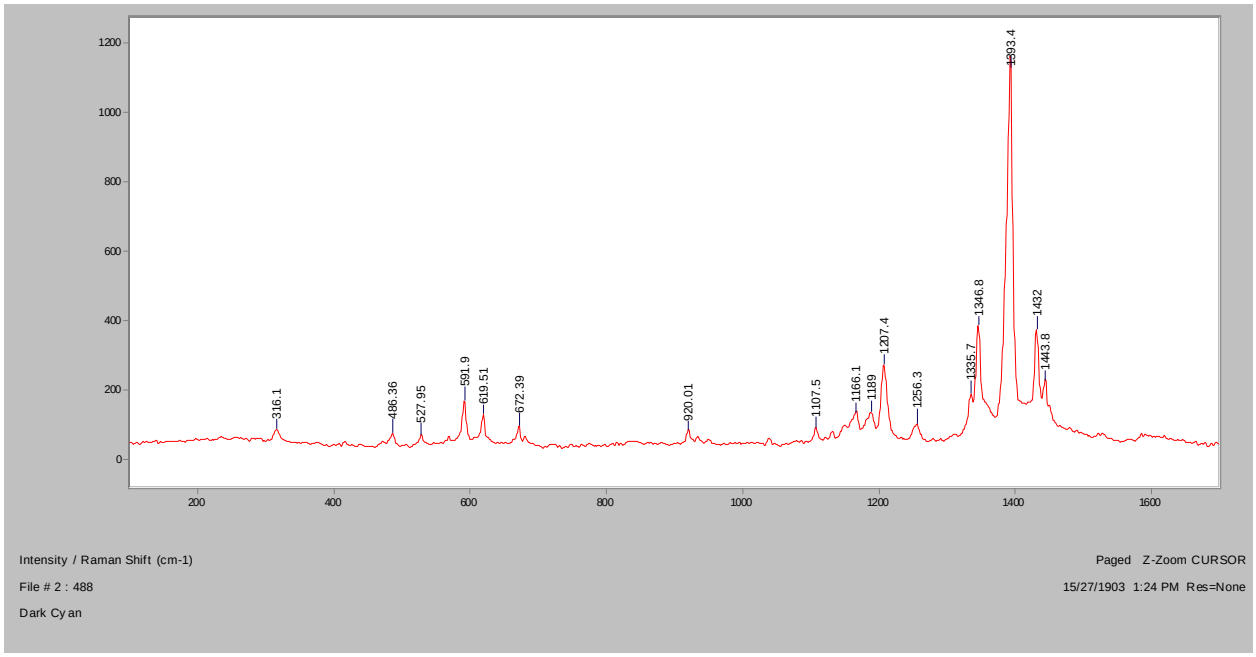

Normal Raman, 633nm

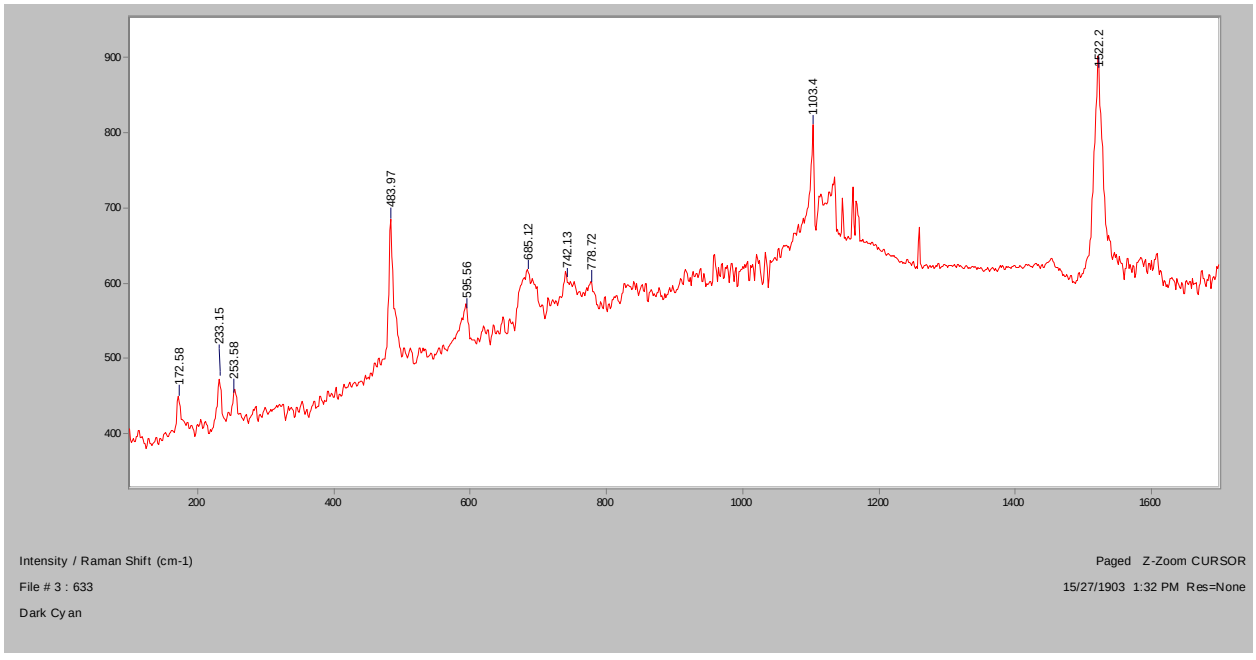

Normal Raman, 785nm

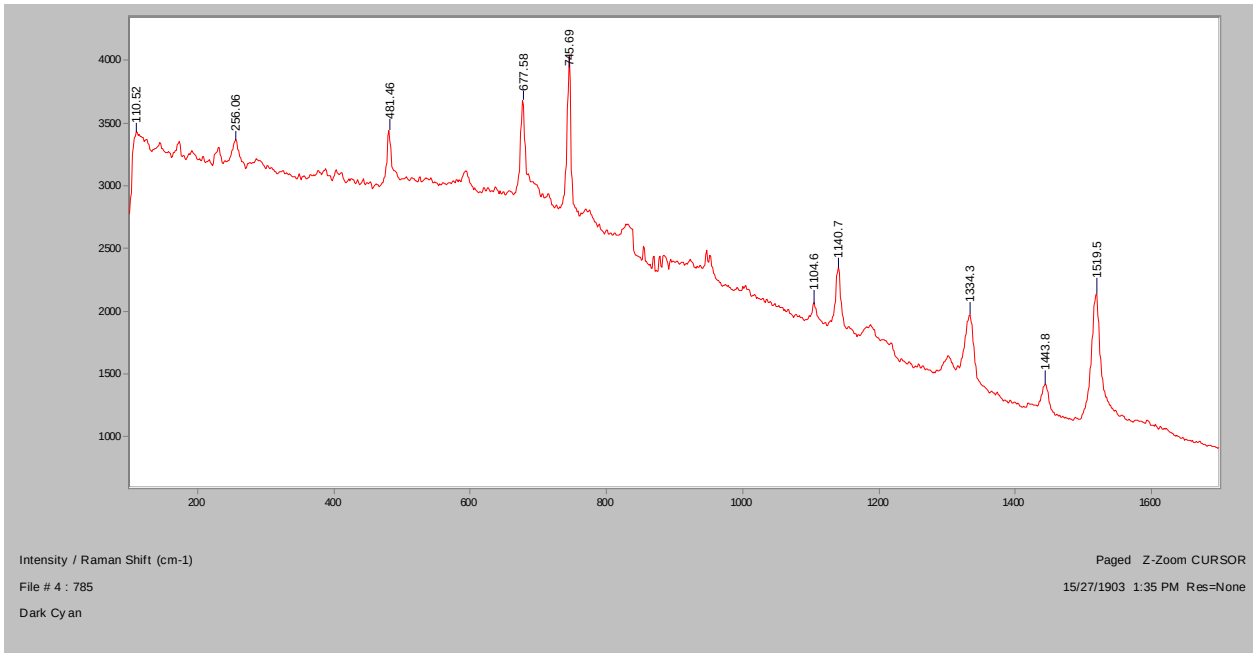

FT-Raman, 1064nm

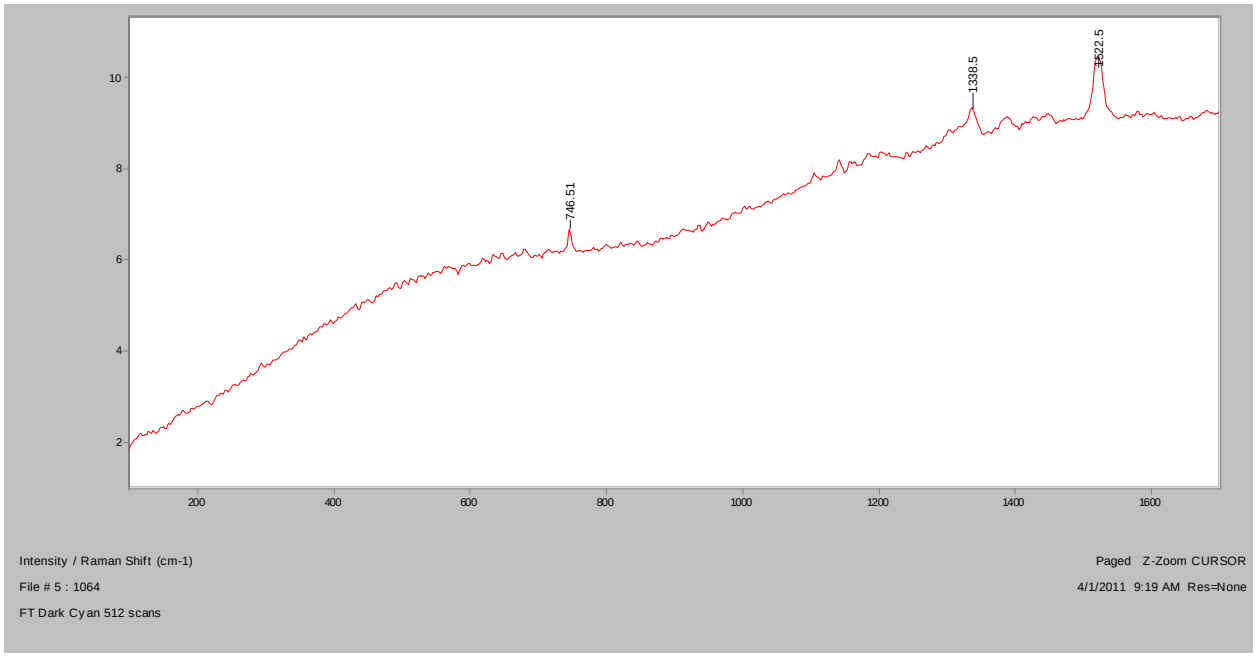

FT-IR (ATR)

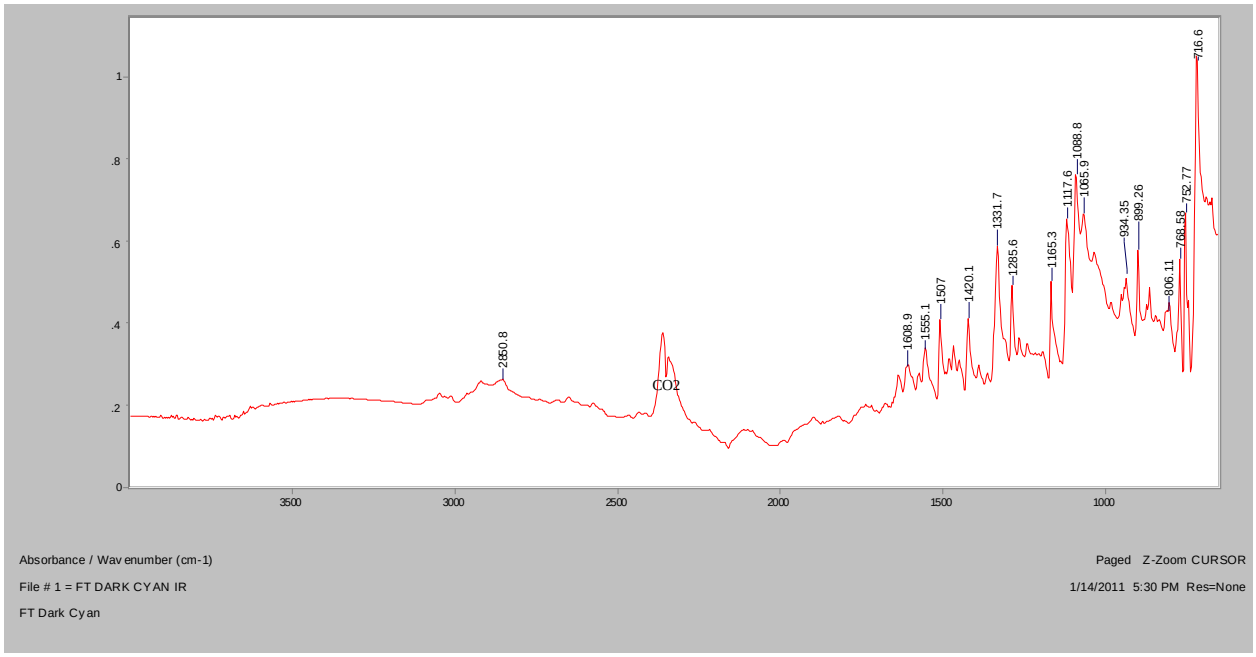
2850.8
CO2
1608.9
1555.1
1507
1420.1
1331.7
1285.6
1165.3
1117.6
1088.8
1065.9
934.35
899.26
806.11
768.58
752.77
716.6
Absorbance / Wavenumber (cm-1)
File # 1 = FT DARK CYAN IR
FT Dark Cyan
Paged Z-Zoom CURSOR
1/14/2011 5:30 PM Res=None

XRF

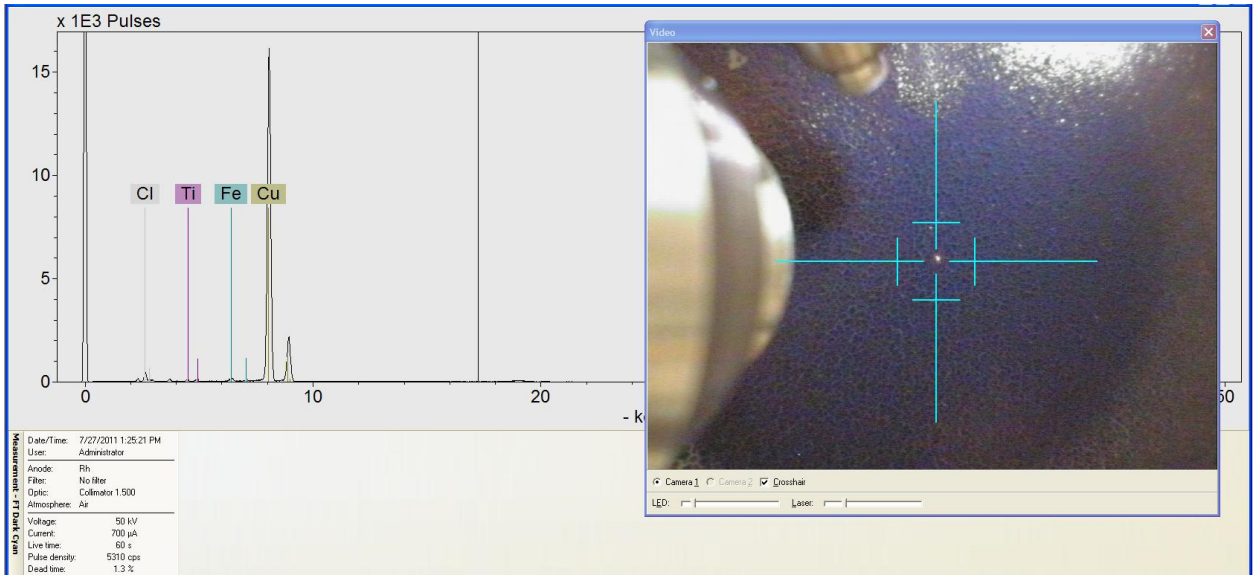
x 1E3 Pulses
Cl
Ti
Fe
Cu
Video
Camera 1
Camera 2
Crosshair
LED:
Laser:
Date/Time: 7/27/2011 1:25:21 PM
User: Administrator
Anode: Rh
Filter: No filter
Optic: Collimator 1.500
Atmosphere: Air
Voltage: 50 kV
Current: 700 µA
Live time: 60 s
Pulse density: 5310 cps
Dead time: 1.3 %

Blue

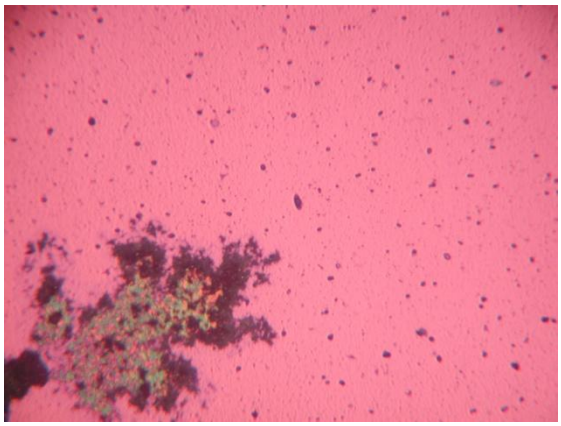

Bright Field, 100x

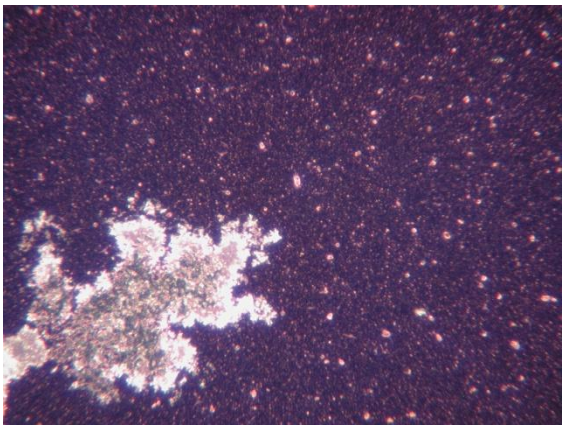

Dark Field, 100x

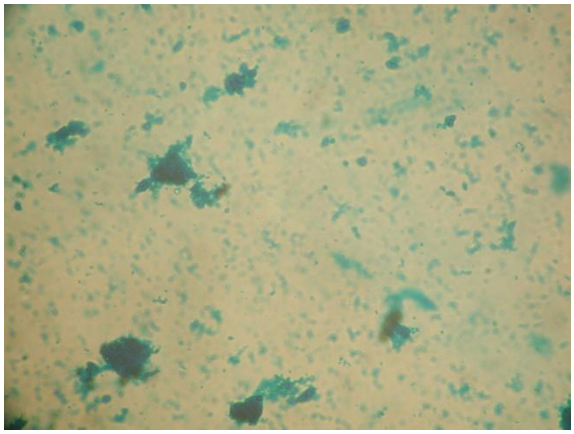

In RI 1.550, 400x

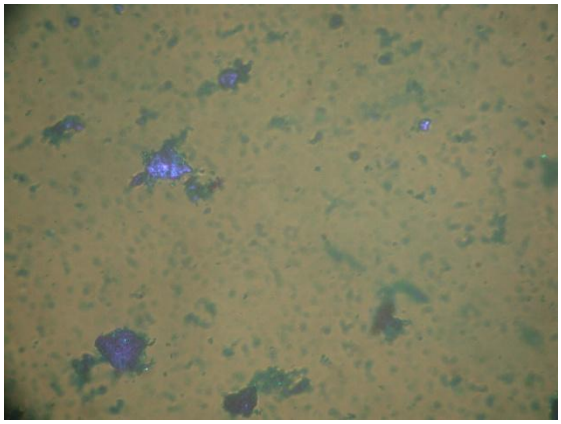

Crossed Polars, In RI 1.550, 400x

Normal Raman, 488nm

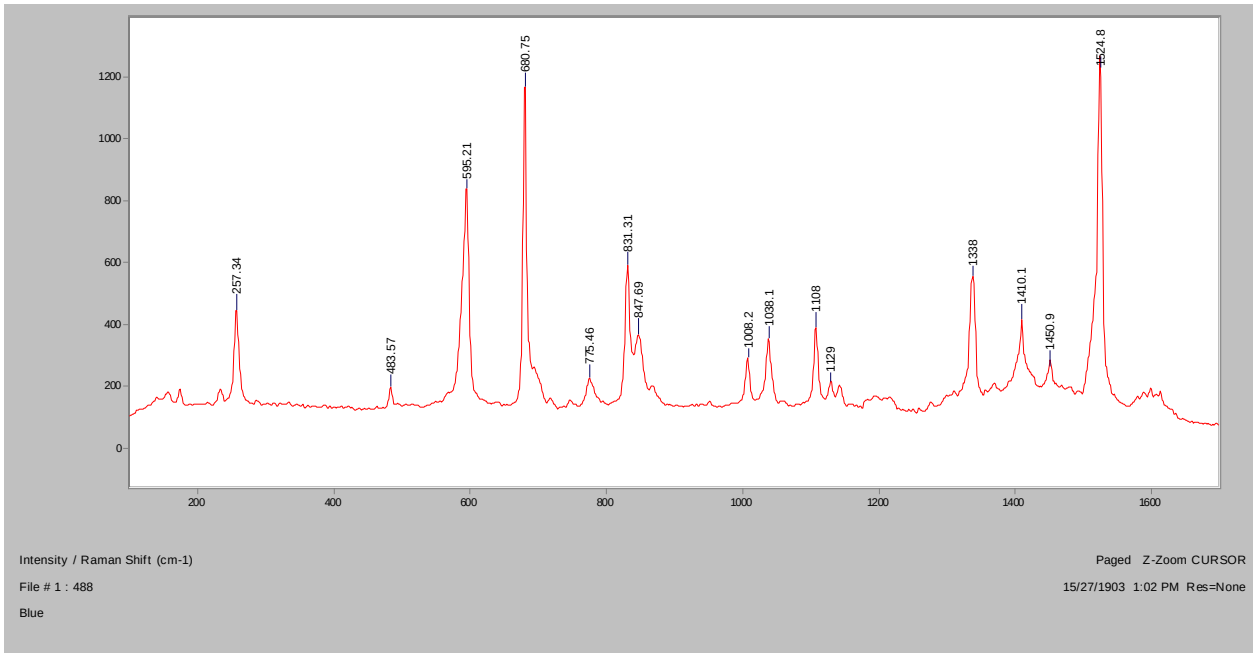

Normal Raman, 633nm

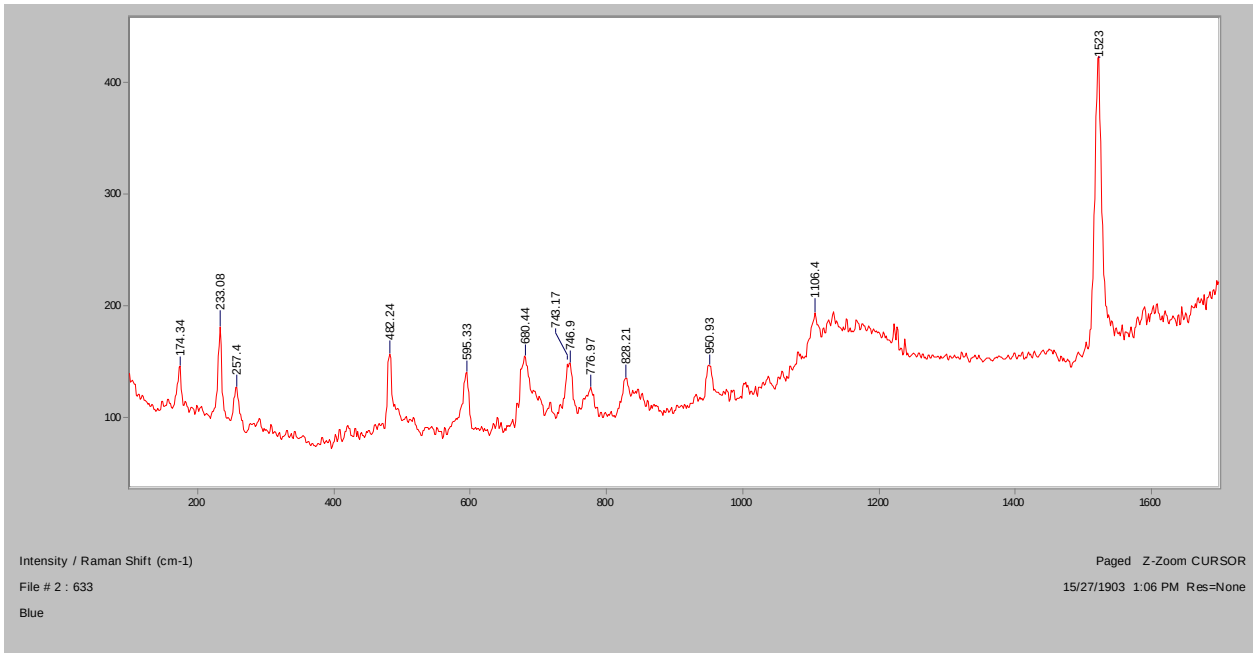

Normal Raman, 785nm

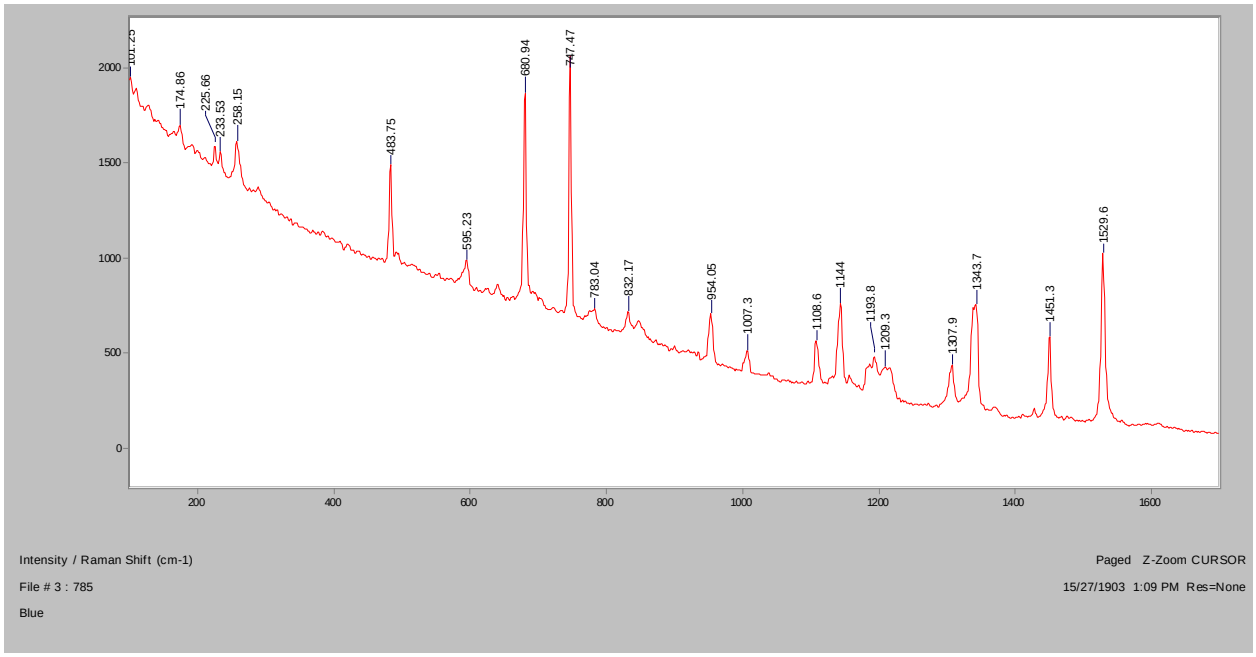

FT-Raman, 1064nm

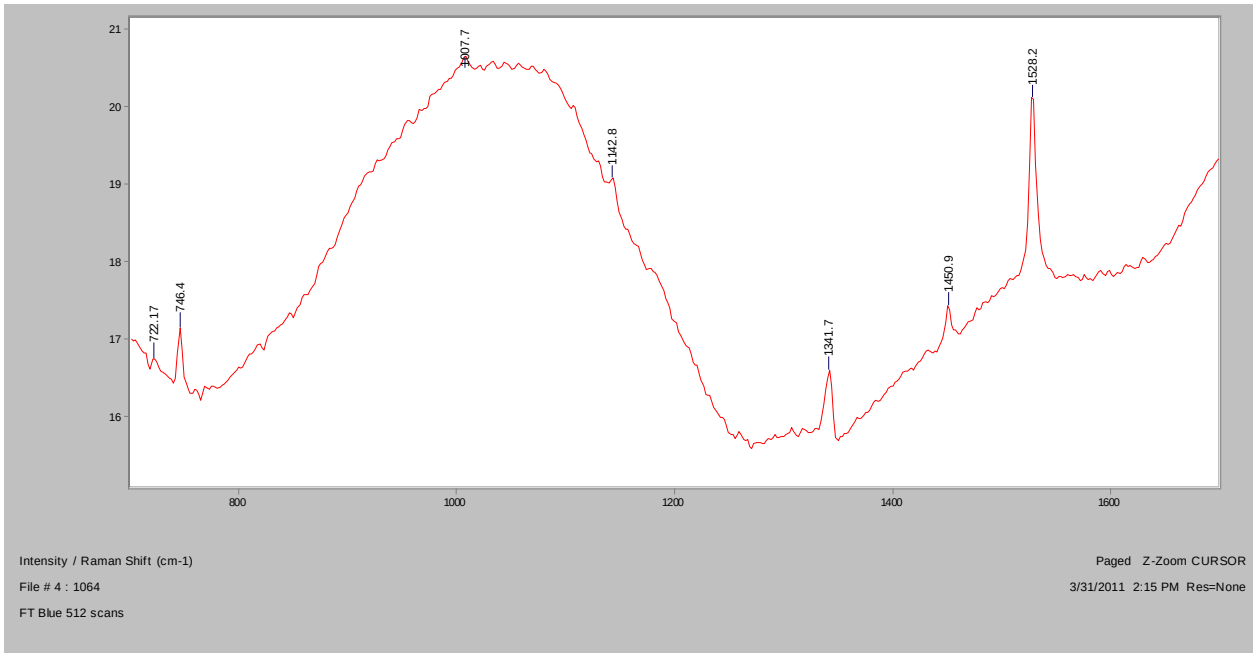

FT-IR (ATR)

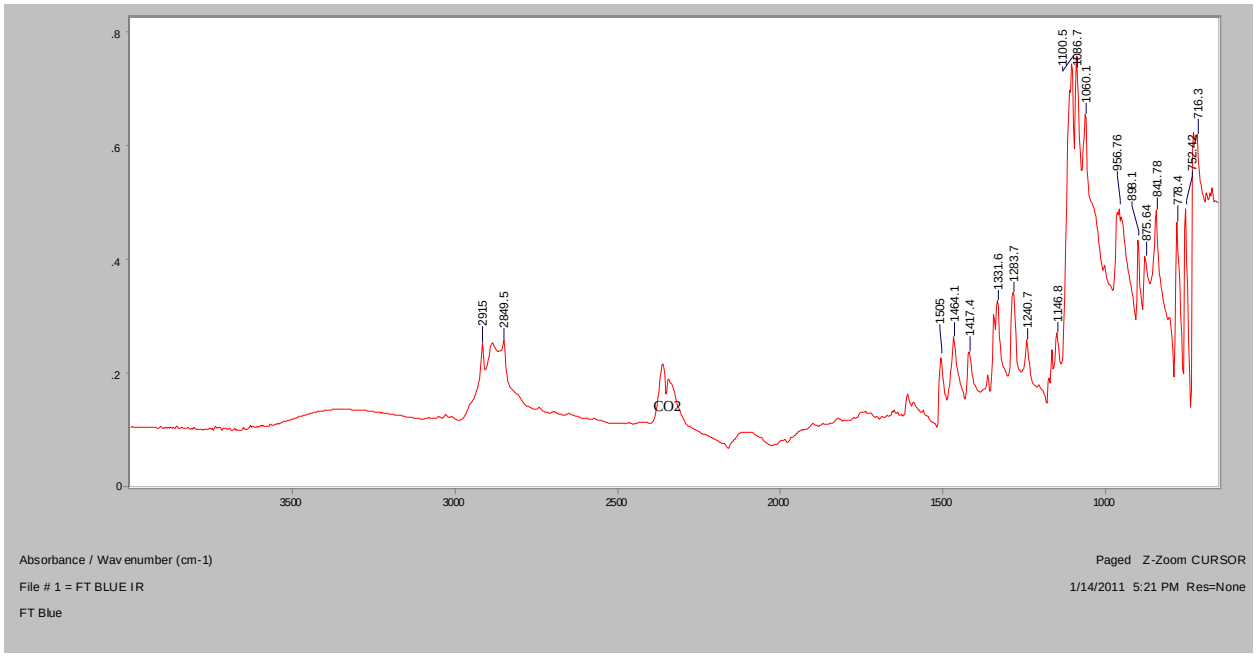
.8
.6
.4
.2
0
3500
3000
2500
2000
1500
1000
2915
2849.5
CO2
1505
1464.1
1417.4
1331.6
1283.7
1240.7
1146.8
1100.5
1086.7
1060.1
956.76
898.1
875.64
841.78
798.4
752.42
716.3
Absorbance / Wavenumber (cm-1)
File # 1 = FT BLUE IR
FT Blue
Paged Z-Zoom CURSOR
1/14/2011 5:21 PM Res=None

XRF

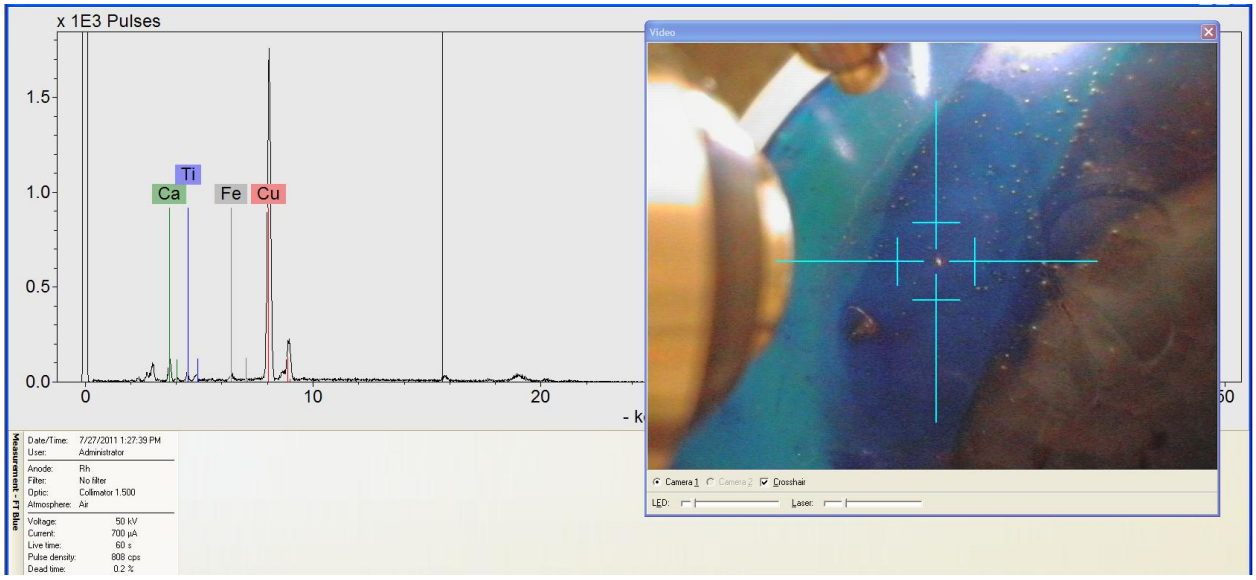
x 1E3 Pulses
1.5
1.0
0.5
0.0
0
10
20
Ti
Ca
Fe
Cu
Video
Camera 1
Camera 2
Crosshair
LED:
Laser:
Date/Time: 7/27/2011 1:27:39 PM
User: Administrator
Anode: Rh
Filter: No filter
Optic: Collimator 1.500
Atmosphere: Air
Voltage: 50 kV
Current: 700 µA
Live time: 60 s
Pulse density: 808 cps
Dead time: 0.2 %

Navy Blue

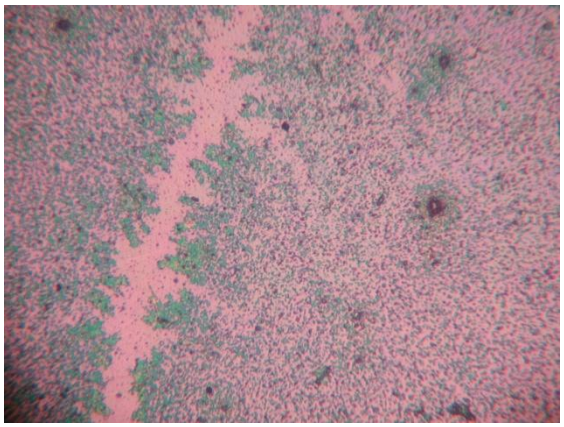

Bright Field, 100x

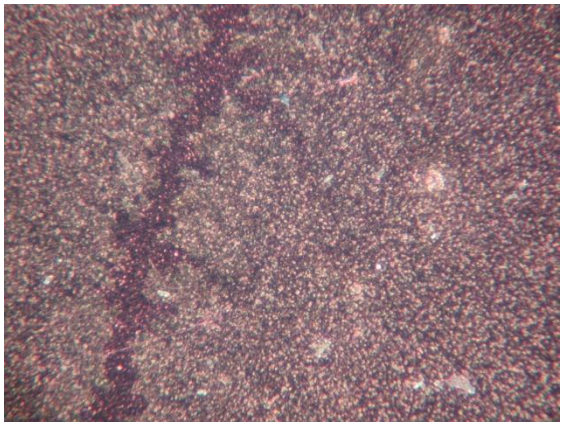

Dark Field, 100x

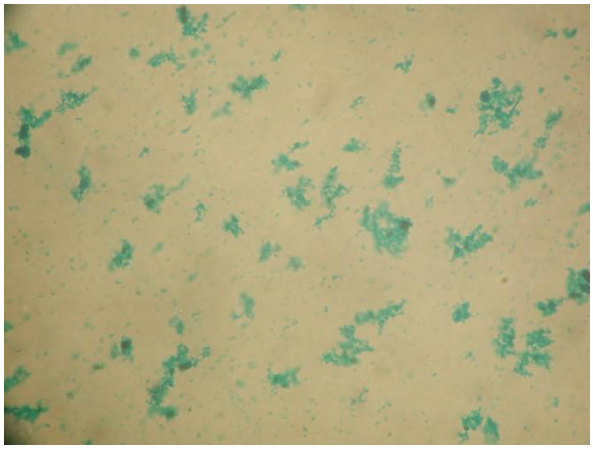

In RI 1.550, 400x

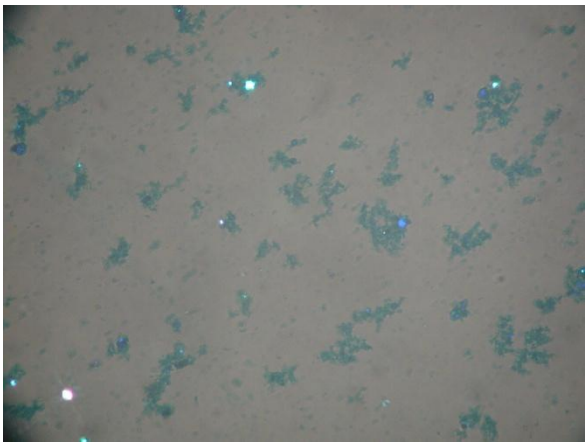

Crossed Polars, In RI 1.550, 400x

Normal Raman, 488nm

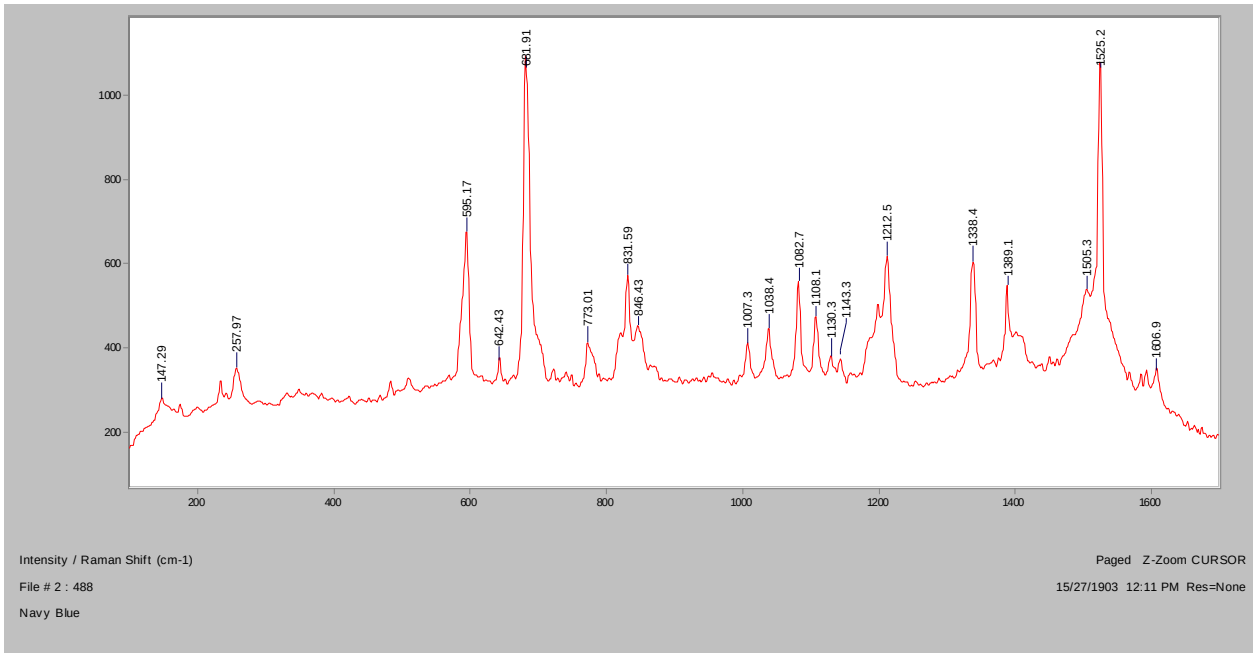

Normal Raman, 633nm

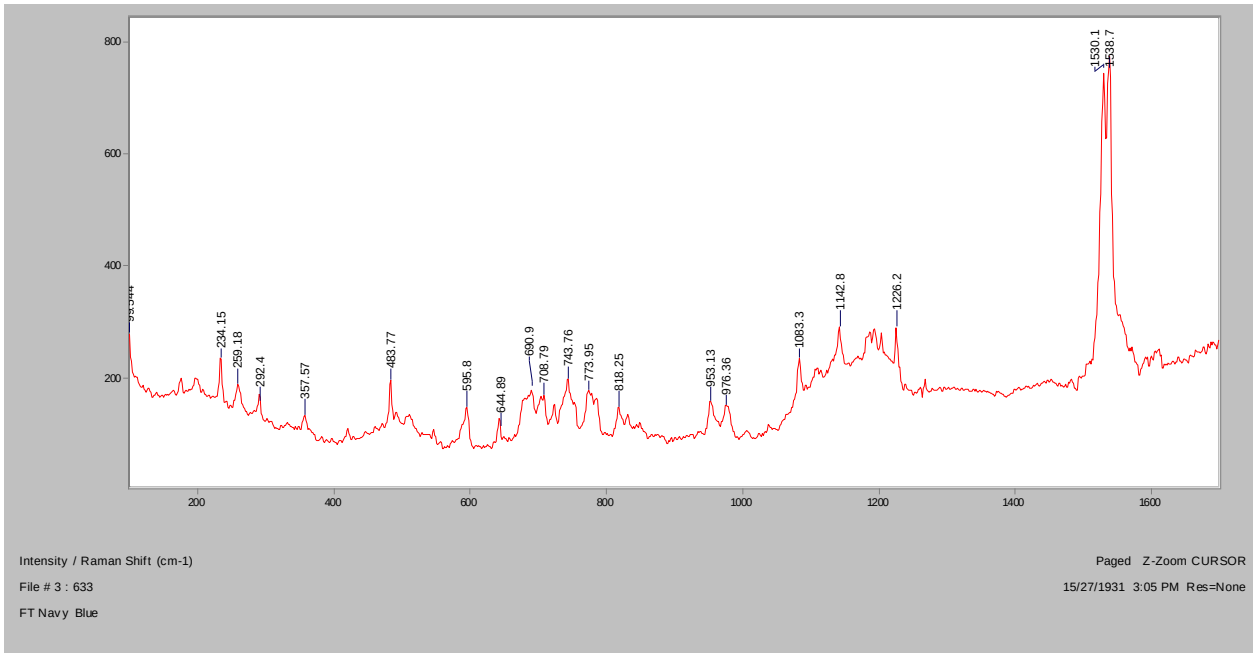

Normal Raman, 785nm

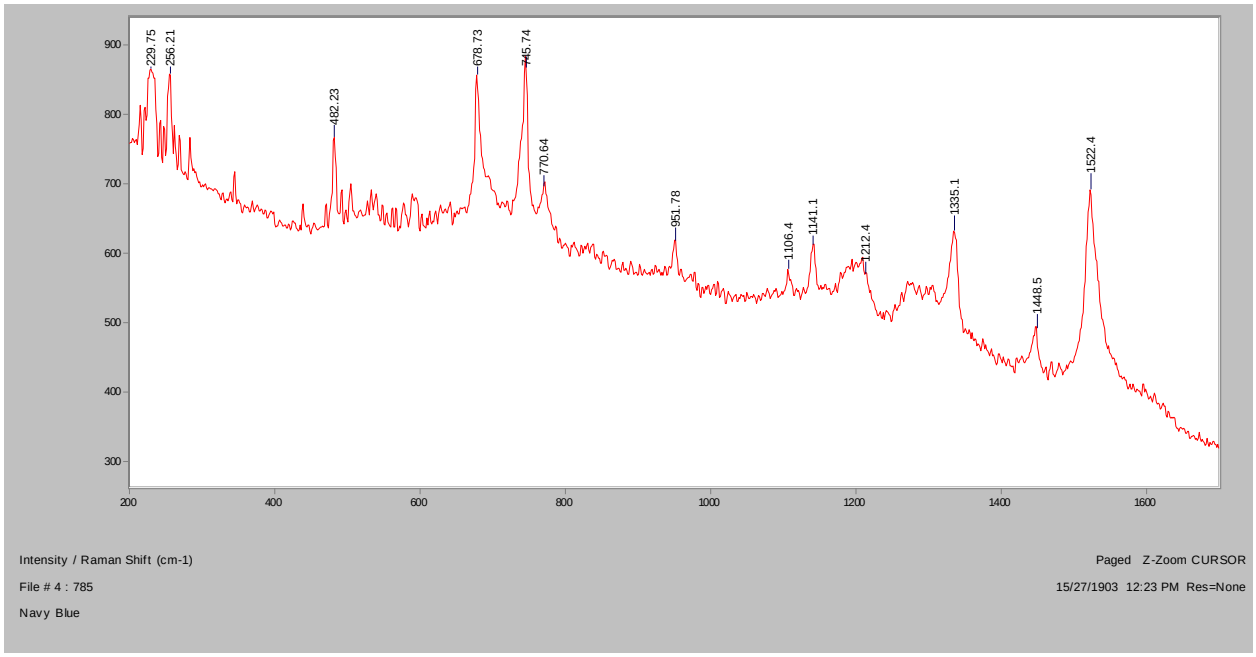

FT-Raman, 1064nm

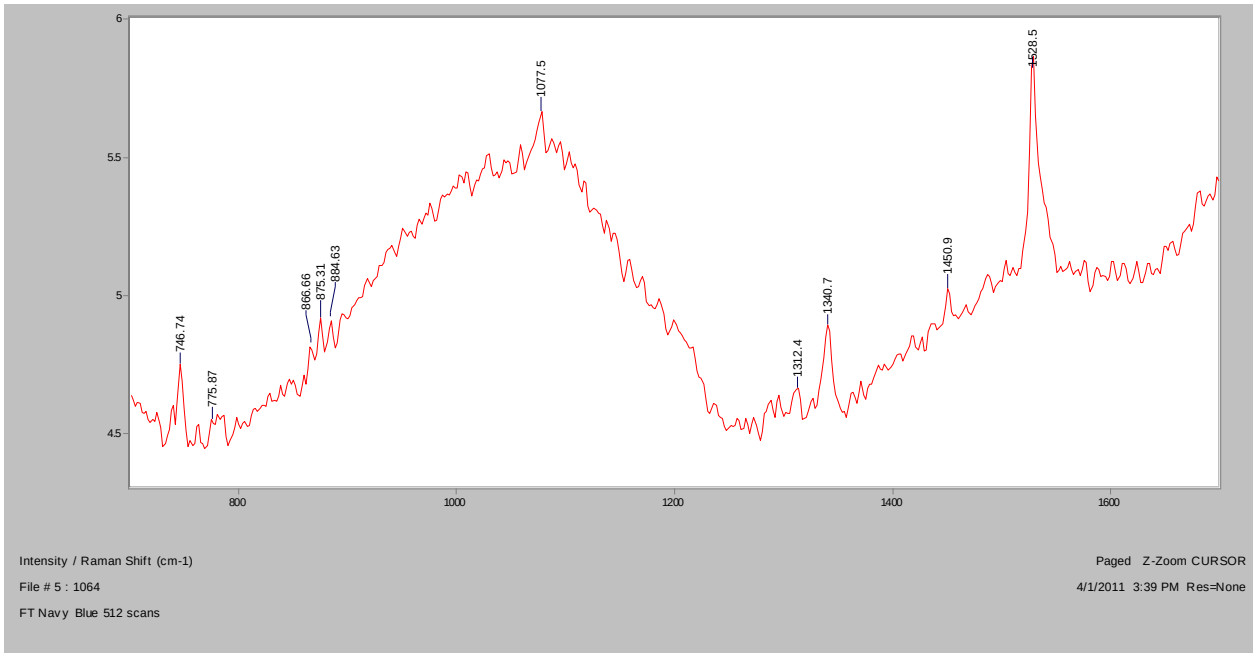

FT-IR (ATR)

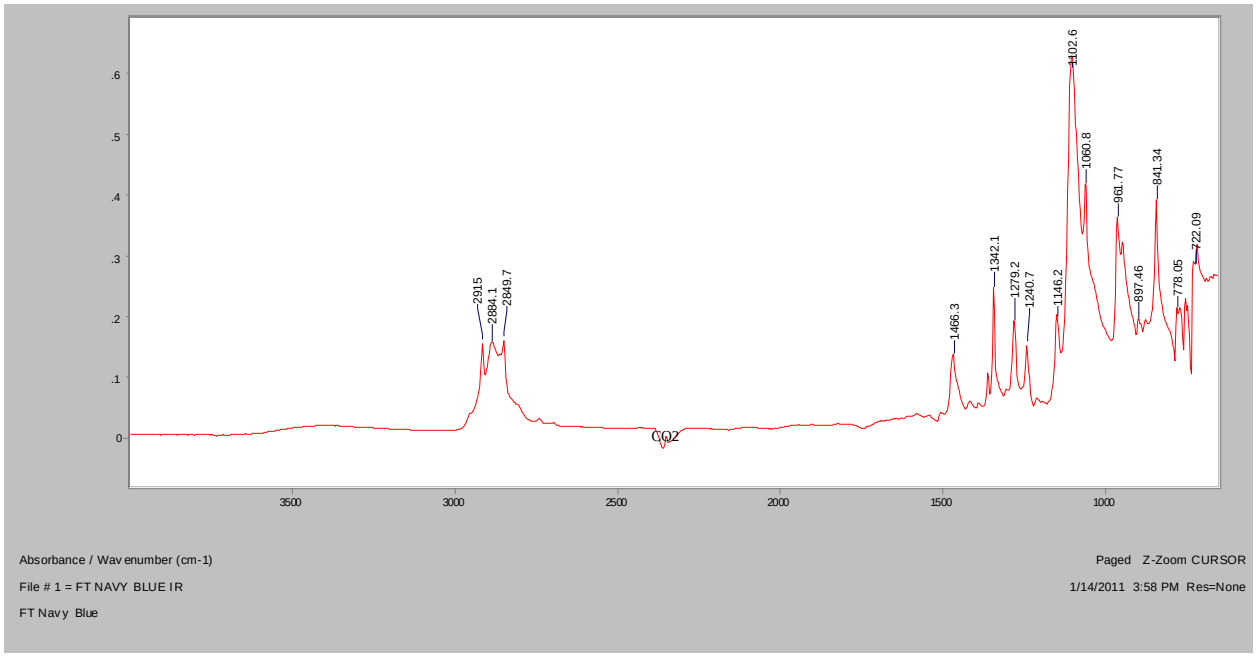
2915
2884.1
2849.7
1466.3
1342.1
1279.2
1240.7
1146.2
1102.6
1060.8
961.77
841.34
897.46
778.05
722.09
CO2
Absorbance / Wavenumber (cm-1)
File # 1 = FT NAVY BLUE IR
FT Navy Blue
Paged Z-Zoom CURSOR
1/14/2011 3:58 PM Res=None

XRF

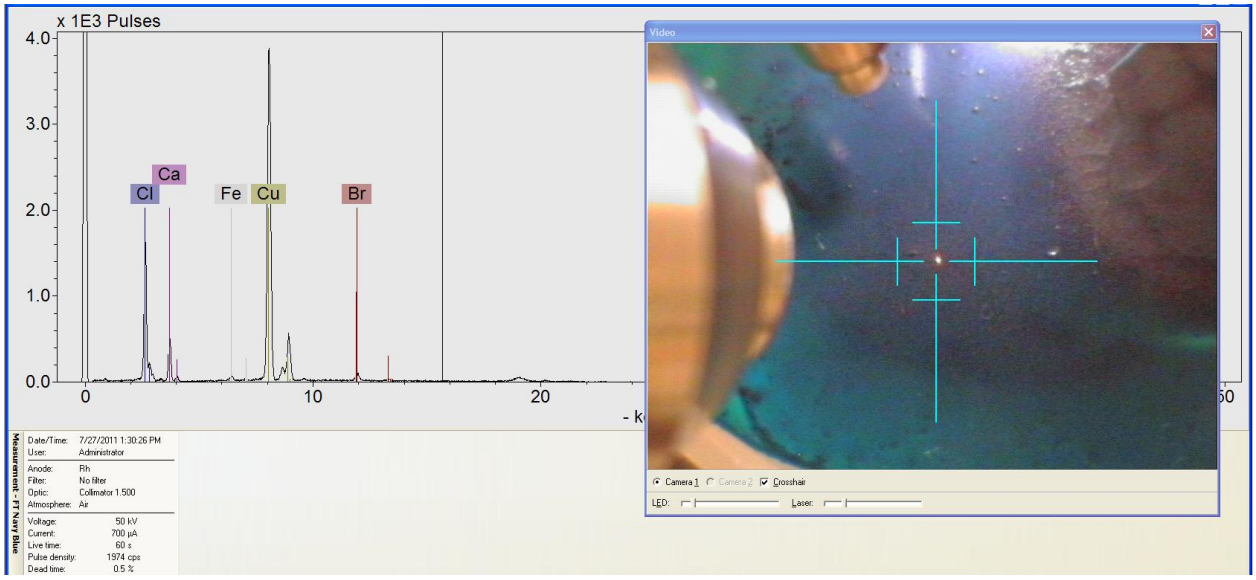
x 1E3 Pulses
Ca
Cl
Fe
Cu
Br
Video
Camera 1
Camera 2
Crosshair
LED:
Laser:
Date/Time: 7/27/2011 1:30:26 PM
User: Administrator
Anode: Rh
Filter: No filter
Optic: Collimator 1.500
Atmosphere: Air
Voltage: 50 kV
Current: 700 µA
Live time: 60 s
Pulse density: 1974 cps
Dead time: 0.5 %

Dark Blue

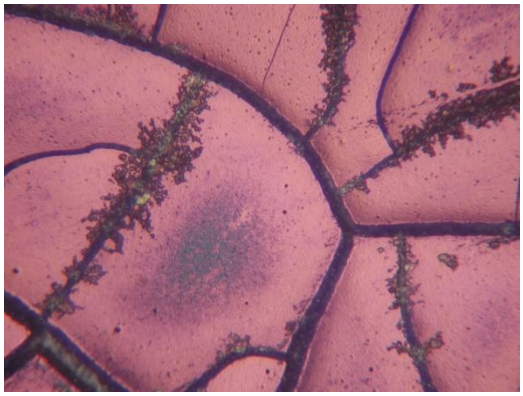

Bright Field, 100x

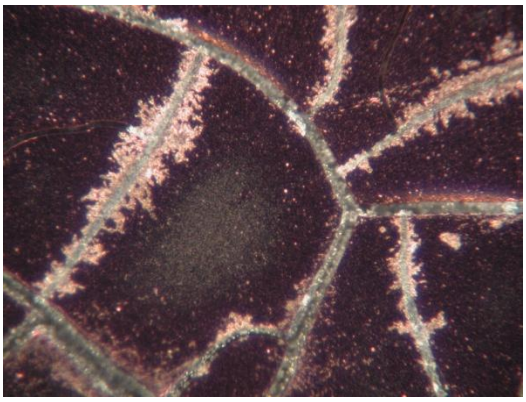

Dark Field, 100x

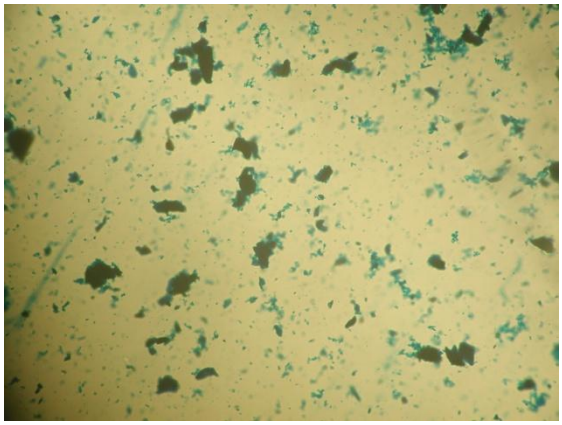

In RI 1.550, 400x

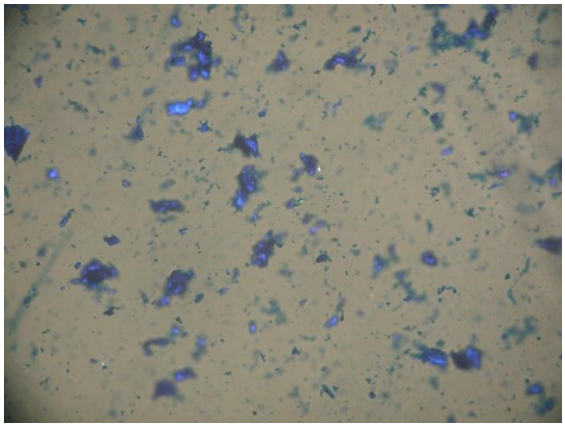

Crossed Polars, In RI 1.550, 400x

Normal Raman, 488nm

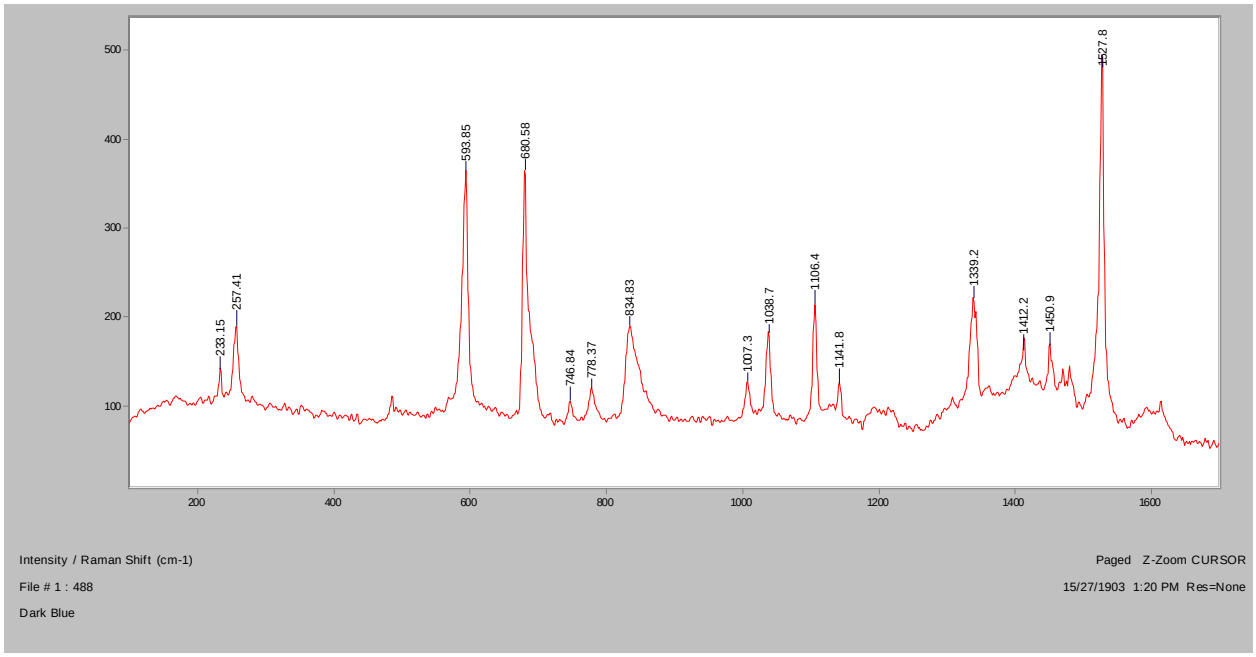

Normal Raman, 633nm

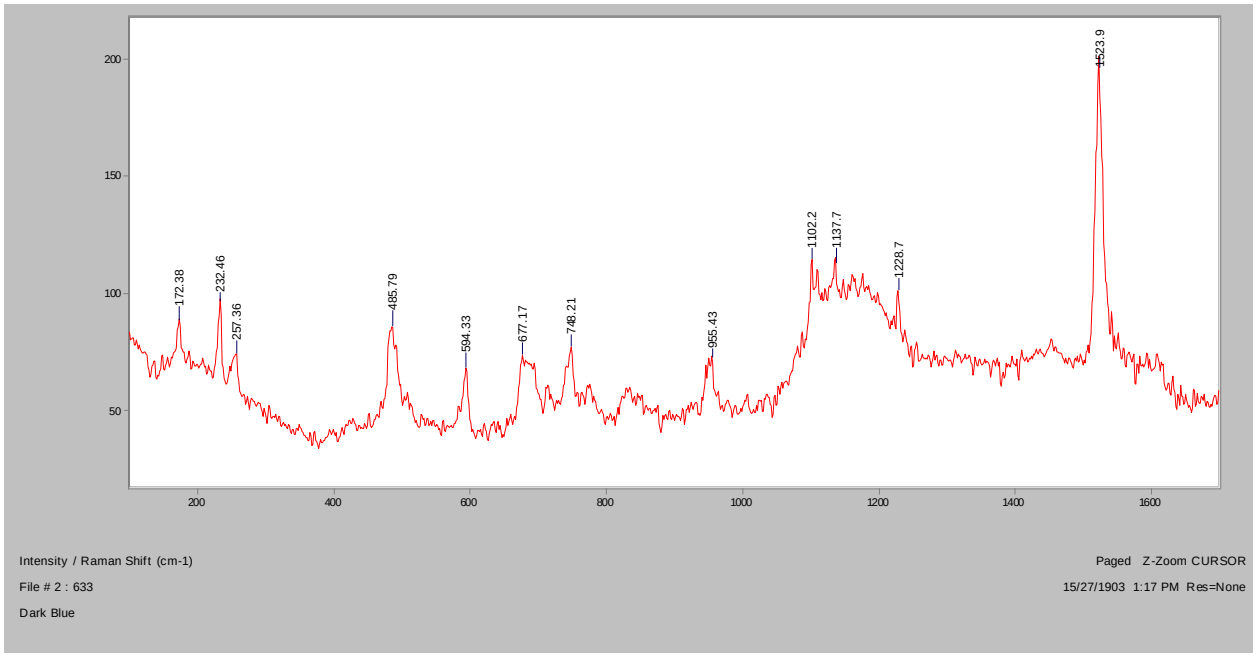

Normal Raman, 785nm

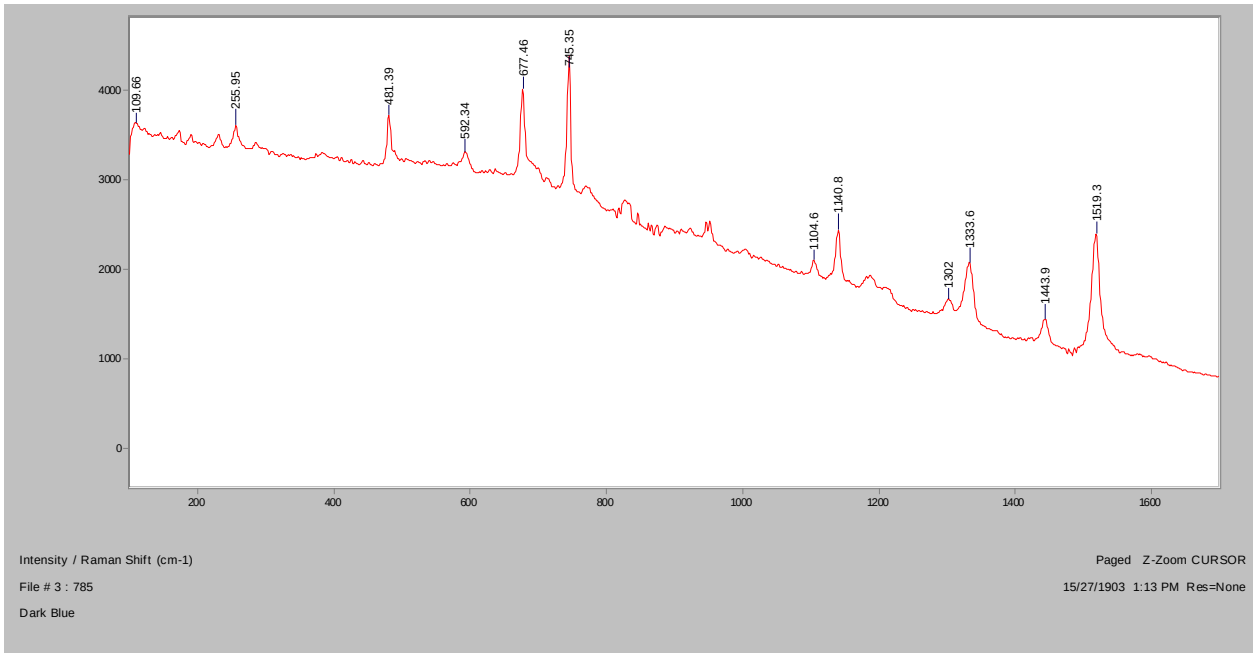

FT-Raman, 1064nm

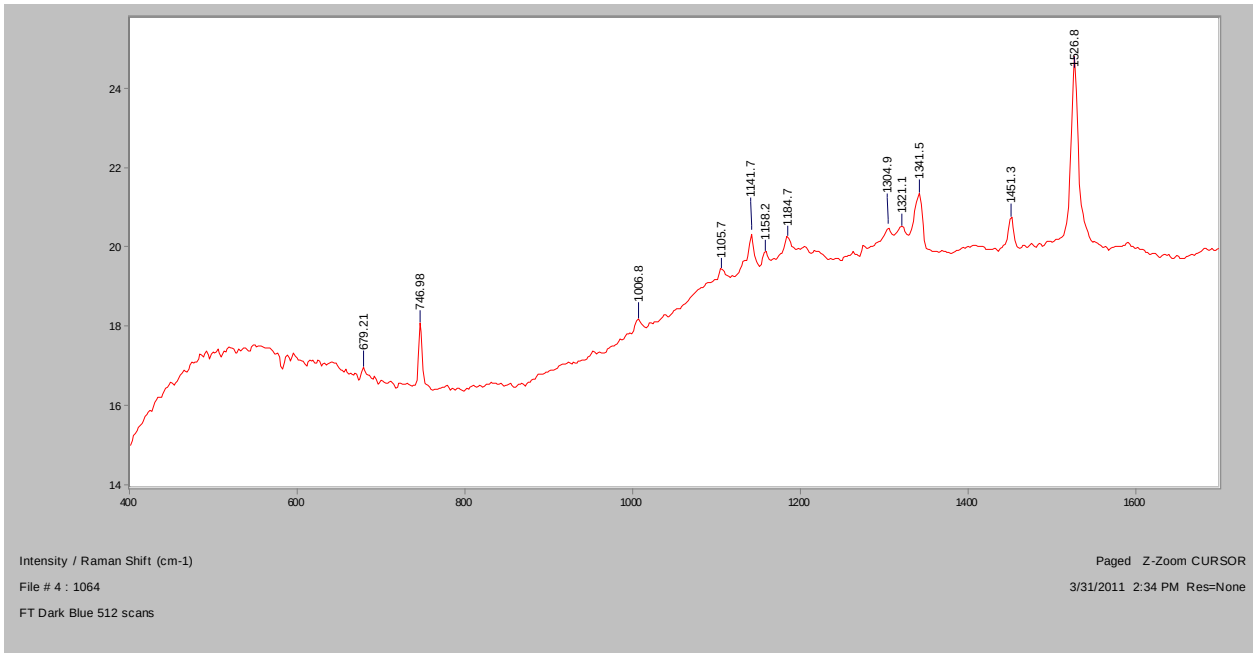

FT-IR (ATR)

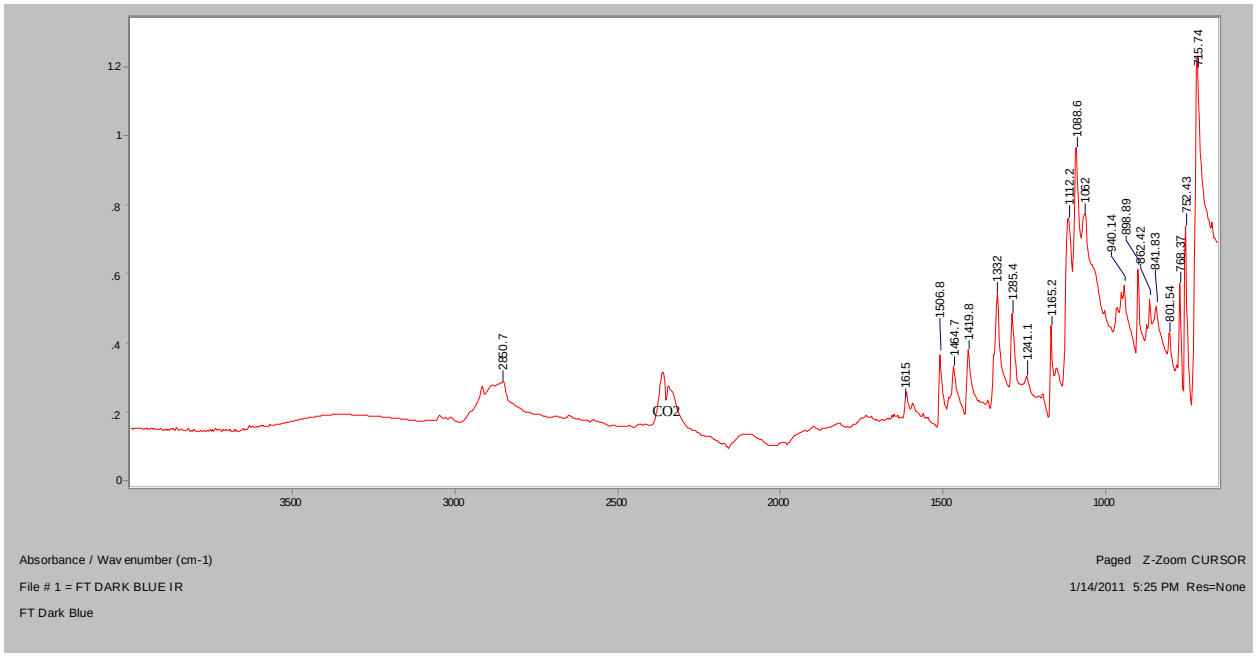
2850.7
CO2
1615
1506.8
1464.7
1419.8
1332
1285.4
1241.1
1165.2
1112.2
1088.6
1062
940.14
898.89
862.42
841.83
801.54
768.37
752.43
715.74
Absorbance / Wavenumber (cm-1)
File # 1 = FT DARK BLUE IR
FT Dark Blue
Paged Z-Zoom CURSOR
1/14/2011 5:25 PM Res=None

XRF

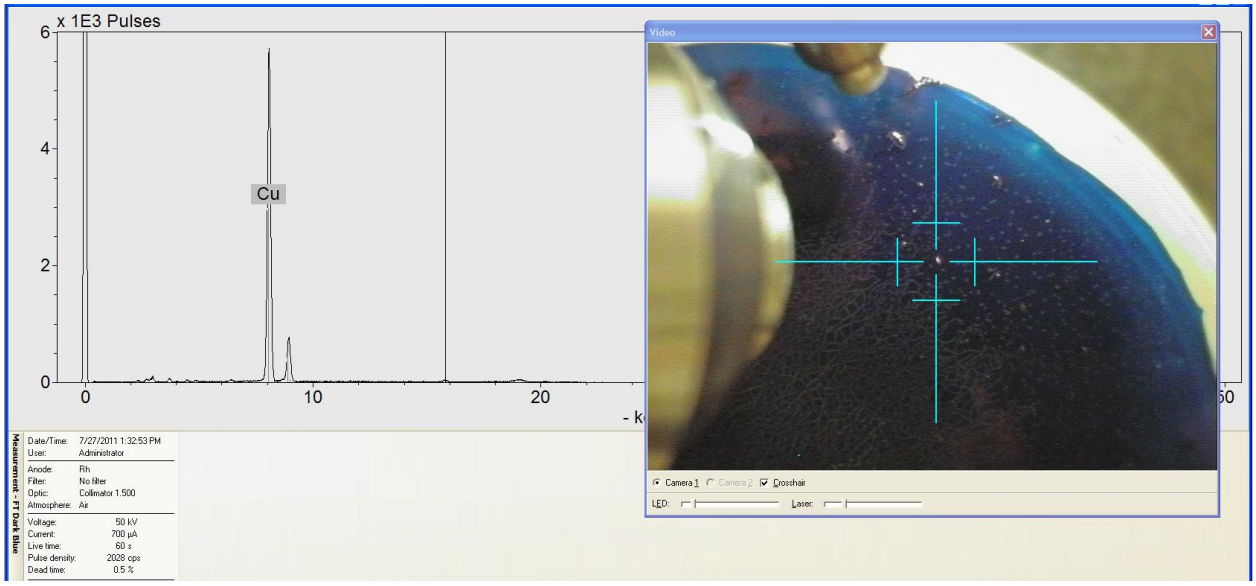
x 1E3 Pulses
Cu
Video
Camera 1
Camera 2
Crosshair
LED:
Laser:
Date/Time: 7/27/2011 1:32:53 PM
User: Administrator
Anode: Rh
Filter: No filter
Optic: Collimator 1.500
Atmosphere: Air
Voltage: 50 kV
Current: 700 µA
Live time: 60 s
Pulse density: 2028 cps
Dead time: 0.5 %

Grape

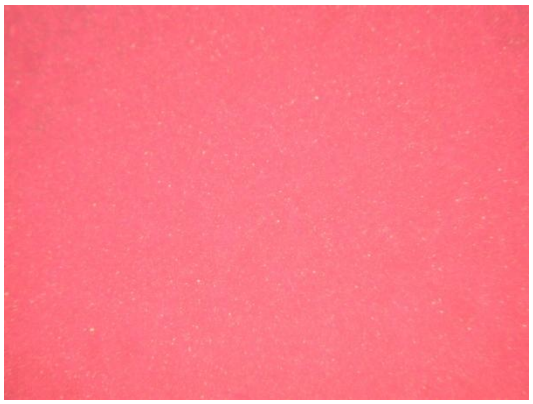

Bright Field, 100x

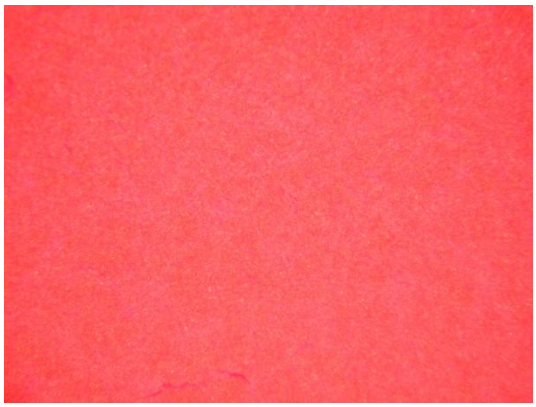

Dark Field, 100x

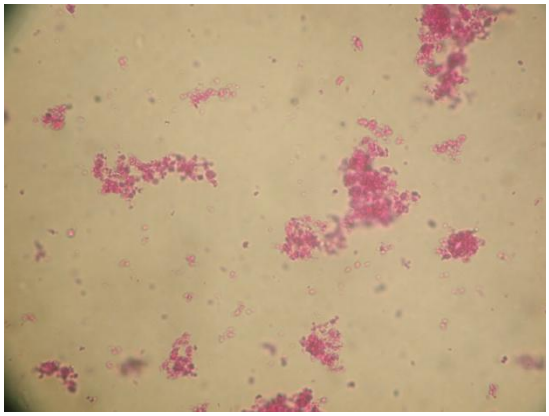

In RI 1.550, 400x

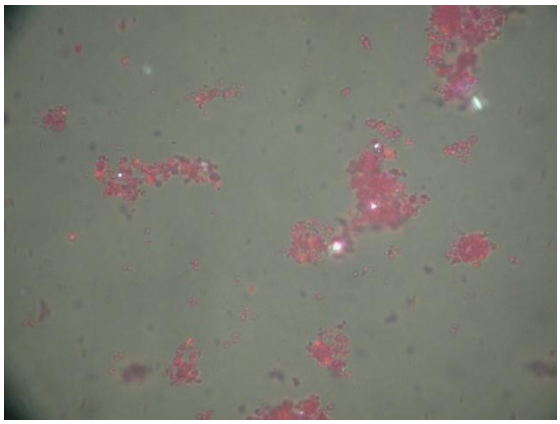

Crossed Polars, In RI 1.550, 400x

Normal Raman, 488nm

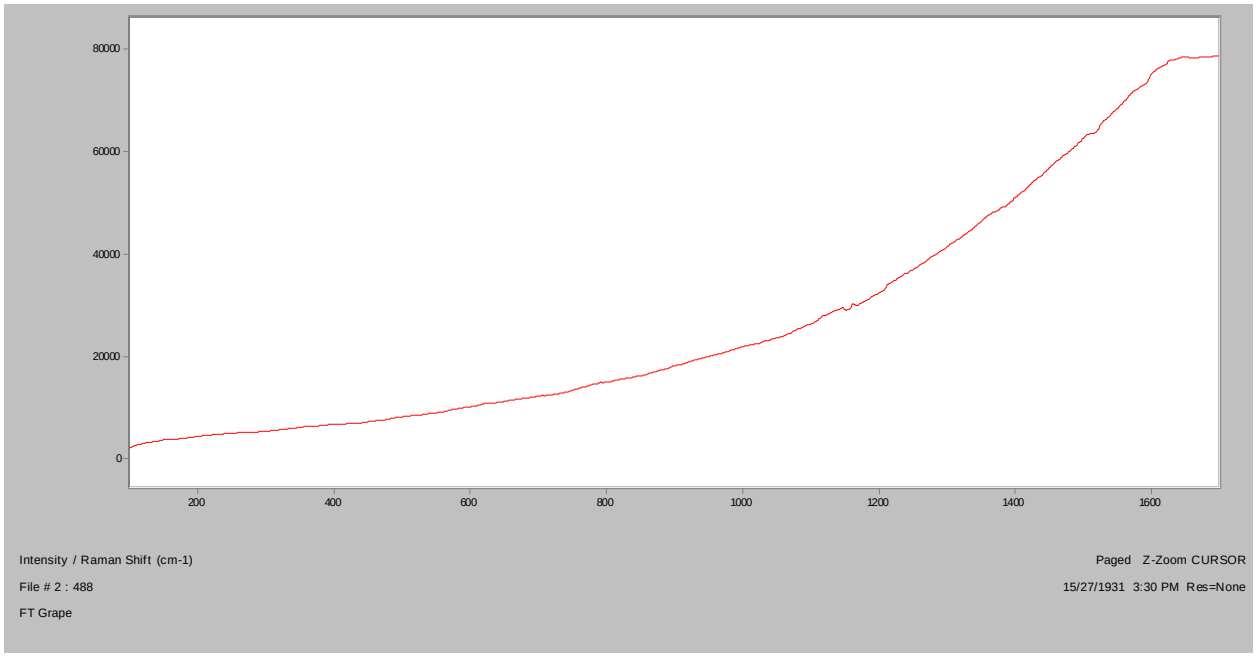

Normal Raman, 633nm

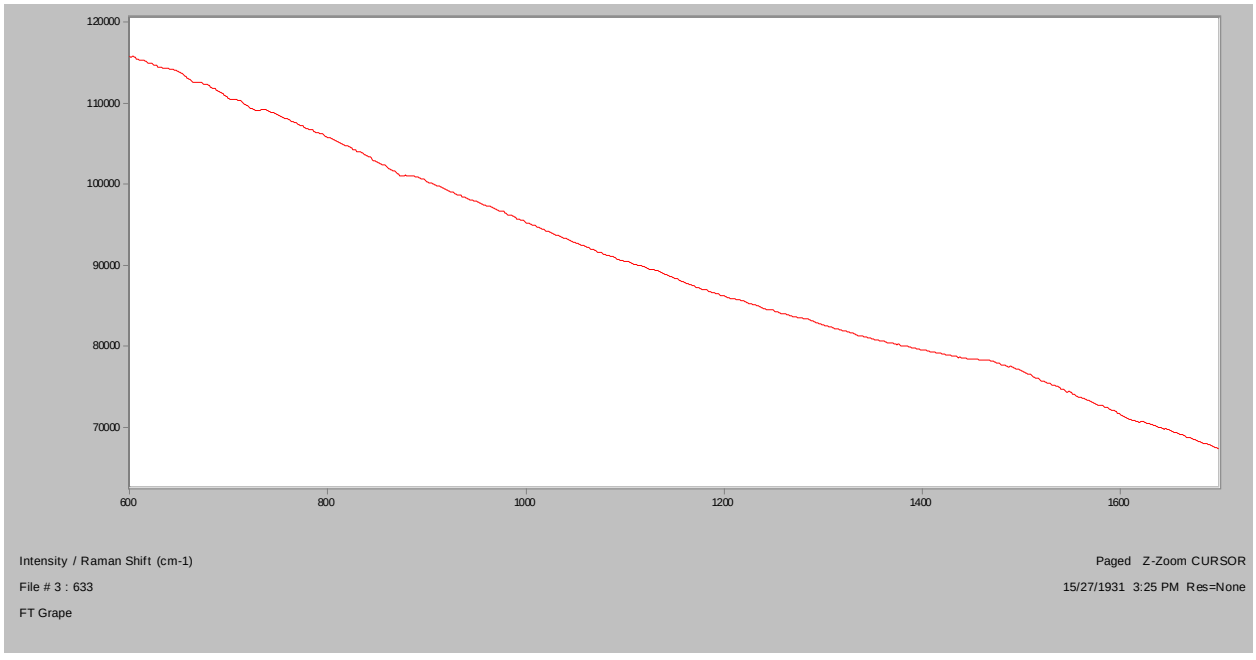

Normal Raman, 785nm

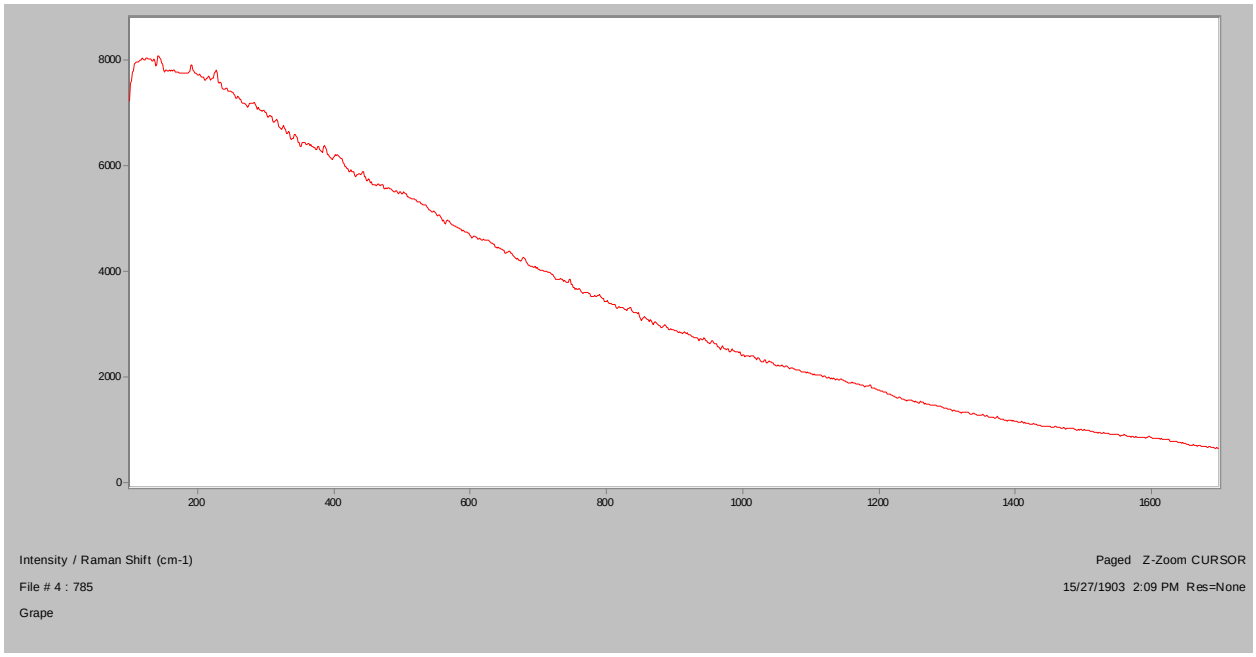

FT-Raman, 1064nm

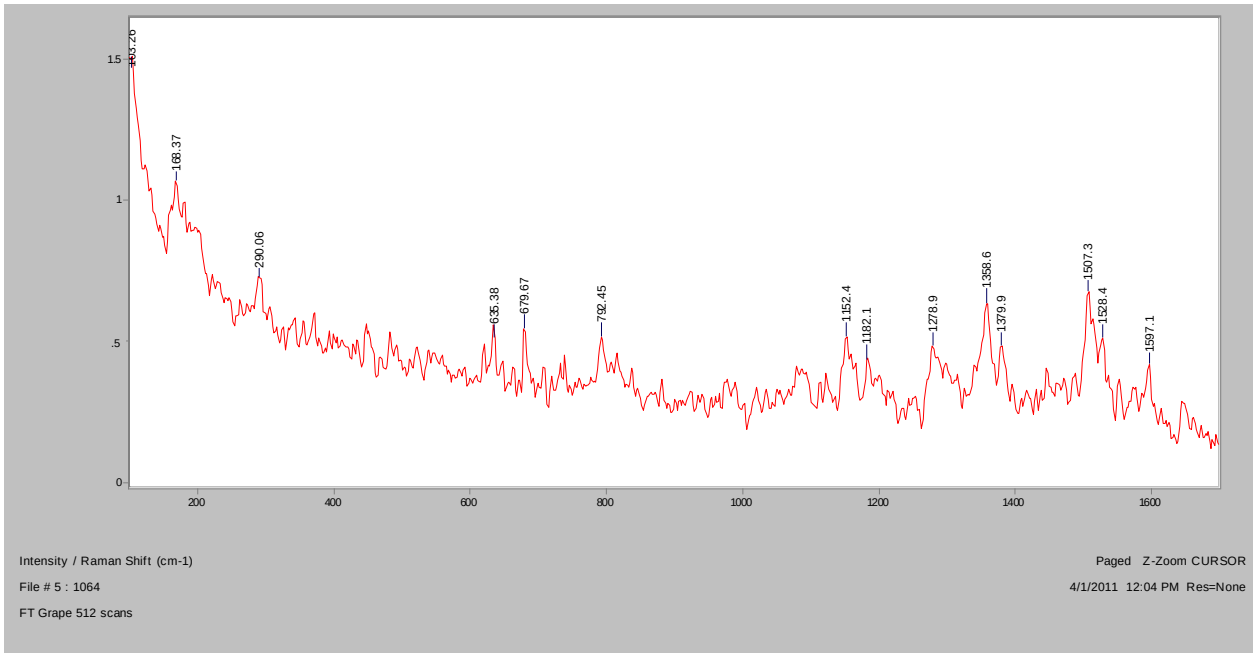

FT-IR (ATR)

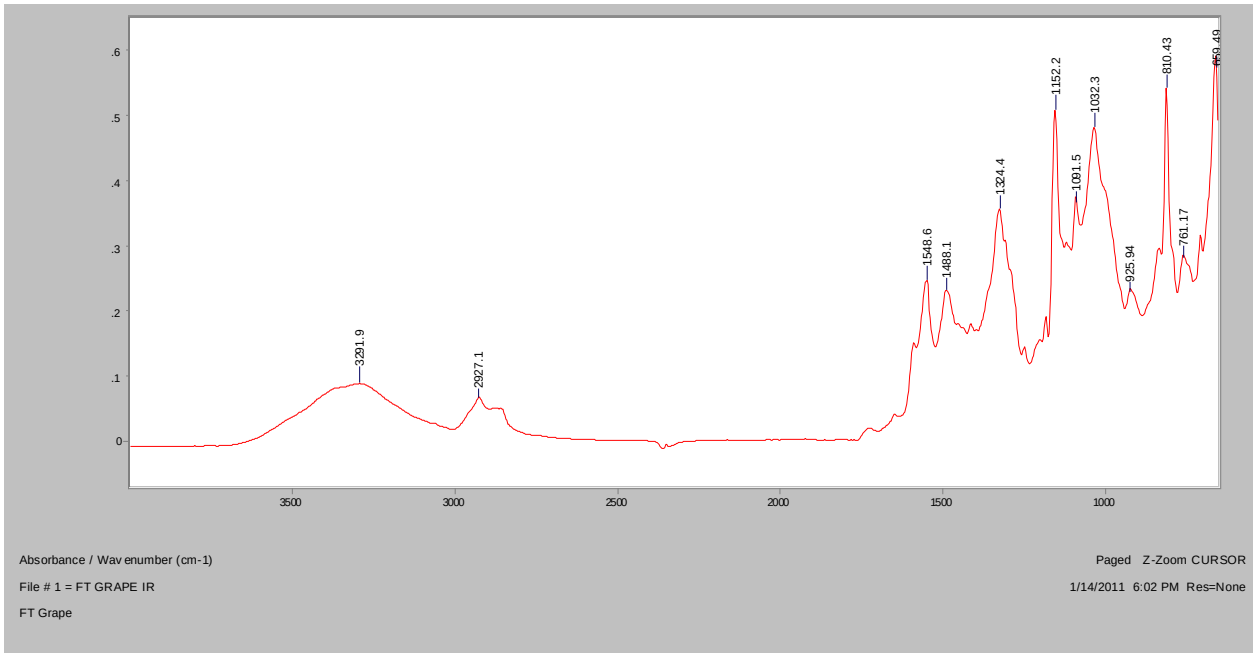
3291.9
2927.1
1548.6
1488.1
1324.4
1152.2
1091.5
1032.3
925.94
810.43
761.17
669.49
Absorbance / Wavenumber (cm-1)
File # 1 = FT GRAPE IR
FT Grape
Paged Z-Zoom CURSOR
1/14/2011 6:02 PM Res=None

XRF

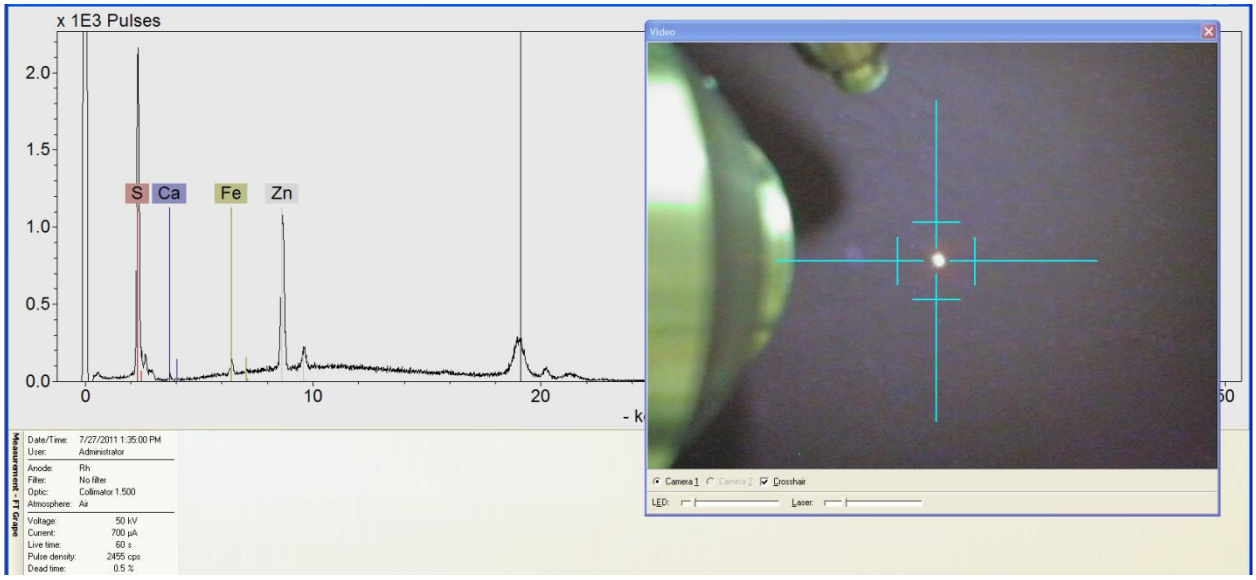
x 1E3 Pulses
S
Ca
Fe
Zn
Video
Camera 1
Crosshair
LED:
Laser:

Purple

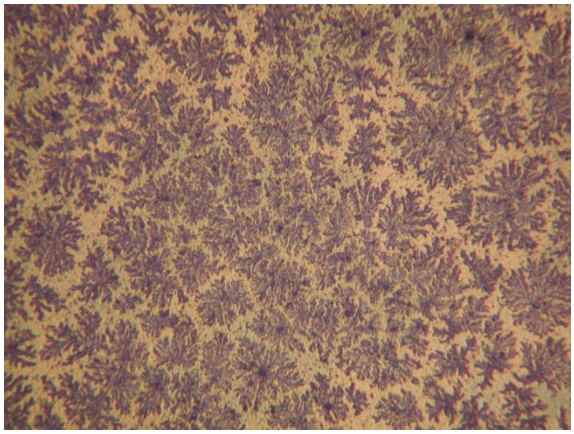

Bright Field, 100x

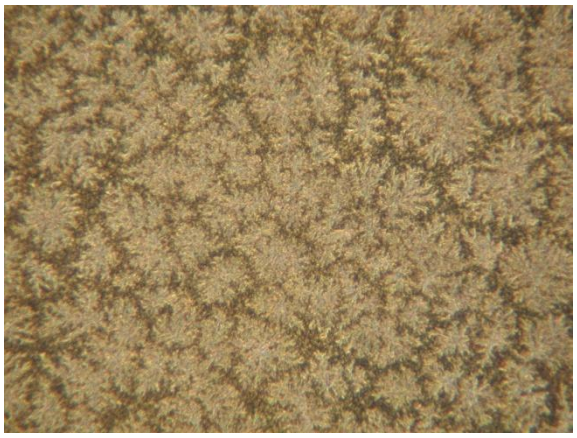

Dark Field, 100x

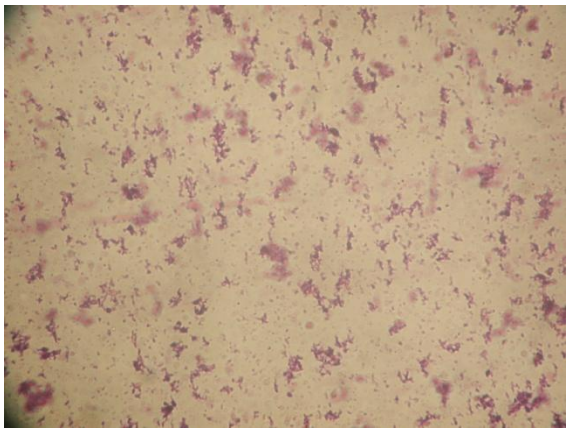

In RI 1.550, 400x

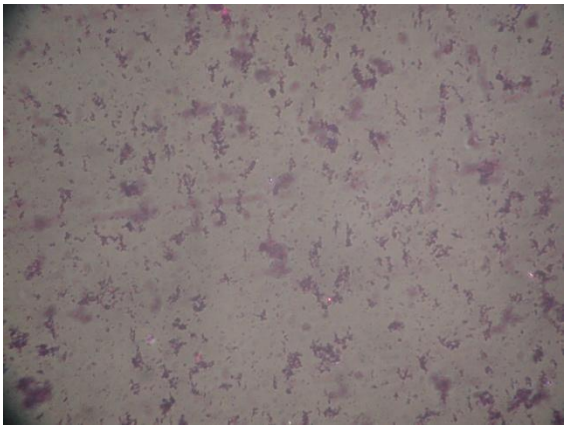

Crossed Polars, In RI 1.550, 400x

Normal Raman, 488nm

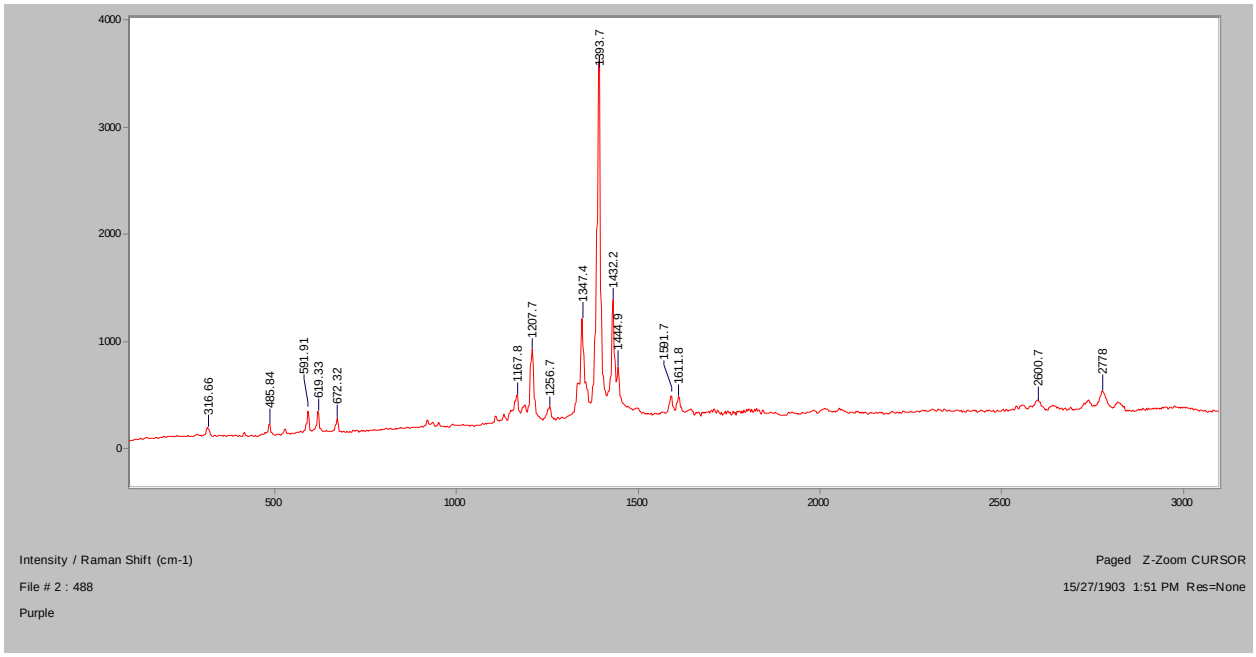

Normal Raman, 633nm

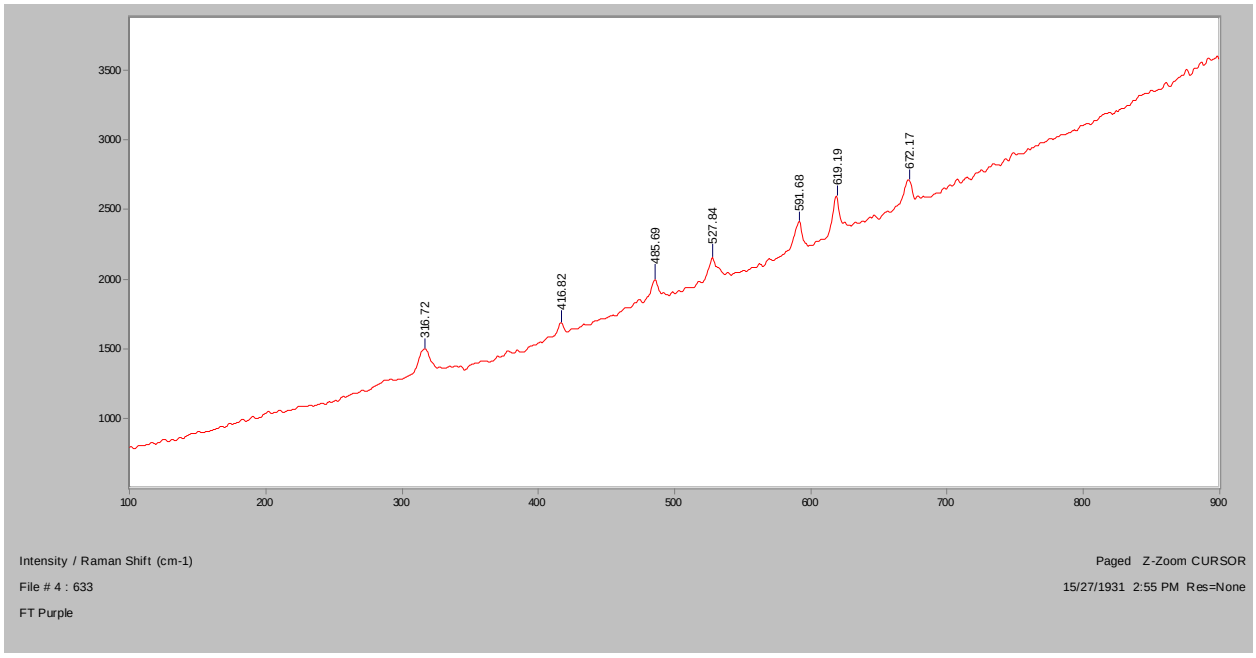

Normal Raman, 785nm

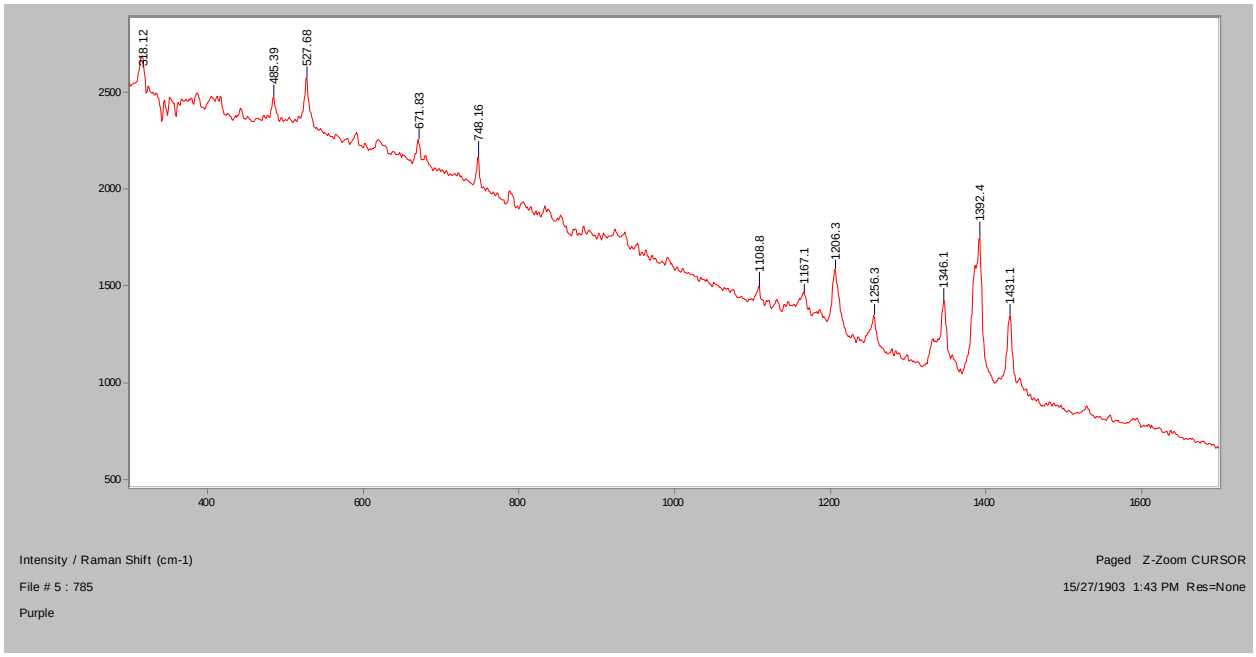

FT-Raman, 1064nm (note: in KBr)

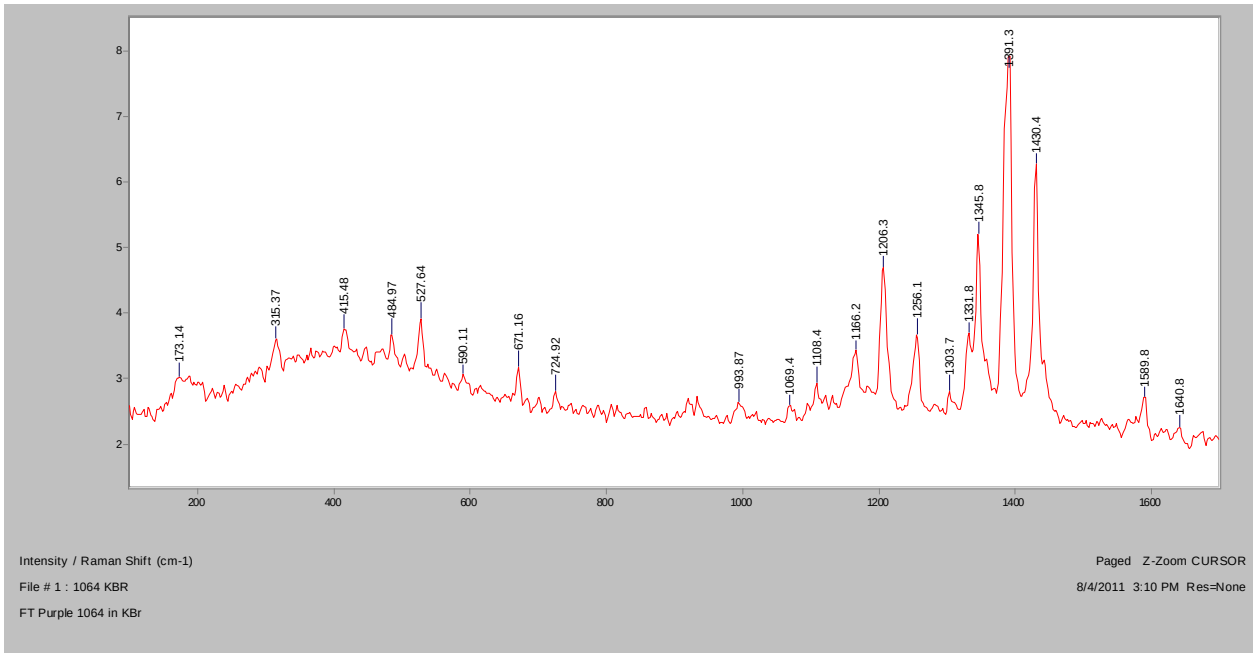

FT-IR (ATR)

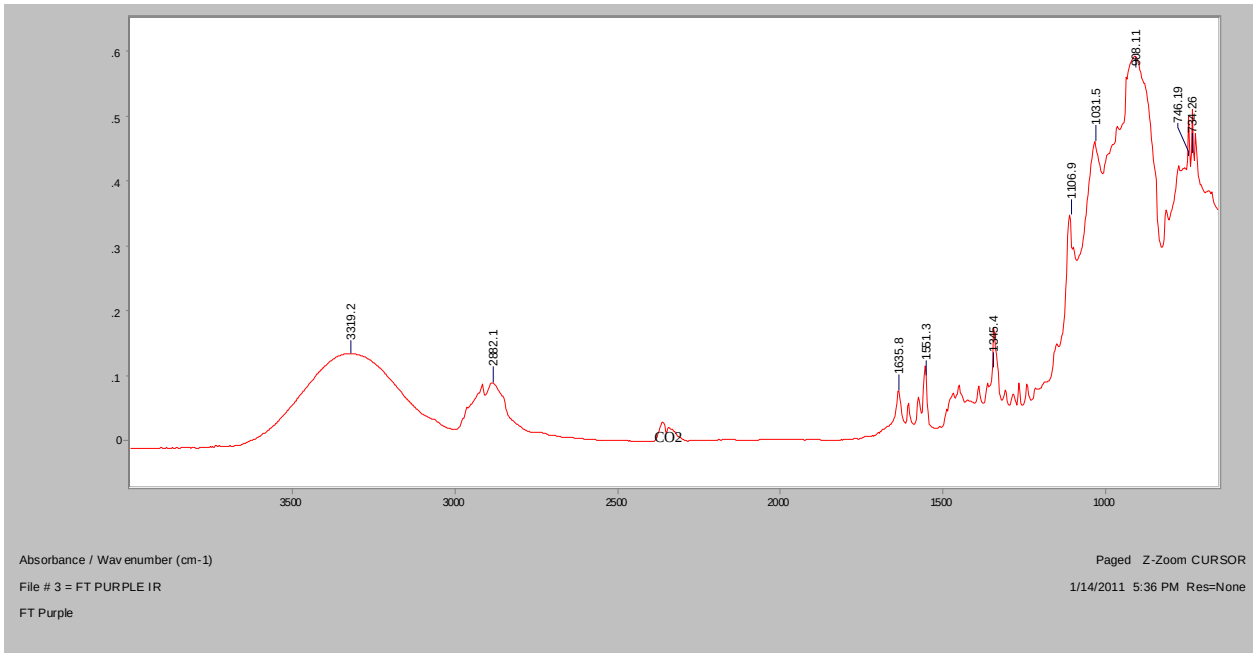
.6
.5
.4
.3
.2
.1
0
3319.2
2882.1
CO2
1635.8
1551.3
1345.4
1106.9
1031.5
968.11
746.19
734.26
3500
3000
2500
2000
1500
1000
Absorbance / Wavenumber (cm-1)
File # 3 = FT PURPLE IR
FT Purple
Paged Z-Zoom CURSOR
1/14/2011 5:36 PM Res=None

XRF

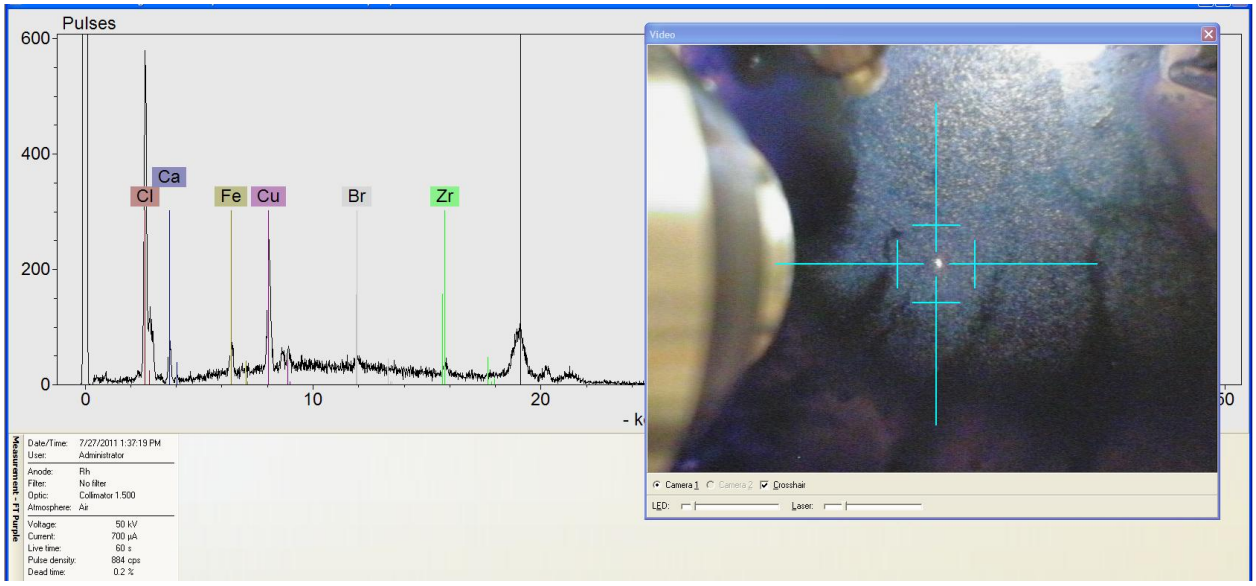
Pulses
600
400
200
0
Ca
Cl
Fe
Cu
Br
Zr
0
10
20
Video
Camera 1
Camera 2
Crosshair
LED:
Laser:
Date/Time: 7/27/2011 1:37:19 PM
User: Administrator
Anode: Rh
Filter: No filter
Optic: Collimator 1.500
Atmosphere: Air
Voltage: 50 kV
Current: 700 µA
Live time: 60 s
Pulse density: 884 cps
Dead time: 0.2 %

Violet

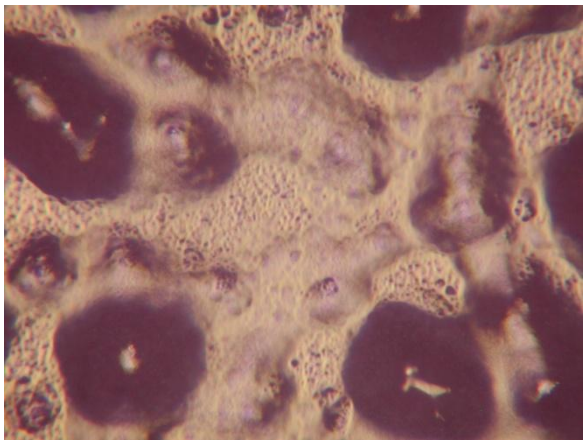

Bright Field, 100x

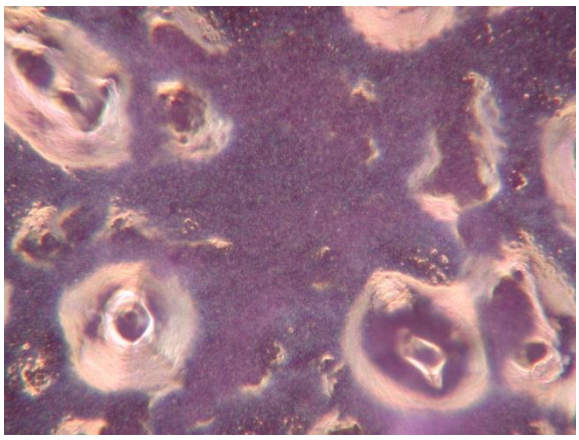

Dark Field, 100x

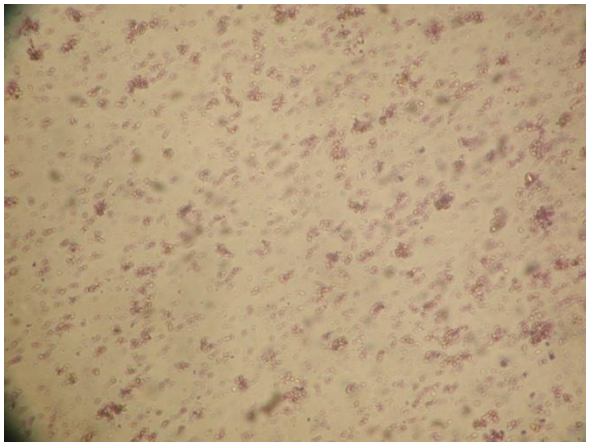

In RI 1.550, 400x

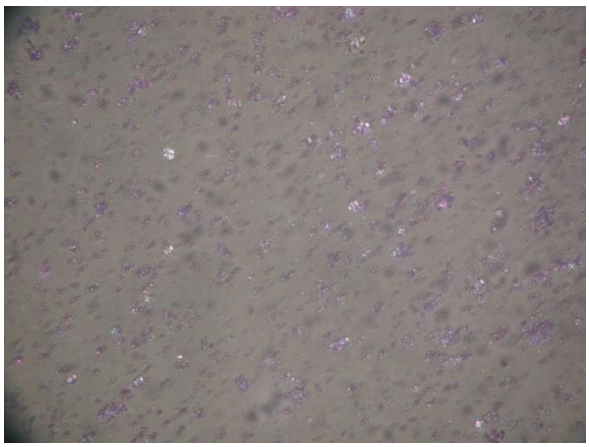

Crossed Polars, In RI 1.550, 400x

Normal Raman, 488nm

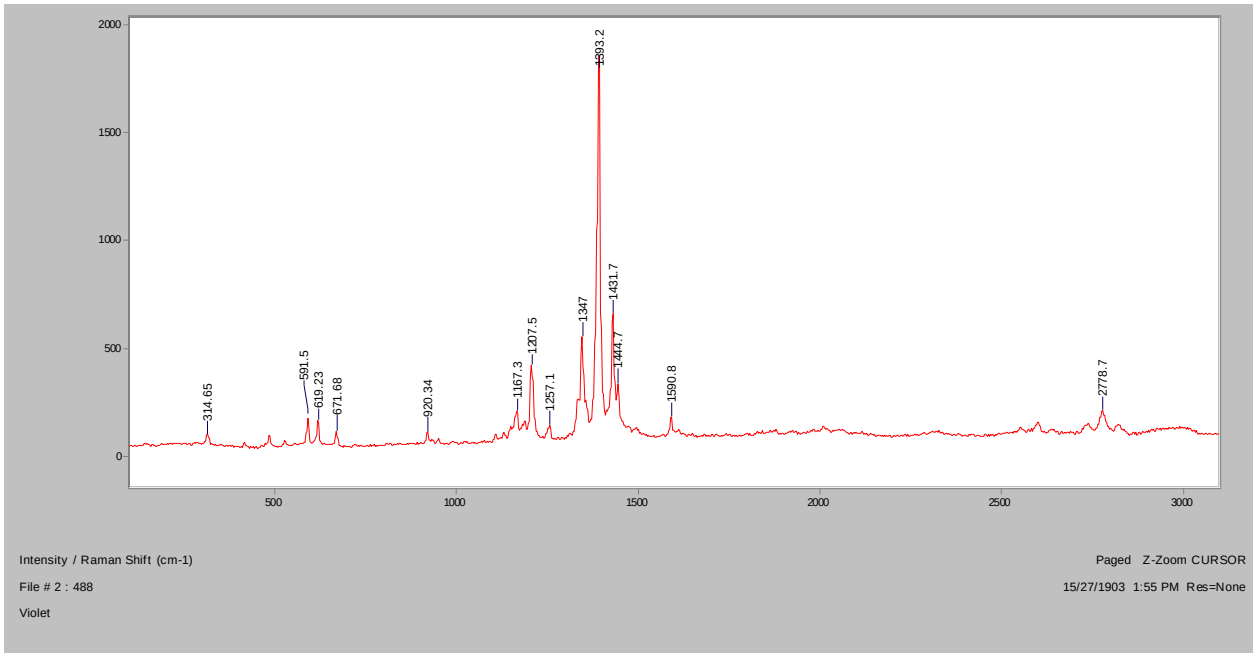

Normal Raman, 633nm

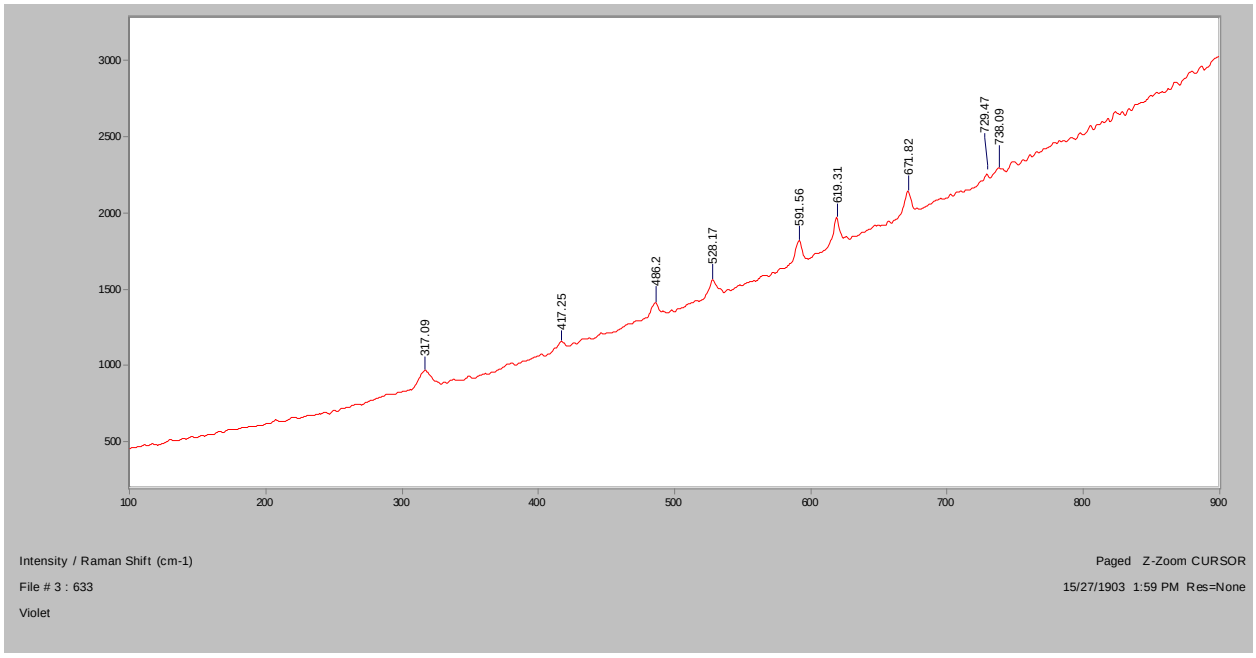

Normal Raman, 785nm

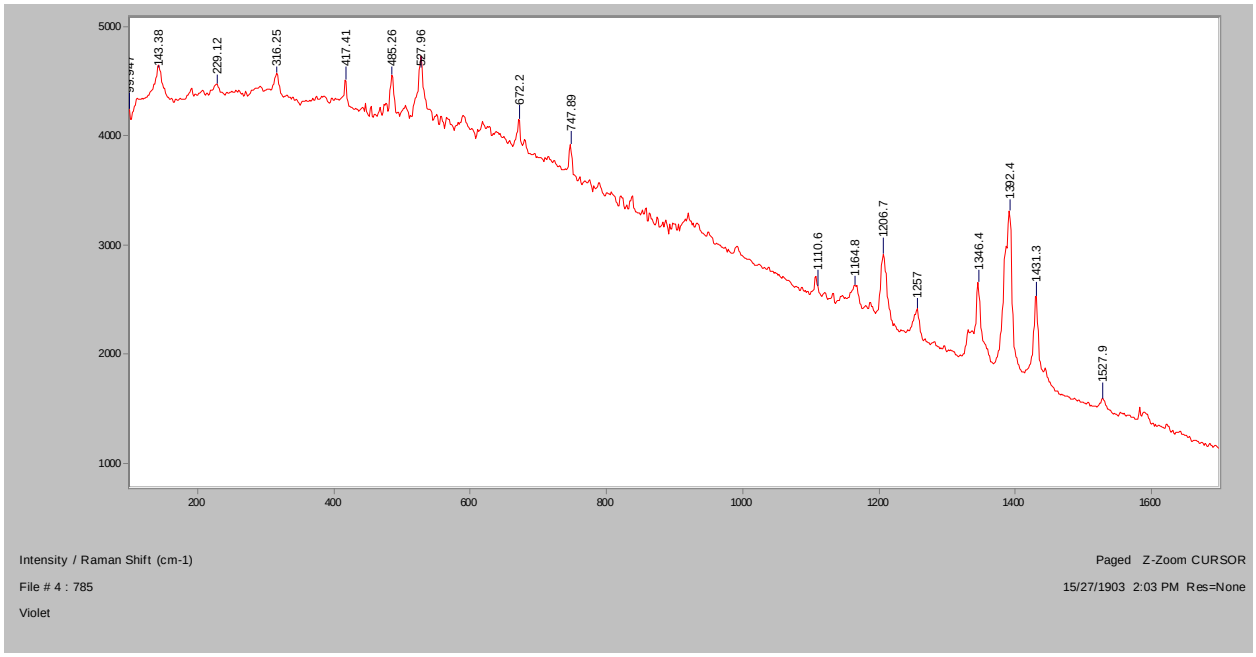

FT-Raman, 1064nm

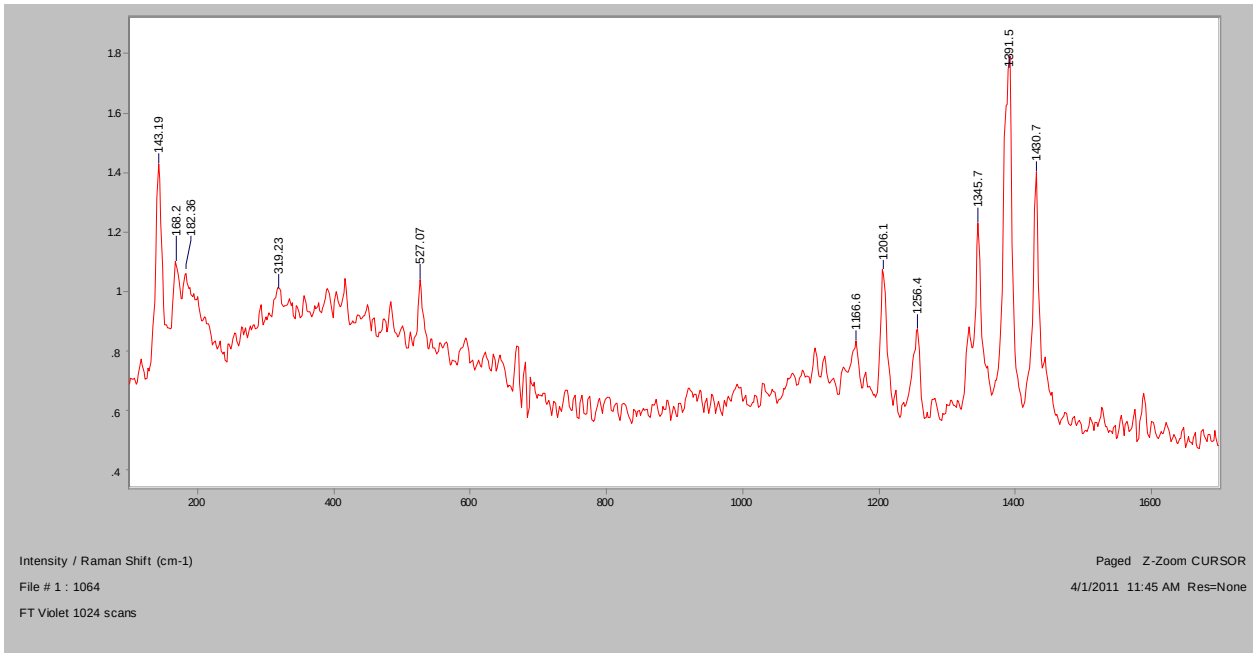

FT-IR (ATR)

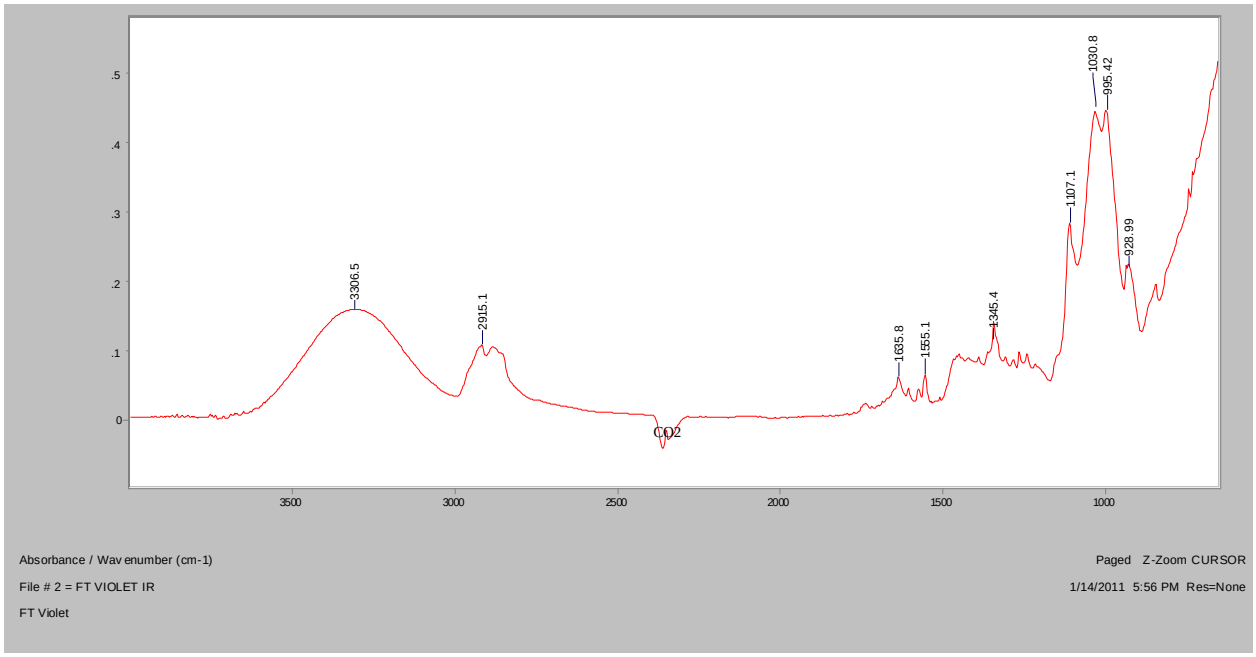
3306.5
2915.1
1635.8
1555.1
1345.4
1107.1
1030.8
995.42
928.99
CO2
.5
.4
.3
.2
.1
0
3500
3000
2500
2000
1500
1000
Absorbance / Wavenumber (cm-1)
File # 2 = FT VIOLET IR
FT Violet
Paged Z-Zoom CURSOR
1/14/2011 5:56 PM Res=None

XRF

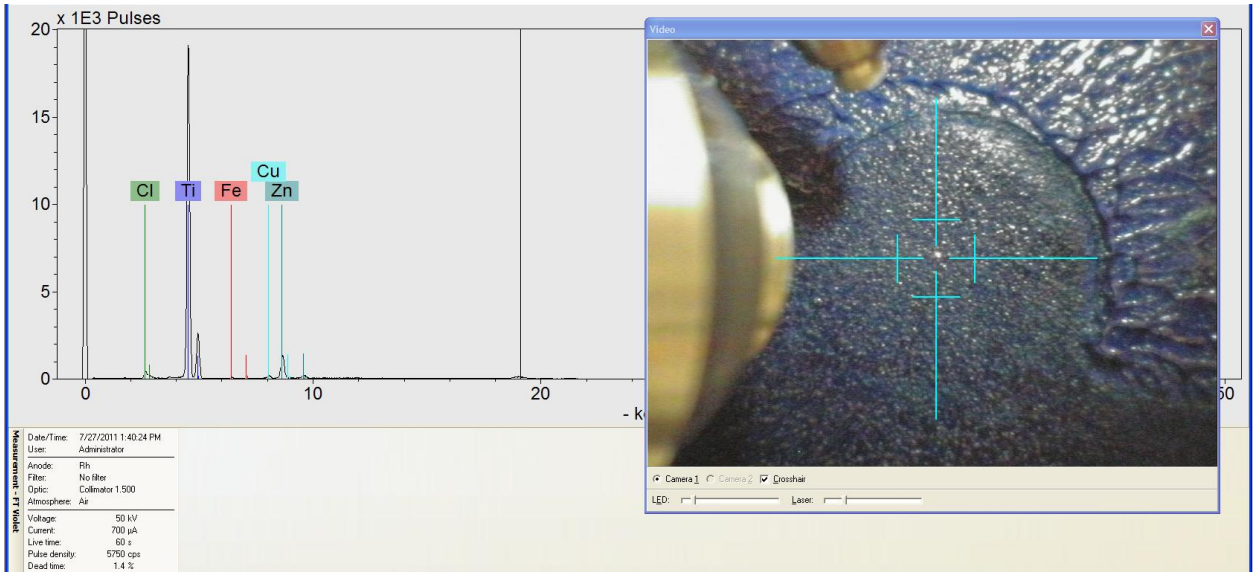
x 1E3 Pulses
20
15
10
5
0
Cl
Ti
Fe
Cu
Zn
0
10
20
Video
Camera 1
Camera 2
Crosshair
LED:
Laser:
Measurement - FT Violet
Date/Time: 7/27/2011 1:40:24 PM
User: Administrator
Anode: Rh
Filter: No filter
Optic: Collimator 1.500
Atmosphere: Air
Voltage: 50 kV
Current: 700 µA
Live time: 60 s
Pulse density: 5750 cps
Dead time: 1.4 %

Grey

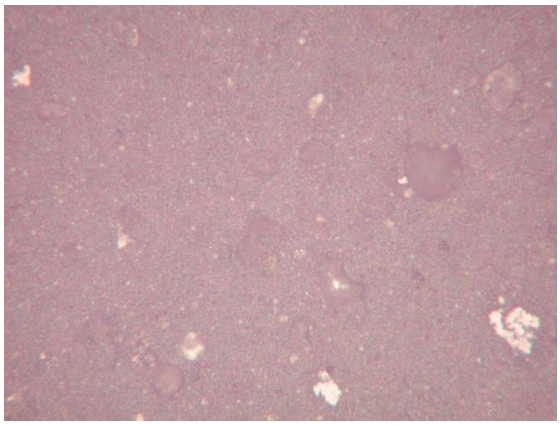

Bright Field, 100x

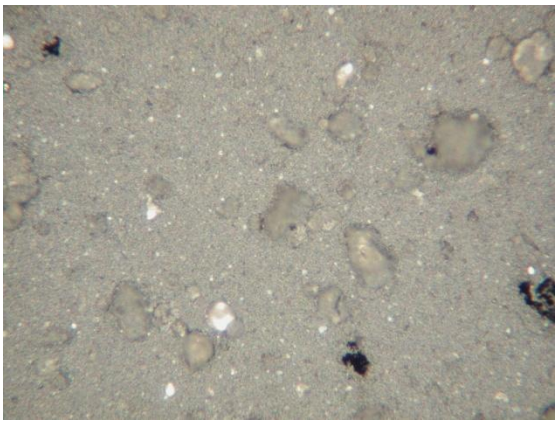

Dark Field, 100x

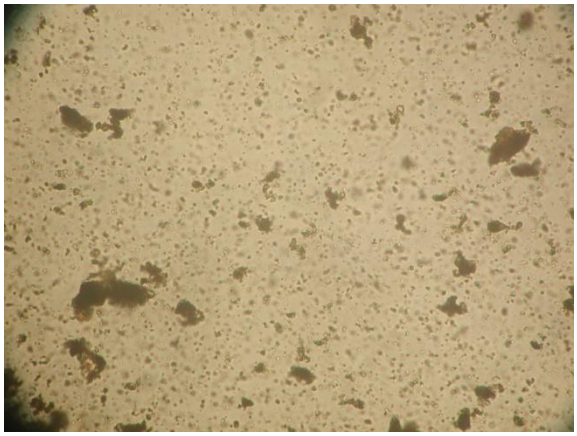

In RI 1.550, 400x

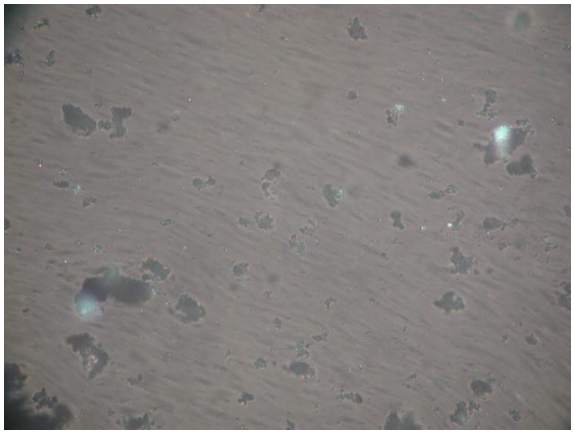

Crossed Polars, In RI 1.550, 400x

Normal Raman, 488nm

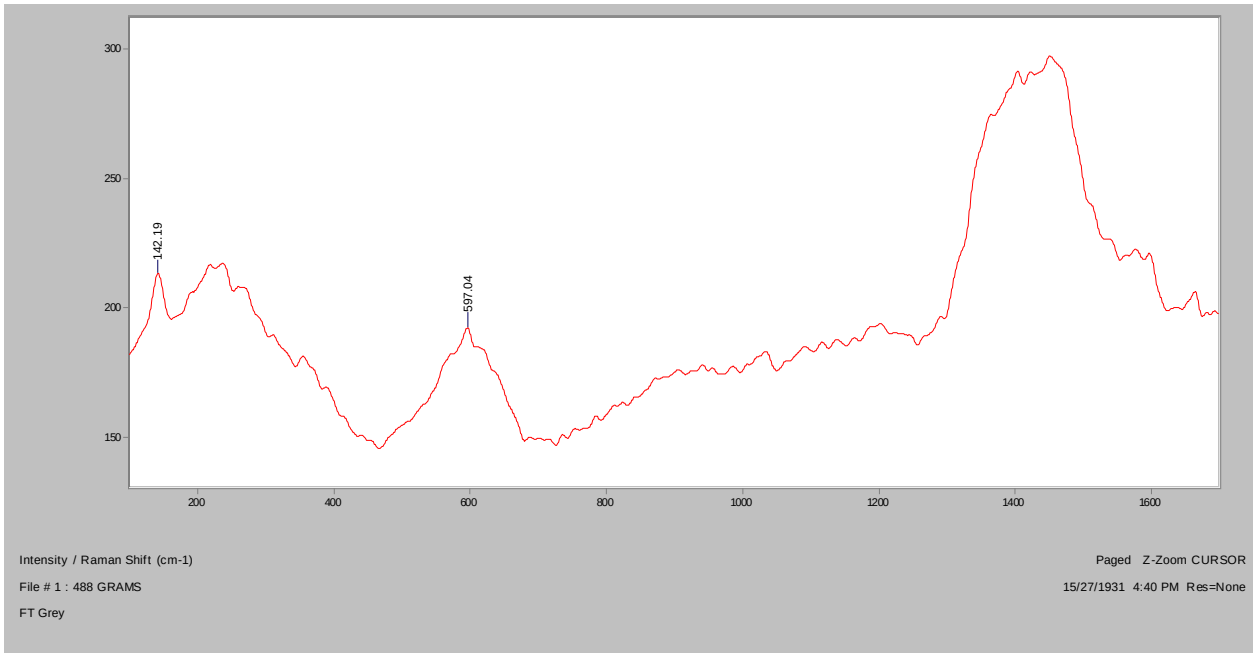

Normal Raman, 633nm

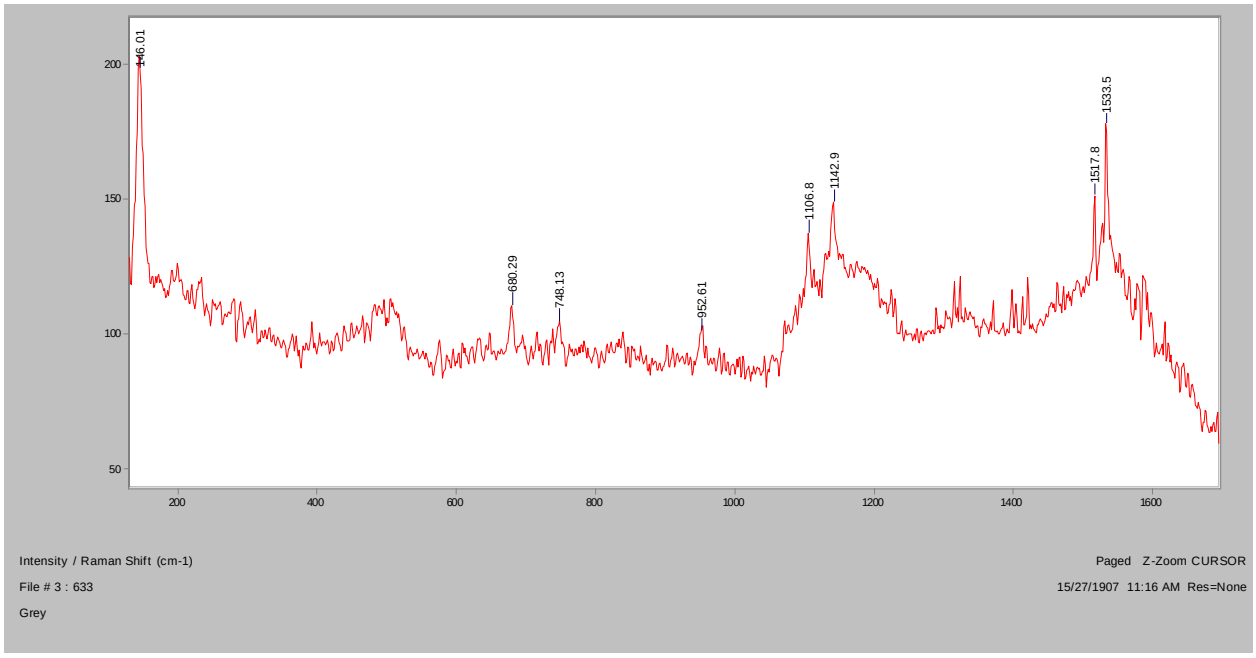

Normal Raman, 785nm

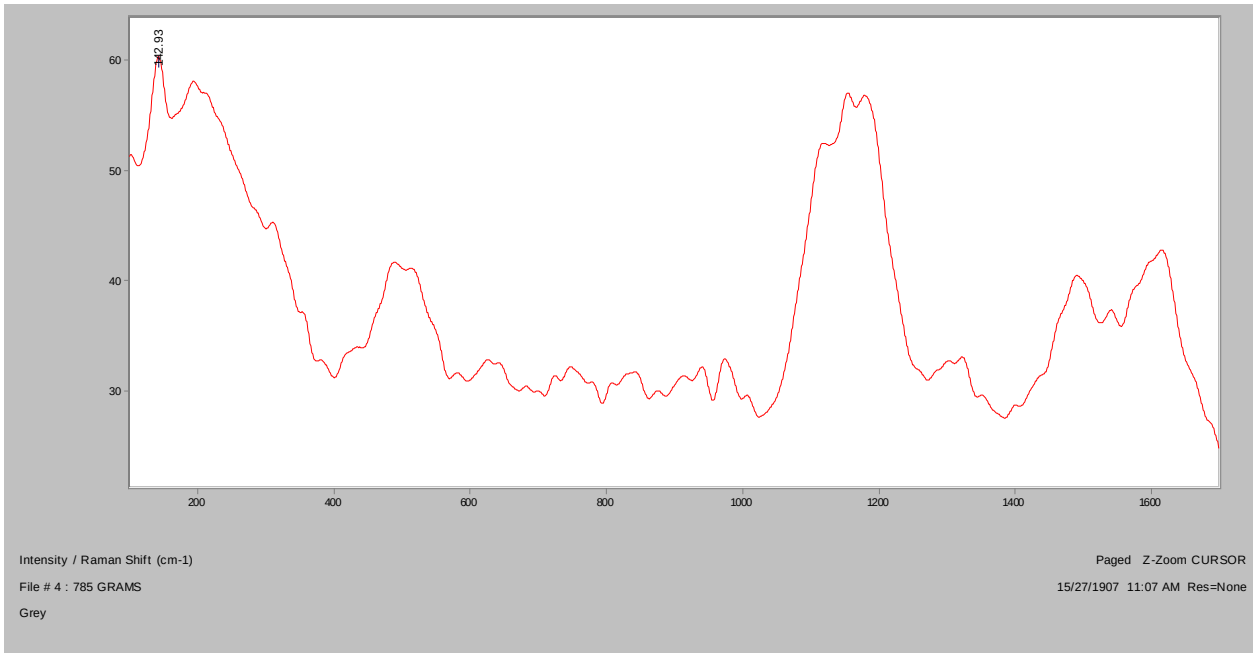

FT-IR (ATR)

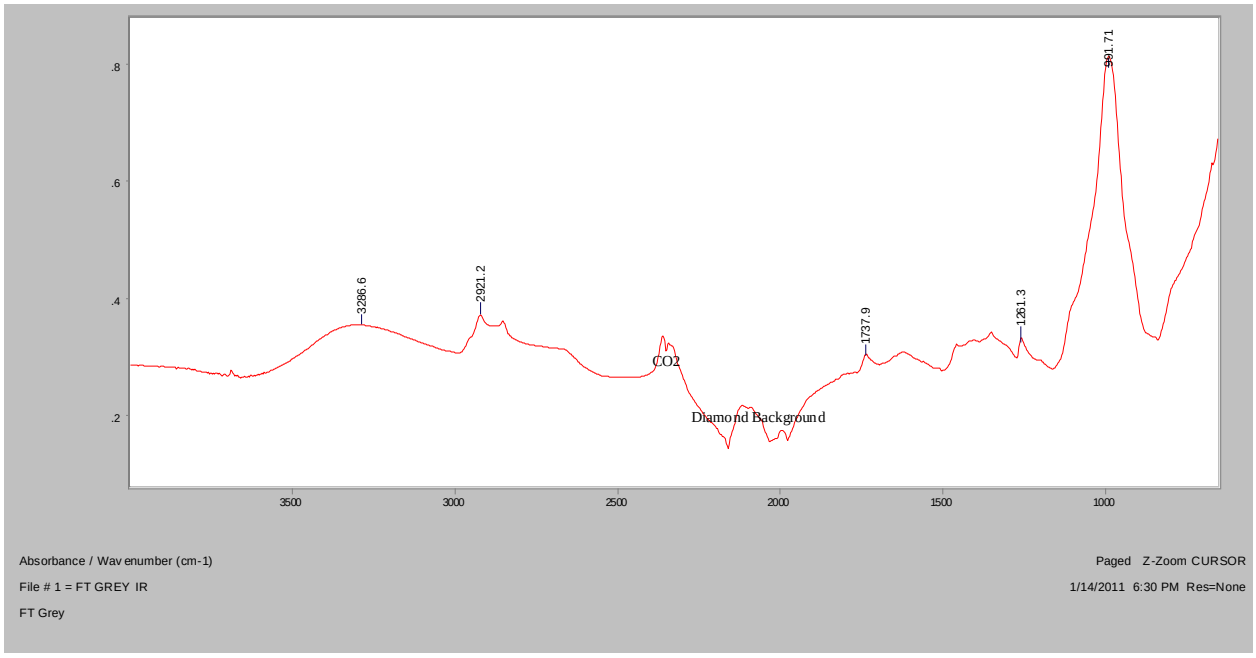

XRF

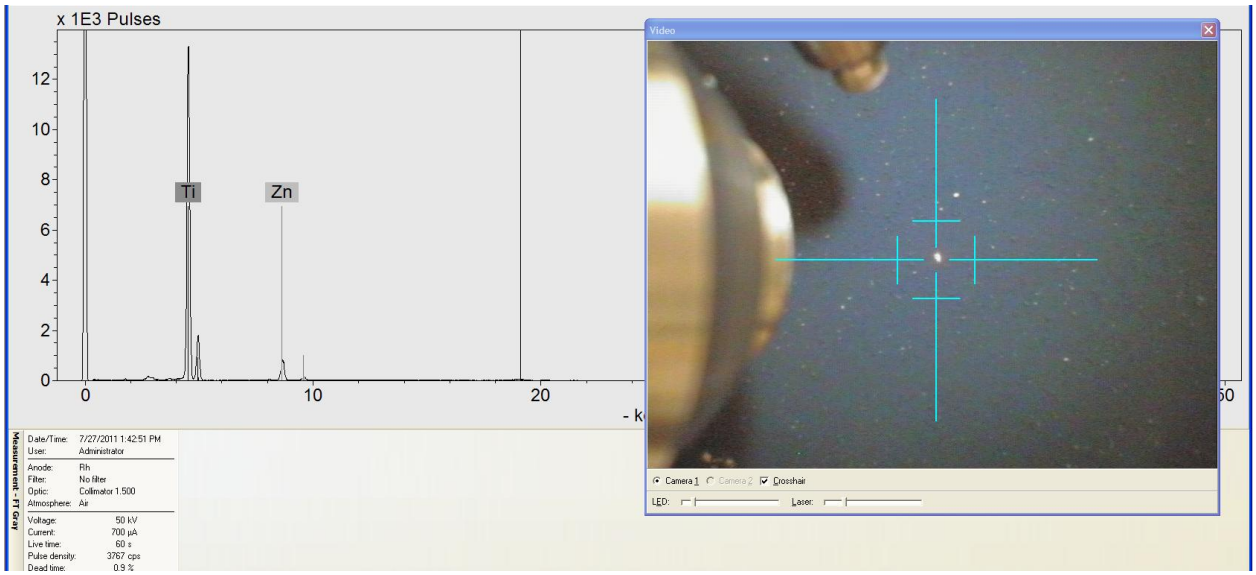
x 1E3 Pulses
12
10
8
6
4
2
0
Ti
Zn
0
10
20
Video
Camera 1
Camera 2
Crosshair
LED:
Laser:
Date/Time: 7/27/2011 1:42:51 PM
User: Administrator
Anode: Rh
Filter: No filter
Optic: Collimator 1.500
Atmosphere: Air
Voltage: 50 kV
Current: 700 µA
Live time: 60 s
Pulse density: 3767 cps
Dead time: 0.9 %

Bright Black

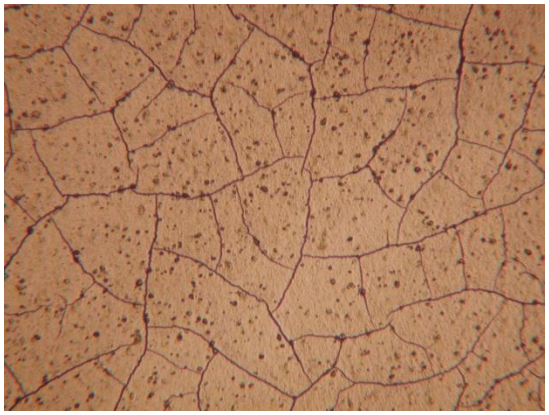

Bright Field, 100x

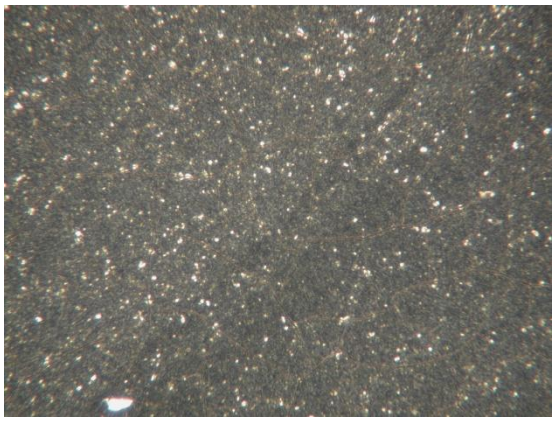

Dark Field, 100x

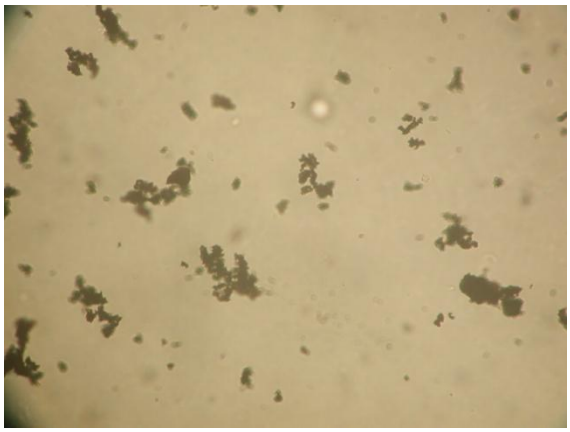

In RI 1.550, 400x

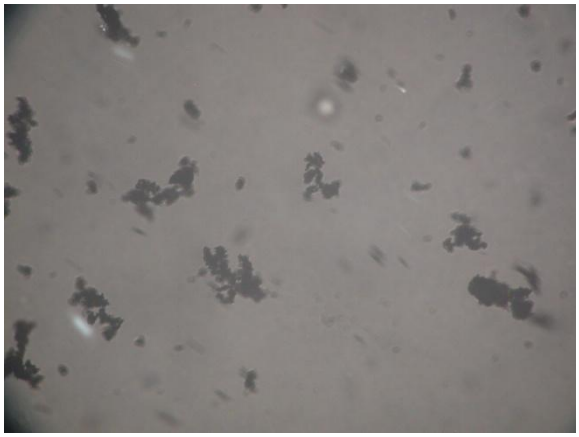

Crossed Polars, In RI 1.550, 400x

Normal Raman, 488nm

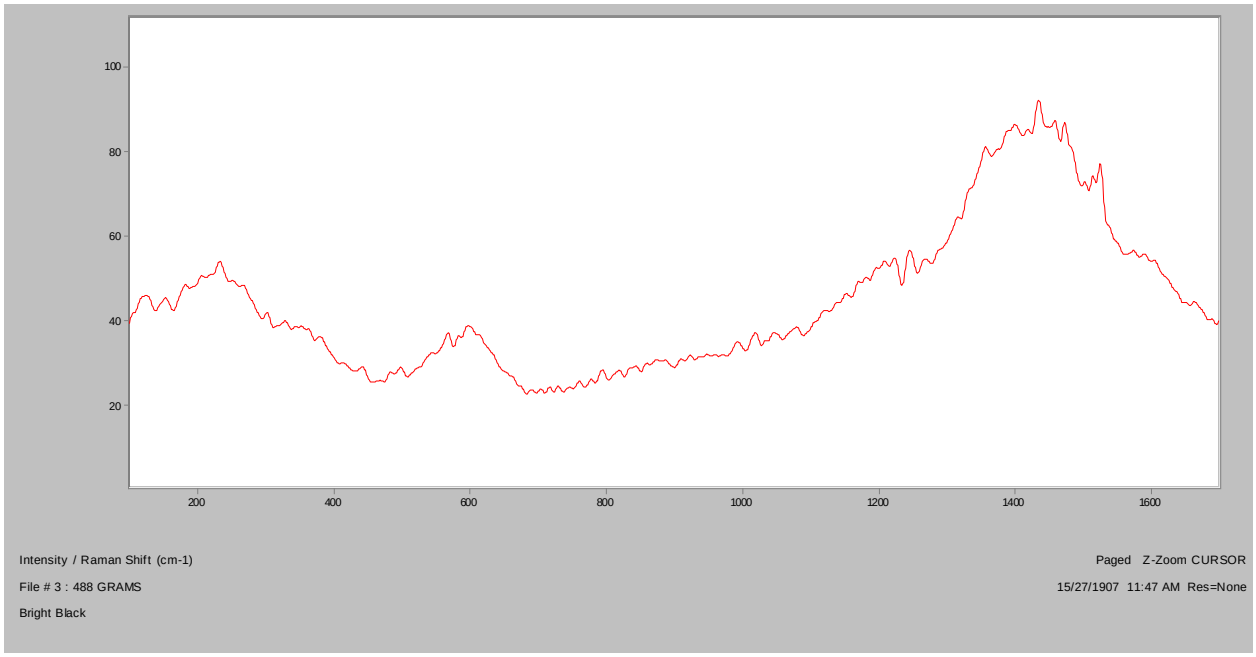

Normal Raman, 633nm

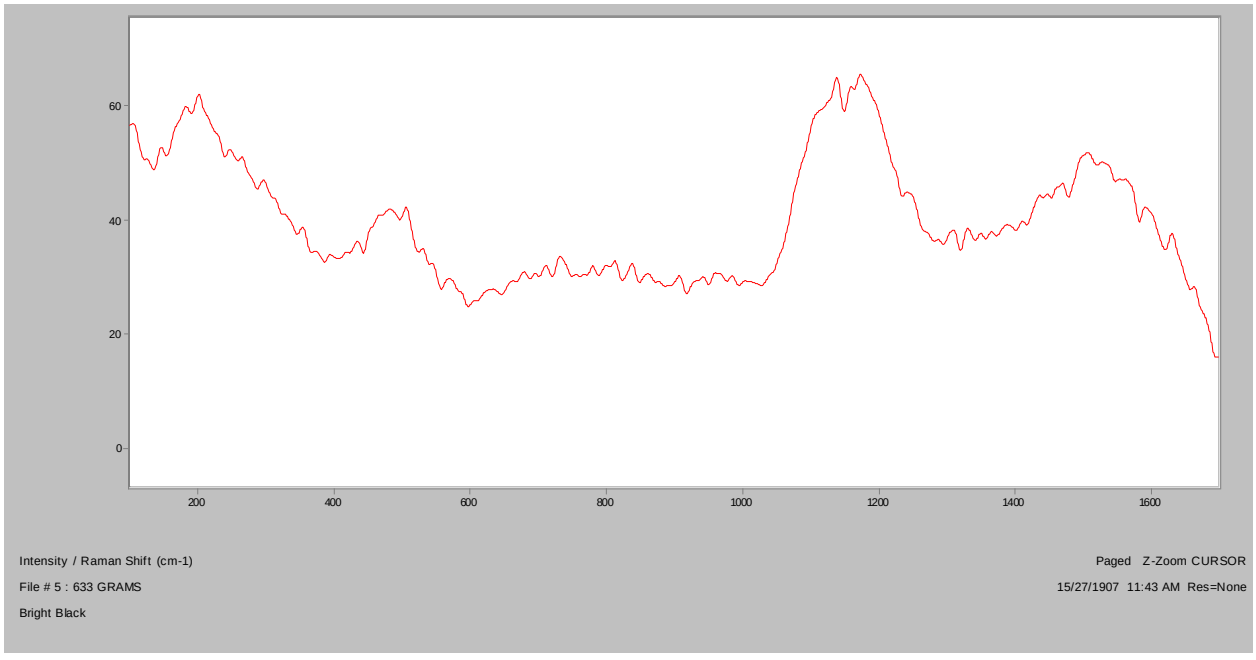

Normal Raman, 785nm

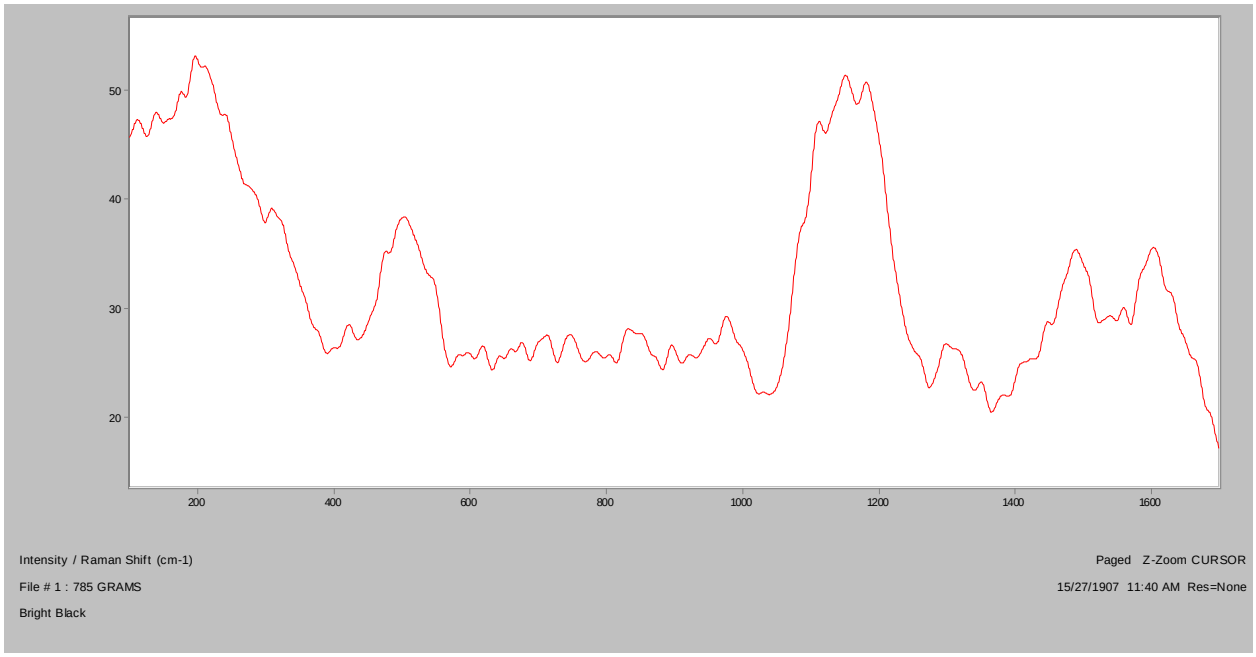

FT-IR (ATR)

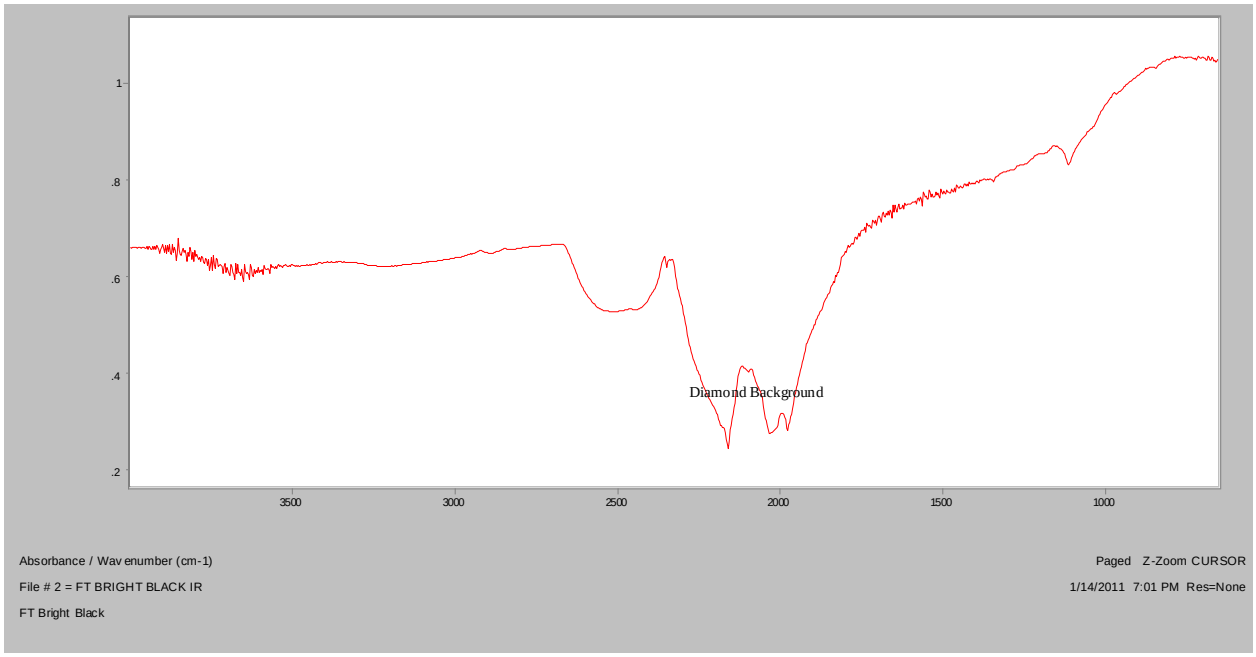

XRF

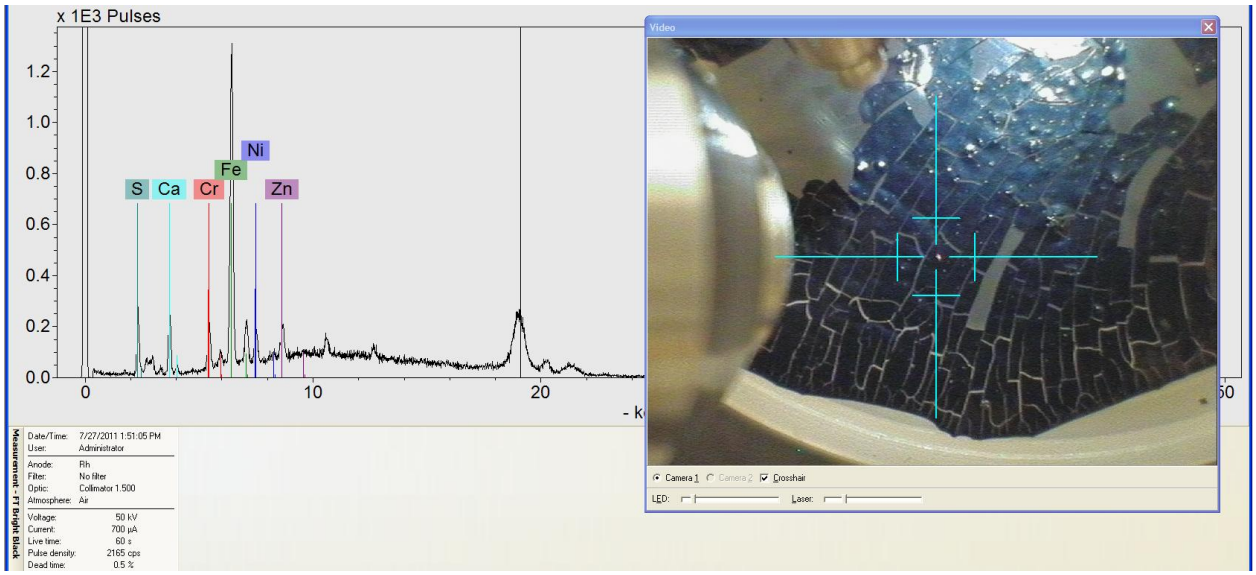
x 1E3 Pulses
1.2
1.0
0.8
0.6
0.4
0.2
0.0
0
10
20
S
Ca
Cr
Fe
Ni
Zn
Video
Camera 1
Camera 2
Crosshair
LED:
Laser:
Date/Time: 7/27/2011 1:51:05 PM
User: Administrator
Anode: Rh
Filter: No filter
Optic: Collimator 1.500
Atmosphere: Air
Voltage: 50 kV
Current: 700 µA
Live time: 60 s
Pulse density: 2165 cps
Dead time: 0.5 %

Black

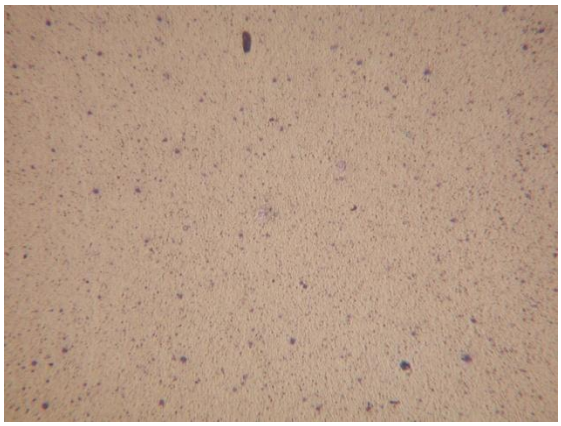

Bright Field, 100x

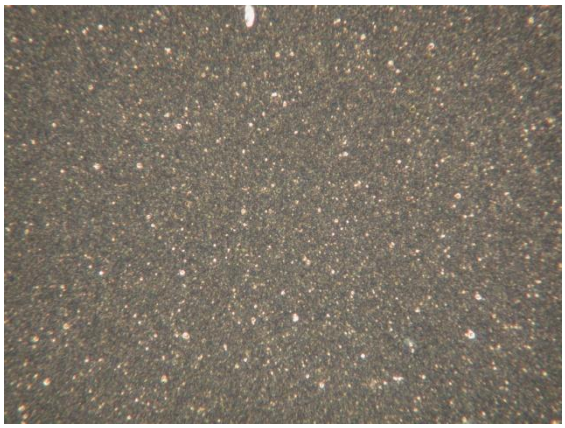

Dark Field, 100x

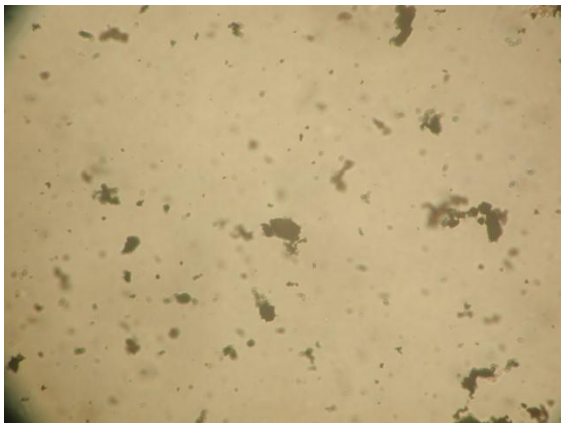

In RI 1.550, 400x

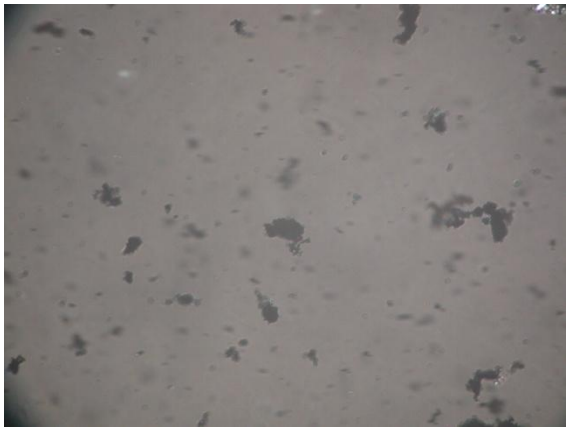

Crossed Polars, In RI 1.550, 400x

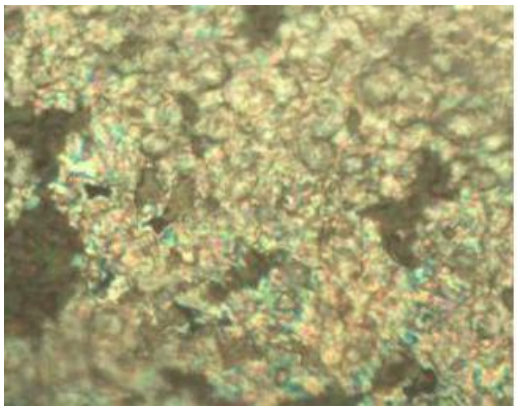

Raman microscope image, 1000x

Normal Raman, 488nm

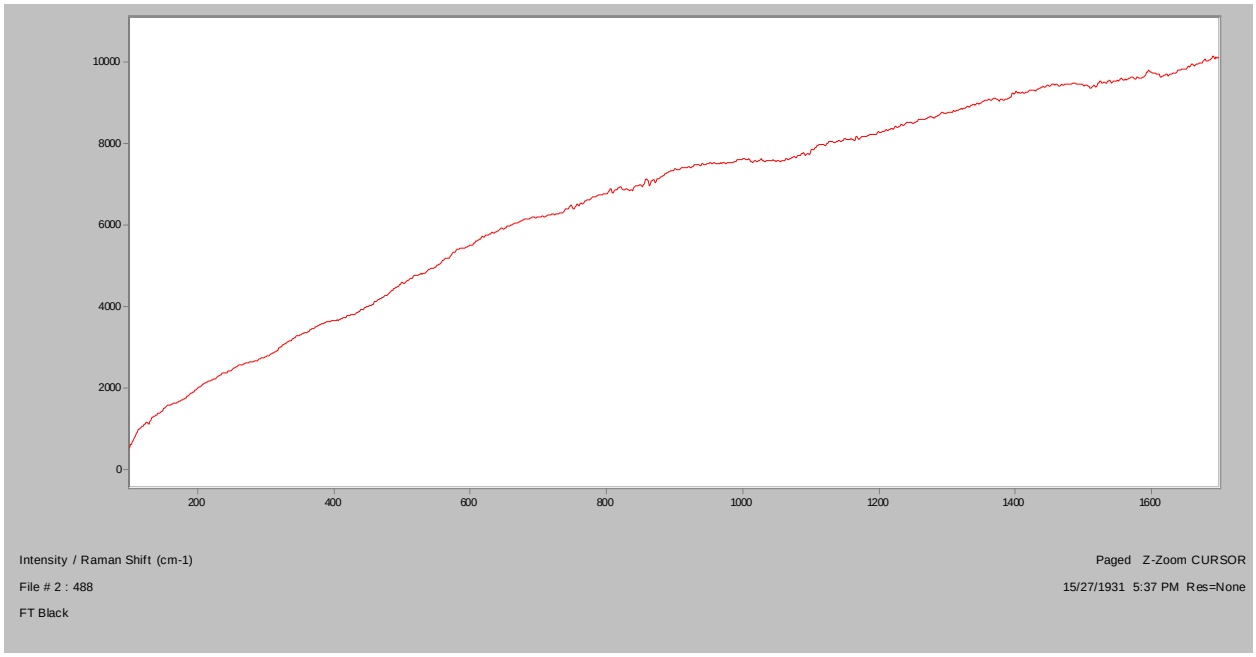

Normal Raman, 633nm

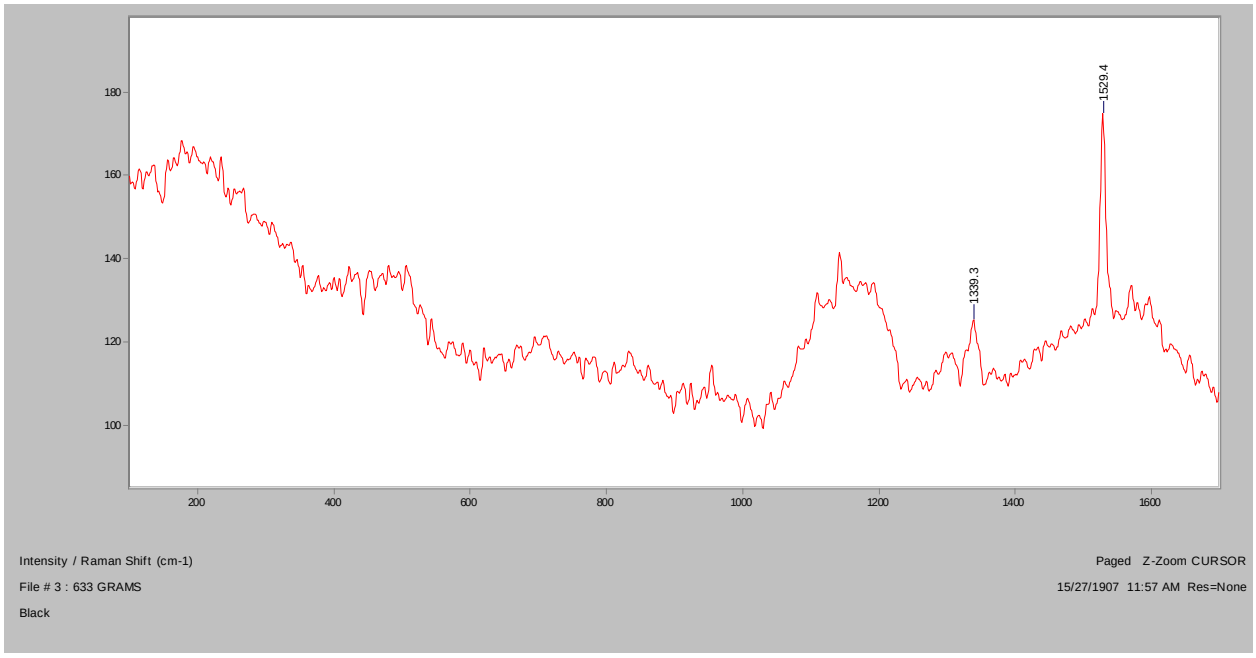

Normal Raman, 785nm

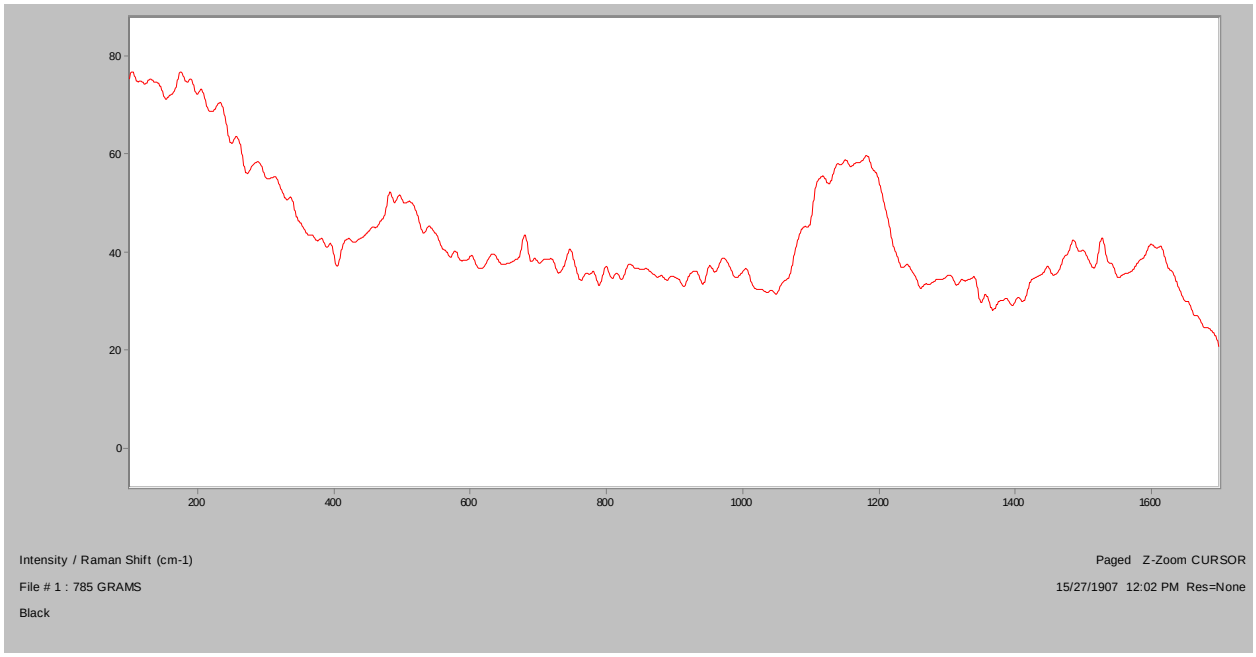

FT-IR (ATR)

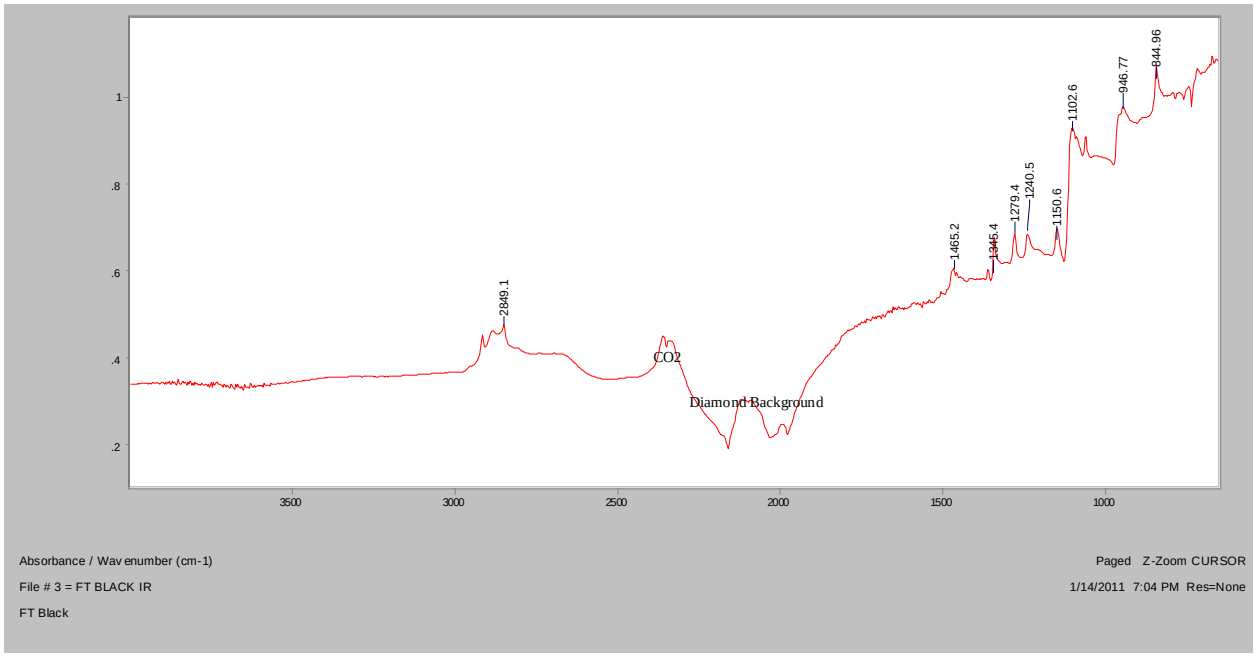

XRF

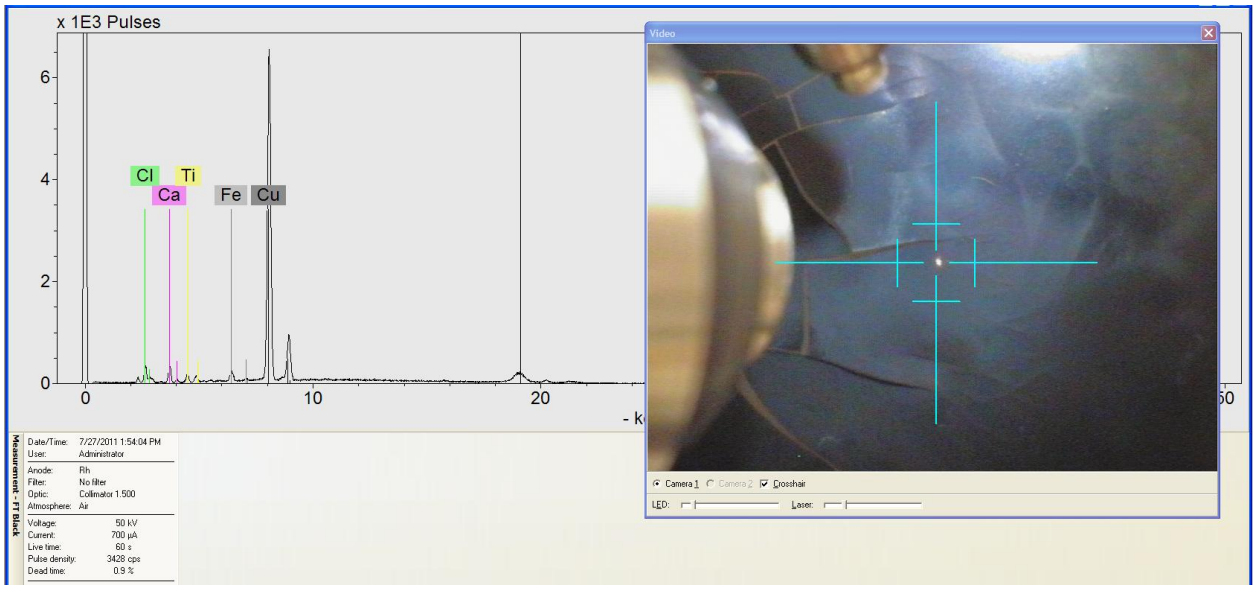
x 1E3 Pulses
6
4
2
0
Cl
Ti
Ca
Fe
Cu
0
10
20
Video
Camera 1
Camera 2
Crosshair
LED:
Laser:
Measurement - FT Black
Date/Time: 7/27/2011 1:54:04 PM
User: Administrator
Anode: Rh
Filter: No filter
Optic: Collimator 1.500
Atmosphere: Air
Voltage: 50 kV
Current: 700 µA
Live time: 60 s
Pulse density: 3428 cps
Dead time: 0.9 %

Eggplant Black

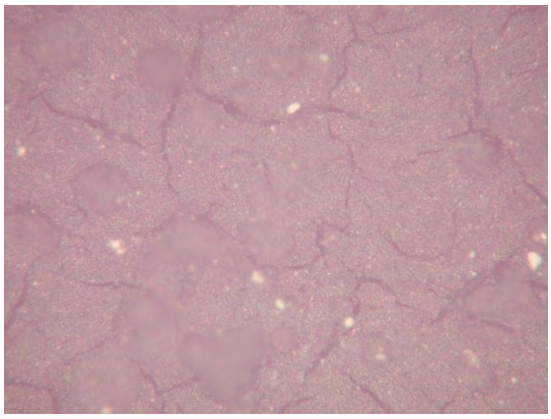

Bright Field, 100x

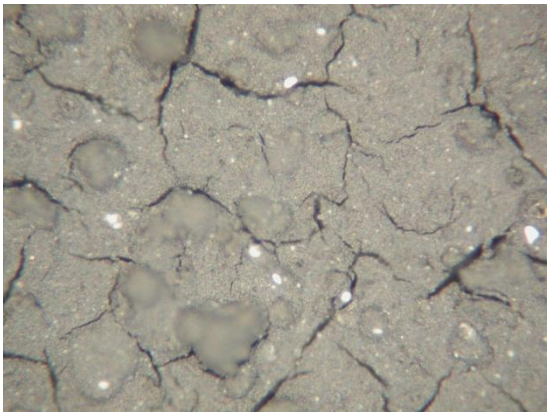

Dark Field, 100x

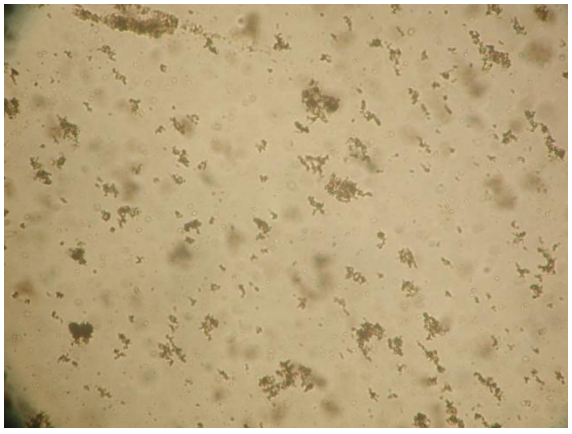

In RI 1.550, 400x

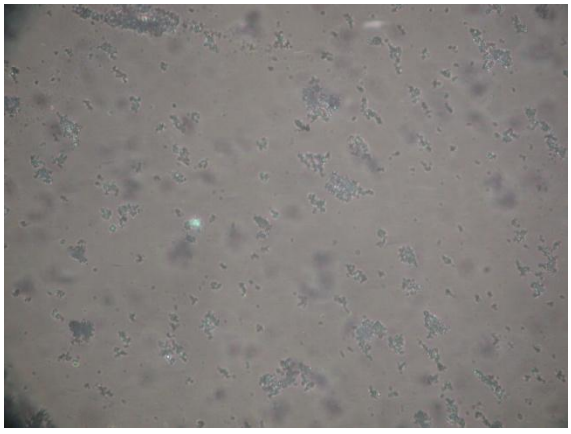

Crossed Polars, In RI 1.550, 400x

Normal Raman, 488nm

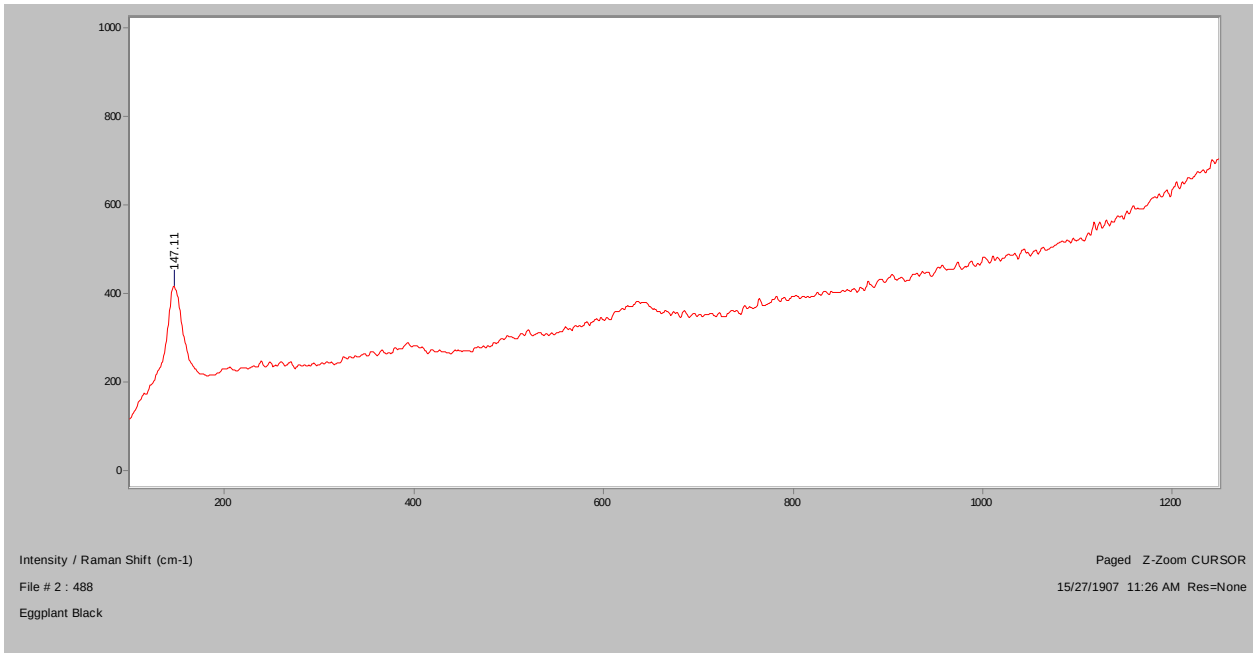

Normal Raman, 633nm

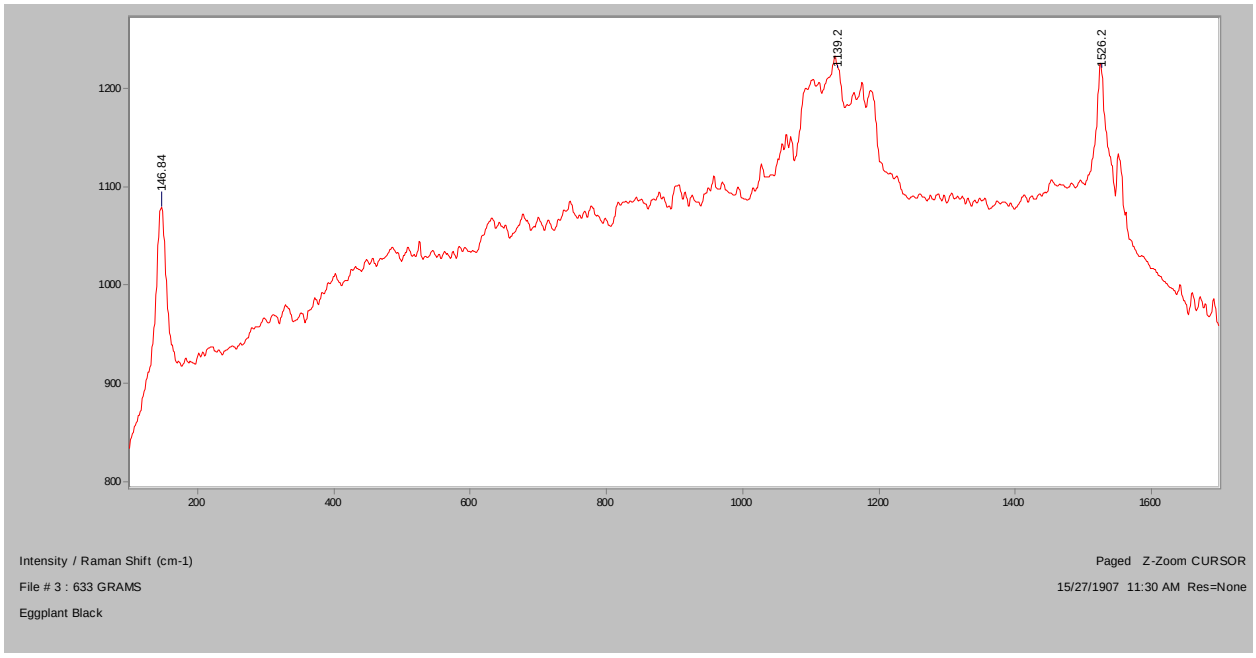

Normal Raman, 785nm

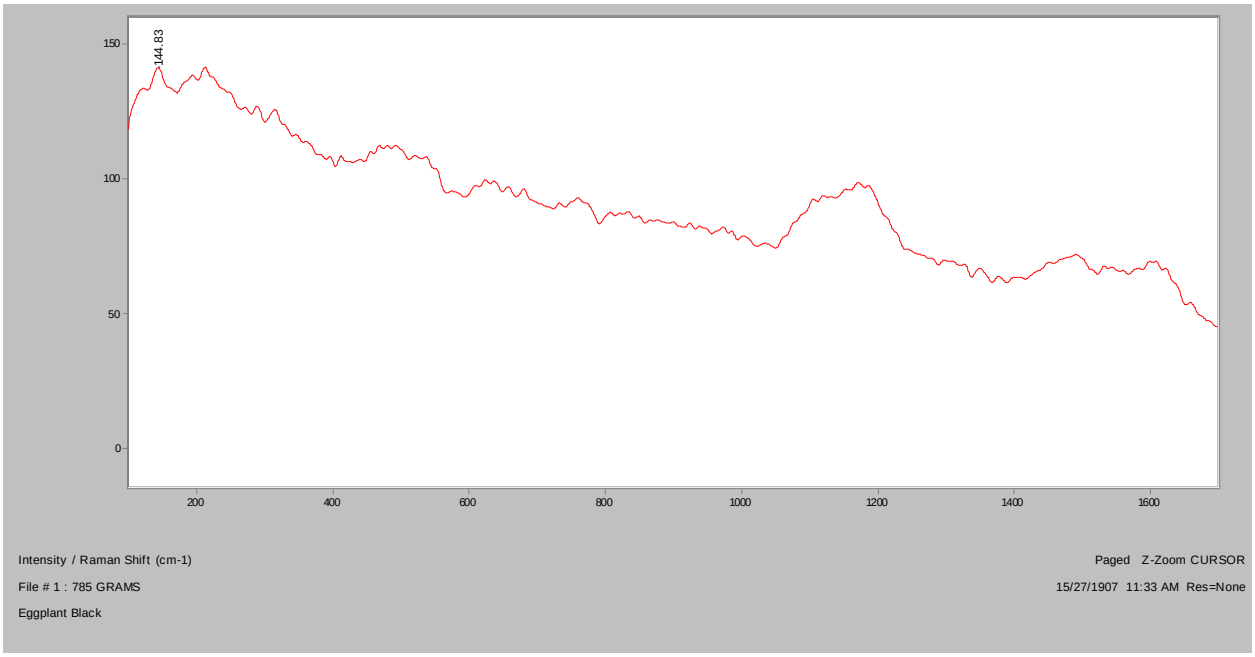

FT-IR (ATR)

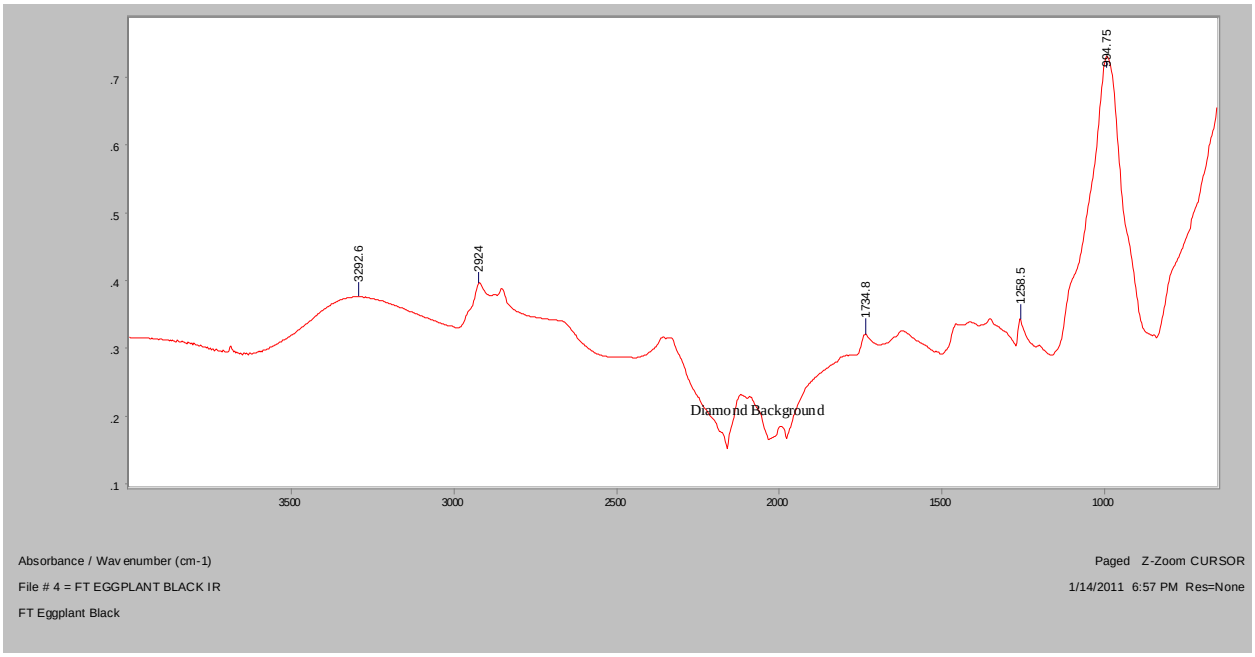

XRF

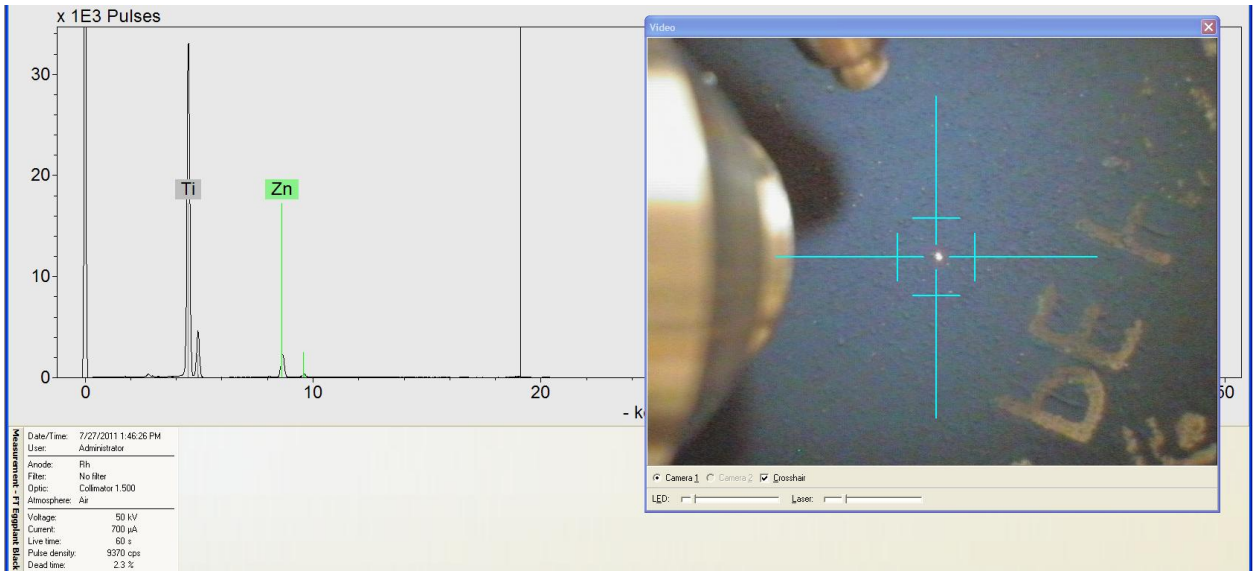
x 1E3 Pulses
30
20
10
0
Ti
Zn
0
10
20
Video
Camera 1
Camera 2
Crosshair
LED:
Laser:
Date/Time: 7/27/2011 1:46:26 PM
User: Administrator
Anode: Rh
Filter: No filter
Optic: Collimator 1.500
Atmosphere: Air
Voltage: 50 kV
Current: 700 µA
Live time: 60 s
Pulse density: 9370 cps
Dead time: 2.3 %

Dark Black

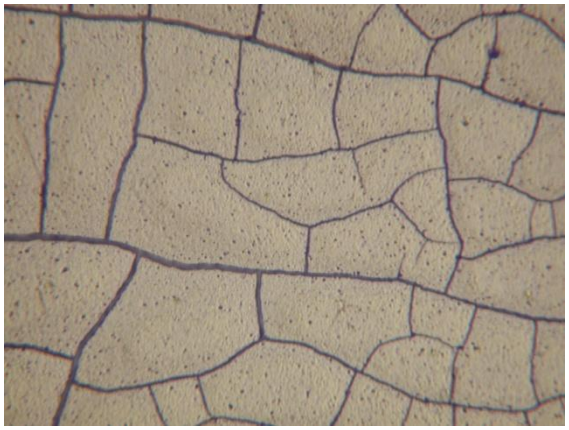

Bright Field, 100x

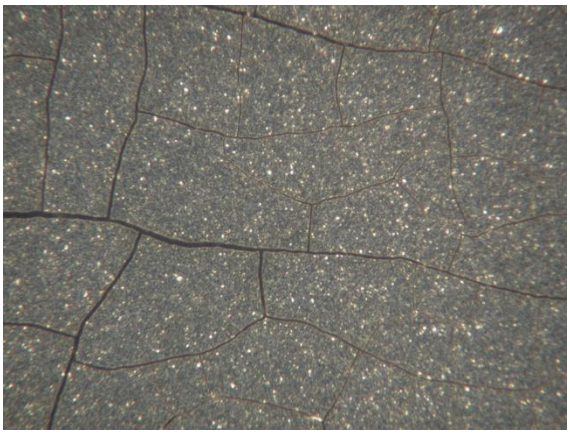

Dark Field, 100x

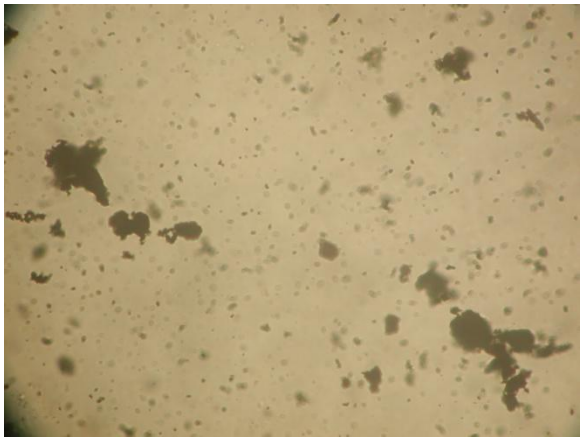

In RI 1.550, 400x

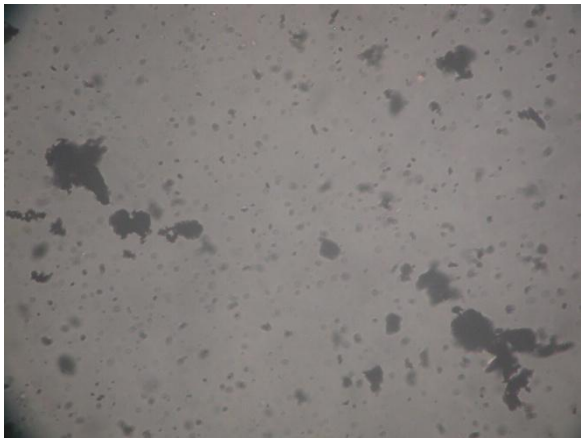

Crossed Polars, In RI 1.550, 400x

Normal Raman, 488nm

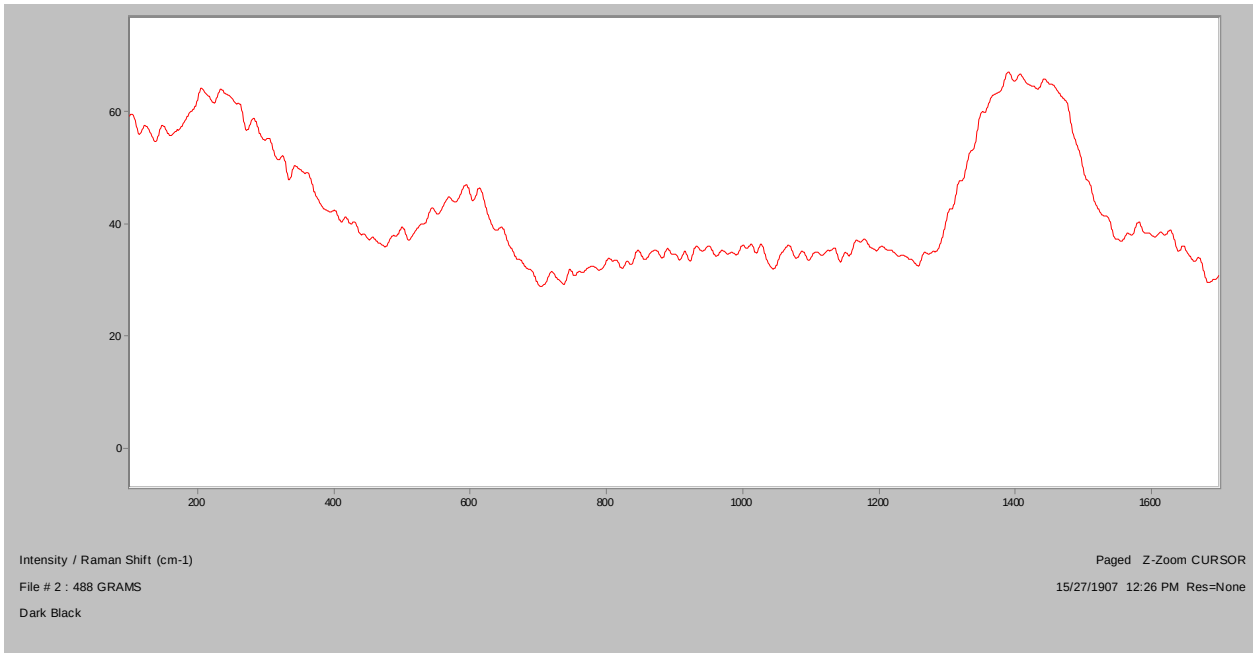

Normal Raman, 633nm

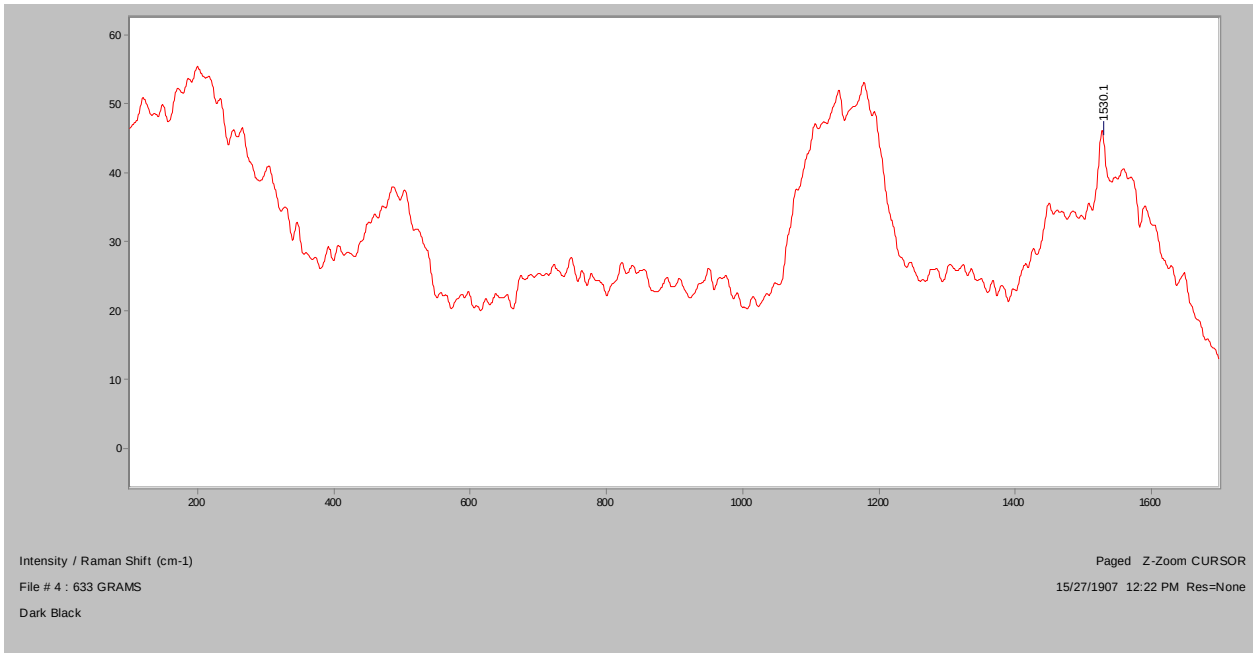

Normal Raman, 785nm

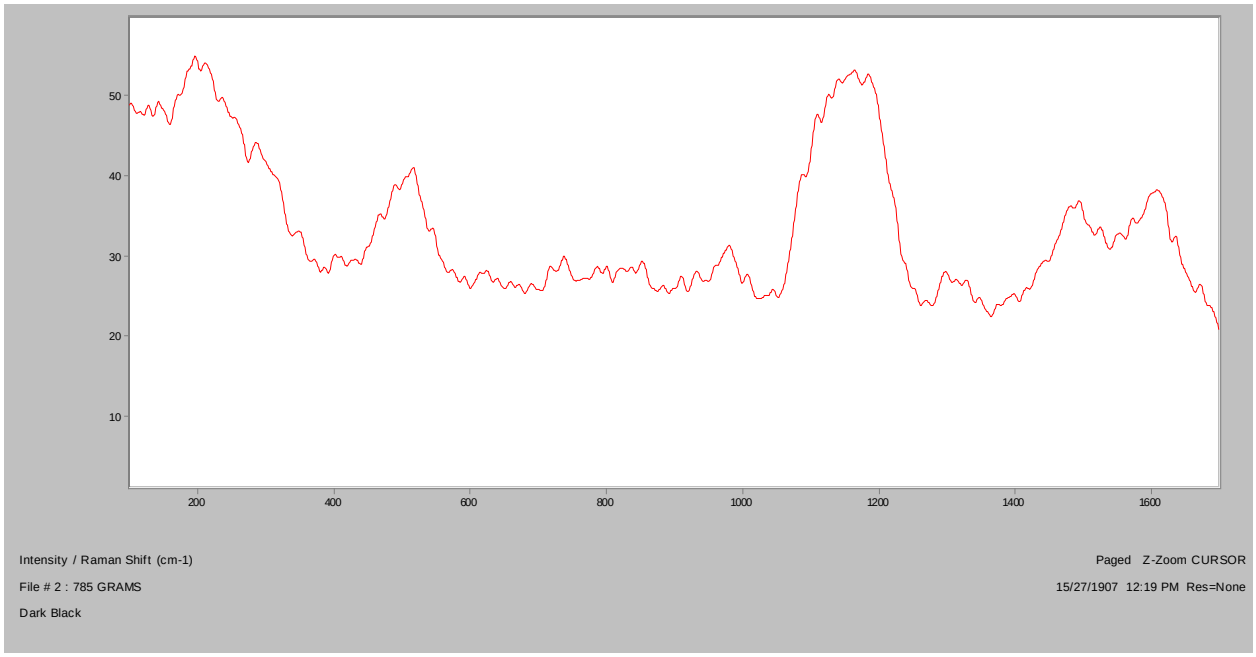

FT-IR (ATR)

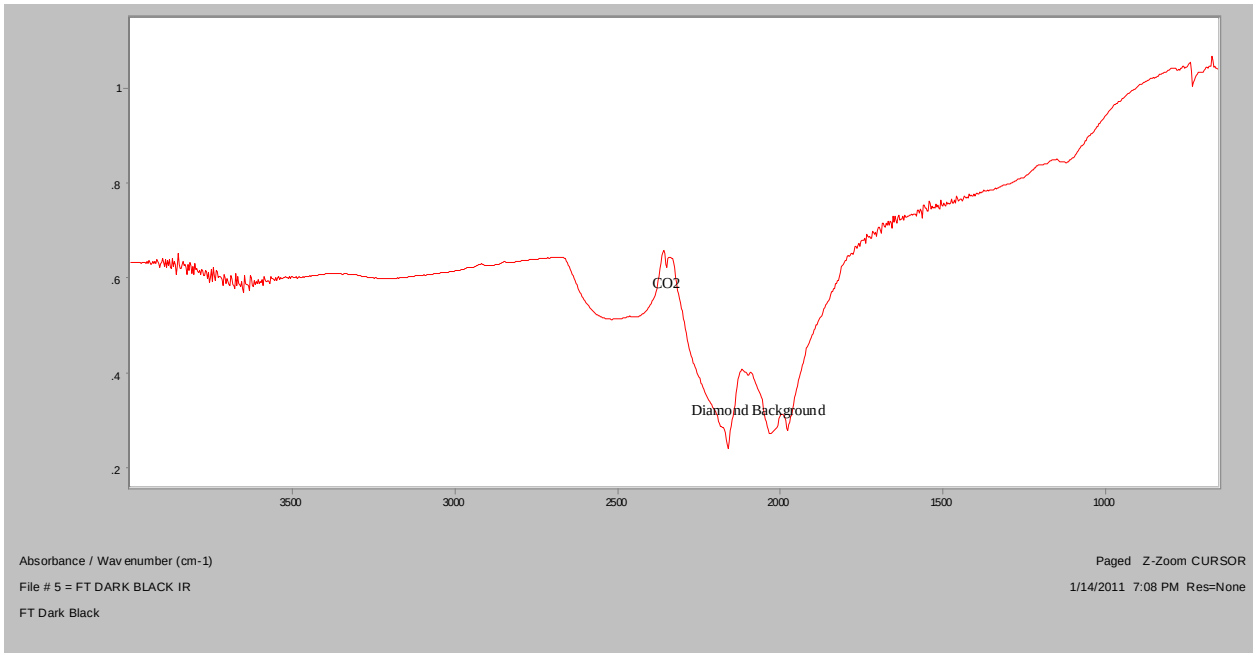

XRF

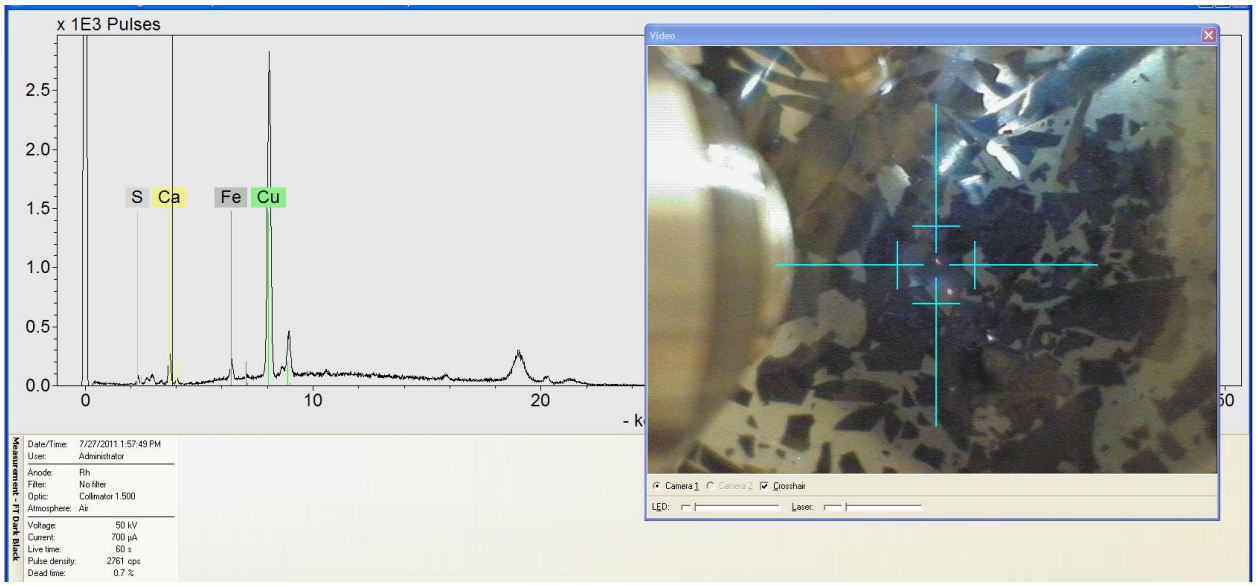
x 1E3 Pulses
2.5
2.0
1.5
1.0
0.5
0.0
S
Ca
Fe
Cu
0
10
20
Video
Camera 1
Camera 2
Crosshair
LED:
Laser:
Measurement - FT Dark Black
Date/Time: 7/27/2011 1:57:49 PM
User: Administrator
Anode: Rh
Filter: No filter
Optic: Collimator 1.500
Atmosphere: Air
Voltage: 50 kV
Current: 700 µA
Live time: 60 s
Pulse density: 2761 cps
Dead time: 0.7 %

Sayonara Suede

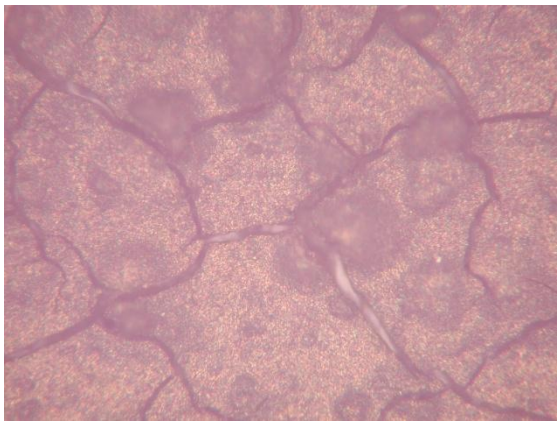

Bright Field, 100x

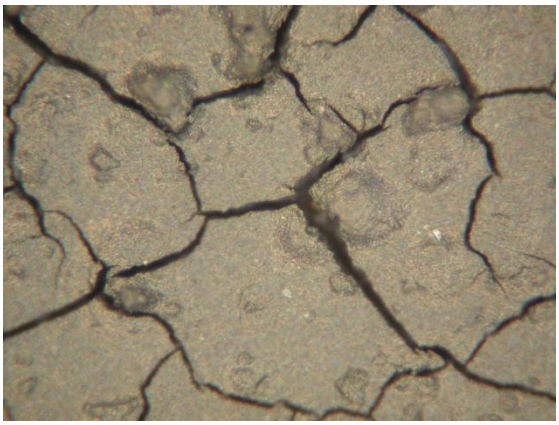

Dark Field, 100x

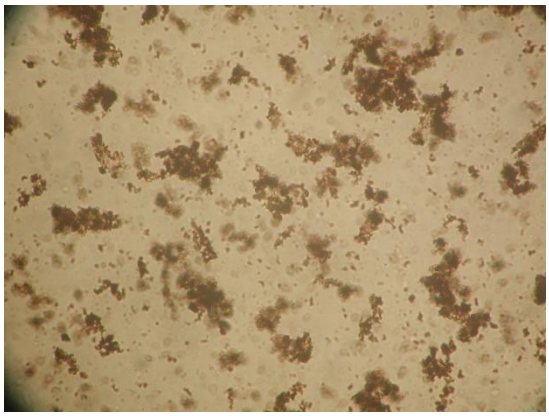

In RI 1.550, 400x

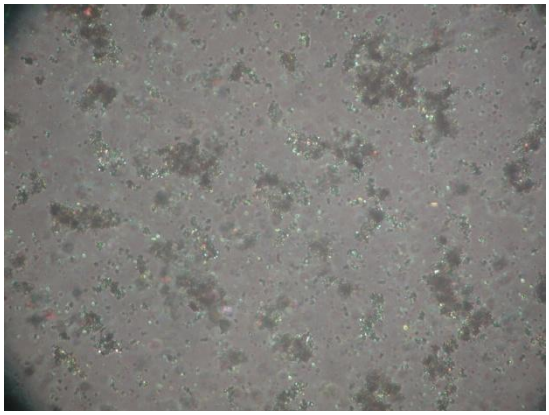

Crossed Polars, In RI 1.550, 400x

Normal Raman, 488nm

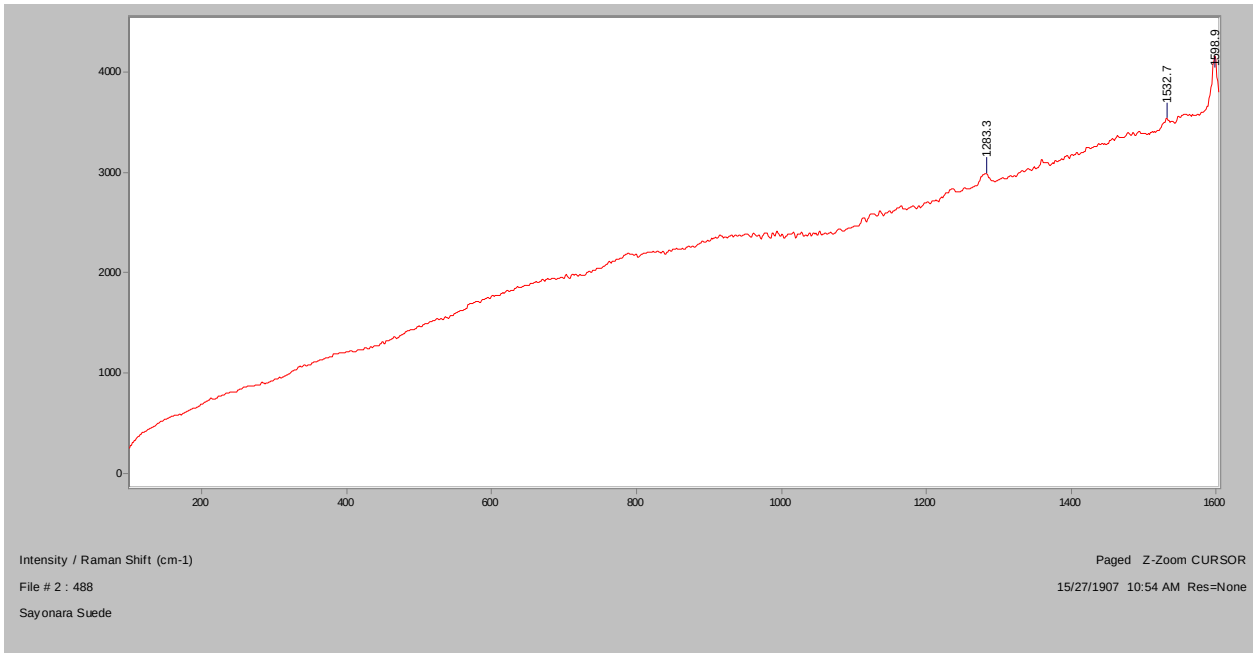

Normal Raman, 633nm

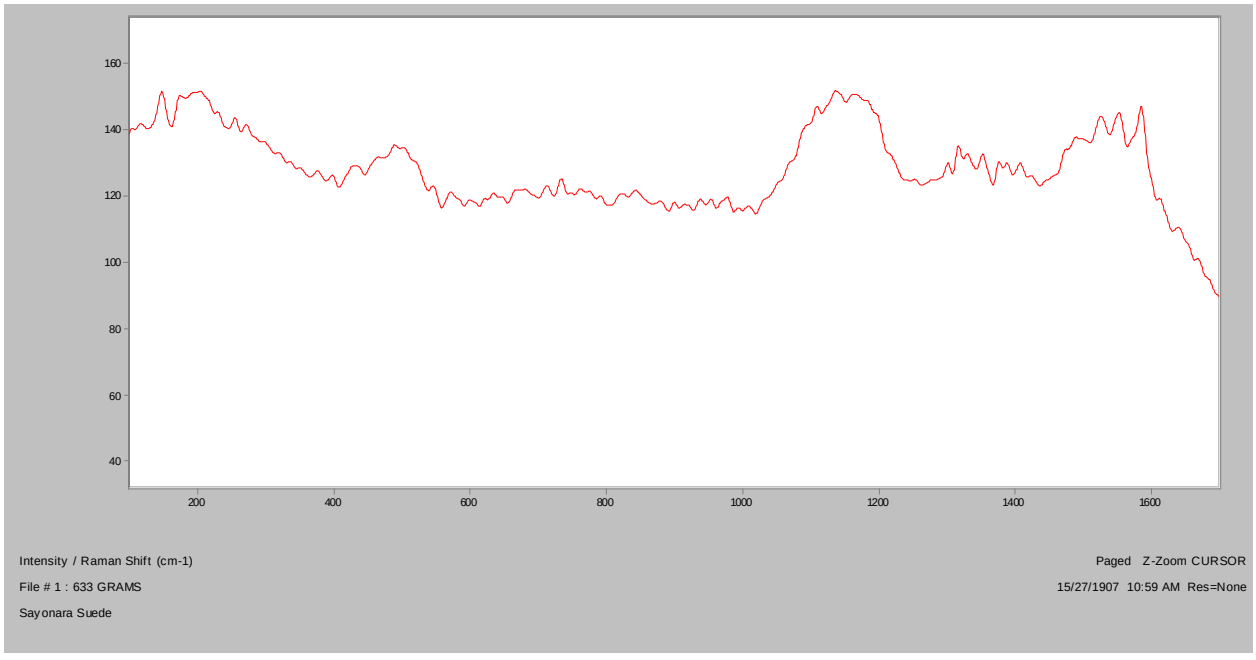

Normal Raman, 785nm

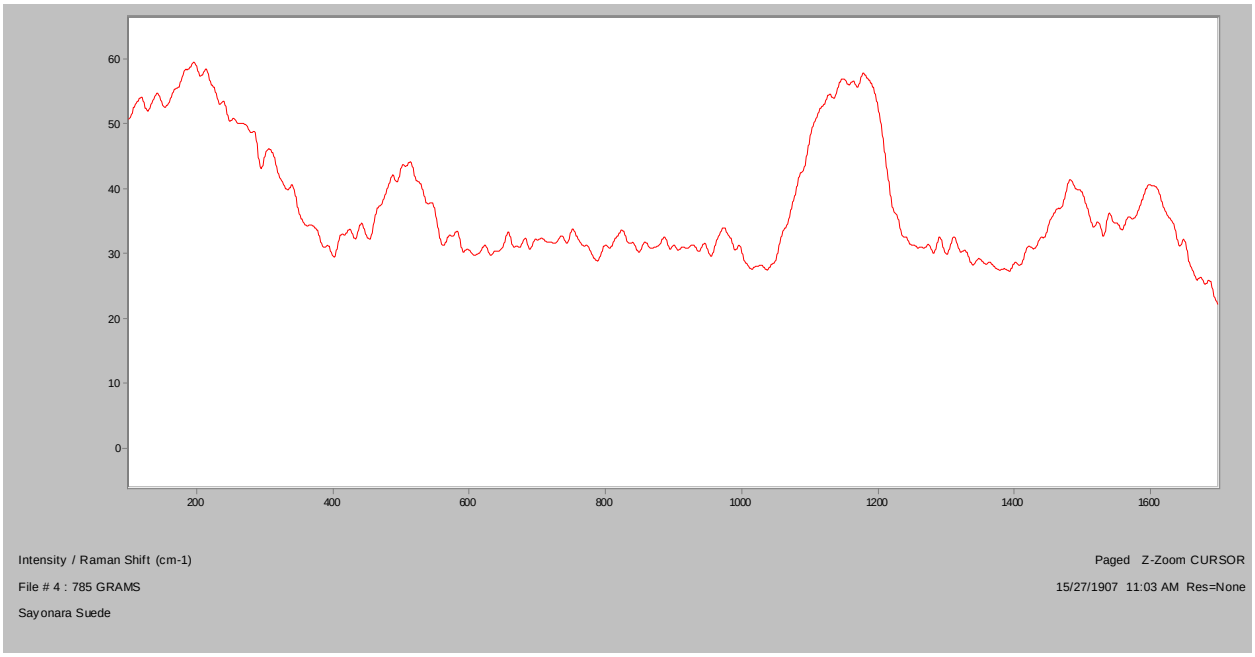

FT-IR (ATR)

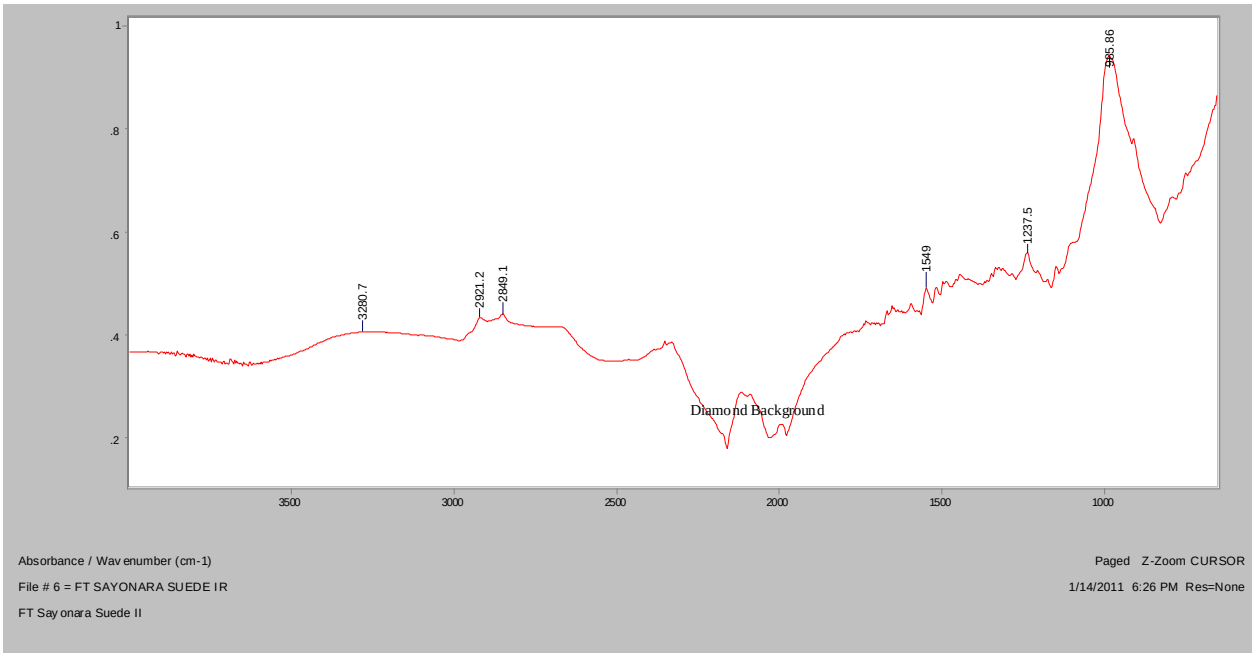

XRF

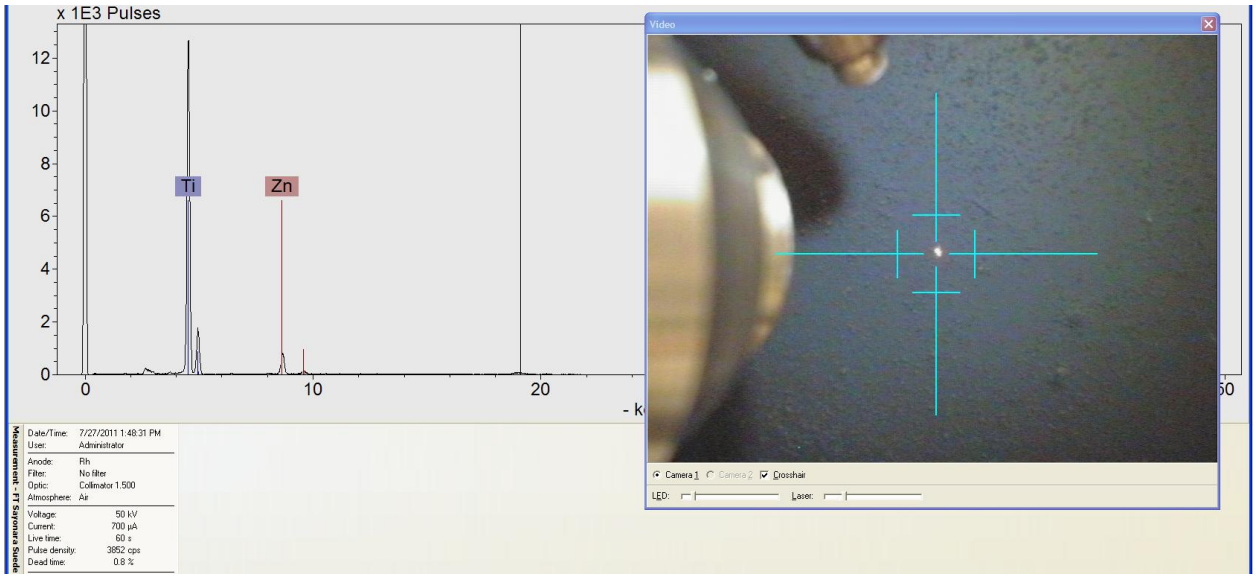
x 1E3 Pulses
12
10
8
6
4
2
0
Ti
Zn
0
10
20
Video
Camera 1
Camera 2
Crosshair
LED:
Laser:
Measurement - FT Silvorna Suede
Date/Time: 7/27/2011 1:48:31 PM
User: Administrator
Anode: Rh
Filter: No filter
Optic: Collimator 1.500
Atmosphere: Air
Voltage: 50 kV
Current: 700 µA
Live time: 60 s
Pulse density: 3852 cps
Dead time: 0.8 %

Dark Brown

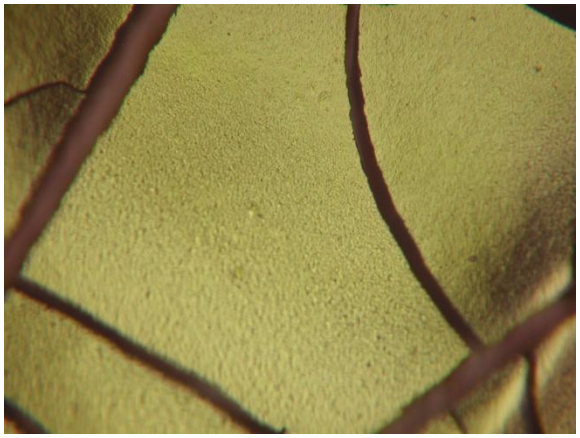

Bright Field, 100x

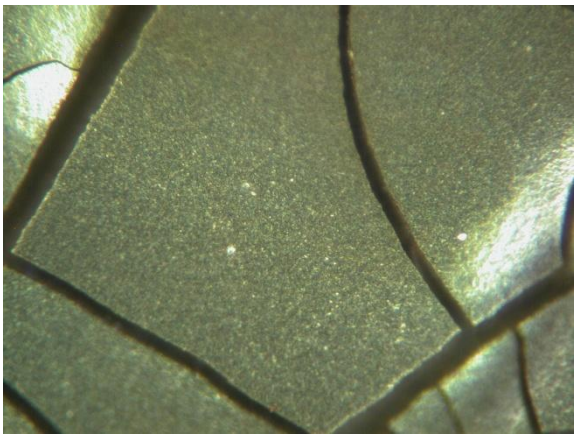

Dark Field, 100x

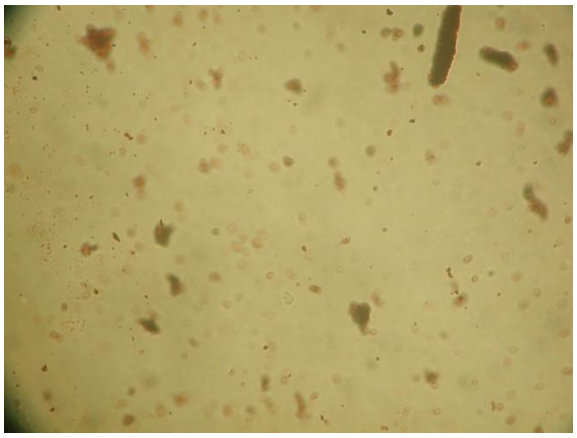

In RI 1.550, 400x

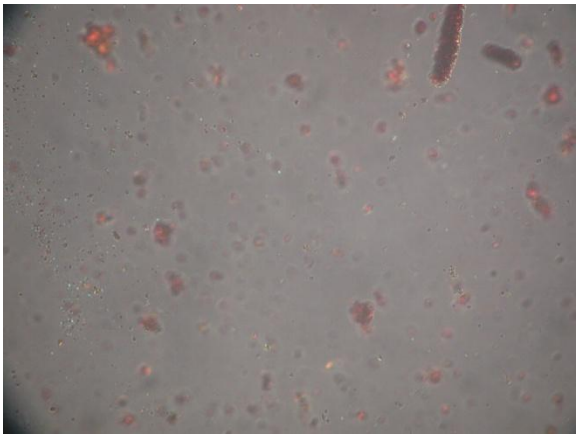

Crossed Polars, In RI 1.550, 400x

Normal Raman, 488nm

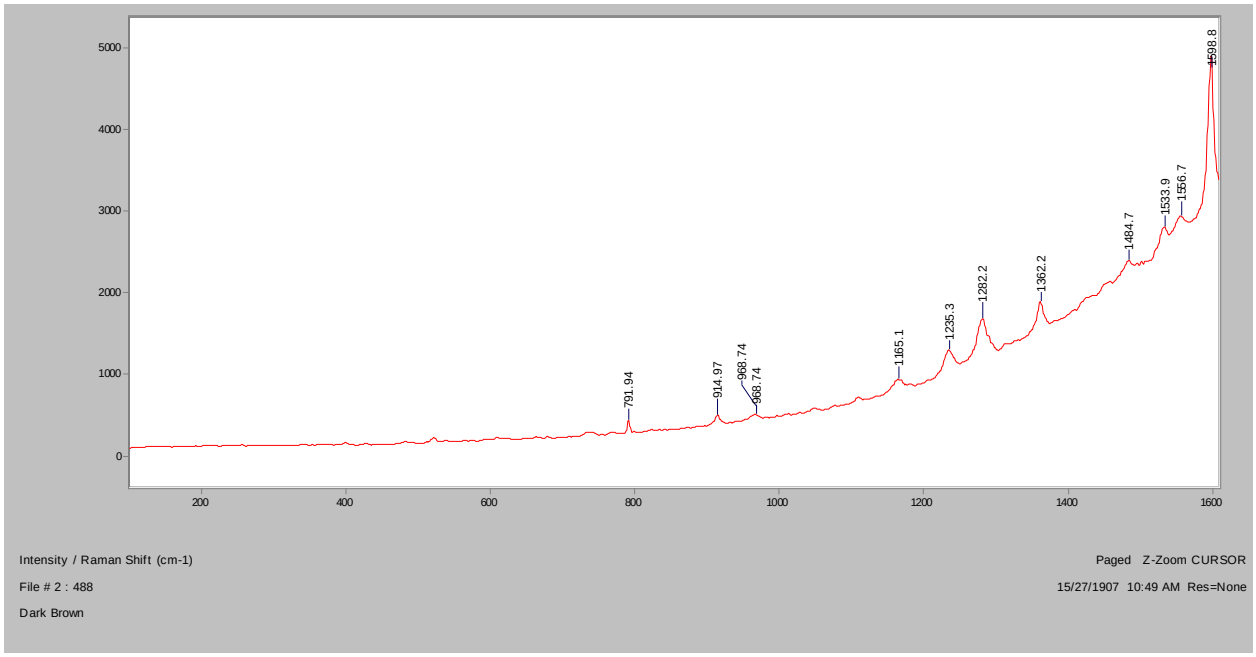

Normal Raman, 633nm

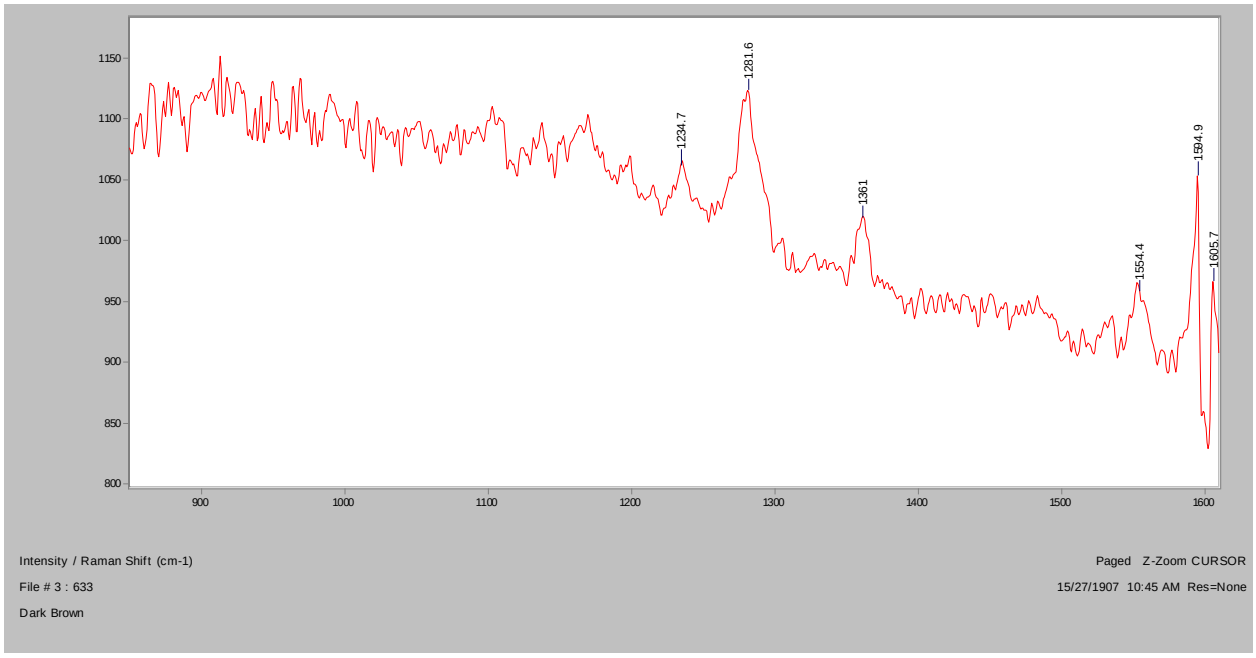

Normal Raman, 785nm

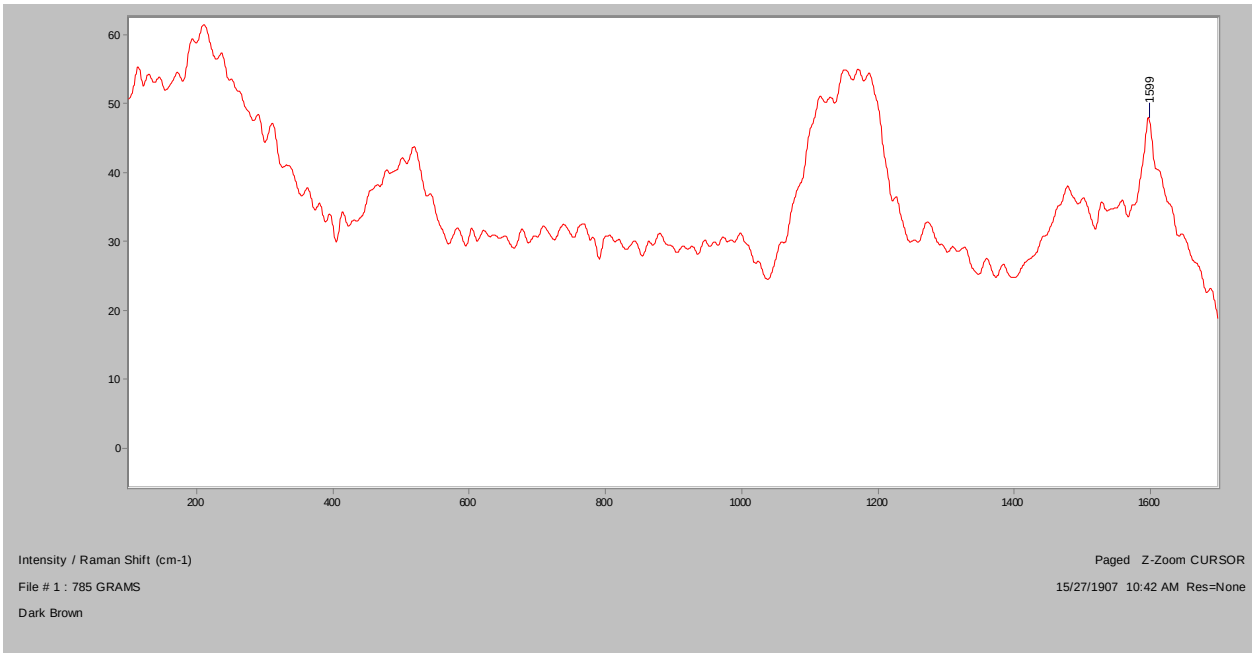

FT-IR (ATR)

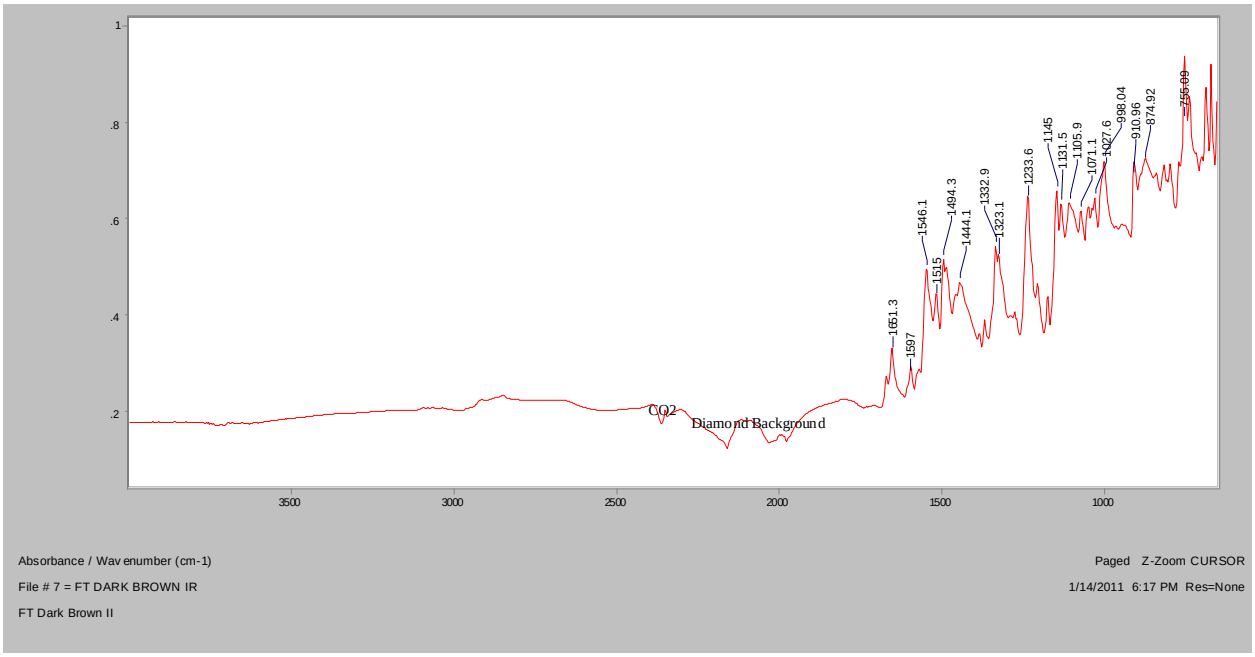

XRF

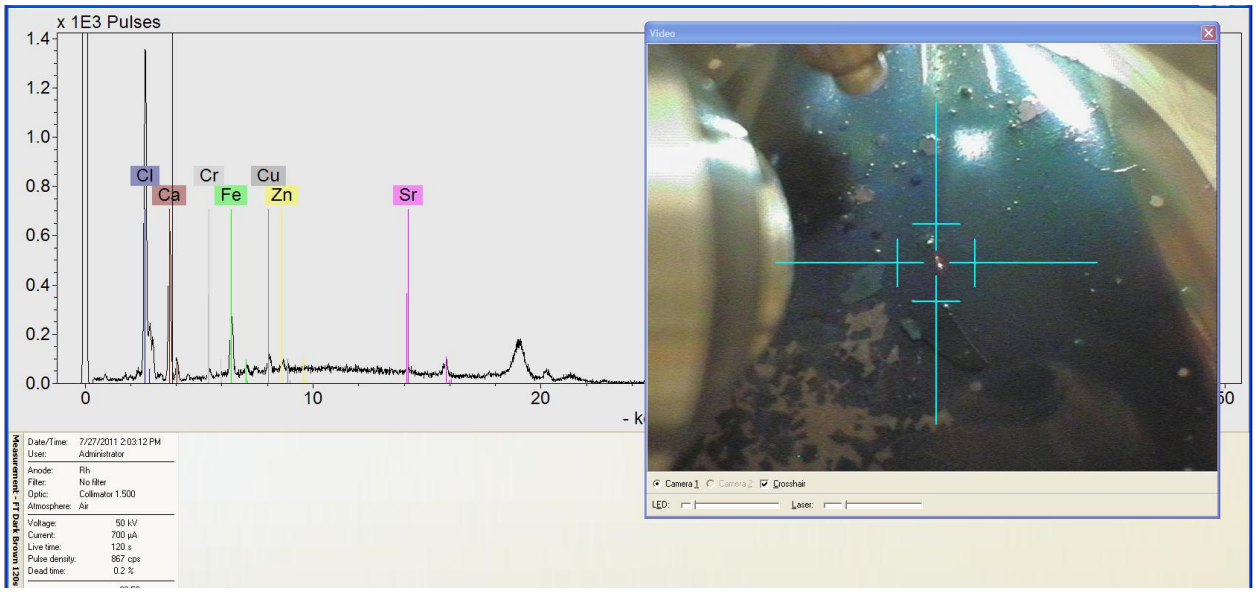
x 1E3 Pulses
1.4
1.2
1.0
0.8
0.6
0.4
0.2
0.0
Cl
Ca
Cr
Fe
Cu
Zn
Sr
0
10
20
Video
Camera 1
Camera 2
Crosshair
LED:
Laser:
Date/Time: 7/27/2011 2:03:12 PM
User: Administrator
Anode: Rh
Filter: No filter
Optic: Collimator 1.500
Atmosphere: Air
Voltage: 50 kV
Current: 700 µA
Live time: 120 s
Pulse density: 867 cps
Dead time: 0.2 %

Light Chocolate

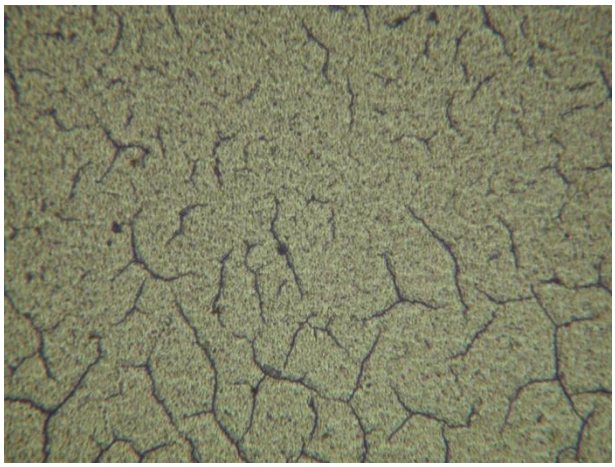

Bright Field, 100x

Dark Field, 100x

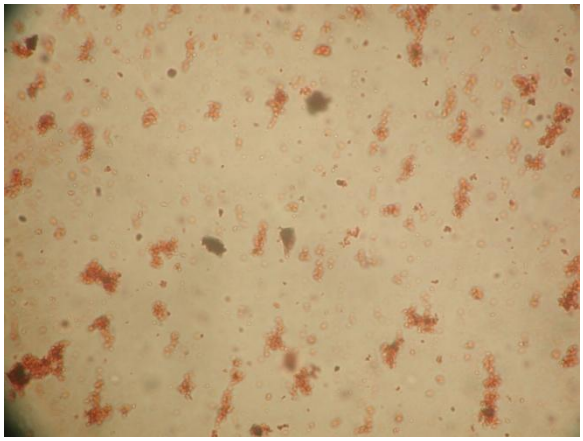

In RI 1.550, 400x

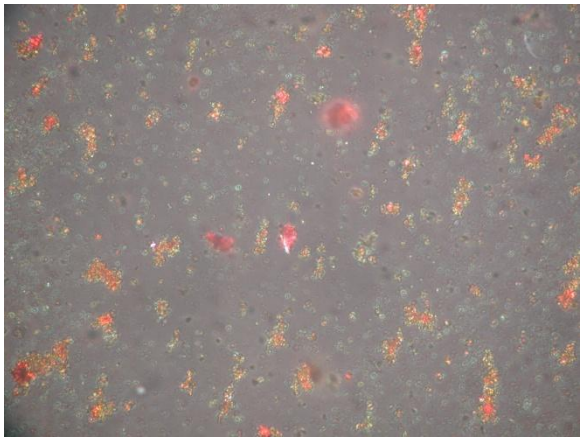

Crossed Polars, In RI 1.550, 400x

Normal Raman, 488nm

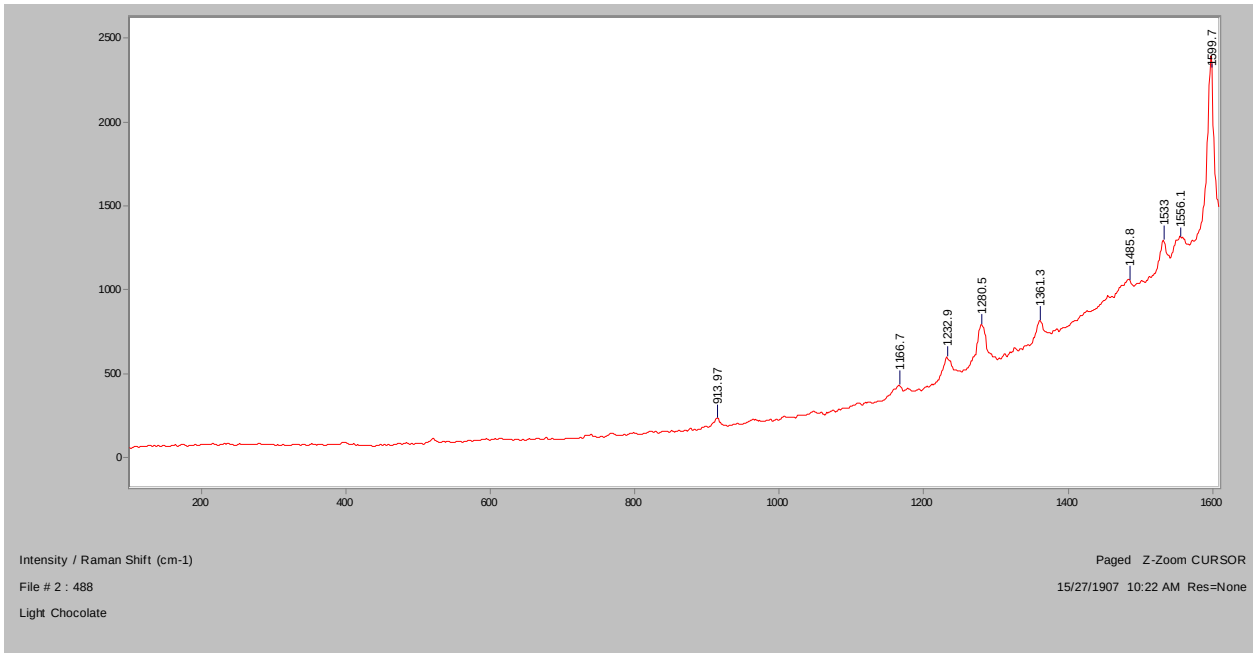

Normal Raman, 633nm

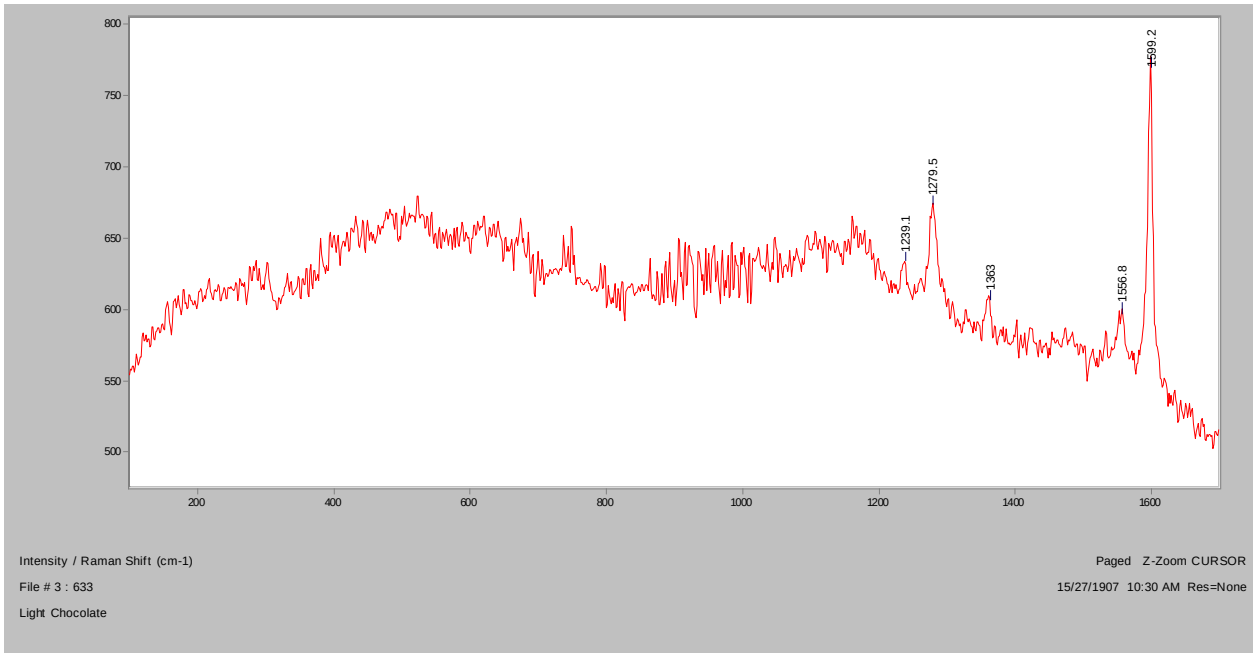

Normal Raman, 785nm

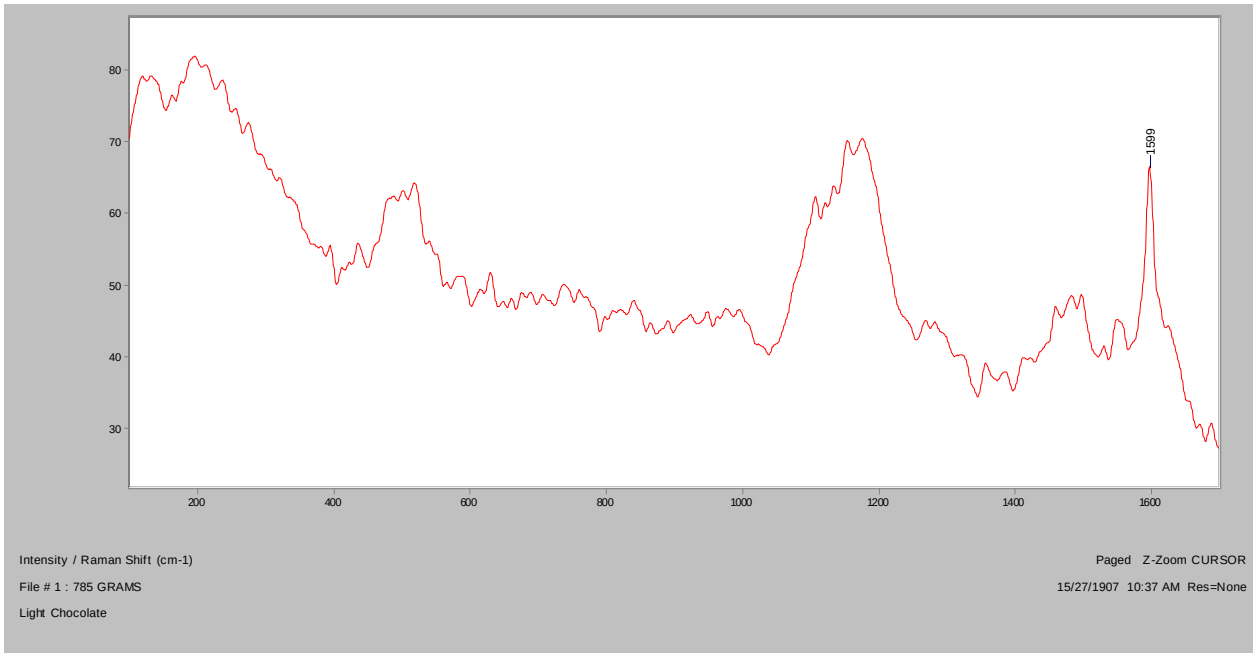

FT-IR (ATR)

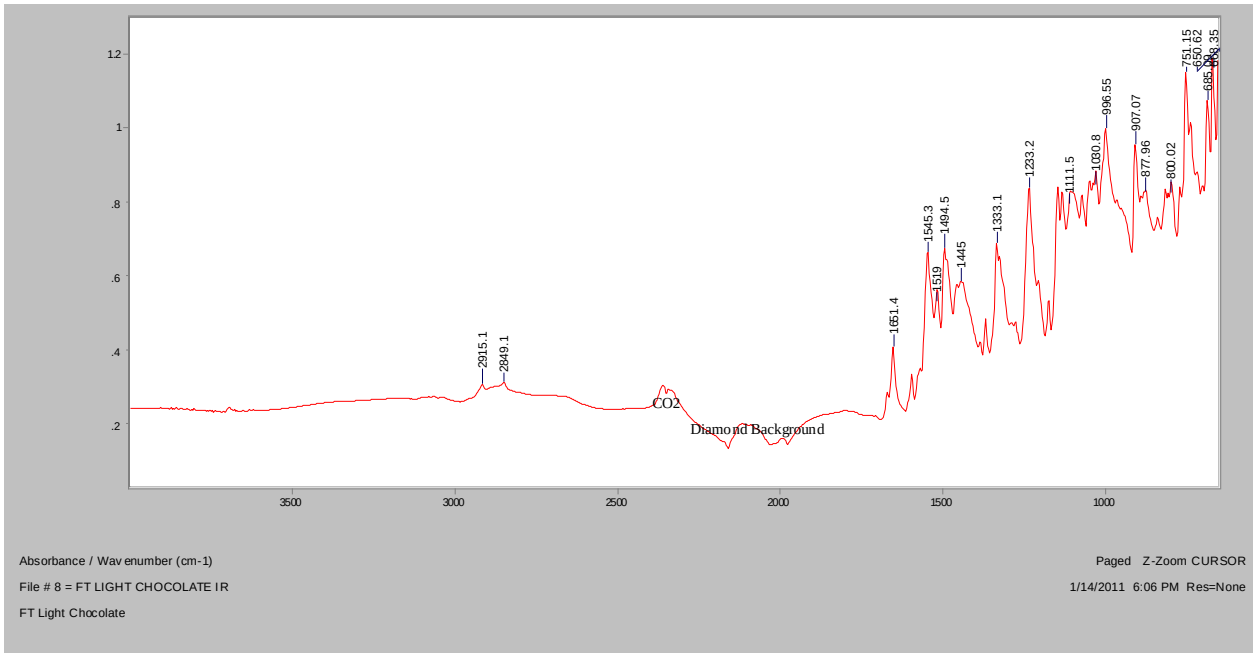

XRF

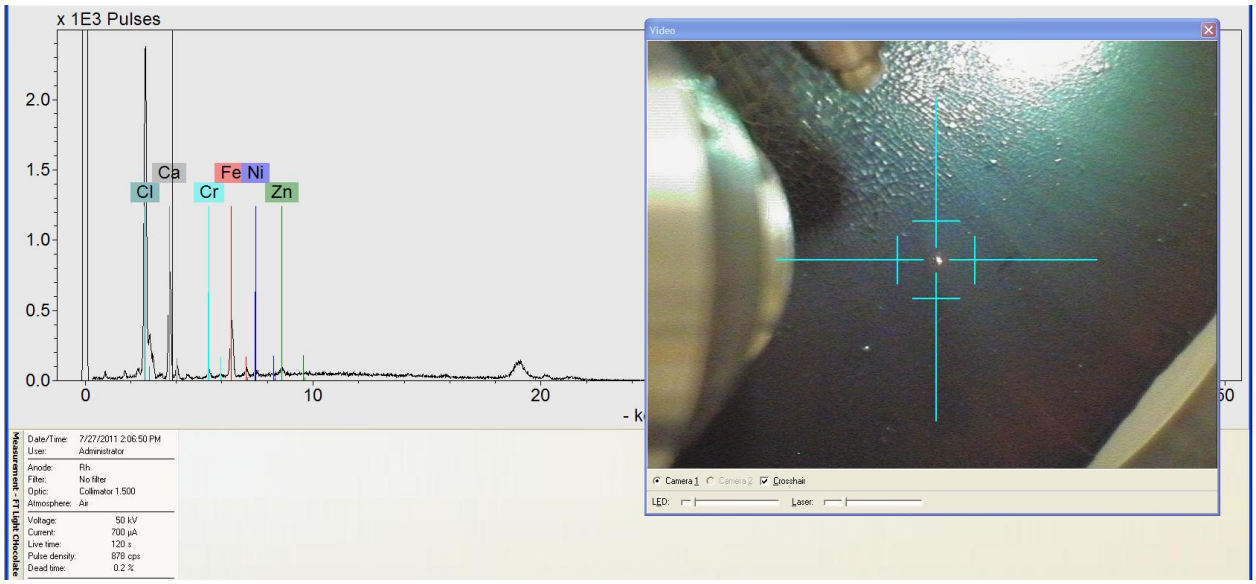
x 1E3 Pulses
2.0
1.5
1.0
0.5
0.0
0
10
20
Cl
Ca
Cr
Fe Ni
Zn
Video
Camera 1
Camera 2
Crosshair
LED:
Laser:
Date/Time: 7/27/2011 2:06:50 PM
User: Administrator
Anode: Rh
Filter: No filter
Optic: Collimator 1.500
Atmosphere: Air
Voltage: 50 kV
Current: 700 µA
Live time: 120 s
Pulse density: 878 cps
Dead time: 0.2 %

Skin Tone

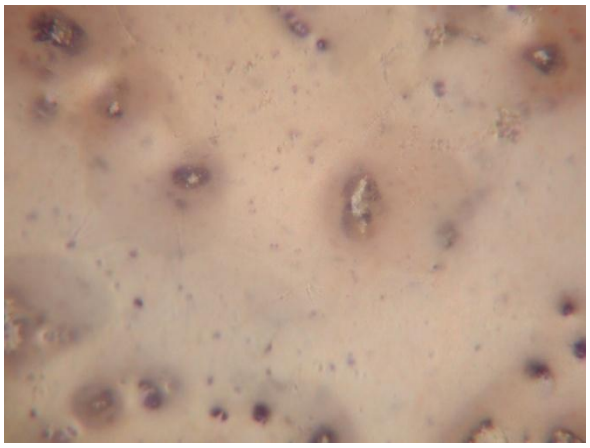

Bright Field, 100x

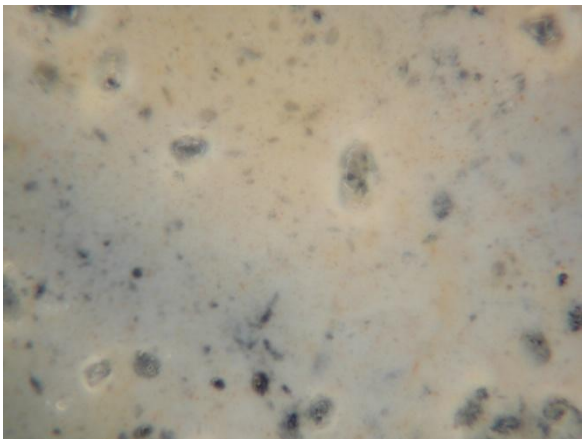

Dark Field, 100x

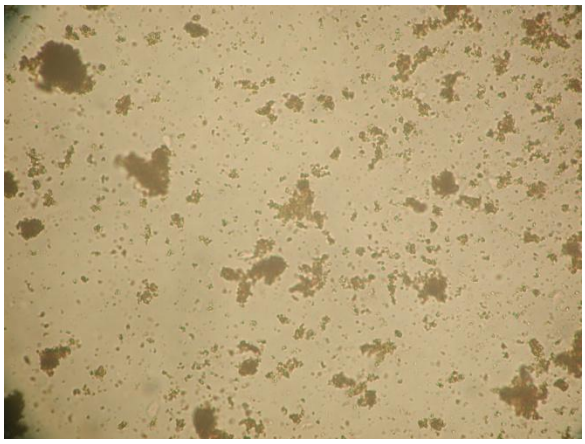

In RI 1.550, 400x

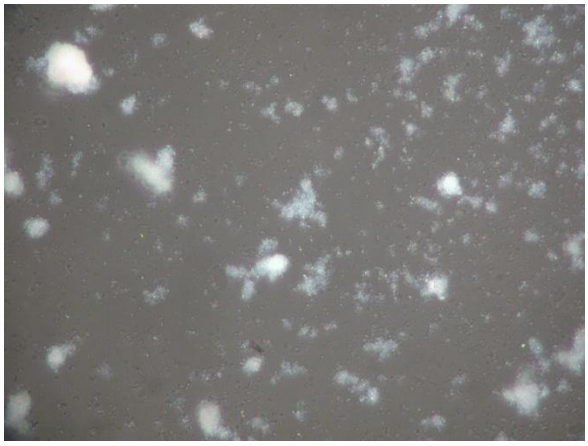

Crossed Polars, In RI 1.550, 400x

Raman microscope image, 1000x

Normal Raman, 488nm

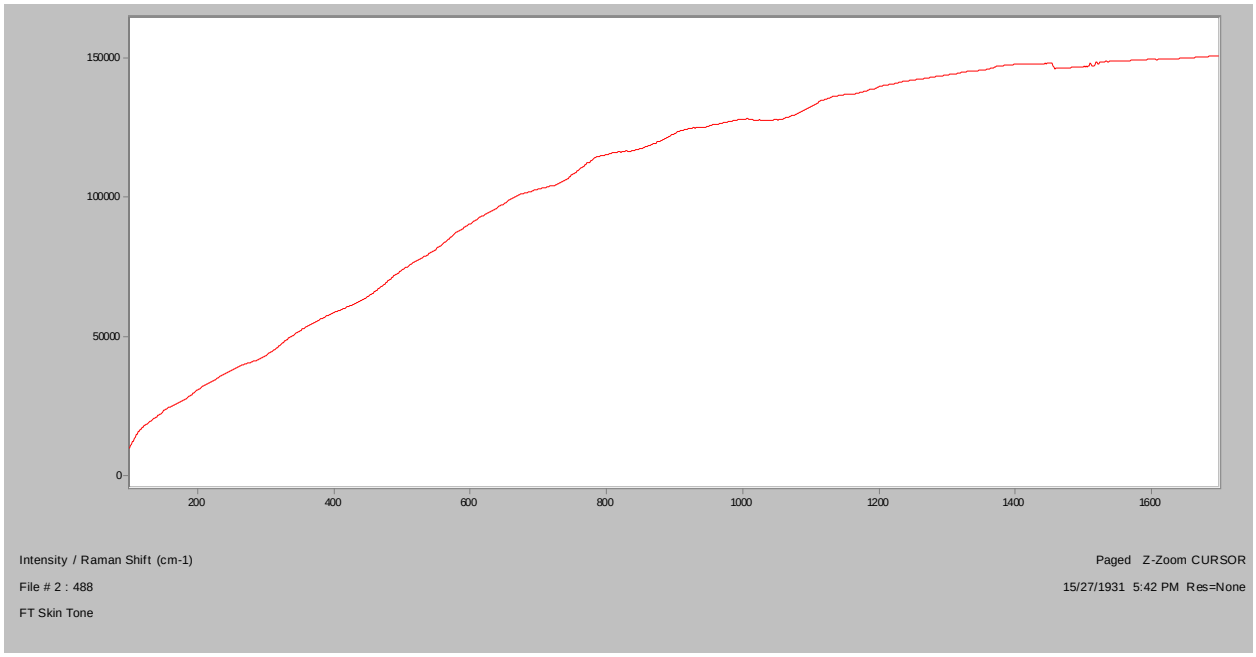

Normal Raman, 633nm

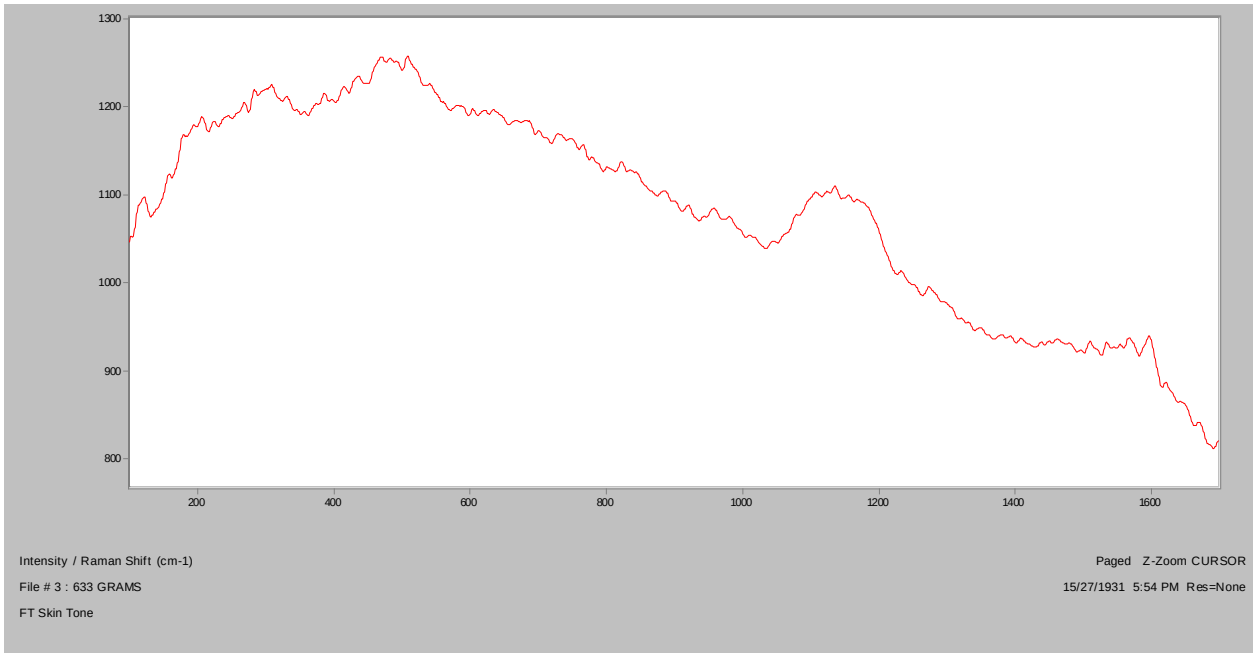

Normal Raman, 785nm

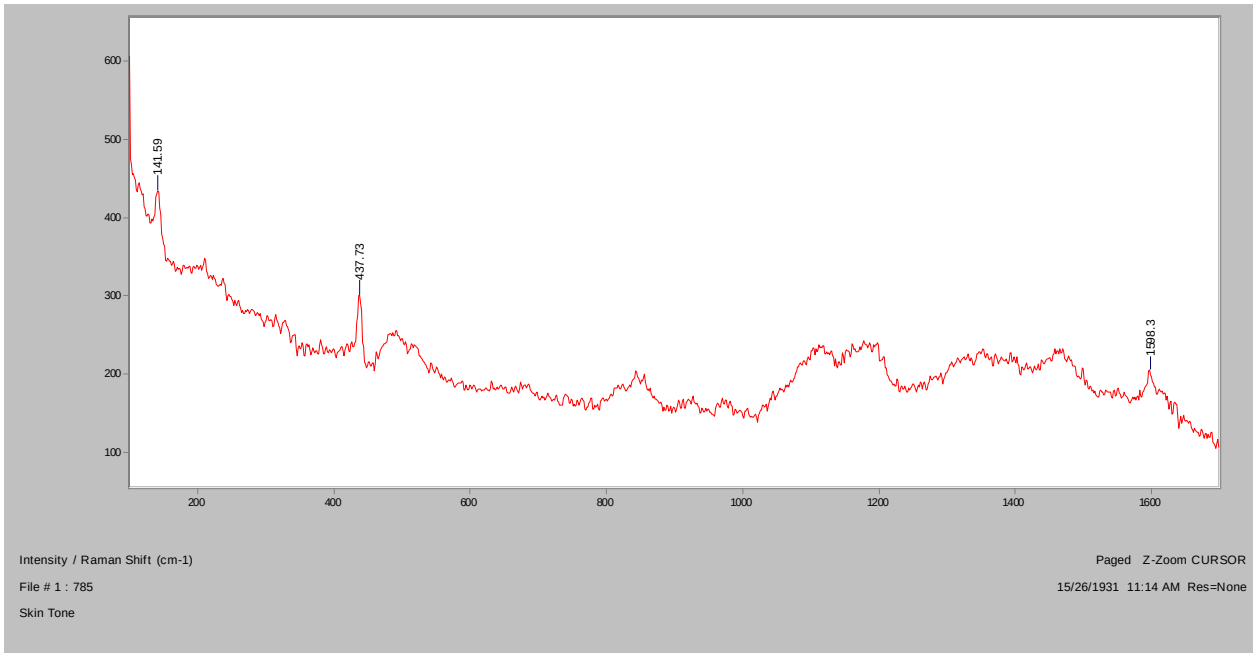

FT-IR (ATR)

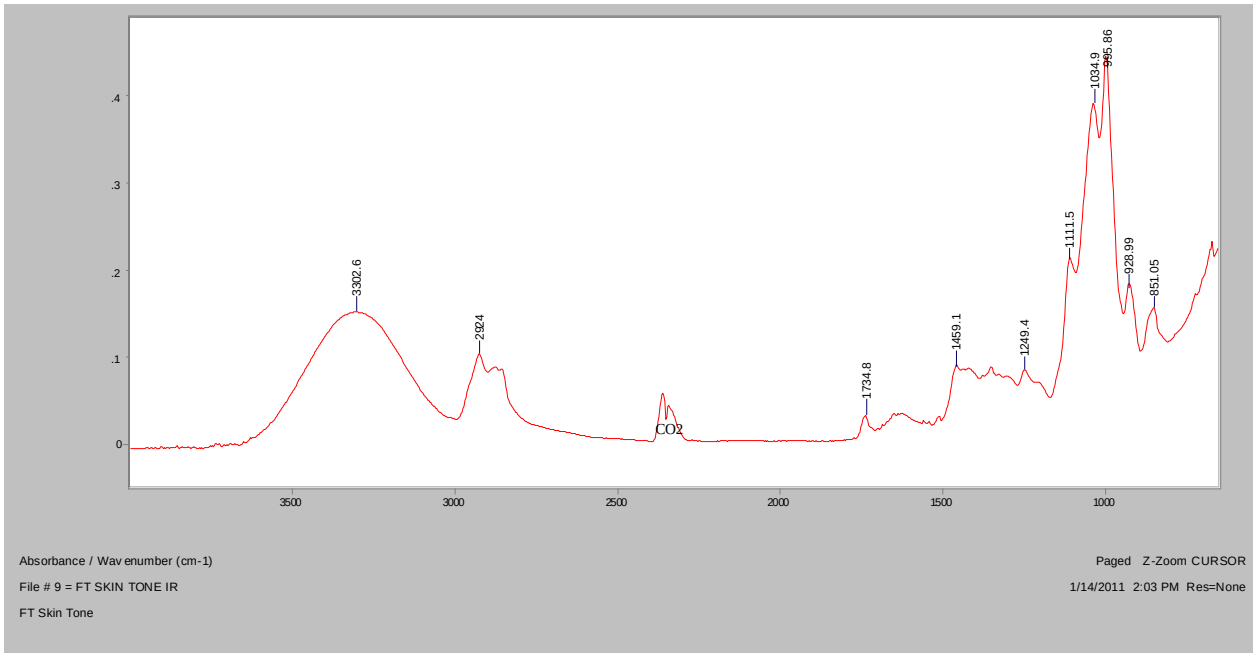

XRF

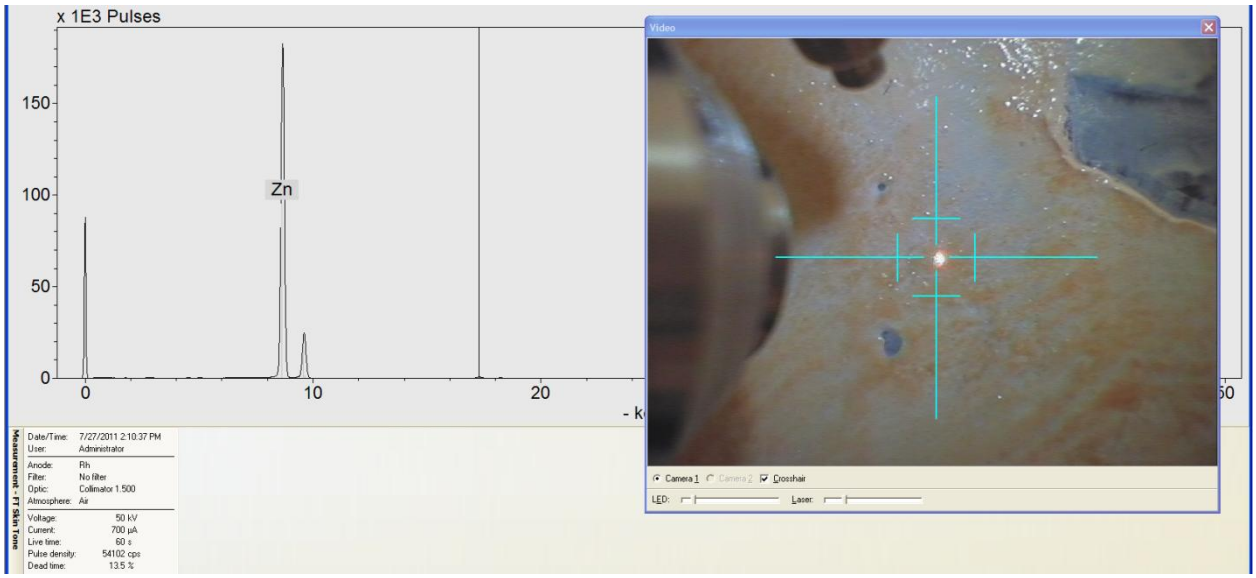
x 1E3 Pulses
150
100
50
0
Zn
0
10
20
Video
Camera 1
Crosshair
LED:
Laser:
Date/Time: 7/27/2011 2:10:37 PM
User: Administrator
Anode: Rh
Filter: No filter
Optic: Collimator 1.500
Atmosphere: Air
Voltage: 50 kV
Current: 700 µA
Live time: 60 s
Pulse density: 54102 cps
Dead time: 13.5 %

White

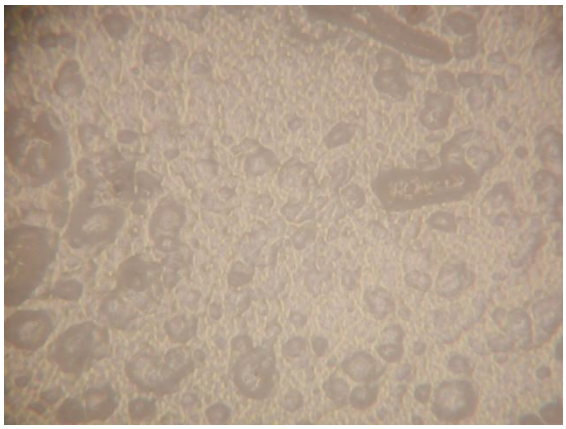

Bright Field, 100x

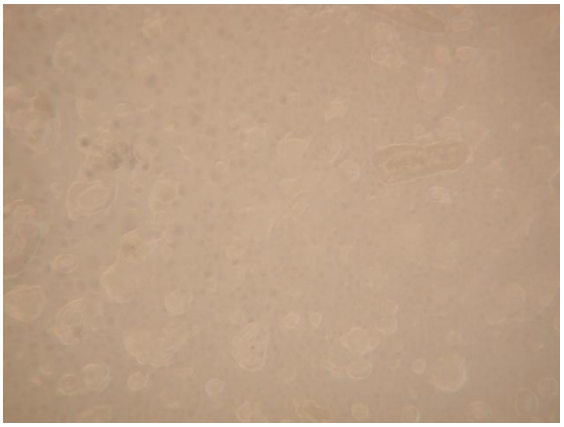

Dark Field, 100x

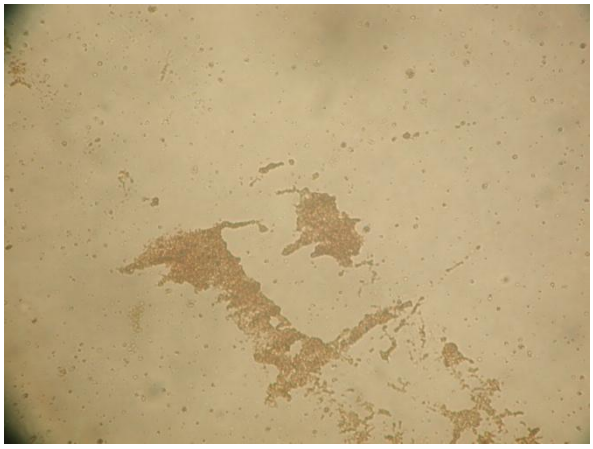

In RI 1.550, 400x

Crossed Polars, In RI 1.550, 400x

Normal Raman, 488nm

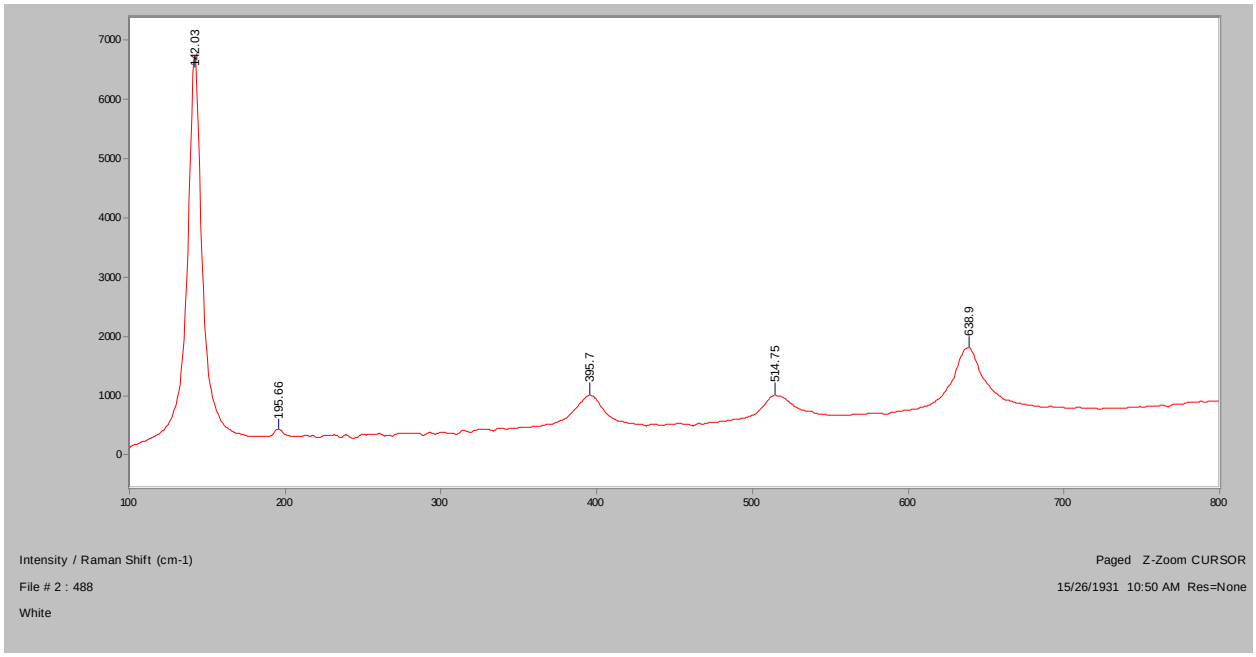

Normal Raman, 633nm

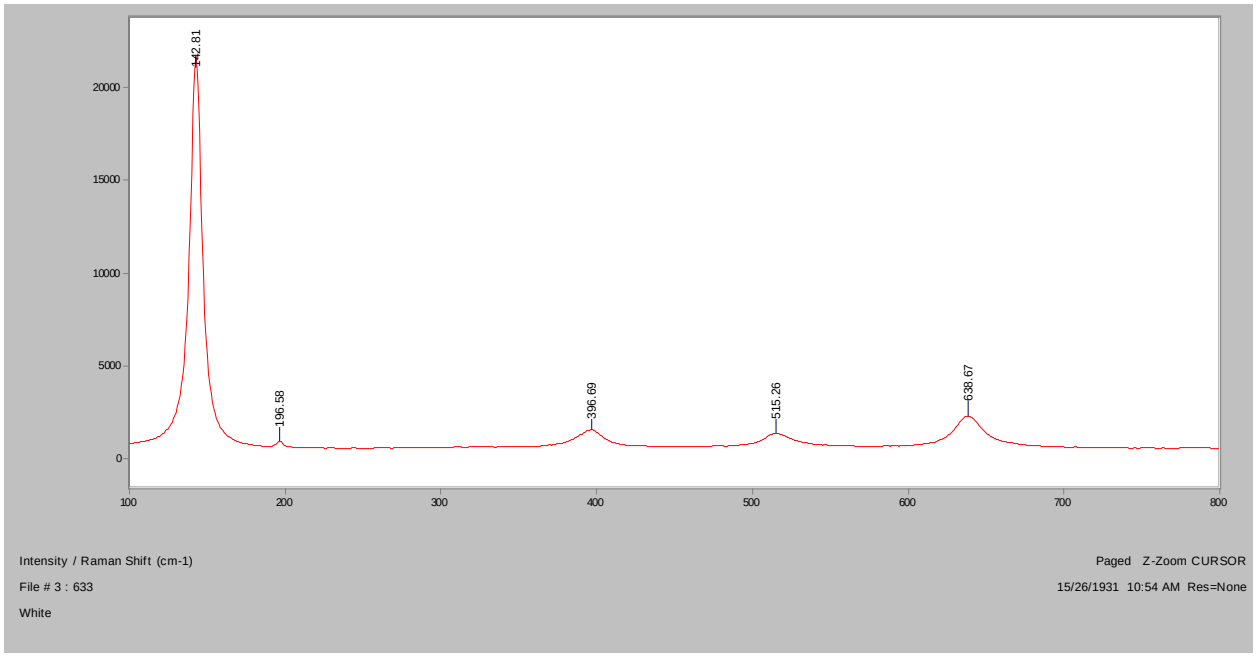

Normal Raman, 785nm

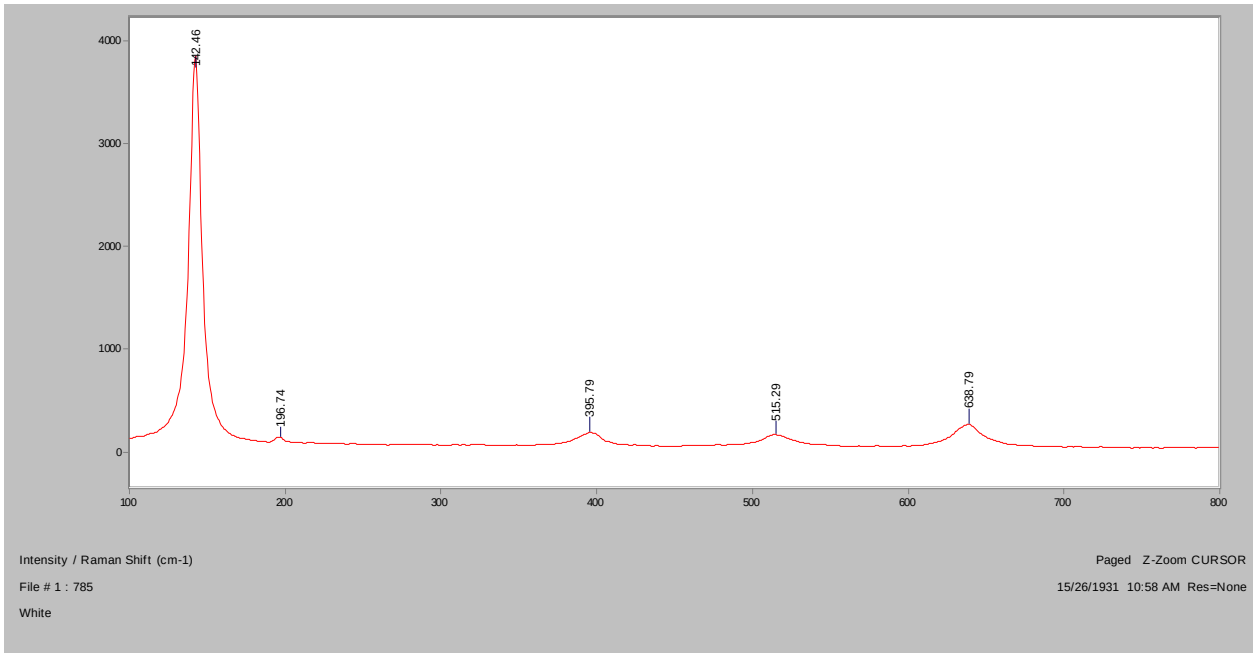

FT-Raman, 1064nm

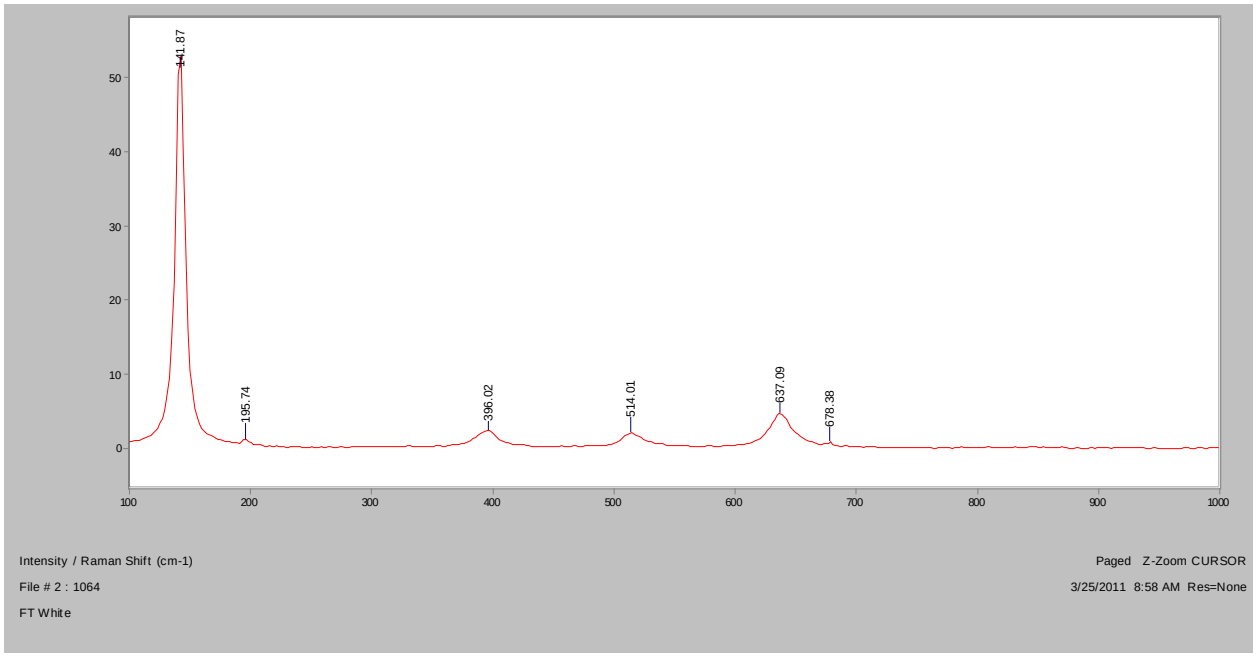

FT-IR (ATR)

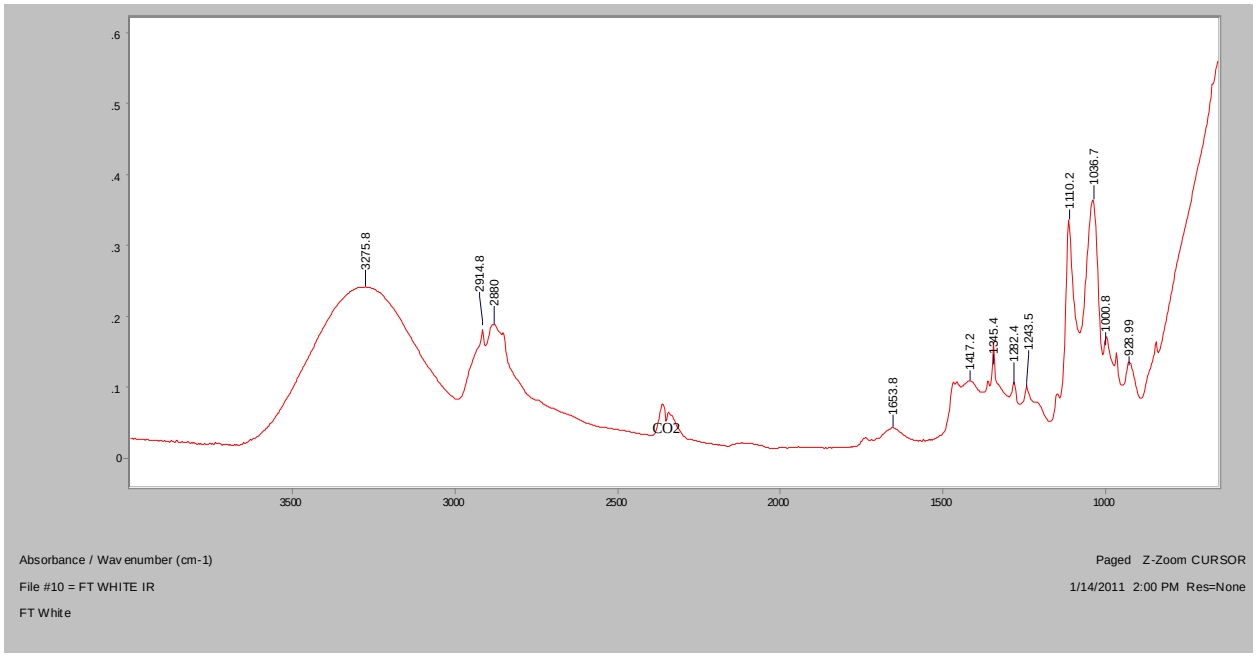
3275.8
2914.8
2880
CO2
1653.8
1417.2
1345.4
1282.4
1243.5
1110.2
1036.7
1000.8
928.99
Absorbance / Wavenumber (cm-1)
File #10 = FT WHITE IR
FT White
Paged Z-Zoom CURSOR
1/14/2011 2:00 PM Res=None

XRF

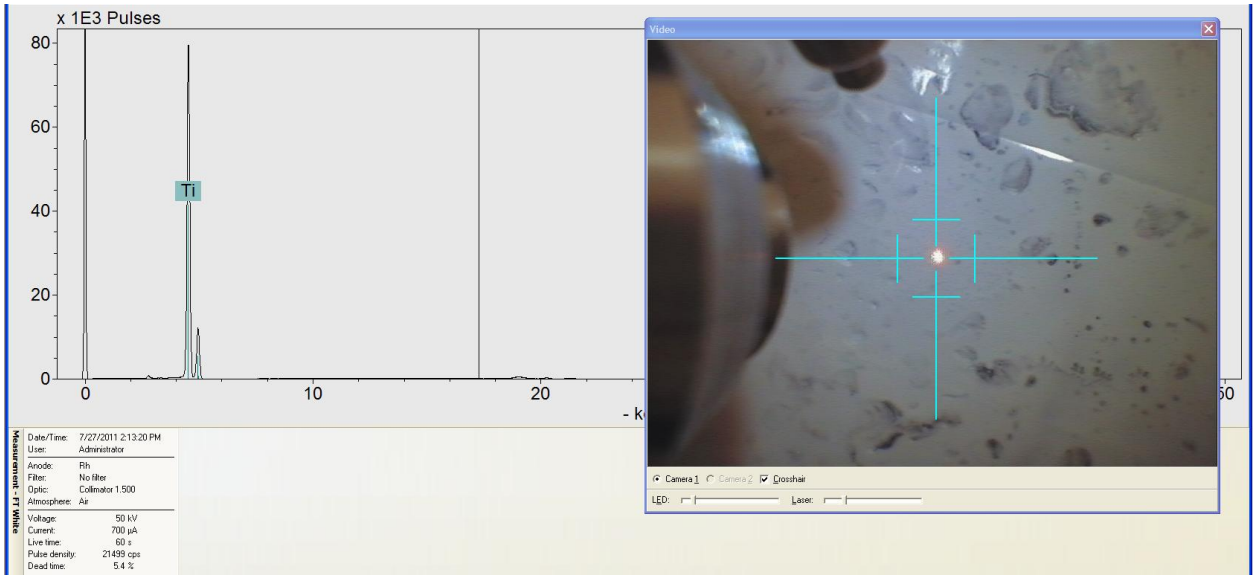
x 1E3 Pulses
Ti
Video
Camera 1
Camera 2
Crosshair
LED:
Laser:
Date/Time: 7/27/2011 2:13:20 PM
User: Administrator
Anode: Rh
Filter: No filter
Optic: Collimator 1.500
Atmosphere: Air
Voltage: 50 kV
Current: 700 µA
Live time: 60 s
Pulse density: 21499 cps
Dead time: 5.4 %

Appendix E: Pigment Extractions

Skin Candy Tattoo Ink

Candy Apple Red

Normal Raman, 488nm

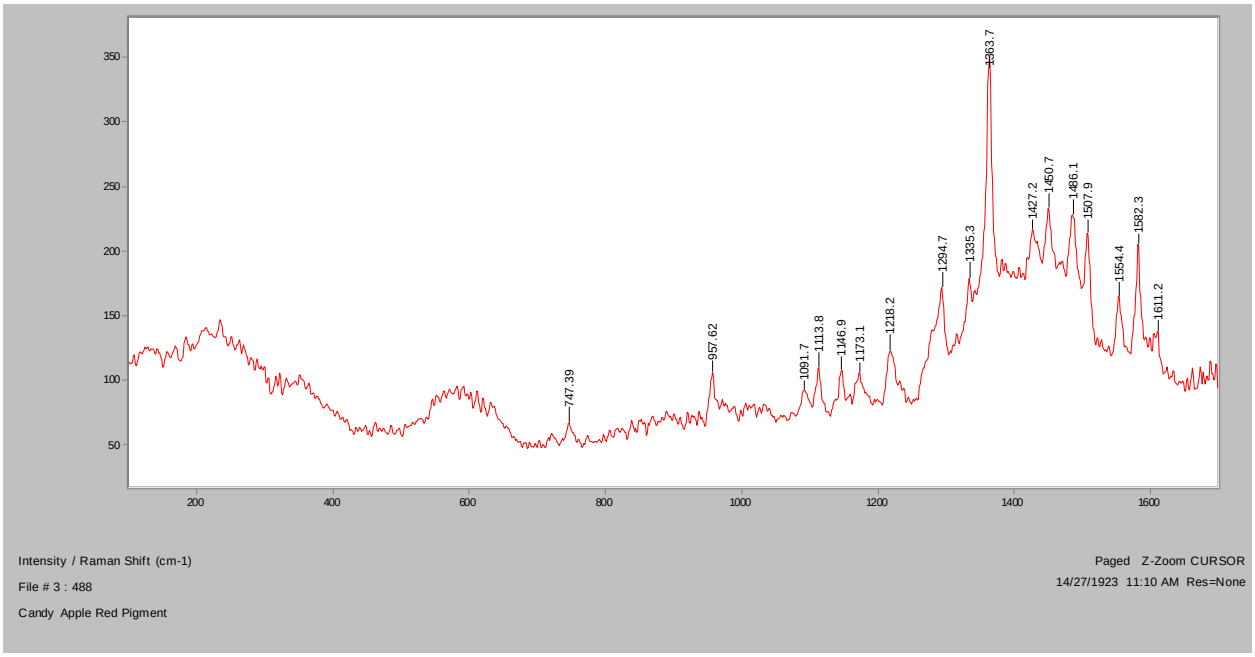

Normal Raman, 633nm

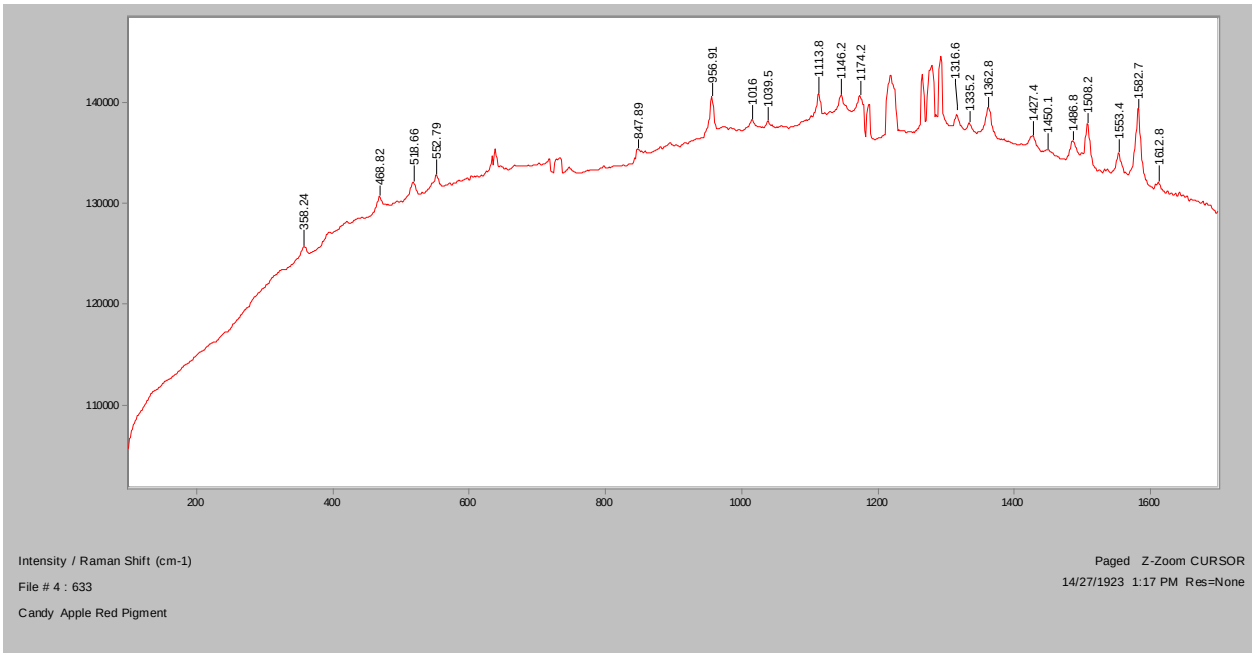

Normal Raman, 785nm

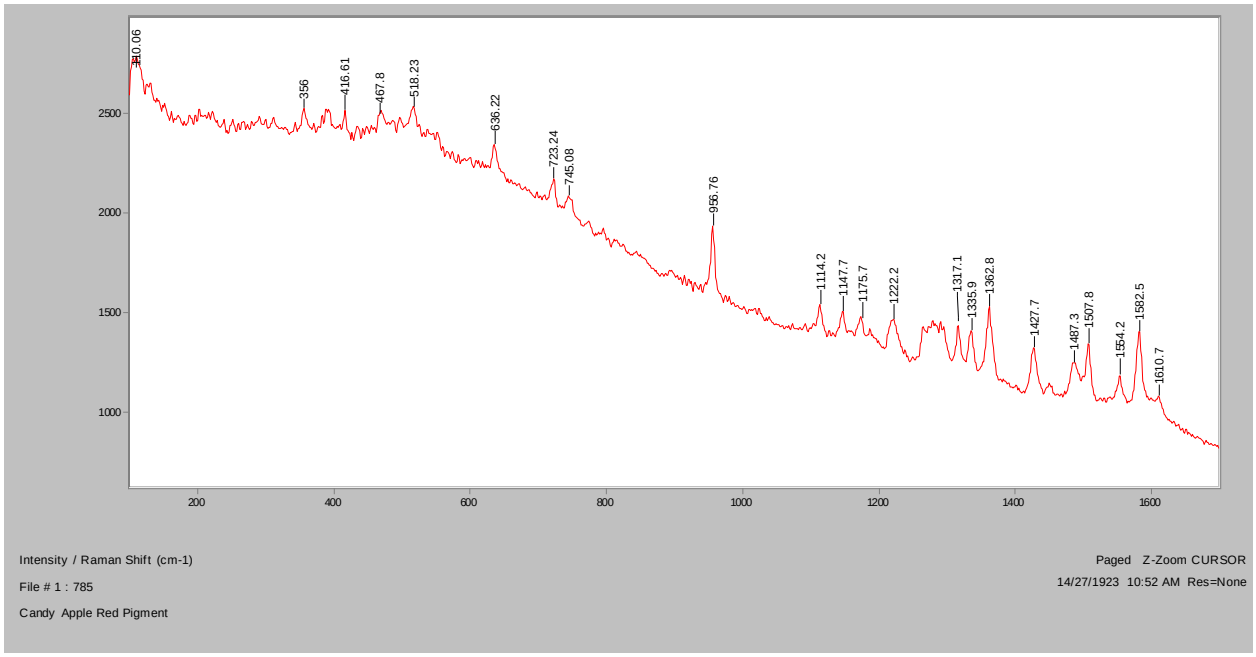

FT-Raman, 1064nm

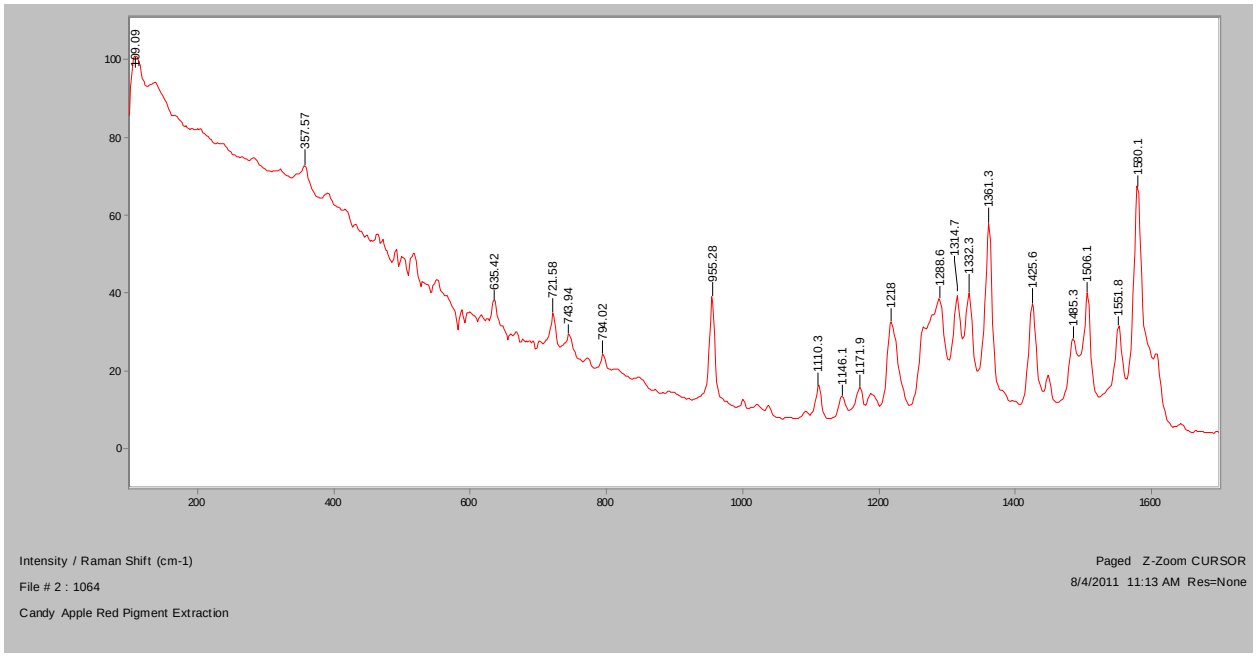

FT-IR (ATR)

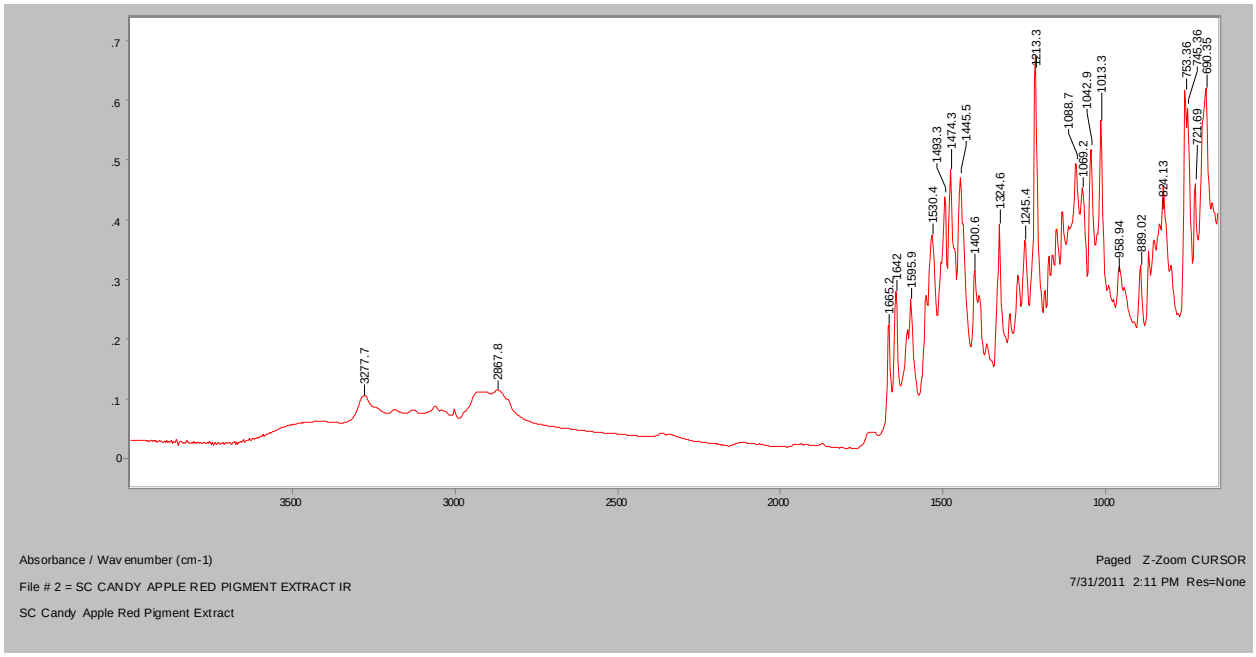

UV-Vis

No.	P/V	Wavelength nm.	Abs.	Description
1		920.50	0.024	
2		889.00	-0.000	
3		857.50	-0.006	
4		787.50	0.005	
5		582.00	0.276	
6		365.00	0.216	
7		299.50	0.390	

Measurement Properties
Wavelength Range (nm.): 200.00 to 1000.00
Scan Speed: Medium
Sampling Interval: 0.5
Auto Sampling Interval: Disabled
Scan Mode: Single

Instrument Properties
Instrument Type: UV-2500PC Series
Measuring Mode: Absorbance
Slit Width: 1.0 nm
Light Source Change Wavelength: 360.0 nm
S/R Exchange: Normal

Attachment Properties
Attachment: None

Sample Preparation Properties
Weight:
Volume:
Dilution:
Path Length:
Additional Information:

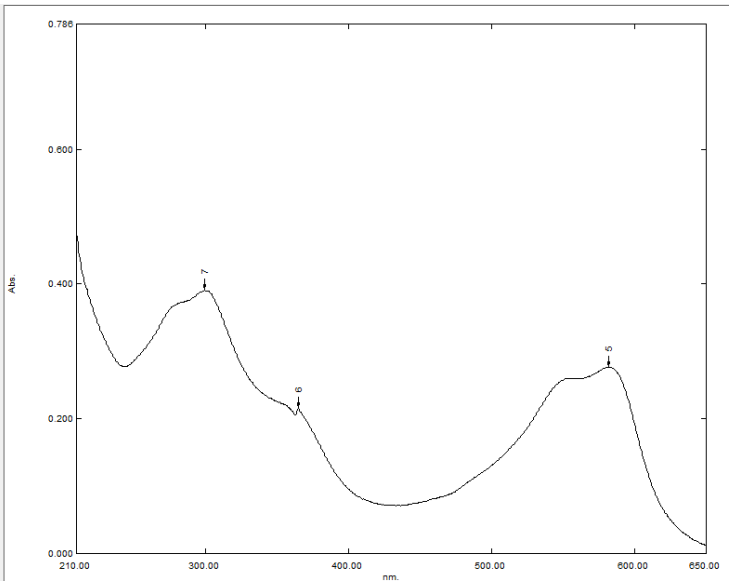

Red Hot

Normal Raman, 488nm

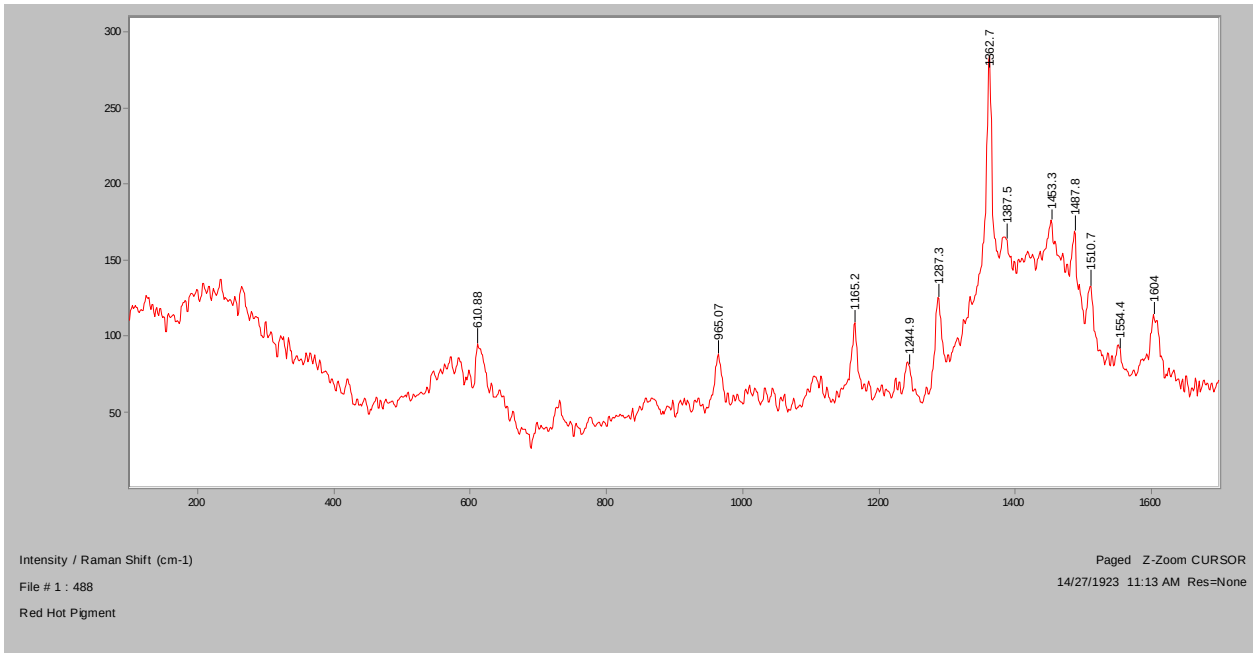

Normal Raman, 633nm

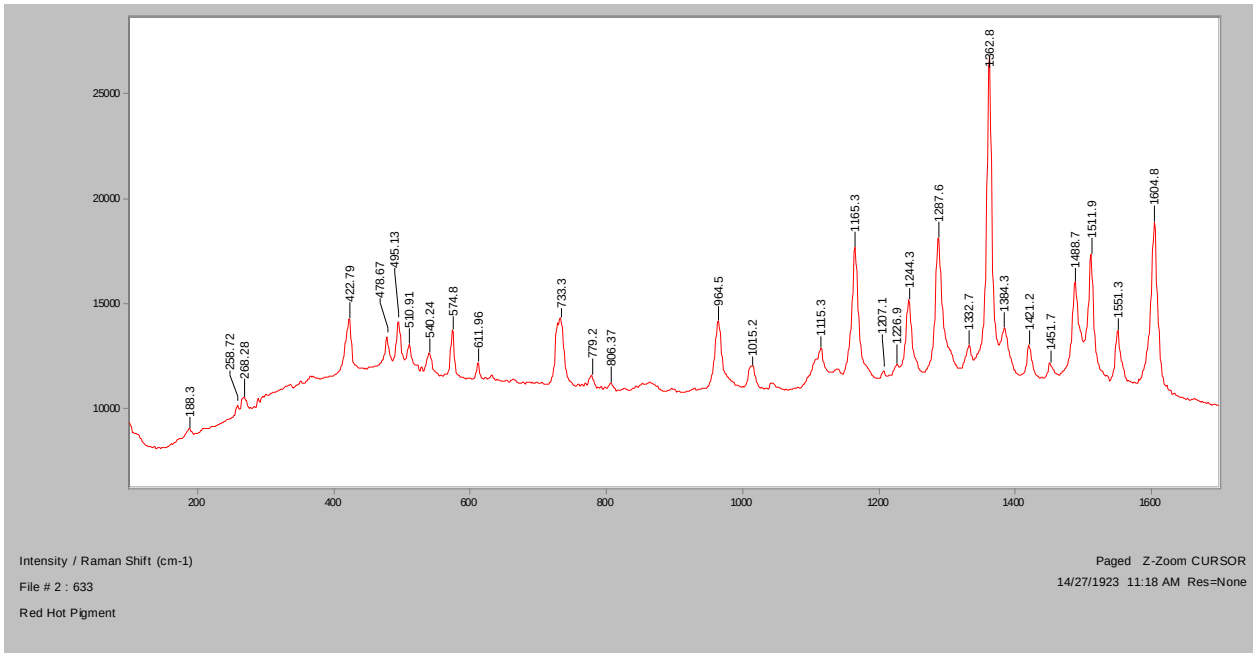

Normal Raman, 785nm

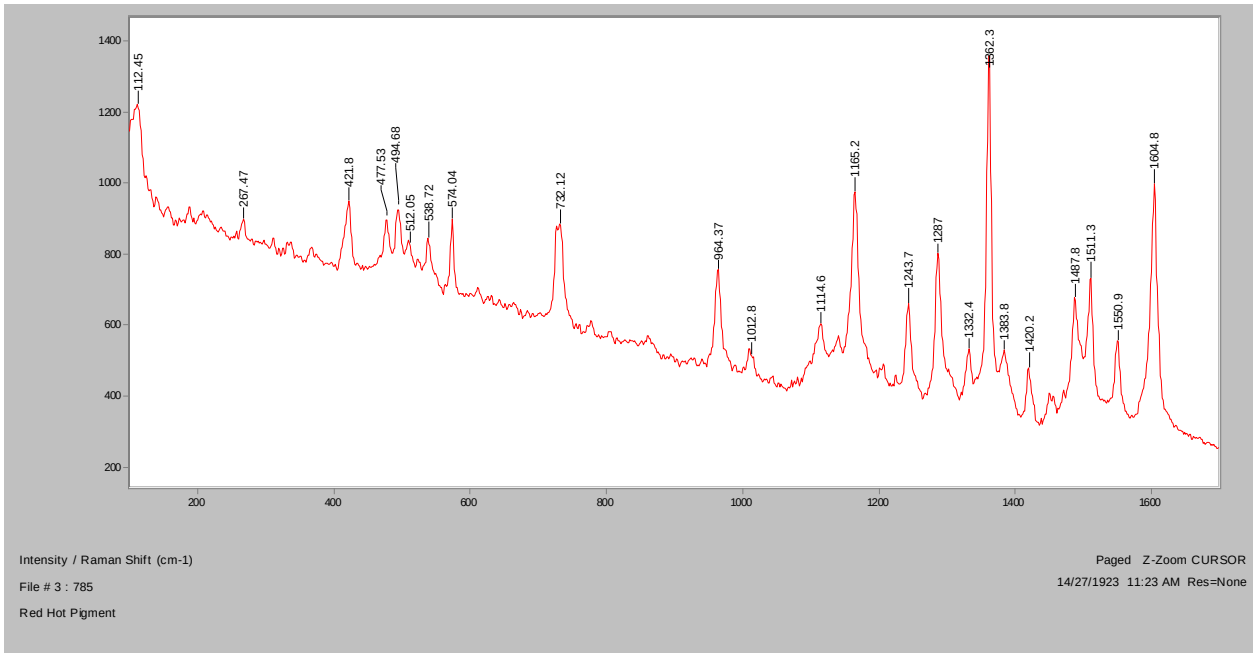

FT-Raman, 1064nm

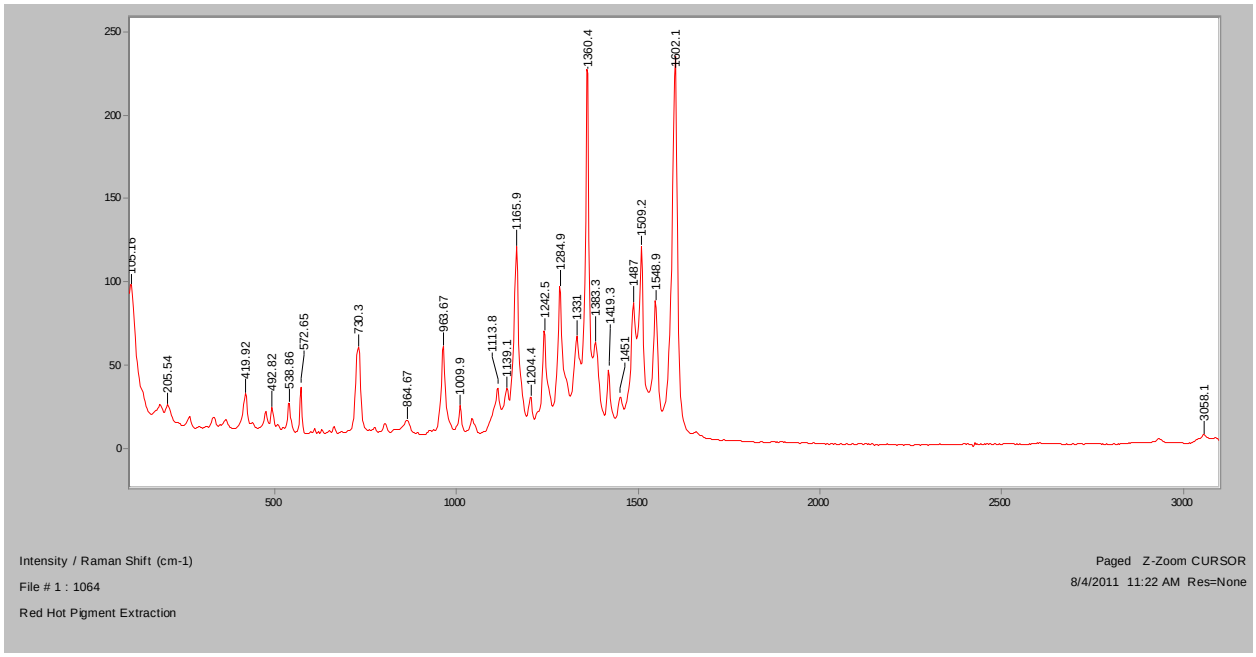

FT-IR (ATR)

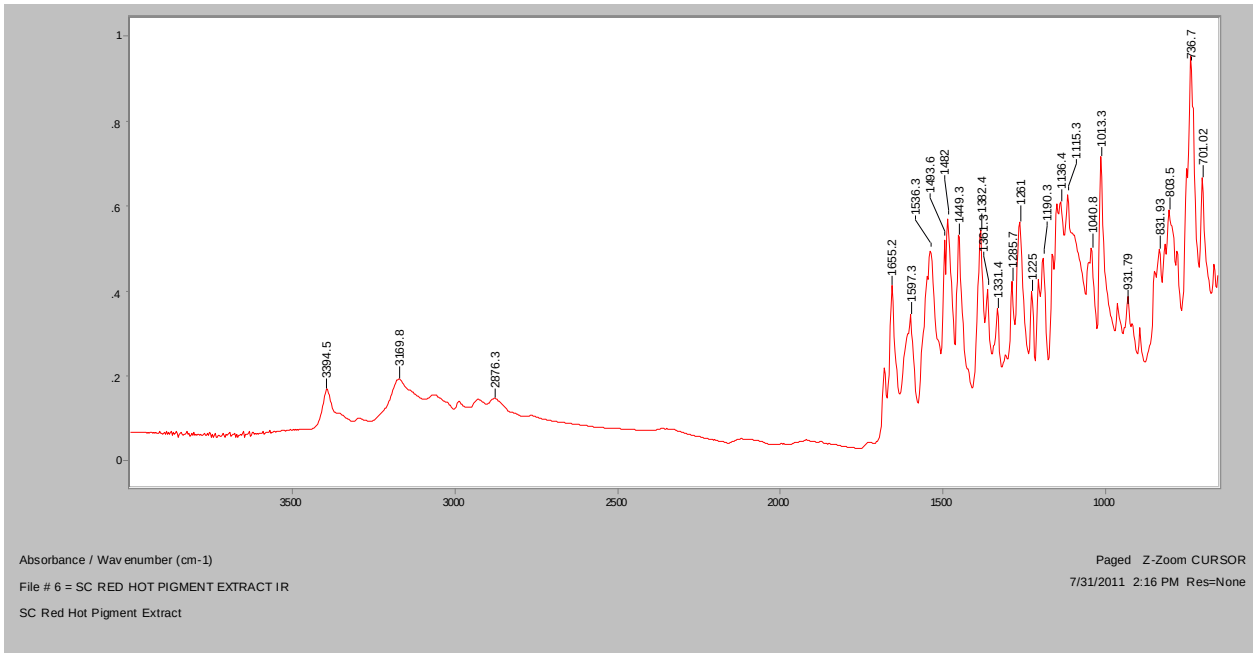

UV-Vis

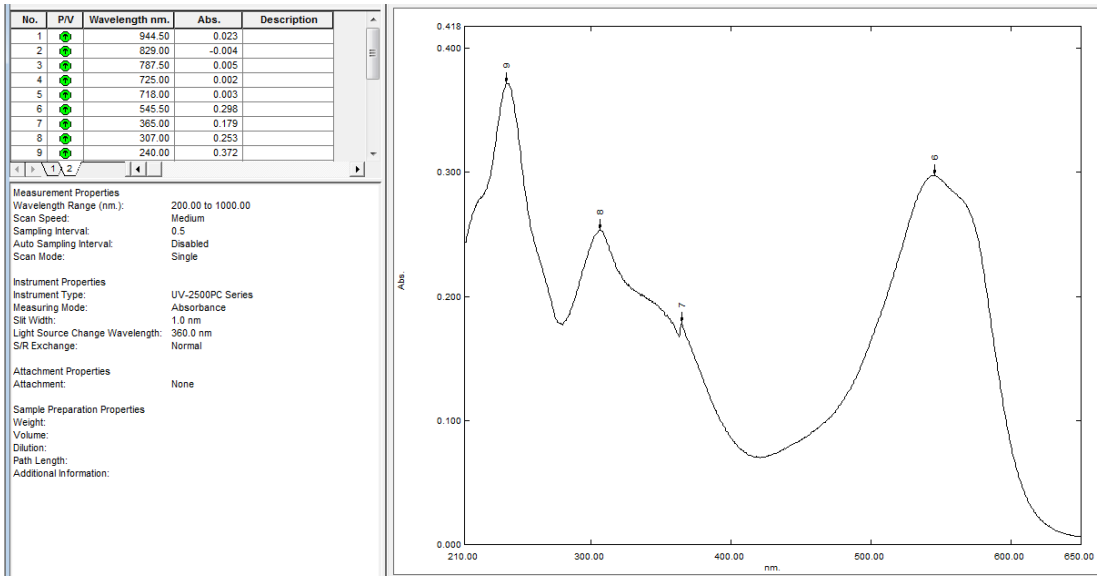

No.	P/V	Wavelength nm.	Abs.	Description
1		944.50	0.023	
2		829.00	-0.004	
3		787.50	0.005	
4		725.00	0.002	
5		718.00	0.003	
6		545.50	0.298	
7		365.00	0.179	
8		307.00	0.253	
9		240.00	0.372	

Measurement Properties
Wavelength Range (nm.): 200.00 to 1000.00
Scan Speed: Medium
Sampling Interval: 0.5
Auto Sampling Interval: Disabled
Scan Mode: Single

Instrument Properties
Instrument Type: UV-2500PC Series
Measuring Mode: Absorbance
Slit Width: 1.0 nm
Light Source Change Wavelength: 360.0 nm
S/R Exchange: Normal

Attachment Properties
Attachment: None

Sample Preparation Properties
Weight:
Volume:
Dilution:
Path Length:
Additional Information:

Marz

Normal Raman, 488nm

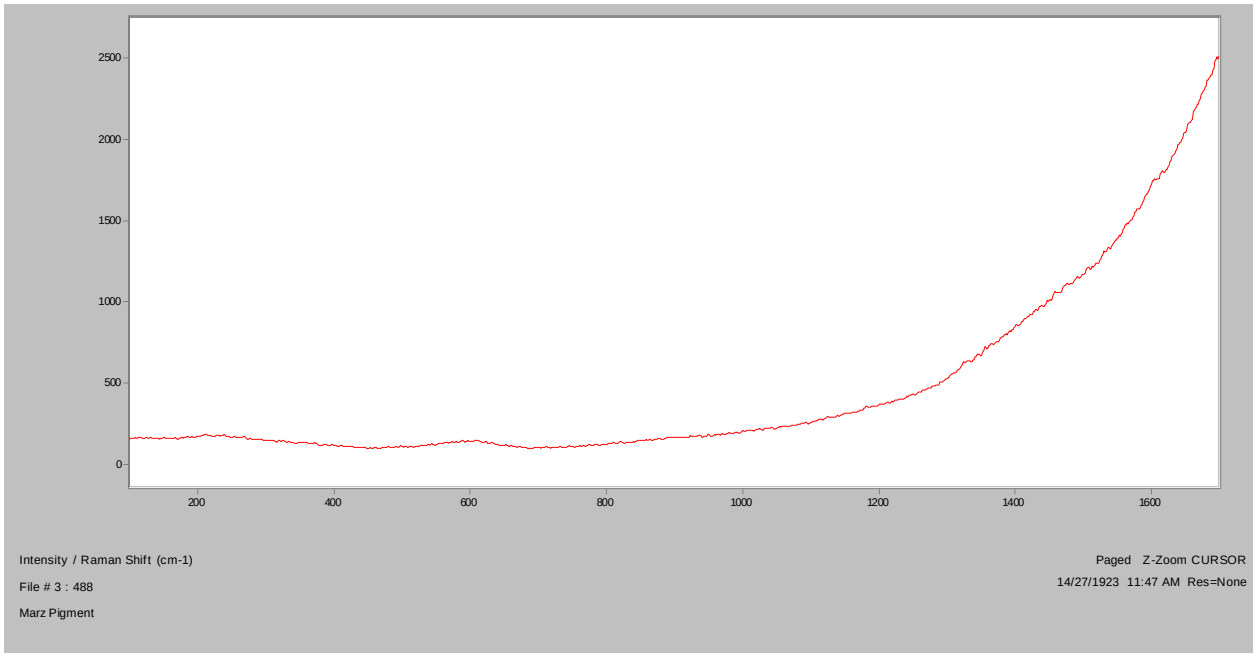

Normal Raman, 633nm

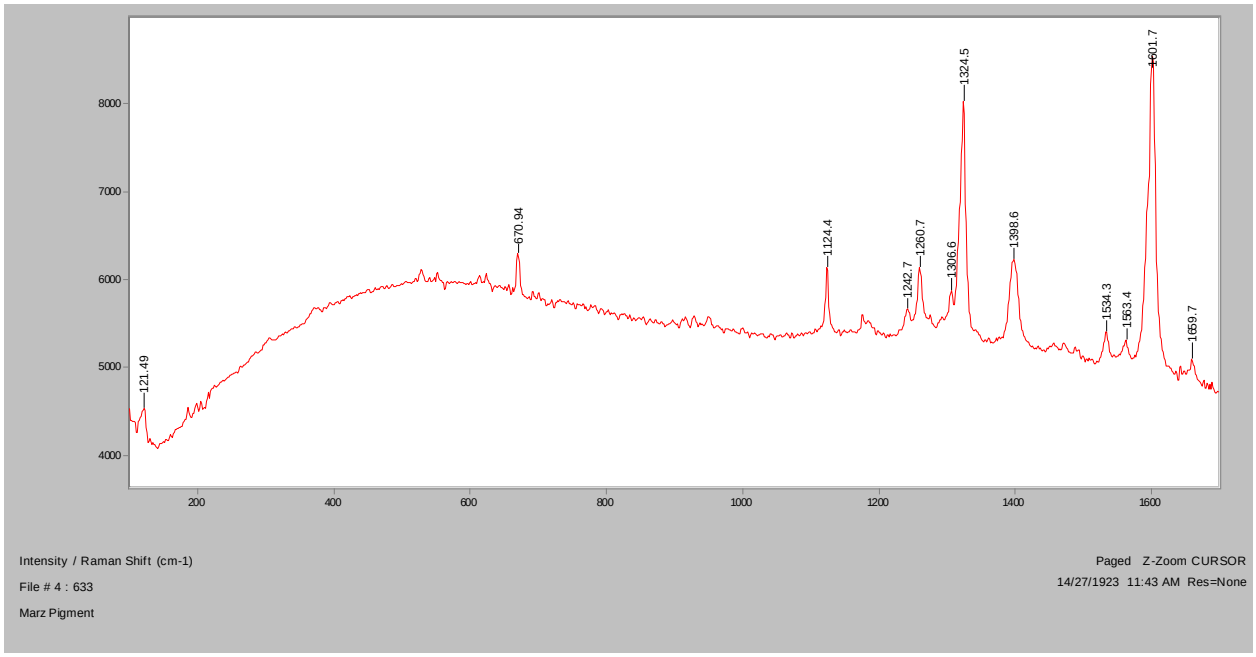

Normal Raman, 785nm

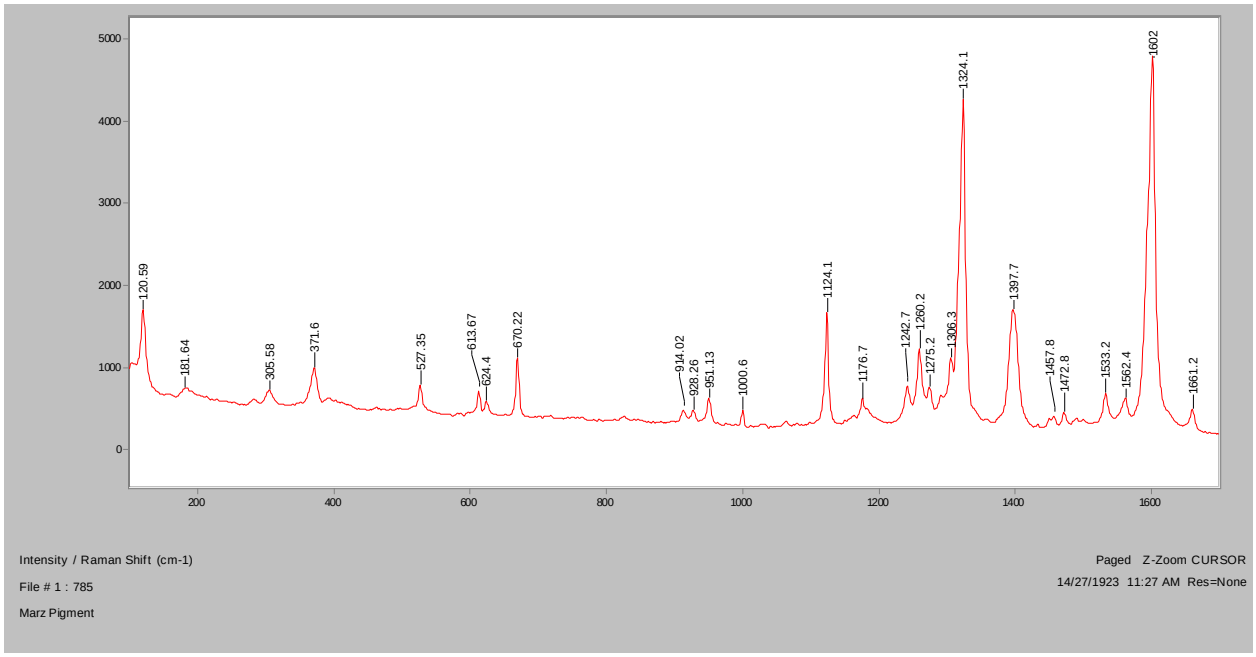

FT-Raman, 1064nm

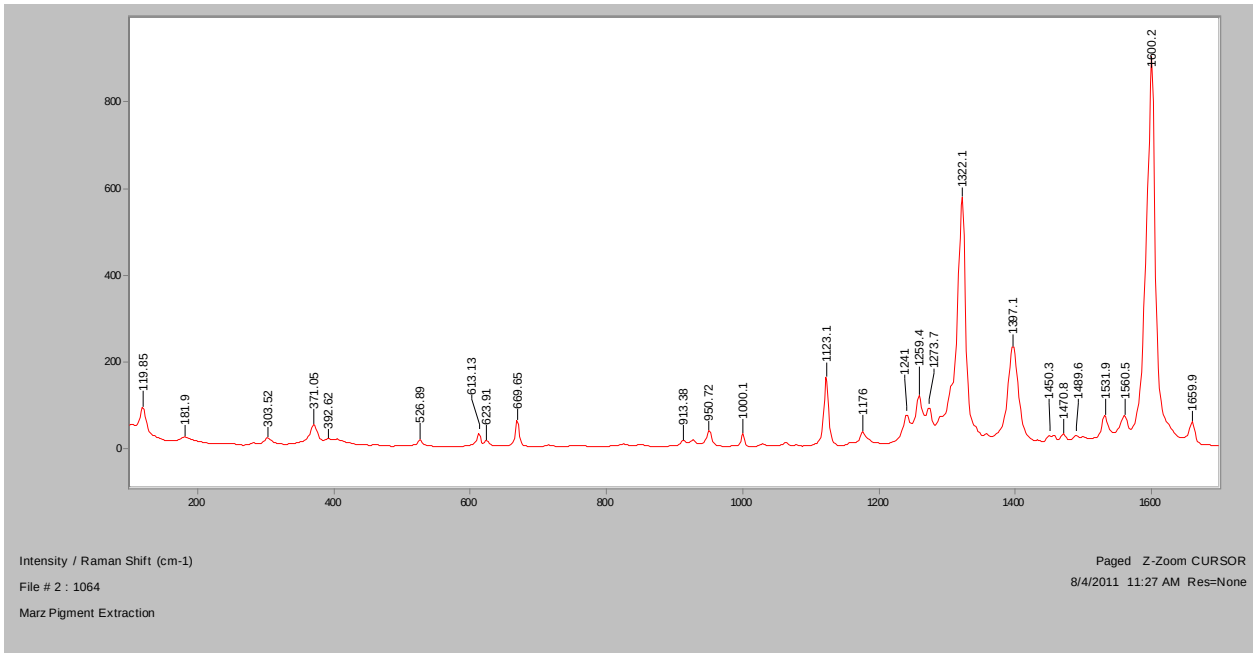

FT-IR (ATR)

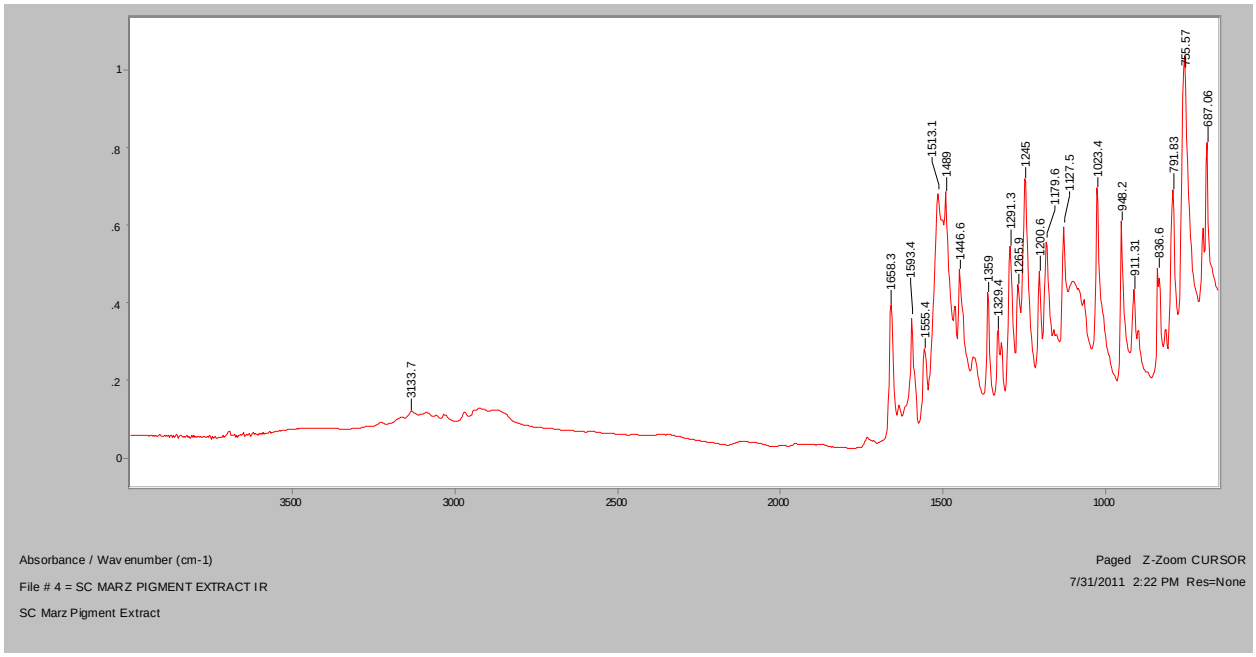

UV-Vis

No.	P/V	Wavelength nm.	Abs.	Description
1		933.50	0.034	
2		878.00	0.009	
3		833.50	0.007	
4		787.50	0.017	
5		749.50	0.020	
6		541.50	0.383	
7		365.50	0.112	
8		312.00	0.123	

Measurement Properties
Wavelength Range (nm.): 200.00 to 1000.00
Scan Speed: Medium
Sampling Interval: 0.5
Auto Sampling Interval: Disabled
Scan Mode: Single

nstrument Properties
nstrument Type: UV-2500PC Series
Measuring Mode: Absorbance
Slit Width: 1.0 nm
Light Source Change Wavelength: 360.0 nm
S/R Exchange: Normal

Attachment Properties
Attachment: None

Sample Preparation Properties
Weight:
Volume:
Dilution:
Path Length:
Additional Information:

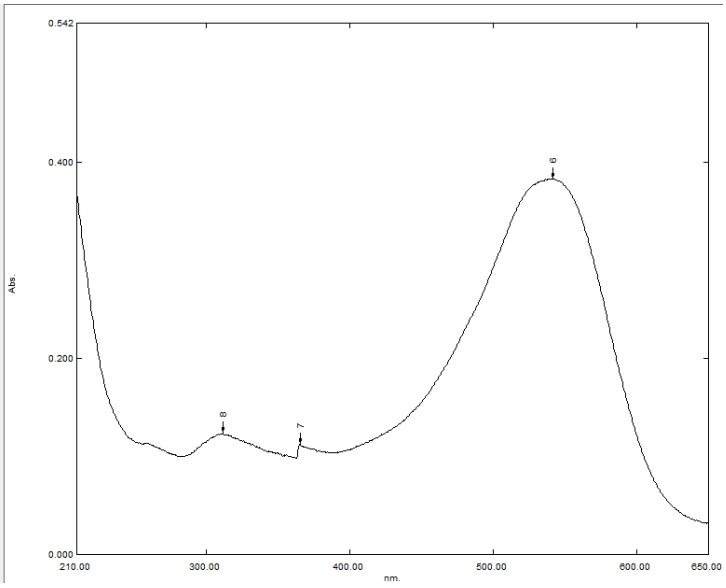

Dolemite

Normal Raman, 488nm

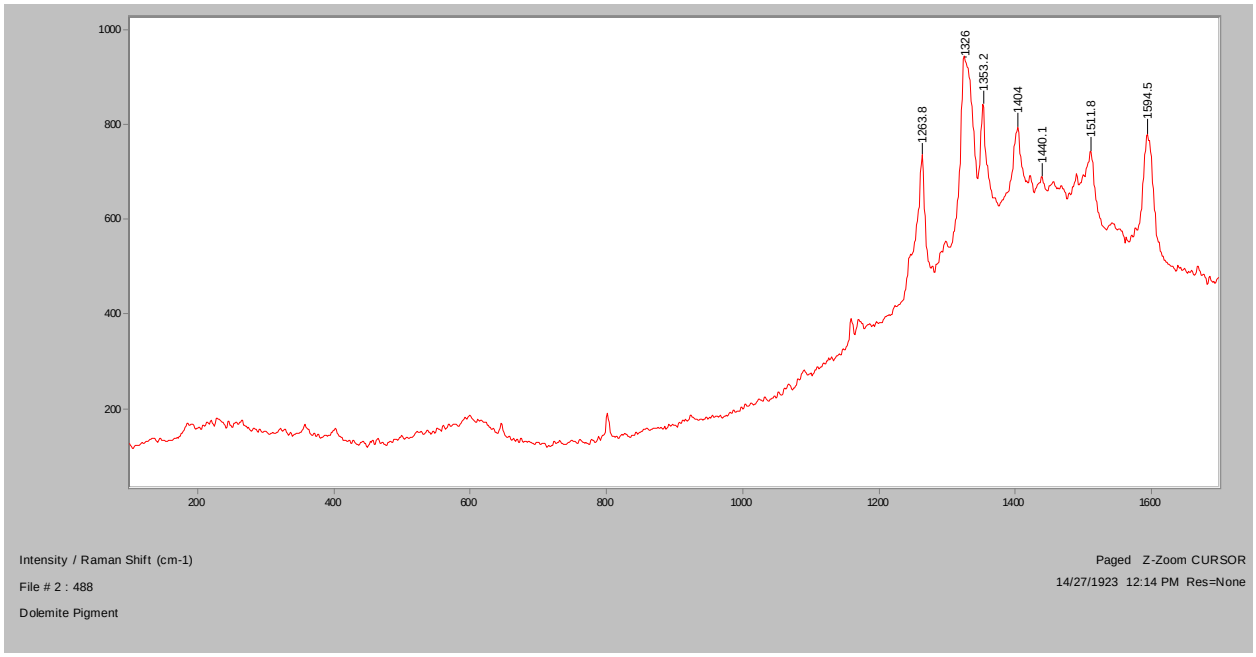

Normal Raman, 633nm

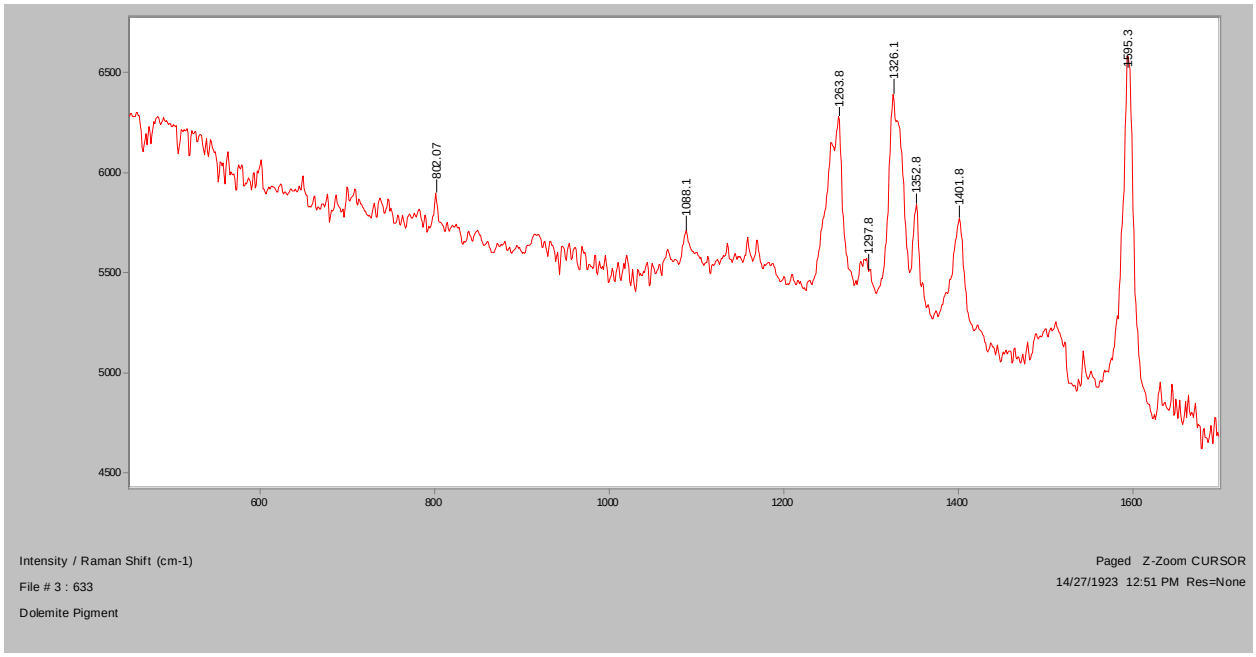

Normal Raman, 785nm

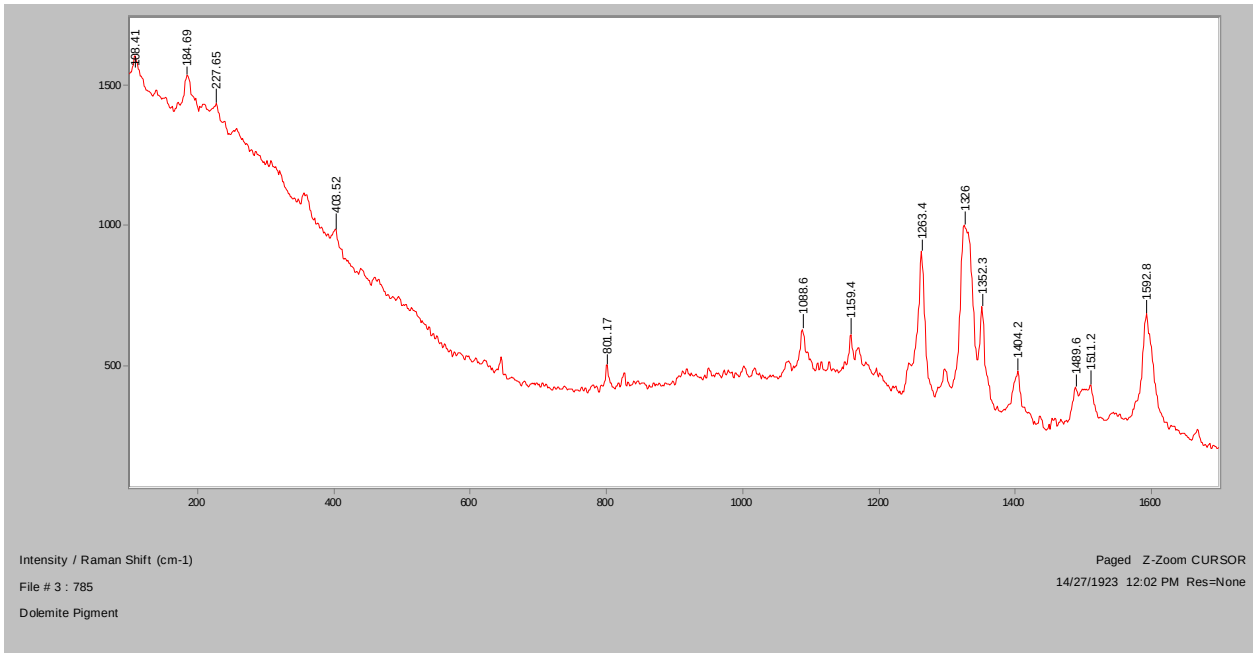

FT-Raman, 1064nm

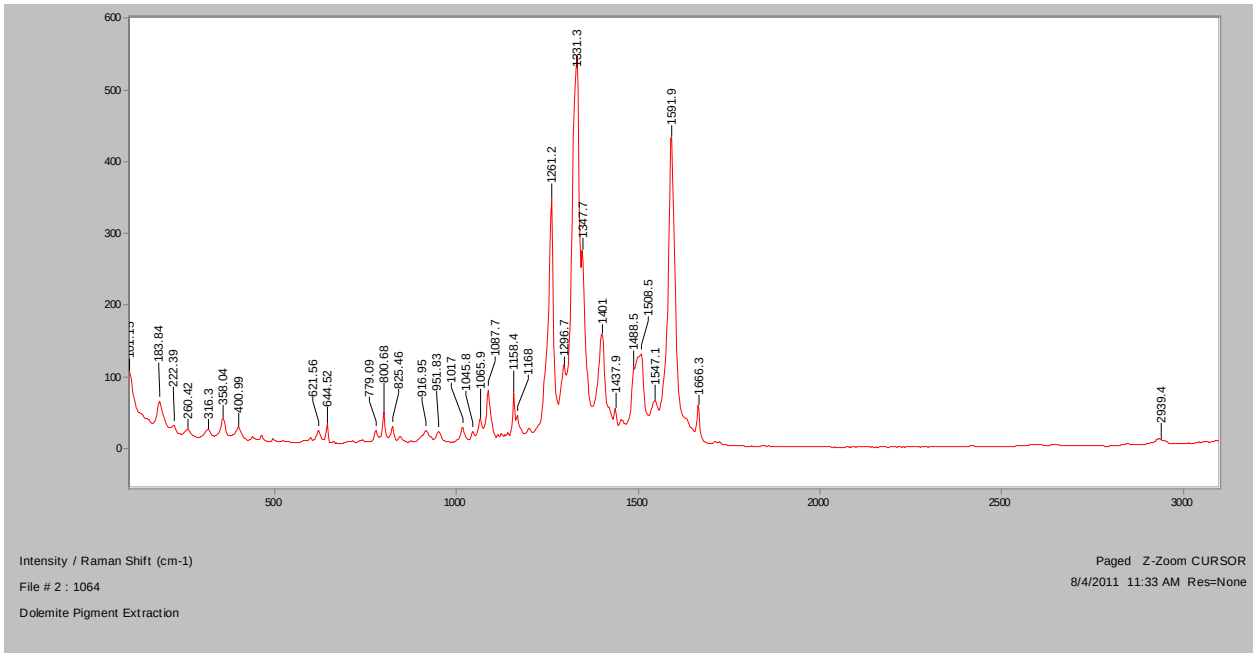

FT-IR (ATR)

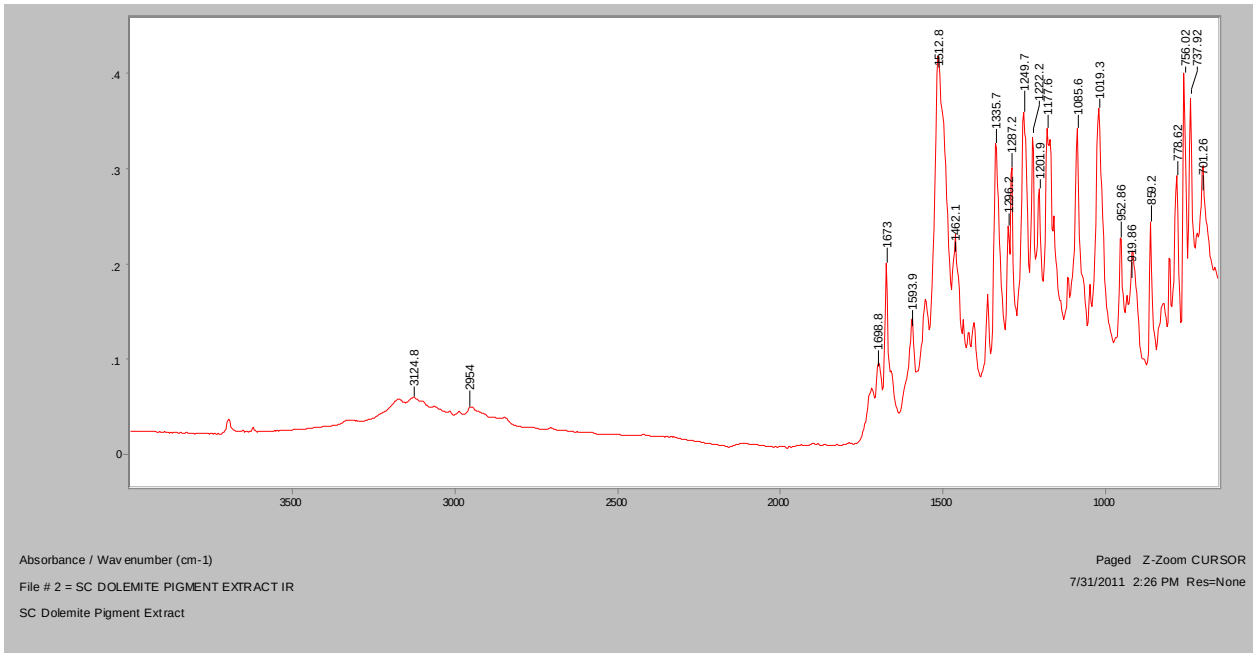

UV-Vis

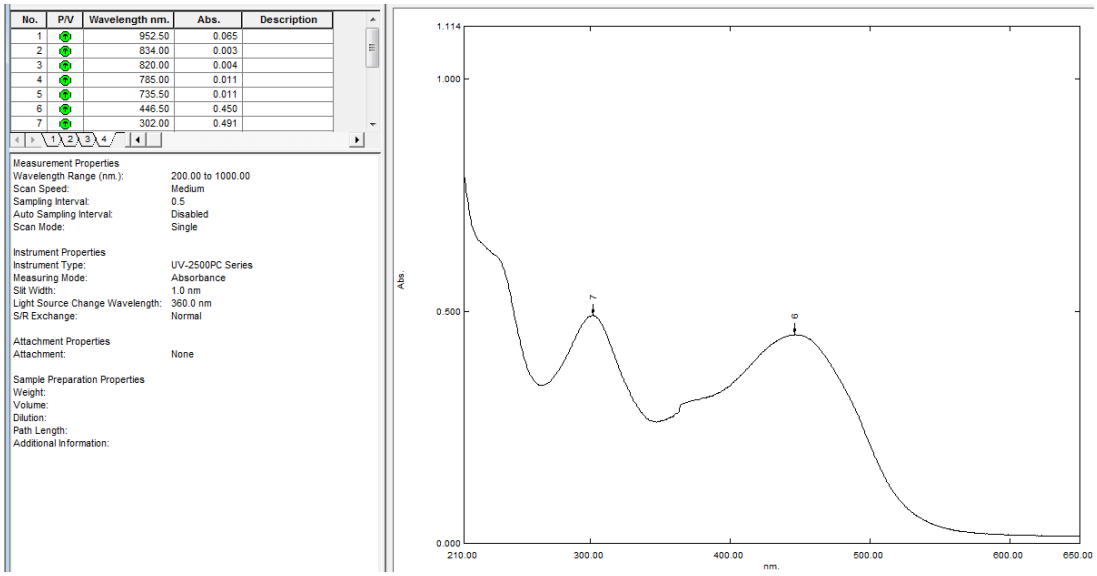

No.	P/V	Wavelength nm.	Abs.	Description
1		952.50	0.065	
2		834.00	0.003	
3		820.00	0.004	
4		785.00	0.011	
5		735.50	0.011	
6		446.50	0.450	
7		302.00	0.491	

Measurement Properties
Wavelength Range (nm.): 200.00 to 1000.00
Scan Speed: Medium
Sampling Interval: 0.5
Auto Sampling Interval: Disabled
Scan Mode: Single

Instrument Properties
Instrument Type: UV-2500PC Series
Measuring Mode: Absorbance
Slit Width: 1.0 nm
Light Source Change Wavelength: 360.0 nm
S/R Exchange: Normal

Attachment Properties
Attachment: None

Sample Preparation Properties
Weight:
Volume:
Dilution:
Path Length:
Additional Information:

Blisterine

Normal Raman, 488nm

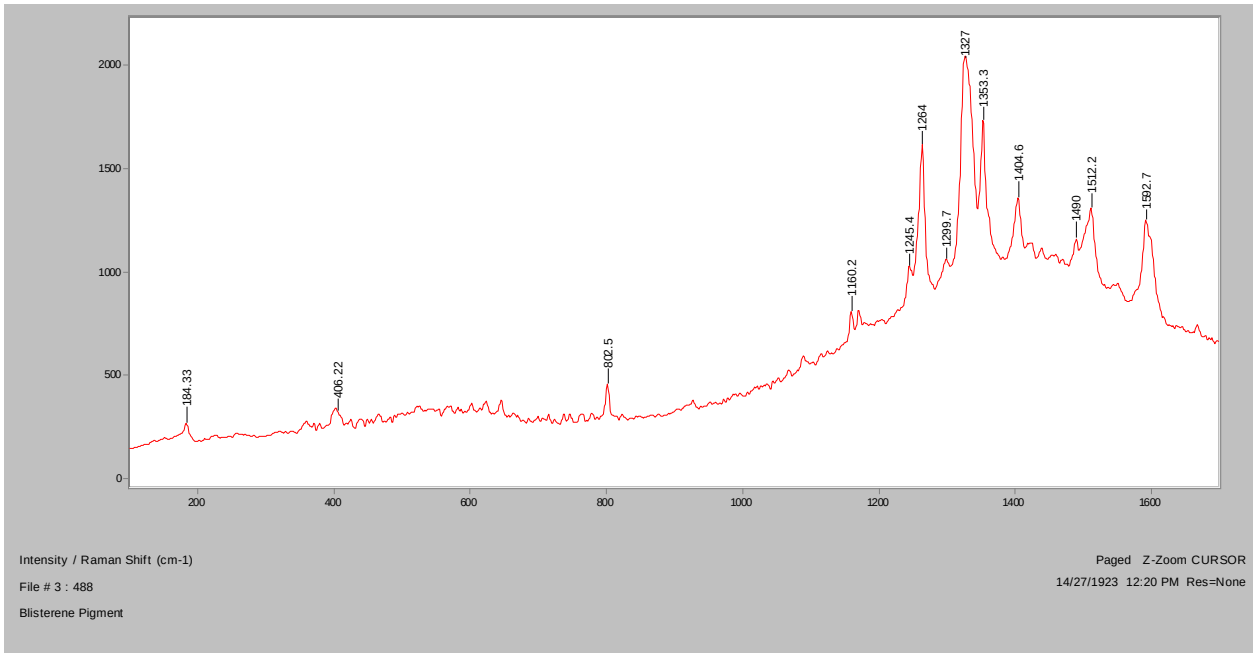

Normal Raman, 633nm

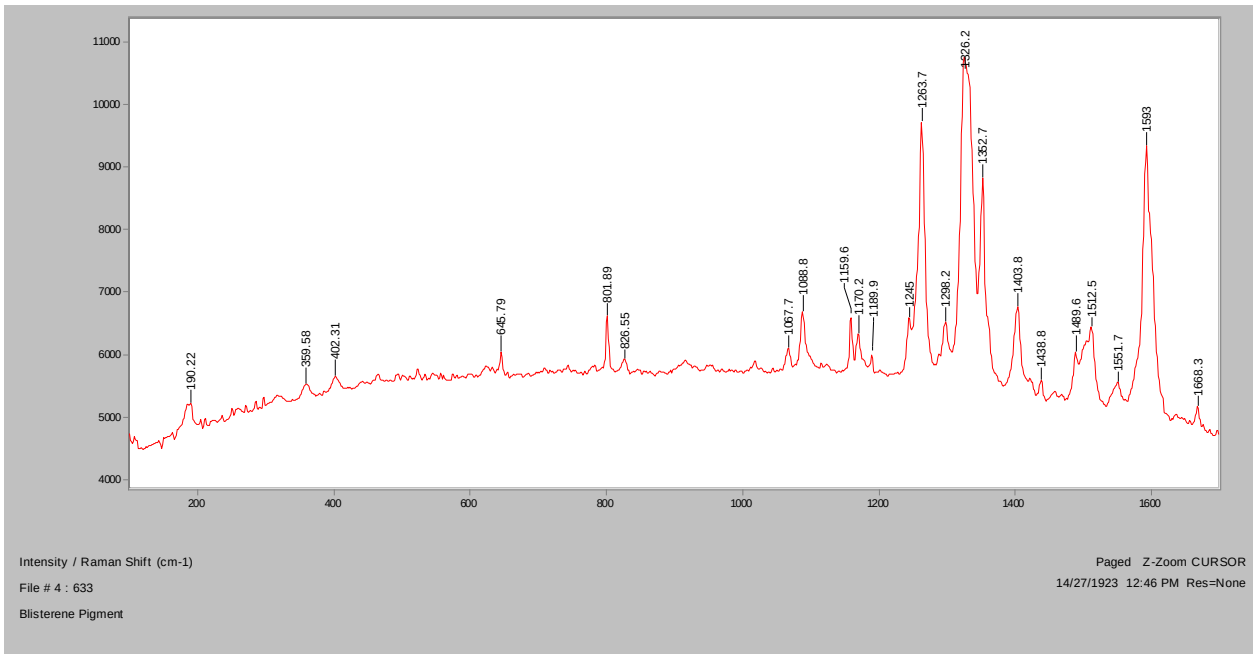

Normal Raman, 785nm

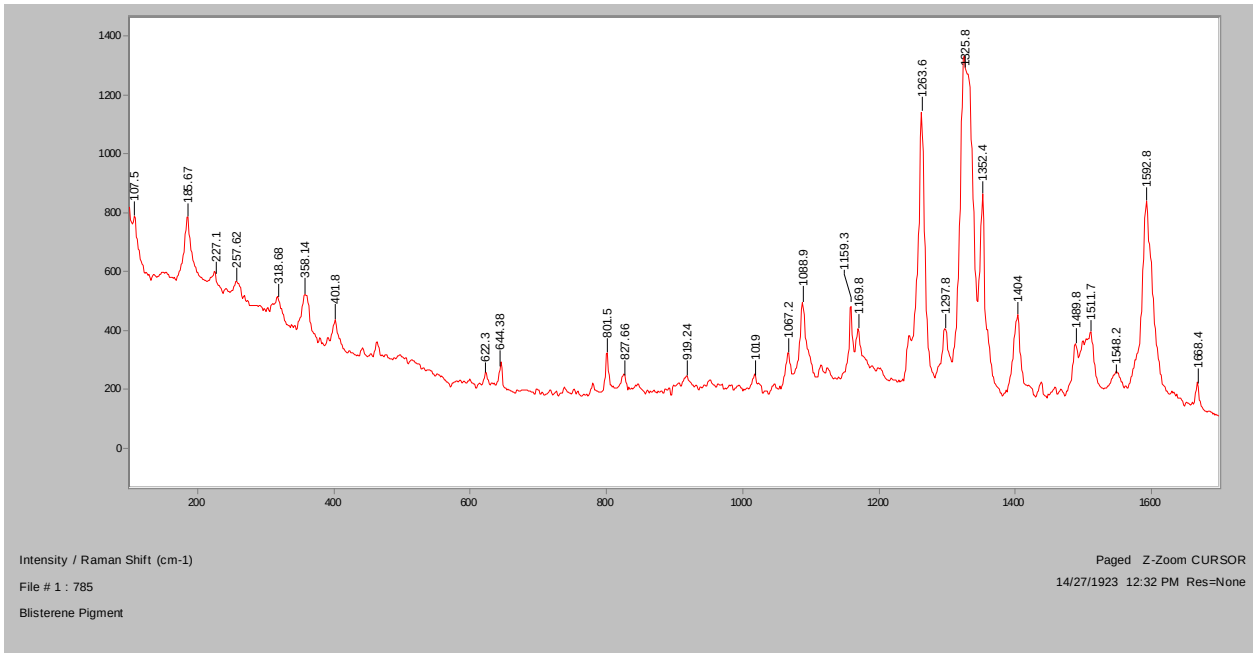

FT-Raman, 1064nm

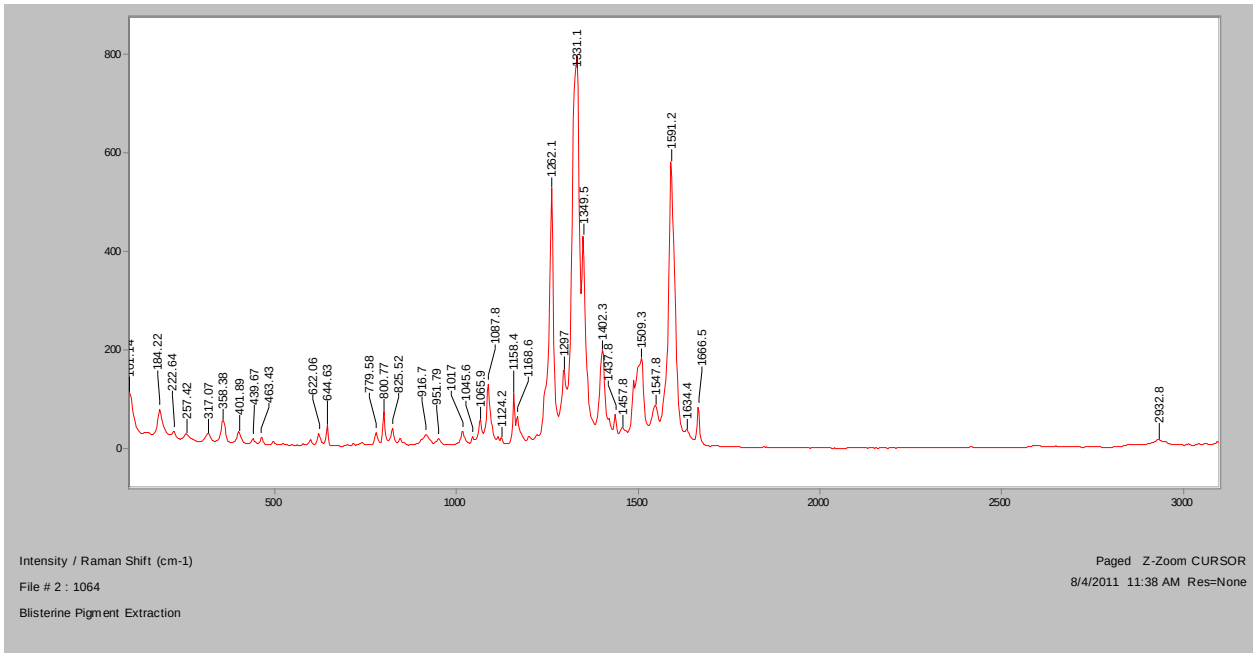

FT-IR (ATR)

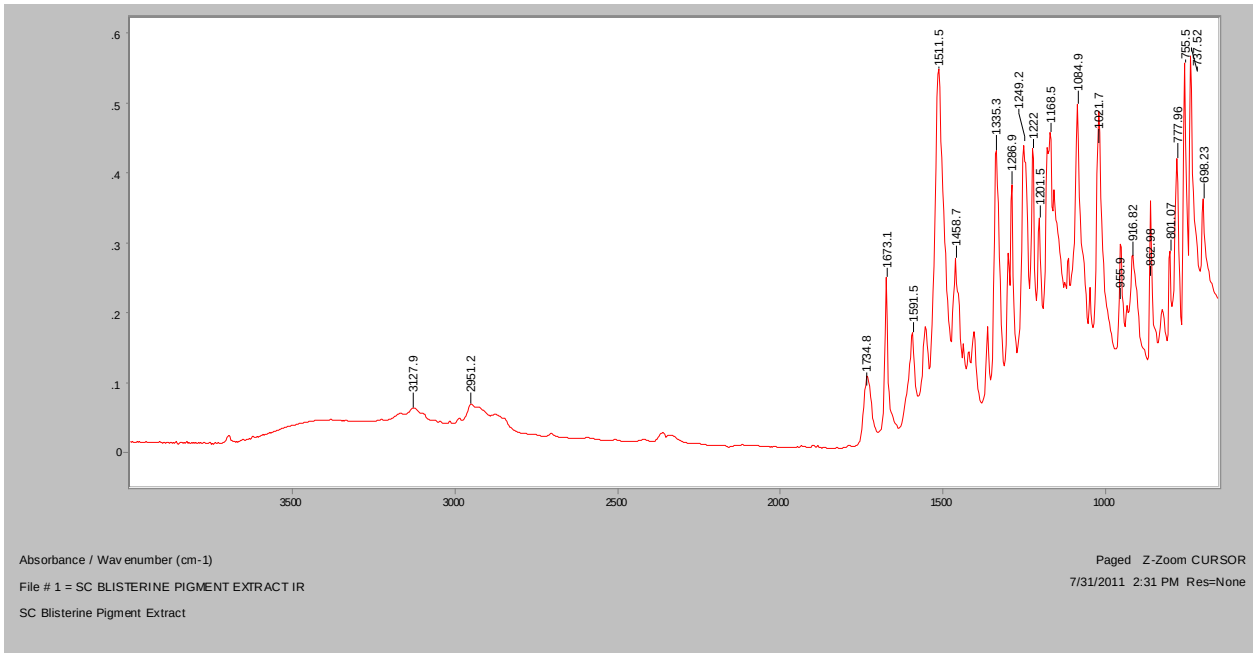

UV-Vis

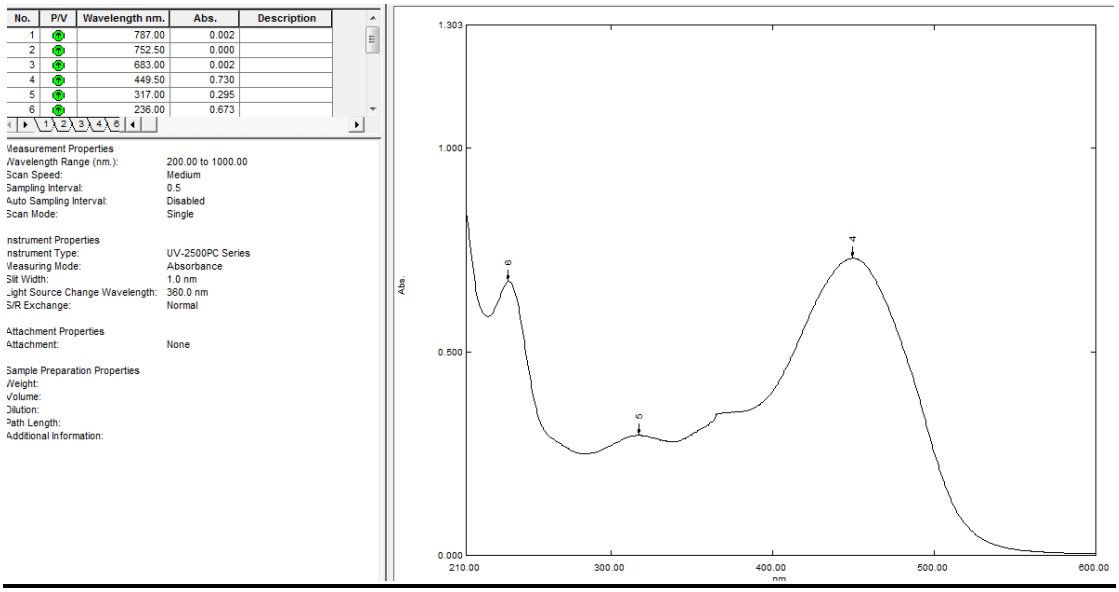

No.	P/V	Wavelength nm.	Abs.	Description
1		787.00	0.002	
2		752.50	0.000	
3		683.00	0.002	
4		449.50	0.730	
5		317.00	0.295	
6		236.00	0.673	

Measurement Properties
Wavelength Range (nm.): 200.00 to 1000.00
Scan Speed: Medium
Sampling Interval: 0.5
Auto Sampling Interval: Disabled
Scan Mode: Single

nstrument Properties
nstrument Type: UV-2500PC Series
Measuring Mode: Absorbance
Slit Width: 1.0 nm
Light Source Change Wavelength: 360.0 nm
S/R Exchange: Normal

Attachment Properties
Attachment: None

Sample Preparation Properties
Weight:
Volume:
Dilution:
Path Length:
Additional Information:

Sassygrass

Normal Raman, 488nm

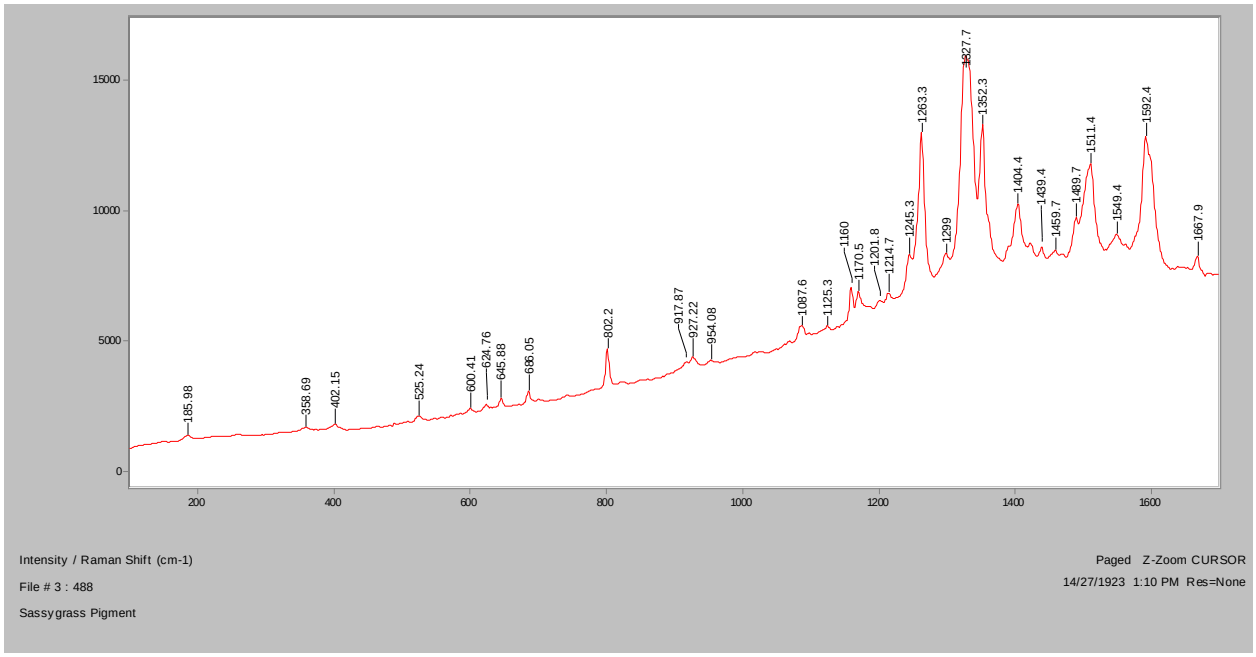

Normal Raman, 633nm

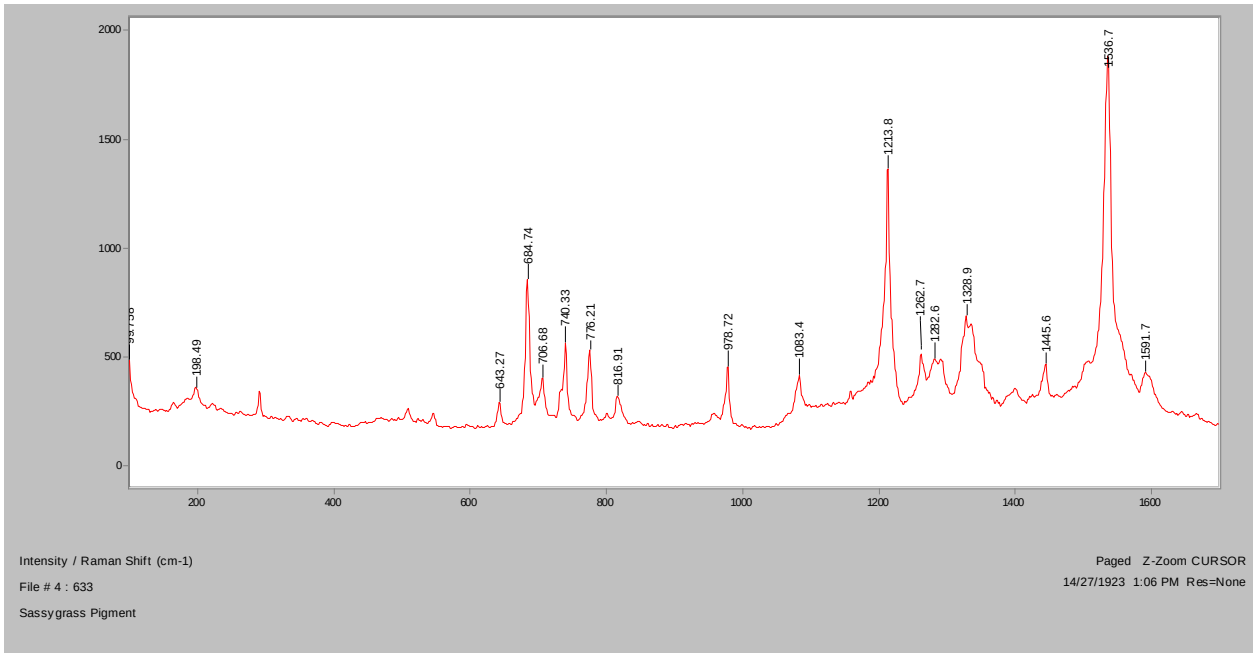

Normal Raman, 785nm

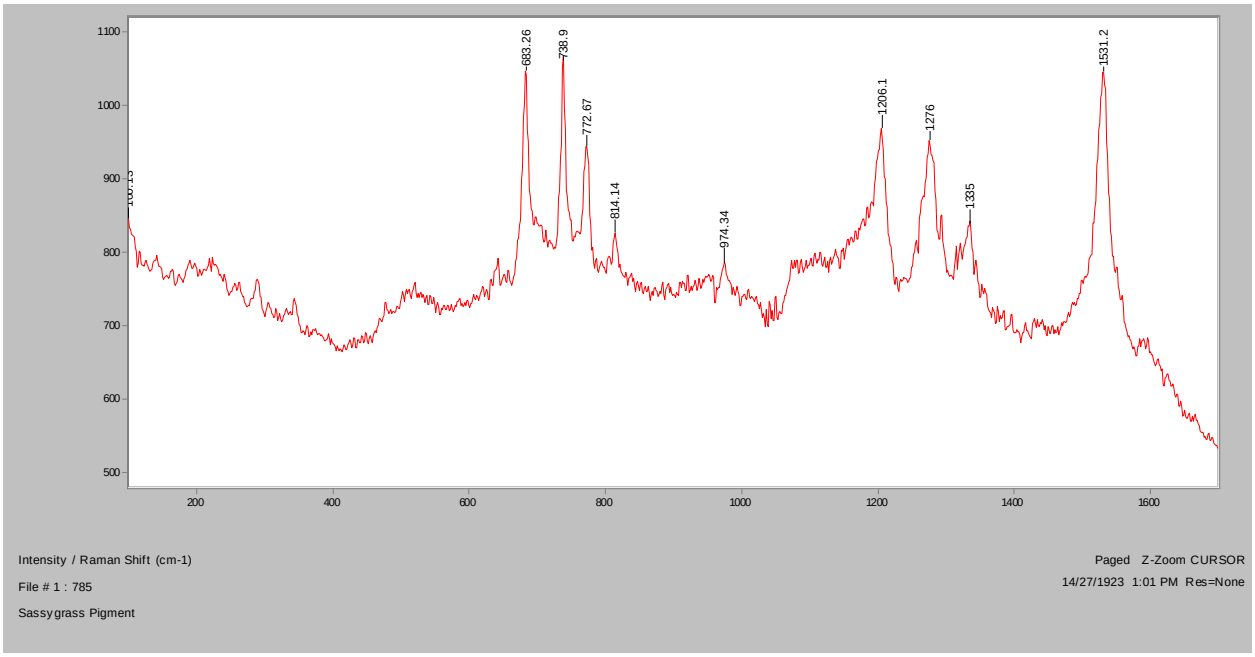

FT-Raman, 1064nm

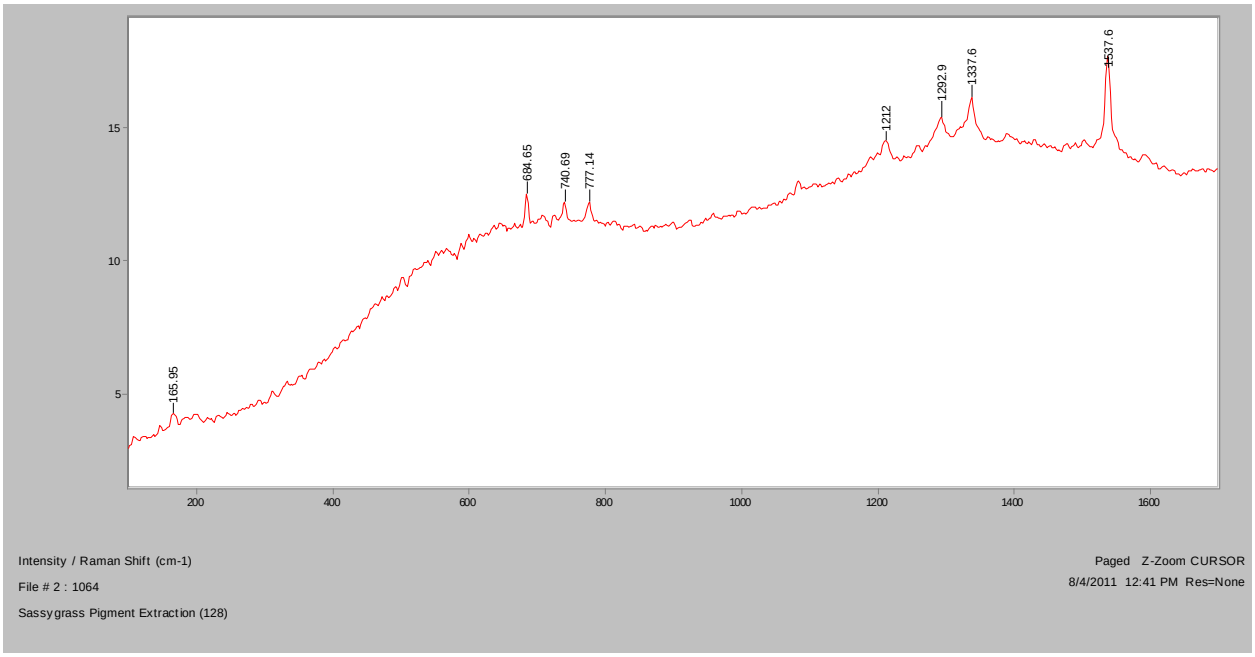

FT-IR (ATR)

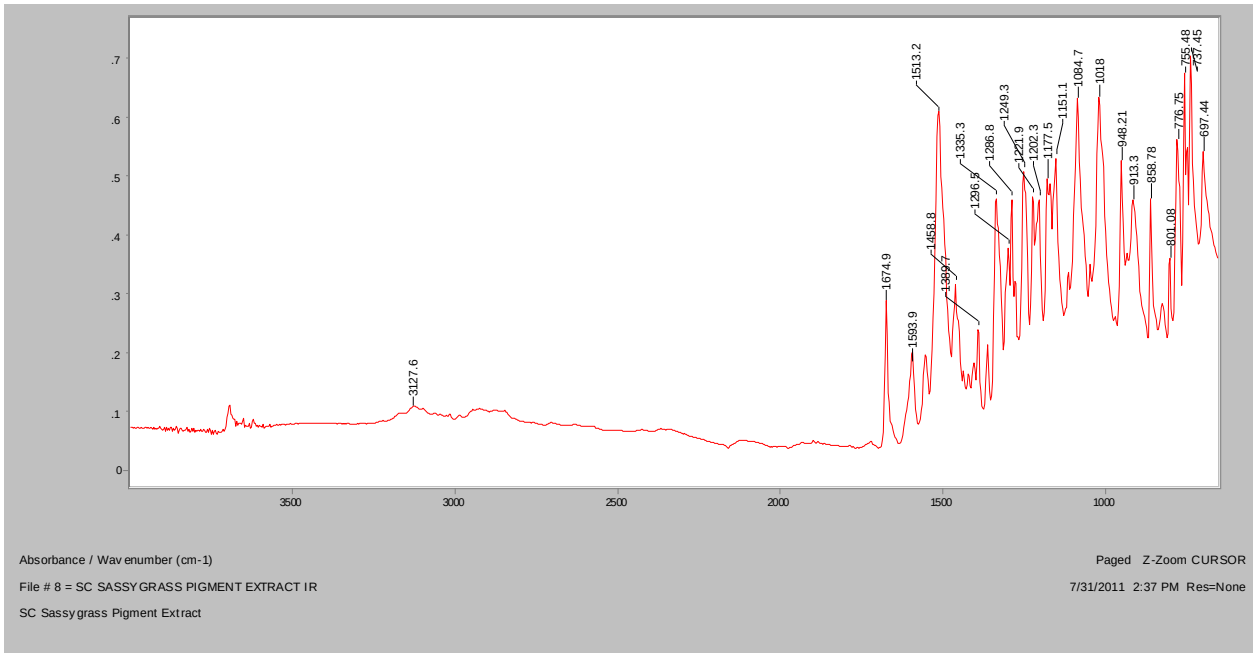

UV-Vis

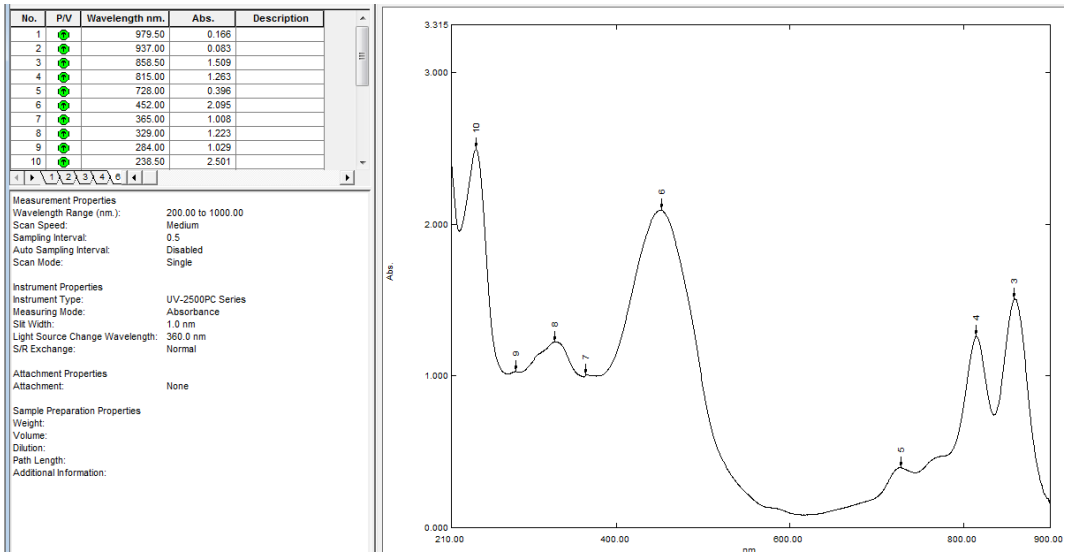

No.	P/V	Wavelength nm.	Abs.	Description
1		979.50	0.166	
2		937.00	0.083	
3		858.50	1.509	
4		815.00	1.263	
5		728.00	0.396	
6		452.00	2.095	
7		365.00	1.008	
8		329.00	1.223	
9		284.00	1.029	
10		238.50	2.501	

Measurement Properties
Wavelength Range (nm.): 200.00 to 1000.00
Scan Speed: Medium
Sampling Interval: 0.5
Auto Sampling Interval: Disabled
Scan Mode: Single

Instrument Properties
Instrument Type: UV-2500PC Series
Measuring Mode: Absorbance
Slit Width: 1.0 nm
Light Source Change Wavelength: 360.0 nm
S/R Exchange: Normal

Attachment Properties
Attachment: None

Sample Preparation Properties
Weight:
Volume:
Dilution:
Path Length:
Additional Information:

Tastywaves

Normal Raman, 488nm

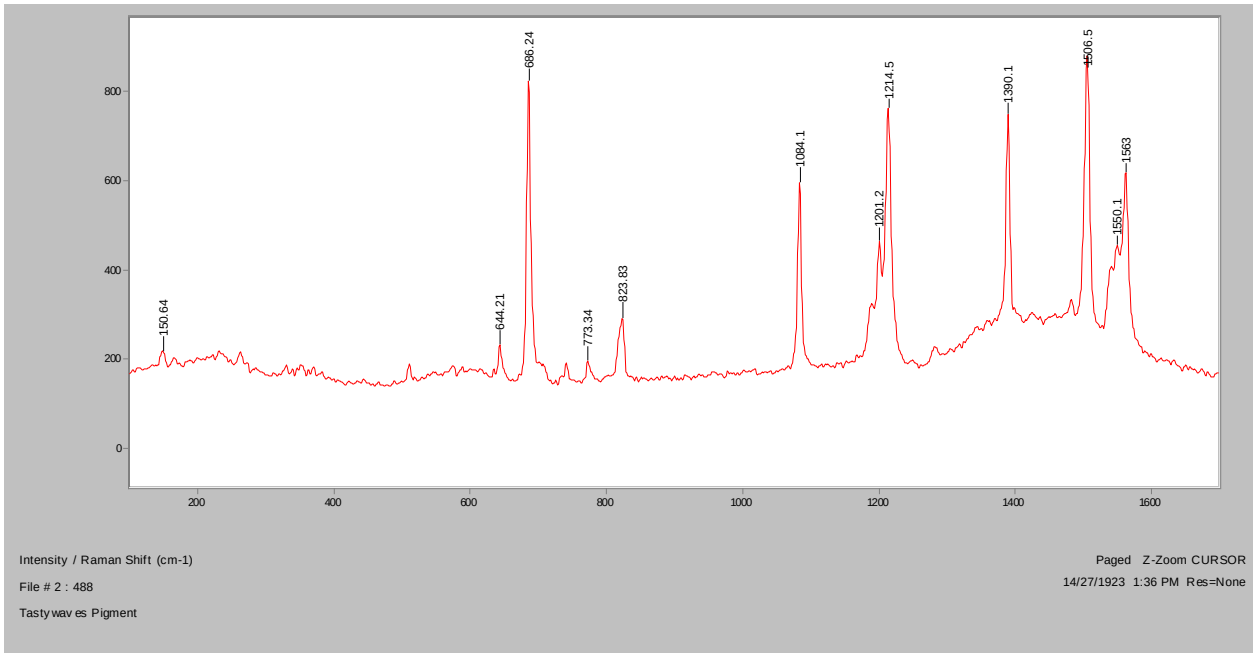

Normal Raman, 633nm

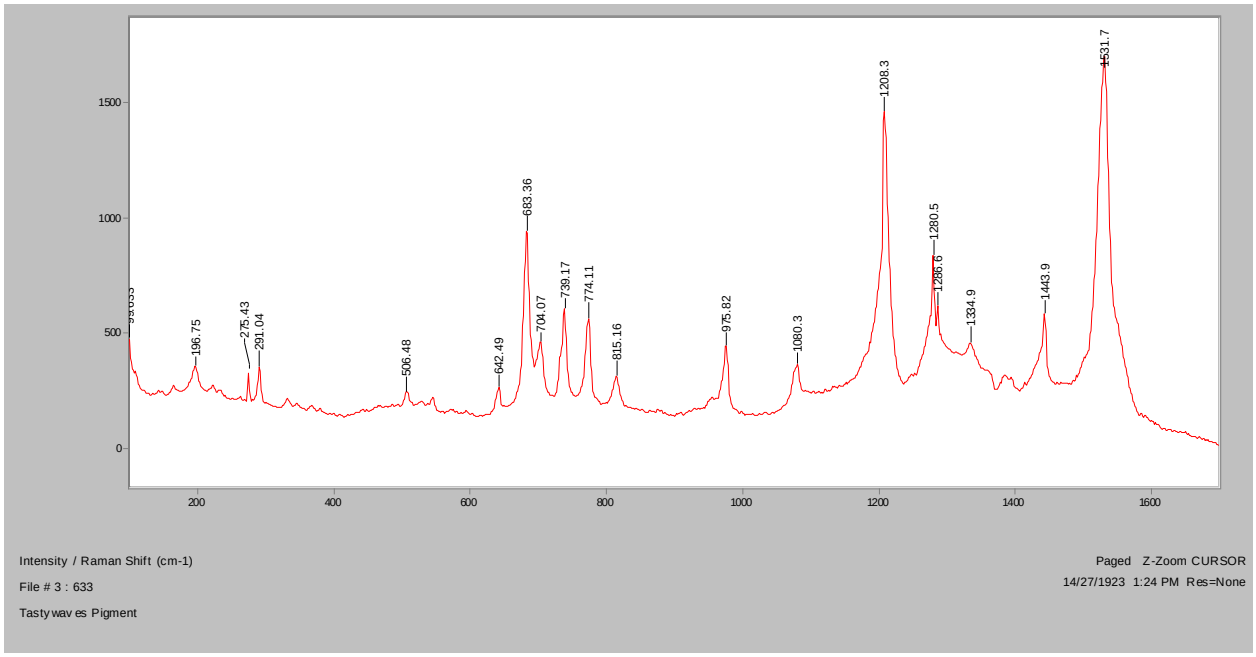

Normal Raman, 785nm

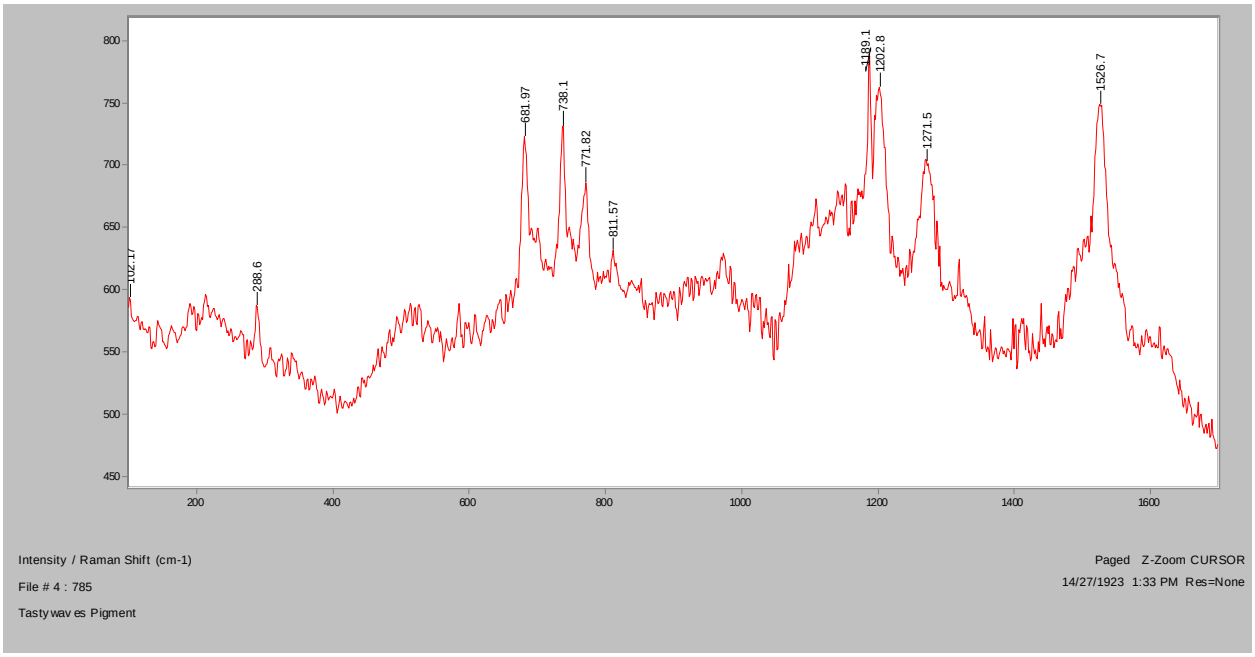

FT-Raman, 1064nm

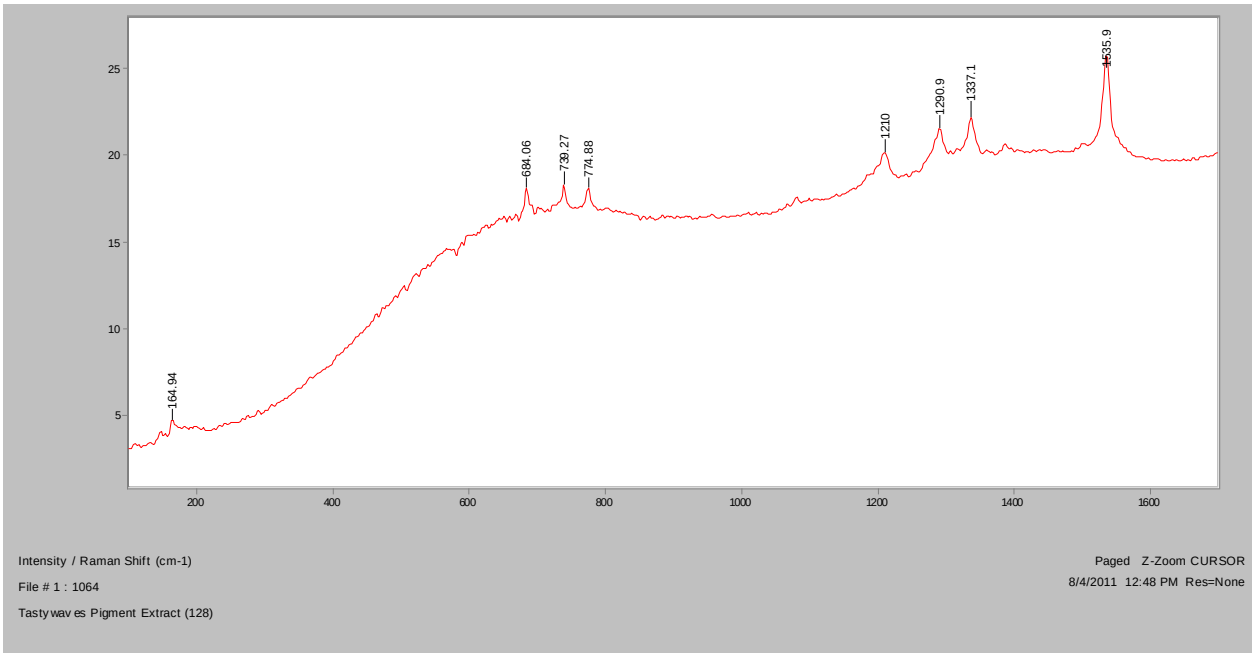

FT-IR (ATR)

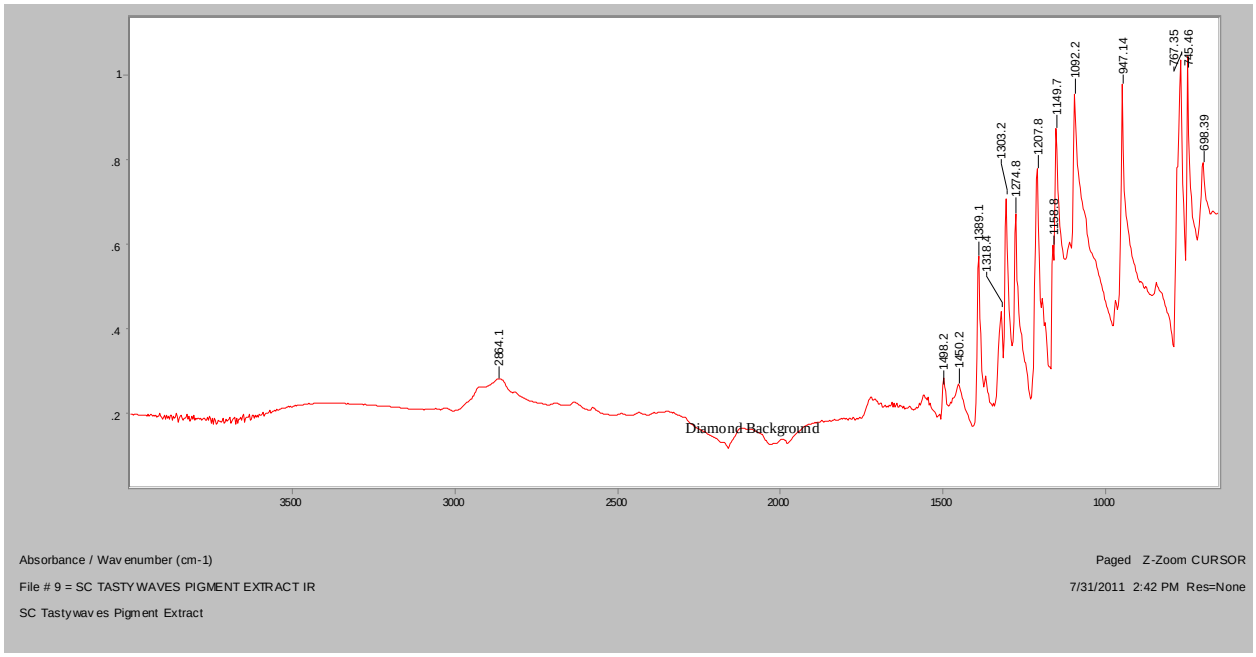

UV-Vis

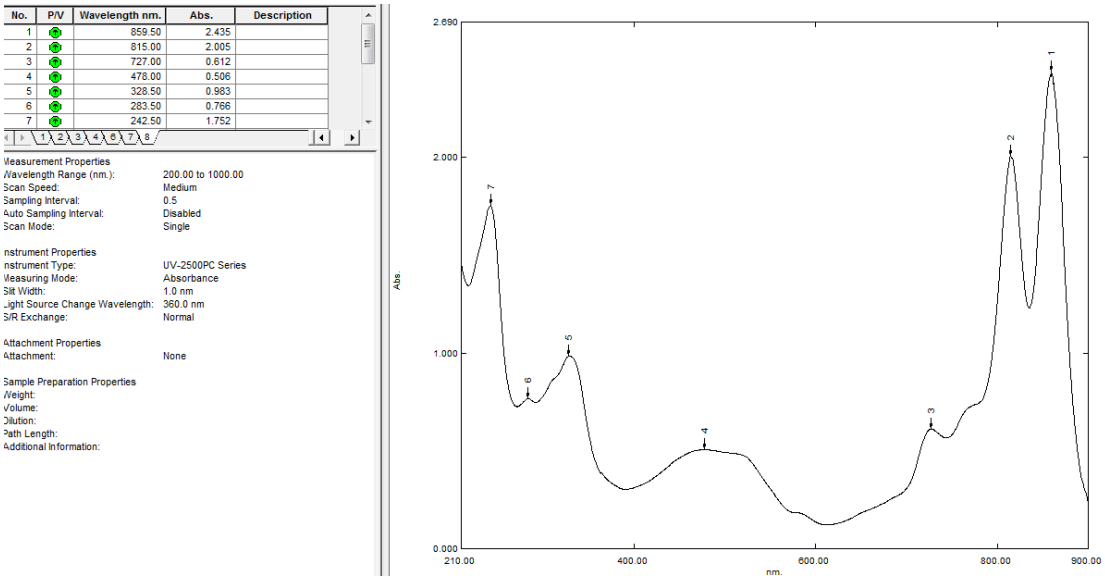

No.	P/V	Wavelength nm.	Abs.	Description
1		859.50	2.435	
2		815.00	2.005	
3		727.00	0.612	
4		478.00	0.506	
5		328.50	0.983	
6		283.50	0.766	
7		242.50	1.752	

Measurement Properties
Wavelength Range (nm.): 200.00 to 1000.00
Scan Speed: Medium
Sampling Interval: 0.5
Auto Sampling Interval: Disabled
Scan Mode: Single

nstrument Properties
nstrument Type: UV-2500PC Series
Measuring Mode: Absorbance
Slit Width: 1.0 nm
Light Source Change Wavelength: 360.0 nm
S/R Exchange: Normal

Attachment Properties
Attachment: None

Sample Preparation Properties
Weight:
Volume:
Dilution:
Path Length:
Additional Information:

Bell Bottom Blue

Normal Raman, 488nm

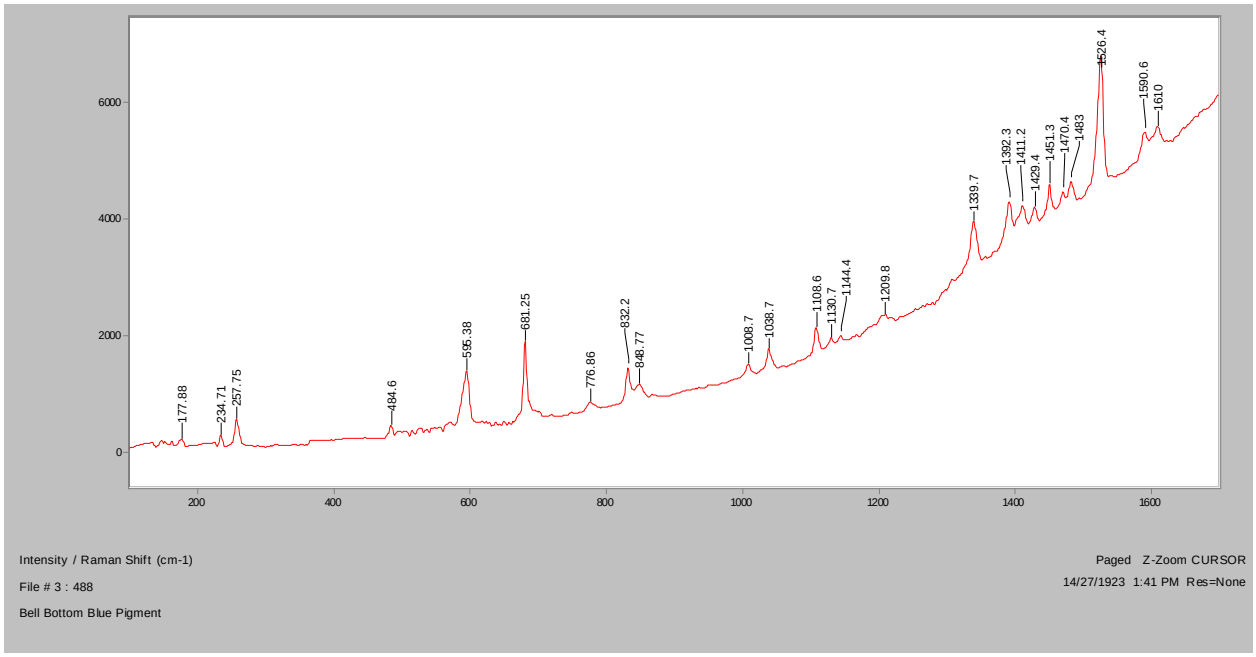

Normal Raman, 633nm

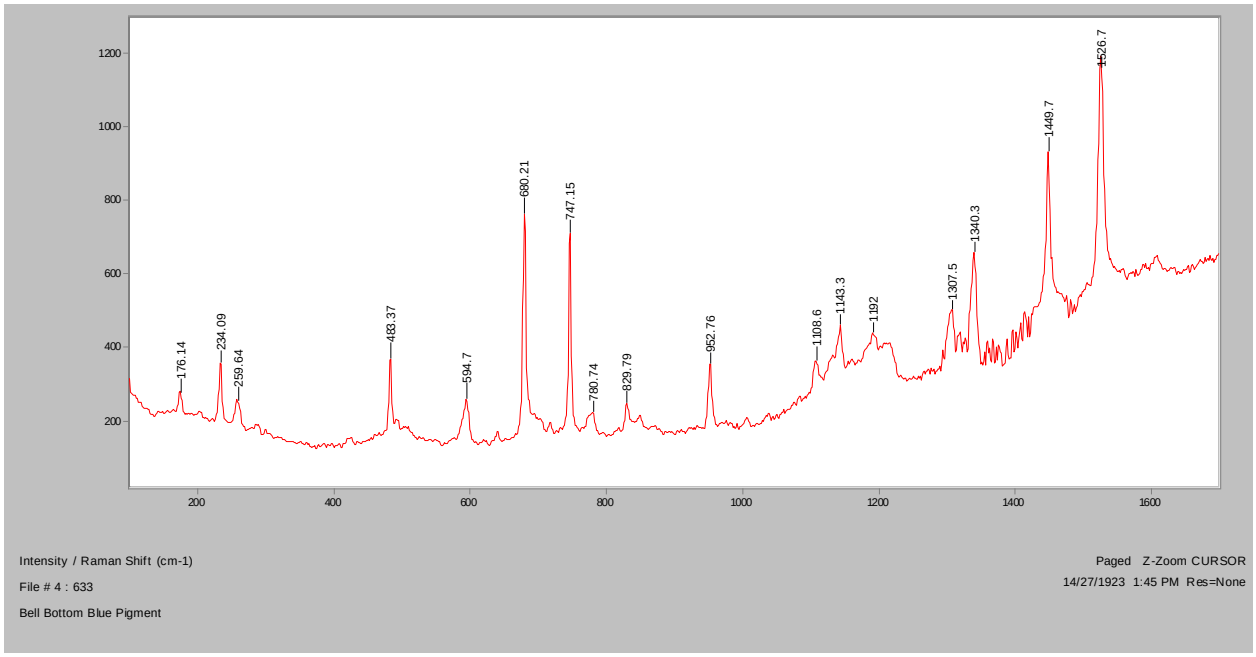

Normal Raman, 785nm

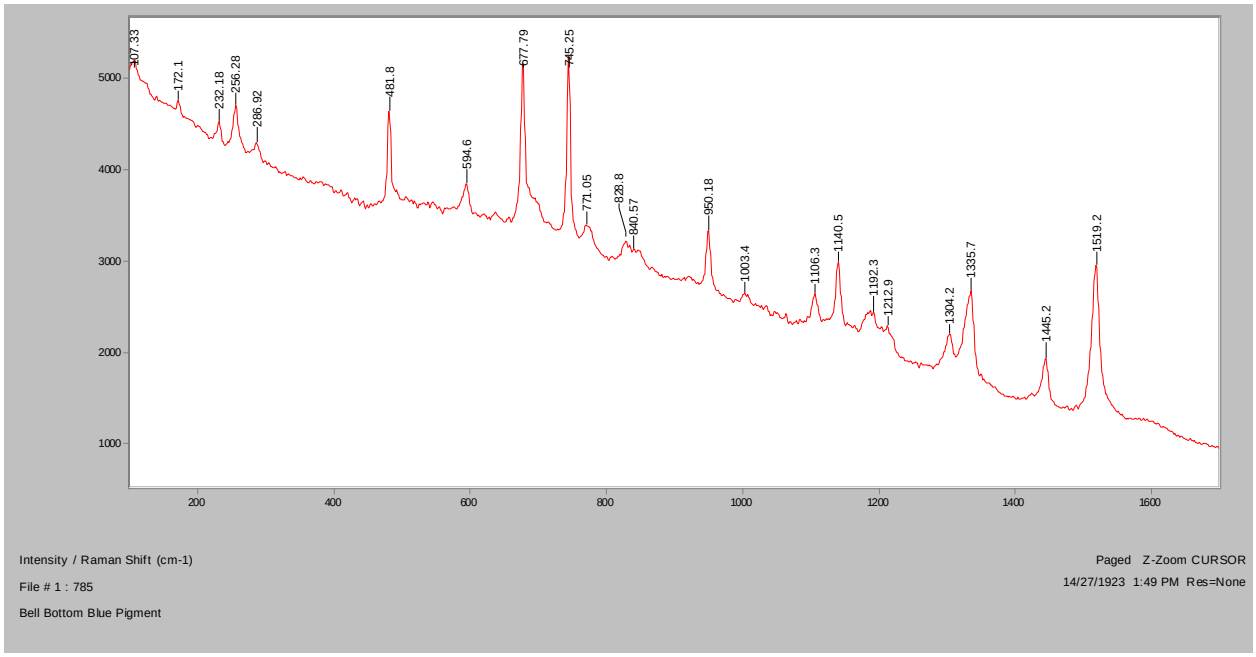

FT-Raman, 1064nm

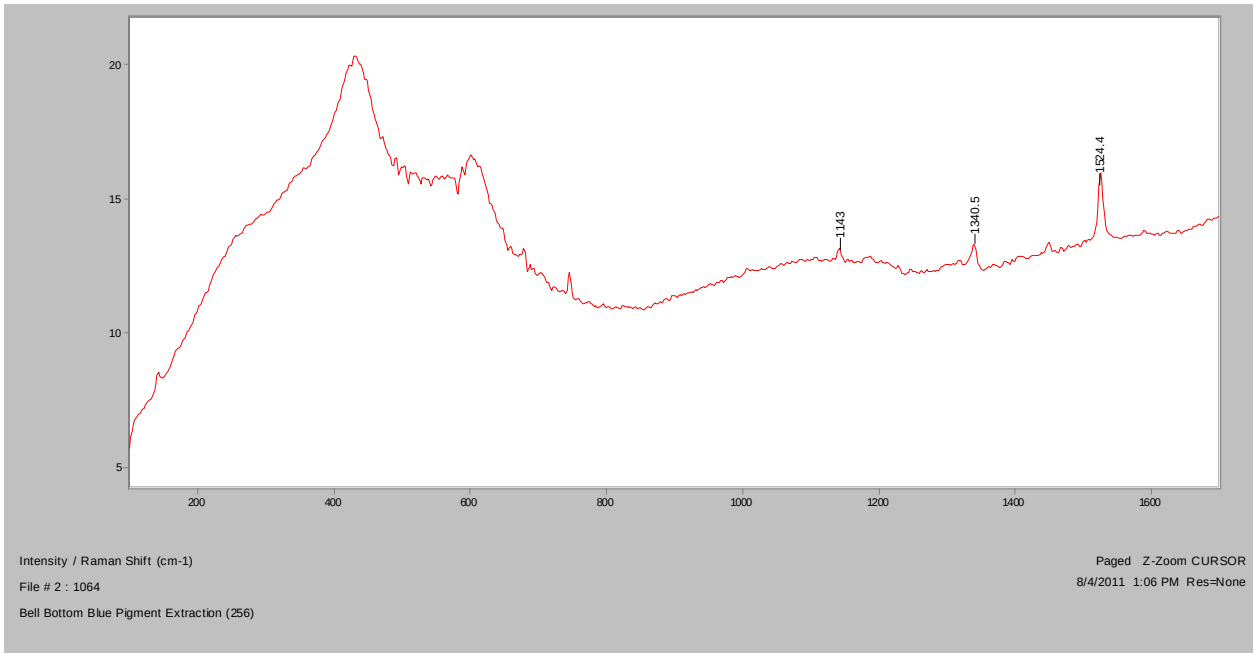

FT-IR (ATR)

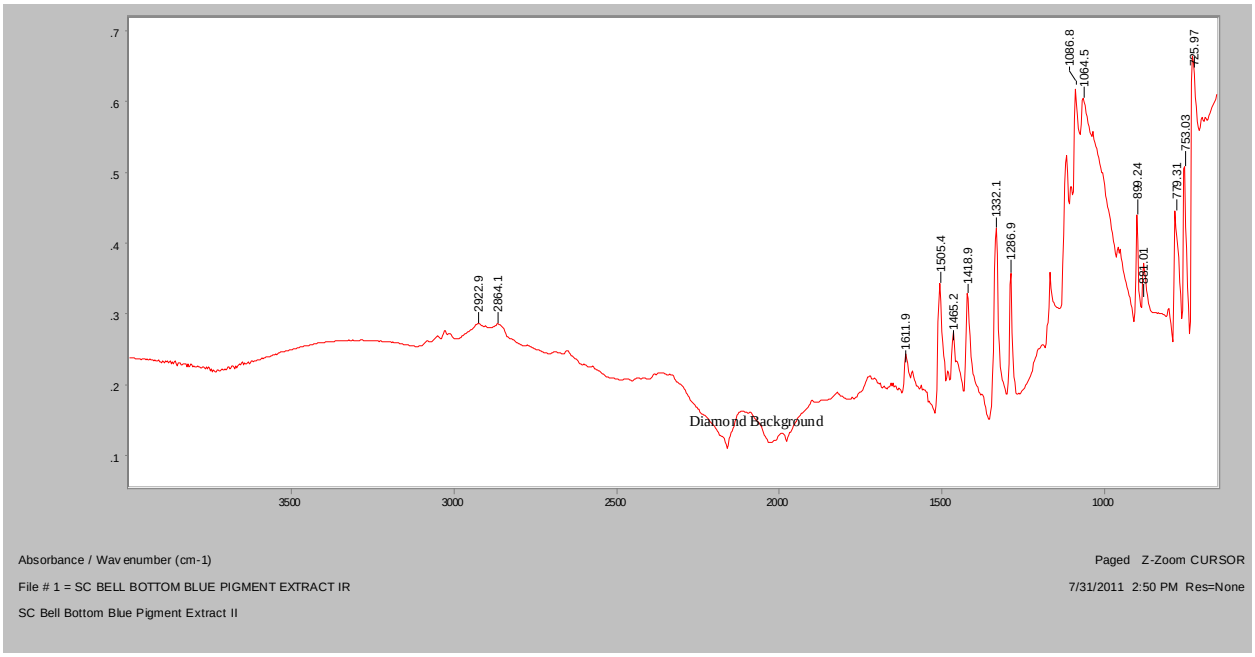

UV-Vis

No.	P/V	Wavelength nm.	Abs.	Description
1		897.50	0.073	
2		867.50	0.064	
3		790.50	2.298	
4		700.00	0.405	
5		439.00	0.365	
6		305.00	0.835	
7		253.00	0.460	
8		222.50	0.734	

Measurement Properties
Wavelength Range (nm.): 200.00 to 1000.00
Scan Speed: Medium
Sampling Interval: 0.5
Auto Sampling Interval: Disabled
Scan Mode: Single

Instrument Properties
Instrument Type: UV-2500PC Series
Measuring Mode: Absorbance
Slit Width: 1.0 nm
Light Source Change Wavelength: 360.0 nm
S/R Exchange: Normal

Attachment Properties
Attachment: None

Sample Preparation Properties
Weight:
Volume:
Dilution:
Path Length:
Additional Information:

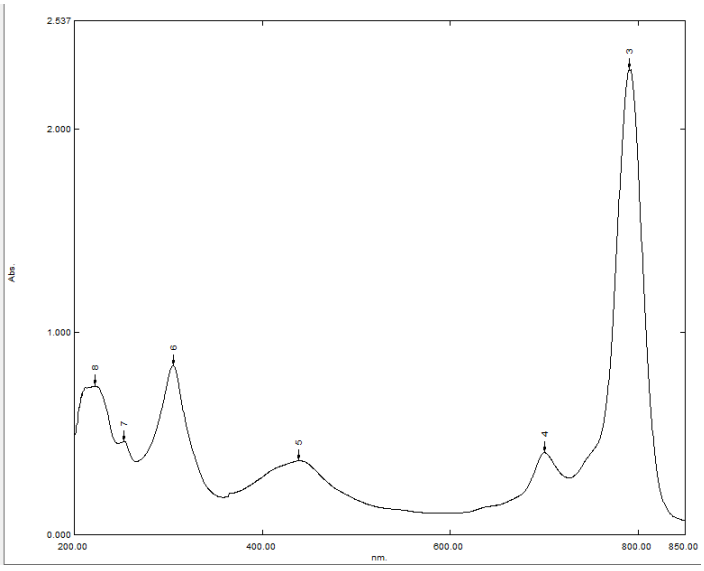

SRV Teal 2

Normal Raman, 488nm

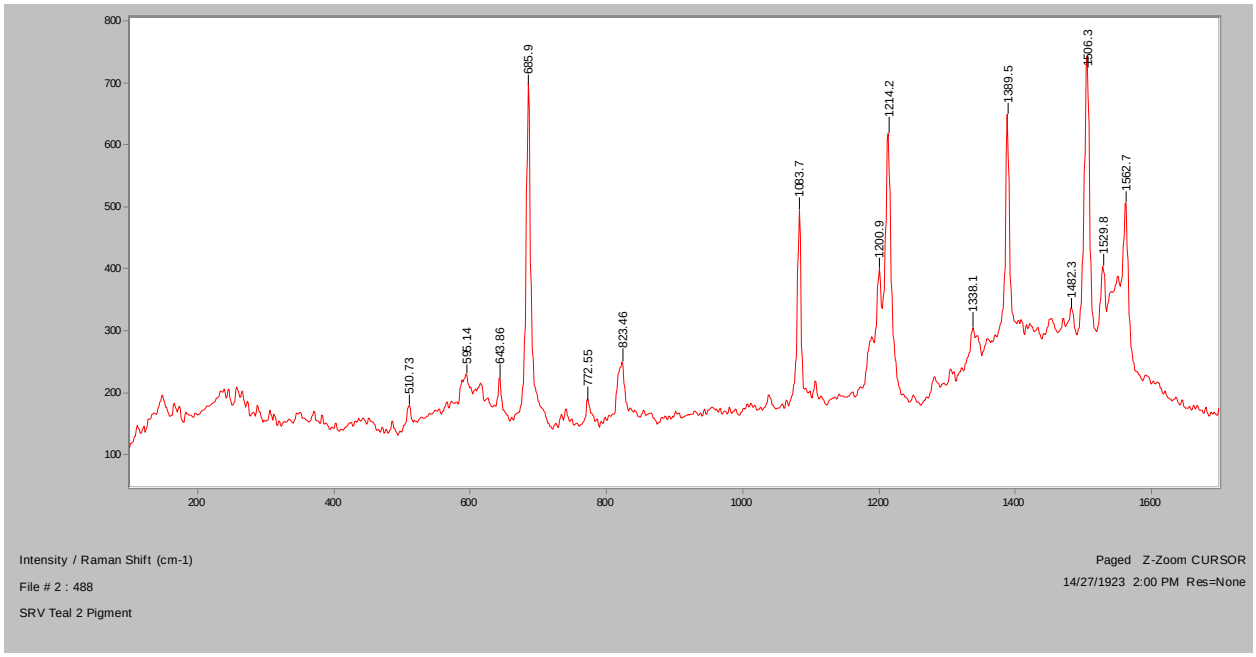

Normal Raman, 633nm

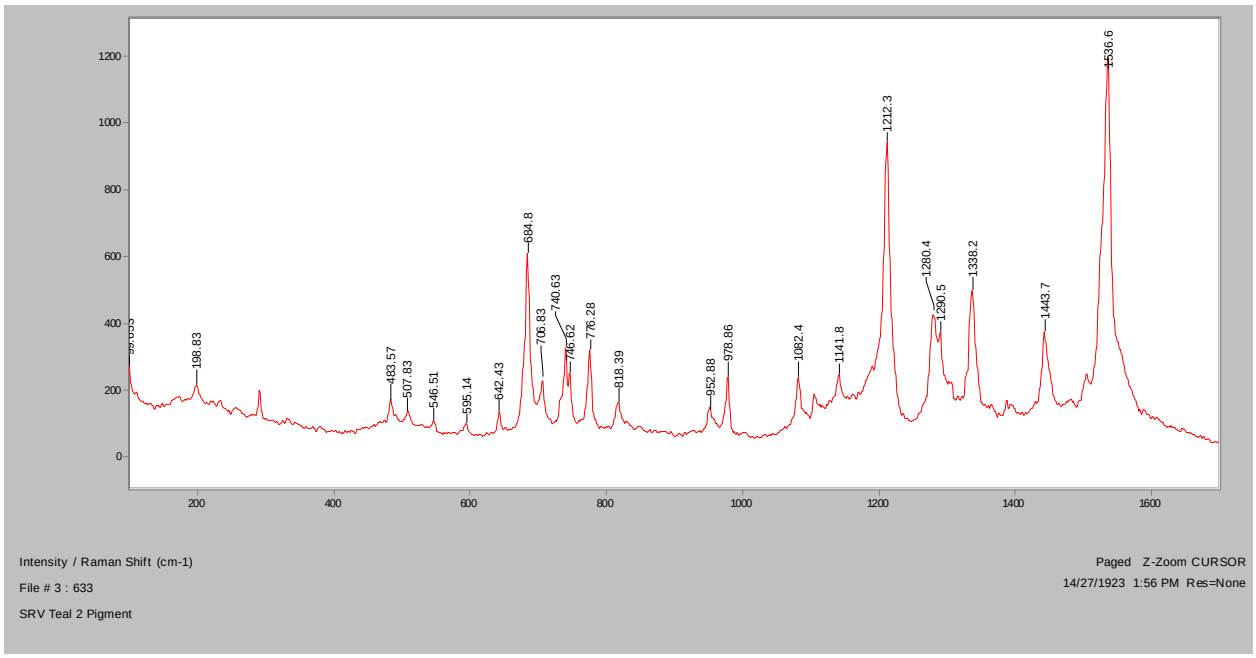

Normal Raman, 785nm

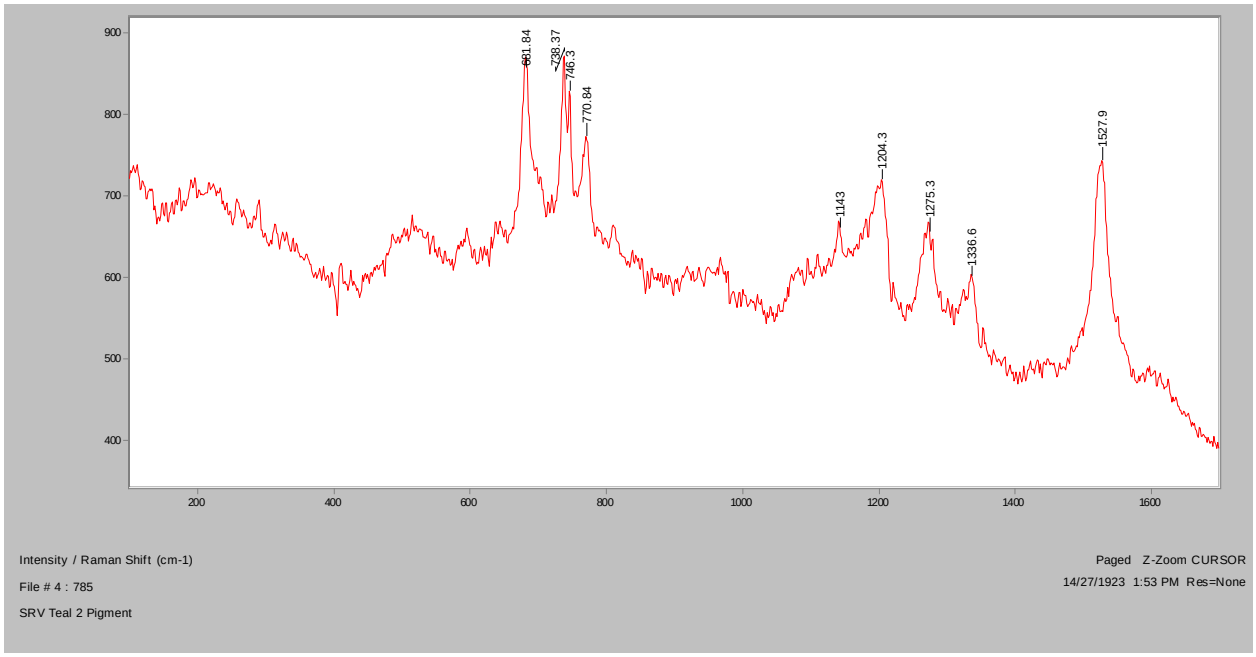

FT-Raman, 1064nm

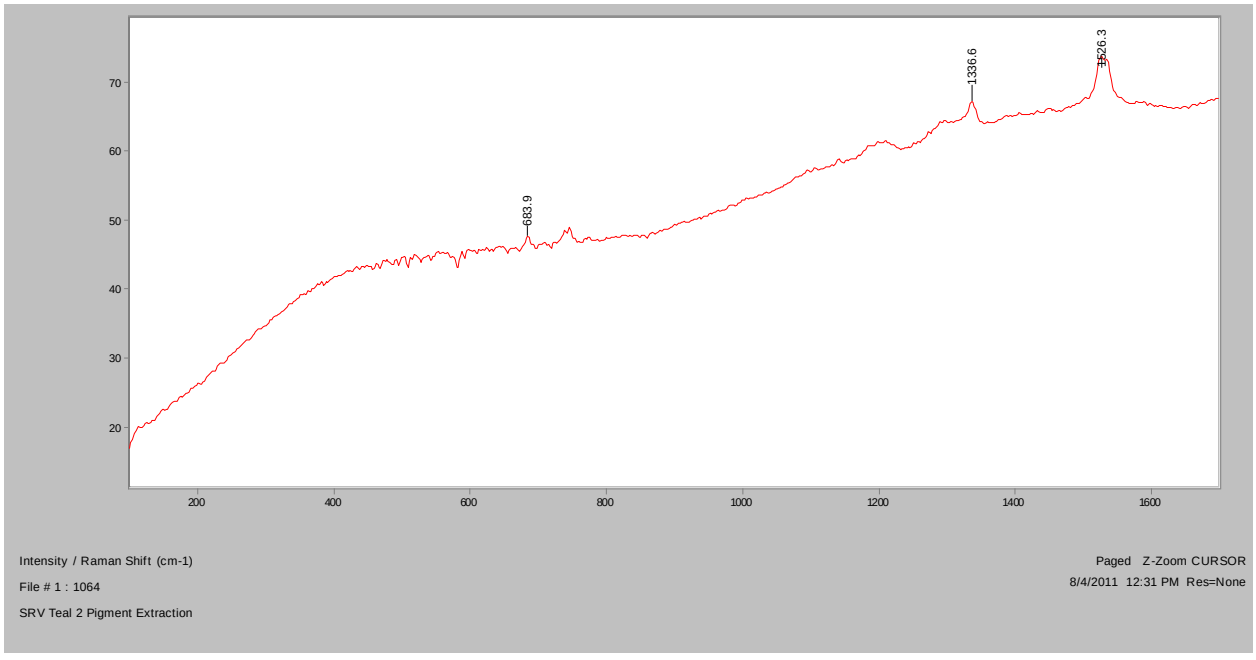

FT-IR (ATR)

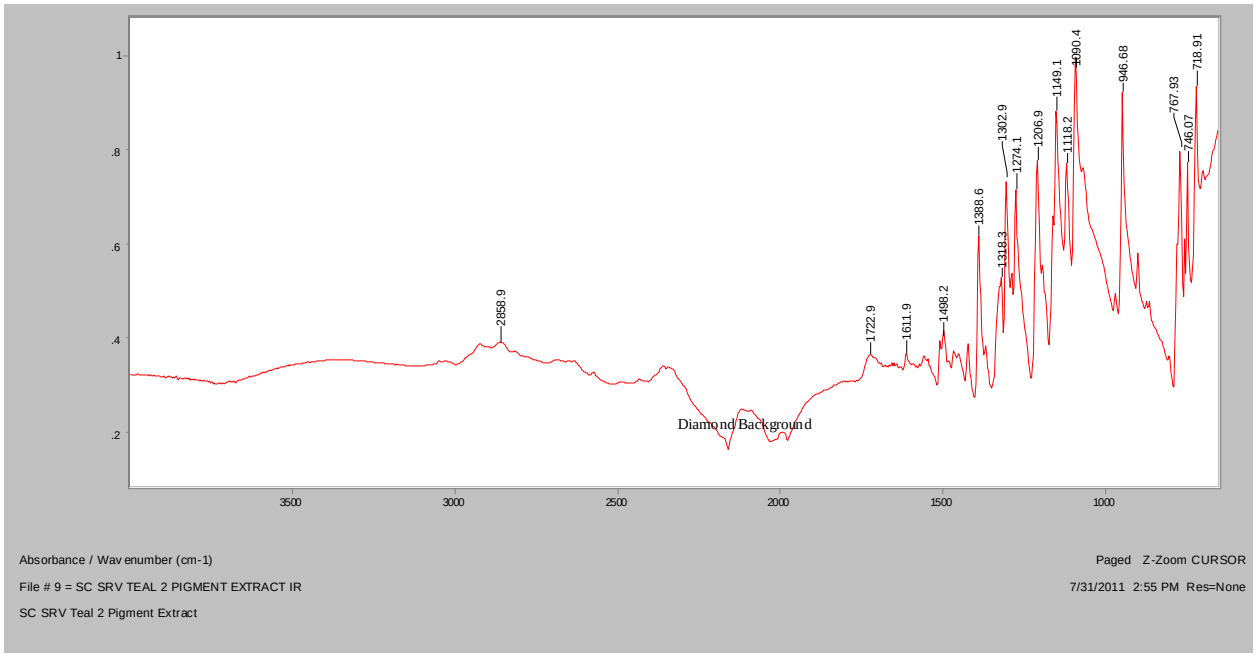

UV-Vis

No.	P/V	Wavelength nm.	Abs.	Description
1		977.50	0.105	
2		859.00	0.677	
3		791.00	2.137	
4		701.50	0.368	
5		443.00	0.318	
6		365.00	0.177	
7		305.50	0.766	
8		208.50	1.002	

Measurement Properties
Wavelength Range (nm.): 200.00 to 1000.00
Scan Speed: Medium
Sampling Interval: 0.5
Auto Sampling Interval: Disabled
Scan Mode: Single

nstrument Properties
nstrument Type: UV-2500PC Series
Measuring Mode: Absorbance
Slit Width: 1.0 nm
Light Source Change Wavelength: 360.0 nm
S/R Exchange: Normal

Attachment Properties
Attachment: None

Sample Preparation Properties
Weight:
Volume:
Dilution:
Path Length:
Additional Information:

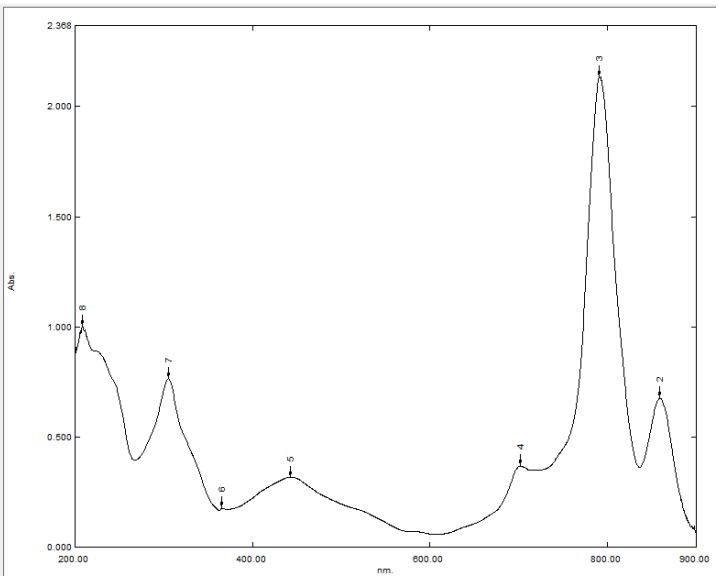

Razberry Creem

Normal Raman, 488nm

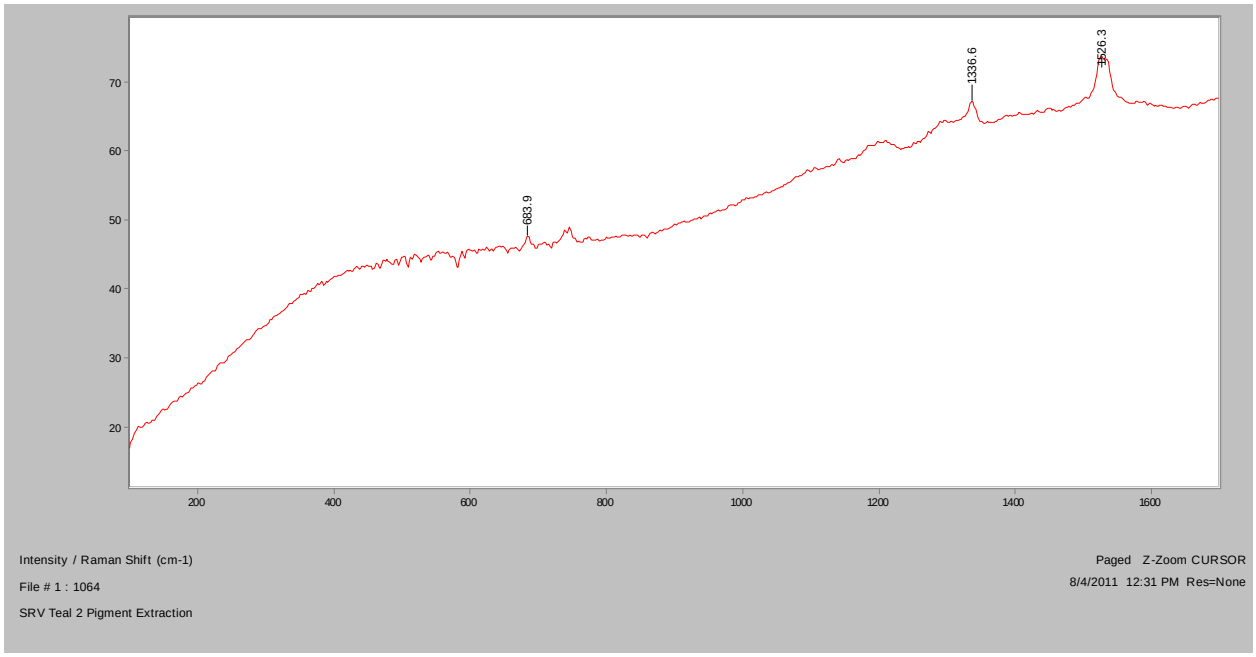

Normal Raman, 633nm

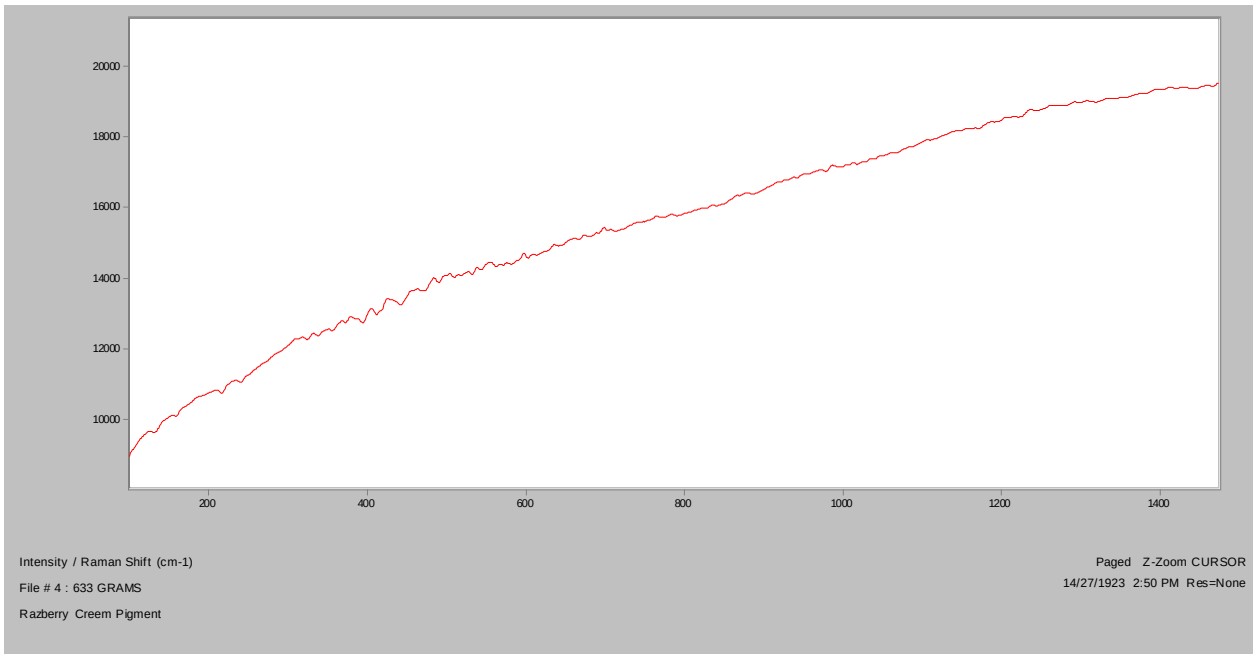

Normal Raman, 785nm

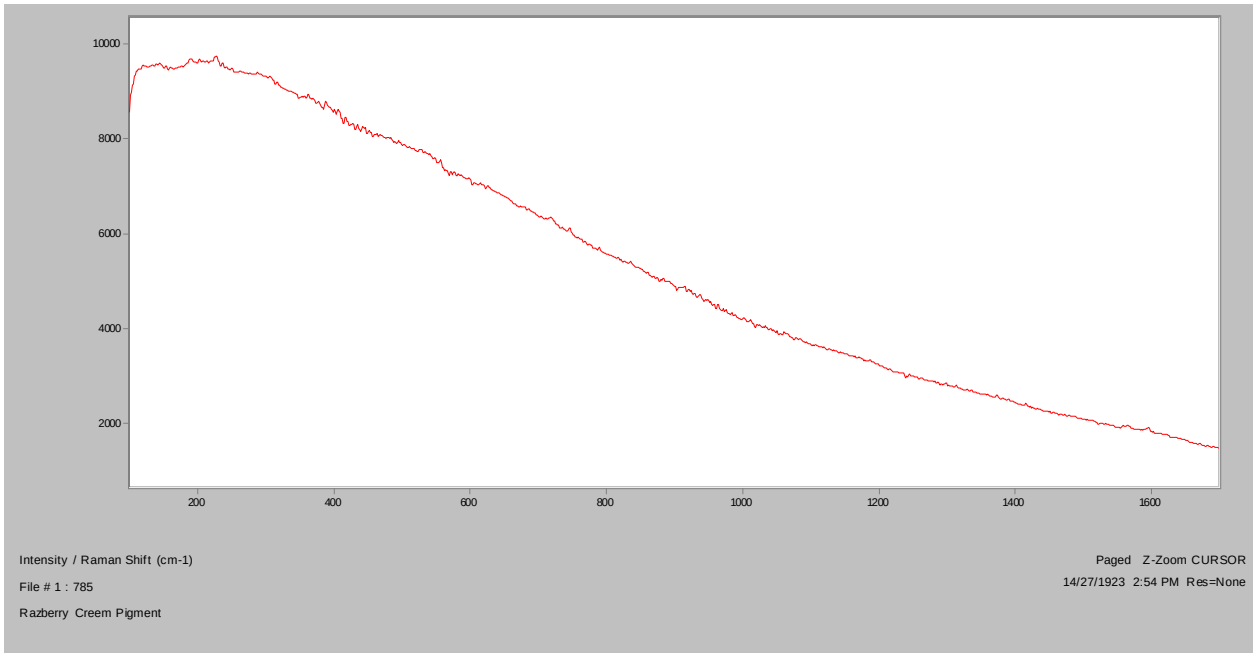

FT-Raman, 1064nm

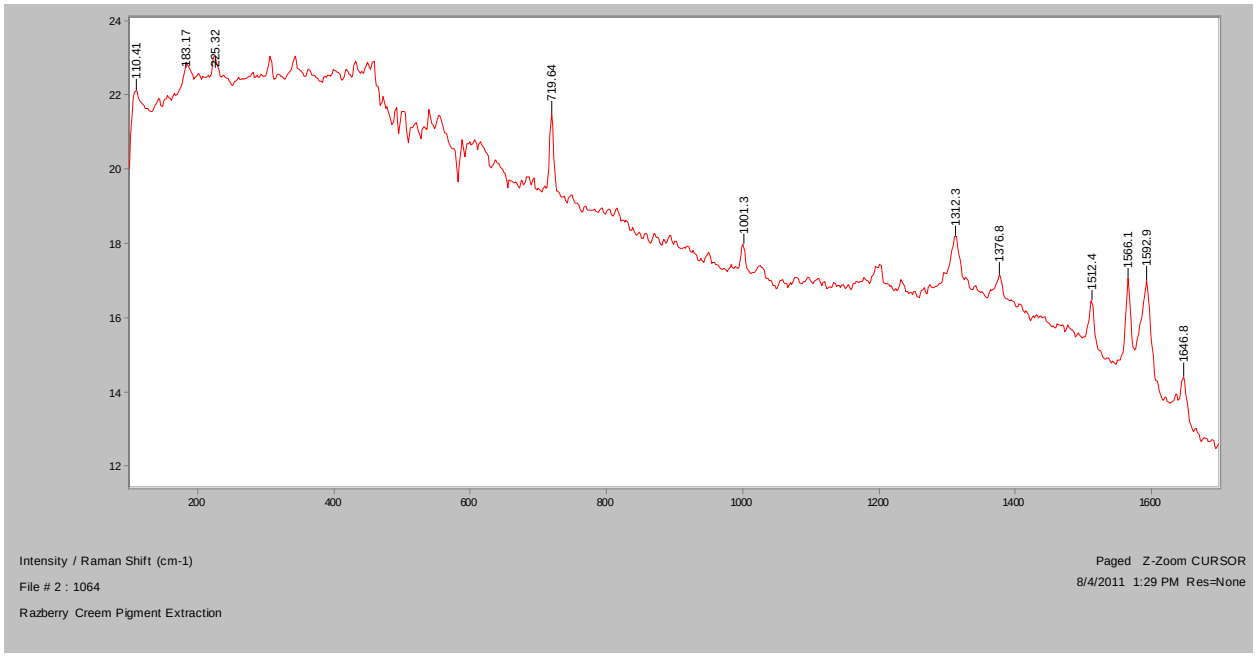

FT-IR (ATR)

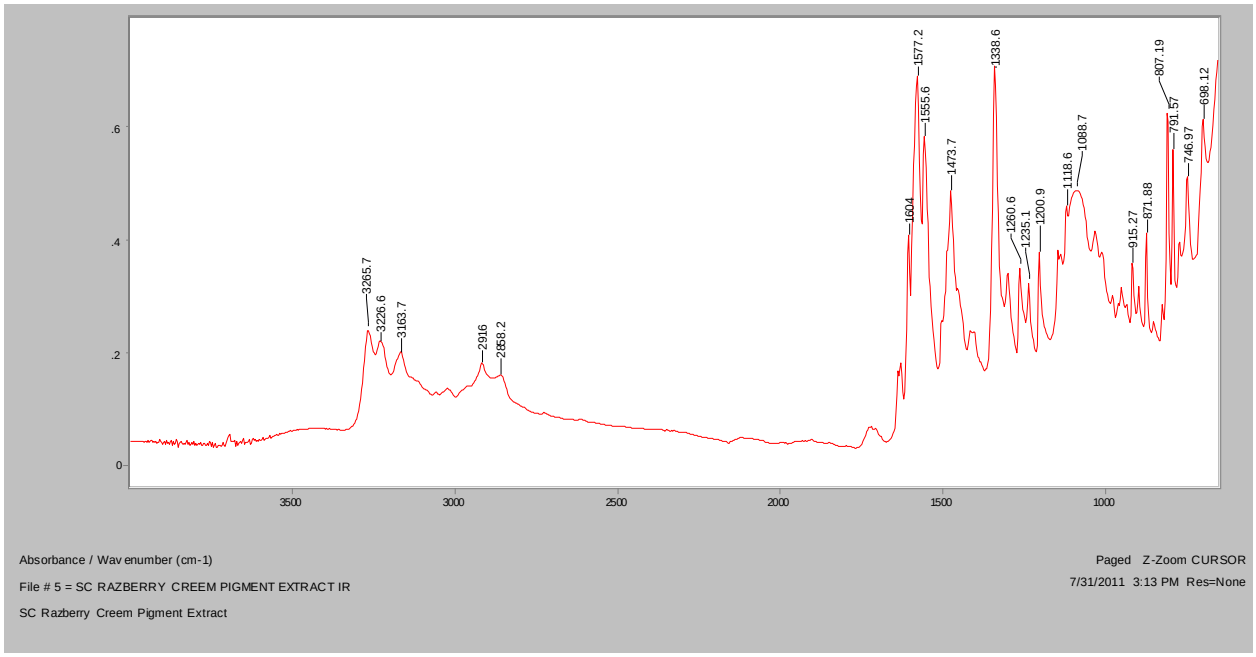

UV-Vis

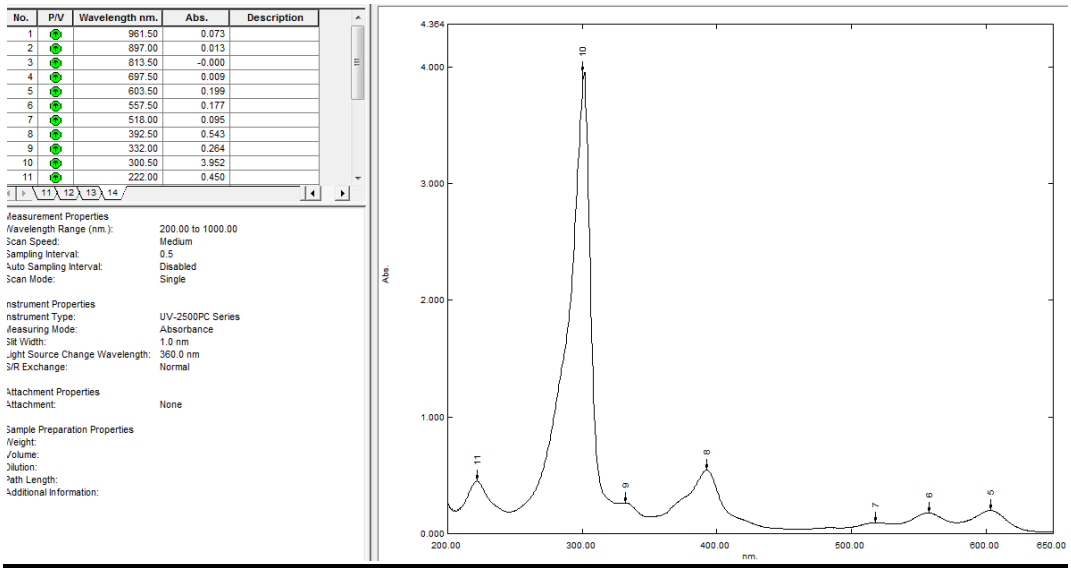

No.	P/V	Wavelength nm.	Abs.	Description
1		961.50	0.073	
2		897.00	0.013	
3		813.50	-0.000	
4		697.50	0.009	
5		603.50	0.199	
6		557.50	0.177	
7		518.00	0.095	
8		392.50	0.543	
9		332.00	0.264	
10		300.50	3.952	
11		222.00	0.450	

11 12 13 14

Measurement Properties
Wavelength Range (nm.): 200.00 to 1000.00
Scan Speed: Medium
Sampling Interval: 0.5
Auto Sampling Interval: Disabled
Scan Mode: Single

Instrument Properties
Instrument Type: UV-2500PC Series
Measuring Mode: Absorbance
Slit Width: 1.0 nm
Light Source Change Wavelength: 360.0 nm
S/R Exchange: Normal

Attachment Properties
Attachment: None

Sample Preparation Properties
Weight:
Volume:
Dilution:
Path Length:
Additional Information:

Muddy Water Blue

Normal Raman, 488nm

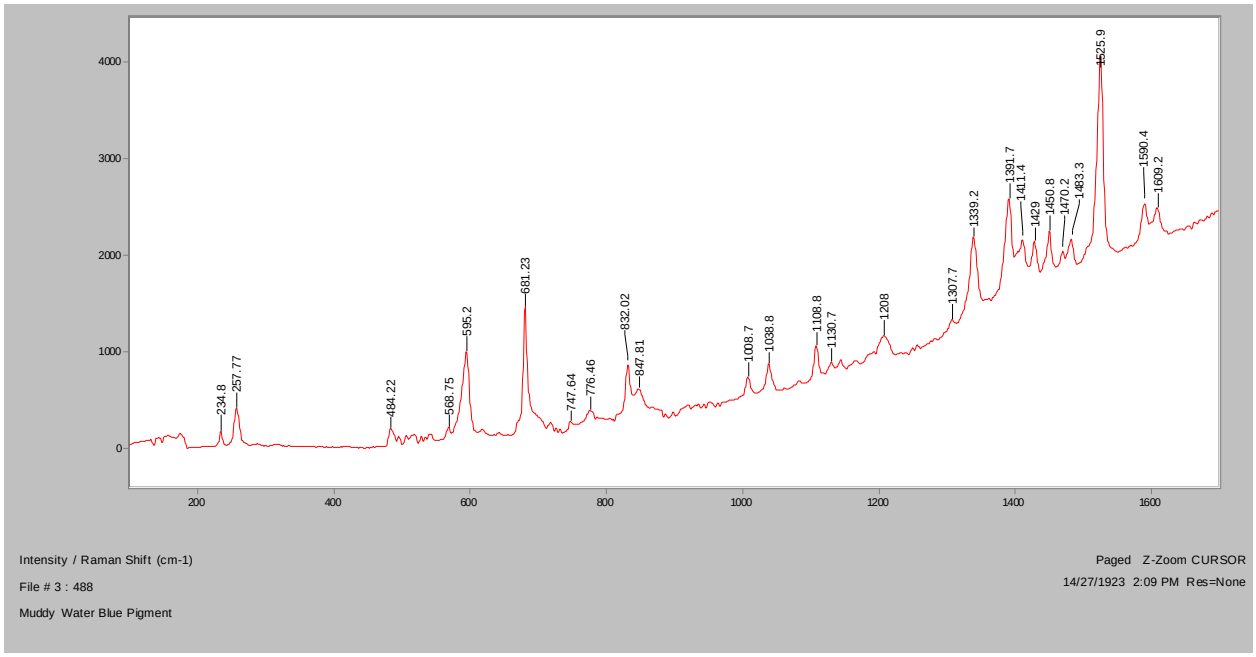

Normal Raman, 633nm

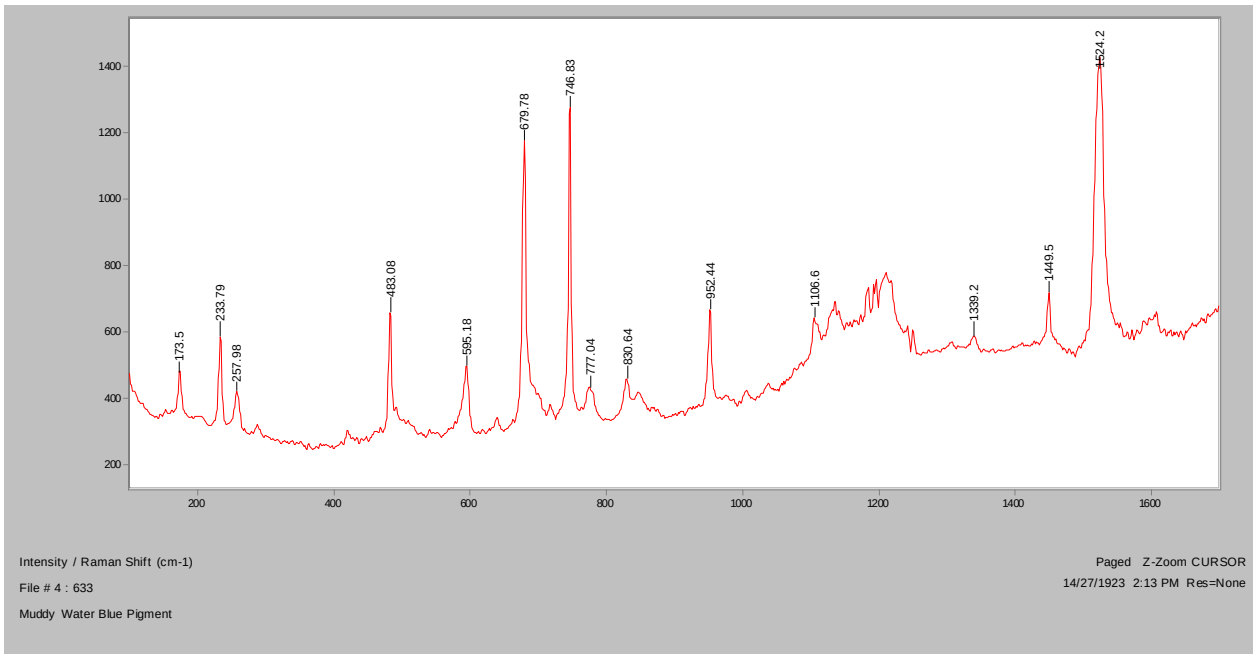

Normal Raman, 785nm

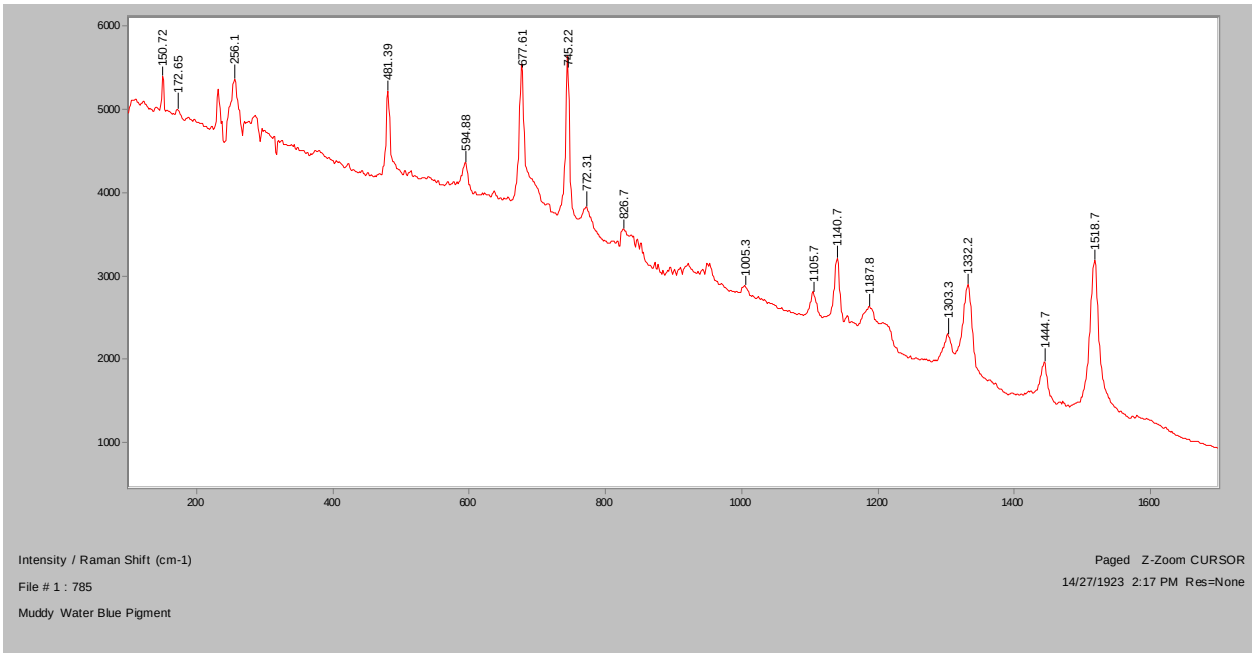

FT-Raman, 1064nm

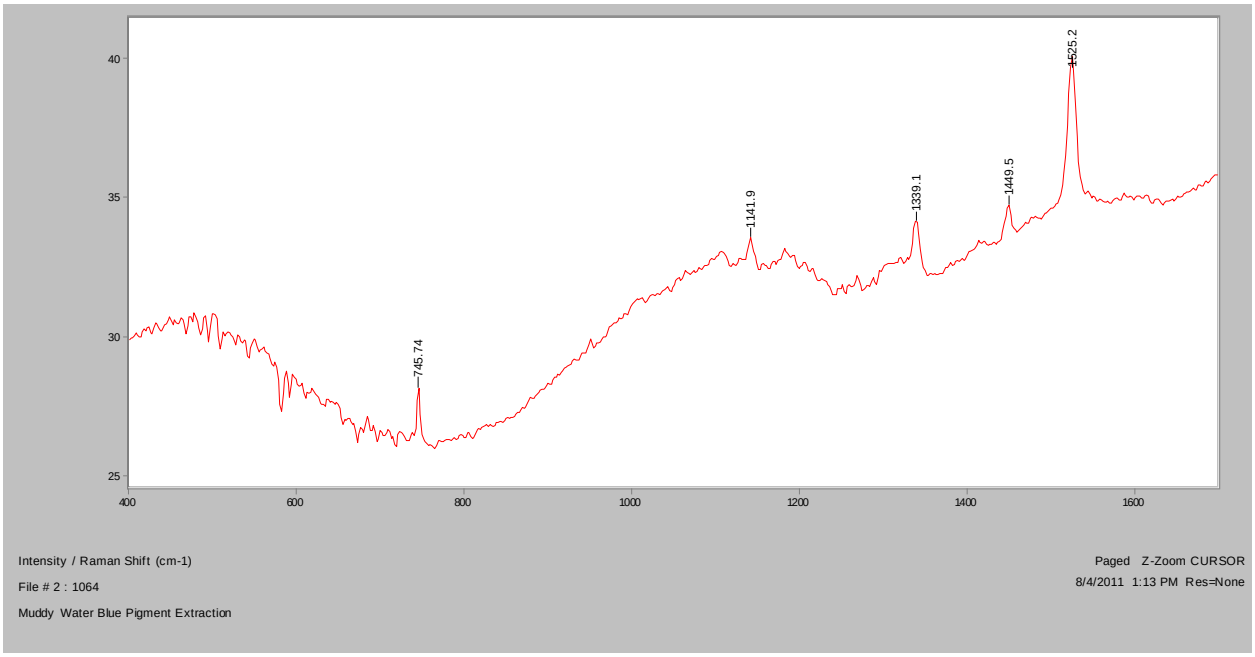

FT-IR (ATR)

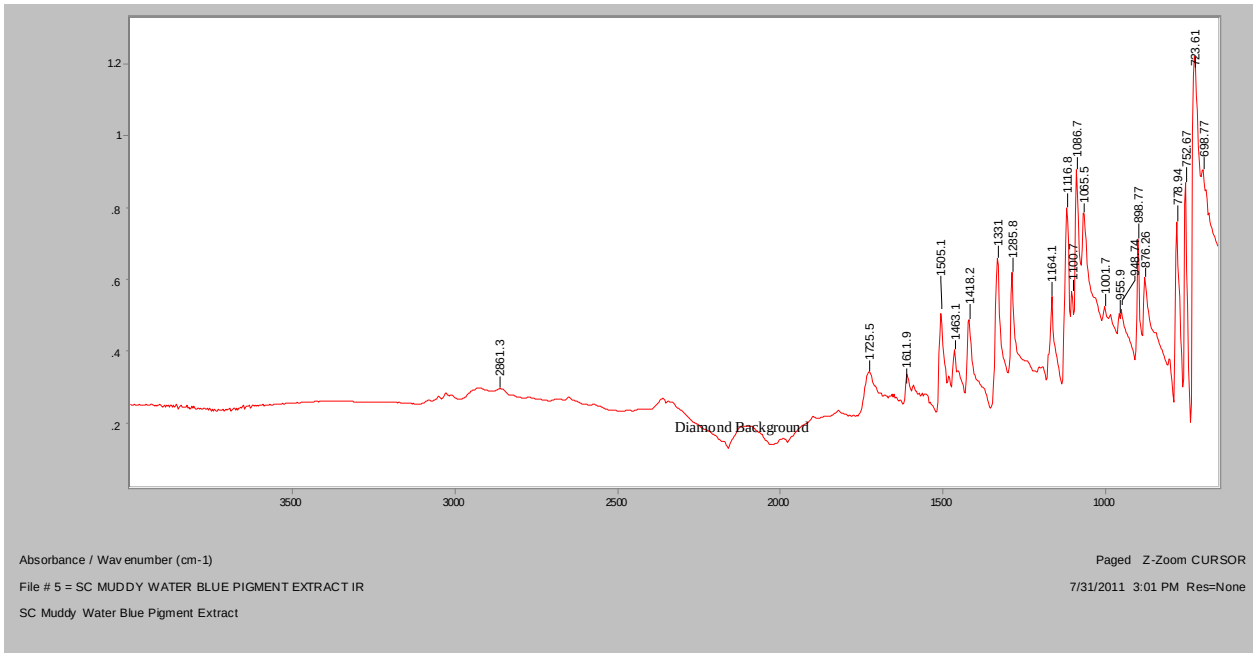

UV-Vis

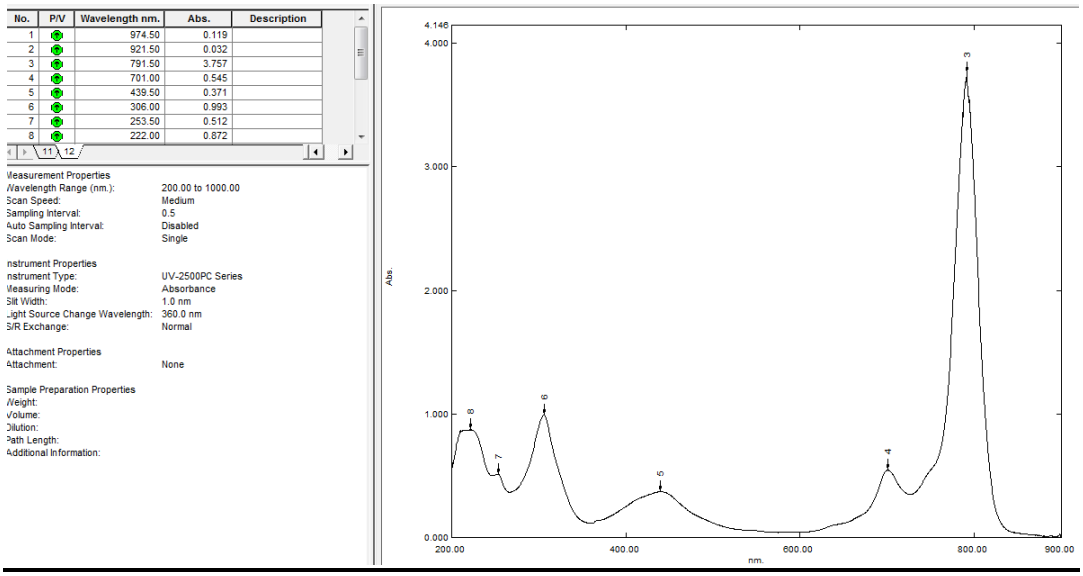

No.	P/V	Wavelength nm.	Abs.	Description
1		974.50	0.119	
2		921.50	0.032	
3		791.50	3.757	
4		701.00	0.545	
5		439.50	0.371	
6		306.00	0.993	
7		253.50	0.512	
8		222.00	0.872	

11 12

Measurement Properties
Wavelength Range (nm.): 200.00 to 1000.00
Scan Speed: Medium
Sampling Interval: 0.5
Auto Sampling Interval: Disabled
Scan Mode: Single

nstrument Properties
nstrument Type: UV-2500PC Series
Measuring Mode: Absorbance
Slit Width: 1.0 nm
_ight Source Change Wavelength: 360.0 nm
S/R Exchange: Normal

Attachment Properties
Attachment: None

Sample Preparation Properties
Weight:
Volume:
Dilution:
Path Length:
Additional Information:

Ripple

Normal Raman, 488nm

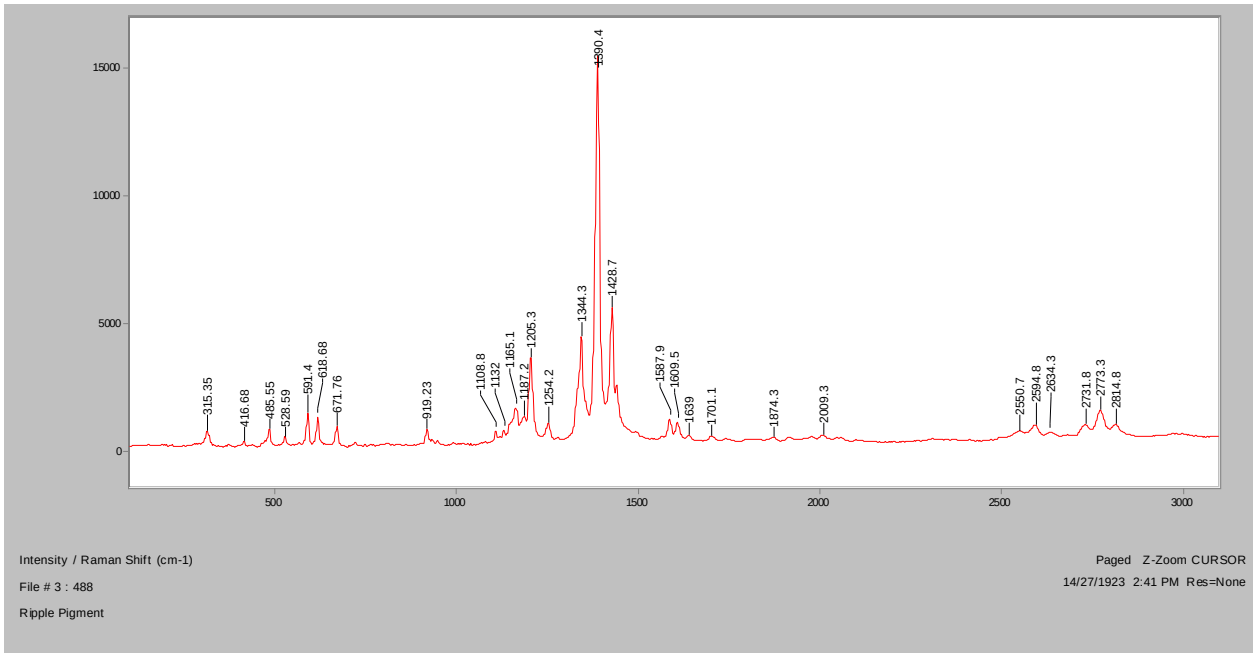

Normal Raman, 633nm

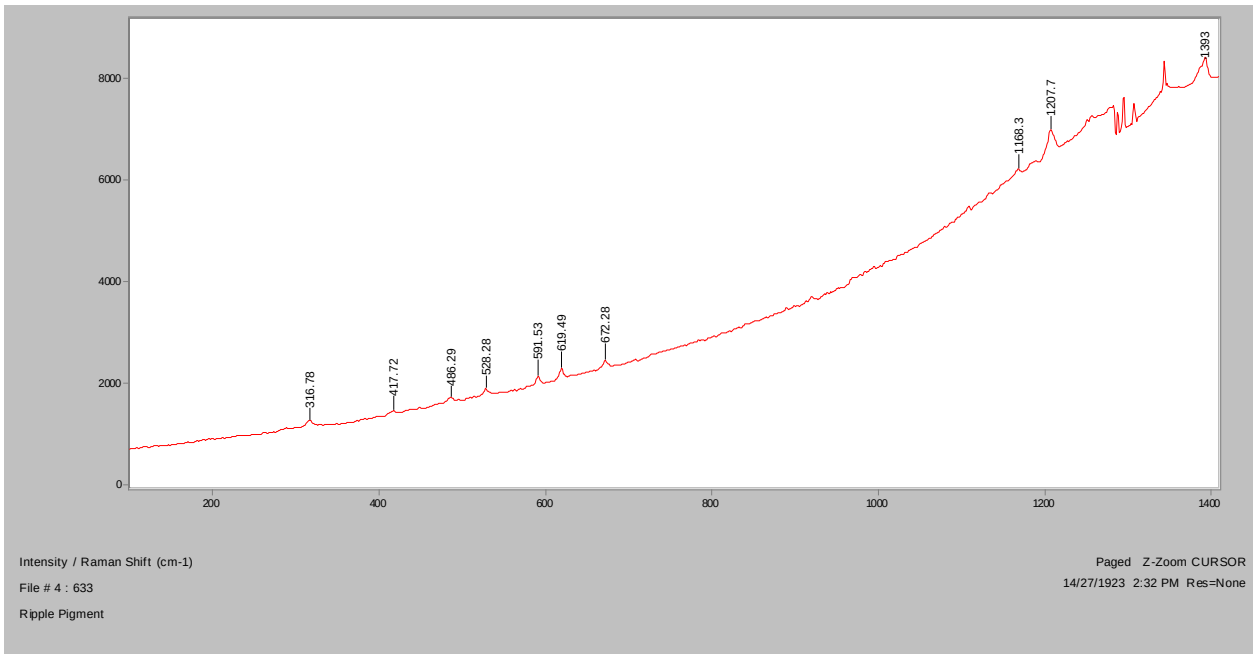

Normal Raman, 785nm

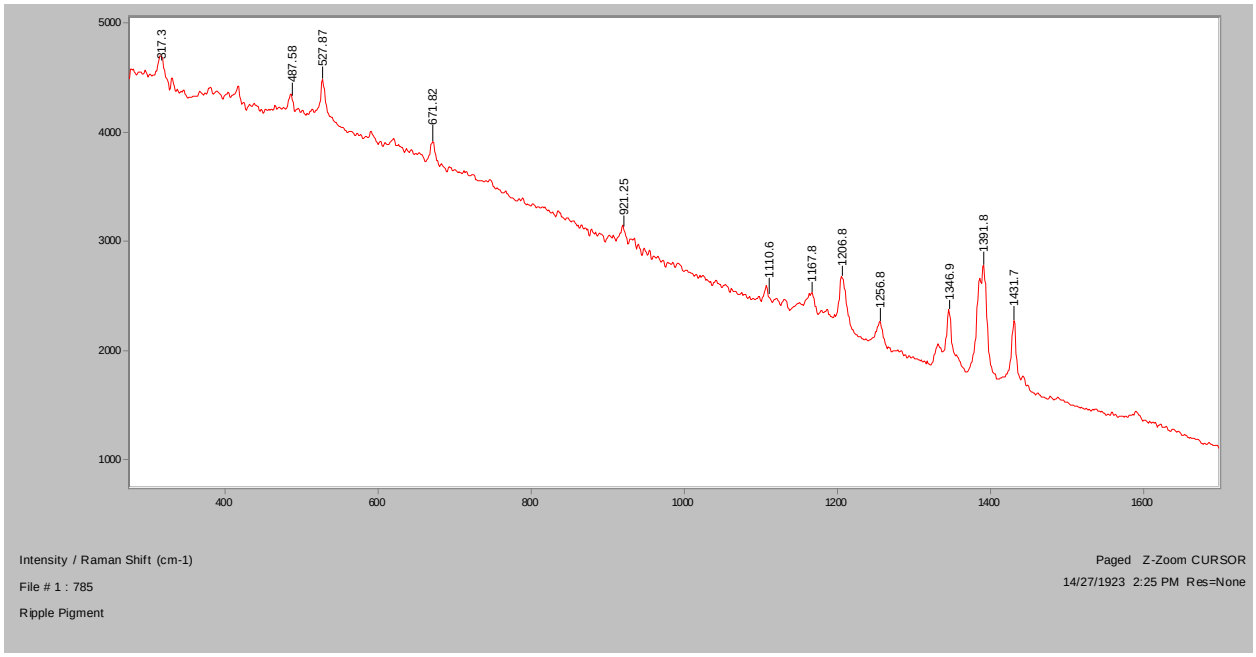

FT-Raman, 1064nm (in KBr)

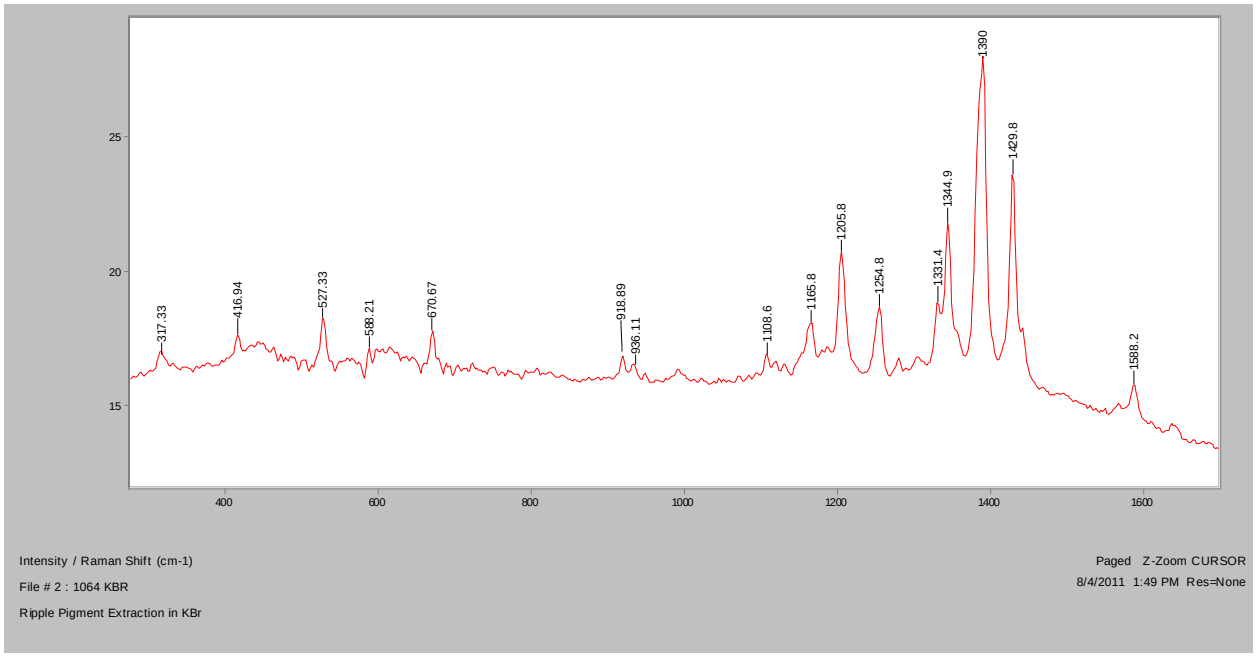

FT-IR (ATR)

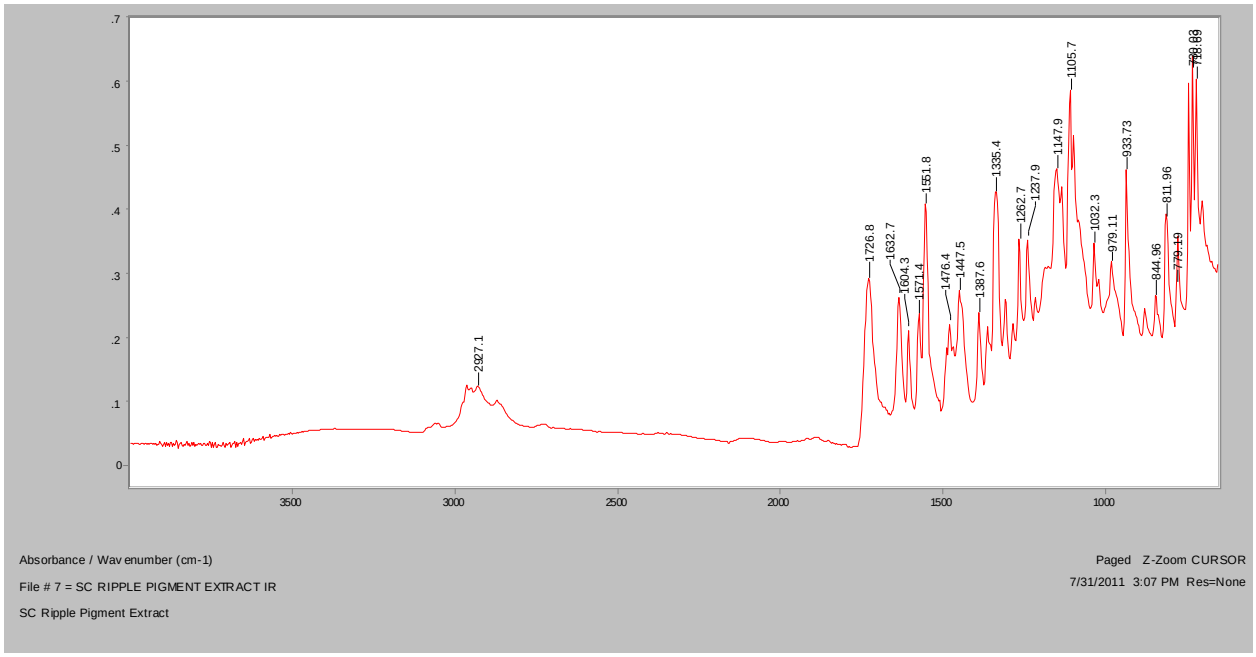

UV-Vis

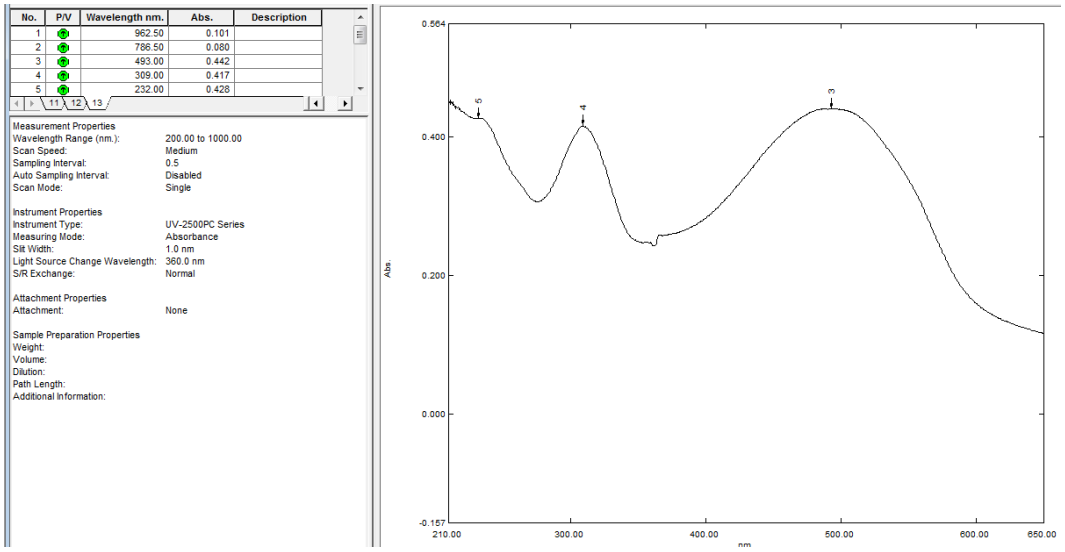

San Brownadino

Normal Raman, 488nm

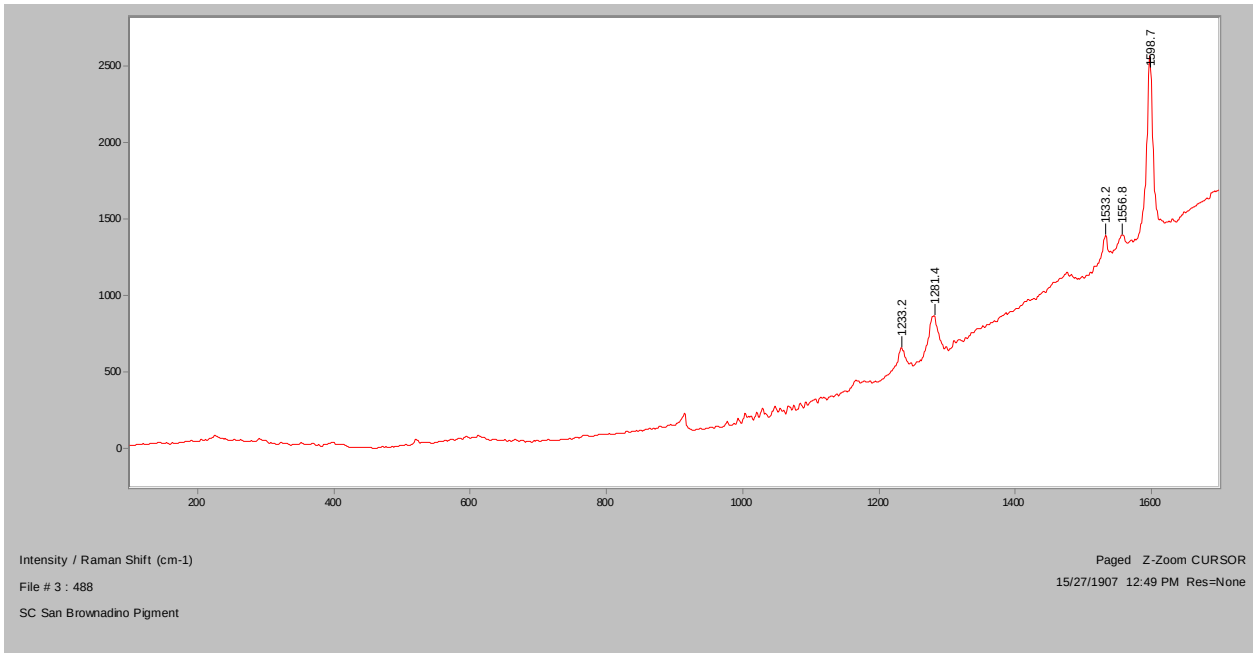

Normal Raman, 633nm

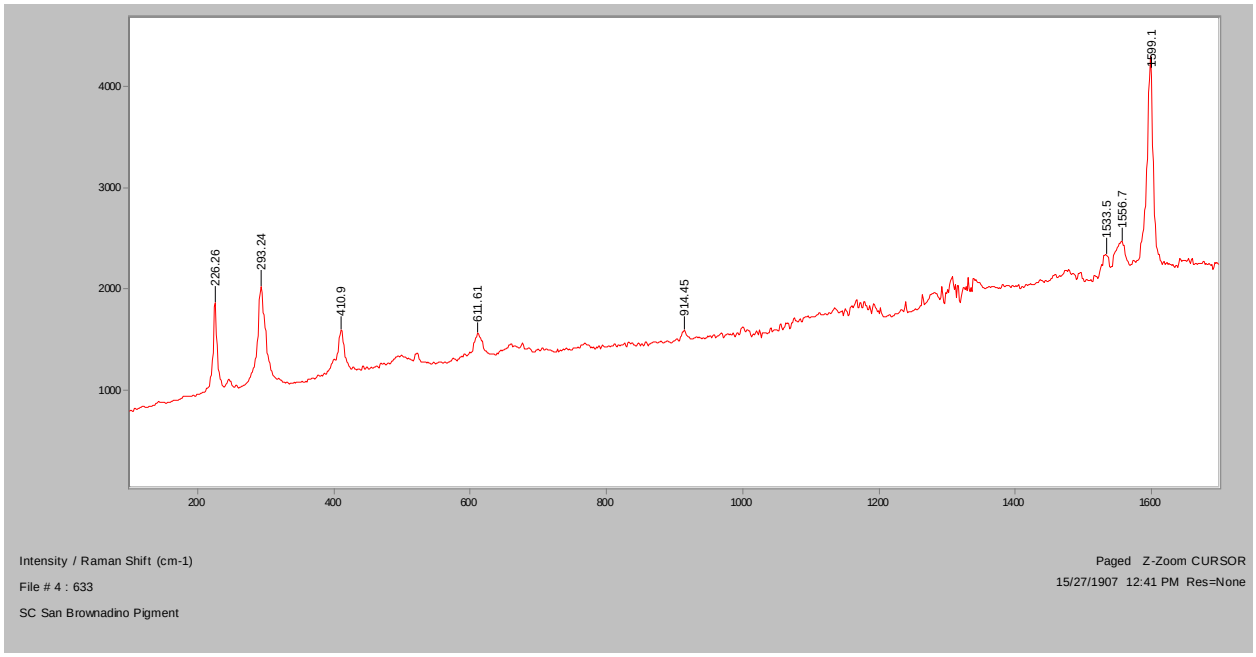

Normal Raman, 785nm

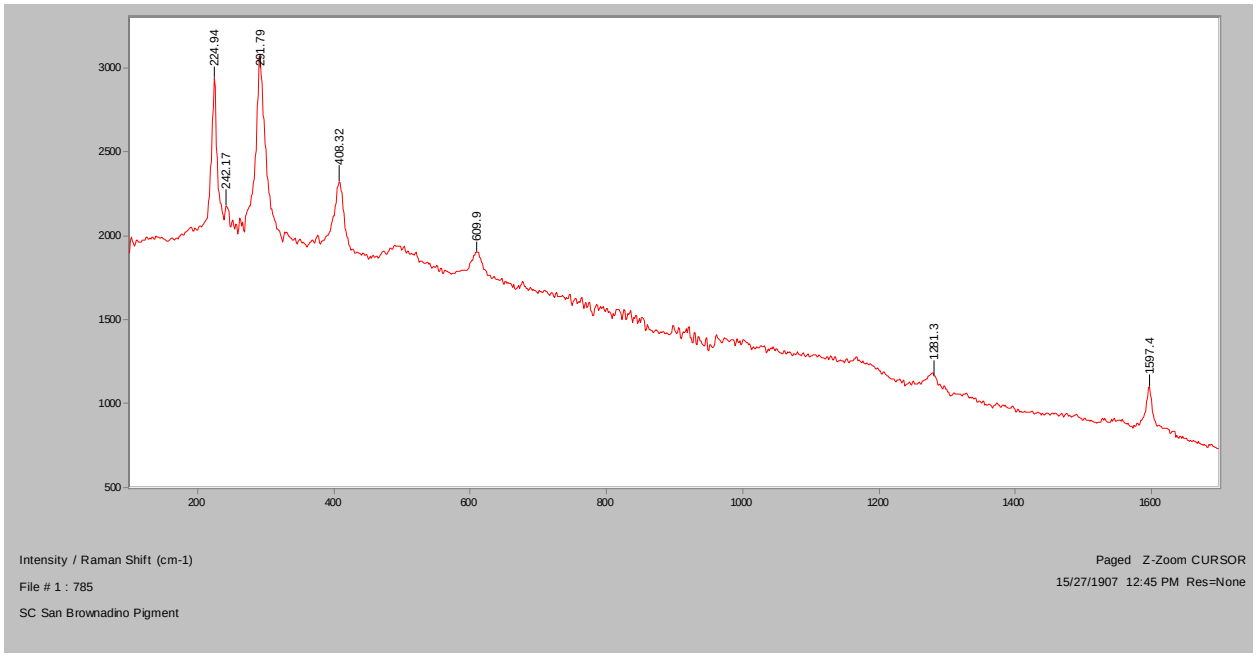

FT-Raman, 1064nm (in KBr)

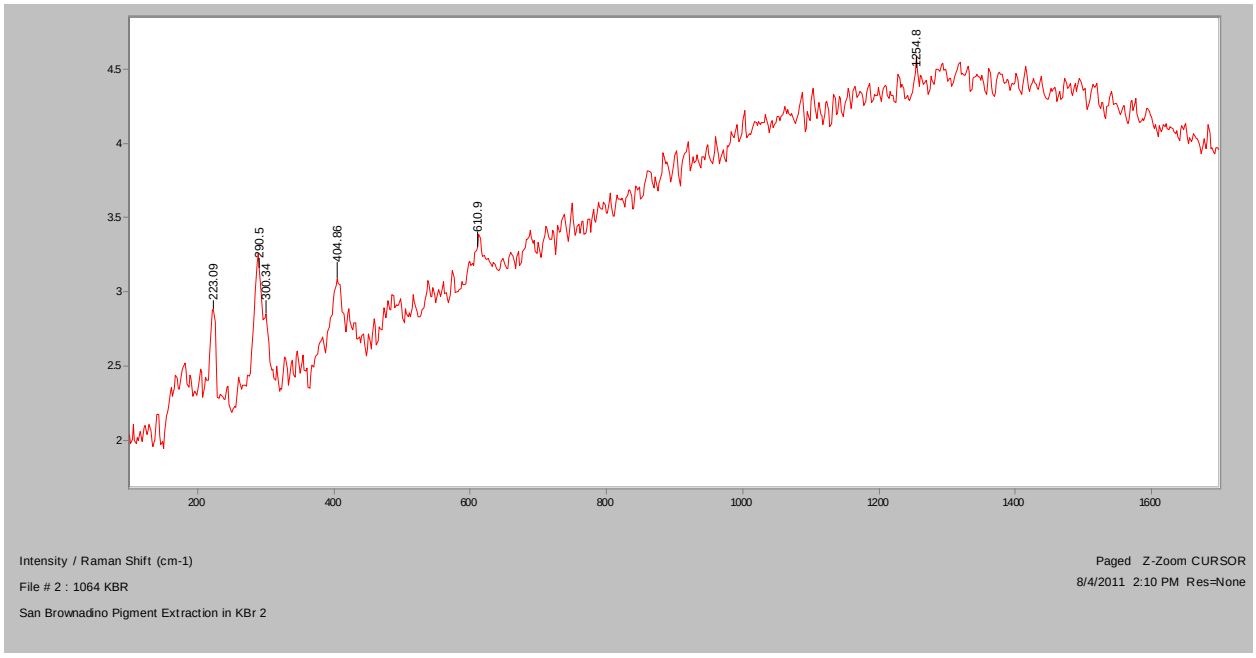

FT-IR (ATR)

UV-Vis

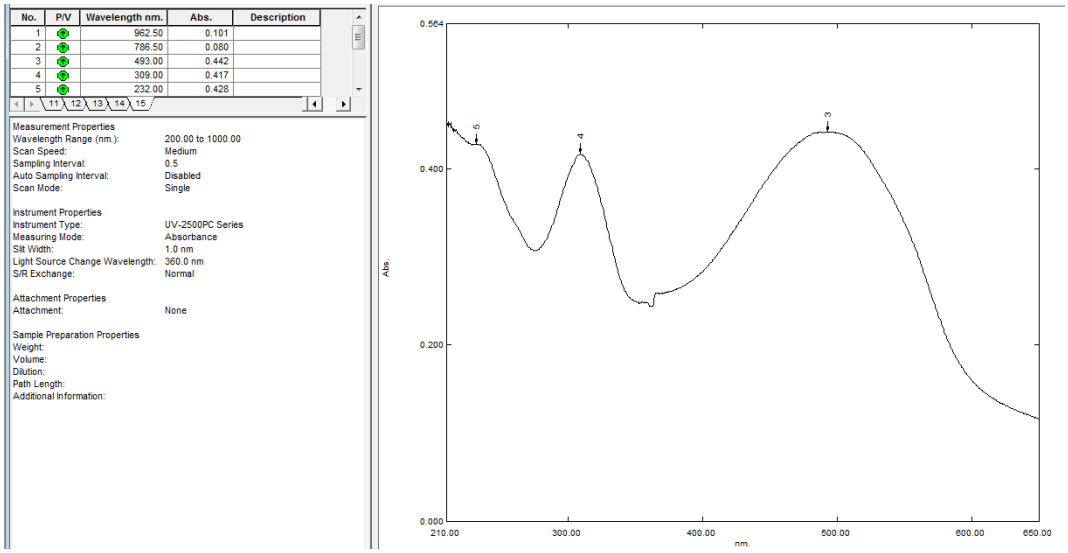

No.	P/V	Wavelength nm.	Abs.	Description
1		962.50	0.101	
2		786.50	0.080	
3		493.00	0.442	
4		309.00	0.417	
5		232.00	0.428	

Measurement Properties
Wavelength Range (nm.): 200.00 to 1000.00
Scan Speed: Medium
Sampling Interval: 0.5
Auto Sampling Interval: Disabled
Scan Mode: Single

Instrument Properties
Instrument Type: UV-2500PC Series
Measuring Mode: Absorbance
Slit Width: 1.0 nm
Light Source Change Wavelength: 360.0 nm
S/R Exchange: Normal

Attachment Properties
Attachment: None

Sample Preparation Properties
Weight:
Volume:
Dilution:
Path Length:
Additional Information:

Roan 2

Normal Raman, 488nm

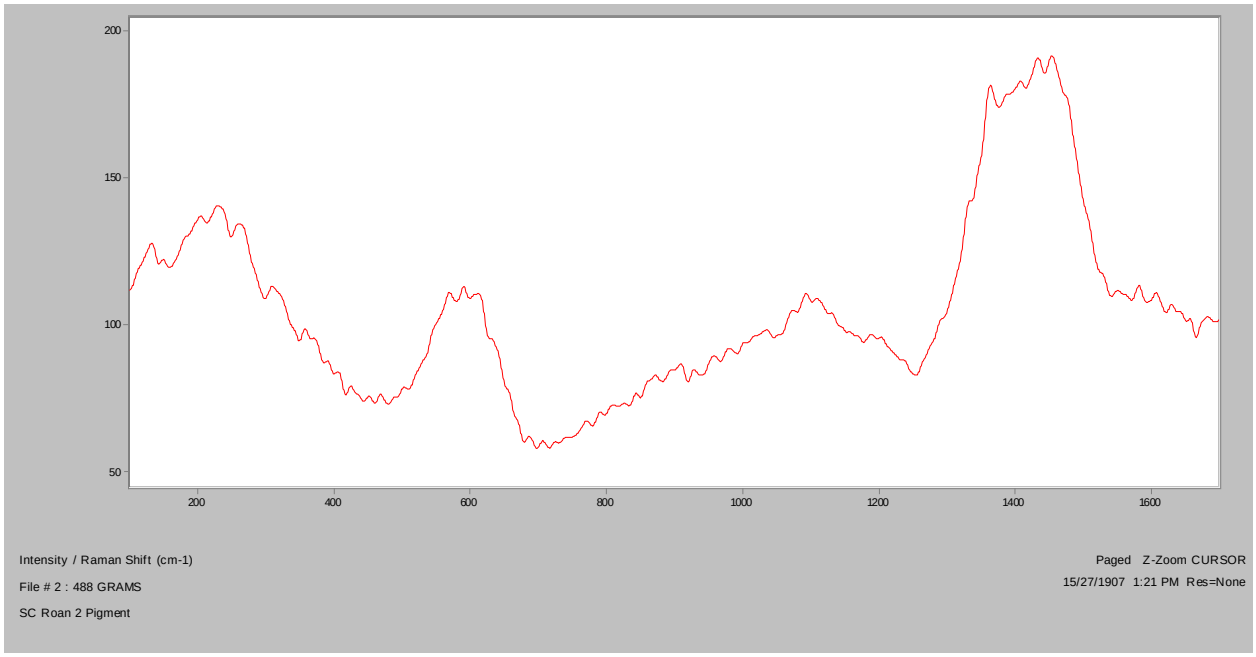

Normal Raman, 633nm

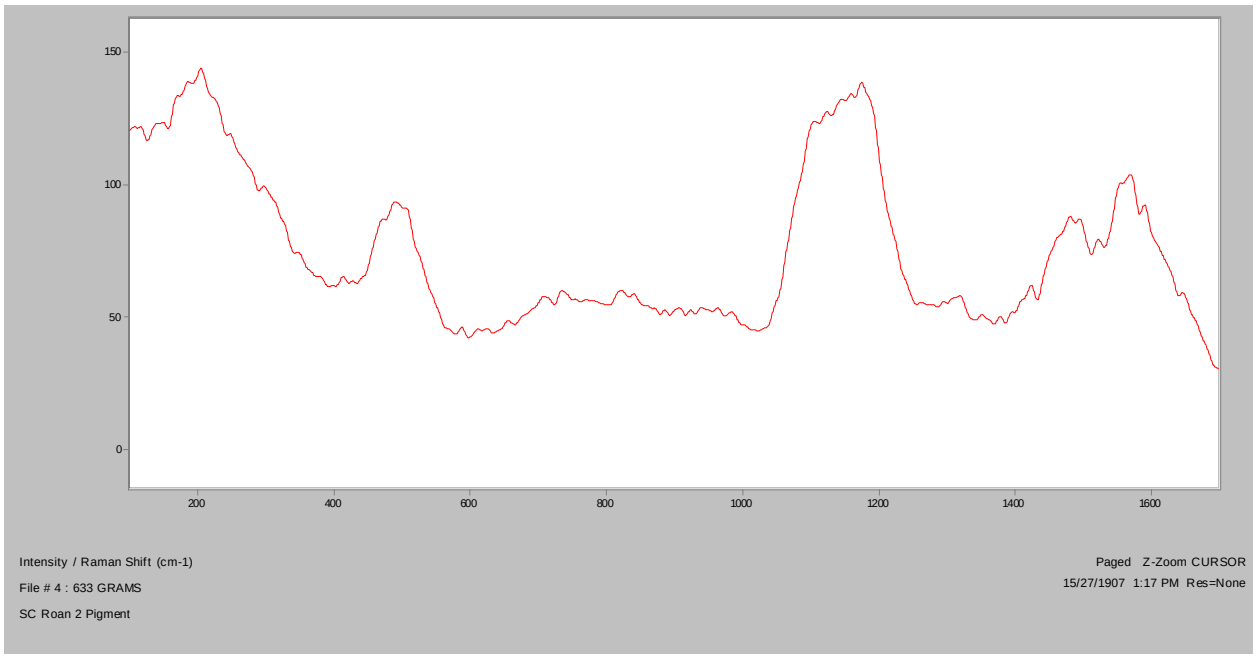

Normal Raman, 785nm

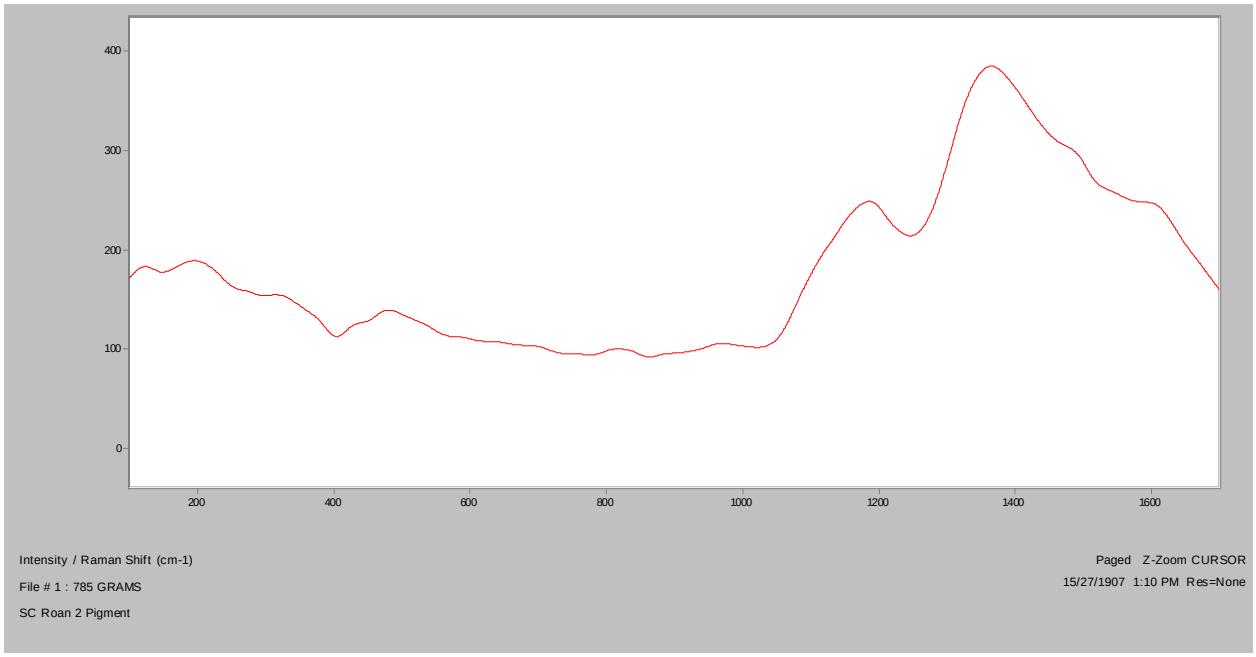

FT-IR (ATR)

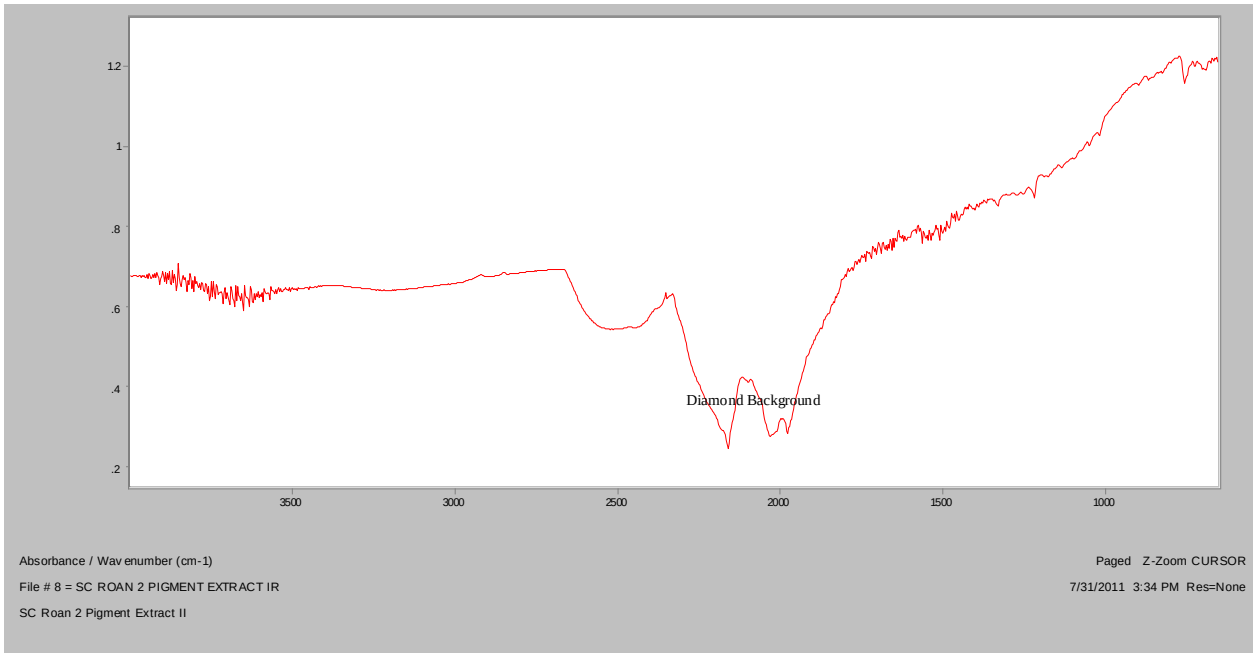

UV-Vis

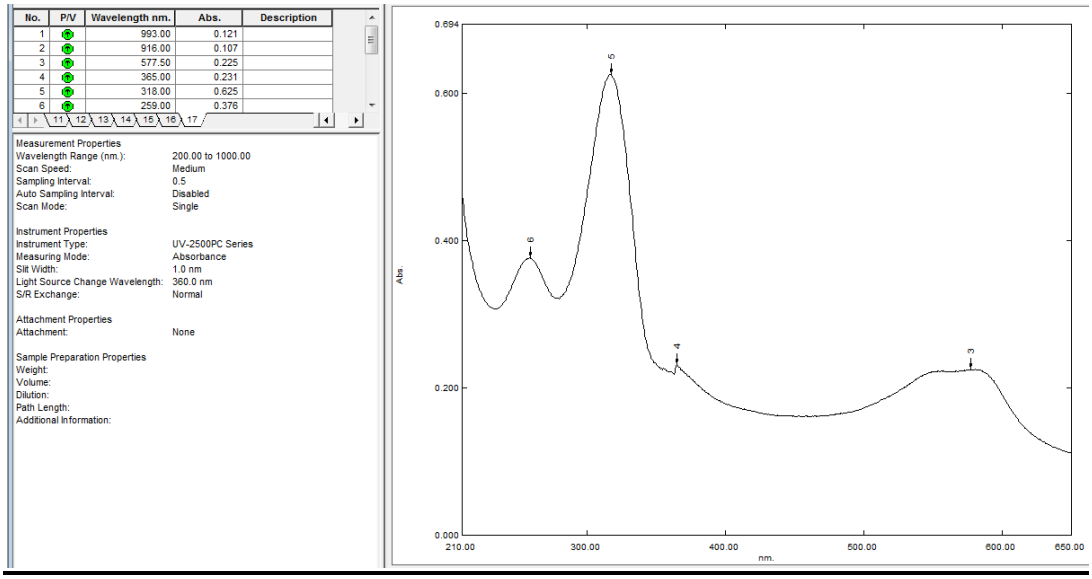

No.	P/V	Wavelength nm.	Abs.	Description
1		993.00	0.121	
2		916.00	0.107	
3		577.50	0.225	
4		365.00	0.231	
5		318.00	0.625	
6		259.00	0.376	

11 12 13 14 15 16 17

Measurement Properties
Wavelength Range (nm.): 200.00 to 1000.00
Scan Speed: Medium
Sampling Interval: 0.5
Auto Sampling Interval: Disabled
Scan Mode: Single

Instrument Properties
Instrument Type: UV-2500PC Series
Measuring Mode: Absorbance
Slit Width: 1.0 nm
Light Source Change Wavelength: 360.0 nm
S/R Exchange: Normal

Attachment Properties
Attachment: None

Sample Preparation Properties
Weight:
Volume:
Dilution:
Path Length:
Additional Information:

Tokyo Pink

Normal Raman, 488nm

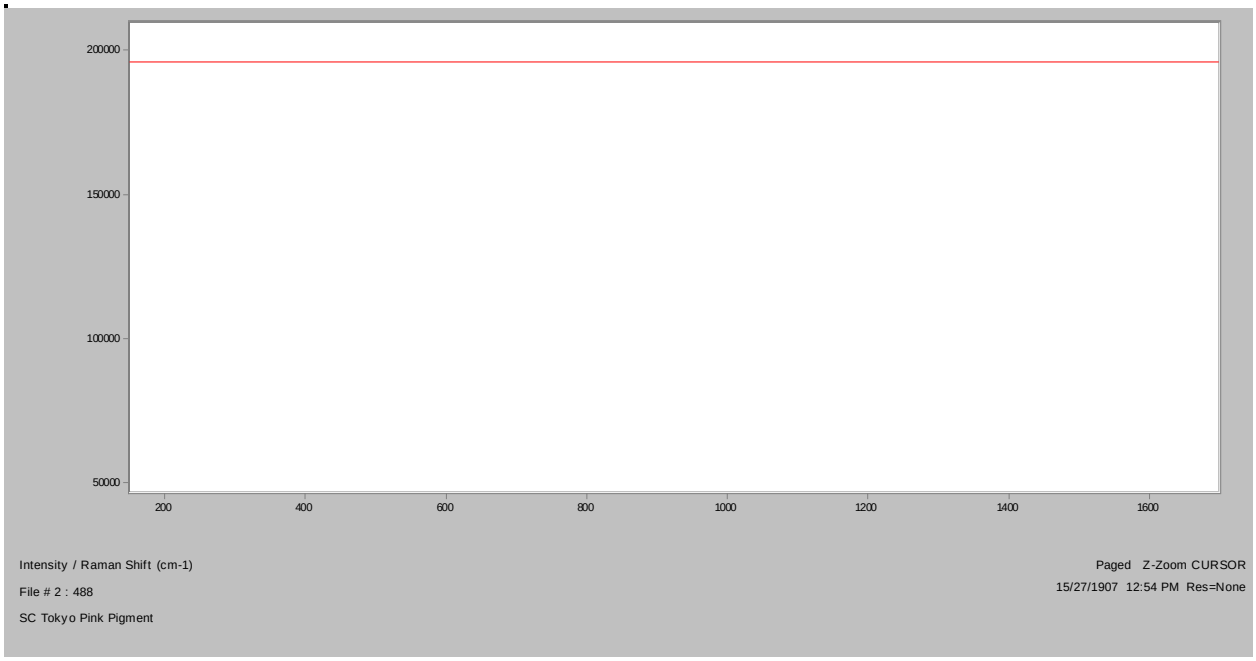

Normal Raman, 633nm

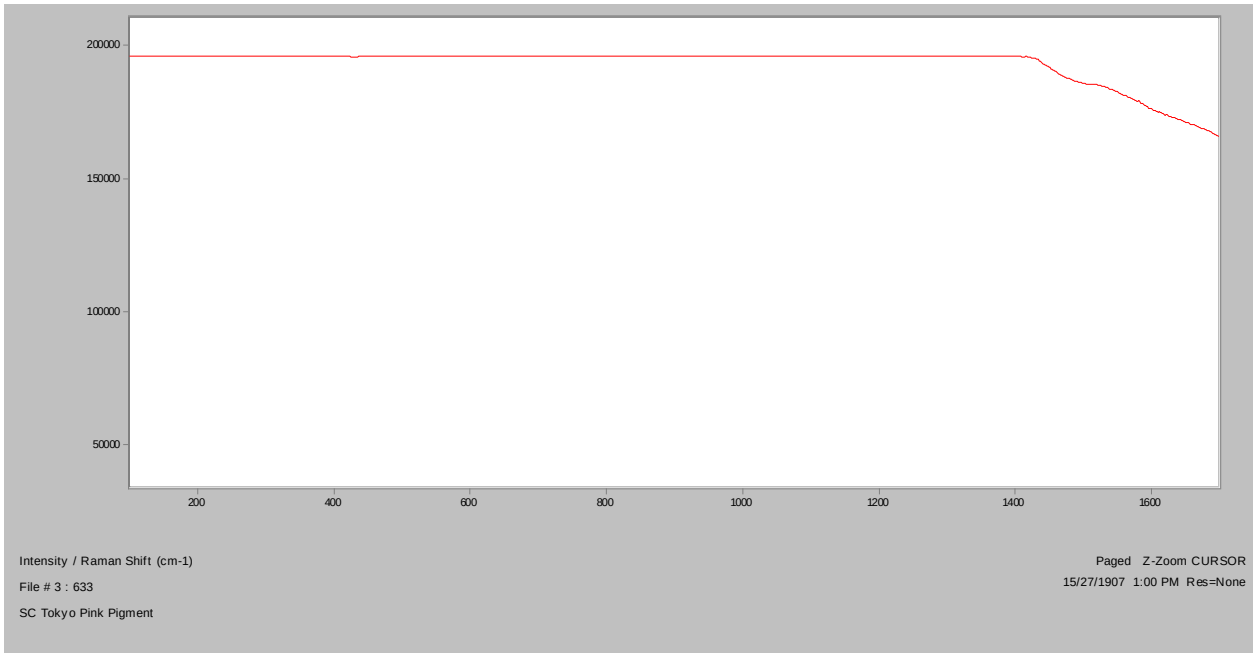

Normal Raman, 785nm

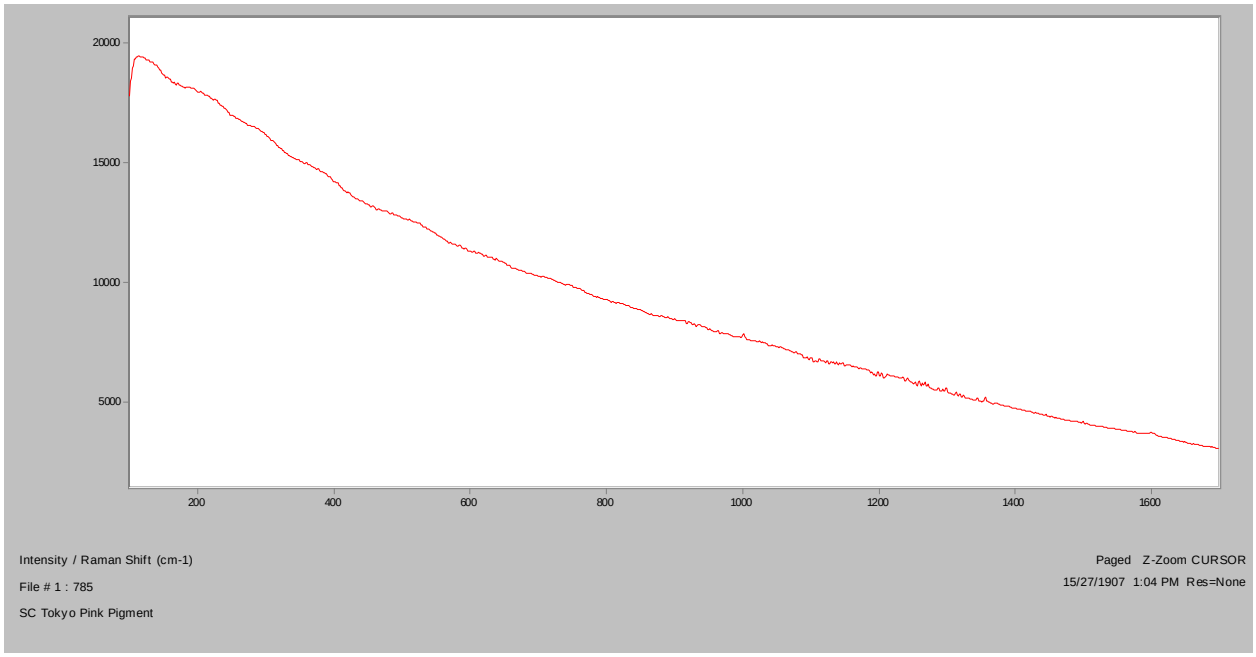

FT-IR (ATR)

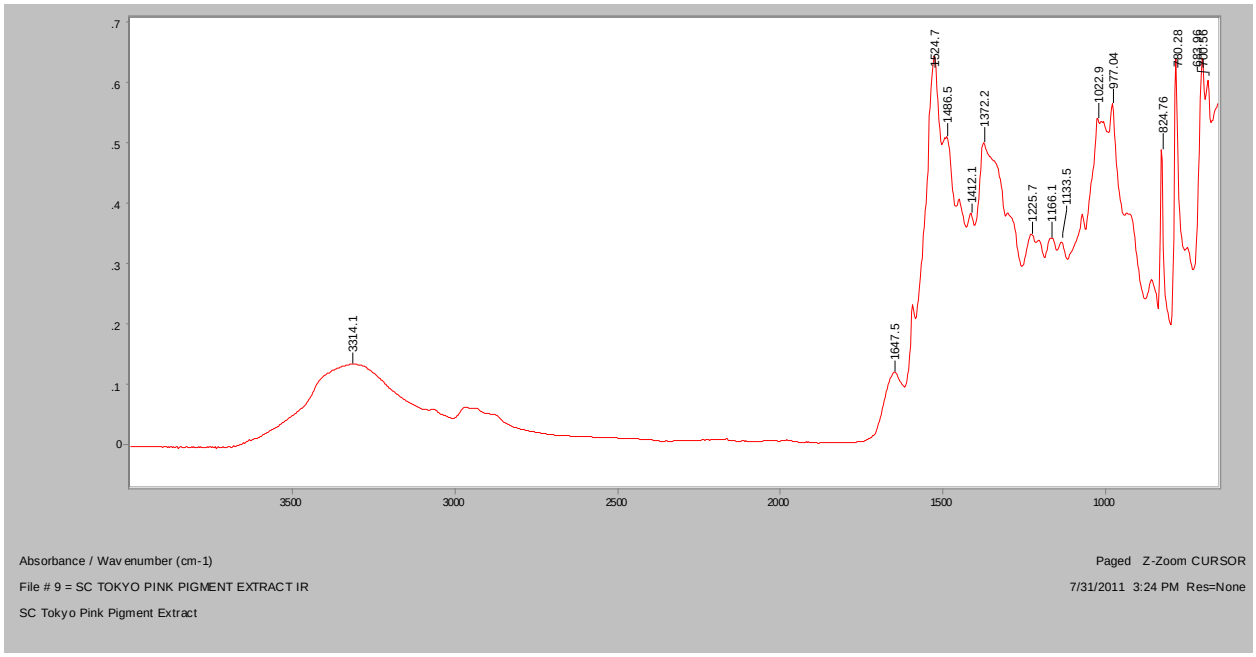

UV-Vis

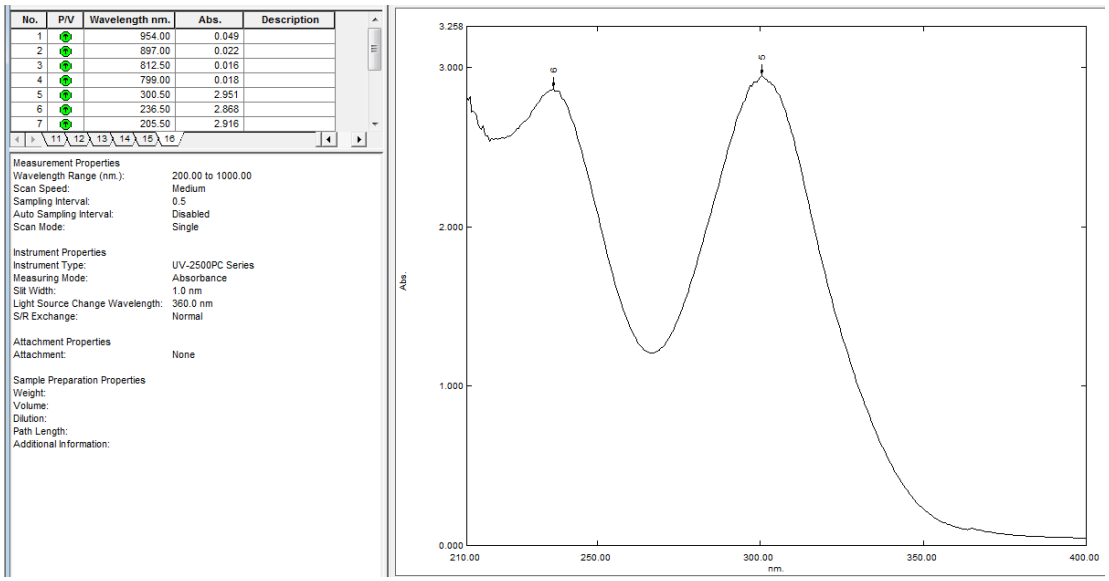

No.	P/V	Wavelength nm.	Abs.	Description
1		954.00	0.049	
2		897.00	0.022	
3		812.50	0.016	
4		799.00	0.018	
5		300.50	2.951	
6		236.50	2.868	
7		205.50	2.916	

11 12 13 14 15 16

Measurement Properties
Wavelength Range (nm.): 200.00 to 1000.00
Scan Speed: Medium
Sampling Interval: 0.5
Auto Sampling Interval: Disabled
Scan Mode: Single

Instrument Properties
Instrument Type: UV-2500PC Series
Measuring Mode: Absorbance
Slit Width: 1.0 nm
Light Source Change Wavelength: 360.0 nm
S/R Exchange: Normal

Attachment Properties
Attachment: None

Sample Preparation Properties
Weight:
Volume:
Dilution:
Path Length:
Additional Information:

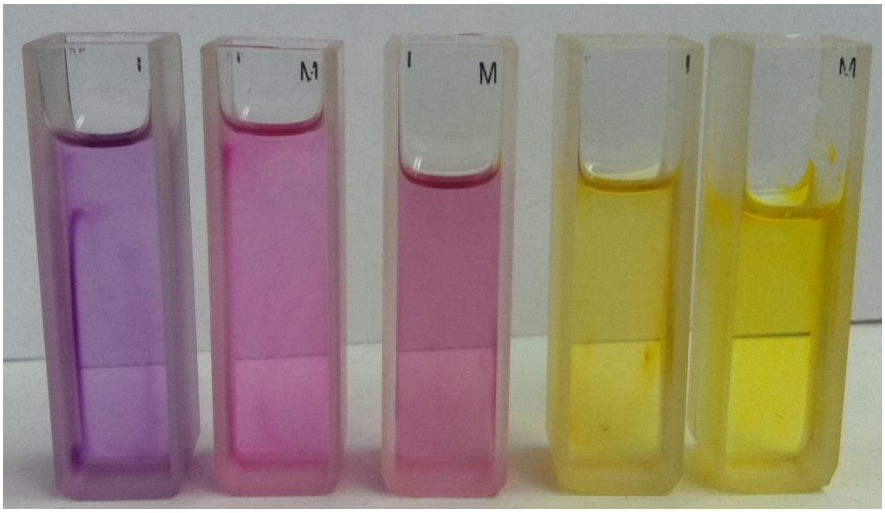

Candy Apple Red, Red Hot, Marz, Dolemite, Blisterine

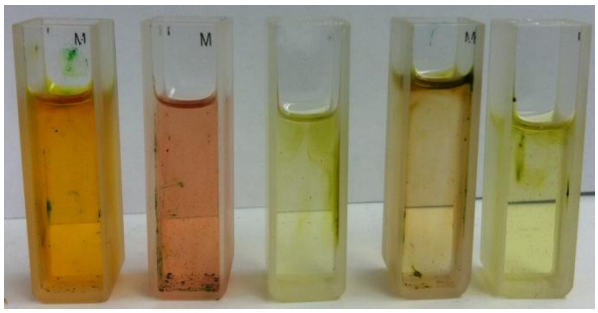

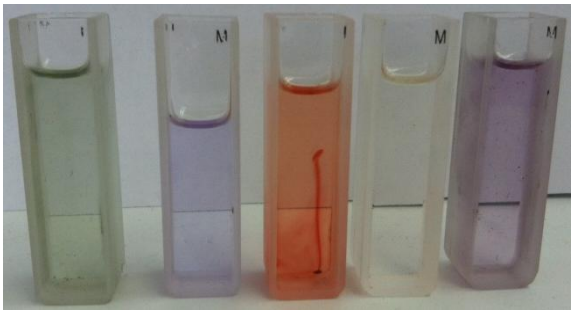

Sassygrass, Tastywaves, Bellbottom Blue, SRV Teal 2, Muddy Water Blue, Ripple, Razberry Creem, San Brownadino, Tokyo Pink, Black Cherry Roan 2

Flying Tigers Tattoo Ink Pigment Extractions

Salmon Pink

Normal Raman, 488nm

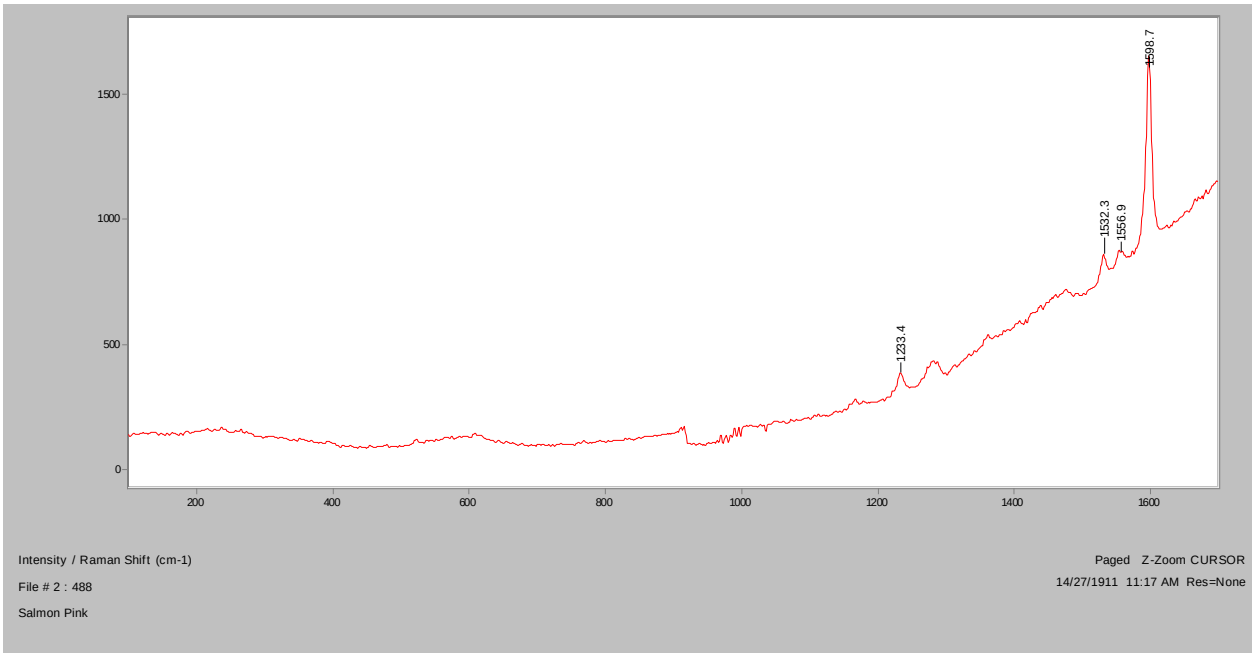

Normal Raman, 633nm

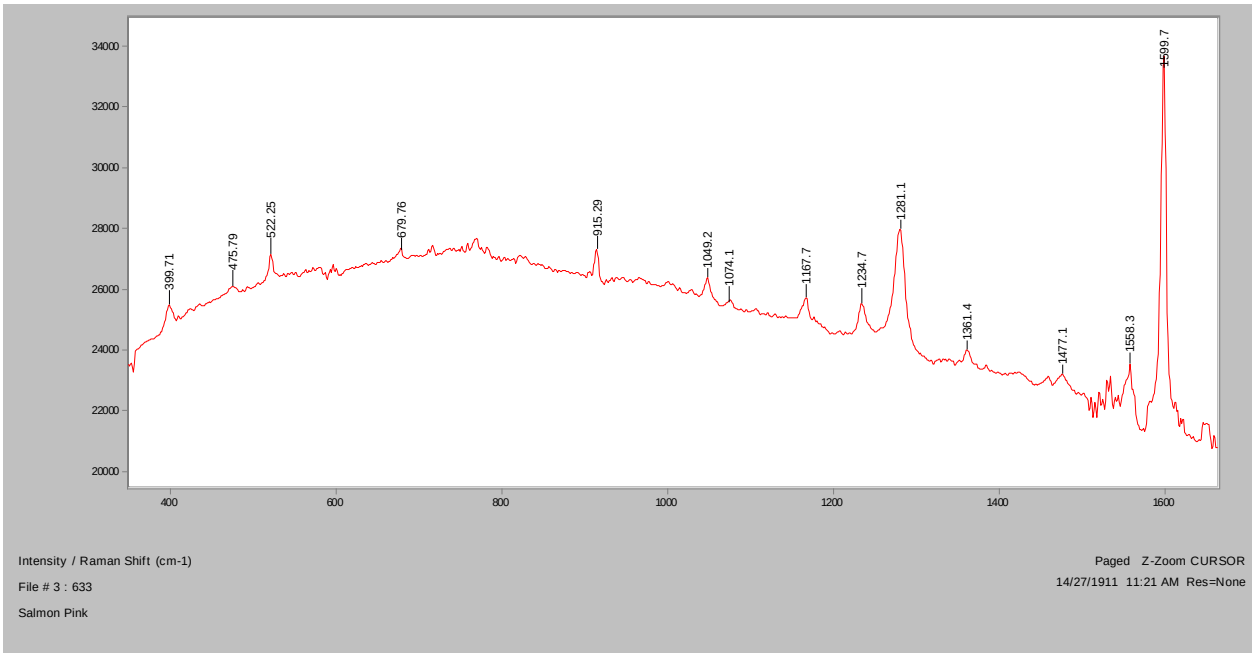

Normal Raman, 785nm

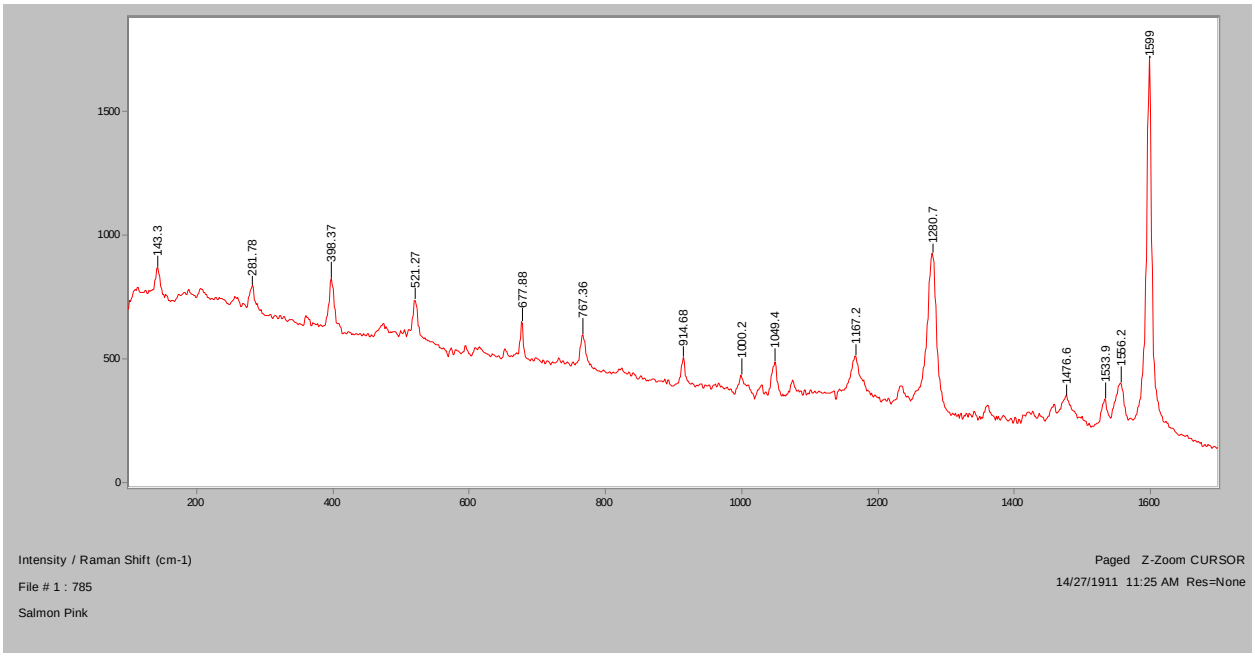

Pink Red

Normal Raman, 488nm

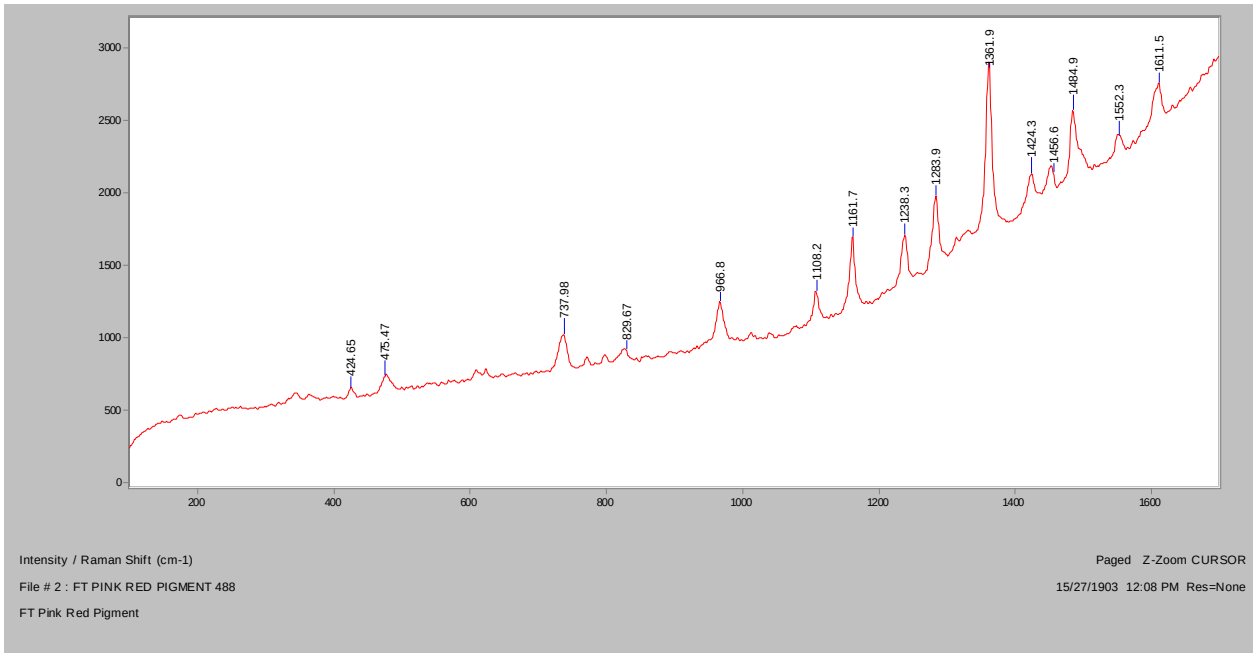

Normal Raman, 633nm

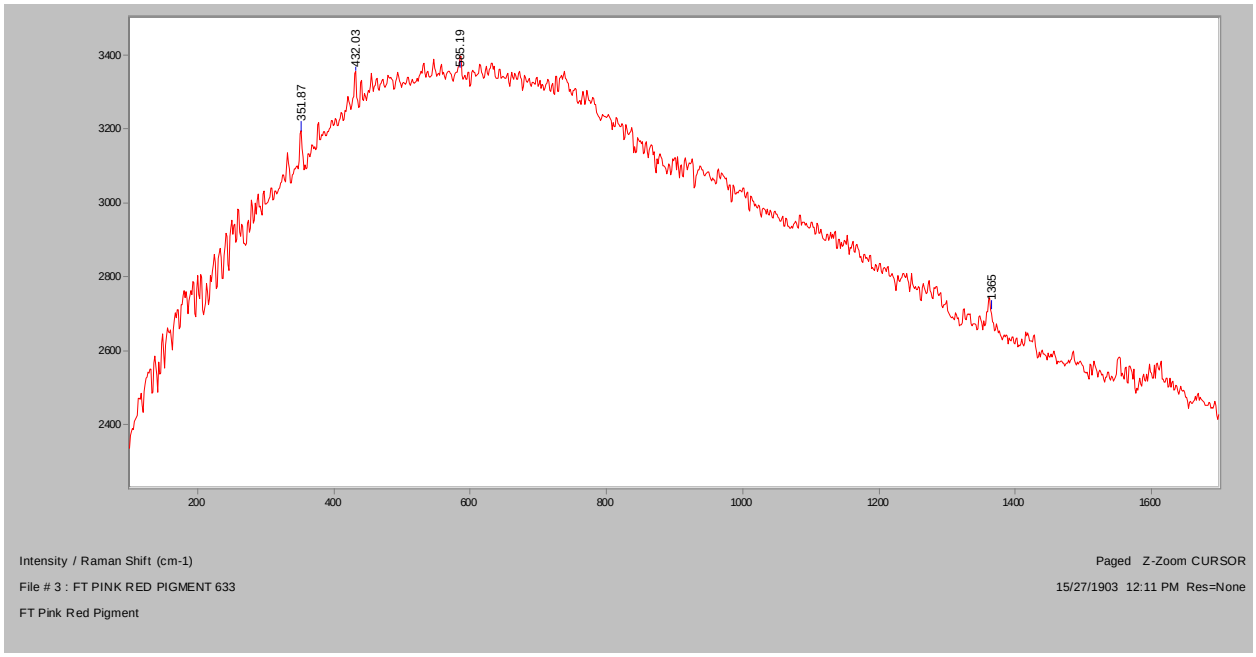

Normal Raman, 785nm

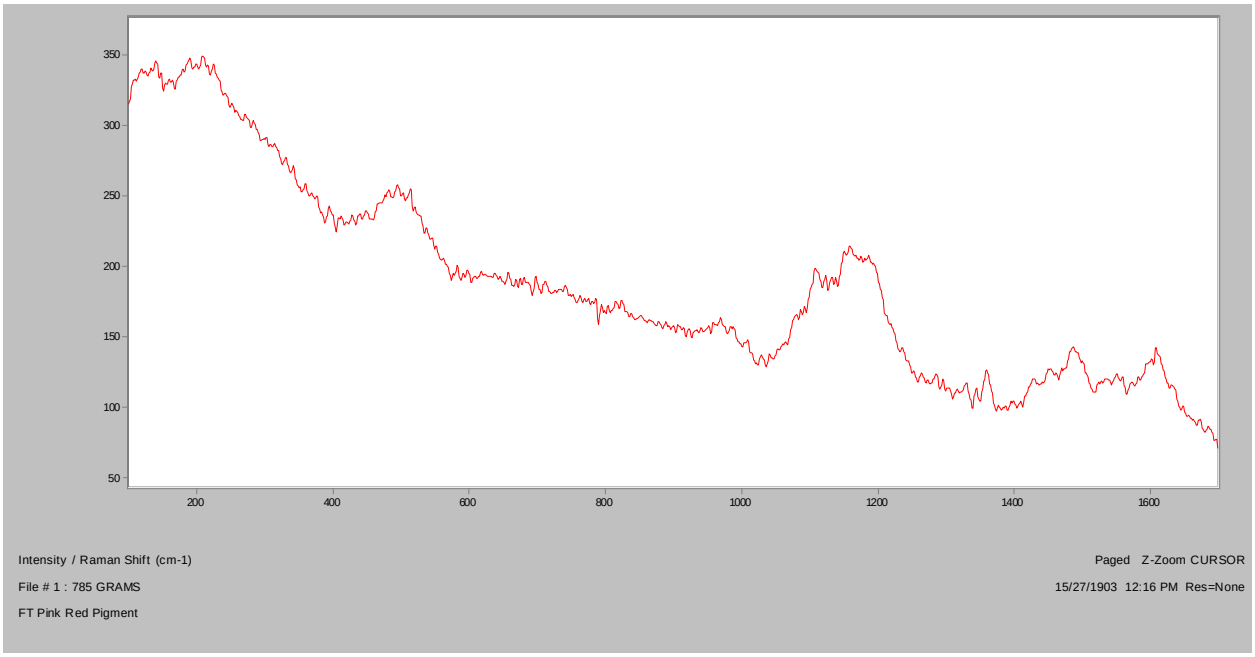

Magenta

Normal Raman, 488nm

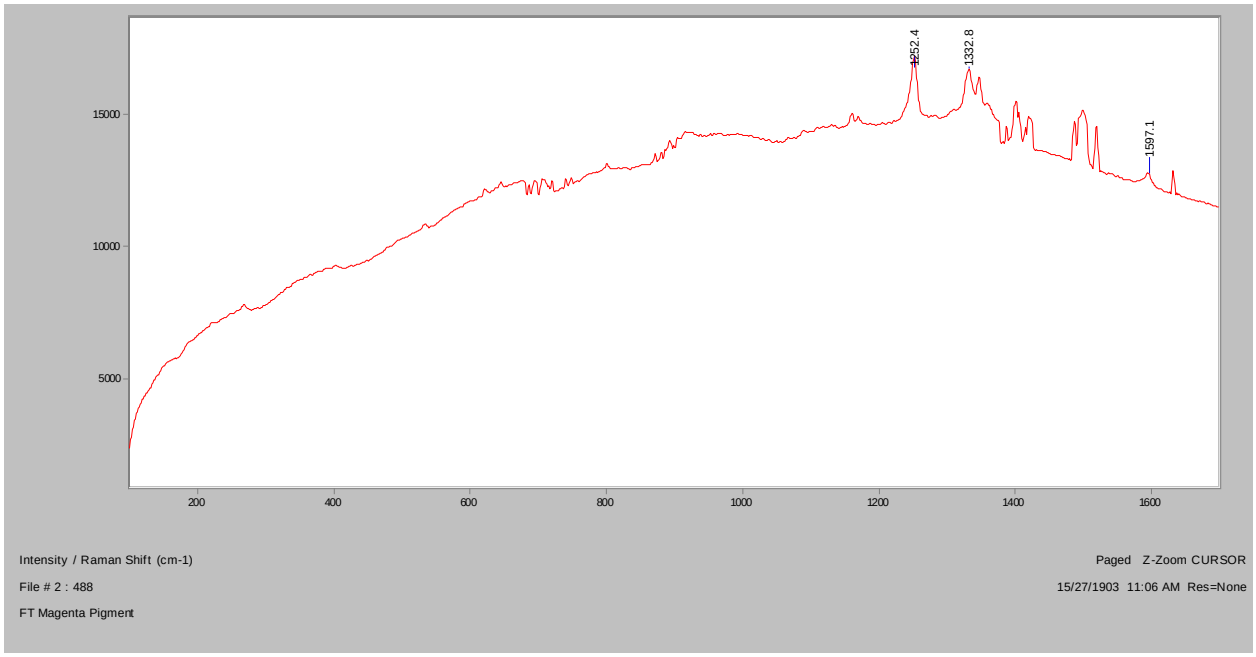

Normal Raman, 633nm

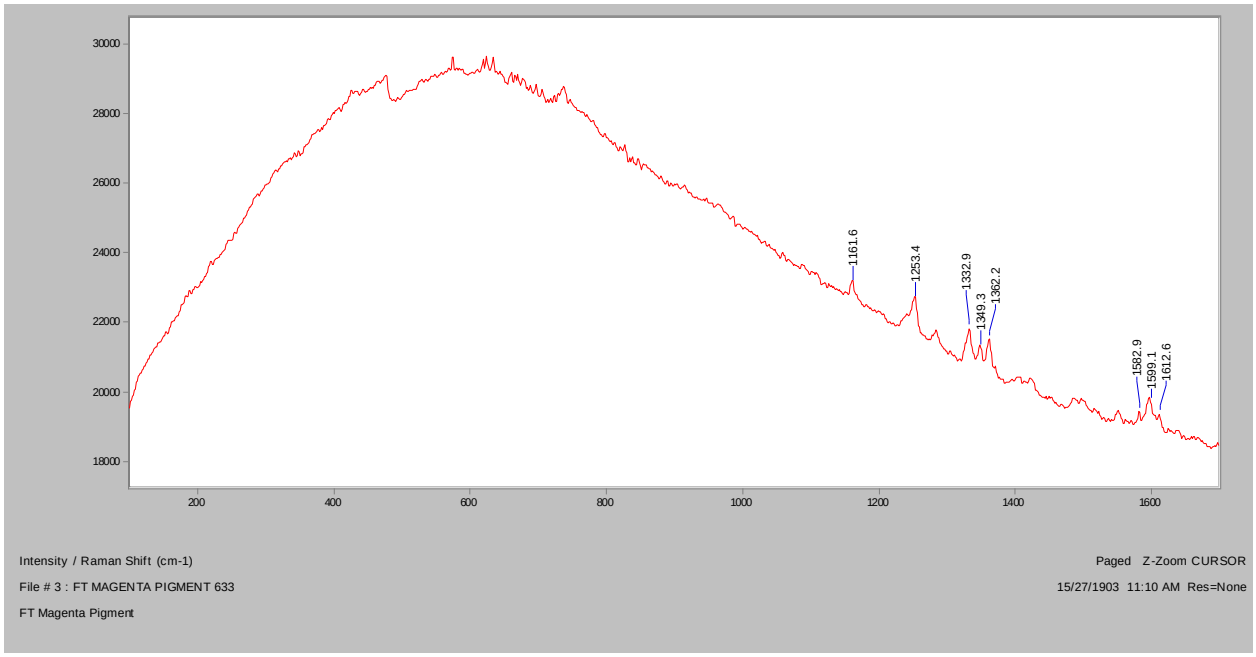

Normal Raman, 785nm

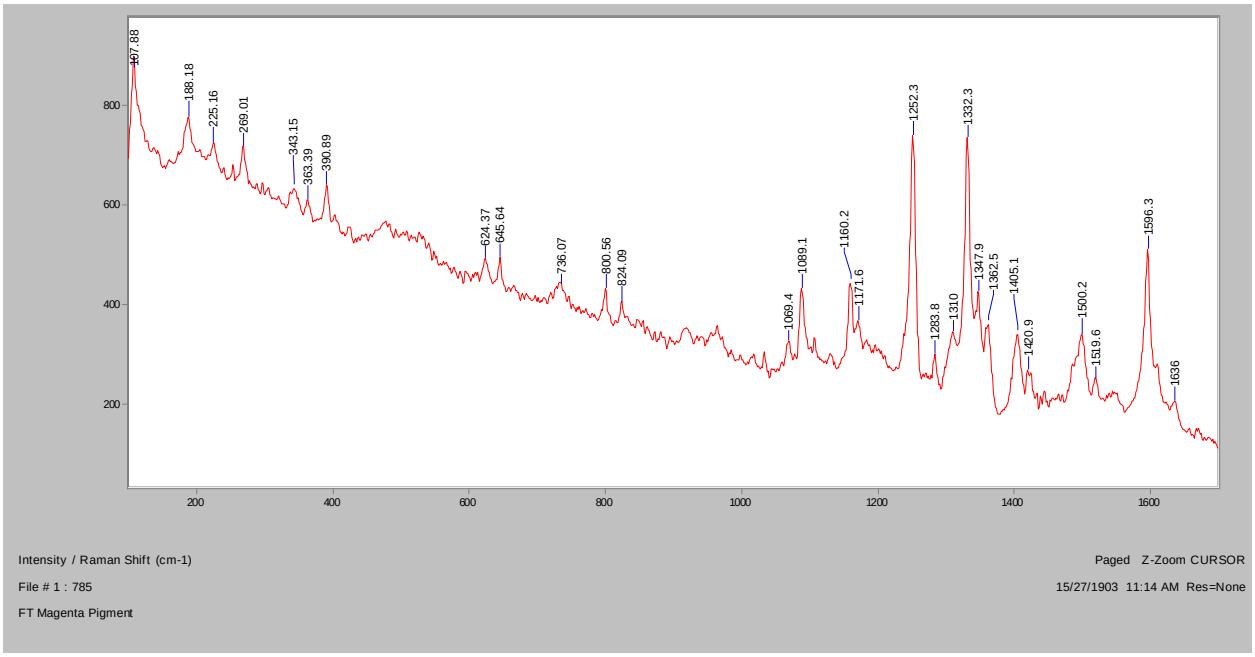

Chinese Red

Normal Raman, 488nm

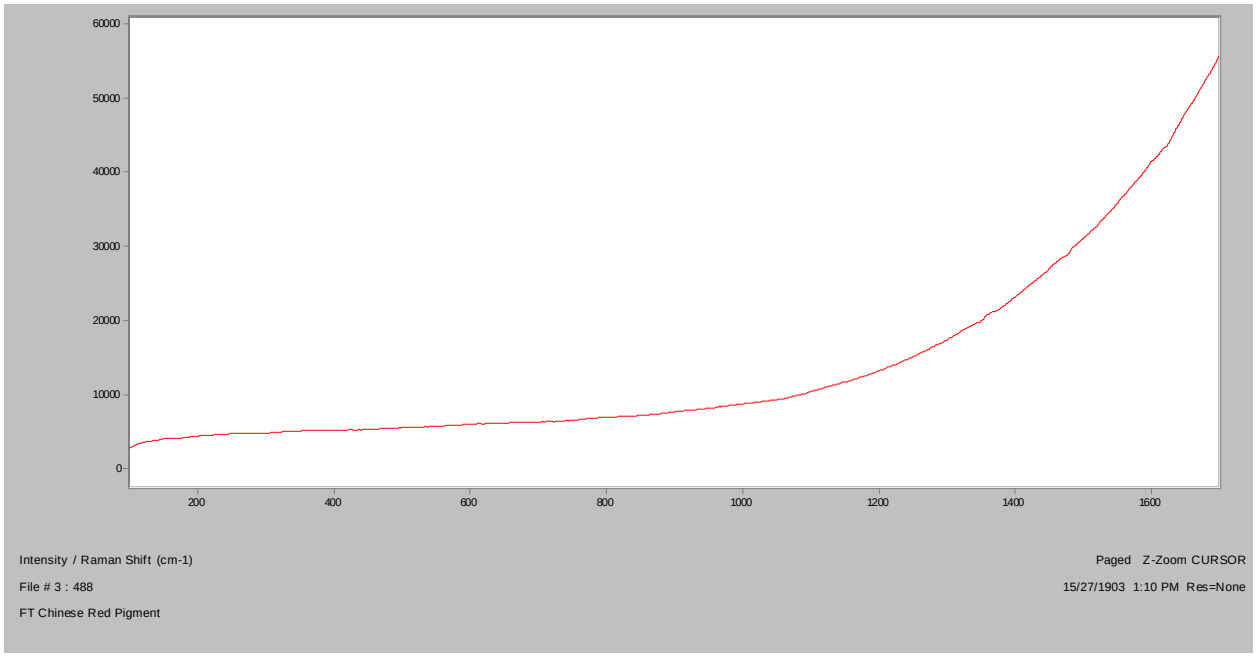

Normal Raman, 633nm

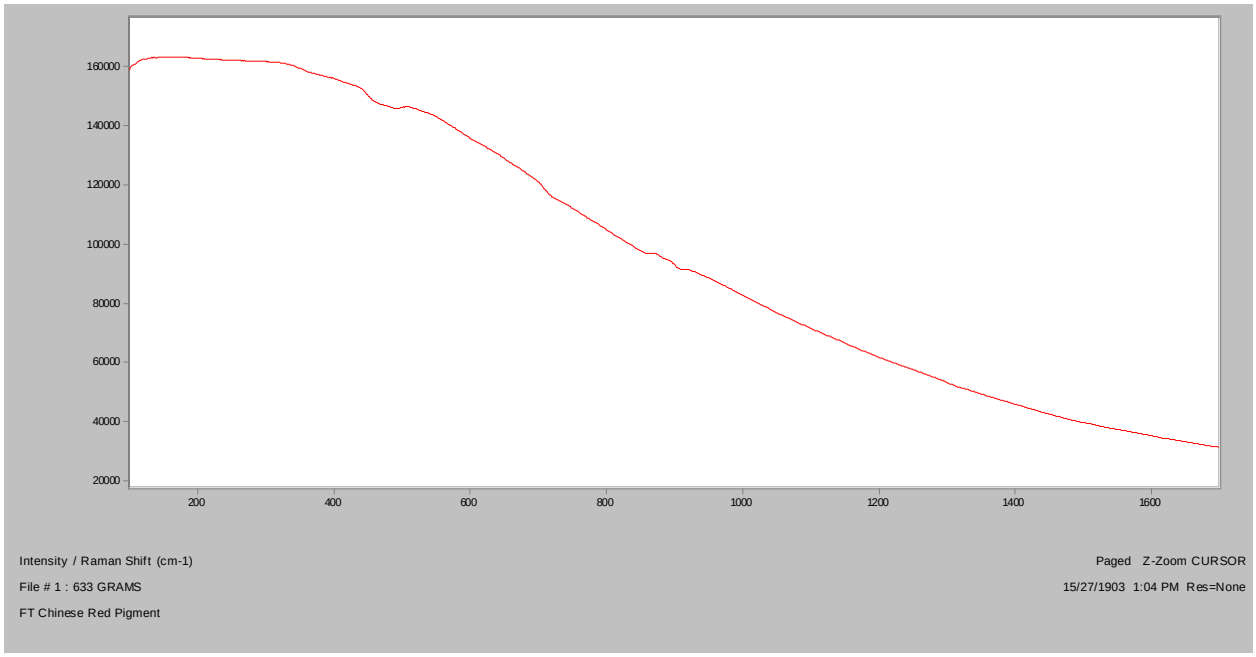

Normal Raman, 785nm

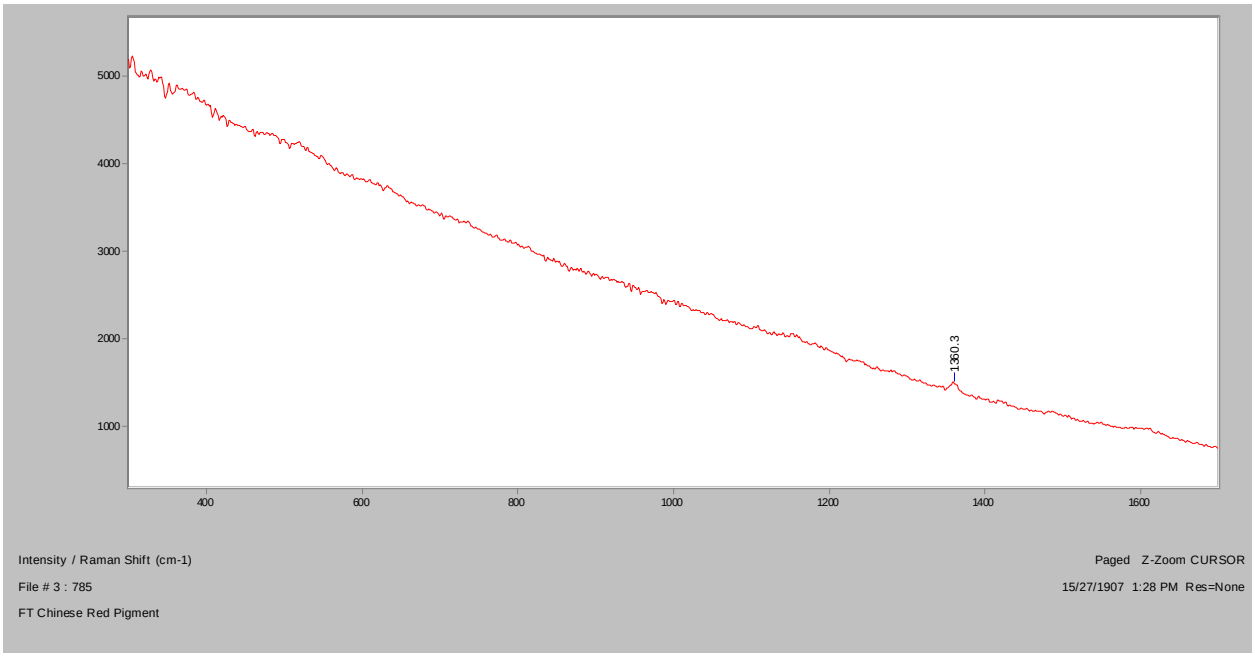

Bright Red

Normal Raman, 488nm

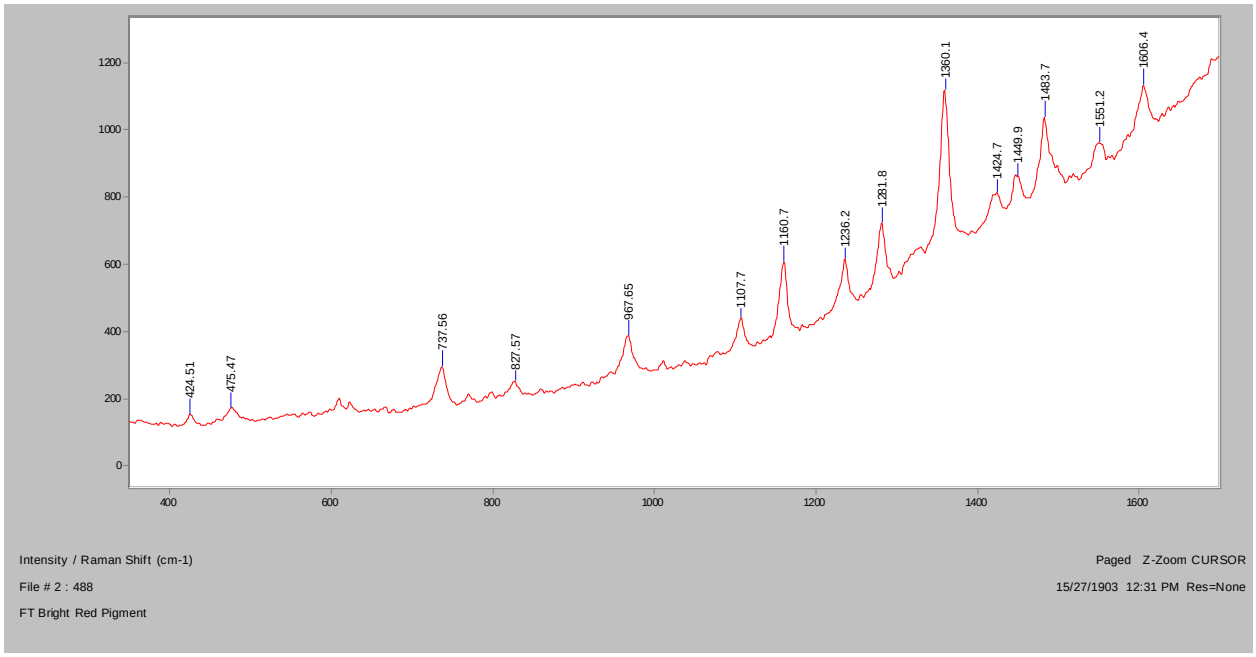

Normal Raman, 633nm

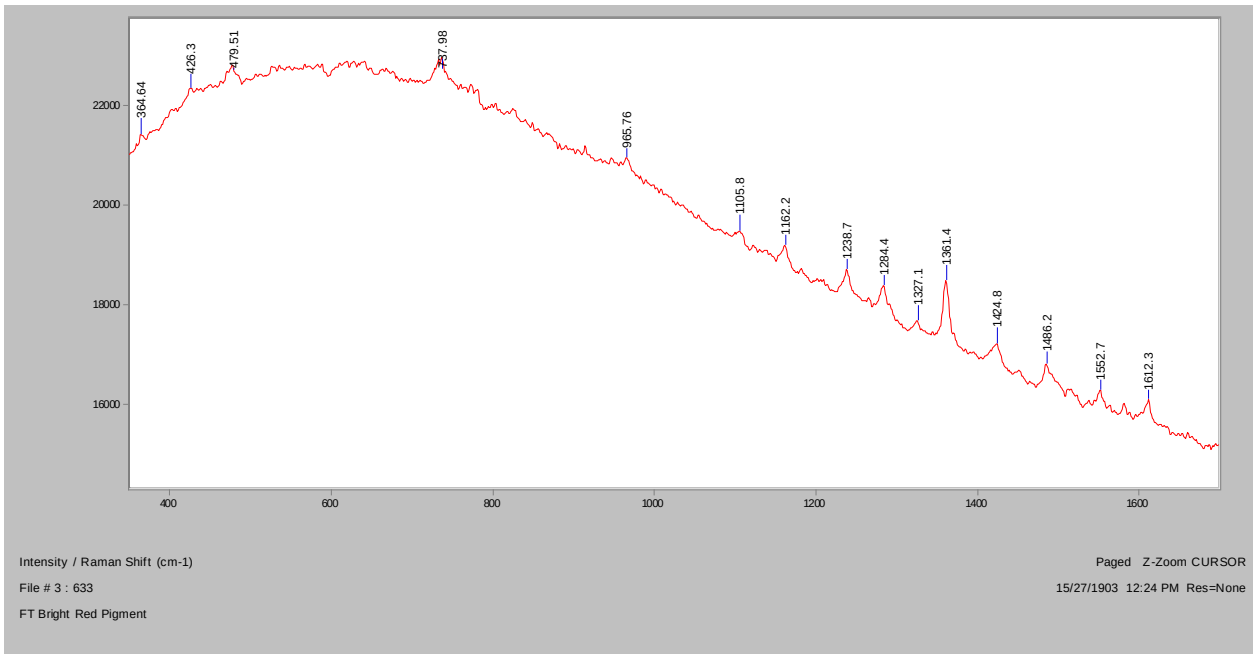

Normal Raman, 785nm

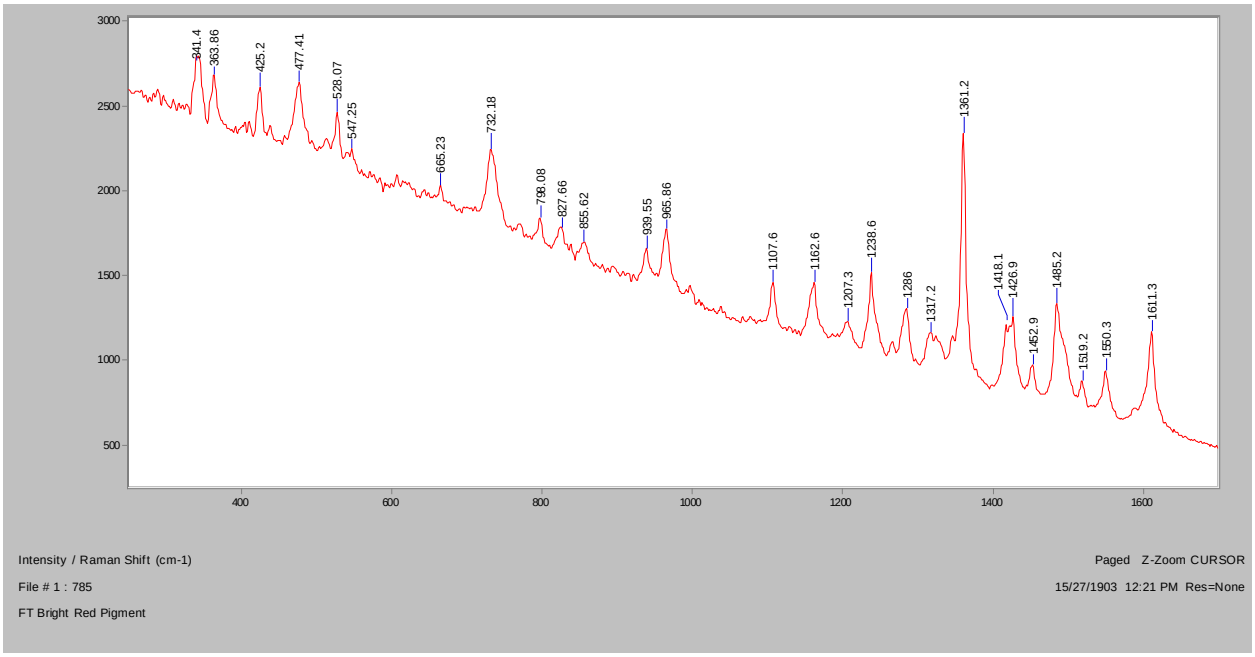

Rose Red

Normal Raman, 488nm

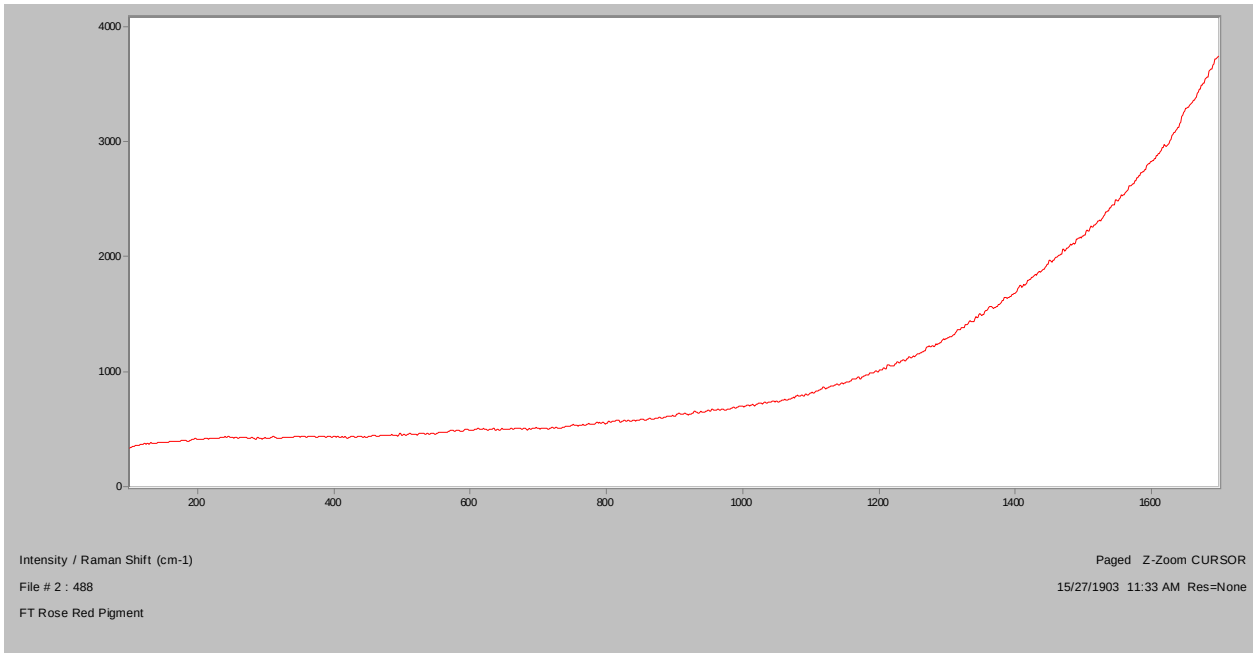

Normal Raman, 633nm

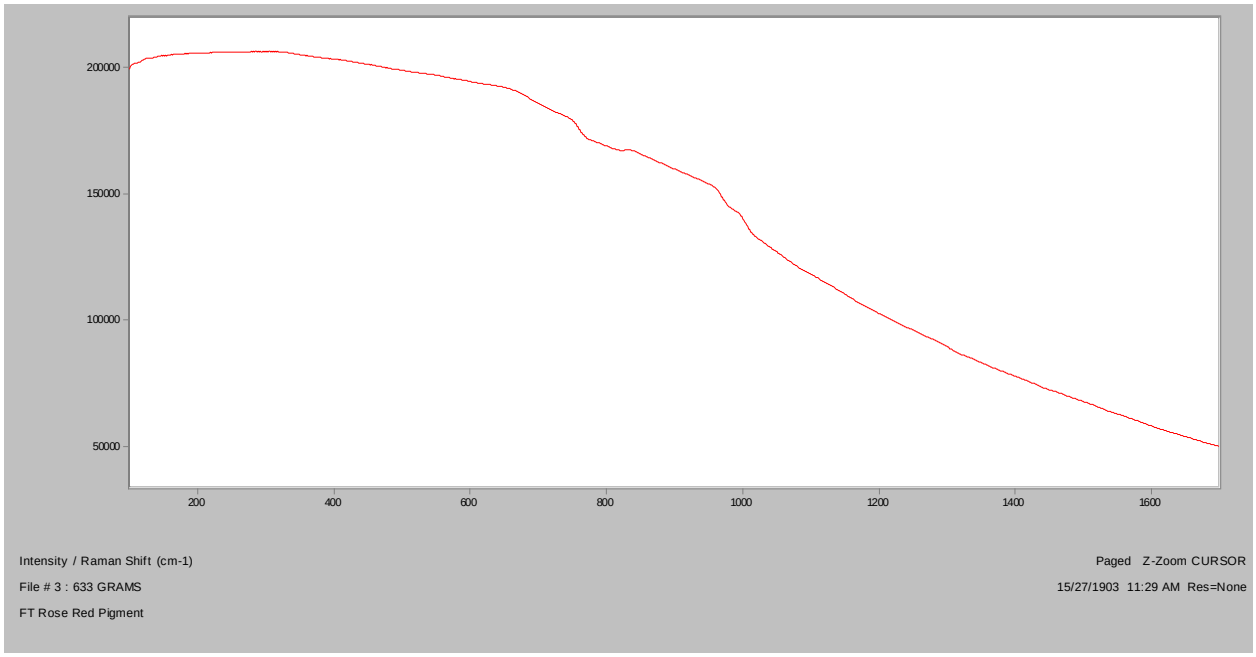

Normal Raman, 785nm

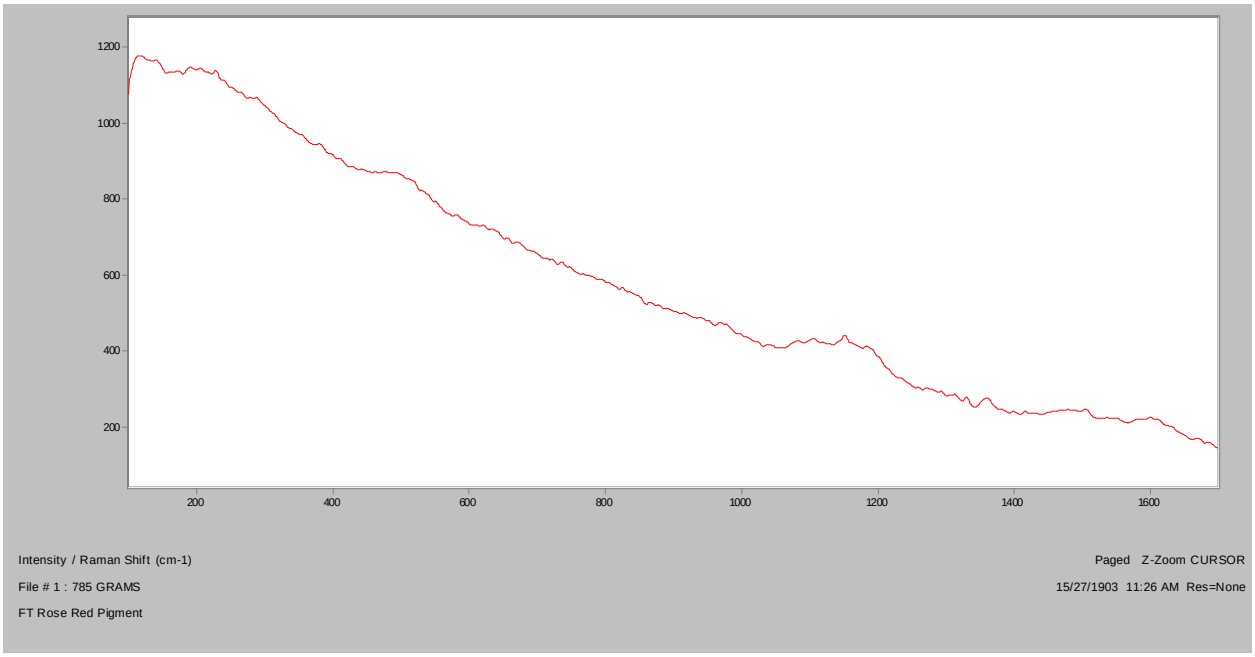

Mulberry

Normal Raman, 488nm

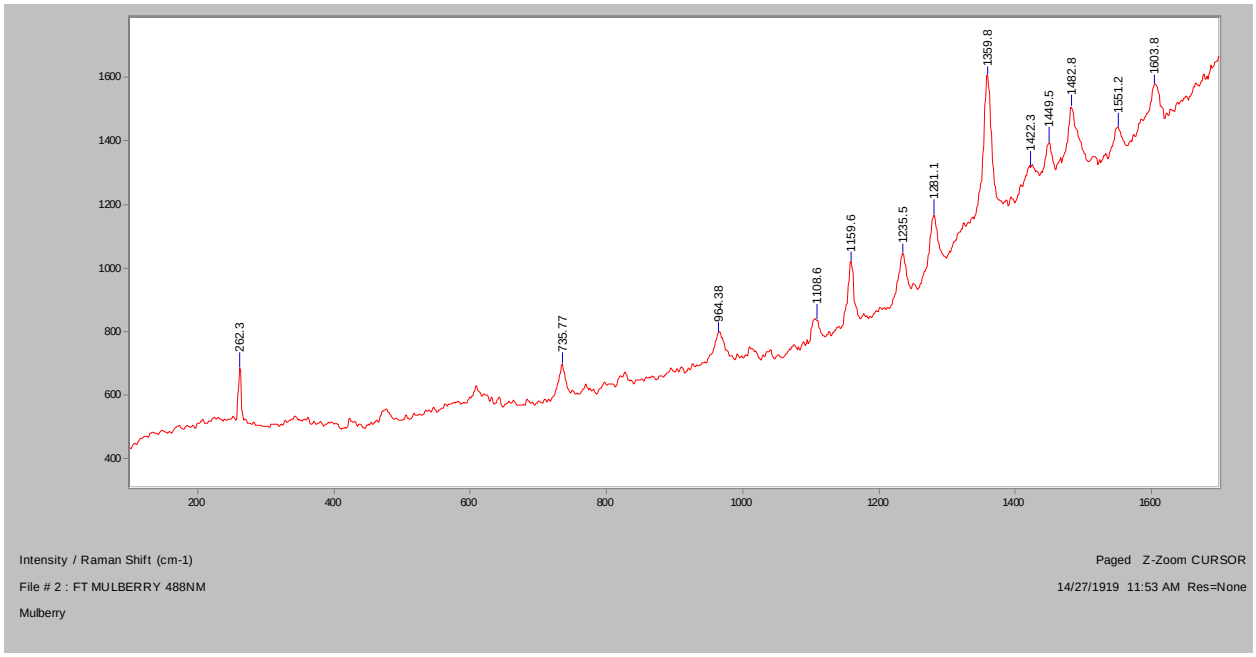

Normal Raman, 633nm

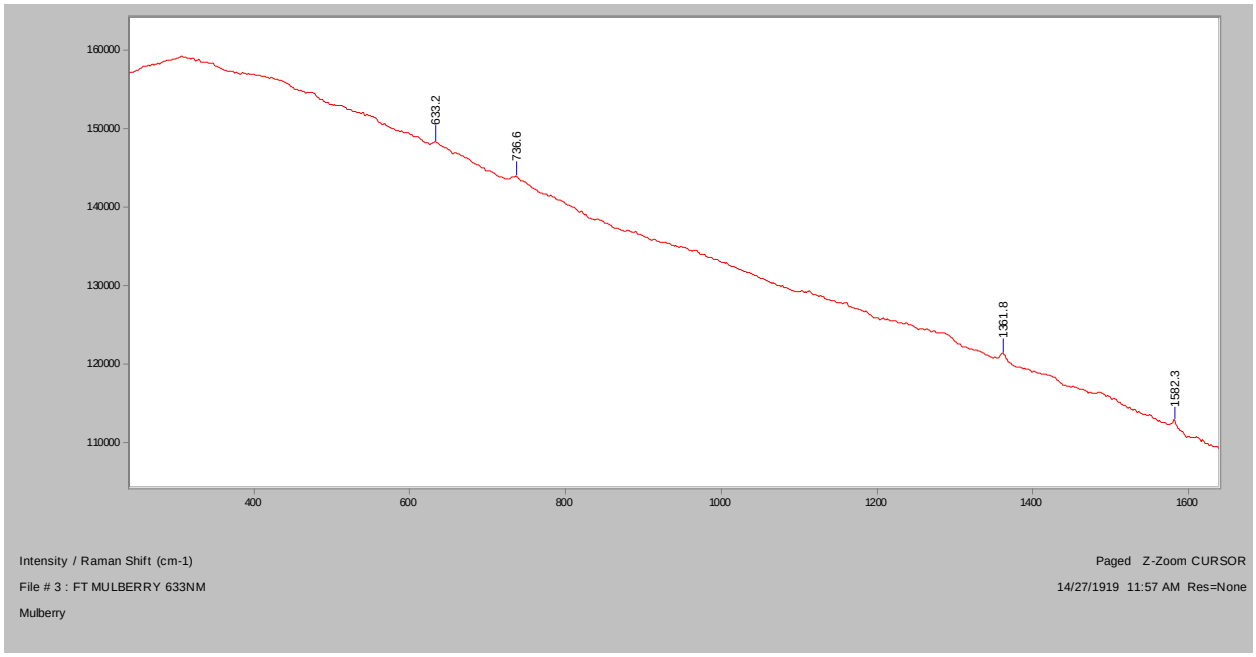

Normal Raman, 785nm

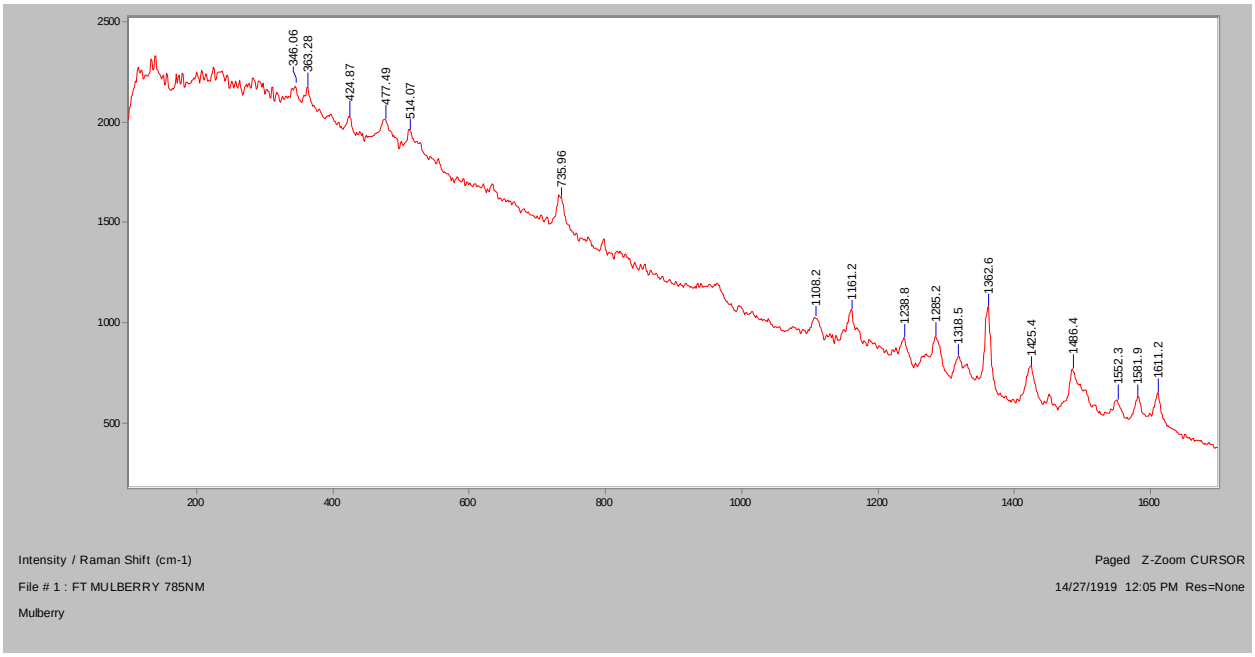

Dark Red

Normal Raman, 488nm

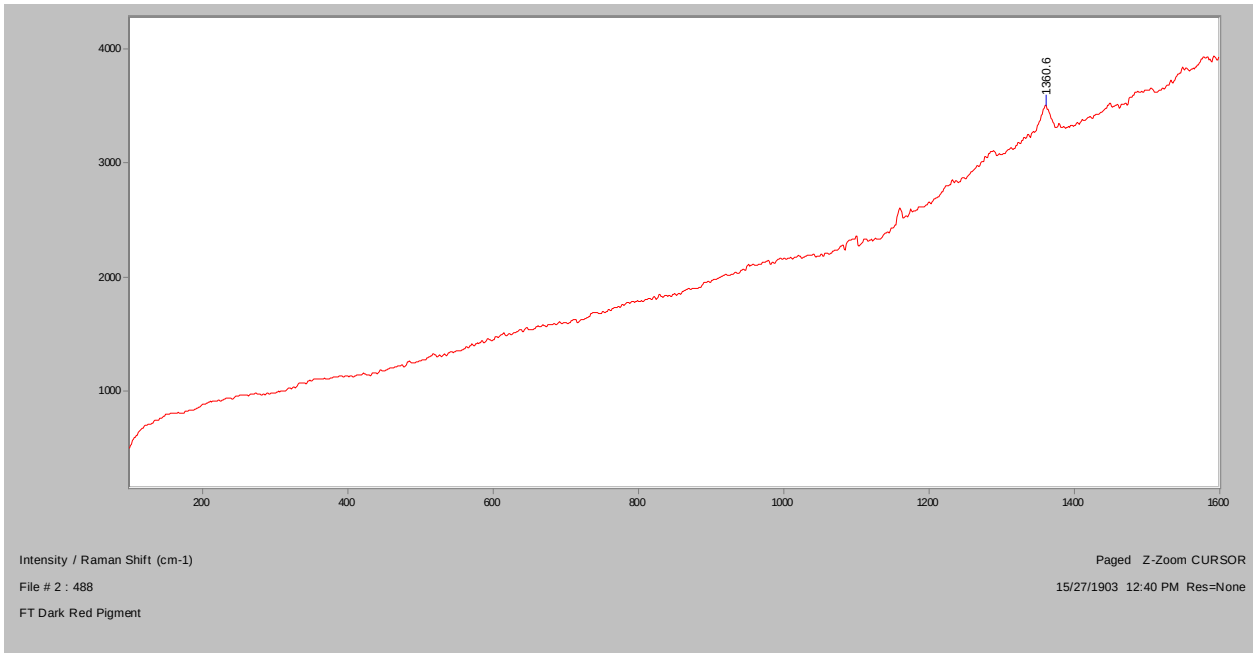

Normal Raman, 633nm

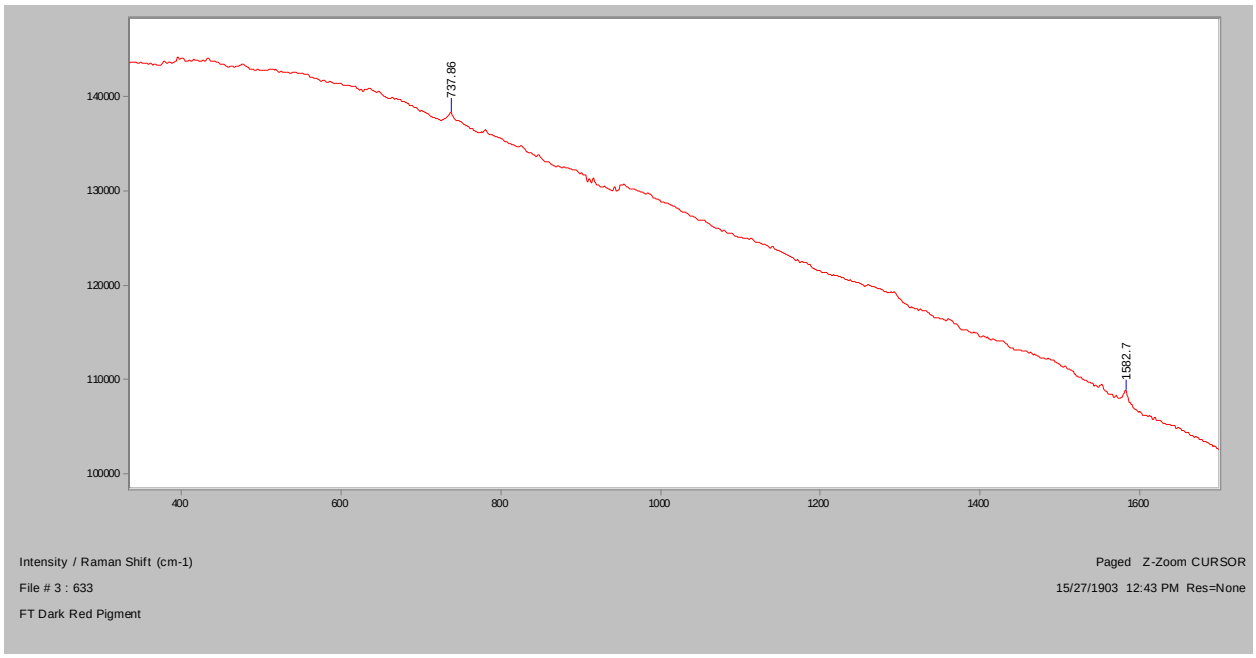

Normal Raman, 785nm

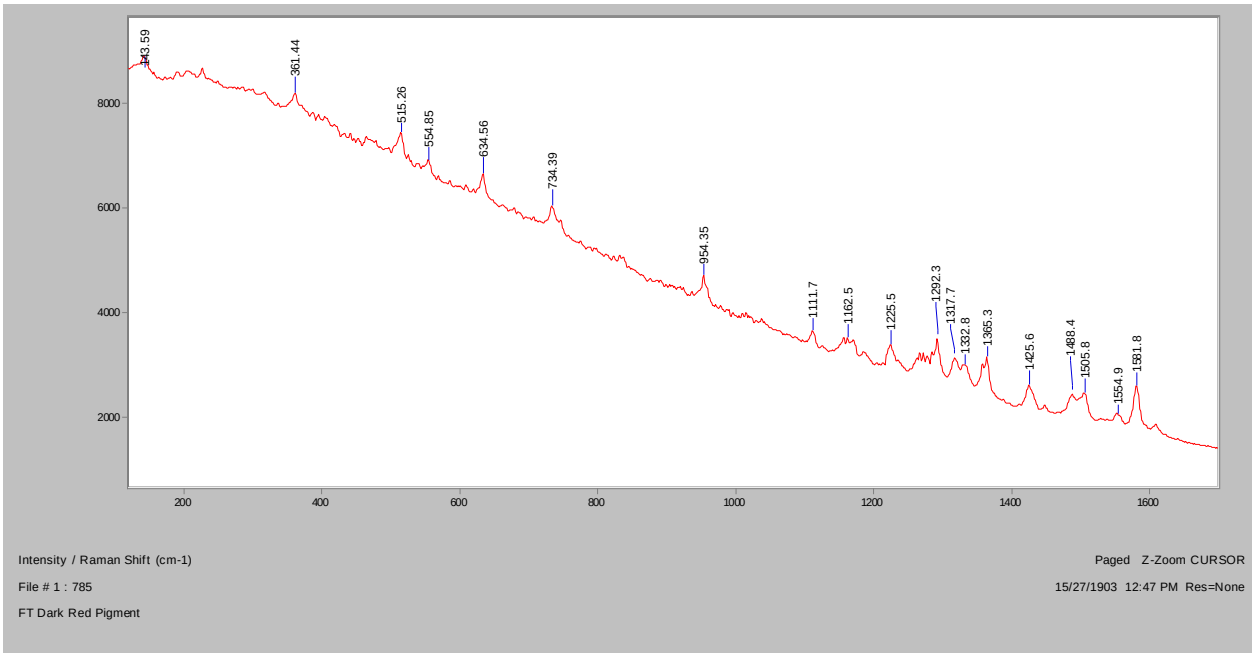

Orange Red

Normal Raman, 488nm

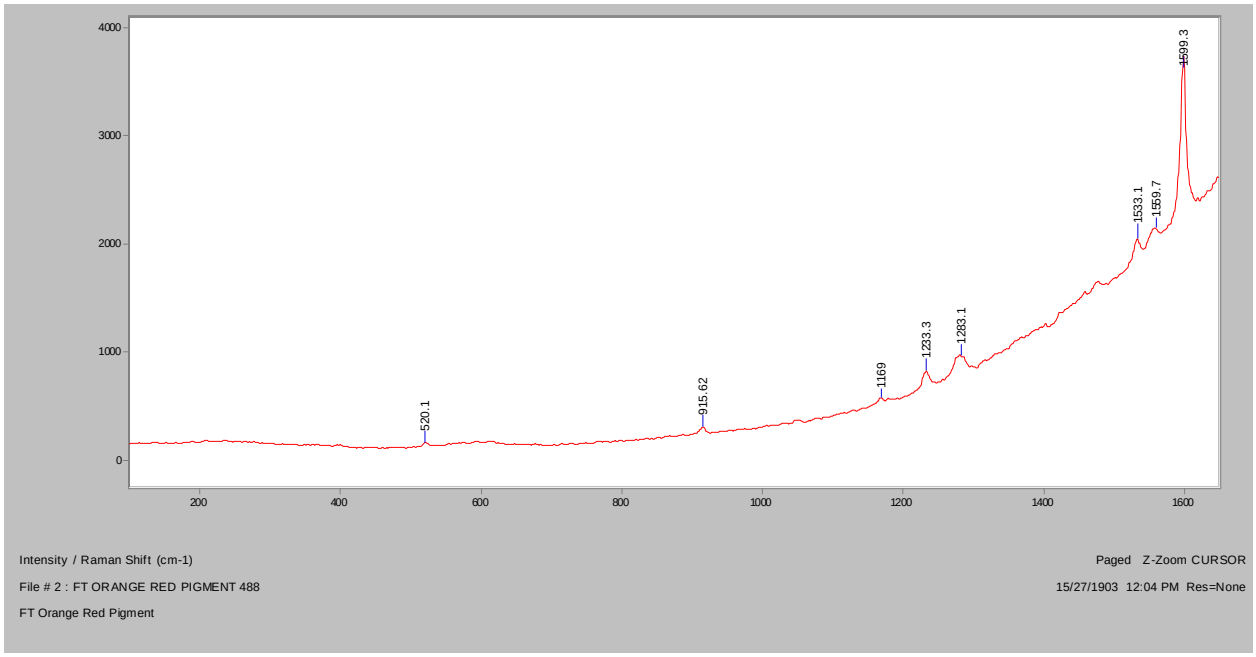

Normal Raman, 633nm

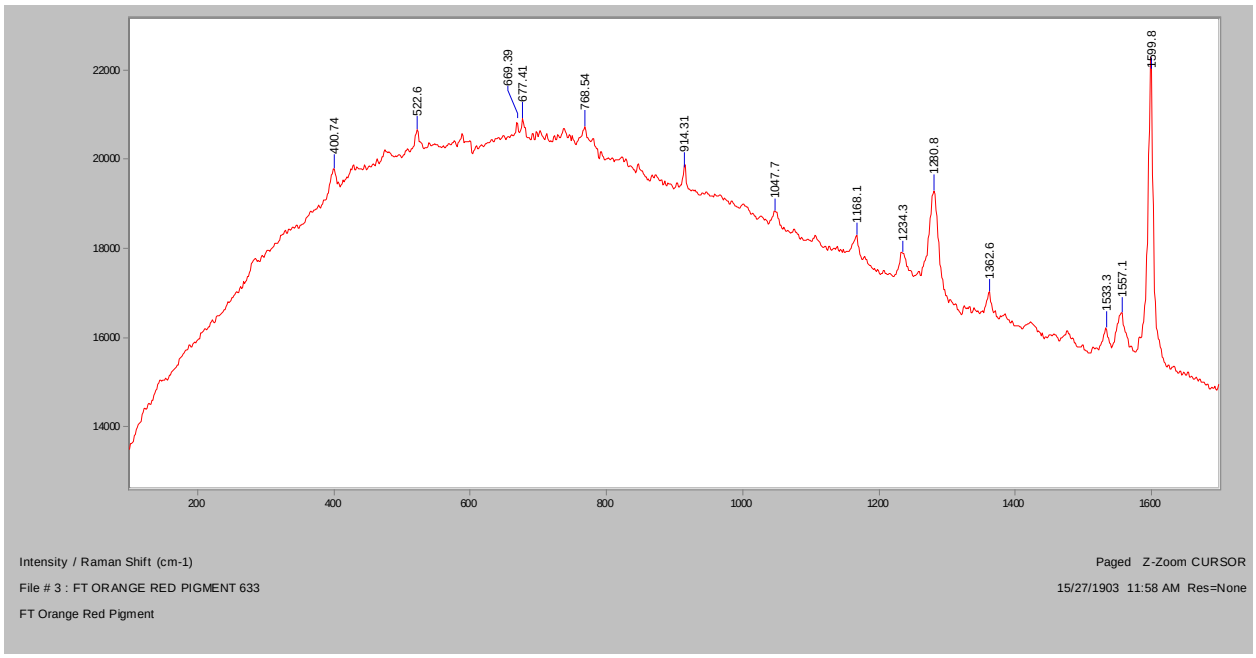

Normal Raman, 785nm

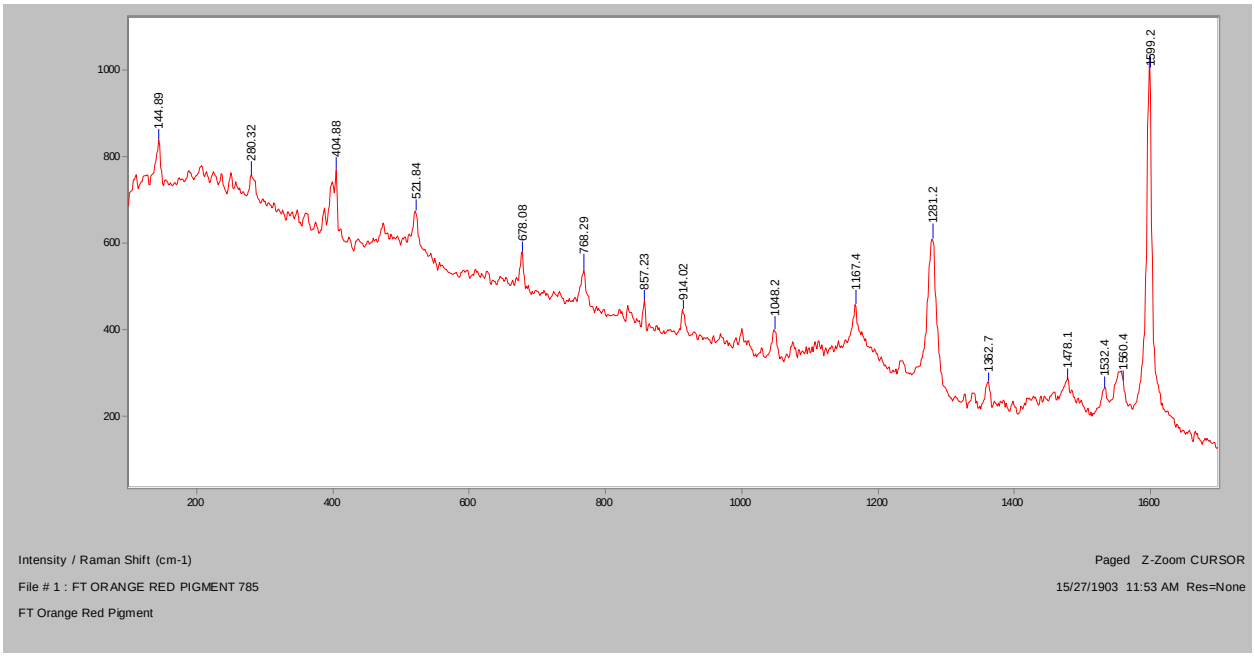

Orange

Normal Raman, 488nm

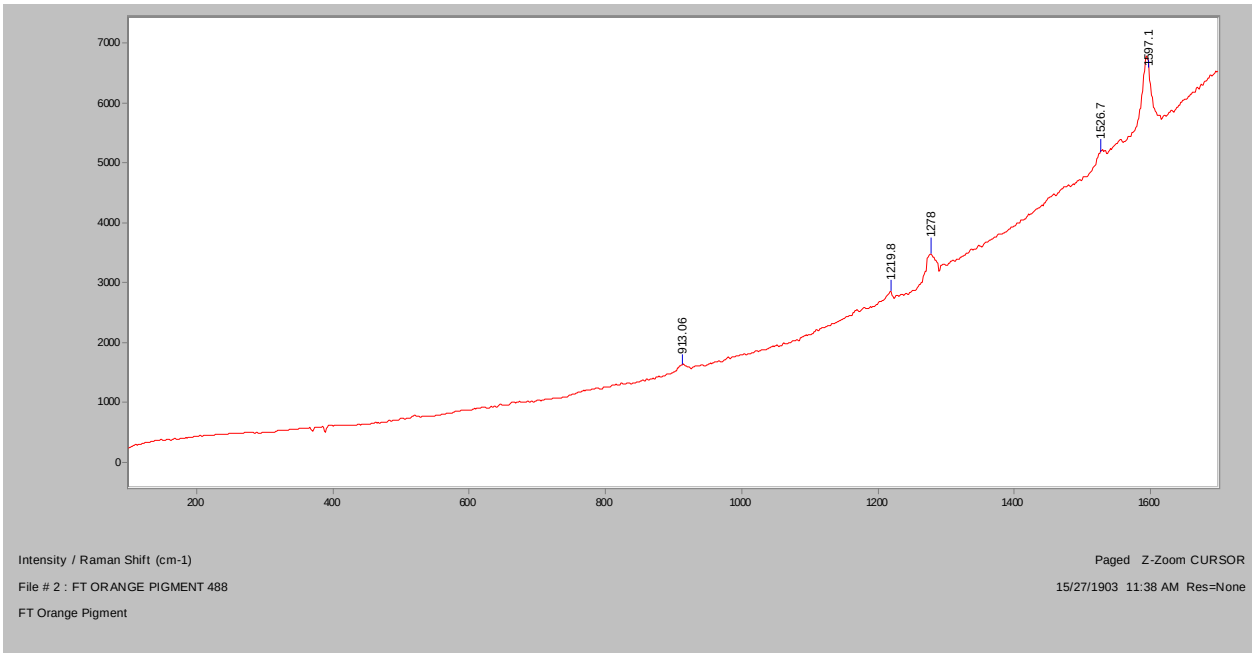

Normal Raman, 633nm

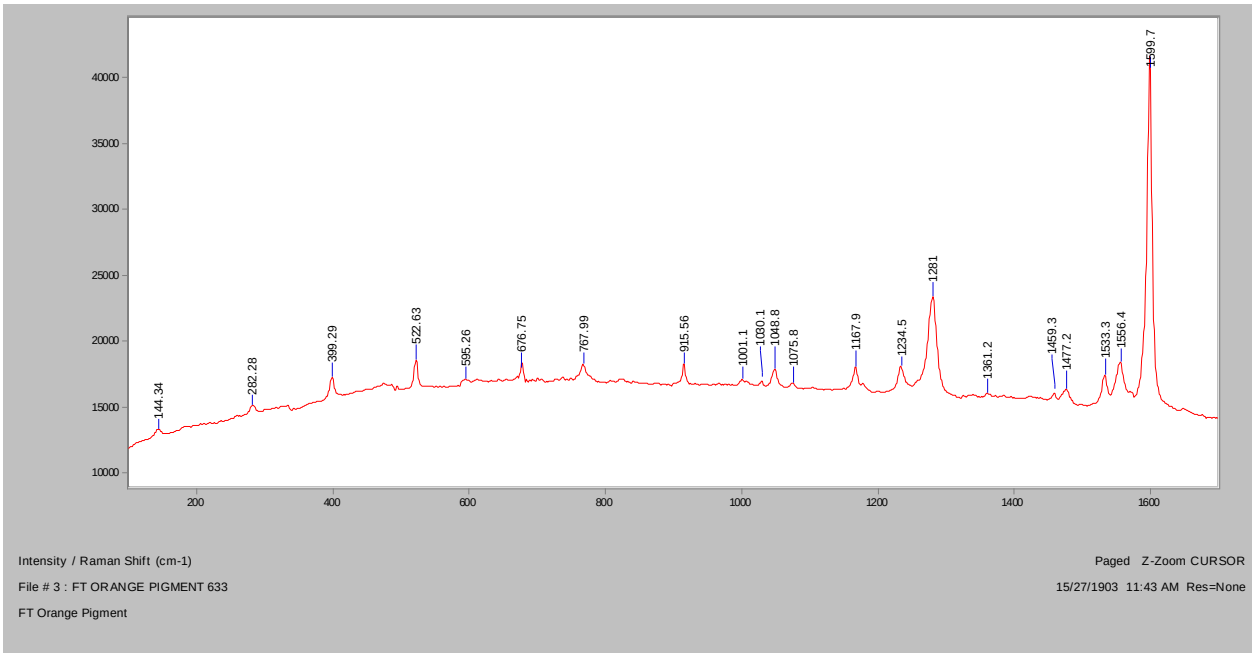

Normal Raman, 785nm

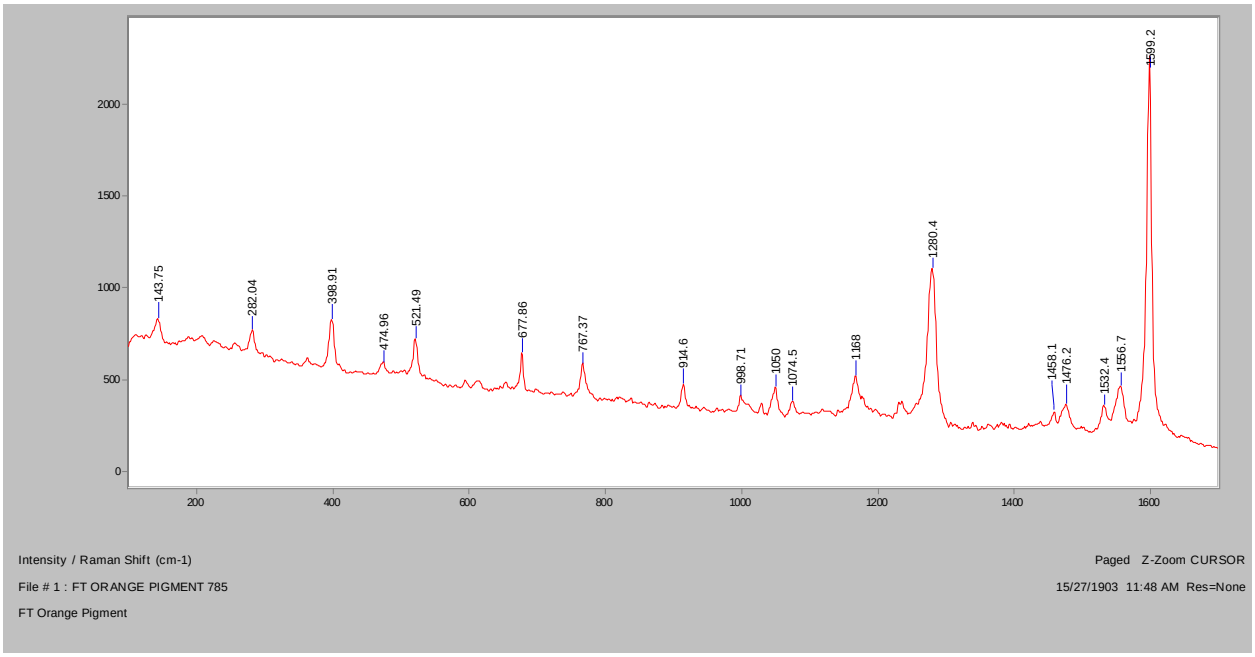

Bright Yellow

Normal Raman, 488nm

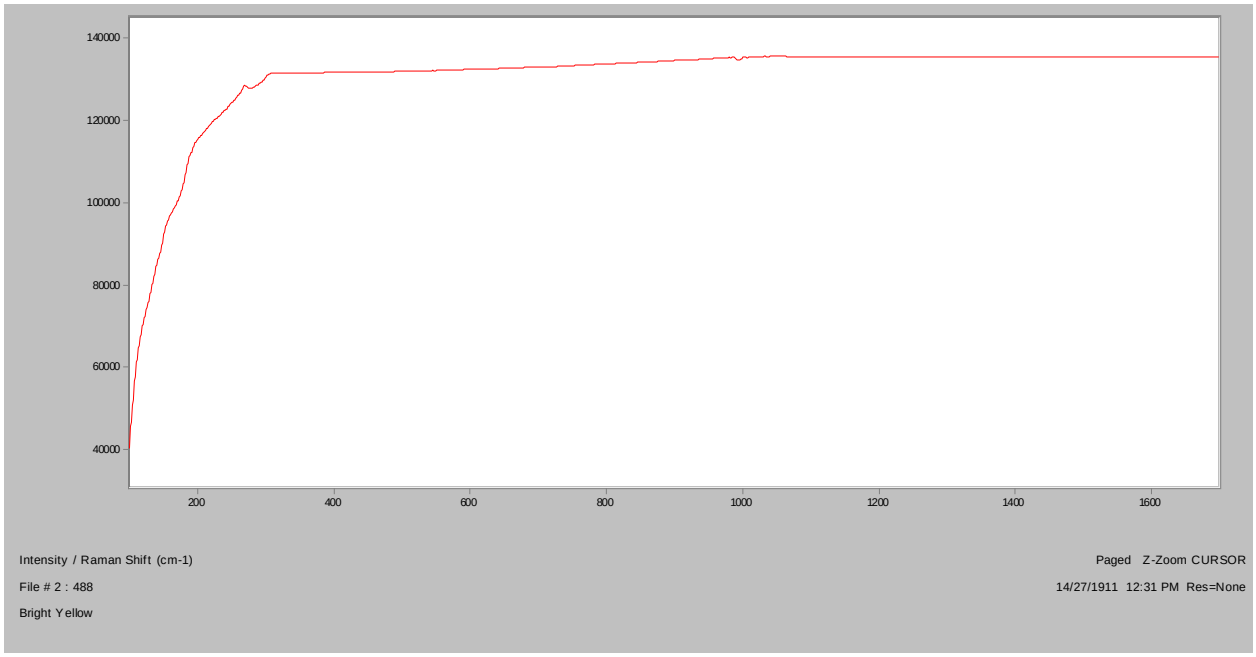

Normal Raman, 633nm

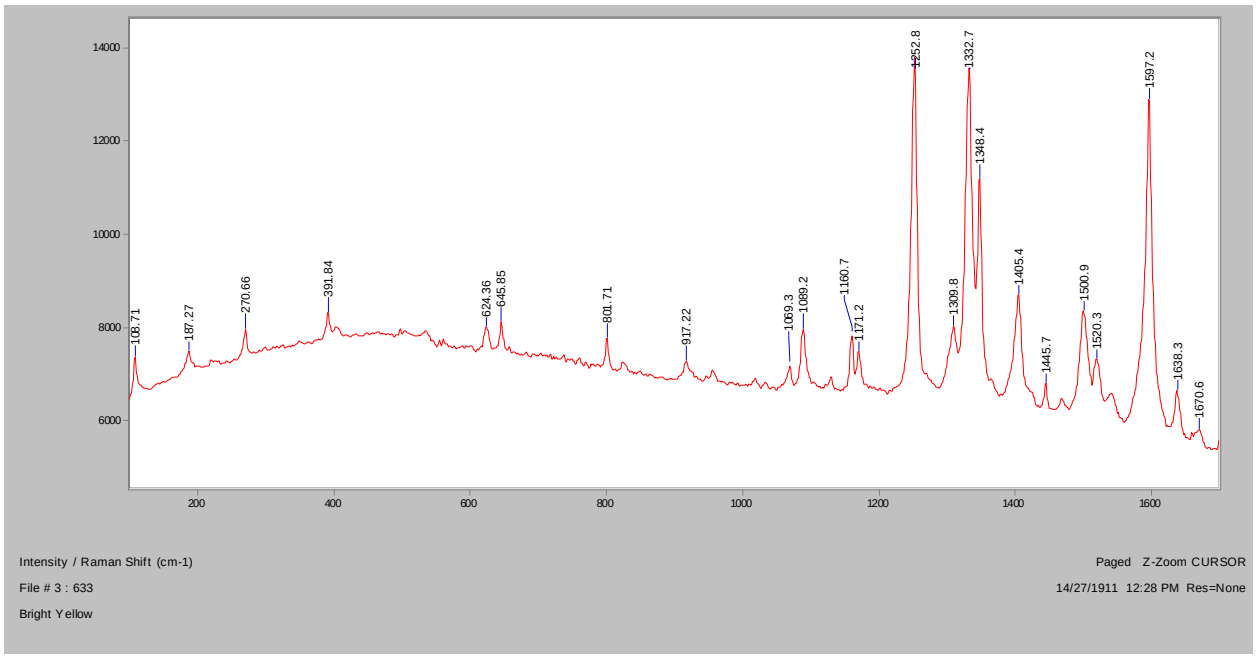

Normal Raman, 785nm

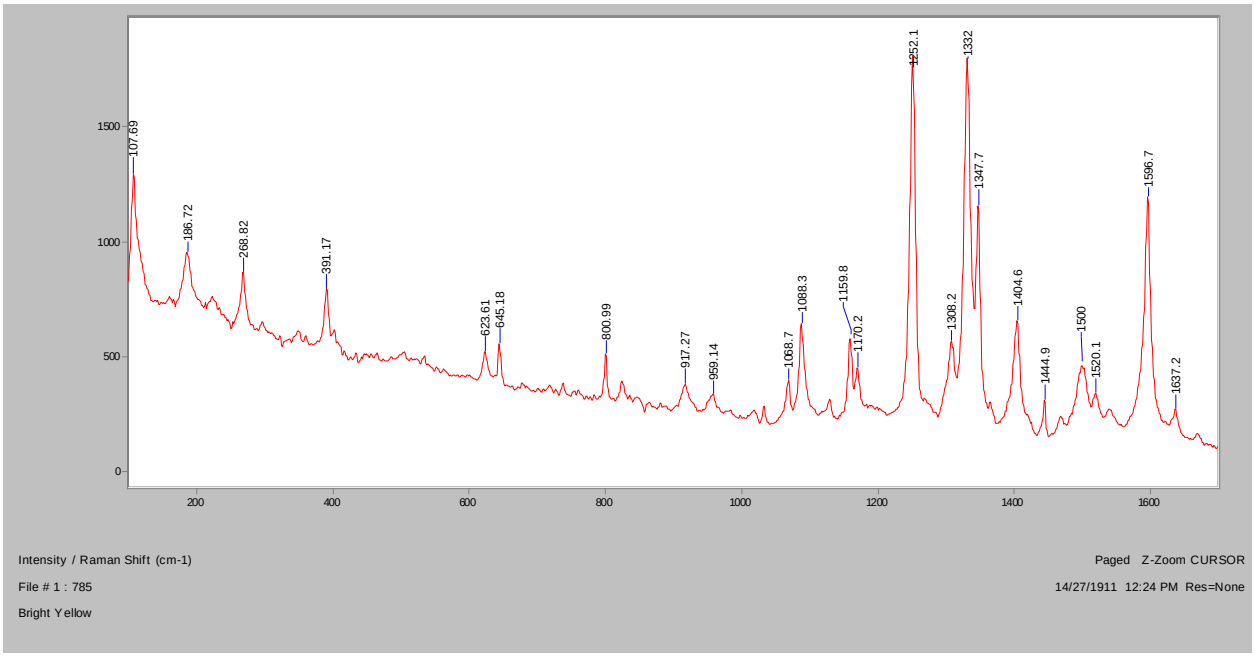

Mid-Yellow

Normal Raman, 488nm

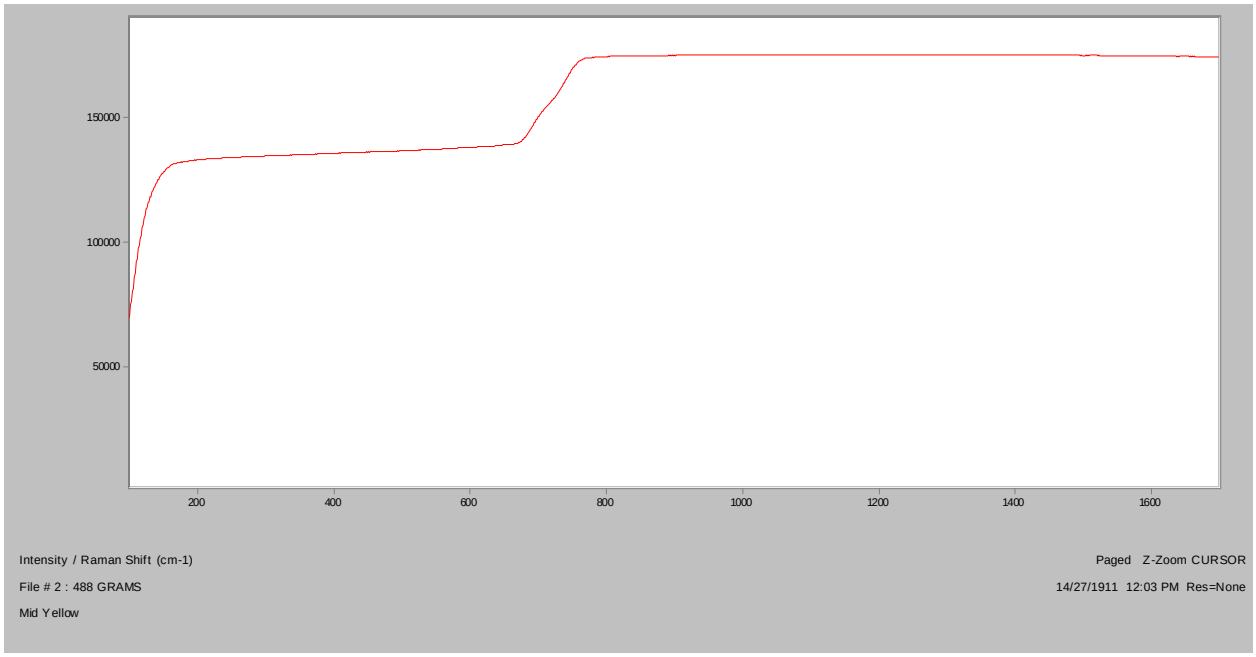

Normal Raman, 633nm

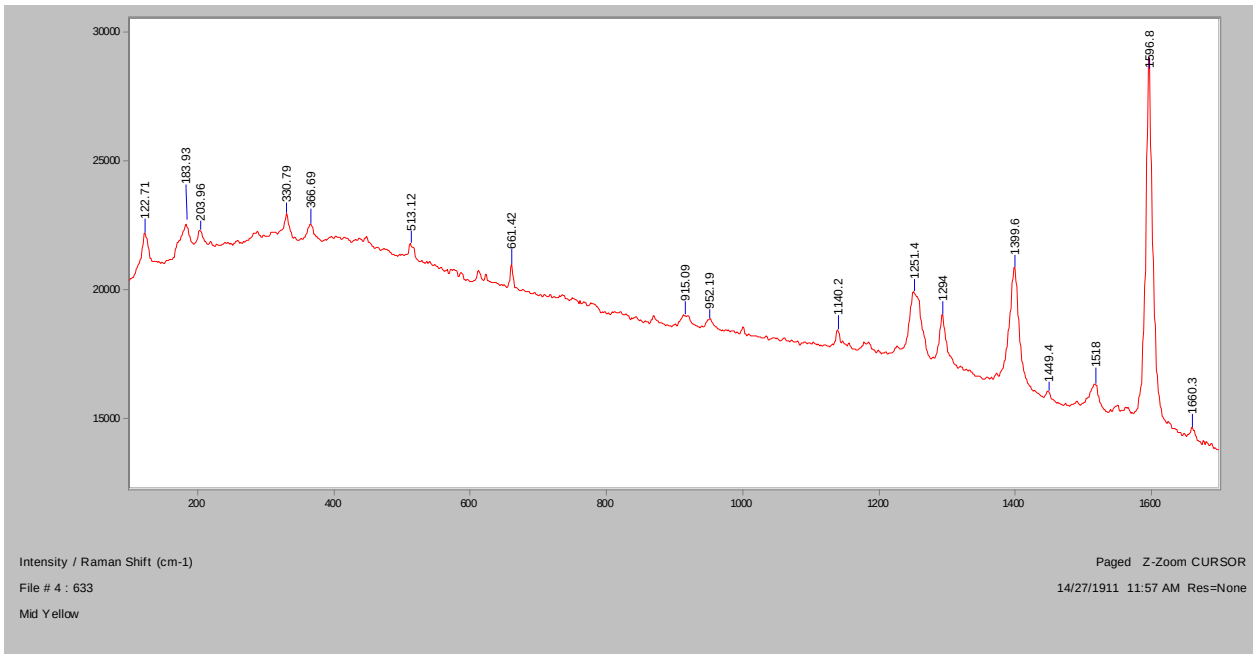

Normal Raman, 785nm

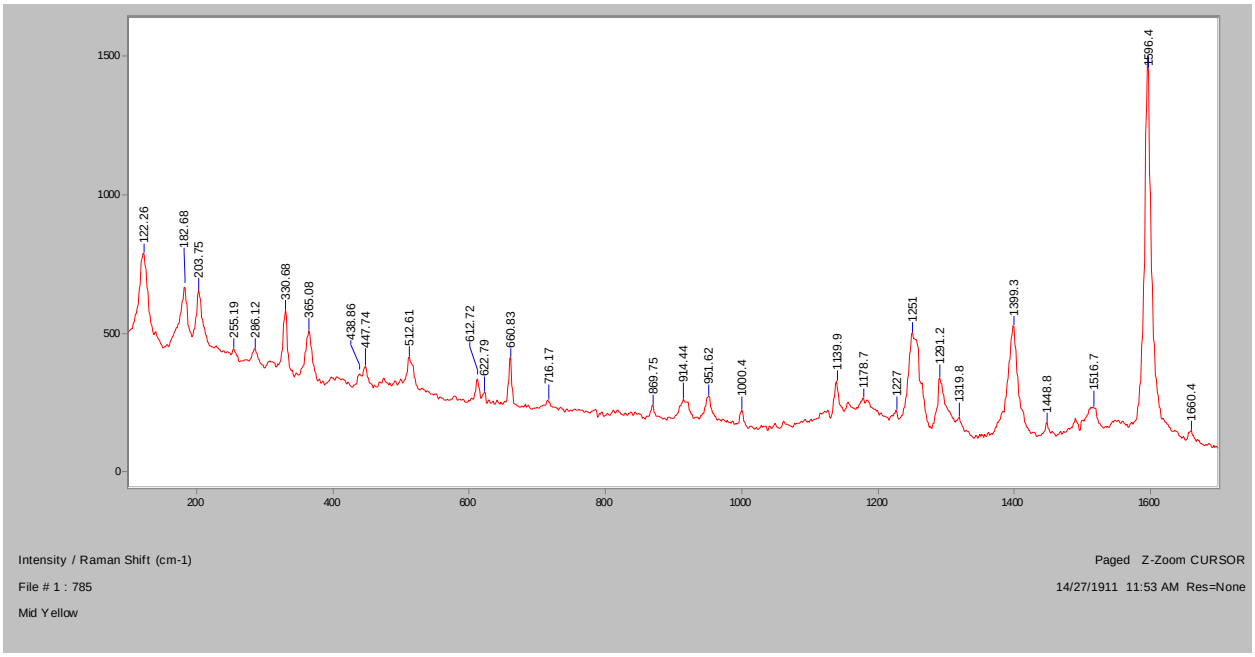

Yellow

Normal Raman, 488nm

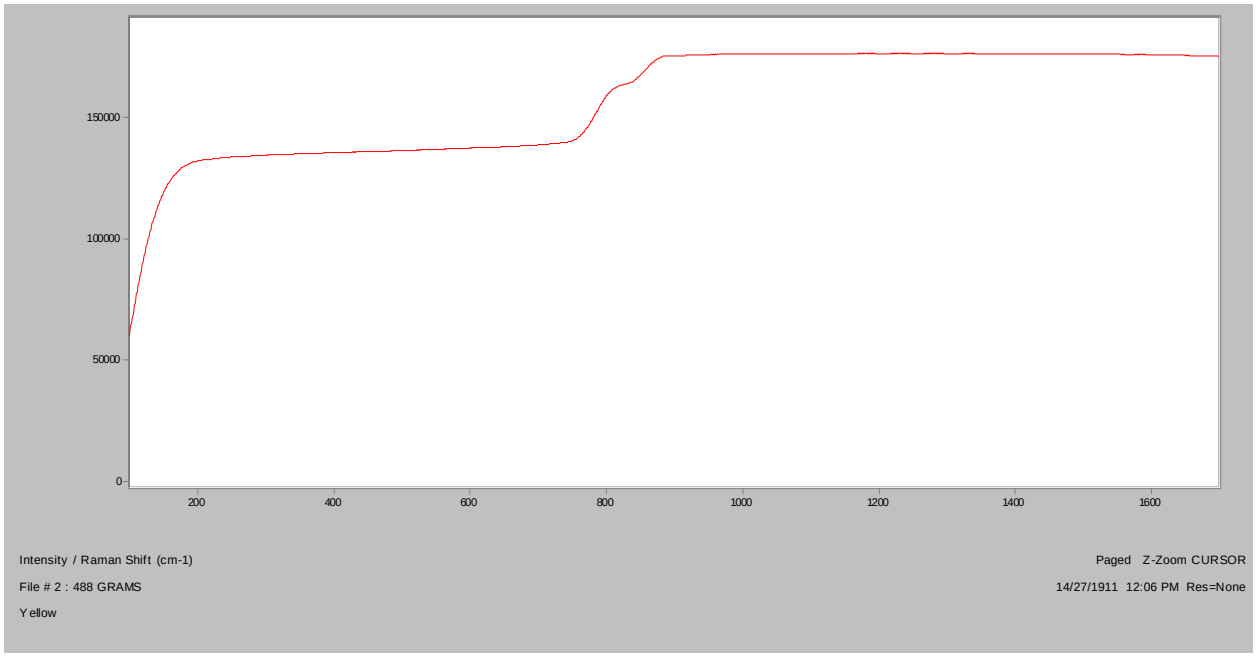

Normal Raman, 633nm

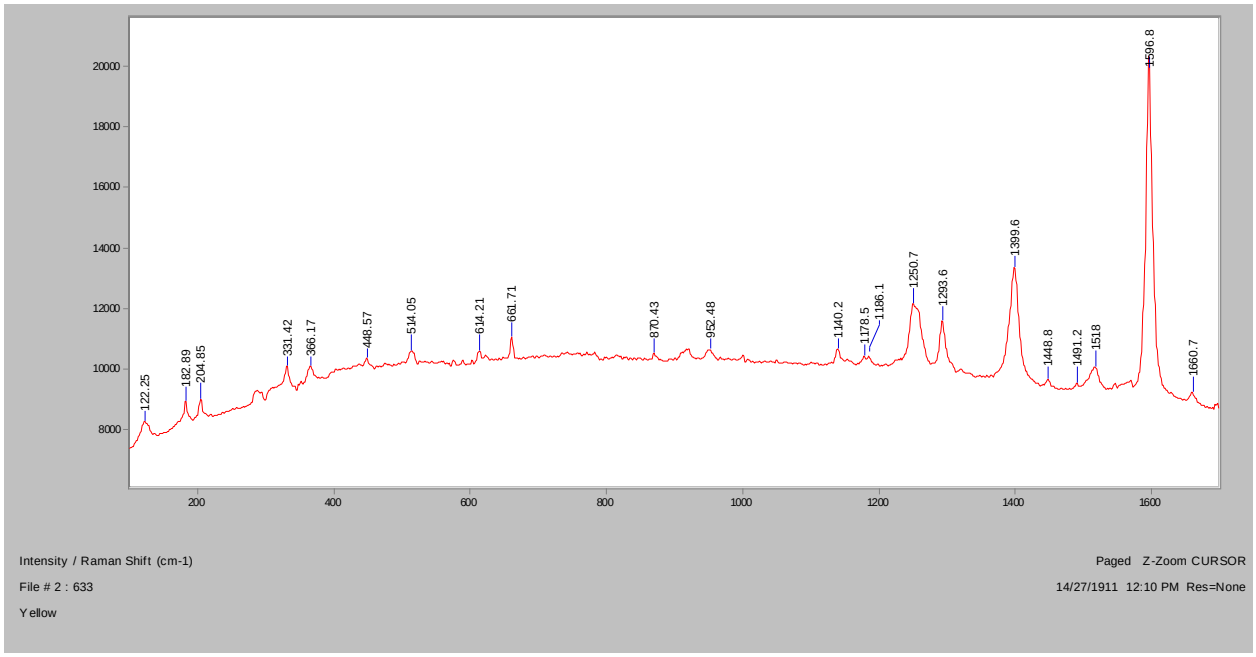

Normal Raman, 785nm

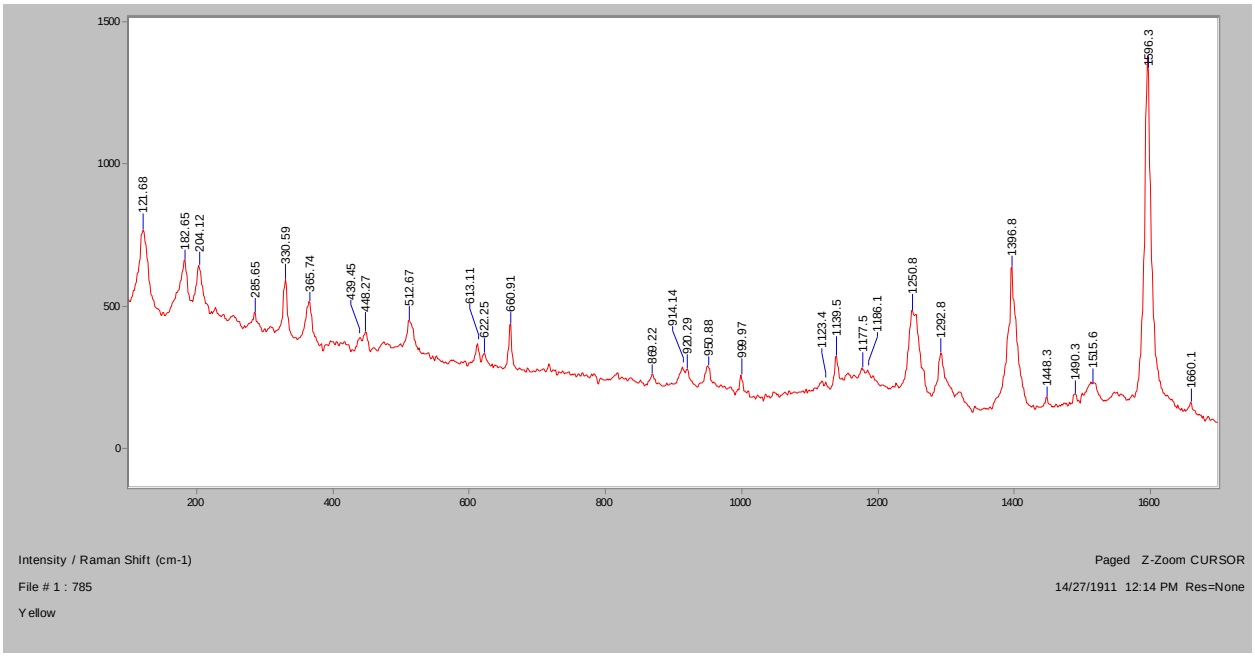

Golden Yellow

Normal Raman, 488nm

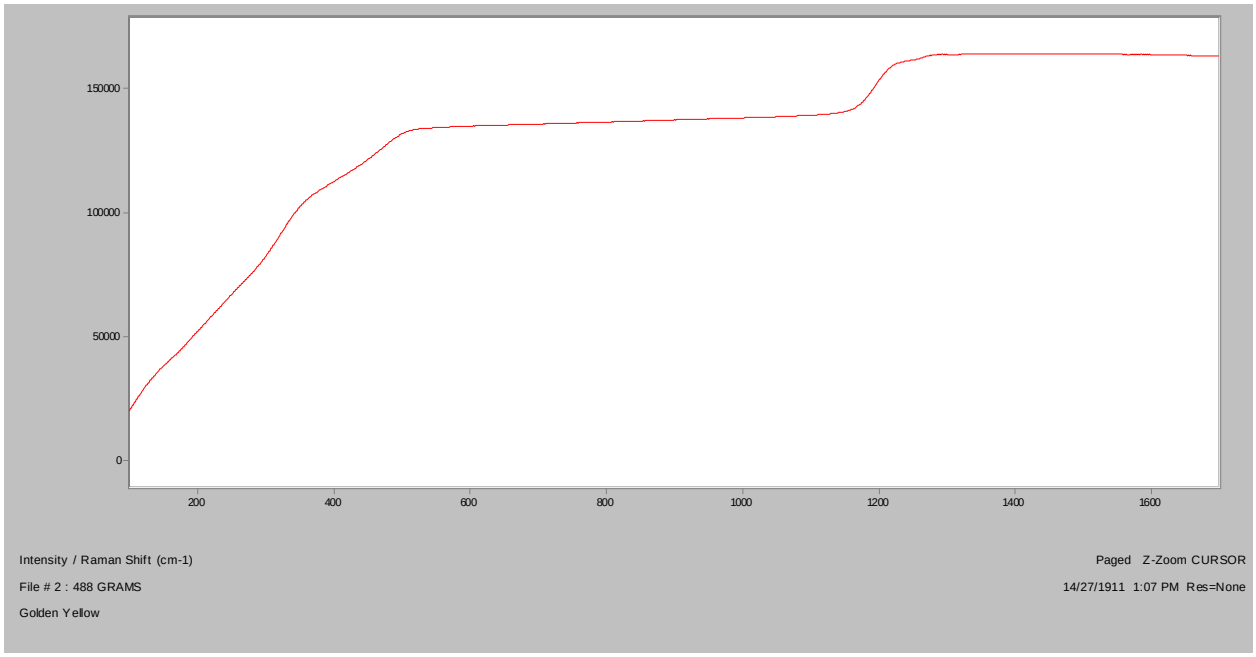

Normal Raman, 633nm

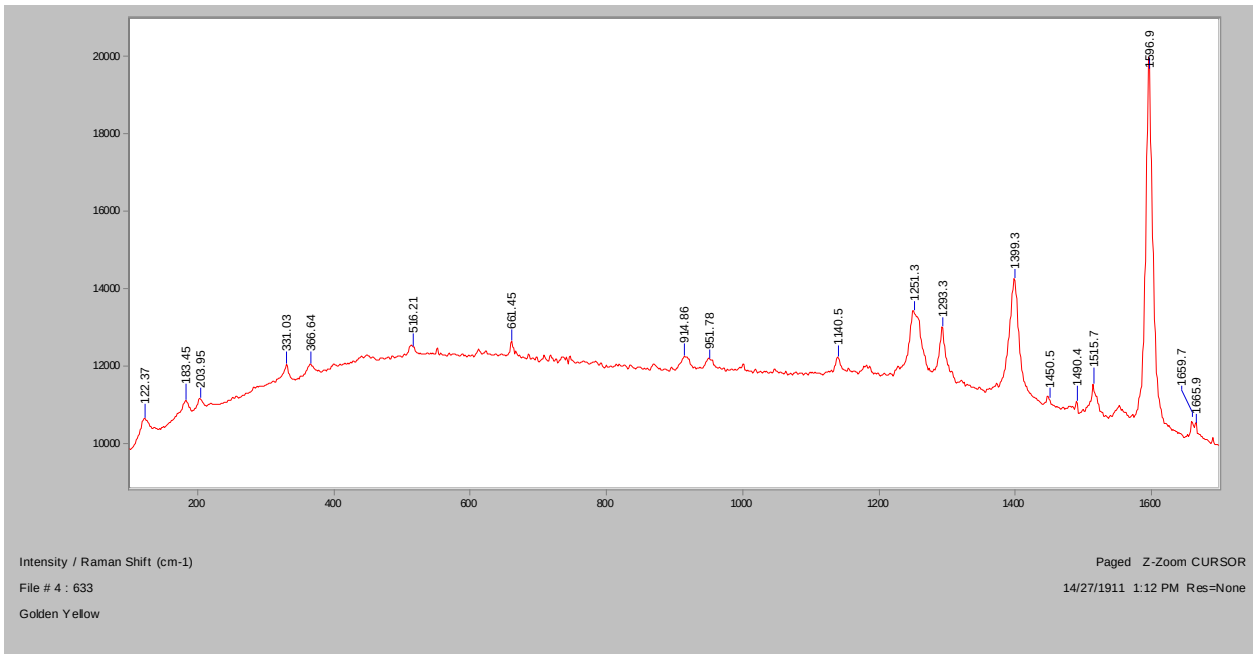

Normal Raman, 785nm

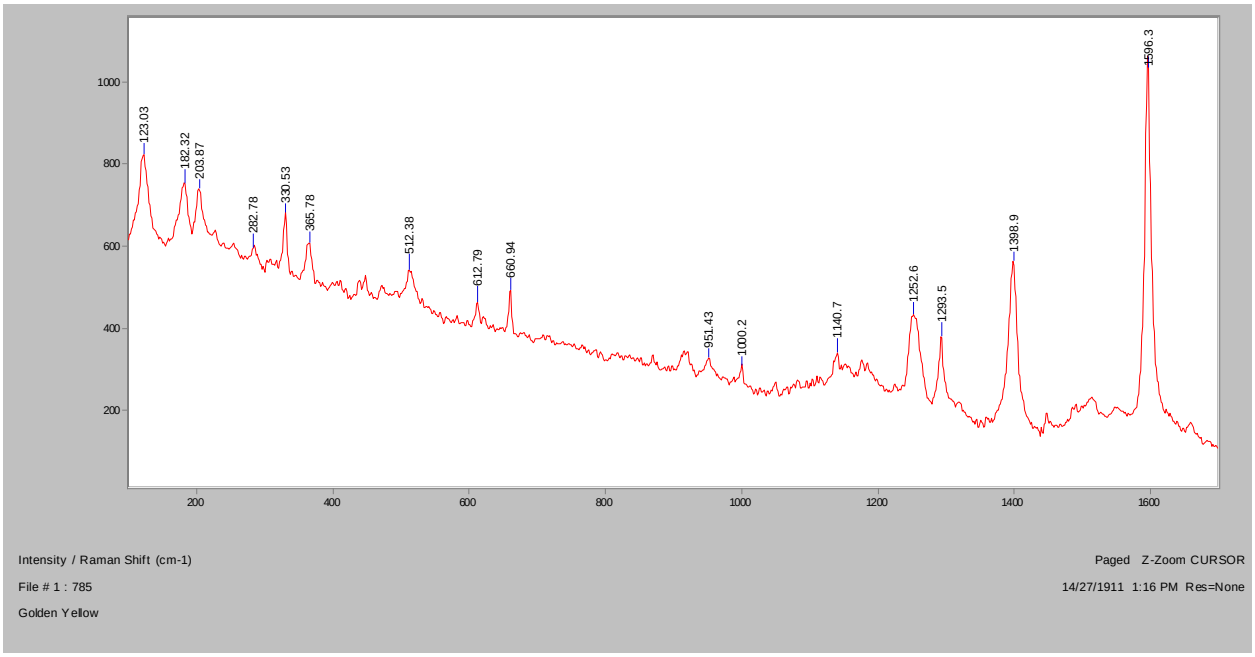

Khaki

Normal Raman, 488nm

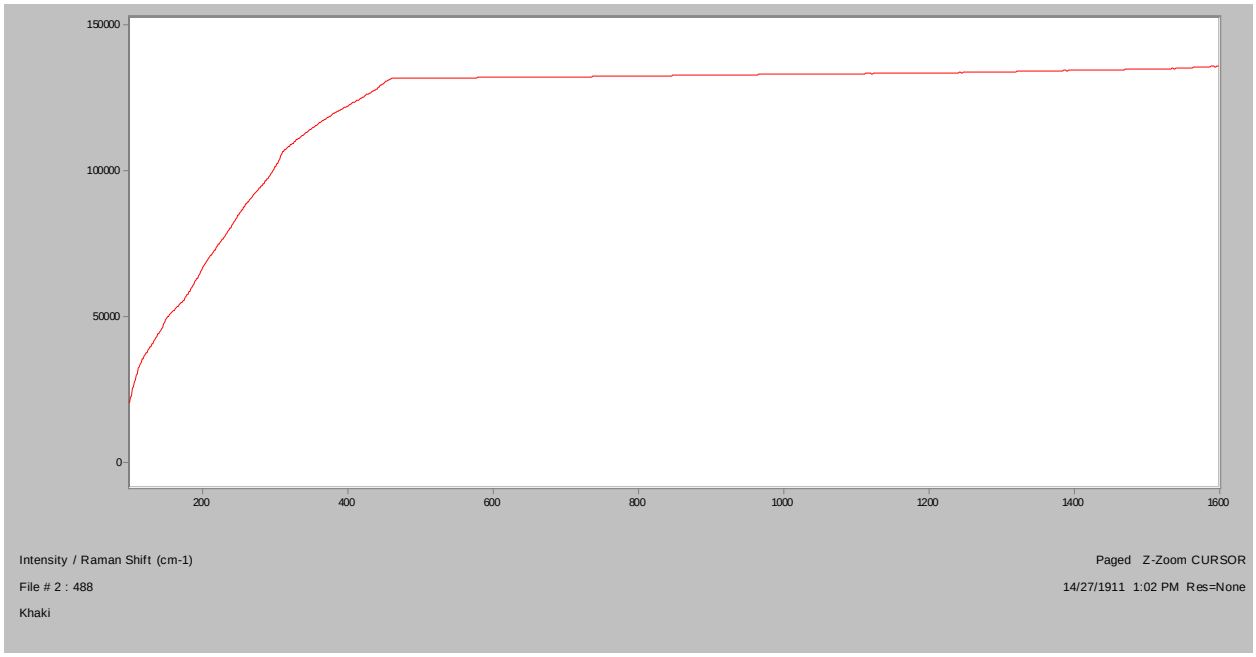

Normal Raman, 633nm

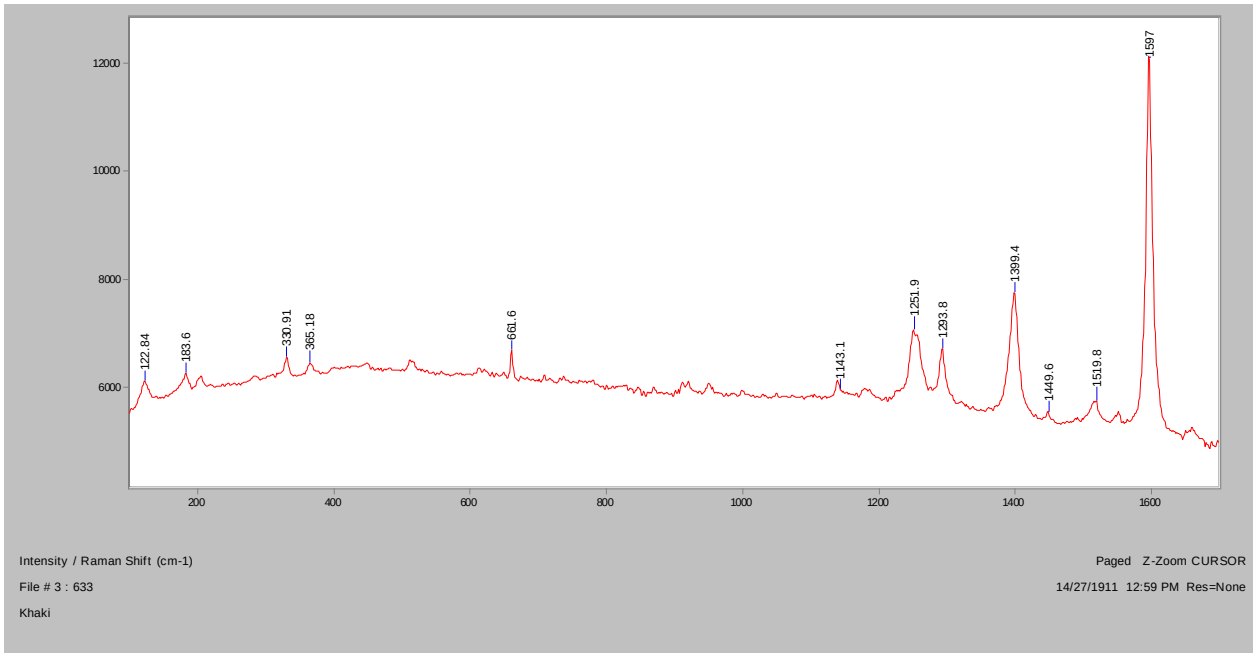

Normal Raman, 785nm

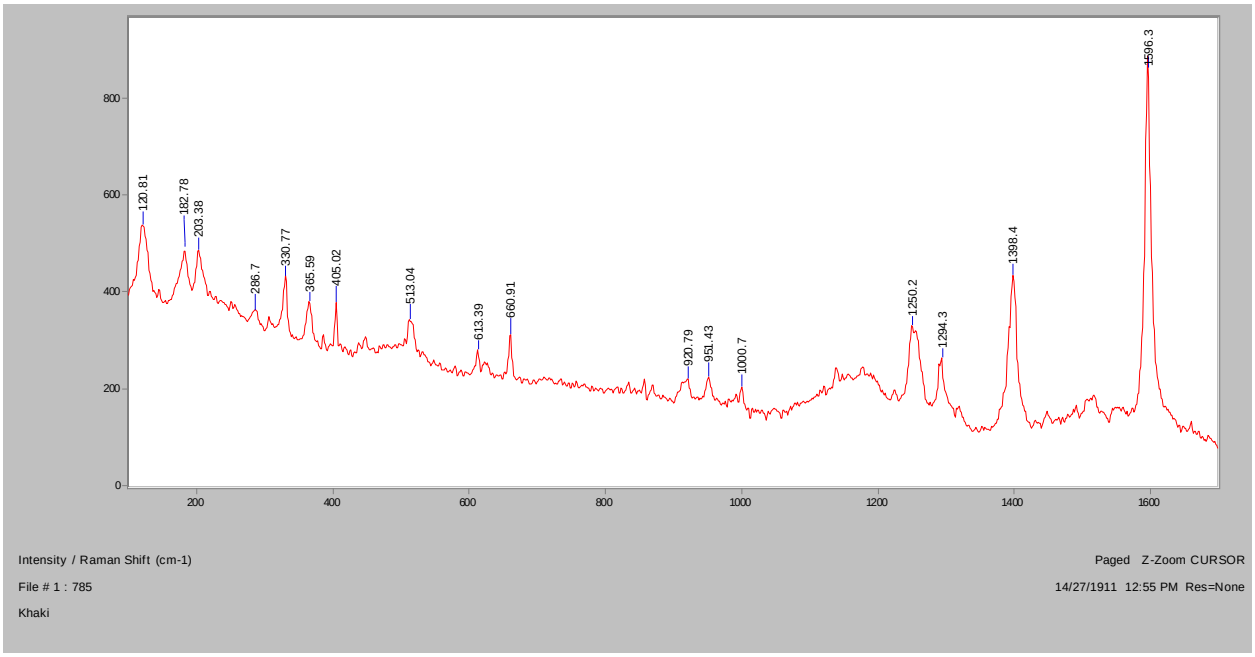

Grass Hopper

Normal Raman, 488nm

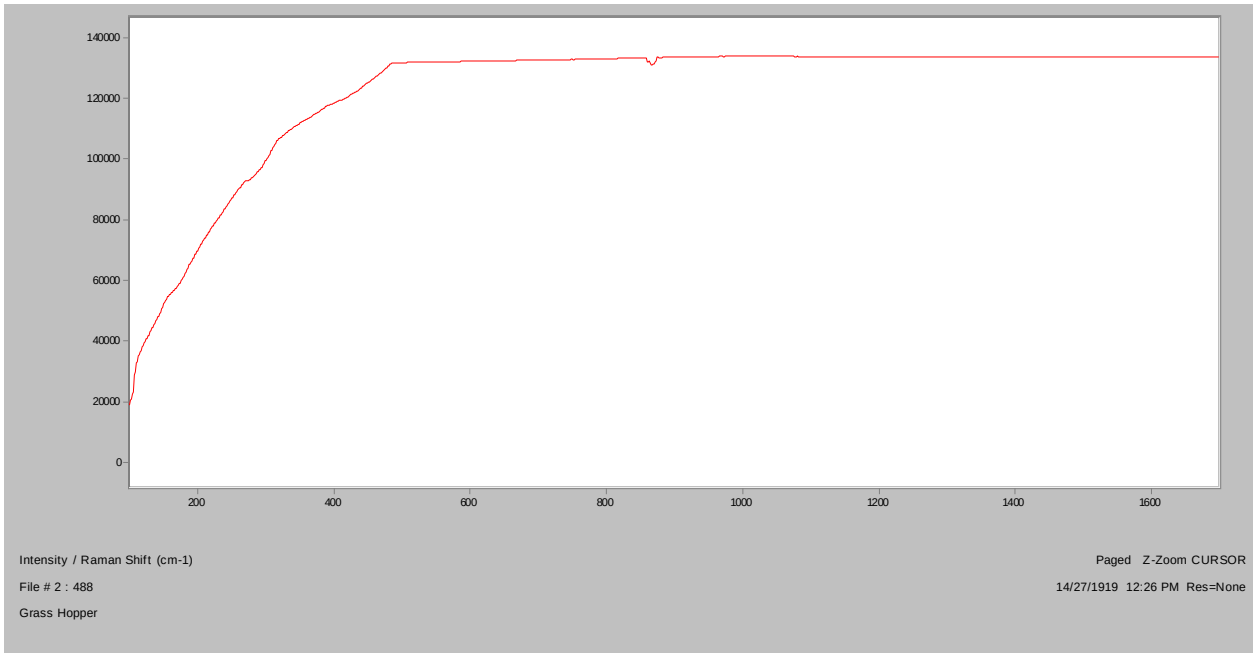

Normal Raman, 633nm

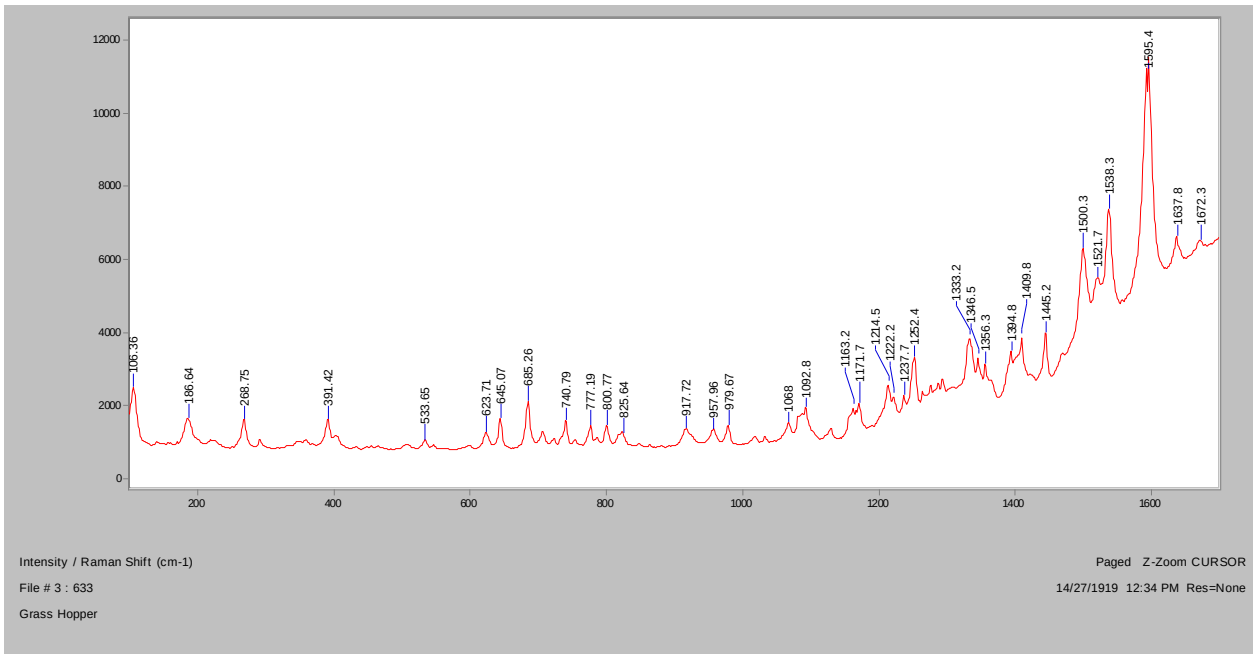

Normal Raman, 785nm

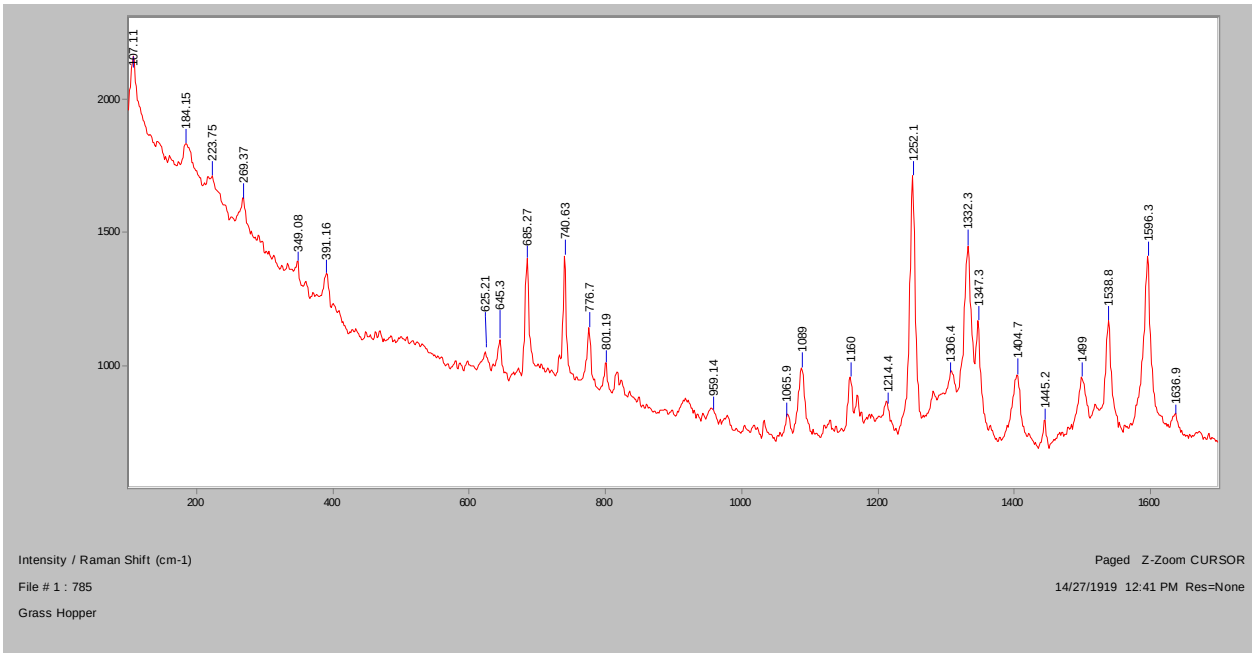

Light Green

Normal Raman, 488nm

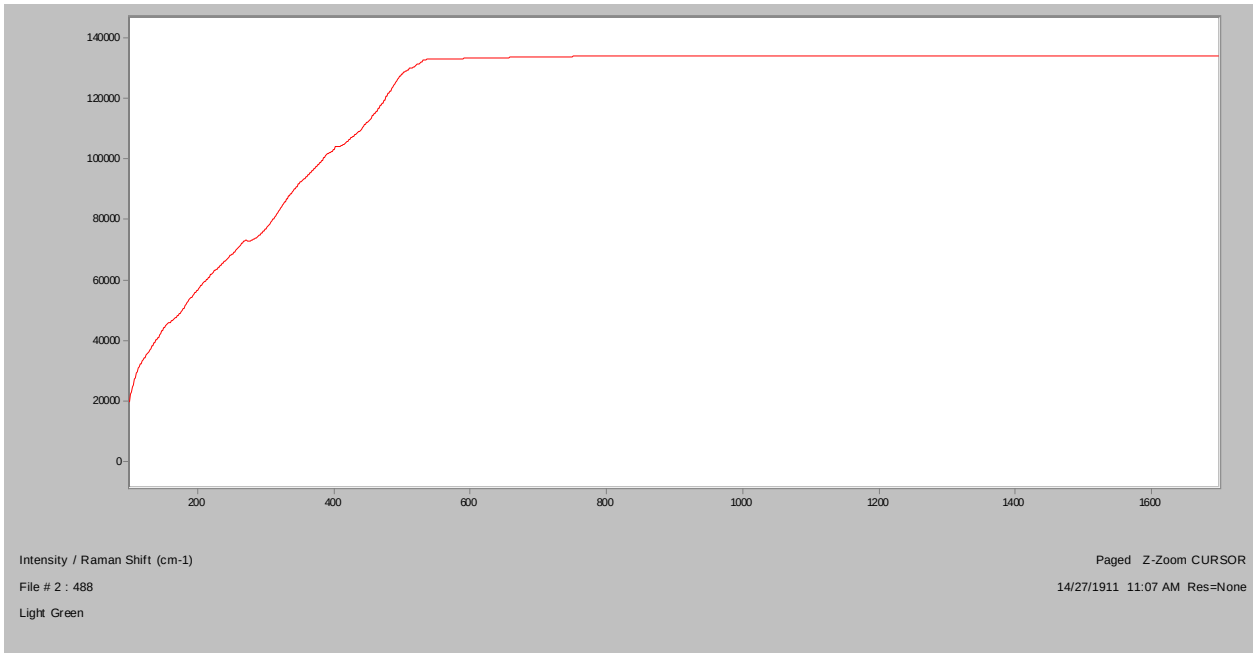

Normal Raman, 633nm

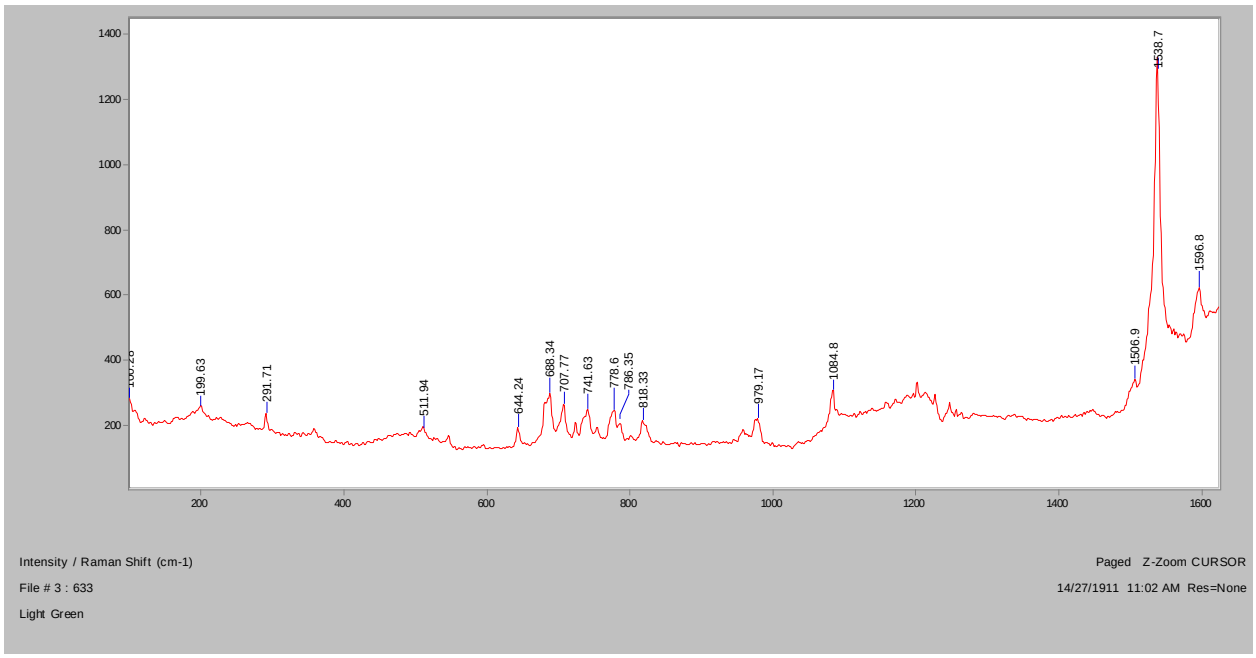

Normal Raman, 785nm

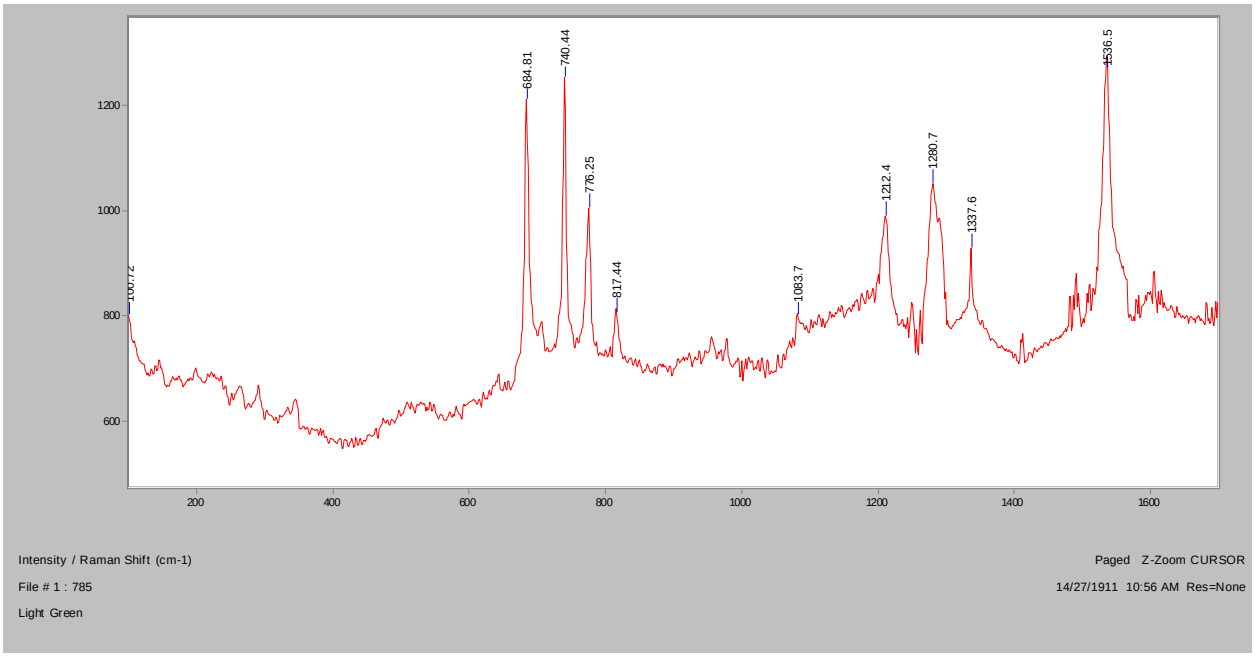

Verdancy

Normal Raman, 488nm

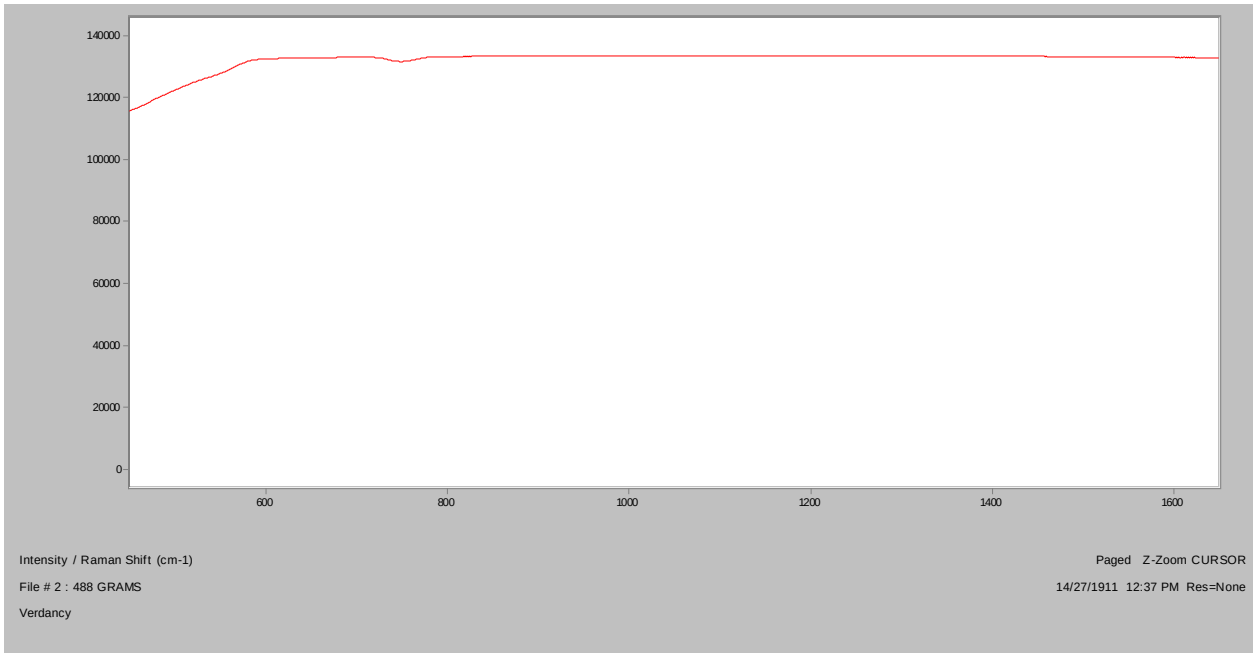

Normal Raman, 633nm

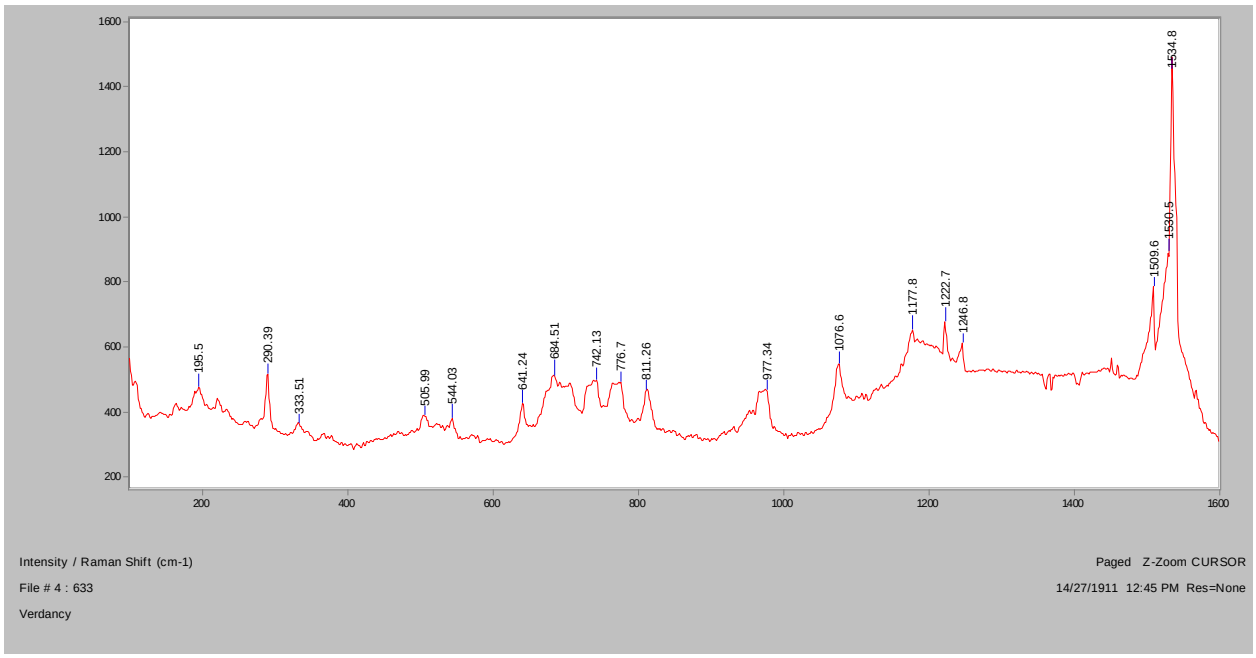

Normal Raman, 785nm

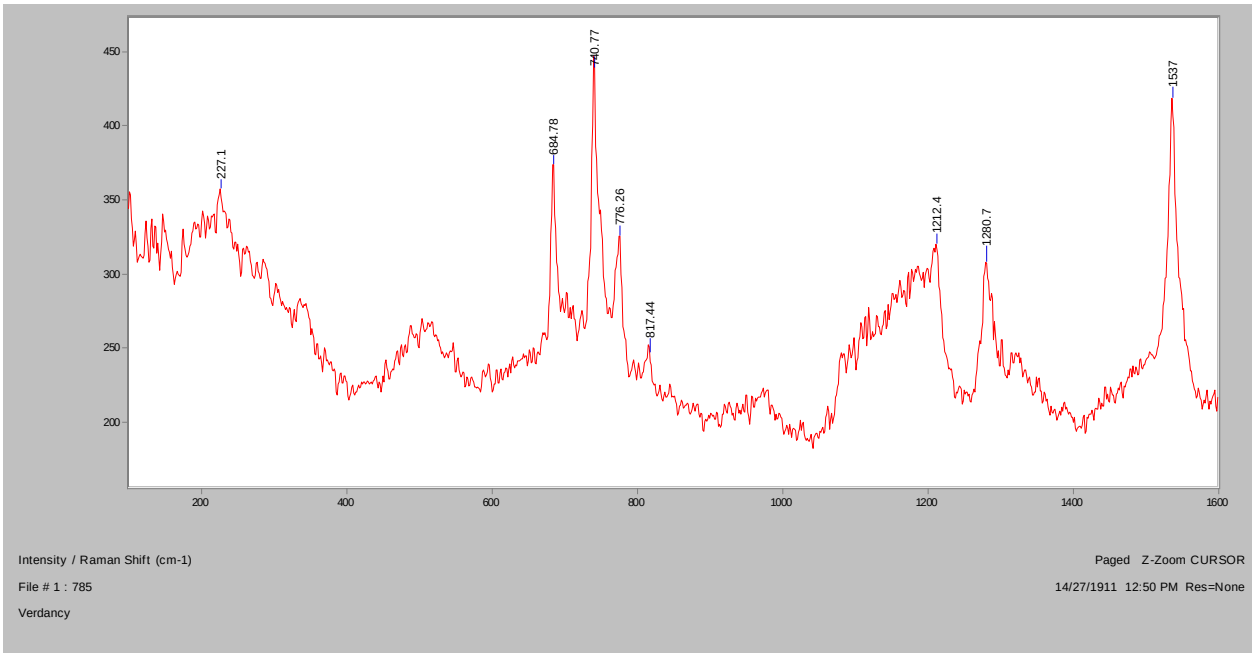

Lawngreen

Normal Raman, 488nm

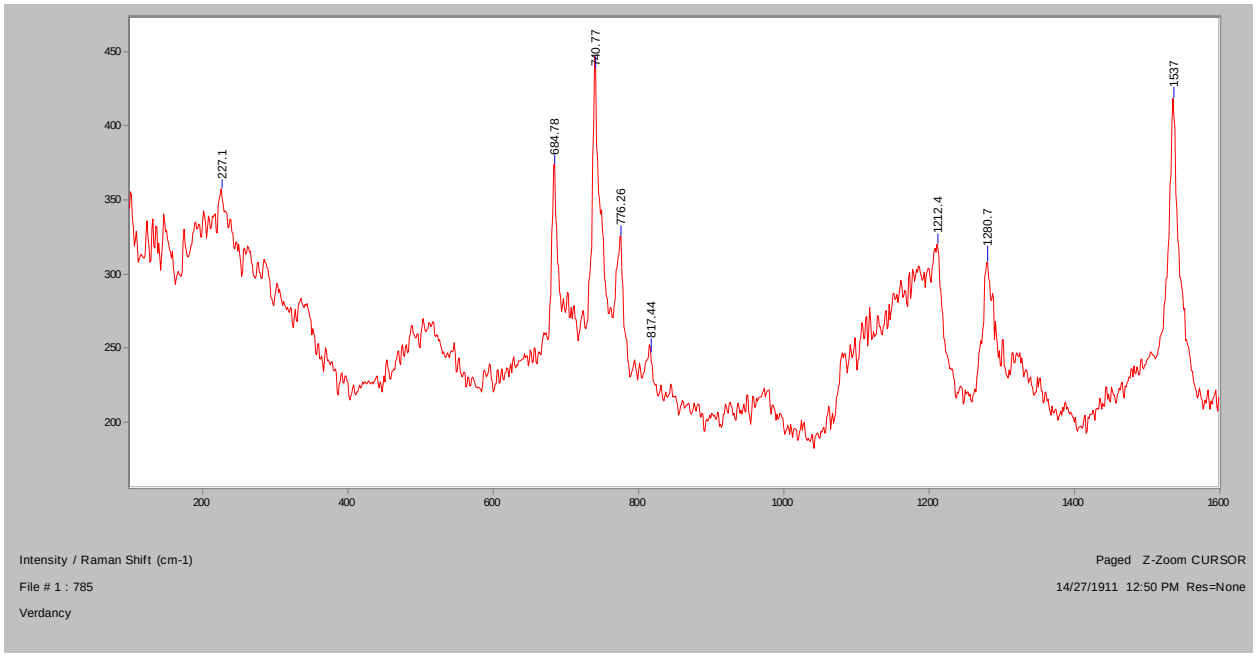

Normal Raman, 633nm

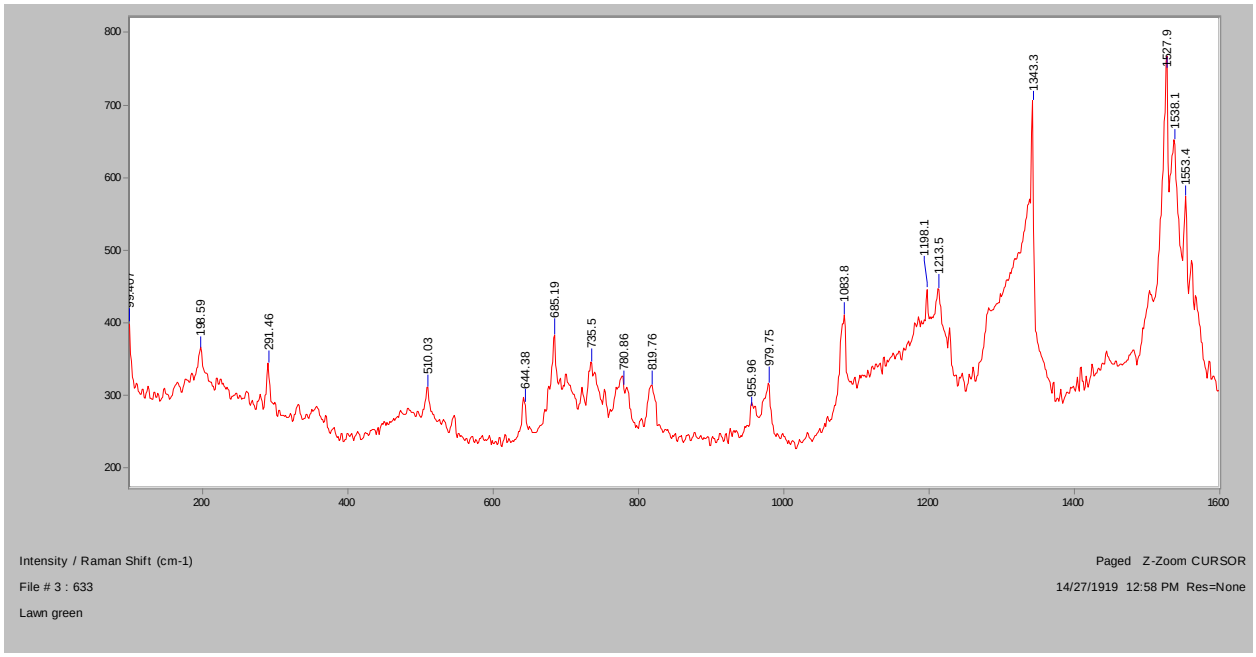

Normal Raman, 785nm

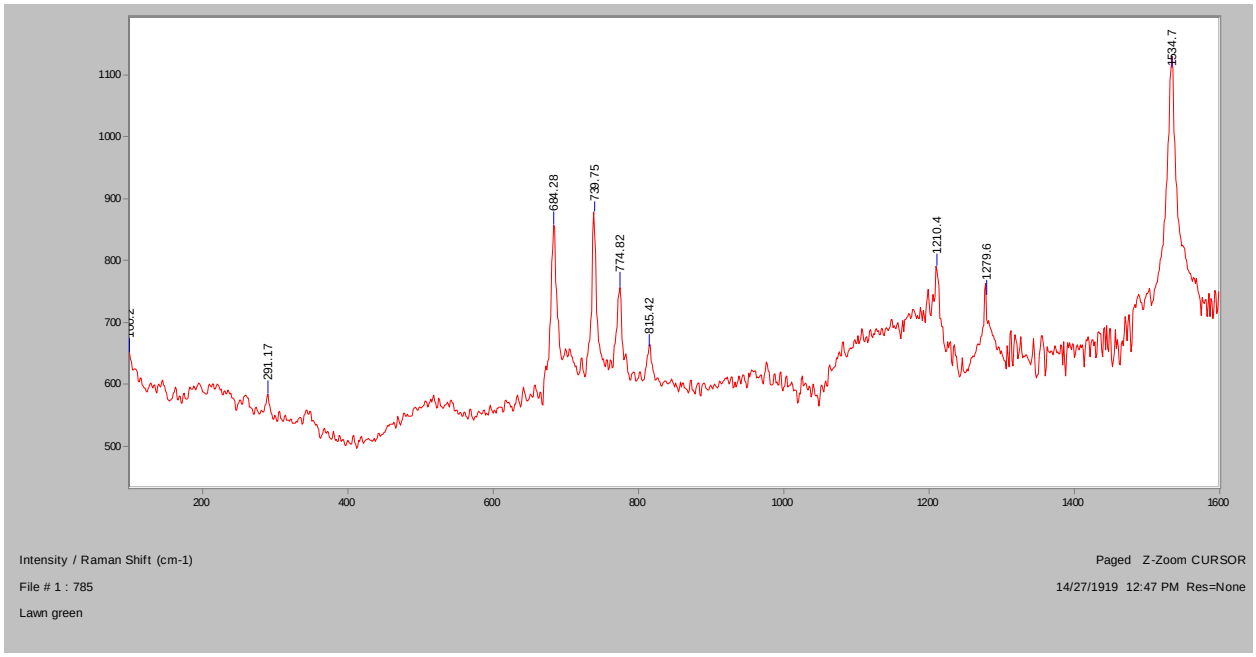

Dark Green

Normal Raman, 488nm

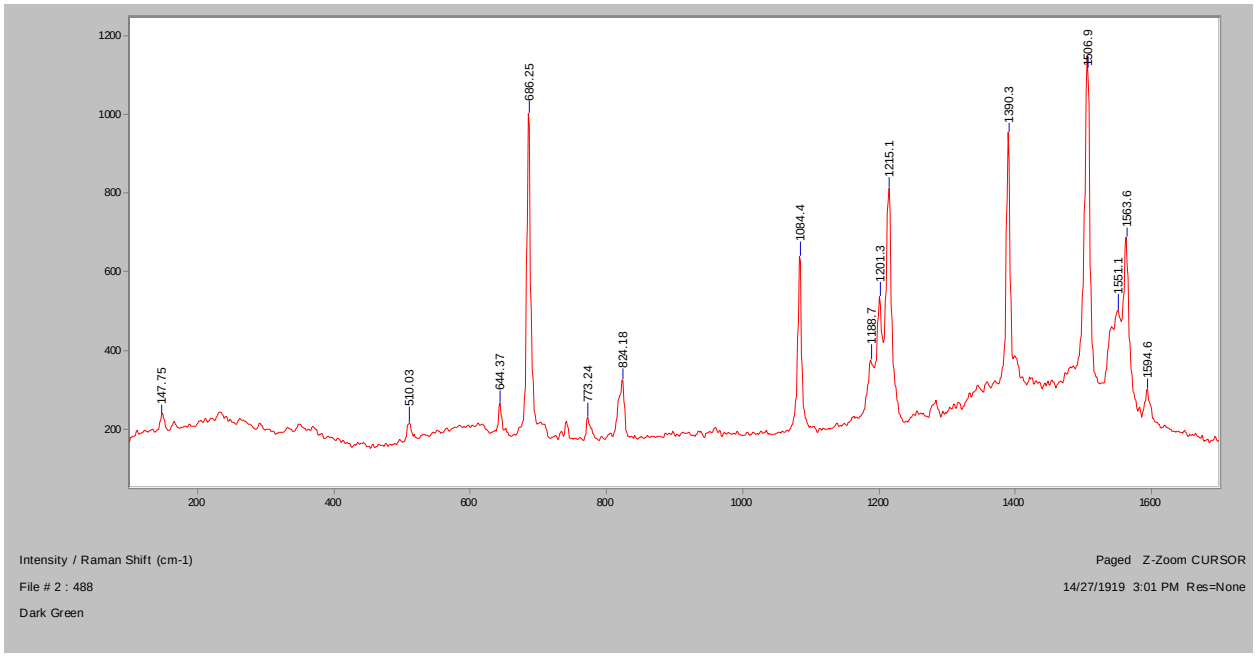

Normal Raman, 633nm

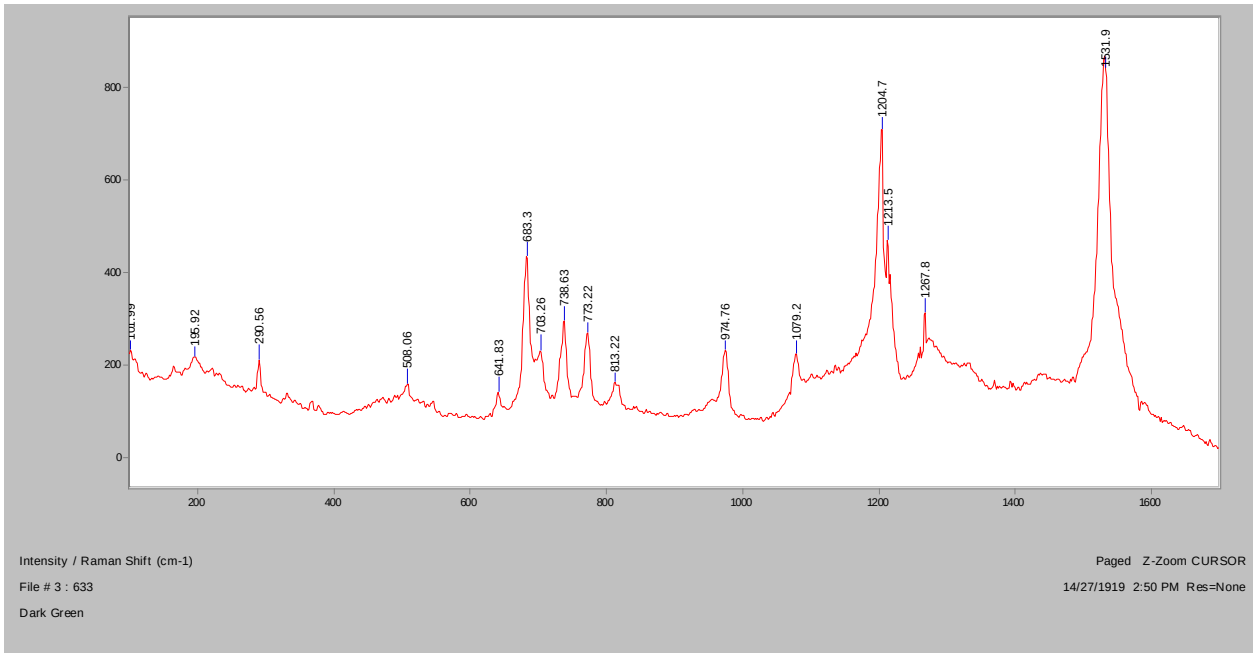

Normal Raman, 785nm

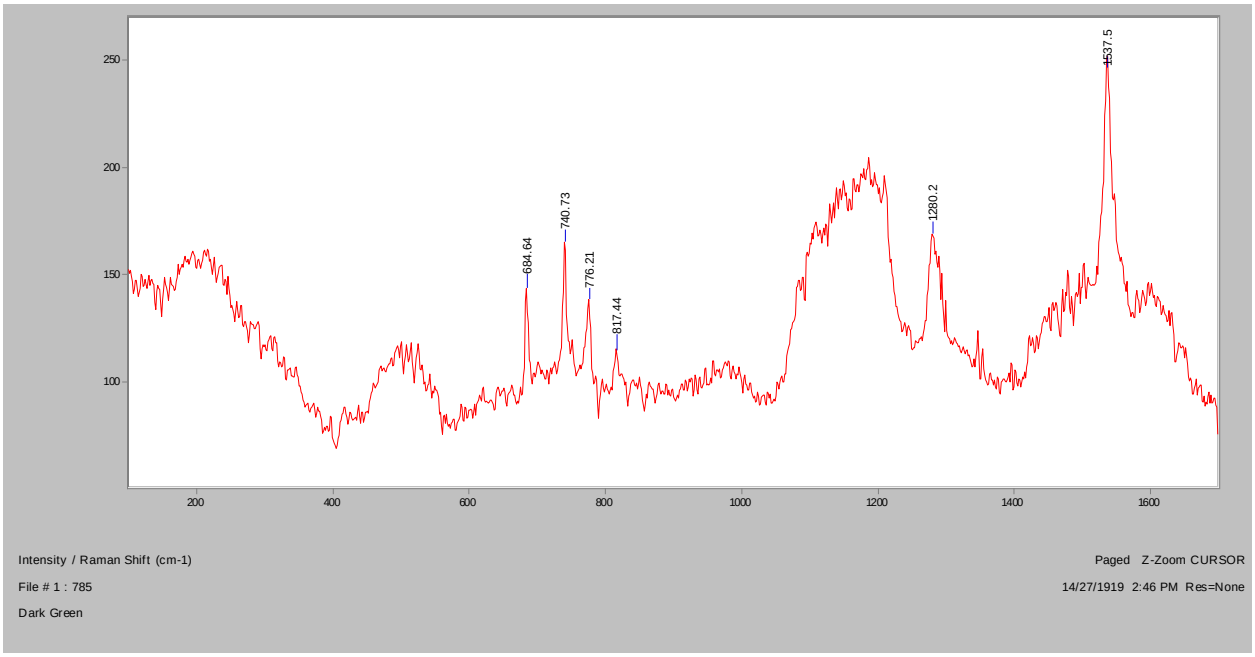

Blue Sky

Normal Raman, 488nm

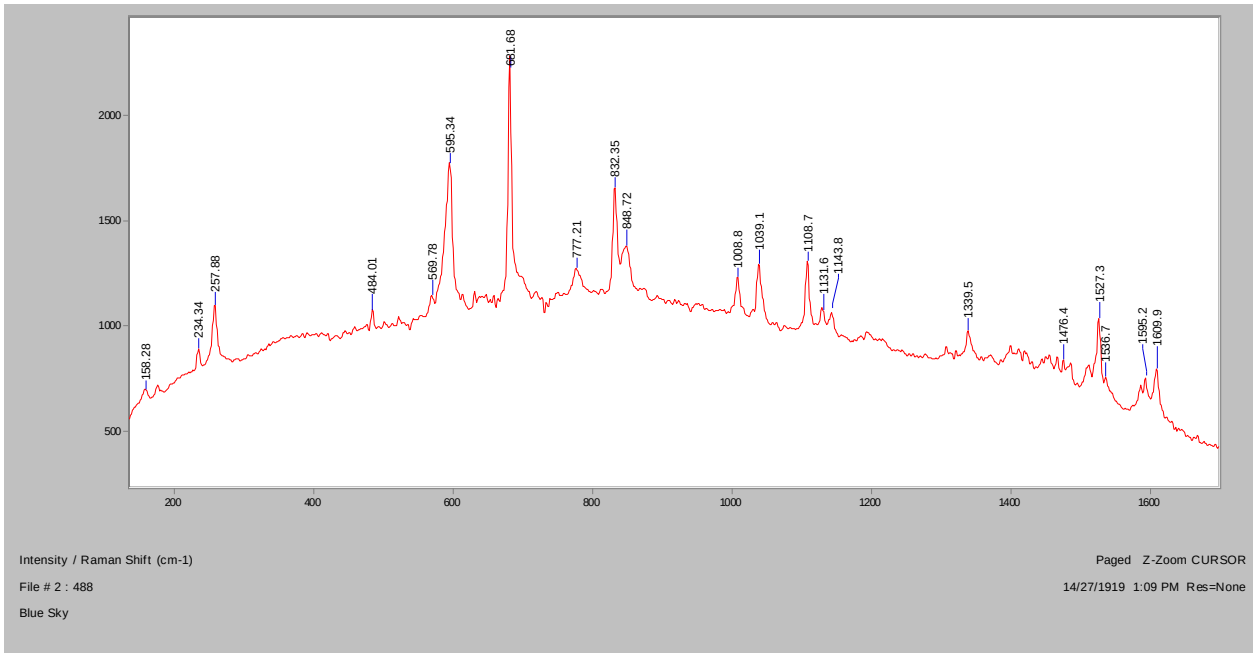

Normal Raman, 633nm

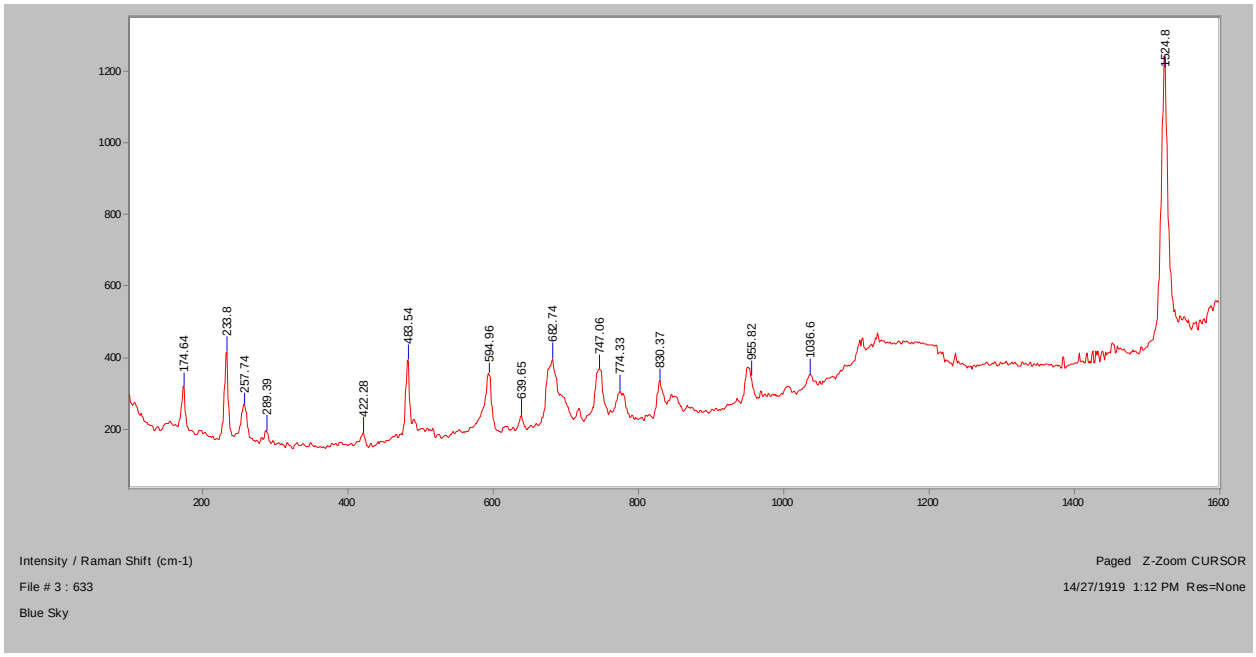

Normal Raman, 785nm

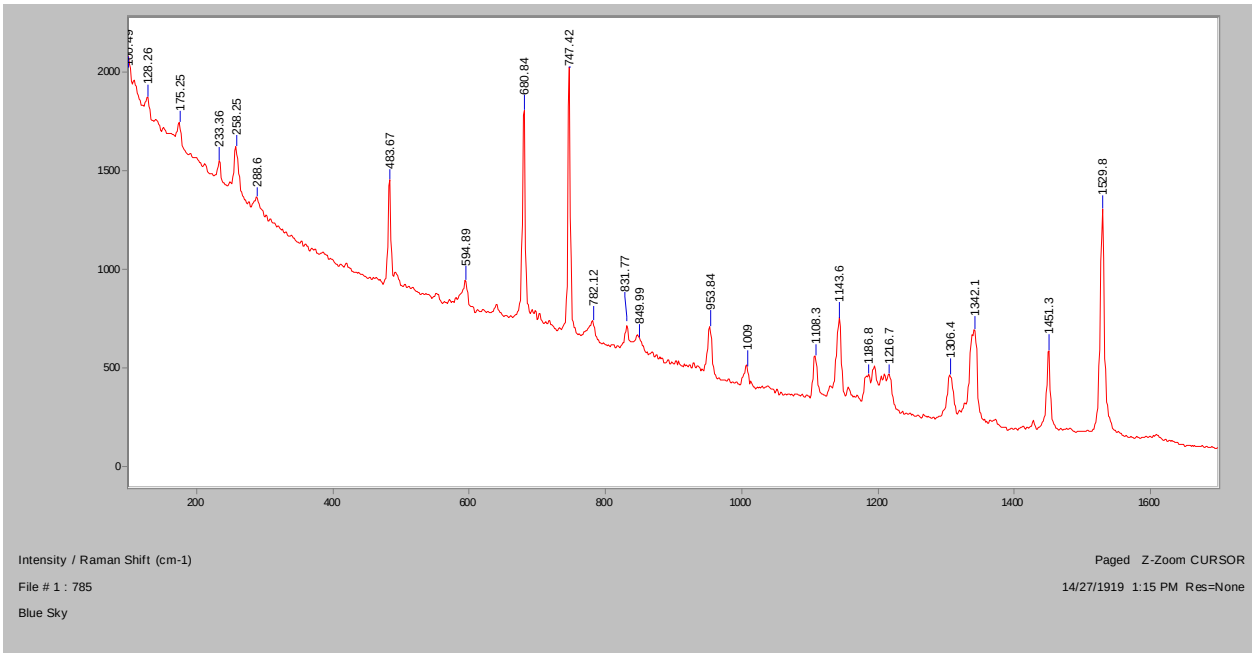

Turquoise Blue

Normal Raman, 488nm

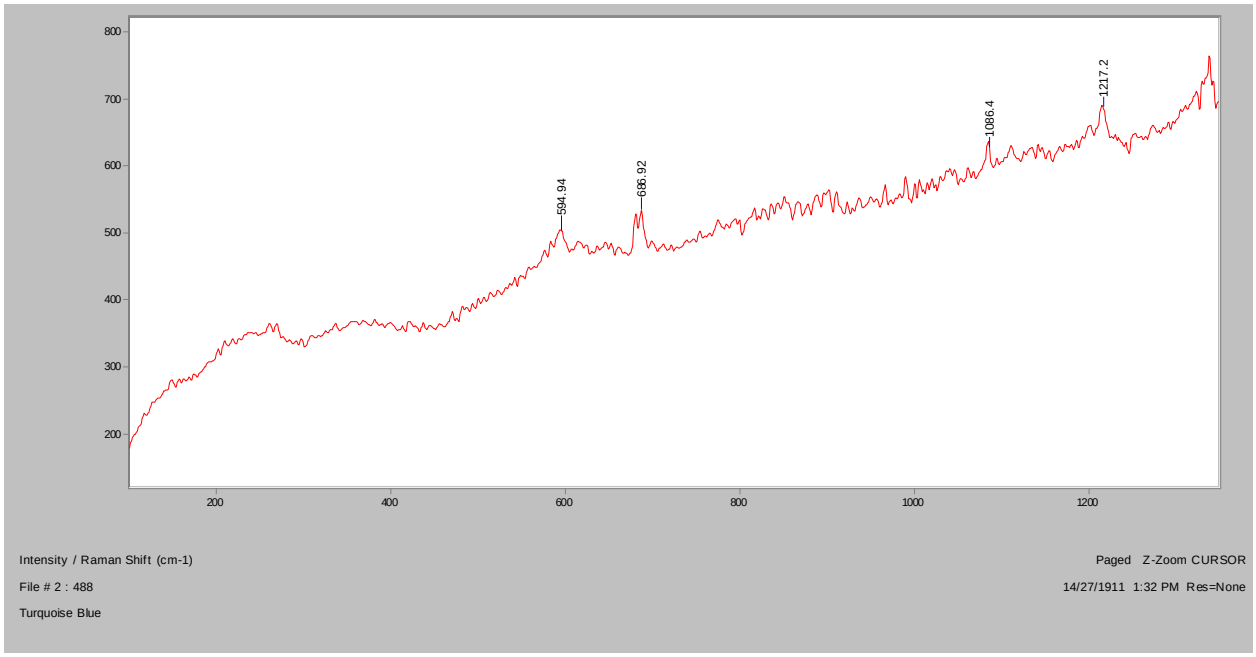

Normal Raman, 633nm

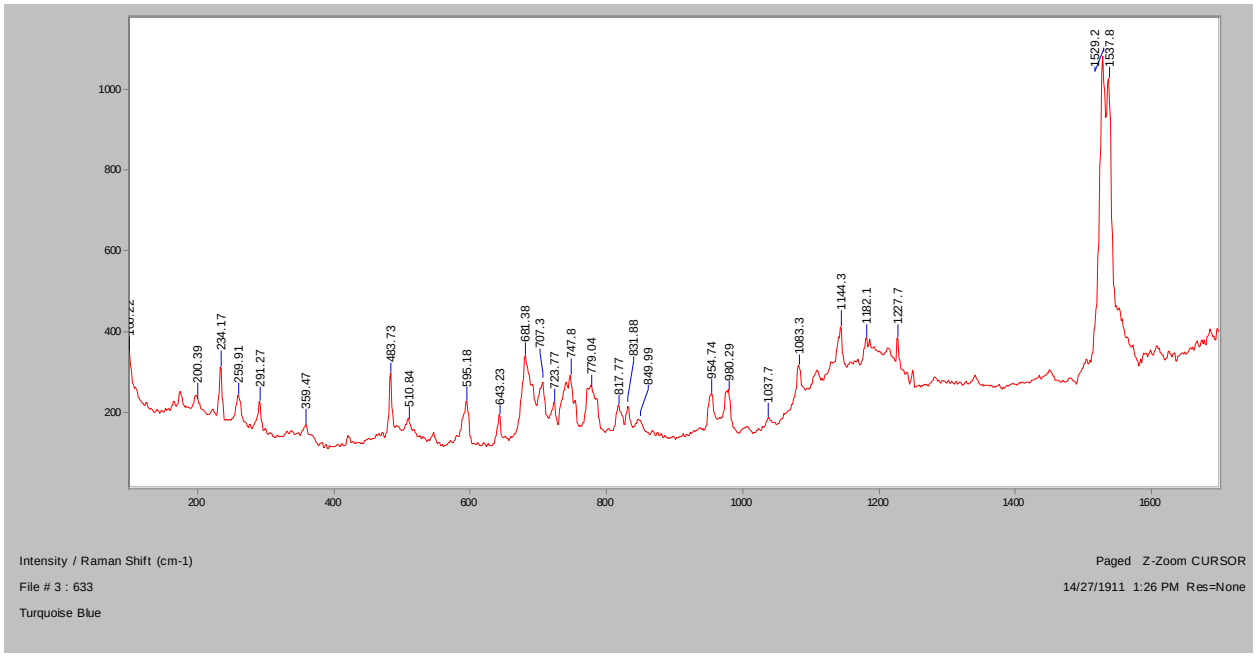

Normal Raman, 785nm

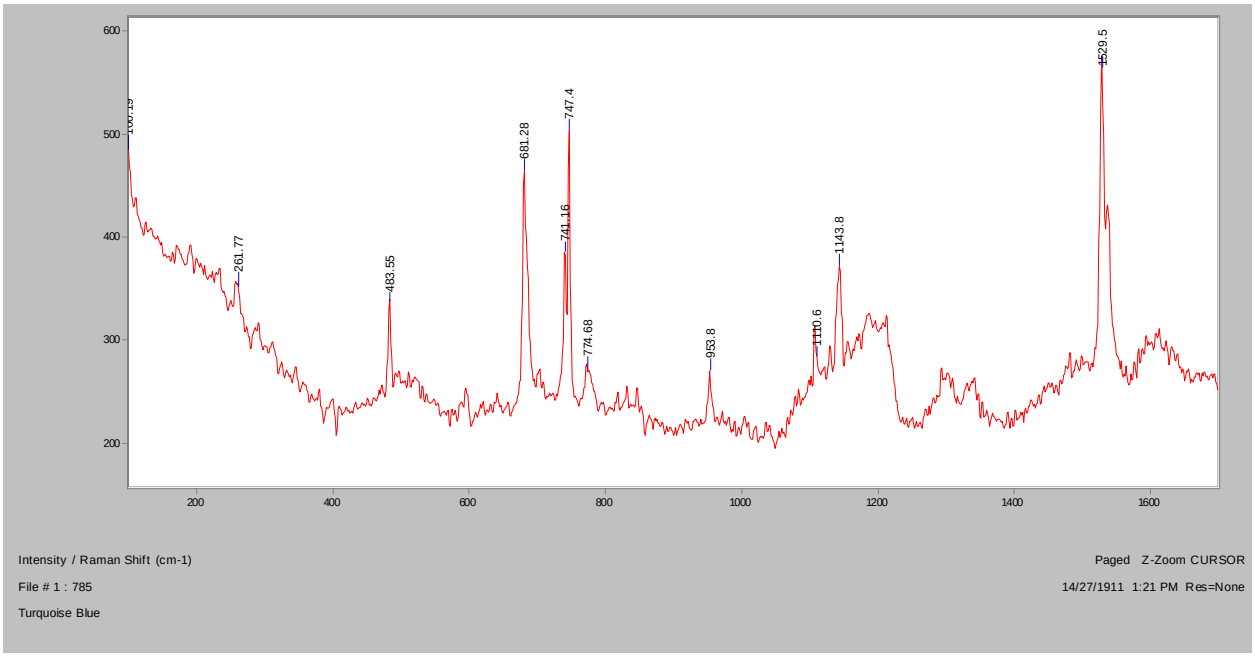

Cyan

Normal Raman, 488nm

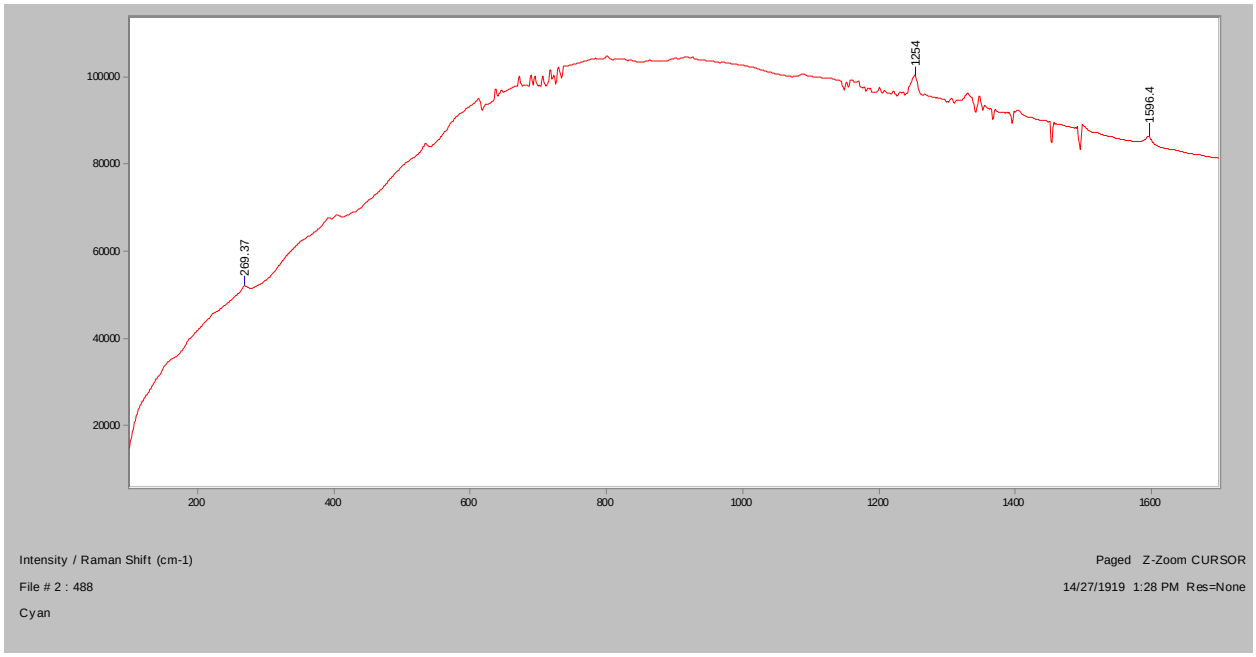

Normal Raman, 633nm

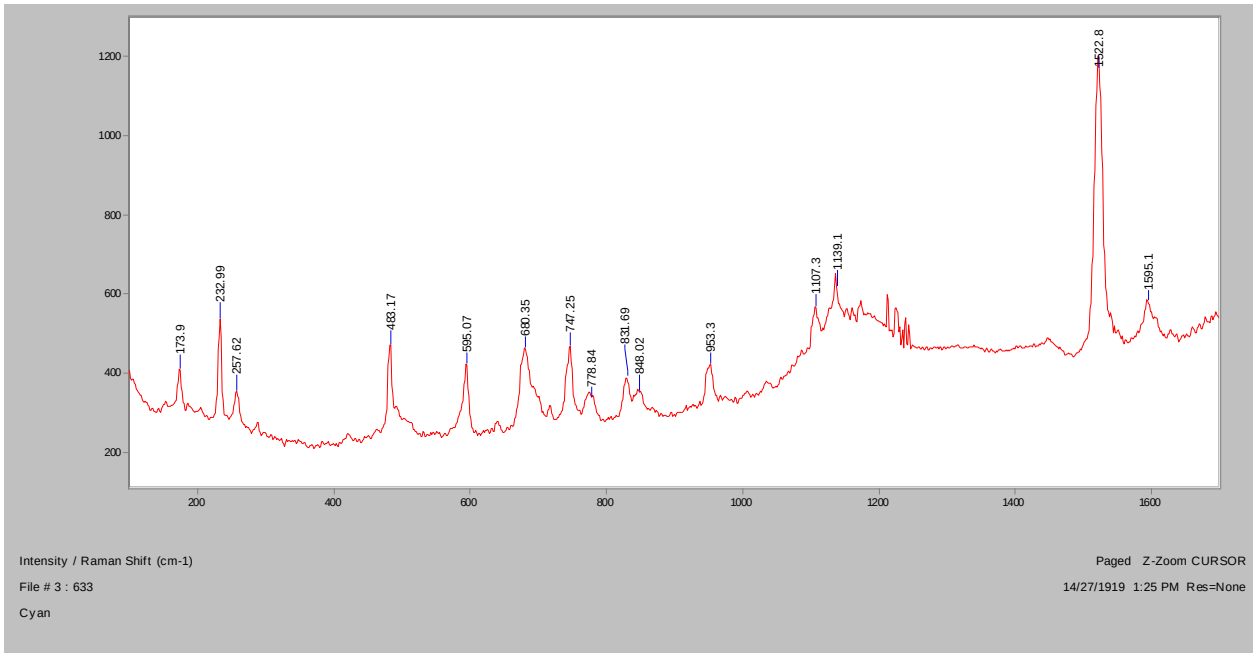

Normal Raman, 785nm

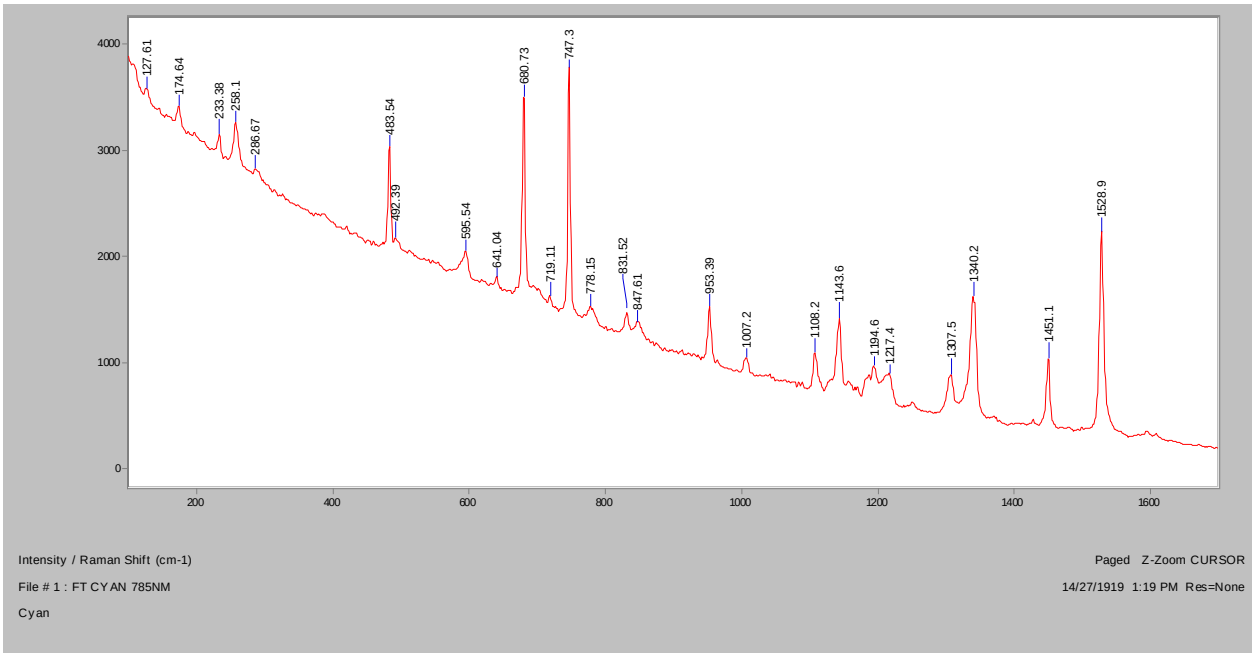

Dark Cyan

Normal Raman, 488nm

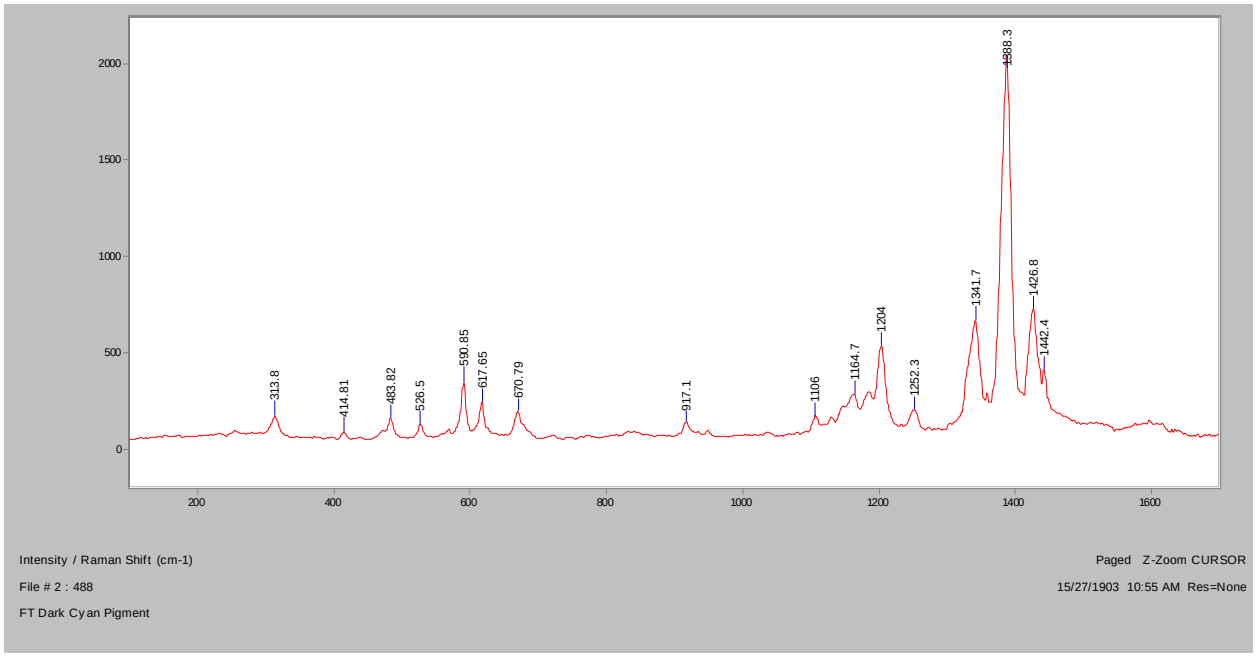

Normal Raman, 633nm

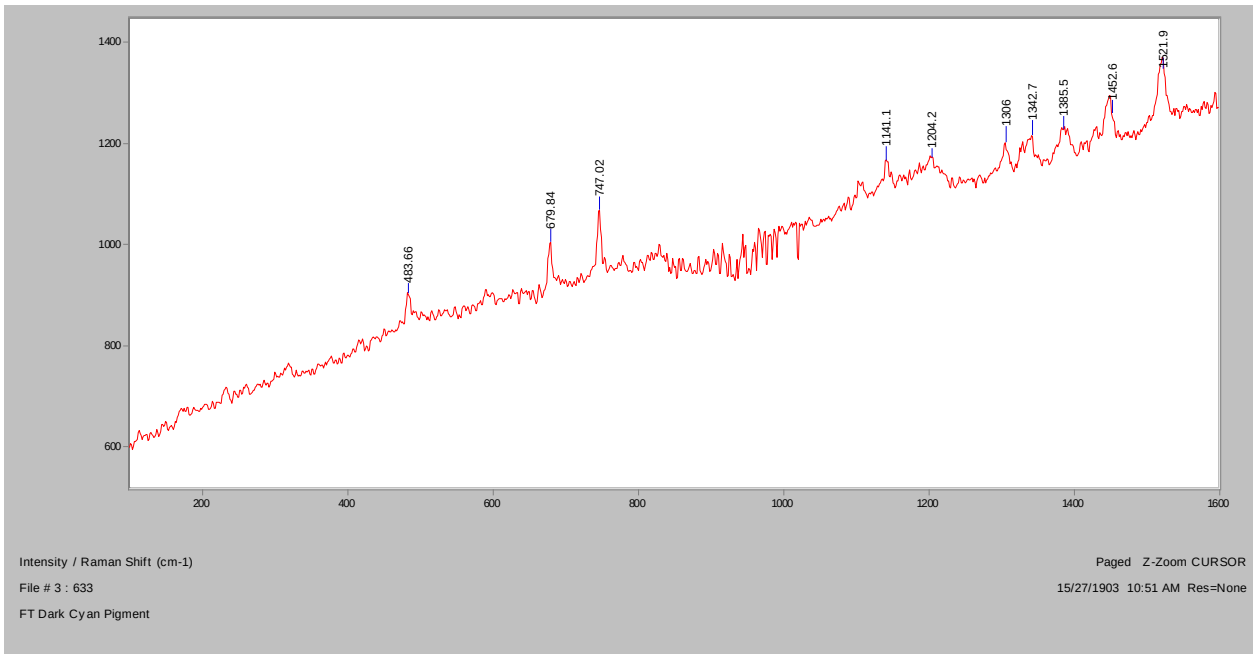

Normal Raman, 785nm

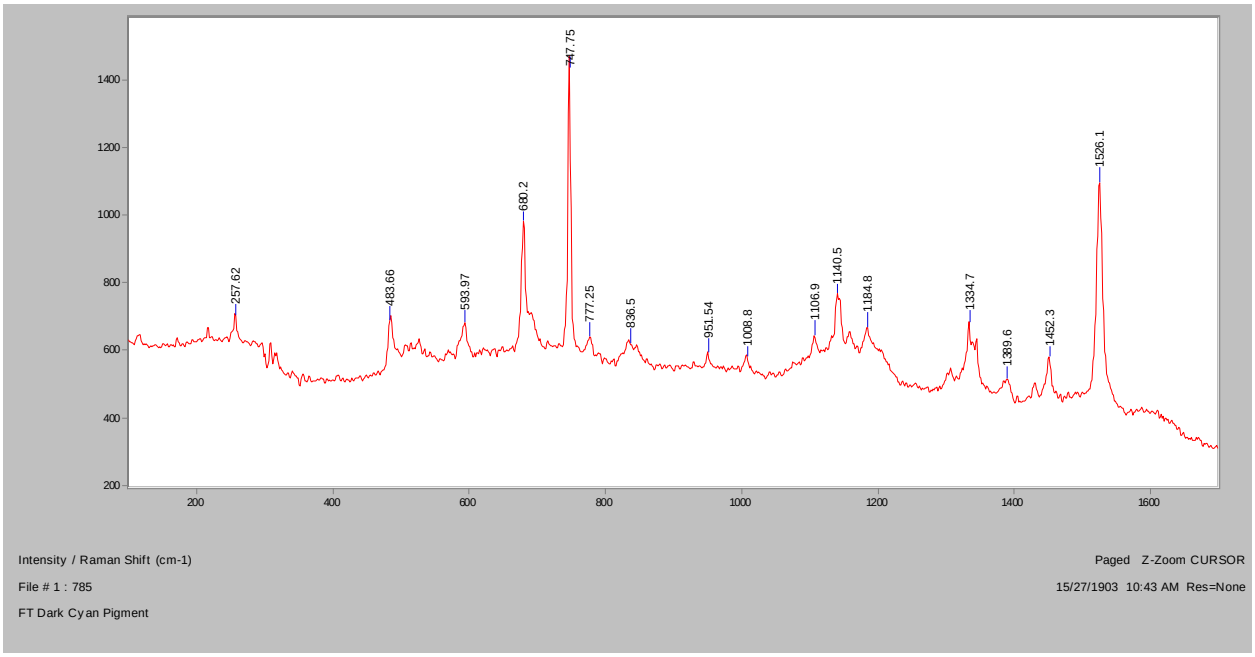

Blue

Normal Raman, 488nm

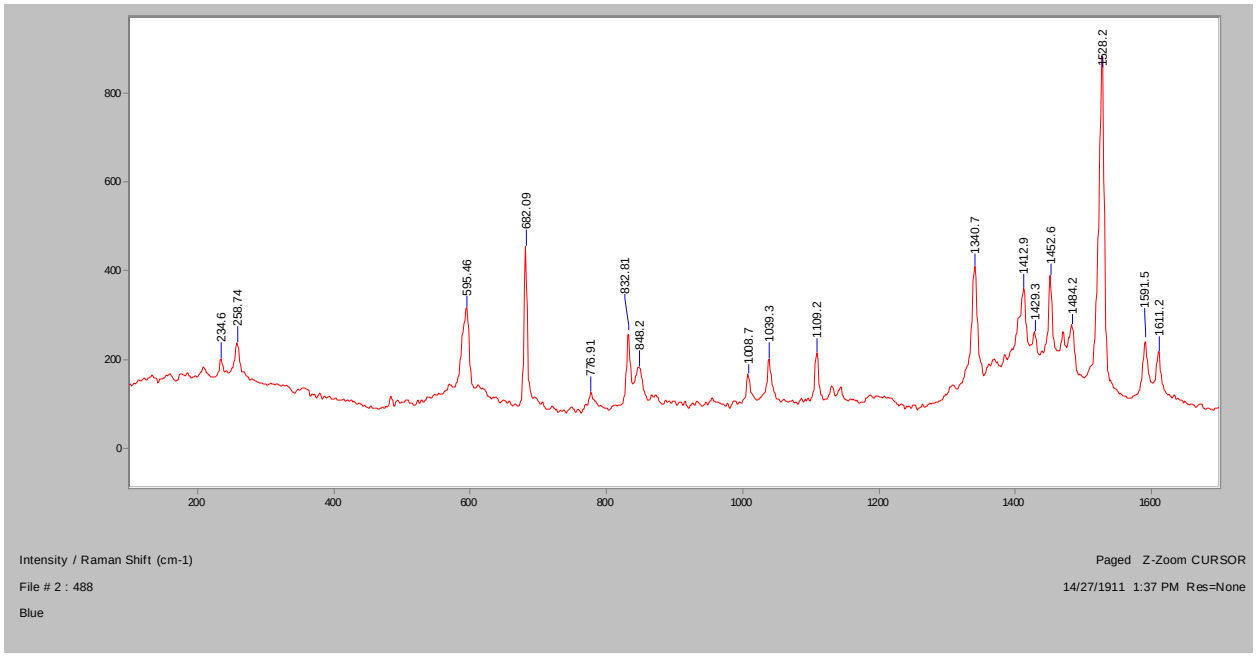

Normal Raman, 633nm

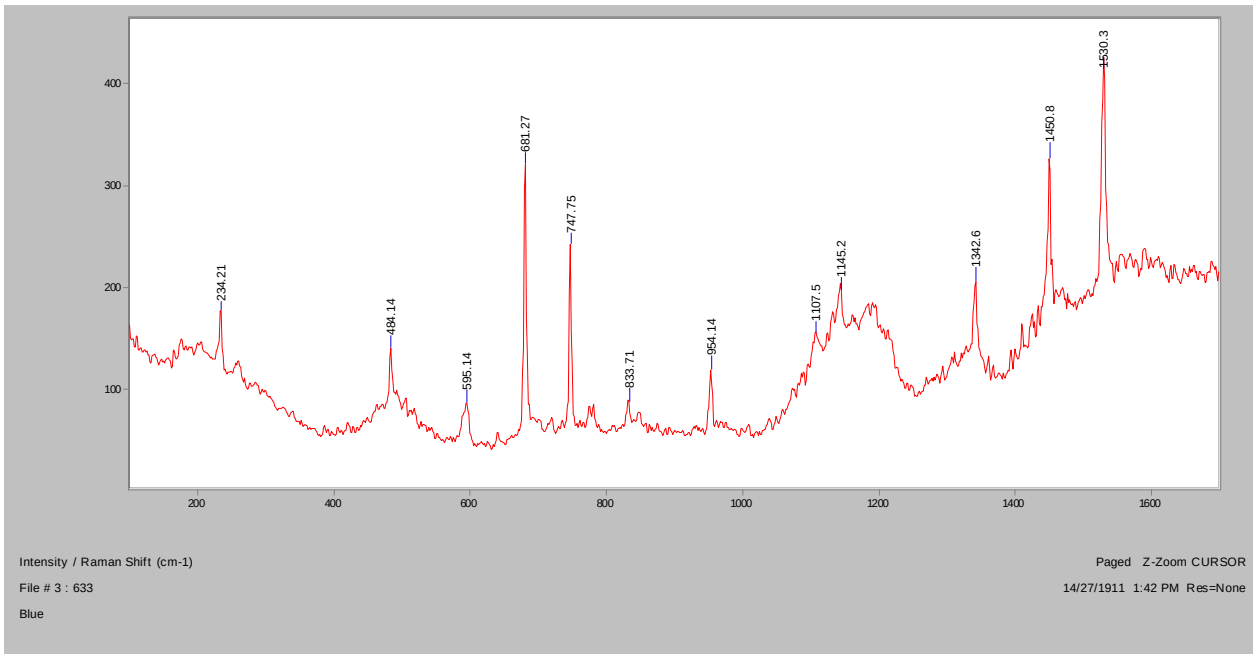

Normal Raman, 785nm

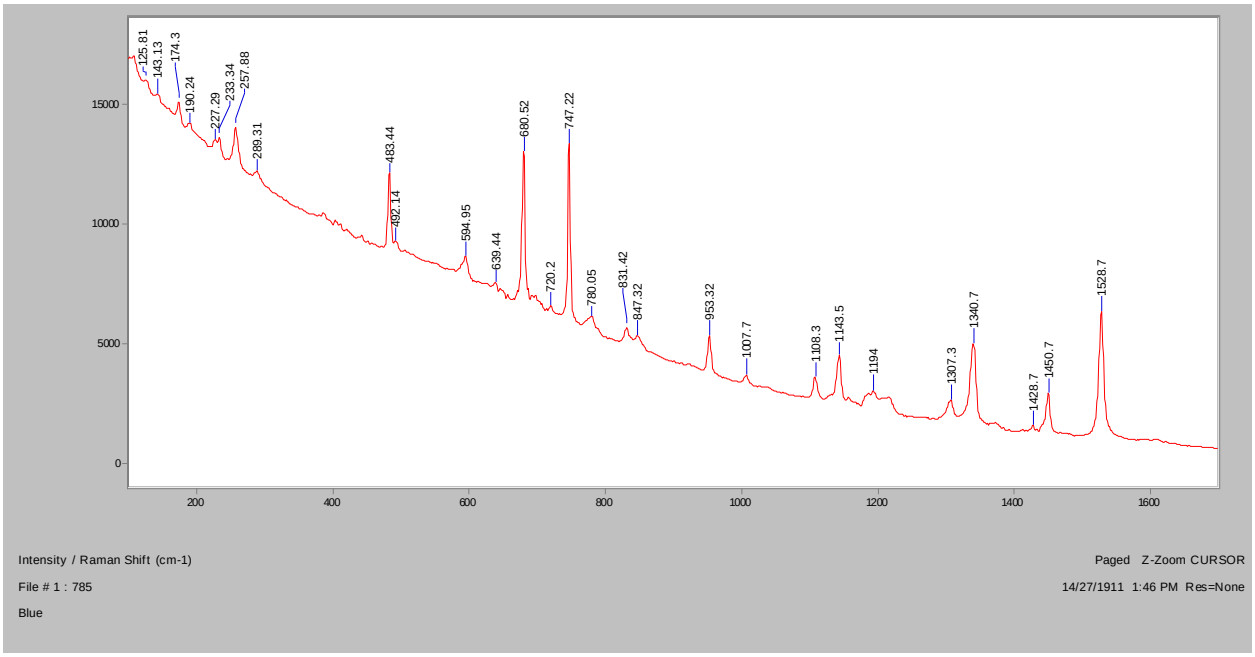

Navy Blue

Normal Raman, 488nm

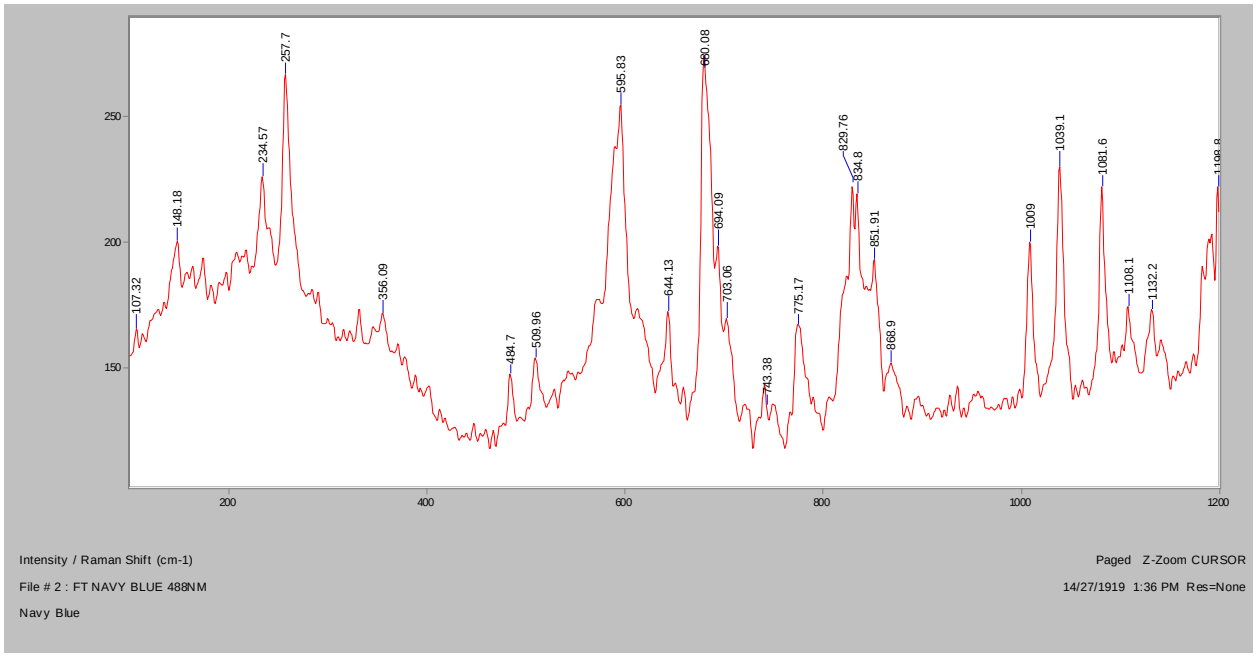

Normal Raman, 633nm

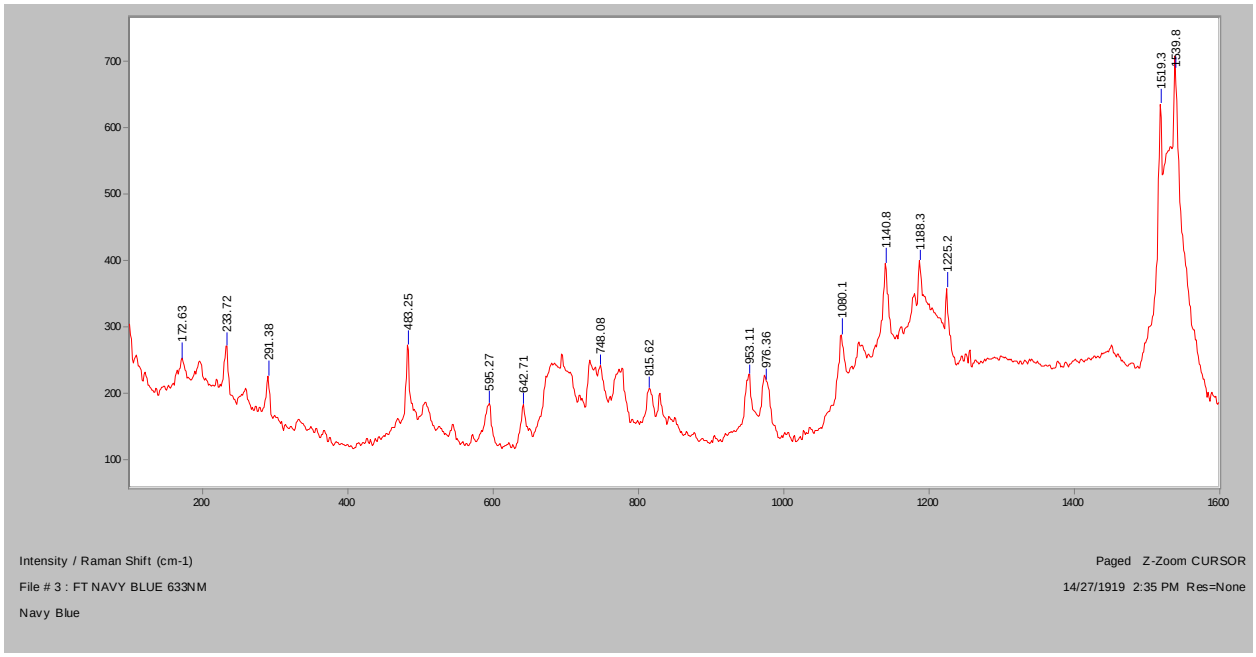

Normal Raman, 785nm

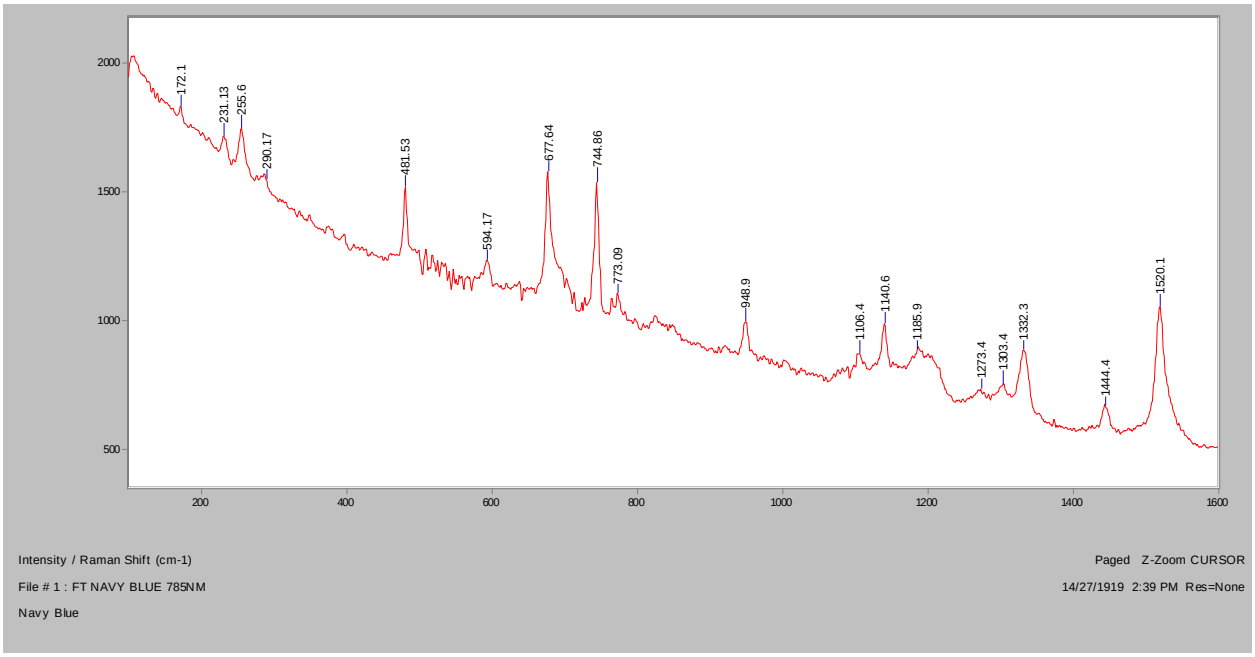

Dark Blue

Normal Raman, 488nm

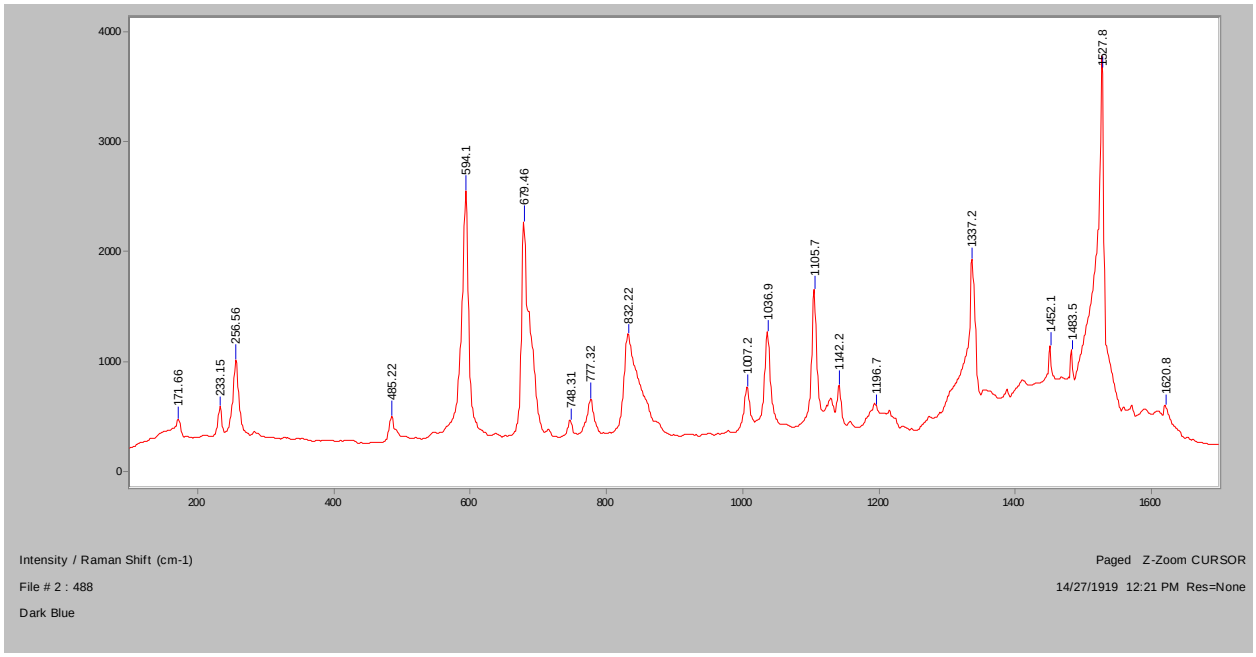

Normal Raman, 633nm

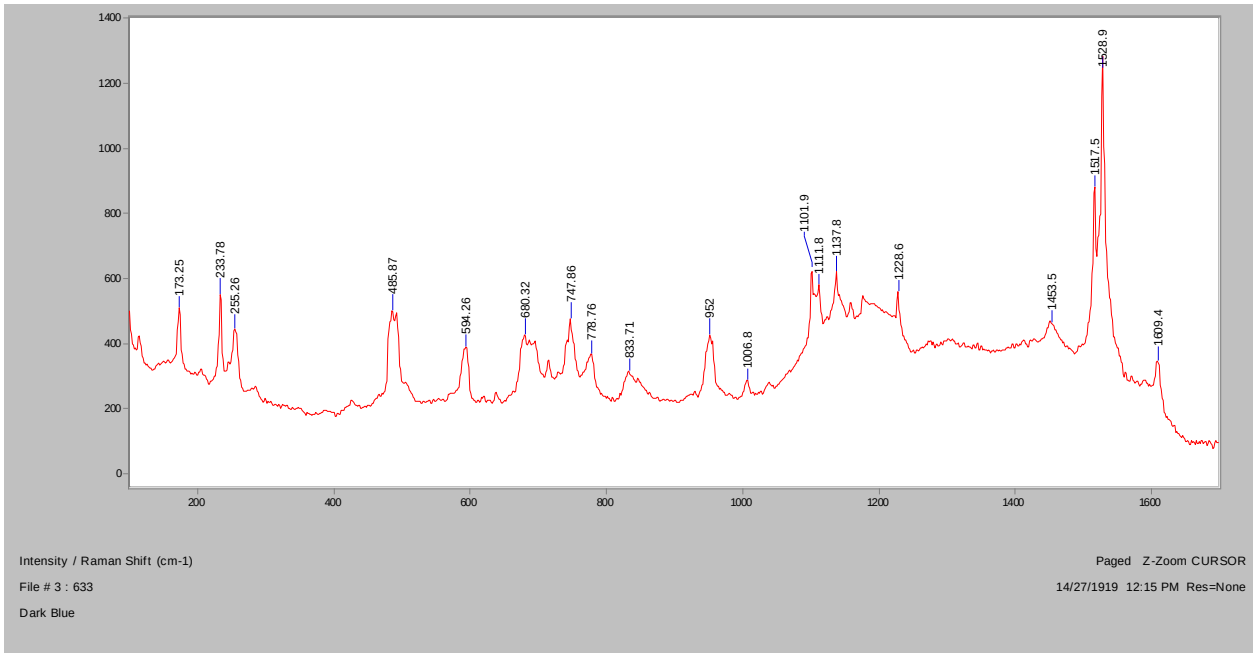

Normal Raman, 785nm

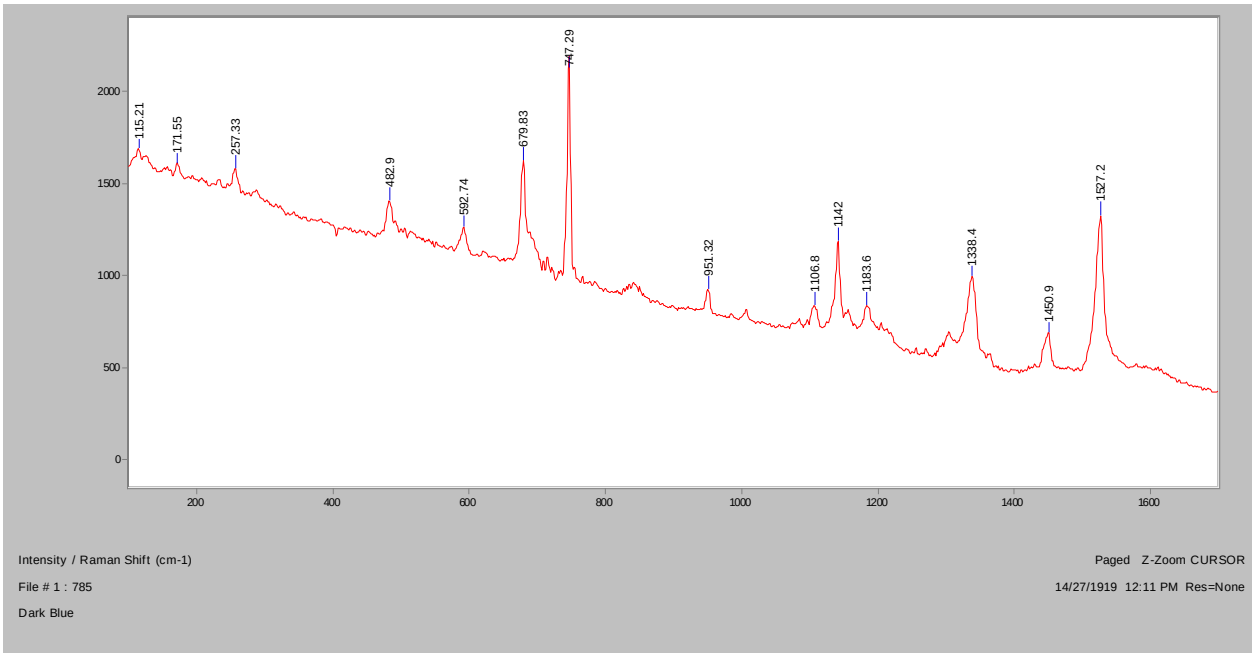

Grape

Normal Raman, 488nm

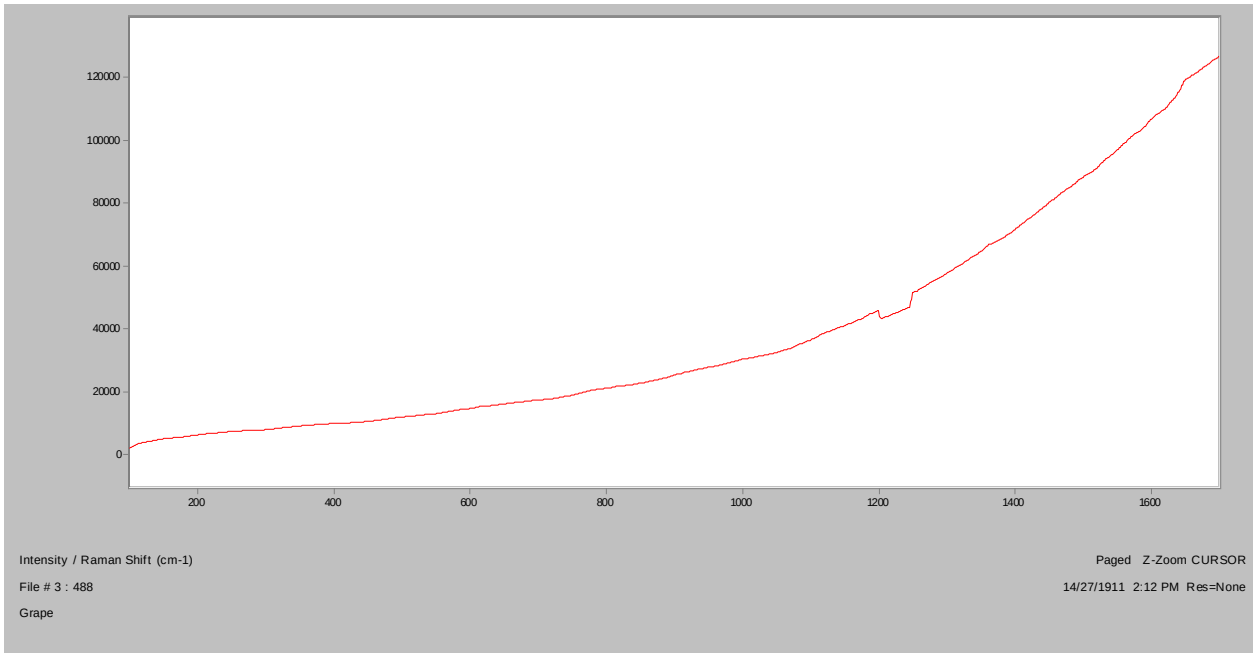

Normal Raman, 633nm

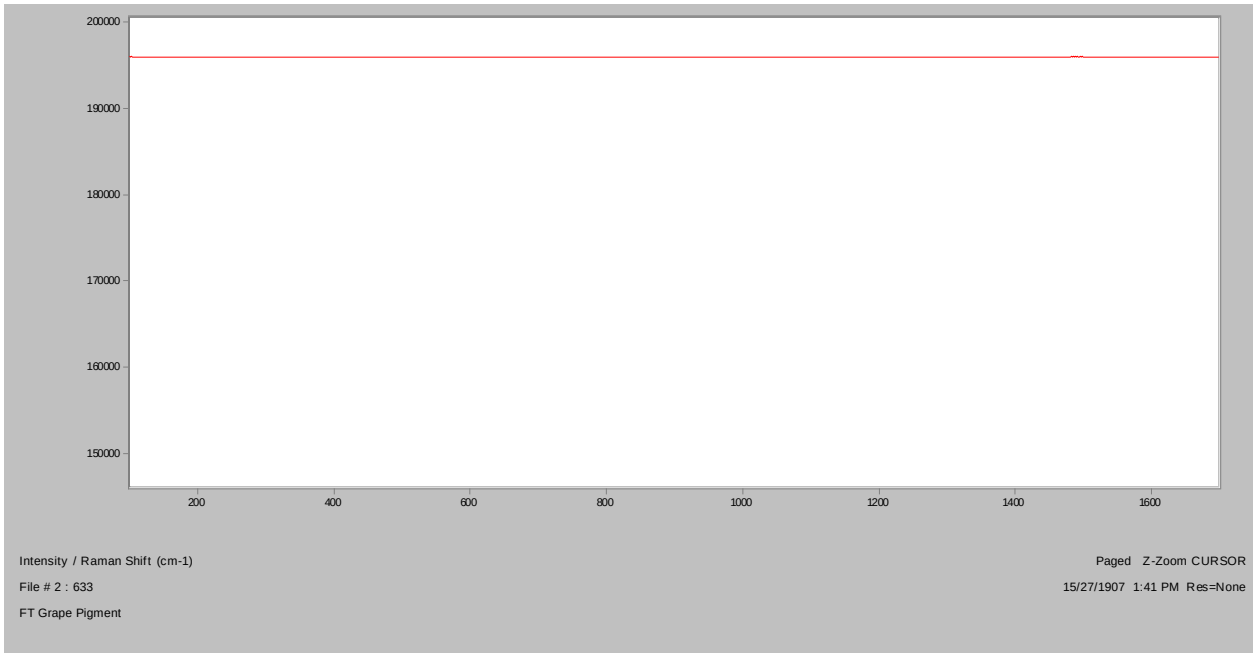

Normal Raman, 785nm

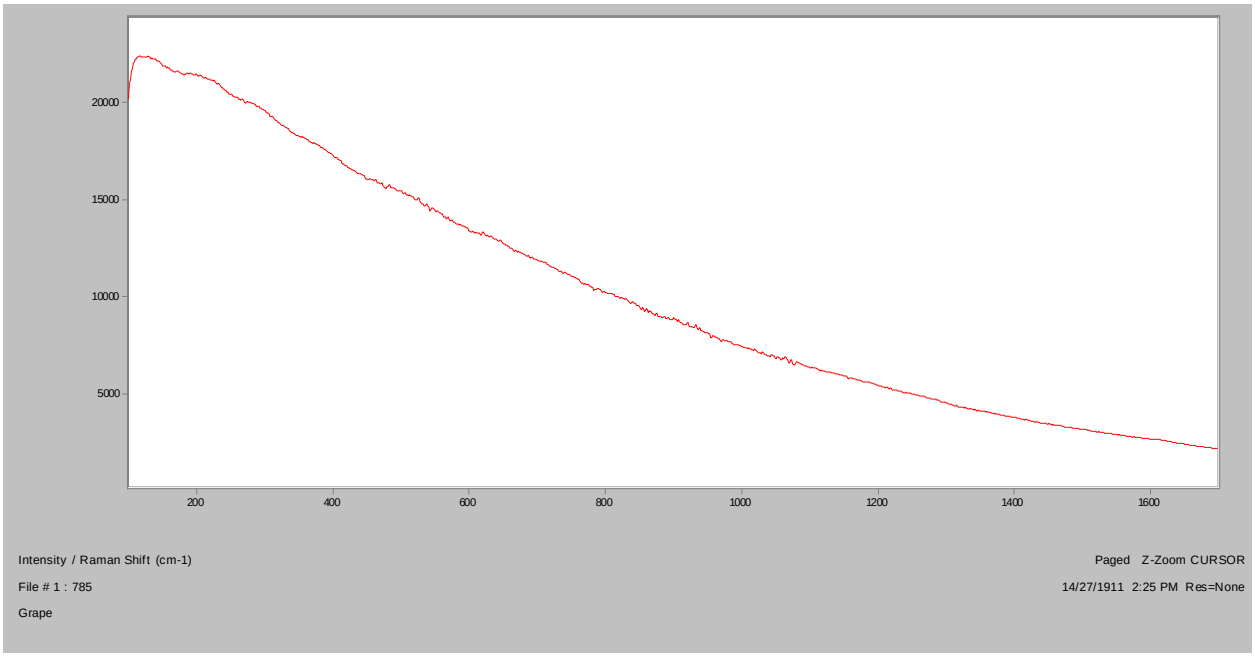

Purple

Normal Raman, 488nm

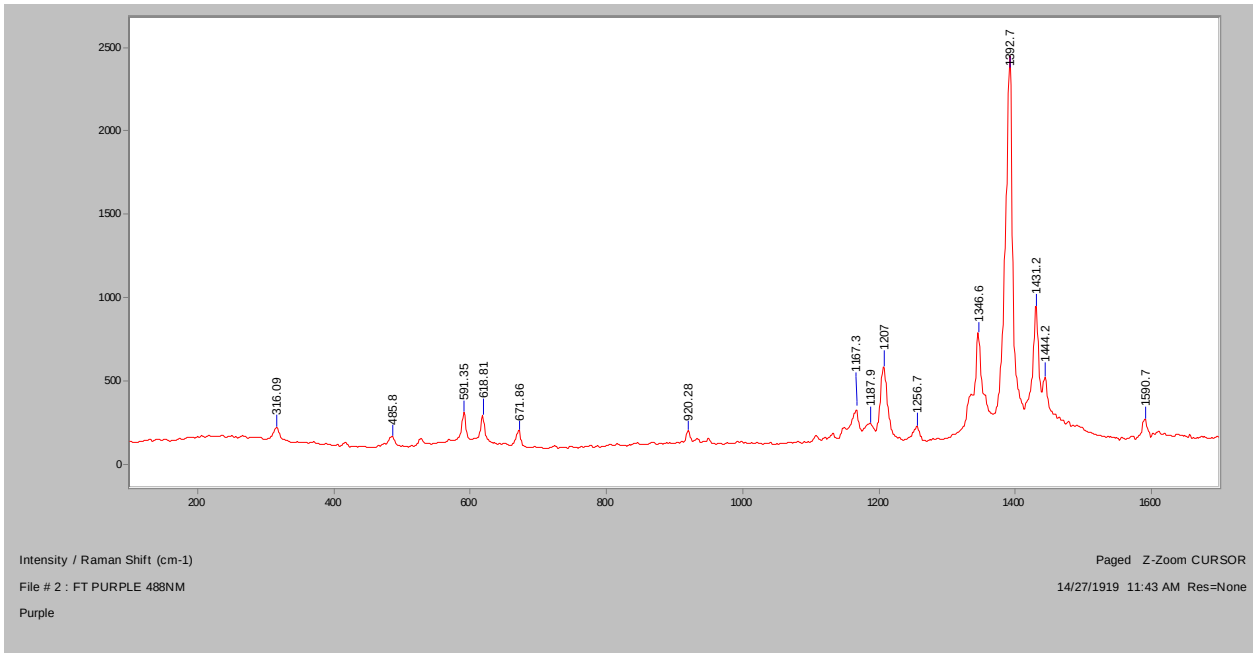

Normal Raman, 633nm

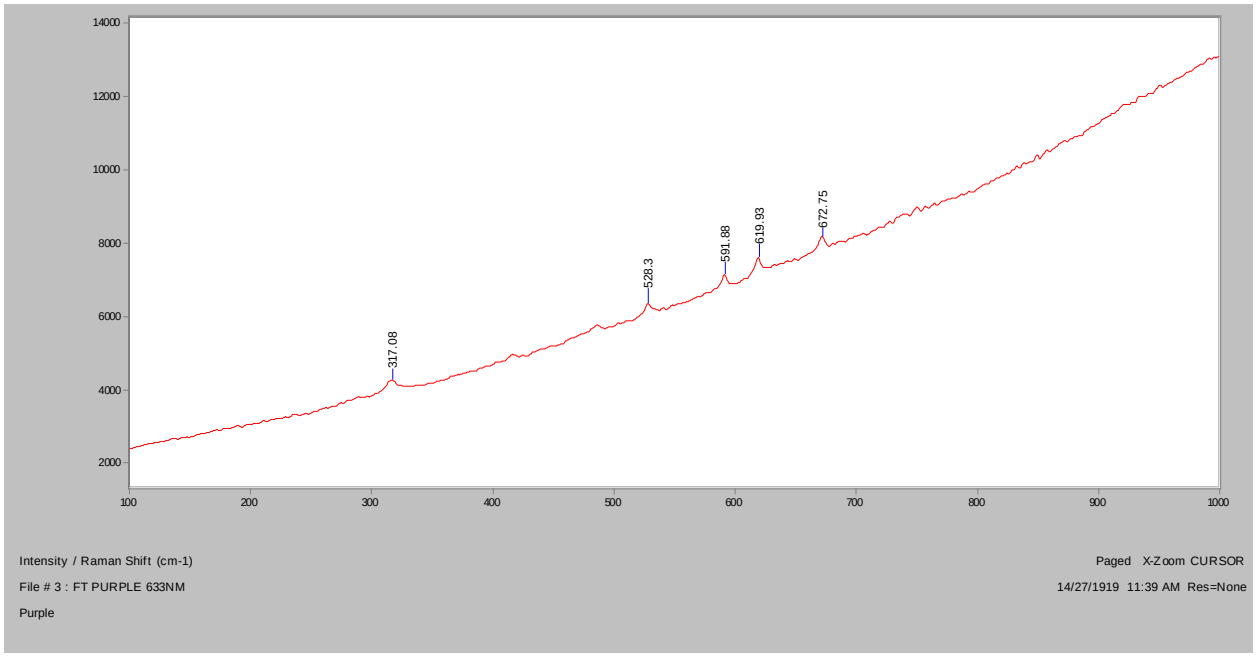

Normal Raman, 785nm

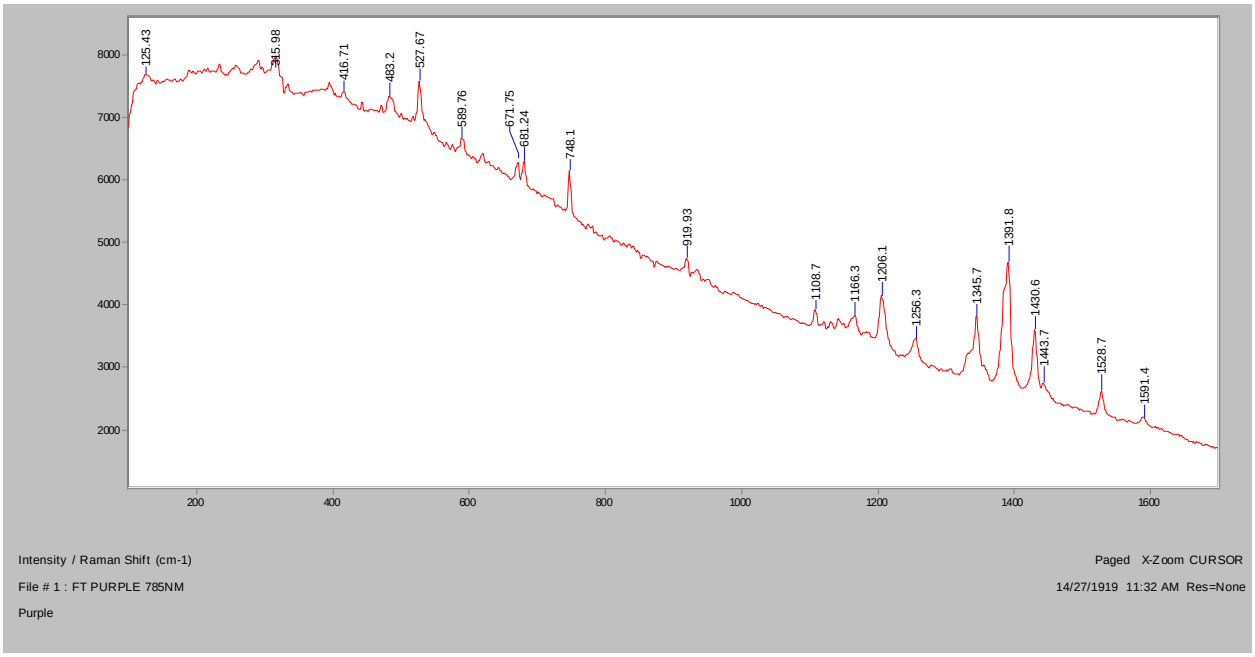

Violet

Normal Raman, 488nm

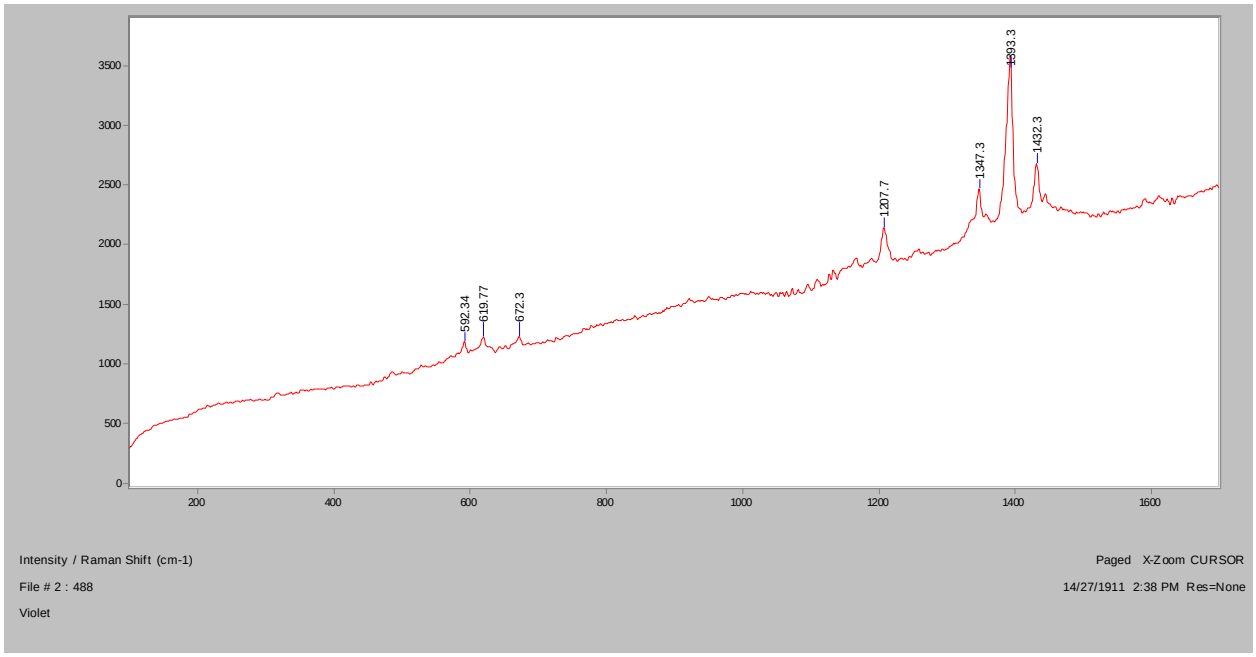

Normal Raman, 633nm

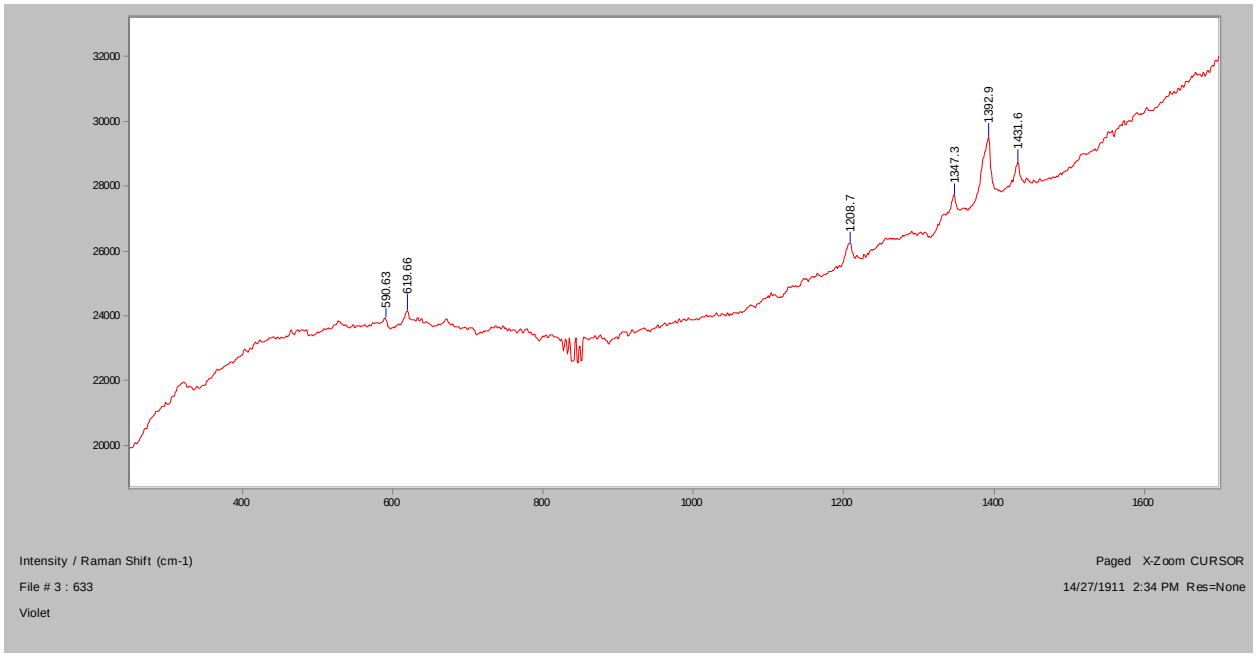

Normal Raman, 785nm

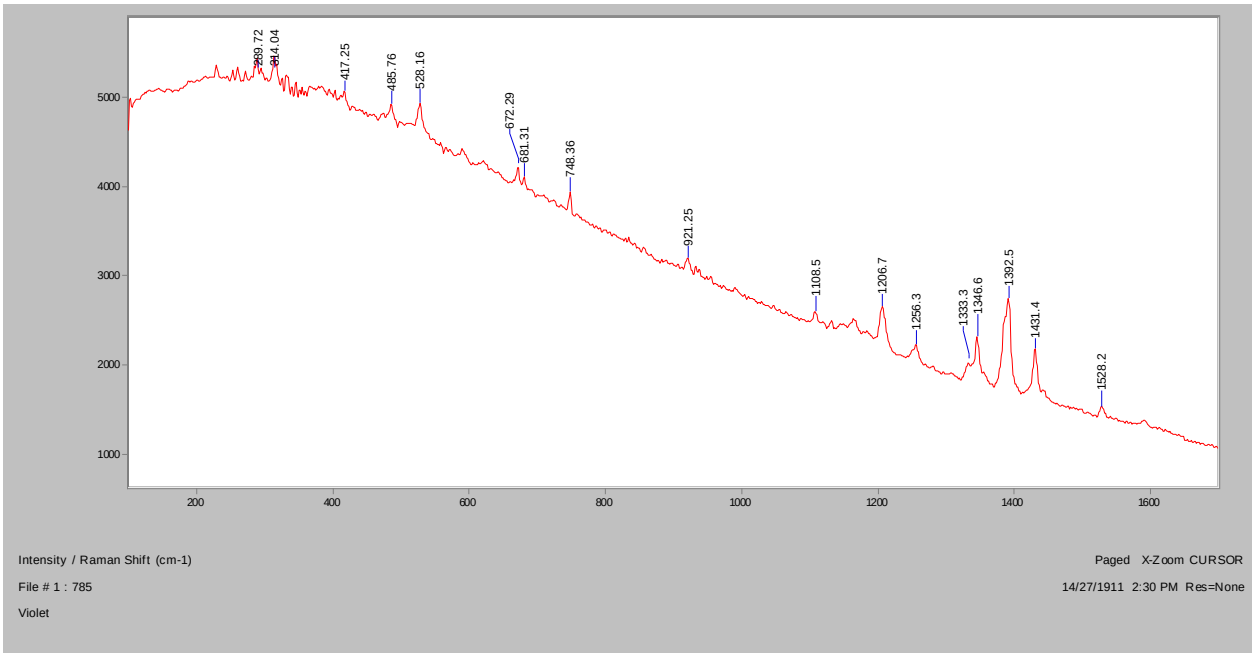

Grey

Normal Raman, 488nm

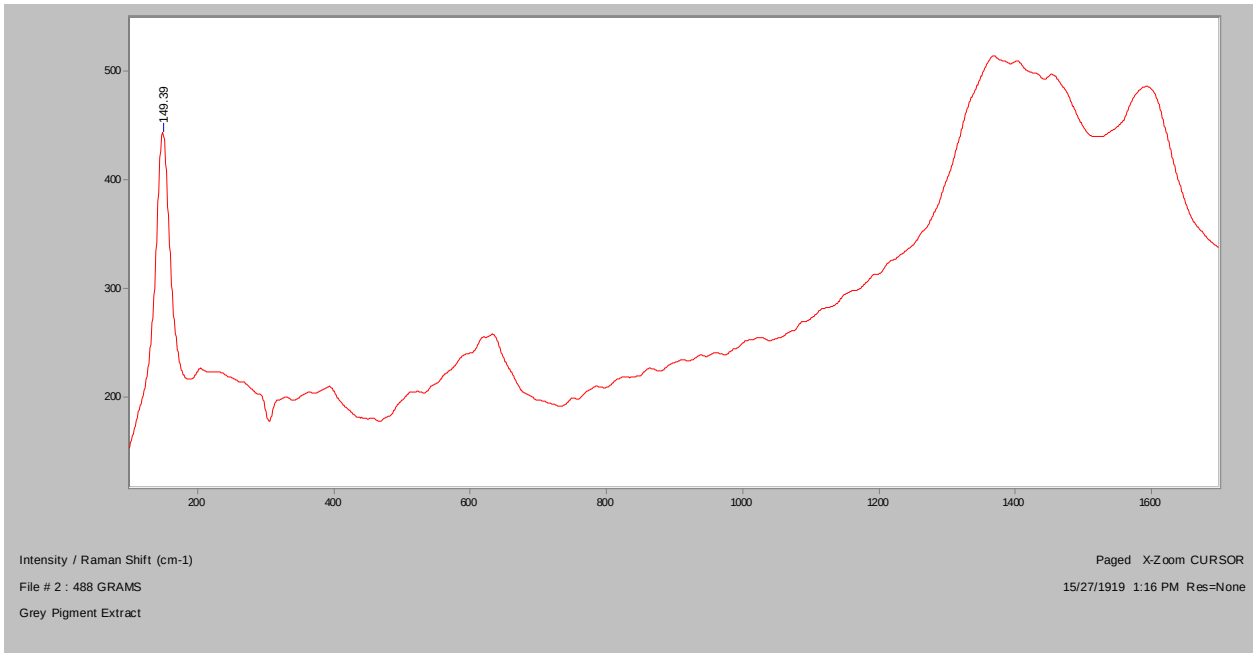

Normal Raman, 633nm

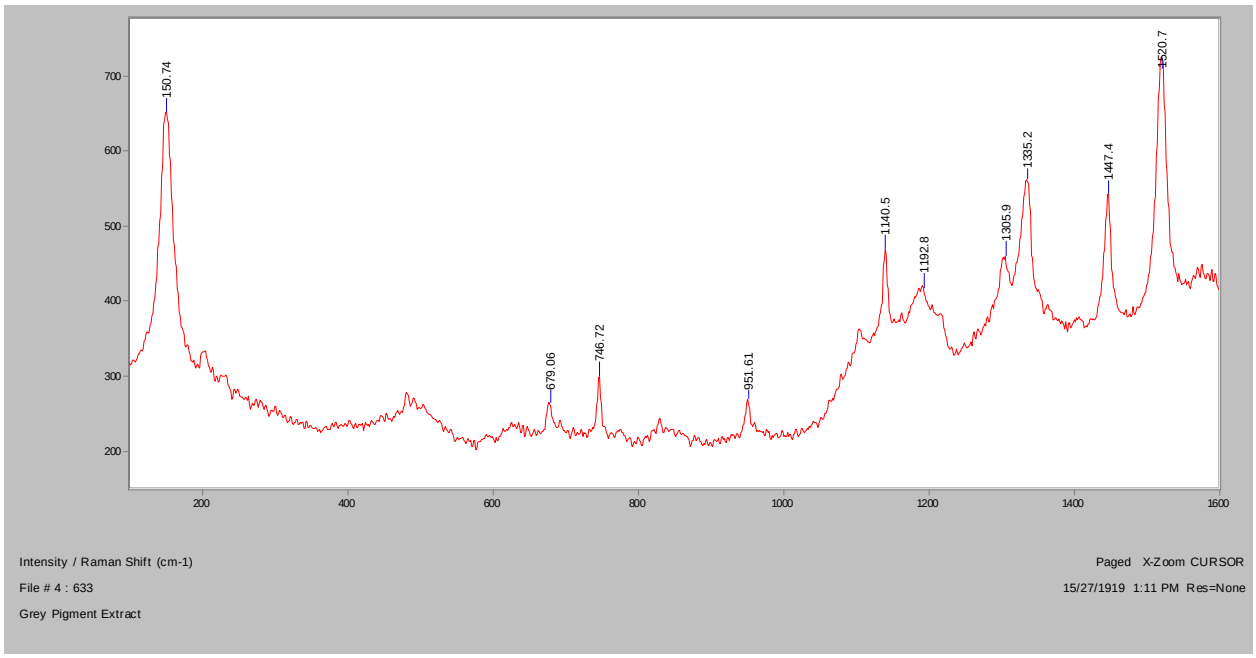

Normal Raman, 785nm

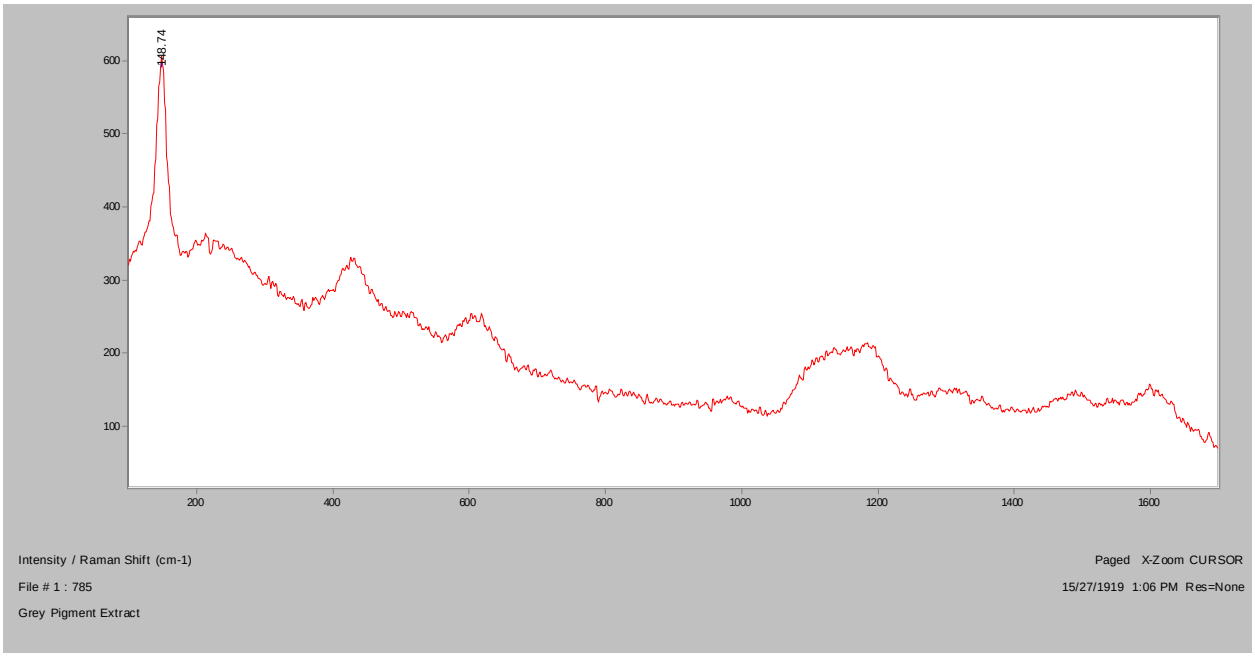

Bright Black

Normal Raman, 488nm

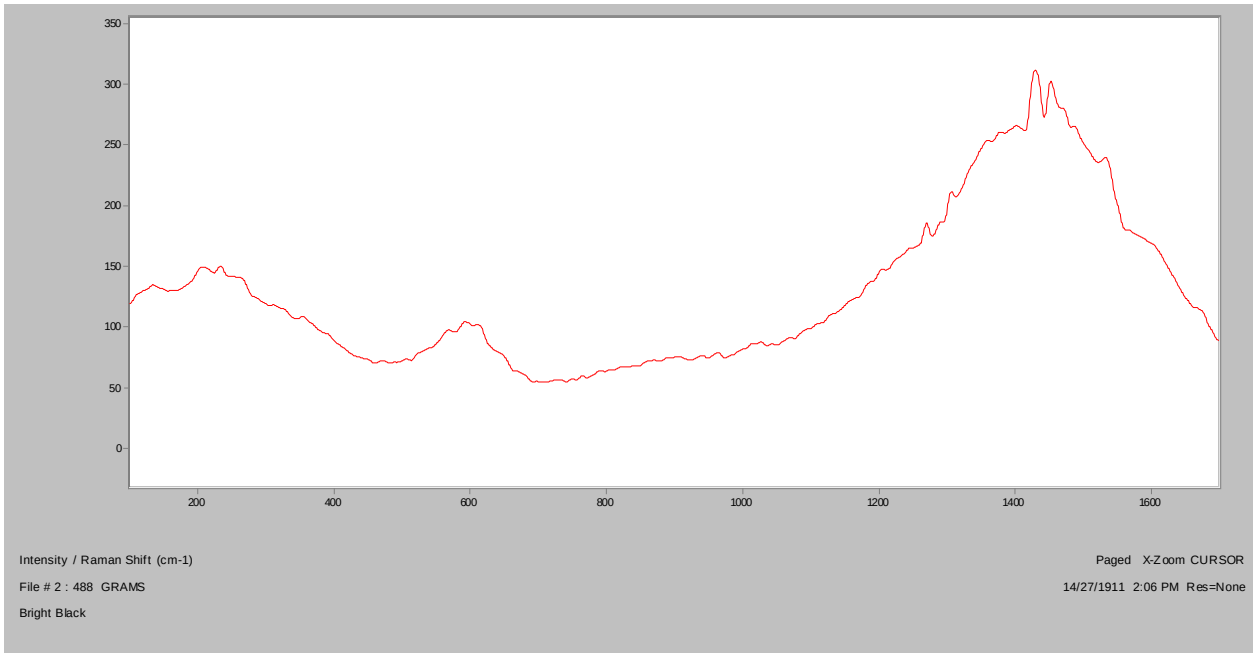

Normal Raman, 633nm

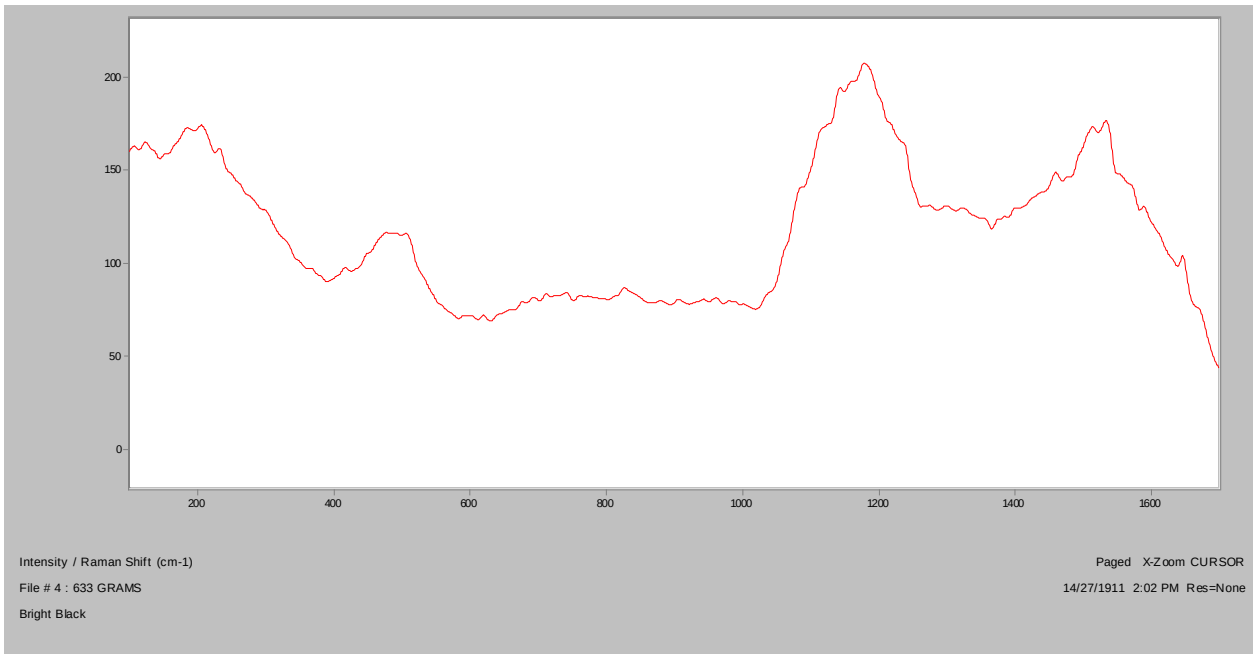

Normal Raman, 785nm

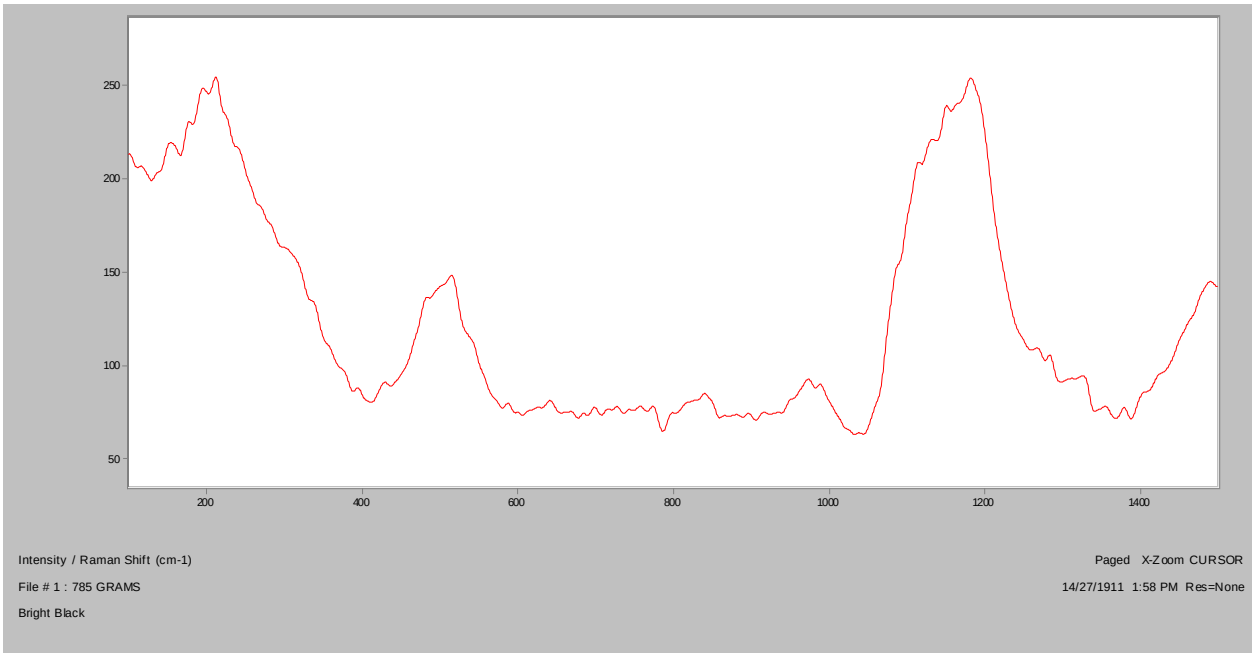

Black

Normal Raman, 488nm

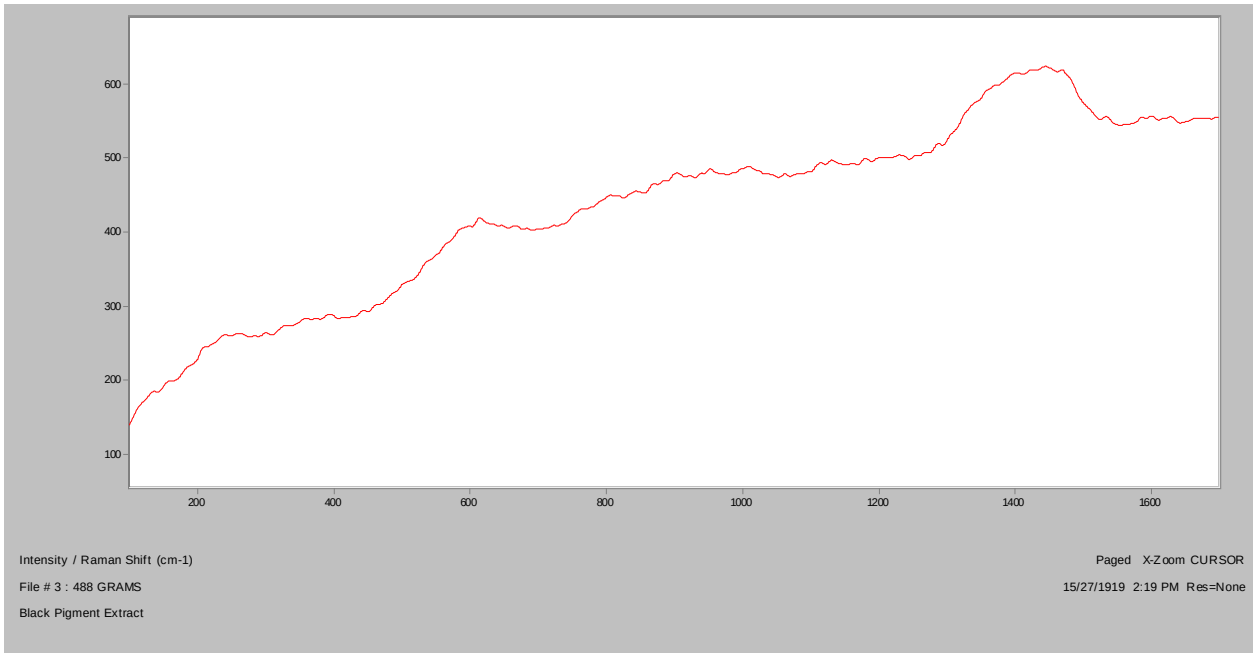

Normal Raman, 633nm

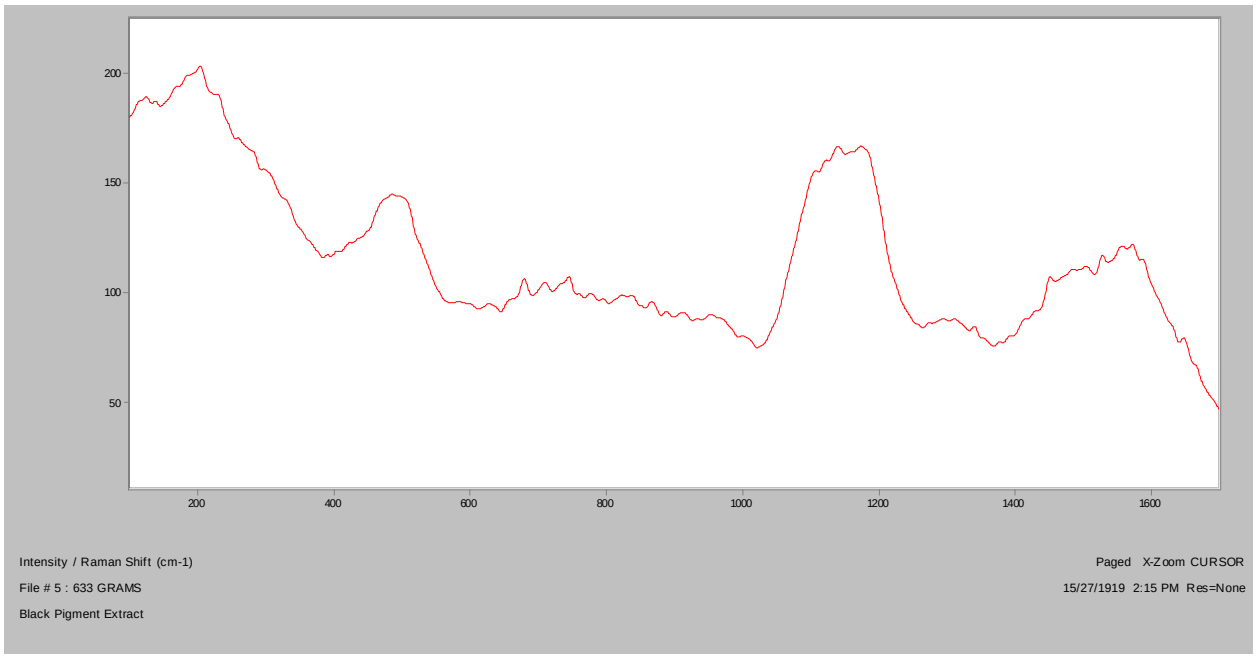

Normal Raman, 785nm

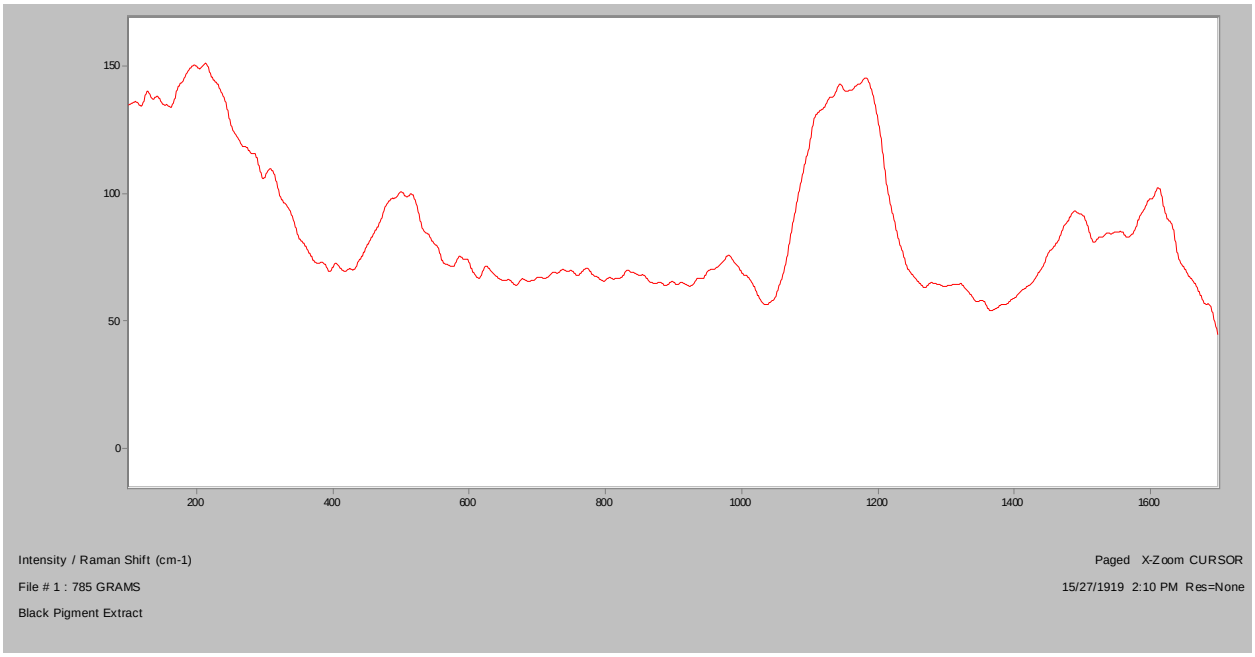

Eggplant Black

Normal Raman, 488nm

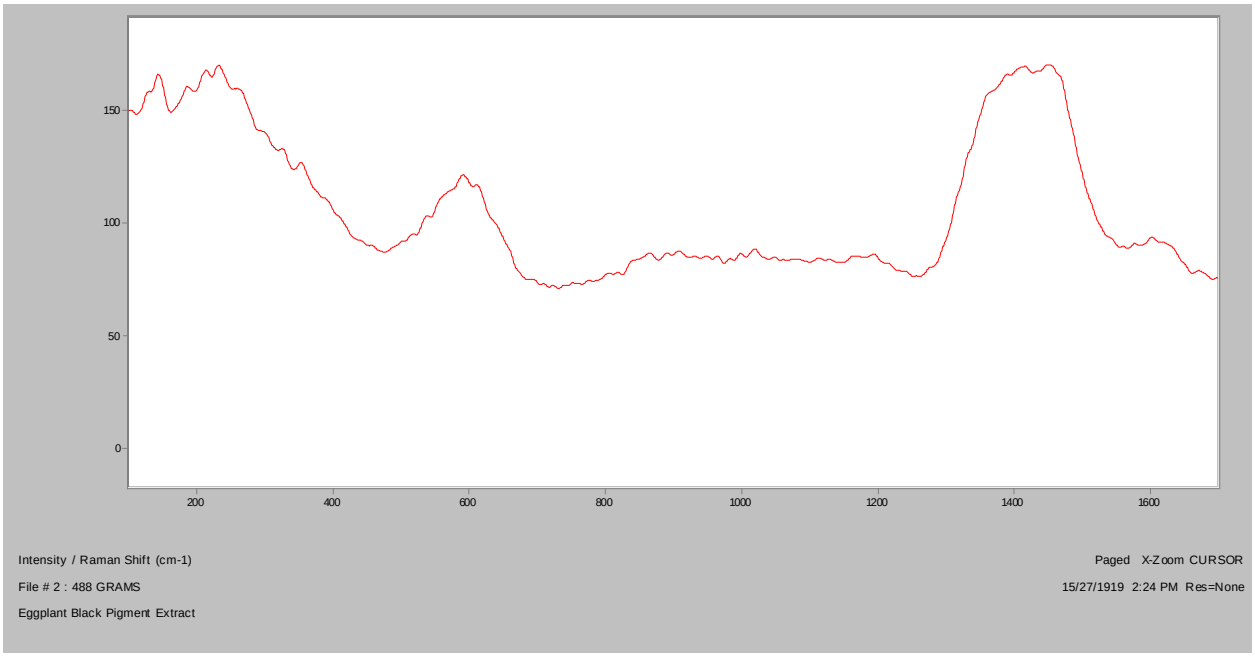

Normal Raman, 633nm

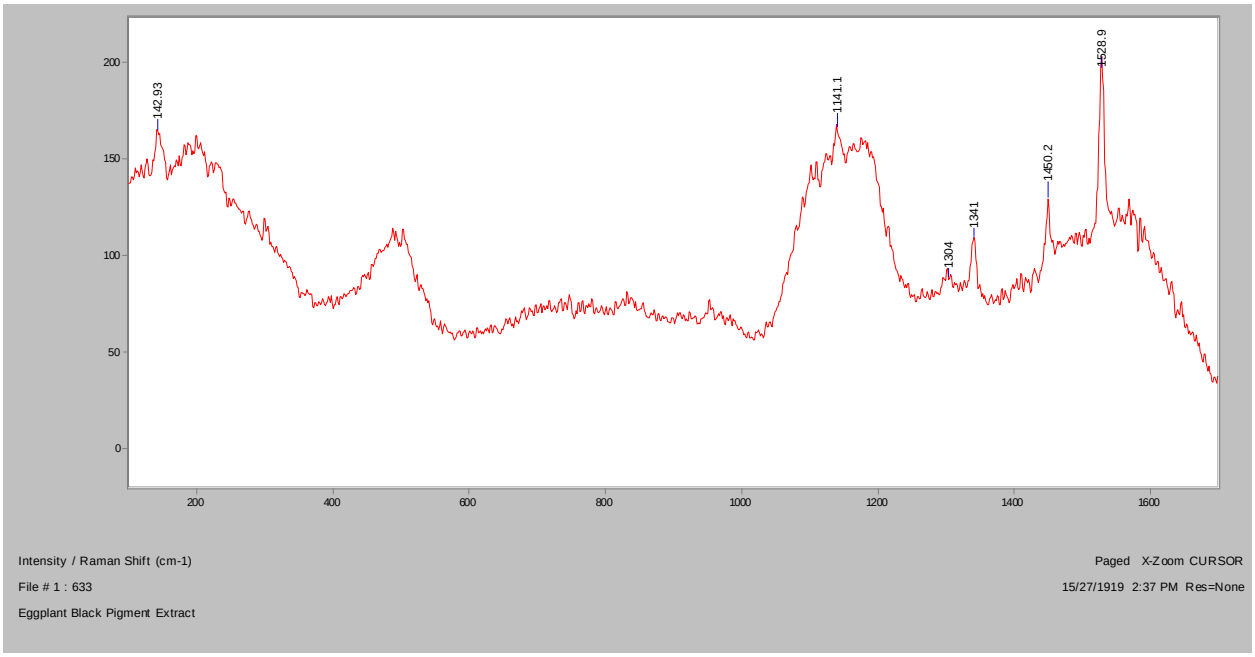

Normal Raman, 785nm

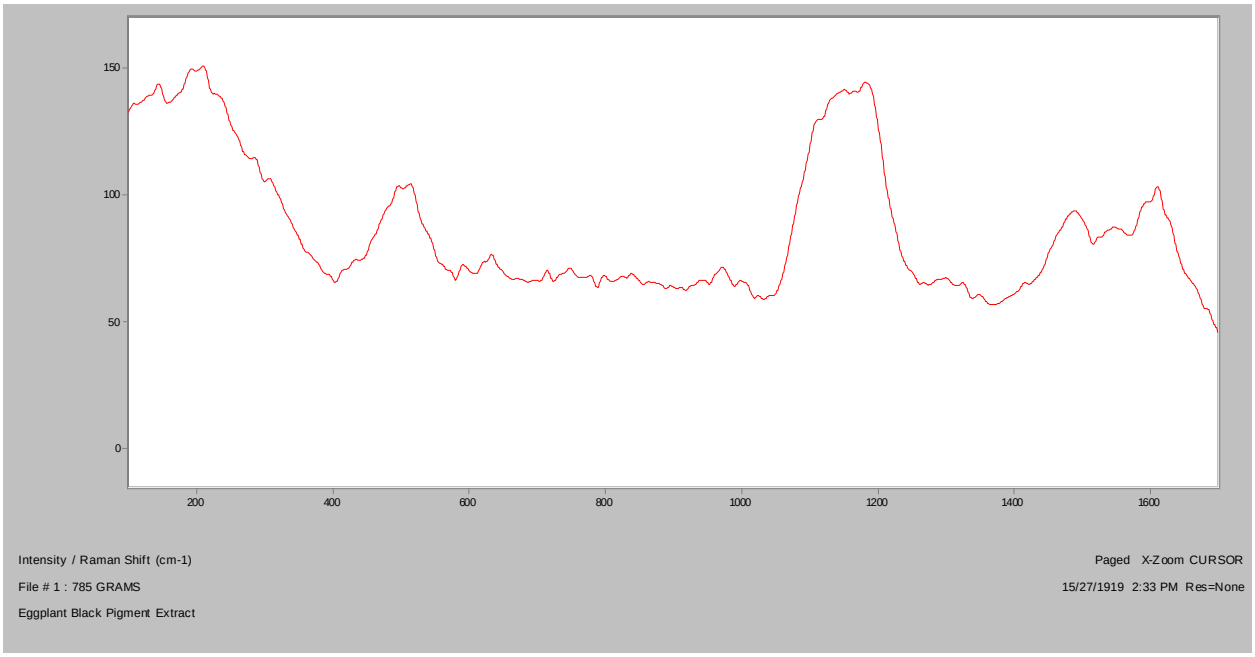

Dark Black

Normal Raman, 488nm

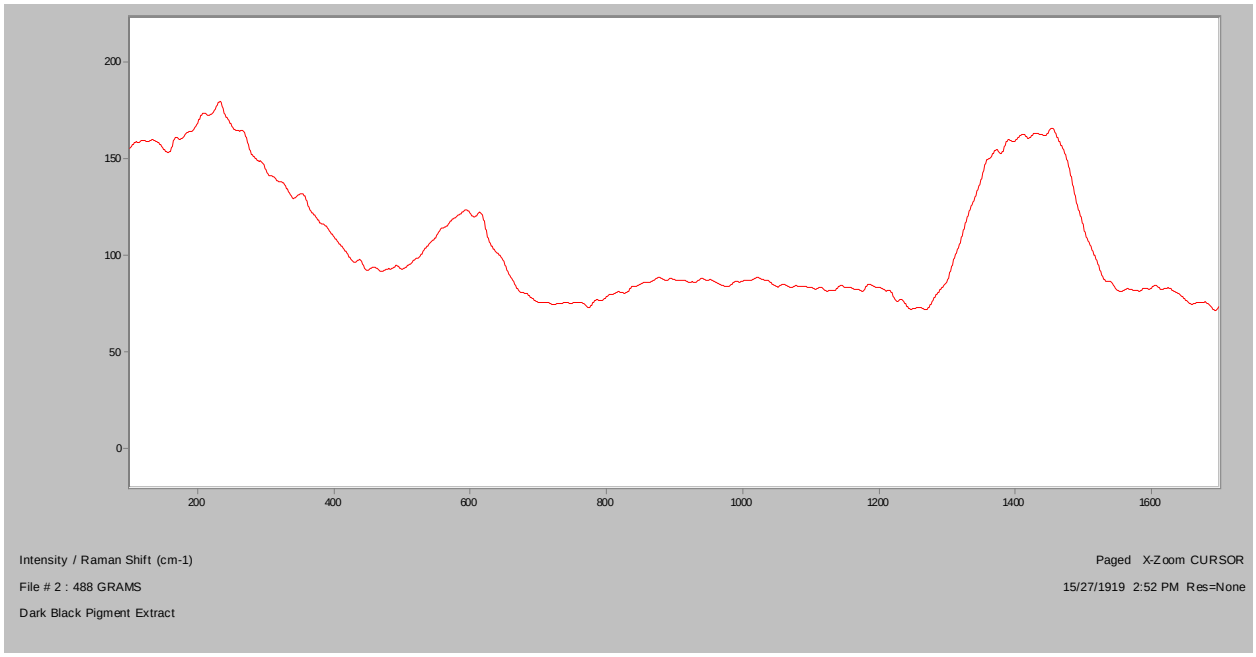

Normal Raman, 633nm

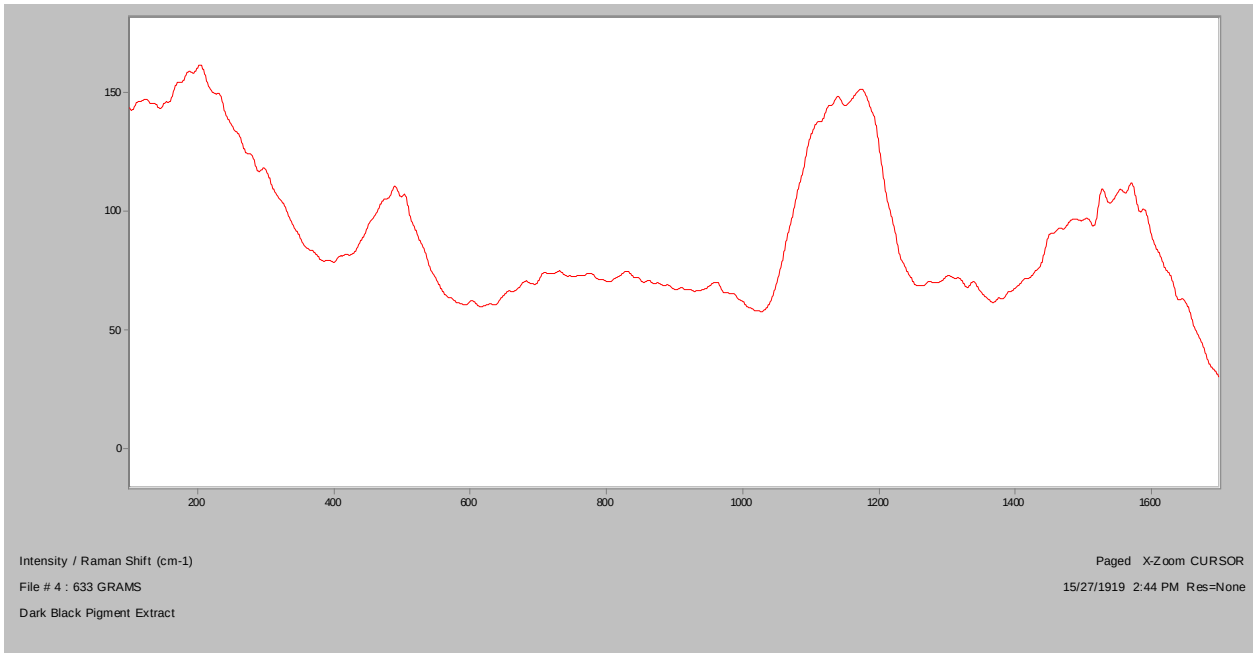

Normal Raman, 785nm

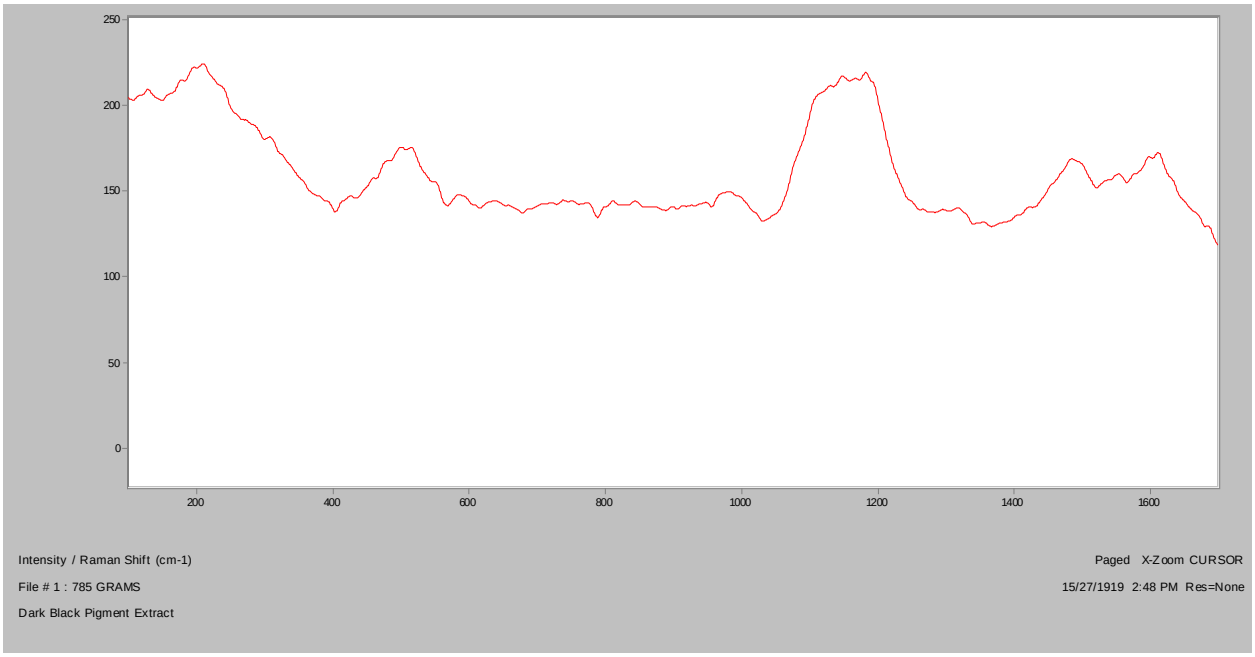

Sayonara Suede

Normal Raman, 488nm

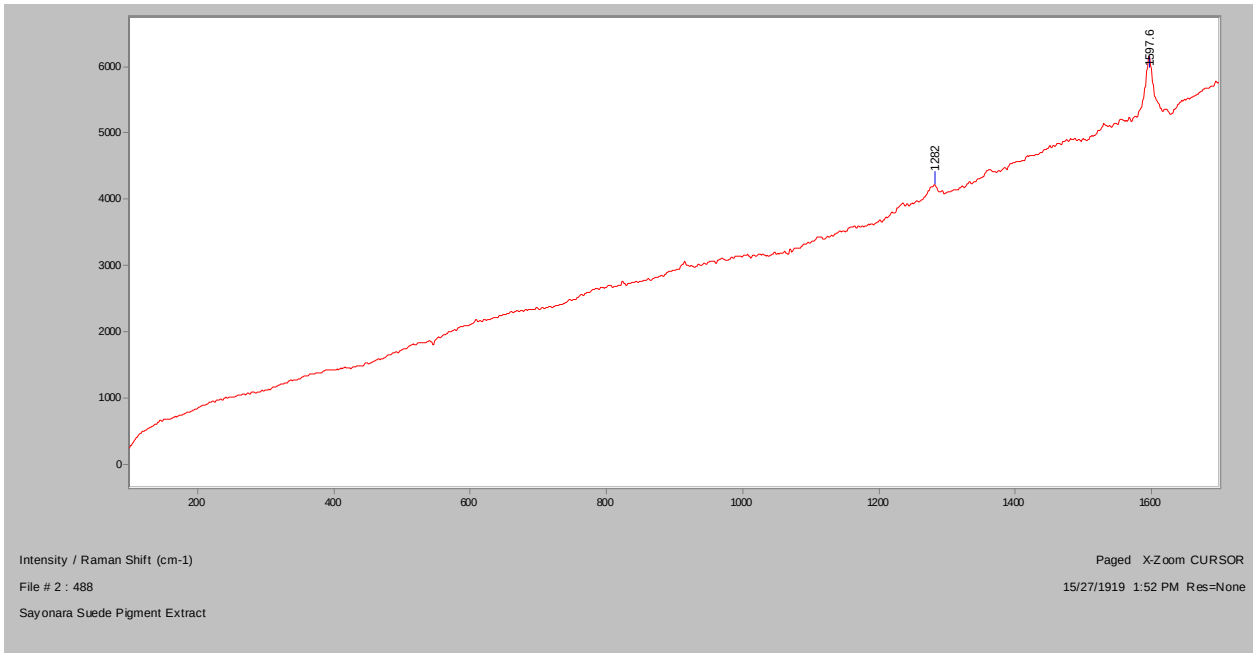

Normal Raman, 633nm

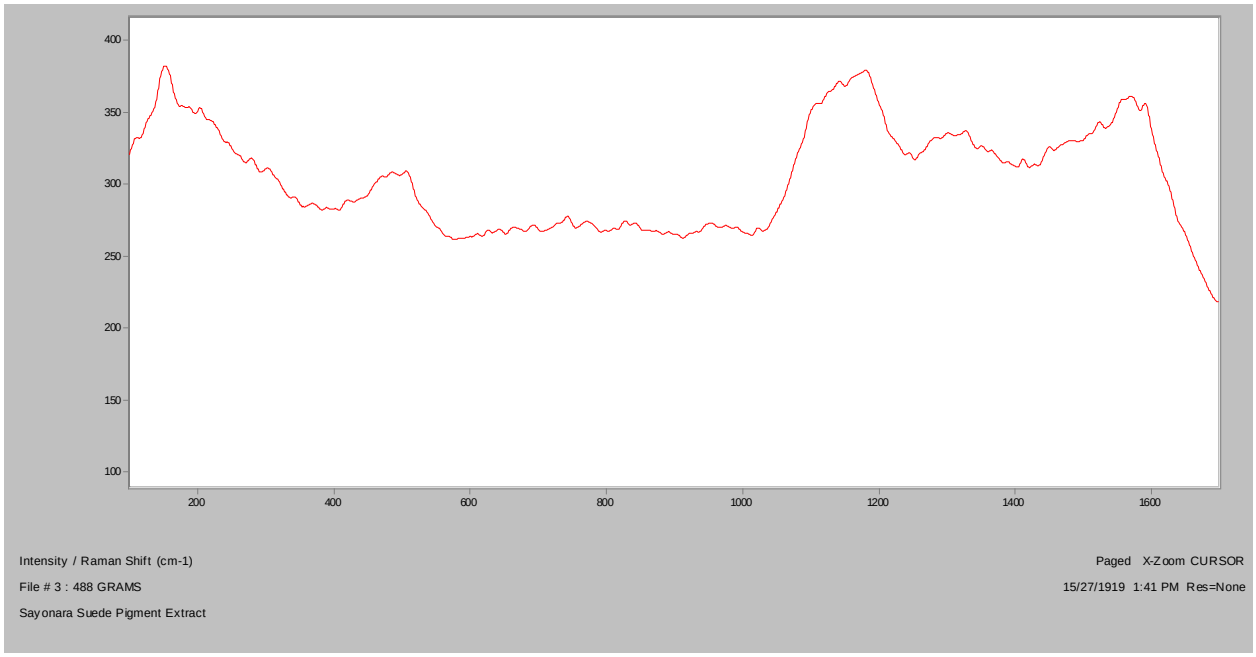

Normal Raman, 785nm

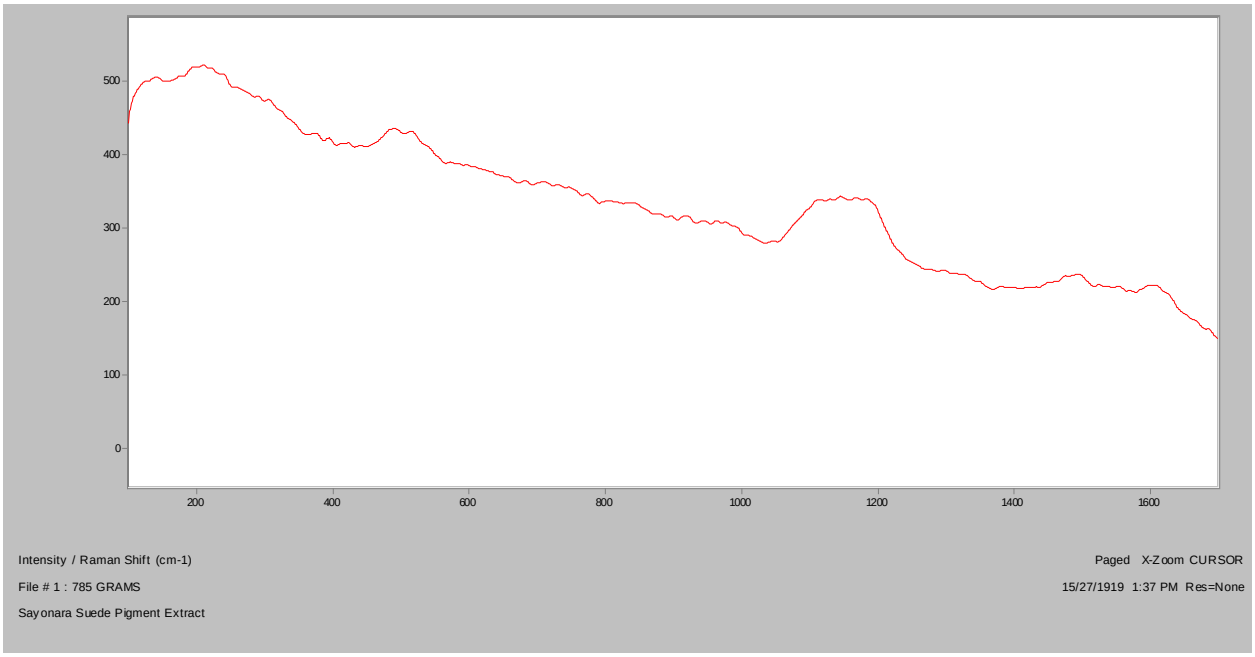

Dark Brown

Normal Raman, 488nm

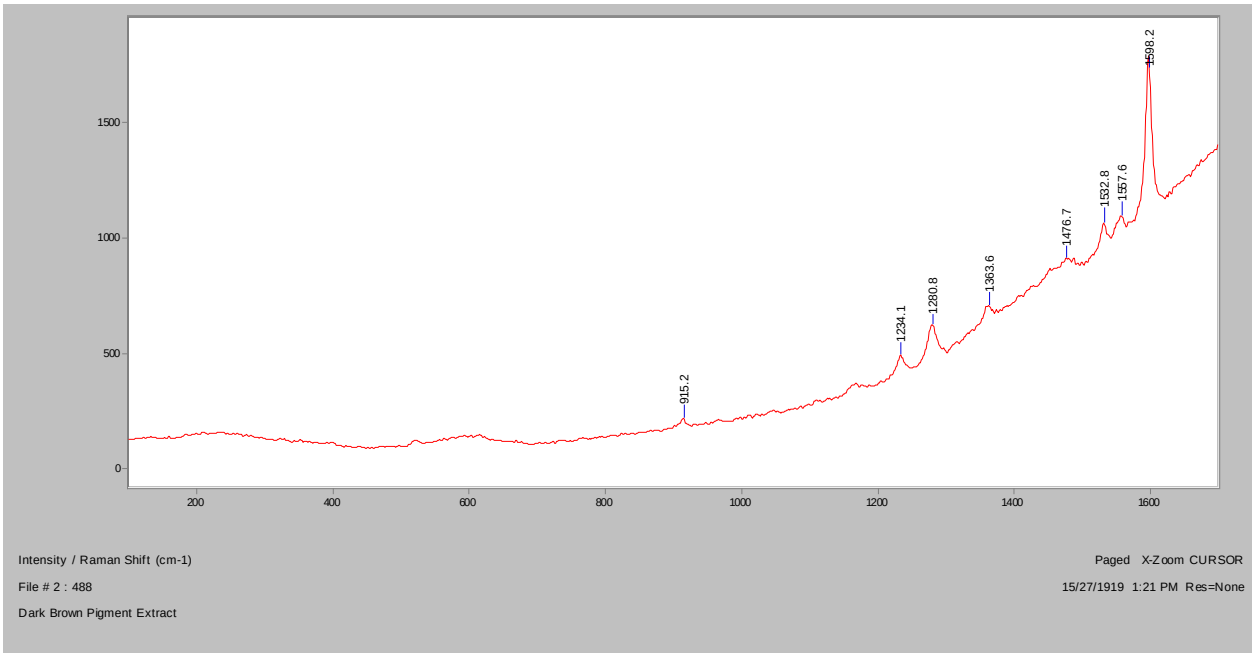

Normal Raman, 633nm

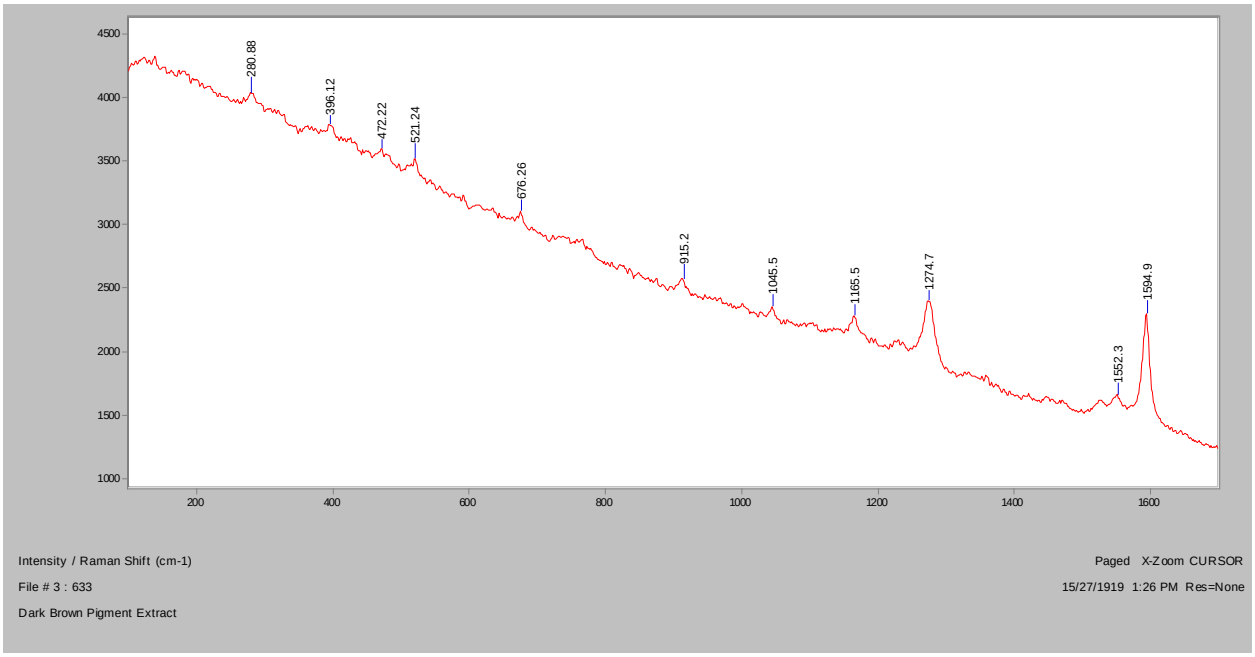

Normal Raman, 785nm

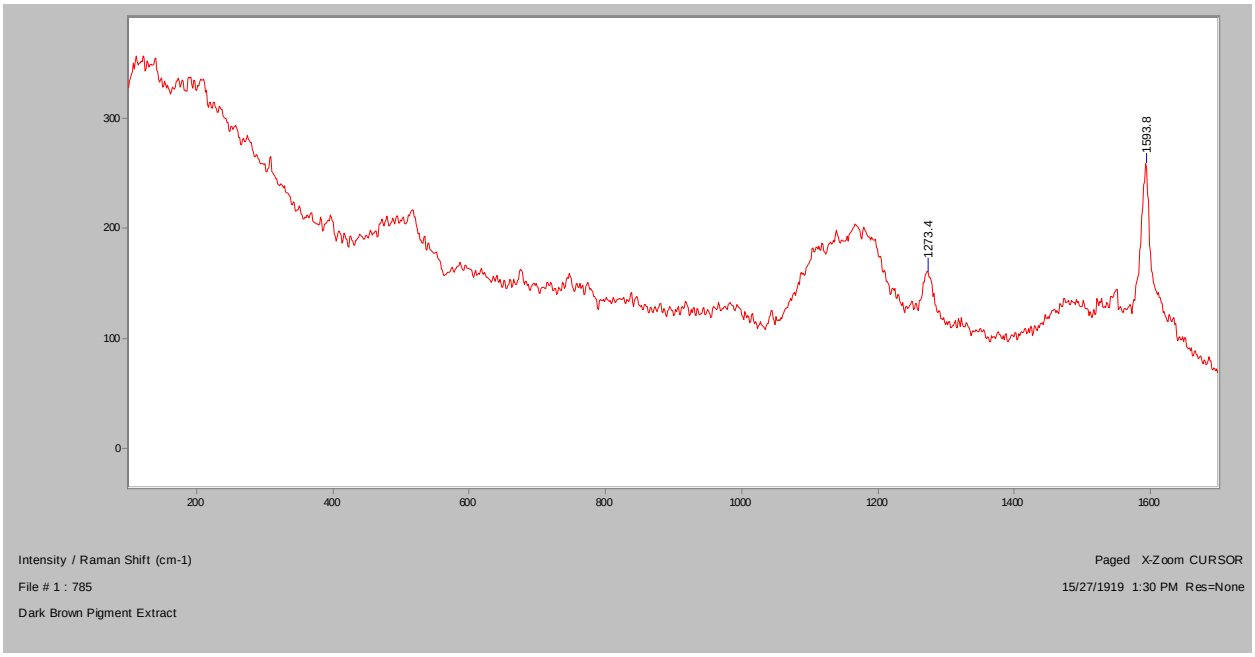

Light Chocolate

Normal Raman, 488nm

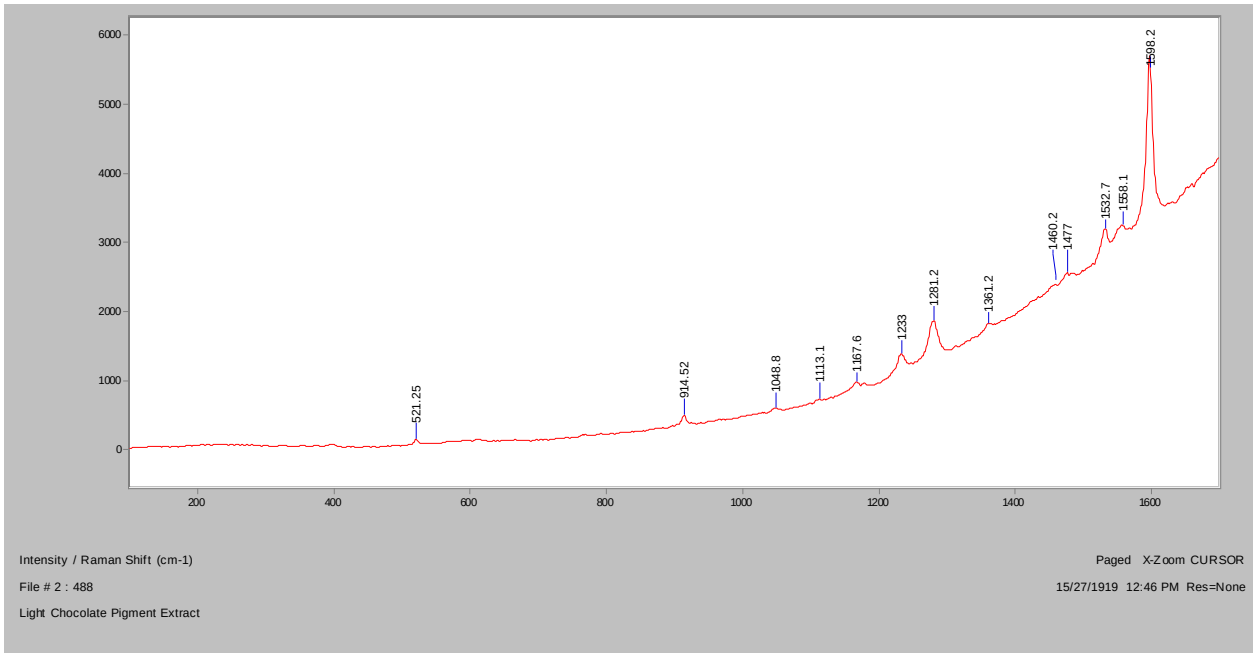

Normal Raman, 633nm

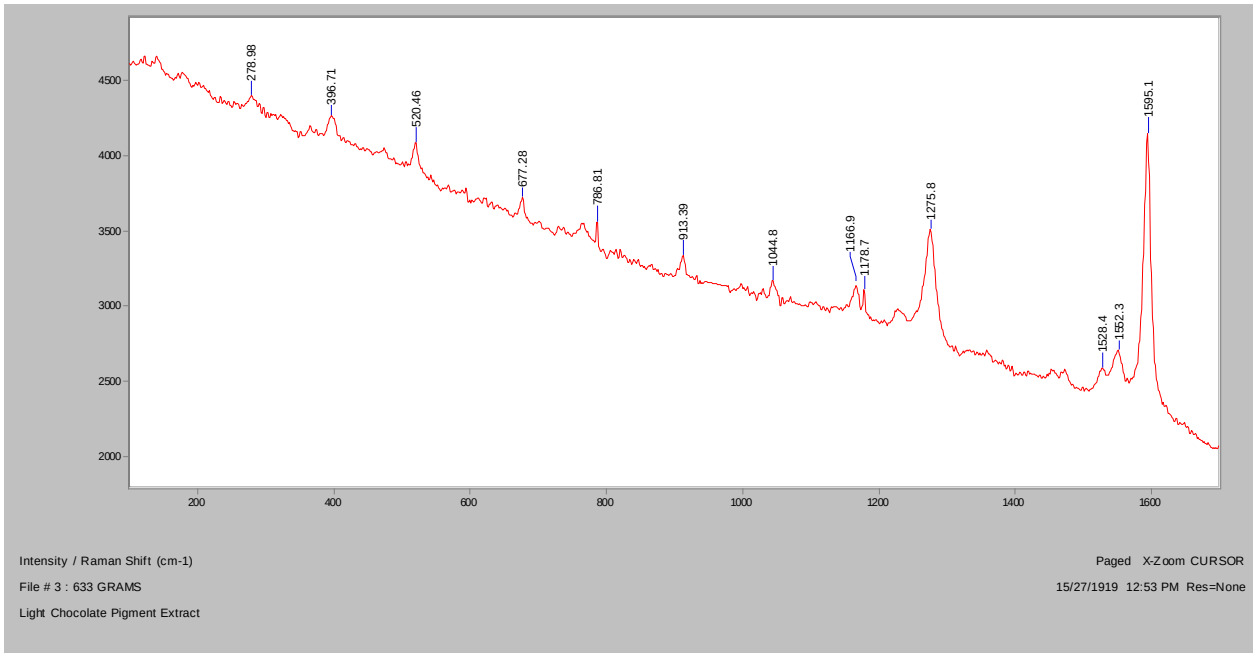

Normal Raman, 785nm

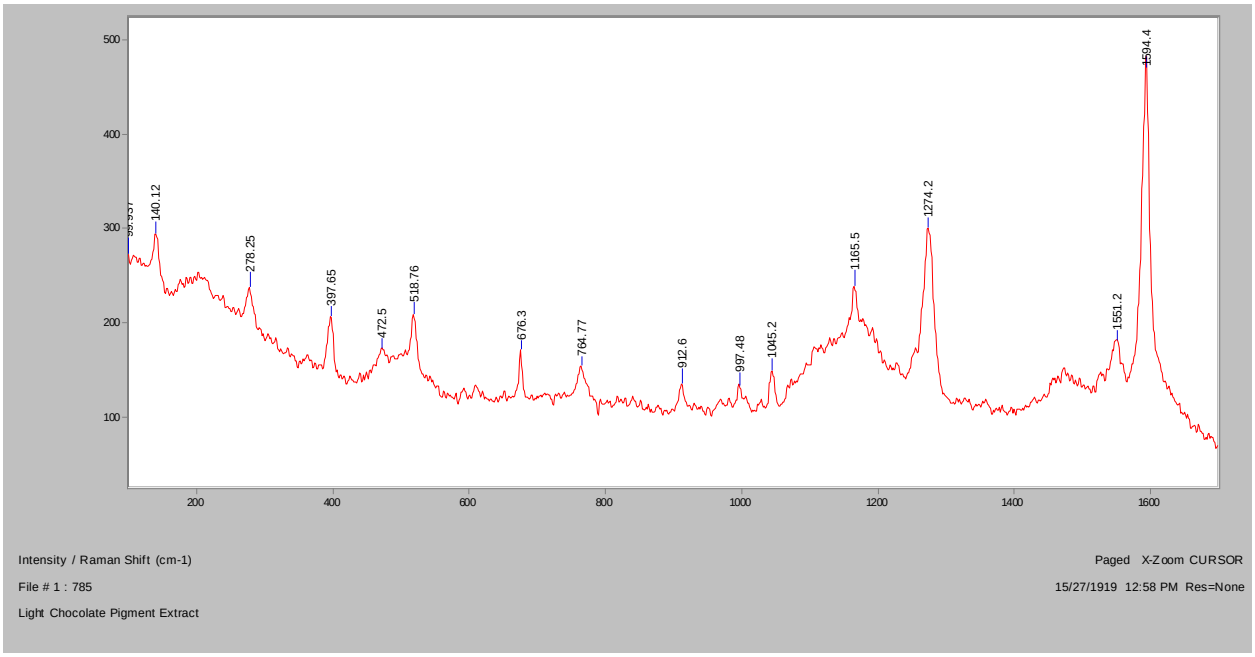

Skin Tone

Normal Raman, 488nm

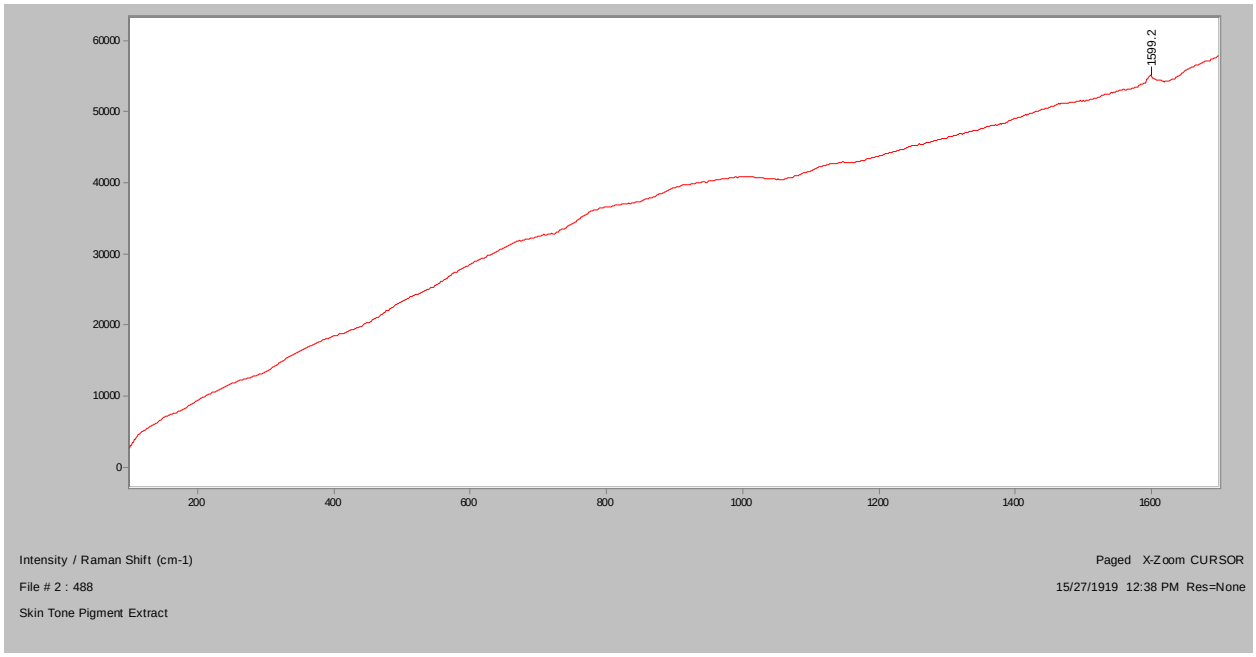

Normal Raman, 633nm

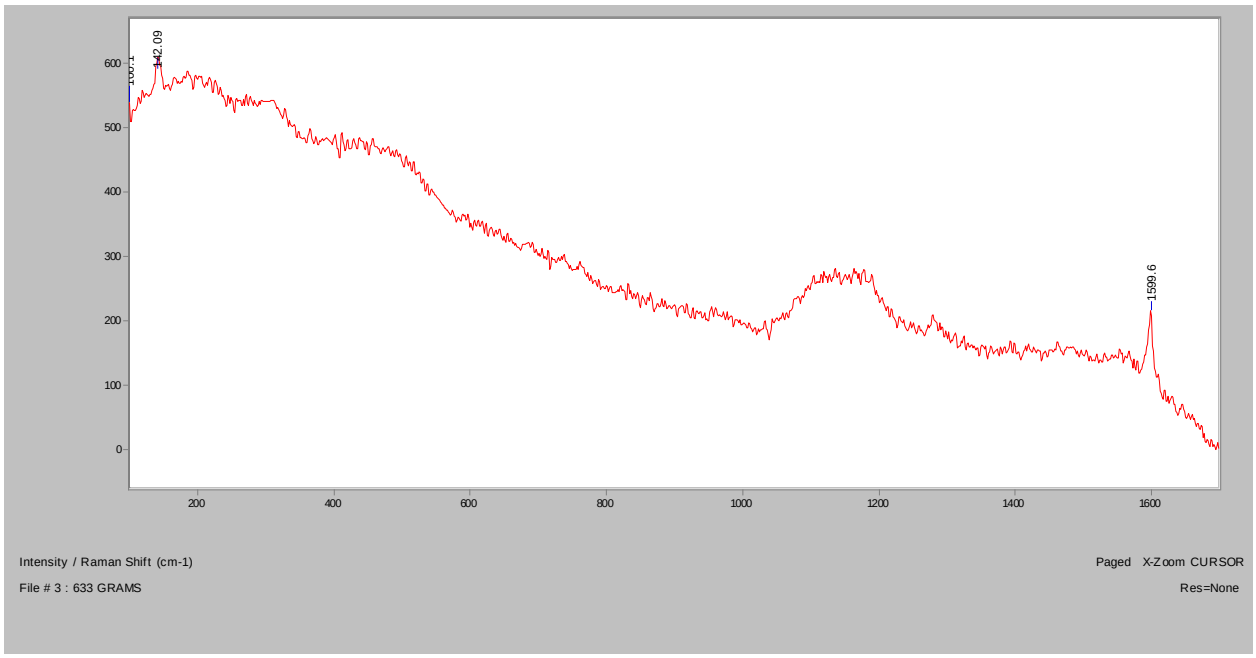

Normal Raman, 785nm

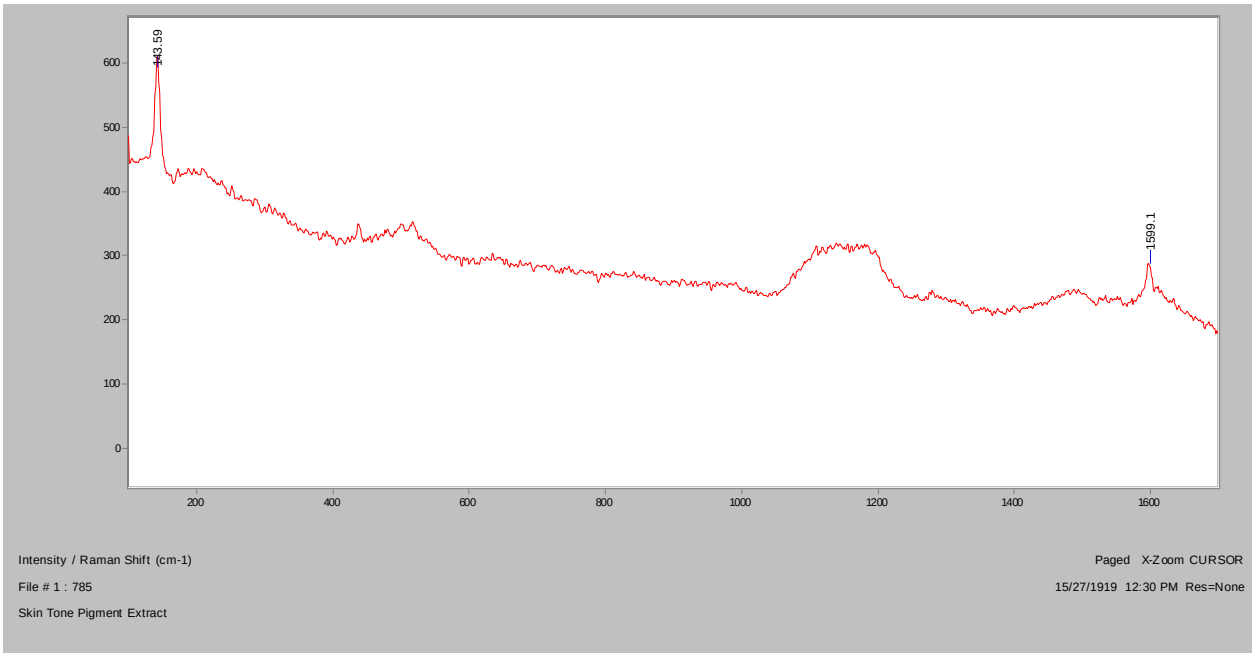

White

Normal Raman, 488nm

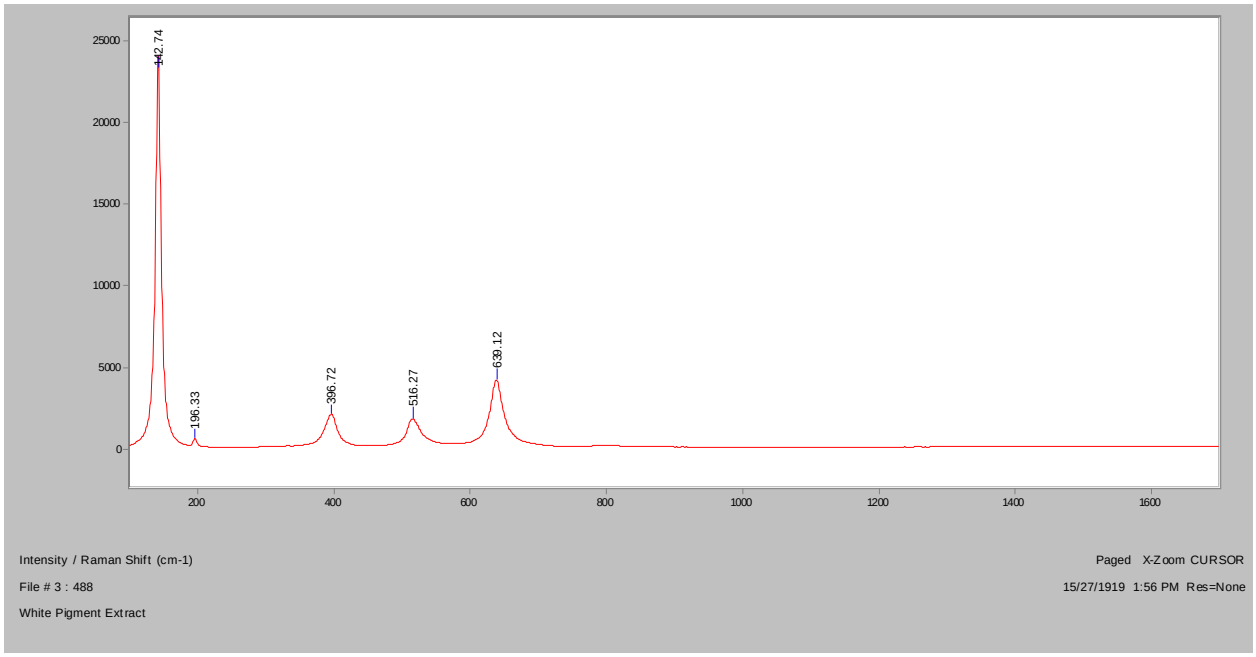

Normal Raman, 633nm

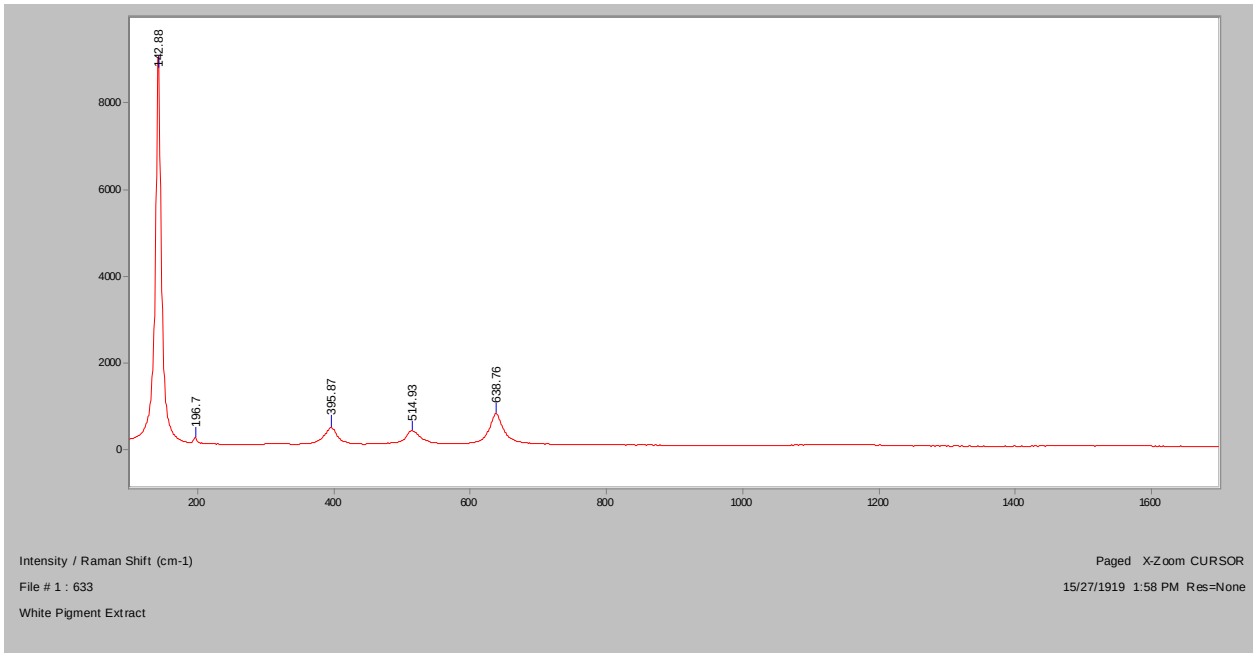

Normal Raman, 785nm

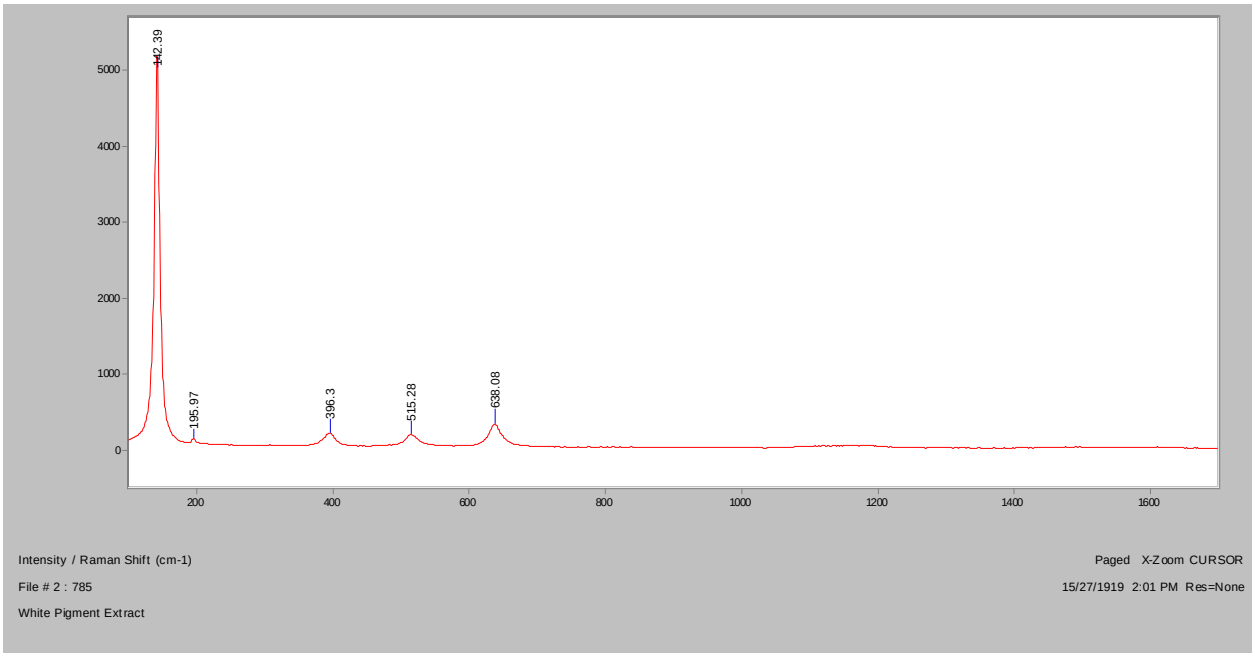

Appendix F: Pigment Standards

Pigment Red 122

Normal Raman, 488nm

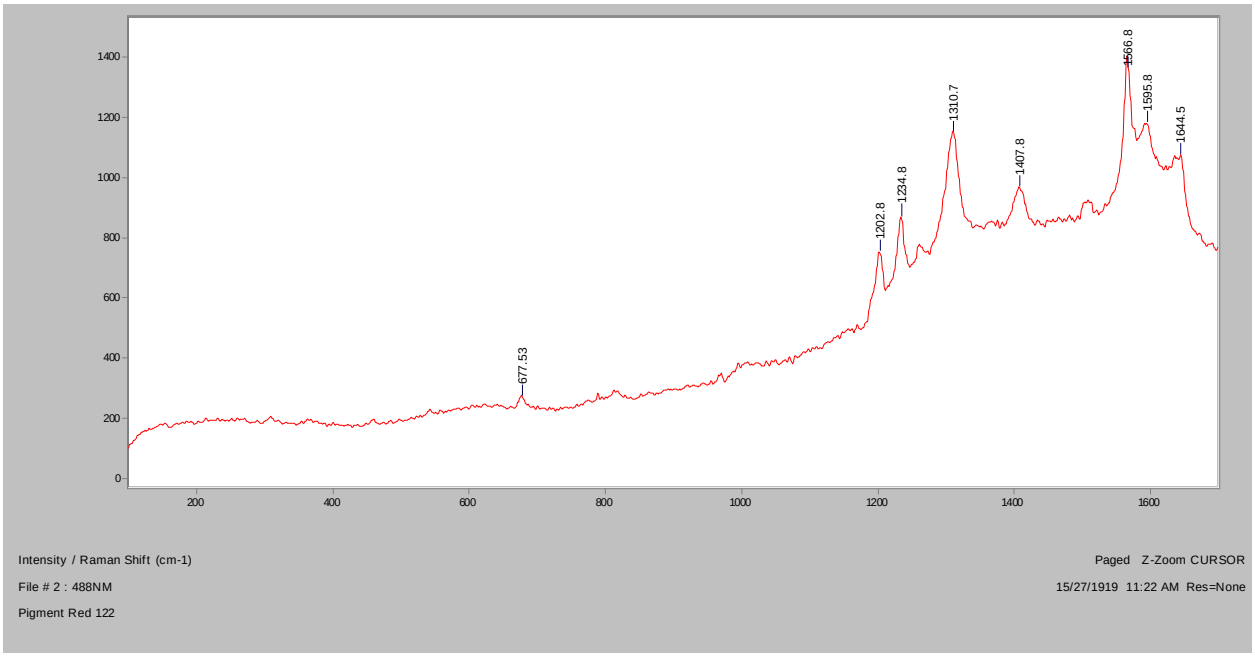

Normal Raman 633nm

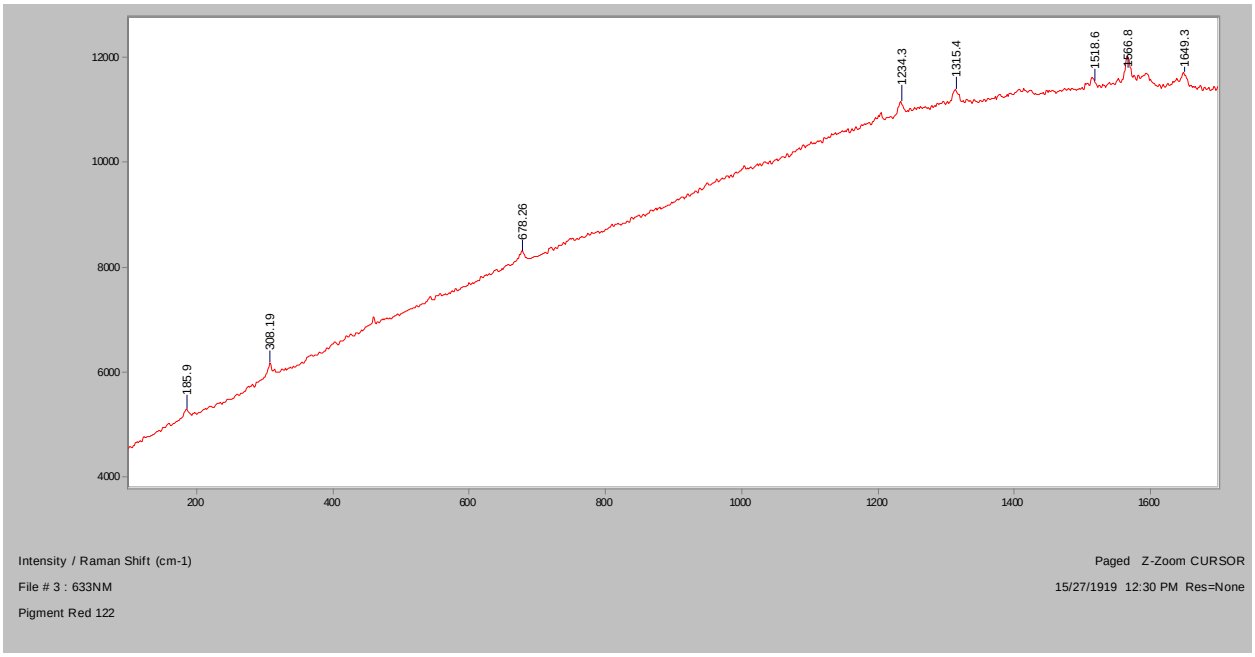

Normal Raman 785nm

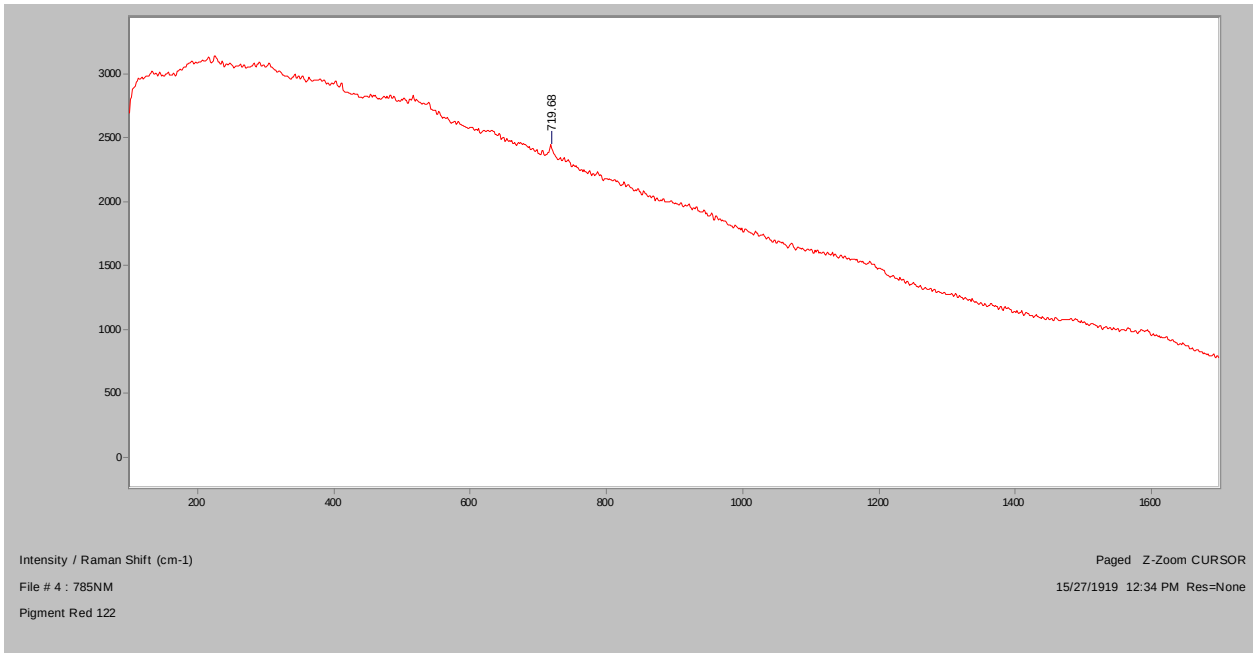

SERS, 488nm

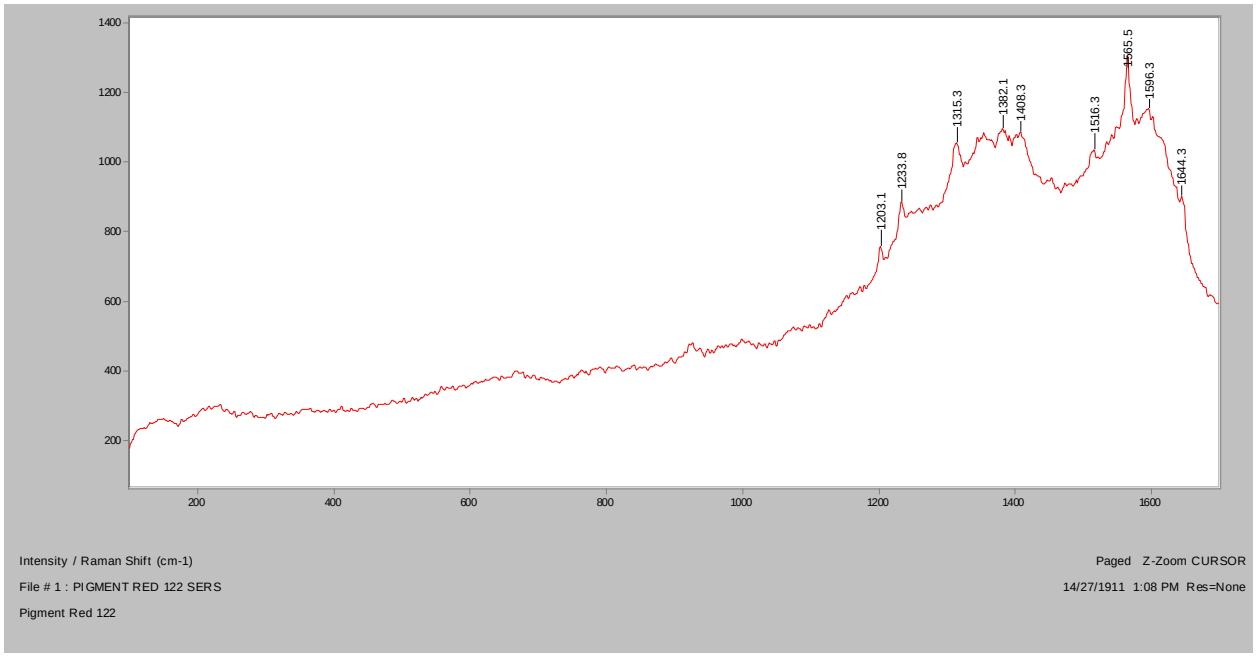

FT-IR (ATR)

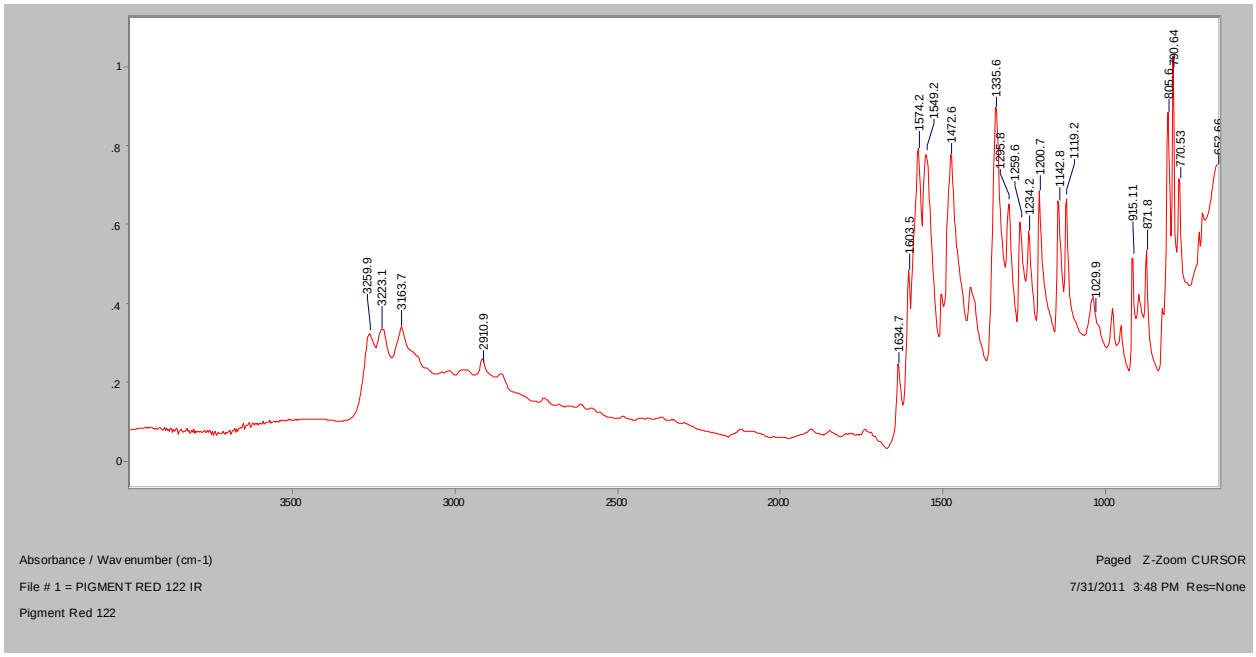

UV-Vis

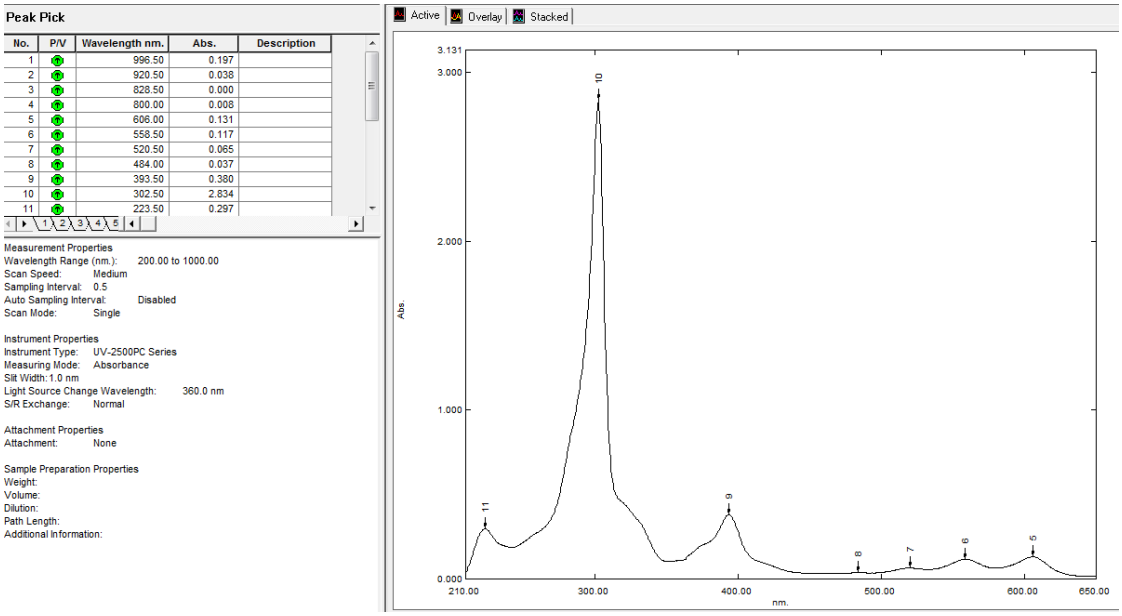

Peak Pick

No.	P/V	Wavelength nm.	Abs.	Description
1		996.50	0.197	
2		920.50	0.038	
3		828.50	0.000	
4		800.00	0.008	
5		606.00	0.131	
6		558.50	0.117	
7		520.50	0.065	
8		484.00	0.037	
9		393.50	0.380	
10		302.50	2.834	
11		223.50	0.297	

Measurement Properties
Wavelength Range (nm.): 200.00 to 1000.00
Scan Speed: Medium
Sampling Interval: 0.5
Auto Sampling Interval: Disabled
Scan Mode: Single

Instrument Properties
Instrument Type: UV-2500PC Series
Measuring Mode: Absorbance
Slit Width:1.0 nm
Light Source Change Wavelength: 360.0 nm
S/R Exchange: Normal

Attachment Properties
Attachment: None

Sample Preparation Properties
Weight:
Volume:
Dilution:
Path Length:
Additional Information:

Pigment Red 146

Normal Raman, 488nm

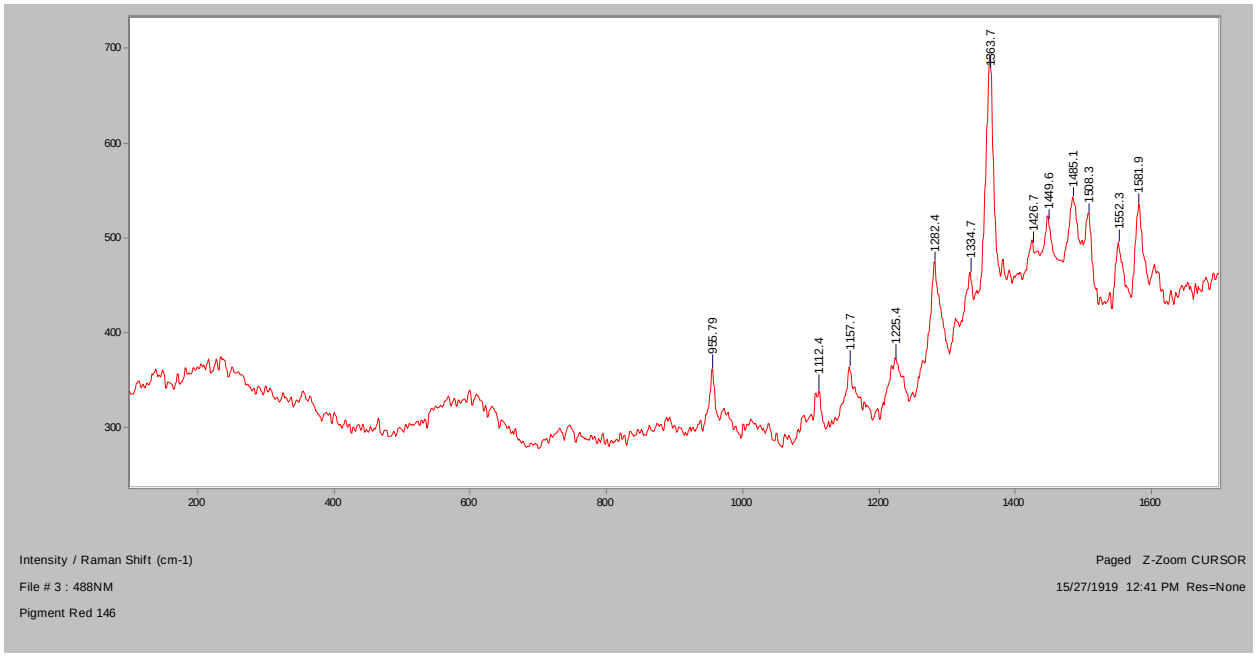

Normal Raman 633nm

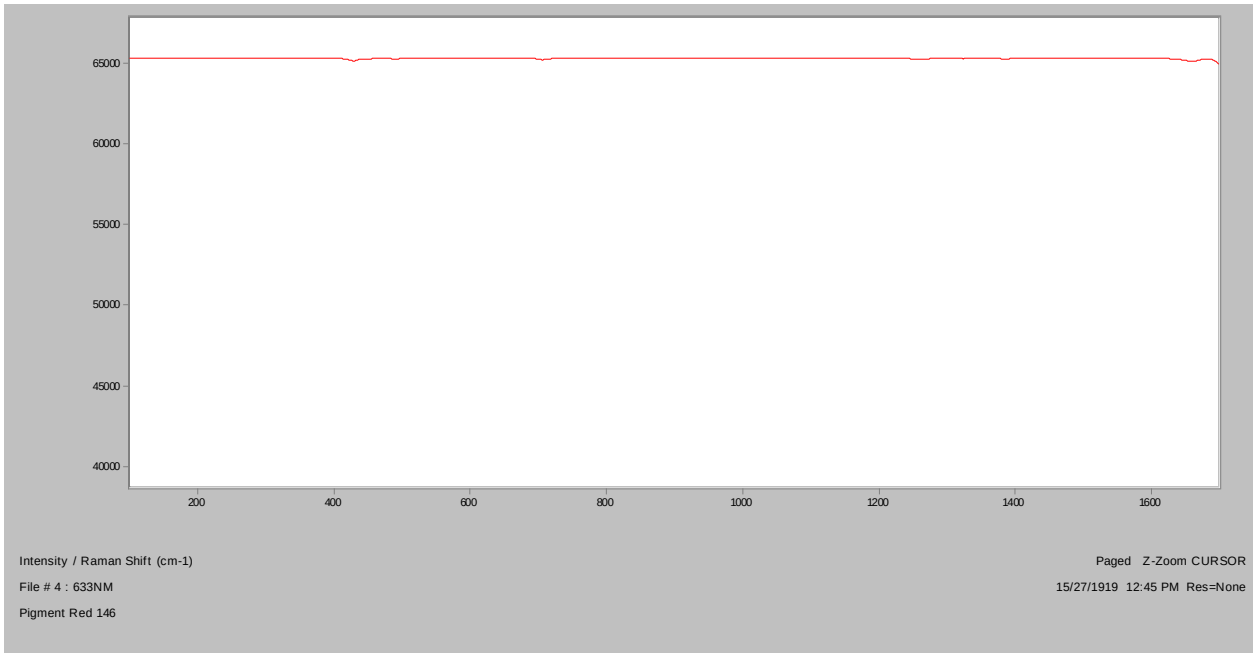

Normal Raman 785nm

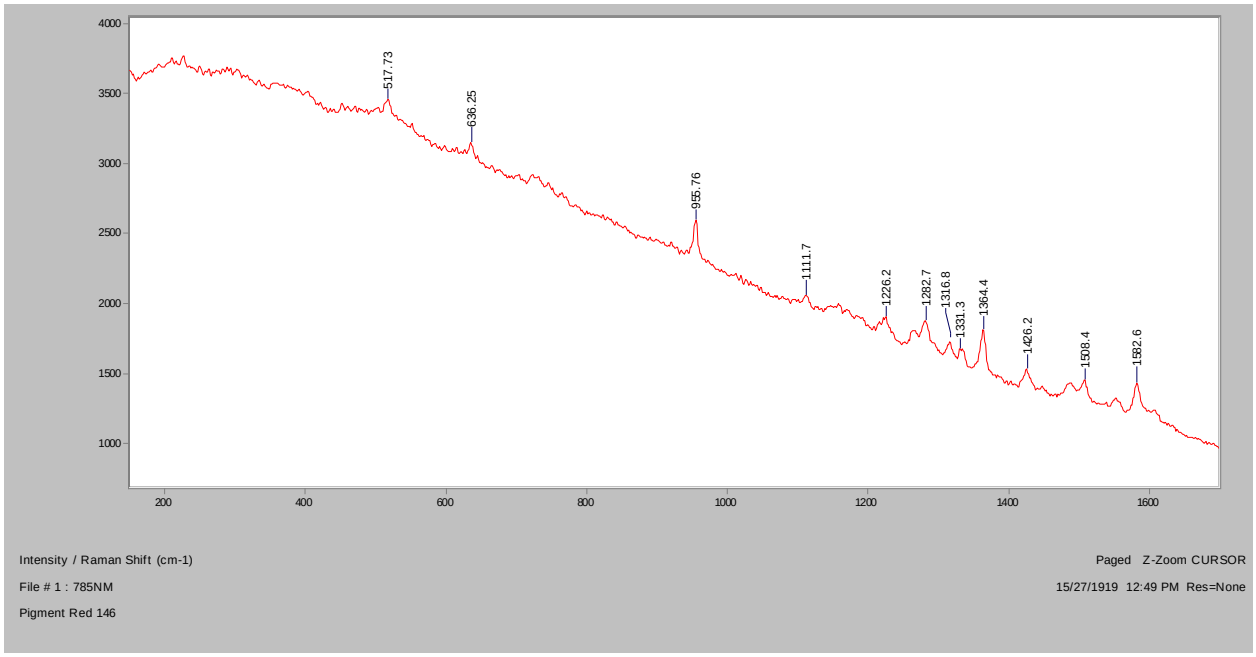

FT Raman, 1064nm

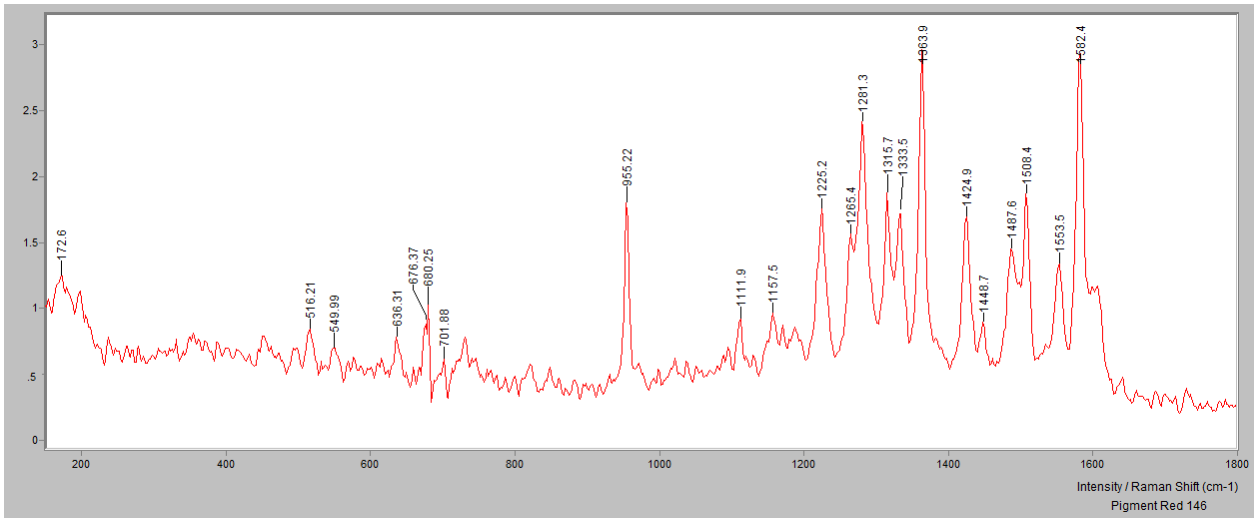

SERS, 488nm

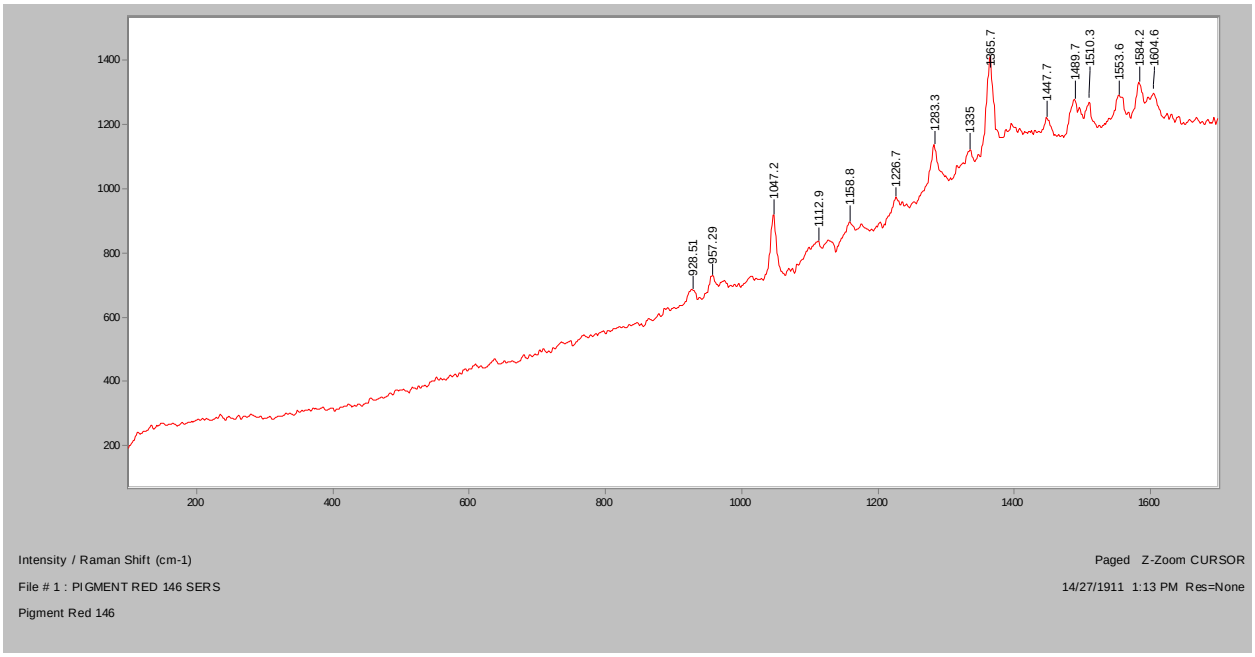

FT-IR (ATR)

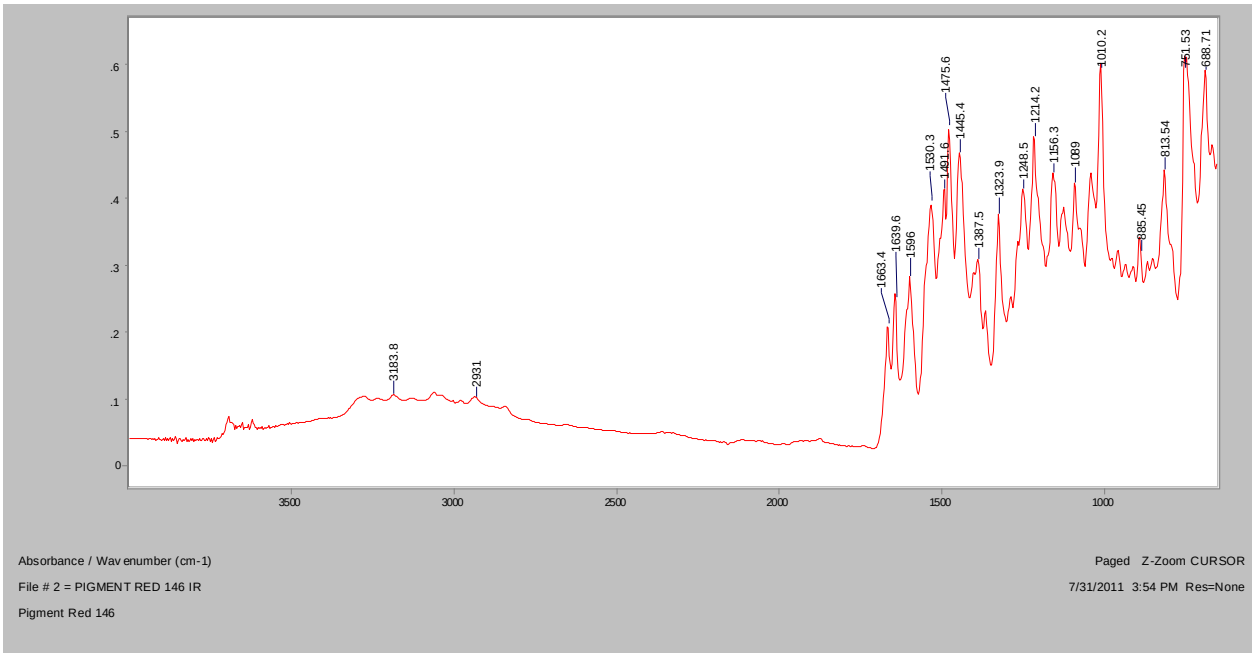

UV-Vis

Peak Pick

No.	P/V	Wavelength nm.	Abs.	Description
1		897.00	0.019	
2		793.50	0.011	
3		579.50	0.128	
4		365.00	0.109	
5		317.00	0.438	
6		251.50	0.252	

1 2 3 4 5 6 7

Measurement Properties
Wavelength Range (nm.): 200.00 to 1000.00
Scan Speed: Medium
Sampling Interval: 0.5
Auto Sampling Interval: Disabled
Scan Mode: Single

Instrument Properties
Instrument Type: UV-2500PC Series
Measuring Mode: Absorbance
Slit Width: 1.0 nm
Light Source Change Wavelength: 360.0 nm
S/R Exchange: Normal

Attachment Properties
Attachment: None

Sample Preparation Properties
Weight:
Volume:
Dilution:
Path Length:
Additional Information:

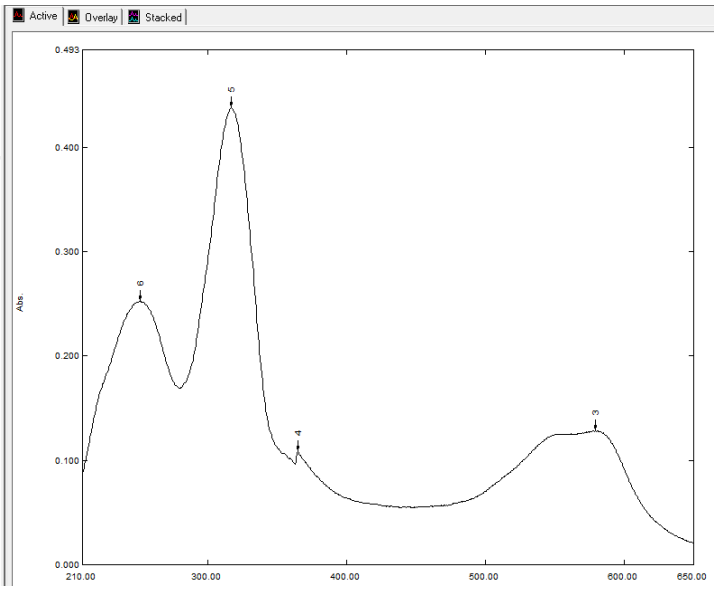

Pigment Red 170

Normal Raman, 488nm

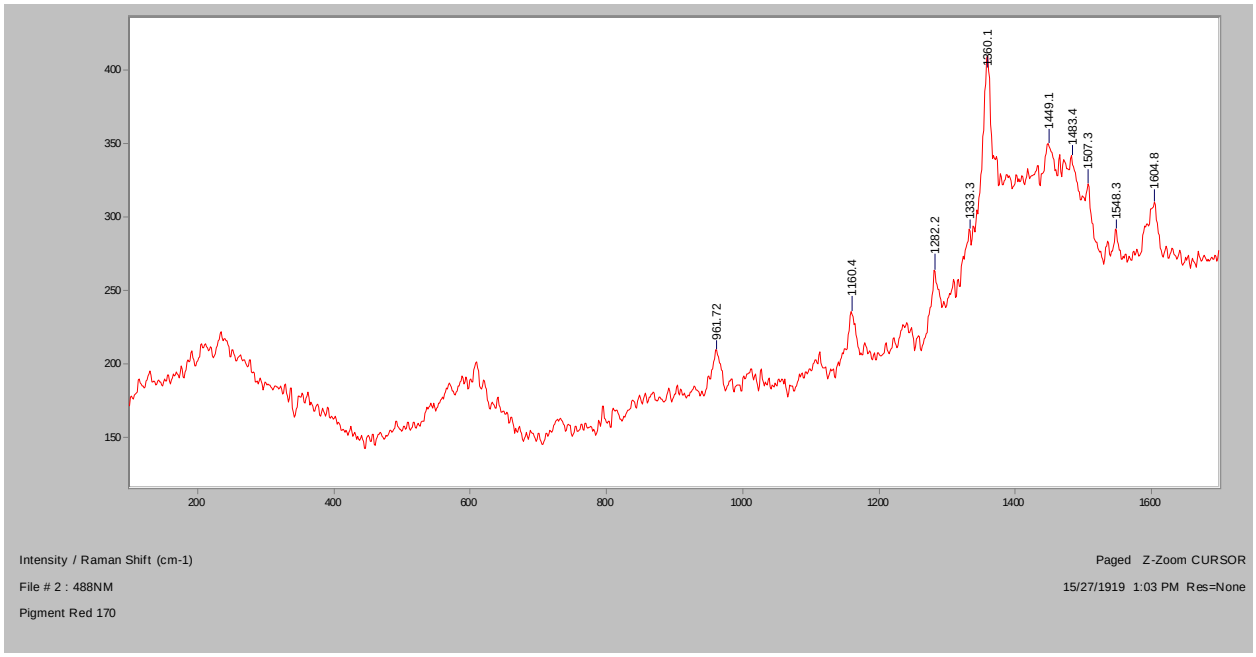

Normal Raman 633nm

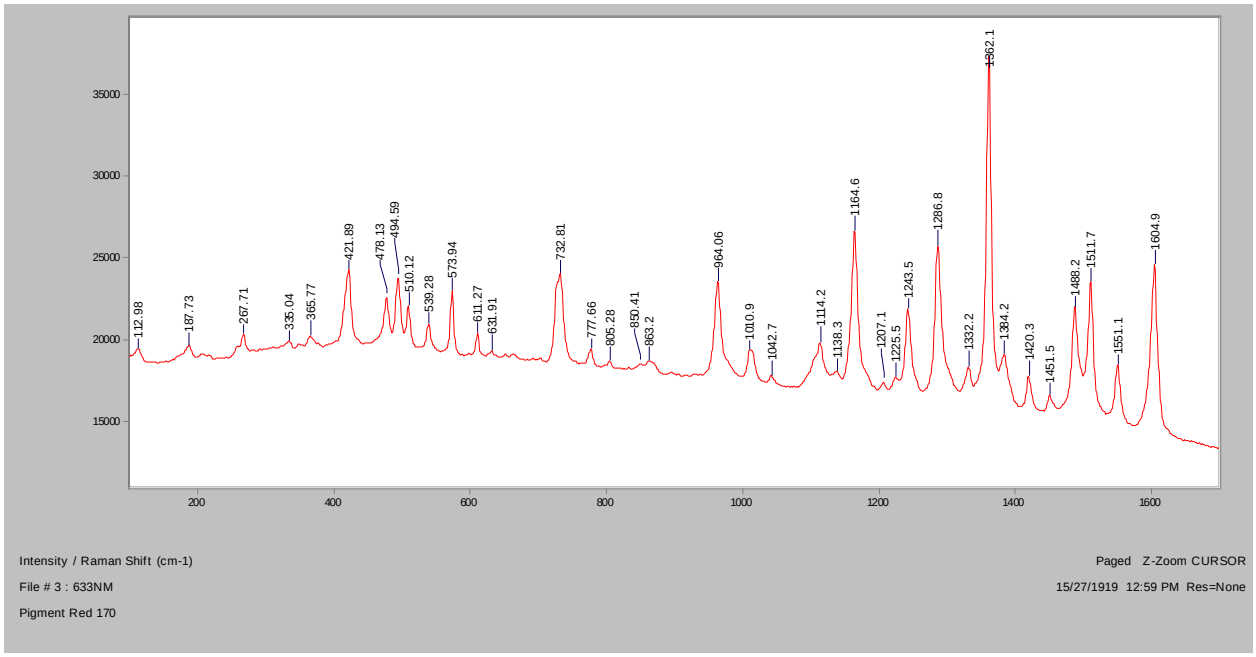

Normal Raman 785nm

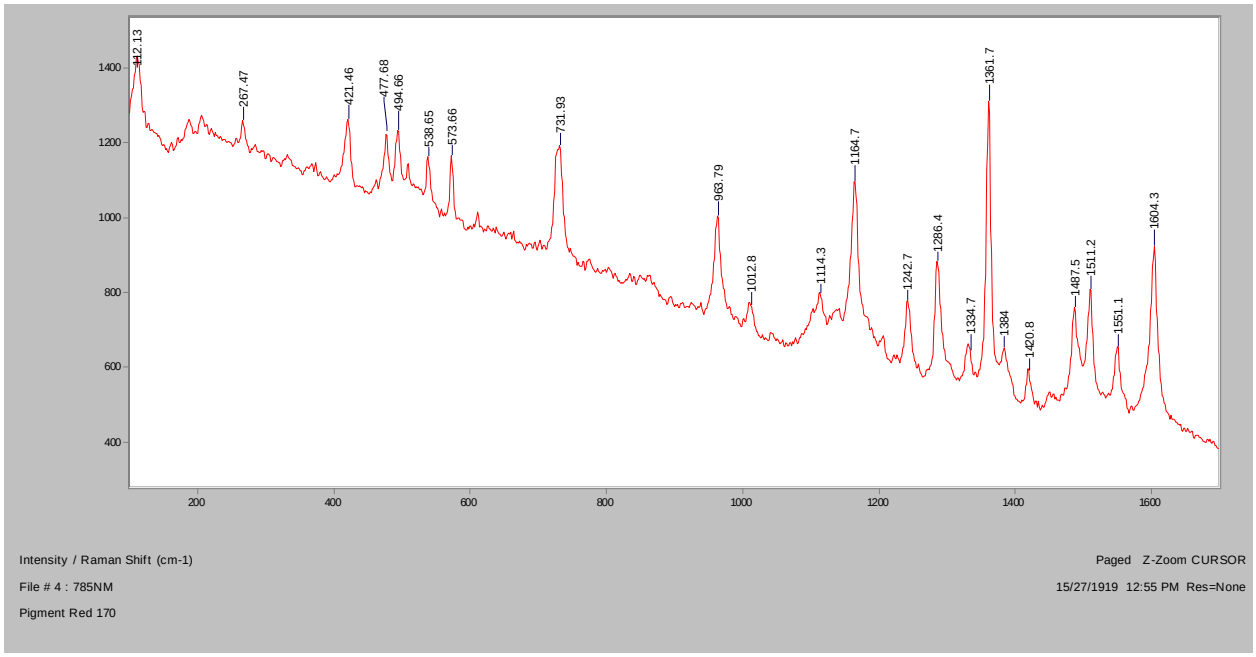

FT Raman, 1064nm

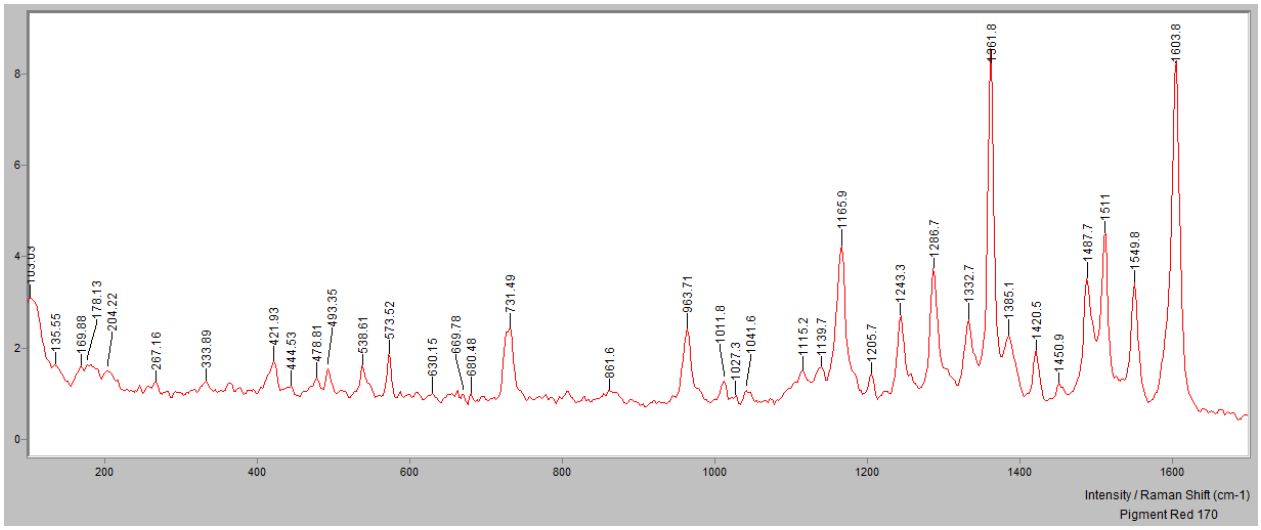

SERS, 488nm

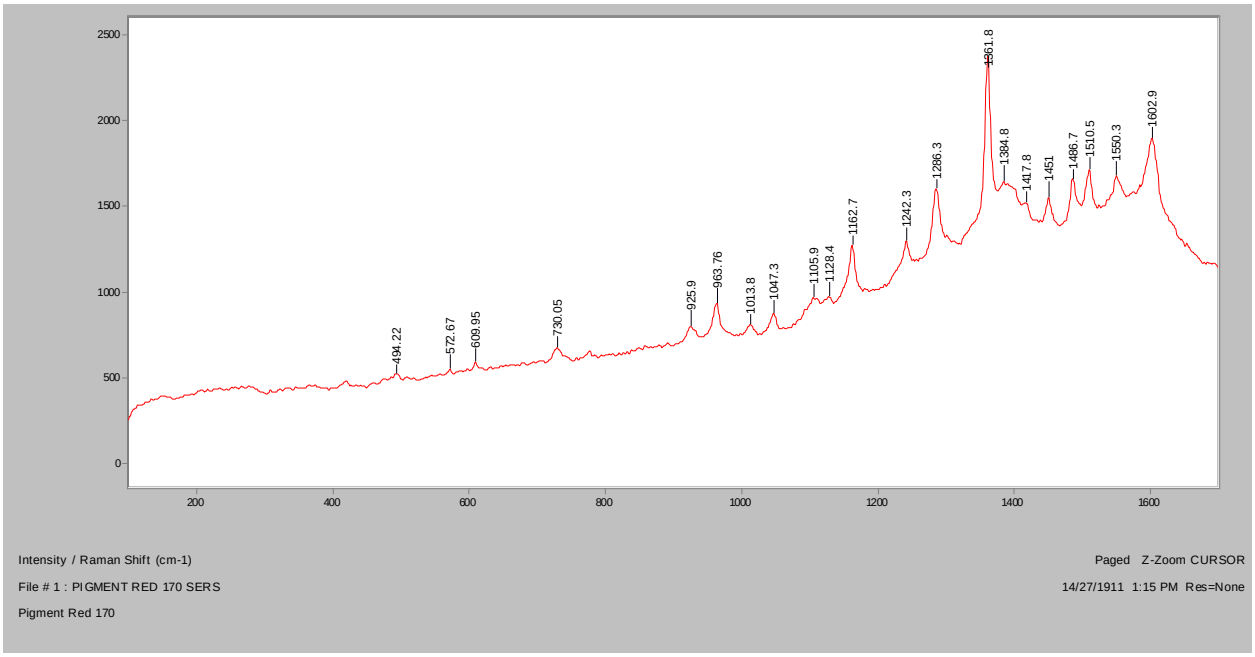

FT-IR (ATR)

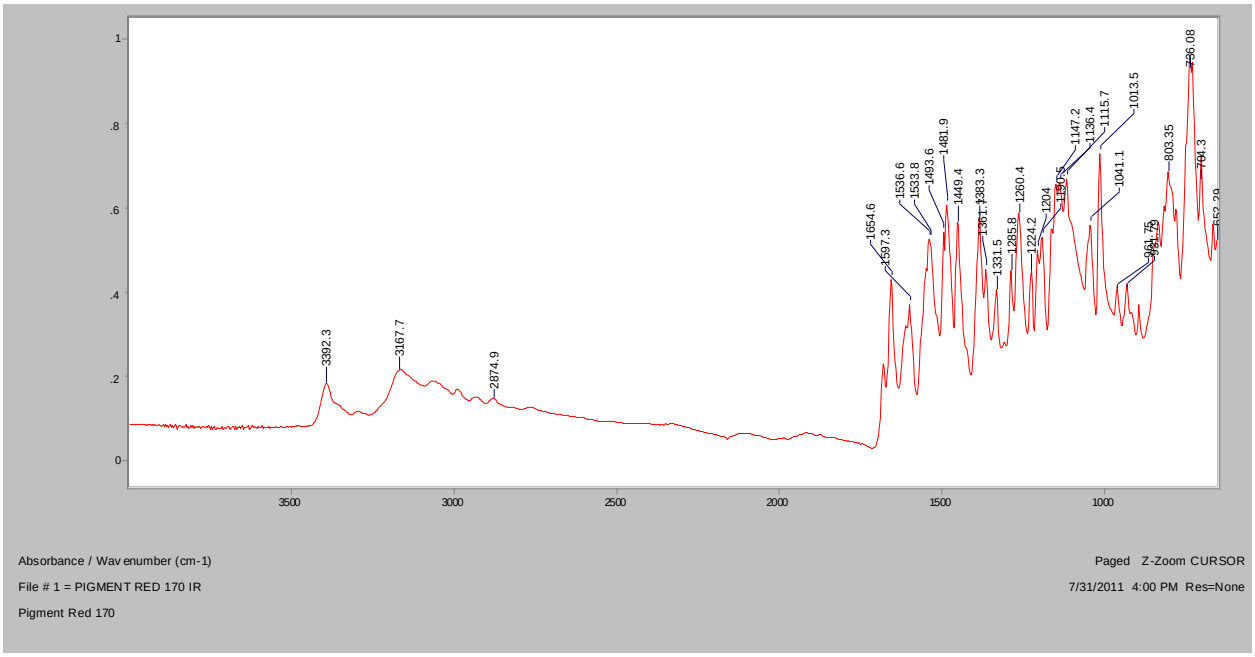

UV-Vis

Peak Pick

No.	P/V	Wavelength nm.	Abs.	Description
1		916.00	0.024	
2		860.50	0.001	
3		780.00	0.007	
4		754.50	0.006	
5		560.50	0.262	
6		365.00	0.158	
7		312.50	0.270	
8		241.50	0.313	

1 2 3 4 5 6 7 8

Measurement Properties
Wavelength Range (nm.): 200.00 to 1000.00
Scan Speed: Medium
Sampling Interval: 0.5
Auto Sampling Interval: Disabled
Scan Mode: Single

Instrument Properties
Instrument Type: UV-2500PC Series
Measuring Mode: Absorbance
Slit Width: 1.0 nm
Light Source Change Wavelength: 360.0 nm
S/R Exchange: Normal

Attachment Properties
Attachment: None

Sample Preparation Properties
Weight:
Volume:
Dilution:
Path Length:
Additional Information:

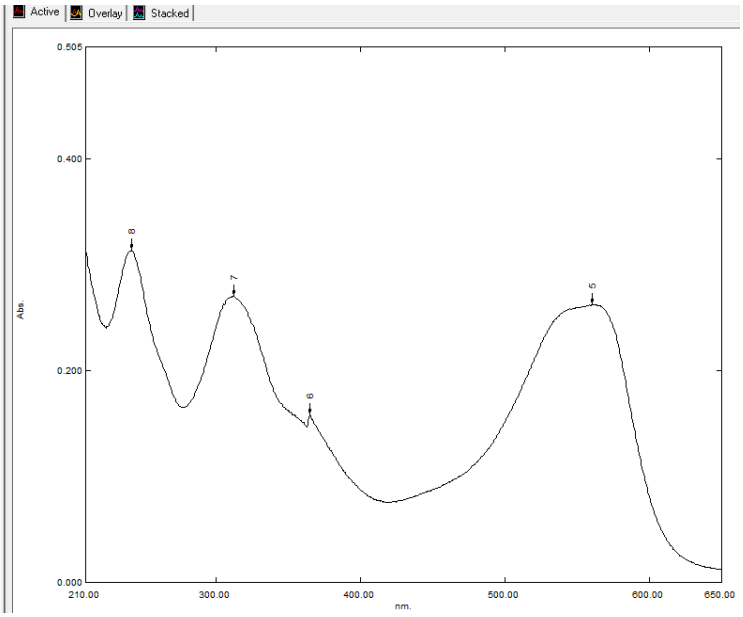

Pigment Red 255

Normal Raman, 488nm

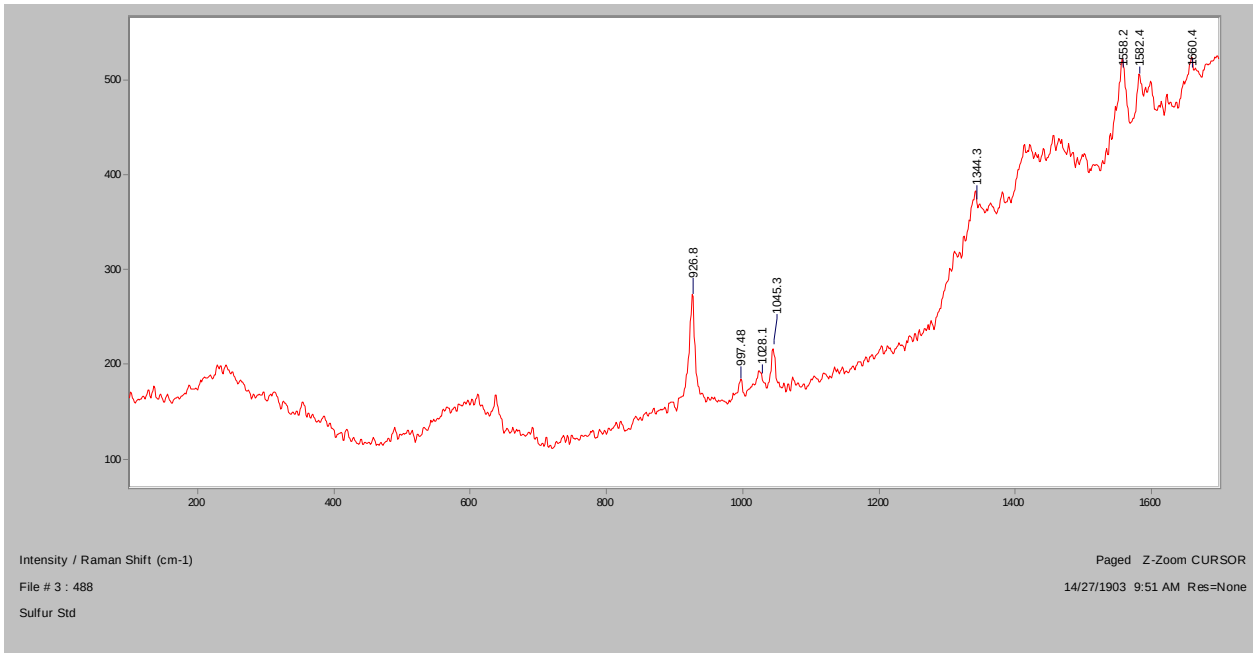

Normal Raman 633nm

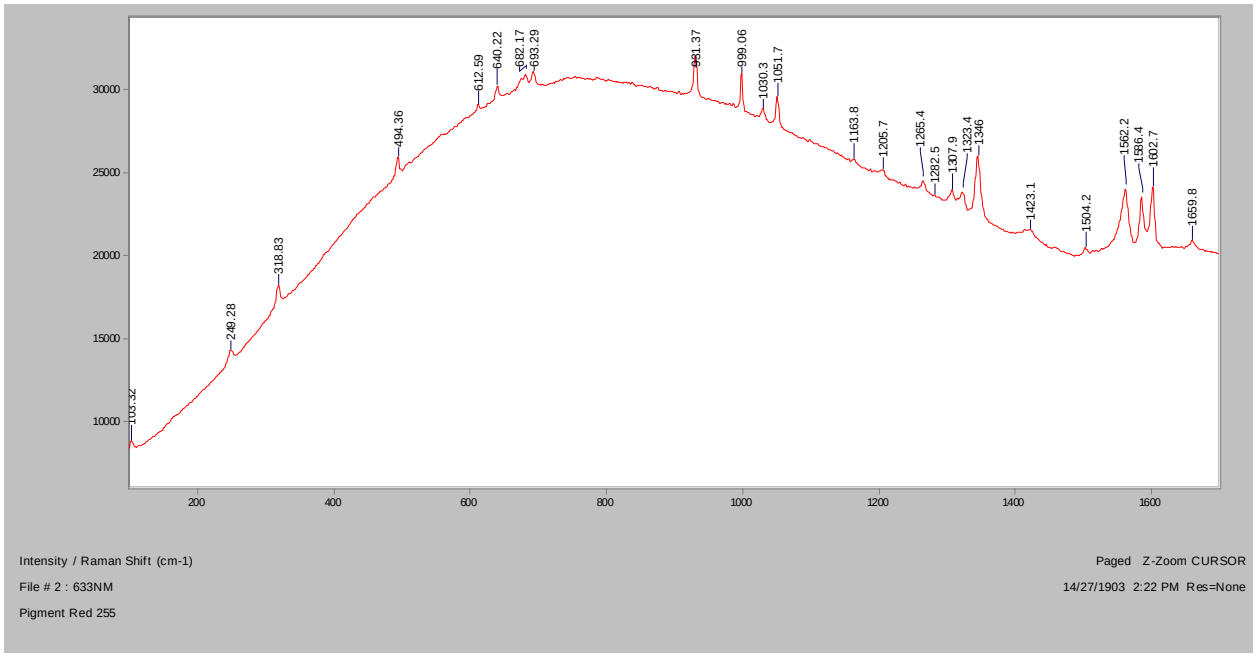

Normal Raman 785nm

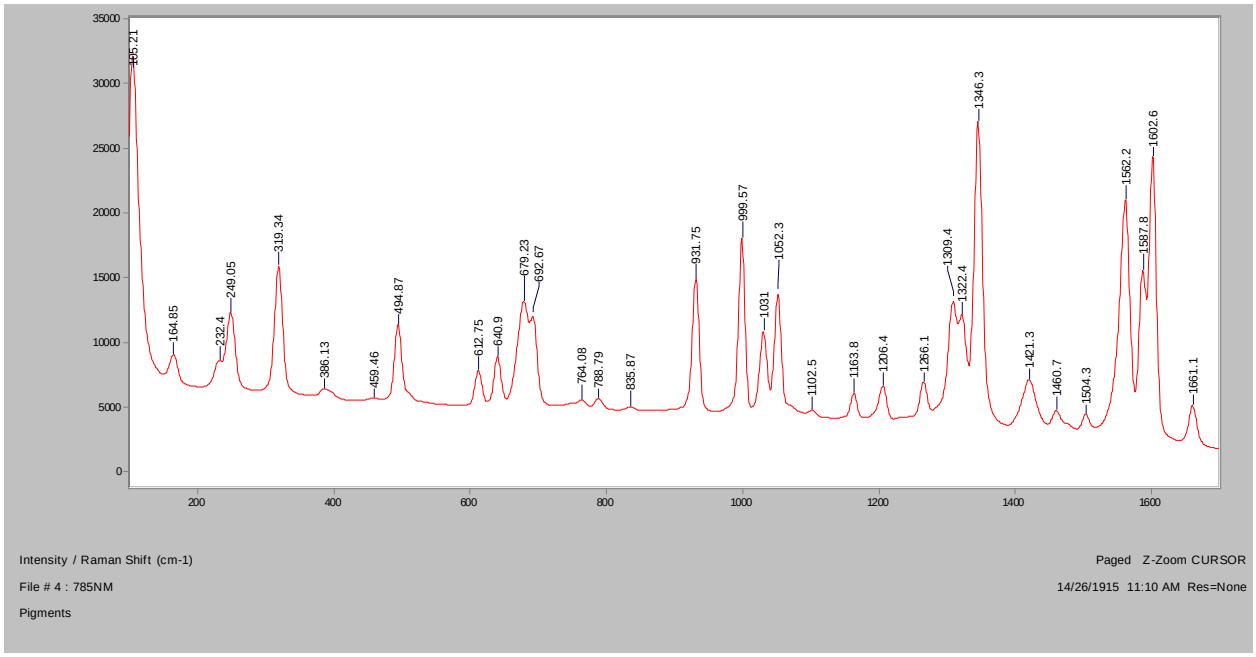

SERS, 488nm

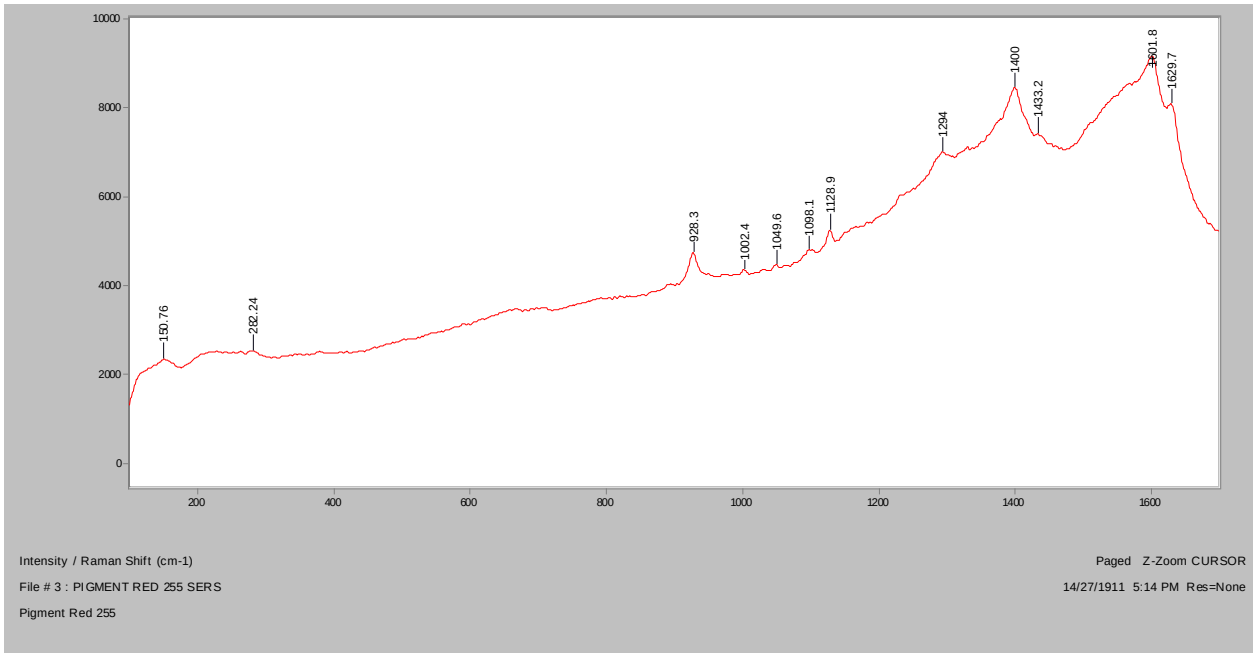

FT-IR (ATR)

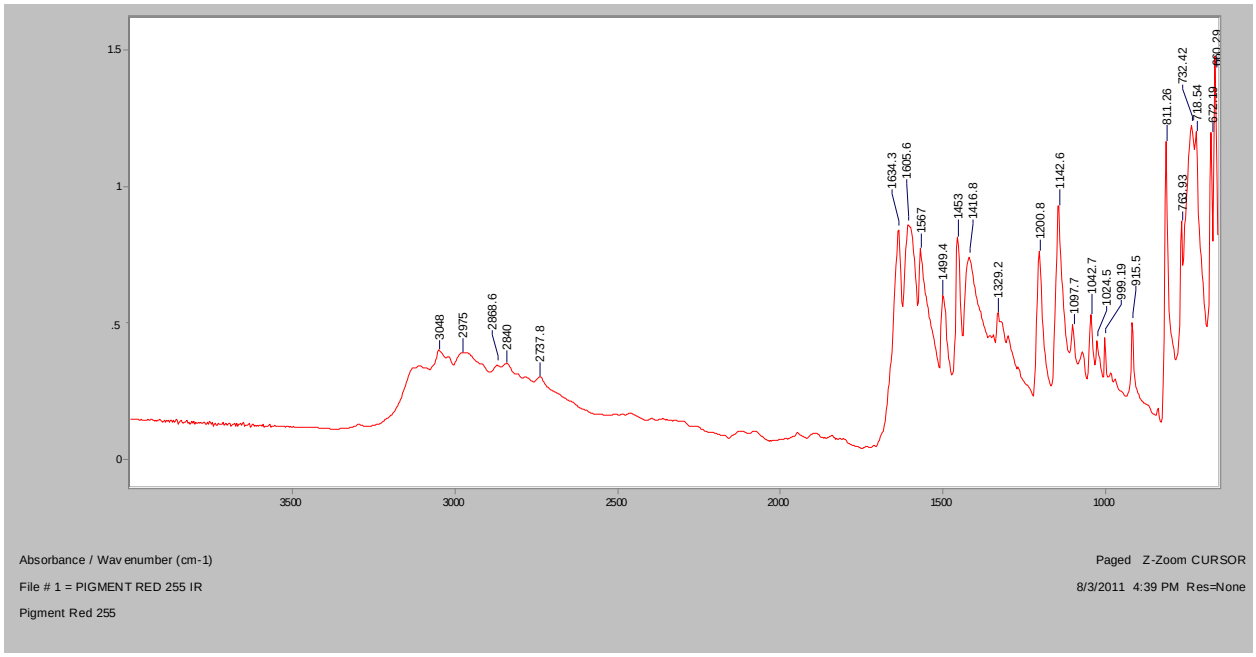

UV-Vis

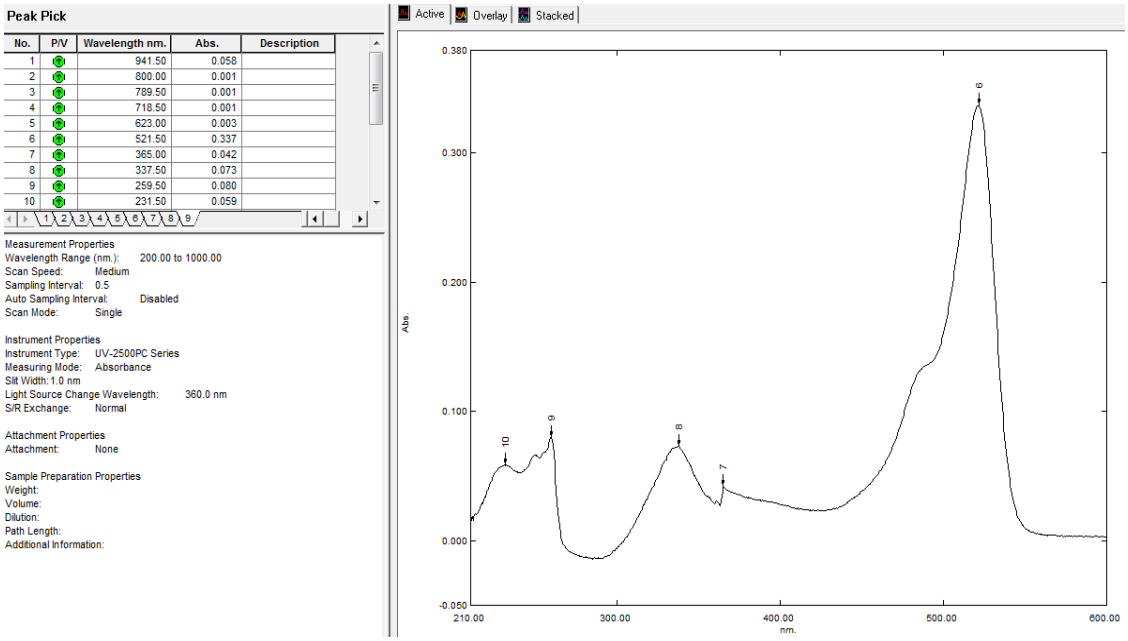

Pigment Orange 16

Normal Raman, 488nm

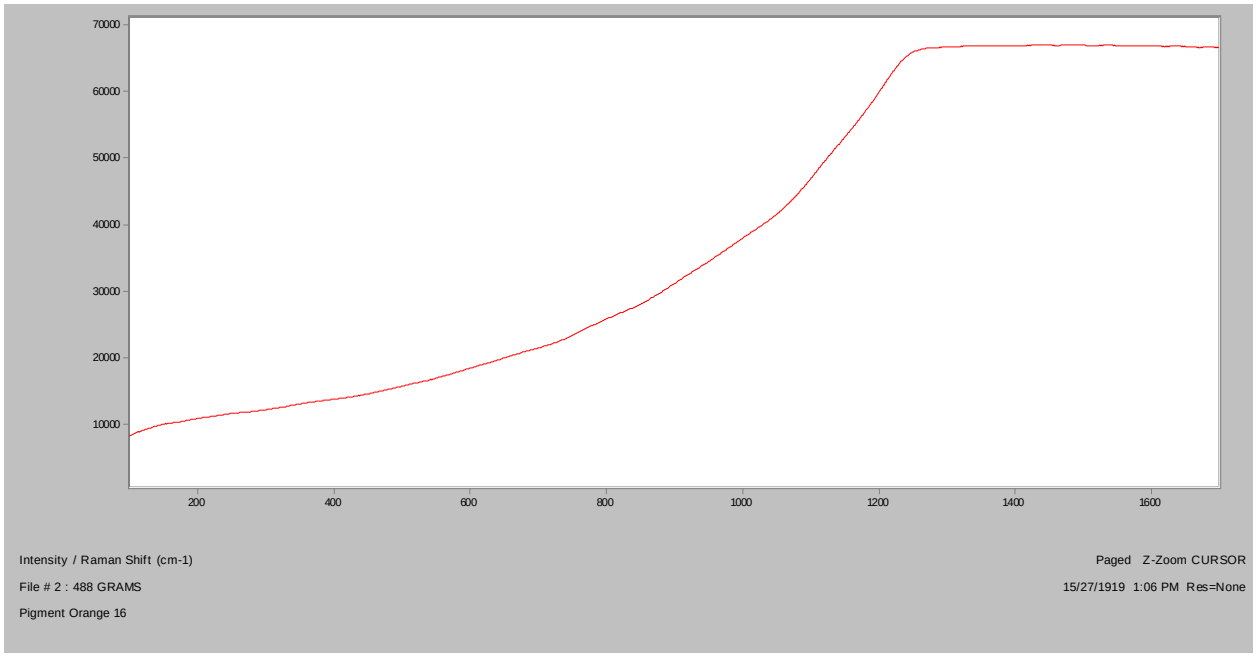

Normal Raman 633nm

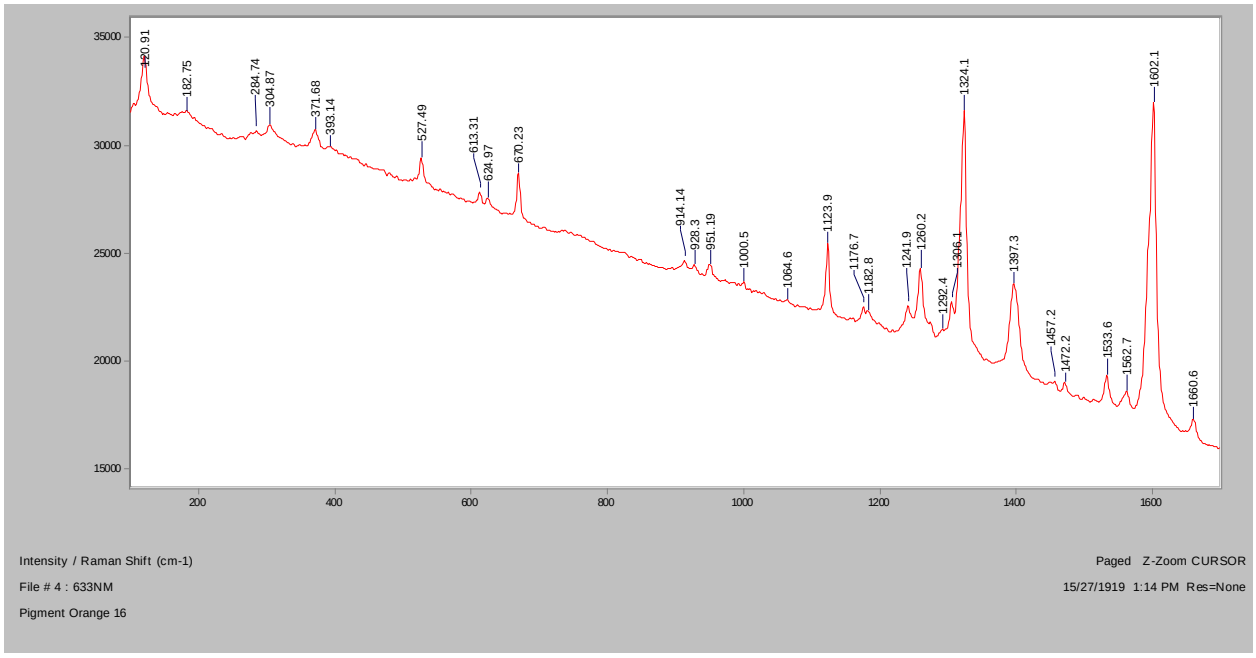

Normal Raman 785nm

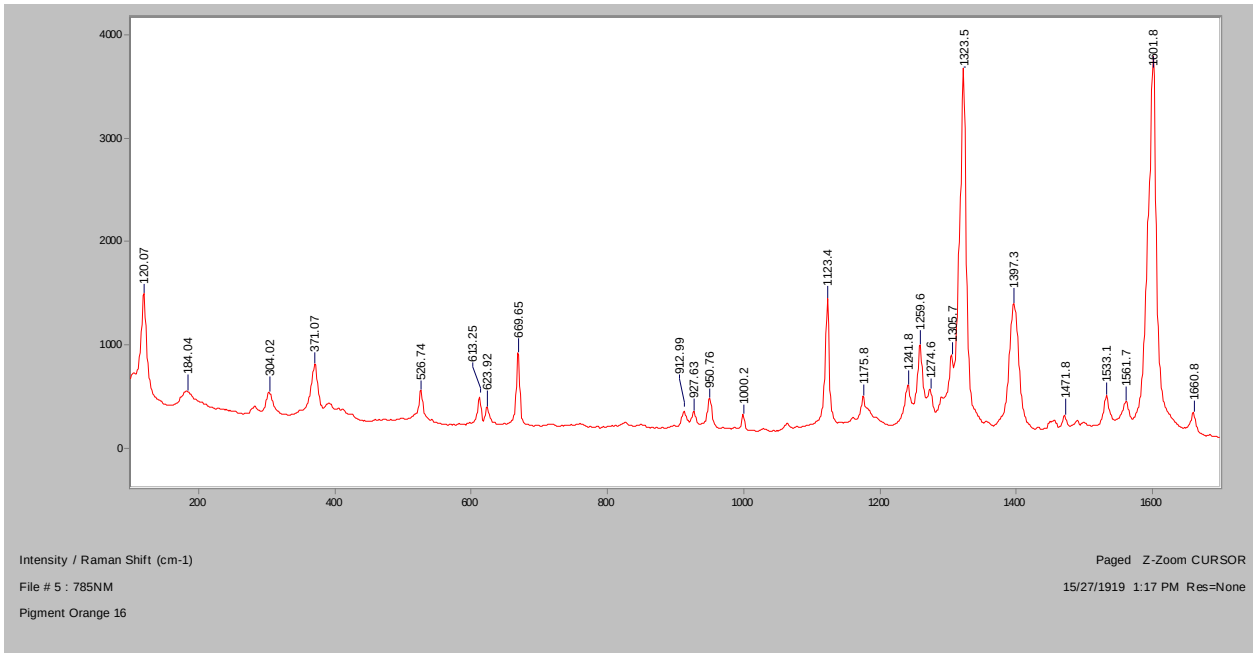

FT Raman, 1064

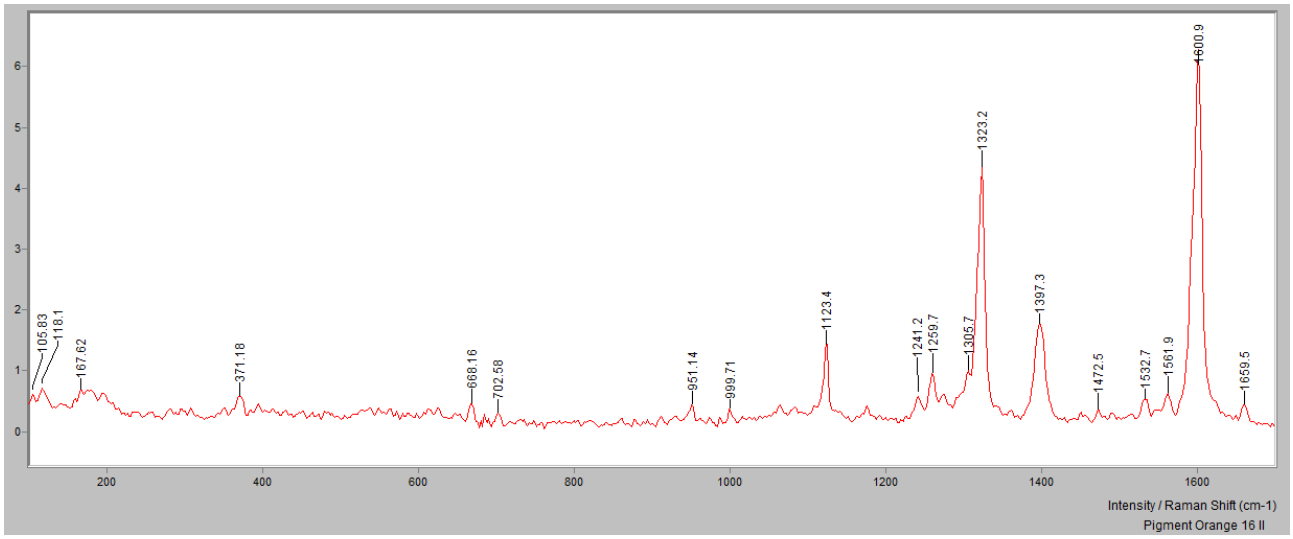

SERS, 488nm

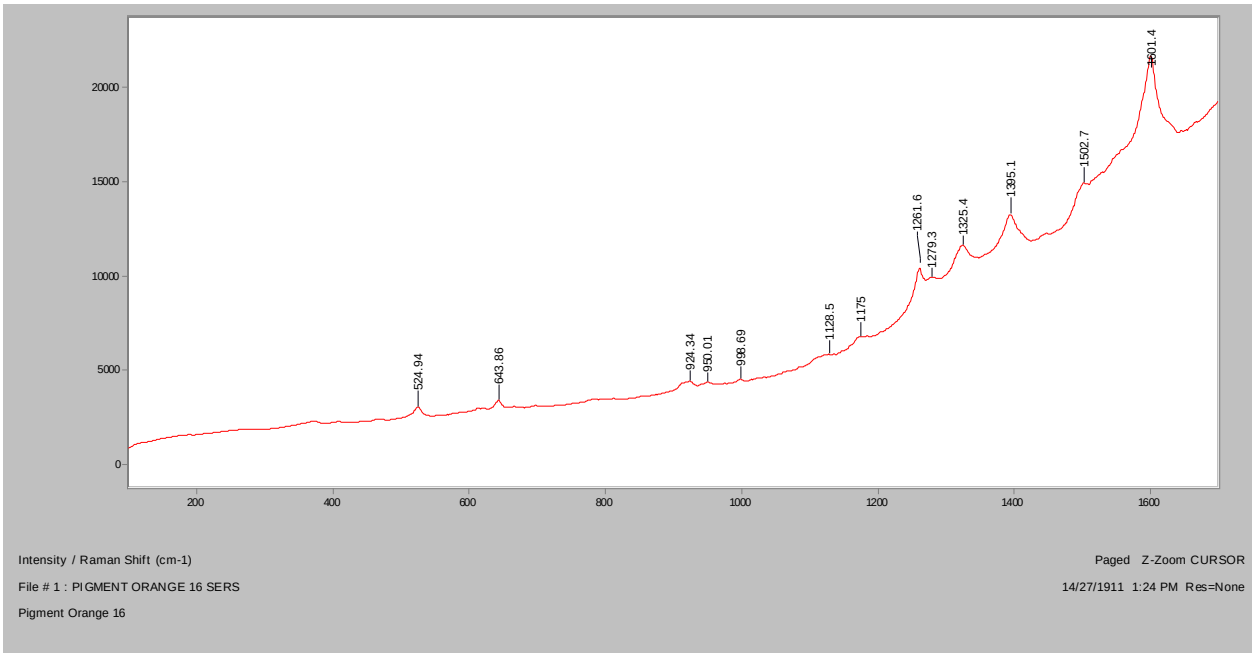

FT-IR (ATR)

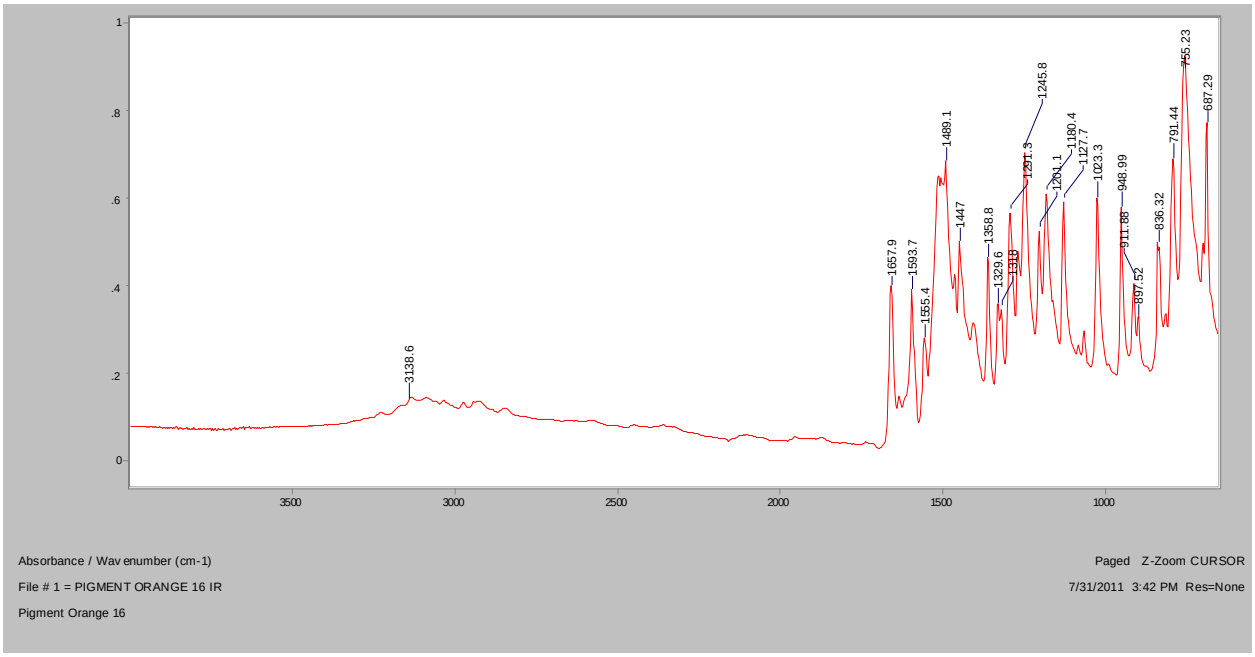

UV-Vis

Peak Pick

No.	P/V	Wavelength nm.	Abs.	Description
1	P	947.50	0.052	
2	P	897.50	0.013	
3	P	759.50	0.007	
4	P	744.50	0.008	
5	P	541.00	0.303	
6	P	318.00	0.143	

1 2 3 4 5

Measurement Properties
Wavelength Range (nm.): 200.00 to 1000.00
Scan Speed: Medium
Sampling Interval: 0.5
Auto Sampling Interval: Disabled
Scan Mode: Single

Instrument Properties
Instrument Type: UV-2500PC Series
Measuring Mode: Absorbance
Slit Width:1.0 nm
Light Source Change Wavelength: 360.0 nm
S/R Exchange: Normal

Attachment Properties
Attachment: None

Sample Preparation Properties
Weight:
Volume:
Dilution:
Path Length:
Additional Information:

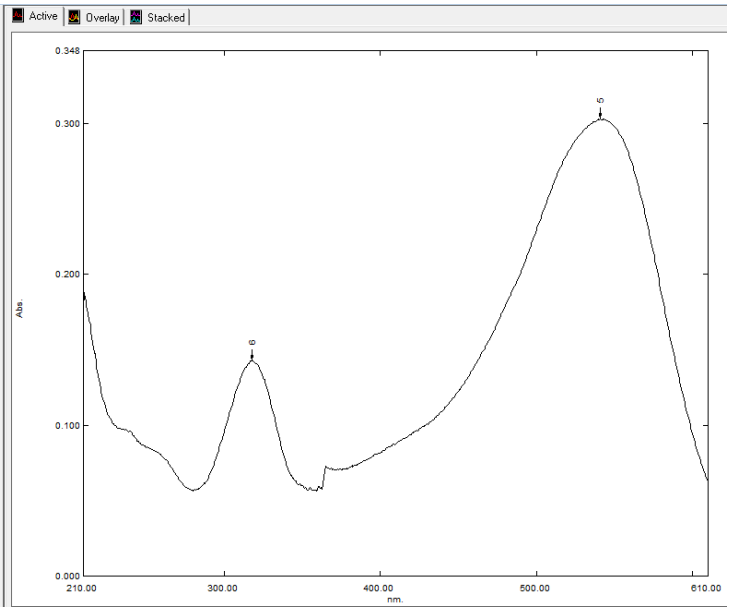

Pigment Orange 34

Normal Raman, 488nm

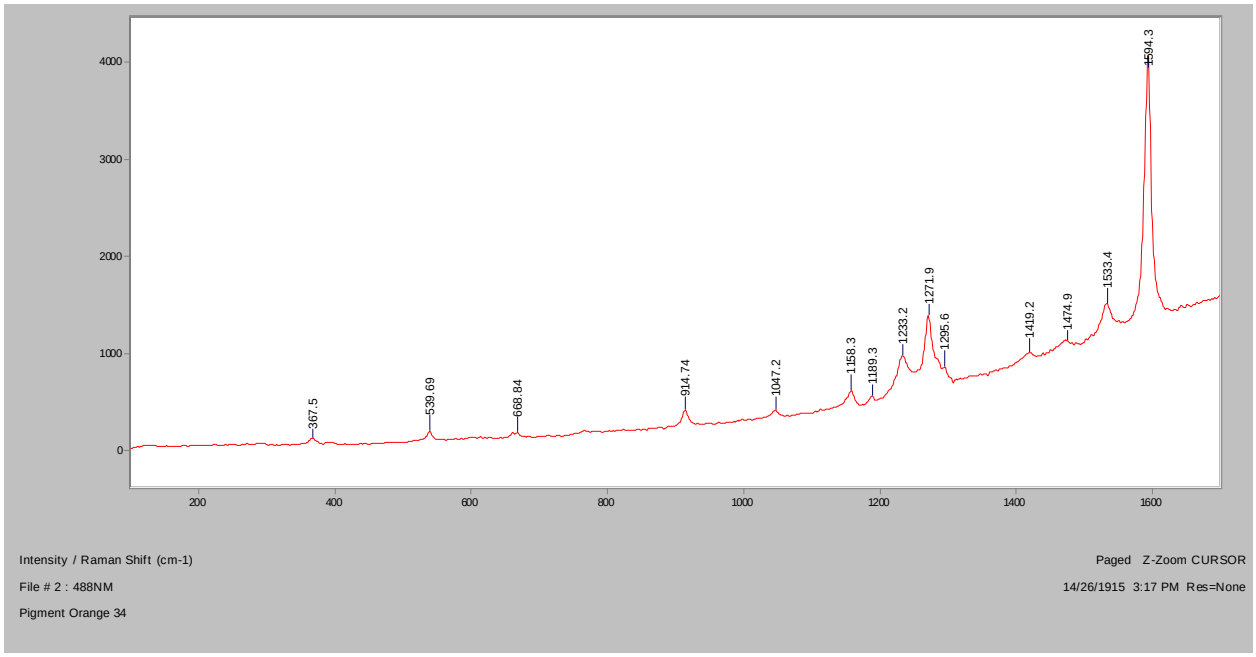

Normal Raman 633nm

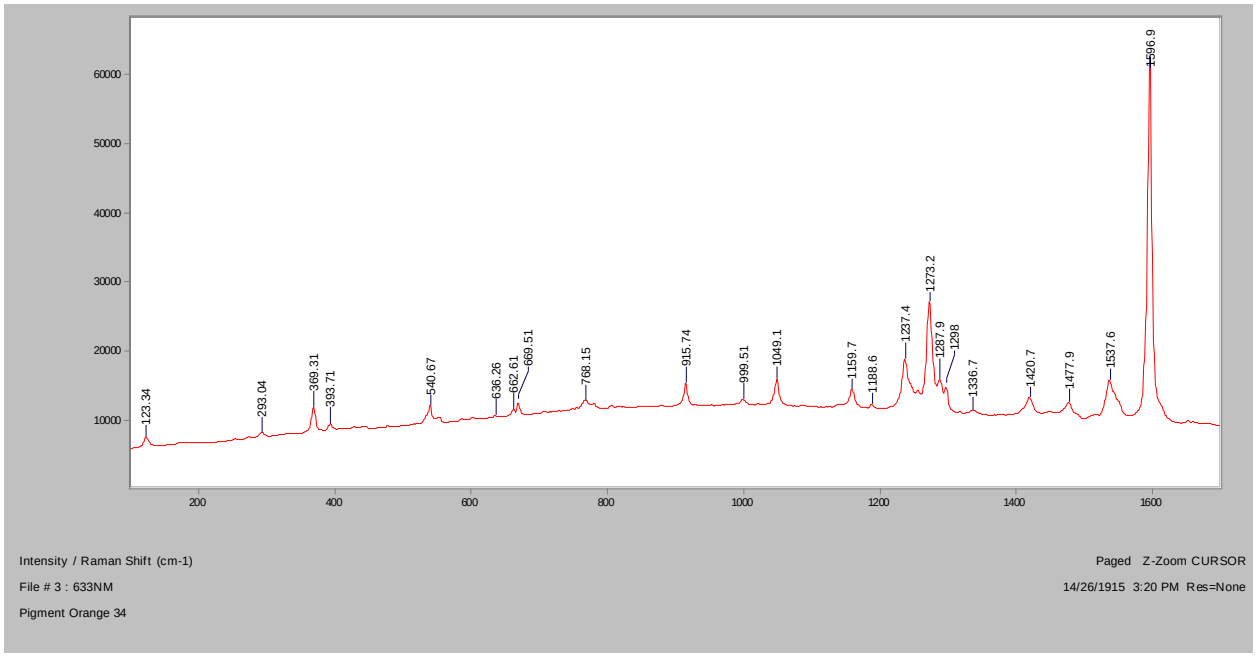

Normal Raman 785nm

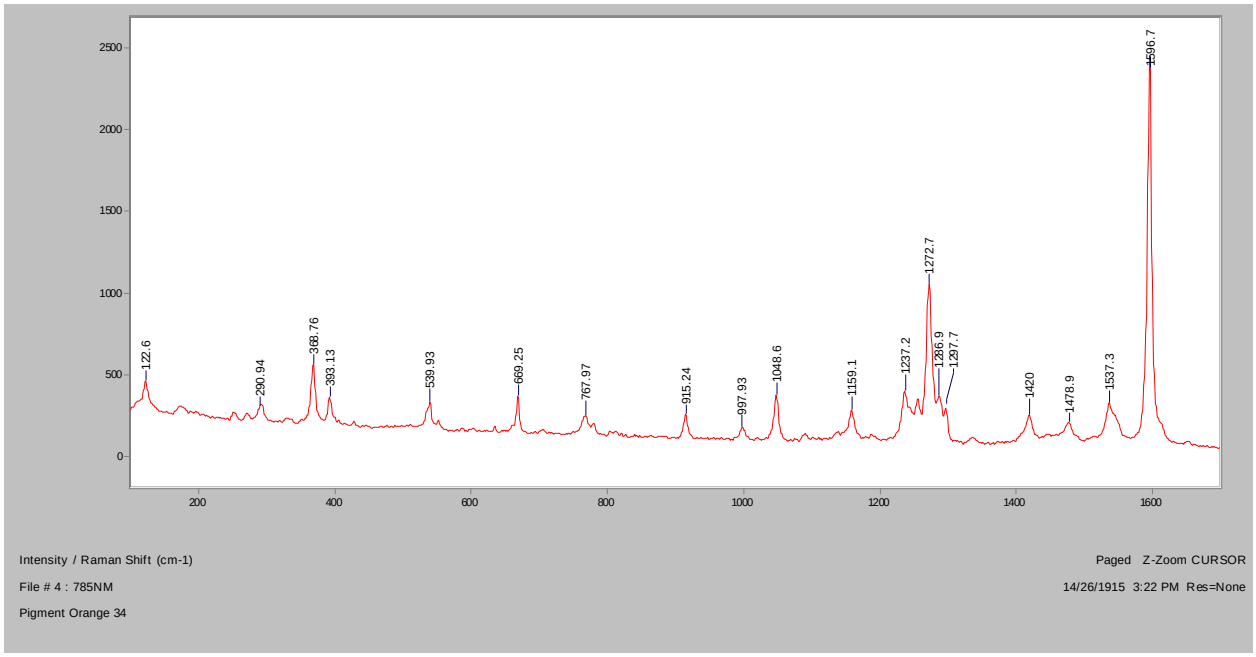

FT Raman, 1064nm

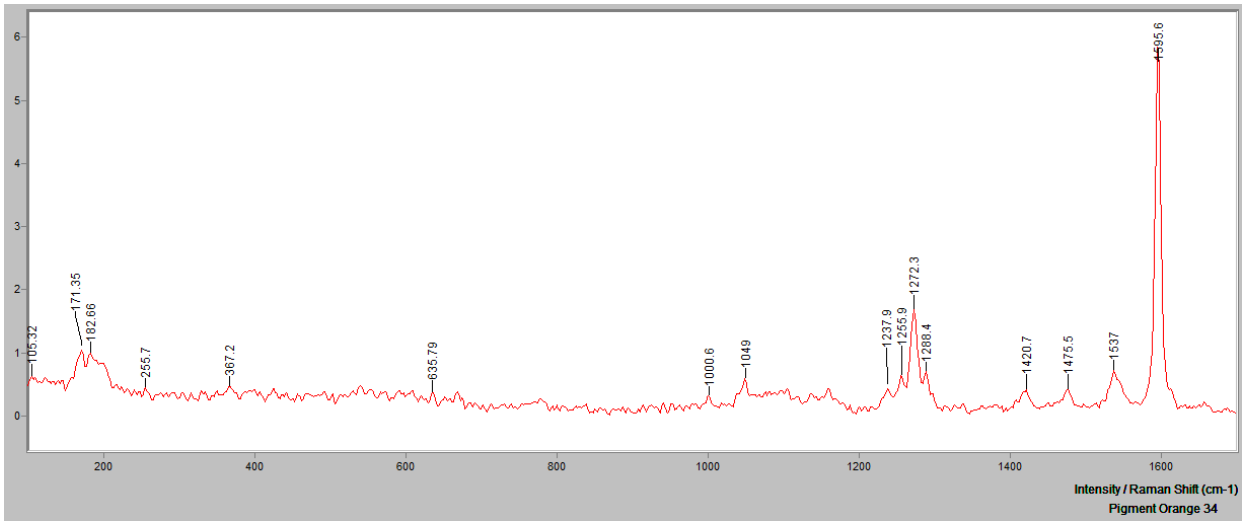

SERS, 488nm

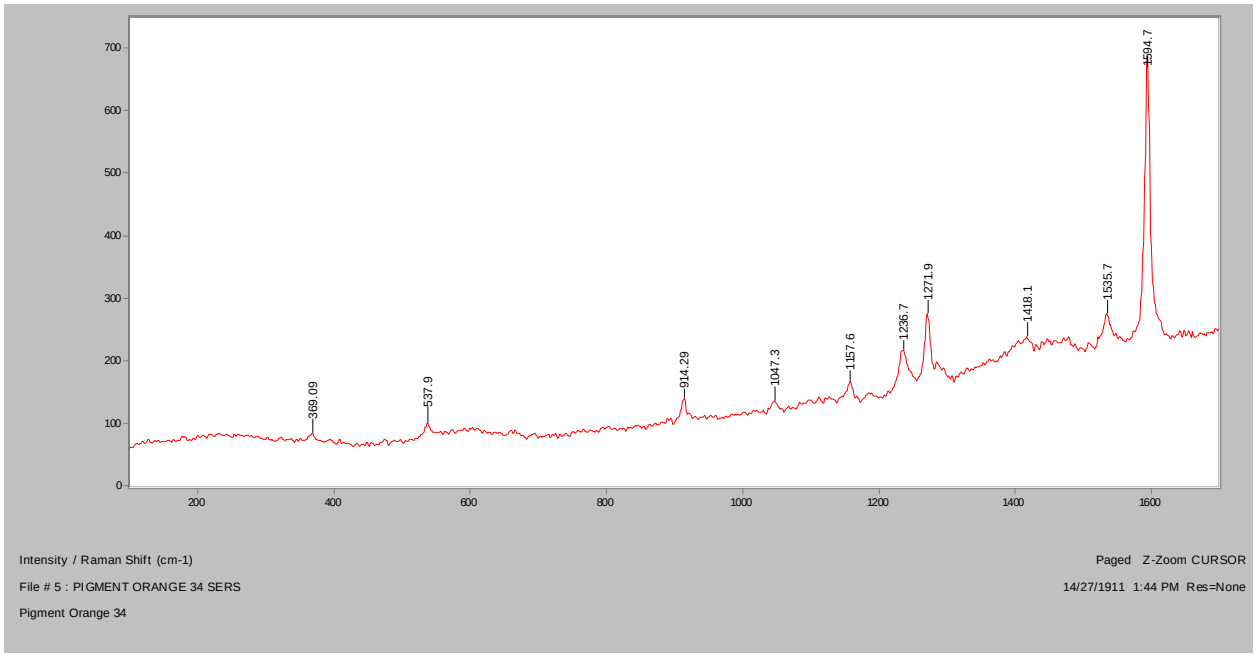

FT-IR (ATR)

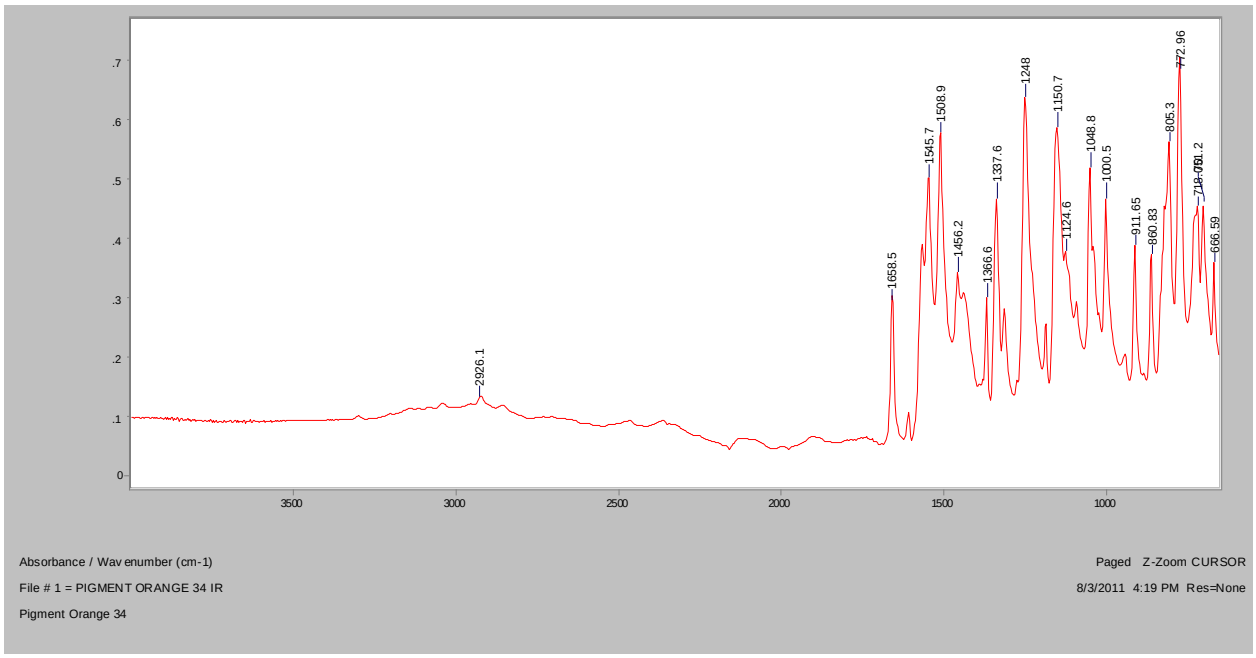

UV-Vis

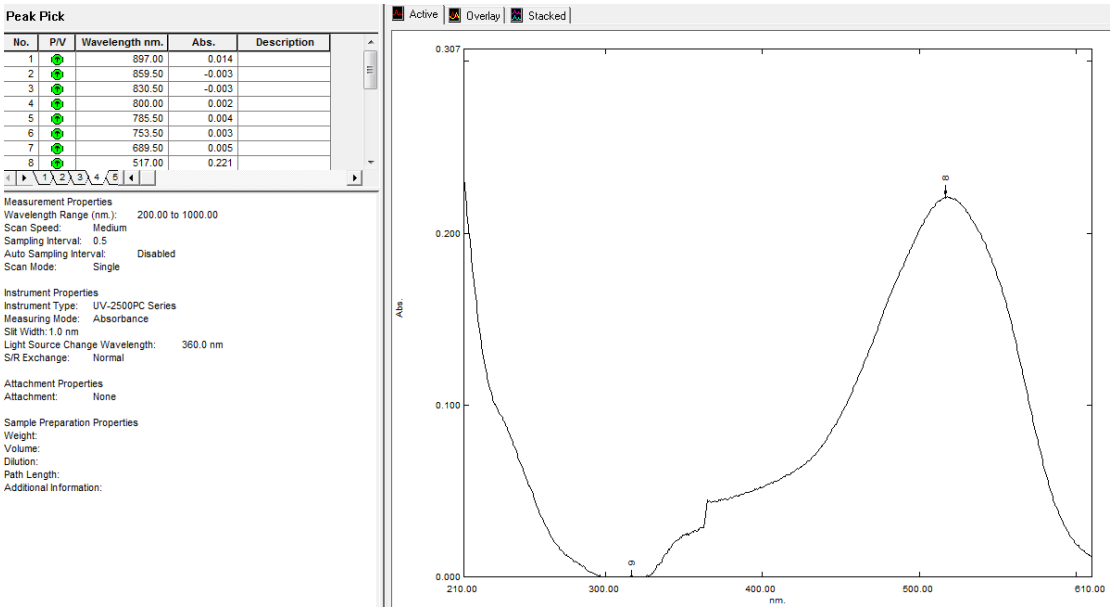

Peak Pick

No.	P/V	Wavelength nm.	Abs.	Description
1		897.00	0.014	
2		859.50	-0.003	
3		830.50	-0.003	
4		800.00	0.002	
5		785.50	0.004	
6		753.50	0.003	
7		689.50	0.005	
8		517.00	0.221	

1 2 3 4 5

Measurement Properties
Wavelength Range (nm.): 200.00 to 1000.00
Scan Speed: Medium
Sampling Interval: 0.5
Auto Sampling Interval: Disabled
Scan Mode: Single

Instrument Properties
Instrument Type: UV-2500PC Series
Measuring Mode: Absorbance
Slit Width:1.0 nm
Light Source Change Wavelength: 360.0 nm
S/R Exchange: Normal

Attachment Properties
Attachment: None

Sample Preparation Properties
Weight:
Volume:
Dilution:
Path Length:
Additional Information:

Active | Overlay | Stacked

Pigment Orange 62

Normal Raman, 488nm

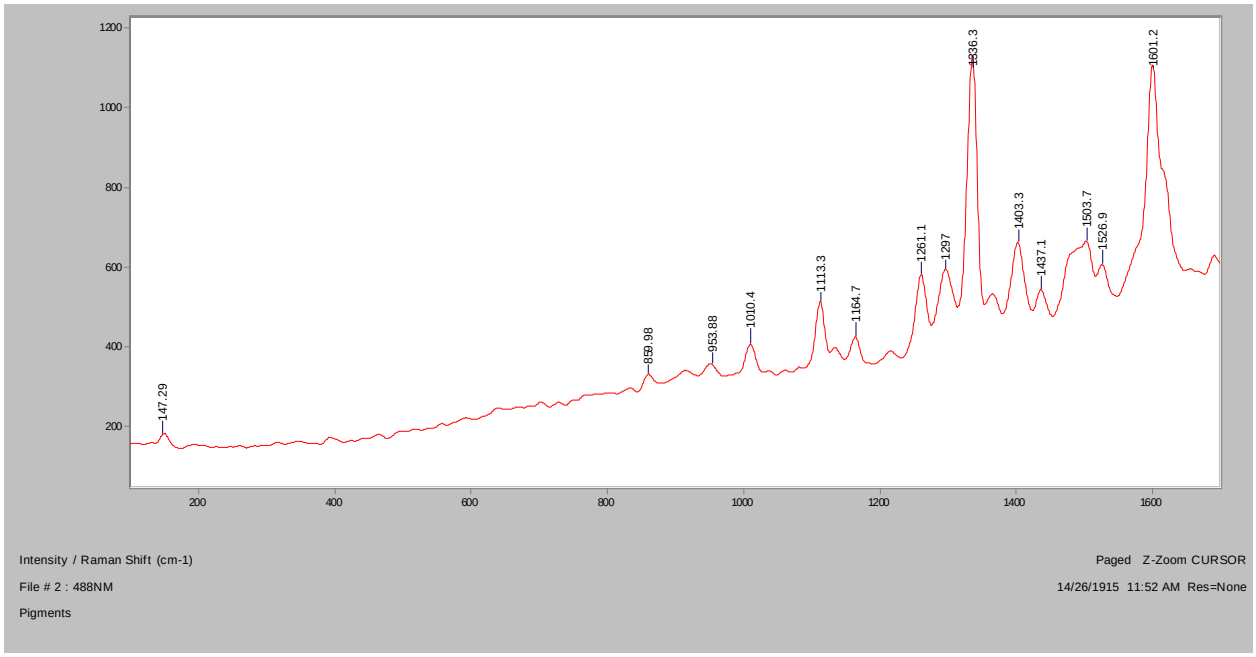

Normal Raman 633nm

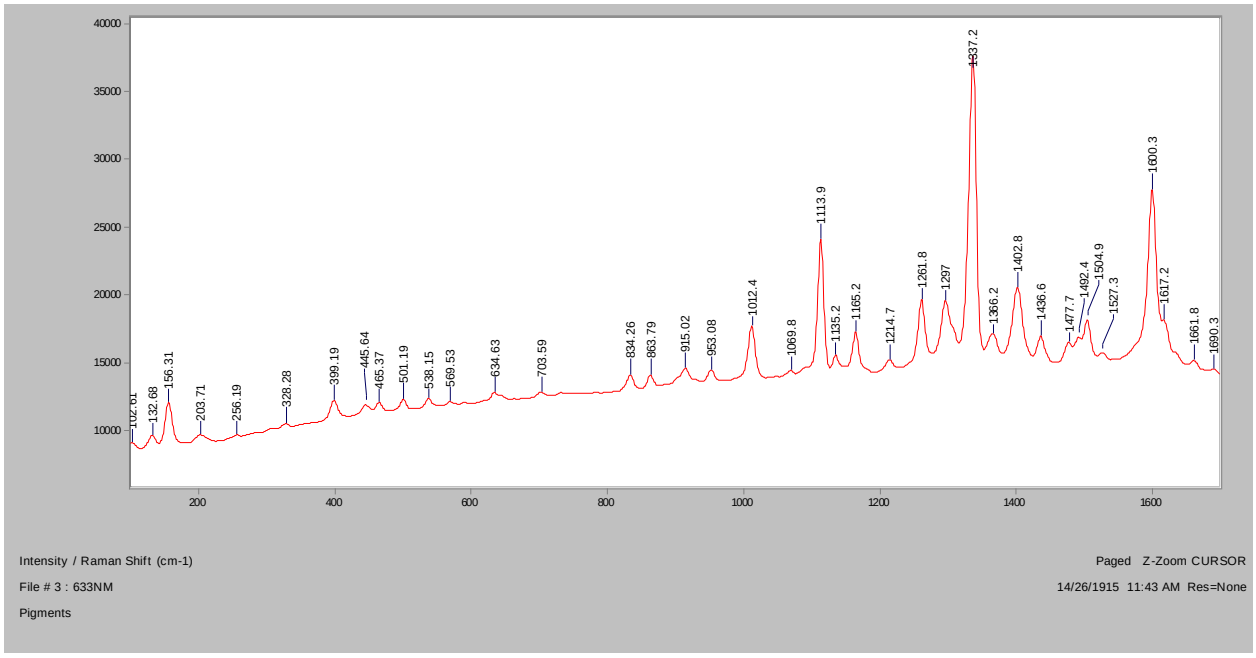

Normal Raman 785nm

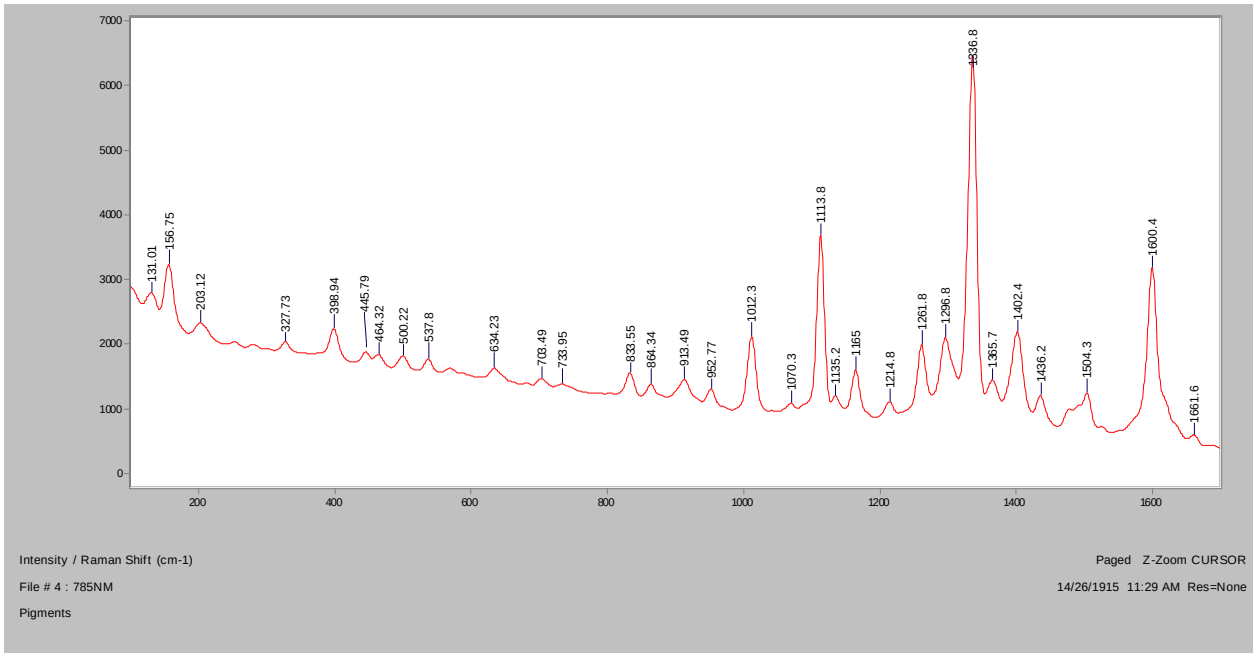

SERS, 488nm

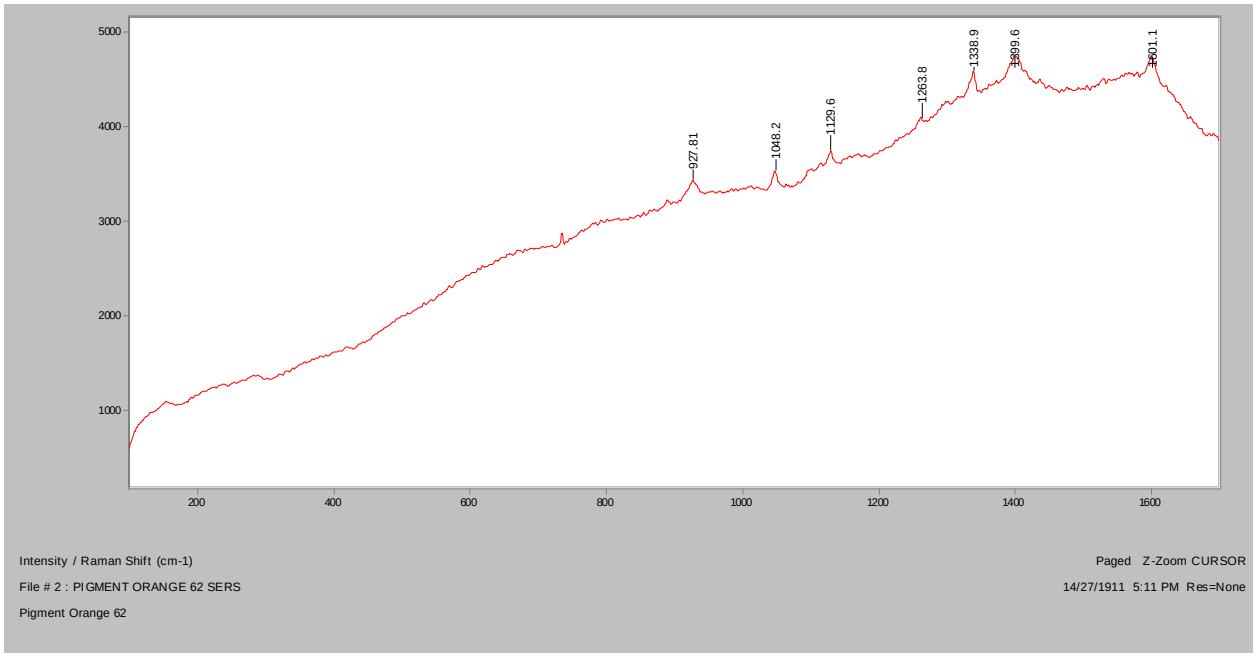

FT-IR (ATR)

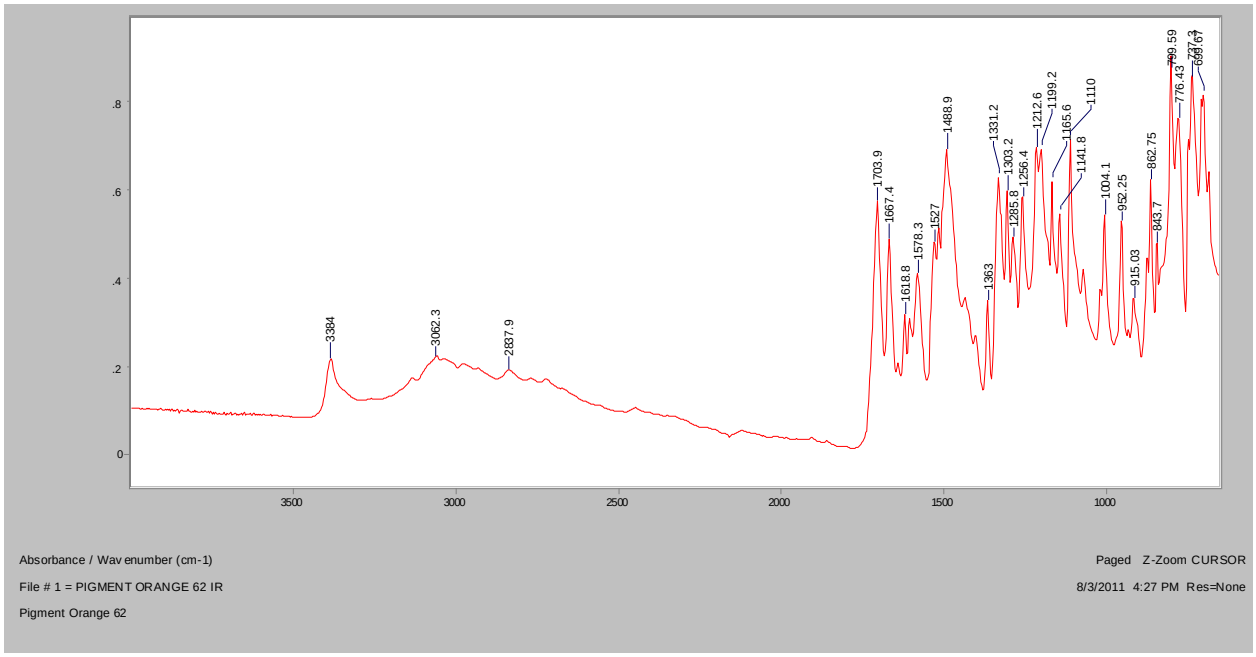

UV-Vis

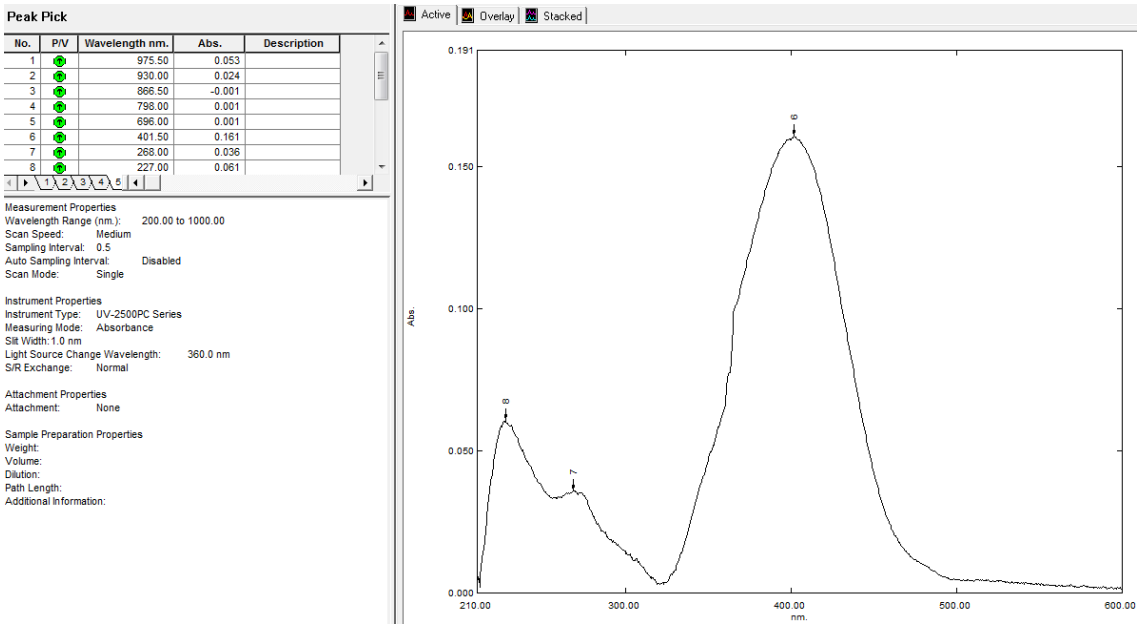

Peak Pick

No.	P/V	Wavelength nm.	Abs.	Description
1		975.50	0.053	
2		930.00	0.024	
3		866.50	-0.001	
4		798.00	0.001	
5		696.00	0.001	
6		401.50	0.161	
7		268.00	0.036	
8		227.00	0.061	

1 2 3 4 5

Measurement Properties
Wavelength Range (nm.): 200.00 to 1000.00
Scan Speed: Medium
Sampling Interval: 0.5
Auto Sampling Interval: Disabled
Scan Mode: Single

Instrument Properties
Instrument Type: UV-2500PC Series
Measuring Mode: Absorbance
Slit Width: 1.0 nm
Light Source Change Wavelength: 360.0 nm
S/R Exchange: Normal

Attachment Properties
Attachment: None

Sample Preparation Properties
Weight:
Volume:
Dilution:
Path Length:
Additional Information:

Pigment Yellow 3

Normal Raman, 488nm

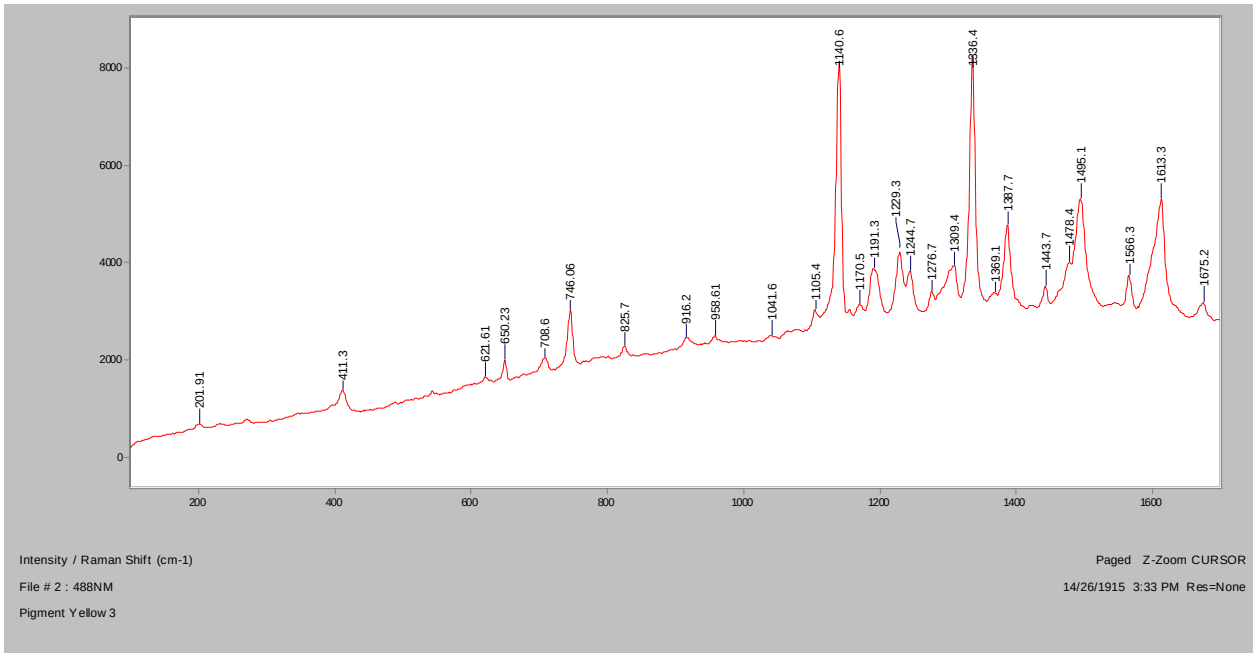

Normal Raman 633nm

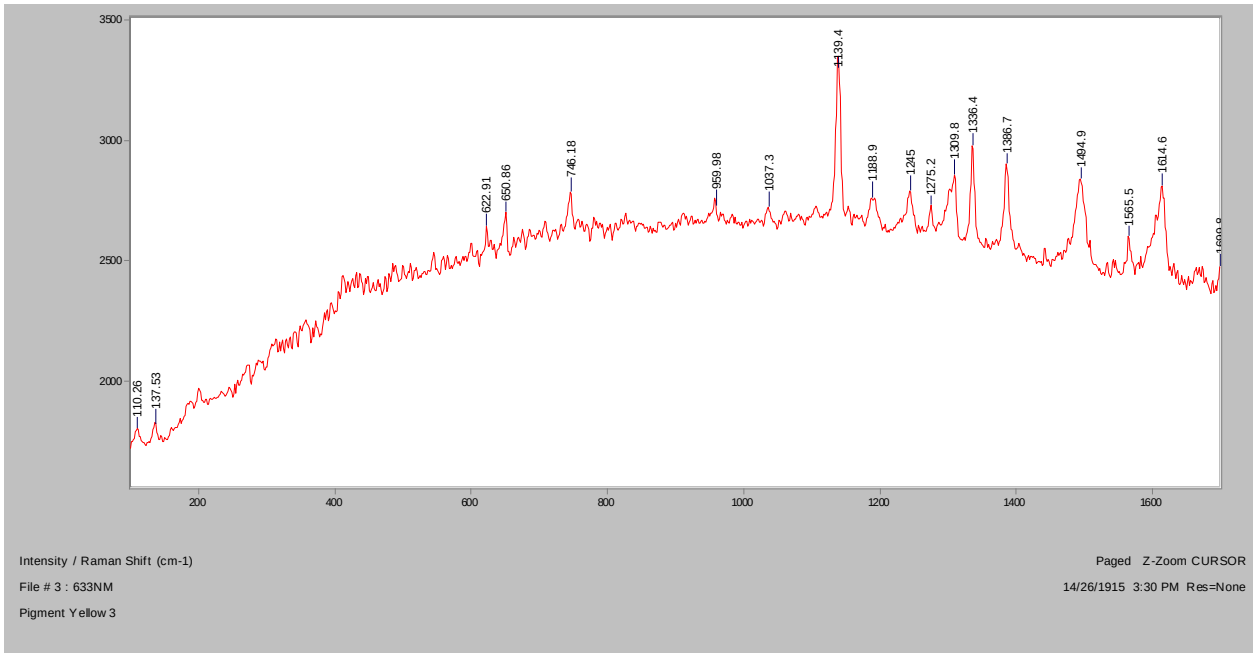

Normal Raman 785nm

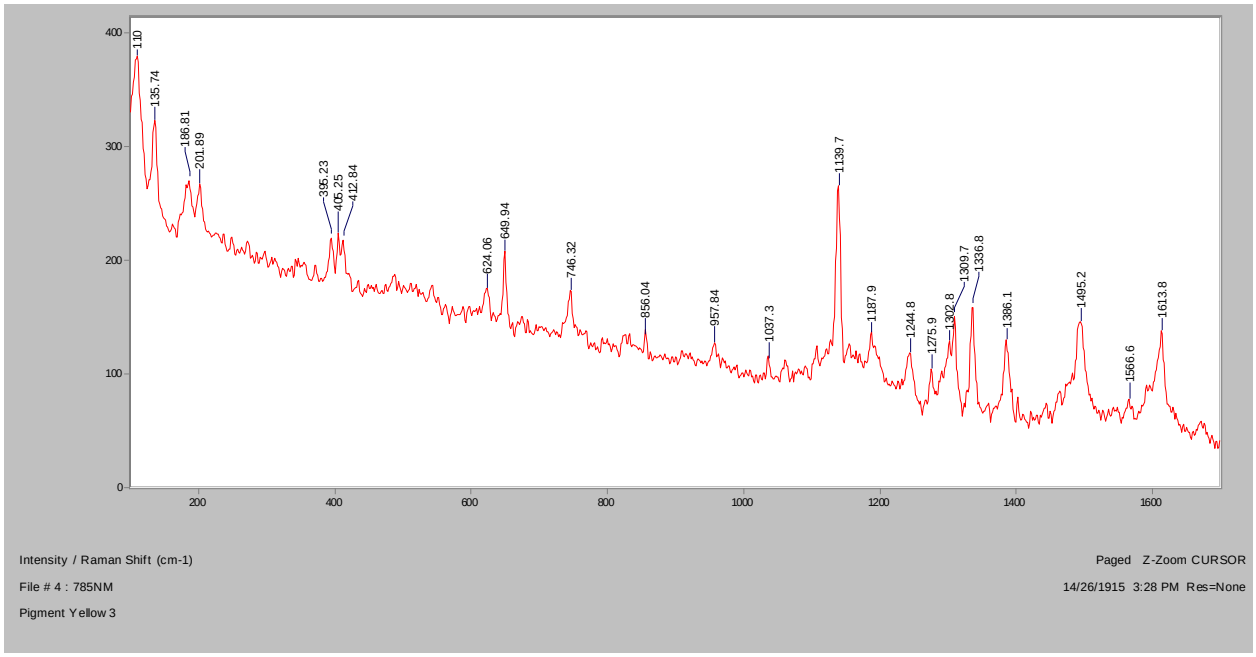

SERS, 488nm

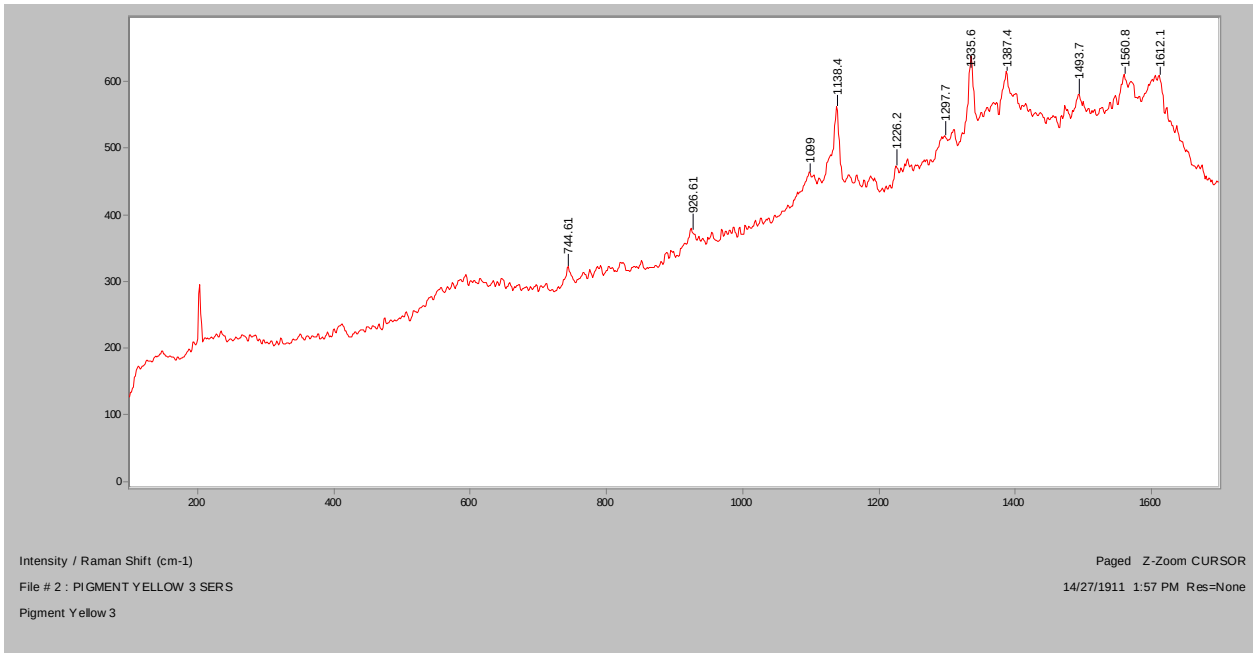

FT-IR (ATR)

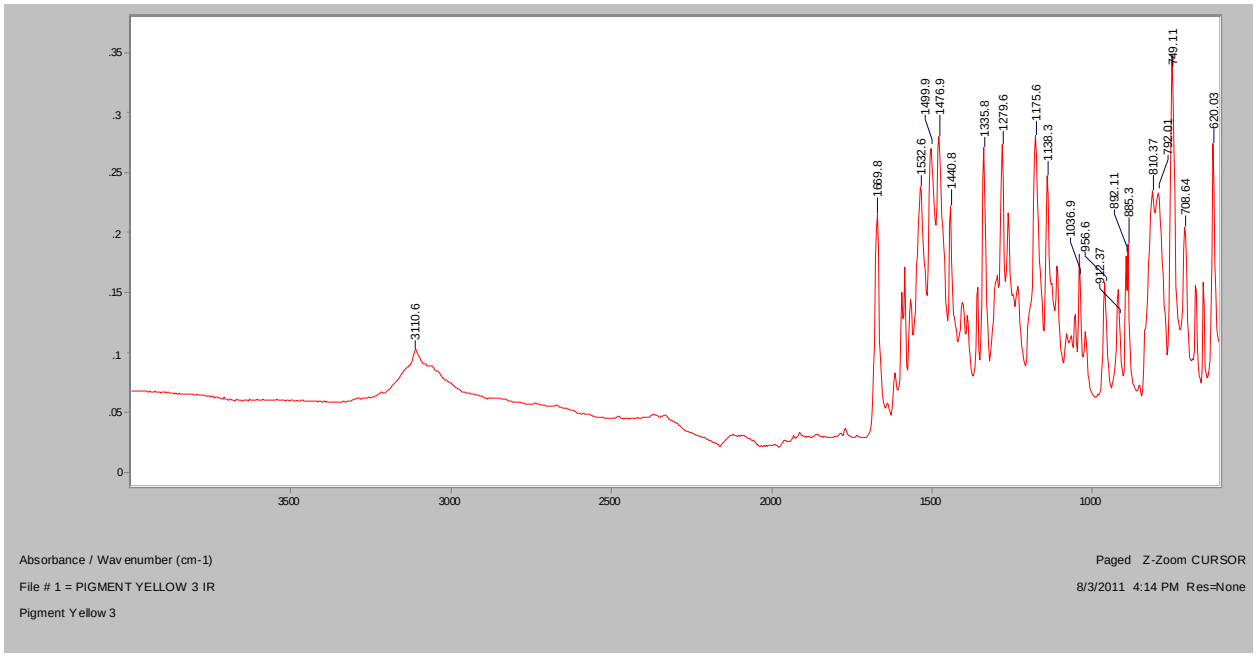

UV-Vis

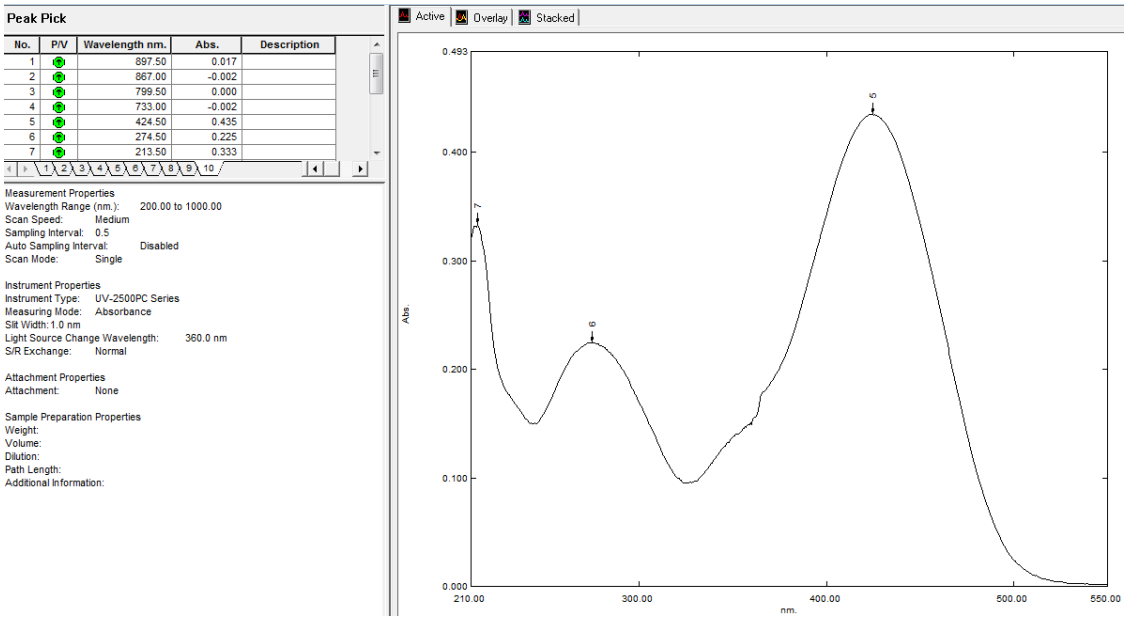

Pigment Yellow 73

Normal Raman, 488nm

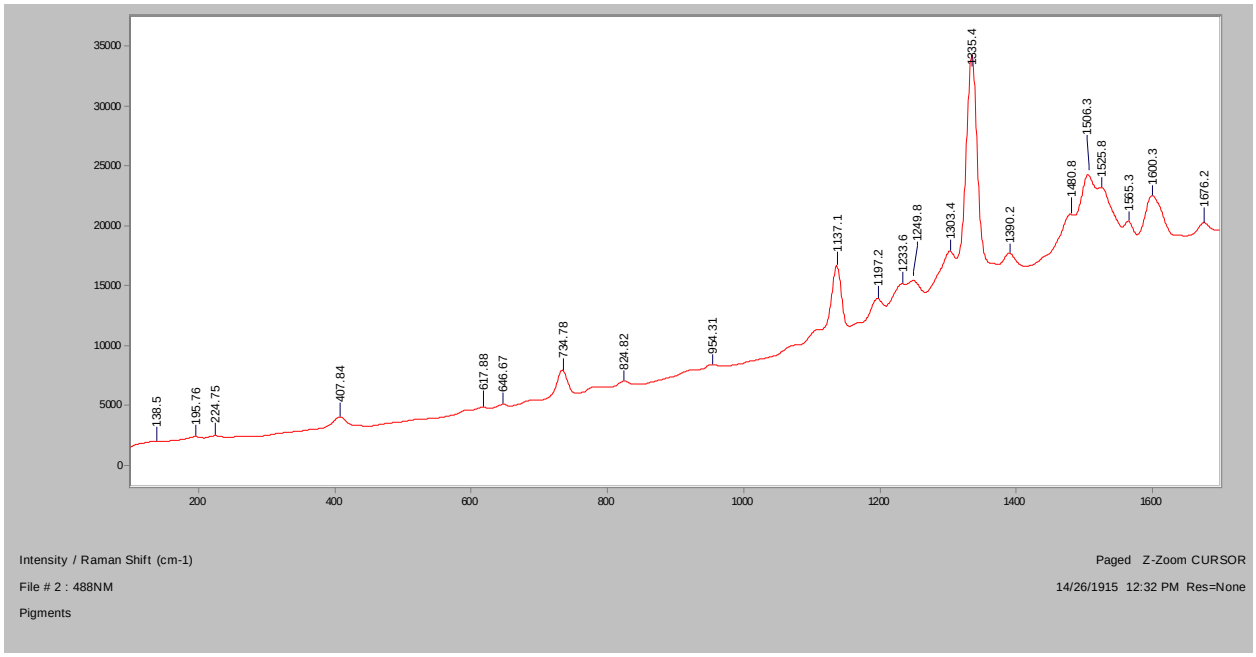

Normal Raman 633nm

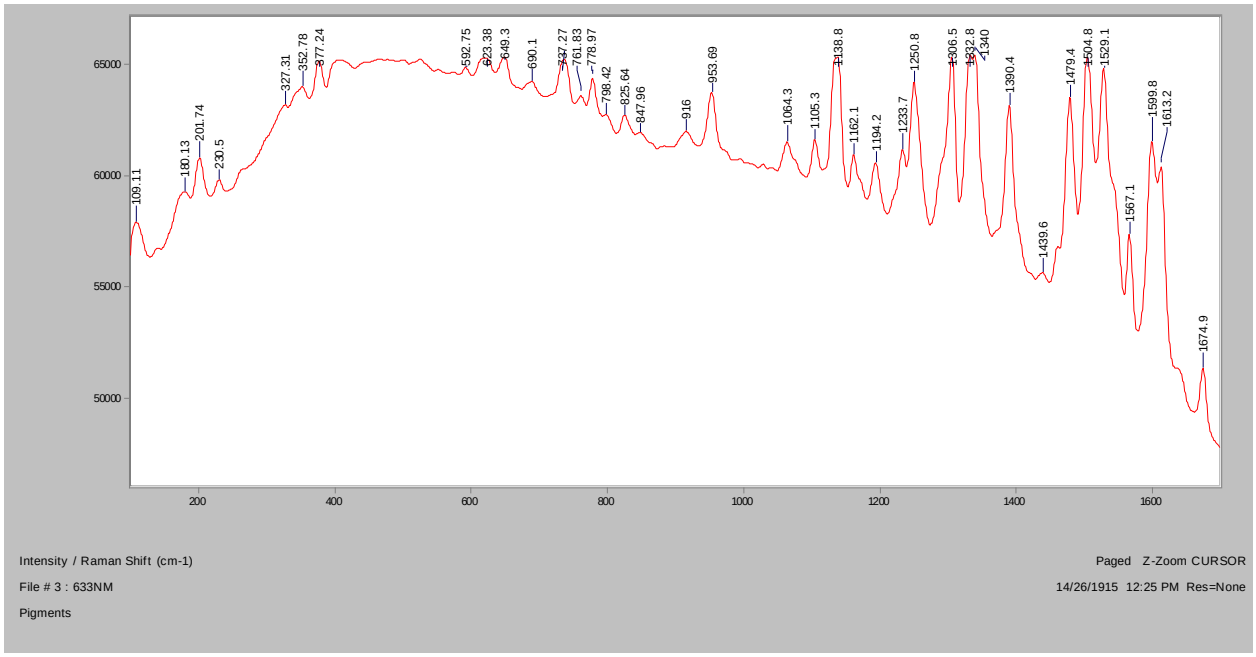

Normal Raman 785nm

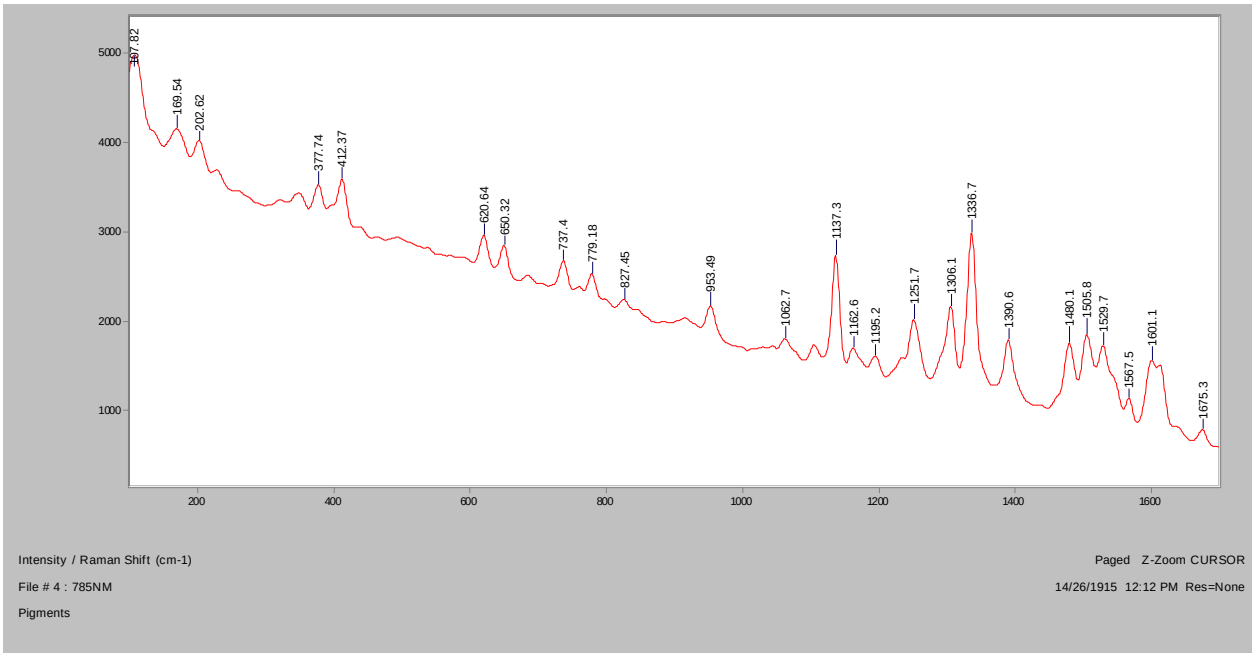

SERS, 488nm

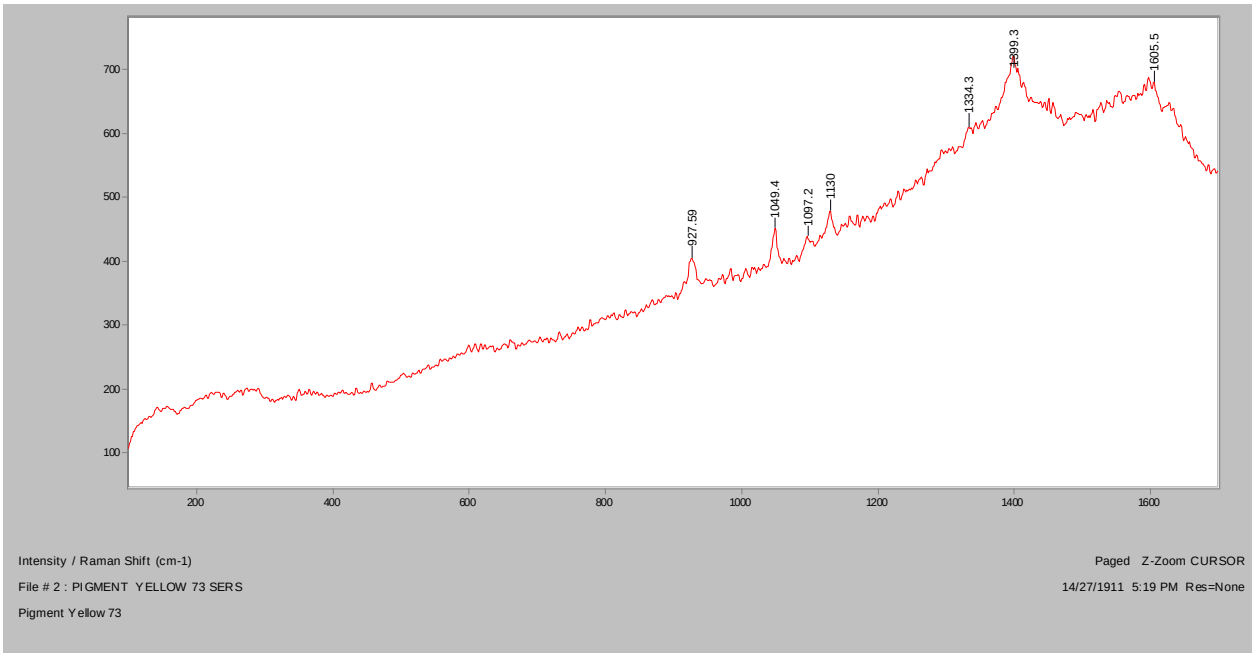

FT-IR (ATR)

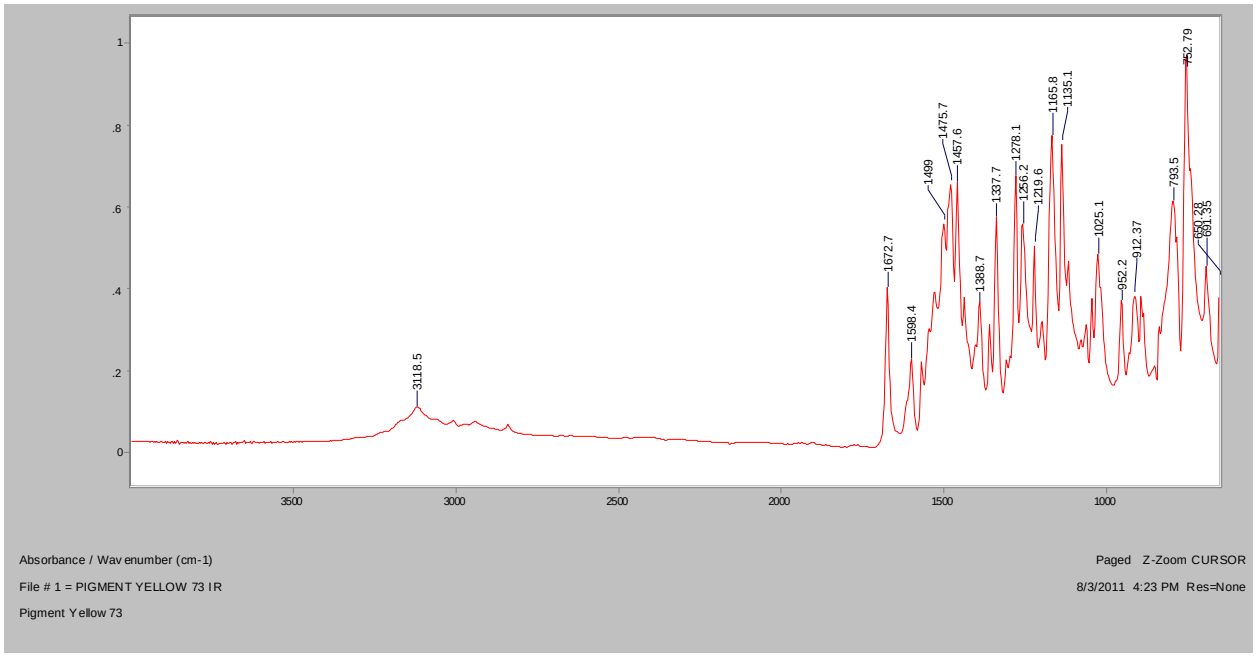

UV-Vis

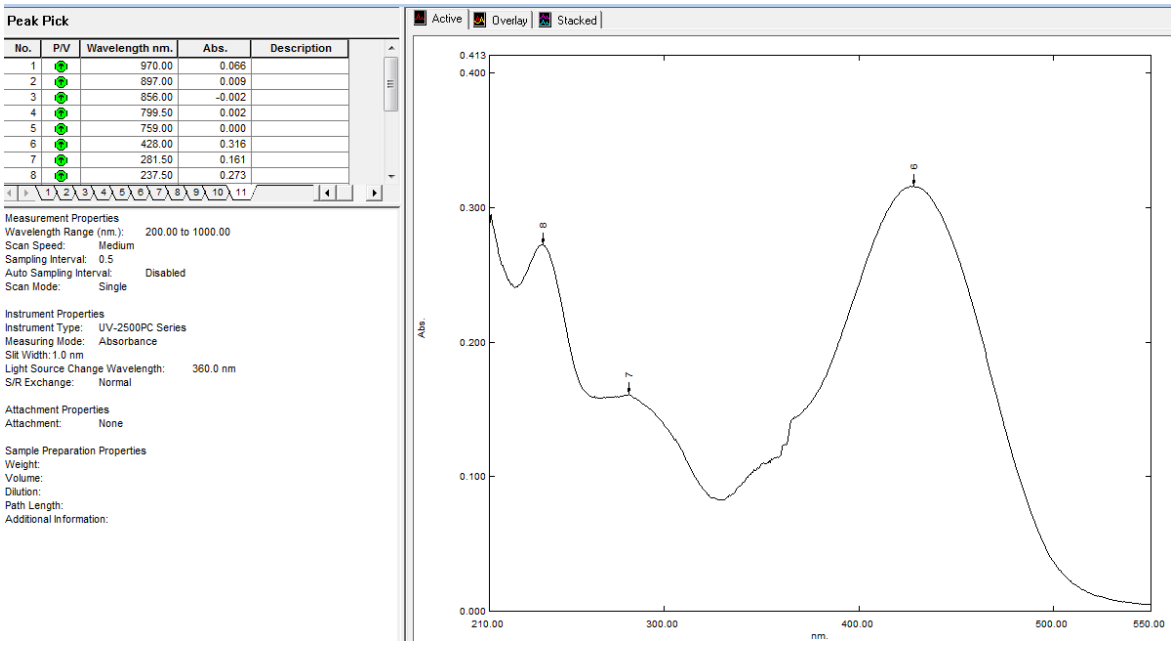

Peak Pick

No.	P/V	Wavelength nm.	Abs.	Description
1		970.00	0.066	
2		897.00	0.009	
3		856.00	-0.002	
4		799.50	0.002	
5		759.00	0.000	
6		428.00	0.316	
7		281.50	0.161	
8		237.50	0.273	

1 2 3 4 5 6 7 8 9 10 11

Measurement Properties
Wavelength Range (nm.): 200.00 to 1000.00
Scan Speed: Medium
Sampling Interval: 0.5
Auto Sampling Interval: Disabled
Scan Mode: Single

Instrument Properties
Instrument Type: UV-2500PC Series
Measuring Mode: Absorbance
Slit Width: 1.0 nm
Light Source Change Wavelength: 360.0 nm
S/R Exchange: Normal

Attachment Properties
Attachment: None

Sample Preparation Properties
Weight:
Volume:
Dilution:
Path Length:
Additional Information:

Pigment Yellow 83

Normal Raman, 488nm

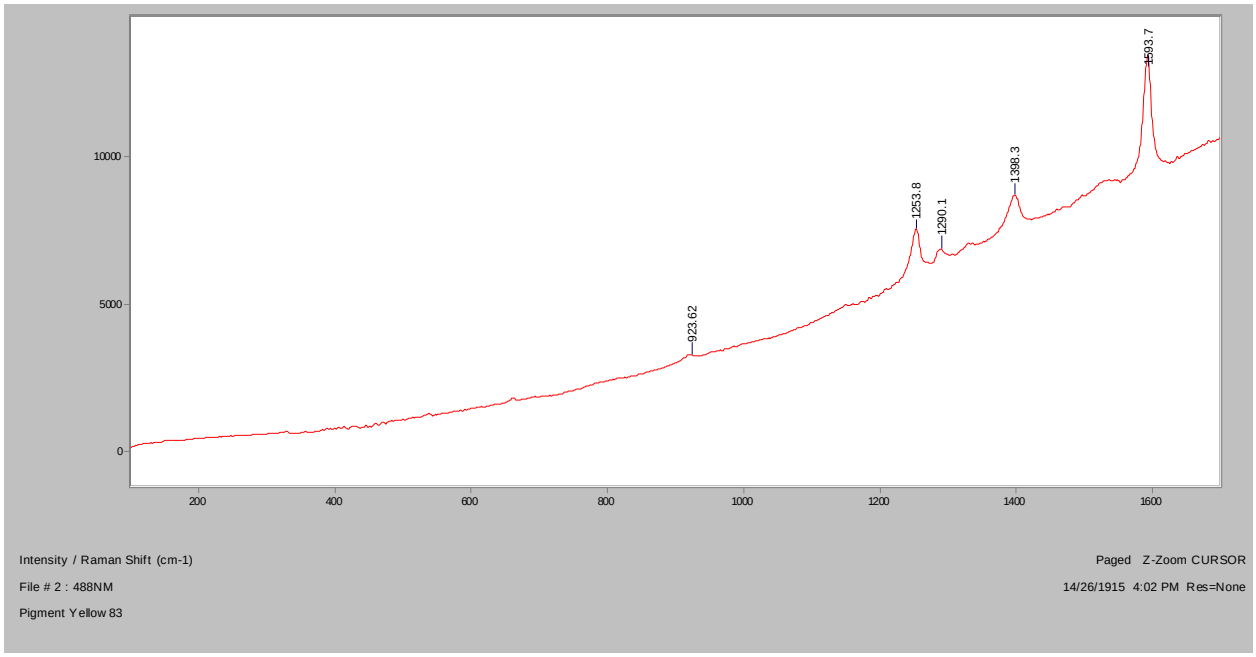

Normal Raman 633nm

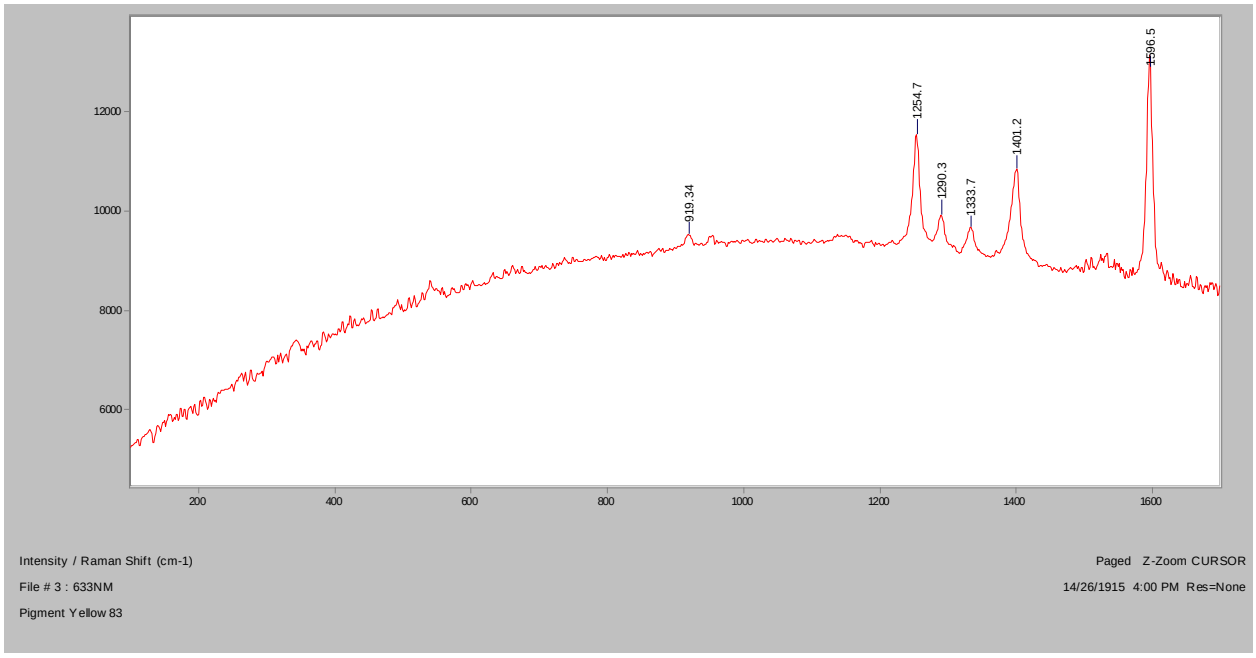

Normal Raman 785nm

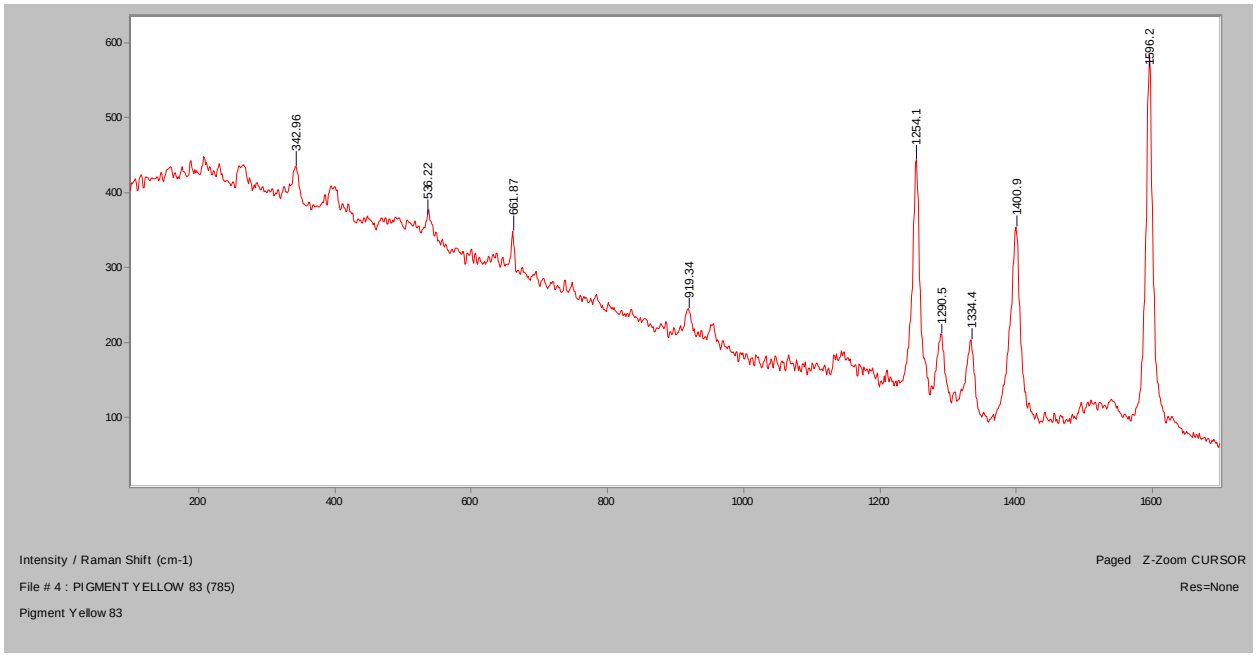

SERS, 488nm

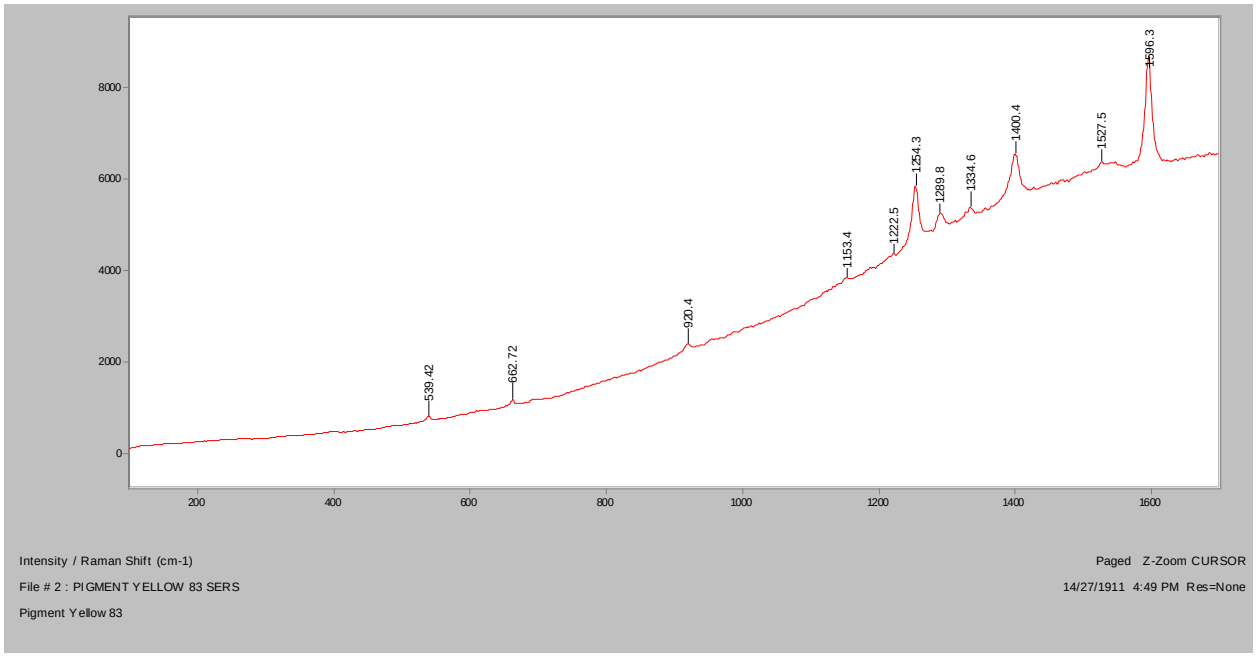

FT-IR (ATR)

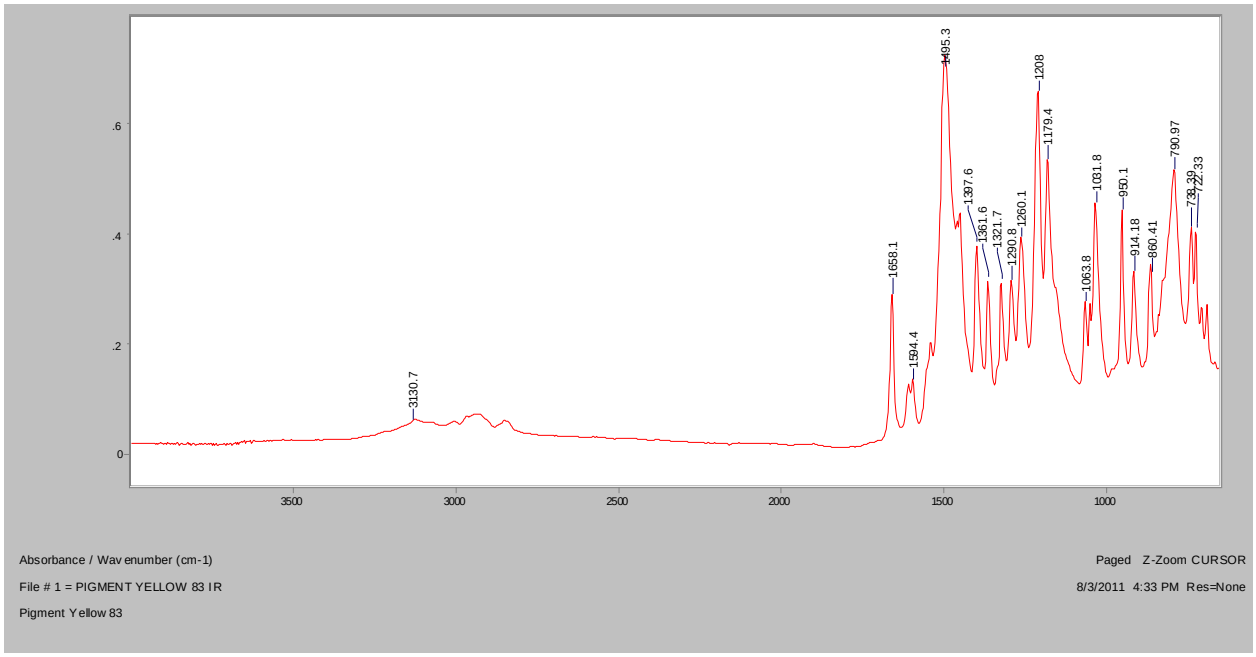

UV-Vis

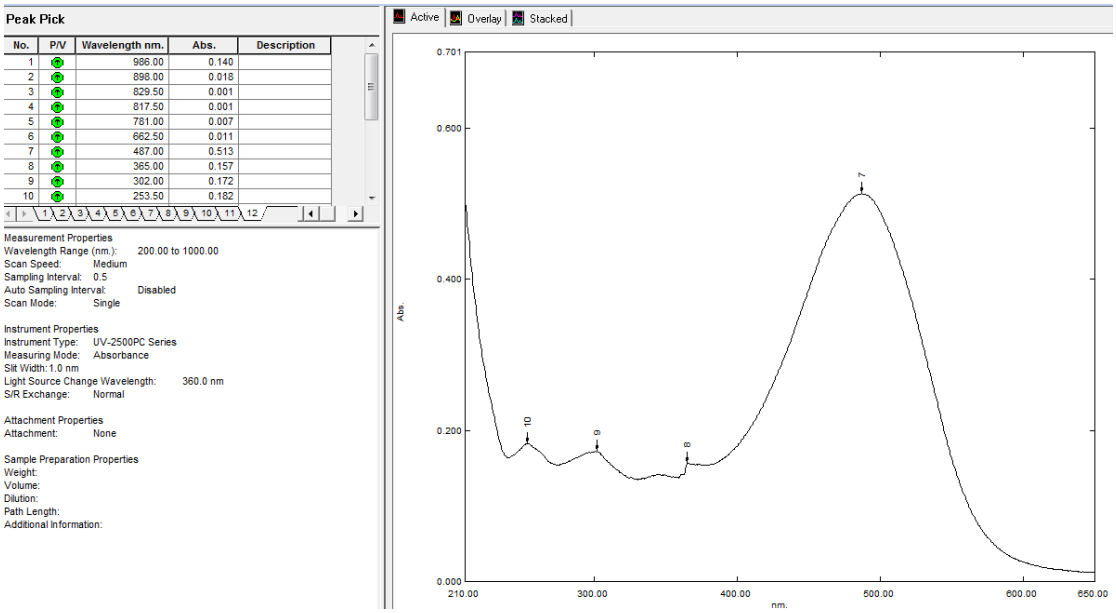

Pigment Yellow 151

Normal Raman, 488nm

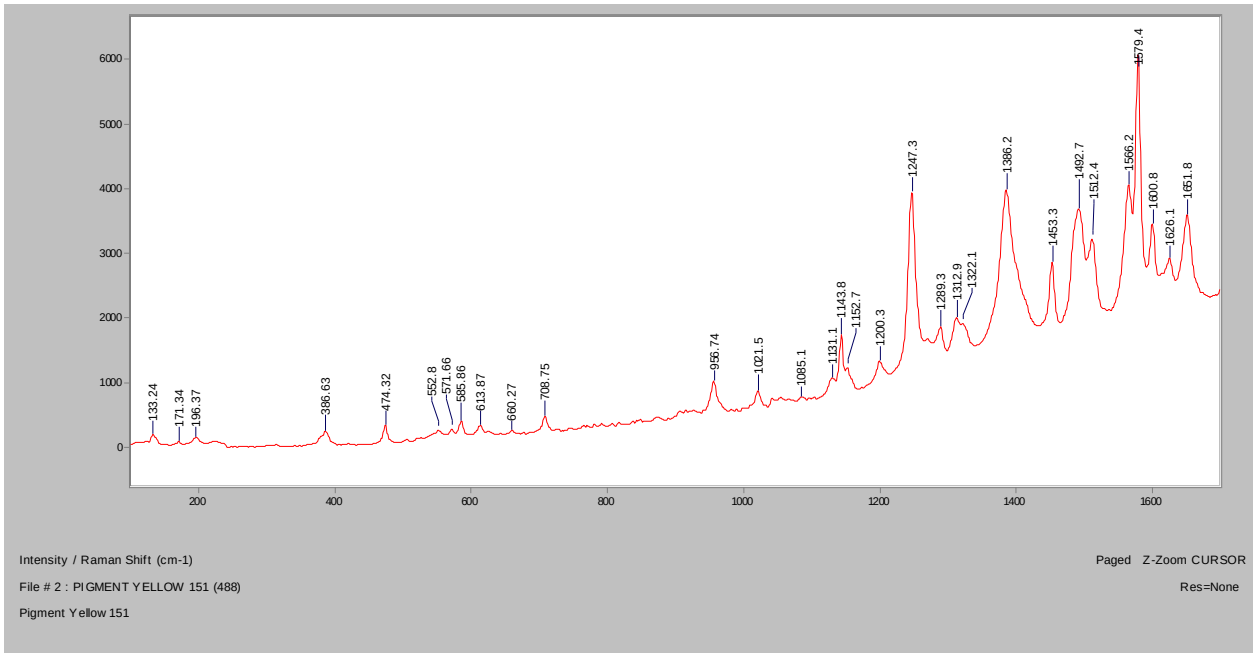

Normal Raman 633nm

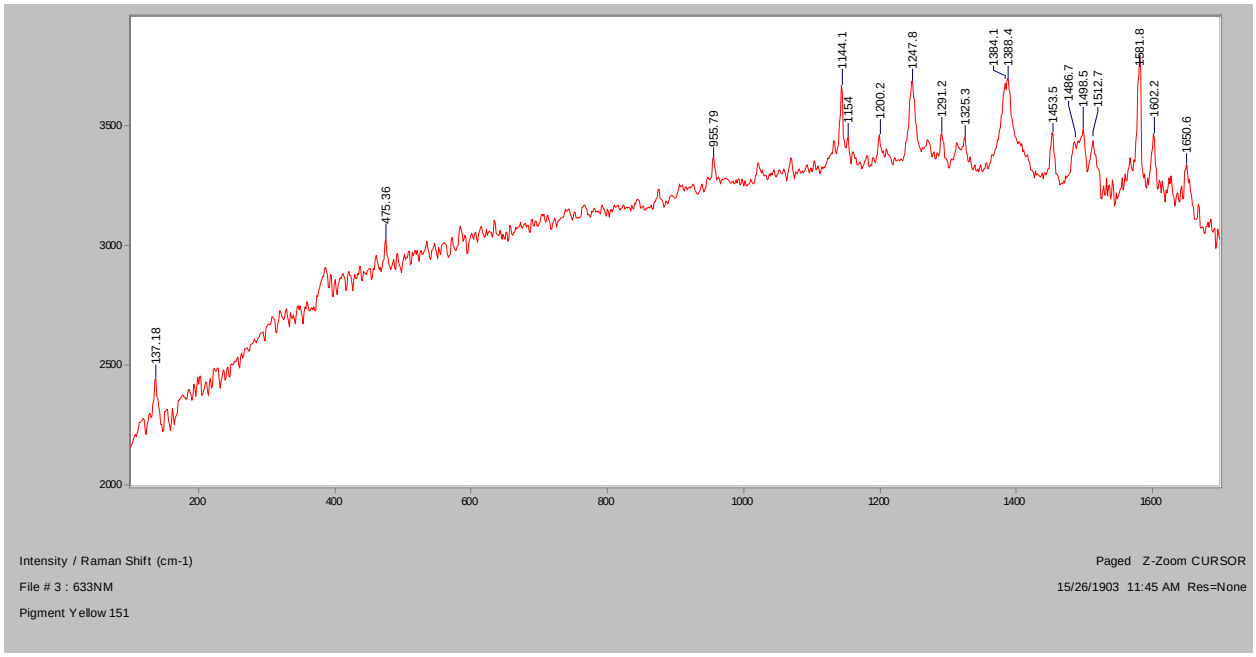

Normal Raman 785nm

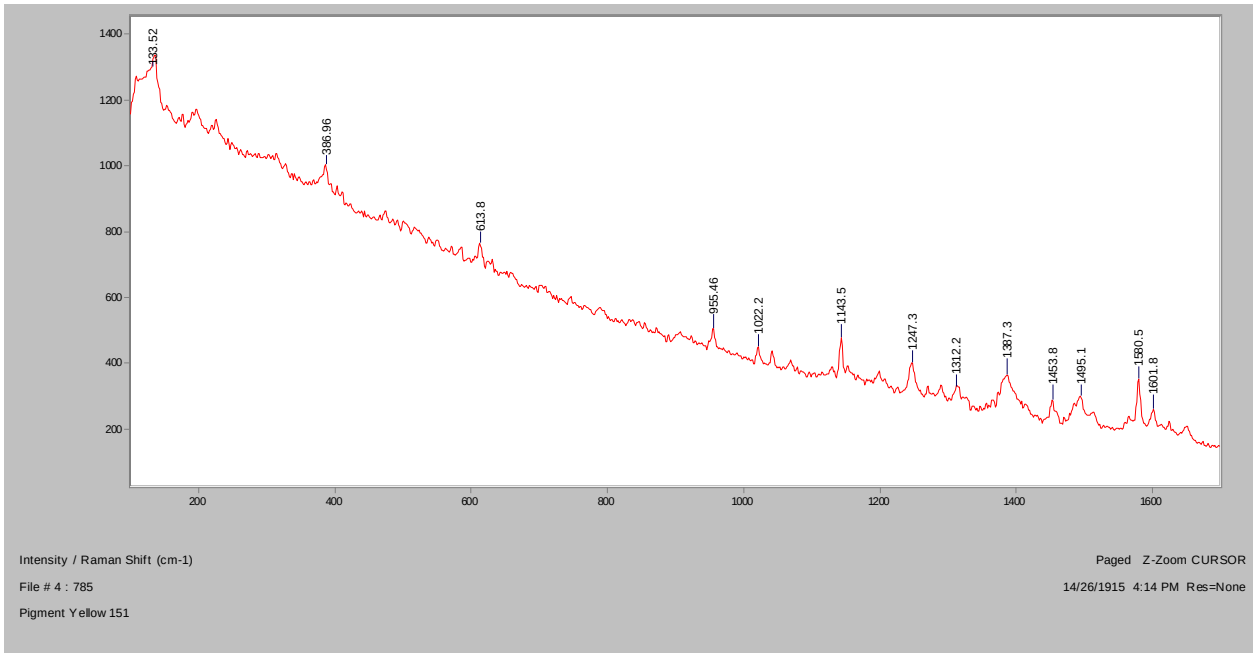

SERS, 488nm

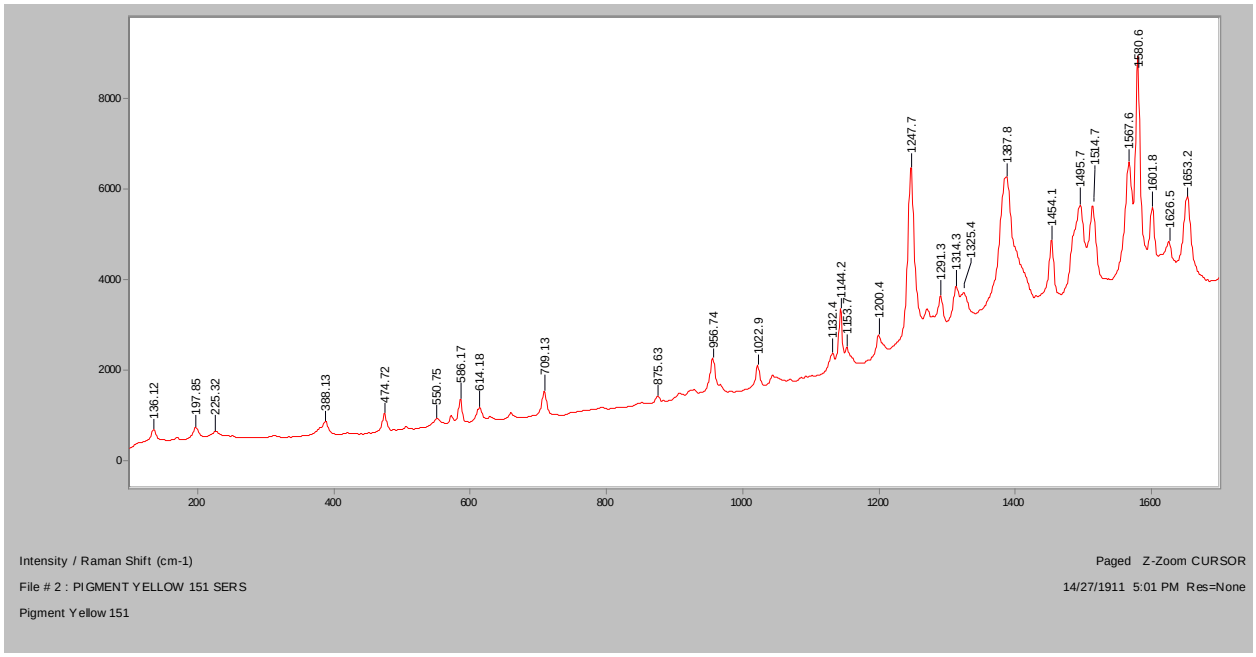

FT-IR (ATR)

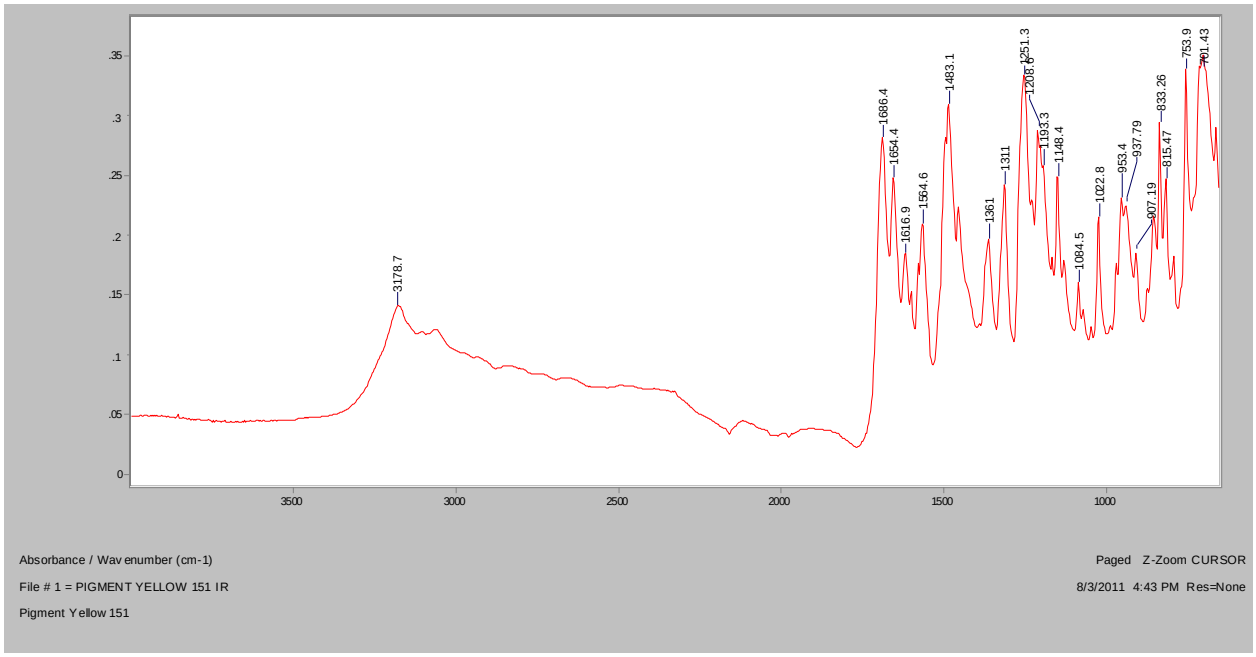

UV-Vis

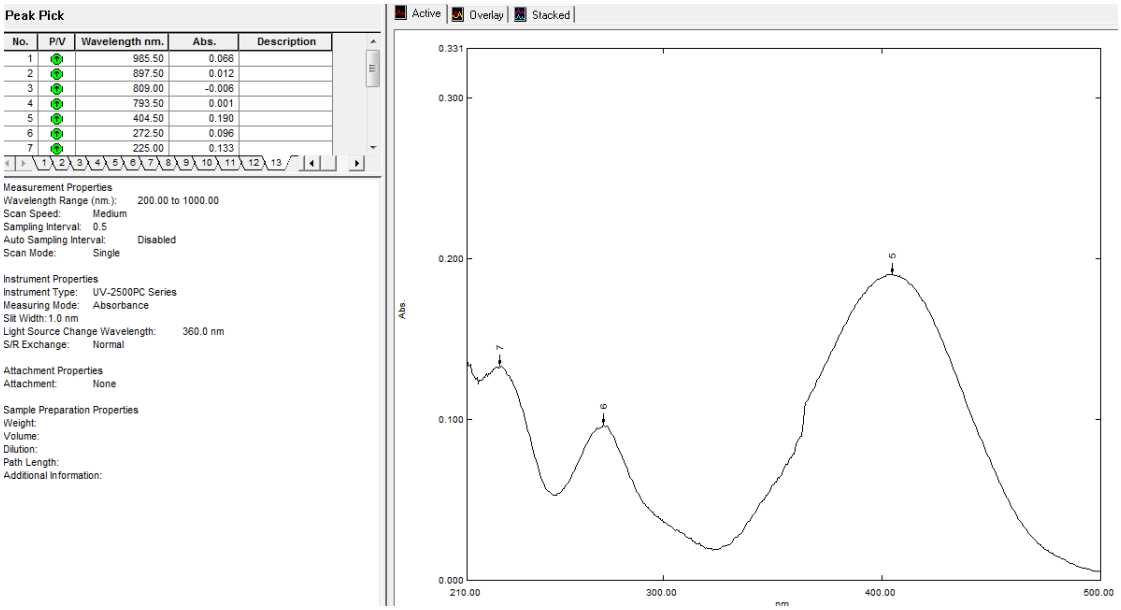

Pigment Green 7

Normal Raman, 488nm

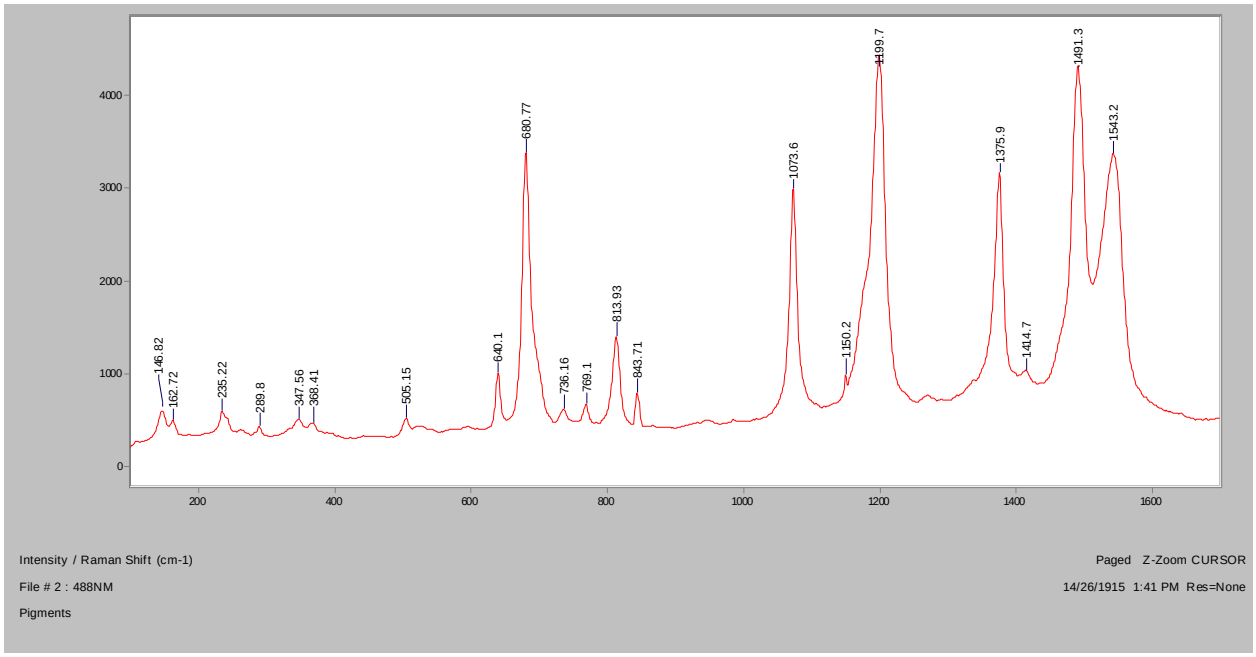

Normal Raman 633nm

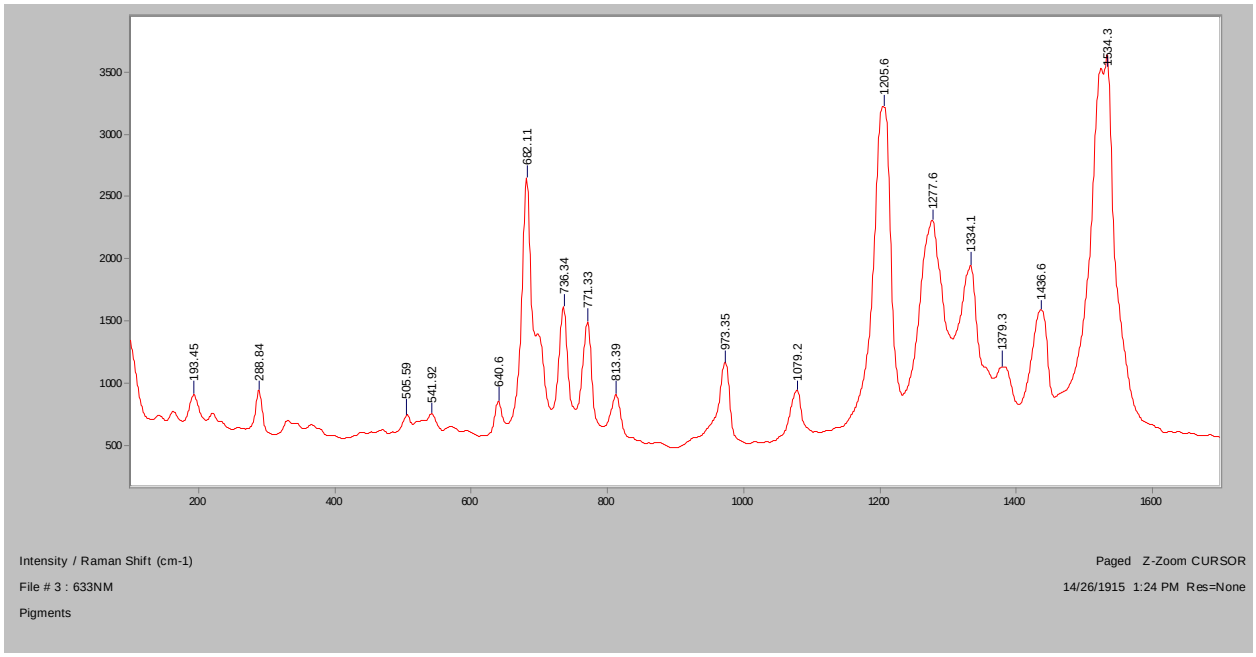

Normal Raman 785nm

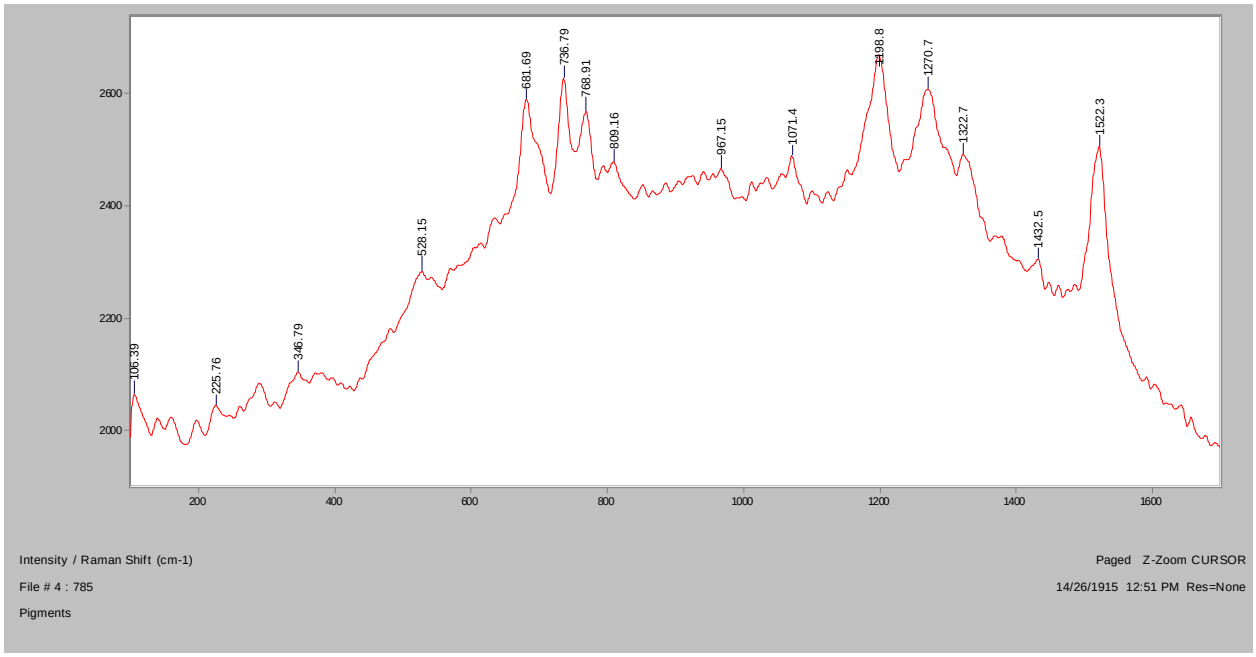

FT Raman, 1064nm

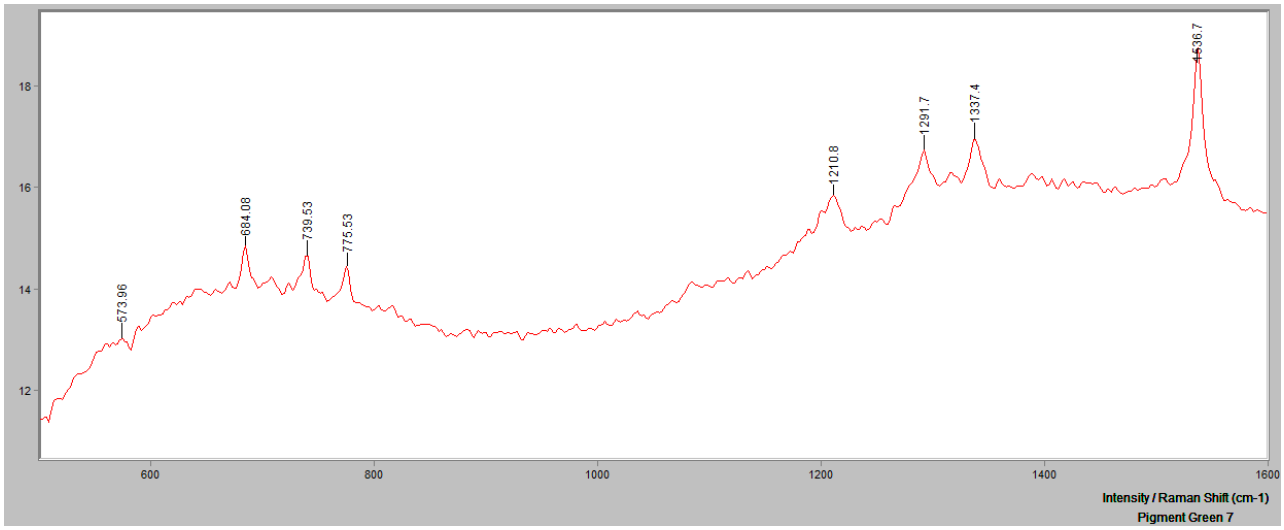

SERS, 488nm

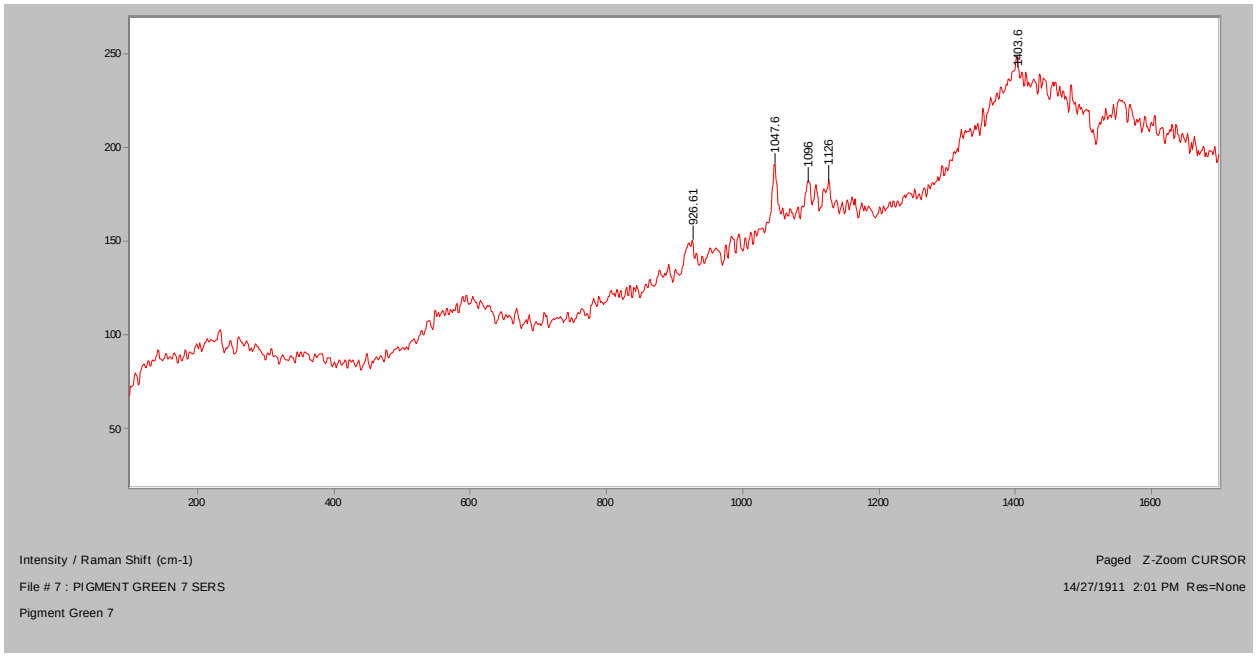

FT-IR (ATR)

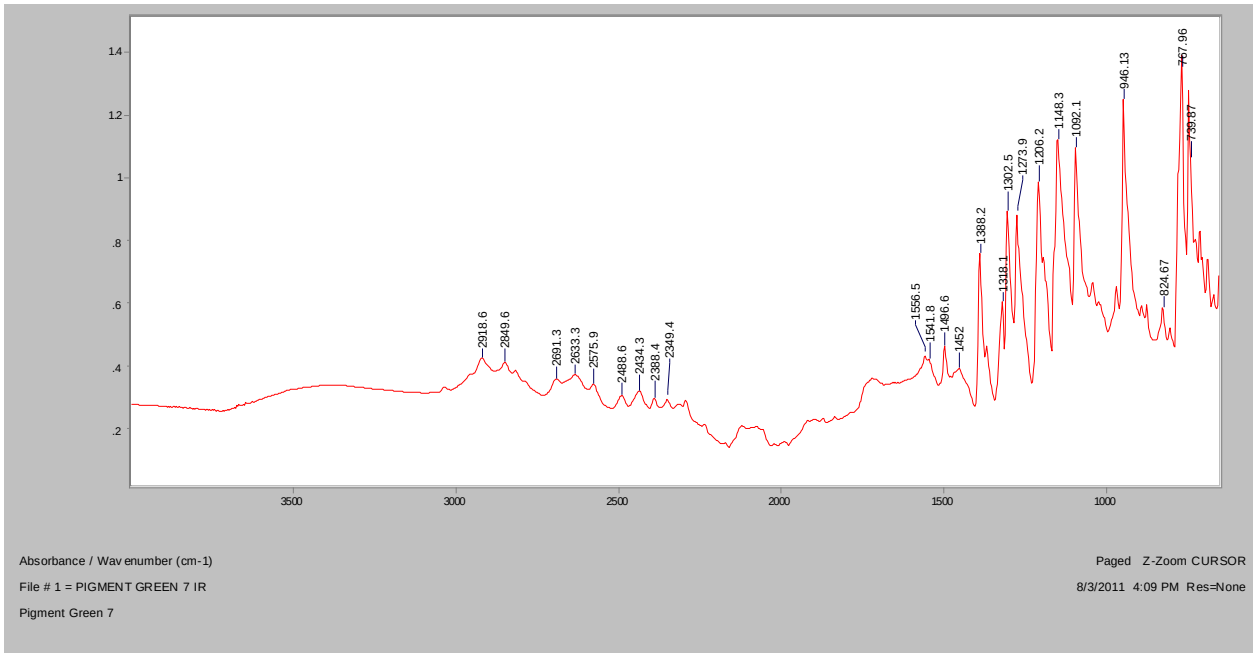

UV-Vis

Peak Pick

No.	P/V	Wavelength nm.	Abs.	Description
1	P	859.50	0.881	
2	P	815.00	0.744	
3	P	727.50	0.253	
4	P	476.00	0.206	
5	P	365.00	0.188	
6	P	333.50	0.336	
7	P	282.00	0.281	
8	P	242.00	0.647	

Measurement Properties
Wavelength Range (nm.): 200.00 to 1000.00
Scan Speed: Medium
Sampling Interval: 0.5
Auto Sampling Interval: Disabled
Scan Mode: Single

Instrument Properties
Instrument Type: UV-2500PC Series
Measuring Mode: Absorbance
Slit Width: 1.0 nm
Light Source Change Wavelength: 360.0 nm
S/R Exchange: Normal

Attachment Properties
Attachment: None

Sample Preparation Properties
Weight:
Volume:
Dilution:
Path Length:
Additional Information:

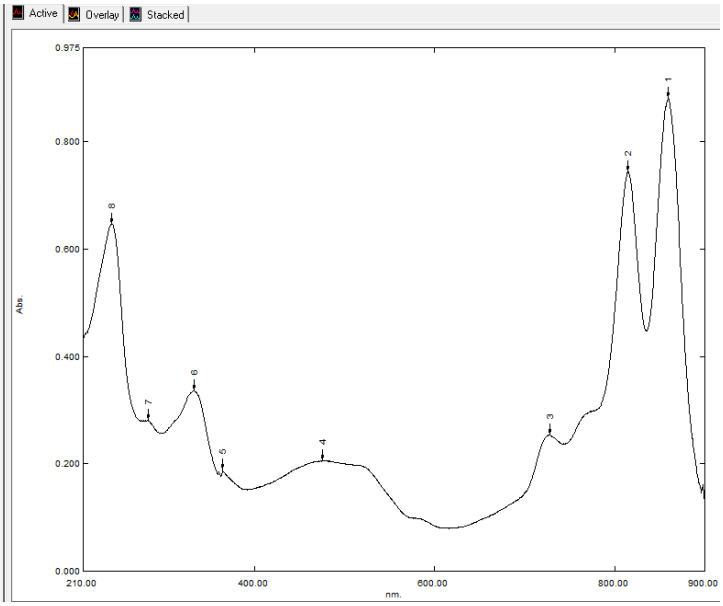

Pigment Blue 15

Normal Raman, 488nm

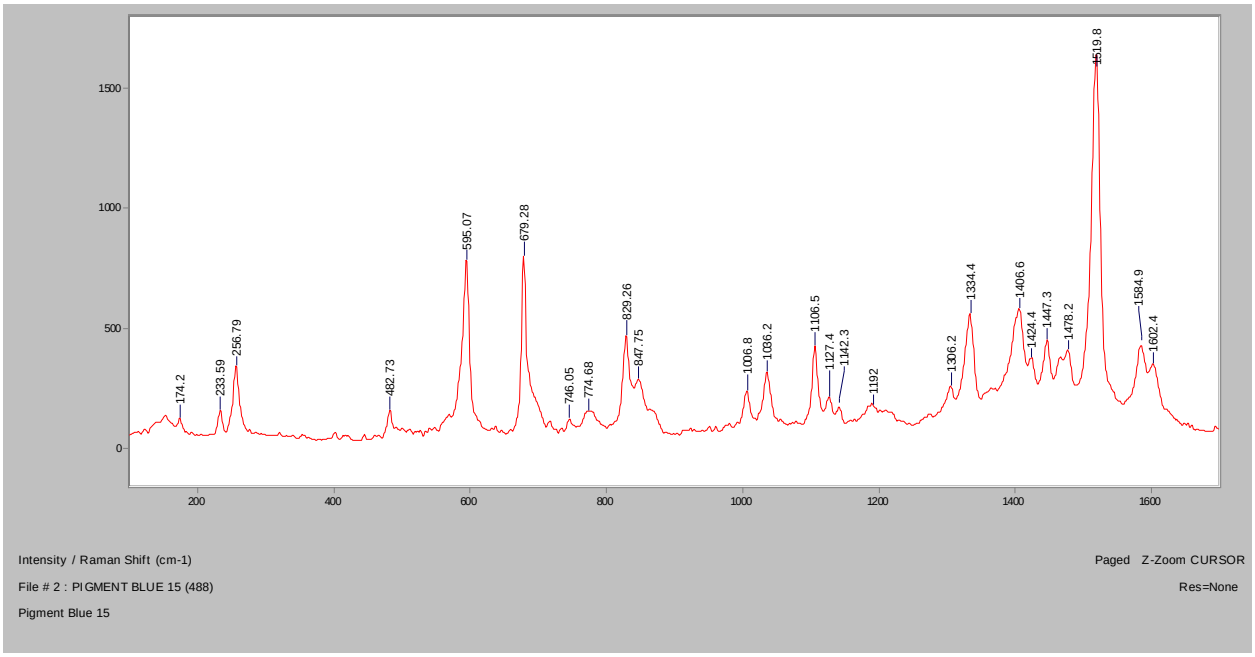

Normal Raman 633nm

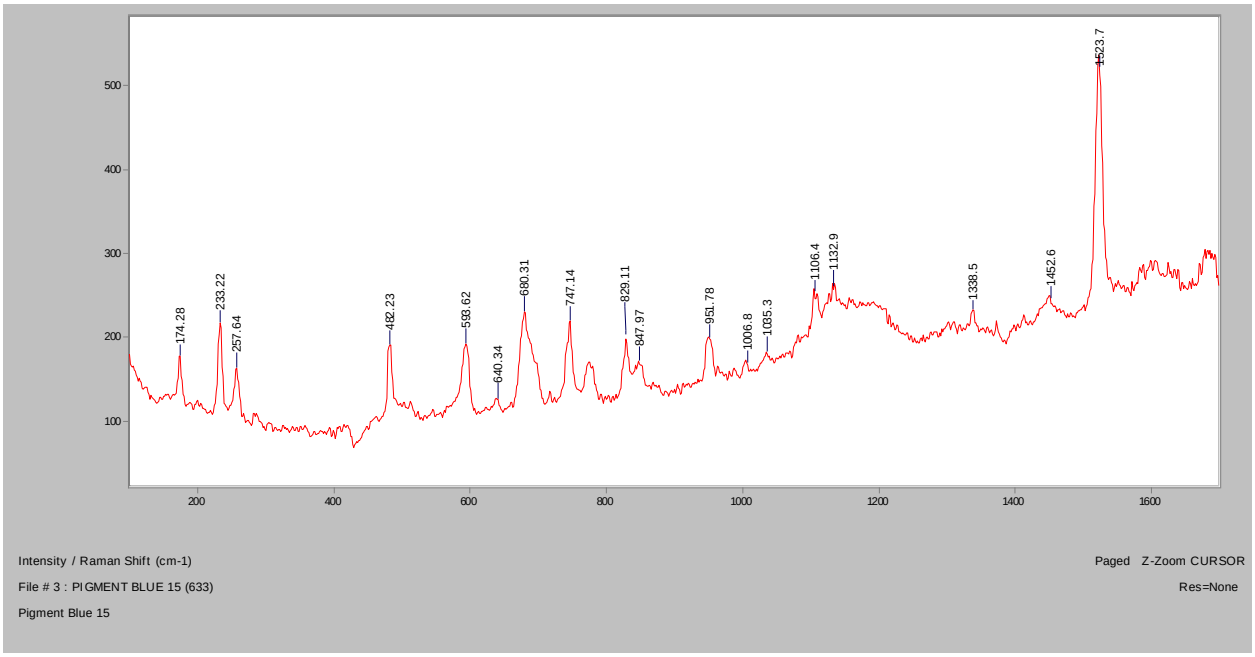

Normal Raman 785nm

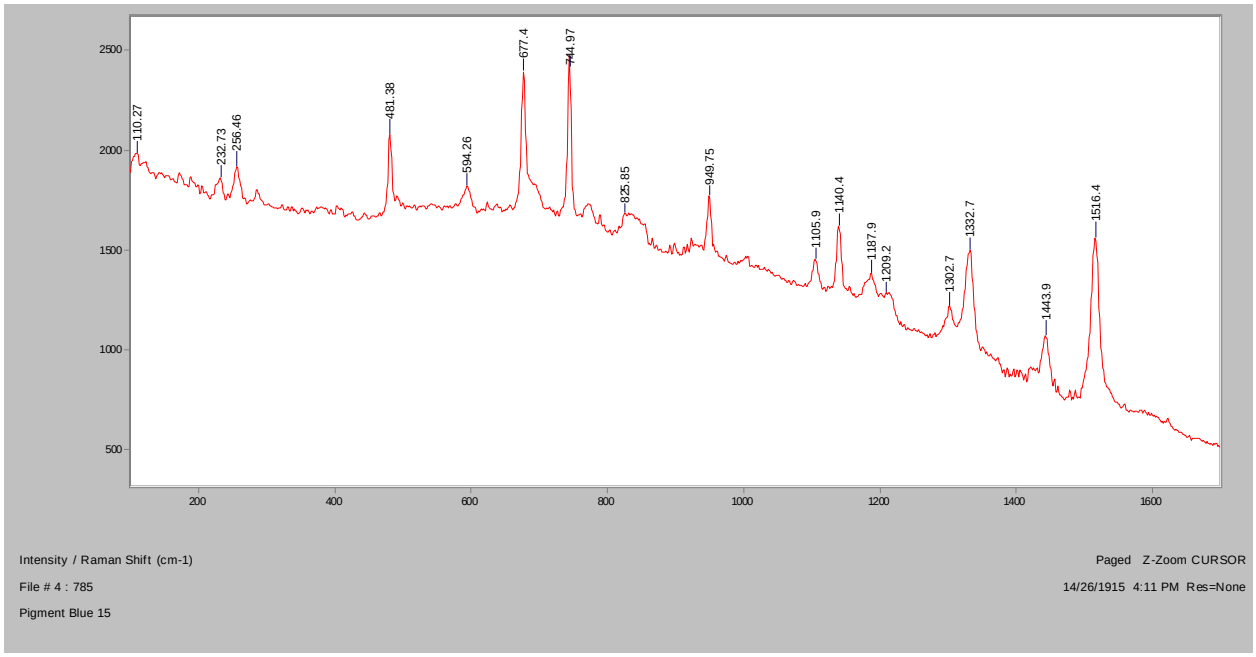

SERS, 488nm

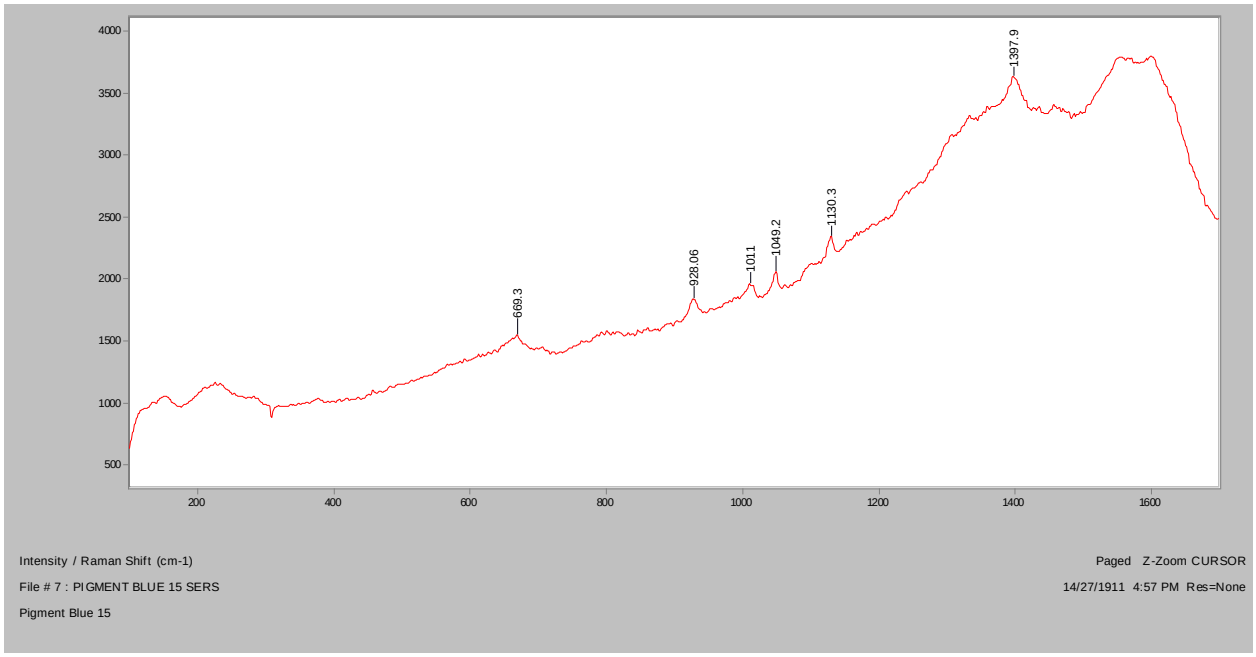

FT-IR (ATR)

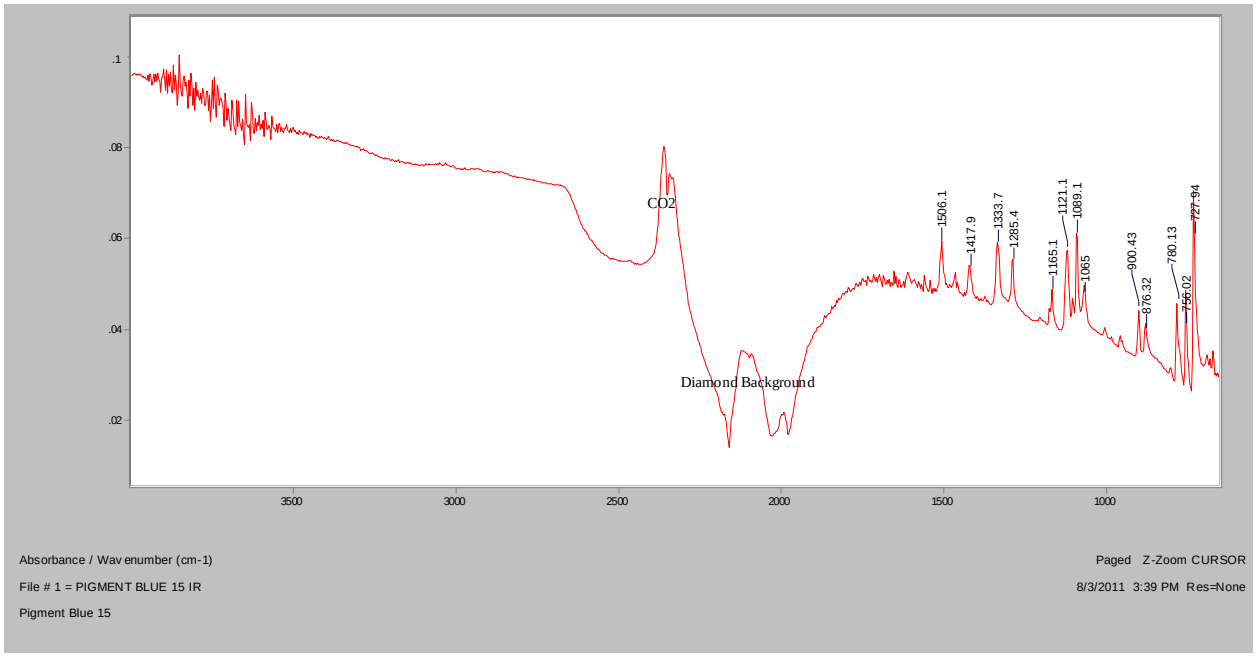

UV-Vis

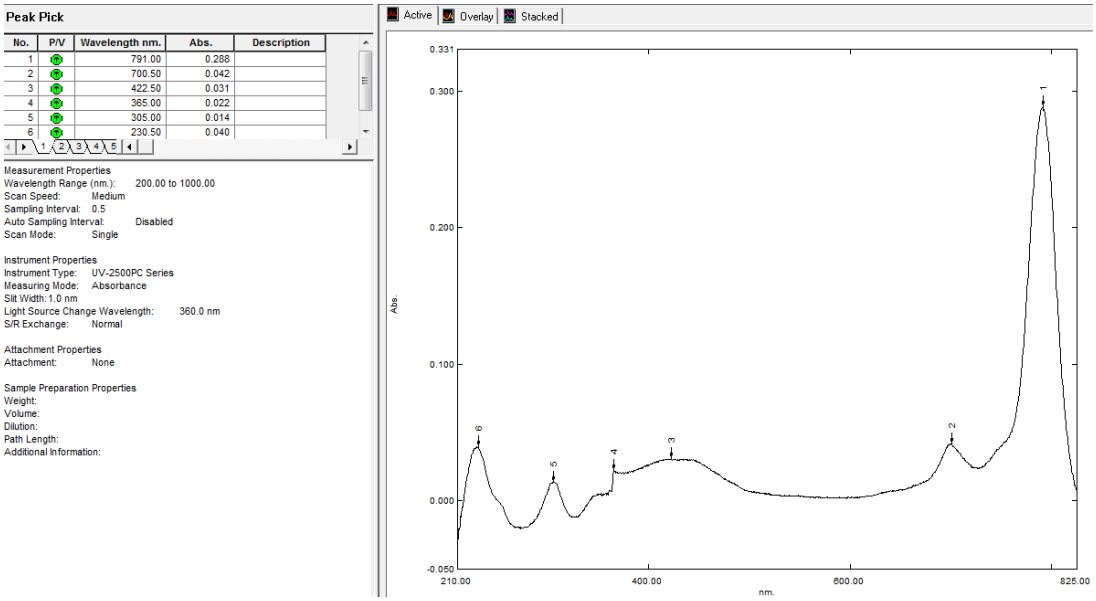

Pigment Blue 15:1

Normal Raman, 488nm

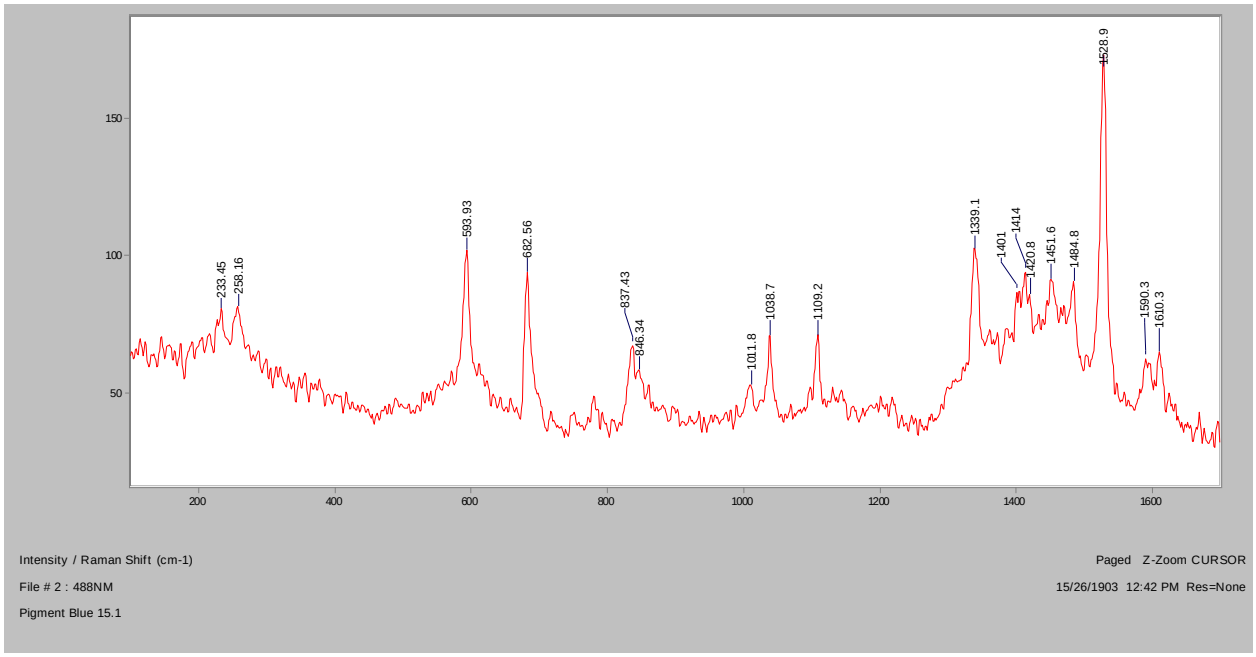

Normal Raman 633nm

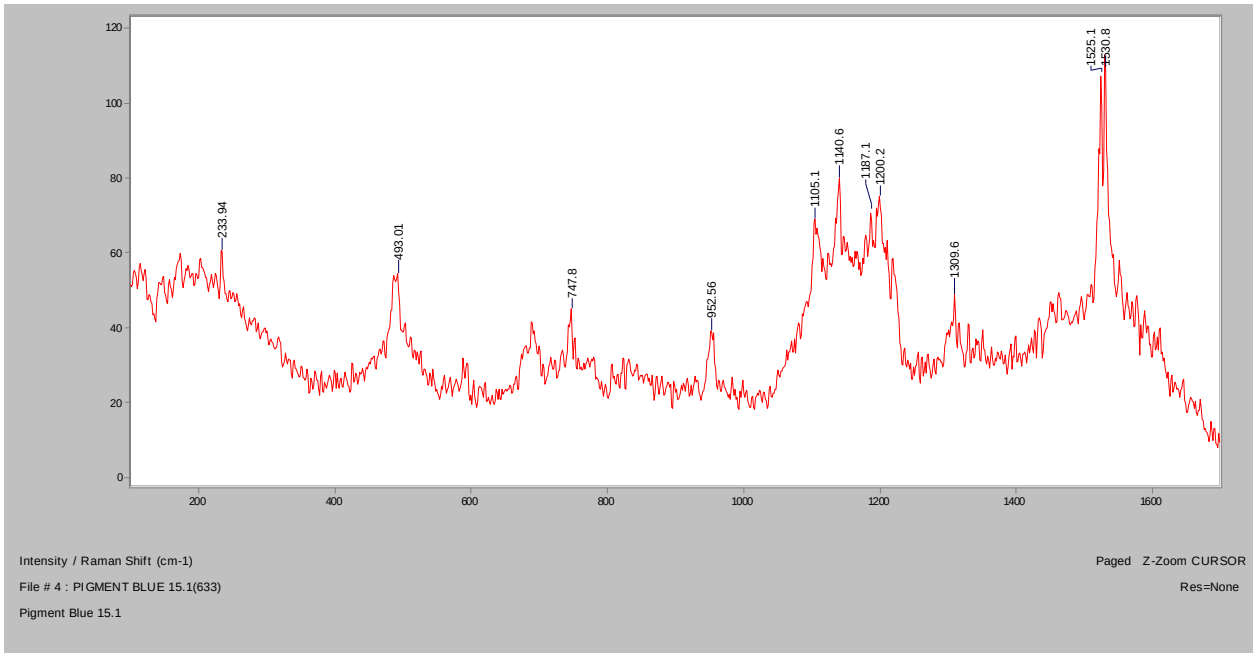

Normal Raman 785nm

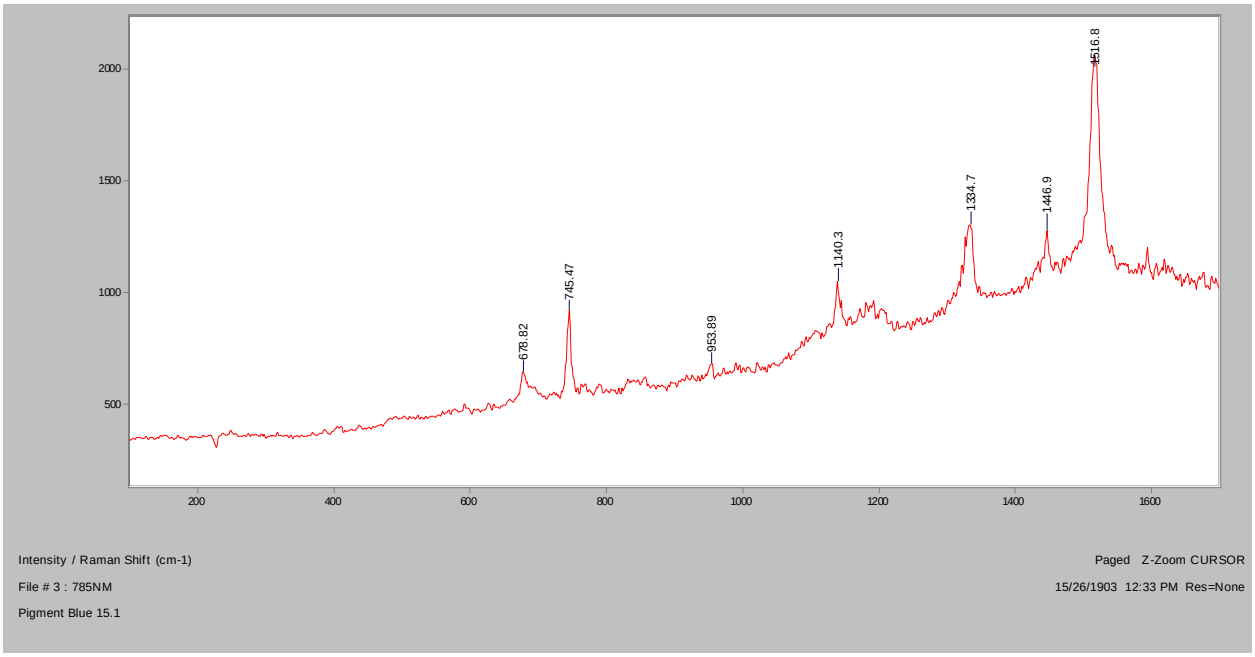

FT-IR (ATR)

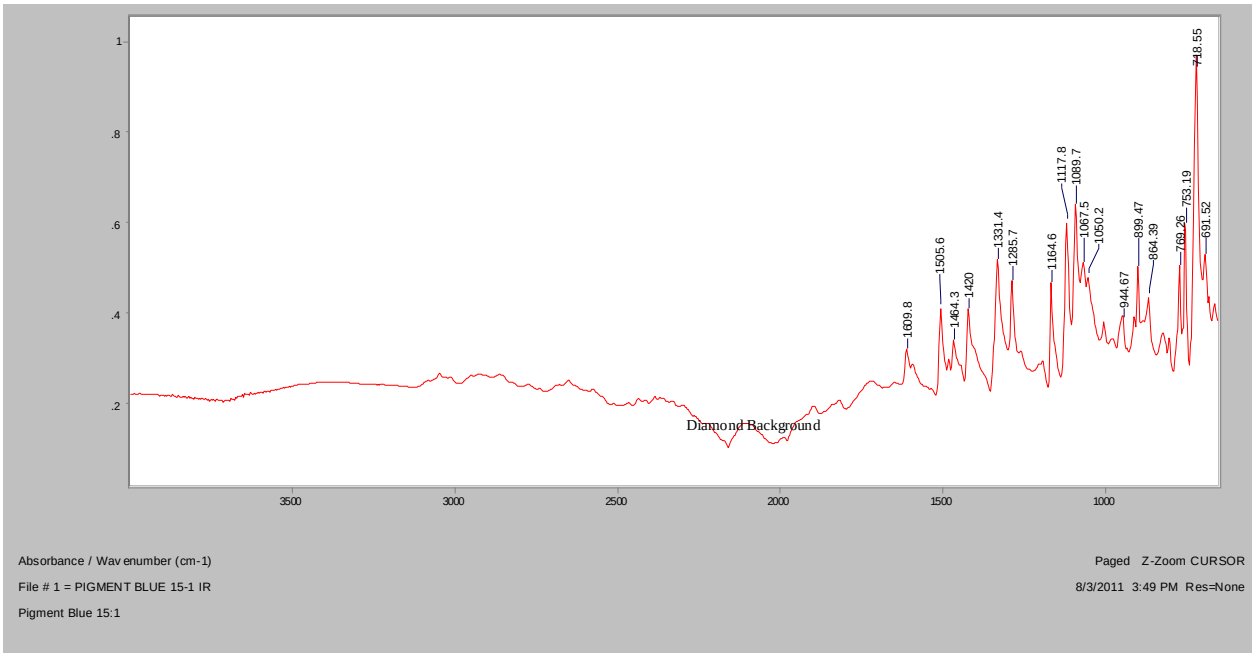

Pigment Blue 15:2

Normal Raman, 488nm

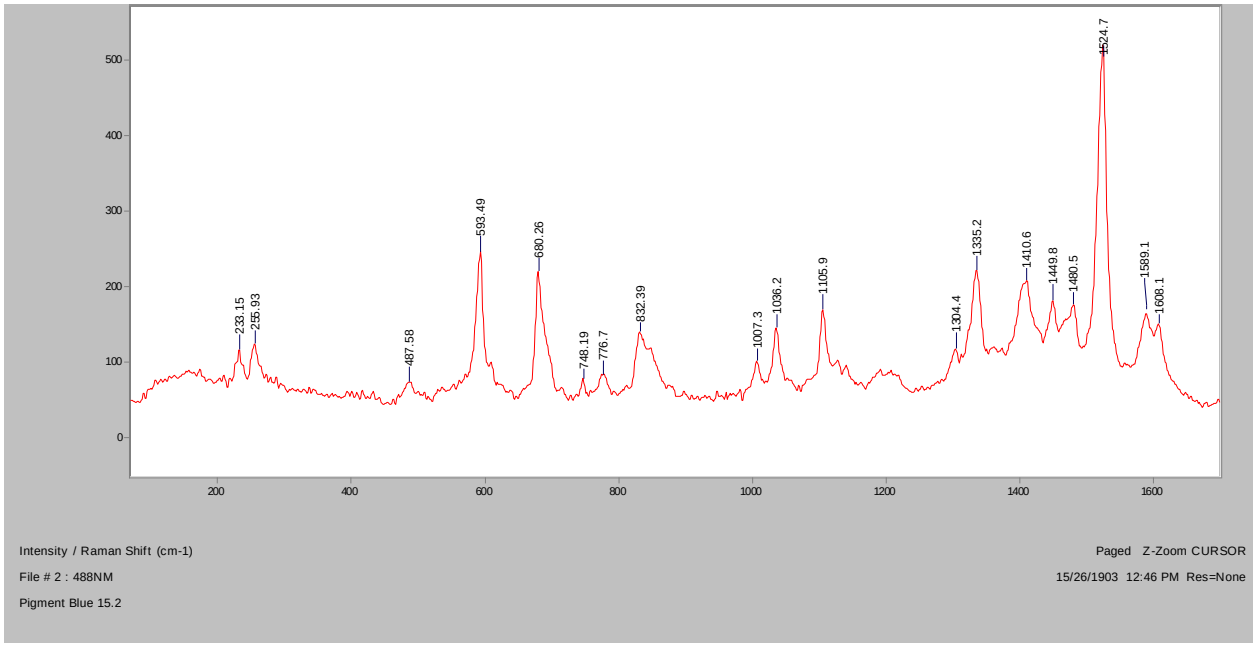

Normal Raman 633nm

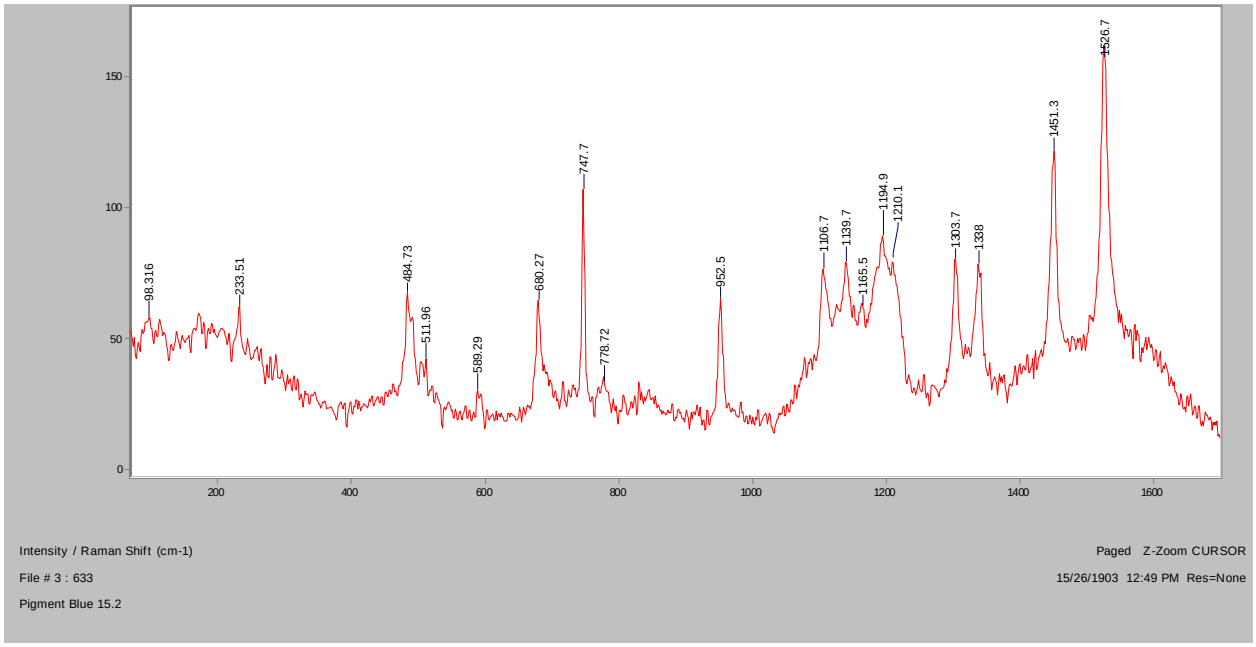

Normal Raman 785nm

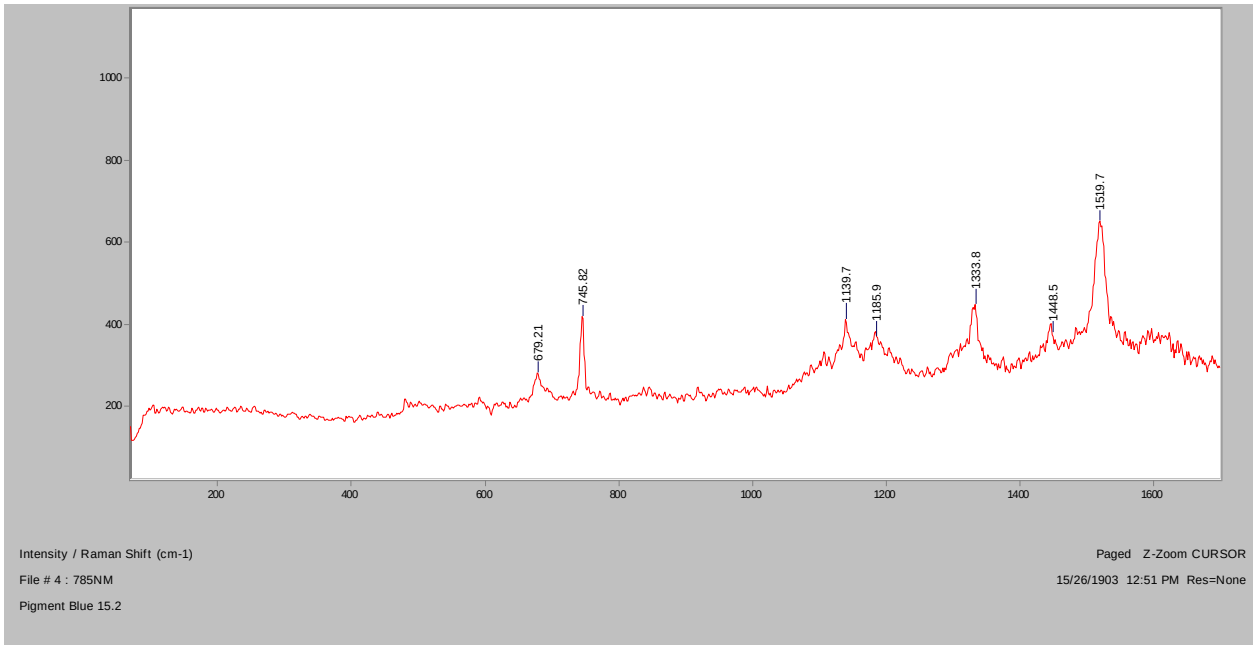

FT-IR (ATR)

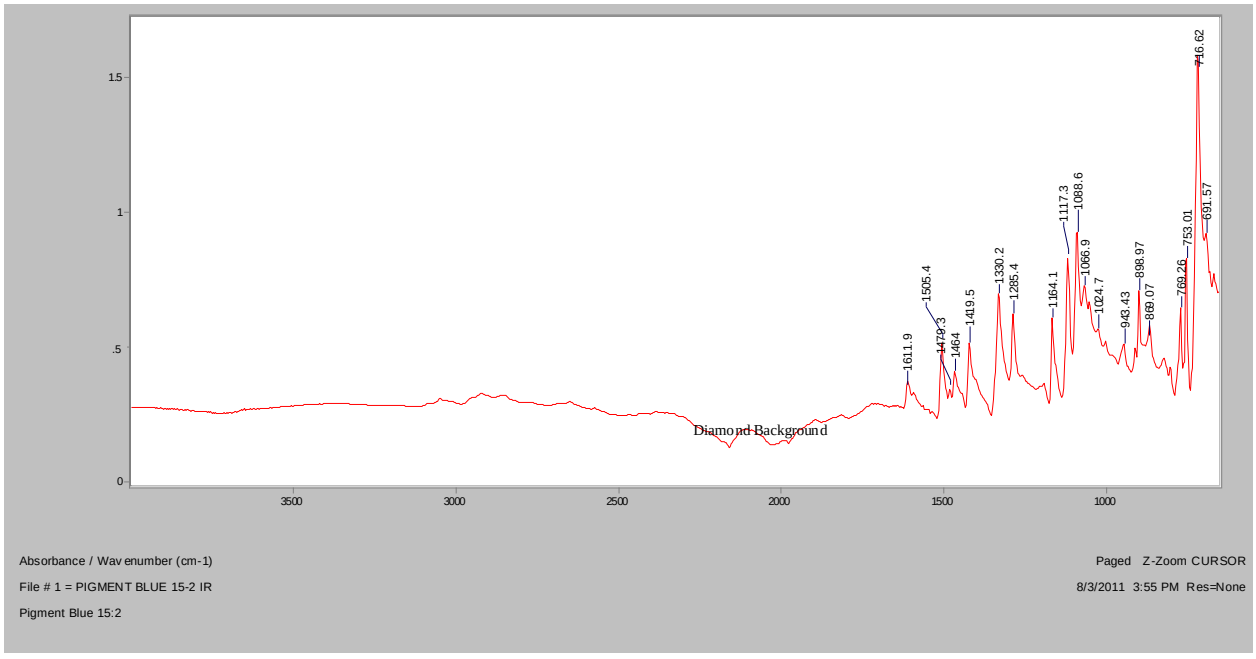

Pigment Blue 15:3

Normal Raman, 488nm

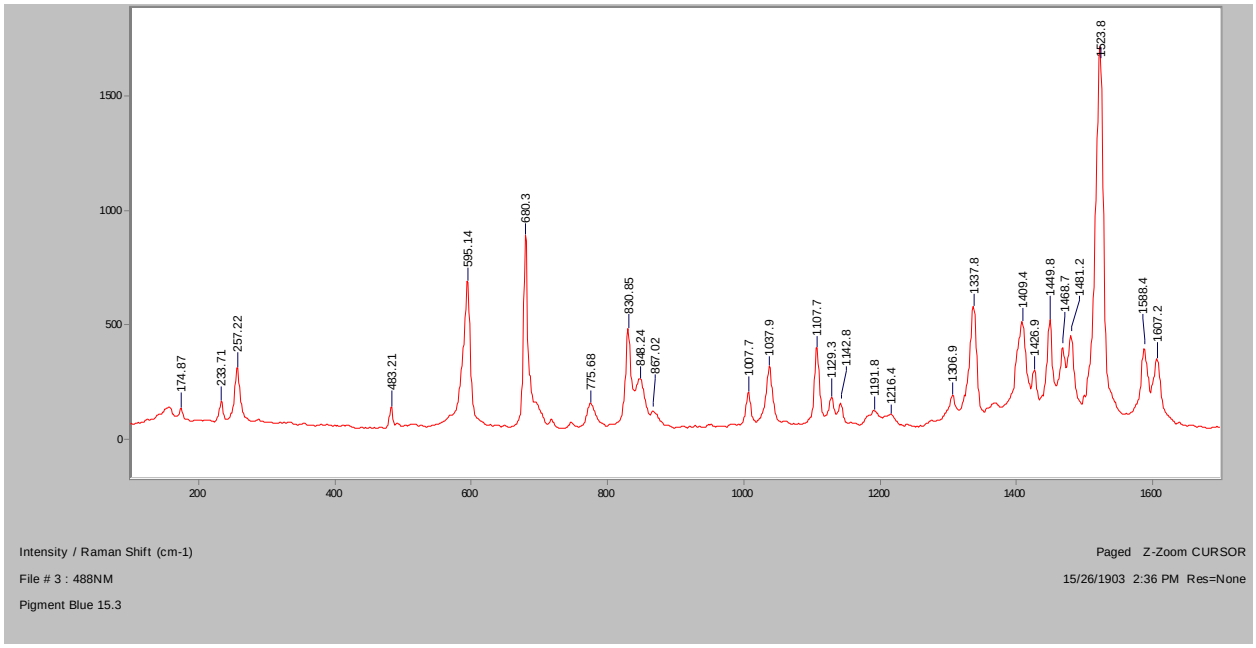

Normal Raman 633nm

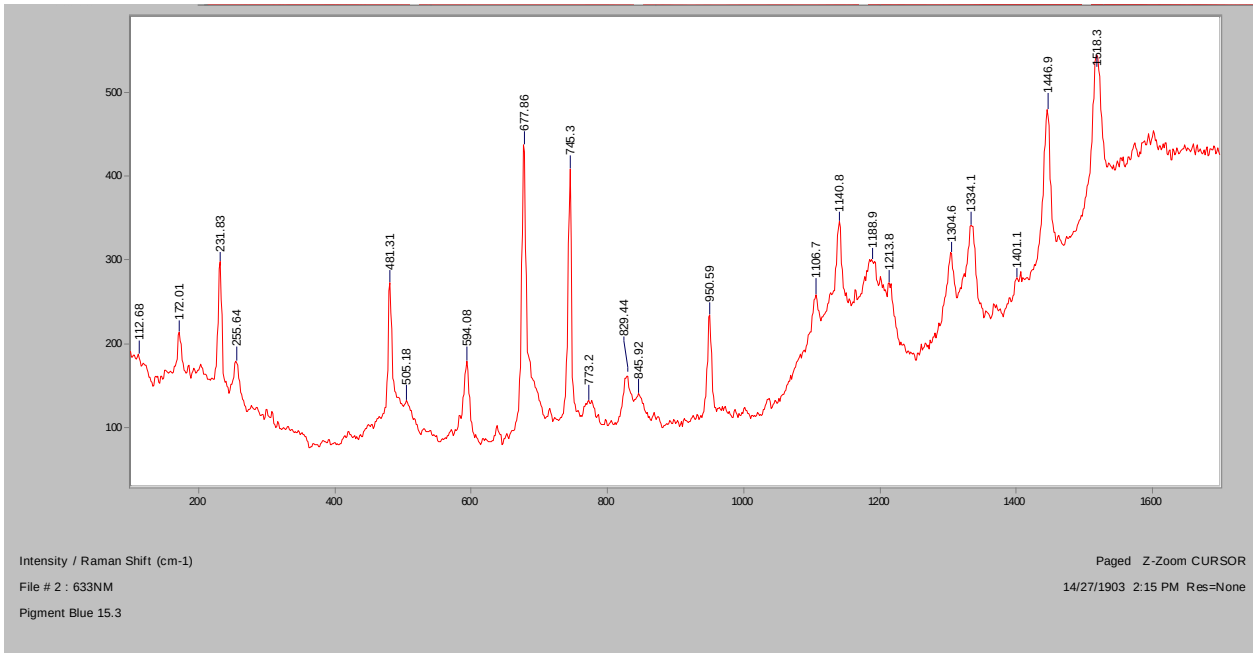

Normal Raman 785nm

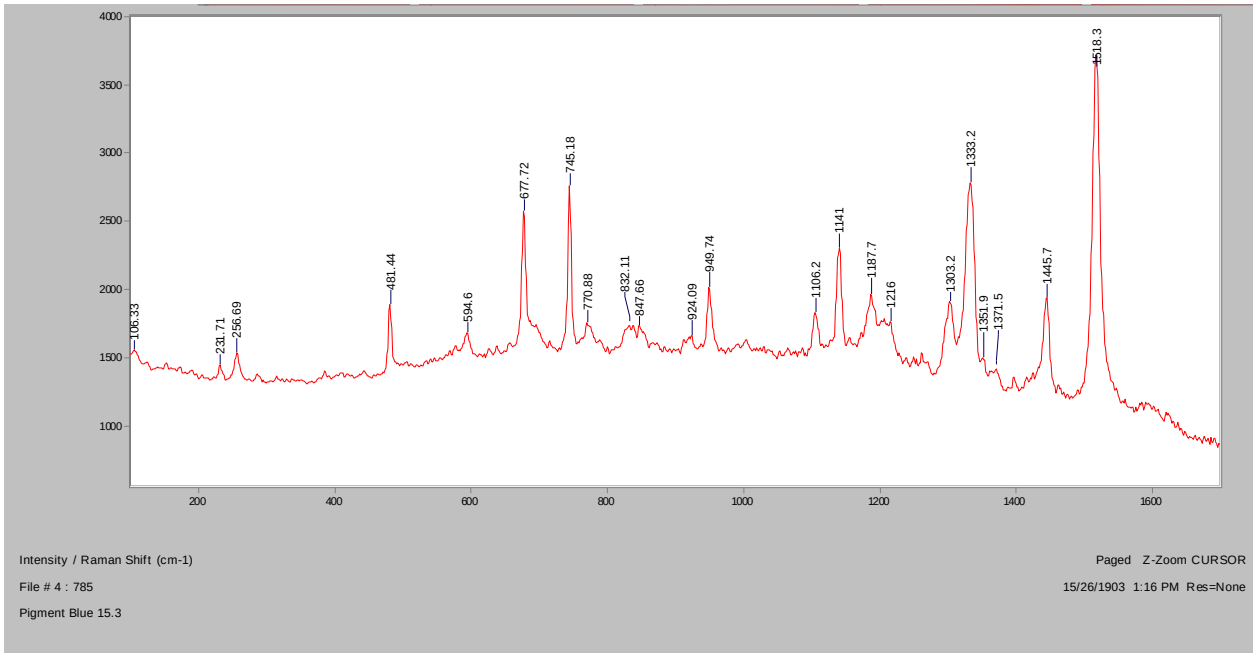

FT-IR (ATR)

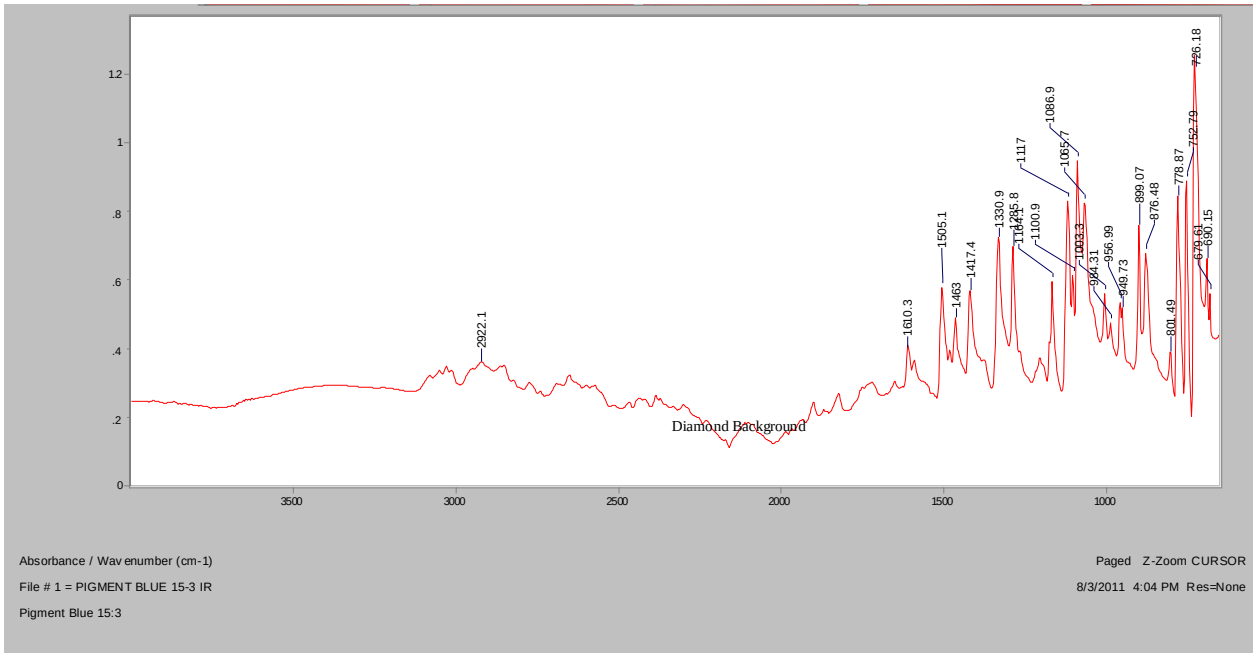

Pigment Violet 23α

Normal Raman, 488nm

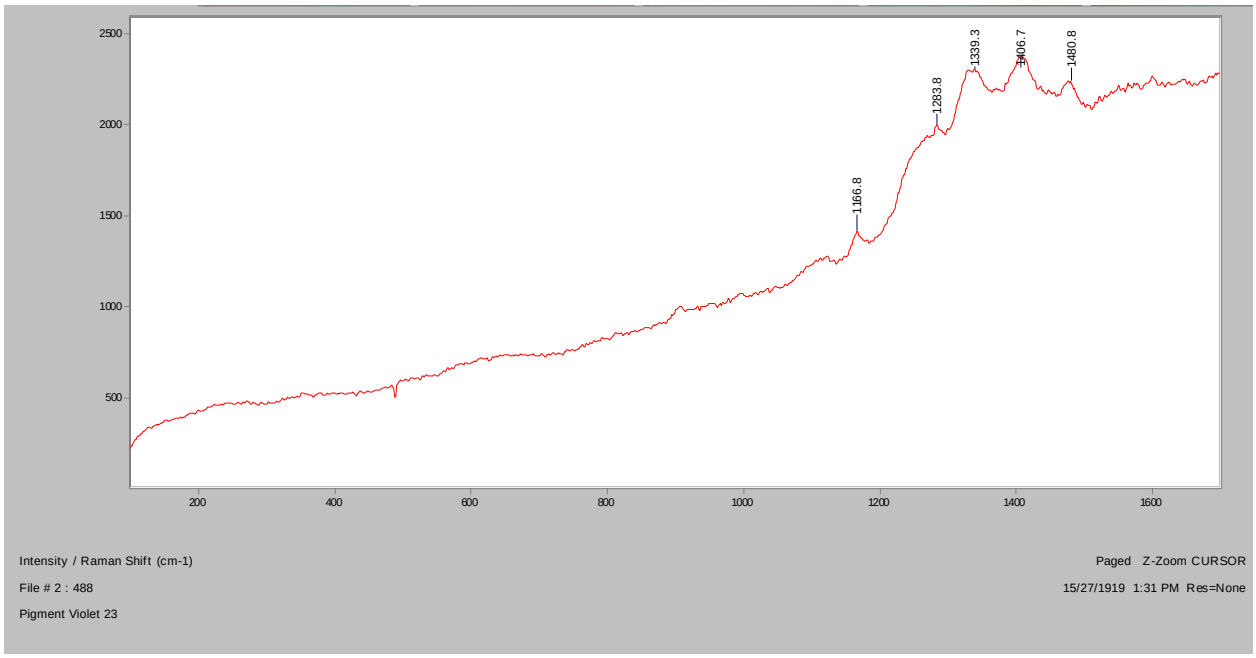

Normal Raman 633nm

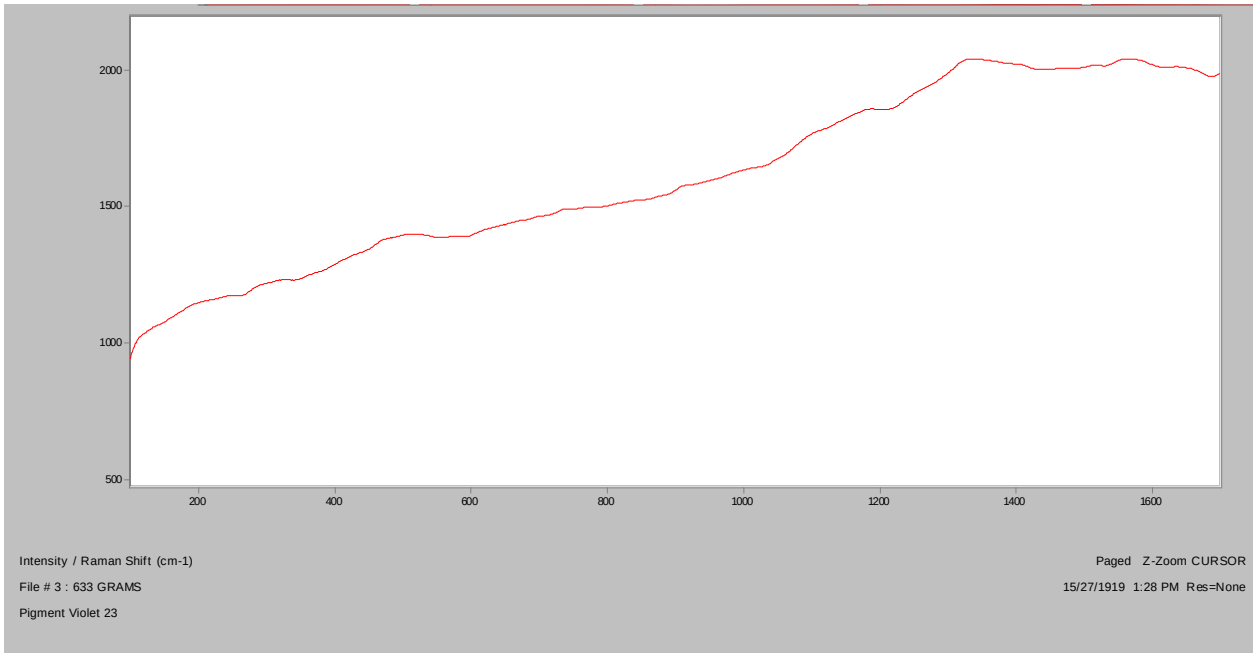

Normal Raman 785nm

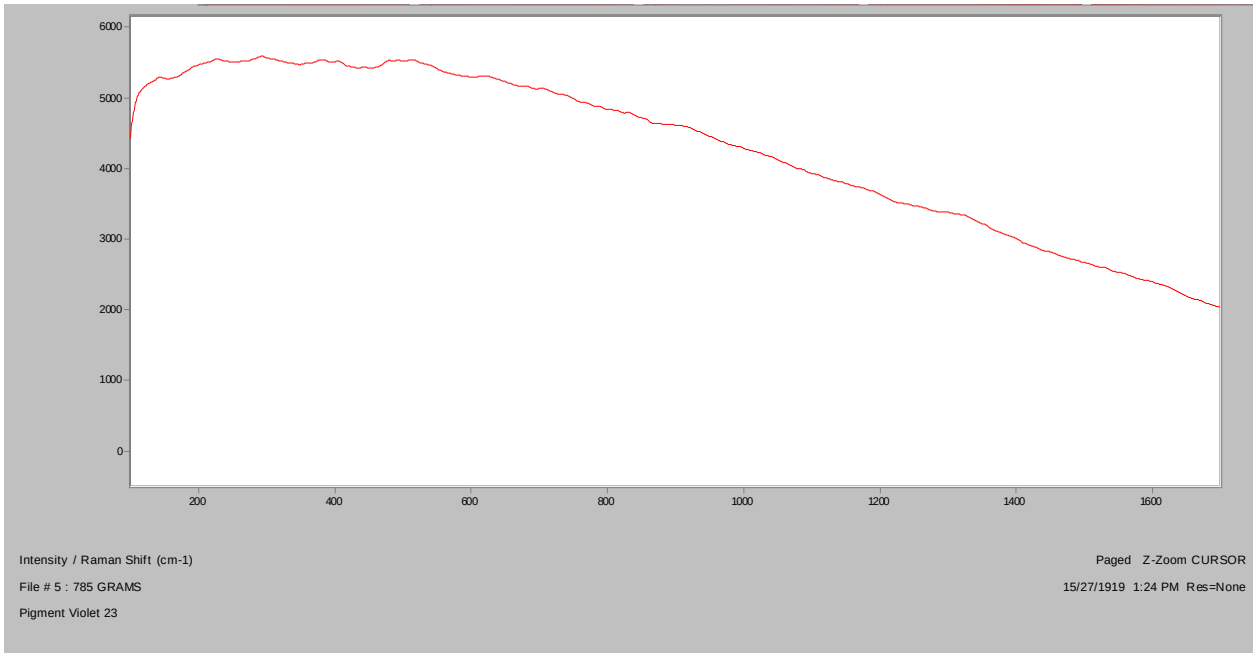

SERS, 488nm

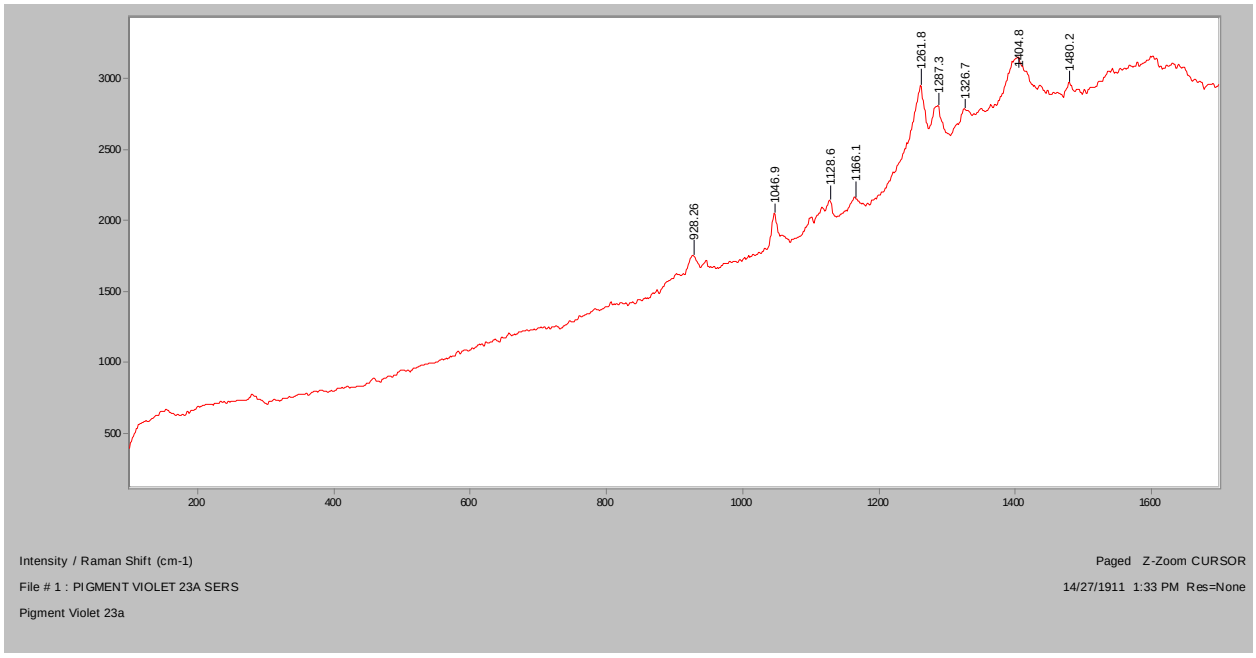

FT-IR (ATR)

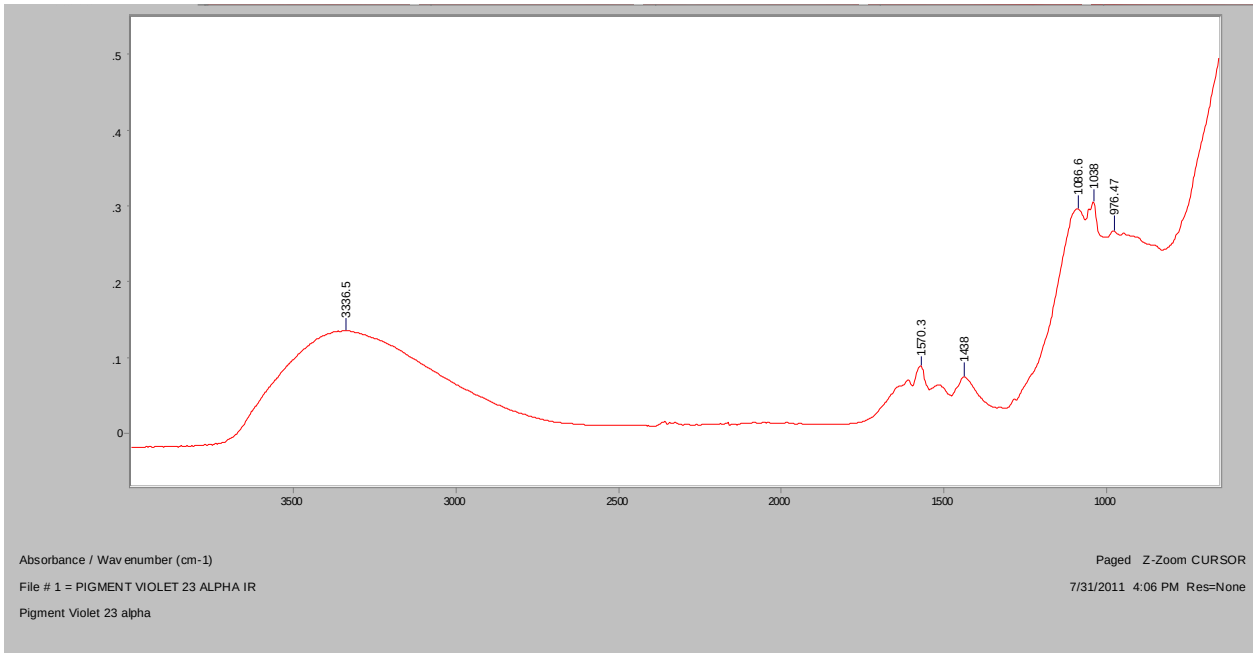

UV-Vis

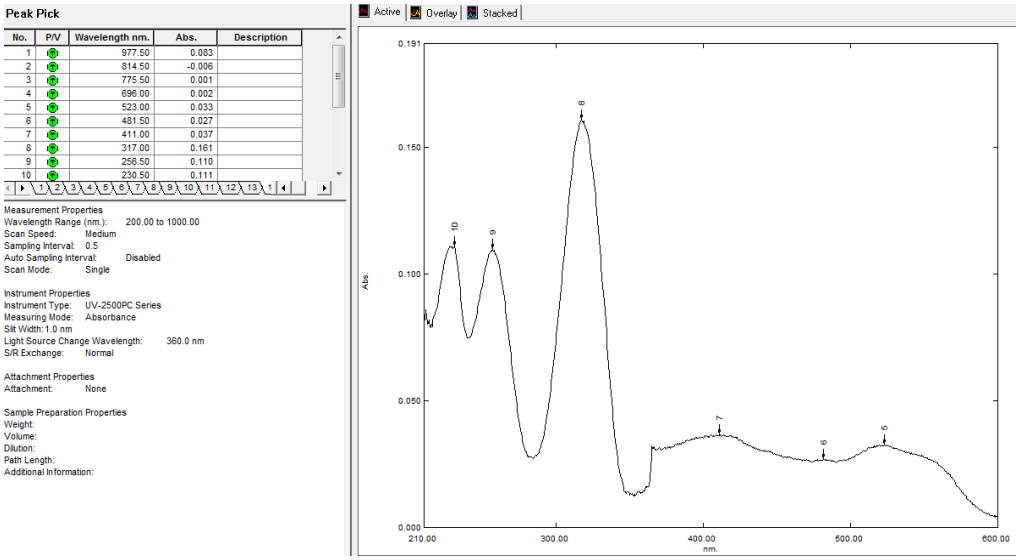

Pigment Violet 23β

Normal Raman, 488nm

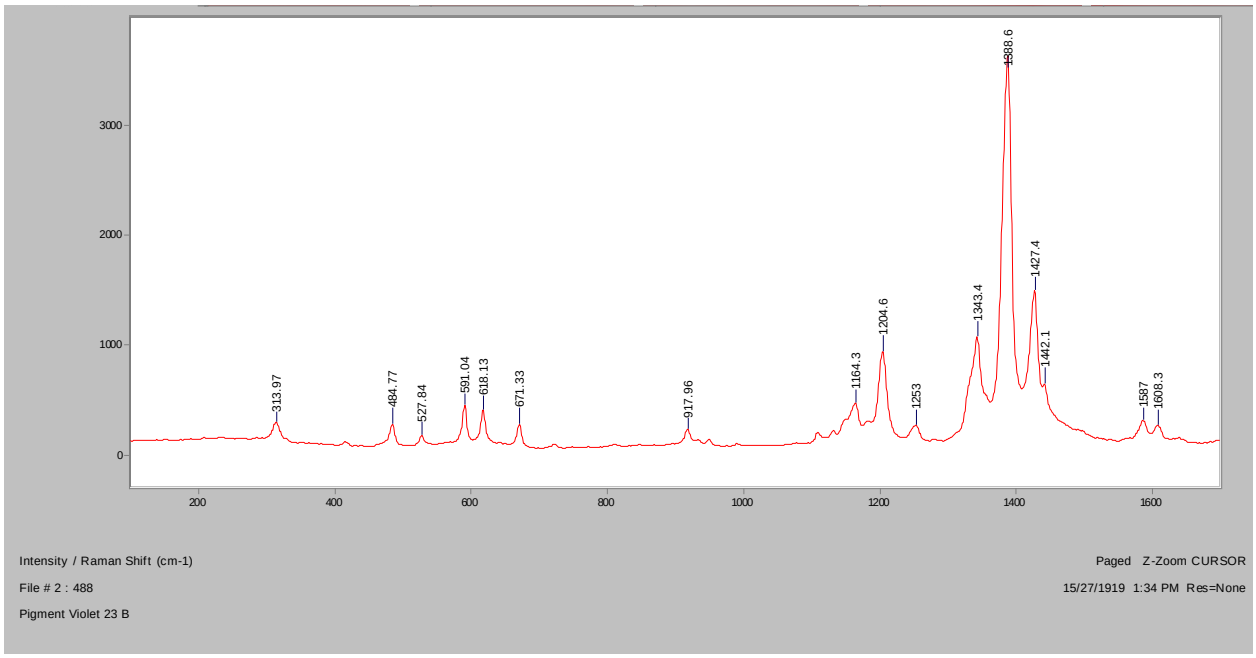

Normal Raman 633nm

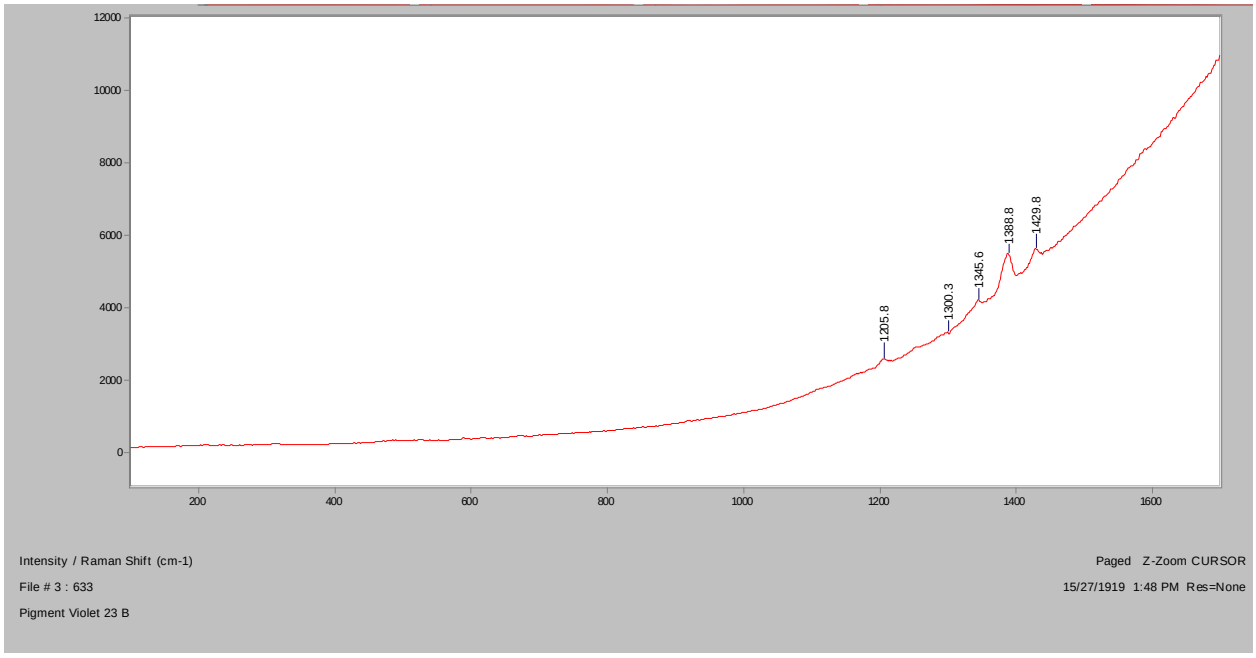

Normal Raman 785nm

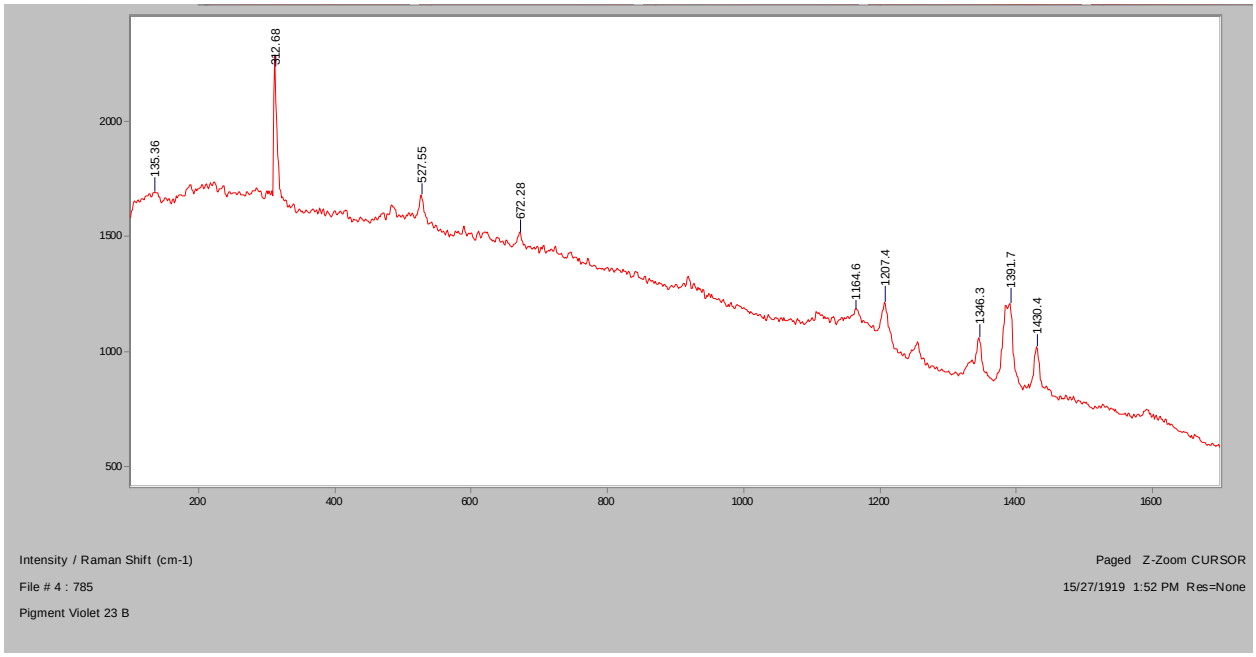

FT Raman, 1064nm

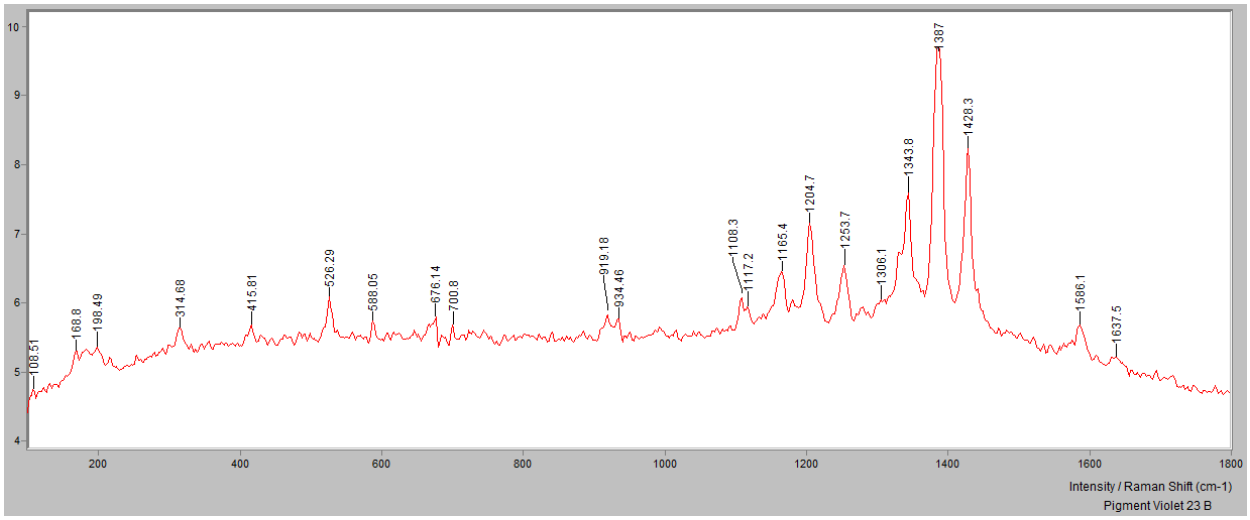

SERS, 488nm

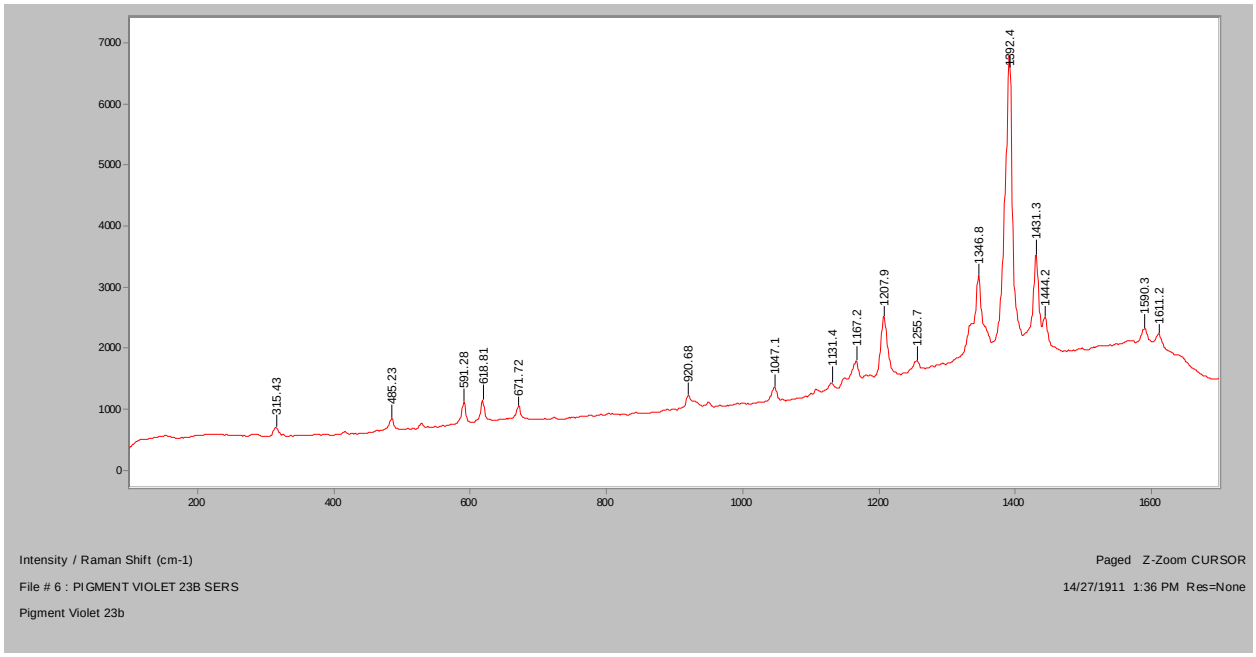

FT-IR (ATR)

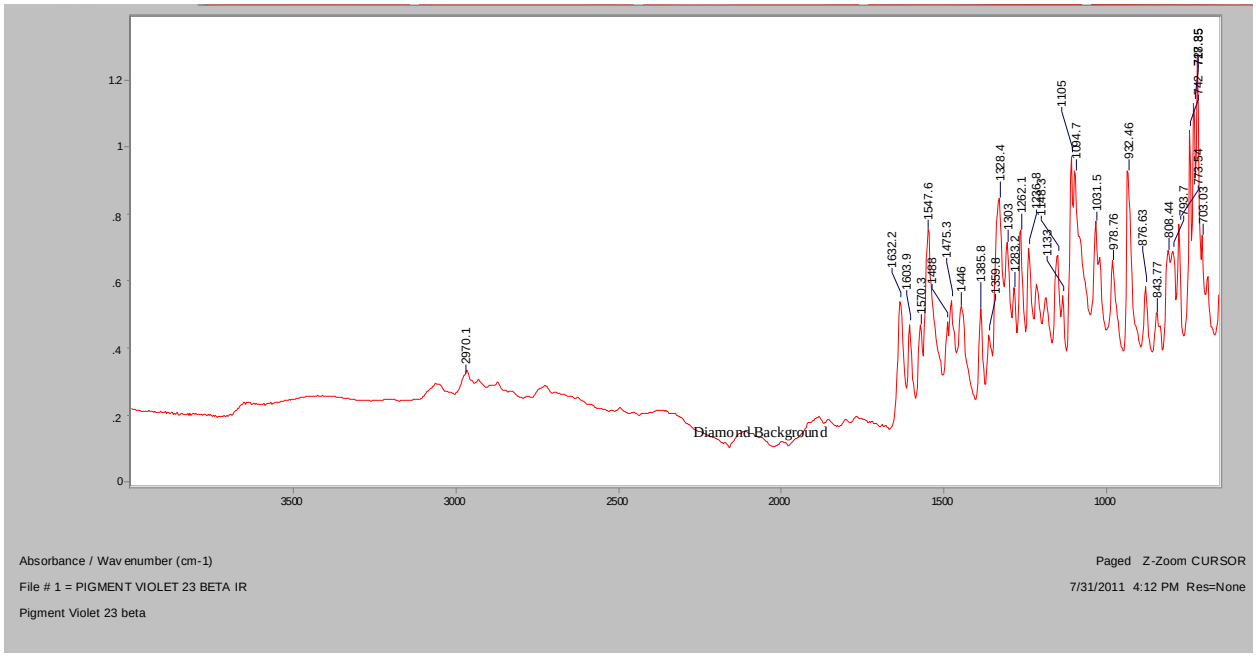

UV-Vis

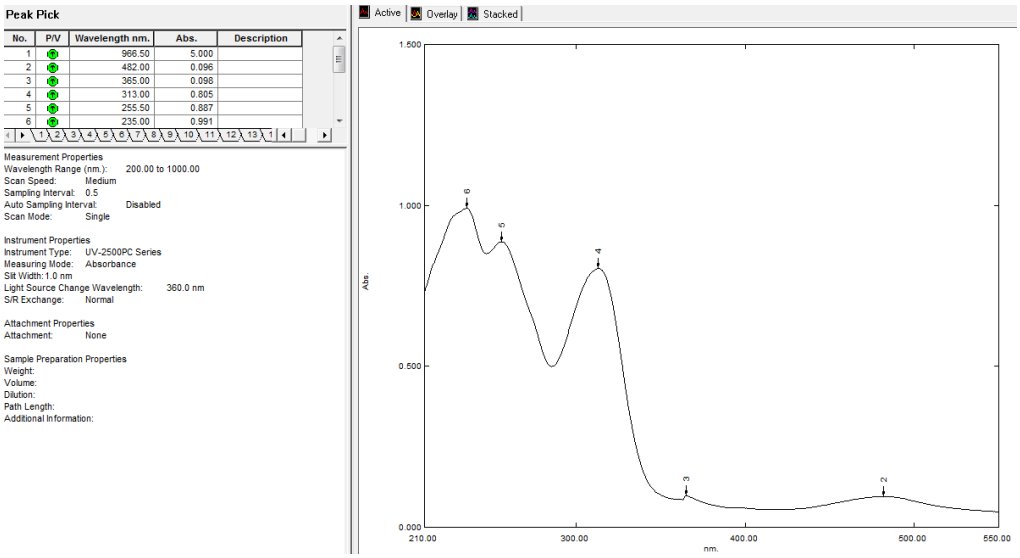

PR 122, PR 146, PR 170, PO 16, PV 23a, PV 23b

PO 34, PY 3, PY 83, PY 151, PG 7, PB 15

PR 255, PO 62, PY 73

Appendix G: Tattoo Inks in Pigskin

Frozen Tissue

White region

Normal Raman, 488nm

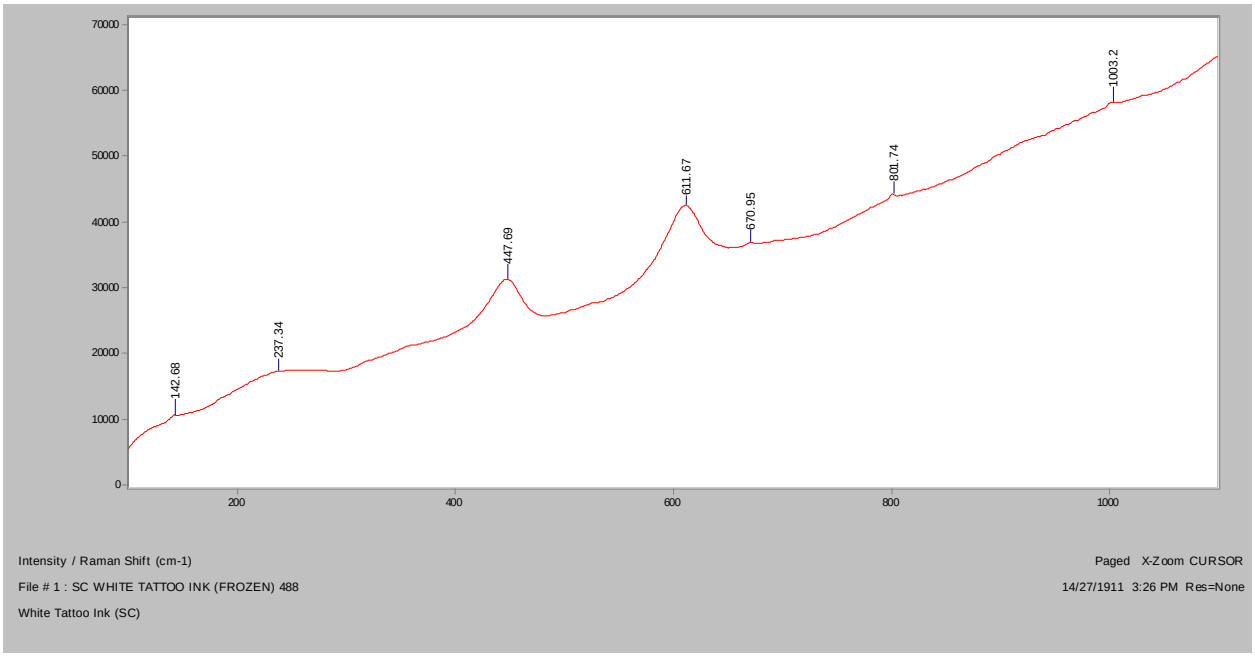

Normal Raman, 785nm

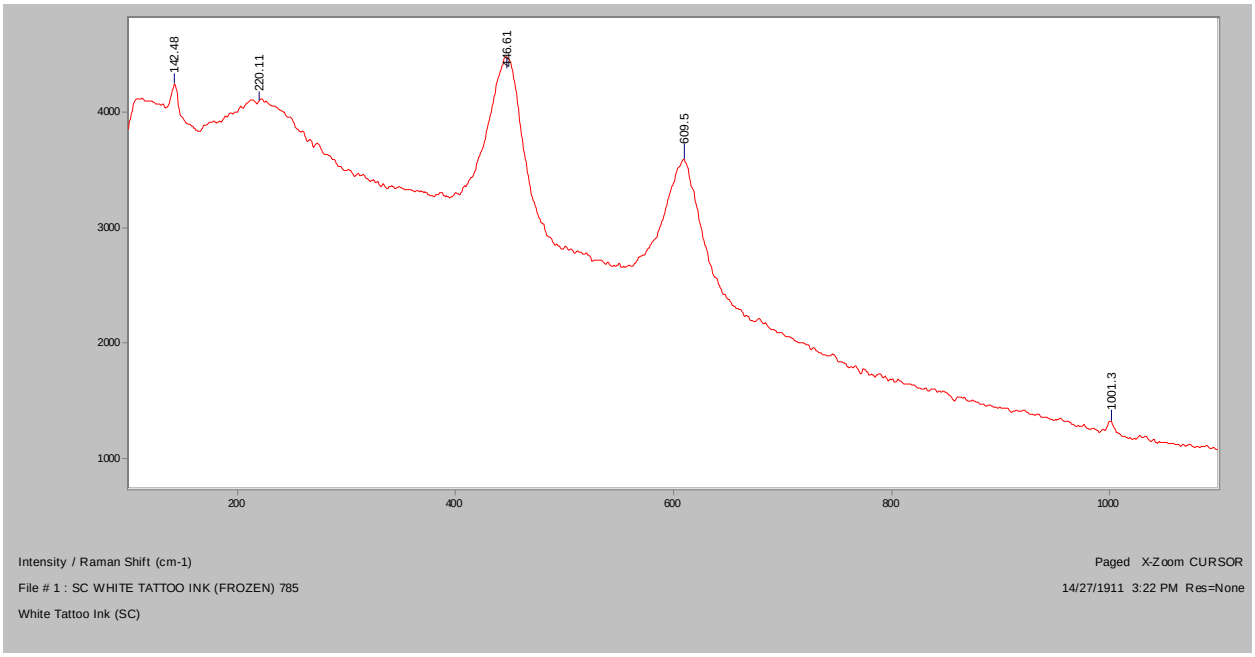

Red region

Normal Raman, 488nm

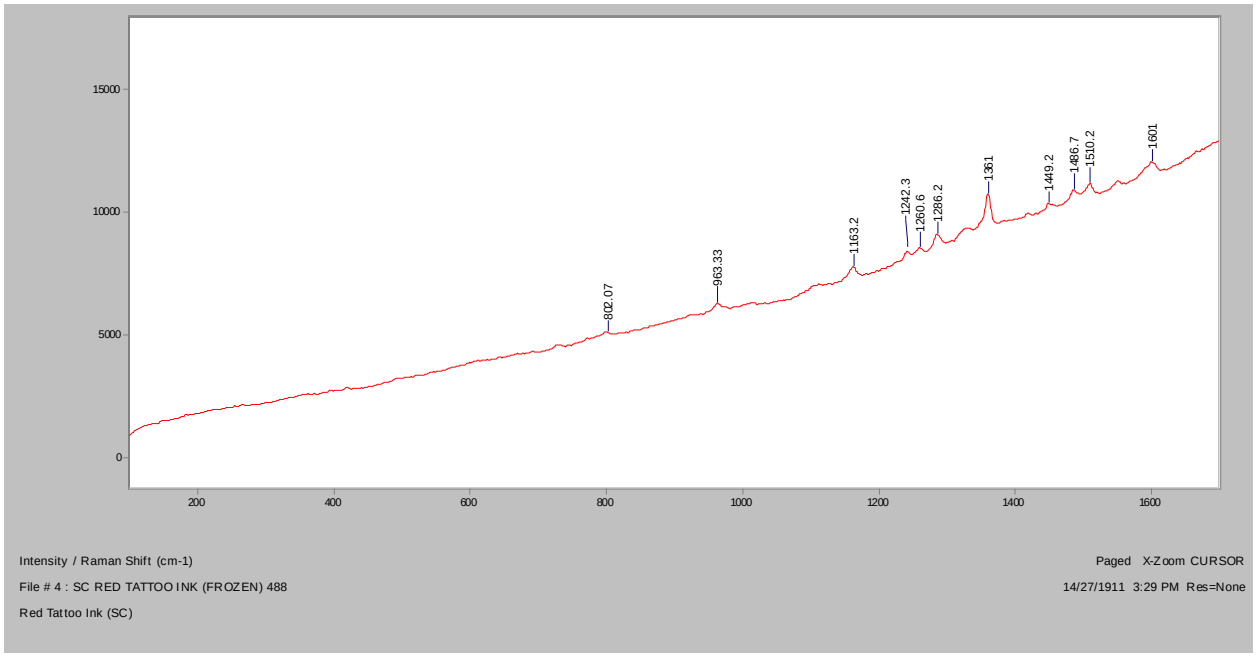

Normal Raman, 785nm

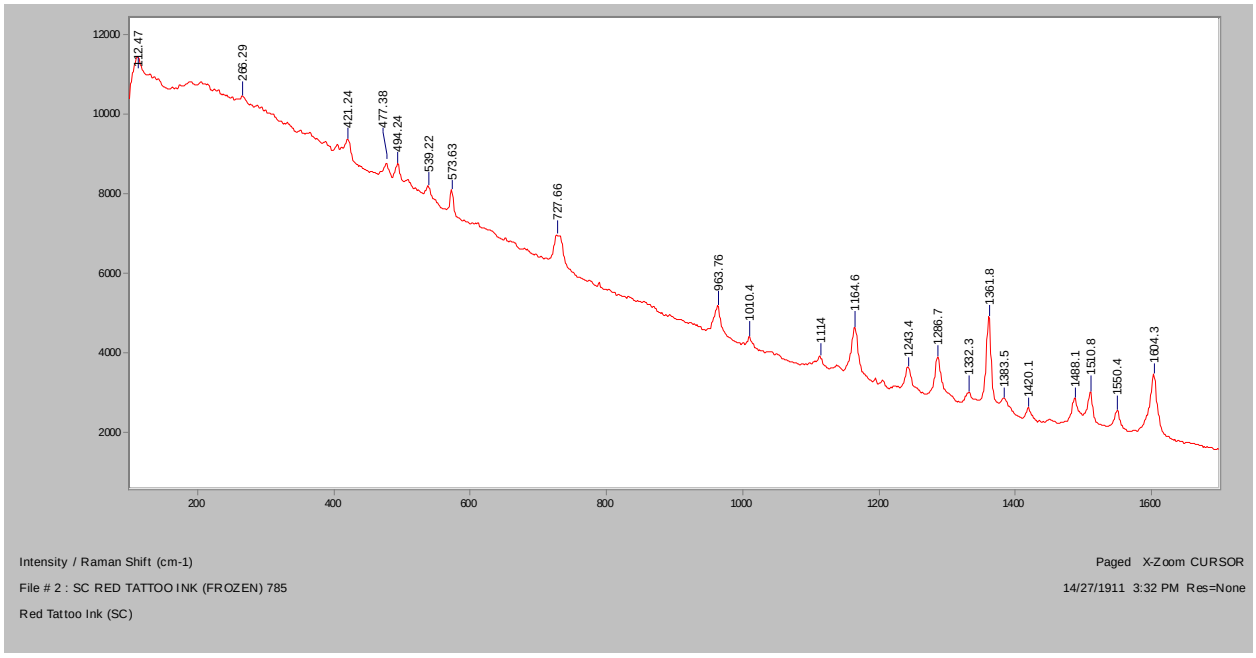

Orange region

Normal Raman, 488nm

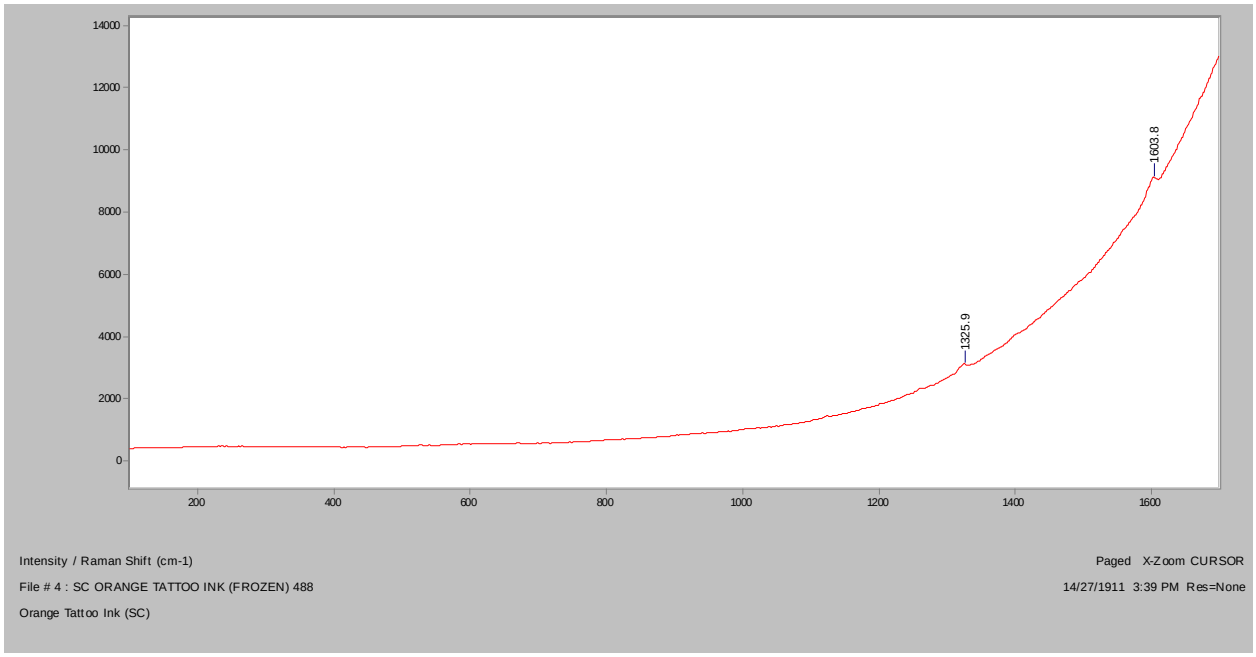

Normal Raman, 785nm

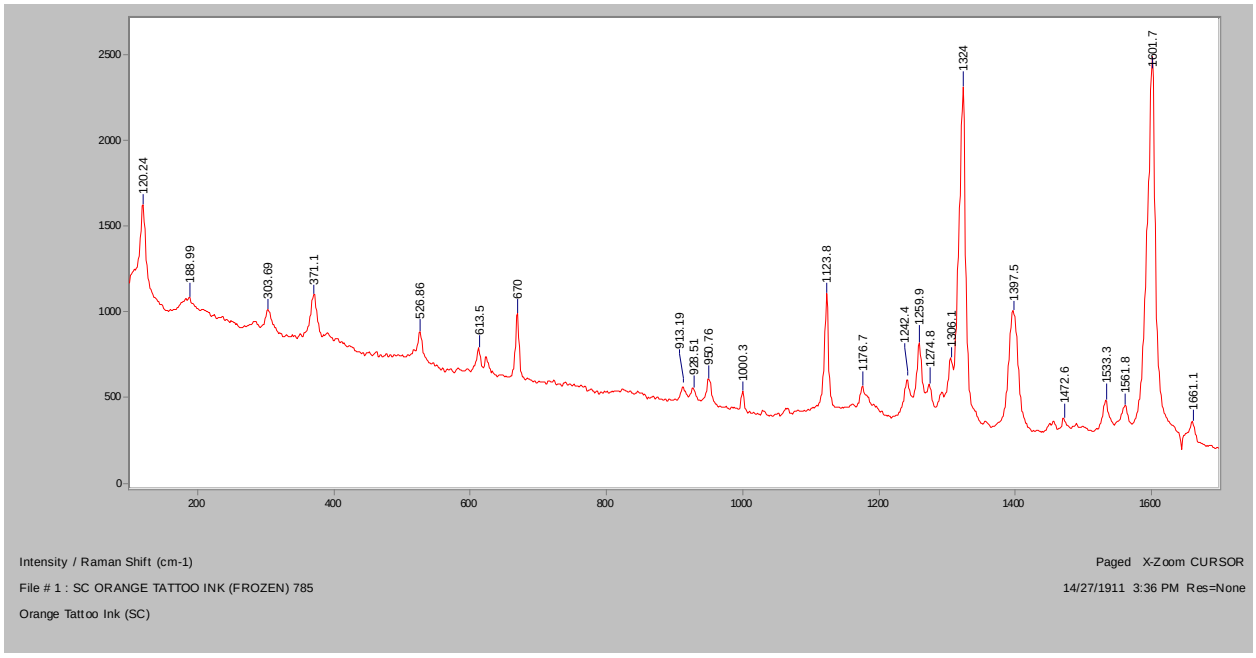

Yellow region

Normal Raman, 488nm

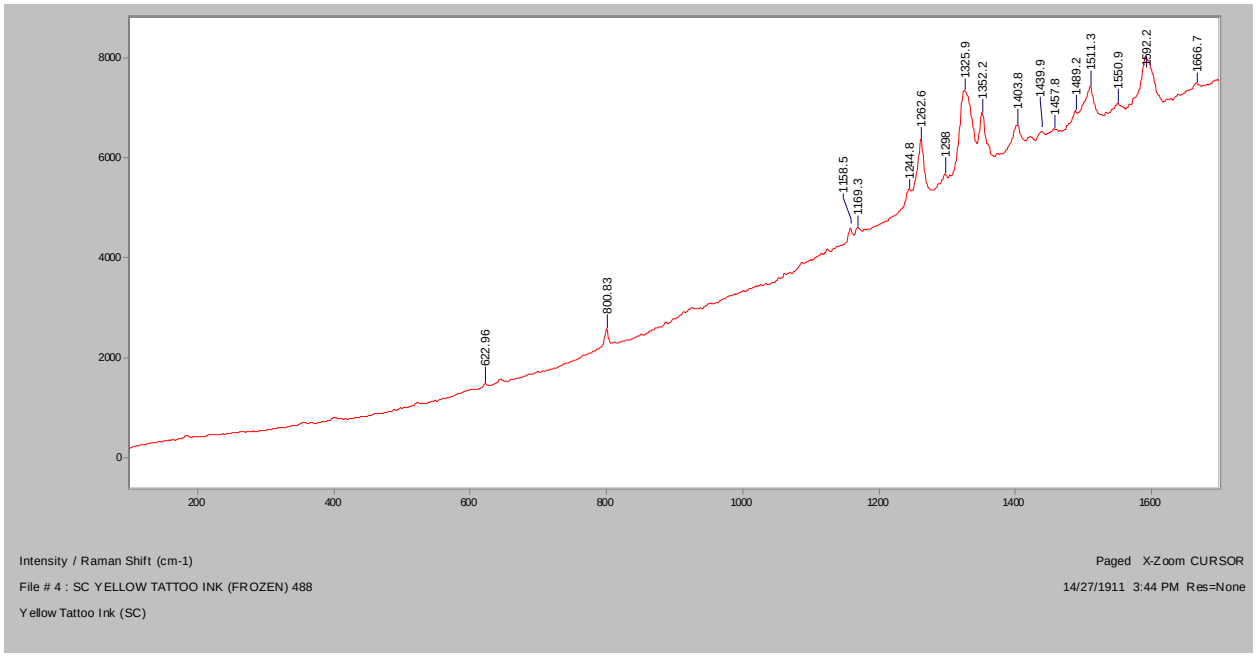

Normal Raman, 785nm

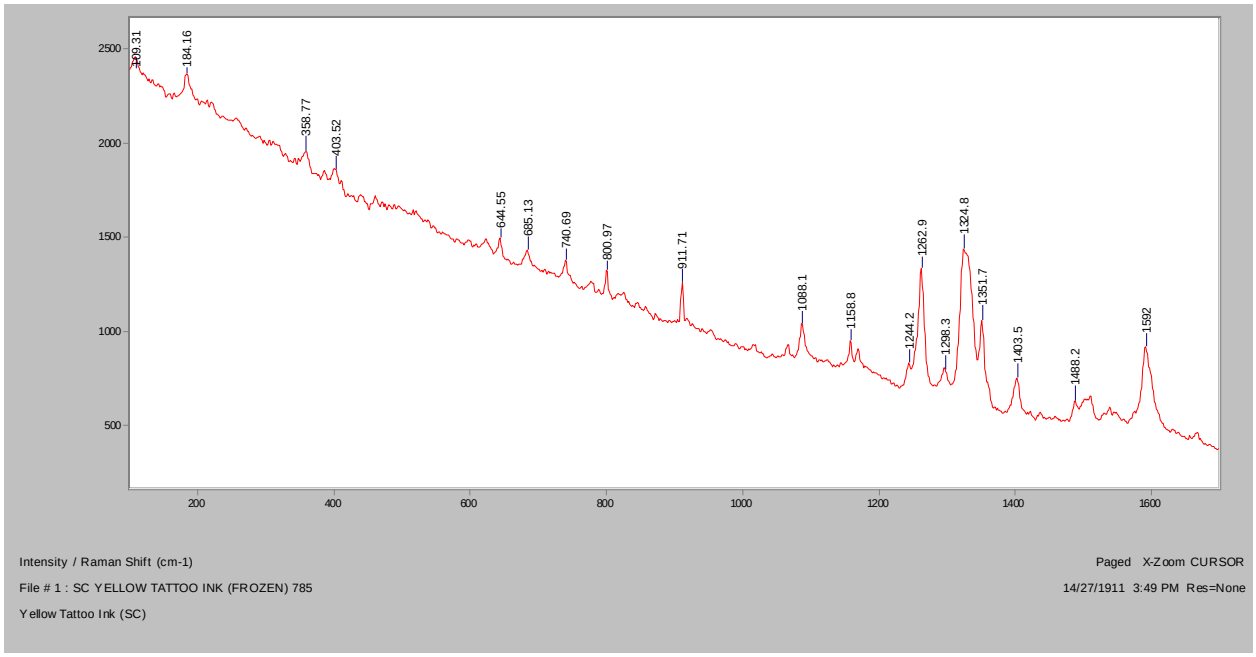

Green region

Normal Raman, 488nm

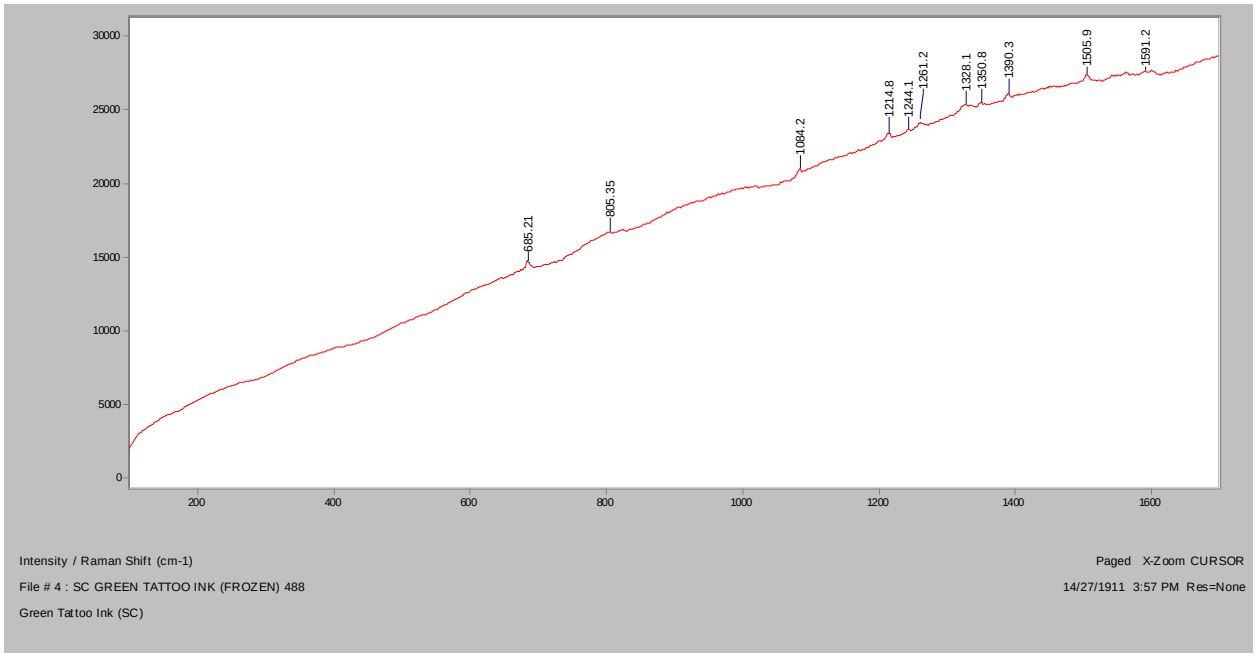

Normal Raman, 785nm

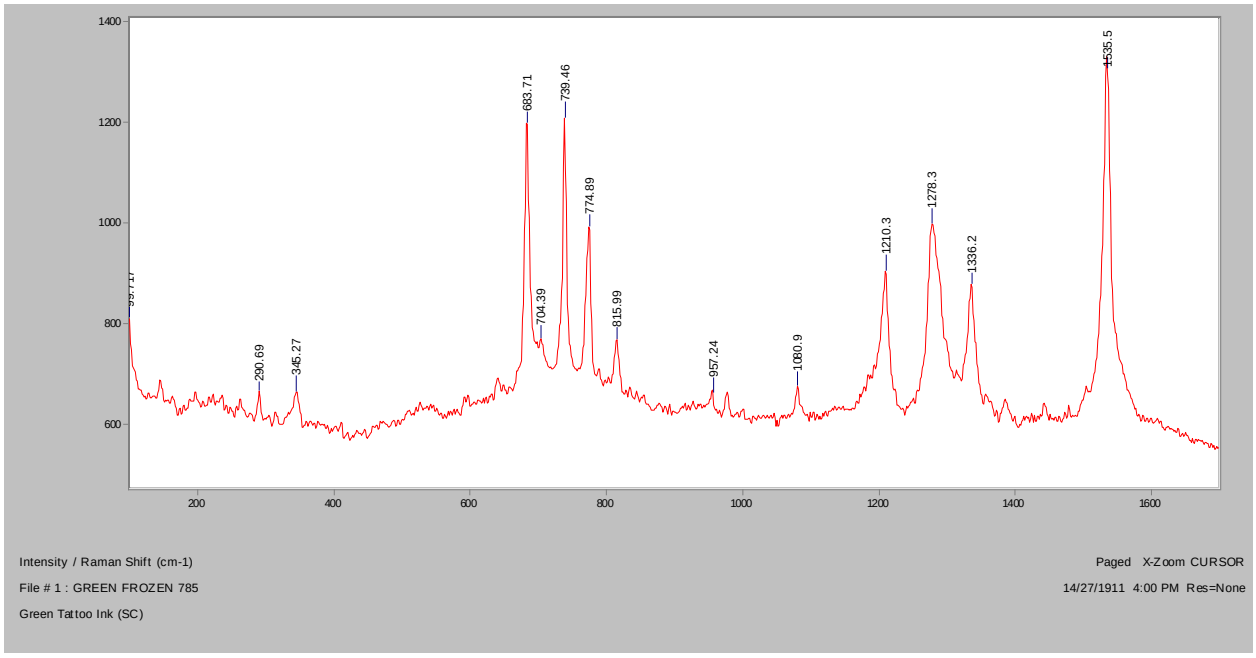

Blue region

Normal Raman, 488nm

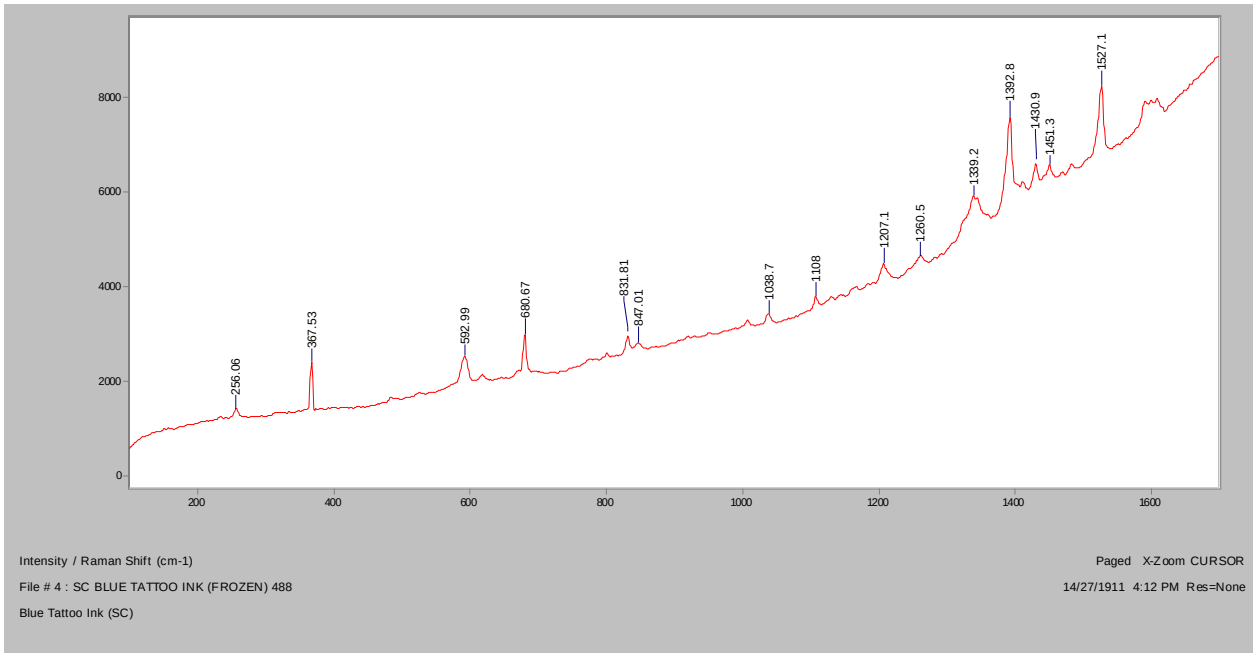

Normal Raman, 785nm

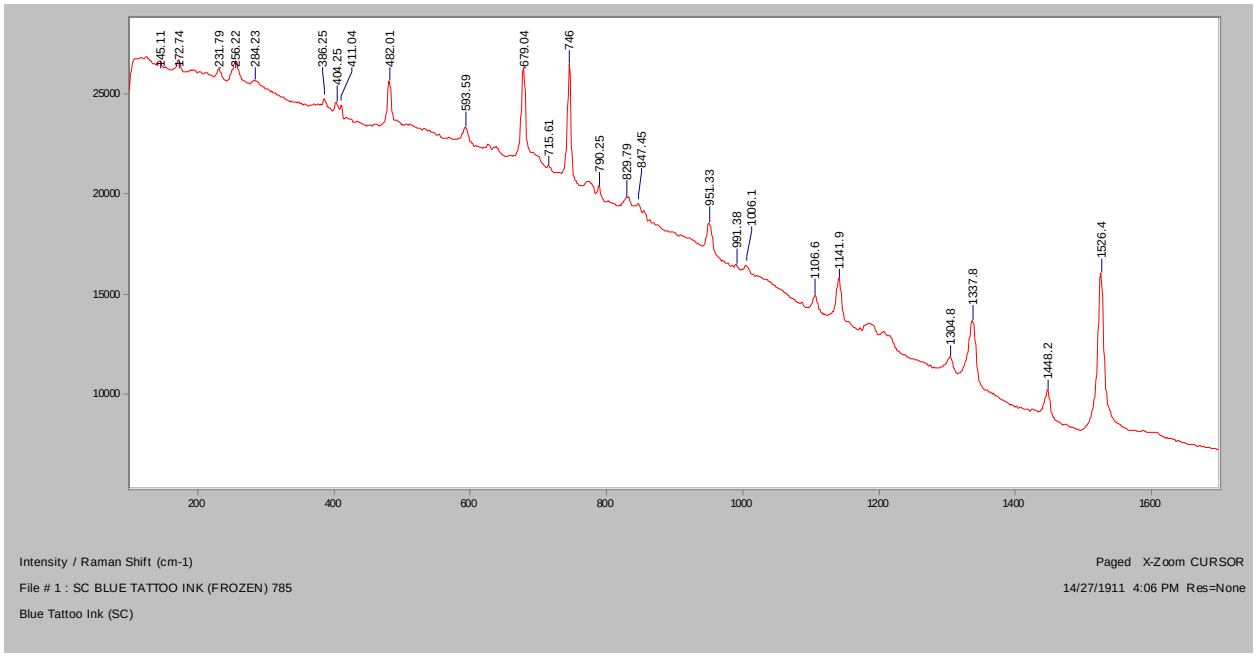

Purple region

Normal Raman, 488nm

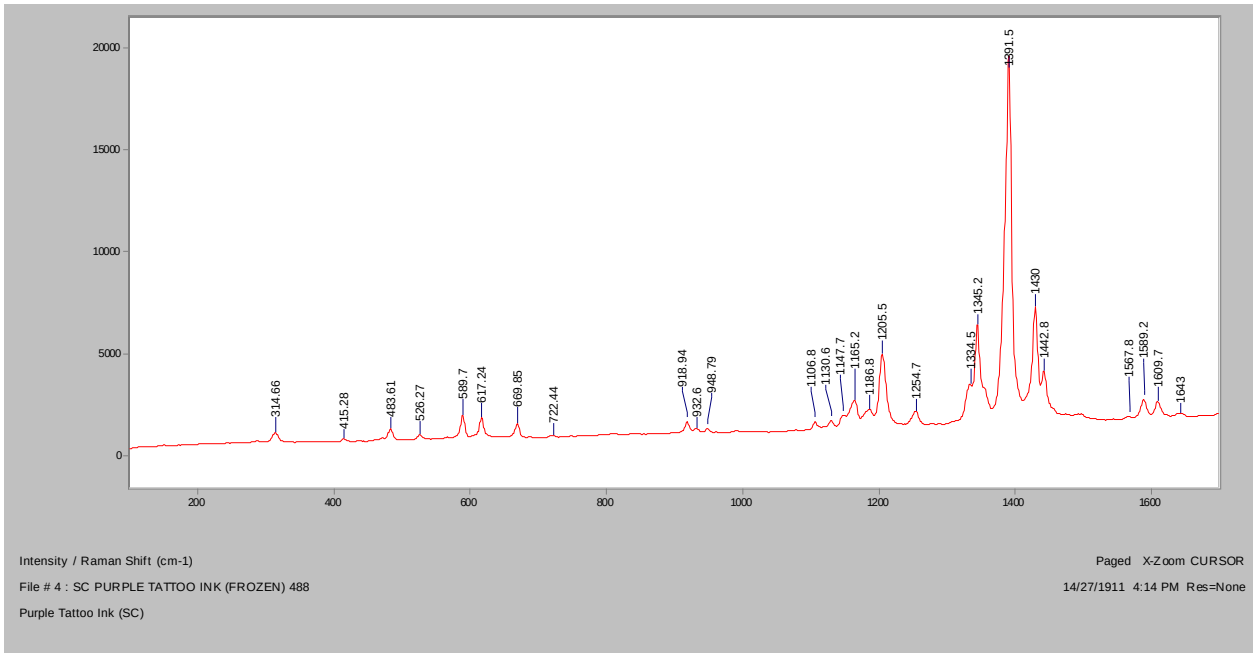

Normal Raman, 785nm

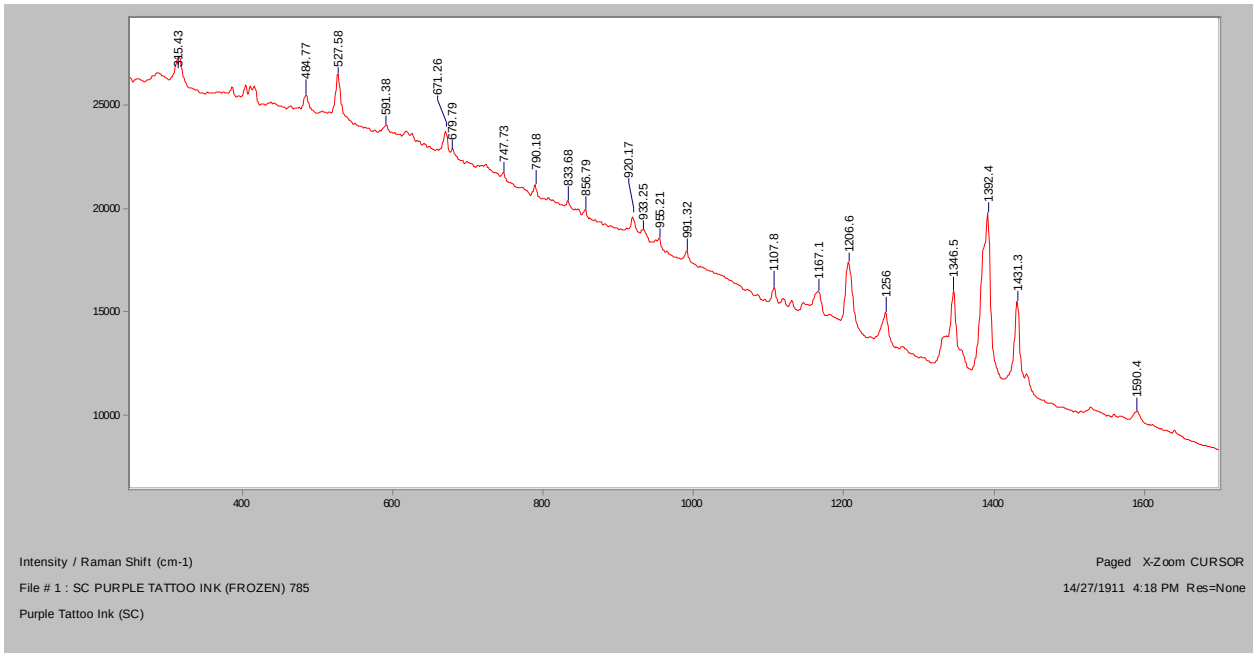

Formalin Fixed Tissue

White region

Normal Raman, 488nm

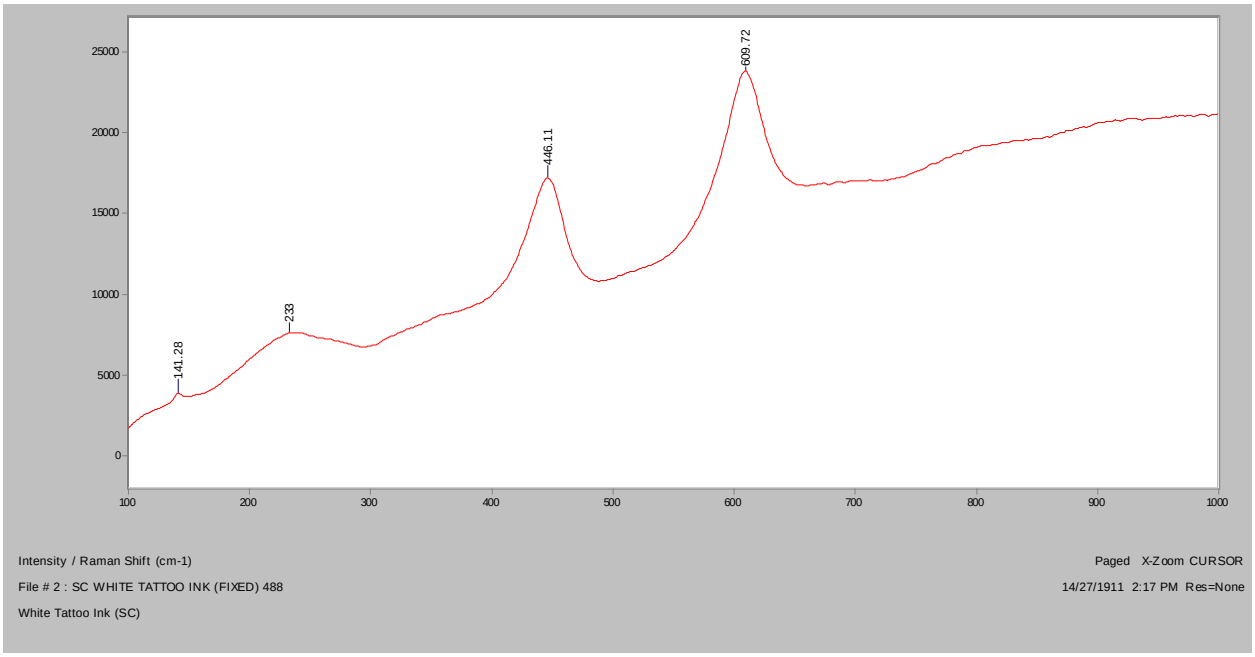

Normal Raman, 785nm

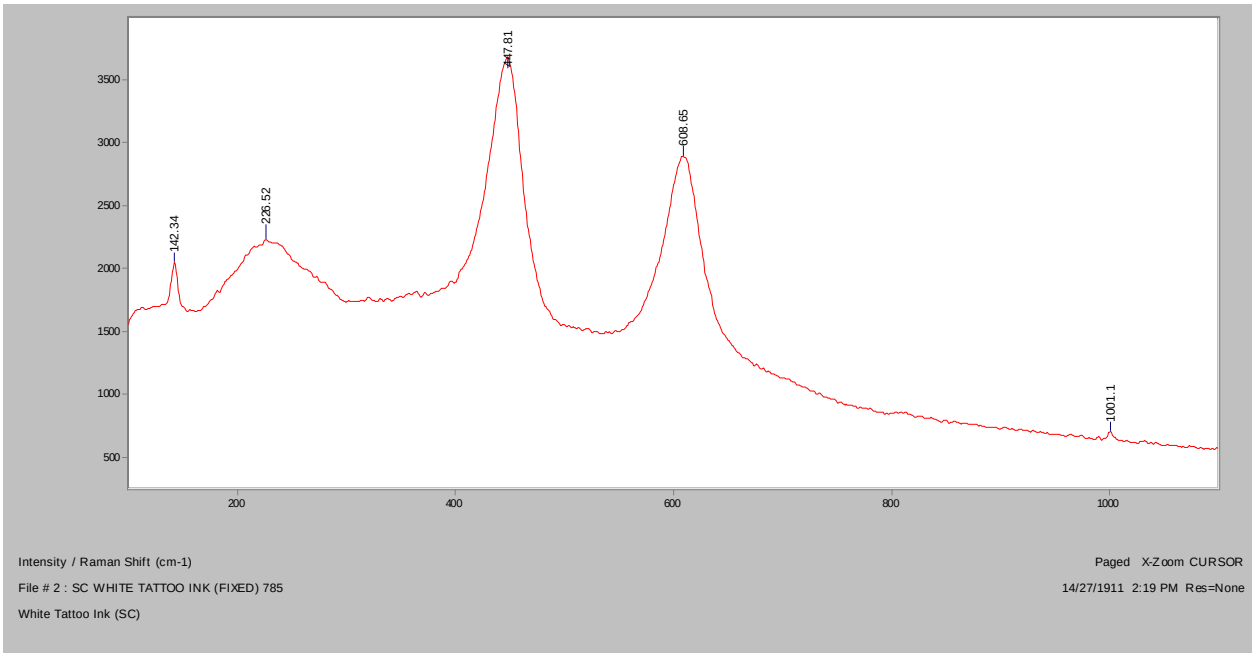

Red region

Normal Raman, 488nm

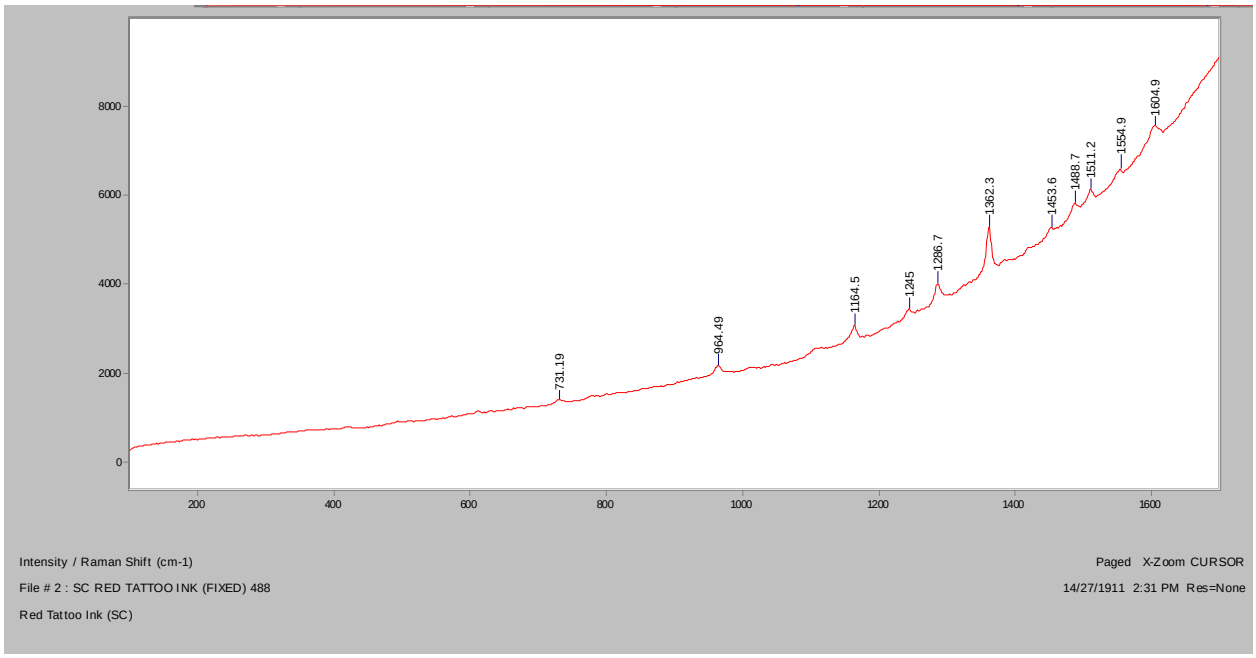

Normal Raman, 785nm

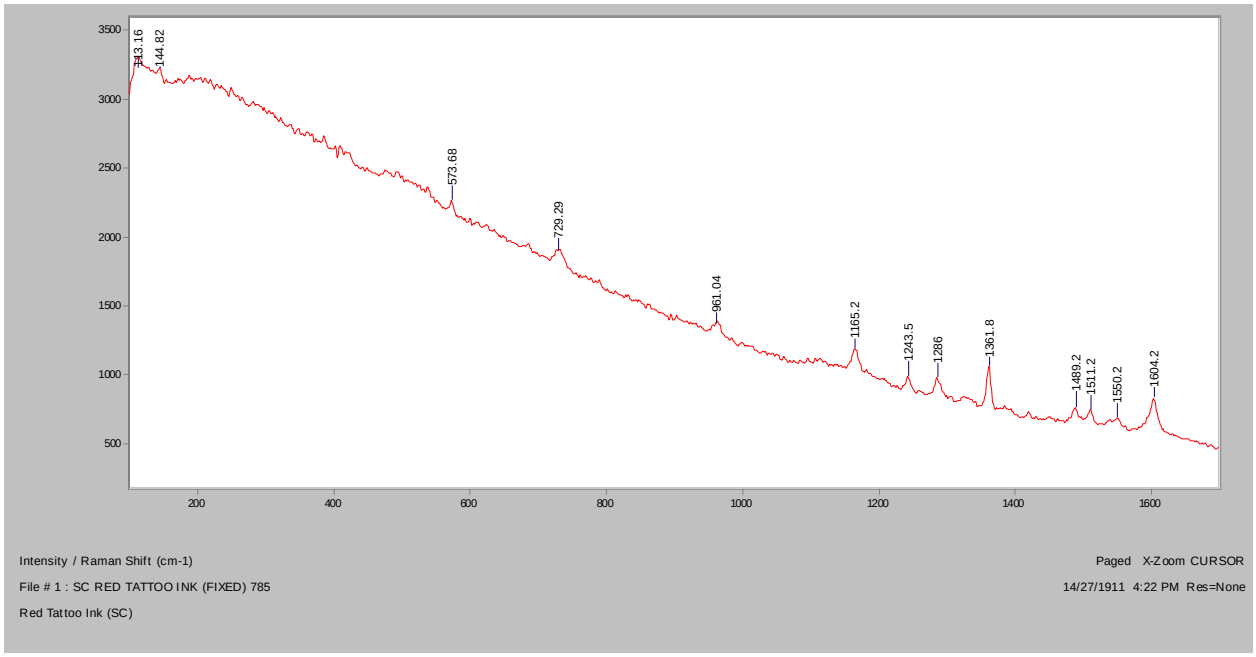

Orange region

Normal Raman, 488nm

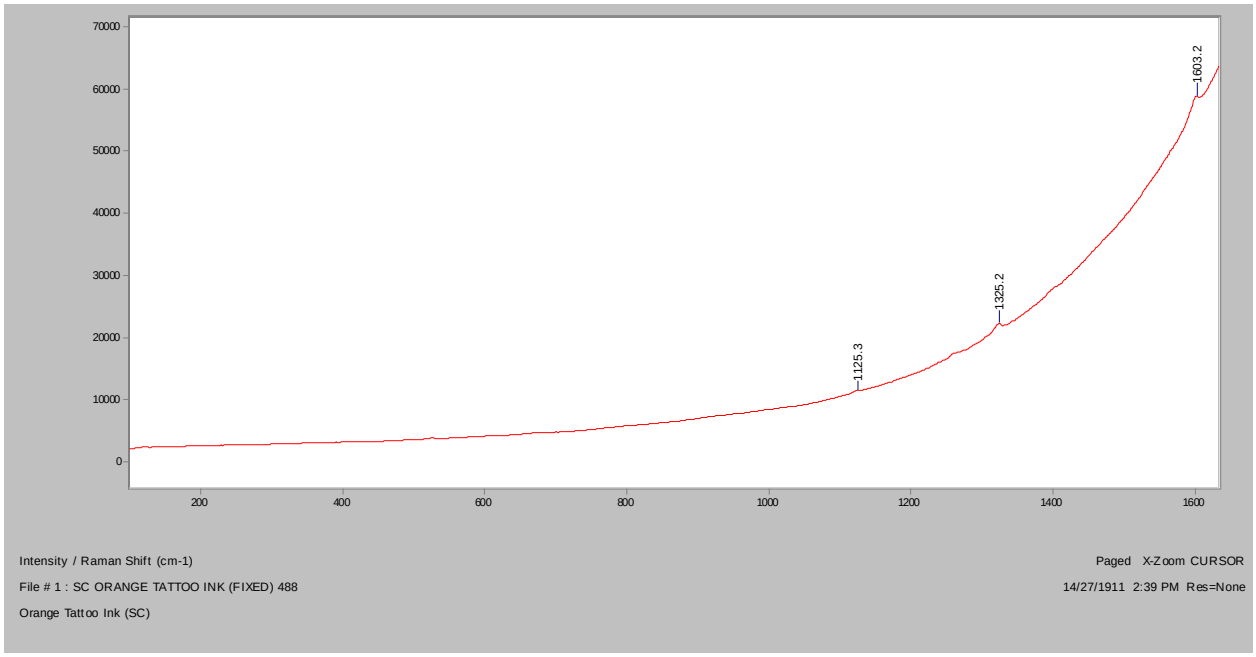

Normal Raman, 785nm

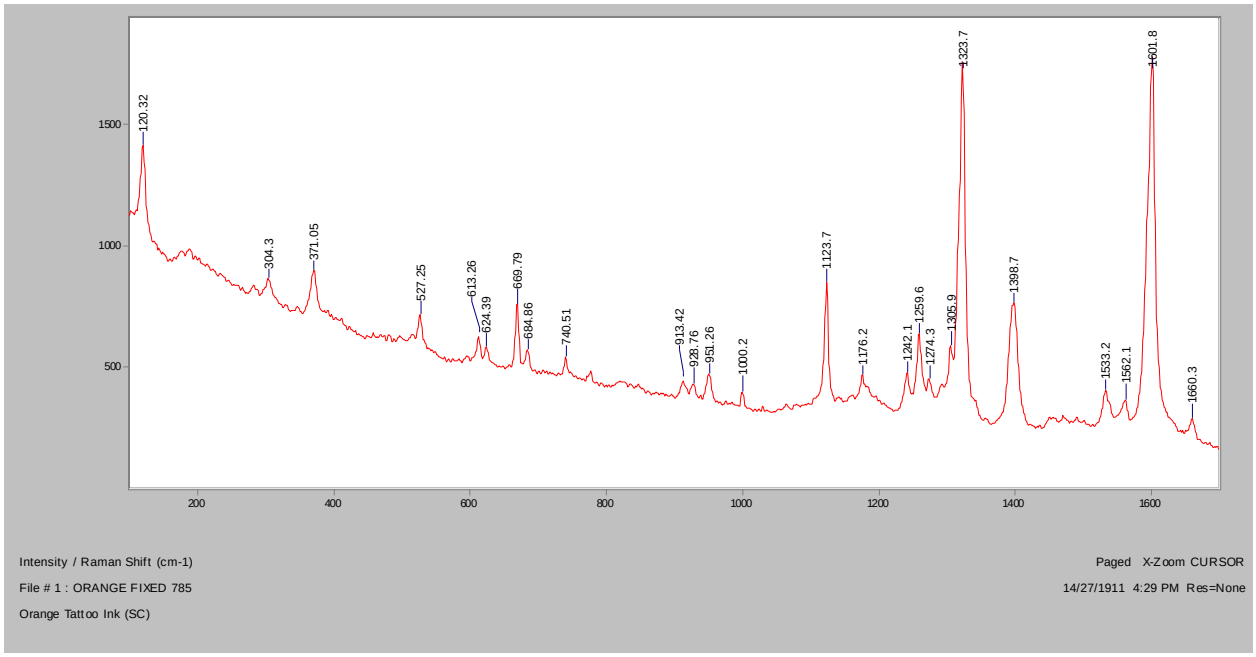

Yellow region

Normal Raman, 488nm

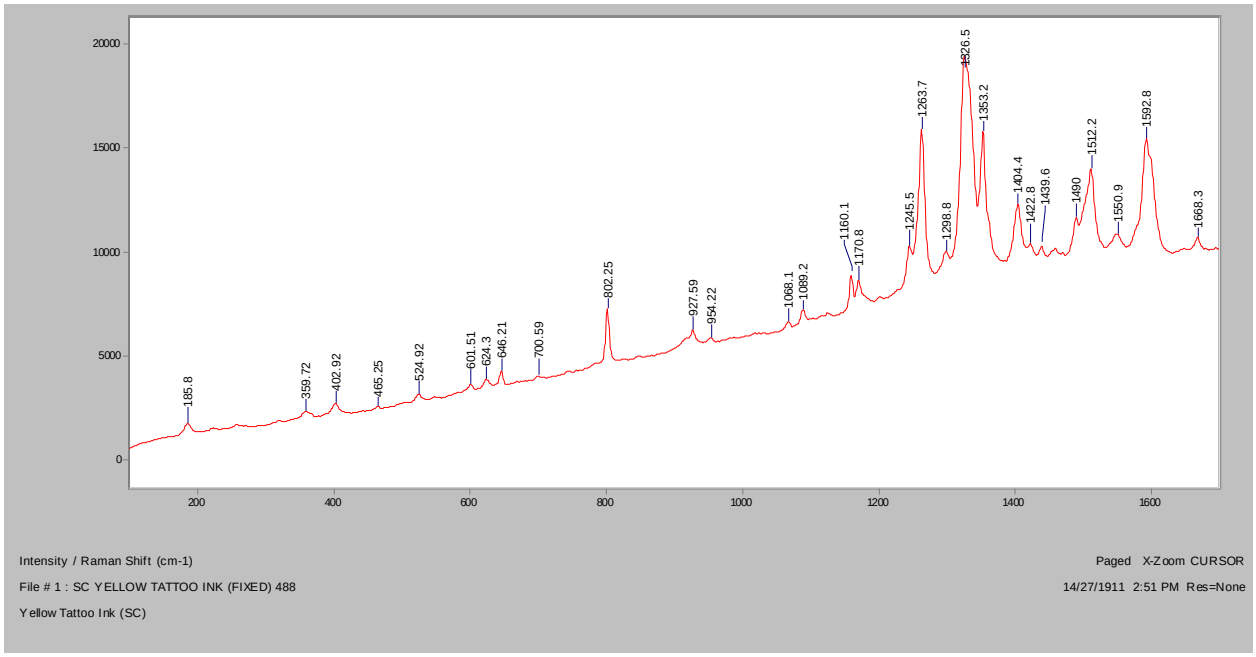

Normal Raman, 785nm

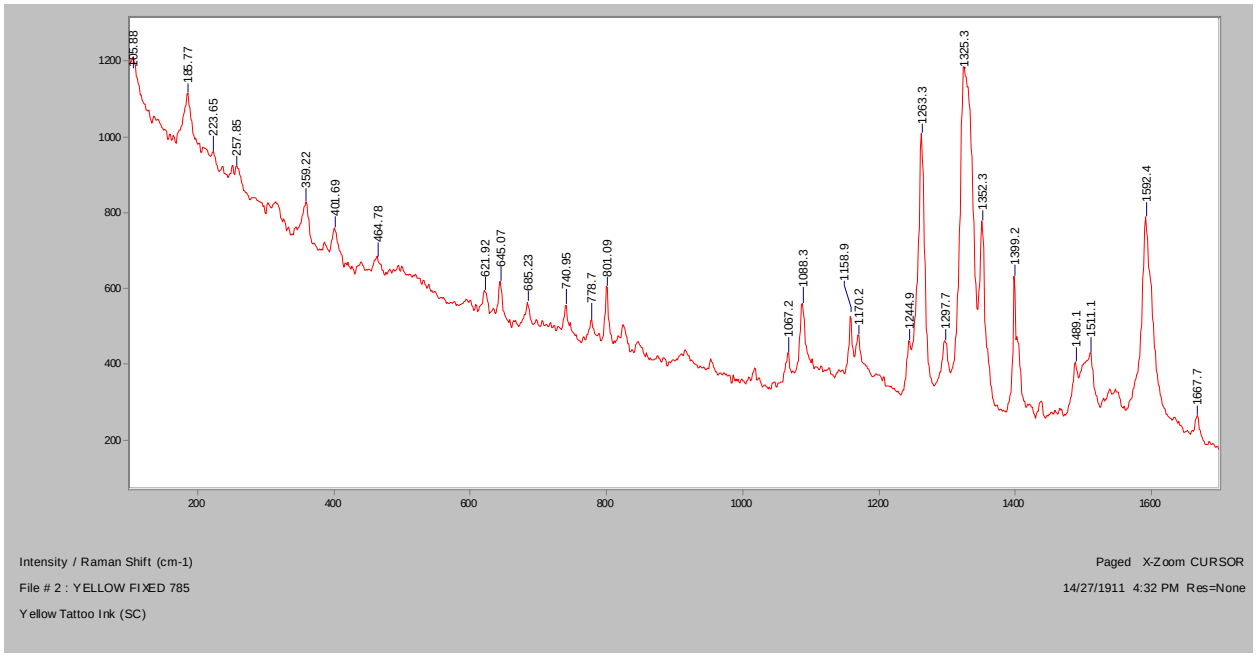

Green region

Normal Raman, 488nm

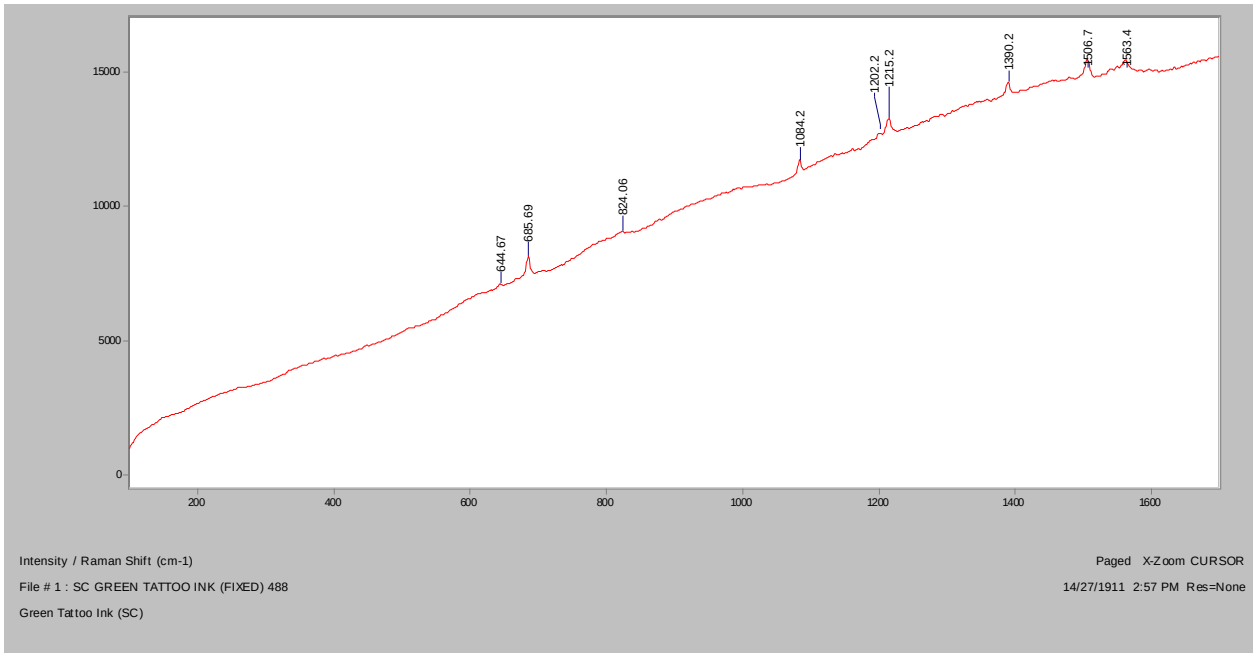

Normal Raman, 785nm

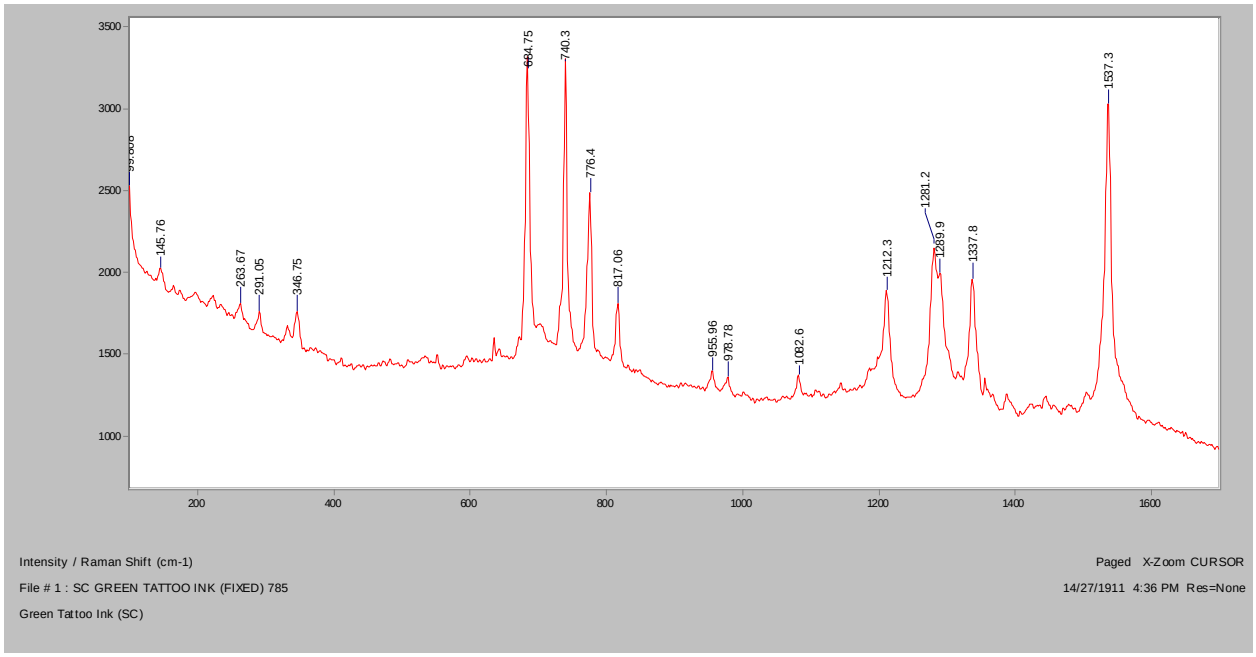

Blue region

Normal Raman, 488nm

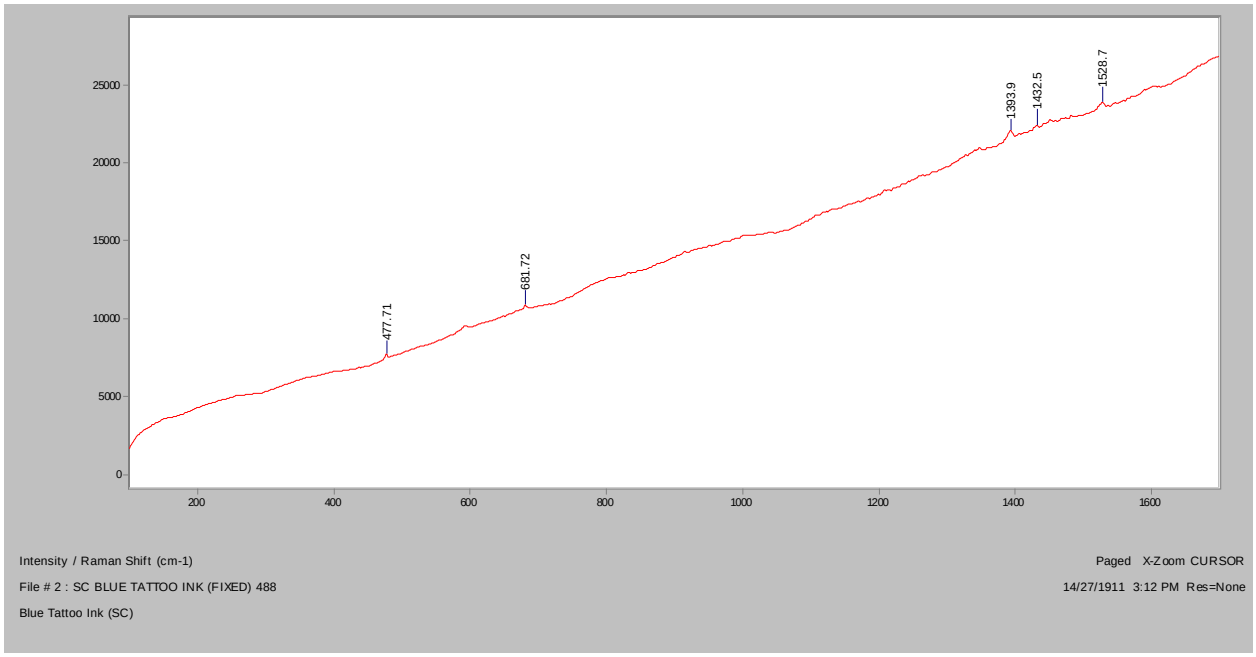

Normal Raman, 785nm

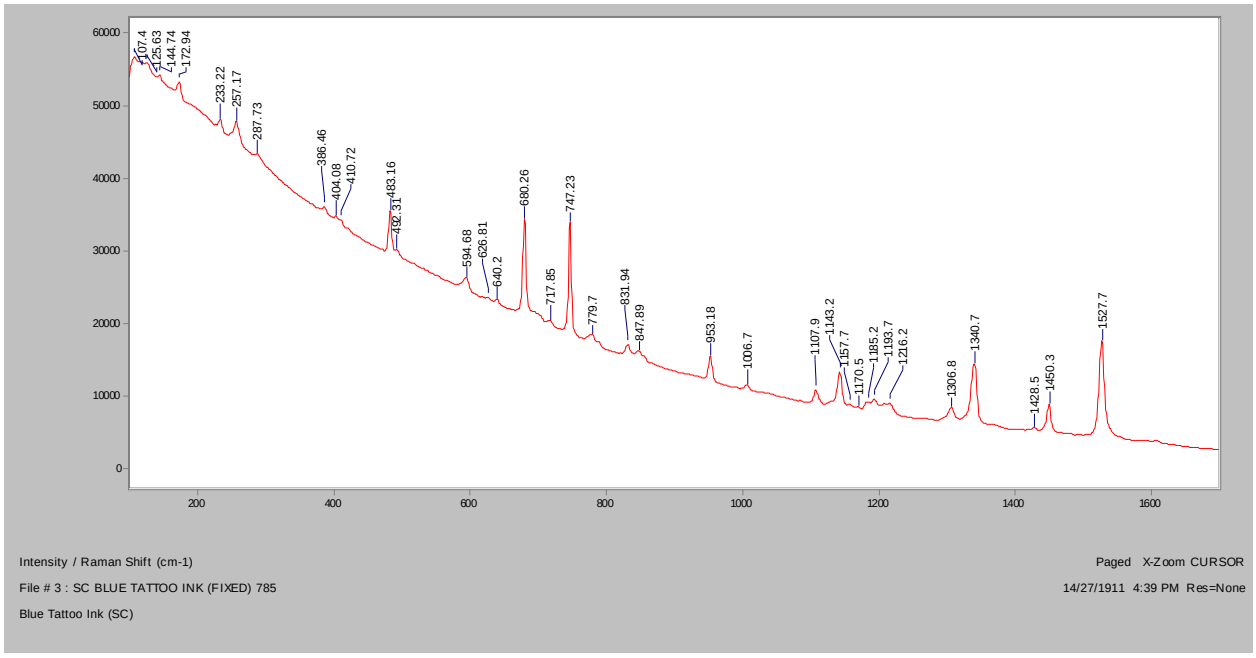

Purple region

Normal Raman, 488nm

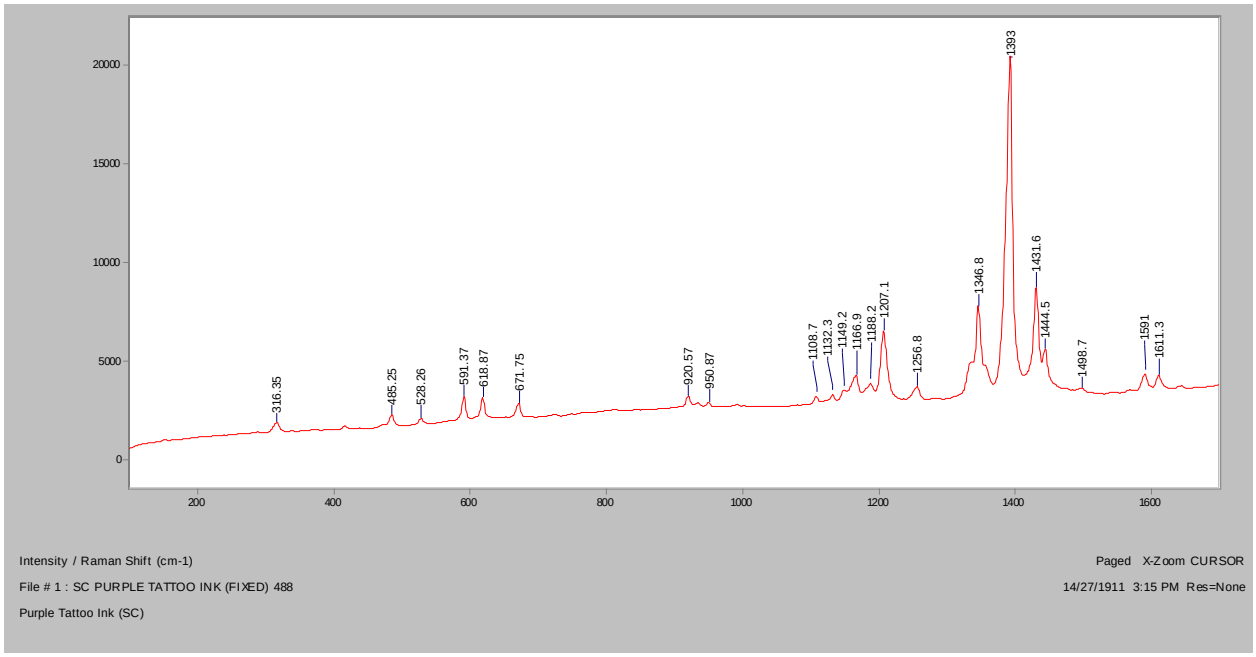

Normal Raman, 785nm

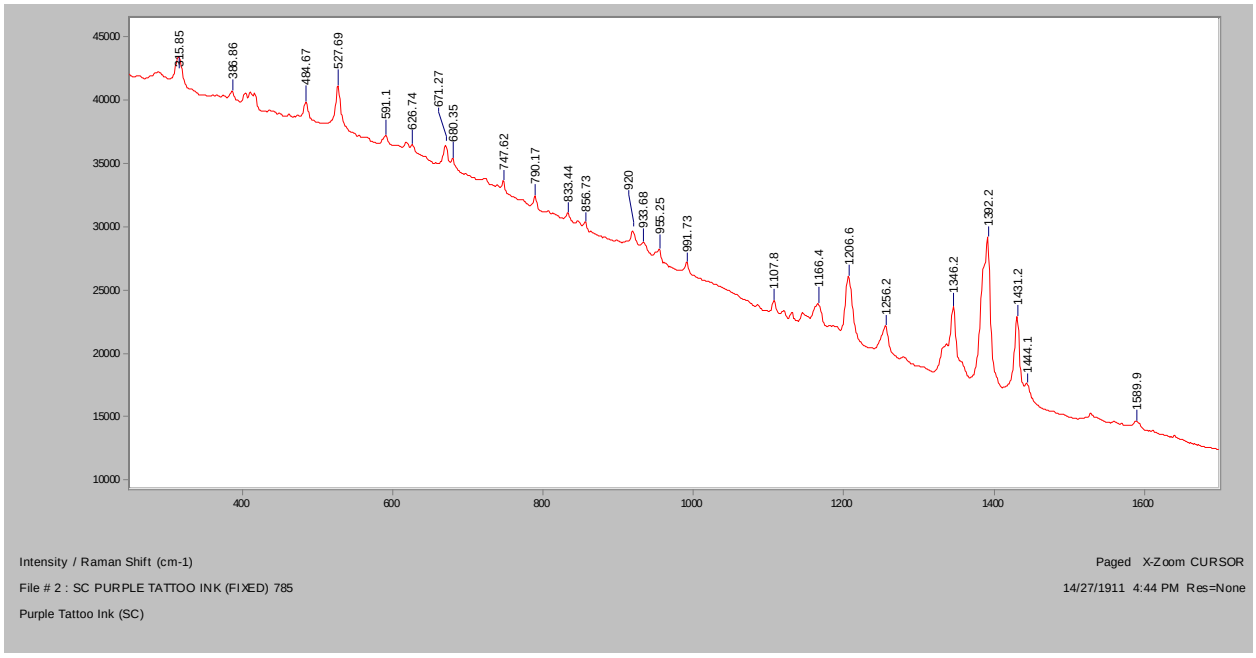

Appendix H: Calibration Standards

Raman Reference Spectra[5,6]

Cyclohexane

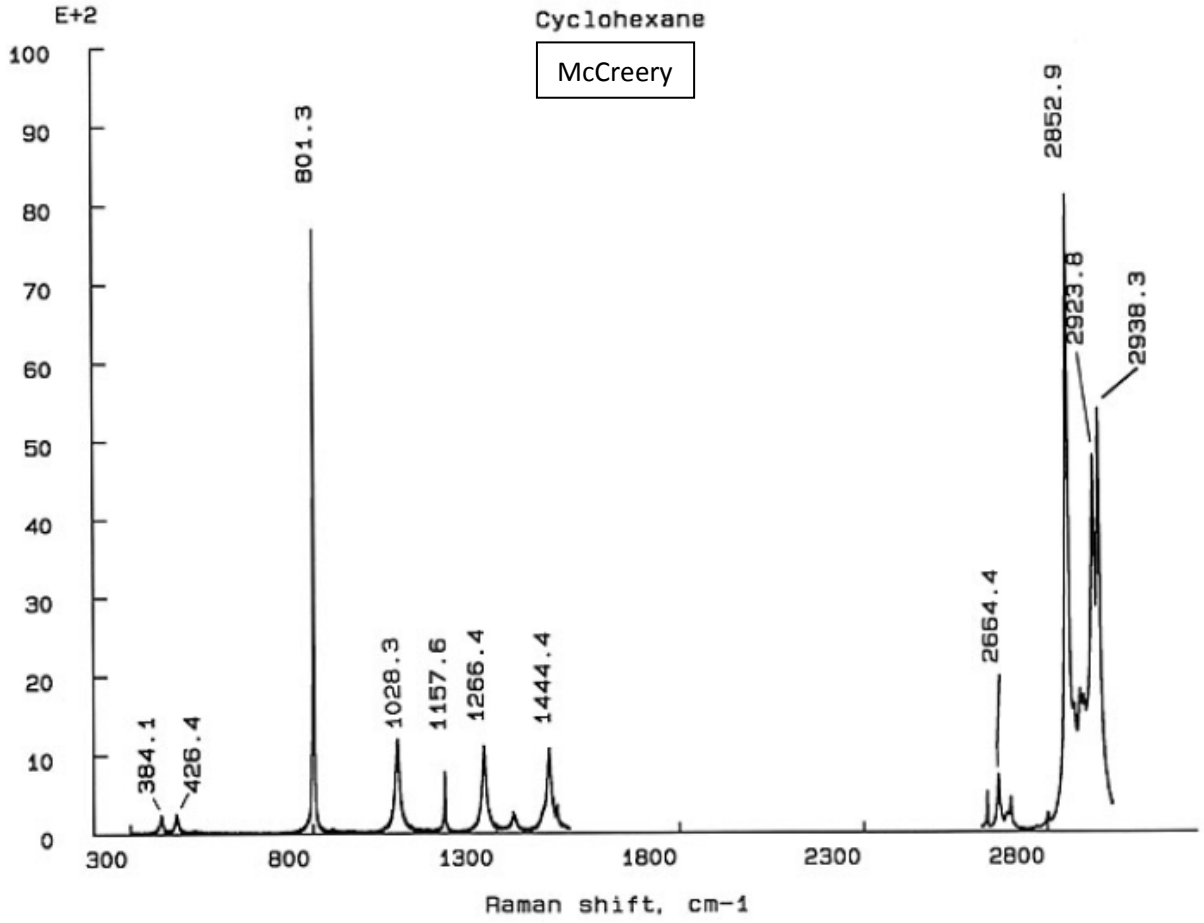

[5] Spectra labeled "McCreery" were obtained from The McCreery Group website: http://www.chem.ualberta.ca/~mccreery/ramanmaterials.html. All spectra generated with an FT-Raman (1064nm laser excitation wavelength)

[6] Spectra labeled "FNB" were obtained from Ferraro, J., K. Nakamoto & C. Brown, Introduction to Raman Spectroscopy, 2nd edition, Elsevier Science, 2003. All spectra were generated with a 488nm laser excitation wavelength.

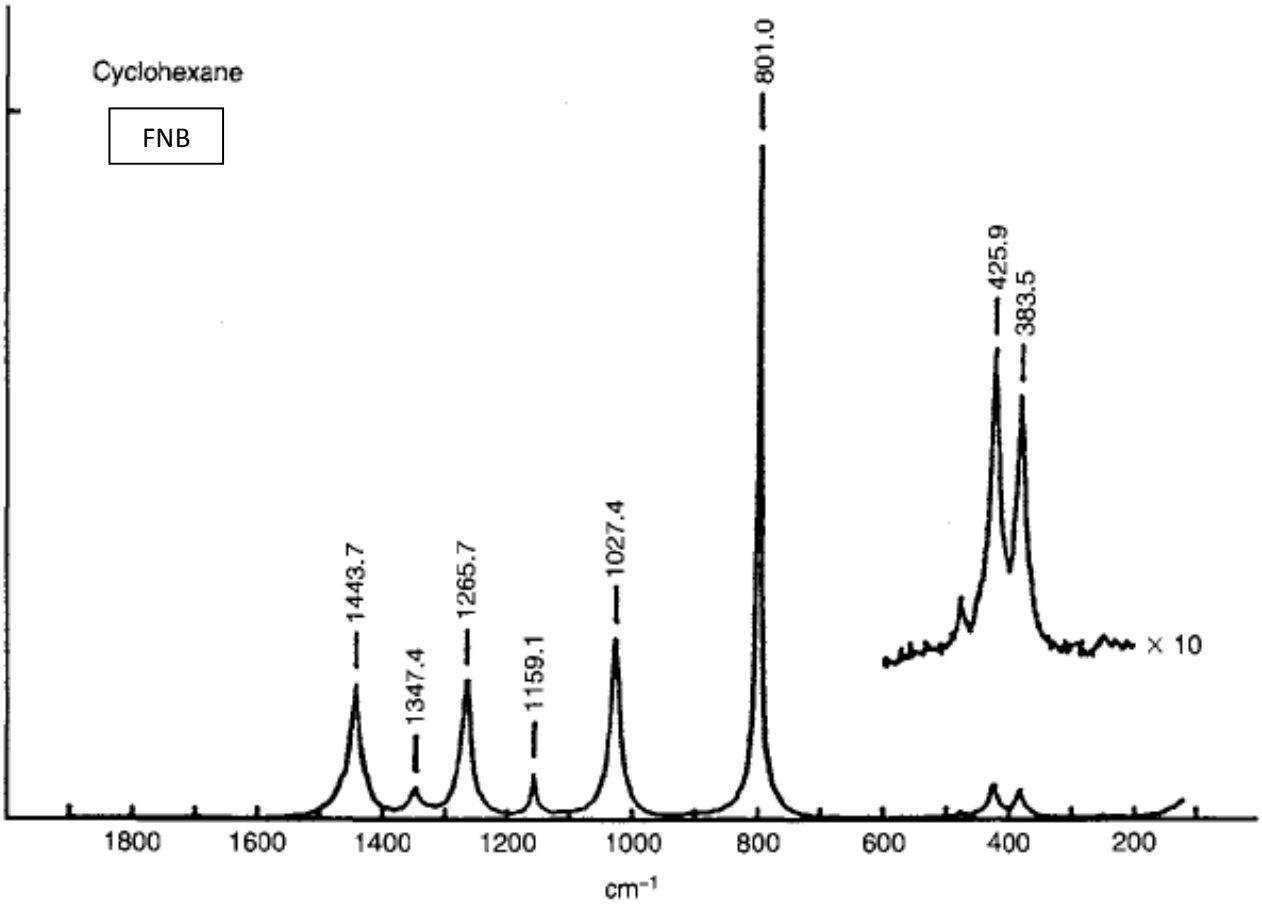
Cyclohexane
FNB
801.0
425.9
383.5
1443.7
1347.4
1265.7
1159.1
1027.4
× 10
1800
1600
1400
1200
1000
800
600
400
200
cm⁻¹

Cyclohexane

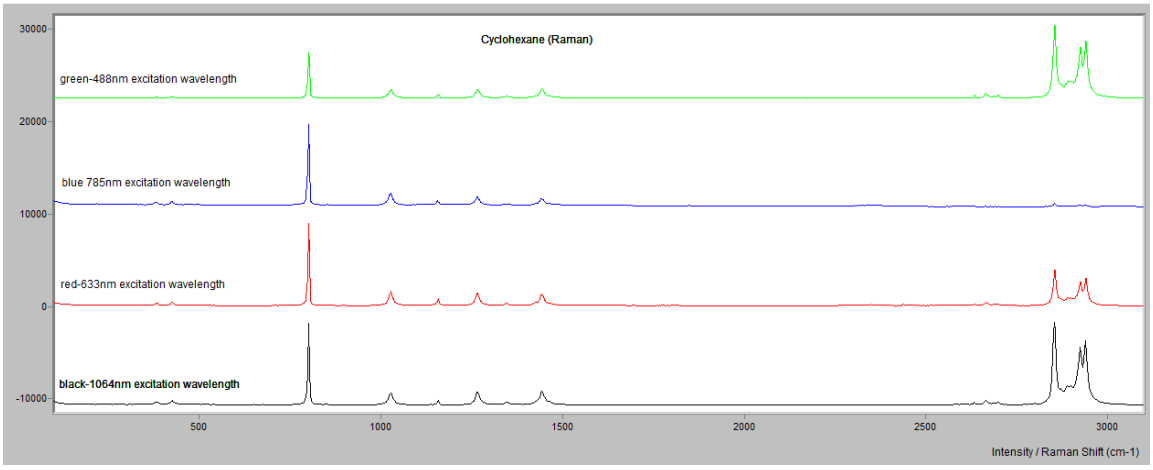

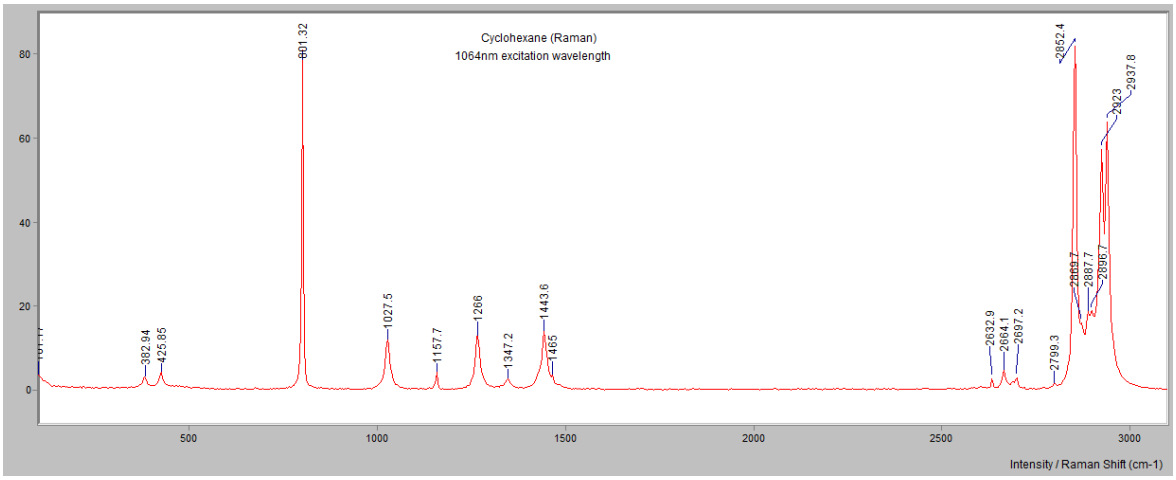

Polystyrene

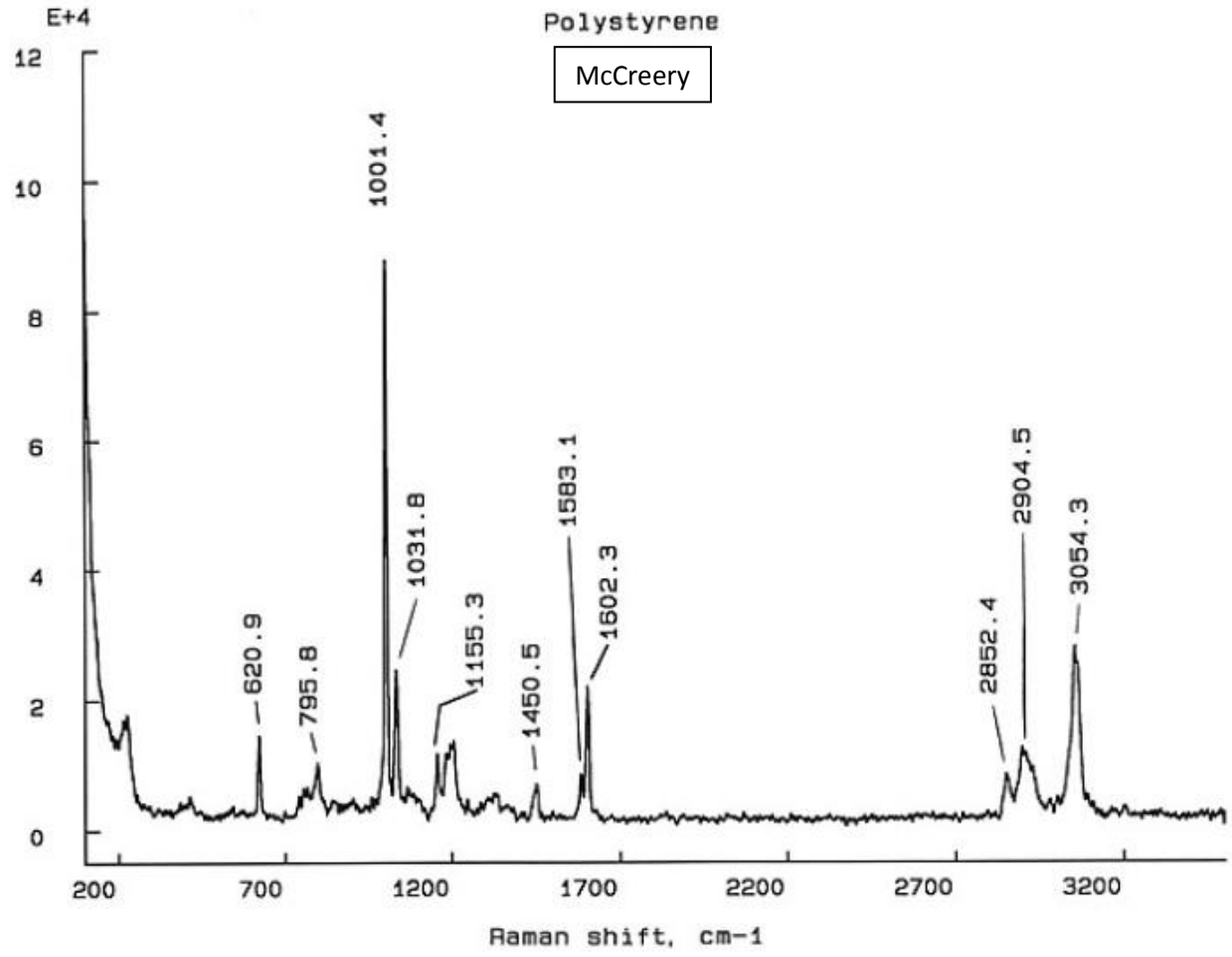

Polystyrene

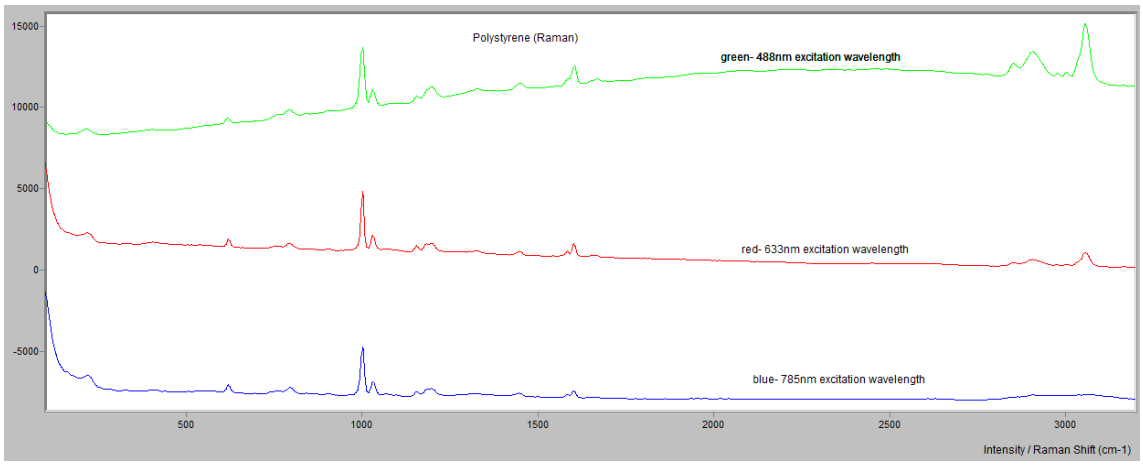

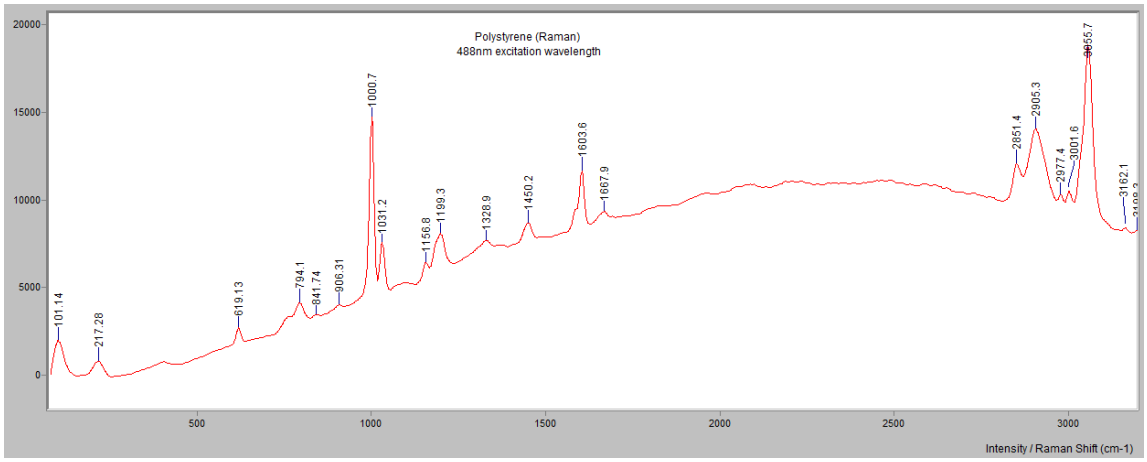

Sulfur

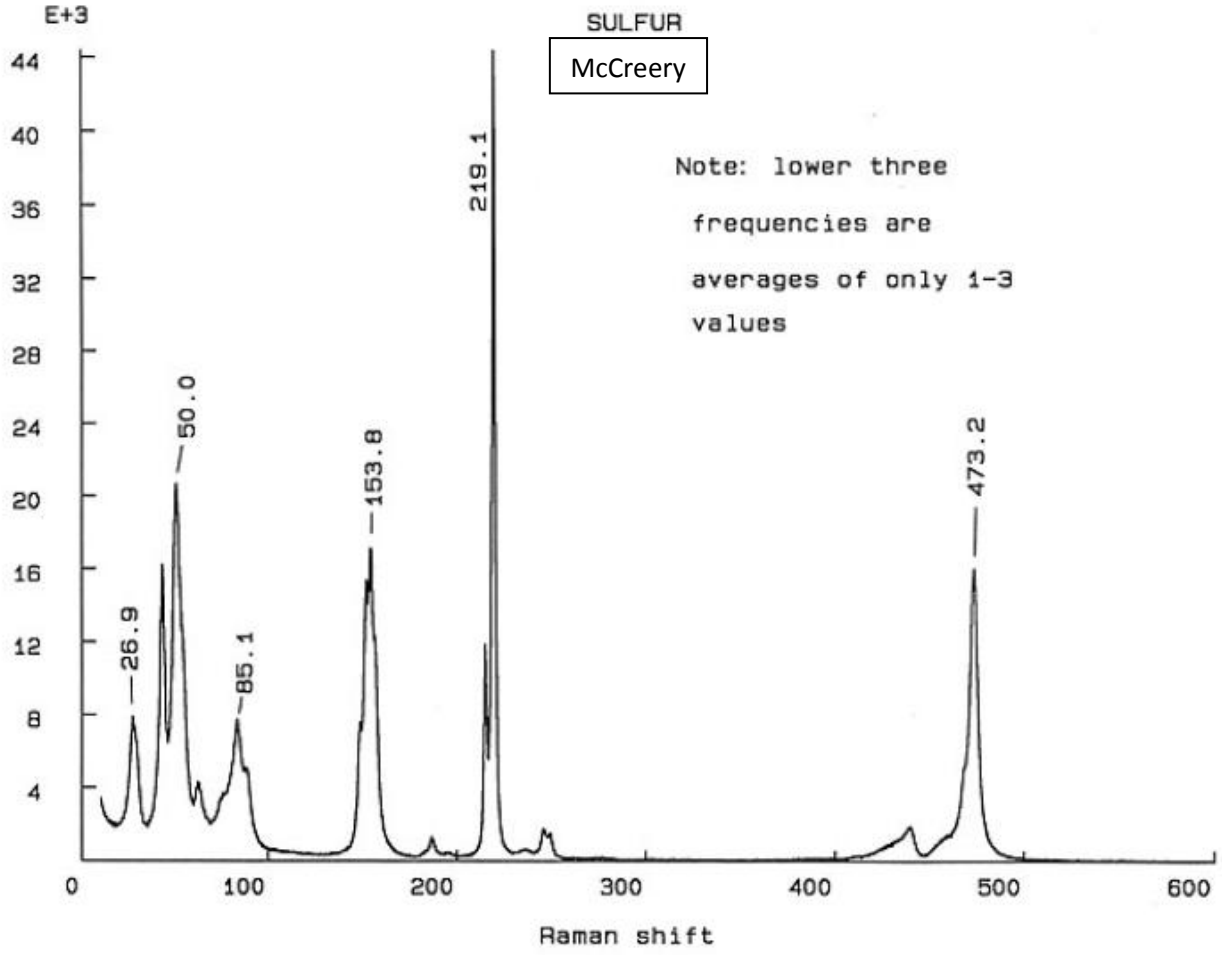
E+3
SULFUR
McCreery
Note: lower three
frequencies are
averages of only 1-3
values
44
40
36
32
28
24
20
16
12
8
4
0
100
200
300
400
500
600
Raman shift
26.9
50.0
85.1
153.8
219.1
473.2

Sulfur

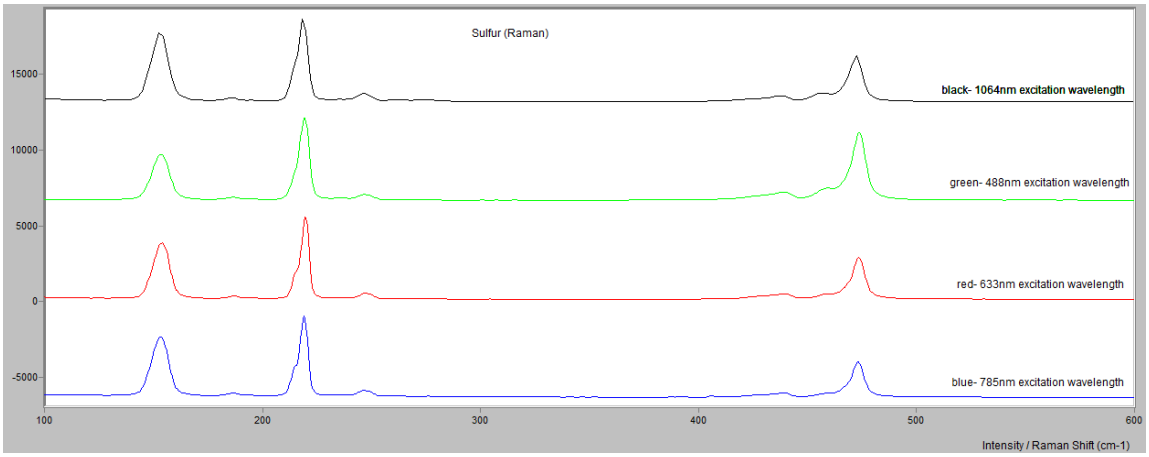
Sulfur (Raman)
black- 1064nm excitation wavelength
green- 488nm excitation wavelength
red- 633nm excitation wavelength
blue- 785nm excitation wavelength
15000
10000
5000
0
-5000
100
200
300
400
500
600
Intensity / Raman Shift (cm-1)

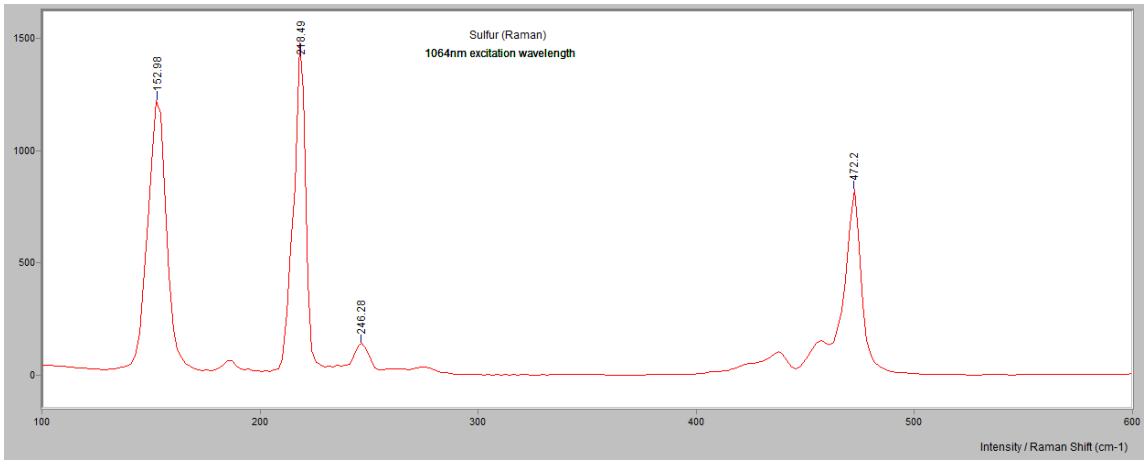
Sulfur (Raman)
1064nm excitation wavelength
152.98
218.49
246.28
472.2
1500
1000
500
0
100
200
300
400
500
600
Intensity / Raman Shift (cm-1)

4-acetomidophenol (Tylenol)

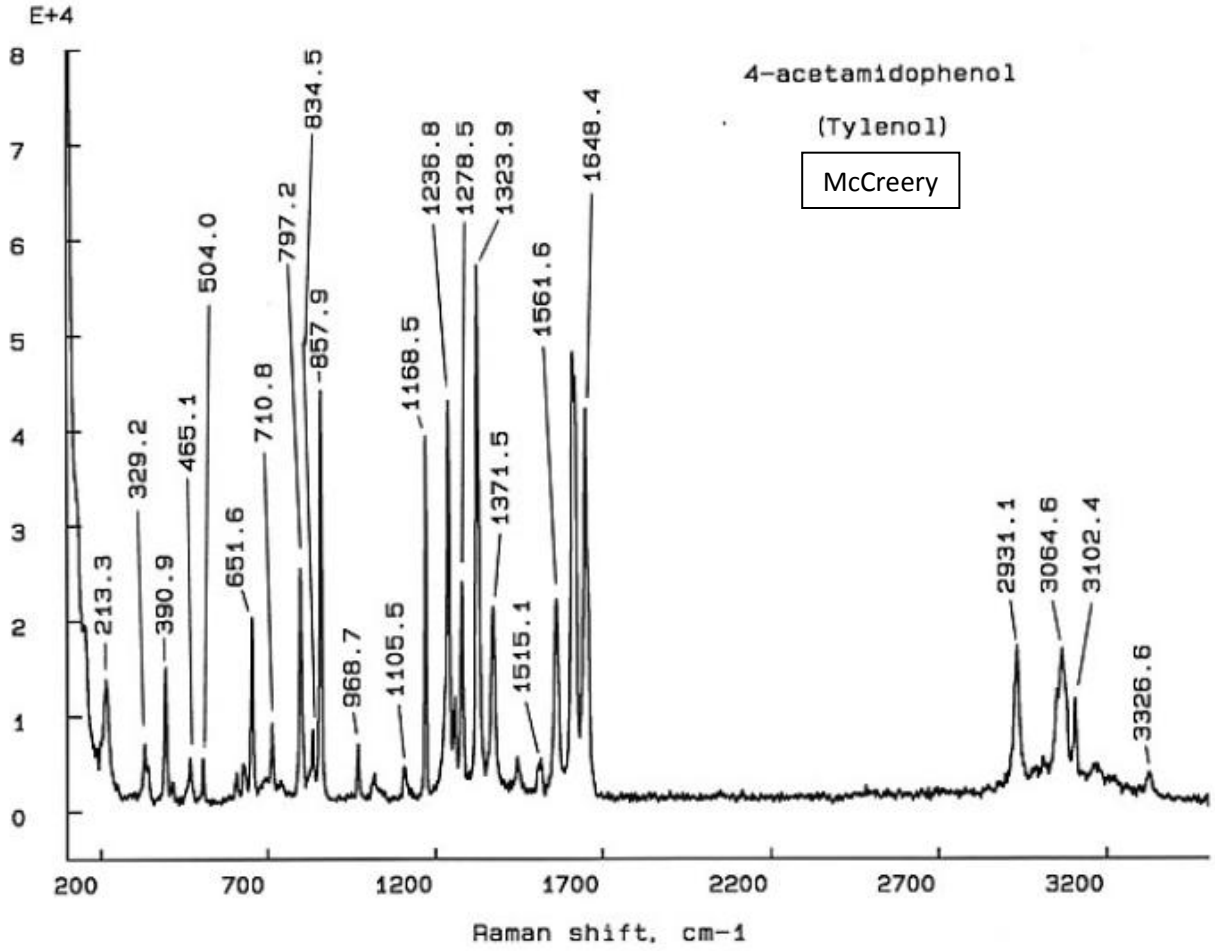

Acetominophen

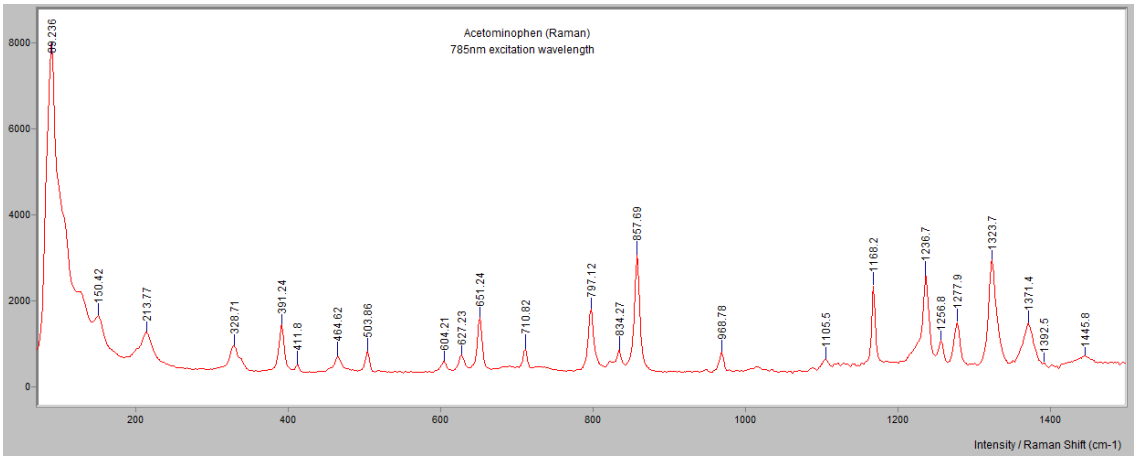

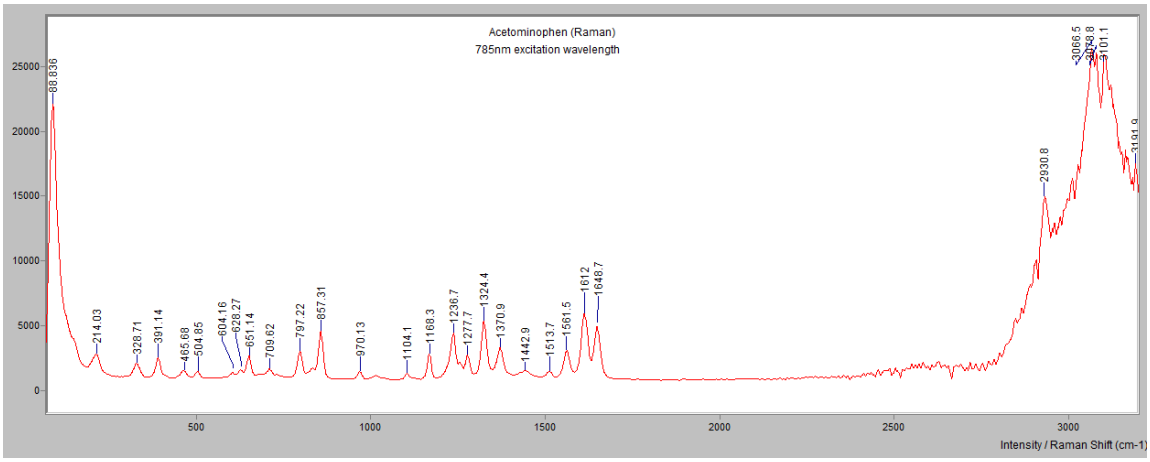

50/50 Toluene: Acetonitrile

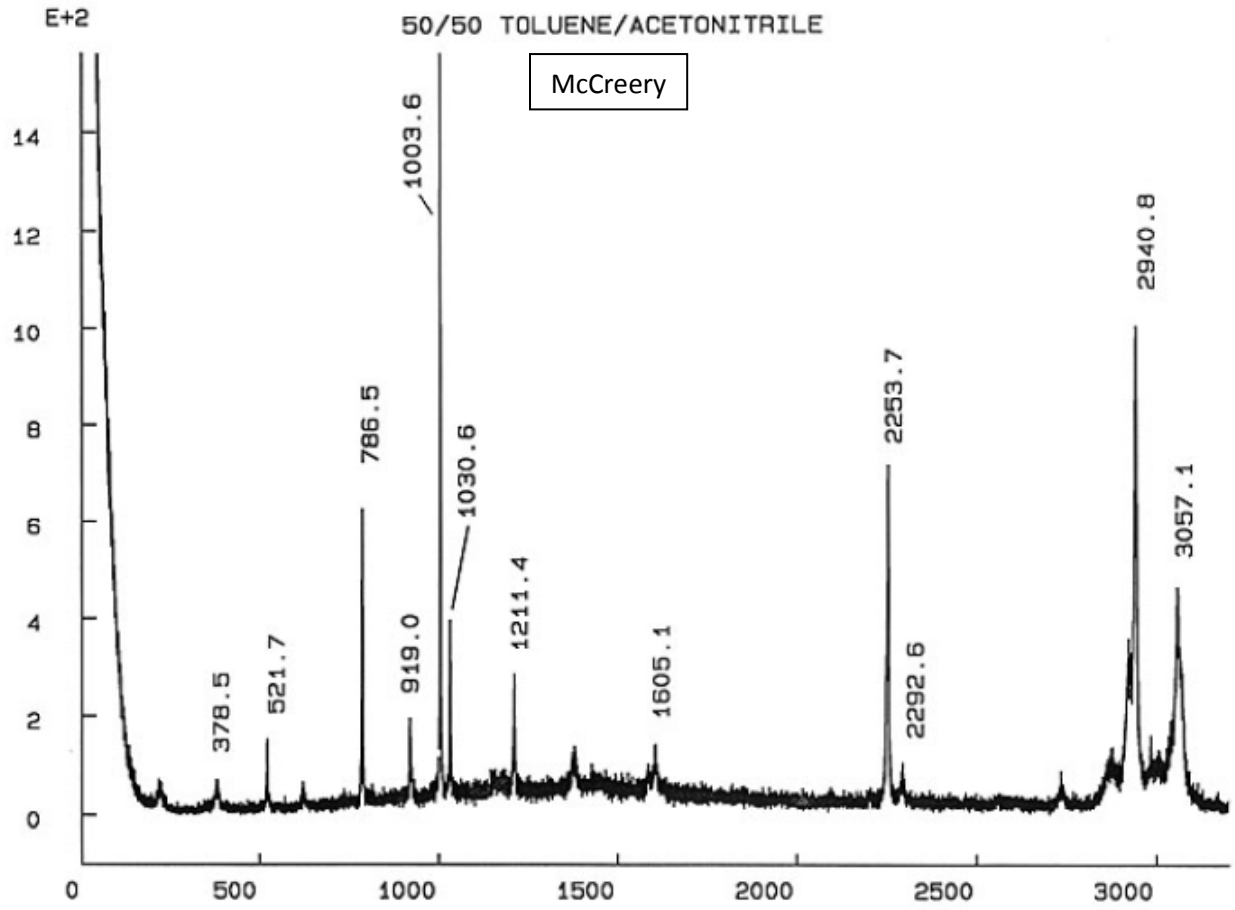

50/50 Toluene: Acetonitrile

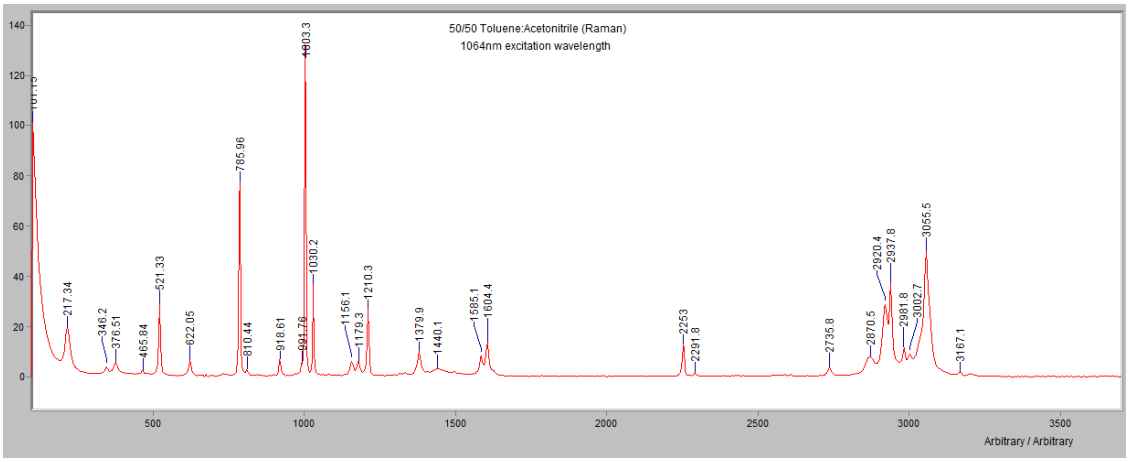

Silicon

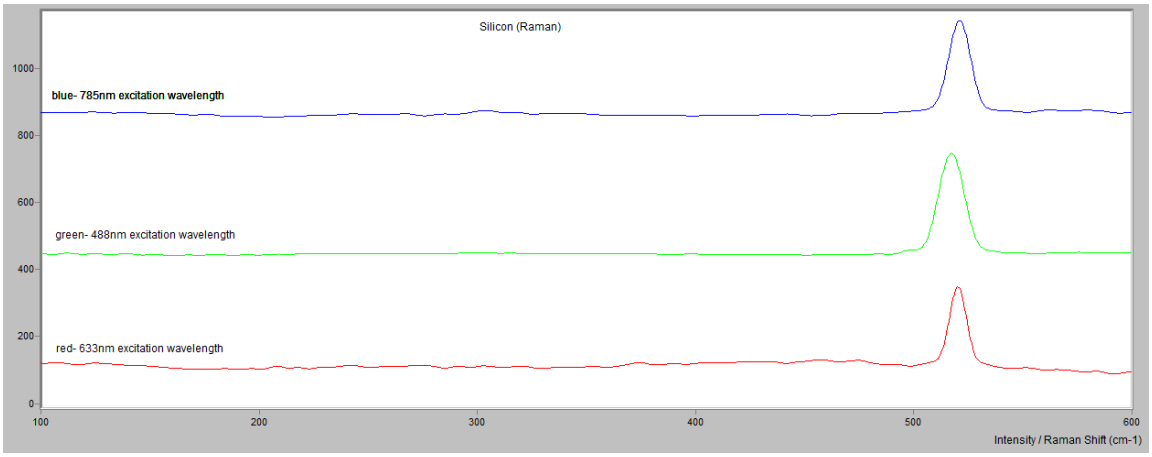
Silicon (Raman)
blue- 785nm excitation wavelength
green- 488nm excitation wavelength
red- 633nm excitation wavelength
1000
800
600
400
200
0
100
200
300
400
500
600
Intensity / Raman Shift (cm-1)

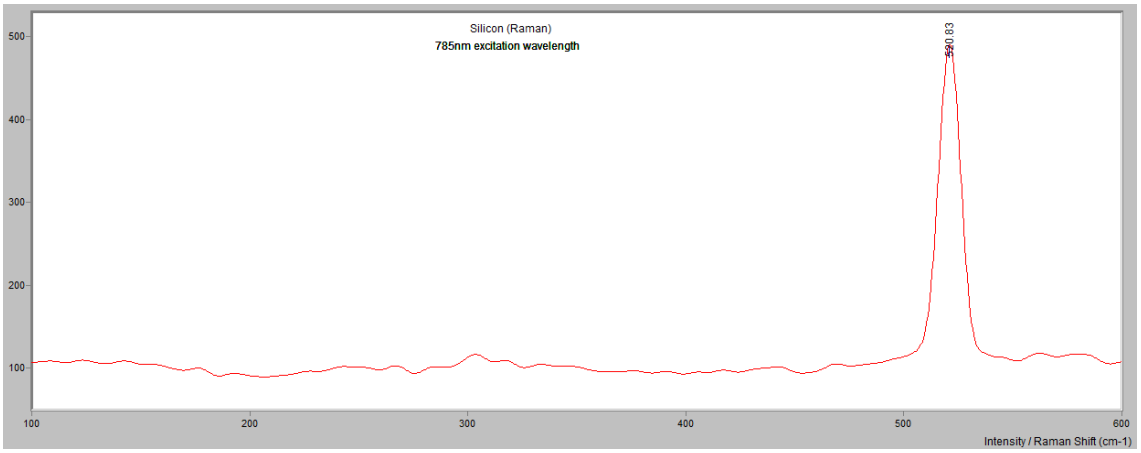
Silicon (Raman)
785nm excitation wavelength
520.83
500
400
300
200
100
100
200
300
400
500
600
Intensity / Raman Shift (cm-1)

Infrared Reference Spectra

Polystyrene- ATR

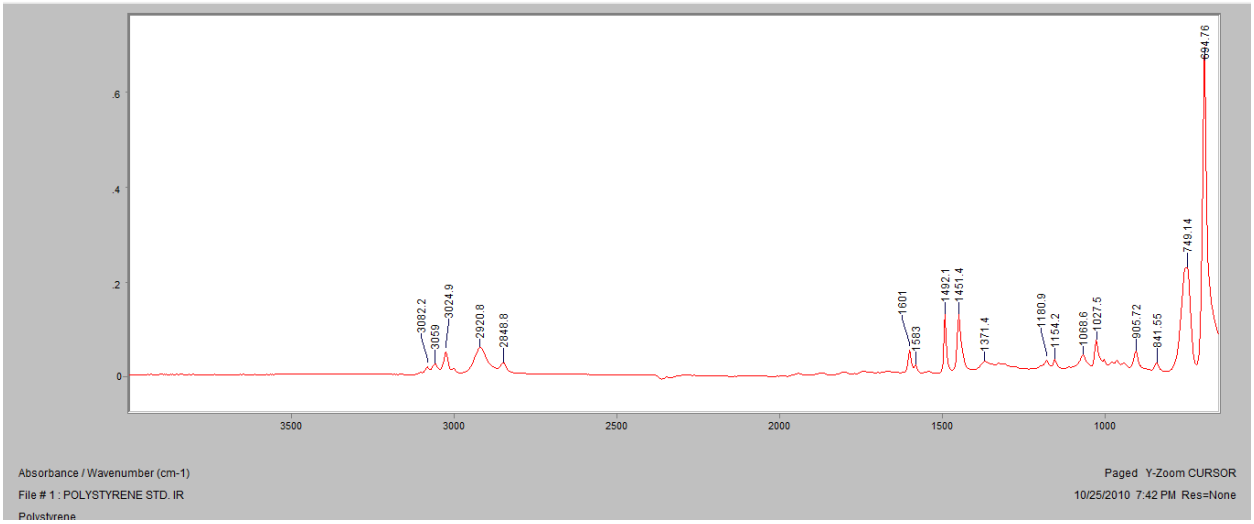

UV-Vis Reference Spectra

Holmium Oxide

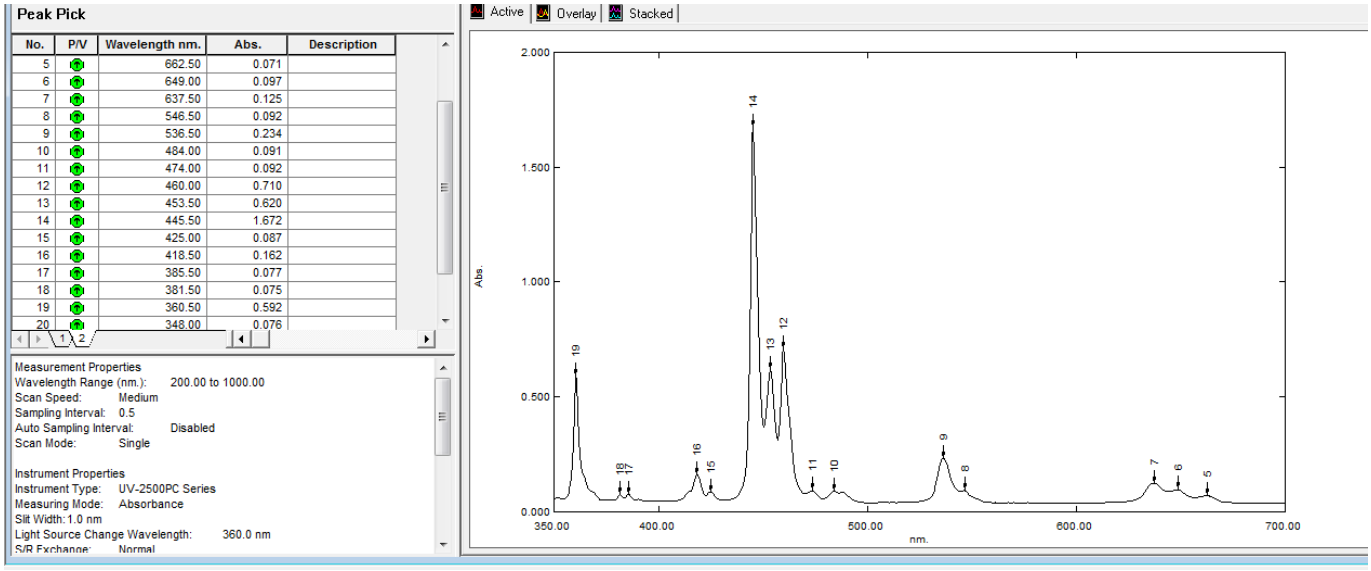

Peak Pick

No.	P/V	Wavelength nm.	Abs.	Description
5		662.50	0.071	
6		649.00	0.097	
7		637.50	0.125	
8		546.50	0.092	
9		536.50	0.234	
10		484.00	0.091	
11		474.00	0.092	
12		460.00	0.710	
13		453.50	0.620	
14		445.50	1.672	
15		425.00	0.087	
16		418.50	0.162	
17		385.50	0.077	
18		381.50	0.075	
19		360.50	0.592	
20		348.00	0.076	

Measurement Properties
Wavelength Range (nm.): 200.00 to 1000.00
Scan Speed: Medium
Sampling Interval: 0.5
Auto Sampling Interval: Disabled
Scan Mode: Single

Instrument Properties
Instrument Type: UV-2500PC Series
Measuring Mode: Absorbance
Slit Width: 1.0 nm
Light Source Change Wavelength: 360.0 nm
S/R Exchange: Normal

Active | Overlay | Stacked

Abs.
2.000
1.500
1.000
0.500
0.000
350.00
400.00
500.00
600.00
700.00
nm.

Didimyum

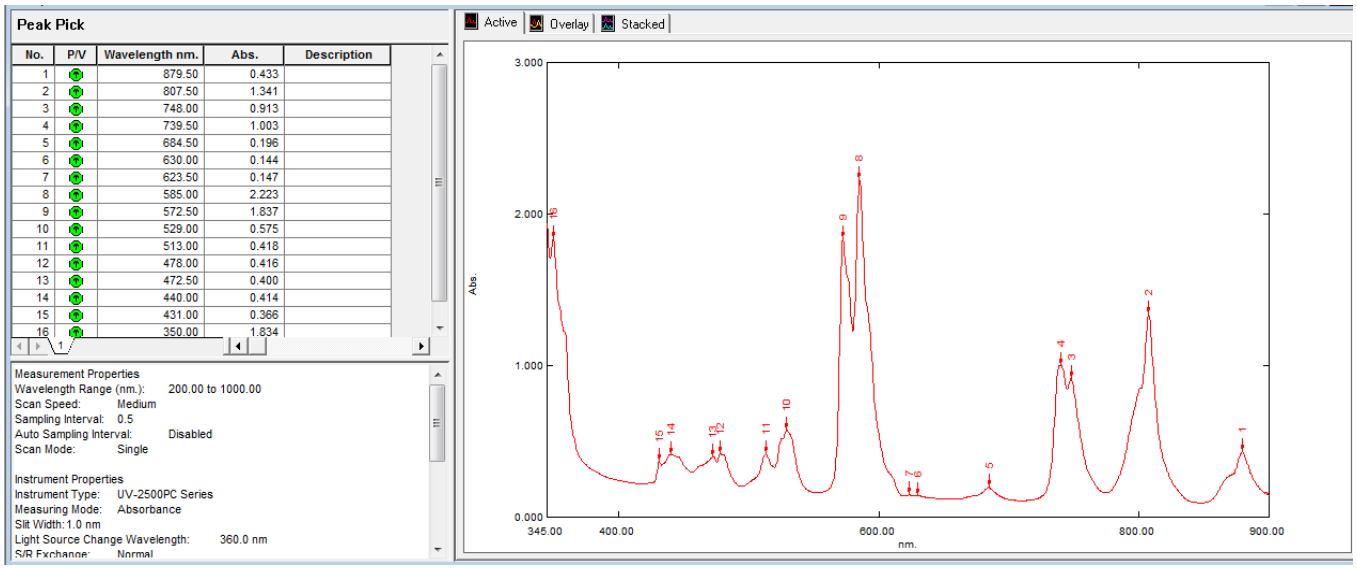

Peak Pick

No.	P/V	Wavelength nm.	Abs.	Description
1		879.50	0.433	
2		807.50	1.341	
3		748.00	0.913	
4		739.50	1.003	
5		684.50	0.196	
6		630.00	0.144	
7		623.50	0.147	
8		585.00	2.223	
9		572.50	1.837	
10		529.00	0.575	
11		513.00	0.418	
12		478.00	0.416	
13		472.50	0.400	
14		440.00	0.414	
15		431.00	0.366	
16		350.00	1.834	

Measurement Properties
Wavelength Range (nm.): 200.00 to 1000.00
Scan Speed: Medium
Sampling Interval: 0.5
Auto Sampling Interval: Disabled
Scan Mode: Single

Instrument Properties
Instrument Type: UV-2500PC Series
Measuring Mode: Absorbance
Slit Width: 1.0 nm
Light Source Change Wavelength: 360.0 nm
S/R Exchange: Normal

Appendix I: Raman Reference Spectra- Pigment Standards

The following tables and spectra from the literature report the pigments and their corresponding Raman shifts. For a more comprehensive file of Raman reference spectra for pigments in addition to experimental conditions, the reader is referred to the publications of Colombini 2010, Scherrer 2009, Schulte 2008, Ropret 2008 and Vandenabeele 2000 (full citations of which can be found in the References section)[7].

7

Relative intensities: vs = very strong; s = strong; m-s = medium to strong; m = medium; m-w = medium to weak; w = weak; vw = very weak; sh = shoulder.

Spectra Reported By Colombini, 2010 (λ_0=785nm):

Colour Index	Raman bands (wavenumber/cm^{-1})
PO34	1600(vs), 1540(m), 1480(m), 1425(m), 1341(w), 1300(m), 1291(m), 1275(s), 1258(m), 1239(m), 1161(m), 1052(m), 1002(w), 916(w), 769(w), 671(w), 542(w), 395(w), 369(w), 294(w)
PO36	1660(m), 1643(m), 1608(vs), 1570(s), 1487(vs), 1391(vs), 1362(m), 1339(m), 1326(m), 1311(m), 1292(s), 1245(vs), 1196(w), 1141(vs), 1113(w), 1063(w), 1011(m), 950(m), 919(w), 876(w), 833(w), 818(w), 740(m), 708(w), 655(m), 626(m), 602(w), 561(m), 479(w), 420(w), 401(m), 358(w), 340(w), 305(w)
PO43	1703(m), 1615(m), 1591(vs), 1547(vs), 1484(w), 1445(m), 1403(vs), 1385(vs), 1344(w), 1315(m), 1283(w), 1250(vs), 1155(m), 1103(w), 1029(m), 1009(m), 875(m), 807(w), 641(w), 550(w), 523(w), 447(w), 399(m), 338(w), 250(w), 213(m)
PO48 & PO49	1671(vs), 1655(ms), 1616(ms), 1591(ms), 1549(s), 1510(w), 1475(w), 1456(m), 1347(vs), 1318(mw), 1270(w), 1203(m), 1150(w), 1075(w), 1020(w), 937(w), 828(ms), 696(m), 645(w), 523(s), 462(vs), 353(w), 283(w), 241(w)
PO59	1676(m), 1602(s), 1535(m), 1423(w), 1359(s), 1336(vs), 1291(w), 1262(s), 1166(w), 1137(w), 1028(w), 836(w), 782(m), 756(w), 717(w), 544(w), 500(w), 448(w), 371(w), 342(w), 310(w), 256(w)
PO61	1673(w), 1592(s), 1493(w), 1445(s), 1403(s), 1307(w), 1237(vs), 1185((m), 1147(s), 1105(s), 1076(w), 939(w), 842(w), 727(m), 682(m), 564(w), 400(w), 291(m), 243(w), 230(w)
PO65	1620(w), 1605(w), 1595(m), 1580(m), 1533(m), 1486(m), 1428(s), 1415(s), 1394(vs), 1370(m), 1346(m), 1285(w), 1262(w), 1236(s), 1193(w), 1164(w), 1114(w), 1050(w), 989(w), 875(w), 773(w), 749(w), 646(w), 585(w), 330(w), 296(w)
PO73	1668(m), 1612(s), 1586(s), 1554(ms), 1523(w), 1448(m), 1408(m), 1352(vs), 1330(m), 1314(ms), 1268(m), 1220(m), 1207(w), 1115(w), 1057(s), 1020(w), 931(s), 749(w), 730(ms), 690(ms), 650(w), 627(ms), 500(m), 358(m), 323(m)
PY1	1672(m), 1622(vs), 1602(s), 1563(s), 1536(s), 1487(vs), 1451(m), 1389(s), 1339(s), 1325(s), 1312(vs), 1257(s), 1218(s), 1195(w), 1179(w), 1170(w), 1139(vs), 1000(s), 952(ms), 925(m), 847(m), 826(m), 786(s), 616(m), 511(w), 460(m), 391(m)
PY3	1674(w), 1614(vs), 1596(vs), 1568(m), 1546(m), 1496(vs), 1445(m), 1388(vs), 1338(vs), 1311(vs), 1276(ms), 1246(s), 1191(m), 1156(m), 1140(vs), 1106(w), 1063(w), 1037(m), 988(vs), 957(m), 825(w), 746(m), 650(ms), 620(m), 461(ms), 452(ms), 410(m), 394(m).
PY16	1673(w), 1633(m), 1592(vs), 1549(ms), 1508(s), 1478(m), 1389(s), 1316(vs), 1276(vs), 1246(m), 1187(w), 1143(m), 1127(m), 1100(w), 1067(ms), 952(m), 940(m), 827(w), 695(m), 661(m), 621(m)
PY24	1663(ms), 1621(m), 1598(s), 1419(m), 1385(vs), 1354(w), 1261(m), 1185(s), 1159(m), 1010(w), 528(m), 456(m), 275(w)
PY74	1673(w), 1596(s), 1516(m), 1403(ms), 1355(s), 1330(vs), 1301(w), 1266(s), 1163(w), 1092(m), 1067(w), 804(m), 647(w), 400(w), 362(w)
PY83	1671(w), 1622(s), 1599(m), 1560(w), 1535(w), 1486(s), 1450(w), 1390(m), 1339(w), 1310(m), 1256(m), 1217(m), 1196(w), 1180(w), 1140(s), 1000(s), 988(s), 952(ms), 926(m), 826(m), 787(s), 616(m), 595(w), 512(m), 461(m), 391(m)
PY109	1671(vs), 1575(m), 1454(w), 1369(m), 1311(m), 1244(s), 1205(m), 1095(w), 1061(w), 820(w), 762(m), 724(m), 623(m), 370(w), 352(w)
PY129	1601(m), 1569(m), 1535(m), 1484(m), 1424(m), 1387(s), 1339(w), 1270(m), 1213(m), 1177(w), 1154(m), 1111(w), 1030(w), 978(w), 939(w), 880(w), 848(w), 604(w), 444(w).
PY138	1787(w), 1672(w), 1486(m), 1462(w), 1418(s), 1371(s), 1353(m), 1282(m), 1188(w), 966(m), 770(w), 655(w), 620(w), 585(w), 525(w), 352(w), 327(w)
PY139	1665(w), 1588(m), 1564(vs), 1381(m), 1259(w), 1246(w), 1185(w), 1141(w), 695(m), 605(m), 294(m), 246-237(ms)
PY151	1715(w), 1653(m), 1628(w), 1603(m), 1582(s), 1516(m), 1497(m), 1455(m), 1388(s), 1320(m), 1292(m), 1273(w), 1249(m), 1202(m), 1145(s), 1070(m), 1044(m), 1023(m), 957(m), 908(w), 876(w), 846(w), 794(w), 703(w), 615(m), 586(w), 475(w), 385(m), 311(w), 225(w), 198(m)
PY154	1660(w), 1615(s), 1589(s), 1503(vs), 1474(m), 1403(s), 1365(ms), 1323(ms), 1298(s), 1266(s), 1160(m), 1134(m), 1070(m), 1038(m), 1006(m), 955(m), 916(w), 878(w), 772(m), 705(w), 612(w), 567(w), 516(w), 480(m), 400(w), 355(m), 285(w)
PY173	1634(m), 1570(m), 1551(m), 1493(m), 1458(m), 1423(w), 1391(vs), 1298(m), 1243(m), 1080(w), 958(w), 903(w), 725(w), 580(m), 375(m)
Fluorescent orange, Sennelier	1590(s), 1550(s), 1511(w), 1428(w), 1363(s), 1233(m), 1204(m), 1158(s), 1094(w), 1049(w), 982(m), 797(w), 773(m), 691(w), 637(m), 289(w)
Fluorescent orange, Kremer	1602(ms), 1551(m), 1509(m), 1429(m), 1381(m), 1368(m), 1310(w), 1234(w), 1205(w), 1153(vs), 1096(m), 1048(w), 977(ms), 798(s), 775(w), 692(m), 660(w), 637(s), 615(w), 544(w), 291(s)
Fluorescent Lumogen orange, Kremer	1711(m), 1596(s), 1573(ms), 1455(m), 1378(s), 1298(vs), 1064(m), 548(m), 451(w), 391(w)
Fluorescent yellow, Sennelier	1697(w), 1599(m), 1587(m), 1383(m), 1366(m), 1156(s), 1094(w), 1049(m), 980(m), 797(m), 691(w), 636(m), 543(w), 291(w)
Fluorescent yellow, Kremer	1695(w), 1602(s), 1548(ms), 1432(m), 1384(m), 1234(m), 1208(m), 1157(vs), 1099(m), 1051(m), 977(ms), 916(w), 801(s), 689(m), 637(ms), 544(m), 474(w), 410(w), 298(ms)
Fluorescent Lumogen yellow, Kremer	1586(vs), 1573(vs), 1525(w), 1464(w), 1355(s), 1314(s), 1301(s), 1227(m), 1125(w), 1083(m), 599(w), 519(m)

Spectra Reported By Scherrer, 2009:

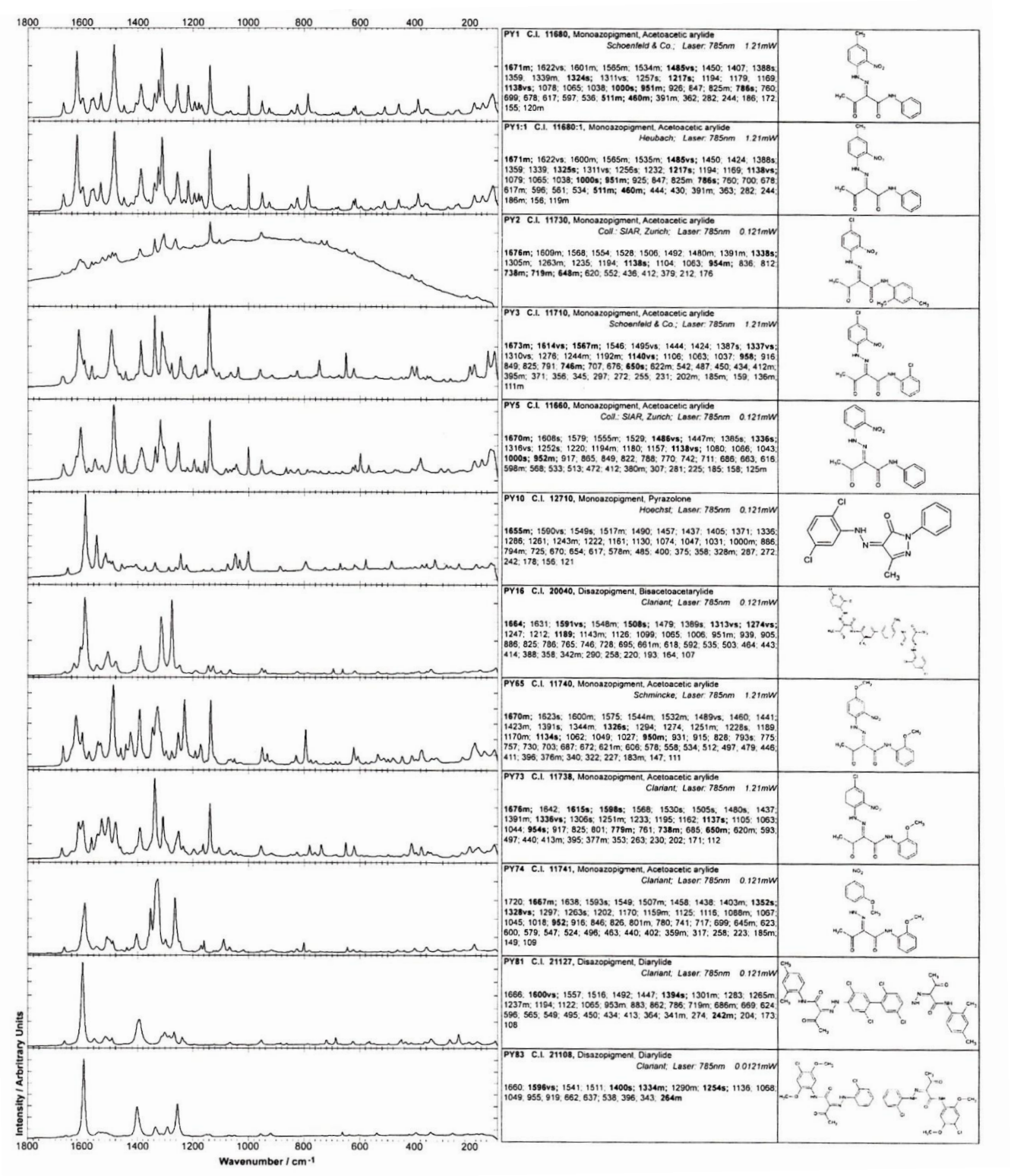

PY1 C.I. 11680, Monoazopigment, Acetoacetic arylide
Schoenfeld & Co.; Laser: 785nm 1.21mW

1671m; 1622vs; 1601m; 1585m; 1534m; **1485vs;** 1450; 1407; 1388s; 1359; 1339m; **1324s;** 1311vs; 1257s; **1217s;** 1194; 1179; 1169; **1138vs;** 1078; 1065; 1038; **1000s; 951m;** 926; 847; 825m; **786s;** 760; 699; 678; 617; 597; 536; **511m; 460m;** 391m; 362; 282; 244; 186; 172; 155; 120m

PY1:1 C.I. 11680:1, Monoazopigment, Acetoacetic arylide
Heubach; Laser: 785nm 1.21mW

1671m; 1622vs; 1600m; 1585m; 1535m; **1485vs;** 1450; 1424; 1388s; 1359; 1339; **1325s;** 1311vs; 1256s; 1232; **1217s;** 1194; 1169; **1138vs;** 1079; 1065; 1038; **1000s; 951m;** 925; 847; 825m; **786s;** 760; 700; 678; 617m; 596; 561; 534; **511m; 460m;** 444; 430; 391m; 363; 282; 244; 186m; 158; 119m

PY2 C.I. 11730, Monoazopigment, Acetoacetic arylide
Coll.: SIAR, Zurich; Laser: 785nm 0.121mW

1676m; 1609m; 1568; 1554; 1528; 1506; 1492; 1480m; 1391m; **1338s;** 1305m; 1263m; 1235; 1194; **1138s;** 1104; 1063; **954m;** 836; 812; **738m; 719m; 648m;** 620; 552; 436; 412; 379; 212; 176

PY3 C.I. 11710, Monoazopigment, Acetoacetic arylide
Schoenfeld & Co.; Laser: 785nm 1.21mW

1673m; 1614vs; 1567m; 1546; 1495vs; 1444; 1424; 1387s; **1337vs;** 1310vs; 1276; 1244m; 1192m; **1140vs;** 1106; 1063; 1037; **958;** 916; 849; 825; 791; **746m;** 707; 676; **650s;** 622m; 542; 487; 450; 434; 412m; 395m; 371; 356; 345; 297; 272; 255; 231; 202m; 185m; 159; 136m; 111m

PY5 C.I. 11660, Monoazopigment, Acetoacetic arylide
Coll.: SIAR, Zurich; Laser: 785nm 0.121mW

1670m; 1608s; 1579; 1555m; 1529; **1486vs;** 1447m; 1385s; **1336s;** 1316vs; 1252s; 1220; 1194m; 1180; 1157; **1138vs;** 1080; 1066; 1043; **1000s; 952m;** 917; 865; 849; 822; 788; 770; 742; 711; 686; 663; 616; 598m; 568; 533; 513; 472; 412; 380m; 307; 281; 225; 185; 158; 125m

PY10 C.I. 12710, Monoazopigment, Pyrazolone
Hoechst; Laser: 785nm 0.121mW

1655m; 1590vs; 1549s; 1517m; 1490; 1457; 1437; 1405; 1371; 1336; 1286; 1261; 1243m; 1222; 1161; 1130; 1074; 1047; 1031; 1000m; 886; 794m; 725; 670; 654; 617; 578m; 485; 400; 375; 358; 328m; 287; 272; 242; 178; 156; 121

PY16 C.I. 20040, Disazopigment, Bisacetoacetarylide
Clariant; Laser: 785nm 0.121mW

1664; 1631; **1591vs;** 1548m; **1508s;** 1479; 1389s; **1313vs; 1274vs;** 1247; 1212; **1189;** 1143m; 1126; 1099; 1065; 1006; 951m; 939; 905; 886; 825; 786; 765; 746; 728; 695; 661m; 618; 592; 535; 503; 464; 443; 414; 388; 358; 342m; 290; 258; 220; 193; 164; 107

PY65 C.I. 11740, Monoazopigment, Acetoacetic arylide
Schmincke; Laser: 785nm 1.21mW

1670m; 1623s; 1600m; 1575; 1544m; 1532m; 1489vs; 1460; 1441; 1423m; 1391s; 1344m; **1326s;** 1294; 1274; 1251m; 1228s; 1189; 1170m; **1134s;** 1062; 1049; 1027; **950m;** 931; 915; 828; 793s; 775; 757; 730; 703; 687; 672; 621m; 606; 578; 558; 534; 512; 497; 479; 446; 411; 396; 376m; 340; 322; 227; 183m; 147; 111

PY73 C.I. 11738, Monoazopigment, Acetoacetic arylide
Clariant; Laser: 785nm 1.21mW

1676m; 1642; **1615s; 1598s;** 1568; 1530s; 1505s; 1480s; 1437; 1391m; **1336vs;** 1306s; 1251m; 1233; 1195; 1162; **1137s;** 1105; 1063; 1044; **954s;** 917; 825; 801; **779m;** 761; **738m;** 685; **650m;** 620m; 593; 497; 440; 413m; 395; 377m; 353; 263; 230; 202; 171; 112

PY74 C.I. 11741, Monoazopigment, Acetoacetic arylide
Clariant; Laser: 785nm 0.121mW

1720; **1667m;** 1638; 1593s; 1549; 1507m; 1458; 1438; 1403m; **1352s; 1328vs;** 1297; 1263s; 1202; 1170; 1159m; 1125; 1116; 1088m; 1067; 1045; 1018; **952;** 916; 846; 826; 801m; 780; 741; 717; 699; 645m; 623; 600; 579; 547; 524; 496; 463; 440; 402; 359m; 317; 258; 223; 185m; 149; 109

PY81 C.I. 21127, Disazopigment, Diarylide
Clariant; Laser: 785nm 0.121mW

1666; **1600vs;** 1557; 1516; 1492; 1447; **1394s;** 1301m; 1283; 1265m; 1237m; 1194; 1122; 1065; 953m; 883; 862; 786; 719m; 686m; 669; 624; 596; 565; 549; 495; 450; 434; 413; 364; 341m; 274; **242m;** 204; 173; 108

PY83 C.I. 21108, Disazopigment, Diarylide
Clariant; Laser: 785nm 0.0121mW

1660; **1596vs;** 1541; 1511; **1400s; 1334m;** 1290m; **1254s;** 1136; 1068; 1049; 955; 919; 662; 637; 538; 396; 343; **264m**

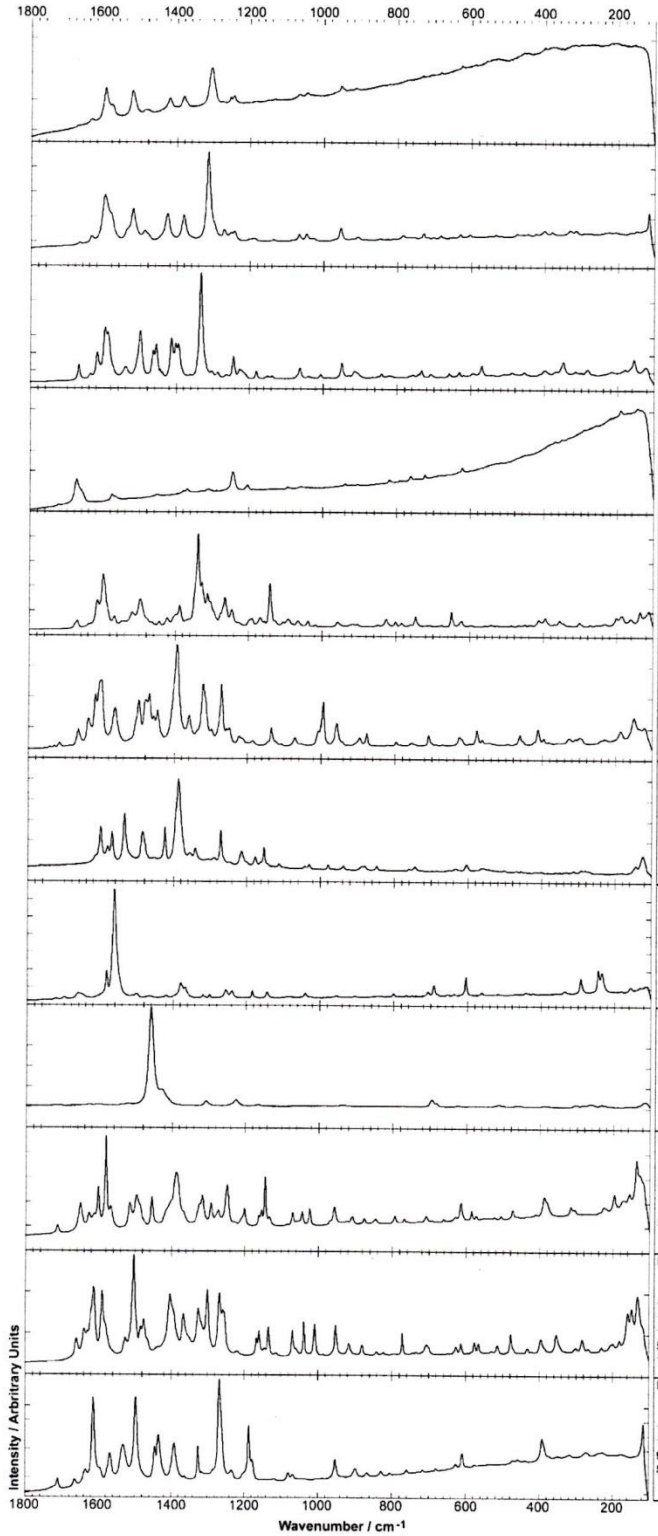

PY93 C.I. 20710, Disazopigment, Condensation
Heubach; Laser: 785nm 0.0121mW

1634; **1596s; 1521s;** 1484; 1420m; **1381m; 1305s;** 1244m; 1067w; 1045w; 952m

PY95 C.I. 20034, Disazopigment, Condensation
Heubach; Laser: 785nm 0.121mW

1667; 1634; **1596s; 1520s;** 1486m; 1426s; **1381s; 1313vs; 1269m;** 1241; 1189; 1135; 1066m; 1045; 1026; 953m; 907; 886; 848; 785; 754; 729; 702; 682; 650; 630; 604; 551; 533; 475; 459; 445; 424; 401; 381; 331; 315; 291; 274; 231; 206; 165; 149; 115m

PY97 C.I. 11767, Monoazopigment, Acetoacetic arylide
Clariant; Laser: 785nm 1.21mW

1668m; 1636; 1617m; 1591s; 1539m; **1499s;** 1455s; 1413s; 1394; **1332vs;** 1301; 1286; 1263; 1243m; 1222; 1180; 1137; 1062m; 1038; 1006; **949m;** 912; 841; 757; 733; 707; 658; 631; 595; 570m; 487; 454; 399; 349m; 315; 282; 216; 179; 155m; 121;

PY109 C.I. 56284, Isoindolinone, Azomethine type
Kremer; Laser: 785nm 0.0121mW

1721; **1672s;** 1575m; 1452; 1368, 1310; **1243s;** 1204m; 1094; 1060; 938; 904; 818; 791; 761; 723; 622; 370; 352; 190; 143

PY111 C.I. 11745, Monoazopigment, Acetoacetic arylide
Clariant; Laser: 785nm 0.121mW

1670m; 1614m; 1596s; 1567; 1546, 1519; 1495m; 1443; 1422; 1387m; **1337vs;** 1310m; 1263m; 1244; 1192; 1167; **1140s;** 1091; 1065; 1037; 1016; **957;** 917; 904; 849; 825; 801; 784; **746;** 708; 675; **649m;** 623; 596, 543; 487; 467; 449; 434; 412; 395m; 355; 301; 272; 234; 201; 185m; 161; 136m

PY120 C.I. 11783, Monoazopigment, Benzimidazolone
Clariant; Laser: 785nm 1.21mW

2590; 1741, 1730; 1715; **1664m;** 1637m; 1603s, 1563s; 1498s, 1469s; 1445m; 1394vs; 1358m; 1319s; 1270s; 1248; 1220; 1184; 1134m; 1107; 1070; 994s; **957m;** 895; 876; 819; 796; 753; **708;** 671; 624; 578m; 563; 544; 494; 461; 412m; 396; 383; 327; 296; 231; 187; 150m

PY129 C.I. 48042, Metal complex, Azomethine metal complex
Kremer; Laser: 785nm 0.0121mW

1601s; 1581; 1569m; 1535s; 1484s; 1424s; **1387vs;** 1355, 1339; 1289; 1270s; 1213; 1176; 1152n; 1111; 1029; 978; 937; 878; 847; 742; 633; 604; 313; 293; 143; 123m

PY139 C.I. 56298, Isoindoline, Methine type
Kremer; Laser: 785nm 0.00605mW

1699; 1658; 1582m; **1561vs;** 1500; 1419, 1379m, 1366; 1317; 1299; 1255; 1238; 1182, 1142; 1039; 954; 801; 765; 707; 690; 654; 637; 604m; 561; 468; 441; 336; 292m; **245m; 234m;** 181; 156

PY150 C.I. 12764, Metal complex, Azo metal complex
Kremer; Laser: 785nm 0.0121mW

1459vs; 1306m; 1224m; 1165w; 935w; **694m;** 624, 514w; 387; 305; 262; 230; 114m

PY151 C.I. 13980, Monoazopigment, Benzimidazolone
Kremer; Laser: 785nm 1.21mW

2938; 1713; **1651m;** 1627; **1602m; 1581vs;** 1515m, 1495m, 1454m; 1387s; 1315m; 1291m; 1272; 1248s; 1200m; 1144s; 1070m, **1043m;** 1023m; **956m;** 923; 908; 875; 845; 792; 768; **708;** 660; 614m; 586; 573; 553; 524; 506; 474; 411; 387m; 315; 225; 197m; 174; 156; 130m

PY154 C.I. 11781, Monoazopigment, Benzimidazolone
Kremer; Laser: 785nm 1.21mW

1660m; 1640m; **1613s; 1589s;** 1527; 1503vs; 1475m; 1402s, 1365m, 1324m; 1300s, 1266s; 1219; 1159m; 1133m; 1113; 1068m; **1037m;** 1008m; 984; **951m;** 915; 880; 840; 822; 793; 771m; 734; **704;** 626; 612; 576, 565; 530; 514; 478m; 432, 395m; 353m, 301; 283; 266; 230; 202; 181; 159s; 147s, 130s

PY155 C.I. 200310, Disazopigment, Bisacetoacetarylide
Clariant; Laser: 785nm 1.21mW

1711; 1664; 1636, **1613vs;** 1567m; **1531m;** 1496vs; **1433s; 1391s;** 1325m; **1266vs;** 1233; **1186s;** 1139; 1118, 1079; 1067; 1037; 1002; 987; 952m; 898; 866; 828; 805, 792; 759, 727; 715; 680; 626; 609m; 575, 518; 472; 457; 437; **391m;** 349; 317; 272; 231; 173; 116m

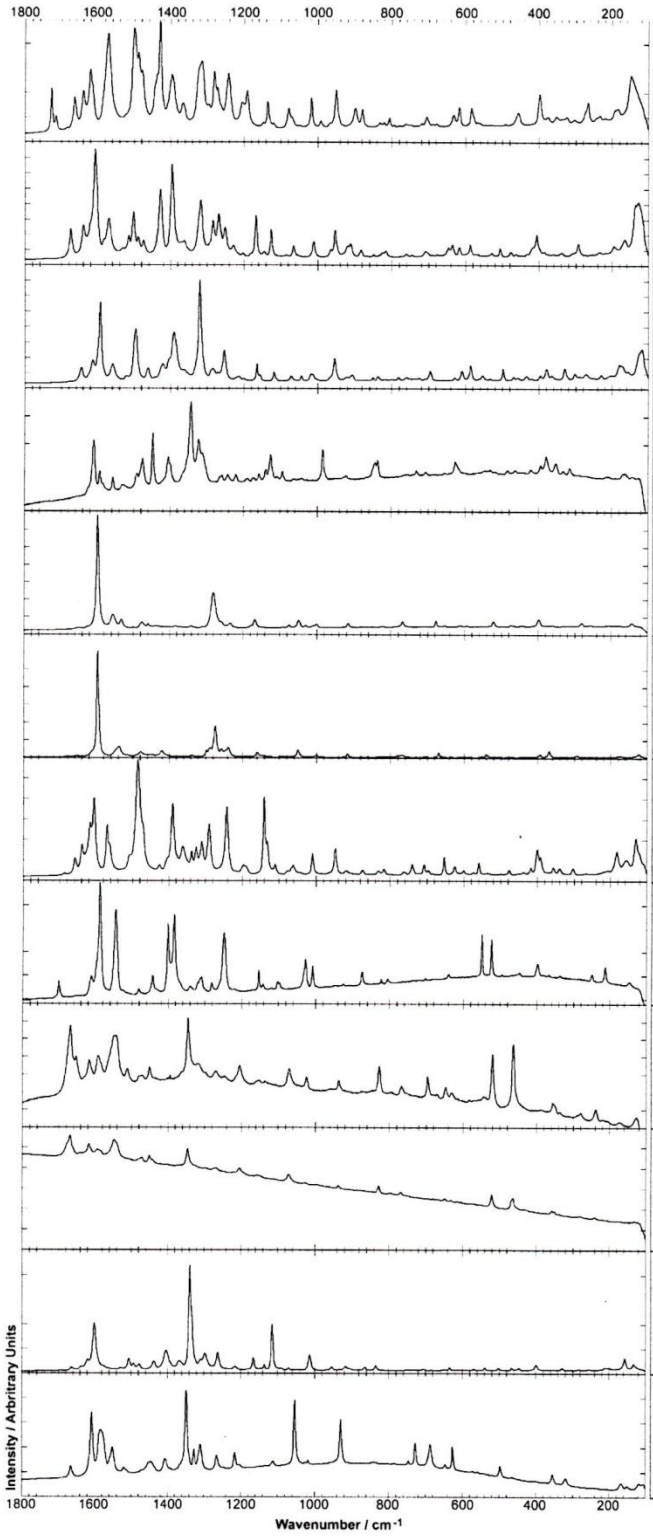

PY175 C.I. 11784, Monoazopigment, Benzimidazolone
Clariant; Laser: 785nm 0.121mW

1727s; 1715; **1663m**; 1640m; 1619s; 1571vs; 1498vs; **1429vs**; 1395m; 1364; 1317s; 1279m; 1241m; 1205; 1190m; 1135m; 1078m; 1016m; 991; **950m**; 898; 878; 831; 820; 805; 760; **705**; 677; 633; 616m; 583m; 456; 398m; 376; 352; 324; 303; 266m; 234; 188; 143s

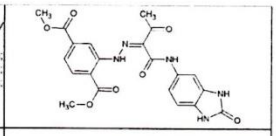

PY181 C.I. 11777, Monoazopigment, Benzimidazolone
Clariant; Laser: 785nm 1.21mW

1674m; **1640m**; 1607vs; 1569m; 1502m; 1474; **1428s**; 1395vs, 1361; 1317s; 1284m; 1267m; 1250m; 1227; 1202; **1167m**; 1144; 1126m; 1065; 1010; **952m**; 911; 882; 848; 815; 760; 744; **707**; 676; 636; 616; 587; 528; 505; 477; 462; 406m; 338; 293m; 235; 194; 165; 129s

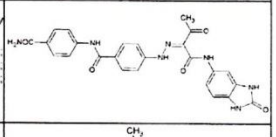

PY194 C.I. 11785, Monoazopigment, Benzimidazolone
Clariant; Laser: 785nm 1.21mW

1645m; 1614m; 1593vs, 1559; 1522; 1496s, 1462; 1422; 1389s; **1319vs**; 1285; 1253m; 1214; 1164m; 1118; 1071; **1043**; 1015; **954m**; 907; 874; 850; 836; 817; 800; 781; 760; 724; **695**; 629; 610; 586m; 553; 532; 497m; 469; 457; 434; 419; 396; 379; 364; 329m; 302; 271; 229; 176m; 154; 121m

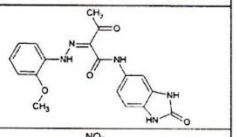

PO5 C.I. 12075, Monoazopigment, B-Naphthol
Clariant; Laser: 785nm 0.0121mW

1610s; 1593; 1557; 1530; 1476m; **1447s**; 1404m; **1343vs**; **1321s**; 1260; 1242; 1220; 1190; 1173; 1157; 1126m; 1093; 1042; **985s**; 922; 836m; 732; 706; 626m; 531; 484; 463; 421; 395; 379m; 352; 332; 314; 209; 166

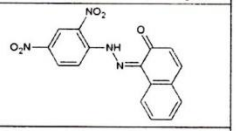

PO13 C.I. 21110, Disazopigment, Pyrazolone
Clariant; Laser: 785nm 0.0121mW

1598vs; **1555m**; 1532; 1476; 1459; 1437; 1384; 1340; **1280s**; 1234; 1167m; 1074; 1048; 1029; 1000; 914; 767m; 677; 653; 612; **521**; 473; 398m; 281; 256; 141

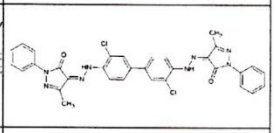

PO34 C.I. 21115, Disazopigment, Pyrazolone
Clariant; Laser: 785nm 0.0121mW

1653; **1597vs**; 1538m; 1478; 1446; 1420; 1374; 1337; 1298; 1289; **1273s**; 1257; 1238; 1189; 1160; 1138; 1091; 1049m; 1000; 916; 805; 781; 768; 706; 669; 636; 602; 587; 553; 539; 446; 429; 393; **369m**; 331; 292; 272; 253; 175; 123

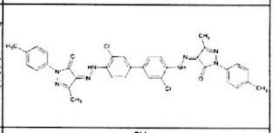

PO36 C.I. 11780, Monoazopigment, Benzimidazolone
Heubach; Laser: 785nm 1.21mW

1687; 1657; 1639m; **1617s**; 1606s; 1570s; 1485vs; 1426; **1390s**; 1361m; 1337; 1325; 1309m; 1290s; **1242s**; 1193; **1140s**; 1110; 1077; 1061; **1009m**; **948m**; 917; 874; 830; 816; 762; 740; 707; 695; 683; 653m; 625; 600; 574; 559; 535; 476; 437; 418; 401m; 390; 356; 339; 302; 267; 207; 182m; 156; 129m

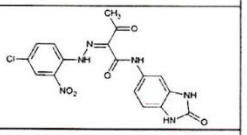

PO43 C.I. 71105, Polycyclic pigment, Perinone
Clariant; Laser: 785nm 0.121mW

1701m; 1612; 1588vs; **1545vs**; 1481; 1442m; **1401s**; **1384vs**; 1339; 1310; 1281; **1248s**; 1153m; 1118; 1102; 1027m; 1007m; 924; 873; 822; 805; 702; 640; **550s**; 523s; 446; 398; 367; 338; 283; 249; **212m**

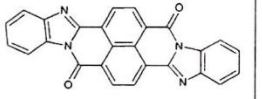

PO48 C.I. 73900, Polycyclic pigment, Quinacridone
Kremer; Laser: 785nm 0.121mW

1669vs; 1616m, 1592m; **1546s**; 1511; 1478; 1450; 1344vs; 1268; 1204m; 1151; **1070m**; 1023; 987; 936; **826m**; 789; 766; **695m**; 646; 589; 583; **519s**; **463vs**; 387; 353; 280; **238m**; 172; 125

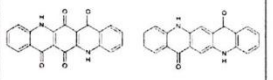

PO49 C.I. 564800, Polycyclic pigment, Quinacridone
Kremer; Laser: 633nm 1.03mW

1669s; 1617m; 1590; **1545s**; 1473; 1450; 1345s; 1294; 1268; 1204; 1153; **1070m**; 1025; 936; **827m**; 795; 767; 648; 632; **520m**; **465m**; 356; 280; **239m**

PO62 C.I. 11775, Monoazopigment, Benzimidazolone
Heubach; Laser: 785nm 0.0605mW

1692; 1663; **1601s**; 1528; 1506; 1492; 1478; 1437; 1403m; 1367; **1338vs**; 1297; 1262m; 1215; 1166; 1136; 1115s; 1070; **1013m**; **953**; 915; 864; 834; 750; 735; 705; 684; 635; 590; 569; 538; 501; 466; 446; 399; 328; 305; 283; 256; 211; 200; 157m; 132

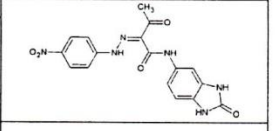

PO73 C.I. 561170, Polycyclic p., Diketopyrrolo-Pyrrole (DPP)
Kremer; Laser: 785nm 0.121mW

1665m; 1608vs; 1582s; **1551m**; 1519; 1447; 1406; 1348vs; 1327; 1309m; 1265; 1216; 1134; 1112; **1053vs**; 1017; **929s**; 839; 783; 746; **727m**; **687m**; 647; **626m**; 571; 559; 497; 463; 403; 354; 319; 241; 166; 150; 118

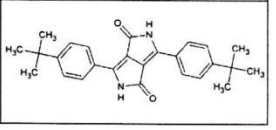

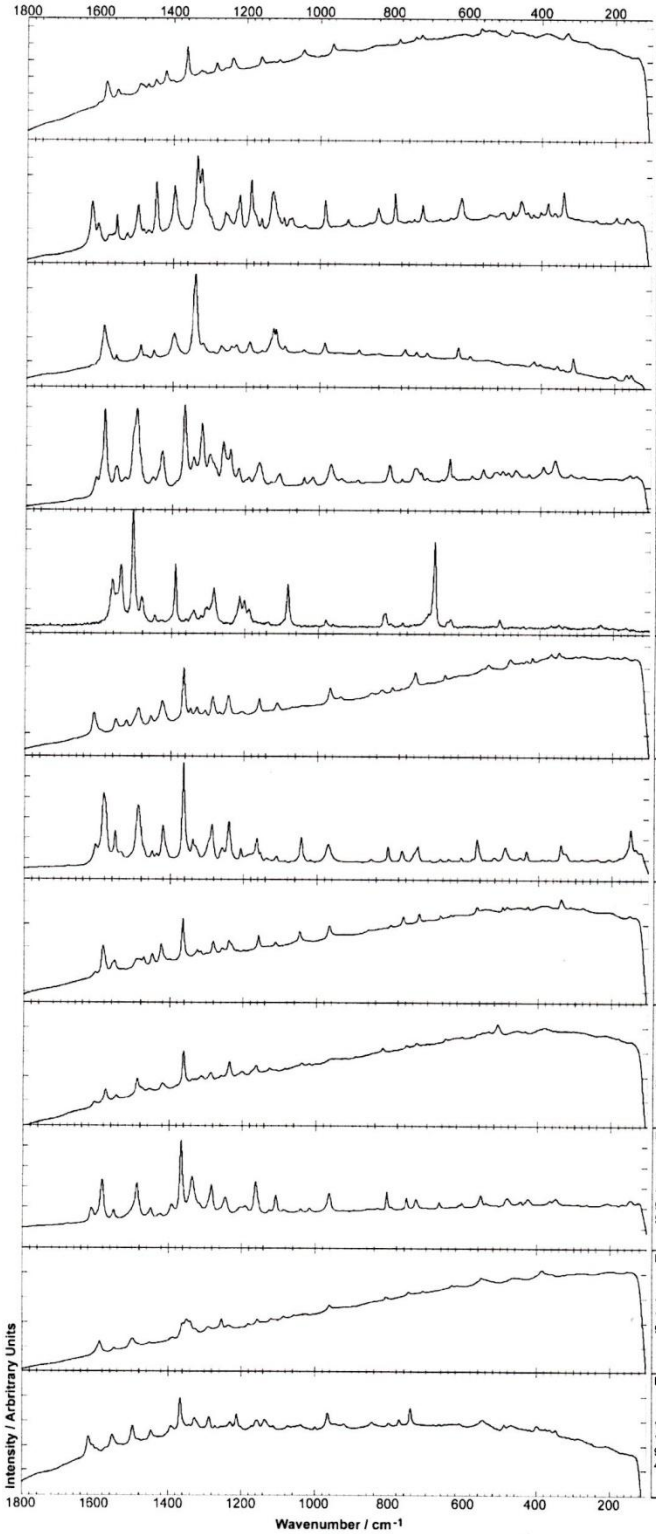

PR2 C.I. 12310, Monoazopigment, Naphthol AS
Coll.: SIAR, Zurich; Laser: 785nm 0.0121mW

1583s; **1553m; 1491m;** 1470; 1448; **1421m; 1362vs;** 1323; **1281m;** 1236m; **1159m;** 1111; 1045m; 966m; **786m;** 742; 725; 566; 484; 385; 332

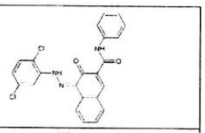

PR3 C.I. 12120, Monoazopigment, B-Naphthol
Clariant; Laser: 785nm 0.121mW

1621s; 1554m; 1526; 1496m; 1470; 1445vs; 1395s; **1333vs;** 1256; **1217s;** 1186s; 1127; 1076; 1057; 1040; 985s; 924; 842m; 797s; 759; 723m; 676; **617m;** 542; 504; 455m; 383m; 340s; 253; 225; 196; 166

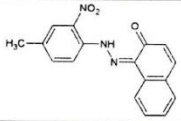

PR4 C.I. 12085, Monoazopigment, B-Naphthol
Hoechst; Laser: 785nm 0.121mW

1587s; 1554; 1487m; 1451; 1396m; **1338vs;** 1288; 1266; 1239; **1224;** 1189; 1156; 1124m; 1093; 1041; 986m; 942; 893; 838; 769; 737; 709; 654; **624m;** 593; 514; 466; 420; 403; 356; 340; 313m; 208; 167

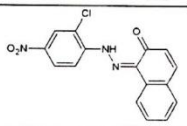

PR5 C.I. 12490, Monoazopigment, Naphthol AS
Heubach; Laser: 785nm 0.121mW

1585vs; **1553m;** 1530; **1498vs;** 1453; **1427m; 1365vs;** 1341m; Pigment Red **1295m;** 1259s; 1239m; 1217; 1190; **1161m;** 1107; 1040; 1016; 967m; 938; 894; 809m; 775; 737; 707; **646m;** 586; 556; 523; 503; 487; 467; 431; 393m; 360m; 318; 283; 215; 157

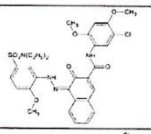

PR7 C.I. 12420, Monoazopigment, Naphthol AS
Kremer; Laser: 785nm 0.0121mW

1601m; 1574s; **1550m; 1481vs;** 1409; **1361vs;** 1329; 1310; **1278s;** 1239s; 1202; **1161s; 1122m;** 1089; 1039; 964m; 842; 760; 728m; 669; 604m; 554m; **497m;** 443; 407; 379; 302

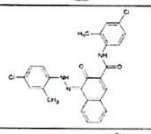

PR8 C.I. 12335, Monoazopigment, Naphthol AS
Schoenfeld & Co.; Laser: 785nm 0.0121mW

1610m; **1550m;** 1521; **1488m;** 1454; **1423m; 1364vs;** 1345; 1327; 1304; **1284m;** 1265; 1241m; 1205; **1158m;** 1109; 965m; 937; 854; 826; 798; 736m; 655; **539m;** 480; 435; 419; 368; 347; 283; 214; 166

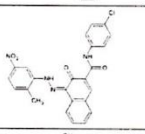

PR9 C.I. 12460, Monoazopigment, Naphthol AS
Kremer; Laser: 785nm 0.121mW

1681; 1605; 1580vs; **1551m;** 1533; **1487s;** 1449; 1437; **1419m; 1363vs;** 1337m; **1285m;** 1258; 1238m; 1206; **1163m;** 1136; 1109; 1086; **1042s;** 1017; 969m; 894; 854; 808m; 770m; 728m; 695; 666; 644; 610; **567s;** 520; 491m; 450; 433; 389; 372; 339m; 301; 282; 255; 240; 209; **148s**

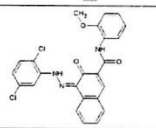

PR10 C.I. 12440, Monoazopigment, Naphthol AS
Coll.: SIAR, Zurich; Laser: 785nm 0.00605mW

1605; 1583s; **1553m; 1491m;** 1471; 1448m; **1423s; 1364vs;** 1325; 1314; **1280m;** 1257; 1236m; **1157m;** 1111; 1045m; 965m; 799; **766m; 722m;** 665; 567; 497; 485; 428; 338m; 278; 157

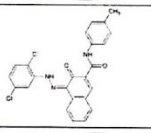

PR11 C.I. 12430, Monoazopigment, Naphthol AS
Hoechst; Laser: 785nm 0.0121mW

1605; 1573m; **1545m; 1486m;** 1453; 1417; **1359vs;** 1311; **1285m;** 1234m; 1200; **1162m;** 1125; 1038; 1018; 819; 754; 727; 650; 605; 533; **509m;** 435; 386

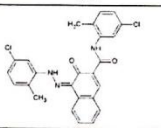

PR12 C.I. 12385, Monoazopigment, Naphthol AS
Schoenfeld & Co.; Laser: 785nm 0.121mW

1677; 1611; 1582s; **1550m; 1486s;** 1448; 1423; 1391; **1365vs; 1335s; 1282s;** 1244m; 1204; 1188; **1161s;** 1125; **1106m;** 1084; 1039; 1015; 962m; 923; 894; 856; 830; 806m; 753; 727; 700; 665; 604; 554m; 537; 512; **481m;** 445; 425; 365; 349; 317; 289; 264; 210; 167; 145

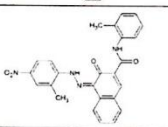

PR16 C.I. 12500, Monoazopigment, Naphthol AS
Hoechst; Laser: 785nm 0.0121mW

1588m; **1548m; 1498m;** 1451; 1389; **1359s; 1349vs; 1340s; 1290m;** 1253m; 1234; 1180; **1156m;** 1141; 1118; 1106; 1085; 1057; 1027; 960m; 807; 748; 707; 629; 615; 549m; 464; 385m; 356; 281

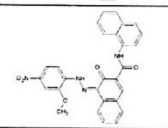

PR18 C.I. 12350, Monoazopigment, Naphthol AS
Imperial Chem. Indust. LDT. UK; Laser: 785nm 0.0605mW

1618m; 1553m; 1497m; 1446; 1391; **1365vs;** 1342; 1326; **1287m;** 1270; 1255; 1229; **1211m; 1157m;** 1134; 1112; 1073; 1038; 998; 965m; 943; 920; 846; 800; **772m;** 741m; 680; 664; 630; 609; 546; 488; 467; 429; 418; 399; 375; 363; 348; 280

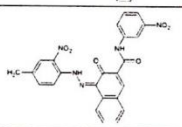

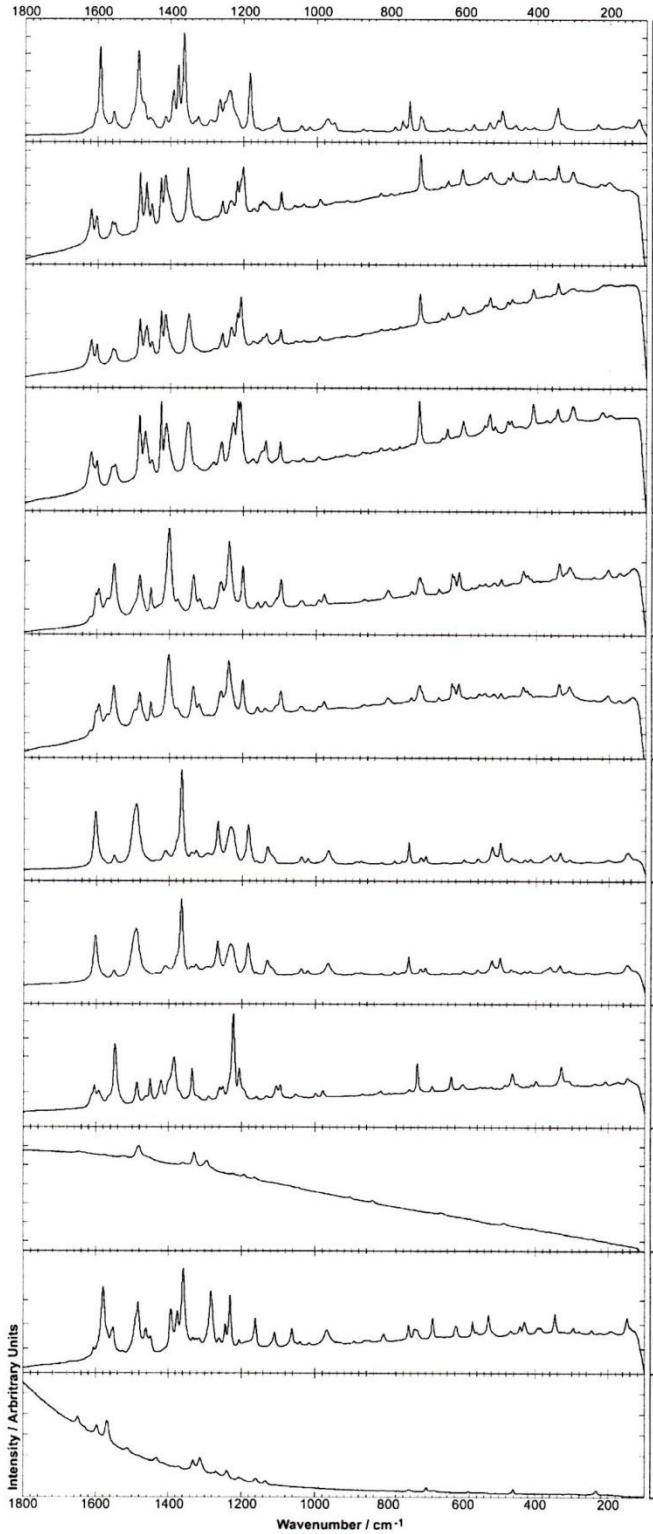

PR48:3 C.I. 15865:3, Monoazopigment, BON lake
Heubach; Laser: 785nm 0.121mW

1593vs; 1555m; 1487vs; 1452; 1412; **1391s; 1378vs;** 1361vs; 1322; 1289; 1264m; 1236m; **1181s;** 1104m; 1041; 1019; 971m; 952; 873; 787; 767; **747m;** 716m; 664; 644; 629; 596; 573; 530; 495m; 459; 433; 409; 344m; 232; 206; 166; 121

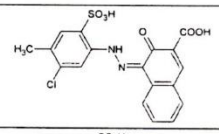

PR49 C.I. 15630, Monoazopigment, B-Naphthol
Coll.: SIAR, Zurich; Laser: 785nm 0.121mW

1618s; 1603m; 1560m; 1551m; 1483vs; 1465vs; 1450m; 1426vs; 1412vs; **1351vs;** 1323; 1257m; 1235; 1216s; **1200vs;** 1172; 1156; 1148; 1097m; 1060; 1035; 991; 918; 826; 800; 775; 719s; 662; 644; **605m;** 545; 528; 480; 468; 411; 377; 359; 343m; **303m;** 225; 201

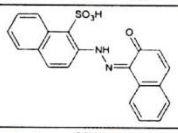

PR49:1 C.I. 15630:1, Monoazopigment, B-Naphthol lake
Coll.: TU Dresden; Laser: 785nm 0.121mW

1618m; 1603m; 1556m; 1483vs; 1466s; 1450m; 1425vs; 1412vs; **1349s;** 1258m; 1233m; 1216s; **1206vs;** 1173; 1136; 1098m; 1057; 1036; 992; 826; 775; 720s; 661; 644; **603m;** 529m; 515; 481; 469; 411m; 343m; **305**

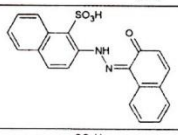

PR49:2 C.I. 15630:2, Monoazopigment, B-Naphthol lake
Coll.: TU Dresden; Laser: 785nm 0.121mW

1617m; 1601m; 1560m; 1550m; 1484vs; 1468s; 1449; 1424vs; 1409s; **1350s;** 1281; 1258m; 1228s; 1215vs; **1207vs;** 1173; 1138m; 1098m; 1067; 1036; 994; 918; 875; 825; 801; 776; 722s; 659; 645; **602m;** 543; 529m; 515; 480; 470; 411m; 375; 344m; **302m;** 221; 198

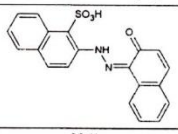

PR53 C.I. 15585, Monoazopigment, B-Naphthol
Coll.: SIAR, Zurich; Laser: 785nm 0.0121mW

1604; 1594m; 1573; 1553vs; 1482s; 1451m; 1401vs; 1376; **1334s;** 1316; 1291; 1260; **1236vs;** 1199s; 1159; 1138; 1095m; 1039; 993; 977; 869; 805; 740; 719m; 667; 631m; **612m;** 578; 557; 540; 516; 497; 436m; 425; 338m; 310; 242; 203; 172; 134

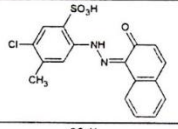

PR53:1 C.I. 15585:1, Monoazopigment, B-Naphthol lake
Coll.: TU Dresden; Laser: 785nm 0.0605mW

1594m; 1573; 1553s; **1497m;** 1481s; 1451m; 1401vs; 1377; **1334s;** 1317; 1293; 1259; **1236vs;** 1199s; 1159; 1138; 1095m; 1040; 977; 869; 804; 740; 719m; 667; 631m; **612m;** 579; 557; 540; 516; 497; 436m; 425; 338m; 310m; 244; 204; 172; 135

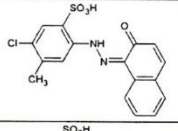

PR57 C.I. 15850, Monoazopigment, BON lake
Coll.: SIAR, Zurich; Laser: 785nm 0.121mW

1603s; 1551; 1491s; 1410; 1365vs; 1338; 1324; 1295; 1265s; 1229s; **1182s;** 1129m; 1038; 1020; 965m; 889; 876; 820; 786; 765; **746m;** 714; 701; 654; 597; 559; 520m; 497m; 467; 431; 415; 362m; 334m; 308; 261; 202; 148m

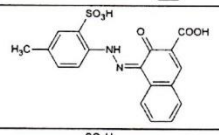

PR57:1 C.I. 15858:1, Monoazopigment, BON lake
Clariant; Laser: 785nm 0.121mW

1603s; 1551; 1492s; 1436; 1409; 1365vs; 1339; 1324; 1296; 1266s; 1229s; **1182s;** 1130m 1039; 1020; 965m, 932; 890; 876; 821; 786; 765; **746m;** 714; 701; 654; 623; 598; 559; 520m; 498m; 467; 431; 416; 362m; 334m; 308; 261; 202; 148m

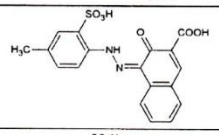

PR68 C.I. 15525, Monoazopigment, B-Naphthol
Hoechst; Laser: 785nm 0.121mW

1605m; 1592; 1547s; 1487m; 1450m; 1421m; 1385s; **1335m;** 1289; 1259; **1222vs**(tw); 1205m; 1159; 1132; 1105m; 1094m; 1052; 998; 979; 872; 822; 799; 744; 722m; 682; **631m;** 599; 553; 538; 522; 484; 463m; 412; 398; 330m; 308; 238; 208; 174; 147

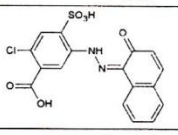

PR83:1 C.I. 58000:1, Polycarbocyclic Anthraquinone
Kremer; Laser: 633nm 0.103mW

1646; 1522; **1481s;** 1358m; **1328vs; 1294s;** 1221m; 1191m; 1163m; **904m;** 843m; 655m; 484m

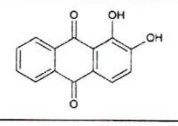

PR112 C.I. 12370, Monoazopigment, Naphthol AS
Heubach; Laser: 785nm 0.0121mW

1579vs; **1552m;** 1526; **1484s;** 1461m; 1448; **1392m; 1375m; 1358vs;** 1332; 1314; **1282s;** 1260; 1243; 1230s; 1205; **1161m;** 1109m, 1061m, 1039; 1015; 967m, 893, 865; 813, 745; 725; 680m, 616; 571; 527m, 467; 442; 429; 389; 346m; 296; 280; 245; 222; 191; 148m

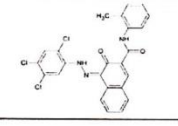

PR122 C.I. 73915, Polycyclic pigment, Quinacridone
Kremer; Laser: 514nm 0.114mW

1649s; 1597s; 1568vs; 1512; 1432; 1370; **1331m;** 1311s; 1267; 1238m; 1204; **1160m;** 1133; 818; 743; 696; 676; 582; 460m; 309; 233m

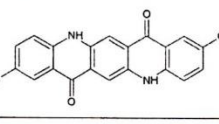

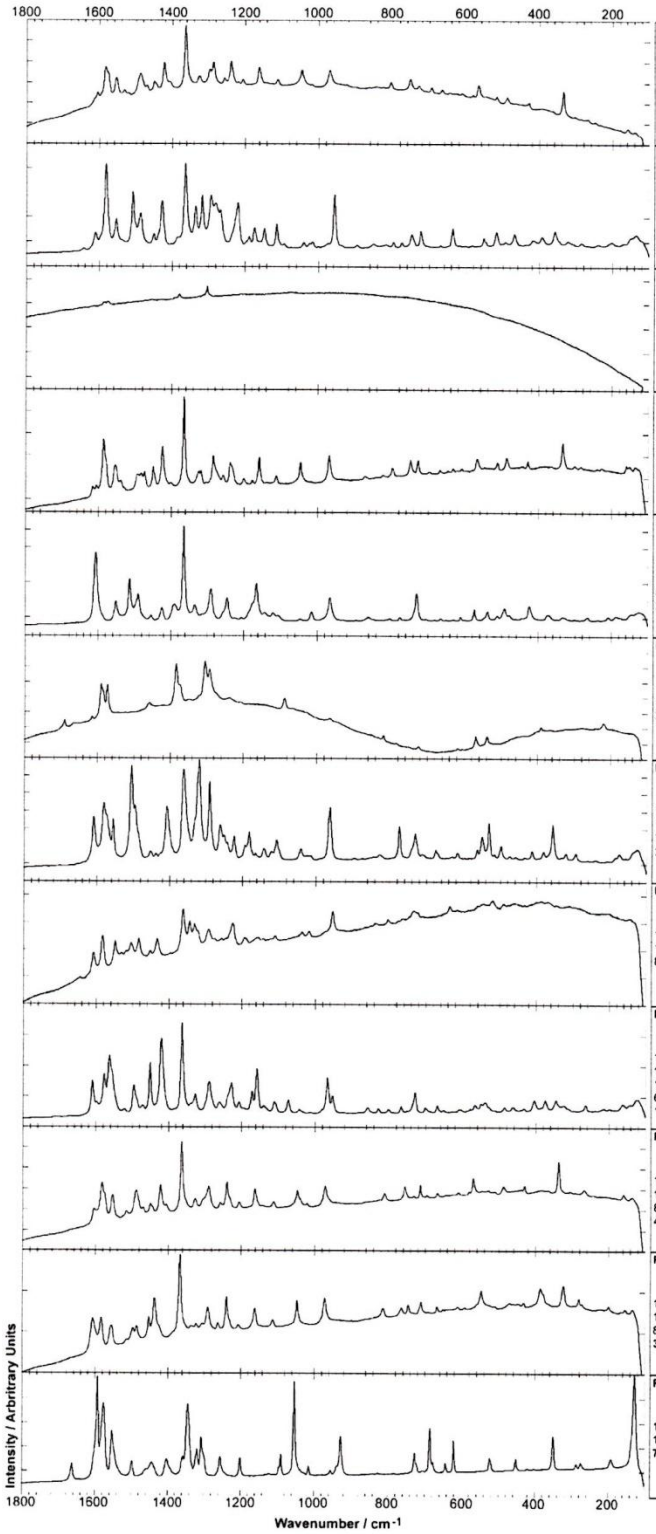

PR144 C.I. 20735, Disazopigment, Condensation
Kremer; Laser: 785nm 0.0605mW

1606; 1581s; **1554m;** 1532; **1487s;** 1448; **1421m; 1362vs;** 1325; **1286m;** 1257; 1238m; 1206; **1161m;** 1110; 1045m; 969m; 923; 844; 824; 804; 751m; 728; 694; 665; 644; 610; 582; 566m; 517; 489; 429; 386; **336s;** 304; 268; 246; 158

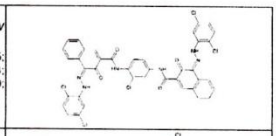

PR146 C.I. 12485, Monoazopigment, Naphthol AS
Clariant; Laser: 785nm 0.121mW

1877; 1643; 1611; 1582vs; **1554m; 1508s; 1486m;** 1450; **1427s; 1363vs;** 1335m; **1316s; 1293s;** 1265m; **1219m;** 1188; **1173m;** 1146m; 1113m; 1092; 1039; 1015; 956s; 895; 851; 817; 796; 774; 746; 722m; 668; 636m; 603; 582; 551; 517m; 493; 467; 417; 392; 357m; 321; 285; 239; 203; 134m

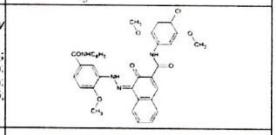

PR149 C.I. 71137, Polycyclic pigment, Perylene & Perinone
Clariant; Laser: 633nm 0.515mW

1585s; 1577s; 1379s; 1302vs

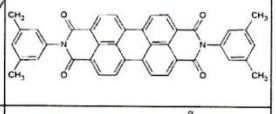

PR166 C.I. 20730, Disazopigment, Condensation
Heubach Laser: 785nm 0.00605mW

1605; 1585s; **1553m; 1492m; 1482m;1472m;** 1449m; 1423s; **1364vs;** 1317; 1283m; 1256; 1235m; 1200; 1177; **1158m;** 1111; 1045m; 968m; 871; 821; 796; 747m; 727m; 667; 632; 609; 567m; 512; 487; 429; 386; **334m;** 301; 226; 159 301; 226; 159

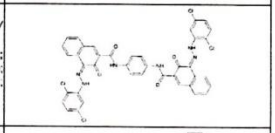

PR170 C.I. 12475, Monoazopigment, Naphthol AS
Kremer; Laser: 785nm 0.121mW

1606vs; **1551m; 1513s; 1489m;** 1453; 1424; 1390; **1363vs;** 1333; **1289s;** 1245m; 1206; **1165s;** 1141; 1119; 1046; 1014; 964m; 893; 861; 803; 775; 730m; 664; 631; 610; 573; 538; 492m; **423m;** 372; 332; 300; 265; 237; 208; 186; 121

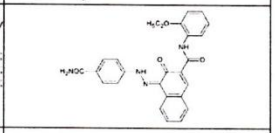

PR179 C.I. 71130, Polycyclic pigment, Perylene & Perinone
Kremer; Laser: 785nm 0.00605mW

1692; 1667; 1615; **1590s;** 1573s; 1458; **1384vs;** 1346; **1304vs; 1291s;** 1237; 1205; 1136; 1087m; 963; 818; 723; 617; **568m;** 538m; 457; 390; 279; 220

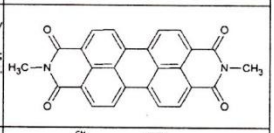

PR185 C.I. 12516, Monoazopigment, Benzimidazolone
Clariant; Laser: 785nm 0.121mW

1609s; 1580s; 1556m; 1505vs; 1452; 1406s; **1360vs; 1319vs; 1289vs;** 1260m; 1222; **1181m;** 1141; 1107m; 1040; 1014; **962s;** 896; 827; 774m; 731m; 675; 616; 550m; 531m; 498; 474; 458; 433; 413; 382; 357m; 322; 295; 239; 175; 125

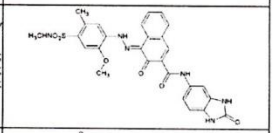

PR187 C.I. 12486, Monoazopigment, Naphthol AS
Clariant; Laser: 785nm 0.0605mW

1646; 1608m; 1583vs; **1548s; 1504m; 1483m;** 1451; 1432m; **1361vs;** 1343s; 1328s; **1291m; 1224s;** 1191; **1158m;** 1109; 1037; 1016; 953s; 837; 803; 733; 636; 546; 520; 491; 460; 366; 202

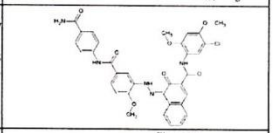

PR188 C.I. 12467, Monoazopigment, Naphthol AS
Clariant; Laser: 785nm 0.121mW

1711; 1672; 1609m; 1578s; **1562s;** 1521; **1495m;** 1471; 1450s; **1419vs; 1363vs;** 1326; **1288m;** 1259; 1227m; 1206; **1157s;** 1137; 1109; 1072; 1041; 1011; 965s; 857; 827; 800; 766; 729m; 700; 668; 606; 566; 538m; 486; 462; 432; 404m; 375m; 346; 323; 265; 216; 199; 162; 121

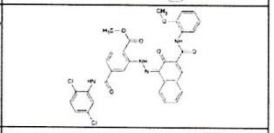

PR214 C.I. 200660, Disazopigment, Condensation
Clariant; Laser: 785nm 0.0605mW

1604; 1582s; **1553m;** 1515; **1487m;** 1448; **1421m; 1362vs;** 1325; **1288m;** 1257; 1238m; 1205; **1161m;** 1111; 1046m; 1020; 971m; 898; 863; 810; 755m; 731; **713m;** 695; 666; 644; 610; 589m; 546; 529; 511; 488; 430; 388; 364; **337s;** 306; 266; 243; 181; 159; 134

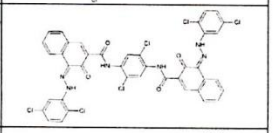

PR242 C.I. 20067, Disazopigment, Condensation
Clariant; Laser: 785nm 0.0605mW

1606m; 1583m; **1556m;** 1496; 1485; 1452; **1436s; 1366vs;** 1336; 1321; **1289m;** 1261; 1238s; 1205; **1160m;** 1111; 1046m; 971m; 898; 813; 764; 744; 711; 666; 651; 643; 610; 592; 547m; 509; 471; 446; 431; **385m; 324m;** 281; 224; 200; 153; 133

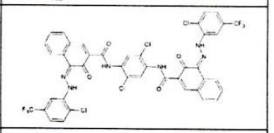

PR254 C.I. 56110, Polycyclic p., Diketopyrrolo-Pyrrole (DPP)
Kremer; Laser: 785nm 0.00605mW

1664m; 1593vs; 1576vs, 1553s; 1498m; 1443m; 1402m; 1344vs, 1319m; 1306s; 1255m; 1200m; 1089m; **1053vs;** 1013; 955; **927s; 727m;** 685s; 643; 621m; **523m;** 451; 420; **350s;** 288; 275; 192; 127vs

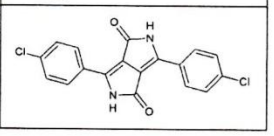

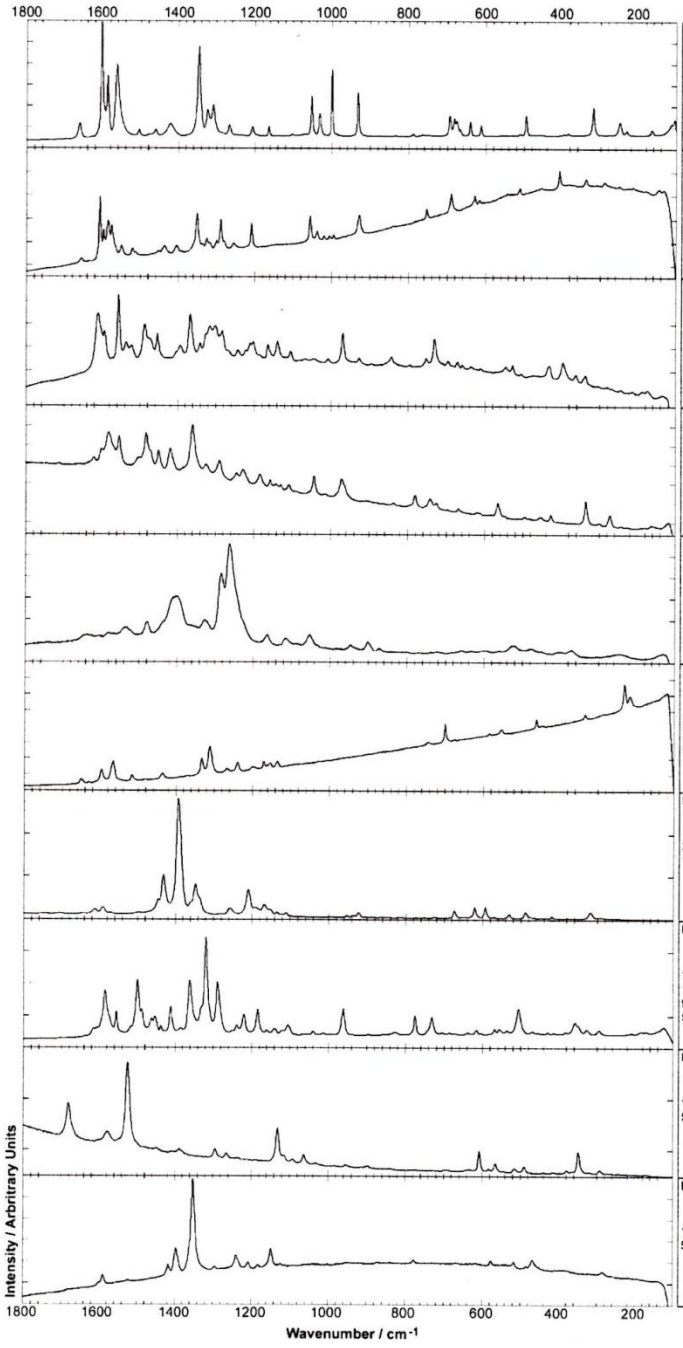

PR255 C.I. **561050,** Polycyclic p., Diketopyrrolo-Pyrrole (DPP)
Kremer; Laser: 785nm 0.121mW

3060; 1660m; 1602vs; 1586s; 1562s; 1503; 1460; 1421m; 1346vs; 1323m; 1308m; 1265; 1206; 1163; 1102; **1051s;** 1030m; **999s; 931s;** 834; 788; 764; 693m; 681m; 640; 612; 494m; 457; 385; **318s;** 248; 230; 164; 107

PR264 C.I. **561300,** Polycyclic p., Diketopyrrolo-Pyrrole (DPP)
Kremer; Laser: 785nm 0.00605mW

1655; 1607vs; 1584vs; 1575s; 1549; 1521; 1437; 1404; 1350vs; 1325; **1288s;** 1255; 1208s; **1055s;** 1037; 1019; 1005; 994; 928s; 752m; 689s; 628m; 615; 510; 455; **406s;** 337m; 288; 249; 212; 145; 131

PBr23 C.I. **20060,** Disazopigment, Condensation
Kremer; Laser: 785nm 0.0605mW

1610vs; 1556vs; 1536m; 1520m; **1487s;** 1453m; 1393; **1366s;** 1341; 1317s; 1300s; 1282m; 1242; 1205; 1163; 1138m; 1104; 1067; 1043; 1007; 969s; 926; 895; 842m; 795; 752; 730s; 696; 671; 635; 611; 545; 527; 504; 472; 432m; 395m; 362; 337; 302; 278; 244; 213; 188; 173

PBr25 C.I. **12510,** Monoazopigment, Benzimidazolone
Clariant; Laser: 633nm 1.03mW

1621; **1582s; 1553s; 1482s;** 1449m; 1418m; **1359vs;** 1324; 1289m; 1245; 1226; 1183; 1157; 1129; 1108; 1043m; 970m; 837; 780m; 741; 725; 668; 619; 565m; 453; 426; 335m; 272; 162; 116

PV5 C.I. **58055,** Polycyclic p., Polycarbocyclic Anthraquinone
Kremer; Laser: 785nm 0.605mW

1641; 1581; 1534; 1479m; **1403s;** 1325m; **1284s; 1260vs;** 1163; 1114; 1052m; 946; **901m;** 871; 721; 659; 597; 524m; 474; 406; 371; 243

PV19 C.I. **73900,** Polycyclic pigment, Quinacridone
Kremer; Laser: 633nm 0.103mW

1650; 1596m; **1566s;** 1516; 1483; 1435; 1369; 1332m; **1310s;** 1266; 1238m; 1198; 1170; 1153; 1134; 743; **699s;** 584; 553; **461m;** 334; **230s;** 215m

PV23 C.I. **51319,** Polycyclic pigment, Dioxazine
Heubach; Laser: 514nm 0.114mW

2819; 2776m; 2733; 2641; 2598m; 2554; 1613; 1591; 1431m; **1391vs; 1347s;** 1256; 1208m; 1167; 922; 673; **621m; 593m;** 530; 487; 317

PV32 C.I. **12517,** Monoazopigment, Benzimidazolone
Clariant; Laser: 785nm 0.121mW

1585s; 1555m; **1499s;** 1453; 1437; 1411m; 1386; 1361s; 1318vs; 1288s; 1238; 1219m; 1184m; 1161; 1139; 1104; 1040; 1013; 994; **961m;** 896; 826; **775m; 731m;** 703; 686; 638; 616; 568; 555; 535; **505m;** 469; 430; 413; 383; 357m; 327; 295; 209; 185; 170; 124

PV36 C.I. **73385,** Polycyclic pigment, Indigoide
Bayer; Laser: 514nm 0.114mW

1680s; 1577m; **1524vs;** 1388; 1293; 1263; **1131s;** 1063; **607m;** 565; 515; 489; **348m;** 292

PV37 C.I. **51345,** Polycyclic pigment, Dioxazine
Kremer; Laser: 785nm 0.121mW

1589m; 1416; **1396s; 1351vs;** 1294; 1237m; 1207; 1182; **1147m;** 777; 576; 517; 467m; 284

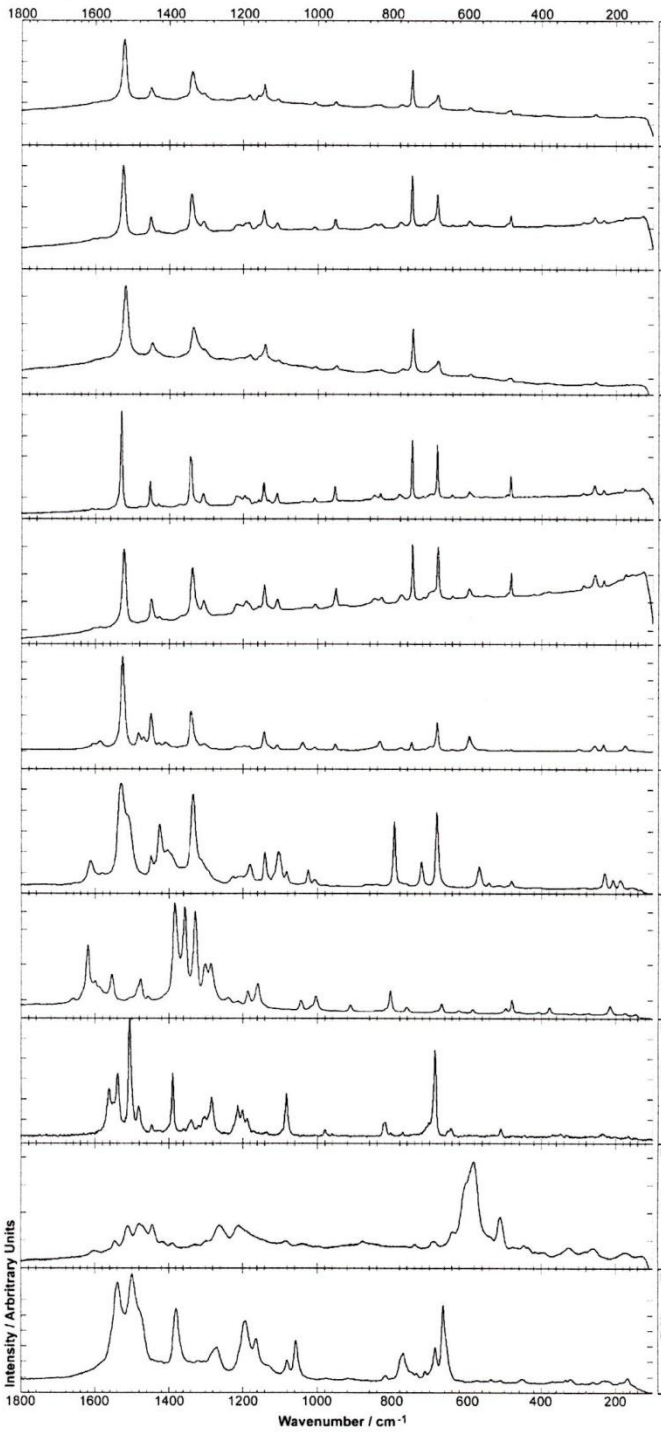

PB15 C.I. 74160, Polycyclic pigment, Phthalocyanine
Kremer; Laser: 785nm 0.0121mW

1522vs; 1448m; **1336s;** 1303; 1256; 1217; 1182; 1141m; 1106; 1006; 951; 830; 776; **746vs; 679s;** 592; **484m;** 255; 172; 123

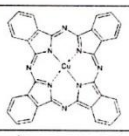

PB15:1 C.I. 74160:1, Polycyclic pigment, Phthalocyanine
Heubach; Laser: 785nm 0.0121mW

1525vs; 1449m; **1338s;** 1306; 1217; 1184; 1143m; 1108; 1007; 952; 848; 830; 778; **747vs; 680s;** 594; **483m;** 383; 288; 257; 233; 174

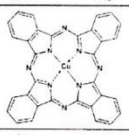

PB15:2 C.I. 74160:2, Polycyclic pigment, Phthalocyanine
Heubach; Laser: 785nm 0.121mW

1518vs; 1446m; **1334s;** 1303; 1181; 1140m; 1105; 1005; 950; 774; **745s; 679m;** 592; **483m;** 255

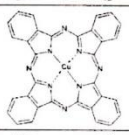

PB15:3 C.I. 74160:3, Polycyclic pigment, Phthalocyanine
Kremer; Laser: 785nm 0.0000121mW

1610; **1530vs;** 1451m; 1429; **1341s;** 1307; 1217; 1195; 1144; 1109; 1008; 954; 849; 832; 781; **747s;** 719; **681s;** 641; 594; **483m;** 289; 258; 233; 175

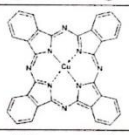

PB15:4 C.I. 74160:4, Polycyclic pigment, Phthalocyanine
Heubach; Laser: 785nm 0.0121mW

2268; **1522vs;** 1448m; 1426; **1336s;** 1305; 1216; 1190; 1142m; 1107; 1037; 1006; 951m; 848; 829; 776; **746s; 679s;** 639; 594; 547; **482m;** 421; 382; 287; 257; 233; 173; 158

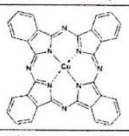

PB15:6 C.I. 74160:6, Polycyclic pigment, Phthalocyanine
Kremer; Laser: 514nm 0.57mW

3051; 2866; 2667; 1587; **1526vs; 1482m;** 1448s; **1408; 1339s;** 1303; 1183; 1142m; 1108; 1039; 1007; 952; 833; 777; **748m; 680s;** 594m; 257; 233; 174

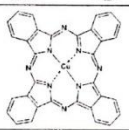

PB16 C.I. 74100, Polycyclic pigment, Phthalocyanine
Imperial Chem. Indust. LDT. UK; Laser: 514nm 5.7mW

3036; 2954; 2867; 2671; 2215; 2009; 1871; 1612m; **1528vs;** 1424s; **1334vs;** 1227; 1180m; 1140m; 1103m; 1024; **794s; 721m; 680s;** 567m; 541; 480; 230; 208; 187; 152

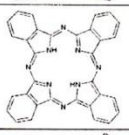

PB60 C.I. 69800, Polycyclic p., Polycarbocyclic Anthraquinone
Kremer; Laser: 514nm 1.14mW

2906; 2739; 2708; 2658; 2593; 2538; 2184; 1660; 1619s; 1554m; 1477m; **1383vs; 1356vs; 1328vs; 1285s;** 1238; 1212; 1185; 1159m; 1043; 1003; **911m;** 804m; 760; 667; 621; 584; 479m; 407; 378; 274; 215; 174; 145

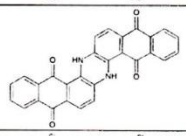

PG7 C.I. 74260, Polycyclic pigment, Phthalocyanine
Kremer; Laser: 514nm 0.114mW

1563s; 1538s; **1506vs;** 1481; 1445; **1389s;** 1338; 1307; **1283s;** 1214m; 1200m; 1187m; 1082s; 979; 820m; 772; **685vs;** 642; 510; 236

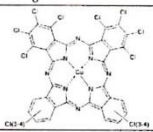

PG9 C.I. 49415, Metal complex, Azo metal complex
Farbwerke Meister Lucius & Brüning; Laser: 785nm 0.121mW

1602; 1546; 1511m; 1479m; 1443m; 1389; 1330; 1262m; 1208m; 1081; 1038; 995; 877; 738; 689; **585vs; 510s;** 446; 391; 327; 260; 173

PG36 C.I. 74265, Polycyclic pigment, Phthalocyanine
Kremer; Laser: 514nm 1.14mW

2600; 1539vs; **1498vs; 1379s;** 1271m; **1193s;** 1162m; 1080w; 1056m; 818; 771m; 685m; **662vs;** 451; 321; 226; 167

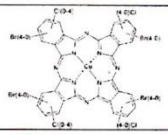

Spectra Reported By Schulte, 2008:

Excitation wavelengths reported as follows:

Excitation Wavelength (nm)	Pigment Analyzed
458	PR 179, PV 19
476	PR 122, PR 123
488	PR 83:1, PB 15:3, PG 7, PV 5:1
514.5	PY 3, PV 1, PV 2
632.8	PY 83
1064	PR 2, PR 49, PR88, PR 146, PR 176, PR 181, PO 13, PO 34, PO 43, PY 109, PY 110

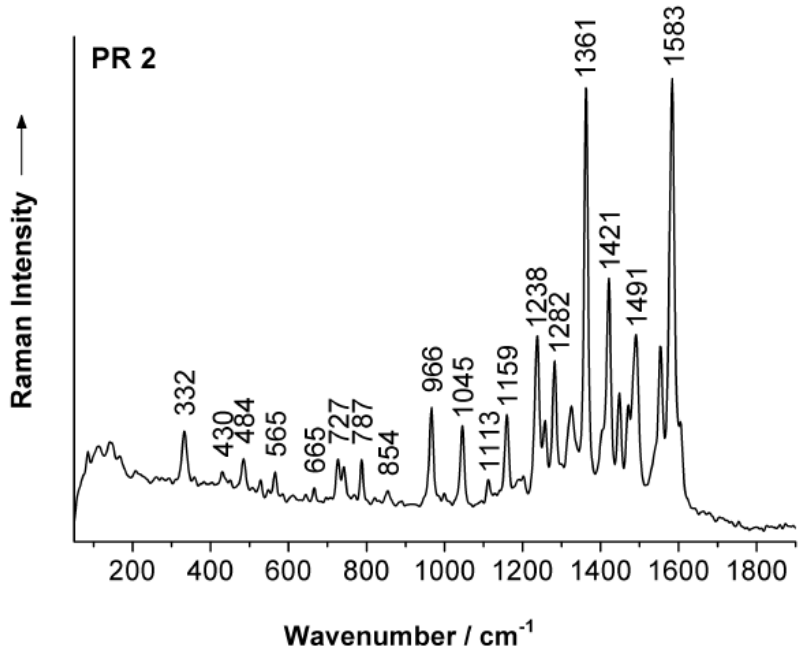

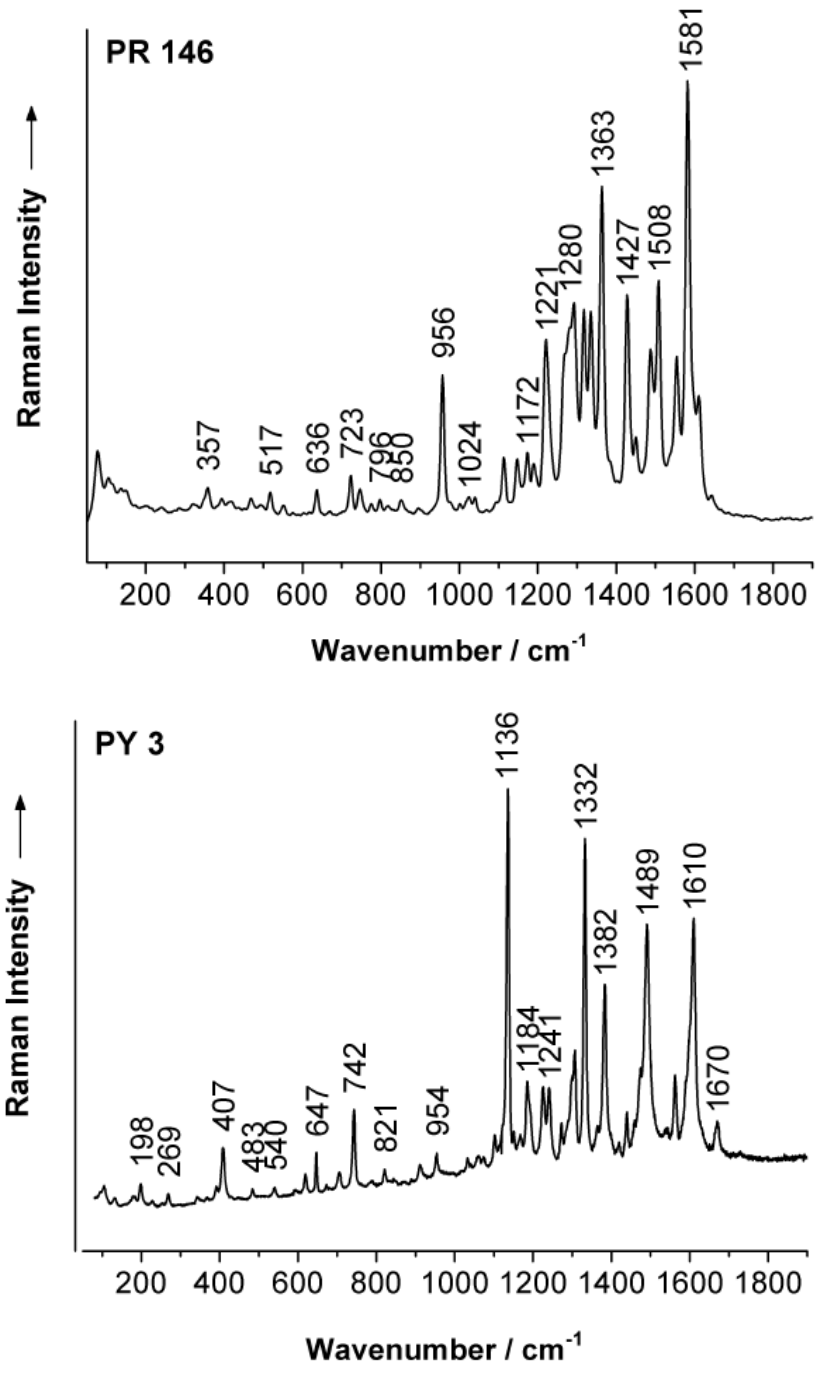
PR 146
Raman Intensity
357
517
636
723
796
850
956
1024
1172
1221
1280
1363
1427
1508
1581
200 400 600 800 1000 1200 1400 1600 1800
Wavenumber / cm-1
PY 3
Raman Intensity
198
269
407
483
540
647
742
821
954
1136
1184
1241
1332
1382
1489
1610
1670
200 400 600 800 1000 1200 1400 1600 1800
Wavenumber / cm-1

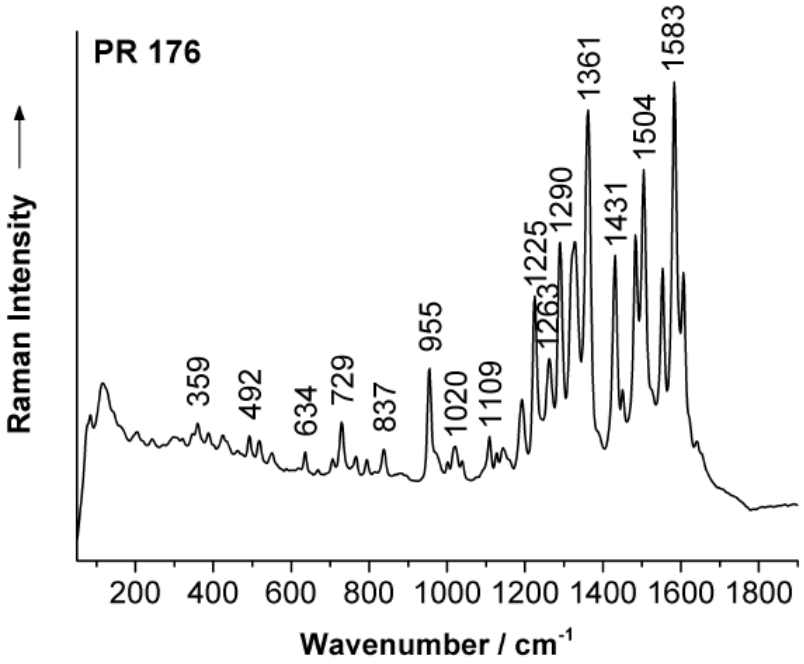
PR 176
Raman Intensity
359
492
634
729
837
955
1020
1109
1225
1263
1290
1361
1431
1504
1583
200 400 600 800 1000 1200 1400 1600 1800
Wavenumber / cm-1

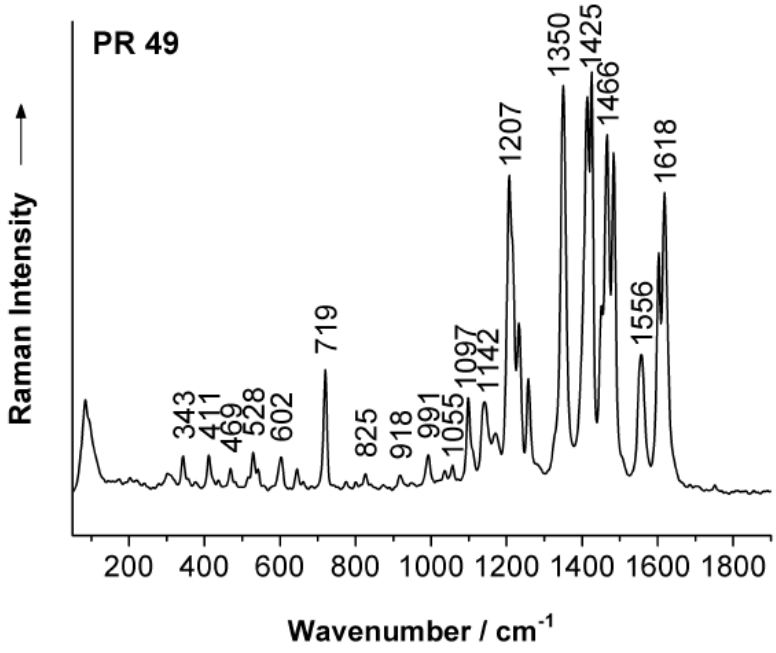
PR 49
Raman Intensity
343
411
469
528
602
719
825
918
991
1055
1097
1142
1207
1350
1425
1466
1556
1618
200 400 600 800 1000 1200 1400 1600 1800
Wavenumber / cm-1

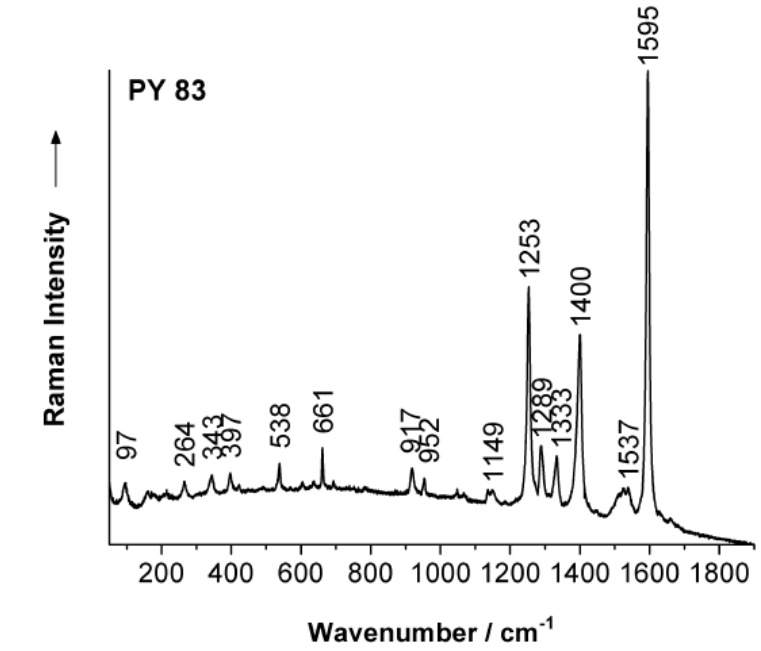
PY 83
Raman Intensity
97
264
343
397
538
661
917
952
1149
1253
1289
1333
1400
1537
1595
200 400 600 800 1000 1200 1400 1600 1800
Wavenumber / cm-1

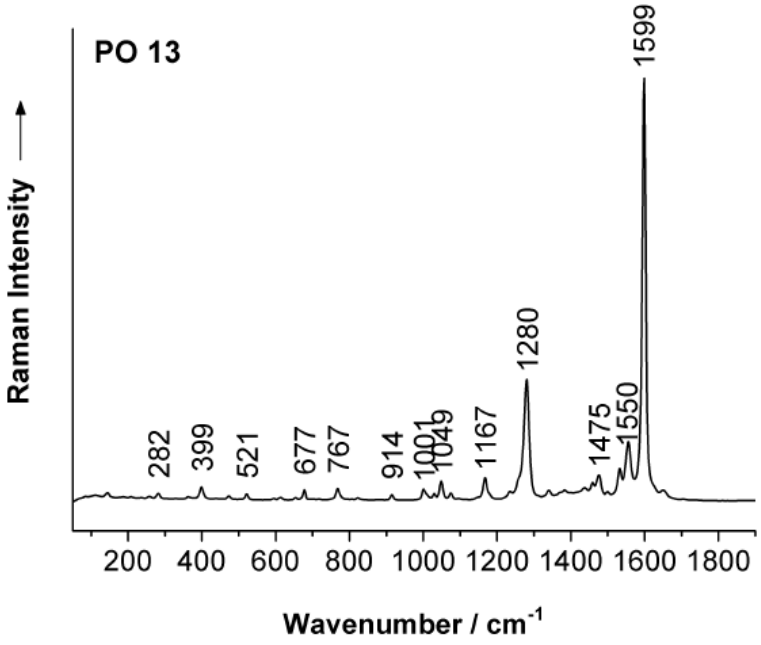
PO 13
Raman Intensity
282
399
521
677
767
914
1001
1049
1167
1280
1475
1550
1599
200 400 600 800 1000 1200 1400 1600 1800
Wavenumber / cm-1

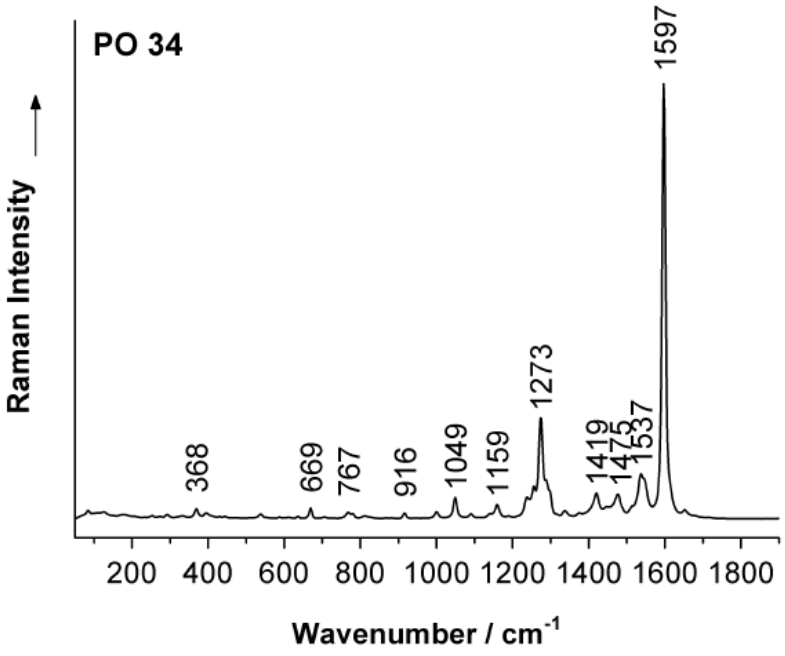
PO 34
Raman Intensity
1597
1273
1537
1475
1419
1159
1049
916
767
669
368
200 400 600 800 1000 1200 1400 1600 1800
Wavenumber / cm-1

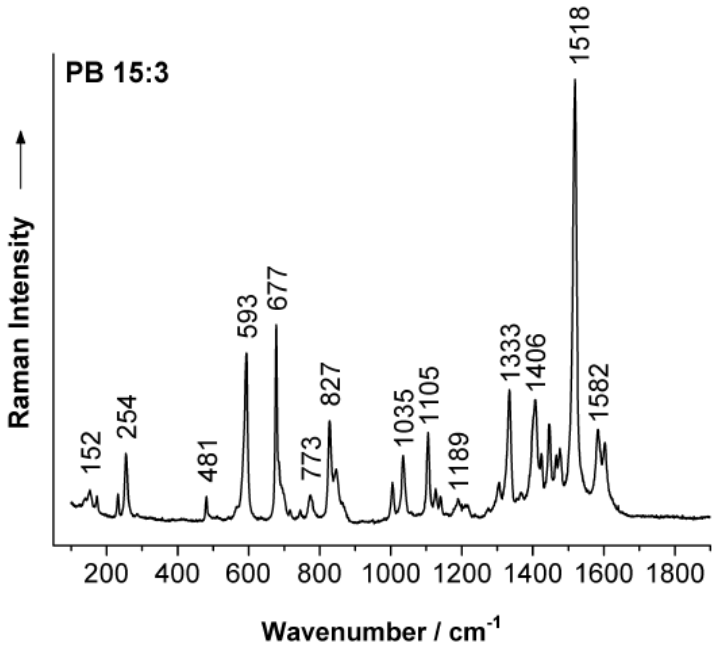
PB 15:3
Raman Intensity
1518
1582
1406
1333
1189
1105
1035
827
773
677
593
481
254
152
200 400 600 800 1000 1200 1400 1600 1800
Wavenumber / cm-1

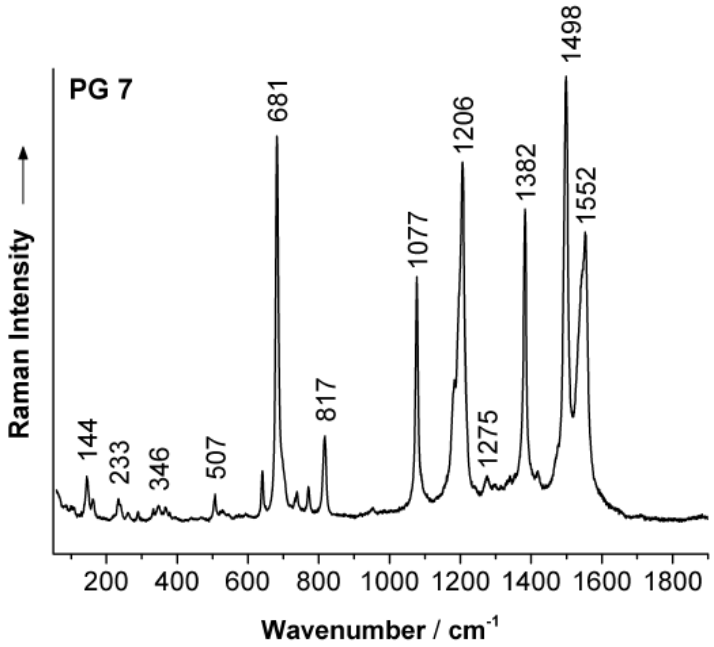
PG 7
Raman Intensity
144
233
346
507
681
817
1077
1206
1275
1382
1498
1552
200 400 600 800 1000 1200 1400 1600 1800
Wavenumber / cm-1

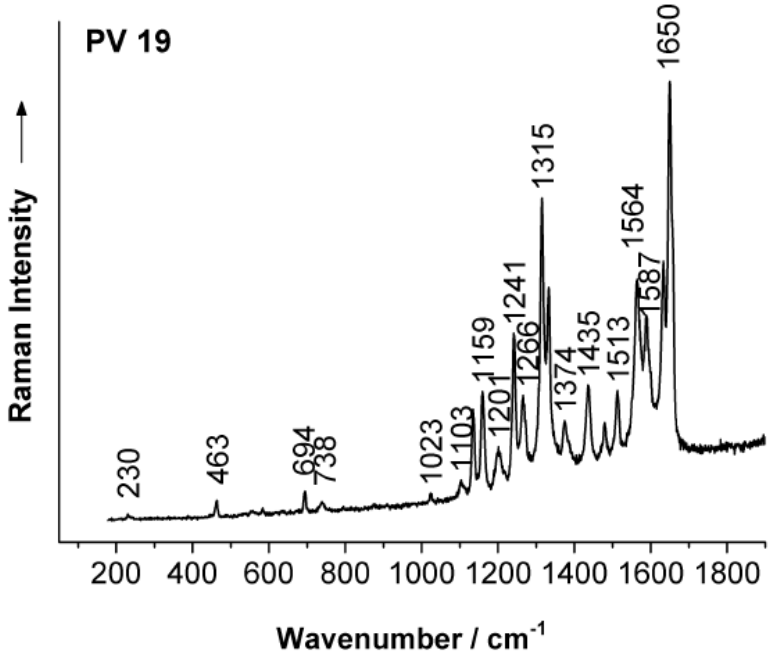
PV 19
Raman Intensity
230
463
694
738
1023
1103
1159
1201
1241
1266
1315
1374
1435
1513
1564
1587
1650
200 400 600 800 1000 1200 1400 1600 1800
Wavenumber / cm-1

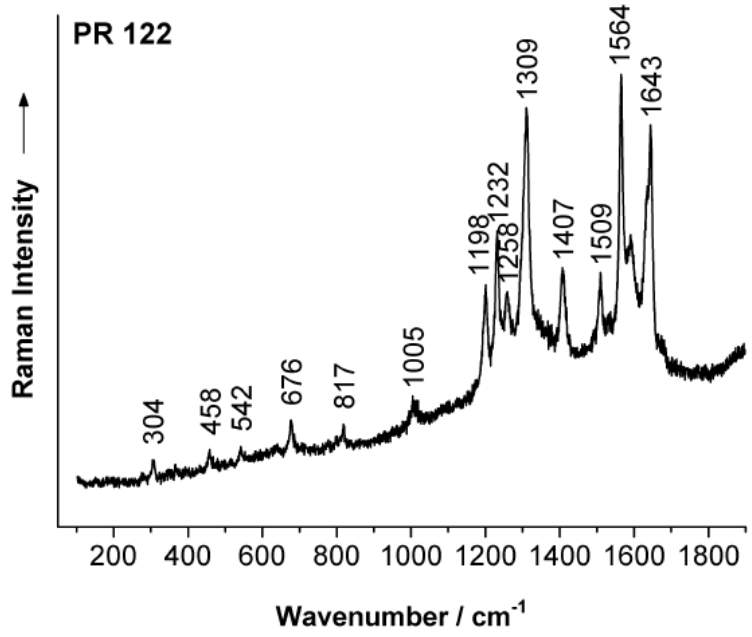
PR 122
Raman Intensity
304
458
542
676
817
1005
1198
1232
1258
1309
1407
1509
1564
1643
200 400 600 800 1000 1200 1400 1600 1800
Wavenumber / cm-1

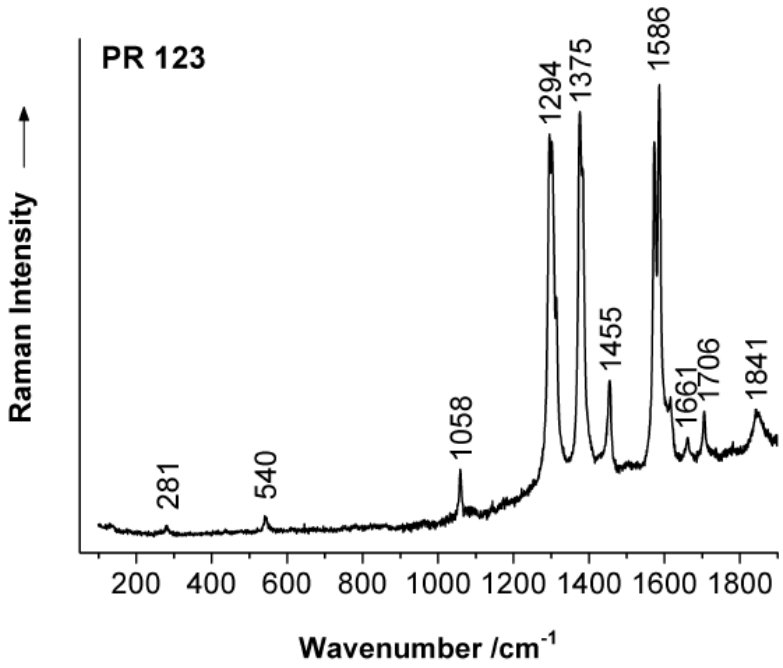
PR 123
Raman Intensity
281
540
1058
1294
1375
1455
1586
1661
1706
1841
200 400 600 800 1000 1200 1400 1600 1800
Wavenumber /cm-1

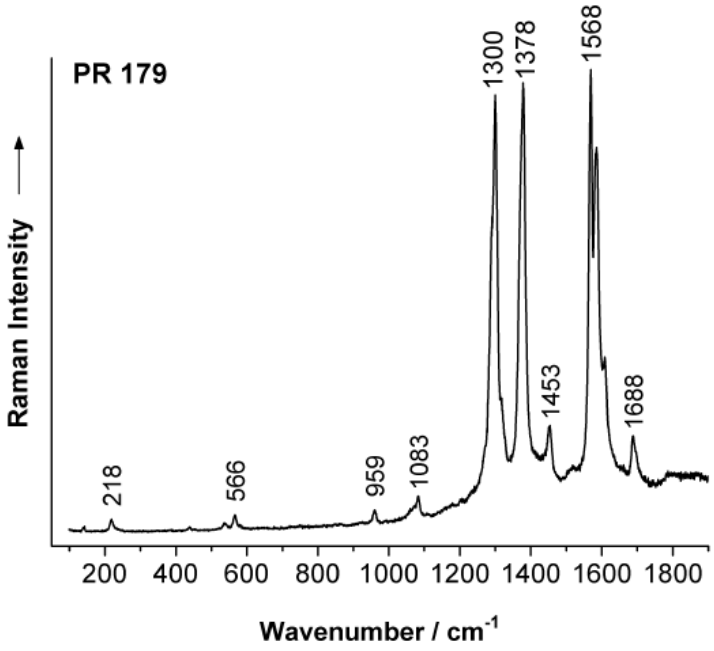
PR 179
Raman Intensity
1300
1378
1568
1453
1688
218
566
959
1083
200 400 600 800 1000 1200 1400 1600 1800
Wavenumber / cm-1

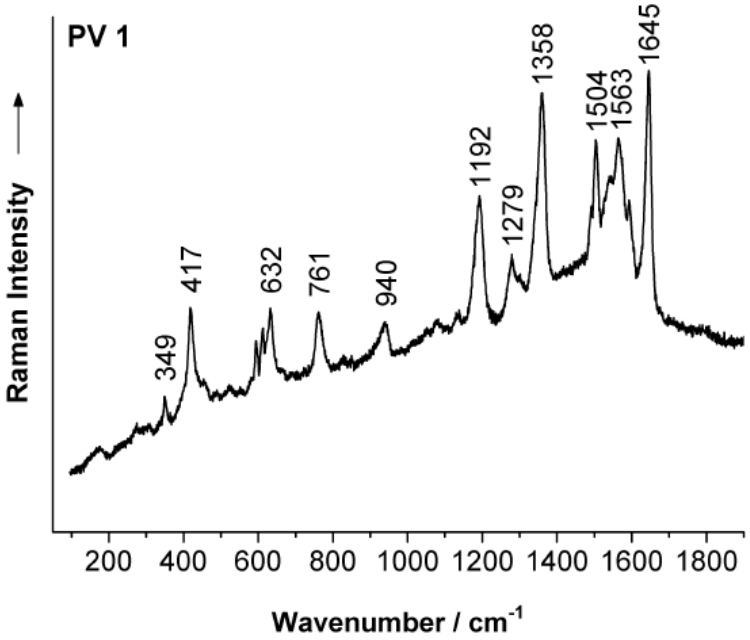
PV 1
Raman Intensity
1358
1645
1504
1563
1192
1279
417
632
761
940
349
200 400 600 800 1000 1200 1400 1600 1800
Wavenumber / cm-1

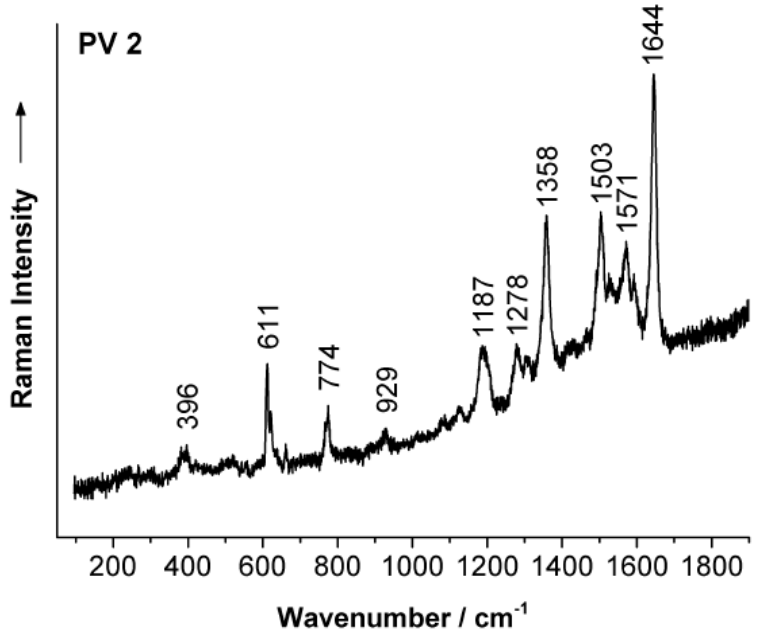
PV 2
Raman Intensity
396
611
774
929
1187
1278
1358
1503
1571
1644
200 400 600 800 1000 1200 1400 1600 1800
Wavenumber / cm-1

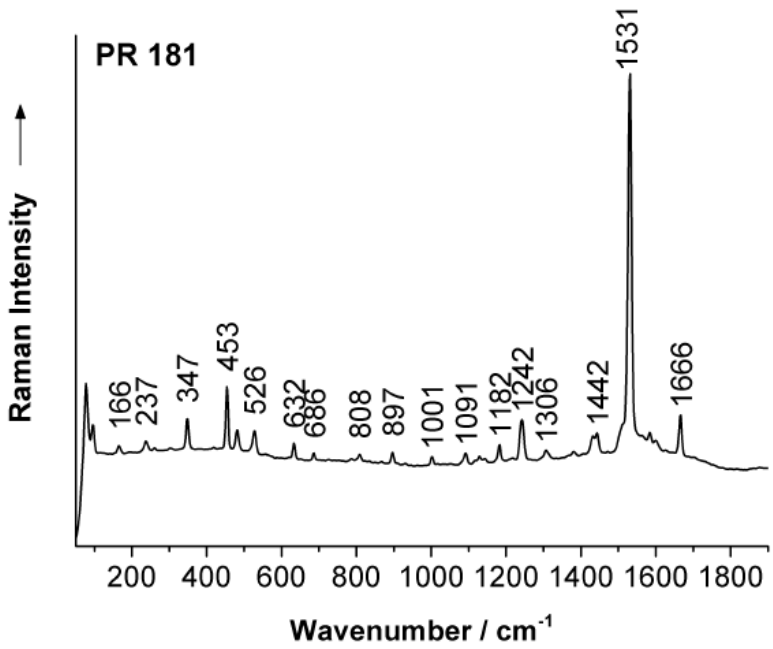
PR 181
Raman Intensity
166
237
347
453
526
632
686
808
897
1001
1091
1182
1242
1306
1442
1531
1666
200 400 600 800 1000 1200 1400 1600 1800
Wavenumber / cm-1

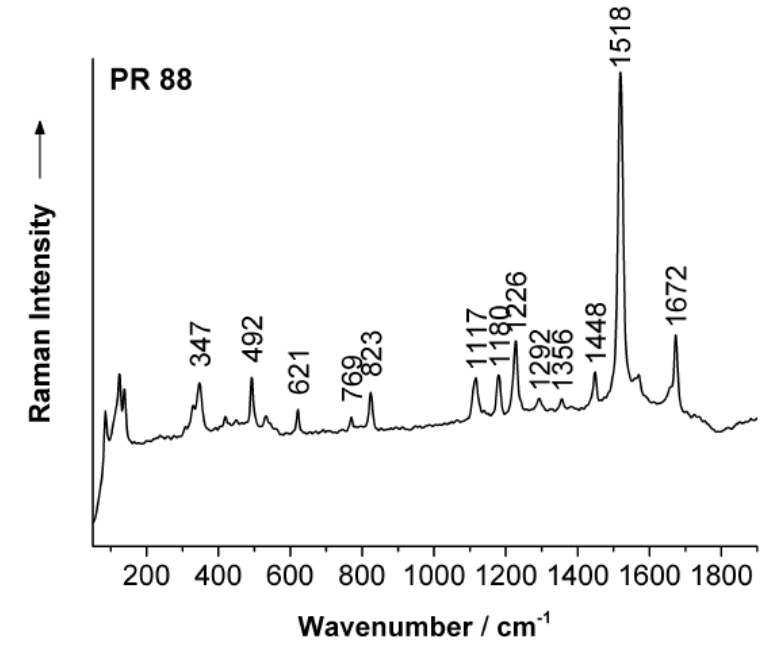
PR 88
Raman Intensity
347
492
621
769
823
1117
1180
1226
1292
1356
1448
1518
1672
200 400 600 800 1000 1200 1400 1600 1800
Wavenumber / cm-1

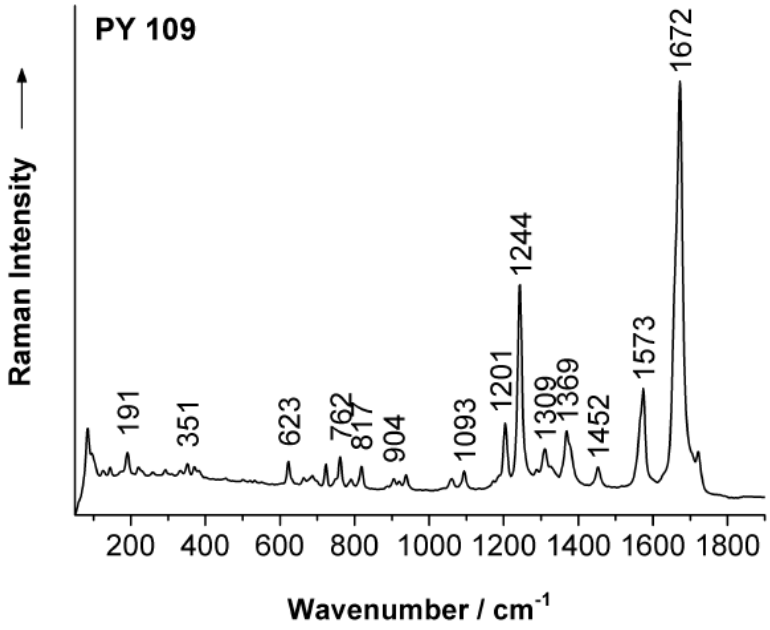
PY 109
Raman Intensity
191
351
623
762
817
904
1093
1201
1244
1309
1369
1452
1573
1672
200 400 600 800 1000 1200 1400 1600 1800
Wavenumber / cm-1

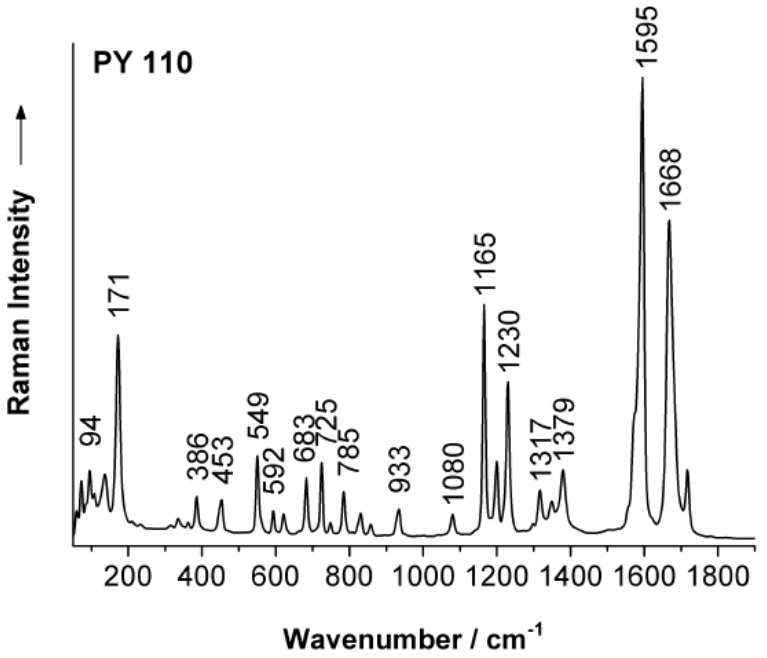
PY 110
Raman Intensity
94
171
386
453
549
592
683
725
785
933
1080
1165
1230
1317
1379
1595
1668
200 400 600 800 1000 1200 1400 1600 1800
Wavenumber / cm-1

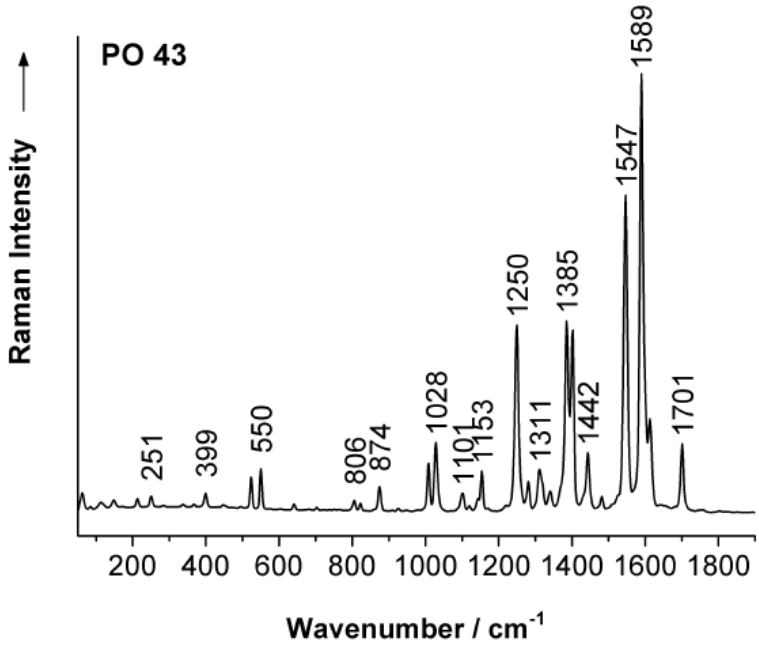
PO 43
Raman Intensity
251
399
550
806
874
1028
1101
1153
1250
1311
1385
1442
1547
1589
1701
200 400 600 800 1000 1200 1400 1600 1800
Wavenumber / cm-1

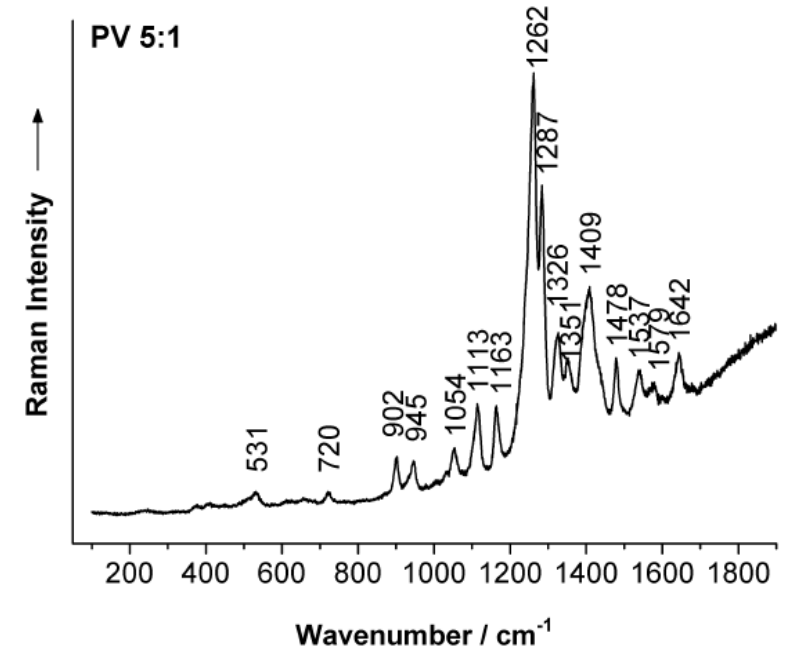
PV 5:1
Raman Intensity
531
720
902
945
1054
1113
1163
1262
1287
1326
1351
1409
1478
1537
1579
1642
200 400 600 800 1000 1200 1400 1600 1800
Wavenumber / cm-1

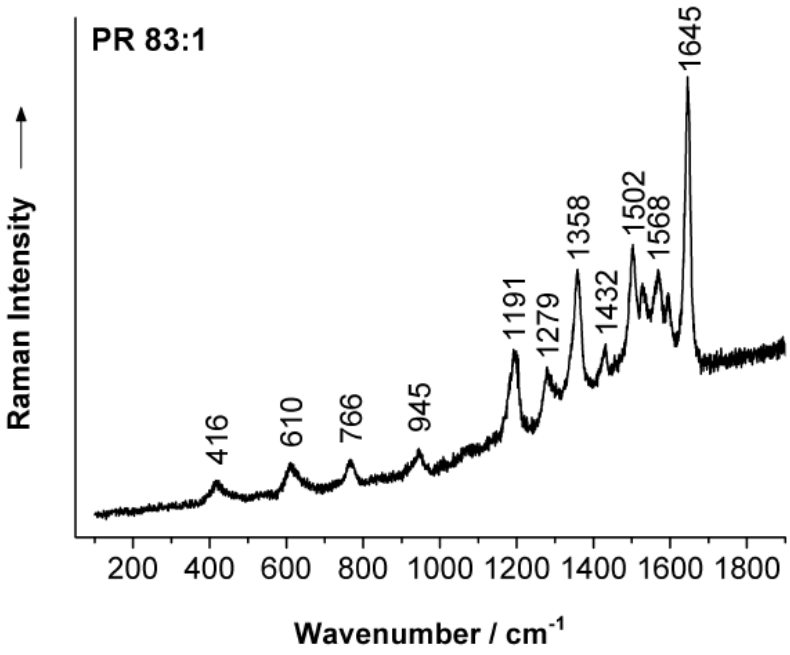
PR 83:1
Raman Intensity
416
610
766
945
1191
1279
1358
1432
1502
1568
1645
200 400 600 800 1000 1200 1400 1600 1800
Wavenumber / cm-1

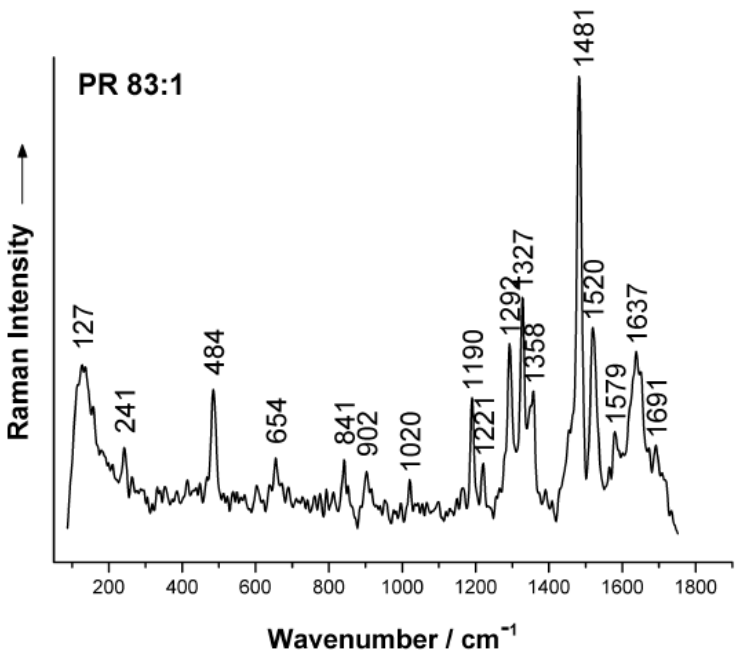
PR 83:1
Raman Intensity
127
241
484
654
841
902
1020
1190
1221
1292
1327
1358
1481
1520
1579
1637
1691
200
400
600
800
1000
1200
1400
1600
1800
Wavenumber / cm-1

Spectra Reported By Ropret, 2008 (λ_0=785nm):

Raman shifts of the reference synthetic organic pigment samples

C.I. name and group	Raman band wave numbers (cm^{-1}) and relative intensities (s, strong; m, medium; w, weak; sh, shoulder; v, very)
Monoazo	
PY6	1673w, 1620m, 1602s, 1569m-w, 1563wsh, 1536vw, 1505msh, 1492s, 1453vw, 1404w, 1388m, 1361vw, 1337m, 1327m, 1308s, 1292wsh, 1288wsh, 1259m, 1235vw, 1193w, 1182w, 1164vw, 1142vs, 1112vw, 1078vw, 1069vw, 1041vw, 1001m, 988vw, 953m-w, 926vw, 917vw, 849vw, 822vw, 785vw, 769vw, 760vw, 742w, 693vw, 685vw, 654w, 625w, 617w, 594vw, 563vw, 532vw, 512vw, 483vw, 443vw, 431vw, 413w, 393wsh, 384w, 370vwsh, 352vw, 331vw, 281vw, 248vwsh, 240vw, 209vw
PY73	1678w, 1641vw, 1616s-m, 1601s-m, 1569m-w, 1546m, 1532s-m, 1507s-m, 1481s-m, 1463vw, 1440vw, 1423vw, 1407wsh, 1392m, 1338vs, 1308s-m, 1296wsh, 1291wsh, 1252m, 1235w, 1224vw, 1196w, 1171vw, 1163w, 1138s, 1117vw, 1106w, 1076vwsh, 1063vw, 1044vw, 1030vw, 955m-w, 917vw, 846vw, 837vw, 826vw, 802vw, 779w, 760vw, 738w, 685vw, 650m-w, 619w, 593vw, 572vw, 525vw, 496vw, 483vw, 467vw, 438vw, 411m-w, 396vw, 377w, 352vw, 343vw, 321vw, 263vw, 228vw, 201vw, 178vw
PY75	1673w, 1611s, 1570m-w, 1561wsh, 1532w, 1522m-w, 1505m, 1479w, 1436vw, 1417vw, 1403vw, 1389m-w, 1357w, 1341vs, 1327m, 1301m, 1300msh, 1260wsh, 1254m, 1247wsh, 1197w, 1166m-w, 1139vs, 1122vw, 1110w, 1063w, 955w, 910vw, 859w, 823w, 758vw, 737m-w, 710vw, 650m-w, 619w, 539vw, 491vw, 438vw, 411w, 379w, 349vw, 315vw, 230vw, 212vw
PY97	1669w, 1637vw, 1618m, 1596s-m, 1589s-m, 1540w, 1500s-m, 1464m, 1456m, 1445vwsh, 1439vw, 1414m, 1402m, 1395m, 1333vs, 1302vw, 1287vw, 1262vw, 1243m-w, 1224w, 1215wsh, 1181vw, 1148vw, 1137vw, 1062w, 1038vw, 1027vw, 1005vw, 985vw, 948m-w, 929vw, 911w, 902vwsh, 841vw, 825vw, 817vw, 765vwsh, 756vw, 740vwsh, 732vw, 706vw, 657vw, 630vw, 617vw, 593vw, 569w, 543vw, 508vw, 486vw, 453vw, 398vw, 368vw, 347w, 314vw, 282vw, 212vw, 176vw, 154vw
PY111	1669vw, 1638vw, 1599s, 1543vw, 1519m-w, 1499w, 1489wsh, 1454vw, 1422w, 1400w, 1361w, 1344ssh, 1336vs, 1327s, 1301m-wsh, 1263s-m, 1244w, 1223vw, 1202vw, 1167w, 1128vw, 1090w, 1066vw, 1016vw, 949vw, 923vw, 903vw, 825vw, 800vw, 783vw, 745vw, 715vw, 645vw, 626vw, 596vw, 557vw, 523vw, 499vw, 466vw, 439vw, 399vw, 387vw, 353vw, 328vw, 300vw, 235vw, 191vw
PY213	1725vw, 1698vw, 1666vw, 1631m-w, 1613vw, 1571w, 1550w, 1491m-w, 1458w, 1446w, 1434w, 1423w, 1405wsh, 1390vs, 1376m, 1319vw, 1293w, 1279vwsh, 1270vw, 1244w, 1234vwsh, 1213vwsh, 1204vw, 1189vw, 1177vw, 1145vw, 1115vw, 1077vw, 1067vwsh, 978vw, 956vw, 940vwsh, 900w, 826vw, 806vw, 763vw, 727vw, 717vwsh, 686vw, 673vw, 627vw, 608vw, 577w, 548vw, 462vw, 417vw, 380vwsh, 373w, 351vw, 340vw, 319vw, 274vw, 261vw, 202vw, 172vw

C.I. name and group	Raman band wave numbers (cm^{-1}) and relative intensities (s, strong; m, medium; w, weak; sh, shoulder; v, very)
Monoazo pigment lakes	
PY100	1682vw, 1602vs, 1566vw, 1506m, 1476m-w, 1415vw, 1353msh, 1346m, 1316vw, 1269vw, 1231vwsh, 1220m-w, 1214wsh, 1178m-w, 1148vwsh, 1126m, 1098w, 1038vw, 1007vw, 989s-m, 982vwsh, 841w, 810w, 763vw, 716vw, 698vw, 647vw, 631w, 615w, 482vw, 461w, 453w, 396vw, 359vw, 282vw, 244vw, 213vw, 185vw
Diarylide	
PY55	1670vw, 1611msh, 1599vs, 1565vw, 1524vw, 1509vw, 1440vw, 1398m, 1326vw, 1308vw, 1287w, 1258s-m, 1242wsh, 1176vw, 1148vw, 1068vw, 1050vw, 1024vw, 951vw, 916vw, 871vw, 856vw, 790vw, 765vw, 705vw, 674vw, 657vw, 619vw, 609vwsh, 575vw, 550vw, 515vw, 491vw, 415vw, 397vw, 375w, 356vw, 329vw, 288vw, 262vw, 225vw, 198vw, 183vw, 163vw
PY81	1668vw, 1602vs, 1558vw, 1518w, 1510wsh, 1494w, 1447vw, 1394m, 1312wsh, 1302m-w, 1285w, 1267m-w, 1238w, 1230vwsh, 1195vw, 1156vw, 1123vw, 1077vwsh, 1066vw, 1058vwsh, 1017vw, 953w, 934vw, 897vw, 890vwsh, 884vw, 862vw, 826vw, 787vw, 740vw, 720vw, 708vwsh, 686vw, 670vw, 624vw, 596vw, 572vw, 565vw, 549vw, 495vw, 455vwsh, 449w, 433vw, 413vw, 386vw, 363vw, 341w, 331vwsh, 273vw, 241w, 215vw, 202vw, 172vw
Bisacetoacetarylide	
PY16	1673vwsh, 1667vw, 1633w, 1610m, 1594vs, 1551w, 1517wsh, 1510m, 1481w, 1430vw, 1415vw, 1391m, 1315s, 1276vs, 1248w, 1214vw, 1191vw, 1144w, 1127w, 1109vwsh, 1100vw, 1067vw, 952vw, 940vw, 907vw, 826vw, 785vw, 764vw, 743vw, 729vw, 696vw, 661vw, 619vw, 592vw, 535vw, 502vw, 464vw, 441vw, 413vw, 399vwsh, 386vw, 357vw, 341vw, 218vw, 190vw
PY155	1712w, 1665vw, 1636w, 1614s, 1596wsh, 1568m-w, 1532m, 1497s, 1445m, 1435s-m, 1391m, 1363vw, 1325m, 1315wsh, 1285wsh, 1266vs, 1232w, 1199wsh, 1186s-m, 1178m-w, 1120vw, 1079vw, 1067vw, 994vw, 952m-w, 897w, 866vw, 828vw, 804vw, 758vw, 715vw, 679vw, 625vw, 608m-w, 574vw, 470vw, 458vw, 435vw, 390m-w, 346vw, 314vw, 272vw, 230vw
Disazo condensation	
PY95	1668vw, 1636vw, 1598s-m, 1583msh, 1537wsh, 1521m, 1489vw, 1425m, 1381m-w, 1314vs, 1298m-wsh, 1270vw, 1252vwsh, 1242vw, 1190vw, 1136vw, 1066vw, 1046vw, 1025vw, 953w, 906vw, 888vw, 847vw, 785vw, 756vw, 728vw, 718vw, 702vw, 681vw, 648vw, 628vw, 602vw, 530vw, 473vw, 445vw, 422vw, 399vw, 379vw, 329vw, 313vw, 274vw, 234vw
PY128	1670vwbr, 1635vw, 1600s-m, 1580m, 1521m, 1480wbr, 1430m, 1384m, 1303s, 1259w, 1075vw, 1047vw, 955w, 915vw, 727vw, 324vw, 207vw, 190vw, 170vwsh, 154vwsh
Benzimidazolone	
PY151	1714vw, 1652m, 1628m-w, 1611wsh, 1602s-m, 1581vs, 1569m, 1515m, 1497m, 1488msh, 1455m, 1404msh, 1388s, 1371wsh, 1324m-wsh, 1315m, 1292m-w, 1272w, 1248s-m, 1207wsh, 1200m-w, 1161wsh, 1554w, 1144s-m, 1133w, 1069w, 1053vwsh, 1043w, 1023w, 967vwsh, 956m-w, 922vwsh, 907vw, 874vw, 844vw, 792vw, 767vw, 707vw, 689vwsh, 659vw, 629vw, 613m-w, 584vw, 572vw, 522vw, 505vw, 473vw, 409vw, 386m-w, 380wsh, 313w, 304vw, 226vw, 195vw
PY154	1661w, 1640m-w, 1630m-wsh, 1613s, 1590s, 1581msh, 1526w, 1503vs, 1484m-w, 1475m, 1439vw, 1403s, 1396m-wsh, 1366m, 1357wsh, 1325s-m, 1319msh, 1300s, 1267s, 1257s-m, 1219vw, 1166w, 1159m-w, 1143vw, 1133m-w, 1111vw, 1068m-w, 1059vwsh, 1036m, 1007m, 951m, 915w, 879w, 840vw, 821vw, 770w, 732vw, 704w, 624vw, 610w, 584vwsh, 574w, 564vw, 528vw, 512vw, 476w, 430vw, 394w, 351w, 298vw, 281w, 263vw, 228vw, 197vw, 179vw, 156w
Azomethine metal complex	
PY129	1615vwsh, 1600m, 1580wsh, 1569m, 1534s-m, 1512vw, 1484m, 1424m, 1385vs, 1353vw, 1339w, 1304vw, 1292vw, 1270m, 1213m-w, 1200vwsh, 1176w, 1153m, 1142vwsh, 1112vw, 1040vwsh, 1030vw, 978vw, 937vw, 922vwsh, 879vw, 845vw, 758vw, 742vw, 651vw, 630vw, 603w, 558vw, 502vw, 465vw, 455vw, 413vw, 289vw, 269vwsh, 233vw, 193vw
PY153	1683m-w, 1633vw, 1603vs, 1554s, 1537s-m, 1495w, 1446s-m, 1433m, 1419m-wsh, 1370s-m, 1358s-m, 1315vs, 1300m, 1263s, 1240s-msh, 1233s, 1176s-m, 1156w, 1132m, 1104vw, 1080vw, 1032w, 999vs, 988m-w, 966m-w, 905vw, 827m, 813wsh, 759m-w, 722m-w, 710vwsh, 686vw, 616w, 564w, 522w, 513vw, 465m-w, 439w, 406vw, 382m-w, 366vw, 358vwsh, 307m-w, 273vw, 259m, 250wsh, 213m, 154vw
Isoindolinone and isoindoline	
PY109	1724vw, 1706vw, 1673vs, 1664s-msh, 1576m-w, 1568wsh, 1454vw, 1376w, 1369m-w, 1325vwsh, 1311w, 1290vw, 1244s, 1204m-w, 1189vw, 1094w, 1060vw, 938vw, 919vw, 905vw, 818w, 791vw, 760m-w, 748vwsh, 722w, 696vwsh, 684vw, 663vw, 631vwsh, 622w, 582vw, 531vw, 498vw, 449vw, 385vwsh, 368vw, 349vw, 330vwsh, 290vw, 258vw, 223vw, 218vwsh, 189vw
PY110	1719w, 1669s-m, 1597vs, 1575m-wsh, 1380m-w, 1350vw, 1318w, 1299vw, 1231s-m, 1200m-w, 1182vw, 1166s, 1080w, 934w, 929vwsh, 858vw, 831vw, 805vw, 784m-w, 747vw, 724m, 682m, 660vw, 620w, 592w, 549s-m, 452m-w, 445wsh, 384w, 360vw, 333vw, 312vw, 233vw, 209vw, 170s-m

C.I. name and group	Raman band wave numbers (cm^{-1}) and relative intensities (s, strong; m, medium; w, weak; sh, shoulder; v, very)
PY173	1708m-w, 1685vs, 1616vw, 1584s, 1572msh, 1470vw, 1374wsh, 1364w, 1313vw, 1270vw, 1253m, 1245m, 1221vw, 1188vw, 1168vw, 1143m, 1053vwsh, 1037w, 1011w, 960vw, 902vw, 889vw, 845w, 825vw, 801vw, 779w, 763vw, 728vw, 708w, 686vw, 655m, 632vw, 610vw, 590w, 553vw, 540vw, 527w, 497s-m, 477vw, 446vw, 389vw, 371vw, 331vw, 304vw, 265vw, 230w, 196m-w
PY139	1724vw, 1700vw, 1662vw, 1650vwsh, 1597vwsh, 1584m-w, 1563vs, 1501vw, 1466vw, 1419vw, 1379w, 1367w, 1318vw, 1300vw, 1256vw, 1239vw, 1183vw, 1142vw, 1089vw, 1038vw, 955vw, 904vw, 837vw, 800vw, 765vw, 706vw, 690w, 654vw, 636vw, 604m-w, 561vw, 515vw, 466vw, 440vw, 421vw, 335vw, 291w, 243m, 233m-w, 179vw, 155vw

Spectra Reported By Vandenabeele, 2000 (λ_0=780nm):

CI name	Supplier	Raman band wavenumbers $\tilde{\nu}$/cm^{-1} (between 1800 and 50 cm^{-1})
PY 1	SunChemicals	1670(w), 1621(vs), 6101(m-w), 1564(w), 1533(w), 1485(vs), 1450(vw), 1406(w), 1386(m), 1337(m-w), 1323(m), 1310(vs), 1255(m), 1216(m), 1192(w), 1178(w), 1168(w), 1138(vs), 1068(vw), 999(m), 951(m-w), 925(w), 845(w), 824(w), 786(m), 616(w), 511(w), 460(w), 410(vw), 390(m-w), 361(w), 353(vw), 186(w)
PY 3	Schmincke, SunChemicals	1671(vw), 1612(m), 1593(w,sh), 1566(vw), 1545(vw), 1494(m), 1442(vw), 1386(m), 1336(m-s), 1309(m), 1275(vw), 1243(w), 1189(w), 1153(vw), 1138(vs), 1105(vw), 1061(vw), 1036(vw), 957(vw), 915(vw), 848(vw), 824(vw), 791(vw), 745(w), 707(vw), 675(vw), 649(m-w), 621(w), 542(vw), 486(vw), 449(vw), 434(vw), 411(w), 394(w), 370(vw), 355(vw), 345(vw), 296(vw), 272(vw), 201(w), 184(w), 136(w), 111(vw)
PY 65	SunChemicals	1670(w), 1623(m), 1601(m-w), 1576(vw), 1543(w), 1534(w,sh), 1488(vs), 1460(vw), 1441(w), 1424(m-w), 1392(m-s), 1344(m), 1326(s), 1316(m,sh), 1295(vw), 1275(vw), 1252(m), 1229(vs), 1190(w), 1171(w), 1135(vs), 1072(vw,sh), 1062(vw), 1049(vw), 1027(vw), 951(w), 932(w), 916(vw), 829(w), 794(m-s), 777(vw), 759(vw), 705(vw), 689(vw), 672(vw), 622(m-w), 607(w), 580(vw), 558(vw), 535(w), 512(vw), 497(vw), 480(vw), 447(w), 411(w), 398(vw), 377(w), 340(vw), 325(w), 229(vw), 184(w), 150(vw), 112(vw)
PY 74	Kremer, SunChemicals	1667(vw), 1593(m), 1549(vw), 1511(w), 1489(w), 1438(vw), 1404(w), 1352(m), 1327(vs), 1298(w), 1263(s), 1202(vw), 1170(vw), 1159(w), 1125(vw), 1117(vw), 1089(w), 1067(vw), 1046(vw), 1019(vw), 954(vw), 917(vw), 846(vw), 826(vw), 802(w), 781(vw), 741(vw), 717(vw), 646(vw), 624(vw), 601(vw), 525(vw), 498(vw), 464(vw), 441(vw), 404(vw), 360(vw), 319(vw), 259(vw), 225(vw), 186(vw)
PR 3	Kremer	1619(m), 1604(w,sh), 1554(w), 1524(vw), 1496(m), 1444(m-s), 1394(m), 1332(vs), 1320(s,sh), 1251(w), 1225(w,sh), 1216(m), 1186(m-s), 1127(m), 1076(w), 986(m), 923(w), 842(m-w), 796(m), 723(m-w), 616(m), 503(w), 479(vw), 454(m-w), 422(vw), 402(vw), 384(w), 340(m-s), 168(w)
PY 12	SunChemicals	1661(vw), 1597(vs), 1554(vw), 1517(vw), 1490(vw), 1449(vw), 1399(m), 1320(vw), 1294(w), 1255(w), 1228(vw), 1179(vw), 1140(vw), 1065(vw), 1050(vw), 1001(vw), 952(vw), 917(vw), 871(vw), 817(vw), 718(vw), 661(vw), 623(vw), 613(vw), 515(vw), 475(vw), 449(vw), 407(vw), 365(vw), 330(vw), 308(vw), 284(vw), 256(vw), 204(vw), 183(vw), 125(vw)
PY 13	SunChemicals	1673(vw), 1598(vs), 1553(vw), 1522(vw), 1491(vw), 1448(vw), 1399(m-w), 1315(vw), 1287(w), 1258(m-w), 1248(w,sh), 1183(vw), 1144(vw), 1067(vw), 1049(vw), 953(vw), 938(vw), 907(vw), 874(vw), 829(vw), 780(vw), 720(vw), 707(vw), 674(vw), 658(vw), 620(vw), 564(vw), 541(vw), 492(vw), 443(vw), 420(vw), 398(vw), 345(vw), 272(vw), 225(vw), 199(vw), 171(vw), 114(vw)
PY 14	SunChemicals	1670(vw), 1597(vs), 1557(vw), 1524(vw), 1481(vw), 1458(vw), 1400(w), 1313(vw), 1287(w), 1258(m), 1180(vw), 1145(vw), 1068(vw), 1049(vw), 954(vw), 918(vw), 798(vw), 769(vw), 709(vw), 659(vw), 623(vw), 539(vw), 512(vw), 477(vw), 444(vw), 422(vw), 396(vw), 344(vw), 280(vw), 203(vw), 172(vw), 120(vw)
PY 17	SunChemicals	1668(vw), 1599(vs), 1546(vw), 1518(vw), 1489(vw), 1461(vw), 1436(vw), 1399(m), 1334(vw), 1292(vw), 1268(w), 1256(w), 1183(vw), 1162(vw), 1067(vw), 1049(vw), 953(vw), 918(vw), 832(vw), 794(vw), 712(vw), 665(vw), 618(vw), 508(vw), 453(vw), 409(vw), 349(vw), 268(vw), 215(vw), 176(vw), 124(vw)
PY 83	Schmincke, SunChemicals	1659(vw), 1595(vs), 1540(vw), 1523(vw), 1511(vw), 1449(vw), 1399(m), 1333(w), 1289(w), 1253(m), 1218(vw), 1148(vw), 1136(vw), 1067(vw), 1049(vw), 956(vw), 920(vw), 692(vw), 661(vw), 638(vw), 538(vw), 421(vw), 394(vw), 342(vw), 265(vw), 211(vw), 176(vw), 158(vw)
PR 49:1	SunChemicals	1617(m), 1602(m-w), 1557(w), 1483(m-s), 1465(m), 1450(w), 1425(m-s), 1413(m-s), 1349(m-s), 1278(vw), 1257(w), 1232(m-w), 1215(m-s,sh), 1206(vs), 1172(vw), 1136(w), 1097(m-w), 1057(vw), 1035(vw), 993(vw), 946(vw), 917(vw), 873(vw), 826(vw), 800(vw), 775(vw), 720(s), 661(vw), 645(w), 604(w), 542(vw), 529(m), 515(vw), 481(vw), 469(w), 411(m-w), 357(w), 343(m-w), 304(vw), 280(vw), 254(vw), 236(vw), 216(vw), 199(vw), 172(vw)

CI name	Supplier	Raman band wavenumbers $\tilde{\nu}$/cm^{-1} (between 1800 and 50 cm^{-1})
PR 53 : 1	SunChemicals	1596(m-w), 1571(w,sh), 1552(m), 1482(m), 1451(w), 1401(vs), 1378(w), 1333(m), 1316(w), 1291(vw), 1259(m-w), 1236(vs), 1199(m-s), 1159(vw), 1138(vw), 1095(m), 1040(vw), 993(vw), 978(w), 871(vw), 805(w), 741(vw), 719(w), 667(vw), 630(m-w), 612(m-w), 577(vw), 557(vw), 540(vw), 515(vw), 497(w), 436(w), 426(w,sh), 338(m-w), 311(m-w), 242(vw), 205(w), 173(vw)
PR 52 : 1	SunChemicals	1598(m), 1575(w,sh), 1554(m), 1488(m), 1456(vw), 1440(vw), 1403(vs), 1362(vs), 1336(vw), 1324(vw), 1294(vw), 1265(m-w), 1237(s), 1179(s), 1159(vw), 1106(w), 1045(w), 1020(vw), 961(s), 871(vw), 802(vw), 786(vw), 744(m-w), 718(vw), 711(vw), 668(vw), 653(vw), 627(vw), 599(vw), 562(w), 528(m-w), 463(w), 434(w), 418(vw), 406(vw), 360(m), 346(m,sh), 325(vw), 240(vw), 210(vw), 182(vw), 138(vw)
PR 57 : 1	SunChemicals	1602(m), 1550(vw), 1490(m-s), 1409(vw), 1365(vs), 1336(vw), 1325(vw), 1294(vw), 1265(m-w), 1230(m-w), 1182(m), 1130(w), 1118(vw,sh), 1038(vw), 1020(vw), 964(vw), 888(vw), 876(vw), 822(vw), 785(vw), 746(w), 714(vw), 701(vw), 597(vw), 559(vw), 520(w), 497(w), 466(vw), 417(vw), 362(vw), 335(w), 309(vw), 253(vw), 150(vw)
PR 8	Kremer	1673(w), 1572(vw), 1519(vs), 1449(w), 1356(vw), 1296(vw), 1227(w), 1180(w), 1119(w), 825(w), 771(w), 620(m-w), 533(w), 492(m), 421(w), 347(m-s), 329(w), 235(vw), 140(vw)
PR 9	Kremer	1604(w), 1579(m-s), 1549(w), 1485(m), 1448(vw), 1362(vs), 1337(w), 1283(m-w), 1257(vw), 1237(m), 1204(vw), 1153(w), 1135(vw), 1108(vw), 1041(w), 1017(vw), 968(w), 853(vw), 807(w), 769(w), 728(w), 665(vw), 642(vw), 609(vw), 565(m-w), 520(vw), 490(w), 448(vw), 432(w), 339(w), 326(vw,sh), 149(w)
PR 17	SunChemicals	1610(m), 1592(vw), 1550(w), 1519(vw), 1488(m), 1454(vw), 1425(m-w), 1362(vs), 1319(vw), 1284(w), 1240(m-w), 1204(vw), 1164(w), 1107(w), 1041(vw), 1015(vw), 997(vw), 966(w), 943(vw,sh), 898(vw), 854(vw), 826(vw), 807(vw), 756(w), 727(w), 666(vw), 620(vw), 539(vw), 516(vw), 483(w), 445(vw), 426(w), 401(vw), 363(w), 343(w)
PR 22	SunChemicals	1611(m-w), 1590(vw,sh), 1550(w), 1519(vw), 1485(m-w), 1453(w), 1424(m-w), 1362(vs), 1347(w), 1318(w), 1283(m-w), 1267(vw), 1238(m-w), 1206(vw), 1161(w), 1107(w), 998(vw), 966(w), 939(w), 856(vw), 826(vw), 798(vw), 771(vw), 734(w), 665(vw), 623(vw), 548(vw), 528(vw), 512(vw), 476(w), 425(w), 399(vw), 363(w), 342(w), 224(vw), 176(vw)
PR 23	SunChemicals	1613(m-w), 1600(w,sh), 1550(w), 1499(vs), 1483(w), 1443(w), 1366(m-s), 1346(vs), 1329(w), 1293(m), 1259(m-w), 1238(m-w), 1172(w), 1160(w), 1108(w), 1078(vw), 1038(vw), 1015(vw), 969(w), 940(w), 837(w), 796(vw), 774(vw), 742(w), 632(w), 610(vw), 496(w), 413(w), 397(w), 370(w), 345(w), 319(vw), 300(vw), 277(vw), 236(vw), 214(vw)
PR 112	Schmincke, Kremer	1604(vw), 1578(s), 1551(w), 1482(m), 1460(w), 1448(w,sh), 1423(vw), 1391(m), 1374(m), 1357(vs), 1331(vw), 1281(s), 1258(vw), 1242(w), 1229(m-s), 1204(vw), 1160(m-w), 1108(w), 1061(w), 1014(vw), 967(w), 892(vw), 865(vw), 813(w), 744(w), 728(w), 679(m-w), 615(w), 571(w), 527(m), 467(vw), 442(w), 429(w), 391(vw), 346(m), 296(vw), 279(vw), 245(vw), 150(vw)
PR 170	Kremer	1605(m-s), 1593(w,sh), 1549(w), 1512(m-w), 1488(w), 1452(vw), 1423(vw), 1388(w), 1363(vs), 1332(w), 1288(m-w), 1244(w), 1164(m), 1142(vw), 1119(vw), 1047(vw), 1013(vw), 964(m-w), 859(vw), 802(vw), 775(vw), 729(m), 665(vw), 610(vw), 573(w), 537(w), 512(vw), 490(w), 479(vw,sh), 423(w), 371(vw), 331(vw), 266(vw), 236(vw), 208(vw), 188(vw), 146(vw)

Appendix J: Density Functional Theory Input and Resultant Spectra

Pigment Orange 16

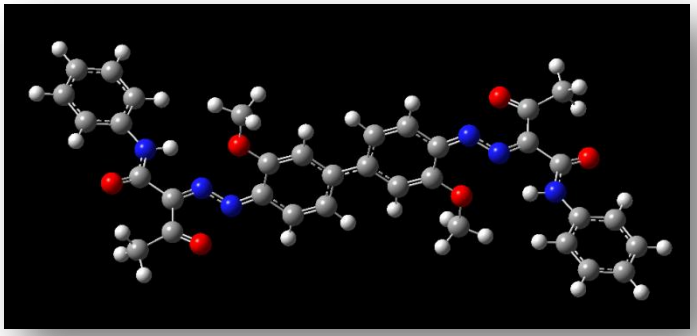

Preprocessing Note: Pigment Orange 16 in vac optandfreq after initial opt with sto

File Name: pigment_orange_16_freq

File Type: .log

Calculation Type: FREQ

Calculation Method: RB3LYP

Basis Set: 6-311G(d,p)

Charge: 0

Spin: Singlet

E(RB3LYP): -2093.95103360a.u.

RMS Gradient Norm: 0.00000188a.u.

Imaginary Freq: 0

Dipole Moment: 0.0006Debye

Point Group: C1

Job cpu time: 1 days 20 hours 15 minutes 40.0 seconds

Pigment Orange 16

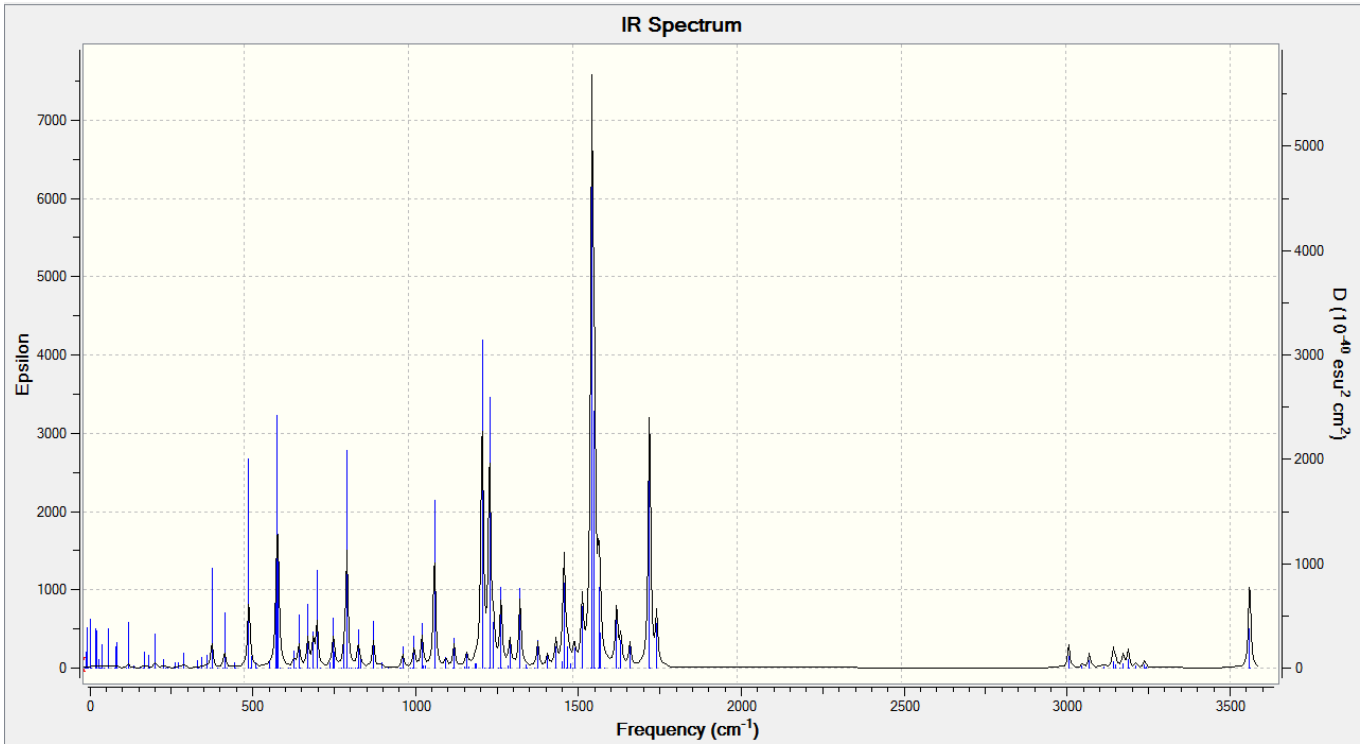

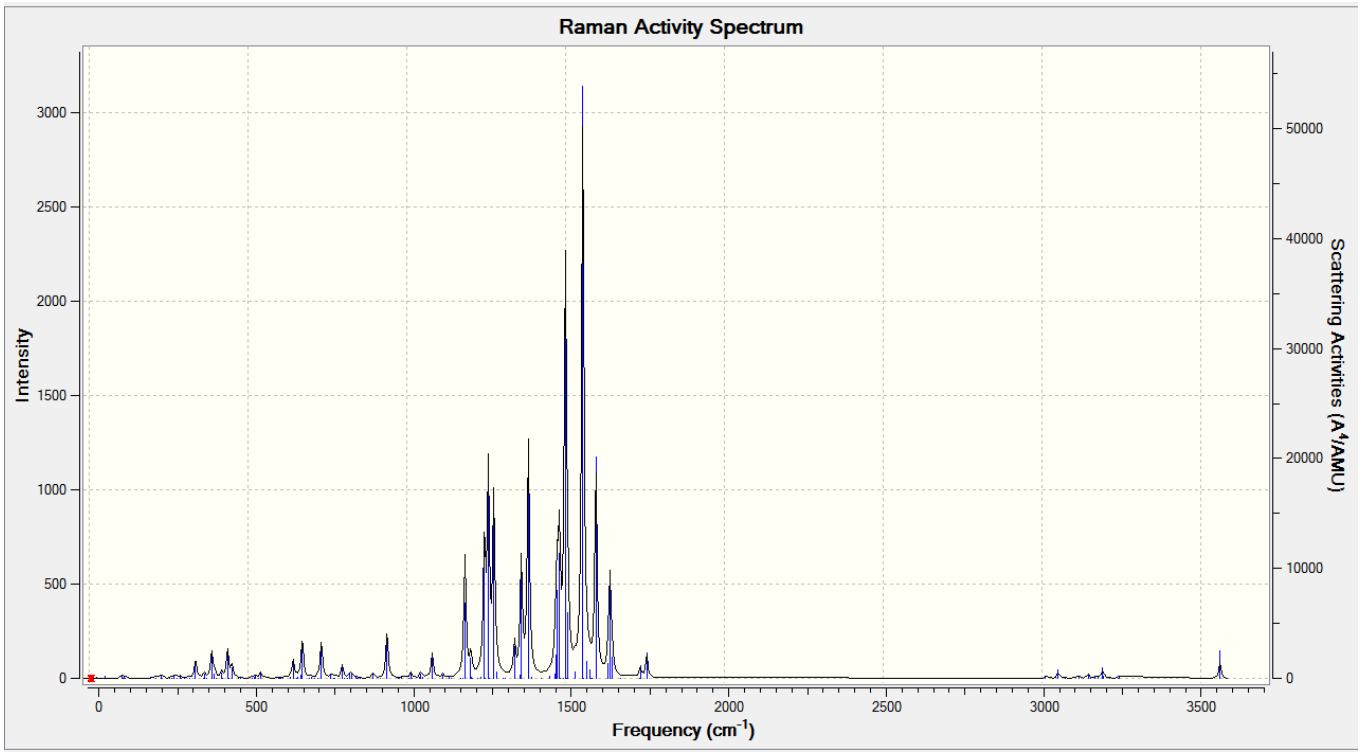

Pigment Red 122

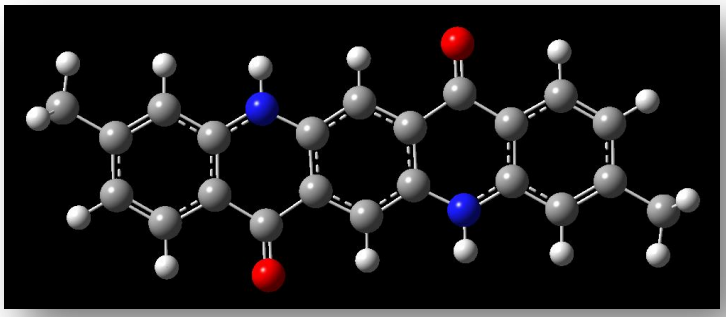

Preprocessing Note: Pigment Red 122_opt in vac optanffreq after opt with sto

File Name: pigment_red_122_freq

File Type: .log

Calculation Type: FREQ

Calculation Method: RB3LYP

Basis Set: 6-311G(d,p)

Charge: 0

Spin: Singlet

E(RB3LYP): -1108.27861652a.u.

RMS Gradient Norm: 0.00001084a.u.

Imaginary Freq: 0

Dipole Moment: 0.0005Debye

Point Group: C1

Job cpu time: 0 days 17 hours 19 minutes 40.7 seconds

Pigment Red 122

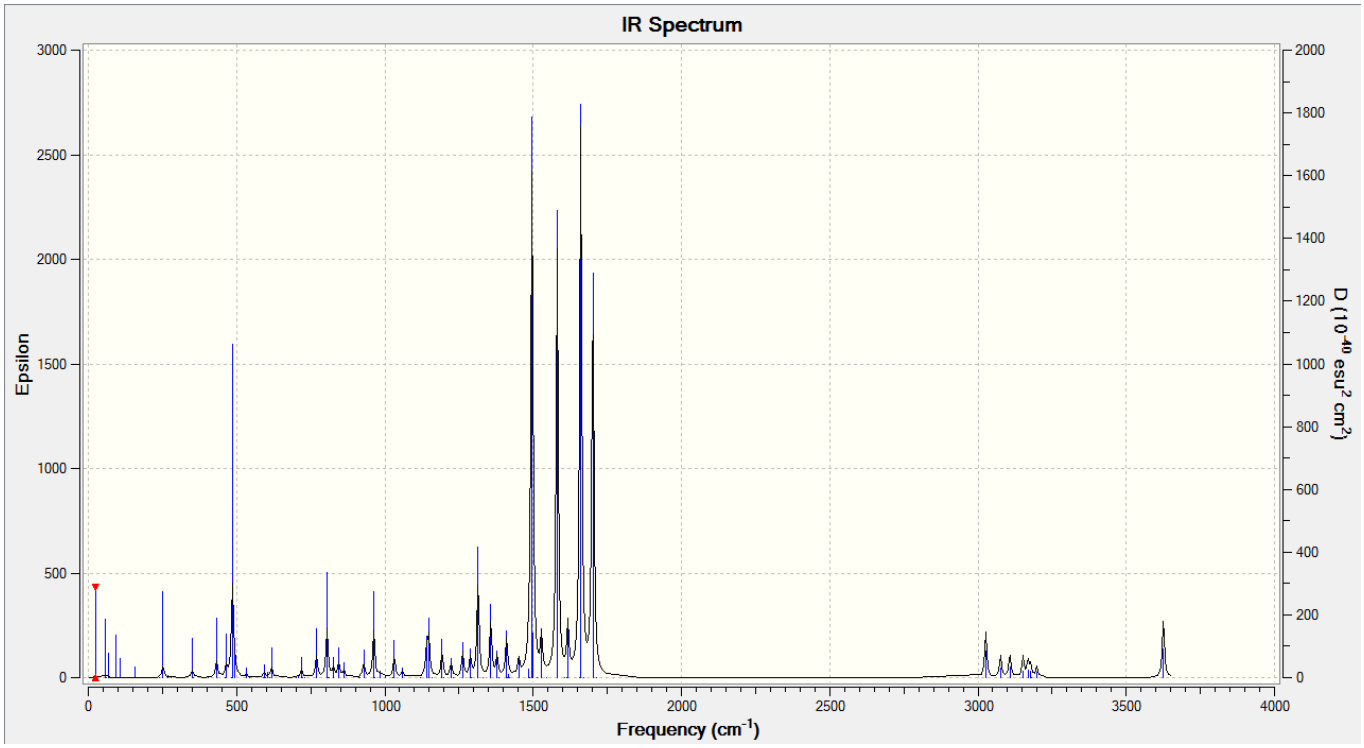

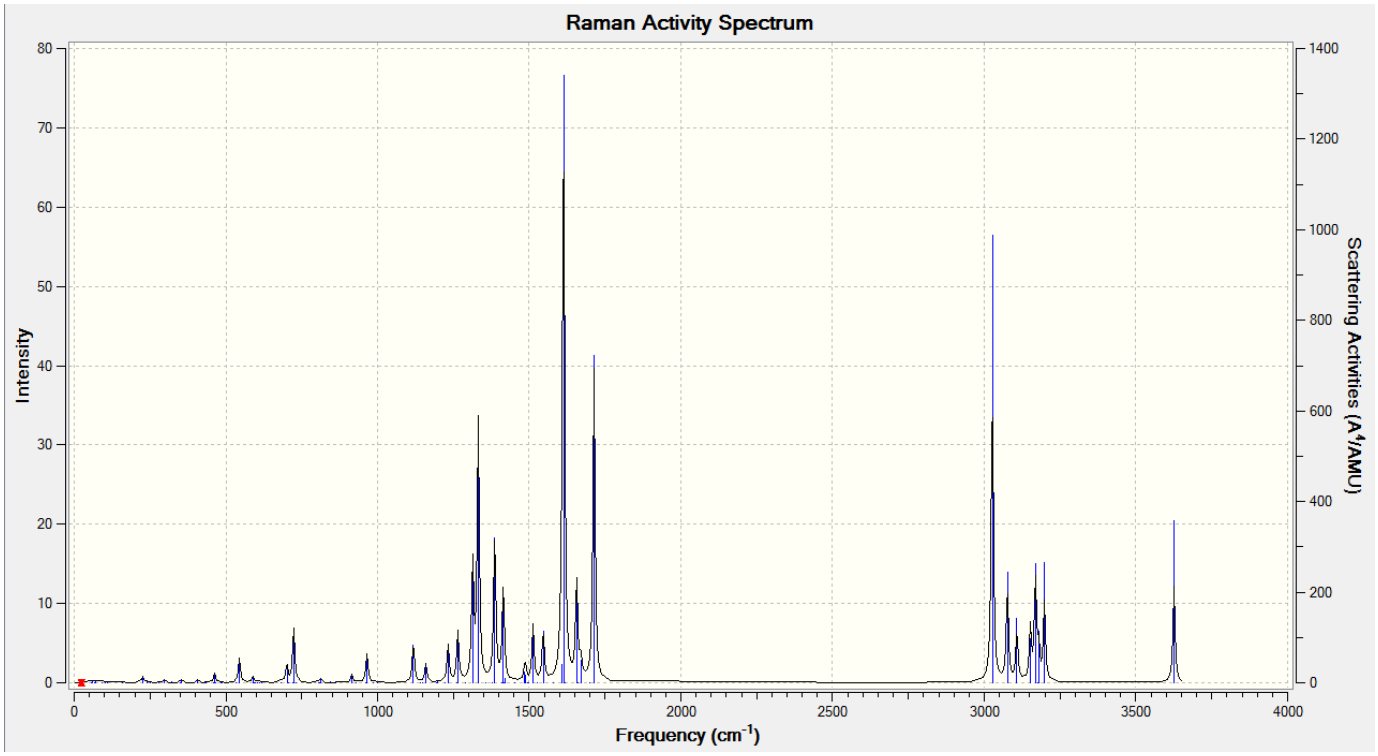

Pigment Red 170

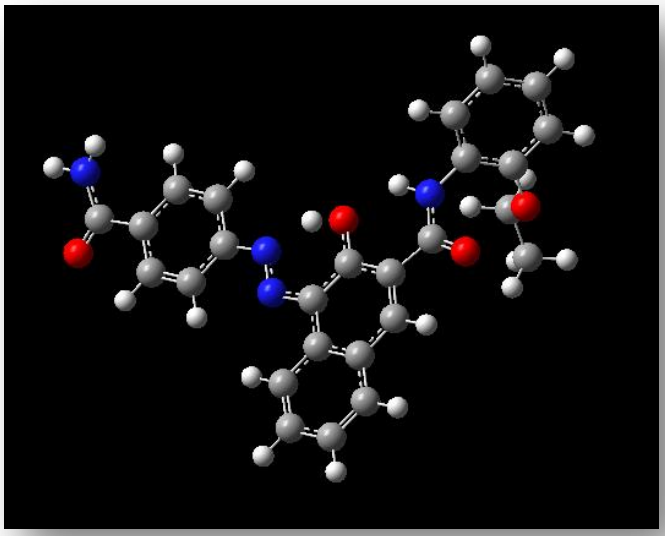

Preprocessing Note: Pigment Red 170 in vac with optandfreq after opt with sto in addition to optimization of the geometry

File Name: pigment_red_170_new_freq2

File Type: .log

Calculation Type: FREQ

Calculation Method: RB3LYP

Basis Set: 6-311G(d,p)

Charge: 0

Spin: Singlet

E(RB3LYP): -1524.31578103a.u.

RMS Gradient Norm 0.00000935a.u.

Imaginary Freq: 0

Dipole Moment: 4.0238Debye

Point Group: C1

Job cpu time: 2 days 4 hours 26 minutes 28.9 seconds

Pigment Red 170

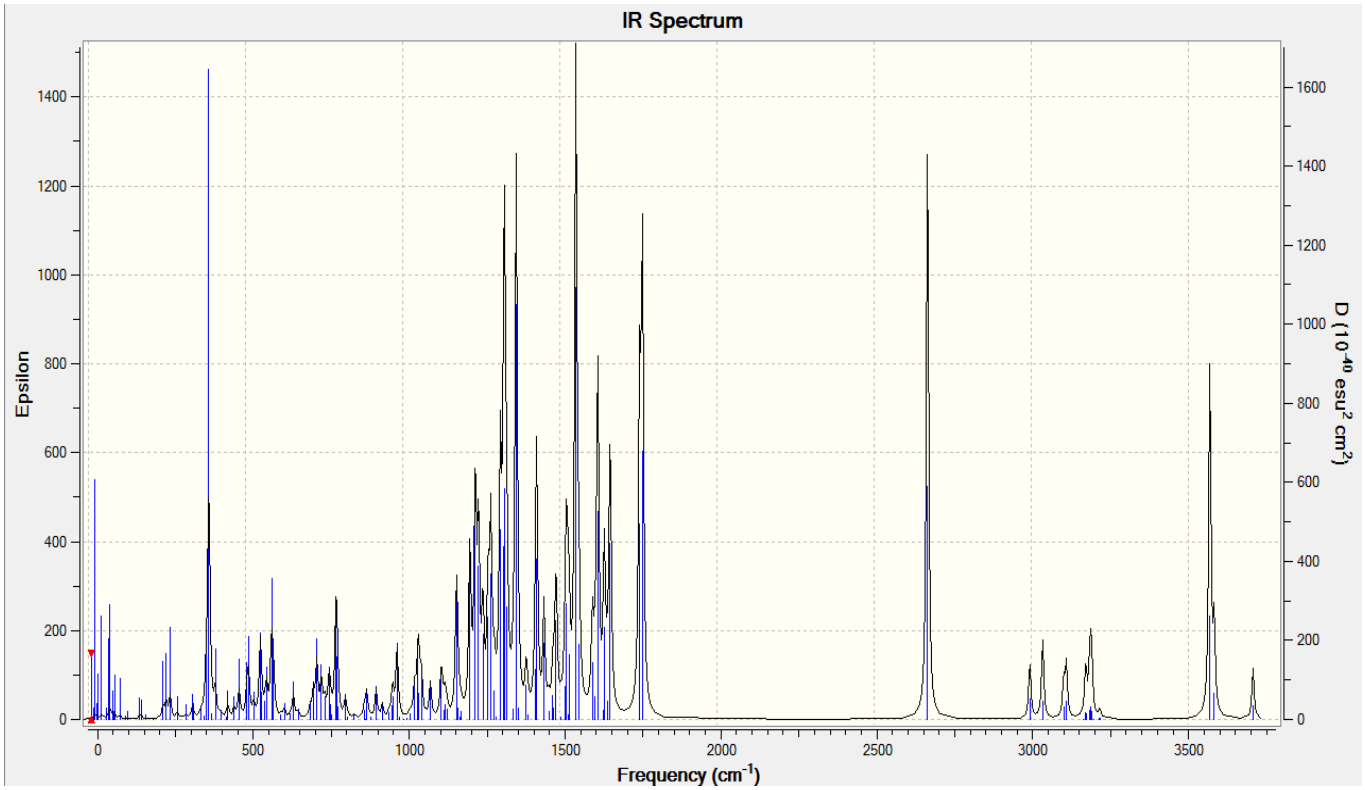

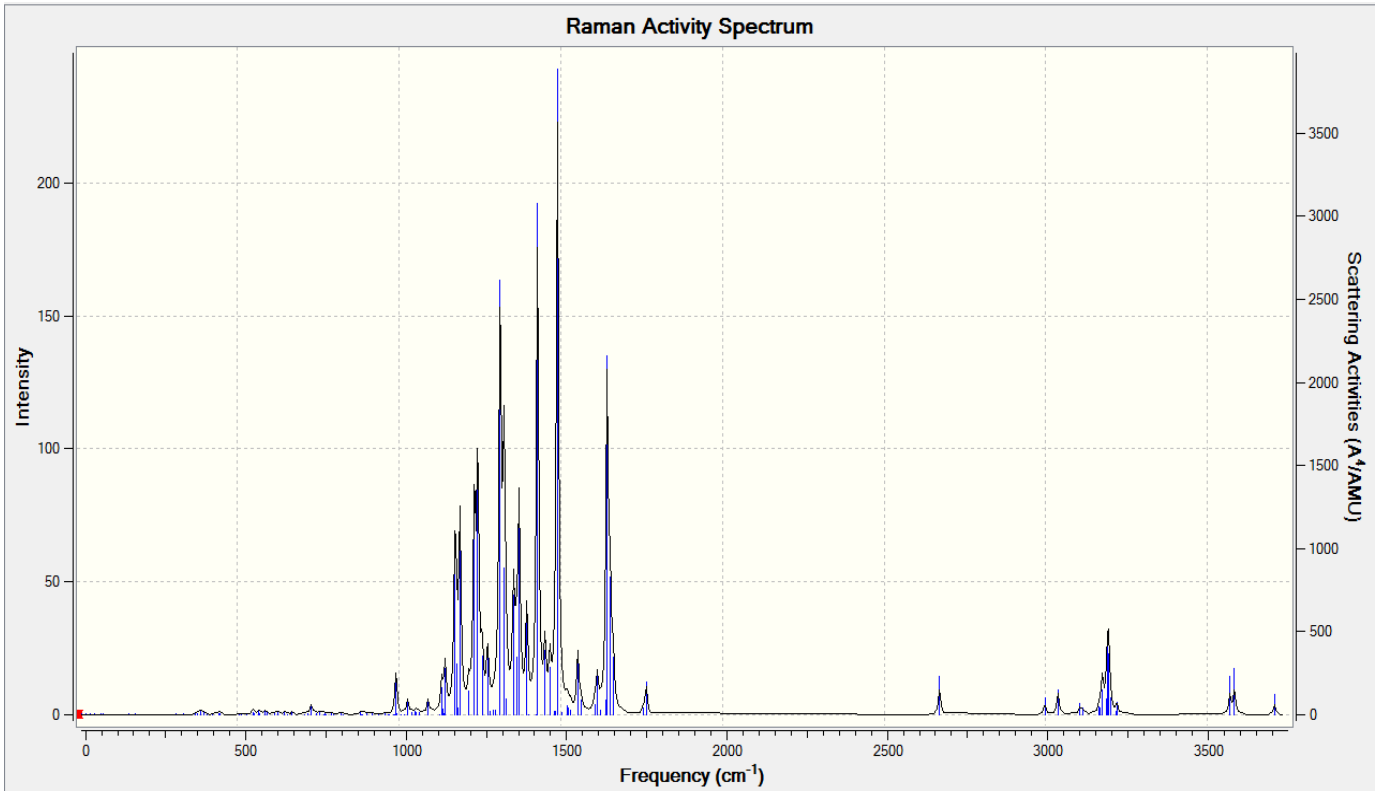

Chapter 7: References

Abbott, L., S. Batchelor, J.L. Smith & J. Moore (2010). Resonance Raman and UV-visible spectroscopy of black dyes on textiles, *Forensic Science International*, *202*(1-3), 54-63.

Adar, F. (2010, March 1). Depth resolution of the Raman microscope: Optical limitations and sample characteristics, *Spectroscopy Magazine Online*. Retrieved from http://spectroscopyonline.findanalytichem.com/spectroscopy/article/articleDetail.jsp?id=662976.

Allen, F.S., J. Zhao, D. Butterfield (2000), United States Patent 6,141,095. Apparatus for measuring and applying instrumentation correction to produce a standard Raman spectrum.

Ambade, V.N., A.N. Keoliya & P.G. Dixit (2011). Decomposed bodies-Still an unrewarding autopsy? *Journal of Forensic and Legal Medicine*, *18*(3), 101-106.

Armelagos, G. (1969). Disease in ancient Nubia, *Science*, *New Series*, *163*(3864), 255-259.

Armstrong, M. (2005). Tattooing, body piercing, and permanent cosmetics: A historical and current view of state regulations with continuing concerns, *Journal of Environmental Health*, *67*(8), 38-43.

ASTM Standard E 1840-96 (2002). Standard Guide for Raman Shift Standards for Spectrometer Calibration.

ASTM Standard E 1683-02 (2006). Standard Practice for Testing the Performance of Screening Raman Spectrometers.

ASTM Standard E 2529-06 (2006). Standard Guide for Testing the Resolution of a Raman Spectrometer.

Baeumler, W., R. Vasold, J. Lundsgaard & H. Talberg (2003). Chemicals used in tattooing and permanent make up products, Proceedings of the European Commission's Workshop on Technical/Scientific and Regulatory Issues on the Safety of Tattoos, Body Piercing and of Related Practices, Italy.

Bäumler, W., E. Eibler, U. Hohenleutner, B. Sens, J. Sauer, & M. Landthaler (2000). Q-switch laser and tattoo pigments: First results of the chemical and photophysical analysis of 41 compounds, *Lasers in Surgery and Medicine*, *26*(1), 13-21.

Basova, T., V. Kiselev, B. Schuster, H. Peisert and T. Chassé (2009). Experimental and theoretical investigation of vibrational spectra of copper phthalocyanine: Polarized single-crystal Raman spectra, isotope effect and DFT calculations, *Journal of Raman Spectroscopy*, 40, 2080-2087.

Basova, T and B. Kolesov (2000). Raman spectra of copper phthalocyanin: Experiment and calculation, *Journal of Structural Chemistry*, 41(5), 770-777.

Bell, I., R. Clark, & P. Gibbs (1997). Raman spectroscopic library of natural and synthetic pigments (pre 1850AD), *Spectrochimica Acta Part A*, *53*(12), 2159-2179.

Bell, S. (1999). Tattooed: A participant observer's exploration of meaning, *Journal of American Culture*, *22*(2), 53-58.

Bell, S., L. Fido, S. Speers, W. Armstrong & S. Spratt (2005). Forensic analysis of architectural finishes using Fourier transform infrared and Raman spectroscopy, part II: white paint, *Applied Spectroscopy*, *59*(11), 1340-1346.

Bell, S., L. Fido, N. Sirimuthu, S. Speers, K. Peters, & S. Cosbey (2007). Screening tablets for DOB using surface-enhanced Raman spectroscopy, *Journal of Forensic Science*, *57*(5), 1063-1067.

Bennett, J. and L. Rockhold (1999). Use of an alternate light source for tattoo recognition in the extended postmortem interval, *Journal of Forensic Sciences*, *44*(1), 182-184.

Beute, T., C. Miller, A. Timko, & E. Ross (2008). *In vitro* spectral analysis of tattoo pigments, *Dermatologic Surgery*, *34*(4), 508-516.

Billmeyer, F., R. Kumar & M. Saltzman (1981). Identification of organic colorants in art objects by solution spectrometry: Pigments, *Journal of Chemical Education*, *58*(4), 307-313.

Birke, R.L. & J.R. Lombardi (1988). Surface enhanced Raman scattering. In R.J. Gale (Ed.), *Spectroelectrochemistry: Theory and practice* (pp. 263-348). New York, NY: Plenum Publishing Corporation.

Bishop, D. (1993). *Group Theory and Chemistry*, New York, NY: Dover Publications, Inc.

Biswas, N. & S. Umapathy (2000). Structures, vibrational frequencies, and normal modes of substituted azo dyes: Infrared, Raman, and density functional calculations, *Journal of Physical Chemistry A*, *104*(12), 2734-2745.

Blanchard, M. (1991). Post-Bourgeois tattoo: Reflections on skin writing in late capitalist societies, *Visual Anthropology Review*, *7*(2), 11-21.

Bouchard, M., R. Rivenc, C. Menke & T. Learner (2009). Micro-FTIR and micro-Raman study of paints used by Sam Francis, *e-Preservation Science*, *6*, 27-37.

Bouchard, M. & D. Smith (2003). Catalogue of 45 reference Raman spectra of minerals concerning research in art history or archaeology, especially on corroded metals and coloured glass, *Spectrochimica Acta Part A*, *59*(10), 2247-2266.

Bovill, A, A. McConell, J. Nimmo and W. Smith (1986). Resonance Raman spectra of α-copper phthalocyanine, *Journal of Physical Chemistry*, 90, 569-575.

Bowie, B., B. Chase & P. Griffiths (2000) Factors affecting the performance of bench-top Raman spectrometers. Part I: Instrumental effects, *Applied Spectroscopy*, *54*(5).

Bowie, B., B. Chase & P. Griffiths (2000). Factors affecting the performance of bench-top Raman spectrometers. Part II: Effect of sample, *Applied Spectroscopy*, 54(6).

Breitman, M., S. Ruiz-Moreno & A. Lopez Gil (2007). Experimental problems in Raman spectroscopy applied to pigment identification in mixtures, *Spectrochimica Acta A*, *68*(4), 1114-1119.

Brennan, J., Y. Wang, R. Dasari & M. Feld (1997). Near-infrared Raman spectrometer systems for human tissue studies, *Applied Spectroscopy*, *51*(2), 201-208.

Brostoff, L. B., S. Centeno, P. Ropret, P. Bythrow & F. Pottier (2009). Combined x-ray diffraction and Raman identification of synthetic organic pigments in works of art: From powder samples to artists' paints, *Analytical Chemistry*, *81*(15), 6096-6106.

Buckland, A. (1888). On tattooing, *The Journal of the Anthropological Institute of Great Britain and Ireland, 17*, 318-328.

Bunker, P. and P. Jensen (1998). *Molecular symmetry and spectroscopy*, Second edition. Ottawa, Canada: NRC Research Press.

Burd, J. (2010, September 22). Man indicted in slaying, body dumping, *The Journal News*.

Burgio L. & R. Clark (2001). Library of FT-Raman spectra of pigments, minerals, pigment media and varnishes, a supplement to existing library of Raman spectra of pigments with visible excitation, *Spectrochimica Acta Part A*, *57*(7), 1491-1521.

Burris, K. & K. Kim (2007). Tattoo removal, *Clinics in Dermatology*, *25*, 388-392.

Campion, A. & P. Kambhampati (1998). Surface-enhanced Raman scattering, *Chemical Society Reviews*, *27*(4), 241-250.

Cañamares, M. & M. Leona (2007). Surface-enhanced Raman scattering study of the red dye laccaic acid, *Journal of Raman Spectroscopy*, *38*(10), 1259-1266.

Cañamares, M., M. Leona, M. Bouchard, C. Grzywacz, J. Wouters, & K. Trentelman (2010). Evaluation of Raman and SERS analytical protocols in the analysis of cape jasmine dye (*Gardenia agusta L.*), *Journal of Raman Spectroscopy*, *41*(4), 391-397.

Cañamares, A., J. Lombardi & M. Leona (2008). Surface-enhanced Raman scattering of photoberberine alkaloids, *Journal of Raman Spectroscopy*, *39*(12), 1907-1914.

Caplan, J. (1997). Speaking Scars: The tattoo in popular practice and medico-legal debate in nineteenth century Europe, *History Workshop Journa*l, No. 44, 106-142.

Caplan, J., Ed. (2000). Written on the body: The tattoo in European and American history, Princeton, NJ: Princeton University Press.

Carter D. & J. Pemberton (1995). Frequency/wavelength calibration of multipurpose multichannel Raman spectrometers, Part I: Instrumental factors affecting precision, *Applied Spectroscopy*, *49*(11), 1550-1560.

Carter, D., W. Thompson, C. Taylor & J. Pemberton (1995). Frequency/wavelength calibration of multipurpose multichannel Raman spectrometers, Part II: calibration fit considerations and calibration standards, *Applied Spectroscopy*, *49*(11), 1561-1576.

Casper, J.L. (1861). A handbook of the practice of forensic medicine based upon personal experience, London: The New Sydenham Society.

Caspers, P., G. Lucassen & G. Puppels (2003). Combined *in vivo* confocal Raman spectroscopy and confocal microscopy of human skin, *Biophysical Journal*, *85*(1), 572-580.

Centeno, S., V. Buisan & P. Ropret (2006). Raman study of synthetic organic pigments and dyes in early lithographic inks (1890-1920), *Journal of Raman Spectroscopy*, *37*(10), 1111-1118.

Chang, J., M. Cañamares, M. Aydin, W. Vetter, M. Schreiner, W. Xu & J. Lombardi (2009). Surface-enhanced Raman spectroscopy of indanthrone and flavanthrone, *Journal of Raman Spectroscopy*, *40*(11), 1557-1563.

Chase, B. (1987). Fourier Transform Raman Spectroscopy, *Analytical Chemistry*, *59*(14), 881A-889A

Chemischen und Veterinäruntersuchungsämter (2010). Tatowierfarben enthalten gefahrliche Stoffe. Daher besteht erhohter Handlunsbedarf. [Freiburg & Karlsruhe], Tatowierfarben rot, orange, gelb. Retrieved from http://www.ua-bw.de/pub/bietrag.asp.

Chen, K., M. Leona, K. Vo-Dinh, F. Yan, M. Wabuyele, & T. Vo-Dinh (2006). Application of surface-enhanced Raman scattering (SERS) for the identification of anthraquinone dyes used in works of art, *Journal of Raman Spectroscopy*, *37*(4), 520-527.

Choquette, S., E. Etz, W. Hurst, D. Blackburn & S. Leigh (2007). Relative intensity correction of Raman spectrometers: NIST SRMs 2241 through 2243 for 785nm, 532nm, and 488nm/514.5nm excitation, *Applied Spectroscopy*, *61*(2), 117-129.

Clark, J.C. (1932). Burmese tatu, *Man*, *32*(82), 67-70.

Clark, R. (2007). The scientific investigation of artwork and archaeological artefacts: Raman microscopy as a structural, analytical and forensic tools, *Applied Physics A*, *89*(4), 833-840.

Clark, R. (2005). Raman microscopy in the identification of pigments on manuscripts and other artwork, Sackler NAS Colloquium, Scientific Examination of Art: Modern Techniques in Conservation and Analysis.

Colombini A. and D. Kaifas (2010). Characterization of some orange and yellow organic and fluorescent pigments by Raman spectroscopy, *e-Preservation Science*, *7*, 14-21.

Colthup N., L. Daly & S. Wiberly (1990). *Introduction to Infrared and Raman Spectroscopy*, Third edition. San Diego, CA: Academic Press, Inc.

Corredor, C., T. Teslova, M. Cañamares, Z. Chen, J. Zhang, J. Lombardi & M. Leona (2009). Raman and surface-enhanced Raman spectra of chrysin, apigenin, luteolin, Vibrational Spectroscopy, 49(2), 190-195.

Cotton, F.A. (1964). *Chemical Applications of Group Theory*, New York, NY: Interscience Publishers (John Wiley and Sons, Inc.).

Crown, D. (1968). *The forensic examination of paints and pigments*. Springfield, Illinois: Charles C Thomas.

Cui, Y., A. Spann, L. Couch, N. Gopee, F. Evans, M. Churchwell, L. Williams, D. Doerge, & P. Howard (2004). Photodecomposition of pigment yellow 74, a pigment used in tattoo inks, *Photochemistry and Photobiology*, *80*(2), 175-184.

Dahlen, M.A. (1939). The phthalocyanines: A new class of synthetic pigments and dyes, *Industrial and Engineering Chemistry*, *31*(7), 839-847

Dangerous Materials Found in Tattoo Ink: German Study (2011, February 18). *Reuters.* Retrieved from http://www.reuters.com/article/2011/02/18/us-germany-tattoo-health-idUSTRE71H4WI20110218.

Daubert v. Merrell Dow Pharmaceuticals, Inc., 509 U.S. 579 (1993) (*Daubert* I)

Daubert v. Merrell Dow Pharmaceuticals, Inc., 43 F.3d 1311 (9th Cir. 1995) (*Daubert* II)

Debnath, N.C. & S. Vaidya (2006). Application of x-ray diffraction technique for characterization of pigments and control of paints quality, *Progress in Organic Coatings*, *56*(2-3), 159-168.

DeCuyper, C. & M. Perez-Cotapos, Eds. (2010). Dermatologic complications with body art: Tattoos, piercings and permanent make-up, Heidelberg: Springer.

De Donno, A., D. Carlucci and F. Introna (2008). The use of infrared rays for identification purposes, *Journal of Forensic Identification*, *58*(2), 193-202.

de Faria, D. & M. de Souza (1999). Raman spectra of human skin and nail excited in the visible region, *Journal of Raman Spectroscopy*, *30*(3), 169-171.

DeGelder, J., P. Vandenabeele, F. Govaret & L. Moens (2005). Forensic analysis of automotive paints by Raman spectroscopy, *Journal of Raman Spectroscopy*, *36*(11), 1059-1067.

Degano, I., Ribechini, F. Modugno & M. Colombini (2009). Analytical methods for the characterization of organic dyes in artworks and in historical textiles, Applied *Spectroscopy Reviews*, *44*, 363-410.

Demello, M. (1993). The convict body: Tattooing among male American prisoners, *Anthropology Today*, *9*(6), 10-13.

Dennington, R., T. Keith & J. Millam (2009). GaussView, Version 5, *Semichem Inc*., Shawnee Mission, KS.

Dorfer, L, M. Moser, K. Spindler, F. Bahr, E. Egarter-Vigl & G. Dohr (1998). 5,200-year-old acupuncture in Central Europe, *Science, New Series*, *282*(5387), 242-243.

Dorfer, L., M. Moser, F. Bahr, K. Spindler, E. Egarter-Vigl, S. Guillen, G. Dohr & T. Kenner (1999). A Medical Report from the stone age? *The Lancet*, *354*(9183), 1023-1025.

Doyle, A.C. (1891). *Adventures of Sherlock Holmes: The red-headed league*, The Original Illustrated Sherlock Holmes, New York, NY: Castle Books.

Dye, I. (1989). The tattoos of early American seafarers, *Proceedings of the American Philosophical Society*, *133*(4), 520-554.

Eastaugh, N., V. Walsh, T. Chaplin, & R. Siddall (2008). *Pigment compendium: A dictionary and optical microscopy of historical pigments*, Oxford, UK: Elsevier Ltd.

Edwards, H.G.M. & J.M Chalmers, Eds. (2005). *Raman spectroscopy in archaeology and art history*. Cambridge UK: Royal Society of Chemistry.

Edwards, H., M. Gniadecka, S. Peterson, J.P. Hart Hansen, O.F. Nielson, D. Christensen, & H. Wilf (2002). NIR-FT Raman spectroscopy as a diagnostic probe for mummified skin and nails, *Vibrational Spectroscopy*, *28*(1), 3-15.

Edwards, H. & T. Munshi (2005). Diagnostic Raman spectroscopy for the forensic detection of biomaterials and the preservation of cultural heritage, *Analytical and Bioanalytical Chemistry*, *382*(6), 1398-1406.

Engel, E. (2007). Tattoo pigments in skin: Determination and quantitative extraction of red tattoo pigments, Ph.D. Dissertation, University of Regensburg.

Engel, E., F. Santarelli, R. Vasold, H. Ulrich, T. Maisch, B. Konig, M. Landthaler, N. Gopee, P. Howard, & W. Baumler (2008). Establishment of an extraction method for the recovery of tattoo pigments from human skin using HPLC diode array detector technology, *Analytical Chemistry*, *78*(18), 6440-6447.

Engel, E., A. Spannberger, R. Vasold, B. Konig, M. Landthaler & W. Bäumler (2007). Photochemical cleavage of a tattoo pigment by UVB radiation or natural sunlight, ***Journal*** *der Deutschen Dermatologischen Gesellschaft*, *5*(7), 583-589.

Fahim, K. (2010, December 10). Experts for defense in police brutality case say evidence is not consistent with claims. *The New York Times*. Available at http://www.nytimes.com/2010/02/10/nyregion/10mineo.html.

Fateley, W., F. Dollish, N. McDevitt & F. Bentley (1972). *Infrared and Raman selection rules for molecular and lattice vibrations: The correlation method*, New York, NY: Wiley-Interscience.

Federal Rules of Evidence (2006), Washington, DC: US Government Printing Office.

Ferraro, J., K. Nakamoto & C. Brown (2003), *Introduction to Raman spectroscopy*, Second edition, San Diego, CA: Academic Press.

Fleming, J. (1997). The renaissance tattoo, *Anthropology and Aesthetics*, No. 31, 34-52.

Friedstein, H. (1981). A short history of the chemistry of painting, *Journal of Chemical Education*, *58*(4), 291-295.

Frisch, M.J., G. W. Trucks, H. B. Schlegel, G. E. Scuseria, M. A. Robb, J. R. Cheeseman, J. A. Montgomery, Jr., T. Vreven, K. N. Kudin, J. C. Burant, J. M. Millam, S. S. Iyengar, J. Tomasi, V. Barone, B. Mennucci, M. Cossi, G. Scalmani, N. Rega, G. A. Petersson, H. Nakatsuji, M. Hada, M. Ehara, K. Toyota, R. Fukuda, J. Hasegawa, M. Ishida, T. Nakajima, Y. Honda, O. Kitao, H. Nakai, M. Klene, X. Li, J. E. Knox, H. P. Hratchian, J. B. Cross, V. Bakken, C. Adamo, J. Jaramillo, R. Gomperts, R. E. Stratmann, O. Yazyev, A. J. Austin, R. Cammi, C. Pomelli, J. W. Ochterski, P. Y. Ayala, K. Morokuma, G. A. Voth, P. Salvador, J. J. Dannenberg, V. G. Zakrzewski, S. Dapprich, A. D. Daniels, M. C. Strain, O. Farkas, D. K. Malick, A. D. Rabuck, K. Raghavachari, J. B. Foresman, J. V.

Ortiz, Q. Cui, A. G. Baboul, S. Clifford, J. Cioslowski, B. B. Stefanov, G. Liu, A. Liashenko, P. Piskorz, I. Komaromi, R. L. Martin, D. J. Fox, T. Keith, M. A. Al-Laham, C. Y. Peng, A. Nanayakkara, M. Challacombe, P. M. W. Gill, B. Johnson, W. Chen, M. W. Wong, C. Gonzalez, and J. A. Pople (2004). Gaussian 03, Revision C.02. Gaussian, Inc., Wallingford CT.

Fryling, M., C. Frank, & R. McCreery (1993). Intensity calibration and sensitivity comparisons for CCD/Raman spectrometers, *Applied Spectroscopy*, *47*(12), 1965-1974.

Frye v. United States, 293 F. 1013 (D.C. Cir. 1923).

Gallucci, J. (2010, July 1). Long Island's Unidentified Murder Victims. *The Long Island Press*. Retrieved from http://www.longislandpress.com/2010/07/01/long-islands-unidentified-murder-victims/.

Geare, R.(1909). How savages ornament their bodies. In Lummis (Ed.) *Out West* (pp. 787-804). 31(3).

Geiman, I., M. Leona & J.R. Lombardi (2009). Application of Raman spectroscopy and surface-enhanced Raman scattering to the analysis of synthetic dyes found in ballpoint pen inks, *Journal of Forensic Science*, *54*(4), 947-952.

General Electric Co. v. Joiner, 522 U.S. 136 (1997).

Gill-King, H. (1996). Chemical and ultrastructural aspects of decomposition. In Haglund & Sorg, (Eds.) *Forensic taphonomy: The postmortem fate of human remains* (pp. 93-108). Boca Raton, FL: CRC Press.

Gniadecka, M., H. Edwards, J. Hart Hansen, O. Nielsen, D. Christensen, S. Guillen & H. Wulf (1999). Near-Infrared Fourier Transform Raman spectroscopy of the mummified skin of the Alpine Iceman, Qilakitsoq Greenland mummies and Chiribaya mummies from Peru, *Journal of Raman Spectroscopy*, *30*(2), 147-153.

Gniadecka, M., O. Nielson, D. Christensen, H. Wulf, (1998). Structure of water, proteins, and lipids in intact human skin, hair and nail, *The Journal of Investigative Dermatology*, 110(4), 393-398.

Gniadecka, M., H. Wulf, O. Neilson, D. Christensen & J. Hart Hansen (1997). Fourier transform Raman spectroscopy of 15th century mummies from Qilakitsoq, Greenland, *Journal of Raman Spectroscopy*, *28*(2-3), 179-184.

Goldstein, N. (2007). Tattoos defined, *Clinics in Dermatology*, *25*(4), 417-420.

Goulet, P. & R. Aroca (2004). Chemical adsorption of salicylate on Silver- A systematic approach to the interpretation of surface enhanced vibrational spectra, *Canadian Journal of Chemistry*, *82*(6), 987-997.

Gross, H. (1924). *Criminal investigation: a practical textbook for magistrates, police officers and lawyers*, London: Sweet & Maxwell.

Guineau, B. (1989). Non-destructive analysis of organic pigments and dyes using Raman microprobe, microfluorometer or absorption microspectrophotometer, *Studies in Conservation*, *34*(1), 38-44.

Haglund, W.D. & Sperry, K. (1993). The use of hydrogen peroxide to visualize tattoos obscured by decomposition and mummification, *Journal of Forensic Science, 38*(1), 147-150.

Harris, D. & M. Bertolucci (1978). *Symmetry and Spectroscopy: An introduction to vibrational and electronic spectroscopy,* New York, NY: Oxford University Press.

Haynes, C., A. McFarland & R. Van Duyne (2005). Surface-enhanced Raman spectroscopy, *Analytical Chemistry*, *77*, 338A-346A.

Hess, M.W., G. Klima, K. Pfaller, K. Kunzel, & O. Gaber (1998). Histological investigations of the Tyrolean Iceman, *American Journal of Physical Anthropology*, *106*(4), 521-532.

Huang, Z., A. McWilliams, S. Lam, J. English, D. McLean, H. Lui & H. Zeng (2003). Effect of formalin fixation on the near-infrared Raman spectroscopy of normal and cancerous human bronchial tissues, *International Journal of Oncology*, *23*(3), 649-655.

Hunger, K. (1999). The effect of crystal structure on colour application properties of organic pigments, *Review of Progress in Coloration and Related Topics*, *29*(1), 71-84.

Hunger, K and W. Herbst (2000). Pigments, organic. In *Ullmann's Encyclopedia of Industrial Chemistry* (Vol. 27, pp. 379-423), Wiley-VCH.

Huzaira, M. & R. Anderson (2002). Magnetite tattoos, *Lasers in Surgery and Medicine*, *31*(2), 121-128.

Ingle J. & S. Crouch (1988). *Spectrochemical analysis*. Englewood Cliffs, NJ: Prentice Hall.

Istvan, K., G. Keresztury, & A. Szep (2003). Normal Raman and surface enhanced Raman spectroscopic experiments with thin layer chromatography spots of essential amino acids using different laser excitation sources, *Spectrochimica Acta Part A*, *59*(8), 1709-1723.

Jones, C. (1987). Stigma: Tattooing and branding in Graeco-Roman antiquity, *The Journal of Roman Studies*, *77*, 139-155.

Juster, N.J. (1962). Color and chemical constitution, *Journal of Chemical Education*, *39*(11), 596-601.

Kappstatter, B., A. Gendar, C. Siemaszko (2011, March 16). Body of missing Bronx mom Tina Adovasio found in woods; husband expected to turn himself in. *New York Daily News*. Retrieved from http://articles.nydailynews.com/2011-03-16/news/29175646_1_sources-housing-cop-bronx-home.

Karsai, S., G. Pfirrmann, S. Hammes & C. Raulin (2008). Treatment of resistant tattoos using a new generation Q-switched Nd:YAG laser: Influence of beam profile and spot size on clearance success, *Lasers in Surgery and Medicine*, *40*(2), 139-145.

Kazandjieva, J., I. Grozdev & N. Tsankov (2007). Temporary henna tattoos, *Clinics in Dermatology*, *25*(4), 383-387.

Kemp, J. (2011, June 22). Cops identify body of woman whose beau killed himself. *New York Daily News*. Retrieved from http://articles.nydailynews.com/2011-06-22/news/29710635_1_bronx-woman-brush-fire-bronx-apartment.

Keren, S., C. Zavaleta, Z. Cheng, A. de la Zerda, O. Gheysens & S. Gambhir (2008). Noninvasive molecular imaging of small living subjects using Raman spectroscopy, *Proceedings of the National Academy of Science*, *105*(15), 5844-5849.

Kim, S. R. Hammaker & W. Fateley (1986). Calibrating Raman spectrometers using a Neon lamp, *Applied Spectroscopy*, *40*(3), 412-415.

Koch, W. & M. Holthausen (2001). A chemist's guide to density functional theory, Weinheim: Wiley-VCH.

Kumho Tire Co. v. Carmichael, 526 U.S. 137, 1999.

Kuperman-Beade, M., V. Levine, & R. Ashinoff (2001). Laser removal of tattoos, *American Journal of Clinical Dermatology, 2*(1), 21-25.

Kuptsov, A. (1994). Applications of Fourier transform Raman spectroscopy in forensic science, *Journal of Forensic Sciences*, *39*(2), 305-318.

Lake, N.C. (1958). Tattooing in the service of surgery, *The British Medical Journal*, *1*(5079), 1084-1087.

Lee, P. & Meisel (1982). Adsorption and surface enhanced Raman of dyes on Silver and Gold sols, *Journal of Physical Chemistry*, *86*(17), 3391-3395.

Leona, M. (2009). Microanalysis of organic pigments and glazes in polychrome works of art by surface-enhanced resonance Raman scattering, *Proceedings of the National Academy of Sciences*, *106*(35), 14757-14762.

Leona, M., P. Decuzzi, T. Kubic, G. Gates & J. Lombardi (2011). Nondestructive Identification of Natural and Synthetic Organic colorants in works of art by surface enhanced Raman scattering, *Analytical Chemistry*, *83*(11), 3990-3993.

Leona, M. & J.R. Lombardi (2007). Identification of berberine in ancient and historical textiles of surface-enhanced Raman scattering, *Journal of Raman Spectroscopy*, *38*(7), 853-858.

Leona, M., J. Stenger, & E. Ferloni (2006). Application of surface-enhanced Raman scattering techniques to the ultrasensitive identification of natural dyes in works of art, *Journal of Raman Spectroscopy*, *37*(10), 981-992.

Li, D., Z. Peng, L. Deng, Y. Shen and Y. Zhou (2005). Theoretical studies on molecular structure and vibrational spectra of copper phthalocyanine, *Vibrational Spectroscopy*, 39, 191-199.

Littleford, R., M. Hughes, G. Dent, D. Tackley & W. Smith (2003). Surface enhanced resonance Raman scattering of black inkjet dyes in solution and *in situ* printed onto paper, *Applied Spectroscopy*, *57*(8), 977-983.

Liu, Z, X. Zhang, Y. Zhang and J. Jiang (2007). Theoretical investigation of the molecular, electronic structures and vibrational spectra of a series of first transition metal phthalocyanines, *Spectrochimica Acta Part A*, 67, 1232-1246.

Lomax, S.Q., & T. Learner (2006). A review of the classes, structures and methods of analysis of synthetic organic pigments, *Journal of the American Institute for Conservation of Historic and Artistic Works*, *45*(2), 107-125.

Lombardi, J.R. & R.L. Birke (2008). A unified approach to surface-enhanced Raman spectroscopy, *Journal of Physical Chemistry C, 112*(14), 5605-5617.

Lombardi, J.R. & R.L. Birke (2009). A unified view of surface-enhanced Raman scattering, *Accounts of Chemical Research*, *42*(6), 734-742.

Lundsgard, J. (2002). Survey of chemical compounds in consumer products: Investigation of pigments in tattoo colors, Danish Environmental Protection Agency.

Lynnerup, N. (2007). Mummies, *Yearbook of Physical Anthropology*, *134*(45S), 162-190.

Lyon, L., C. Keating, A. Fox, B. Baker, L. He, S. Nicewarner, S. Mulvaney & M. Natan (1998). Raman Spectroscopy, *Analytical Chemistry, 70*(12), 341R-361R.

MacDill, M. (1927). Tattoo marks yield to chemical treatment, *The Science News-Letter*, *12*(338), 209-214.

Majoube, M. & M. Henry (1991). Fourier transform Raman and infrared and surface enhanced Raman spectra for Rhodamine 6G, *Spectrochimica Acta*, *47A*(9/10), 1459-1466.

Martinez, R. & C. Wetli (1989). Tattoos of the Marielitos, *The American Journal of Forensic Medicine and Pathology*, *10*(4), 315-325.

Matthews, D. (1947). Technique and value of tattooing in plastic surgery, *Proceedings of the Royal Society of Medicine*, *40*(14) 881-883.

Mazzella, W. & P. Buzzini (2005). Raman spectroscopy of blue gel pen inks, *Forensic Science International*, *152*(2-3), 241-247.

McCreery, R. (2000). *Raman Spectroscopy for Chemical Analysis*. Danvers, MA: Wiley-Interscience, John Wiley and Sons, Inc. (see also The McCreery Group website: http://www.chem.ualberta.ca/~mccreery/ramanmaterials.html.).

McCreery, R. (2002). Photometric standards for Raman spectroscopy, In Chalmers and Griffiths, (Eds.), *Handbook of Vibrational Spectroscopy*, Chichester: John Wiley & Sons.

McGowan, G. & J. Prangnell (2006). The Significance of Viviante in archaeological settings, *Geoarchaeology: An International Journal*, *21*(1), 93-111.

McKechnie, M., G. Porter & N. Langlois (2008). The detection of latent residue tattoo ink pigments in skin using invisible radiation photography, *Australian Journal of Forensic Sciences*, *40*(1), 65-72.

McQuarrie, D. & J. Simon (1997). *Physical chemistry: A molecular approach*. Sausalito, CA: University Science Books.

The Merck Index of Chemicals and Drugs: An encyclopedia for the chemist, pharmacist, physician and allied professions (1952). Sixth edition, Rahway NJ : Merck & Co, Inc,.

Miller, F. & G. Kauffman (1989). C.V. Raman and the discovery of the Raman effect, *Journal of Chemical Education*, *66*(10), 795-801.

Miller, L., & R. McEvoy, Jr. (2011). *Police Photography*, Sixth edition, Burlington, MA: Anderson Publishing.

Miranda, M.D. (2003). Infrared analysis of forensic evidence: A comparison of transmission and reflection methods, M.S. Thesis, John Jay College of Criminal Justice, The City University of New York.

Moenssens, Andre (1993). Novel Scientific Evidence in Criminal Cases: Some Words of Caution, *The Journal of Criminal Law and Criminology*, *84*(1), 1-21.

Morgan, B. (1974).Tattoos, *British Medical Journal*, *3*, 34-36.

Moskovits, M. (2005). Surface-enhanced Raman spectroscopy: a brief retrospective, *Journal of Raman Spectroscopy*, *36*(6-7), 485-496.

MSDS- Material Safety Data Sheets, Infinitink Tattoo Inks. Available at http://www.infinitink.com/consumer/c_ink.php.

MSDS- Material Safety Data Sheets, Skin Candy Tattoo Inks. Available at http://skincandytattoosupply.com/.

Naito, S., Y. Min, K. Sugata, O. Osanai, T. Kitahara, H. Hiruma & H. Hamaguchi (2008). *In vivo* measurement of human dermis by 1064nm- excited fiber Raman spectroscopy, *Skin Research and Technology*, *14*(1), 18-25.

National Academy of Sciences Report, *Strengthening forensic science in the United States: A path forward* (2009), Washington DC: National Academies Press.

OPUS Spectroscopy Software User Manual (2006). OVP Raman, Version 6, Bruker Optik.

Orna, M.V. (1980). Chemistry or artists' colors: Part II Structural features of colored compounds, *Journal of Chemical Education*, *57*(4), 264-267.

Pabst, M.A., I. Leftrosky, Papst, E. Bock, M. Moser, L. Dorfer, E. Egarter-Vigl, & F. Hofer (2009). The tattoos of the Tyrolean Iceman: a light microscopical, ultrastructural and element analytical study, *Journal of Archaeological Science*, *36*(10), 2335-2341.

Pages-Camagna, A. Duval & H. Guicharnaud (2004). Study of Gustave Moreau's black drawings: identification of the graphic materials by Raman microspectrometry and PIXIE, *Journal of Raman Spectroscopy*, *35*(8-9), 628-632.

Panina, N. R. van de Ven, P. Verwer, H. Meekes, E. Vlieg and G. Deroover (2008). Polymorph prediction of organic pigments, *Dyes and Pigments*, 79, 183-192.

Parker v. Mobil Oil Corporation, et. al., 2006 NY Slip Op 7391 Court of Appeals New York, 2006.

Parker, S., K. Williams, P. Hendra & A. Turner (1988). Fourier Transform Raman Spectroscopy using a bench-top FT-IR spectrometer, *Applied Spectroscopy*, *42*(5), 796-800.

Pauling, L., & E. Wilson, Jr. (1985), *Introduction to quantum mechanics with applications to chemistry*, New York, NY: Dover Publications, Inc.

Petersen, S., O. Nielson, D. Christensen, H. Edwards, D. Farwell, R. David, P. Lambert, M. Gniadecka & H. Wulf (2003). Near-infrared Fourier transform Raman spectroscopy of skin samples from the 'Tomb of the two brothers' Khnum-Nakht and Nekt-Ankh, XIIth Dynasty Egyptian mummies (ca 2000 BC), *Journal of Raman Spectroscopy*, *34*(5), 375-379.

Pfirrmann, G., S. Karsai, S. Roos, S. Hammes and C. Raulin (2007). Tattoo removal-state of the art, *Journal der Deutschen Dermatologischen*, 10(5), 889-898.

Poon, K., I. Dadour, & A. McKinley (2008). *In situ* chemical analysis of modern organic tattooing inks and pigments by micro-Raman spectroscopy, *Journal of Raman Spectroscopy*, *39*(9), 1227-1237.

Poon, K.W.C. (2008). *In situ* chemical analysis of tattooing inks and pigments-Modern organic and traditional pigments in ancient mummified remains, M.S./Ph.D. Thesis, The University of Western Australia.

Radley, J.A. (1948). *Photography in crime detection*, London: Chapman and Hall, Ltd.

Raman, C.V. & K.S. Krishnan (1929). The production of new radiations by light scattering-Part I, *Proceedings of the Royal Society of London Series A*, *122*(789), 23-35.

Rana, V., M. Canamares, T. Kubic, M. Leona & J. Lombardi (2011). Surface-enhanced Raman spectroscopy for trace identification of controlled substances: Morphine, Codeine and Hydrocodone, *Journal of Forensic Sciences*, *56*(1), 200-207.

Ray, K. & R. McCreery (1997). Simplified calibration of instrument response function for Raman spectrometers based on luminescent intensity standards, *Applied Spectroscopy*, *51*(1), 108-116.

Reed, C. (2000). Tattoo in early China, *Journal of the American Oriental Society*, *120*(3), 360-376.

Regensburger, J., K. Lehner, T. Maisch, R. Vasold, F. Santerelli, E. Engel, A. Gollmer, B. Konig, M. Landthaler and W. Bäumler (2010). Tattoo inks contain polycyclic aromatic hydrocarbons that additionally generate deleterious singlet oxygen, *Experimental Dermatology*, 19, e275-e281.

Riegel, E. (1942). *Industrial chemistry: An elementary treatise for the student and general reader*, New York, NY: Reinhold Publishing Co.

Robinson, E. (2010). *Crime scene photography*, Second edition, Burlington, MA: Academic Press.

Rodger, C., G. Dent, J. Watkinson & W. Smith (2000). Surface-enhanced resonance Raman scattering and near-infrared Fourier transform Raman scattering as *in situ* probes for ink jet dyes printed on paper, *Applied Spectroscopy*, *54*(11), 1567-1576.

Rodger, C., V. Rutherford, D. Broughton, P. White, & W. Smith (1998). The *in situ* analysis of lipsticks by surface enhanced resonance Raman scattering, *Analyst*, *123*(9), 1823-1826.

Ropret, P., S. Centeno, & P. Bukovec (2008). Raman identification of yellow synthetic organic pigments in modern and contemporary paintings: Reference spectra and case studies, *Spectrochimica Acta Part A*, *69*(2), 486-497.

Roth, H.L. (1901) Maori tatu and moko, *The Journal of the Anthropological Institute of Great Britain and Ireland*, *31*, 29-64.

Roth, H.L. (1905). Tatu in the Society Islands, *The Journal of the Anthropological Institute of Great Britain and Ireland*, *35*, 283-294.

Rykhlinskaya, K. & S. Fritzsche (2004). Use of group theory for the analysis of vibrational spectra, *Computer Physics Communications*, *162*(2), 124-142.

Scherrer, N., Z. Stefan, D. Francoise, F. Annette & K. Renate (2009). Synthetic organic pigments of the 20th and 21st century relevant to artist's paints: Raman spectra reference collection, *Spectrochimica Acta Part A*, *73*(3), 505-524.

Schildkrout, E. (2004). Inscribing the body, *Annual Review of Anthropology*, *33*, 319-344.

Schmitt, M., J. Popp (2006). Raman spectroscopy at the beginning of the twenty-first century, *Journal of Raman Spectroscopy*, *37*(1-3), 20-28.

Schulte, F., K Brzezinka, K. Lutzenberger, H. Stege, & U. Panne (2008). Raman Spectroscopy of synthetic organic pigments used in 20th century works of art, *Journal of Raman Spectroscopy*, *39*(10), 1455-1463.

Sequin-Frey, M. (1981). The chemistry of paint and animal dyes, *Journal of Chemical Education*, *58*(4), 301-305.

Skoog, D., F. Holler & Nieman (1998). *Principles of instrumental analysis*, Fifth edition. Philadelphia, PA: Harcourt Brace College Publishers.

Slater, D. & T. Durrant (1984) Tattoos: light and transmission electron microscopy studies with x-ray microanalysis, *Clinical and Experimental Dermatology*, *9*(2), 167-173.

Smeaton, W. (1937). Tattooing among the Arabs of Iraq, *American Anthropologist*, *39*(1), 53-61.

Smith E. & G. Dent (2005). *Modern Raman spectroscopy-A practical approach*, Chichester, England: John Wiley and Sons, Ltd.

Smith, G. & M. Zimmerman (1975). Tattooing found on a 1600 year old frozen, mummified body from St. Lawrence island, Alaska, *American Antiquity*, *40*(4), 433-437.

Society of Dyers and Colourists (1971). *The Colour Index*, Third Edition. American Association of Textile Chemists and Colorists, Bradford, England.

Sowden, J., J. Byrne, A. Smith, C. Hiley, V. Suarez, B. Wagner & D. Slater (1991). Red tattoo reactions: x-ray microanalysis and patch-test studies, *British Journal of Dermatology*, *124*(6), 576-580.

Sperry, K. (1991). Tattoos and tattooing part I: History and methodology, *The American Journal of Forensic Medicine and Pathology*, *12*(4), 313-319.

Sperry, K. (1992). Tattoos and tattooing part II: Gross pathology, histopathology, medical complications and applications, *The American Journal of Forensic Medicine and Pathology*, *13*(1), 7-17.

Stallmann, O. (1960). Use of metal complexes in organic dyes and pigments, *Journal of Chemical Education*, *37*(5), 220-230.

Sullivan, L. (2004). Tattooing. In M. Bosworth, (Ed.), *Encyclopedia of Prisons and Correctional Facilities*. (Vol. 2, pp. 947-949). Thousand Oaks, CA: Sage Publications Inc.

Szabo, A. & N. Ostlund (1996). *Modern quantum chemistry: Introduction to advanced electronic structure theory*, New York, NY: Dover Publications, Inc.

Taplin, F. (2011). Application of Raman spectroscopy, surface enhanced Raman scattering (SERS) and density functional theory for the identification of phenylethylamine and its analogs, Master's Thesis, John Jay College of Criminal Justice- The City University of New York.

Teslova, T., C. Corredor, R. Livingstone, T. Spataru, R. Birke, J. Lombardi, M. Cañamares & M. Leona (2007). Raman and surface-enhanced Raman spectra of flavones and several hydroxyl derivatives, *Journal of Raman Spectroscopy*, *38*(7), 802-818.

Thomas, J., P. Buzzini, G. Massonnet, B. Reedy & C. Roux (2005). Raman spectroscopy and the forensic analysis of black/grey and blue cotton fibers, Part I: Investigation of the effects of varying laser wavelength, *Forensic Science International*, *152*(2-3), 189-197.

Thomson, J. (1977). Identification of organic pigments on substrates other than textile fibers. In Venkataraman, K.,(Ed.) *The analytical chemistry of synthetic dyes* (pp. 431-464) New York, NY: John Wiley and Sons.

Timko, A., C. Miller, F. Johnson, & E. Ross (2001). *In vitro* quantitative chemical analysis of tattoo pigments, *Archives of Dermatology*, *137*(2) 143-147.

Tran, C. (1984). *In situ* identification of paper chromatogram spots by surface enhanced Raman spectroscopy, *Journal of Chromatography*, *292*, 432-438.

Tseng, C., J. Ford, C. Mann & T. Vickers (1993). Wavelength calibration of a multichannel spectrometer, *Applied Spectroscopy*, *47*(11), 1808-1813.

Turrell, G. & J. Corset, Eds. (1996). *Raman microscopy: Developments and applications*, London: Academic Press, Harcourt Brace & Company.

Vandenabeele, P, L. Moens, H. Edwards & R. Dams (2000). Raman spectroscopic database of azo pigments and application to modern art studies, *Journal of Raman Spectroscopy*, *31*(6), 509-517.

Vandenabeele, P., H. Edwards, & L. Moens (2007). A Decade of Raman Spectroscopy in Art and Archaeology, *Chemical Reviews*, *107*(3), 675-686.

Vasold, R., N. Naarmann, H. Ulrich, D. Fischer, B. Konig, M. Landthaler & W. Baumler (2004). Tattoo pigments are cleaved by laser light-The chemical analysis *in vitro* provide evidence for hazardous compounds, *Photochemistry and Photobiology*, *80*(2), 185-190.

Verbov, J. (1983). Mummified Skin-An exercise in preservation, *International Journal of Dermatology*, *22*(1), 46-60.

Vickers, T & C. Mann (1999). Raman shift calibration of a compact multichannel spectrometer, *Applied Spectroscopy*, *53*(12), 1617-1622.

Wang, H., G. Provan and K. Helliwell (2003). Identification of hamamelitannin, catechins and gallic acid in witch hazel bark, twig and leaf by HPLC, *Journal of Pharmaceutical and Biomedical Analysis*, *33*(4), 539-544.

White, P., C. Rodger, V. Rutherford, Y. Finnon, W. Smith, & M. Fitzgerald (1998). Surface enhanced resonance Raman scattering (SERRS) spectroscopy. A powerful technique for

the forensic analysis of colourants? SPIE Conference on Investigation and Forensic Science Technologies.

Wilson, E.B., J. Decius and P. Cross (1955). *Molecular Vibrations: The theory of infrared and Raman vibrational spectra*, New York, NY: Dover Publications, Inc.

Wright, F.D. & G.S. Golden (2010). The use of full spectrum digital photography for evidence collection and preservation in cases involving forensic odontology, *Forensic Science International*, *201*(1-3), 59-67.

Zieba-Palus, J. & M. Kunicki (2006). Application of the micro-FTIR spectroscopy, Raman spectroscopy and XRF method examination of inks, *Forensic Science International*, *158*(2-3), 164-172.

Zieba-Palus, A. Michalska & A. Weselucha-Birczynska (2011). Characterisation of paint samples by infrared and Raman spectroscopy for criminalistic purposes, *Journal of Molecular Structure*, *993*(1-3), 134-141.

Zollinger, H. (2003). *Color chemistry: Syntheses, properties, and applications of organic dyes and pigments*, 3rd ed. Switzerland: Wiley-VCH.